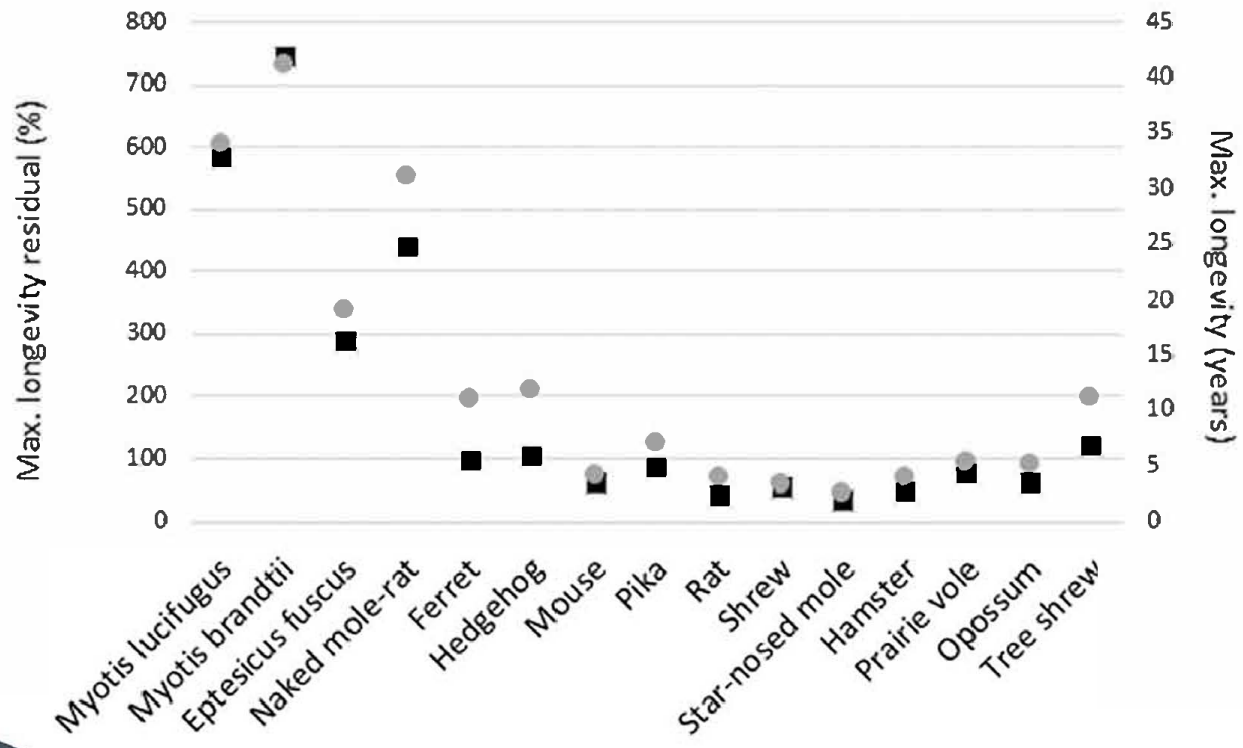

Special Collection on Tumor Suppressors

Small-bodied mammals that display exceptional longevity, see Lambert et al. - "Adaptive sequence convergence of the tumor suppressor ADAMTS9 between small-bodied mammals displaying exceptional longevity."

Tumor Suppressors | AgING

ONLINE ISSN: 1945-4589

AGING

www.aging-us.com

Aging (ISSN: 1945 - 4589) is published monthly by Impact Journals, LLC.
6666 East Quaker St., Suite 1B, Orchard Park, NY 14127

Abstracted and/or indexed in: PubMed/Medline (abbreviated as "Aging (Albany NY)"), PubMed Central (abbreviated as "Aging (Albany NY)"), Web of Science/Science Citation Index Expanded (abbreviated as Aging-US) & listed in the Cell Biology-SCIE and Geriatrics & Gerontology category, Scopus /Rank Q1(the highest rank) (abbreviated as Aging)- Aging and Cell Biology category, Biological Abstracts, BIOSIS Previews, EMBASE, META (Chan Zuckerberg Initiative), Dimensions (Digital Science's).

Editorial and Publishing Office Aging
6666 E. Quaker St., Suite 1,
Orchard Park, NY 14127
Phone: 1-800-922-0957
Fax: 1-716-508-8254
e-Fax: 1-716-608-1380

Submission
Please submit your manuscript on-line at http://aging.msubmit.net

Editorial
For editorial inquiries, please call us or email editors@impactaging.com

Production
For questions related to preparation of your article for publication, please call us or email krasnova@impactaging.com

Indexing
If you have questions about the indexing status of your paper, please email kurenova@impactaging.com

Billing/Payments
If you have questions about billing/invoicing or would like to make a payment, please call us or email payment@impactaging.com

Media
If you have questions about post publication promotion, Altmetric, video interviews or social media, please email media@impactjournals.com

Printing
Each issue or paper can be printed on demand. To make a printing request, please call us or email printing@impactjournals.com

Publisher's Office
Aging is published by Impact Journals, LLC
To contact the Publisher's Office, please email: publisher@impactjournals.com, visit www.impactjournals.com, or call 1-800-922-0957

Aging (ISSN: 1945 - 4589) is published twice a month by Impact Journals, LLC.
6666 East Quaker St., Suite 1B, Orchard Park, NY 14127

Abstracted and/or indexed in: PubMed/Medline (abbreviated as "Aging (Albany NY)"), PubMed Central (abbreviated as "Aging (Albany NY)"), Web of Science/Science Citation Index Expanded (abbreviated as Aging-US) & listed in the Cell Biology-SCIE and Geriatrics & Gerontology category, Scopus /Rank Q1(the highest rank) (abbreviated as Aging) - Aging and Cell Biology category, Biological Abstracts, BIOSIS Previews, EMBASE, META (Chan Zuckerberg Initiative), Dimensions (Digital Science's).

IMPACT JOURNALS

Table of Contents

Overexpression of hsa_circ_0002874 promotes resistance of non-small cell lung cancer to paclitaxel by modulating miR-1273f/MDM2/p53 pathway

Originally published in Volume 13, Issue 4 pp 5986-6009

ITPKA induces cell senescence, inhibits ovarian cancer tumorigenesis and can be downregulated by miR-203

Originally published in Volume 13, Issue 8 pp 11822-11832

Expression profile, molecular functions, and prognostic significance of miRNAs in primary colorectal cancer stem cells

Originally published in Volume 13, Issue 8 pp 12067-12085

Cdkn1a transcript variant 2 is a marker of aging and cellular senescence

Originally published in Volume 13, Issue 10 pp 13380-13392

LHX9, a p53-binding protein, inhibits the progression of glioma by suppressing glycolysis

Originally published in Volume 13, Issue 18 pp 22109-22119

Metformin-induced chemosensitization to cisplatin depends on P53 status and is inhibited by Jarid1b overexpression in non-small cell lung cancer cells

Originally published in Volume 13, Issue 18 pp 21914-21940

The telomere-mitochondrial axis of aging in newborns

Originally published in Volume 14, Issue 4 pp 1627-1650

TP53/BRAF mutation as an aid in predicting response to immune-checkpoint inhibitor across multiple cancer types

Originally published in Volume 14, Issue 6 pp 2868-2879

Wild type and gain of function mutant TP53 can regulate the sensitivity of pancreatic cancer cells to chemotherapeutic drugs, EGFR/Ras/Raf/MEK, and PI3K/mTORC1/GSK-3 pathway inhibitors, nutraceuticals and alter metabolic properties

Originally published in Volume 14, Issue 8 pp 3365-3386

Research Paper

Integrated analysis of colorectal cancer microRNA datasets: identification of microRNAs associated with tumor development

Luca Falzone[1,*], Letizia Scola[2,*], Antonino Zanghì[3], Antonio Biondi[4,5], Antonio Di Cataldo[3,5], Massimo Libra[1,5], Saverio Candido[1,5]

[1]Department of Biomedical and Biotechnological Sciences, University of Catania, Catania 95123, Italy
[2]Department of Pathobiology and Medical Biotechnologies, University of Palermo, Palermo 90127, Italy
[3]Department of Medical and Surgical Sciences and Advanced Technology "G.F. Ingrassia", University of Catania, Catania 95125, Italy
[4]Department of General Surgery, Vittorio Emanuele Hospital, University of Catania, Catania 95124, Italy
[5]Research Center for Prevention, Diagnosis and Treatment of Cancer (PreDiCT), University of Catania, Catania 95123, Italy
[*]Equal contribution

Correspondence to: Massimo Libra; **email:** mlibra@unict.it
Keywords: colorectal cancer, microRNA, bioinformatics, dataset, biomarker
Received: April 4, 2018 **Accepted:** May 7, 2018 **Published:** May 18, 2018

ABSTRACT

Colorectal cancer (CRC) is one of the leading cause of cancer death worldwide. Currently, no effective early diagnostic biomarkers are available for colorectal carcinoma. Therefore, there is a need to discover new molecules able to identify pre-cancerous lesions. Recently, microRNAs (miRNAs) have been associated with the onset of specific pathologies, thus the identification of miRNAs associated to colorectal cancer may be used to detect this pathology at early stages. On these bases, the expression levels of miRNAs were analyzed to compare the miRNAs expression levels of colorectal cancer samples and normal tissues in several miRNA datasets. This analysis revealed a group of 19 differentially expressed miRNAs. To establish the interaction between miRNAs and the most altered genes in CRC, the mirDIP gene target analysis was performed in such group of 19 differentially expressed miRNAs. To recognize miRNAs able to activate or inhibit genes and pathways involved in colorectal cancer development, DIANA-mirPath prediction analysis was applied. Overall, these analyses showed that the up-regulated hsa-miR-183-5p and hsa-miR-21-5p, and the down-regulated hsa-miR-195-5p and hsa-miR-497-5p were directly related to colorectal cancer through the interaction with the Mismatch Repair pathway and Wnt, RAS, MAPK, PI3K, TGF-β and p53 signaling pathways involved in cancer development.

INTRODUCTION

Colorectal carcinoma (CRC) is the most frequent tumor affecting the entire digestive tract. According to the data reported by GLOBOCAN 2012, CRC is the second most frequent cancer in women and the third most frequent in males. Overall, it is the fourth most frequent cancer in both sexes preceded only by breast, prostate and lung cancers. This tumor is usually diagnosed at the average age of 69 years, in which 60% are over the age of 65 and 36% are over 75 years. Although many therapeutic approaches for CRC are available today, this pathology is still responsible for a high number of deaths, representing the fourth cause of mortality due to cancer diseases (693.933 deaths, 8.5% of all tumor deaths in 2012) [1, 2]. Over the years, the geographical

distribution of CRC has changed, showing today a higher incidence and mortality rates mainly in the more developed countries (Australia/New Zealand/Europe) and in the less developed areas (Eastern Europe/Russia/ South America) respectively [3]. Despite the epidemiological data described above, CRC mortality rate is declining in many developed countries world-wide thanks to the improvement of anti-neoplastic treatments and the new screening programs adopted [4].

Several factors, mainly related to eating habits or lifestyles, contribute to the development of colorectal cancer. Among these risk factors, a leading role is played by obesity [5], cigarette smoking [6], alcohol abuse [7] and by a diet rich in fats and red meat and low in fiber and vegetables [8]. In addition to these risk factors, there are also several physiological and pathological predisposing conditions, such as age over 50 years, family history of CRC, inflammatory bowel disease (IBD) and inherited syndromes (Lynch syndrome, Familial adenomatous polyposis, etc.) [9, 10].

Beside these well-recognized risk factors, CRC onset is often associated with several genetic mutations affecting key genes involved in the regulation of cell cycle, cell proliferation and apoptosis. Among these, mutations occurring in *KRAS*, *APC*, *TP53* and *PIK3CA* genes are the most observed in CRC [11-13]. Other inactivating mutations affect genes involved in the Mismatch Repair system leading to an accumulation of somatic mutations that promote cells' neoplastic transformation [14, 15]. Finally, several studies indicate that CRC development is age-related and that aging is associated with the loss of gene regulation mechanisms that lead to a further accumulation of oncogene mutations [16, 17]. Recently, aging has also been linked to epigenetic modifications capable of altering cellular homeostasis thus favoring the development of tumor pathologies [17-19].

Although colorectal cancer mortality is lower when compared to those of other cancers, the clinical management of CRC is often complicated by several associated comorbidities resulting in a negative health economics impact [20]. The main critical aspects for the management of colorectal cancer are the high rate of tumor relapses after surgery and the frequent and invasive diagnostic tests performed during the follow-up. Other issues are related to the high costs and the low compliance rates of colonoscopy [21] and the low specificity and sensitivity of the screening tests, such as the faecal occult blood test or the detection of CEA and CA 19.9 biomarkers, which often fail to early identify CRC tumor lesions [22,23].

On these bases, the discovery of new markers and the implementation of new diagnostic screening tests for CRC may be helpful to improve the effectiveness of diagnostic strategies, especially in individuals with high risk of tumor development [24].

In the last decade, several studies hypothesized that the development of cancer is associated with the deregulation of microRNAs (miRNAs), small non-coding RNA sequences that inhibit gene expression by binding to mRNAs inducing their degradation or the blocking of translation [25]. In particular, miRNAs can be detected in different biological samples, including serum, saliva and stool, and used as biomarkers with high specificity and sensitivity for the identification of pre-cancerous lesions [26-30]. However, conflicting data were generated on this matter. Such contradictory results may be caused by the difficulty in analyzing the huge amount of information available derived from the genome sequencing analysis [31].

The identification of novel biomarkers, linked to tumor development, is one of the main challenges of cancer research. Accordingly, the computational discovery of over-expressed or down-regulated miRNAs in CRC represents the first step of this process.

To our best knowledge, no previous studies have analyzed simultaneously all microRNA profiling datasets available on tissue samples from CRC patients. In order to identify miRNAs differentially expressed in CRC patients compared to healthy controls, a broad computational analysis of all microRNA profiling datasets, available on the Gene Expression Omnibus DataSets (GEO DataSets), was performed. Furthermore, the interaction between such miRNAs and the main genes altered in CRC were investigated along with their role in the modulation of molecular pathways known to be involved in cancer onset and progression.

RESULTS

microRNA profiling datasets selection

The analysis performed on GEO DataSets allowed to identify 114 microRNA profiling by array datasets (published until December 2017) concerning the CRC. However, most of these did not meet the inclusion and exclusion criteria described above because they were constructed with miRNA expression data obtained from tumor cell lines and not from CRC patients. Therefore, the used criteria allowed to select only 10 datasets in which the subsequent analyses were carried out. All the information about the selected datasets is reported in Table 1.

Table 1. Characteristics of the datasets selected for the study.

Series Accession	Normal n.	Cancer n.	Paired Samples	Defective MMR Samples	Sample Type	Platform	Author ref.	Identified miRNAs
GSE18392	29	116	Yes	19	Fresh frozen tissue	Illumina GPL8178	Sarver, A. L. et al, 2009 [64]	miR-31, miR-135b, miR-552, miR-592, miR-503, miR-1, miR-622, miR-10b, miR-147, miR-33b, miR-143, miR-21
GSE108153	21	21	Yes	Not Defined	Fresh frozen tissue	Agilent GPL19730	Zeng, Z. et al, 2017	Not Reported
GSE30454	20	54	No	35	FFPE tissue	Illumina GPL8179	Balaguer, F. et al, 2011 [65]	miR-1238, miR-192*, miR-362-5p, miR-938, miR-622, miR-133b, miR-16-2*, miR-30a*, miR-183, miR-486-5p
GSE35834	23	31	Yes	Not Defined	Fresh frozen tissue	Affymetrix GPL8786	Pizzini, S. et al, 2013 [66]	miR-143, miR-145, miR-125b, miR-21, miR-17, miR-92, miR-20, miR-100, miR-183, miR-31, miR-150, miR-139-5p, miR-244, miR-10b, miR-99a, miR-182, miR-145, miR-195, miR-497
GSE38389	71	69	Yes	Not Defined	Fresh frozen tissue	Exiqon miRCURY LNA GPL11039	Gaedcke, J. et al, 2012 [67]	miR-135b, miR-492, miR-542-5p, miR-584, miR-483-5p, miR-144, miR-2110, miR-652*, miR-375, miR-147b, miR-148a, miR-190, miR-26a/b, miR-338-3p
GSE41012	15	20	Yes	Not Defined	Fresh frozen tissue	Exiqon miRCURY LNA GPL7724	Li, X. et al, 2015	Not Reported
GSE41655	15	33	No	Not Defined	Fresh frozen tissue	Agilent GPL11487	Shi, X. et al, 2015	Not Reported
GSE49246	40	40	Yes	Not Defined	FFPE tissue	Sun Yat-Sen University Cancer Center GPL17496	Zhang, J. X. et al, 2013 [68]	miR-21-5p, miR-20a-5p, miR-103a-3p, miR-106b-5p, miR-143-5p, miR-215
GSE68204	8	37	Yes	Not Defined	FFPE tissue	Agilent GPL10850	Millino, C. et al, 2017 [69]	miR-572, miR-939, miR-630, miR-638, miR-575, miR-374b, miR-32, miR-186, miR-30e*, miR-150, miR-155, miR-33a, miR-324-5p, miR-200b*, miR-142-3p, miR-210, miR-1260, miR-574-3p, miR-192*, miR-29b, miR-26b, miR-30c, miR-193a-3p, miR-142-5p, miR-29c, miR-7g, miR-7, miR-200a, miR-2015
GSE83924	20	20	Yes	Not Defined	Fresh frozen tissue	Affymetrix GPL16384	Nagy, Z. B. et al, 2016	miR-375, miR-378, miR-139-5p, miR-133a, and miR-422a, miR-503, miR-375, miR-378, miR-139-5p, miR-133a, and miR-422a

Of these datasets, 3 were developed by Agilent (Agilent Human miRNA Microarray), 2 developed by Affymetrix (Affymetrix miRNA Array), 2 developed by Illumina (Illumina Human MicroRNA expression beadchip), 2 developed by Exiqon – Qiagen (Exiqon miRCURY LNA microRNA array v.9.2 Extended Version), and 1 datasets was a custom platform used by Sun Yat-Sen University. Overall, the bioinformatics analysis was carried out on 703 samples of which 262 normal and 441 samples of colorectal carcinoma.

Identification of putative miRNAs involved in CRC development

The differential analysis between colorectal cancer patients and related healthy controls or tissues revealed 20 different TOP 20 miRNAs ($p < 0.01$) that were differentially expressed in at least 3 of the 10 datasets analyzed (> 30% of all datasets). For each differentially expressed miRNA were reported the logFC value (Figure 1). Among these 20 miRNAs, 10 were up-regulated (hsa-miR-1246, hsa-miR-1308, hsa-miR-135b-5p, hsa-miR-183-5p, hsa-miR-18a-5p, hsa-miR-18b-5p, hsa-miR-21-5p, hsa-miR-223-3p, hsa-miR-224-5p, hsa-miR-503-5p) and 10 were down-regulated (hsa-miR-1-3p, hsa-miR-133b, hsa-miR-143-3p, hsa-miR-145-5p, hsa-miR-150-5p, hsa-miR-195-5p, hsa-miR-215-5p, hsa-miR-375, hsa-miR-378-3p and hsa-miR-497-5p). Among up-regulated miRNAs, hsa-miR-18a-5p (5 of 10 datasets) and hsa-miR-135b-5p and hsa-miR-21-5p (4 of 10 datasets) showed higher levels of expression in CRC, while among the down-regulated miRNAs remarkable were hsa-miR-375 and hsa-miR-133b (down-regulated in 5 of 10 datasets).

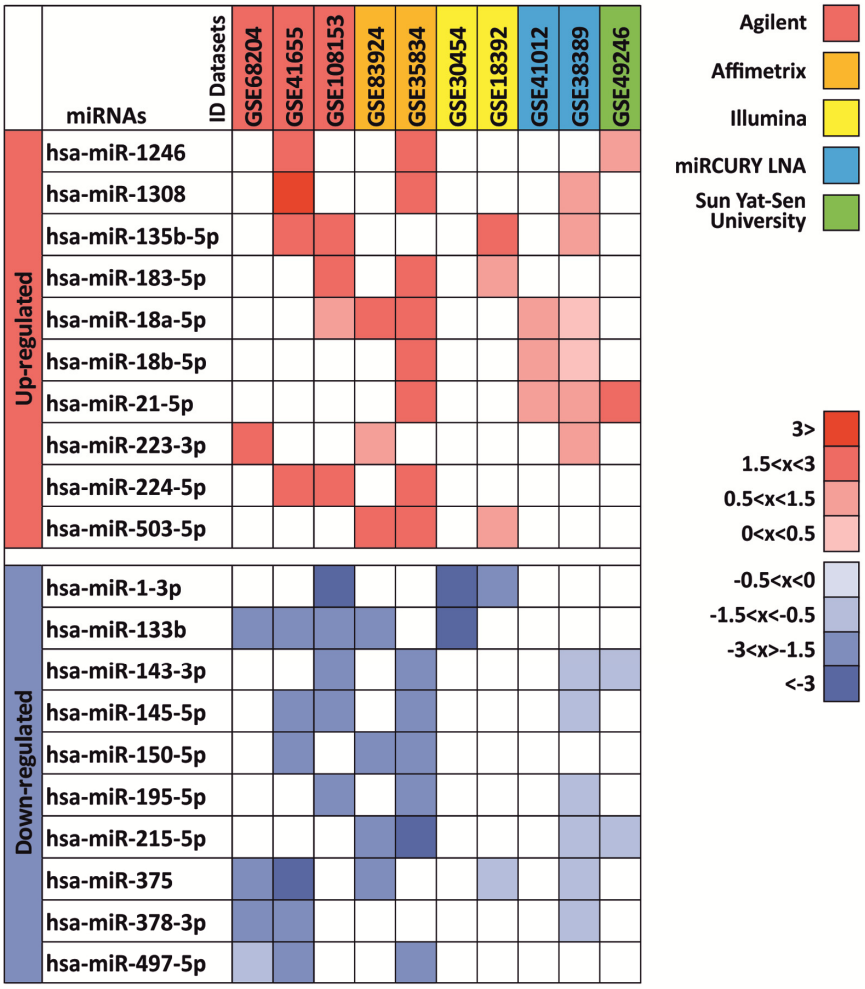

Figure 1. Differentially expressed miRNAs between colorectal cancer samples and normal tissues in at least 3 of 10 datasets. logFC values are reported with red scale boxes for up-regulated miRNAs and blue scale boxes for the down-regulated miRNAs. lgFC values were divided in "highly" (logFC ≥ 3), "moderately" (logFC 1.5 <x< 3), "lightly" (logFC 0.5 <x< 1.5) and "poorly" (logFC 0 <x< 0.5) up-regulated or down-regulated (negative logFC values). ID Datasets boxes were colored in a different manner according to the different microarray platform adopted in the dataset.

The up-regulated miRNA hsa-miR-1308 was excluded from the subsequent gene target and prediction pathway analyses because according to miRBase this is not a miRNA but a fragment of a tRNA.

Gene target analysis of selected miRNAs

Gene target analysis performed by the bioinformatics tool mirDIP showed the level of interaction of the 19 computationally identified miRNAs (hsa-miR-1308 was excluded from this analysis because it is a fragment of a tRNA) with the main gene mutated or altered in CRC.

As shown in Figure 2, we take into account 10 different genes obtained from COSMIC and the mirDIP analysis revealed that all selected miRNAs were able to interact with all genes involved in CRC with high levels of specificity. In particular, for each miRNA were reported the specificity of the interaction, from low to very high specificity. Several miRNAs, such as the up-regulated hsa-miR-223-3p and the down-regulated hsa-miR-195-5p and hsa-miR-497-5p, showed very high and high interaction levels with all genes analyzed suggesting a possible role of these miRNAs in the development of colorectal cancer, while the down-regulated hsa-miR-378a-3p showed the lower level of interaction among all miRNAs. Furthermore, some genes showed to be linked with miRNAs, as in the case of *BRAF* where the only levels of high interaction are with the miRNAs up-regulated hsa-miR-21-5p and the down-regulated hsa-miR-150-5p, hsa-miR-195-5p and hsa-miR-497-5p. On the contrary, the genes linked with higher levels of specificity by miRNAs were found to be *ZHFX3* and *KRAS*, which showed in most cases high or very high levels of interaction (Figure 2).

According to this analysis, hsa-miR-223-3p, hsa-miR-195-5p, hsa-miR-497-5p are able to target and modulate

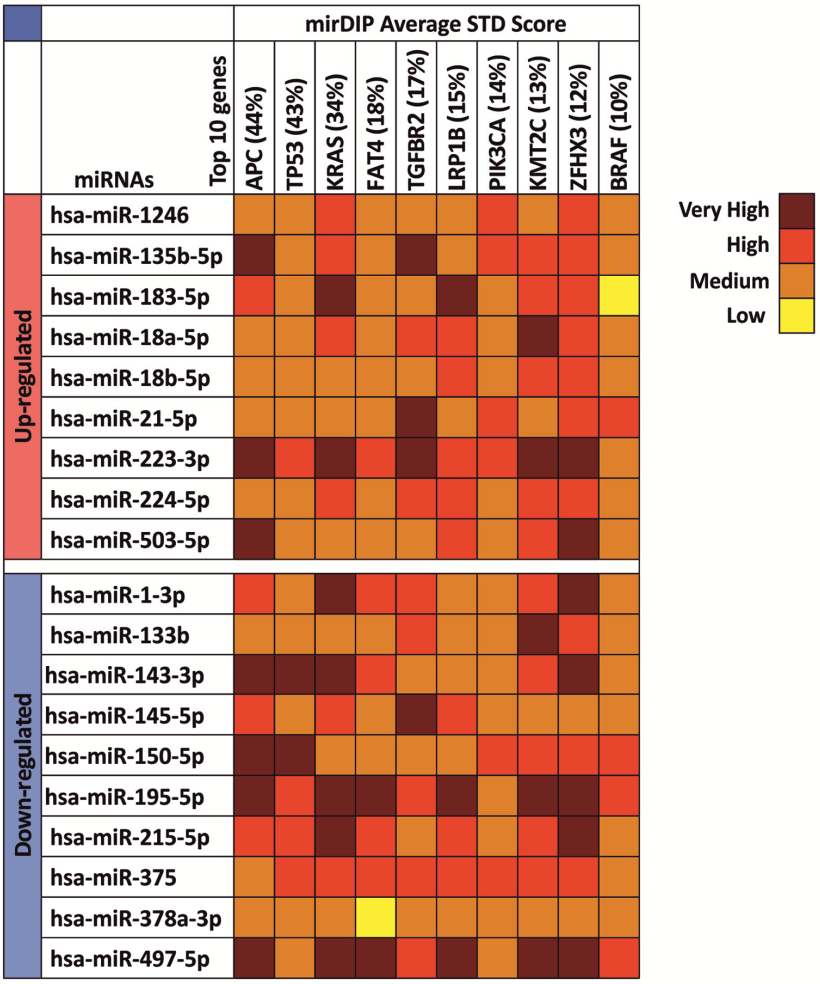

Figure 2. mirDIP gene target analysis – Interaction between selected miRNAs and main altered genes in CRC. For each miRNA the level of interaction with the 10 genes involved in CRC is reported. The intensity of interaction is highlighted with a color scale ranging from dark red (very high interaction) to yellow (low interaction).

both oncogene and tumor suppressor genes playing a possible key role in tumor cell development and progression.

Two-approaches pathway prediction analysis of selected miRNAs

To understand the role of miRNAs in cancer development, the DIANA-mirPath analysis of the 19 selected highly-modulated miRNAs was performed. The two-approaches analysis was independently applied. In the first approach a prediction pathway analysis, by searching for CRC altered molecular pathways, was considered taking into account 7 different pathways (KEGG pathway), as indicated by TCGA Network. In the second approach, the same analysis, by searching for the 19 computationally selected miRNAs, was assessed.

As shown in Figure 3, almost all the selected miRNAs were able to modulate the Wnt signaling pathway (hsa04310), RAS-MAPK signaling pathways (hsa04041 and hsa04010 respectively), PI3K-AKT signaling pathway (hsa04151), TGF-β and p53 signaling pathways (hsa04350 and hsa04115 respectively) and the mismatch repair pathway (hsa03430). In particular, the most modulated pathways are the PI3K-AKT signaling pathway (hsa04151) and the MAPK signaling pathways (hsa04010), while the up-regulated miRNAs hsa-miR-183-5p and hsa-miR-21-5p and the down-regulated miRNAs hsa-miR-195-5p and hsa-miR-497-5p, showed to target the higher number of genes (214) within the 7 previously mentioned pathways (Figure 3). These miRNAs were thus able to target key genes involved in these pathways and in cancer development such as *TP53*, *APC*, several proteins of the WNT family (WNT3A, WNT5A and WNT9A) and of the MAPK family (MAPK1, MAPK8 and MAPK9), *VEGFA* and *MYC* suggesting their possible use in diagnostic and clinical practice.

On the contrary, the mismatch repair pathway (hsa03430) it was found to be the least modulated pathway from the selected miRNAs. In the same way, the miRNAs with minor gene targets were found to be hsa-miR-215-5p (11 targeted genes), hsa-miR-135b-5p (13 targeted genes), hsa-miR-223-3p (15 targeted genes) and hsa-miR-133b (16 targeted genes) (Figure 3). In Table S1 are reported the targeted gene by selected miRNAs within the aforementioned pathways (Table S1). The Figure 3 shows the number of genes targeted by the computationally selected miRNAs within several colorectal cancer related-pathway. In particular, dark red boxes indicate those miRNAs able to target more 30-40 genes. The Table S1 contains all the genes targeted by selected miRNAs and the statistical significance (p_value) of these interactions.

Subsequently, the opposite analysis was performed carrying out the second approach by entering individually the selected miRNAs. This analysis showed that the selected miRNAs were able to modulate the expression of over 1420 genes directly involved in several molecular cancer and signaling pathways, however, each gene can be targeted by several miRNAs, therefore the real number of genes regulated by the selected miRNA is 460. In Figure 4 are summarized the predicted pathways involved in cancer development and targeted by the 19 computationally selected miRNAs and their interaction with all genes of

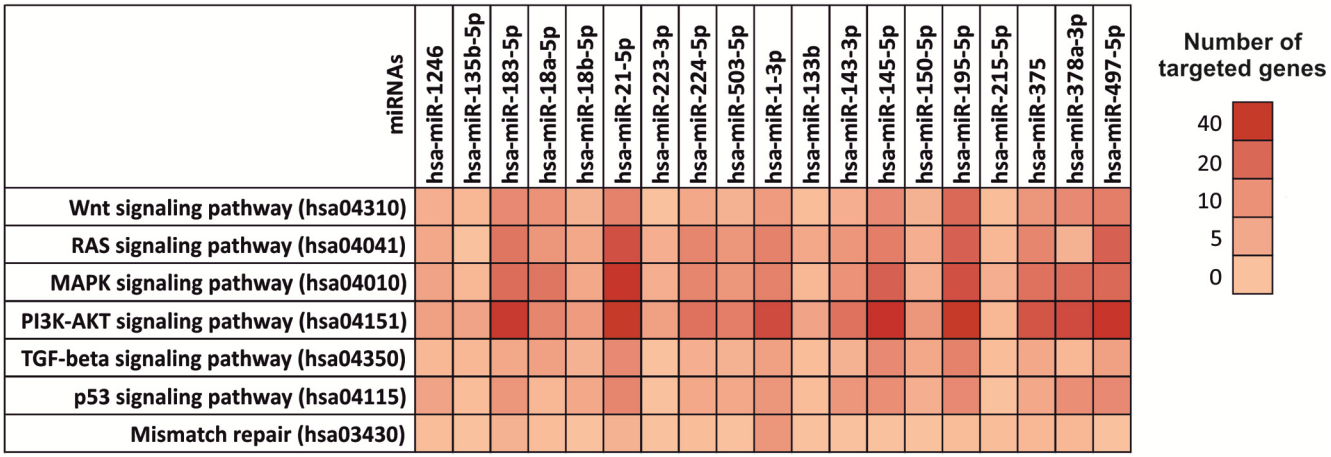

Figure 3. Diana-mirPath pathway analysis – Interaction between selected miRNAs and TCGA colorectal cancer pathways. Prediction pathway analysis of the interaction between selected miRNAs and the main genes and pathways involved in CRC development according to The Cancer Genome Atlas Network. For each miRNA the number of targeted gene within a specific pathway is indicated by highlighting the corresponding box with a color scale ranging from red (40 genes targeted) to light red (0 genes targeted).

these pathways (Figure 4). All miRNAs showed to modulate the molecular pathways involved in cancer development, excluding the miRNAs hsa-miR-503-5p, hsa-miR-1-3p and hsa-miR-215-5p that have not shown interactions with any pathways. In addition, this approach confirmed the weak interaction of hsa-miR-215-5p, hsa-miR-135b-5p, hsa-miR-223-3p and hsa-miR-133b with the molecular pathways taken into account (Figure 4). Hence, this second approach confirmed the results previously obtained with the first approach. All the selected miRNAs may alter the transcriptional levels of several genes grouped in different pathways. Therefore, such miRNAs have not only a role as diagnostic markers of CRC, but could also mediate directly the processes that lead to the development colorectal cancer.

In Table S2 are reported the targeted gene by selected miRNAs within the 15 selected pathways involved in cancer development (Table S2).

DISCUSSION

Recently, a growing body of evidence indicated the improvement of therapeutic strategies for colorectal carcinoma [32, 33]. However, such improvement was not observed regarding screening and diagnostic approaches [34,35]. Conflicting data were obtained for the identification of sensitive molecular biomarkers in the context of early diagnosis [36], while promising results derived from the analysis of miRNAs.

In particular, the discovery of extracellular miRNAs, stable in several biological samples, generated a significant interest in the field of biomarker discovery and cancer treatment because the alterations of miRNAs expression levels can be used as specific and sensitive indicator for different kinds of disease, including cancer, and for the development of new personalized therapeutic strategies [37-39].

Currently, no effective biomarkers are available for the early detection of colorectal cancer. In this context, the analysis of specific miRNAs may represent a good strategy for the early diagnosis and prognosis of different tumor types, including colorectal cancer.

In previous studies it was speculated the potential role of a bioinformatics approach to identify miRNAs with high diagnostic and prognostic significance in cancer development and progression [40-44].

On these bases, in the present study a broad computational analysis taking into account all microRNA

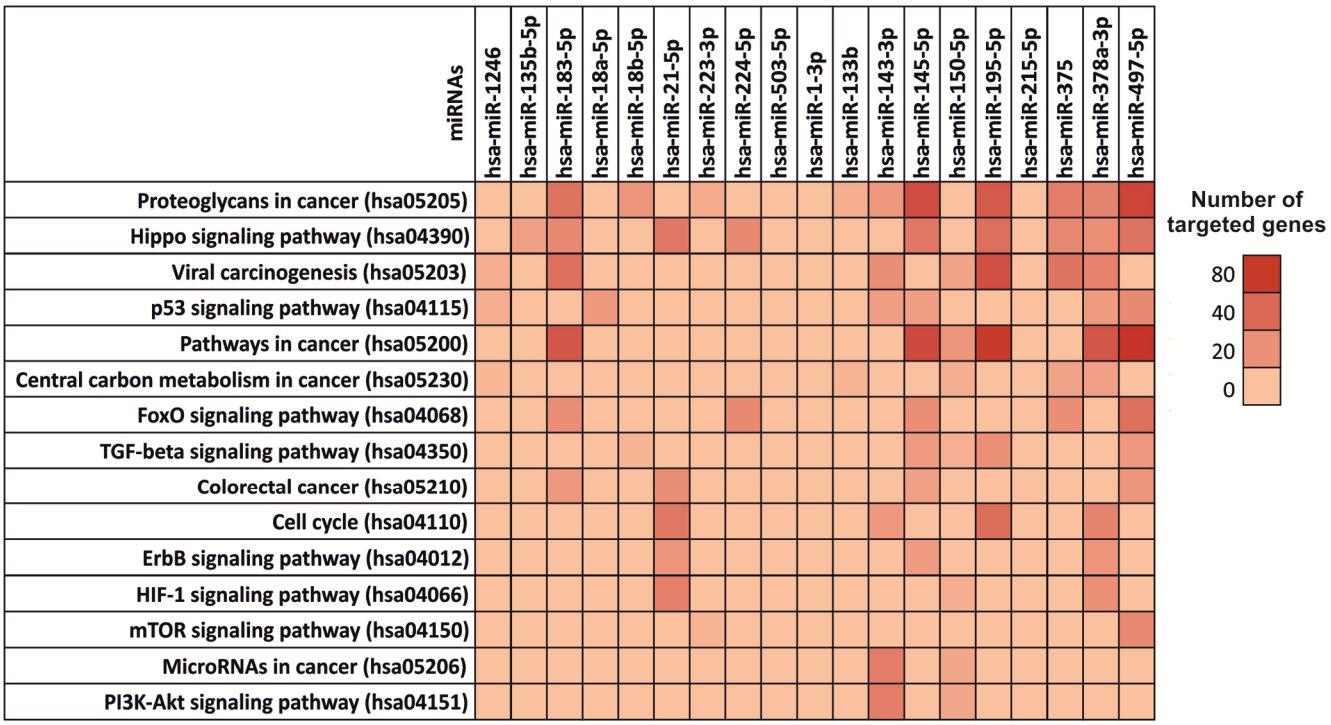

Figure 4. Diana-mirPath pathway analysis – Interaction between selected miRNAs and several molecular pathways involved in cancer development. Prediction pathway analysis of the interaction between individually selected miRNAs and the molecular and signaling pathways involved in CRC development. For each miRNA is indicated the number of targeted gene within a specific pathway by highlighting the corresponding box with a color scale ranging from red (80 genes targeted) to light red (0 genes targeted).

profiling by array datasets containing the miRNAs expression data of CRC biopsies and normal tissues was performed.

The analysis was conducted in 10 microRNA profiling by array datasets to identify putative miRNAs differentially expressed in CRC patients compared to healthy controls. This preliminary bioinformatics approach allowed us to identify 20 different miRNAs involved in colorectal cancer of which 10 were up-regulated and 10 down-regulated. The up-regulated miRNA hsa-miR-1308 was subsequently excluded for the gene target and pathway analyses because according to miRBase it was a fragment of a tRNA.

This preliminary analysis showed that the up-regulated hsa-miR-18a-5p and hsa-miR-21-5p and the down-regulated hsa-miR-133b and hsa-miR-375 were the most frequently found miRNAs within the 10 analyzed datasets. All these frequently modulated miRNAs in CRC are already described in literature thus high-lighting the consistency and effectiveness of the performed computational analysis [45-48].

Subsequently, the gene target analysis between all the computationally identified miRNAs and the main genes mutated or altered in CRC (according to the data contained in COSMIC) was performed. Although, miRNAs are not directly involved in mutagenesis phenomena not either in reducing or favoring the onset of mutations, this analysis was important because the role of miRNAs is crucial in inhibiting over-expressed mRNAs of genes harboring activating mutations. This analysis revealed a direct and high-level interaction between selected miRNAs and several genes known to be important for CRC development and prognosis, such as *APC*, *TP53*, *KRAS* and *BRAF* [49].

In particular, the gene target analysis revealed that the miRNAs hsa-miR-223-3p, hsa-miR-195-5p and hsa-miR-497-5p showed the highest interaction levels among all selected miRNAs, with a particular specificity for the *APC*, *KRAS*, *KMT2C* and *ZFHX3*. Interestingly, the interaction values of the hsa-miR-195-5p and hsa-miR-497-5 were almost completely over-lapping (9 of 10 gene interaction were the same). Of note, these 2 miRNAs were organized in a genomic cluster at the chromosome 17 in position p13.1 and this analysis suggested the same functional roles of these 2 miRNAs [50].

These 3 miRNAs were also already correlated to CRC and reported in literature. The authors described the diagnostic value of hsa-miR-223 and its role in CRC progression [51] and the importance of the miR-497∼195 cluster that were down-regulated in CRC [52-54].

Finally, the two-approaches DIANA-mirPath analysis showed that all the computational selected miRNAs have an effective role in the modulation of different colorectal cancer pathways highlighting their possible involvement in CRC development. In particular, the first approach revealed that the selected miRNAs modulate the expression levels of key genes known to be involved in the colorectal cancer pathways indicated by the TCGA Network and in the development of CRC, such as AKT family, BCL2, Cyclin family (*CCND1*, *CCND2*, *CCND3*, etc), Cyclin-dependent kinase family (*CDK4* and *CDK6*), *EGFR*, MAPK family, *TP53*, *VEGFA*, PIK3 family, etc [55-57]. In addition, the second approach confirmed the previously obtained results showing that the selected miRNAs are capable of modulating 83 different pathways, of which 15 are directly related to tumor development, interacting with more than 1400 genes. This second approach revealed a wide number of miRNAs able to target more genes compared to the first approach. The second analysis, performed by searching for a single miRNA, is a much more robust analysis that also takes into account the genes, not directly involved in the pathway, of which regulation indirectly determines a de-regulation of the analyzed pathway. Furthermore, the number of miRNAs and genes found in the second approach appears to be higher because in the second approach are also considered miRNA-gene interactions only predicted, but not yet validated. On these bases, in this study both analyses were performed to have a more comprehensive knowledge of those miRNAs able to inhibit the expression of genes involved in different cancer-related pathways. Although some of these interactions are only predicted but not yet validated, the results of this dual computational approach can provide important information on which to conduct new validation studies.

Overall, according to the gene target analysis, the analysis of the pathways showed that the up-regulated miRNAs hsa-miR-21-5p and the down-regulated miRNAs hsa-miR-195-5p and hsa-miR-497-5p are able to target the higher number of genes within the pathways reported in Tables S1 and S2. All these miRNAs are well described in the literature and have been related to several cancer types. However, through a computational integrated analysis, for the first time was recognized a set of miRNAs strongly related to colorectal cancer gene and pathways.

Overall, these observations led us to hypothesize that such miRNAs may induce the increase of cell proliferation and inhibition of tumor cell death leading to tumor development and progression by directly inhibiting or activating (in the case of down-regulated miRNAs) key genes. Furthermore, these results represent the basis for additional studies in which define

sensitivity, specificity and effectiveness of the putative miRNAs, here identified, showing highly specific interactions with genes and molecular pathways of particular interest in colorectal cancer development.

MATERIALS AND METHODS

Colorectal cancer microRNA profiling datasets analysis

The colorectal cancer datasets of microRNA profiling by array were selected by consulting the Gene Expression Omnibus DataSets portal (GEO DataSets) publicly available on NCBI (www.ncbi.nlm.nih.gov/geo/). In particular, the selection of the CRC datasets was carried out by entering as search terms in the advanced research tool "((("non coding rna profiling by array"[DataSet Type]) AND colorectal cancer) AND "Homo sapiens"[porgn:__txid9606]". This preliminary research allowed to identify all CRC datasets containing miRNA expression levels information of both healthy controls and colorectal cancer patients.

This research allowed to identify several colorectal carcinoma datasets, and among these were selected only those datasets that respected the following inclusion and exclusion criteria:

Inclusion criteria, i) datasets containing the miRNA expression levels information of both cancer patients and healthy controls or containing the expression data of pathological biopsy samples and of healthy tissue counterpart; ii) datasets containing the miRNA expression data of at least 30 samples (both tumor and normal).

Exclusion criteria, i) datasets containing information only regarding cancer patients; ii) datasets containing information on the expression levels of miRNAs of tumor and normal cell lines, without considering cancer patients; iii) datasets containing information on miRNAs expression levels of serum samples; iv) datasets with obsolete miRNA annotations, datasets with no available reading keys and datasets with data not normalized and centered.

To identify the down-regulated or up-regulated miRNAs in CRC, for each selected dataset, the data matrix was downloaded to perform the differential analysis of miRNAs expression levels (fold change value) between cancer and normal samples by using GEO2R tool available on GEO DataSets. Before calculating the fold change, the miRNAs contained in all the datasets were annotated according to the last nomenclature published by miRBase (miRBase V 21) (http://www.mirbase.org/) because of the different microarray platforms taken into account [58].

The fold change values (FC) were reported as base-2 logarithm of FC (logFC) to normalize the different scales of values due to the different microarray platforms by which the datasets were constructed.

Finally, for each dataset the TOP 20 list of the most statistically significant ($p < 0.01$) up-regulated or down-regulated miRNAs was performed. This analysis allowed to identify the 10 most up-regulated and down-regulated miRNAs in colorectal cancer patients compared to healthy controls.

Identification of putative miRNAs involved in colorectal cancer development

The previously obtained TOP 20 lists for each dataset were merged by using a bioinformatics tool, Venn Diagrams of the Bioinformatics & Evolutionary Genomics (BEG) (http://bioinformatics.psb.ugent.be/webtools/Venn/), for the comparison of sets. This approach allowed to identify only the miRNAs strongly up-regulated or down-regulated in at least 3 of the previously selected datasets. For each miRNA over-expressed or down-regulated in multiple datasets was reported the level of up-regulation and down-regulation using respectively red boxes and blue boxes. miRNAs were thus divided according to their expression levels in "highly" (logFC ≥ 3), "moderately" (logFC $1.5 < x < 3$), "lightly" (logFC $0.5 < x < 1.5$) and "poorly" (logFC $0 < x < 0.5$) up-regulated or down-regulated (negative logFC values).

Interaction between selected putative miRNAs and the main genes involved in colorectal cancer development and progression

By consulting the Catalogue Of Somatic Mutation In Cancer (COSMIC) (http://cancer.sanger.ac.uk/cosmic) it was possible to identify the 10 most mutated genes that are known to be involved in colorectal carcinoma development and therefore have a dysregulated expression.

These genes are *APC* (44%), *TP53* (43%), *KRAS* (34%), *FAT4* (18%), *TGFBR2* (17%), *LRP1B* (15%), *PIK3CA* (14%), *KMT2C* (13%), *ZFHX3* (12%), *BRAF* (10%).

Subsequently, using the bioinformatics prediction tool microRNA Data Integration Portal (mirDIP – V 4.1.1.6, Nov 2017) (http://ophid.utoronto.ca/mirDIP) [59,60], the interaction between the miRNA previously identified by computational analysis and the main genes mutated and altered in CRC was evaluated. For this analysis the tool mirDIP was chosen because it allows to integrate 30 different resources of human miRNA–target prediction tools thus allowing to centralize all data related to miRNAs-targets interactions.

Interaction between selected miRNAs and main pathways in cancer

The selected miRNAs are not only involved in the alteration of the aforementioned genes, but are also involved in the regulation of a wide number of genetic targets and in the modulation of key molecular pathways of cell proliferation and cancer progression. On these bases, a pathway prediction analysis was performed to explore the implication of the selected computational miRNAs in the modulation of pathways notoriously involved in cancer development.

For this purpose, the bioinformatics prediction tool DIANA-mirPath (v.3) [61] was used to analyze the differentially expressed miRNA common in at least 3 of the 10 selected datasets and to predict miRNA targets in 3′-UTR gene regions according to experimentally validated miRNA interactions derived from DIANA-TarBase v7.0 algorithm [62]. These interactions (predicted and/or validated) were subsequently combined with sophisticated merging and meta-analysis algorithms by DIANA-mirPath and giving as a result the genes and pathways targeted by a specific miRNAs and the statistical significance of this interaction.

A two-approaches analysis was performed. In the first approach, the analysis of the main pathways leading to tumor development was carried out. In particular, specific pathways for colon cancer were used as search terms and analyzed, following the indications given by The Cancer Genome Atlas Network in reference to CRC [63].

To confirm this first approach, a second analysis was carried out by entering the selected computational miRNAs individually as search terms in order to identify all the genes and the pathways inhibited by them. Cancer pathways of other tumor types and the molecular pathways not directly involved in cancer development or in cell cycle and homeostasis, such as Hepatitis B pathway (hsa05161), Axon guidance pathway (hsa04360), Lysine degradation pathway (hsa00310), etc, were excluded from this analysis.

Statistical analysis

All miRNA expression level data were already normalized by GEO2R software, therefore, no additional normalization procedures were applied to data obtained from all datasets included in this study. The p_Values of miRNAs of the gene target analysis and of the prediction pathway analysis were already calculated by mirDIP and DIANA-miPath respectively.

CONFLICTS OF INTEREST

The authors declare that they have no competing interests.

FUNDING

This study was funded in part by the Lega Italiana per la Lotta contro i Tumori and by the FIR 2015 – University of Catania.

REFERENCES

1. Ferlay J, Soerjomataram I, Dikshit R, Eser S, Mathers C, Rebelo M, Parkin DM, Forman D, Bray F. Cancer incidence and mortality worldwide: sources, methods and major patterns in GLOBOCAN 2012. Int J Cancer. 2015; 136:E359–86. https://doi.org/10.1002/ijc.29210
2. Torre LA, Siegel RL, Ward EM, Jemal A. Global Cancer Incidence and Mortality Rates and Trends--An Update. Cancer Epidemiol Biomarkers Prev. 2016; 25:16–27. https://doi.org/10.1158/1055-9965.EPI-15-0578
3. Favoriti P, Carbone G, Greco M, Pirozzi F, Pirozzi RE, Corcione F. Worldwide burden of colorectal cancer: a review. Updates Surg. 2016; 68:7–11. https://doi.org/10.1007/s13304-016-0359-y
4. Siegel RL, Miller KD, Fedewa SA, Ahnen DJ, Meester RG, Barzi A, Jemal A. Colorectal cancer statistics, 2017. CA Cancer J Clin. 2017; 67:177–93. https://doi.org/10.3322/caac.21395
5. Ortega LS, Bradbury KE, Cross AJ, Morris JS, Gunter MJ, Murphy N. A Prospective Investigation of Body Size, Body Fat Composition and Colorectal Cancer Risk in the UK Biobank. Sci Rep. 2017; 7:17807. https://doi.org/10.1038/s41598-017-17997-5
6. Drew DA, Nishihara R, Lochhead P, Kuchiba A, Qian ZR, Mima K, Nosho K, Wu K, Wang M, Giovannucci E, Fuchs CS, Chan AT, Ogino S. A Prospective Study of Smoking and Risk of Synchronous Colorectal Cancers. Am J Gastroenterol. 2017; 112:493–501. https://doi.org/10.1038/ajg.2016.589
7. Svensson T, Yamaji T, Budhathoki S, Hidaka A, Iwasaki M, Sawada N, Inoue M, Sasazuki S, Shimazu T, Tsugane S. Alcohol consumption, genetic variants in the alcohol- and folate metabolic pathways and colorectal cancer risk: the JPHC Study. Sci Rep. 2016; 6:36607. https://doi.org/10.1038/srep36607
8. Gilsing AM, Schouten LJ, Goldbohm RA, Dagnelie PC, van den Brandt PA, Weijenberg MP. Vegetarianism, low meat consumption and the risk of colorectal

cancer in a population based cohort study. Sci Rep. 2015; 5:13484. https://doi.org/10.1038/srep13484

9. Johnson CM, Wei C, Ensor JE, Smolenski DJ, Amos CI, Levin B, Berry DA. Meta-analyses of colorectal cancer risk factors. Cancer Causes Control. 2013; 24:1207–22. https://doi.org/10.1007/s10552-013-0201-5

10. Butterworth AS, Higgins JP, Pharoah P. Relative and absolute risk of colorectal cancer for individuals with a family history: a meta-analysis. Eur J Cancer. 2006; 42:216–27. https://doi.org/10.1016/j.ejca.2005.09.023

11. Stoffel EM, Koeppe E, Everett J, Ulintz P, Kiel M, Osborne J, Williams L, Hanson K, Gruber SB, Rozek LS. Germline Genetic Features of Young Individuals With Colorectal Cancer. Gastroenterology. 2018; 154:897–905.e1. https://doi.org/10.1053/j.gastro.2017.11.004

12. Du L, Kim JJ, Shen J, Chen B, Dai N. KRAS and TP53 mutations in inflammatory bowel disease-associated colorectal cancer: a meta-analysis. Oncotarget. 2017; 8:22175–86. https://doi.org/10.18632/oncotarget.14549

13. Chang PY, Chen JS, Chang SC, Wang MC, Chang NC, Wen YH, Tsai WS, Liu WH, Liu HL, Lu JJ. Acquired somatic *TP53* or *PIK3CA* mutations are potential predictors of when polyps evolve into colorectal cancer. Oncotarget. 2017; 8:72352–62. https://doi.org/10.18632/oncotarget.20376

14. Zhang Y, Sun Z, Mao X, Wu H, Luo F, Wu X, Zhou L, Qin J, Zhao L, Bai C. Impact of mismatch-repair deficiency on the colorectal cancer immune microenvironment. Oncotarget. 2017; 8:85526–36. https://doi.org/10.18632/oncotarget.20241

15. Peña-Diaz J, Rasmussen LJ. Approaches to diagnose DNA mismatch repair gene defects in cancer. DNA Repair (Amst). 2016; 38:147–54. https://doi.org/10.1016/j.dnarep.2015.11.022

16. Leonardi GC, Accardi G, Monastero R, Nicoletti F, Libra M. Ageing: from inflammation to cancer. Immun Ageing. 2018; 15:1. https://doi.org/10.1186/s12979-017-0112-5

17. Badiola I, Santaolalla F, Garcia-Gallastegui P, Ana SD, Unda F, Ibarretxe G. Biomolecular bases of the senescence process and cancer. A new approach to oncological treatment linked to ageing. Ageing Res Rev. 2015; 23:125–38. https://doi.org/10.1016/j.arr.2015.03.004

18. Lanceta J, Prough RA, Liang R, Wang E. MicroRNA group disorganization in aging. Exp Gerontol. 2010; 45:269–78. https://doi.org/10.1016/j.exger.2009.12.009

19. Chen LH, Chiou GY, Chen YW, Li HY, Chiou SH. MicroRNA and ageing: a novel modulator in regulating the ageing network. Ageing Res Rev. 2010; 9:59–66. https://doi.org/10.1016/j.arr.2010.08.002

20. Sharp L, O'Leary E, O'Ceilleachair A, Skally M, Hanly P. Financial Impact of Colorectal Cancer and Its Consequences: Associations Between Cancer-Related Financial Stress and Strain and Health-Related Quality of Life. Dis Colon Rectum. 2018; 61:27–35. https://doi.org/10.1097/DCR.0000000000000923

21. Gauci C, Lendzion R, Phan-Thien KC, King D, Perera DS. Patient compliance with surveillance colonoscopy: patient factors and the use of a graded recall system. ANZ J Surg. 2018; 88:311–15. https://doi.org/10.1111/ans.14296

22. Rim JH, Youk T, Kang JG, Park BK, Gee HY, Kim JH, Yoo J. Fecal Occult Blood Test Results of the National Colorectal Cancer Screening Program in South Korea (2006-2013). Sci Rep. 2017; 7:2804. https://doi.org/10.1038/s41598-017-03134-9

23. Cappellani A, Di Vita M, Zanghi A, Veroux P, Cavallaro A, Lo Menzo E, Cacopardo B, Canzonieri V, Murabito P, Tirelli U, Berretta M. Biological and clinical markers in colorectal cancer: state of the art. Front Biosci (Schol Ed). 2010; 2:422–31. https://doi.org/10.2741/s75

24. Kanth P, Grimmett J, Champine M, Burt R, Samadder NJ. Hereditary Colorectal Polyposis and Cancer Syndromes: A Primer on Diagnosis and Management. Am J Gastroenterol. 2017; 112:1509–25. https://doi.org/10.1038/ajg.2017.212

25. Fabian MR, Sonenberg N, Filipowicz W. Regulation of mRNA translation and stability by microRNAs. Annu Rev Biochem. 2010; 79:351–79. https://doi.org/10.1146/annurev-biochem-060308-103103

26. Carter JV, Galbraith NJ, Yang D, Burton JF, Walker SP, Galandiuk S. Blood-based microRNAs as biomarkers for the diagnosis of colorectal cancer: a systematic review and meta-analysis. Br J Cancer. 2017; 116:762–74. https://doi.org/10.1038/bjc.2017.12

27. Yan S, Han B, Gao S, Wang X, Wang Z, Wang F, Zhang J, Xu D, Sun B. Exosome-encapsulated microRNAs as circulating biomarkers for colorectal cancer. Oncotarget. 2017; 8:60149–58. https://doi.org/10.18632/oncotarget.18557

28. Dumache R. Early Diagnosis of Oral Squamous Cell Carcinoma by Salivary microRNAs. Clin Lab. 2017; 63:1771–76. https://doi.org/10.7754/Clin.Lab.2017.170607

29. Bhome R, Goh RW, Bullock MD, Pillar N, Thirdborough SM, Mellone M, Mirnezami R, Galea D, Veselkov K, Gu Q, Underwood TJ, Primrose JN, De Wever O, et al. Exosomal microRNAs derived from colorectal cancer-associated fibroblasts: role in driving cancer progression. Aging (Albany NY). 2017; 9:2666–94. https://doi.org/10.18632/aging.101355

30. Wu CW, Ng SS, Dong YJ, Ng SC, Leung WW, Lee CW, Wong YN, Chan FK, Yu J, Sung JJ. Detection of miR-92a and miR-21 in stool samples as potential screening biomarkers for colorectal cancer and polyps. Gut. 2012; 61:739–45. https://doi.org/10.1136/gut.2011.239236

31. Ciombor KK, Haraldsdottir S, Goldberg RM. How Can Next-Generation Sequencing (Genomics) Help Us in Treating Colorectal Cancer? Curr Colorectal Cancer Rep. 2014; 10:372–79. https://doi.org/10.1007/s11888-014-0244-3

32. Xu W, Kuang M, Gong Y, Cao C, Chen J, Tang C. Survival benefit and safety of the combinations of FOLFOXIRI ± bevacizumab versus the combinations of FOLFIRI ± bevacizumab as first-line treatment for unresectable metastatic colorectal cancer: a meta-analysis. OncoTargets Ther. 2016; 9:4833–42. https://doi.org/10.2147/OTT.S104981

33. Akhtar R, Chandel S, Sarotra P, Medhi B. Current status of pharmacological treatment of colorectal cancer. World J Gastrointest Oncol. 2014; 6:177–83. https://doi.org/10.4251/wjgo.v6.i6.177

34. Monahan KJ, Alsina D, Bach S, Buchanan J, Burn J, Clark S, Dawson P, De Souza B, Din FV, Dolwani S, Dunlop MG, East J, Evans DG, et al. Urgent improvements needed to diagnose and manage Lynch syndrome. BMJ. 2017; 356:j1388. https://doi.org/10.1136/bmj.j1388

35. Chang LC, Shun CT, Hsu WF, Tu CH, Tsai PY, Lin BR, Liang JT, Wu MS, Chiu HM. Fecal Immunochemical Test Detects Sessile Serrated Adenomas and Polyps With a Low Level of Sensitivity. Clin Gastroenterol Hepatol. 2017; 15:872–879.e1. https://doi.org/10.1016/j.cgh.2016.07.029

36. Diamandis EP. Cancer biomarkers: can we turn recent failures into success? J Natl Cancer Inst. 2010; 102:1462–67. https://doi.org/10.1093/jnci/djq306

37. Baldassarre A, Felli C, Prantera G, Masotti A. Circulating microRNAs and Bioinformatics Tools to Discover Novel Diagnostic Biomarkers of Pediatric Diseases. Genes (Basel). 2017; 8:E234. https://doi.org/10.3390/genes8090234

38. Thind A, Wilson C. Exosomal miRNAs as cancer biomarkers and therapeutic targets. J Extracell Vesicles. 2016; 5:31292. https://doi.org/10.3402/jev.v5.31292

39. Cho WC. MicroRNAs: potential biomarkers for cancer diagnosis, prognosis and targets for therapy. Int J Biochem Cell Biol. 2010; 42:1273–81. https://doi.org/10.1016/j.biocel.2009.12.014

40. Polo A, Crispo A, Cerino P, Falzone L, Candido S, Giudice A, De Petro G, Ciliberto G, Montella M, Budillon A, Costantini S. Environment and bladder cancer: molecular analysis by interaction networks. Oncotarget. 2017; 8:65240–52. https://doi.org/10.18632/oncotarget.18222

41. Falzone L, Candido S, Salemi R, Basile MS, Scalisi A, McCubrey JA, Torino F, Signorelli SS, Montella M, Libra M. Computational identification of microRNAs associated to both epithelial to mesenchymal transition and NGAL/MMP-9 pathways in bladder cancer. Oncotarget. 2016; 7:72758–66. https://doi.org/10.18632/oncotarget.11805

42. Hafsi S, Candido S, Maestro R, Falzone L, Soua Z, Bonavida B, Spandidos DA, Libra M. Correlation between the overexpression of Yin Yang 1 and the expression levels of miRNAs in Burkitt's lymphoma: A computational study. Oncol Lett. 2016; 11:1021–25. https://doi.org/10.3892/ol.2015.4031

43. Zhao M, Liu Y, Huang F, Qu H. A gene browser of colorectal cancer with literature evidence and pre-computed regulatory information to identify key tumor suppressors and oncogenes. Sci Rep. 2016; 6:30624. https://doi.org/10.1038/srep30624

44. Kou Y, Qiao L, Wang Q. Identification of core miRNA based on small RNA-seq and RNA-seq for colorectal cancer by bioinformatics. Tumour Biol. 2015; 36:2249–55. https://doi.org/10.1007/s13277-014-2832-x

45. McCubrey JA, Lertpiriyapong K, Steelman LS, Abrams SL, Yang LV, Murata RM, Rosalen PL, Scalisi A, Neri LM, Cocco L, Ratti S, Martelli AM, Laidler P, et al. Effects of resveratrol, curcumin, berberine and other nutraceuticals on aging, cancer development, cancer stem cells and microRNAs. Aging (Albany NY). 2017; 9:1477–536. https://doi.org/10.18632/aging.101250

46. Wang X, Bu J, Liu X, Wang W, Mai W, Lv B, Zou J, Mo X, Li X, Wang J, Niu B, Fan Y, Hou B. miR-133b suppresses metastasis by targeting HOXA9 in human colorectal cancer. Oncotarget. 2017; 8:63935–48. https://doi.org/10.18632/oncotarget.19212

47. Wei R, Yang Q, Han B, Li Y, Yao K, Yang X, Chen Z, Yang S, Zhou J, Li M, Yu H, Yu M, Cui Q. microRNA-375 inhibits colorectal cancer cells proliferation by downregulating JAK2/STAT3 and MAP3K8/ERK signaling pathways. Oncotarget. 2017; 8:16633–41. https://doi.org/10.18632/oncotarget.15114

48. Yau TO, Wu CW, Dong Y, Tang CM, Ng SS, Chan FK, Sung JJ, Yu J. microRNA-221 and microRNA-18a identification in stool as potential biomarkers for the non-invasive diagnosis of colorectal carcinoma. Br J Cancer. 2014; 111:1765–71. https://doi.org/10.1038/bjc.2014.484

49. Shen Y, Han X, Wang J, Wang S, Yang H, Lu SH, Shi Y. Prognostic impact of mutation profiling in patients with stage II and III colon cancer. Sci Rep. 2016; 6:24310. https://doi.org/10.1038/srep24310

50. Flavin RJ, Smyth PC, Laios A, O'Toole SA, Barrett C, Finn SP, Russell S, Ring M, Denning KM, Li J, Aherne ST, Sammarae DA, Aziz NA, et al. Potentially important microRNA cluster on chromosome 17p13.1 in primary peritoneal carcinoma. Mod Pathol. 2009; 22:197–205. https://doi.org/10.1038/modpathol.2008.135

51. Li ZW, Yang YM, Du LT, Dong Z, Wang LL, Zhang X, Zhou XJ, Zheng GX, Qu AL, Wang CX. Overexpression of miR-223 correlates with tumor metastasis and poor prognosis in patients with colorectal cancer. Med Oncol. 2014; 31:256. https://doi.org/10.1007/s12032-014-0256-5

52. Yang M, Li CJ, Sun X, Guo Q, Xiao Y, Su T, Tu ML, Peng H, Lu Q, Liu Q, He HB, Jiang TJ, Lei MX, et al. MiR-497∼195 cluster regulates angiogenesis during coupling with osteogenesis by maintaining endothelial Notch and HIF-1α activity. Nat Commun. 2017; 8:16003. https://doi.org/10.1038/ncomms16003

53. Qiu Y, Yu H, Shi X, Xu K, Tang Q, Liang B, Hu S, Bao Y, Xu J, Cai J, Peng W, Cao Q, Yin P. microRNA-497 inhibits invasion and metastasis of colorectal cancer cells by targeting vascular endothelial growth factor-A. Cell Prolif. 2016; 49:69–78. https://doi.org/10.1111/cpr.12237

54. Zhang X, Xu J, Jiang T, Liu G, Wang D, Lu Y. MicroRNA-195 suppresses colorectal cancer cells proliferation via targeting FGF2 and regulating Wnt/β-catenin pathway. Am J Cancer Res. 2016; 6:2631–40.

55. Lin SH, Raju GS, Huff C, Ye Y, Gu J, Chen JS, Hildebrandt MA, Liang H, Menter DG, Morris J, Hawk E, Stroehlein JR, Futreal A, et al. The somatic mutation landscape of premalignant colorectal adenoma. Gut. 2017gutjnl-2016-313573. https://doi.org/10.1136/gutjnl-2016-313573

56. Wee P, Wang Z. Epidermal Growth Factor Receptor Cell Proliferation Signaling Pathways. Cancers (Basel). 2017; 9:52. https://doi.org/10.3390/cancers9050052

57. Jiang BH, Liu LZ. PI3K/PTEN signaling in angiogenesis and tumorigenesis. Adv Cancer Res. 2009; 102:19–65. https://doi.org/10.1016/S0065-230X(09)02002-8

58. Kozomara A, Griffiths-Jones S. miRBase: annotating high confidence microRNAs using deep sequencing data. Nucleic Acids Res. 2014; 42:D68–73. https://doi.org/10.1093/nar/gkt1181

59. Tokar T, Pastrello C, Rossos AE, Abovsky M, Hauschild AC, Tsay M, Lu R, Jurisica I. mirDIP 4.1-integrative database of human microRNA target predictions. Nucleic Acids Res. 2018; 46:D360–70. https://doi.org/10.1093/nar/gkx1144

60. Shirdel EA, Xie W, Mak TW, Jurisica I. NAViGaTing the micronome--using multiple microRNA prediction databases to identify signalling pathway-associated microRNAs. PLoS One. 2011; 6:e17429. https://doi.org/10.1371/journal.pone.0017429

61. Vlachos IS, Zagganas K, Paraskevopoulou MD, Georgakilas G, Karagkouni D, Vergoulis T, Dalamagas T, Hatzigeorgiou AG. DIANA-miRPath v3.0: deciphering microRNA function with experimental support. Nucleic Acids Res. 2015; 43:W460-6. https://doi.org/10.1093/nar/gkv403

62. Vlachos IS, Paraskevopoulou MD, Karagkouni D, Georgakilas G, Vergoulis T, Kanellos I, Anastasopoulos IL, Maniou S, Karathanou K, Kalfakakou D, Fevgas A, Dalamagas T, Hatzigeorgiou AG. DIANA-TarBase v7.0: indexing more than half a million experimentally supported miRNA:mRNA interactions. Nucleic Acids Res. 2015; 43:D153–59. https://doi.org/10.1093/nar/gku1215

63. Muzny DM, Bainbridge MN, Chang K, Dinh HH, Drummond JA, Fowler G, Kovar CL, Lewis LR, Morgan MB, Newsham IF, Reid JG, Santibanez J, Shinbrot E, et al, and Cancer Genome Atlas Network. Comprehensive molecular characterization of human colon and rectal cancer. Nature. 2012; 487:330–37. https://doi.org/10.1038/nature11252

64. Sarver AL, French AJ, Borralho PM, Thayanithy V, Oberg AL, Silverstein KA, Morlan BW, Riska SM, Boardman LA, Cunningham JM, Subramanian S, Wang L, Smyrk TC, et al. Human colon cancer profiles show differential microRNA expression depending on mismatch repair status and are characteristic of undifferentiated proliferative states. BMC Cancer. 2009; 9:401. https://doi.org/10.1186/1471-2407-9-401

65. Balaguer F, Moreira L, Lozano JJ, Link A, Ramirez G, Shen Y, Cuatrecasas M, Arnold M, Meltzer SJ, Syngal S, Stoffel E, Jover R, Llor X, et al. Colorectal cancers with microsatellite instability display unique miRNA profiles. Clin Cancer Res. 2011; 17:6239–49. https://doi.org/10.1158/1078-0432.CCR-11-1424

66. Pizzini S, Bisognin A, Mandruzzato S, Biasiolo M, Facciolli A, Perilli L, Rossi E, Esposito G, Rugge M, Pilati P, Mocellin S, Nitti D, Bortoluzzi S, Zanovello P.

Impact of microRNAs on regulatory networks and pathways in human colorectal carcinogenesis and development of metastasis. BMC Genomics. 2013; 14:589. https://doi.org/10.1186/1471-2164-14-589

67. Gaedcke J, Grade M, Camps J, Søkilde R, Kaczkowski B, Schetter AJ, Difilippantonio MJ, Harris CC, Ghadimi BM, Møller S, Beissbarth T, Ried T, Litman T. The rectal cancer microRNAome--microRNA expression in rectal cancer and matched normal mucosa. Clin Cancer Res. 2012; 18:4919–30. https://doi.org/10.1158/1078-0432.CCR-12-0016

68. Zhang JX, Song W, Chen ZH, Wei JH, Liao YJ, Lei J, Hu M, Chen GZ, Liao B, Lu J, Zhao HW, Chen W, He YL, et al. Prognostic and predictive value of a microRNA signature in stage II colon cancer: a microRNA expression analysis. Lancet Oncol. 2013; 14:1295–306. https://doi.org/10.1016/S1470-2045(13)70491-1

69. Millino C, Maretto I, Pacchioni B, Digito M, De Paoli A, Canzonieri V, D'Angelo E, Agostini M, Rizzolio F, Giordano A, Barina A, Rajendran S, Esposito G, et al. Gene and MicroRNA Expression Are Predictive of Tumor Response in Rectal Adenocarcinoma Patients Treated With Preoperative Chemoradiotherapy. J Cell Physiol. 2017; 232:426–35. https://doi.org/10.1002/jcp.25441

SUPPLEMENTARY MATERIAL

Please browse Full text version to see the data of Supplementary Tables related to this manuscript:

Table S1. DIANA-mirPath pathway analysis - First Approach: interaction between selected miRNAs and TGCA colorectal cancer pathways.

Table S2. DIANA-mirPath pathway analysis - Second Approach: interaction between selected miRNAs and several molecular and signaling pathways involved in cancer development.

Editorial

Is MDMX the better target?

Ning Kon and Wei Gu

The functions of tumor suppressor p53 are much appreciated in combating tumorigenesis when cells encounter genotoxic and other deleterious stresses. Under those circumstances, p53 stabilities and transcriptional activities increase dramatically and often lead to activation of genes and trigger pathways that cause terminal and irreversible fate for the damaged cells. Meanwhile, the p53 functions in metabolic regulation have gained attractions for their roles in normal conditions and in tumor suppression. To dissect the physiological role of acetylation in modulating p53 functions, we previously established a *p53-3KR* mutant mice where the acetylation defective p53 mutant losses its ability to activate apoptosis, senescence and growth arrest [1]. Importantly, the *p53-3KR* mice do not succumb to early onset tumor formation compared to *p53* knockout mice, which allow us to uncover p53 activities beyond those canonical tumor suppression functions of p53. To further enhance the remaining functions of p53, *p53-3KR* mutant mice are crossed with *mdm2* or *mdmx* knockout mice individually, to study the stability and transcriptional activation of p53-3KR mutant in the absence of either MDM2 or MDMX.

Although *p53-3KR* mutant only partially rescued the lethality of *mdm2* knockout mice, p53-3KR protein levels dramatically increased in the absence of MDM2, demonstrating again that MDM2 is critical for p53 stability (Figure 1). Since p53-3KR mutant is unable to induce apoptosis, senescence and cell growth arrest, the embryonic lethality in *p53-3KR/mdm2*$^{-/-}$ mice led us to discovery of the p53 mediated downregulation of SLC7A11 and subsequent activation of ferroptosis, a form of cell death in response to ROS stress [2]. In contrast, *p53-3KR* mutant was able to completely rescue the lethality of *Mdmx* knockout mice (Figure 1), suggesting the ferroptotic functions of p53-3KR are not activated in the absence of MDMX. Interestingly, there was a modest increase of p53-3KR levels in the absence of MDMX, indicating MDMX only has a limited role in regulating p53 stability, revealing that the Mdm2/Mdmx heterodimer is not absolutely required for p53 degradation [3]. Nevertheless, a number of genes were activated and resulted in metabolic phenotypes. The *p53-3KR/mdmx*$^{-/-}$ mice became skinny even though they had no obvious developmental defects. The analysis of these mice revealed that p53 activities were enhanced in *p53-3KR/mdmx*$^{-/-}$ mice, which resulted in resistance to fat accumulation in adipose tissues upon high fat diet in these mice [3]. These anti-obesity phenotypes in *p53-3KR/mdmx*$^{-/-}$ mice were caused in part by modulation of lipid metabolism and thermogenic programs in adipose tissues. These results elucidate unknown beneficial effects of the p53/MDMX axis in adipose tissue remodeling, and revealed a surprising role of MDMX inhibition in anti-obesity effects beyond, commonly expected, tumor suppression.

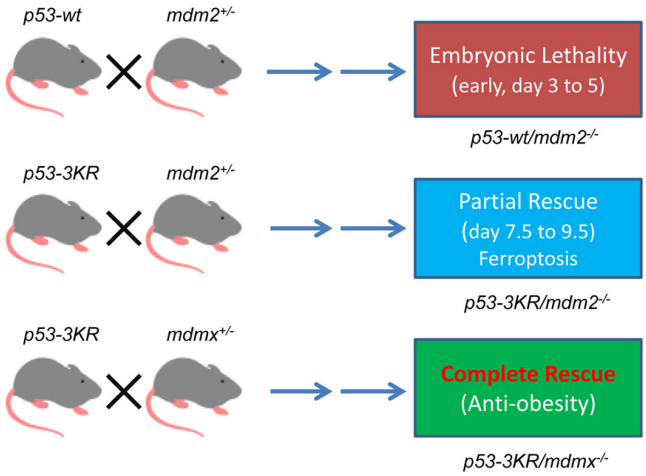

Figure 1. Differential effects of p53 function by inactivation of *mdm2* or *mdmx* by using mouse models.

Restoration of p53 activity remains an important goal in the quest for more effective cancer therapeutics. Indeed, small molecule inhibitors of MDM2 such as Nutlin-3, are able to activate p53, and exhibits anti-tumor efficacy in cancer cells that express wild-type p53. Nevertheless, the usage of MDM2 inhibitors in clinics has significant limitations with high toxicity in normal cells [4]. Based on our study, loss of MDMX induces p53 activation but apparently has much less destructive effects than MDM2 inactivation *in vivo*. Thus, it is very likely that targeting MDMX alone might be the better approach in cancer therapy since much less toxicity was observed upon MDMX inactivation. Moreover, specific inhibitors of MDMX may have both tumor suppression and anti-obesity effects.

REFERENCES

1. Li T, et al. Cell. 2012; 149:1269–83. https://doi.org/10.1016/j.cell.2012.04.026 2. Jiang L, et al. Nature. 2015; 520:57–62. https://doi.org/10.1038/nature14344
3. Kon N, et al. Oncotarget. 2018; 9:7282–97. https://doi.org/10.18632/oncotarget.23837
4. Li Q, Lozano G. Clin Cancer Res. 2013; 19:34–41. https://doi.org/10.1158/1078-0432.CCR-12-0053

Wei Gu: Institute for Cancer Genetics, College of Physicians and Surgeons of Columbia University, New York, NY 10032, USA

Correspondence: *Wei Gu*
Email: *wg8@columbia.edu*

Keywords: *p53 3KR mutant, mdm2 KO, mdmx KO*

Received: June 1, 2018
Published: June 13, 2018

Research Paper

ZNF185 is a p53 target gene following DNA damage

Artem Smirnov[1], Angela Cappello[1], Anna Maria Lena[1], Lucia Anemona[1], Alessandro Mauriello[1], Nicola Di Daniele[2], Margherita Annicchiarico-Petruzzelli[3], Gerry Melino[1,4], Eleonora Candi[1,3]

[1] Department of Experimental Medicine, TOR, University of Rome "Tor Vergata", 00133 Rome, Italy
[2] Department of Systems Medicine, University of Rome "Tor Vergata", 00133 Rome, Italy;
[3] Istituto Dermopatico dell'Immacolata-IRCCS, 00163 Rome, Italy
[4] MRC-Toxicology Unit, University of Cambridge, Cambridge, UK

Correspondence to: Gerry Melino, Eleonora Candi; **email:** gm614@mrc-tox.cam.ac.uk, candi@uniroma2.it
Keywords: p53, ZNF185, DNA damage, cytoskeleton, skin, epithelial cancer
Received: August 10, 2018 **Accepted:** November 1, 2018 **Published:** November 16, 2018

ABSTRACT

The transcription factor p53 is a key player in the tumour suppressive DNA damage response and a growing number of target genes involved in these pathways has been identified. p53 has been shown to be implicated in controlling cell motility and its mutant form enhances metastasis by loss of cell directionality, but the p53 role in this context has not yet being investigated. Here, we report that ZNF185, an actin cytoskeleton-associated protein from LIM-family of Zn-finger proteins, is induced following DNA-damage. ChIP-seq analysis, chromatin crosslinking immune-precipitation experiments and luciferase assays demonstrate that *ZNF185* is a *bona fide* p53 target gene. Upon genotoxic stress, caused by DNA-damaging drug etoposide and UVB irradiation, ZNF185 expression is up-regulated and in etoposide-treated cells, ZNF185 depletion does not affect cell proliferation and apoptosis, but interferes with actin cytoskeleton remodelling and cell polarization. Bioinformatic analysis of different types of epithelial cancers from both TCGA and GTEx databases showed a significant decrease in *ZNF185* mRNA level compared to normal tissues. These findings are confirmed by tissue micro-array IHC staining. Our data highlight the involvement of ZNF185 and cytoskeleton changes in p53-mediated cellular response to genotoxic stress and indicate ZNF185 as potential biomarker for epithelial cancer diagnosis.

INTRODUCTION

To counteract DNA damage, specific mechanisms have been evolved, these are activated by specific signal transduction pathways, such as the phosphatidylinositol 3-kinase-like protein kinases (PIKKs) family, ATM, ATR and DNA-PK, and the members of the poly(ADP)ribose polymerase (PARP) family [1–7]. Among the effectors, a key role is played by the tumour suppressor protein p53 [8–15]. Indeed, DNA damage leads to p53 stabilisation by inhibition of interaction with its ubiquitin ligase, MDM2 [9], and as consequence, p53 transcriptionally induces cell cycle arrest, apoptosis or senescence. Among p53 targets in response to DNA damage, there are the CDK inhibitor p21, the pro-apoptotic proteins BAX and PUMA [16]. Moreover, p53 directly activates repair pathways such as nucleotide excision repair (NER) through regulation of the NER factors XPC and DDB2 and induces dNTP synthesis [17].

In addition to its roles in cell death, p53 has also been implicated in cytoskeleton assembly, cell motility and mechanosignaling, as negative regulator of cancer cell mobility, invasion and metastasis [18–20]. Integrin expression and signalling pathways, which play a key

role in tumour cell invasion and metastasis, have been reported to be regulated indirectly by p53 [18]. For instance, Nutlin-3a, an MDM2 antagonist that acts as p53 activator, decreases the expression of integrin *alpha*5 in colorectal cancer and glioma cells [21,22]; also the expression of integrin *beta*3 decreases upon DNA-damage in wild-type p53 expressing cells [23]. p53 also regulates focal adhesion and Rho signalling pathways by regulating Rho GTPase activity [24] and effector protein genes of RhoA/RhoC and Cdc42 pathways [25–28]. In addition, F-actin formation is negatively or positively regulated by p53 in response to DNA damage depending on the anti-tumour drug used and cell type. For instance, while doxorubicin increases the expression of RhoC and LIM kinase 2 in a p53-dependent manner promoting actin stress fibers formation [29], etoposide and camptothecin attenuate this process through p53-dependent expression of RhoE [30]. It has been also reported that upon etoposide-mediated DNA damage, p53 alters actin cytoskeleton by transcriptionally induction of the expression of the cytoskeleton adaptor protein ankyrin-1 [31]. The relevance of cytoskeleton remodelling and cell mobility in tumours is evidenced by the fact that mutant p53 promotes tumour cell invasion and results in loss of directionality during migration [32]. Cytoskeleton remodelling and cell migration in cancer is a complex process and is controlled by many proteins and pathways, the specific role of p53 in these mechanisms is not yet completely understood.

Here, we describe a novel p53 target gene, *ZNF185*, which codifies for a Zn-finger protein belonging to LIM-family, activated upon genotoxic stress caused by DNA-damaging drug etoposide. ZNF185 itself is not necessary for p53-dependent cell cycle arrest and apoptosis, yet its silencing affects actin cytoskeleton changes and cell polarity upon etoposide treatment. At mRNA and protein level, ZNF185 is strongly reduced in different types of epithelial tumours, including skin and head and neck squamous cell carcinomas, suggesting that depletion of ZNF185 in cancer cells facilitate cancer cell migration and spreading.

RESULTS

ZNF185 is a p53 target gene

We have previously shown that the p53 family member p63, using a novel promoter region and a specific enhancer, directly regulated ZNF185 expression in keratinocytes [33]. To investigate whether also p53 could regulate ZNF185 expression and expand the p53 target genes involved in cytoskeleton regulation and cell polarity, we further analysed *ZNF185* promoter region using UCSC genome browser (Fig 1A). We observed several regions showing high accessibility and conservation between the species, and an enrichment in different transcription factors (TF) binding. Analysis of the publicity available ChIP-seq data for p53 performed in MCF7 cells after p53 stabilization by nutlin (GSE86164, [34]), revealed a strong peak within *ZNF185* promoter only in nutlin-treated cells (Fig 1B), suggesting p53 involvement in regulation of *ZNF185* transcription. Using previously described bioinformatic tool for p53 binding site (bs) prediction [35], we identified a putative binding site for p53 within the genomic region corresponding to the peak from the ChIP seq shown in Fig 1B (Fig 1C). Interestingly, this region is conserved only in primates and is absent in other species (Fig 1C). To confirm physical binding of p53 on *ZNF185* promoter, we performed ChIP assay in p53 Tet-On inducible SaOs-2 cells previously generated in the laboratory [36]. As a positive control, we used the promoter of *CDKN1A*, the gene coding for p21 (Fig 1D). To confirm if p53 could directly regulate *ZNF185* expression binding its promoter, we cloned the genomic locus harbouring p53 bs up-stream of the luciferase reporter gene. Luciferase activity assay showed a strong activation (120-fold, $P<0.01$) upon p53 overexpression. Interestingly, the overexpression of the two different p53 mutants frequently found in human cancers (R175H and R273H) did not show any strong activation compared to the control (Fig 1E), indicating that *ZNF185* is target of wild-type p53. Furthermore, the substitution of cytosines and guanines to adenines within *ZNF185* promoter sequence led to dramatic decrease of the luciferase activity (83% reduction, $P<0.01$) upon p53 overexpression (Fig 1F). To investigate if p53 is able to regulate *ZNF185* transcription, we induced p53 expression by doxycycline in SaOs-2 Tet-On cells and measured by RT-qPCR a significant increase of *ZNF185* mRNA after p53 induction paralleling *CDKN1A* increases (15-fold for *ZNF185* and 5-fold for *CDKN1A* at 24 h of induction, $P<0.05$; Fig 1G). We also confirmed this result changing cellular system. Indeed, overexpression of p53 in H1299 also led to a 20-fold increase of *ZNF185* mRNA, meanwhile the overexpression of two p53 mutants didn't show any significant modulation (Fig 1H). Altogether, these data indicate *ZNF185* as a *bona fide* transcriptional target of wild-type p53.

ZNF185 is up-regulated upon DNA damage

We investigated whether *ZNF185* is transcribed as consequence of p53 activation following DNA damage. Using two different carcinoma cell lines harbouring wild-type p53 (HCT116 and MCF7), we analysed ZNF185 expression after 0, 8, 16, and 24 hours of etoposide treatment. In both cases, we saw p53 stabilization as indicated by the western blots (Fig 2 A-

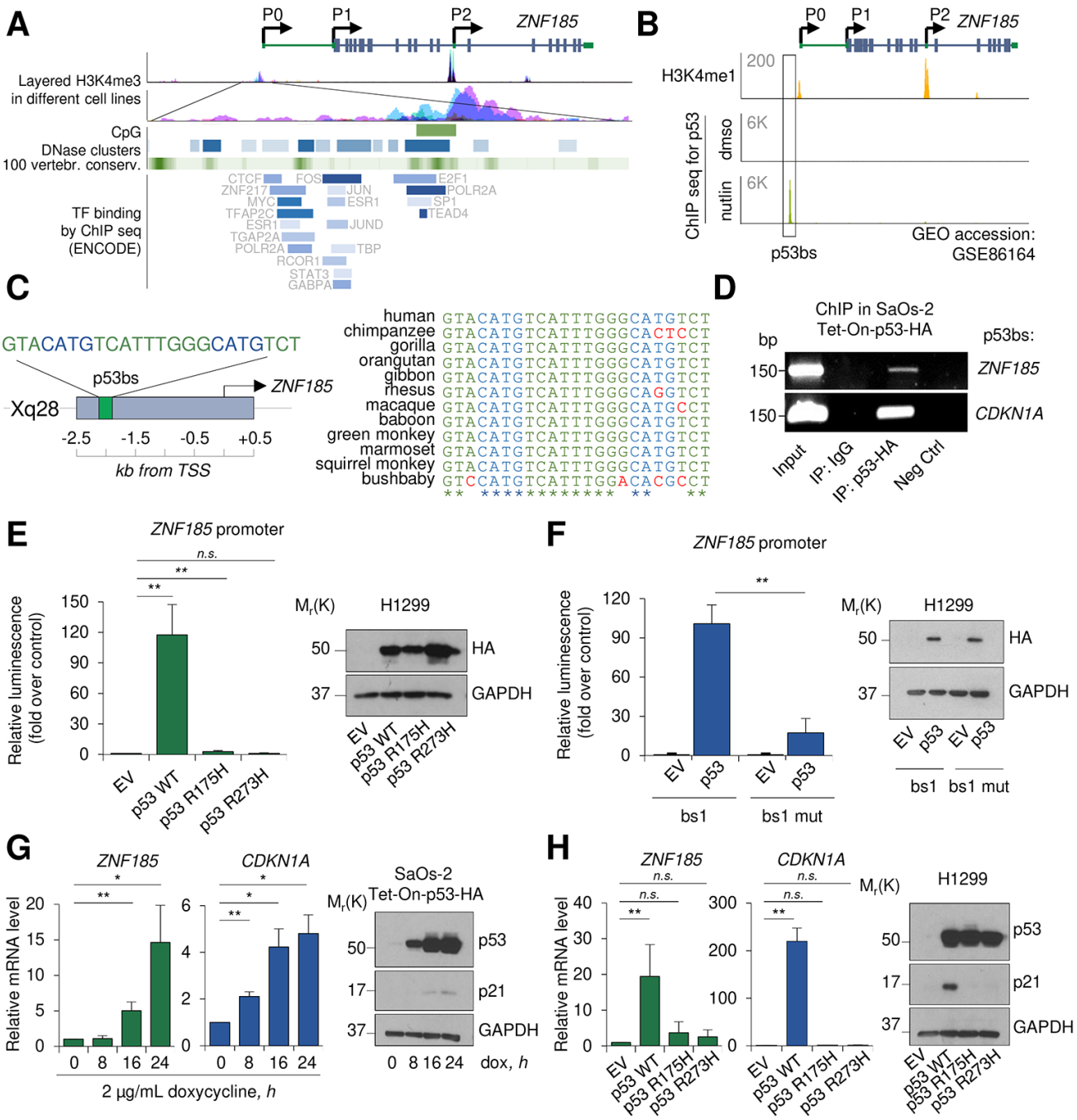

Figure 1. ZNF185 is a transcription target of p53. (**A**) UCSC genome browser analysis showing layered H3K4me3 mark in different cell lines, CpG islands, DNase clusters, conservation in vertebrates, and TF binding within *ZNF185* promoter. (**B**) Genomic locus of *ZNF185* showing the promoter region with H3K4me1 and p53 ChIP-seq signals after MCF7 treatment with either DMSO or nutlin. (**C**) Identified p53 binding site (p53 bs) within *ZNF185* promoter region and conservation analysis among primates. (**D**) Amplification of specific DNA fragments after ChIP performed in SaOs-2 Tet-On-p53-HA cells using HA antibody. (**E**) Luciferase activity assay in H1299 after transfection of pGL3-*ZNF185* promoter and either empty vector, p53 WT, p53-R175H, or p53-R273H expression vectors. ** $P<0.01$, $n=4$. Western blot analysis of cell lysates confirms p53 overexpression. (**F**) Luciferase activity assay in H1299 after transfection of pGL3-*ZNF185* promoter with either WT of mutated p53 bs and either empty vector or p53 WT expression vectors. ** $P<0.01$, $n=3$. Western blot analysis of cell lysates to confirm p53 overexpression. (**G**) RT-qPCR analysis of *ZNF185* and *CDKN1A* mRNA levels in SaOs-2 Tet-On-p53-HA after induction of p53 expression with 2 µg/mL doxycycline. * $P<0.05$, ** $P<0.01$, $n=3$. Western blot shows p53 and p21 levels. (**H**) RT-qPCR analysis of *ZNF185* and *CDKN1A* mRNA levels in H1299 after transfection with empty vector, p53 WT, p53 R175H, or p53 R273H expression vectors. ** $P<0.01$, $n=3$. Western blot shows p53 and p21 levels.

B) and, as a consequence of p53 activation, significant up-regulation of *ZNF185* mRNA (3-4-fold over control at 24 h of etoposide treatment, $P<0.05$), and p21 as positive control, both at mRNA and protein levels (Fig 2A-B). Interestingly, analysis of publicity available ChIP seq data (GSE56674, [37]) for p53 performed in keratinocytes showed that p53 binds to the locus within *ZNF185* promoter identified by us in this study. Moreover, this binding is observed only upon cisplatin or doxorubicin treatment (Fig 2C). As a model of basal layer keratinocytes, we used the commercial cell line of immortalized keratinocytes, Ker-CT. We confirmed that also in Ker-CT cells etoposide treatment leads to p53 stabilization and ZNF185 up-regulation both at mRNA (3-fold, $P<0.01$) and protein levels (Fig 2D). To confirm that ZNF185 up-regulation is p53-dependent, we performed siRNA-mediated knock-down of p53 in Ker-CT cells. As expected, depletion of p53 abolished up-regulation of ZNF185 upon etoposide treatment (Fig 2E). Since the major source of DNA damage in the human keratinocytes is UV irradiation, we irradiated Ker-CT cells and analysed ZNF185 level. Also in this case, we saw an up-regulation of ZNF185 at protein level. Altogether, these findings show that upon DNA damage we detected up-regulation of ZNF185 expression in p53-dependent manner both in tumour cell lines and in normal human keratinocytes.

ZNF185 is involved in the cytoskeleton remodelling upon DNA damage

Since the major functions of p53 activation upon DNA damage relate to the cell cycle arrest and apoptosis, we asked whether depletion of ZNF185 could alter cell

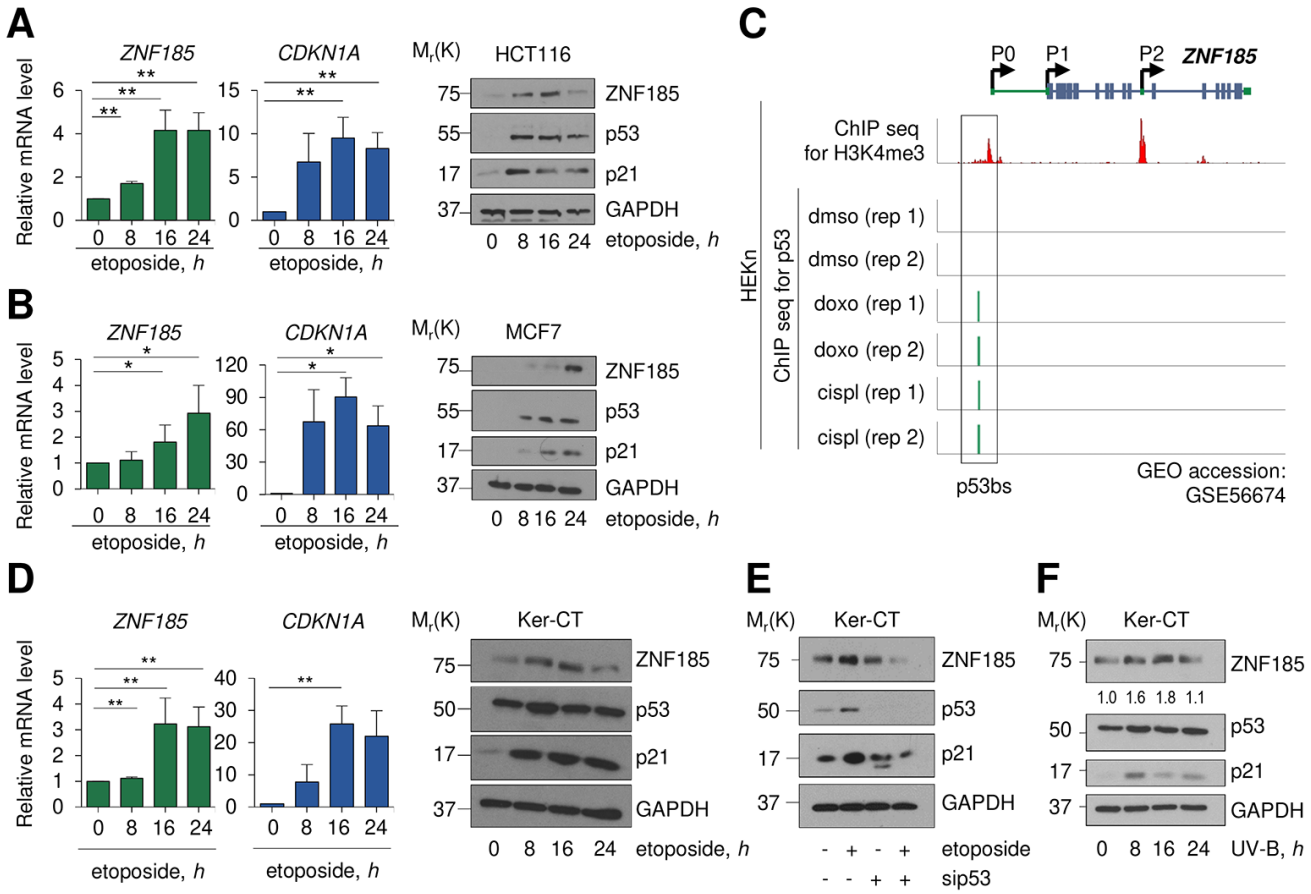

Figure 2. ZNF185 is up-regulated upon DNA damage. (**A**) qPCR analysis of *ZNF185* and *CDKN1A* mRNA levels in HCT116 after 25 µM etoposide treatment. **$P<0.01$. Western blot shows ZNF185, p53, and p21 levels. (**B**) qPCR analysis of *ZNF185* and *CDKN1A* mRNA levels in MCF7 after 25 µM etoposide treatment. Western blot shows ZNF185, p53, and p21 levels. *$P<0.05$ (**C**) Genomic locus of *ZNF185* showing the promoter region with H3K4me3 and p53 ChIP-seq signals after HEKn treatment with either DMSO, doxorubicin, or cisplatin. (**D**) qPCR analysis of *ZNF185* and *CDKN1A* mRNA levels in Ker-CT after 100 µM etoposide treatment. **P 0.05, n=3 (for *ZNF185*) and n=2 (for *CDKN1A*). Western blot shows ZNF185, p53, and p21 levels. (**E**) Western blot analysis of ZNF185, p53, and p21 levels after 100 µM etoposide treatment and p53 knock-down in Ker-CT cells. (**F**) Western blot analysis of ZNF185, p53, and p21 levels after 10 mJ·cm^{-2} UV-B treatment in Ker-CT cells for indicated times. Densitometry values of ZNF185 expression levels, normalized to GAPDH level, are shown.

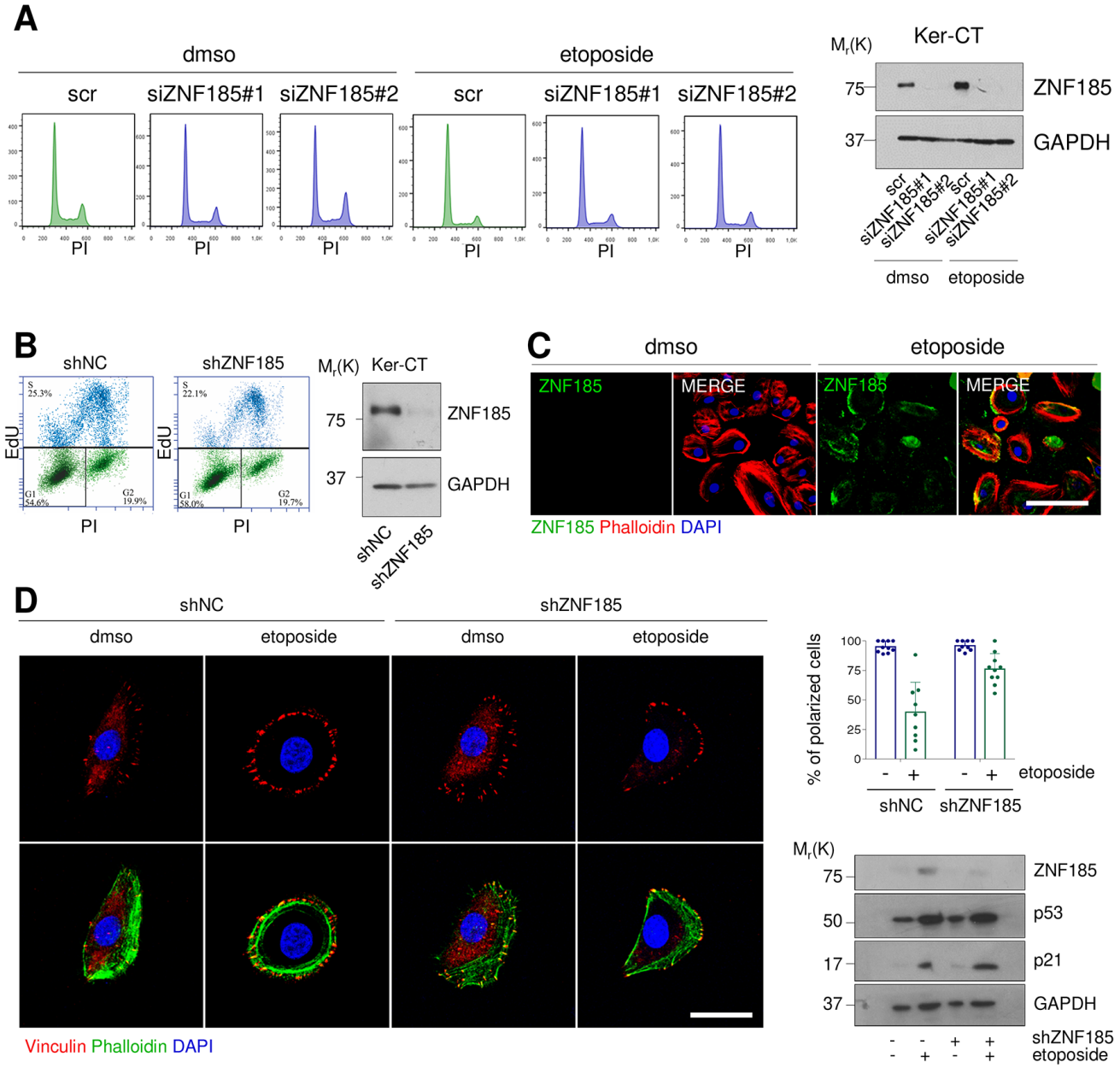

Figure 3. ZNF185 is involved in the cytoskeleton remodelling upon DNA damage. (**A**) FACS analysis of cell cycle content of the Ker-CT treated with either DMSO or 100 µM etoposide for 24 h after ZNF185 knock-down with two different siRNAs. Western blot confirms ZNF185 silencing. (**B**) EdU-incorporation assay by FACS showing % of EdU-positive Ker-CT shZNF185 cells. Western blot confirms the ZNF185 knock-down. (**C**) Immunofluorescence analysis of ZNF185 expression in Ker-CT treated with either DMSO or 100 µM etoposide for 16 h. Phalloidin was used for cytoskeleton staining. Scale bar: 50 µm. (**D**) Immunofluorescence analysis of vinculin distribution in Ker-CT treated with either DMSO or 100 µM etoposide and knocked-down for ZNF185. Phalloidin was used for cytoskeleton staining. Scale bar: 20 µm. In the right panel is shown the quantification of % of polarized cells in ten random fields. Western blot shows ZNF185, p53, and p21 levels.

cycle content under this specific stress condition. We performed siRNA mediated knock-down of ZNF185 in Ker-CT cells with two different siRNAs and treated the cells with etoposide. Cytofluorimetric analysis did not reveal any significant modulation in cell cycle distribution and apoptosis respect to the control (Fig 3A). It was previously reported that ZNF185 regulates proliferation of prostate cancer cells [38], to further investigate this point we generated Ker-CT cell line, stably expressing shRNA against ZNF185 (shZNF185).

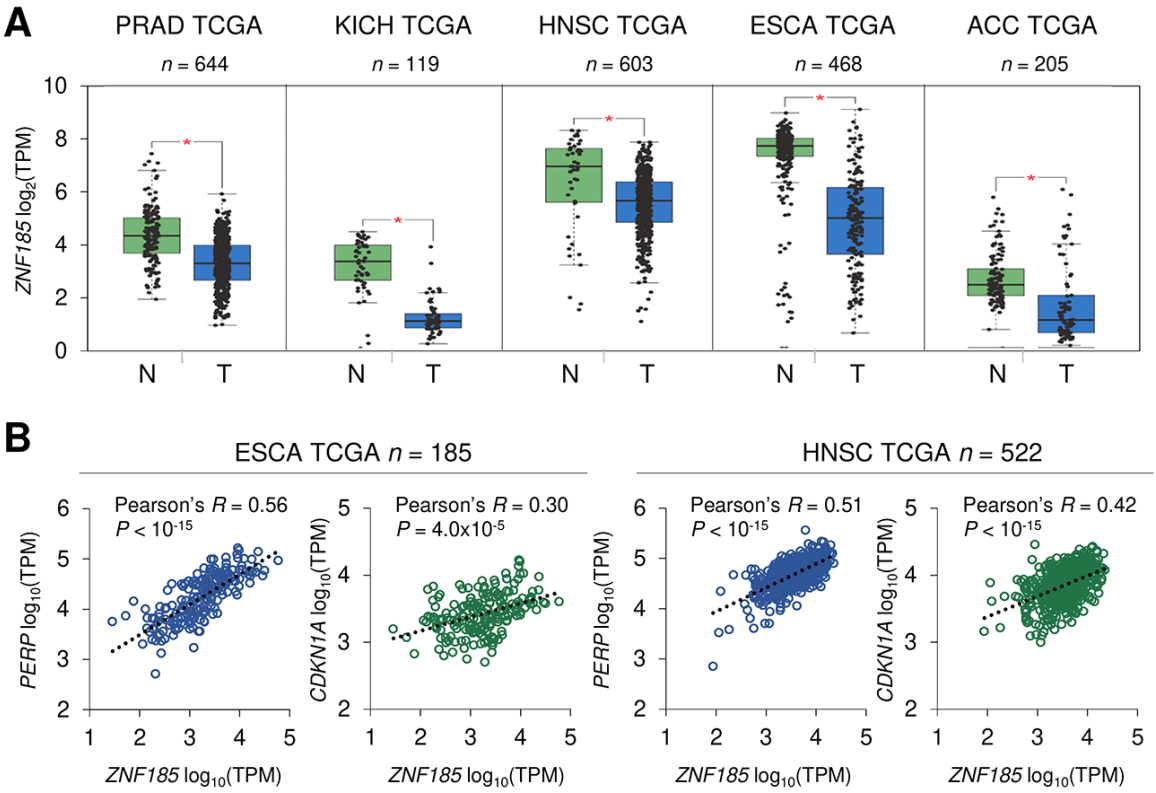

Figure 4. ZNF185 mRNA is down-regulated in epithelial cancer. (**A**) Box-plot showing expression of ZNF185 mRNA in different types of cancer from the GTEx/TCGA datasets for normal samples (N) and TCGA datasets for tumour samples (T). * *P*<0.05. (**B**) Correlation analysis between the expression of *ZNF185* and either *PERP* or *CDKN1A* in ESCA and HNSC tumour samples from TCGA.

We performed the EdU-incorporation assay to evaluate the number of cells in S-phase, but we did not observe any significant difference in cell proliferation respect to the control (Fig 3B). Given that several LIM-domain Zn-fingers can migrate into the nucleus under stress conditions [39], we asked whether DNA damage can alter ZNF185 localisation. We found that ZNF185 localised in the cytoplasm and at the cell periphery (Fig 3C) also after etoposide treatment. Due to the presence of the actin-interacting domain within ZNF185 protein, we hypothesised that ZNF185 could be involved in cytoskeleton remodelling upon DNA damage. To this aim, we performed immunofluorescence analysis using phalloidin as a marker of filamentous actin and vinculin as a marker of focal adhesion. Under normal conditions, most of the cells had migratory phenotype showing vinculin accumulation on the leading edge. After etoposide treatment, cells lost planar polarity as visualised by homogeneous vinculin distribution on the cell periphery (percentage of polarized cells from 100% to 35%). Surprisingly, this phenotype was abolished in the shZNF185 cells which retained planar polarization also upon etoposide treatment (percentage of polarized cells from 100% to 82%) (Fig 3D). Altogether, these results suggest that ZNF185 is involved in the loss of the planar polarity of cells upon DNA damage.

ZNF185 is down-regulated in epithelial cancers

p53 is frequently mutated in human cancers and we have shown that ZNF185 is positively regulated by wild-type p53, therefore we asked if ZNF185 level is decreased in epithelial cancers and particularly in the skin carcinomas. Firstly, we analysed *ZNF185* mRNA expression in different types of epithelial cancers from TCGA collection. Five cancer types - prostate adenocarcinoma (*PRAD*), chromophobe renal cell carcinoma (*KICH*), head and neck squamous cell carcinoma (*HNSC*), oesophageal carcinoma (*ESCA*), and adenoid cystic carcinoma (*ACC*) – showed a significant decrease in *ZNF185* mRNA level respect to the normal tissues from both TCGA and GTEx database (Fig 4A). Furthermore, we analysed correlation between the expression of *ZNF185* and two distinct targets of p53 – *PERP* and *CDKN1A*. Interestingly, a strong positive correlation was observed only in the cancers

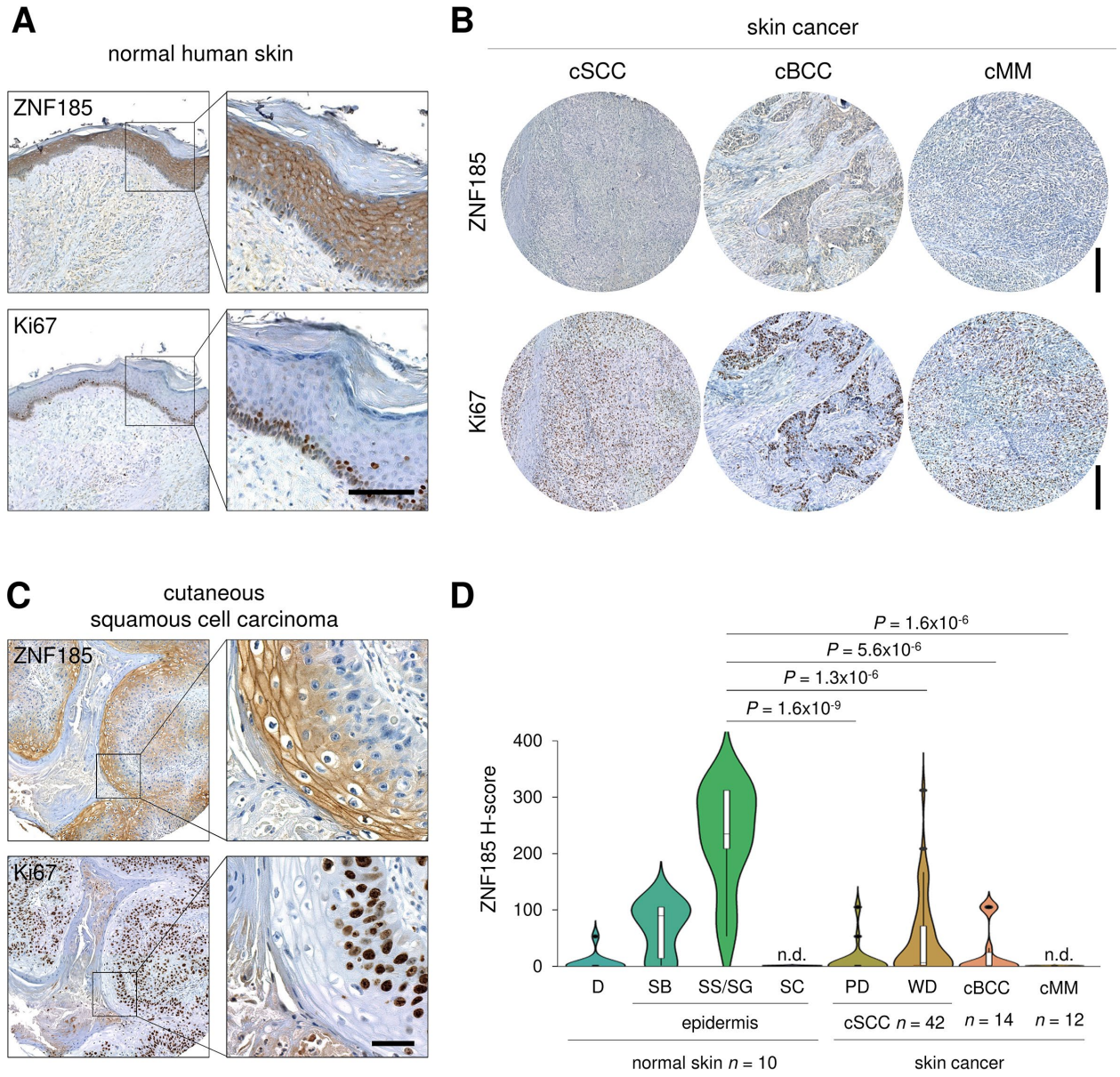

Figure 5. ZNF185 is down-regulated in skin cancer. (**A**) Immunohistochemical analysis of ZNF185 expression in normal skin. Ki67 was used as a marker of proliferation. Scale bar: 100 µm. (**B**) Immunohistochemical analysis of ZNF185 expression in skin cancer: cutaneous basal cell (cBCC), squamous cell carcinoma (cSCC), and malignant melanoma (cMM). Ki67 was used as a marker of proliferation. Scale bar: 250 µm. (**C**) Immunohistochemical analysis of ZNF185 expression in cutaneous squamous cell carcinoma (well differentiated). Ki67 was used as a marker of proliferation. Scale bar: 50 µm. (**D**) Violin plot showing H-score of protein expression level of ZNF185 in the normal skin (D – dermis, SB – basal layer, SS/SG – spinous and granular layers, SC – cornified layer) and skin cancer (cSCC (cSCC subpopulations: PD – poorly-differentiated cells, WD – well-differentiated cells), cBCC, and cMM).

arising from squamous epithelia – oesophageal and head and neck carcinomas (Fig. 4B). Since there are only few datasets of skin cancer with a very low number of samples, we decided to analyse ZNF185 expression in skin cancer by immunohistochemistry using tissue microarray, containing 42 samples of the cutaneous squamous cell carcinoma (cSCC), 14 samples of the cutaneous basal cell carcinoma (cBCC), 12 samples of cutaneous malignant melanoma (cMM), and 10 samples of the normal skin. As a marker of proliferation, we used Ki67. Analysis of ZNF185 expression pattern at protein level in the normal skin confirmed previously published data from our laboratory [33], in which ZNF185 highest expression occurs in the differentiated spinous and granular layers ("SS/SG") of the epidermis with low expression in the proliferating basal layer

("SB"). Cornified layer ("SC") and dermis ("D") were found negative for ZNF185 (Figure 5A). Analysis of skin cancer samples revealed that ZNF185 expression is dramatically down-regulated in the cutaneous squamous and basal cell carcinoma ("cSCC" and "cBCC") and malignant melanoma ("cMM") samples (Figure 5B). Furthermore, ZNF185 was found only in well-differentiated subpopulations of squamous cell carcinoma ("WD" of cSCC) in contrast to poorly-differentiated basal-like subpopulations ("PD" of cSCC) (Figure 5C). All the tumour samples showed a significant decrease ($P<1x10^{-5}$) of ZNF185 H-score respect to the differentiated layers of the normal epidermis (Figure 5D). These findings reveal a dramatic down-regulation of ZNF185 at protein level in the skin cancer and suggest that ZNF185 could be a potential biomarker for epithelial cancer diagnosis and prognosis.

DISCUSSION

Aging is complex set of genetic [40,41], epigenetic [42–46], immunological [47–51], and metabolic [52–58] rearrangements, involving several cellular signalling pathways [59–63] able to regulate metabolism, ROS formation [64–71] and DNA Damage Response (DDR) [72–74] in all organs [75–77]. Therefore, the identification of novel pathways involving p53-mediated responses [78,79] is of crucial interest. TP53 has been extensively studied in development and differentiation [14,80–82] as well as in cancer progression [83,84] and specifically in DDR [85–87]. The situation involves additional complexity if we consider that also the p53-related family members [88,89], that is p63 [90–92] and p73 [93], may be involved in DDR. TP63 is a gene primarily related to skin development [94], metabolism [36,95,96] and epithelial homeostasis [97,98] however, there is compelling evidence that it is also involved in cancer [27,47,99–103]. Similarly, TP73 is clearly involved in cancer [104], while the knockout studies [105,106] indicate a clear involvement in metabolism [107–109], neuro-development [104,110,111] and cancer progression [112,113]. Therefore, while the potential involvement of p73 with ZNF185 remains to be elucidated, the identification of a novel pathways of p53 regulating DDR via ZNF185 is of relevance.

Recently, the importance of actin-cytoskeleton remodelling and cell polarity during cancer cell spreading and metastasis has emerged [114–117], and p53 is in part involved in counteracting this specific aspect. Indeed, wild-type p53 can influence actin cytoskeleton dynamics controlling integrin and cadherin signalling and extracellular matrix degradation, suppressing EMT via different pathways [20,23,118–120]. Interestingly, also tumour microenvironment influences actin cytoskeleton [121,122], in part repressing wild-type p53 functions [123]. In fact, when p53 is inactivated, cancer cells invasion increases [124]. Here, we demonstrated that p53 wild-type transcriptionally activates *ZNF185* in cells upon DNA damage, which could make part of p53 negative regulation of cancer cell mobility, invasion and metastasis. Interestingly, similarly to another p53 target gene Rap2B [125], down-regulation of ZNF185 does not affect cell cycle progression or cell death, but its silencing abolishes the actin cytoskeleton rearrangements and cell polarity changes upon etoposide treatment.

ZNF185 is an actin-cytoskeleton-associated Lin-l 1, Isl-1 and Mec-3 (LIM) domain-containing protein [126]. The domain interacting with actin is located at the N-terminus, and it is necessary to mediate actin-cytoskeleton targeting of ZNF185, while the C-terminus LIM domain is dispensable for actin binding [38]. The LIM domain is a protein-protein interaction domain found in a wide range of proteins whose functions are related to the dynamics of the cytoskeleton [39,127,128]. In keratinocytes and epidermis ZNF185 has been described highly expressed in differentiating conditions, physically interacting with E-cadherin, a component of the adherens junctions, one of the critical cell-cell adhesive complexes crucial in the pluristratified epithelia [33]. ZNF185 involvement in pathologies, such as cancer [38], has not been completely investigated yet. Few studies reported ZNF185 as an unfavourable prognostic marker in ductal carcinoma of pancreas [129]. Its expression was found upregulated in colon cancer and likely correlated with liver metastasis [130]. On the other hand, other studies described epigenetic silencing of *ZNF185* associated with high grade and metastatic prostate tumours [131], lung tumours and head and neck squamous cell carcinomas [33,132–134]. Recently, it was reported that ZNF185 expression is negatively correlated with lymph node metastasis of lung adenocarcinoma and its overexpression leads to down-regulation of p-AKT, p-GSK3β, VEGF and MMP-9 expression [135]. These studies suggest a possible tumour-specific contribution of ZNF185 expression in tumour formation.

We confirmed ZNF185 down-regulation in different epithelial tumours and, by analysing the expression of ZNF185 at protein level, we found a significant decrease of ZNF185 in all the tumour samples analysed. Moreover, we found ZNF185 positive signal only in well-differentiated subpopulations of squamous cell carcinoma in contrast to poorly-differentiated basal-like aggressive subpopulations, suggesting a tumour-suppressor role of ZNF185. The possible involvement of ZNF185 in cytoskeleton remodelling upon DNA

damage suggests its role in the metastasis promotion which is in line with previous reports [135]. The identification of p53-ZNF185 axis could contribute to determine how p53 controls cell spreading by actin cytoskeletal remodelling, in which both the mechanical properties of the cytoskeleton of the cell as well as the microenvironment of the tumour cells seem to play an important role. Further investigation on the mechanisms by which p53 controls actin cytoskeleton reorganization and cell polarity, including the identification of novel target genes and pathways, would possibly be useful in developing new anti-cancer strategies and therapies.

MATERIALS AND METHODS

Cell culture, transfection, and treatments

Immortalized human epidermal keratinocytes Ker-CT (ATCC, Manassas, VA, USA) were cultured in EpiLife medium with addition of Human Keratinocyte Growth Supplements (HKGS, LifeTechnologies, Carlsbad, CA, USA). Human Non-Small-Cell Lung Carcinoma cells H1299 (ATCC), Human Osteosarcoma cells SaOs-2 inducible for p53 expression (SaOs-2 Tet-on p53), Human Colorectal Carcinoma cells HCT116 (ATCC), and mammary gland adenocarcinoma cells MCF7 (ATCC) were grown in DMEM medium with the addition of 10% FBS, 100 U penicillin, and 100 µg/mL streptomycin (Gibco, LifeTechnologies). For siRNA-mediated knock-down experiments, $2.5x10^5$ of cells were seeded on 60 mm culture dishes and the day after transfected with 80 pmol of specific siRNAs (Supplementary Table 1) by Lipofectamine RNAiMAX transfection reagent (Invitrogen, Carlsbad, CA, USA). Cells were collected 48h posttransfection. For overexpression experiments, $1x10^6$ of cells were seeded in 100 mm culture dishes and the day after were transfected with 5 µg of plasmidic DNA using Lipofectamine 2000 transfection reagent (Invitrogen). Cells were collected 24 h later. For shRNA-mediated knock-down, $2.5x10^5$ of Ker-CT were infected at m.o.i. 10 with lentiviral particles carrying either scramble control shRNA (NC, Cat. No. VSC7078, Dharmacon, Lafayette, CO, USA) or specific shRNA for *ZNF185* (shZNF185, Cat. No. V3SVHSHC_5107270, Dharmacon). Transduced cells were selected by puromycin addiction to culture medium (1.5 µg/mL, Sigma, St. Louis, MO, USA). To induce DNA damage, cells were treated with either 25 µM or 100 µM etoposide (Sigma) or 0.02-0.40% DMSO (Sigma) for the indicated times or for 16 h if not otherwise indicated. Ker-CT cells were irradiated for indicated times with 10 $mJ \cdot cm^{-2}$ UV-B rays. p53 expression was induced in SaOs-2 Tet-On p53 cells by adding of 2 µg/mL doxycycline (Sigma) for the indicated times.

Western blotting

The cells were collected by trypsinization, washed in PBS and lysed in RIPA buffer (50 mM Tris-cl pH 7.4, 150 mM NaCl, 1 % NP40, 0.25 % Na-deoxycholate, 1 mM AEBSF, 1 mM DTT). 20-50 µg of total protein extracts were resolved in SDS polyacrylamide gel using the Mini-PROTEAN Tetra cell System (Bio-Rad, Hercules, CA, USA) and blotted onto a Hybond PVDF membrane (GE Healthcare, Chicago, IL, USA) using the Bio-Rad Mini Trans-Blot Cell system Bio-Rad). Membranes were blocked with 5 % non-fat dry milk (Bio-Rad) in PBS/0.1 % Tween-20 buffer, for 1 h at room temperature in agitation. Membranes were incubated with primary antibodies over night at +4 °C, washed and hybridized for 1 h at room temperature with the appropriate horseradish peroxidase-conjugated secondary antibodies (goat anti-rabbit and goat anti-mouse antibodies, Bio-Rad). Detection was performed with the ECL chemiluminescence kit (Perkin Elmer, Waltham, MA, USA). The following antibodies were used: anti-ZNF185 (1:300, Cat. No. HPA000400, Sigma), anti-GAPDH (1:15000, Cat. No. G8795, Sigma), anti-p53 (1:500, Cat. No. SC-126, Santa Cruz, Dallas, TX, USA), anti-p21 (1:300, Cat. No. SC-756, Santa Cruz), anti-HA (1:1000, Cat. No. 901502, BioLegend, San Diego, CA, USA).

RNA extraction and RT-qPCR analysis

Total RNA was isolated using the RNeasy Mini Kit (Qiagen, Hilden, Germany) following the manufacturer's protocol. Total RNA (1 µg) was used for cDNA synthesis by GoScript Reverse Transcription System kit (Promega, Madison, WI, USA). RT-qPCRs were performed using the GoTaq Real-Time PCR System (Promega) in Applied Biosystems 7500 Real-Time PCR System (Applied Biosystems, Foster City, CA, USA) using appropriate qPCR primers (Supplementary Table 1). *TBP* was used as housekeeping gene for normalization. The expression of each gene was defined from the threshold cycle (C_t), and relative expression levels were calculated using the $2^{-\Delta\Delta Ct}$ method. All reactions were run in triplicate.

Analysis of *ZNF185* genomic locus

To analyse *ZNF185* genomic locus, different publicity accessible high-throughput sequencing data from ENCODE database (ChIP seq for H3K4me3 in different cell lines, CpG islands, DNase clusters, vertebrate conservation, TF binding) were visualised in the UCSC Genome Browser. Several ChIP-seq data from NCBI GEO database were analysed to assess p53 binding to the *ZNF185* promoter locus (GSE56674 ([37]) and

GSE86164 ([34])). To identify putative p53 binding sites was used the "p53 scan" software [136]. The conservation analysis of *ZNF185* promoter locus was performed within UCSC genome browser.

Chromatin immunoprecipitation assay

$1x10^6$ of SaOs Tet-On p53 cells, induced to overexpress p53 for 16 h, were used for ChIP assay. Cells were collected, fixed in 1% formaldehyde, and subjected to sonication for DNA shearing. The chromatin immunoprecipitation was performed with HA antibody (BioLegend) or unspecific immunoglobulin G (IgG, Invitrogen) using the MAGnify ChIP Kit (Invitrogen). Specific primers were used to amplify the putative p53 response element identified within *ZNF185* promoter region (Supplementary Table 1).

Luciferase activity assay

Promoter region of *ZNF185* containing the putative p53 binding site was amplified from human genomic DNA using specific primers (Supplementary Table 1). PCR products were digested by Kpn1/Nhe1 restriction enzymes (New England Biolabs, Ipswich, MA, USA) and subcloned into the pGL3-Promoter reporter vector (Promega). The constructs were completely sequenced. For luciferase activity assay, a total of $1.2x10^5$ H1299 cells were seeded in 12-well dishes 24 h before transfection. 100 ng of pGL3 reporter vector, 2 ng of pRL-CMV-Renilla luciferase vector (Promega) and 300 ng of either pcDNA-HA-p53, pcDNA-HA-p53-R175H, pcDNA-HA-p53-R273H, or empty pcDNA-HA vector (as a control) were cotransfected using Effectene transfection reagent according to the manufacturer's instructions (Qiagen). The luciferase activity was measured 24 h after transfection using a Dual Luciferase Reporter Assay System (Promega). The light emission was measured over 10 sec using a Lumat LB9507 luminometer (EG&GBerthold, Bad Wildbad, Germany). The transfection efficiency was normalized to Renilla luciferase activity. The overexpression of p53 was confirmed by western blotting.

Mutagenesis

For mutagenesis of p53 binding site was performed a PCR on 100 ng of pGL3 vector carrying p53 binding site using specific primers (Supplementary Table 1). PCR product was digested with DpnI restriction enzyme (New England Biolabs). The presence of mutated site was confirmed by sequencing.

Immunohistochemical staining and TMA

The immunohistochemical staining of the skin cancer tissue microarray sections (US Biomax, Rockville, MD, USA) was performed using the BenchMark ULTRA slide staining system (Roche Diagnostics, Risch-Rotkreuz, Switzerland). The staining for Ki67 was performed using anti-Ki67 antibody (Cat. No. 790-4286, Ventana) following manufacturer's indications. For ZNF185 staining, samples were incubated at 95°C for 76 min in the Cell Conditioning solution CC1 (Roche) and stained with anti-ZNF185 antibody (1:100, Sigma) for 40 min. Sections were counterstained with Mayer's haematoxylin, dehydrated and mounted. Samples were scored using a semi-quantitative method. Cases were analysed for staining intensity, which was scored as 0 (not detected), 1+ (weak), 2+ (intermediate), and 3+ (strong). For each case, the histological "H-score" (0-300) was calculated by multiplying the percentage of positive cells (0%-100%) by the intensity (0-3).

Immunofluorescence

Ker-CT cells were seeded on 5 mm coverslips, fixed for 10 min in 10% formalin buffered solution, washed with PBS and permeabilized in 0.2% triton X-100 solution in PBS for 10 min. Sections were incubated for 1 h in 10% goat serum in PBS at room temperature and overnight at 4 ºC with primary antibodies. Following antibodies were used: anti-ZNF185 (1:50, Sigma) and anti-vinculin (1:300, BD Biosciences, Franklin Lakes, NJ, USA). Sections were incubated for 1 h at room temperature with secondary anti-mouse and anti-rabbit 488- or 568-AlexaFluor conjugated antibodies (Invitrogen, 1:1000) together with 1 µg/mL DAPI (Sigma) for nuclear DNA staining. For cytoskeleton staining, 488- or 568-AlexaFluor conjugated phalloidin was used (1:1000, Thermo Fisher Scientific, Waltham, MA, USA). Images were acquired by Nikon A1 confocal laser microscope using NIS elements software (Nikon, Tokyo, Japan).

Cell proliferation

The incorporation of EdU during DNA synthesis was evaluated using the Click-iT EdU flow cytometry assay kit according to the manufacturer's protocol (Thermo Fisher Scientific). The cell cycle was analysed using an Accuri C6 flow cytometer (BD Biosciences). Fifteen thousand events were evaluated using the Accuri C6 (BD Biosciences) software. For cell cycle analysis, cells were fixed in 50% methanol/acetone 4:1 mix for 30 min at +4 °C, then treated with 13 Kunitz U/mL RNase for 15 min and stained with 50 µg/mL of propidium iodide for 20 min. Twelve thousand events were acquired using FACScalibur (BD Biosciences). Cell cycle distribution was calculated using FloxJo software.

Bioinformatic analysis

Analysis of ZNF185 expression in normal and tumour samples from TCGA/GTEx databases was performed using GEPIA [137]. *ZNF185*, *PERP*, and *CDKN1A*

expression data in ESCA and HNSC samples from TCGA collection were obtained using R2: Genomics Analysis and Visualization Platform (http://r2.amc.nl/).

Statistical analysis

The significance of differences between two experimental groups was calculated using unpaired, two-tailed Student's t-test. Values of $P < 0.05$ were considered significant. For RT-qPCR and luciferase assay, values reported are the mean ± SD. For statistical analysis of TMA scoring was used Mann–Whitney U test. All statistical analyses were performed using GraphPad Prism 7.0 Software. Violin plots were generated in R using ggplot2 package.

Abbreviations

LIM domain: Lin-l 1, Isl-1 and Mec-3 domain; bs: binding site; TMA: tissue micro-array; ChIP: chromatin immuno-precipitation; cBCC: cutaneous basal cell carcinoma; cSCC: cutaneous squamous cell carcinoma; cMM: cutaneous malignant melanoma.

AUTHOR CONTRIBUTIONS

AS, AC, AML and LA performed the research, EC designed the research, EC, AM, NDD, MAP and GM analysed the data, EC wrote the paper and all the authors read the paper and made comments.

CONFLICTS OF INTEREST

The authors declare no conflict of interest.

FUNDING

This work has been supported by grants from Associazione Italiana per la Ricerca contro il Cancro (AIRC): IG15653 (to G.M.), and by Istituto Dermopatico dell'Immacolata, IRCCS, RC to EC and joint research program Italia-Cina. This work has been also partially supported by the Medical Research Council, UK.

REFERENCES

1. Harper JW, Elledge SJ. The DNA damage response: ten years after. Mol Cell. 2007; 28:739–45. https://doi.org/10.1016/j.molcel.2007.11.015
2. Jackson SP, Bartek J. The DNA-damage response in human biology and disease. Nature. 2009; 461:1071–78. https://doi.org/10.1038/nature08467
3. Houtgraaf JH, Versmissen J, van der Giessen WJ. A concise review of DNA damage checkpoints and repair in mammalian cells. Cardiovasc Revasc Med. 2006; 7:165–72. https://doi.org/10.1016/j.carrev.2006.02.002
4. Ciccia A, Elledge SJ. The DNA damage response: making it safe to play with knives. Mol Cell. 2010; 40:179–204. https://doi.org/10.1016/j.molcel.2010.09.019
5. Hawley BR, Lu WT, Wilczynska A, Bushell M. The emerging role of RNAs in DNA damage repair. Cell Death Differ. 2017; 24:1989. https://doi.org/10.1038/cdd.2017.146
6. Baran K, Yang M, Dillon CP, Samson LL, Green DR. The proline rich domain of p53 is dispensable for MGMT-dependent DNA repair and cell survival following alkylation damage. Cell Death Differ. 2017; 24:1925–36. https://doi.org/10.1038/cdd.2017.116
7. Delbridge AR, Grabow S, Strasser A. Loss of BIM augments resistance of ATM-deficient thymocytes to DNA damage-induced apoptosis but does not accelerate lymphoma development. Cell Death Differ. 2017; 24:1987–88. https://doi.org/10.1038/cdd.2017.138
8. Zhou BB, Elledge SJ. The DNA damage response: putting checkpoints in perspective. Nature. 2000; 408:433–39. https://doi.org/10.1038/35044005
9. Lakin ND, Jackson SP. Regulation of p53 in response to DNA damage. Oncogene. 1999; 18:7644–55. https://doi.org/10.1038/sj.onc.1203015
10. Kruiswijk F, Labuschagne CF, Vousden KH. p53 in survival, death and metabolic health: a lifeguard with a licence to kill. Nat Rev Mol Cell Biol. 2015; 16:393–405. https://doi.org/10.1038/nrm4007
11. Kubbutat MH, Jones SN, Vousden KH. Regulation of p53 stability by Mdm2. Nature. 1997; 387:299–303. https://doi.org/10.1038/387299a0
12. Gurley KE, Ashley AK, Moser RD, Kemp CJ. Synergy between Prkdc and Trp53 regulates stem cell proliferation and GI-ARS after irradiation. Cell Death Differ. 2017; 24:1853–60. https://doi.org/10.1038/cdd.2017.107
13. Nayak D, Kumar A, Chakraborty S, Rasool RU, Amin H, Katoch A, Gopinath V, Mahajan V, Zilla MK, Rah B, Gandhi SG, Ali A, Kumar LD, Goswami A. Inhibition of Twist1-mediated invasion by Chk2 promotes premature senescence in p53-defective cancer cells. Cell Death Differ. 2017; 24:1275–87. https://doi.org/10.1038/cdd.2017.70
14. Van Nostrand JL, Bowen ME, Vogel H, Barna M, Attardi LD. The p53 family members have distinct roles during mammalian embryonic development.

Cell Death Differ. 2017; 24:575–79. https://doi.org/10.1038/cdd.2016.128

15. Solomon H, Bräuning B, Fainer I, Ben-Nissan G, Rabani S, Goldfinger N, Moscovitz O, Shakked Z, Rotter V, Sharon M. Post-translational regulation of p53 function through 20S proteasome-mediated cleavage. Cell Death Differ. 2017; 24:2187–98. https://doi.org/10.1038/cdd.2017.139

16. Riley T, Sontag E, Chen P, Levine A. Transcriptional control of human p53-regulated genes. Nat Rev Mol Cell Biol. 2008; 9:402–12. https://doi.org/10.1038/nrm2395

17. Ford JM. Regulation of DNA damage recognition and nucleotide excision repair: another role for p53. Mutat Res. 2005; 577:195–202. https://doi.org/10.1016/j.mrfmmm.2005.04.005

18. Ebata T, Hirata H, Kawauchi K. Functions of the Tumor Suppressors p53 and Rb in Actin Cytoskeleton Remodeling. BioMed Res Int. 2016; 2016:9231057. https://doi.org/10.1155/2016/9231057

19. Roger L, Gadea G, Roux P. Control of cell migration: a tumour suppressor function for p53? Biol Cell. 2006; 98:141–52. https://doi.org/10.1042/BC20050058

20. Araki K, Ebata T, Guo AK, Tobiume K, Wolf SJ, Kawauchi K. p53 regulates cytoskeleton remodeling to suppress tumor progression. Cell Mol Life Sci. 2015; 72:4077–94. https://doi.org/10.1007/s00018-015-1989-9

21. Janouskova H, Maglott A, Leger DY, Bossert C, Noulet F, Guerin E, Guenot D, Pinel S, Chastagner P, Plenat F, Entz-Werle N, Lehmann-Che J, Godet J, et al. Integrin α5β1 plays a critical role in resistance to temozolomide by interfering with the p53 pathway in high-grade glioma. Cancer Res. 2012; 72:3463–70. https://doi.org/10.1158/0008-5472.CAN-11-4199

22. Janouskova H, Ray AM, Noulet F, Lelong-Rebel I, Choulier L, Schaffner F, Lehmann M, Martin S, Teisinger J, Dontenwill M. Activation of p53 pathway by Nutlin-3a inhibits the expression of the therapeutic target α5 integrin in colon cancer cells. Cancer Lett. 2013; 336:307–18. https://doi.org/10.1016/j.canlet.2013.03.018

23. Bon G, Di Carlo SE, Folgiero V, Avetrani P, Lazzari C, D'Orazi G, Brizzi MF, Sacchi A, Soddu S, Blandino G, Mottolese M, Falcioni R. Negative regulation of beta4 integrin transcription by homeodomain-interacting protein kinase 2 and p53 impairs tumor progression. Cancer Res. 2009; 69:5978–86. https://doi.org/10.1158/0008-5472.CAN-09-0244

24. Muller PA, Vousden KH, Norman JC. p53 and its mutants in tumor cell migration and invasion. J Cell Biol. 2011; 192:209–18. https://doi.org/10.1083/jcb.201009059

25. Gadea G, de Toledo M, Anguille C, Roux P. Loss of p53 promotes RhoA-ROCK-dependent cell migration and invasion in 3D matrices. J Cell Biol. 2007; 178:23–30. https://doi.org/10.1083/jcb.200701120

26. Lefort K, Mandinova A, Ostano P, Kolev V, Calpini V, Kolfschoten I, Devgan V, Lieb J, Raffoul W, Hohl D, Neel V, Garlick J, Chiorino G, Dotto GP. Notch1 is a p53 target gene involved in human keratinocyte tumor suppression through negative regulation of ROCK1/2 and MRCKalpha kinases. Genes Dev. 2007; 21:562–77. https://doi.org/10.1101/gad.1484707

27. Guo F, Gao Y, Wang L, Zheng Y. p19Arf-p53 tumor suppressor pathway regulates cell motility by suppression of phosphoinositide 3-kinase and Rac1 GTPase activities. J Biol Chem. 2003; 278:14414–19. https://doi.org/10.1074/jbc.M300341200

28. Gadéa G, Lapasset L, Gauthier-Rouvière C, Roux P. Regulation of Cdc42-mediated morphological effects: a novel function for p53. EMBO J. 2002; 21:2373–82. https://doi.org/10.1093/emboj/21.10.2373

29. Croft DR, Crighton D, Samuel MS, Lourenco FC, Munro J, Wood J, Bensaad K, Vousden KH, Sansom OJ, Ryan KM, Olson MF. p53-mediated transcriptional regulation and activation of the actin cytoskeleton regulatory RhoC to LIMK2 signaling pathway promotes cell survival. Cell Res. 2011; 21:666–82. https://doi.org/10.1038/cr.2010.154

30. Ongusaha PP, Kim HG, Boswell SA, Ridley AJ, Der CJ, Dotto GP, Kim YB, Aaronson SA, Lee SW. RhoE is a pro-survival p53 target gene that inhibits ROCK I-mediated apoptosis in response to genotoxic stress. Curr Biol. 2006; 16:2466–72. https://doi.org/10.1016/j.cub.2006.10.056

31. Hall AE, Lu WT, Godfrey JD, Antonov AV, Paicu C, Moxon S, Dalmay T, Wilczynska A, Muller PA, Bushell M. The cytoskeleton adaptor protein ankyrin-1 is upregulated by p53 following DNA damage and alters cell migration. Cell Death Dis. 2016; 7:e2184. https://doi.org/10.1038/cddis.2016.91

32. Muller PA, Caswell PT, Doyle B, Iwanicki MP, Tan EH, Karim S, Lukashchuk N, Gillespie DA, Ludwig RL, Gosselin P, Cromer A, Brugge JS, Sansom OJ, et al. Mutant p53 drives invasion by promoting integrin recycling. Cell. 2009; 139:1327–41. https://doi.org/10.1016/j.cell.2009.11.026

33. Smirnov A, Lena AM, Cappello A, Panatta E, Anemona L, Bischetti S, Annicchiarico-Petruzzelli M, Mauriello A, Melino G, Candi E. ZNF185 is a p63 target gene critical for epidermal differentiation and squamous cell carcinoma development. Oncogene. 2018 Oct 18. doi: 10.1038/s41388-018-0509-4. [Epub ahead of print]

34. Andrysik Z, Galbraith MD, Guarnieri AL, Zaccara S, Sullivan KD, Pandey A, MacBeth M, Inga A, Espinosa JM. Identification of a core TP53 transcriptional program with highly distributed tumor suppressive activity. Genome Res. 2017; 27:1645–57. https://doi.org/10.1101/gr.220533.117

35. Kouwenhoven EN, van Heeringen SJ, Tena JJ, Oti M, Dutilh BE, Alonso ME, de la Calle-Mustienes E, Smeenk L, Rinne T, Parsaulian L, Bolat E, Jurgelenaite R, Huynen MA, et al. Genome-wide profiling of p63 DNA-binding sites identifies an element that regulates gene expression during limb development in the 7q21 SHFM1 locus. PLoS Genet. 2010; 6:e1001065. https://doi.org/10.1371/journal.pgen.1001065

36. Gressner O, Schilling T, Lorenz K, Schulze Schleithoff E, Koch A, Schulze-Bergkamen H, Lena AM, Candi E, Terrinoni A, Catani MV, Oren M, Melino G, Krammer PH, et al. TAp63α induces apoptosis by activating signaling via death receptors and mitochondria. EMBO J. 2005; 24:2458–71. https://doi.org/10.1038/sj.emboj.7600708

37. McDade SS, Patel D, Moran M, Campbell J, Fenwick K, Kozarewa I, Orr NJ, Lord CJ, Ashworth AA, McCance DJ. Genome-wide characterization reveals complex interplay between TP53 and TP63 in response to genotoxic stress. Nucleic Acids Res. 2014; 42:6270–85. https://doi.org/10.1093/nar/gku299

38. Zhang JS, Gong A, Young CY. ZNF185, an actin-cytoskeleton-associated growth inhibitory LIM protein in prostate cancer. Oncogene. 2007; 26:111–22. https://doi.org/10.1038/sj.onc.1209769

39. Kadrmas JL, Beckerle MC. The LIM domain: from the cytoskeleton to the nucleus. Nat Rev Mol Cell Biol. 2004; 5:920–31. https://doi.org/10.1038/nrm1499

40. Stoll EA, Karapavlovic N, Rosa H, Woodmass M, Rygiel K, White K, Turnbull DM, Faulkes CG. Naked mole-rats maintain healthy skeletal muscle and Complex IV mitochondrial enzyme function into old age. Aging (Albany NY). 2016; 8:3468–85. https://doi.org/10.18632/aging.101140

41. Ticinesi A, Tana C, Nouvenne A, Prati B, Lauretani F, Meschi T. Gut microbiota, cognitive frailty and dementia in older individuals: a systematic review. Clin Interv Aging. 2018; 13:1497–511. https://doi.org/10.2147/CIA.S139163

42. Kaestner L, Minetti G. The potential of erythrocytes as cellular aging models. Cell Death Differ. 2017; 24:1475–77. https://doi.org/10.1038/cdd.2017.100

43. Kuro-O M. Molecular Mechanisms Underlying Accelerated Aging by Defects in the FGF23-Klotho System. Int J Nephrol. 2018; 2018:9679841. https://doi.org/10.1155/2018/9679841

44. Pollard AK, Ortori CA, Stöger R, Barrett DA, Chakrabarti L. Mouse mitochondrial lipid composition is defined by age in brain and muscle. Aging (Albany NY). 2017; 9:986–98. https://doi.org/10.18632/aging.101204

45. Regina C, Compagnone M, Peschiaroli A, Lena AM, Melino G, Candi E. ΔNp63α modulates histone methyl transferase SETDB1 to transcriptionally repress target genes in cancers. Cell Death Dis. 2016; 2:16015. https://doi.org/10.1038/cddiscovery.2016.15

46. Smirnov A, Panatta E, Lena A, Castiglia D, Di Daniele N, Melino G, Candi E. FOXM1 regulates proliferation, senescence and oxidative stress in keratinocytes and cancer cells. Aging (Albany NY). 2016; 8:1384–97. https://doi.org/10.18632/aging.100988

47. Xu-Monette ZY, Zhang S, Li X, Manyam GC, Wang XX, Xia Y, Visco C, Tzankov A, Zhang L, Montes-Moreno S, Dybkaer K, Chiu A, Orazi A, et al. p63 expression confers significantly better survival outcomes in high-risk diffuse large B-cell lymphoma and demonstrates p53-like and p53-independent tumor suppressor function. Aging (Albany NY). 2016; 8:345–65. https://doi.org/10.18632/aging.100898

48. Lareau CA, DeWeese CF, Adrianto I, Lessard CJ, Gaffney PM, Iannuzzi MC, Rybicki BA, Levin AM, Montgomery CG. Polygenic risk assessment reveals pleiotropy between sarcoidosis and inflammatory disorders in the context of genetic ancestry. Genes Immun. 2017; 18:88–94. https://doi.org/10.1038/gene.2017.3

49. Messemaker TC, Mikkers HM, Huizinga TW, Toes RE, van der Helm-van Mil AH, Kurreeman F. Inflammatory genes TNFα and IL6 display no signs of increased H3K4me3 in circulating monocytes from untreated rheumatoid arthritis patients. Genes Immun. 2017; 18:191–96. https://doi.org/10.1038/gene.2017.20

50. Nikolic T, Woittiez NJ, van der Slik A, Laban S, Joosten A, Gysemans C, Mathieu C, Zwaginga JJ, Koeleman B, Roep BO. Differential transcriptome of

tolerogenic versus inflammatory dendritic cells points to modulated T1D genetic risk and enriched immune regulation. Genes Immun. 2017; 18:176–83. https://doi.org/10.1038/gene.2017.18

51. Liu S, Hou XL, Sui WG, Lu QJ, Hu YL, Dai Y. Direct measurement of B-cell receptor repertoire's composition and variation in systemic lupus erythematosus. Genes Immun. 2017; 18:22–27. https://doi.org/10.1038/gene.2016.45

52. Uzhachenko R, Boyd K, Olivares-Villagomez D, Zhu Y, Goodwin JS, Rana T, Shanker A, Tan WJ, Bondar T, Medzhitov R, Ivanova AV. Mitochondrial protein Fus1/Tusc2 in premature aging and age-related pathologies: critical roles of calcium and energy homeostasis. Aging (Albany NY). 2017; 9:627–49. https://doi.org/10.18632/aging.101213

53. Baraibar MA, Hyzewicz J, Rogowska-Wrzesinska A, Bulteau AL, Prip-Buus C, Butler-Browne G, Friguet B. Impaired energy metabolism of senescent muscle satellite cells is associated with oxidative modifications of glycolytic enzymes. Aging (Albany NY). 2016; 8:3375–89. https://doi.org/10.18632/aging.101126

54. Honrath B, Matschke L, Meyer T, Magerhans L, Perocchi F, Ganjam GK, Zischka H, Krasel C, Gerding A, Bakker BM, Bünemann M, Strack S, Decher N, et al. SK2 channels regulate mitochondrial respiration and mitochondrial Ca2+ uptake. Cell Death Differ. 2017; 24:761–73. https://doi.org/10.1038/cdd.2017.2

55. Ingram T, Chakrabarti L. Proteomic profiling of mitochondria: what does it tell us about the ageing brain? Aging (Albany NY). 2016; 8:3161–79. https://doi.org/10.18632/aging.101131

56. Kagan VE, Jiang J, Huang Z, Tyurina YY, Desbourdes C, Cottet-Rousselle C, Dar HH, Verma M, Tyurin VA, Kapralov AA, Cheikhi A, Mao G, Stolz D, et al. NDPK-D (NM23-H4)-mediated externalization of cardiolipin enables elimination of depolarized mitochondria by mitophagy. Cell Death Differ. 2016; 23:1140–51. https://doi.org/10.1038/cdd.2015.160

57. Kaufman DM, Wu X, Scott BA, Itani OA, Van Gilst MR, Bruce JE, Crowder CM. Ageing and hypoxia cause protein aggregation in mitochondria. Cell Death Differ. 2017; 24:1730–38. https://doi.org/10.1038/cdd.2017.101

58. Giacomello M, Pellegrini L. The coming of age of the mitochondria-ER contact: a matter of thickness. Cell Death Differ. 2016; 23:1417–27. https://doi.org/10.1038/cdd.2016.52

59. Choi JY, Hwang CY, Lee B, Lee SM, Bahn YJ, Lee KP, Kang M, Kim YS, Woo SH, Lim JY, Kim E, Kwon KS. Age-associated repression of type 1 inositol 1, 4, 5-triphosphate receptor impairs muscle regeneration. Aging (Albany NY). 2016; 8:2062–80. https://doi.org/10.18632/aging.101039

60. Jęśko H, Stępień A, Lukiw WJ, Strosznajder RP. The Cross-Talk Between Sphingolipids and Insulin-Like Growth Factor Signaling: Significance for Aging and Neurodegeneration. Mol Neurobiol. 2018. https://doi.org/10.1007/s12035-018-1286-3

61. Lee SJ, Hwang J, Jeong HJ, Yoo M, Go GY, Lee JR, Leem YE, Park JW, Seo DW, Kim YK, Hahn MJ, Han JW, Kang JS, Bae GU. PKN2 and Cdo interact to activate AKT and promote myoblast differentiation. Cell Death Dis. 2016; 7:e2431. https://doi.org/10.1038/cddis.2016.296

62. Oh J, Sinha I, Tan KY, Rosner B, Dreyfuss JM, Gjata O, Tran P, Shoelson SE, Wagers AJ. Age-associated NF-κB signaling in myofibers alters the satellite cell niche and re-strains muscle stem cell function. Aging (Albany NY). 2016; 8:2871–96. https://doi.org/10.18632/aging.101098

63. Shao AW, Sun H, Geng Y, Peng Q, Wang P, Chen J, Xiong T, Cao R, Tang J. Bclaf1 is an important NF-κB signaling transducer and C/EBPβ regulator in DNA damage-induced senescence. Cell Death Differ. 2016; 23:865–75. https://doi.org/10.1038/cdd.2015.150

64. Knupp J, Martinez-Montañés F, Van Den Bergh F, Cottier S, Schneiter R, Beard D, Chang A. Sphingolipid accumulation causes mitochondrial dysregulation and cell death. Cell Death Differ. 2017; 24:2044–53. https://doi.org/10.1038/cdd.2017.128

65. Lalia AZ, Dasari S, Robinson MM, Abid H, Morse DM, Klaus KA, Lanza IR. Influence of omega-3 fatty acids on skeletal muscle protein metabolism and mitochondrial bioenergetics in older adults. Aging (Albany NY). 2017; 9:1096–129. https://doi.org/10.18632/aging.101210

66. Lang A, Anand R, Altinoluk-Hambüchen S, Ezzahoini H, Stefanski A, Iram A, Bergmann L, Urbach J, Böhler P, Hänsel J, Franke M, Stühler K, Krutmann J, et al. SIRT4 interacts with OPA1 and regulates mitochondrial quality control and mitophagy. Aging (Albany NY). 2017; 9:2163–89. https://doi.org/10.18632/aging.101307

67. Marini A, Rotblat B, Sbarrato T, Niklison-Chirou MV, Knight JR, Dudek K, Jones C, Bushell M, Knight RA, Amelio I, Willis AE, Melino G. TAp73 contributes to the oxidative stress response by regulating protein

synthesis. Proc Natl Acad Sci USA. 2018; 115:6219–24. https://doi.org/10.1073/pnas.1718531115

68. Pinto M, Pickrell AM, Wang X, Bacman SR, Yu A, Hida A, Dillon LM, Morton PD, Malek TR, Williams SL, Moraes CT. Transient mitochondrial DNA double strand breaks in mice cause accelerated aging phenotypes in a ROS-dependent but p53/p21-independent manner. Cell Death Differ. 2017; 24:288–99. https://doi.org/10.1038/cdd.2016.123

69. Qi Y, Liu H, Daniels MP, Zhang G, Xu H. Loss of Drosophila i-AAA protease, dYME1L, causes abnormal mitochondria and apoptotic degeneration. Cell Death Differ. 2016; 23:291–302. https://doi.org/10.1038/cdd.2015.94

70. Ohkusu-Tsukada K, Yamashita T, Tsukada T, Takahashi K. Low expression of a Ddm7/Ldm7-hybrid mutant (D/Ldm7) in the novel haplotype H-2nc identified in atopic dermatitis model NC/Nga mice. Genes Immun. 2017. [Epub ahead of print] https://doi.org/10.1038/s41435-017-0003-y

71. Tak H, Eun JW, Kim J, Park SJ, Kim C, Ji E, Lee H, Kang H, Cho DH, Lee K, Kim W, Nam SW, Lee EK. T-cell-restricted intracellular antigen 1 facilitates mitochondrial fragmentation by enhancing the expression of mitochondrial fission factor. Cell Death Differ. 2017; 24:49–58. https://doi.org/10.1038/cdd.2016.90

72. Galluzzi L, Vitale I, Aaronson SA, Abrams JM, Adam D, Agostinis P, Alnemri ES, Altucci L, Amelio I, Andrews DW, Annicchiarico-Petruzzelli M, Antonov AV, Arama E, et al. Molecular mechanisms of cell death: recommendations of the Nomenclature Committee on Cell Death 2018. Cell Death Differ. 2018; 25:486–541. https://doi.org/10.1038/s41418-017-0012-4

73. Gross A, Zaltsman Y, Maryanovich M. The ATM-BID pathway plays a critical role in the DNA damage response by regulating mitochondria metabolism. Cell Death Differ. 2016; 23:182. https://doi.org/10.1038/cdd.2015.154

74. Lovat PE, Ranalli M, Annichiarrico-Petruzzelli M, Bernassola F, Piacentini M, Malcolm AJ, Pearson AD, Melino G, Redfern CP. Effector mechanisms of fenretinide-induced apoptosis in neuroblastoma. Exp Cell Res. 2000; 260:50–60. https://doi.org/10.1006/excr.2000.4988

75. Belle JI, Petrov JC, Langlais D, Robert F, Cencic R, Shen S, Pelletier J, Gros P, Nijnik A. Repression of p53-target gene Bbc3/PUMA by MYSM1 is essential for the survival of hematopoietic multipotent progenitors and contributes to stem cell maintenance. Cell Death Differ. 2016; 23:759–75. https://doi.org/10.1038/cdd.2015.140

76. Brzeszczyńska J, Johns N, Schilb A, Degen S, Degen M, Langen R, Schols A, Glass DJ, Roubenoff R, Greig CA, Jacobi C, Fearon KC, Ross JA. Loss of oxidative defense and potential blockade of satellite cell maturation in the skeletal muscle of patients with cancer but not in the healthy elderly. Aging (Albany NY). 2016; 8:1690–702. https://doi.org/10.18632/aging.101006

77. Greschik H, Duteil D, Messaddeq N, Willmann D, Arrigoni L, Sum M, Jung M, Metzger D, Manke T, Günther T, Schüle R. The histone code reader Spin1 controls skeletal muscle development. Cell Death Dis. 2017; 8:e3173. https://doi.org/10.1038/cddis.2017.468

78. Aggarwal M, Saxena R, Sinclair E, Fu Y, Jacobs A, Dyba M, Wang X, Cruz I, Berry D, Kallakury B, Mueller SC, Agostino SD, Blandino G, et al. Reactivation of mutant p53 by a dietary-related compound phenethyl isothiocyanate inhibits tumor growth. Cell Death Differ. 2016; 23:1615–27. https://doi.org/10.1038/cdd.2016.48

79. Alexandrova EM, Moll UM. Depleting stabilized GOF mutant p53 proteins by inhibiting molecular folding chaperones: a new promise in cancer therapy. Cell Death Differ. 2017; 24:3–5. https://doi.org/10.1038/cdd.2016.145

80. Artigas N, Gámez B, Cubillos-Rojas M, Sánchez-de Diego C, Valer JA, Pons G, Rosa JL, Ventura F. p53 inhibits SP7/Osterix activity in the transcriptional program of osteoblast differentiation. Cell Death Differ. 2017; 24:2022–31. https://doi.org/10.1038/cdd.2017.113

81. Baldelli S, Ciriolo MR. Altered S-nitrosylation of p53 is responsible for impaired antioxidant response in skeletal muscle during aging. Aging (Albany NY). 2016; 8:3450–67. https://doi.org/10.18632/aging.101139

82. Cam H, Griesmann H, Beitzinger M, Hofmann L, Beinoraviciute-Kellner R, Sauer M, Hüttinger-Kirchhof N, Oswald C, Friedl P, Gattenlöhner S, Burek C, Rosenwald A, Stiewe T. p53 family members in myogenic differentiation and rhabdomyosarcoma development. Cancer Cell. 2006; 10:281–93. https://doi.org/10.1016/j.ccr.2006.08.024

83. Ghosh S, Salot S, Sengupta S, Navalkar A, Ghosh D, Jacob R, Das S, Kumar R, Jha NN, Sahay S, Mehra S, Mohite GM, Ghosh SK, et al. p53 amyloid formation leading to its loss of function: implications in cancer

pathogenesis. Cell Death Differ. 2017; 24:1784–98. https://doi.org/10.1038/cdd.2017.105

84. Nicolai S, Rossi A, Di Daniele N, Melino G, Annicchiarico-Petruzzelli M, Raschellà G. DNA repair and aging: the impact of the p53 family. Aging (Albany NY). 2015; 7:1050–65. https://doi.org/10.18632/aging.100858

85. Seitz SJ, Schleithoff ES, Koch A, Schuster A, Teufel A, Staib F, Stremmel W, Melino G, Krammer PH, Schilling T, Müller M. Chemotherapy-induced apoptosis in hepatocellular carcinoma involves the p53 family and is mediated via the extrinsic and the intrinsic pathway. Int J Cancer. 2010; 126:2049–66.

86. Charni M, Aloni-Grinstein R, Molchadsky A, Rotter V. p53 on the crossroad between regeneration and cancer. Cell Death Differ. 2017; 24:8–14. https://doi.org/10.1038/cdd.2016.117

87. Amelio I, Knight RA, Lisitsa A, Melino G, Antonov AV. p53MutaGene: an online tool to estimate the effect of p53 mutational status on gene regulation in cancer. Cell Death Dis. 2016; 7:e2148. https://doi.org/10.1038/cddis.2016.42

88. Levine AJ, Tomasini R, McKeon FD, Mak TW, Melino G. The p53 family: guardians of maternal reproduction. Nat Rev Mol Cell Biol. 2011; 12:259–65. https://doi.org/10.1038/nrm3086

89. De Laurenzi V, Melino G. Evolution of functions within the p53/p63/p73 family. Ann N Y Acad Sci. 2000; 926:90–100. https://doi.org/10.1111/j.1749-6632.2000.tb05602.x

90. Memmi EM, Sanarico AG, Giacobbe A, Peschiaroli A, Frezza V, Cicalese A, Pisati F, Tosoni D, Zhou H, Tonon G, Antonov A, Melino G, Pelicci PG, Bernassola F. p63 Sustains self-renewal of mammary cancer stem cells through regulation of Sonic Hedgehog signaling. Proc Natl Acad Sci USA. 2015; 112:3499–504. https://doi.org/10.1073/pnas.1500762112

91. Novelli F, Lena AM, Panatta E, Nasser W, Shalom-Feuerstein R, Candi E, Melino G. Allele-specific silencing of EEC p63 mutant R304W restores p63 transcriptional activity. Cell Death Dis. 2016; 7:e2227. https://doi.org/10.1038/cddis.2016.118

92. Rivetti di Val Cervo P, Lena AM, Nicoloso M, Rossi S, Mancini M, Zhou H, Saintigny G, Dellambra E, Odorisio T, Mahé C, Calin GA, Candi E, Melino G. p63-microRNA feedback in keratinocyte senescence. Proc Natl Acad Sci USA. 2012; 109:1133–38. https://doi.org/10.1073/pnas.1112257109

93. Melino G, De Laurenzi V, Vousden KH. p73: Friend or foe in tumorigenesis. Nat Rev Cancer. 2002; 2:605–15. https://doi.org/10.1038/nrc861

94. Candi E, Schmidt R, Melino G. The cornified envelope: a model of cell death in the skin. Nat Rev Mol Cell Biol. 2005; 6:328–40. https://doi.org/10.1038/nrm1619

95. Viticchiè G, Agostini M, Lena AM, Mancini M, Zhou H, Zolla L, Dinsdale D, Saintigny G, Melino G, Candi E. p63 supports aerobic respiration through hexokinase II. Proc Natl Acad Sci USA. 2015; 112:11577–82. https://doi.org/10.1073/pnas.1508871112

96. Candi E, Smirnov A, Panatta E, Lena AM, Novelli F, Mancini M, Viticchiè G, Piro MC, Di Daniele N, Annicchiarico-Petruzzelli M, Melino G. Metabolic pathways regulated by p63. Biochem Biophys Res Commun. 2017; 482:440–44. https://doi.org/10.1016/j.bbrc.2016.10.094

97. Candi E, Terrinoni A, Rufini A, Chikh A, Lena AM, Suzuki Y, Sayan BS, Knight RA, Melino G. p63 is upstream of IKK alpha in epidermal development. J Cell Sci. 2006; 119:4617–22. https://doi.org/10.1242/jcs.03265

98. Martin SE, Temm CJ, Goheen MP, Ulbright TM, Hattab EM. Cytoplasmic p63 immunohistochemistry is a useful marker for muscle differentiation: an immunohistochemical and immunoelectron microscopic study. Mod Pathol. 2011; 24:1320–26. https://doi.org/10.1038/modpathol.2011.89

99. Compagnone M, Gatti V, Presutti D, Ruberti G, Fierro C, Markert EK, Vousden KH, Zhou H, Mauriello A, Anemone L, Bongiorno-Borbone L, Melino G, Peschiaroli A. ΔNp63-mediated regulation of hyaluronic acid metabolism and signaling supports HNSCC tumorigenesis. Proc Natl Acad Sci USA. 2017; 114:13254–59. https://doi.org/10.1073/pnas.1711777114

100. Di Franco S, Sala G, Todaro M. p63 role in breast cancer. Aging (Albany NY). 2016; 8:2256–57. https://doi.org/10.18632/aging.101042

101. Flores ER, Lozano G. The p53 family grows old. Genes Dev. 2012; 26:1997–2000. https://doi.org/10.1101/gad.202648.112

102. Flores ER, Sengupta S, Miller JB, Newman JJ, Bronson R, Crowley D, Yang A, McKeon F, Jacks T. Tumor predisposition in mice mutant for p63 and p73: evidence for broader tumor suppressor functions for the p53 family. Cancer Cell. 2005; 7:363–73. https://doi.org/10.1016/j.ccr.2005.02.019

103. Latina A, Viticchiè G, Lena AM, Piro MC, Annicchiarico-Petruzzelli M, Melino G, Candi E.

ΔNp63 targets cytoglobin to inhibit oxidative stress-induced apoptosis in keratinocytes and lung cancer. Oncogene. 2016; 35:1493–503. https://doi.org/10.1038/onc.2015.222

104. Niklison-Chirou MV, Steinert JR, Agostini M, Knight RA, Dinsdale D, Cattaneo A, Mak TW, Melino G. TAp73 knockout mice show morphological and functional nervous system defects associated with loss of p75 neurotrophin receptor. Proc Natl Acad Sci USA. 2013; 110:18952–57. https://doi.org/10.1073/pnas.1221172110

105. Rufini A, Niklison-Chirou MV, Inoue S, Tomasini R, Harris IS, Marino A, Federici M, Dinsdale D, Knight RA, Melino G, Mak TW. TAp73 depletion accelerates aging through metabolic dysregulation. Genes Dev. 2012; 26:2009–14. https://doi.org/10.1101/gad.197640.112

106. Tomasini R, Tsuchihara K, Wilhelm M, Fujitani M, Rufini A, Cheung CC, Khan F, Itie-Youten A, Wakeham A, Tsao MS, Iovanna JL, Squire J, Jurisica I, et al. TAp73 knockout shows genomic instability with infertility and tumor suppressor functions. Genes Dev. 2008; 22:2677–91. https://doi.org/10.1101/gad.1695308

107. Amelio I, Inoue S, Markert EK, Levine AJ, Knight RA, Mak TW, Melino G. TAp73 opposes tumor angiogenesis by promoting hypoxia-inducible factor 1α degradation. Proc Natl Acad Sci USA. 2015; 112:226–31. https://doi.org/10.1073/pnas.1410609111

108. Agostini M, Romeo F, Inoue S, Niklison-Chirou MV, Elia AJ, Dinsdale D, Morone N, Knight RA, Mak TW, Melino G. Metabolic reprogramming during neuronal differentiation. Cell Death Differ. 2016; 23:1502–14. https://doi.org/10.1038/cdd.2016.36

109. Tóth B, Garabuczi E, Sarang Z, Vereb G, Vámosi G, Aeschlimann D, Blaskó B, Bécsi B, Erdõdi F, Lacy-Hulbert A, Zhang A, Falasca L, Birge RB, et al. Transglutaminase 2 is needed for the formation of an efficient phagocyte portal in macrophages engulfing apoptotic cells. J Immunol. 2009; 182:2084–92. https://doi.org/10.4049/jimmunol.0803444

110. Agostini M, Tucci P, Steinert JR, Shalom-Feuerstein R, Rouleau M, Aberdam D, Forsythe ID, Young KW, Ventura A, Concepcion CP, Han YC, Candi E, Knight RA, et al. microRNA-34a regulates neurite outgrowth, spinal morphology, and function. Proc Natl Acad Sci USA. 2011; 108:21099–104. https://doi.org/10.1073/pnas.1112063108

111. Agostini M, Tucci P, Killick R, Candi E, Sayan BS, Rivetti di Val Cervo P, Nicotera P, McKeon F, Knight RA, Mak TW, Melino G. Neuronal differentiation by TAp73 is mediated by microRNA-34a regulation of synaptic protein targets. Proc Natl Acad Sci USA. 2011; 108:21093–98. https://doi.org/10.1073/pnas.1112061109

112. Martin-Lopez M, Maeso-Alonso L, Fuertes-Alvarez S, Balboa D, Rodríguez-Cortez V, Weltner J, Diez-Prieto I, Davis A, Wu Y, Otonkoski T, Flores ER, Menéndez P, Marques MM, Marin MC. p73 is required for appropriate BMP-induced mesenchymal-to-epithelial transition during somatic cell reprogramming. Cell Death Dis. 2017; 8:e3034. https://doi.org/10.1038/cddis.2017.432

113. Matin RN, Chikh A, Chong SL, Mesher D, Graf M, Sanza' P, Senatore V, Scatolini M, Moretti F, Leigh IM, Proby CM, Costanzo A, Chiorino G, et al. p63 is an alternative p53 repressor in melanoma that confers chemoresistance and a poor prognosis. J Exp Med. 2013; 210:581–603. https://doi.org/10.1084/jem.20121439

114. Schmitz AA, Govek EE, Böttner B, Van Aelst L. Rho GTPases: signaling, migration, and invasion. Exp Cell Res. 2000; 261:1–12. https://doi.org/10.1006/excr.2000.5049

115. Nagano M, Hoshino D, Koshikawa N, Akizawa T, Seiki M. Turnover of focal adhesions and cancer cell migration. Int J Cell Biol. 2012; 2012:310616. https://doi.org/10.1155/2012/310616

116. Halaoui R, McCaffrey L. Rewiring cell polarity signaling in cancer. Oncogene. 2015; 34:939–50. https://doi.org/10.1038/onc.2014.59

117. Sgrò F, Bianchi FT, Falcone M, Pallavicini G, Gai M, Chiotto AM, Berto GE, Turco E, Chang YJ, Huttner WB, Di Cunto F. Tissue-specific control of midbody microtubule stability by Citron kinase through modulation of TUBB3 phosphorylation. Cell Death Differ. 2016; 23:801–13. https://doi.org/10.1038/cdd.2015.142

118. Wu DW, Lee MC, Wang J, Chen CY, Cheng YW, Lee H. DDX3 loss by p53 inactivation promotes tumor malignancy via the MDM2/Slug/E-cadherin pathway and poor patient outcome in non-small-cell lung cancer. Oncogene. 2014; 33:1515–26. https://doi.org/10.1038/onc.2013.107

119. Schubert J, Brabletz T. p53 Spreads out further: suppression of EMT and stemness by activating miR-200c expression. Cell Res. 2011; 21:705–07. https://doi.org/10.1038/cr.2011.62

120. Kim T, Veronese A, Pichiorri F, Lee TJ, Jeon YJ, Volinia S, Pineau P, Marchio A, Palatini J, Suh SS, Alder H, Liu CG, Dejean A, Croce CM. p53 regulates epithelial-mesenchymal transition through microRNAs

targeting ZEB1 and ZEB2. J Exp Med. 2011; 208:875–83. https://doi.org/10.1084/jem.20110235

121. Cianfrocca R, Rosanò L, Tocci P, Sestito R, Caprara V, Di Castro V, De Maria R, Bagnato A. Blocking endothelin-1-receptor/β-catenin circuit sensitizes to chemotherapy in colorectal cancer. Cell Death Differ. 2017; 24:1811–20. https://doi.org/10.1038/cdd.2017.121

122. Delaidelli A, Negri GL, Jan A, Jansonius B, El-Naggar A, Lim JK, Khan D, Zarni Oo H, Carnie CJ, Remke M, Maris JM, Leprivier G, Sorensen PH. MYCN amplified neuroblastoma requires the mRNA translation regulator eEF2 kinase to adapt to nutrient deprivation. Cell Death Differ. 2017; 24:1564–76. https://doi.org/10.1038/cdd.2017.79

123. Bao W, Strömblad S. Integrin alphav-mediated inactivation of p53 controls a MEK1-dependent melanoma cell survival pathway in three-dimensional collagen. J Cell Biol. 2004; 167:745–56. https://doi.org/10.1083/jcb.200404018

124. Mak AS. p53 in cell invasion, podosomes, and invadopodia. Cell Adhes Migr. 2014; 8:205–14. https://doi.org/10.4161/cam.27841

125. D i J, Huang H, Wang Y, Qu D, Tang J, Cheng Q, Lu Z, Zhang Y, Zheng J. p53 target gene Rap2B regulates the cytoskeleton and inhibits cell spreading. J Cancer Res Clin Oncol. 2015; 141:1791–98. https://doi.org/10.1007/s00432-015-1948-8

126. Heiss NS, Gloeckner G, Bächner D, Kioschis P, Klauck SM, Hinzmann B, Rosenthal A, Herman GE, Poustka A. Genomic structure of a novel LIM domain gene (ZNF185) in Xq28 and comparisons with the orthologous murine transcript. Genomics. 1997; 43:329–38. https://doi.org/10.1006/geno.1997.4810

127. Dawid IB, Breen JJ, Toyama R. LIM domains: multiple roles as adapters and functional modifiers in protein interactions. Trends Genet. 1998; 14:156–62. https://doi.org/10.1016/S0168-9525(98)01424-3

128. Bach I. The LIM domain: regulation by association. Mech Dev. 2000; 91:5–17. https://doi.org/10.1016/S0925-4773(99)00314-7

129. Furukawa D, Chijiwa T, Matsuyama M, Mukai M, Matsuo EI, Nishimura O, Kawai K, Suemizu H, Nakagohri T, Ozawa S, Shimada K, Hiraoka N, Nakamura M. Plasma membrane expression of ZNF185 is a prognostic factor in pancreatic ductal carcinoma. Oncol Lett. 2017; 14:3633–40. https://doi.org/10.3892/ol.2017.6633

130. Furukawa D, Chijiwa T, Matsuyama M, Mukai M, Matsuo EI, Nishimura O, Kawai K, Suemizu H, Hiraoka N, Nakagohri T, Yasuda S, Nakamura M. Zinc finger protein 185 is a liver metastasis-associated factor in colon cancer patients. Mol Clin Oncol. 2014; 2:709–13. https://doi.org/10.3892/mco.2014.298

131. Vanaja DK, Cheville JC, Iturria SJ, Young CY. Transcriptional silencing of zinc finger protein 185 identified by expression profiling is associated with prostate cancer progression. Cancer Res. 2003; 63:3877–82.

132. Gonzalez HE, Gujrati M, Frederick M, Henderson Y, Arumugam J, Spring PW, Mitsudo K, Kim HW, Clayman GL. Identification of 9 genes differentially expressed in head and neck squamous cell carcinoma. Arch Otolaryngol Head Neck Surg. 2003; 129:754–59. https://doi.org/10.1001/archotol.129.7.754

133. Medina PP, Carretero J, Ballestar E, Angulo B, Lopez-Rios F, Esteller M, Sanchez-Cespedes M. Transcriptional targets of the chromatin-remodelling factor SMARCA4/BRG1 in lung cancer cells. Hum Mol Genet. 2005; 14:973–82. https://doi.org/10.1093/hmg/ddi091

134. Krøigård AB, Larsen MJ, Lænkholm AV, Knoop AS, Jensen JD, Bak M, Mollenhauer J, Thomassen M, Kruse TA. Identification of metastasis driver genes by massive parallel sequencing of successive steps of breast cancer progression. PLoS One. 2018; 13:e0189887. https://doi.org/10.1371/journal.pone.0189887

135. Wang J, Huang HH, Liu FB. ZNF185 inhibits growth and invasion of lung adenocarcinoma cells through inhibition of the akt/gsk3β pathway. J Biol Regul Homeost Agents. 2016; 30:683–91.

136. Oti M, Kouwenhoven EN, Zhou H. Genome-wide p63-regulated gene expression in differentiating epidermal keratinocytes. Genom Data. 2015; 5:159–63. https://doi.org/10.1016/j.gdata.2015.06.002

137. Tang Z, Li C, Kang B, Gao G, Li C, Zhang Z. GEPIA: a web server for cancer and normal gene expression profiling and interactive analyses. Nucleic Acids Res. 2017; 45:W98–102. https://doi.org/10.1093/nar/gkx247

SUPPLEMENTARY MATERIAL

Supplementary Table 1. List of siRNAs and primers sequences.

siRNAs		
Name	**Company**	**Cat. No.**
Neg CTRL	Dharmacon	D-001810-10
h*ZNF185* #1	Qiagen	SI04156320
h*ZNF185* #2	Qiagen	SI04309137
h*TP53*	Qiagen	SI00011655
Primers for qPCR		
TBP-For	TCAAACCCAGAATTGTTCTCCTTAT	
TBP-Rev	CCTGAATCCCTTTAGAATAGGGTAG	
ZNF185-For	TCAAGCAGATGAAAGTGCGAACC	
ZNF185-Rev	CTCCCCAGCTGATGAAAAGGATG	
CDKN1A-For	GTCACTGTCTTGTACCCTTGTG	
CDKN1A-Rev	CGGCGTTTGGAGTGGTAGAAA	
Primers for ChIP		
ZNF185-p53bs-For	TACTGCTGAGAGAAAGTGGAGG	
ZNF185-p53bs-Rev	CCAGGGCACCTCTAGTCACC	
CDKN1A-p53bs-For	GCTCCCTCATGGGCAAACTCACT	
CDKN1A-p53bs-Rev	TGGCTGGTCTACCTGGCTCCTCT	
Primers for luciferase activity assay		
ZNF185-promoter-For	GTACTCGAGTGCTGCCTAAGCTGGAG	
ZNF185-promoter-Rev	GTAAAGCTTGGGCCTCAAGCTCTTC	
Primers for mutagenesis		
ZNF185-bsMUT-For	CTATCTGGGTAAATATCATTTGGGAATATCTGGTGCTTGAAG	
ZNF185-bsMUT-Rev	CTTCAAGCACCAGATATTCCCAAATGATATTTACCCAGATAG	

Research Paper

TAp73 regulates ATP7A: possible implications for ageing-related diseases

Piervito Lopriore[1,2], Nazzareno Capitanio[2], Emanuele Panatta[1], Nicola Di Daniele[3], Alessandra Gambacurta[4], Gerry Melino[1,4], Ivano Amelio[1]

[1] MRC Toxicology Unit, University of Cambridge, Leicester LE1 7HB, United Kingdom
[2] Department of Clinical & Experimental Medicine, University of Foggia, Foggia, Italy
[3] Department of Systems Medicine, Nephrology and Hypertension Unit, Tor Vergata University Hospital, Rome, Italy
[4] Department of Experimental Medicine and Surgery, University of Rome Tor Vergata, Rome, Italy

Correspondence to: Ivano Amelio; **email:** ia348@mrc-tox.cam.ac.uk
Keywords: neurodegeneration, ageing, p53 family, copper, cancer
Received: October 4, 2018 **Accepted:** November 15, 2018 **Published:** December 8, 2018

ABSTRACT

The p53 family member p73 controls a wide range of cellular function. Deletion of p73 in mice results in increased tumorigenesis, infertility, neurological defects and altered immune system. Despite the extensive effort directed to define the molecular underlying mechanism of p73 function a clear definition of its transcriptional signature and the extent of overlap with the other p53 family members is still missing. Here we describe a novel TAp73 target, ATP7A a member of a large family of P-type ATPases implicated in human neurogenerative conditions and cancer chemoresistance. Modulation of TAp73 expression influences basal expression level of ATP7A in different cellular models and chromatin immunoprecipitation confirmed a physical direct binding of TAp73 on ATP7A genomic regions. Bioinformatic analysis of expression profile datasets of human lung cancer patients suggests a possible implication of TAp73/ATP7A axis in human cancer. These data provide a novel TAp73-dependent target which might have implications in ageing-related diseases such as cancer and neurodegeneration.

INTRODUCTION

p53 family is one of the most powerful families of genes due to the large spectrum of role that plays from tumour suppression, maintenance of the cellular homeostasis, contribution to development, reproduction and ageing [1-11]. As transcription factors, the three members, p53, p63 and p73, sharing high degree of structural homology, especially in their DNA-binding domains [12], regulate the expression of genes crucial for a wide range of cellular processes, including cell cycle arrest/apoptosis, senescence, metabolism[13-19], autophagy as well as terminal differentiation in specific cell types, such as neurons for p73[20-22] and keratinocytes for p63[23-27]. The functional and physical interplay within the family members is also thought to play biological roles and the interaction with the mutated forms of p53 can have implications in cancer [28-36].

Similar to 95% of human genes [37, 38] *TP73* gene generates multiple protein isoforms, which arise as a result of alternative promoter (P1 and P2) control and differential mRNA splicing at the 3'end. P2 activity generates ΔNp73 isoforms that lack the transactivation (TA) domain present in the N terminus of the full length p73 protein (TAp73); alternative splicing, instead, leads to 7 isoforms (α- η) varying in activity and specificity [39-41].

p73 plays critical functions in cellular processes such as neuronal development and differentiation [32, 42-48], and metabolic control [42, 49-57]. Mimicking p53 function, TAp73 controls cell cycle arrest and apoptosis as well as genome integrity protection in germline and somatic cells, impacting fertility and cancer [9, 29, 58-61]. Differently from *TP53* gene, in cancer cells p73 is rarely mutated, but shows often dysregulated expressions. Isoform-specific knockout mice revealed that the two major N-terminal p73 isoforms, TAp73 and ΔNp73, play opposite role in cancer [6, 62]. TAp73 deficiency predisposes to spontaneous cancer and increases the susceptibility to carcinogens [62], whereas the absence of ΔNp73 decreases tumour growth [63]. The impact of p73 deregulation on cancer cell biology can indeed depend on the relative expression of TAp73 and ΔNp73 isoforms [64]. As a result, most studies in cancer-related fields focus their attention on the analysis of changes in TAp73 and ΔNp73 expression levels. ΔNp73 is thought to inhibit the activity of the transcriptional competent isoform TAp73, with a fine molecular tuning. ΔNp73 can indeed counteract TAp73 tetramerization or compete for promoter binding. The TAp73/ΔNp73 ratio in cells subjected to chemotherapeutic agents could therefore be crucial. TAp73 contributes to genomic stability of somatic and germline cells by controlling the mitotic checkpoints. Furthermore, TAp73 interacts with kinetochore proteins Bub1 and Bub3 to control the spindle assembly. Deregulation of TAp73 in cancer are consequentially expected to impact on polyploidy [6]. More recent work showed that TAp73 can physically bind and control stability of the hypoxia-inducible factor 1α (HIF-1α). In hypoxic tumour, expression of TAp73 represses activation of HIF-1, thus limiting tumour angiogenesis and therefore progression towards advanced stages [60, 65-67]. Additional contribution of p73 to tumour cell biology might be mediated by its support to cellular anti-oxidant defence and anabolic processes. This is partially mediated by a TAp73-dependent regulation on mitochondrial proteins synthesis under oxidative stress [14] and by a transcriptional control of metabolic enzymes responsible for GSH synthesis, such as glutaminase-2 (GLS-2) [50, 52] and glucose-6-phosphate-dehydrogenase (G6PD) [53].

However, despite the important effort placed by scientific community, we are very far from a dissection of p73 transcriptional programme and a clear discrimination of this from the transcriptome of the siblings p53 and p63. By re-analysing previously published high throughput genomic screening approach (gene microarrays) and filtering data by using bioinformatic tools we aimed to identify novel p73 transcriptional targets. Our analysis, supported by *in vitro* data and clinical analysis identified a previously unknown relationship between TAp73 and ATP7A (or *MNK*), a gene encoding for a transmembrane P-type ATPase transporter required for copper homeostasis in mammals [68]. ATP7A is recognized as a critical copper-transport protein with multiple important cellular functions. Mutations is ATP7A are responsible for Menkes disease, a X-linked recessive disorder characterized by growth retardation, neurodegeneration, and peculiar hair [69]. In addition, over-expression of ATP7A is observed in multiple cancers, and recent studies suggest that this copper efflux transporter play an important role in platinum drug resistance [70-76]. Our data demonstrate a TAp73-dependent *ATP7A* transcription control and a possible clinical relevance of this axis for lung cancer patients. Our finding might delineate the possible underlining mechanisms of different ageing-related conditions, such as cancer and neurodegeneration, where alterations of the TAp73/ATP7A axis might play a direct impact.

RESULTS

ATP7A is within the top TAp73 candidate target genes

To further deepen TAp73 functions as transcriptional factor we firstly started analysing two previously reported global gene expression analysis in TAp73 silenced cells, *p53*-null human non-small cell lung carcinoma cell line H1299 [65] and human embryonic kidney cell line 293T [14]. Crossing the two lists and considering the top ranked genes, in terms of fold change, we selected the ones with established role or suspected involvement in tumour biology. Hence, we tested the synergist effect of the expression of each individual gene (from a list including 175 genes) with p73 expression on survival outcome in different cancer datasets by a bioinformatic datamining tool we previously established, Syntarget [77]. Not surprisingly the most represented cancer type was lung cancer: 20 of the 21 genes found clinically synergize with *TP73* ($p<0.05$) in Lung Adenocarcinoma stage I-II (GSE31210) and Lung Cancer (GSE30219) datasets. Indeed, previous studies have showed that TAp73$^{-/-}$ mice spontaneously develop lung carcinomas, and altered ratio TAp73/ΔNp73 is frequently reported in human lung cancer [62, 78]. Thus, we selected 5 genes of these (*SPP1*, *TET2*, *CABLES1*, *JPH1* and *ATP7A*) that more significantly synergize with *TP73*, influencing more robustly oncological patients overall survival. A representative work flow of the followed rationale is shown in Figure 1a.

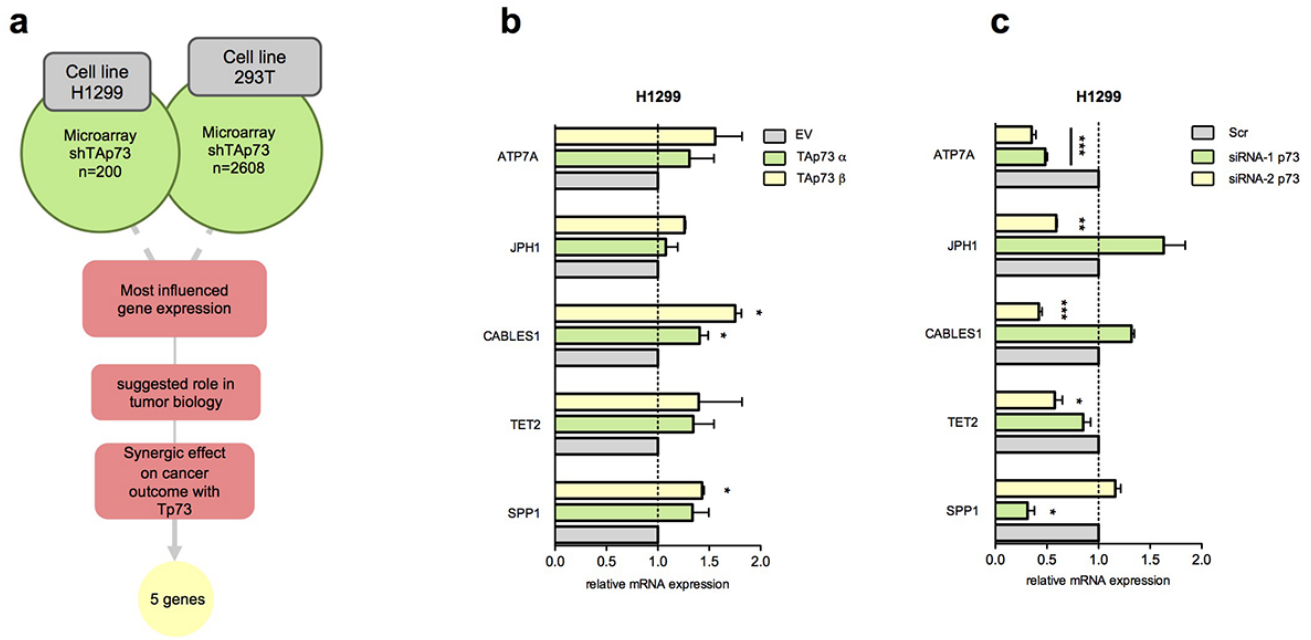

Figure 1. Identification of new TAp73 transcriptional targets. (**a**) Schematic workflow of putative TAp73 transcriptional target analysis; most influenced genes in H1299 (Amelio et al.) [65] and 293T (Marini et al.) [14] (shTAp73) were analysed by filtering ones more related with tumor biology; searching for previous evidence were done on PubMed (NCBI). Gene expressions effect on oncological patients survival and synergical effect with Tp73 on cancer outcome were analysed studying KM curves in all available datasets in web based online tool Syntarget. (**b**) mRNA levels of SPP1, TET2, CABLES1, JPH1, ATP7A were analysed by quantitative PCR after HA-TAp73 α and β overexpression. Relative expression of genes was normalized against TBP and calculated as fold change to the control treatment (empty vector, EV). Data is reported as mean ± s.d. of three experiments. * $p < 0.05$ (Student's T-test). (**c**) mRNA levels of genes of interest were analysed by quantitative PCR after siRNA-1 p73 and siRNA-2 p73 treatment. Relative expression of genes was normalized against TBP and calculated as fold change to the control treatment (siCTRL, Scr). Data is reported as mean ± s.d. of three experiments. *** $p < 0.0001$, ** $p < 0.001$, * $p < 0.05$ (Student's T-test).

TAp73 silencing influences ATP7A expression level

To explore potential downstream targets of TAp73 we analysed the expression level of the top 5 candidate genes following overexpression and silencing of TAp73 by transfection of pcDNA HA-TAp73 α-β and siRNA-1/2 p73 in both H1299 and 293T cell lines. p73 silencing in both cell lines resulted in a significant ATP7A transcript downregulation (Figure 1c, Figure 2a). In H1299 overexpression assay only *CABLES1*, a gene encoding for a protein well-known involved in the cell cycle regulation [79], showed slight mRNA level increase (1.5-2-fold increase) (Figure 1b). This data, however, was not confirmed in 293T cells overexpressing TAp73 (Supplementary Figure 1c). The remaining genes showed similar mRNA level fluctuation, however not always high consistency was observed in both models (Figure 1b, c and Supplementary Figure 1a, b). p73 and p21 expression levels were measured by RT-qPCR to verify efficiency of TAp73 overexpression and silencing (Figure 2b and Supplementary Figure 1c).

We decided to focus on ATP7A due to the more significant and consistent regulation observed. ATP7A mRNA reduction in p73 knocked-down cells was accompanied by a significant decrease of the protein level, more evident in the 293T model (Figure 2c,d). In addition, H1299 showed also a moderated, but consistent upregulation of ATP7A protein upon TAp73 overexpression (Figure 2e).

Collectively, these data demonstrate a TAp73-dependent regulation of *ATP7A* expression at both protein and mRNA level.

TAp73 binds ATP7A genomic regions

The above results suggested a relationship between TAp73 and ATP7A transcript. Hence, we asked whether a TAp73-dependent transcriptional regulation of ATP7A was associated to a direct physical binding of TAp73 to ATP7A promoter region.

In addition to the canonical upstream promoter, found by using Eukaryotic Promoter Database (labelled

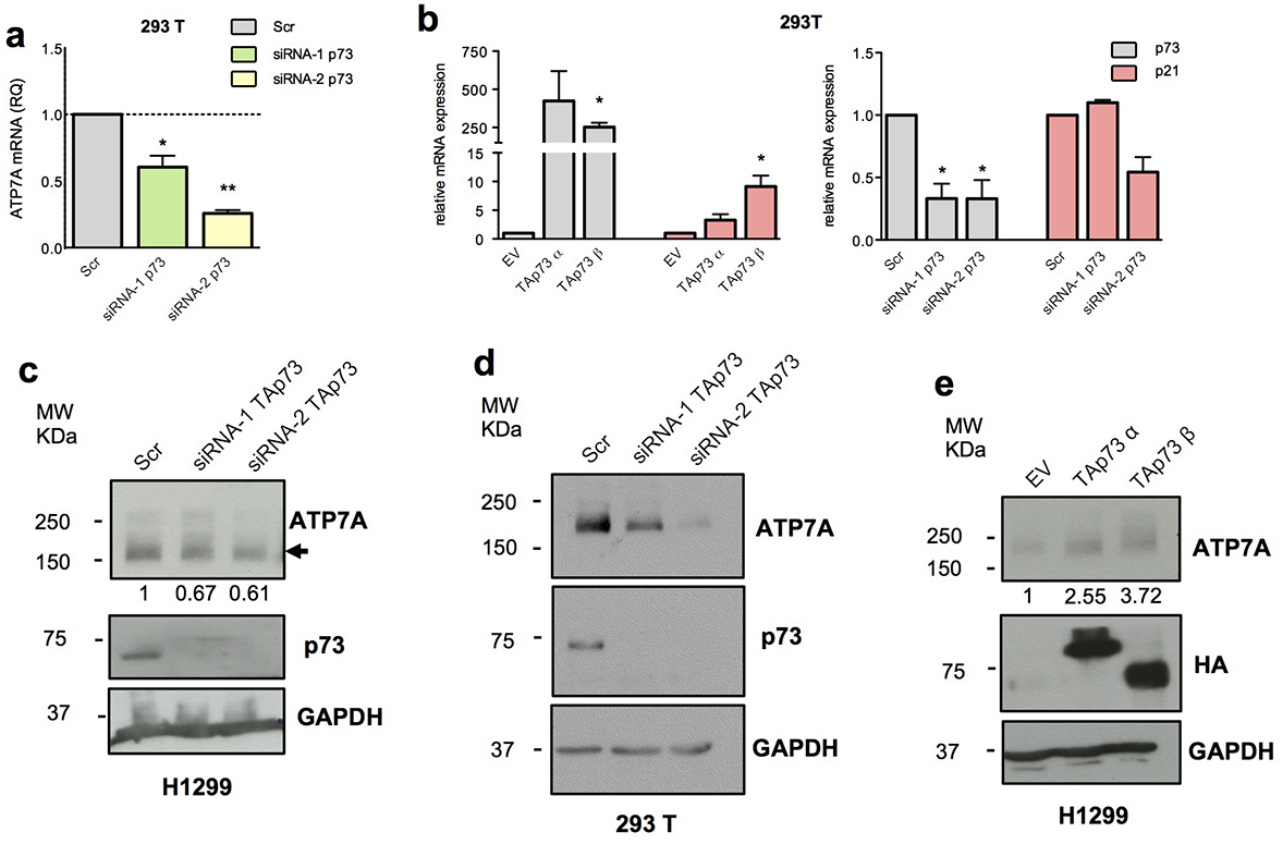

Figure 2. TAp73 regulates ATP7A expression level. (**a**) ATP7A mRNA levels were analysed by quantitative PCR after TAp73 silencing (siRNA-1/2 p73). Relative mRNA expression was normalized against TBP and calculated as fold change to the control treatment (Scr). Data is reported as mean ± s.d. of three experiments. ** $p < 0.001$, * $p < 0.05$ (Student's T-test). (**b**) p73 and p21 mRNA levels were analysed by quantitative PCR after TAp73 overexpression (HA-TAp73 α-β) and p73 silencing (siRNA-1/2 p73). Up- and downregulation of p21, a TAp73 transcriptional target, confirmed p73 transcriptional activity modulation. Relative expression of genes was normalized against TBP and calculated as fold change to the control treatments (EV and Scr). Data is reported as mean ± s.d. of two experiments. * $p < 0.05$ (Student's T-test). (**c-e**) Protein levels of ATP7A, HA-TAp73 or endogenous TAp73 and GAPDH were analysed by WB in cell overexpressing or depleted for TAp73. Figure shows a representative replicate of three independent experiments.

yellow in Figure 3a), MatInspector Professional Software *in silico* analysis identified 2 regions containing responsive elements (REs) for p53-family proteins. One of these two (labelled in red in Figure 3a) included a 25 nucleotides sequence (ChrX: 77,961,553-77,962,65 – intron 1/21) with a 0.947 value of matrix similarity. Due to lower matrix similarity, we decided not to consider the other one, containing potentially 6 REs, four of them specific for p63 protein.

Immunoprecipitated chromatin with anti-HA antibody from HA-TAp73 overexpressing H1299 and 293 T cells showed specific binding of TAp73 on the REs identified in the promoter region (Eukaryotic Promoter Database) and in the intron 1 (MatInspector Professional Software) (Figure 3b). MDM2 was tested as positive control of TAp73 binding, whereas SAT2 represented a negative control.

Overall our data demonstrate a relationship between TAp73 and ATP7A. TAp73 directly binds *ATP7A* promoter region and the RE localized in intron 1, suggesting a potential direct transcriptional control, and depletion of TAp73 impact on the basal expression level of ATP7A. However, TAp73 overexpression appears not sufficient to strongly promote *ATP7A* expression level.

p73/ATP7A axis in human cancer

In order to better understand the clinical relevance of p73-dependent regulation of ATP7A in human cancer,

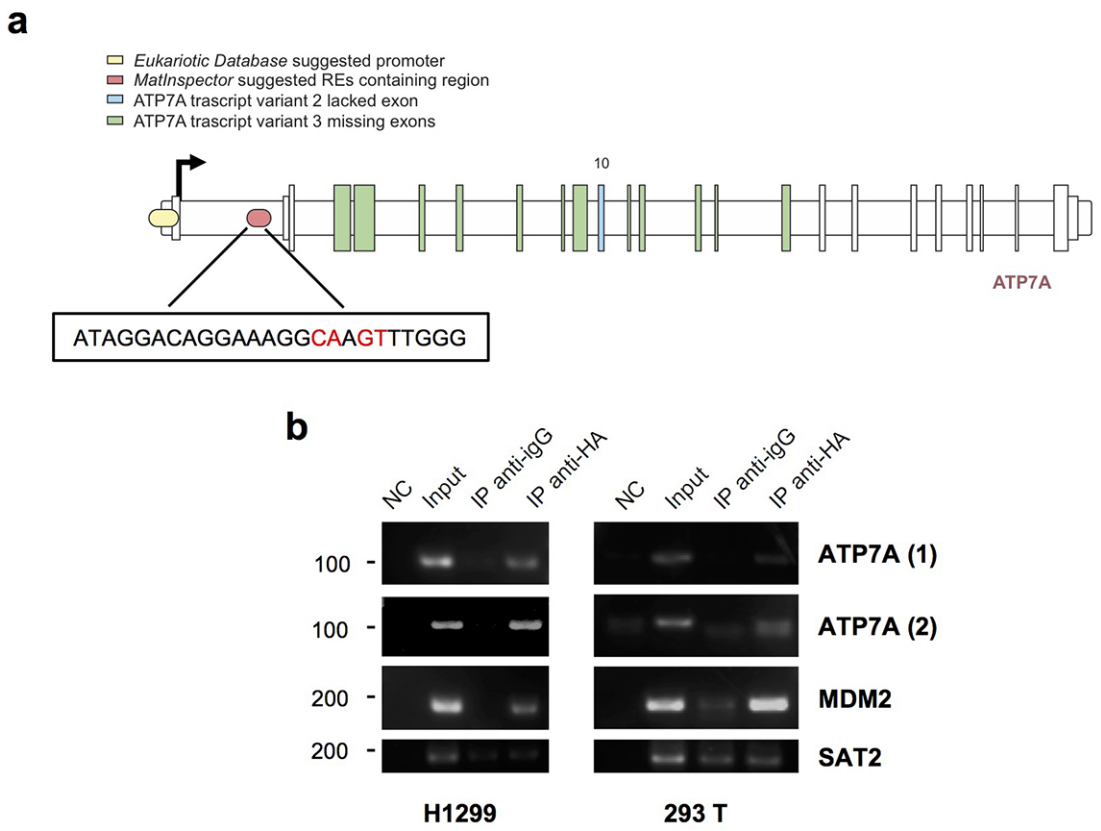

Figure 3. TAp73 physically binds *ATP7A* genomic areas. (**a**) Schematic map of the human ATP7A gene. MatInspector professional software suggested promoter region containing p53 family members-response elements is indicated in red; the insert shows the sequence of the p53 family member-RE chosen, the nearest to the TSS (ChrX: 77,961,553-77,962,65). In yellow ATP7A promoter region found on *Eukaryotic Promoter Database* by selecting a region from -1000 to 100 bp relative to TSS CAGEseq derived (ChrX: 77,909,608- 77,910,867) [Human Dec. 2013 (GRCh38/hg38)]. (**b**) A tagged TAp73 was overexpressed in H1299 and 293T cell lines for 24h. The sonicated chromatin was incubated with anti-HA or IgG antibodies. Immunoprecipitated DNA was amplified by PCR with ATP7A primers, one (ATP7A1) amplifying Eukaryotic Database suggested promoter, the other (ATP7A2) recognizing the p53-response element found on MatInspector. ChIP on MDM2 promoter was performed as a positive control, and ChIP on SAT2 promoter as a negative control. NC: PCR negative control. Figure shows a representative replicate of two independent experiments.

we evaluated by computational webtools the impact of the correlation between p73 and ATP7A in different publicly available datasets of expression profiling of oncologic patients.

Using human lung cancer datasets we assessed the impact of the expressions of the individual genes and the combination of both on the patient survival. Unexpectedly ATP7A high expression positively impacted on patient's survival (*P* value 1.4e-10) (Figure 4a), whereas high p73 expression had a marginal but negative impact (*P* value 0.0023) (Figure 4b). However interestingly the combination of high expression of both genes together highly significantly influenced the overall survival of lung cancer patients (*P* value 3.6e-13) (Figure 4c).

An important major difference was observed when the lung cancer datasets were selected for the different histological subtype. ATP7A expression was importantly discriminating good and bad prognosis in lung adenocarcinoma patients (*P* value 9.2e-15), but no effect was observed in the subset of samples belonging to the squamous cell carcinoma histological subtype (Figure 4d, e).

Despite a potential unexpected result, this analysis indicated a possible implication of p73/ATP7A axis in human lung cancer. According to previously observed role of ATP7A in chemoresistance, a high expression level would have been expected to define a poor prognosis cohort, however unexpectedly our result indicates that high level of ATP7A positively influences

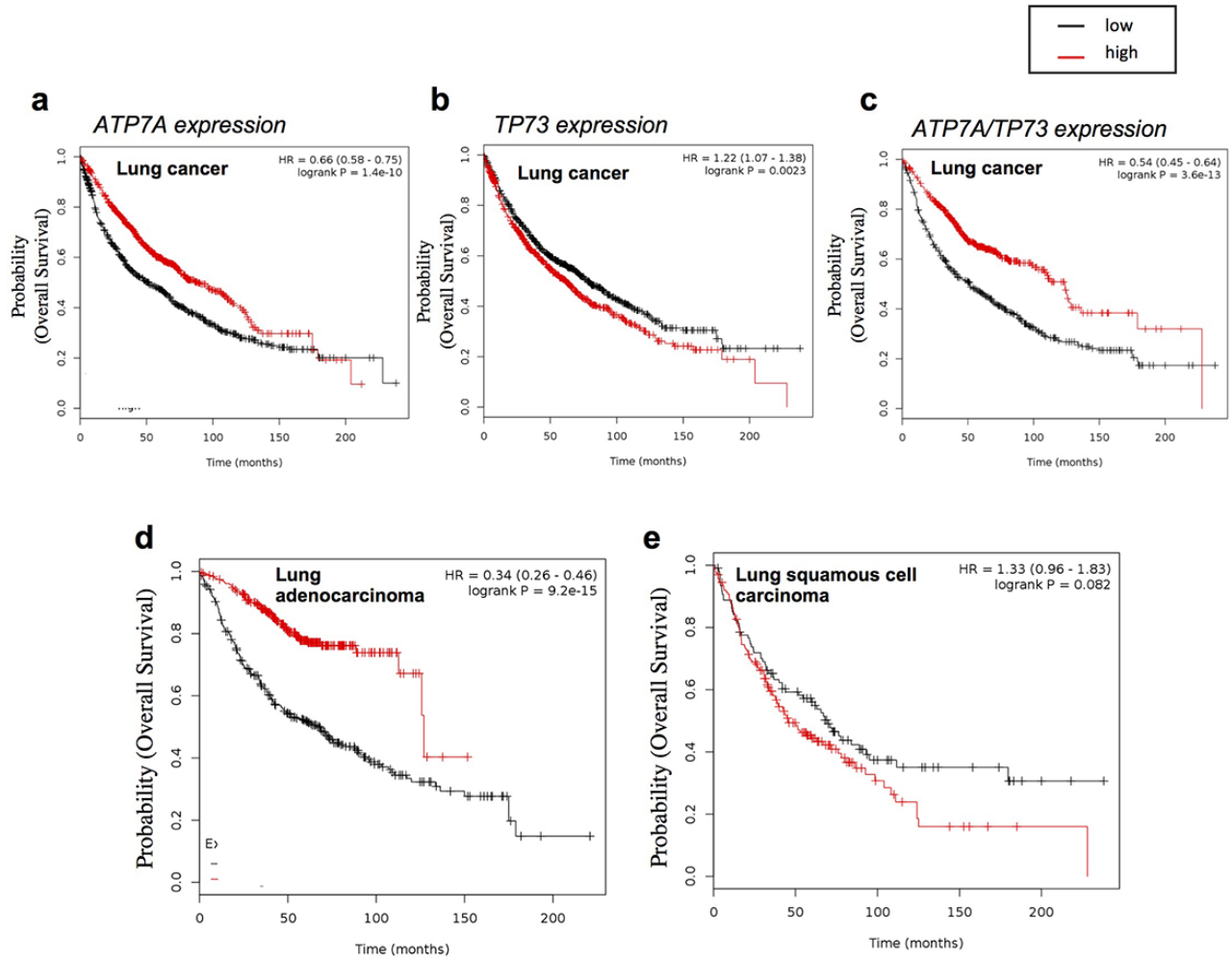

Figure 4. ATP7A expression affect lung cancer patient's outcome. Overall survival analysis of lung cancer datasets (see Material and Methods for full list) relative to (**a**) Tp73 expression (232546_at probe, mean expression) (n=1926), (**b**) ATP7A expression (205198_s_at probe, mean expression) (n=1145), (**c**) Tp73 and ATP7A probes mean expression (n=1145). HGU133A probe set. Patients splitted by median. P values showed on the top. Overall survival analysis of lung cancer datasets relative to ATP7A expression (205198_s_at probe, mean expression) obtained filtering the results with (**d**) "Adenocarcinoma" (n=673) and (**e**) "squamous cell carcinoma" histology type (n=271). HGU133A probe set. Patients split by median. P values showed on the top.

patient's prognosis. In addition, high expression of both ATP7A and p73 is defining a subgroup with a significant better prognosis compared to the individual contribution of ATP7A and p73. This result indicates that the activation of p73/ATP7a axis could play a tumour suppressor role in a subgroup of lung cancer patients.

DISCUSSION

20 years after the discovery of the p53 homologue, p73, we still lack a clear definition of its transcriptional signature and the extent of overlap with the ones controlled by the other p53 family members [80-82]. Here we reanalyse previously published transcriptional analysis of TAp73 depleted cells, trying to investigate potential novel transcriptional targets responsible for TAp73 function.

We describe a novel TAp73 target, ATP7A, that in our cellular models appears to require TAp73 expression in order to maintain its basal expression level. However, following TAp73 overexpression despite we observe TAp73 accumulation on ATP7A genomic region, no strong effects are observed on ATP7a transcript and protein level. This result might have multiple explanations. For a certain extent this highlights the complexity of specific transcriptional networks. TAp73-dependent ATP7A regulation could indeed not simply rely on the direct TAp73 binding on the ATP7A

genomic sites, but require the interplay with additional transcriptional factors. Previous studies in zebrafish models have showed that *SOD1* transcription is affected by ATP7A in a copper responsive manner through the transcription factor Sp1 [83-85]. Moreover, Sp1 itself binds *ATP7A* promoter in human intestinal epithelial cells being fundamental for the HIF2α-mediated induction of gene transcription during iron deficiency/hypoxia to regulate iron balance [86]. Interplay between TAp73 and HIF family proteins [65], Sp1 transcription factor [87, 88] or a hierarchical genetic regulation mediated by copper could be therefore involved in this regulatory mechanism. Downstream pathways altered by TAp73 need to be elucidated in the specific context of ATP7A regulation to fully clarify all the participants of this signalling. An alternative explanation of our results could be that TAp73 has the capacity of controlling alternative transcriptional signatures in a dosage-dependent manner. High expression level of TAp73 could be responsible for upregulation of pro-apoptotic/cell cycle arrest genes in contexts such as genotoxic stress. Basal expression level of TAp73 instead might be responsible for the control of homeostatic and/or metabolic regulators. These two transcriptional programmes might be completely distinguished and might be determined by the expression level of TAp73. This would represent a potential similarity with p53 functions in DNA damage response and basal conditions [89-93].

The biological significance of our findings is strictly associated to the lack of clarity regarding the implications of p73 for human diseases. KO mouse models for p73 show a range of defects that include tumour suppression, infertility, neurological defects and altered immune system [47, 94]. The complexity of p73 functions is therefore obviously highlighted by the phenotype of the genetic mouse models. The control of genomic stability is central to all family members, and TAp73 deficiency is associated with genomic instability that emerged to be important not only in tumorigenesis but also in maturation of oocytes. In addition to this, more recently a defective ciliogenesis of multiciliated epithelia, such as the upper airway tract, further expanded the range of defects observed in p73 mouse models. However, despite that, a clear connection of p73 with human disease never emerged. p73 deficiency in mice is also associated to premature ageing.

The altered mitochondrial metabolism is a root cause for premature ageing and mitochondrial dysfunction in TAp73 KO mice plays a key role in this context [95-101]. Oxidative damage promotes cellular senescence *in vitro* and ageing *in vivo*. TAp73-null MEFs and silenced cells are sensitive to oxidative damaging agents such as hydrogen peroxide (H2O2). On the other hand, TAp73-null MEFs grow well in low-oxygen conditions or with the addition of antioxidants, conditions that dampen oxidative damage [54, 102, 103]. These indicates that an important part of p73 functions depends on its control of cellular metabolism.

ATP7A is a member of a large family of P-type ATPases, which are energy-utilizing membrane proteins that pumps ions and lipids across cellular membranes [104]. ATP7A has a dual homeostatic and biosynthetic functions: exporting copper in excess outside the cell, and transporting copper to cuproenzymes at the secretory pathway [105]. Depending on the copper intracellular concentration and the cellular states, ATP7A can be shuttled from the endoplasmic reticulum to the plasma membrane, facilitating copper extrusion from the cell. Mutations in ATP7A leads to Menkes Disease, a lethal paediatric multisystemic disorder associated to progressive neurodegeneration [106].

The TAp73/ATP7A axis might play a role in different biological contexts, with a potential high interest in ageing-associated diseases, such as cancer and neurodegeneration. Our computational analysis of expression profiling datasets of human cancer highlighted a potential correlation of TAp73/ATP7A with cancer pathogenesis; further studies will determine if this is a simple correlative connection, or an actual causative relationship. Despite a role in human cancer of ATP7A has been identified in drug-resistance (drug extrusion from cancer cells), our data indicate that high level of ATP7A is a positive prognostic factor, which becomes even stronger when concurrent with high TAp73 expression. The data are therefore suggestive of a potential implication of TAp73/ATP7A axis in tumour suppression.

Implication of TAp73 in mouse neurodevelopment and deregulation of TAp73 expression in human neurodegenerative conditions might be suggestive of role of TAp73/ATP7A axis also in neuro-biology. Possibly the altered TAp73-dependent regulation of ATP7A during ageing could produce neuro-toxic effects responsible for progressive neurodegeneration similar to the severe manifestations observed in Menkes Disease. However, in absence of any experimental evidence these speculations might only indicate potential future research directions aimed to better define p73 implications in human diseases.

MATERIALS AND METHODS

Cell Culture

The human non-small cell lung carcinoma cell line NCI-H1299 were cultivated in RPMI medium 1640

(Gibco, Life Technologies, Carlsbad, CA, USA) containing 4.5 g/L D-Glucose, 2.383 g/L HEPES Buffer, L-Glutamine, 1.5 g/L Sodium Bicarbonate, and 110 mg/L Sodium Pyruvate, supplemented with 50 units/mL Penicillin, 50 mg/mL Streptomycin (Gibco), and 10% (vol/vol) FBS (Labtech, Heathfield, UK). The human embryonic kidney cell line HEK-293 were cultivated in Dulbecco's Modified Eagle Medium (Gibco) containing 4.5 g/L D-Glucose, L-Glutamine, and Pyruvate, supplemented with 50 units/ mL Penicillin, 50 mg/mL Streptomycin (Gibco), and 10 % (v/v) FBS (Labtech). All cell cultures were maintained 37 °C with 5% CO2 in a humidified incubator.

Cell transfection

For overexpression, H1299 cells were seeded 24 h before transfection. Transfection was performed with 10 µg DNA (pcDNA empty, pcDNA HA-TAp73α, pcDNA HA-TAp73β) per 10 cm dish with 1.2×10^6 cells seeded using Lipofectamine 2000 Reagent (Invitrogen). Cells were collected 24 h after transfection. For 293T cells transfection was performed with 3 µg DNA per 10 cm dish with 2.5×10^6 cells seeded using Effectene reagent (Qiagen, Manchester, UK) and cells collected 24 h after transfection. For p73 knockdown in H1299 and 293 T 1.2×10^6 and 2.5×10^6 cells, respectively, were seeded per 10 cm dish 24 h before transfection. Transfection was performed using 50 nM siRNA [control siRNA, siRNA-2 p73-1 and siRNA-2 p73-2 (Ambion)] and Lipofectamine RNAiMAX (Invitrogen). Cells were collected 48 h after transfection.

RNA extraction and analysis

Total RNA was isolated from cells using the RNEasy Mini Kit (Qiagen), according to the Qiagen company protocol. 2 µg of total RNA was used to prepare cDNA using RevertAid H minus First strand cDNA Synthesis kit (ThermoScientific), using Random primers and the protocol from the kit. qPCR was performed using 1/10 of the prepared cDNA and Power SYBR Green PCR Master Mix (Applied Biosystems). Relative gene expression was analyzed in accordance with 7500 Software version 2.0.6 of Applied Biosystems. Gene expression levels were quantified according to the comparative ΔΔCt method and normalized to expression of the TBP housekeeping gene. Sequences of the primers used for the qPCR are:

TAp73 Fw CAGACAGCACCTACTTCGACCTT, Rev CCGCCCACCACCTCATTA;
p21 Fw CCTGTCACTGTCTTGTACCCT, Rev GCGTTTGGAGTGGTAGAAATCT;
TBP Fw TCAAACCCAGAATTGTTCTCCTTAT, Rev CCTGAATCCCTTTAGAATAGGGTAGA;
SPP1 Fw GAGGGCTTGGTTGTCAGC, Rev CAATTCTCATGGTAGTGAGTTTTCC;
CABLES1(transcript variant 2) Fw TCGCGACAGTACCCAAGTC, Rev TCAAACTCACTGCACCAGTTG;
TET2 Fw AAAGATGAAGGTCCTTTTTATACCC, Rev ATAGCTTTACCCTTCTGTCCAAAC;
JPH1 Fw GACATCGCGAGAGCTGTG, Rev TTCCTGAAATCTCTGTTTGACG;
ATP7A (transcript variant 1) Fw TCTTCCAGGATTGTCTGTTATGAA, Rev ACCAGCTCCGAAAAACTG;
ATP7A (transcript variant 2) Fw TCTTCCAGGATTGTCTGTTATGAA, Rev CCTCTGATGTTTTGCCCTGTA;
ATP7A (transcript variant 3) Fw TGTGCATCACATTAAGGTAAAGGTA, Rev AGTTCCCACAATGGCCAAGA.

Western blotting

For protein extraction, cells were lysed in RIPA buffer with protease inhibitor cocktail tablets Complete, EDTA-free (Roche) and phosphatase inhibitor cocktail tablets PhosSTOP (Roche). Lysates were measured for protein concentration by using the Bio-Rad Protein Assay (Bio-Rad), then mixed with Laemmli loading buffer, electrophoresed on SDS-PAGE gels and separated proteins transferred to PVDF blotting membranes (Amersham, GE Healthcare). Membranes were blocked for 1 h in 10% (m/vol) dry milk dissolved in TBS with 1% (vol/vol) Tween-20 (TBSt); incubated with primary antibodies overnight and with secondary antibodies conjugated with horseradish peroxidase, for 1 h. Antibodies were diluted in 10% dry milk in TBSt: anti-HA 1:1000 (Covance), anti-GAPDH 1:40000 (Sigma), anti-p21, anti-p73 1:3000 (Bethyl), anti-ATP7A 1:500 (Santa Cruz). To detect the signal ECL Western Blotting Detection Reagent (Amersham, GE Healthcare) or SuperSignal West Dura Chemiluminescent Substrate (Thermo Scientific) was used.

Promoter region analysis

Analysis of promoter region was performed using MatInspector Professional software by Genomatix (https://www.genomatix.de) and the Eukariotic Promoter Database (https://epd.vital-it.ch/index.php).

Chromatin Immunoprecipitation assay

TAp73α was overexpressed for 24 h in H1299 and 293T cell lines (see cell transfection section for details). Cells were collected fixed in 37% formaldehyde and

subjected to sonication for DNA shearing. Chromatin was sonicated (around 500 bp) and immunoprecipitated with/without 10 µL anti-HA antibodies (Covance) or 10 µL nonspecific immunoglobulin G (IgG) antibodies (Invitrogen) using the MAGnify ChIP System kit (Invitrogen). The co-immunoprecipitated DNA fragments were amplified by PCR. MDM2 was used as positive control. SAT2 was used as negative control.

ATP7A (1) Fw GGTTTCGCTTTTGTCGTGGG, Rev TGAAAAGGAACGCGTGGTCT;
ATP7A (2) Fw ATACCCTTGTACTGCTTCCCAC, Rev TAGGATGAGTTCAGGTGGCG;
MDM2 Fw GGTTGACTCAGCTTTTCCTCTTG, Rev GGAAAATGCATGGTTTAAATAGCC;
SAT2 Fw CTGCAATCATCCAATGGTCG, Rev GATTCCATTCGGGTCCATTC.

Bioinformatic analyses

First bioinformatic analysis, to test gene synergy in cancer, was performed using *Syntarget* by ChemoProfiling (http://www.chemoprofiling.org). All available datasets had been checked. Survival analysis on lung cancer patients was performed by Kaplan-Meier Plotter (http://kmplot.com/analysis/). Datasets considered were: CAARRAY, GSE14814, GSE19188, GSE29013, GSE30219, GSE31210, GSE3141, GSE31908, GSE37745, GSE43580, GSE4573, GSE50081, GSE8894, TGCA.

Statistics

Technical as well as biological triplicates of each experiment were performed. Error bars indicate ±S.D. in each figure. Statistical significance was determined using the unpaired two-tailed Student's *t*-test using GraphPad Software. A p-value ≤0.05 was considered statistically significant.

CONFLICTS OF INTEREST

The authors declare no conflict of interest.

FUNDING

This work was supported by the Medical Research Council (MRC intramural funding).

REFERENCES

1. Melino G, De Laurenzi V, Vousden KH. p73: Friend or foe in tumorigenesis. Nat Rev Cancer. 2002; 2:605–15. https://doi.org/10.1038/nrc861

2. Billant O, Léon A, Le Guellec S, Friocourt G, Blondel M, Voisset C. The dominant-negative interplay between p53, p63 and p73: A family affair. Oncotarget. 2016; 7:69549–64. https://doi.org/10.18632/oncotarget.11774

3. Celardo I, Grespi F, Antonov A, Bernassola F, Garabadgiu AV, Melino G, Amelio I. Caspase-1 is a novel target of p63 in tumor suppression. Cell Death Dis. 2013; 4:e645. https://doi.org/10.1038/cddis.2013.175

4. Gebel J, Luh LM, Coutandin D, Osterburg C, Löhr F, Schäfer B, Frombach AS, Sumyk M, Buchner L, Krojer T, Salah E, Mathea S, Güntert P, et al. Mechanism of TAp73 inhibition by ΔNp63 and structural basis of p63/p73 hetero-tetramerization. Cell Death Differ. 2016; 23:1930–40. https://doi.org/10.1038/cdd.2016.83

5. Robbins D, Bakke J, Cherian MT, Wu J, Chen T. PXR interaction with p53: a meeting of two masters. Cell Death Dis. 2016; 7:e2218. https://doi.org/10.1038/cddis.2016.122

6. Tomasini R, Mak TW, Melino G. The impact of p53 and p73 on aneuploidy and cancer. Trends Cell Biol. 2008; 18:244–52. https://doi.org/10.1016/j.tcb.2008.03.003

7. Velletri T, Xie N, Wang Y, Huang Y, Yang Q, Chen X, Chen Q, Shou P, Gan Y, Cao G, Melino G, Shi Y. P53 functional abnormality in mesenchymal stem cells promotes osteosarcoma development. Cell Death Dis. 2016; 7:e2015. https://doi.org/10.1038/cddis.2015.367

8. Amelio I, Grespi F, Annicchiarico-Petruzzelli M, Melino G. p63 the guardian of human reproduction. Cell Cycle. 2012; 11:4545–51. https://doi.org/10.4161/cc.22819

9. Inoue S, Tomasini R, Rufini A, Elia AJ, Agostini M, Amelio I, Cescon D, Dinsdale D, Zhou L, Harris IS, Lac S, Silvester J, Li WY, et al. TAp73 is required for spermatogenesis and the maintenance of male fertility. Proc Natl Acad Sci USA. 2014; 111:1843–48. https://doi.org/10.1073/pnas.1323416111

10. Alexandrova EM, Moll UM. Depleting stabilized GOF mutant p53 proteins by inhibiting molecular folding chaperones: a new promise in cancer therapy. Cell Death Differ. 2017; 24:3–5. https://doi.org/10.1038/cdd.2016.145

11. Candi E, Amelio I, Agostini M, Melino G. MicroRNAs and p63 in epithelial stemness. Cell Death Differ. 2015; 22:12–21. https://doi.org/10.1038/cdd.2014.113

12. Yang A, Walker N, Bronson R, Kaghad M, Oosterwegel M, Bonnin J, Vagner C, Bonnet H, Dikkes P, Sharpe A, McKeon F, Caput D. p73-deficient mice have neurological, pheromonal and inflammatory defects but lack spontaneous tumours. Nature. 2000; 404:99–103. https://doi.org/10.1038/35003607

13. Vikhreva P, Petrova V, Gokbulut T, Pestlikis I, Mancini M, Di Daniele N, Knight RA, Melino G, Amelio I. TAp73 upregulates IL-1β in cancer cells: potential biomarker in lung and breast cancer? Biochem Biophys Res Commun. 2017; 482:498–505. https://doi.org/10.1016/j.bbrc.2016.10.085

14. Marini A, Rotblat B, Sbarrato T, Niklison-Chirou MV, Knight JR, Dudek K, Jones C, Bushell M, Knight RA, Amelio I, Willis AE, Melino G. TAp73 contributes to the oxidative stress response by regulating protein synthesis. Proc Natl Acad Sci USA. 2018; 115:6219–24. https://doi.org/10.1073/pnas.1718531115

15. Charni M, Aloni-Grinstein R, Molchadsky A, Rotter V. p53 on the crossroad between regeneration and cancer. Cell Death Differ. 2017; 24:8–14. https://doi.org/10.1038/cdd.2016.117

16. Lowe JM, Nguyen TA, Grimm SA, Gabor KA, Peddada SD, Li L, Anderson CW, Resnick MA, Menendez D, Fessler MB. The novel p53 target TNFAIP8 variant 2 is increased in cancer and offsets p53-dependent tumor suppression. Cell Death Differ. 2017; 24:181–91. https://doi.org/10.1038/cdd.2016.130

17. Guirguis AA, Slape CI, Failla LM, Saw J, Tremblay CS, Powell DR, Rossello F, Wei A, Strasser A, Curtis DJ. PUMA promotes apoptosis of hematopoietic progenitors driving leukemic progression in a mouse model of myelodysplasia. Cell Death Differ. 2016; 23:1049–59. https://doi.org/10.1038/cdd.2015.159

18. Saint-Germain E, Mignacca L, Vernier M, Bobbala D, Ilangumaran S, Ferbeyre G. SOCS1 regulates senescence and ferroptosis by modulating the expression of p53 target genes. Aging (Albany NY). 2017; 9:2137–62. https://doi.org/10.18632/aging.101306

19. Renner G, Janouskova H, Noulet F, Koenig V, Guerin E, Bär S, Nuesch J, Rechenmacher F, Neubauer S, Kessler H, Blandin AF, Choulier L, Etienne-Selloum N, et al. Integrin α5β1 and p53 convergent pathways in the control of anti-apoptotic proteins PEA-15 and survivin in high-grade glioma. Cell Death Differ. 2016; 23:640–53. https://doi.org/10.1038/cdd.2015.131

20. Velletri T, Romeo F, Tucci P, Peschiaroli A, Annicchiarico-Petruzzelli M, Niklison-Chirou MV, Amelio I, Knight RA, Mak TW, Melino G, Agostini M. GLS2 is transcriptionally regulated by p73 and contributes to neuronal differentiation. Cell Cycle. 2013; 12:3564–73. https://doi.org/10.4161/cc.26771

21. Killick R, Niklison-Chirou M, Tomasini R, Bano D, Rufini A, Grespi F, Velletri T, Tucci P, Sayan BS, Conforti F, Gallagher E, Nicotera P, Mak TW, et al. p73: a multifunctional protein in neurobiology. Mol Neurobiol. 2011; 43:139–46. https://doi.org/10.1007/s12035-011-8172-6

22. Niklison-Chirou MV, Killick R, Knight RA, Nicotera P, Melino G, Agostini M. How does p73 cause neuronal defects? Mol Neurobiol. 2016; 53:4509–20. https://doi.org/10.1007/s12035-015-9381-1

23. Lena AM, Cipollone R, Amelio I, Catani MV, Ramadan S, Browne G, Melino G, Candi E. Skn-1a/Oct-11 and ΔNp63α exert antagonizing effects on human keratin expression. Biochem Biophys Res Commun. 2010; 401:568–73. https://doi.org/10.1016/j.bbrc.2010.09.102

24. Vanbokhoven H, Melino G, Candi E, Declercq W. p63, a story of mice and men. J Invest Dermatol. 2011; 131:1196–207. https://doi.org/10.1038/jid.2011.84

25. Blanpain C, Fuchs E. p63: revving up epithelial stem-cell potential. Nat Cell Biol. 2007; 9:731–33. https://doi.org/10.1038/ncb0707-731

26. Novelli F, Lena AM, Panatta E, Nasser W, Shalom-Feuerstein R, Candi E, Melino G. Allele-specific silencing of EEC p63 mutant R304W restores p63 transcriptional activity. Cell Death Dis. 2016; 7:e2227. https://doi.org/10.1038/cddis.2016.118

27. Xu-Monette ZY, Zhang S, Li X, Manyam GC, Wang XX, Xia Y, Visco C, Tzankov A, Zhang L, Montes-Moreno S, Dybkaer K, Chiu A, Orazi A, et al. p63 expression confers significantly better survival outcomes in high-risk diffuse large B-cell lymphoma and demonstrates p53-like and p53-independent tumor suppressor function. Aging (Albany NY). 2016; 8:345–65. https://doi.org/10.18632/aging.100898

28. Kehrloesser S, Osterburg C, Tuppi M, Schäfer B, Vousden KH, Dötsch V. Intrinsic aggregation propensity of the p63 and p73 TI domains correlates with p53R175H interaction and suggests further significance of aggregation events in the p53 family. Cell Death Differ. 2016; 23:1952–60. https://doi.org/10.1038/cdd.2016.75

29. Levine AJ, Tomasini R, McKeon FD, Mak TW, Melino G. The p53 family: guardians of maternal reproduction. Nat Rev Mol Cell Biol. 2011; 12:259–65. https://doi.org/10.1038/nrm3086

30. Ortiz GJ, Lozano G. SNPing away at mutant p53 activities. Genes Dev. 2018; 32:195–96.

https://doi.org/10.1101/gad.312934.118

31. Tashakori M, Zhang Y, Xiong S, You MJ, Lozano G. p53 activity dominates that of p73 upon Mdm4 loss in development and tumorigenesis. Mol Cancer Res. 2016; 14:56–65. https://doi.org/10.1158/1541-7786.MCR-15-0346

32. Vargas L, Alvarez A. P73 and P63: the siblings that work together in neurodevelopment. Cell Cycle. 2015; 14:3671–72. https://doi.org/10.1080/15384101.2015.1112615

33. Aggarwal M, Saxena R, Sinclair E, Fu Y, Jacobs A, Dyba M, Wang X, Cruz I, Berry D, Kallakury B, Mueller SC, Agostino SD, Blandino G, et al. Reactivation of mutant p53 by a dietary-related compound phenethyl isothiocyanate inhibits tumor growth. Cell Death Differ. 2016; 23:1615–27. https://doi.org/10.1038/cdd.2016.48

34. Alam SK, Yadav VK, Bajaj S, Datta A, Dutta SK, Bhattacharyya M, Bhattacharya S, Debnath S, Roy S, Boardman LA, Smyrk TC, Molina JR, Chakrabarti S, et al. DNA damage-induced ephrin-B2 reverse signaling promotes chemoresistance and drives EMT in colorectal carcinoma harboring mutant p53. Cell Death Differ. 2016; 23:707–22. https://doi.org/10.1038/cdd.2015.133

35. Morrison CD, Chang JC, Keri RA, Schiemann WP. Mutant p53 dictates the oncogenic activity of c-Abl in triple-negative breast cancers. Cell Death Dis. 2017; 8:e2899. https://doi.org/10.1038/cddis.2017.294

36. Oren M, Tal P, Rotter V. Targeting mutant p53 for cancer therapy. Aging (Albany NY). 2016; 8:1159–60. https://doi.org/10.18632/aging.100992

37. Wang ET, Sandberg R, Luo S, Khrebtukova I, Zhang L, Mayr C, Kingsmore SF, Schroth GP, Burge CB. Alternative isoform regulation in human tissue transcriptomes. Nature. 2008; 456:470–76. https://doi.org/10.1038/nature07509

38. Pan Q, Shai O, Lee LJ, Frey BJ, Blencowe BJ. Deep surveying of alternative splicing complexity in the human transcriptome by high-throughput sequencing. Nat Genet. 2008; 40:1413–15. https://doi.org/10.1038/ng.259

39. Solomon H, Sharon M, Rotter V. Modulation of alternative splicing contributes to cancer development: focusing on p53 isoforms, p53β and p53γ. Cell Death Differ. 2014; 21:1347–49. https://doi.org/10.1038/cdd.2014.99

40. Grespi F, Amelio I, Tucci P, Annicchiarico-Petruzzelli M, Melino G. Tissue-specific expression of p73 C-terminal isoforms in mice. Cell Cycle. 2012; 11:4474–83. https://doi.org/10.4161/cc.22787

41. Vikhreva P, Melino G, Amelio I. p73 alternative splicing: exploring a biological role for the C-terminal isoforms. J Mol Biol. 2018; 430:1829–38. https://doi.org/10.1016/j.jmb.2018.04.034

42. Agostini M, Romeo F, Inoue S, Niklison-Chirou MV, Elia AJ, Dinsdale D, Morone N, Knight RA, Mak TW, Melino G. Metabolic reprogramming during neuronal differentiation. Cell Death Differ. 2016; 23:1502–14. https://doi.org/10.1038/cdd.2016.36

43. A gostini M, Tucci P, Killick R, Candi E, Sayan BS, Rivetti di Val Cervo P, Nicotera P, McKeon F, Knight RA, Mak TW, Melino G. Neuronal differentiation by TAp73 is mediated by microRNA-34a regulation of synaptic protein targets. Proc Natl Acad Sci USA. 2011; 108:21093–98. https://doi.org/10.1073/pnas.1112061109

44. Basu S, Murphy ME. p53 family members regulate cancer stem cells. Cell Cycle. 2016; 15:1403–04. https://doi.org/10.1080/15384101.2016.1171649

45. Turnquist C, Horikawa I, Foran E, Major EO, Vojtesek B, Lane DP, Lu X, Harris BT, Harris CC. p53 isoforms regulate astrocyte-mediated neuroprotection and neurodegeneration. Cell Death Differ. 2016; 23:1515–28. https://doi.org/10.1038/cdd.2016.37

46. Xie N, Vikhreva P, Annicchiarico-Petruzzelli M, Amelio I, Barlev N, Knight RA, Melino G. Integrin-β4 is a novel transcriptional target of TAp73. Cell Cycle. 2018; 17:589–94. https://doi.org/10.1080/15384101.2017.1403684

47. Nemajerova A, Amelio I, Gebel J, Dötsch V, Melino G, Moll UM. Non-oncogenic roles of TAp73: from multiciliogenesis to metabolism. Cell Death Differ. 2018; 25:144–53. https://doi.org/10.1038/cdd.2017.178

48. Carpentieri A, Cozzoli E, Scimeca M, Bonanno E, Sardanelli AM, Gambacurta A. Differentiation of human neuroblastoma cells toward the osteogenic lineage by mTOR inhibitor. Cell Death Dis. 2016; 7:e2202. https://doi.org/10.1038/cddis.2016.60

49. Agostini M, Annicchiarico-Petruzzelli M, Melino G, Rufini A. Metabolic pathways regulated by TAp73 in response to oxidative stress. Oncotarget. 2016; 7:29881–900. https://doi.org/10.18632/oncotarget.8935

50. Amelio I, Antonov AA, Catani MV, Massoud R, Bernassola F, Knight RA, Melino G, Rufini A. TAp73 promotes anabolism. Oncotarget. 2014; 5:12820–934. https://doi.org/10.18632/oncotarget.2667

51. Amelio I, Cutruzzolá F, Antonov A, Agostini M, Melino G. Serine and glycine metabolism in cancer. Trends Biochem Sci. 2014; 39:191–98. https://doi.org/10.1016/j.tibs.2014.02.004

52. Amelio I, Markert EK, Rufini A, Antonov AV, Sayan BS, Tucci P, Agostini M, Mineo TC, Levine AJ, Melino G. p73 regulates serine biosynthesis in cancer. Oncogene. 2014; 33:5039–46. https://doi.org/10.1038/onc.2013.456

53. Du W, Jiang P, Mancuso A, Stonestrom A, Brewer MD, Minn AJ, Mak TW, Wu M, Yang X. TAp73 enhances the pentose phosphate pathway and supports cell proliferation. Nat Cell Biol. 2013; 15:991–1000. https://doi.org/10.1038/ncb2789

54. Rufini A, Niklison-Chirou MV, Inoue S, Tomasini R, Harris IS, Marino A, Federici M, Dinsdale D, Knight RA, Melino G, Mak TW. TAp73 depletion accelerates aging through metabolic dysregulation. Genes Dev. 2012; 26:2009–14. https://doi.org/10.1101/gad.197640.112

55. Sharif T, Ahn DG, Liu RZ, Pringle E, Martell E, Dai C, Nunokawa A, Kwak M, Clements D, Murphy JP, Dean C, Marcato P, McCormick C, et al. The NAD(+) salvage pathway modulates cancer cell viability via p73. Cell Death Differ. 2016; 23:669–80. https://doi.org/10.1038/cdd.2015.134

56. Teoh PJ, Bi C, Sintosebastian C, Tay LS, Fonseca R, Chng WJ. PRIMA-1 targets the vulnerability of multiple myeloma of deregulated protein homeostasis through the perturbation of ER stress via p73 demethylation. Oncotarget. 2016; 7:61806–19. https://doi.org/10.18632/oncotarget.11241

57. Velletri T, Romeo F, Tucci P, Peschiaroli A, Annicchiarico-Petruzzelli M, Niklison-Chirou M, Amelio I, Knight R, Mak T, Melino G, Agostini M. GLS2 is transcriptionally regulated by p73 and contributes to neuronal differentiation. Cell Cycle. 2015; 14:1611–12.

58. Holembowski L, Kramer D, Riedel D, Sordella R, Nemajerova A, Dobbelstein M, Moll UM. TAp73 is essential for germ cell adhesion and maturation in testis. J Cell Biol. 2014; 204:1173–90. https://doi.org/10.1083/jcb.201306066

59. Fouchécourt S, Livera G, Messiaen S, Fumel B, Parent AS, Marine JC, Monget P. Apoptosis of Sertoli cells after conditional ablation of murine double minute 2 (Mdm2) gene is p53-dependent and results in male sterility. Cell Death Differ. 2016; 23:521–30. https://doi.org/10.1038/cdd.2015.120

60. Amelio I, Melino G. The p53 family and the hypoxia-inducible factors (HIFs): determinants of cancer progression. Trends Biochem Sci. 2015; 40:425–34. https://doi.org/10.1016/j.tibs.2015.04.007

61. Thakur AK, Nigri J, Lac S, Leca J, Bressy C, Berthezene P, Bartholin L, Chan P, Calvo E, Iovanna JL, Vasseur S, Guillaumond F, Tomasini R. TAp73 loss favors Smad-independent TGF-β signaling that drives EMT in pancreatic ductal adenocarcinoma. Cell Death Differ. 2016; 23:1358–70. https://doi.org/10.1038/cdd.2016.18

62. Tomasini R, Tsuchihara K, Wilhelm M, Fujitani M, Rufini A, Cheung CC, Khan F, Itie-Youten A, Wakeham A, Tsao MS, Iovanna JL, Squire J, Jurisica I, et al. TAp73 knockout shows genomic instability with infertility and tumor suppressor functions. Genes Dev. 2008; 22:2677–91. https://doi.org/10.1101/gad.1695308

63. Wilhelm MT, Rufini A, Wetzel MK, Tsuchihara K, Inoue S, Tomasini R, Itie-Youten A, Wakeham A, Arsenian-Henriksson M, Melino G, Kaplan DR, Miller FD, Mak TW. Isoform-specific p73 knockout mice reveal a novel role for delta Np73 in the DNA damage response pathway. Genes Dev. 2010; 24:549–60. https://doi.org/10.1101/gad.1873910

64. Rufini A, Agostini M, Grespi F, Tomasini R, Sayan BS, Niklison-Chirou MV, Conforti F, Velletri T, Mastino A, Mak TW, Melino G, Knight RA. p73 in Cancer. Genes Cancer. 2011; 2:491–502. https://doi.org/10.1177/1947601911408890

65. Amelio I, Inoue S, Markert EK, Levine AJ, Knight RA, Mak TW, Melino G. TAp73 opposes tumor angiogenesis by promoting hypoxia-inducible factor 1α degradation. Proc Natl Acad Sci USA. 2015; 112:226–31. https://doi.org/10.1073/pnas.1410609111

66. Petrova V, Annicchiarico-Petruzzelli M, Melino G, Amelio I. The hypoxic tumour microenvironment. Oncogenesis. 2018; 7:10. https://doi.org/10.1038/s41389-017-0011-9

67. Petrova V, Mancini M, Agostini M, Knight RA, Annicchiarico-Petruzzelli M, Barlev NA, Melino G, Amelio I. TAp73 transcriptionally represses BNIP3 expression. Cell Cycle. 2015; 14:2484–93. https://doi.org/10.1080/15384101.2015.1044178

68. Voskoboinik I, Camakaris J. Menkes copper-translocating P-type ATPase (ATP7A): biochemical and cell biology properties, and role in Menkes disease. J Bioenerg Biomembr. 2002; 34:363–71. https://doi.org/10.1023/A:1021250003104

69. Kaler SG. Translational research investigations on ATP7A: an important human copper ATPase. Ann N Y

Acad Sci. 2014; 1314:64–68. https://doi.org/10.1111/nyas.12422

70. Zheng MD, Wang ND, Li XL, Yan J, Tang JH, Zhao XH, Zhang Z. Toosendanin mediates cisplatin sensitization through targeting Annexin A4/ATP7A in non-small cell lung cancer cells. J Nat Med. 2018; 72:724–33. https://doi.org/10.1007/s11418-018-1211-0

71. Yang T, Chen M, Chen T, Thakur A. Expression of the copper transporters hCtr1, ATP7A and ATP7B is associated with the response to chemotherapy and survival time in patients with resected non-small cell lung cancer. Oncol Lett. 2015; 10:2584–90. https://doi.org/10.3892/ol.2015.3531

72. Xiao F, Li Y, Wan Y, Xue M. MircroRNA-139 sensitizes ovarian cancer cell to cisplatin-based chemotherapy through regulation of ATP7A/B. Cancer Chemother Pharmacol. 2018; 81:935–47. https://doi.org/10.1007/s00280-018-3548-1

73. Song L, Li Y, Li W, Wu S, Li Z. miR-495 enhances the sensitivity of non-small cell lung cancer cells to platinum by modulation of copper-transporting P-type adenosine triphosphatase A (ATP7A). J Cell Biochem. 2014; 115:1234–42. https://doi.org/10.1002/jcb.24665

74. Li ZH, Qiu MZ, Zeng ZL, Luo HY, Wu WJ, Wang F, Wang ZQ, Zhang DS, Li YH, Xu RH. Copper-transporting P-type adenosine triphosphatase (ATP7A) is associated with platinum-resistance in non-small cell lung cancer (NSCLC). J Transl Med. 2012; 10:21. https://doi.org/10.1186/1479-5876-10-21

75. Aaboud M, Aad G, Abbott B, Abdallah J, Abdinov O, Abeloos B, Abidi SH, AbouZeid OS, Abraham NL, Abramowicz H, Abreu H, Abreu R, Abulaiti Y, et al, and ATLAS Collaboration. Performance of the ATLAS track reconstruction algorithms in dense environments in LHC Run 2. Eur Phys J C Part Fields. 2017; 77:673. https://doi.org/10.1140/epjc/s10052-017-5225-7

76. Inoue Y, Matsumoto H, Yamada S, Kawai K, Suemizu H, Gika M, Takanami I, Iwazaki M, Nakamura M. Association of ATP7A expression and in vitro sensitivity to cisplatin in non-small cell lung cancer. Oncol Lett. 2010; 1:837–40. https://doi.org/10.3892/ol_00000147

77. Amelio I, Tsvetkov PO, Knight RA, Lisitsa A, Melino G, Antonov AV. SynTarget: an online tool to test the synergetic effect of genes on survival outcome in cancer. Cell Death Differ. 2016; 23:912. https://doi.org/10.1038/cdd.2016.12

78. Flores ER, Sengupta S, Miller JB, Newman JJ, Bronson R, Crowley D, Yang A, McKeon F, Jacks T. Tumor predisposition in mice mutant for p63 and p73: evidence for broader tumor suppressor functions for the p53 family. Cancer Cell. 2005; 7:363–73. https://doi.org/10.1016/j.ccr.2005.02.019

79. Shi Z, Park HR, Du Y, Li Z, Cheng K, Sun SY, Li Z, Fu H, Khuri FR. Cables1 complex couples survival signaling to the cell death machinery. Cancer Res. 2015; 75:147–58. https://doi.org/10.1158/0008-5472.CAN-14-0036

80. Lozano G. The Enigma of p53. Cold Spring Harb Symp Quant Biol. 2016; 81:37–40. https://doi.org/10.1101/sqb.2016.81.031062

81. Wu M, Ye H, Tang Z, Shao C, Lu G, Chen B, Yang Y, Wang G, Hao H. p53 dynamics orchestrates with binding affinity to target genes for cell fate decision. Cell Death Dis. 2017; 8:e3130. https://doi.org/10.1038/cddis.2017.492

82. Fuschi P, Carrara M, Voellenkle C, Garcia-Manteiga JM, Righini P, Maimone B, Sangalli E, Villa F, Specchia C, Picozza M, Nano G, Gaetano C, Spinetti G, et al. Central role of the p53 pathway in the noncoding-RNA response to oxidative stress. Aging (Albany NY). 2017; 9:2559–86. https://doi.org/ 10.18632/aging.101341

83. Chen HR, Yang HC, Hsieh DJ, Liu Z, Tsai KJ. Zebrafish sod1 and sp1 expression are modulated by the copper ATPase gene atp7a in response to intracellular copper status. Chem Biol Interact. 2011; 189:192–97. https://doi.org/10.1016/j.cbi.2010.12.003

84. Xiao B, Deng X, Lim GG, Xie S, Zhou ZD, Lim KL, Tan EK. Superoxide drives progression of Parkin/PINK1-dependent mitophagy following translocation of Parkin to mitochondria. Cell Death Dis. 2017; 8:e3097. https://doi.org/10.1038/cddis.2017.463

85. Wang R, Yin C, Li XX, Yang XZ, Yang Y, Zhang MY, Wang HY, Zheng XF. Reduced SOD2 expression is associated with mortality of hepatocellular carcinoma patients in a mutant p53-dependent manner. Aging (Albany NY). 2016; 8:1184–200. https://doi.org/10.18632/aging.100967

86. Xie L, Collins JF. Transcription factors Sp1 and Hif2α mediate induction of the copper-transporting ATPase (Atp7a) gene in intestinal epithelial cells during hypoxia. J Biol Chem. 2013; 288:23943–52. https://doi.org/10.1074/jbc.M113.489500

87. Logotheti S, Michalopoulos I, Sideridou M, Daskalos A, Kossida S, Spandidos DA, Field JK, Vojtesek B, Liloglou T, Gorgoulis V, Zoumpourlis V. Sp1 binds to

the external promoter of the p73 gene and induces the expression of TAp73gamma in lung cancer. FEBS J. 2010; 277:3014–27. https://doi.org/10.1111/j.1742-4658.2010.07710.x

88. Oppenheim A, Lahav G. The puzzling interplay between p53 and Sp1. Aging (Albany NY). 2017; 9:1355–56. https://doi.org/ 10.18632/aging.101238

89. Tajan M, Hock AK, Blagih J, Robertson NA, Labuschagne CF, Kruiswijk F, Humpton TJ, Adams PD, Vousden KH. A Role for p53 in the adaptation to glutamine starvation through the expression of SLC1A3. Cell Metab. 2018; 28:721–736.e6. https://doi.org/10.1016/j.cmet.2018.07.005

90. Hock AK, Vousden KH. Tumor suppression by p53: fall of the triumvirate? Cell. 2012; 149:1183–85. https://doi.org/10.1016/j.cell.2012.05.024

91. Humpton TJ, Vousden KH. Regulation of cellular metabolism and hypoxia by p53. Cold Spring Harb Perspect Med. 2016; 6:a026146. https://doi.org/10.1101/cshperspect.a026146

92. Isaac R, Goldstein I, Furth N, Zilber N, Streim S, Boura-Halfon S, Elhanany E, Rotter V, Oren M, Zick Y. TM7SF3, a novel p53-regulated homeostatic factor, attenuates cellular stress and the subsequent induction of the unfolded protein response. Cell Death Differ. 2017; 24:132–43. https://doi.org/10.1038/cdd.2016.108

93. Horikawa I, Park KY, Isogaya K, Hiyoshi Y, Li H, Anami K, Robles AI, Mondal AM, Fujita K, Serrano M, Harris CC. Δ133p53 represses p53-inducible senescence genes and enhances the generation of human induced pluripotent stem cells. Cell Death Differ. 2017; 24:1017–28. https://doi.org/10.1038/cdd.2017.48

94. Martin-Lopez M, Maeso-Alonso L, Fuertes-Alvarez S, Balboa D, Rodríguez-Cortez V, Weltner J, Diez-Prieto I, Davis A, Wu Y, Otonkoski T, Flores ER, Menéndez P, Marques MM, Marin MC. p73 is required for appropriate BMP-induced mesenchymal-to-epithelial transition during somatic cell reprogramming. Cell Death Dis. 2017; 8:e3034. https://doi.org/10.1038/cddis.2017.432

95. Pinto M, Pickrell AM, Wang X, Bacman SR, Yu A, Hida A, Dillon LM, Morton PD, Malek TR, Williams SL, Moraes CT. Transient mitochondrial DNA double strand breaks in mice cause accelerated aging phenotypes in a ROS-dependent but p53/p21-independent manner. Cell Death Differ. 2017; 24:288–99. https://doi.org/10.1038/cdd.2016.123

96. Giacomello M, Pellegrini L. The coming of age of the mitochondria-ER contact: a matter of thickness. Cell Death Differ. 2016; 23:1417–27. https://doi.org/10.1038/cdd.2016.52

97. Vila MC, Rayavarapu S, Hogarth MW, Van der Meulen JH, Horn A, Defour A, Takeda S, Brown KJ, Hathout Y, Nagaraju K, Jaiswal JK. Mitochondria mediate cell membrane repair and contribute to Duchenne muscular dystrophy. Cell Death Differ. 2017; 24:330–42. https://doi.org/10.1038/cdd.2016.127

98. Gross A, Zaltsman Y, Maryanovich M. The ATM-BID pathway plays a critical role in the DNA damage response by regulating mitochondria metabolism. Cell Death Differ. 2016; 23:182. https://doi.org/10.1038/cdd.2015.154

99. Kaestner L, Minetti G. The potential of erythrocytes as cellular aging models. Cell Death Differ. 2017; 24:1475–77. https://doi.org/10.1038/cdd.2017.100

100. Wang X, Huang N, Yang M, Wei D, Tai H, Han X, Gong H, Zhou J, Qin J, Wei X, Chen H, Fang T, Xiao H. FTO is required for myogenesis by positively regulating mTOR-PGC-1α pathway-mediated mitochondria biogenesis. Cell Death Dis. 2017; 8:e2702. https://doi.org/10.1038/cddis.2017.122

101. Wang ZB, Hao JX, Meng TG, Guo L, Dong MZ, Fan LH, Ouyang YC, Wang G, Sun QY, Ou XH, Yao YQ. Transfer of autologous mitochondria from adipose tissue-derived stem cells rescues oocyte quality and infertility in aged mice. Aging (Albany NY). 2017; 9:2480–88. https://doi.org/10.18632/aging.101332

102. Kaufman DM, Wu X, Scott BA, Itani OA, Van Gilst MR, Bruce JE, Crowder CM. Ageing and hypoxia cause protein aggregation in mitochondria. Cell Death Differ. 2017; 24:1730–38. https://doi.org/10.1038/cdd.2017.101

103. Caputa G, Zhao S, Criado AE, Ory DS, Duncan JG, Schaffer JE. RNASET2 is required for ROS propagation during oxidative stress-mediated cell death. Cell Death Differ. 2016; 23:347–57. https://doi.org/10.1038/cdd.2015.105

104. Palmgren MG, Nissen P. P-type ATPases. Annu Rev Biophys. 2011; 40:243–66. https://doi.org/10.1146/annurev.biophys.093008.131331

105. Lutsenko S, Barnes NL, Bartee MY, Dmitriev OY. Function and regulation of human copper-transporting ATPases. Physiol Rev. 2007; 87:1011–46. https://doi.org/10.1152/physrev.00004.2006

106. Tümer Z. An overview and update of ATP7A mutations leading to Menkes disease and occipital horn syndrome. Hum Mutat. 2013; 34:417–29. https://doi.org/10.1002/humu.22266

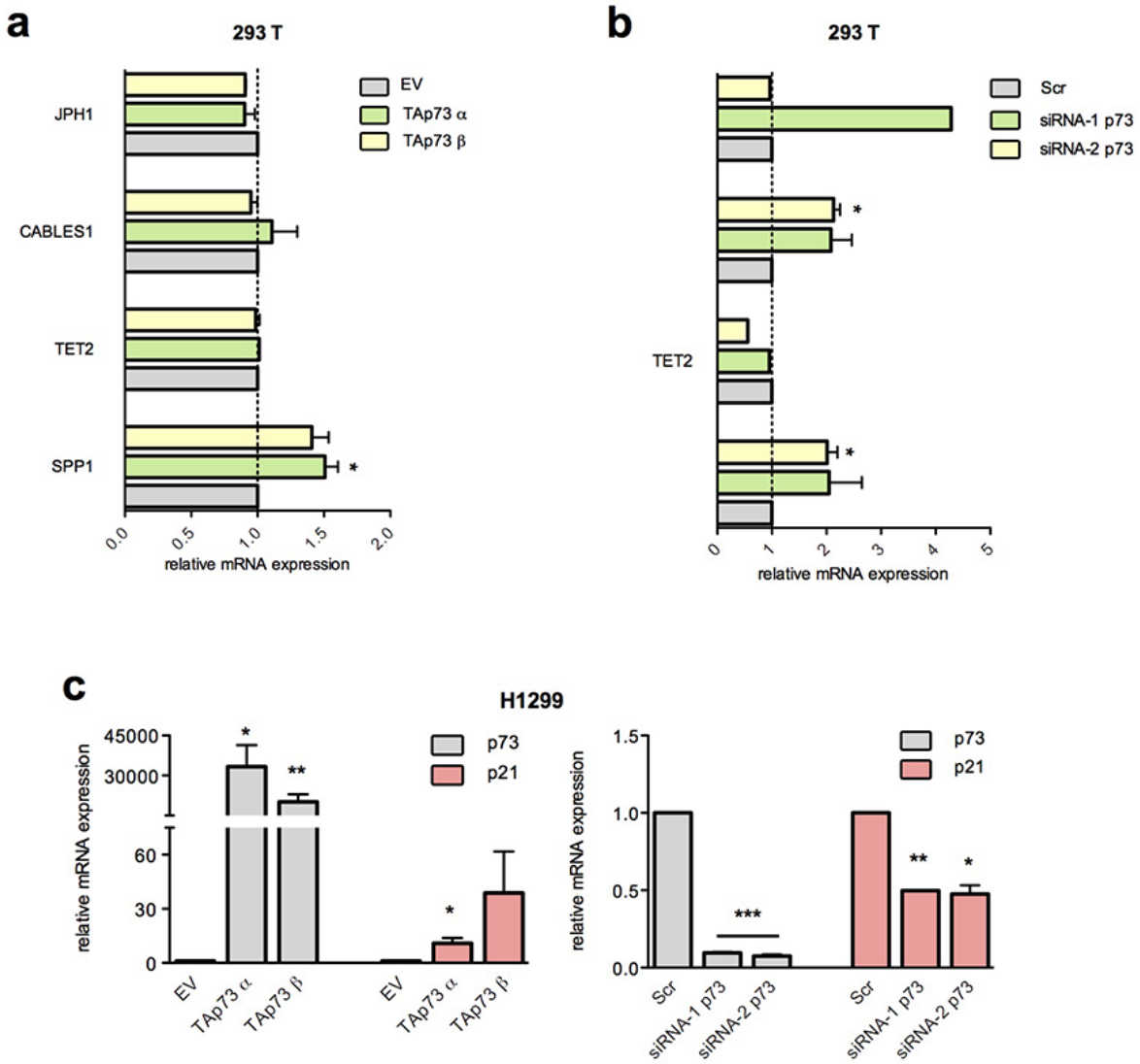

Supplementary Figure 1. TAp73 overexpression and silencing in 293T cells and H1299. (**a**) mRNA levels of SPP1, TET2, CABLES1, JPH1, ATP7A were analysed by quantitative PCR after HA-Tap73 α and β induction. Relative expression of genes was normalized against TBP and calculated as fold change to the control treatment (empty vector, EV). Data is reported as mean ± s.d. of two experiments. * $p < 0.05$ (Student's T-test). (**b, c**) mRNA levels of genes of interest were analysed by quantitative PCR after siRNA-1 p73 and siRNA-2 p73 treatment. Relative expression of genes was normalized against TBP and calculated as fold change to the control treatment (siCTRL, Scr) Data is reported as mean ± s.d. of two experiments. * $p < 0.05$ (Student's T-test). (**c**) p73 and p21 mRNA levels were analysed by quantitative PCR after TAp73 overexpression (HA-Tap73 α-β) and p73 silencing (siRNA-1/2 p73). Up- and downregulation of p21, a TAp73 transcriptional target, confirmed p73 transcriptional activity modulation. Relative expression of genes was normalized against TBP and calculated as fold change to the control treatments (EV and Scr). Data is reported as mean ± s.d. of three experiments. *** $p < 0.0001$, ** $p < 0.001$, * $p < 0.05$ (Student's T-test).

Research Paper

ΔNp63 promotes IGF1 signalling through IRS1 in squamous cell carcinoma

Valentina Frezza[1], Claudia Fierro[1], Elena Gatti[2], Angelo Peschiaroli[3], Anna Maria Lena[1], Margherita Annicchiarico Petruzzelli[4], Eleonora Candi[1,4], Lucia Anemona[1], Alessandro Mauriello[1], Pier Giuseppe Pelicci[2], Gerry Melino[1,5], Francesca Bernassola[1]

[1]Department of Experimental Medicine, TOR, University of Rome "Tor Vergata", Rome 00133 Italy
[2]Department of Experimental Oncology, European Institute of Oncology, Milan 20139 Italy
[3]National Research Council of Italy, Institute of Translational Pharmacology (IFT-CNR), Rome 00133 Italy
[4]Istituto Dermopatico dell'Immacolata, IRCCS, Rome 00163 Italy
[5]Medical Research Council, Toxicology Unit, University of Cambridge, Leicester LE1 9HN, UK

Correspondence to: Francesca Bernassola, Gerry Melino; **email:** bernasso@uniroma2.it, melino@uniroma2.it
Keywords: p53 family, p63, IGF system, IRS1, head and neck tumours
Received: October 24, 2018 **Accepted:** December 12, 2018 **Published:** December 28, 2018

ABSTRACT

Accumulating evidence has proved that deregulation of ΔNp63 expression plays an oncogenic role in head and neck squamous cell carcinomas (HNSCCs). Besides p63, the type 1-insulin-like growth factor (IGF) signalling pathway has been implicated in HNSCC development and progression. Most insulin/IGF1 signalling converges intracellularly onto the protein adaptor insulin receptor substrate-1 (IRS-1) that transmits signals from the receptor to downstream effectors, including the PI3K/AKT and the MAPK kinase pathways, which, ultimately, promote proliferation, invasion, and cell survival. Here we report that p63 directly controls IRS1 transcription and cellular abundance and fosters the PI3K/AKT and MAPK downstream signalling pathways. Inactivation of ΔNp63 expression indeed reduces tumour cell responsiveness to IGF1 stimulation, and inhibits the growth potential of HNSCC cells. In addition, a positive correlation was observed between p63 and IRS1 expression in human HNSCC tissue arrays and in publicly available gene expression data. Our findings indicate that aberrant expression of ΔNp63 in HNSSC may act as an oncogenic stimulus by altering the IGF signalling pathway.

INTRODUCTION

Head and neck squamous cell carcinoma (HNSCC), the sixth most frequent malignancy worldwide, is a heterogeneous disease that develops from the stratified epithelium of the upper aerodigestive tract [1]. Despite recent diagnostic and therapeutic advances, the prognosis and survival of HNSCC patients remain poor. In response to the increase in the number of new HNSCC cases worldwide, further knowledge of tumour biology and the identification of novel clinical biomarkers are needed to improve prognostic stratification and optimise the anti-cancer therapies.

The p53 family of transcription factors includes p53, p63 and p73, which are all involved in tumorigenesis [2-8] as well as in fertility [9, 10], metabolism [11], and aging [12-17] regulation. In addition, a developmental or differentiation function has been described for all the family members [18-32]. Many of these features are compatible with the genetic [33-37] and metabolic [38-45] events described in aging [46-55]. A common feature of the p53 family members is the presence of two distinct promoters that can be differentially used to transcribe the full-length (TA isoforms) or the N-terminal-shorter (ΔN isoforms) proteins, exerting distinct functions [56]. ΔNp63 is the predominant isoform

transcribed from the TP63 gene. It is expressed in the basal compartments of several ectoderm-derived tissues [57-60], in which, it acts as a master regulator of epithelial development and maintenance [61, 62]. In addition, ΔNp63 promotes the survival and sustains the self-renewal potential of epithelial cancer stem cells [63, 64]. Genomic amplification and overexpression of TP63, as a result of decreased methylation of CpGs at the ΔNp63 promoter, is frequent in HNSCCs [65-67], in which ΔNp63 promotes cancer cell survival, proliferation and chemoresistance [59, 66, 68, 69]. ΔNp63 overexpression is an adverse prognostic factor for HNSCC patients [66, 70]. Although some ΔNp63 targets and molecular pathways relevant for its pro-tumorigenic activities have been identified [59, 66, 71, 72], there still need to uncover the molecular basis of its oncogenic function.

The Insulin-like Growth Factor (IGF) axis is composed of the tyrosine kinase IGF type 1 receptor (IGF1R), its ligands, insulin, IGF1 and IGF2, the adaptor protein Insulin Receptor Substrate 1 (IRS1) and a family of six ligand-binding proteins (IGFBPs) that regulate the bioavailability and half-life of circulating IGF1. Among the IGFBPs, IGFBP3 binds to more than 95% of circulating IGF. The IGF1R binds IGF1 and IGF2 with high affinity, as well as insulin, though with lower affinity. Upon ligation, IGF1R recruits and phosphorylates IRS1. Phosphorylated IRS1 acts as docking site for intracellular adaptor proteins that, ultimately, activate two downstream signalling cascades: the PI3K/AKT and the MAPK pathways, both of which have mitogenic and pro-survival roles.

Reduced responsiveness to IGF1/insulin can occur as a result of diminished total or phosphorylated amounts of IGF1R or IRS1, and results in decreased activation of the PI3K/AKT and MAPK pathways [73].

Deregulation of the IGF axis has been implicated in the development and progression of several human cancers. Elevated serum IGF1 levels, and increased levels or constitutive activation of IGF1R and IRS1 are associated with increased risk of a variety of epithelial cancers, metastasis and therapeutic resistance [74-80]. Hence, it has been proposed that reduction of IGF signalling ~~in~~ may have a prognostic impact and a therapeutic benefit in some cancer types. In HNSCC, IGF1R overexpression is associated with adverse survival, HPV negativity and high tumour T-stage [76, 81, 82]. High IGF1 levels and both lower and higher levels of IGFBP3 are predictor risk factors for secondary tumour development in patients with HNSCC [83, 84]. In addition, increased IRS1 expression was found in nasopharyngeal carcinoma patients, where it correlated with lymph node metastasis [80].

Notably, the existence of a possible crosstalk between p63 and the IGF system has been reported. The tumour suppressive TAp63 isoforms negatively control *Igf1r* transcription [85], whereas *Igfbp3* is a target of transcriptional repression by ΔNp63 [86]. Here we report, that ΔNp63 affects the transcription and the cellular abundance of *Irs1* in HNSCC cells and, that, as a result, p63 down-regulation impairs the activation of the intracellular signalling pathways following IGF1R stimulation.

RESULTS

p63 controls IRS1 expression levels in HNSCC cells

By exploiting RNA sequencing (RNA-seq) transcriptome profiling, we identified genes regulated by ΔNp63 in normal human epidermal keratinocytes (NHEKs) (E.C. unpublished data). The analysis of RNA-Seq data obtained from p63-depleted cells revealed almost 50% reduction in IRS1 expression levels relatively to control cells (Fig. 1A). We then sought to test whether IRS1 expression is regulated by p63 in HNSCC cells. HNSCC cell lines display moderate/high levels of p63 expression (Fig. 1B, upper panel). In particular, the predominantly expressed isoform of p63 in HNSCC cells is ΔNp63, with TAp63 being undetectable in the majority of the cell lines (Fig. 1C). We observed a consistent correlation between ΔNp63 protein levels and the gene expression pattern of IRS1 in most of the HNSCC cell lines analysed (Fig. 1B, lower panel). Validation of RNA-seq data showed that, following p63 knockdown, IRS1 transcript and protein levels were reduced in NHEK and in a panel of HNSCC cell lines (Fig. 1D).

p63 induces IRS1 expression by binding directly to the regulatory region of the *Irs1* gene

Genome-wide profiling of p63 binding sites by Chromatin IP Sequencing (ChIP-seq) analysis of NHEKs [87] revealed peaks of p63 binding to regions downstream the *Irs1* locus (Fig. 2A). The algorithm p63scan identified a putative p63 responsive element (RE) in the most distant enriched peak. To validate direct interaction of p63 with this putative RE, we examined p63 occupancy at the site identified in the ChIP-seq analysis. By ChIP experiments in HNSCC cells, we found binding of p63 to a regulatory region located downstream the *Irs1* locus (+148 kbps from the TSS) (Fig. 2B). In addition, by performing luciferase activity reporter assays in H1299 cells, we found that the ΔNp63 isoforms activate a luciferase reporter gene driven by the p63 RE located in the regulatory region of the *Irs1* locus (Fig. 2C). Site-specific mutagenesis of the p63 RE almost completely abrogated the transactivating

ability of ΔNp63 (Fig. 2C). Overall, these data demonstrate that *Irs1* is a direct transcriptional target of ΔNp63.

p63 inactivation impairs cellular sensitivity of HNSCC cells to IGF1/insulin stimulation

We next tested whether knockdown of ΔNp63 affects the level of activated IRS1. To assess whether down-regulation of IRS1 in p63-depletd HNSCC cells would impair cellular responsiveness to receptor stimulation, we treated serum starved Fadu cells with both IGF1 and insulin. Stimulation of the IGF1R resulted in reduced levels of phosphorylated (Ser612) IRS1 in p63-depleted relatively to control cells (Fig. 3A). To rule out off-target effects, two independent siRNAs against p63 and one specific ΔNp63 siRNA were employed (Fig. 3A, Fig. S1A, and S1B).

To examine whether alteration of IRS1 and phospho-IRS1 levels induced by p63 silencing may affect downstream IGF signal transduction, we measured the activation of PI3K/AKT and MAPK downstream signalling pathways in p63-depleted cells. Upon p63 knock-down, we observed desensitization of HNSCC cells to IGF1 stimulation, as assessed by decreased amounts of phospho-AKT (Ser473) and phospho-S6 (Ser235/236) (Fig. 3B). Activation of MAPK (phospho-Erk1/2; Thr202/Tyr204) signalling pathway in response

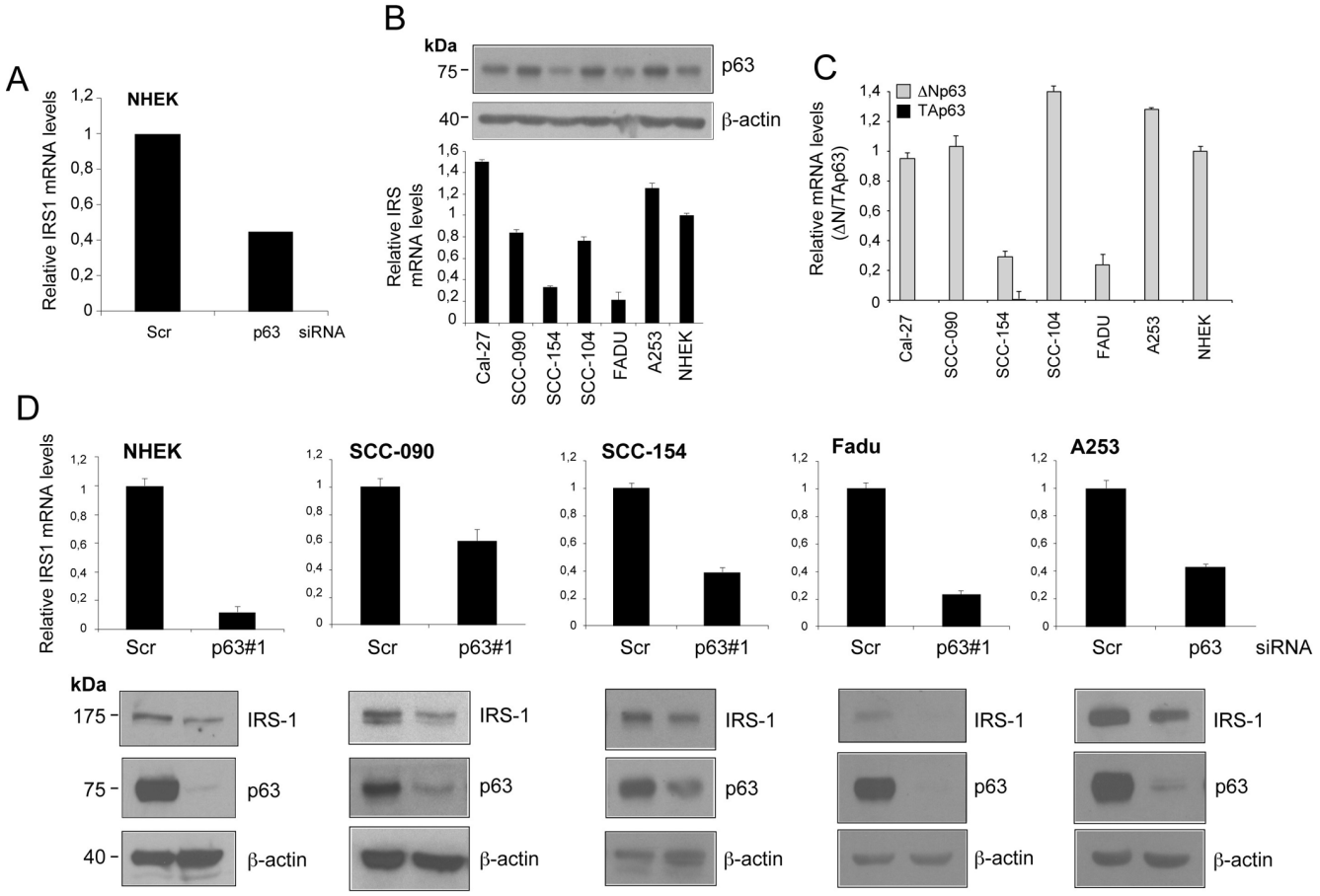

Figure 1. IRS1 expression is decreased upon down-regulation of p63 in HNSCC cell lines. (**A**) Relative expression levels of *Irs1* as measured by RNA-Seq analysis of p63-depleted NHEK. Cells were transfected with p63 (sip63#1) or scrambled control (siScr) siRNAs. P-value = 0,005. (**B**) The amount of p63 was measured in NHEK and HNSCC cell lines by western blot analysis (upper panel). IRS1 transcript levels were analysed by RT-qPCR (lower panel). RT-qPCR was performed in duplicate. IRS1 expression was normalized on *Tbp* housekeeper and plotted relative to NHEK cells (mean ± s.d.). (**C**) The transcript levels of TAp63 (black box) and ΔNp63 (grey box) were measured in NHEK and HNSCC cell lines by RT-qPCR. RT-qPCR was performed as above. Gene expression was normalized on *Tbp* housekeeper and plotted relative to NHEK cells (mean ± s.d.). (**D**) RT-qPCR analysis (upper panels) of two independent experiments performed in duplicates for *Irs1* transcripts in NHEK and HNSCC cells transfected with scrambled control (siScr) or p63 (sip63#1) siRNAs. Cells were harvested 48 h after transfection. qRT-PCR was performed as above. Values are normalized to *Tbp* and plotted relative to control cells (mean ± s.d.). Western Blot analysis for IRS1 and p63 in HNSCC cells transfected as above. Cells were harvested 48 h after transfection. β-actin served as loading control.

to IGF-1 stimulation was also markedly reduced in p63-depleted cells (Fig. 3B), further proving that p63 affects cellular sensitivity to IGF1/insulin stimulation through the regulation of IRS1 cellular abundance. Notably, knockdown of IRS1 hampered the proliferation of HNSCC cells, mimicking the effect of p63 inactivation (Fig. 3C). These findings indicate that the p63/IRS1 functional axis positively regulates the growth potential of HNSCC cells.

p63 and IRS1 expression correlates in HNSCC patients

To examine possible correlations between the expres-sion levels of □Np63 and IRS1 in NHSCC primary tumours, clinical NHSCC tumour specimens sample sand related benign controls were examined for p63 and IRS1 staining on tissue microarray slides. Consistent with previous reports [65, 66], the majority of the patients (63%) showed high levels of p63 expression (Fig. 4A; represen-tative staining patterns are seen in Fig. 4C, top panels). High and moderate tumour cell IRS1 expression was observed in 27% and 10%, respectively of the cases (Fig. 4B, representative staining patterns are seen in Fig. 4C, bottom panels). Significant correlation of p63 and IRS1 expression was observed in 23 out of 60 HNSCC samples (38%, Fig. 4C and Table S1).

To further investigate the expression levels of p63 and IRS1, we analysed publicly available transcriptome sequencing data of 522 HNSCC patients from the TCGA repository [88]. Overall, the transcript levels of p63 and IRS1 are significantly higher in tumour speci-mens than in normal samples (Fig. 4D, and 4E). On the basis of their expression levels, for each gene, we stratified tumour patients into two distinct groups, displaying either up-regulation or down-regulation relatively to normal subjects. Notably, we found that 66.2% of tumour samples with p63 up-regulation also exhibited high levels of IRS1 expressiA similar correlation was observed in samples with p63 down-regulation, in which 58% of the patients concomitantly

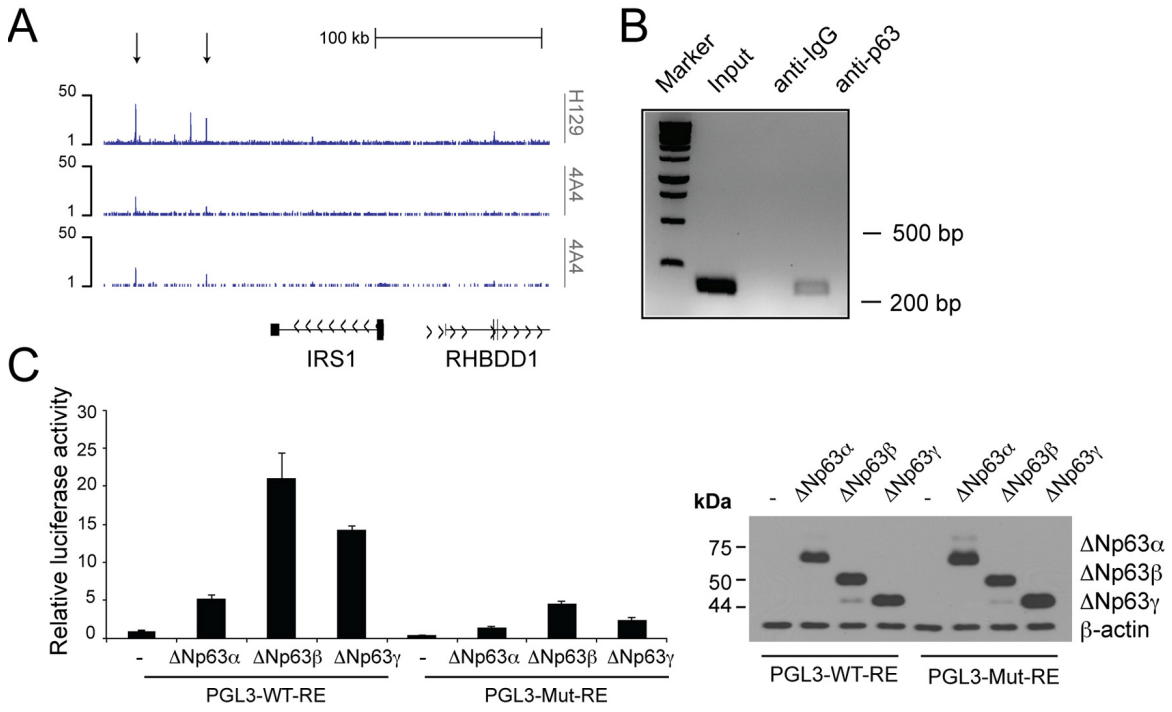

Figure 2. p63 binds to the regulatory region of the *Irs1* gene. (**A**) p63 DNA-binding profiles in the *Irs1* locus, obtained in NHEKs by ChIP-sequencing (ChIP-seq) using 4A4 and H129 anti-p63 antibodies in two normal human primary keratinocyte cell lines (K1 and K2) [87]. (**B**) ChIP analysis of p63 occupancy at the regulatory regions of the *Irs1* gene. ChIP assays were performed in Fadu HNSCC cells using H129 anti-p63 antibody and control IgGs. PCR validation was performed using primers spanning the p63-binding sites located within the genomic regions identified by ChIP-seq assays. (**C**) Luciferase reporter assays of *Irs1* regulatory regions (left panel). The pGL3 reporter vector (30 ng) and the pRL-CMV-*Renilla* luciferase plasmid (5 ng) were cotransfected with the empty pcDNA-HA vector or plasmids coding ΔNp63α, ΔNp63β, and ΔNp63γ (150 ng) into the p53 null human H1299 cell line. The luciferase activities of cellular extracts were measured 24 h after transfection. Cellular lysates were also analysed by western blot (right panel). Data are presented as mean ± SD and are representative of three independent experiments.

displayed low levels of IRS1 transcripts (Fig. 4F, p-value= 4.293e-07). Overall, these findings demonstrate that a statistical significant positive association exists between p63 and IRS1 expression inHNSCC patients.

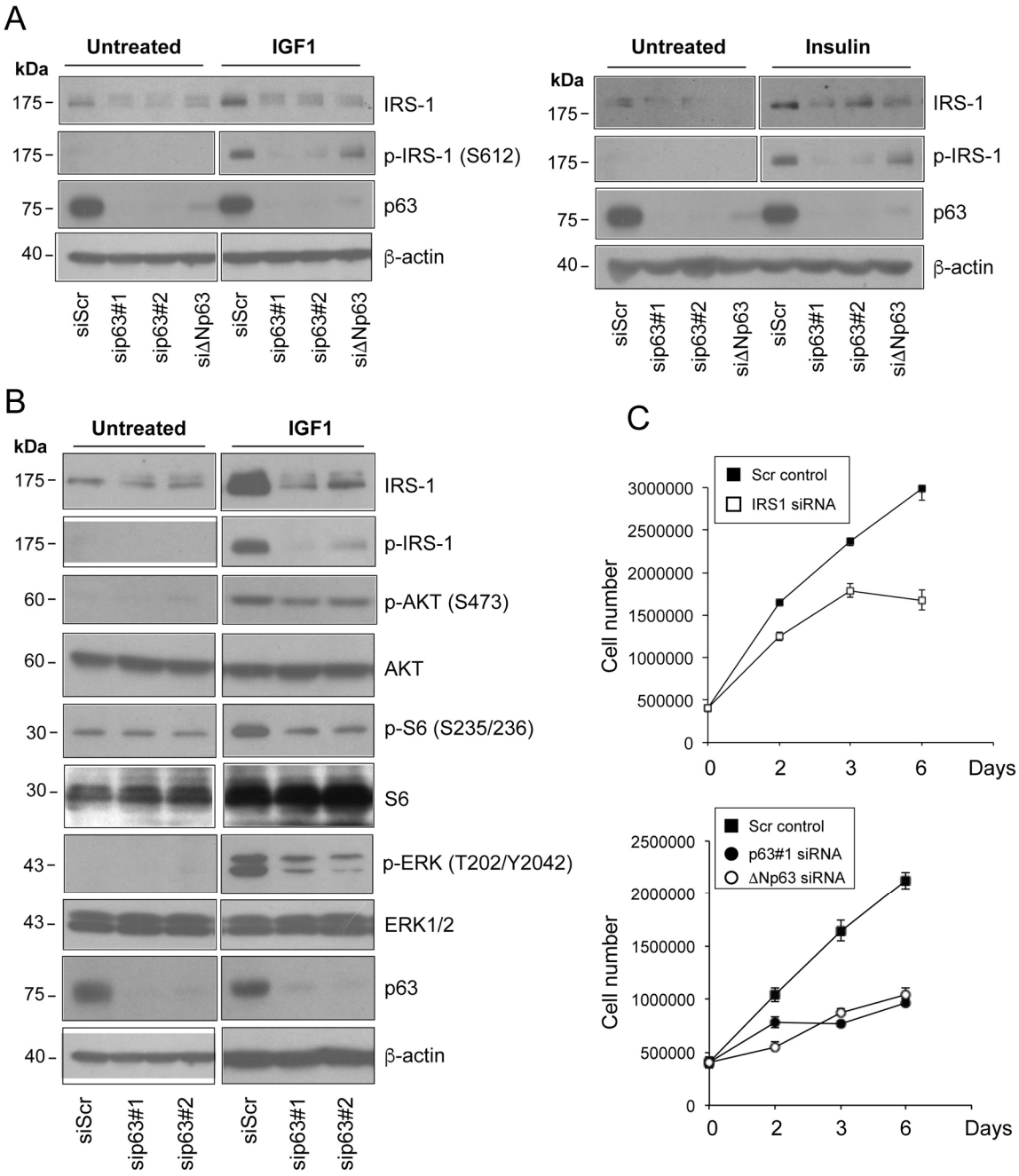

Figure 3. **Depletion of p63 reduces the responsiveness of HNSCC cells to ligand stimulation.** (**A**) Fadu cells were transfected with siScr or different p63 (sip63#1, sip63#2, siΔNp63) siRNAs. Forty-eight h after transfection, cells were serum starved for 4 h, and then stimulated with 5 nM IGF1 (upper panel) or 500 ng/ml insulin (lower panel) for 10 min. Protein amounts of p63, IRS1 and p-IRS1 were detected by western blot analysis. β-actin served as loading control. Blots are representative of three individual experiments. (**B**) Fadu cells were transfected with siScr, sip63#1 and sip63#2, serum starved for 4 h and then stimulated with 5 nM IGF1 for 10 min. Cellular extracts were analysed with the following antibodies: anti-IRS1, anti-p-IRS1, anti-p-AKT, anti-AKT, anti-p-S6 Ribosomal Protein, anti-S6, anti-p44/42 MAPK (p-ERK1/2), anti-ERK1/2, p63 and β-actin as loading control. Blots are representative of three individual experiments. (**C**) Fadu cells were transfected with siScr or siIRS1 (upper panel) and with sip63#1, ΔNp63, or siScr (lower panel). Forty-eight h after transfection, cells were seeded in 6-cm plates at 500,000/plate and growth was followed until day 6.

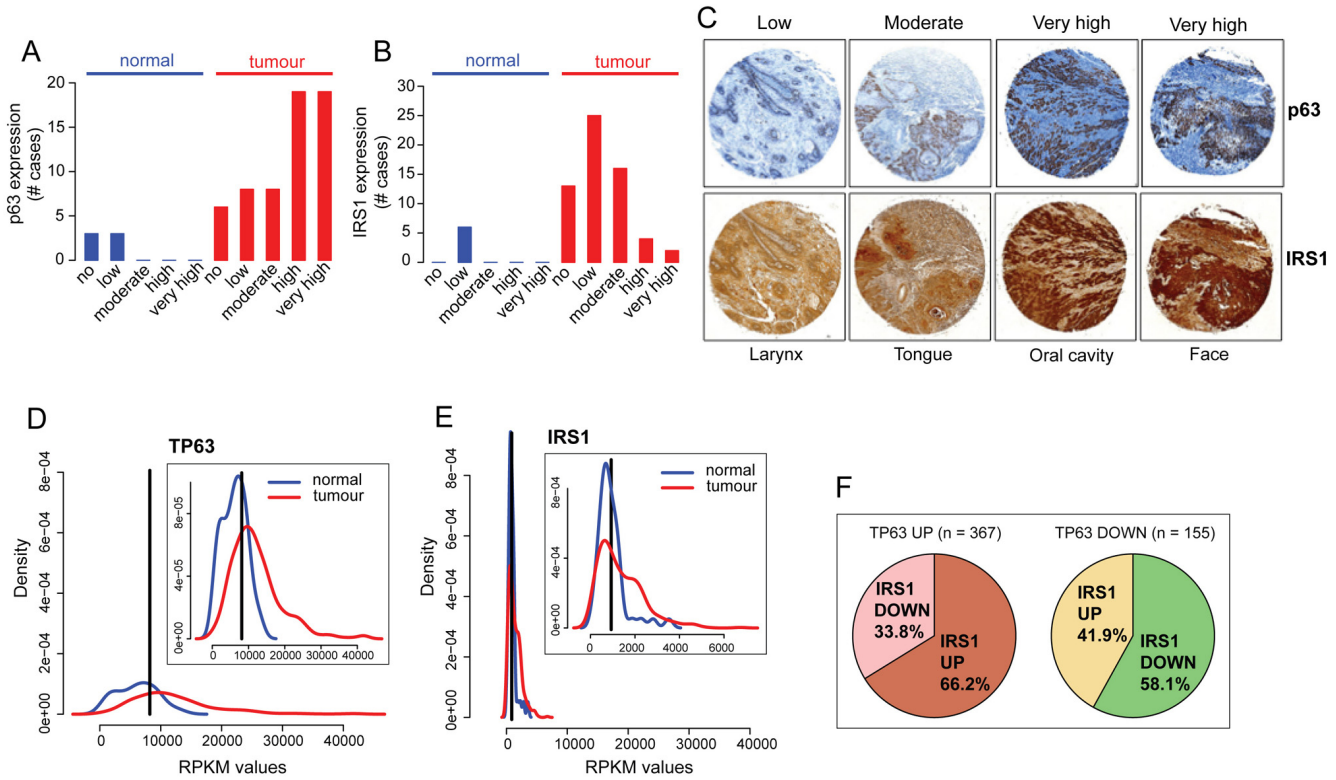

Figure 4. p63 and IRS1 expression patterns are positively correlated in HNSCC patients. (**A-C**) Tissue sections were stained with anti-p63 and IRS1 antibodies. The scores for the percentage of p63 and IRS1 positive cells and those for the expression intensities were combined to calculate immunoreactive scores (IRSs) summarised in Table S1. According to the IRS, patients were assigned to five groups: 0 (no expression), 0,5 (low expression), 1 (moderate expression), 1,5-2 (high expression), and 2,5-3 (very high expression). The distribution of p63 and IRS1 expression in HNSCC specimens and normal tissues is shown in **A, B**. (**C**) Representative micrographs of immunohistochemical staining of p63 and IRS1 in HNSCC primary tumours (magnification: 40x). (**D-E**) Density distribution of RPKM values in normal (n=44; blue) and tumour (n=522: red) samples for p63 and IRS1 transcripts. Top right panels show an enlargement of the overlapping curves. Vertical black line indicates the optimal cutpoint between tumour and normal RPKM distributions, identified using *OptimalCutpoints* R package [96] *P-value* < 1.074e-10 for p63 and *P-value* < 0.004 for IRS1. (**F**) Pie charts representing the proportion of tumour samples with IRS1 up- or down-regulated in p63 up (left) and p63 down-regulated (right) tumour samples. Statistical significance of the contingency table represented by the 4 sub-dataset of tumour samples is p-value= 4.293e-07 (Fisher's exact test). Statistical tests (Wilcoxon and Fisher's exact tests) on TCGA gene expression data were performed in R.

DISCUSSION

It has been originally hypothesized that, ΔNp63 mainly exerts its oncogenic functions by acting as a dominant negative repressor of the tumour suppressive members of the p53 family, including TAp63. As a consequence of preventing access to their DNA binding sites, ΔNp63 would impinge on the transcription of genes involved in cell cycle control and cell death. In addition, emerging evidence has unveiled key tumour-related signalling pathways that are transcriptionally regulated by ΔNp63, in a p53 independent manner [89]. For instance, by acting in concert with the chromatin remodelling factor ACTL6A, p63 controls chromatin accessibility and functions as a direct transcriptional repressor of the Hippo/YAP regulator WWC1 in SCC [66]. Further-more, ΔNp63 controls a transcriptional program com-prising the hyaluronic acid (HA) synthase HAS3 and two hyaluronidase genes, HYAL-1 and HYAL-3, thus sustaining the pro-tumorigenic HA metabolism and signalling [59]. Abraham and collaborators [90] have recently identified components of the transforming growth factor-β signalling and the RHOA GTPase as targets and mediators of ΔNp63-dependent cell pro-liferation in SCCs.

Our data demonstrate that IRS1 is a direct target of transcriptional activation by ΔNp63 in HNSCC cells. Coherently, ΔNp63 and IRS1 expression patterns are positively correlated in primary tumours, suggesting

that the interaction of p63 and IRS1 might contribute to the pathogenesis of HNSCC. More broadly, in ΔNp63 overexpressing SSC tumours, unbalanced expression of the TAp63/ΔNp63 isoforms may lead to enhanced *Igfr1/Irs1* transcriptional activation, resulting in augmented protein abundance of IGFR1 and IRS1, which may increase sensitivity of cancer cells to growth factor stimulation (Figure 5). In addition, over-expression of ΔNp63 prevents expression of *Igfbp3* thus, ultimately, enhancing circulating IGF-1 (Fig. 5). Thus, the existence of a crosstalk between p63 and the IGF1 system may represent a mechanism by which tumours that overexpress ΔNp63 escape apoptosis and acquire a proliferative advantage.

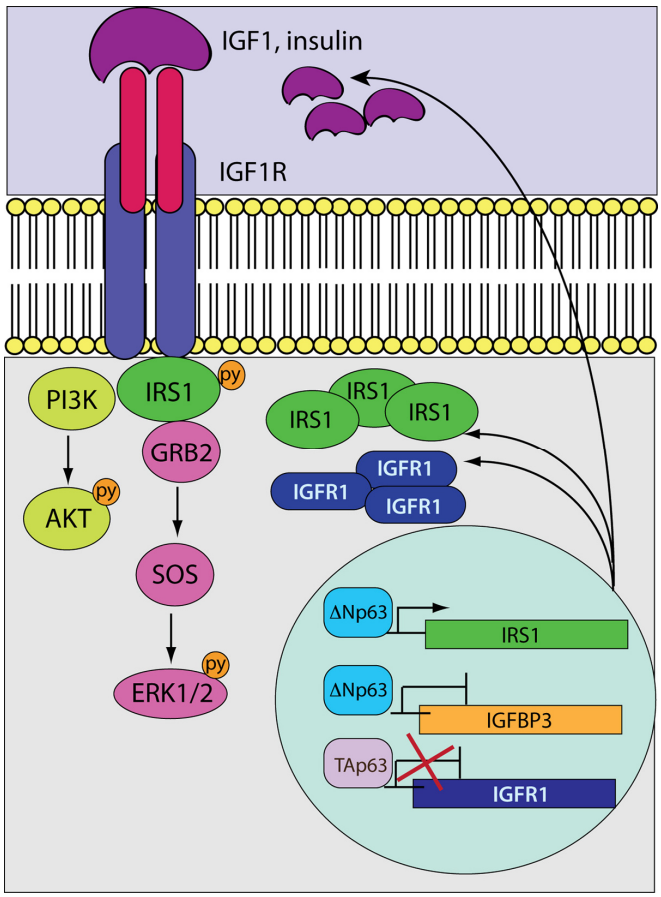

Figure 5. A model depicting the crosstalk between p63 and the IGF system. While the tumour suppressive TAp63 isoforms negatively control *Igf-1r* transcription, the oncogenic ΔNp63 variants induce and repress the expression of the *Irs1* and *Igfbp3* genes, respectively. In HNSCC cells overexpressing ΔNp63, the transcription of *Igf1r* would be stimulated as a result of the unbalanced ratio between the TA/ΔN p63 proteins. Aberrant accumulation of IGF1R and its docking protein IRS1 would enhance signalling activation in response to receptor stimulation. On the other hand, reduced expression levels of *Igfbp3* would increase the availability of circulating IGF1 that could further potentiate receptor activation.

Elevated levels of IRS1 have been reported to contribute to cancer development and progression [78, 80, 91, 92]. Notably, high expression of IRS1 in breast cancer cells was positively correlated with aberrant phosphorylation of AKT, which was significantly associated with lymph node metastasis [93]. Coherently, we observed reduced ligand-stimulated activation of AKT in p63-depleted cells, implying that reducing the cellular abundance of IRS1 could be a strategy to diminish the mitogenic potential of the IGF system. Acting as an adaptor protein that conveys signals originating from different receptors to multiple downstream signalling molecules, IRS1 represents a potentially relevant predictive clinical biomarkers for cancers susceptible to IGF-IR targeting.

Several reports have showed a correlation between the IGF pathway and HNSCC clinical parameters [80-84]. On the other hand, IGF pathway-related proteins have not been implemented as cancer biomarkers yet, due to the existence of contradictory findings on their prognostic impact. Indeed, negative correlations between levels of IGF1/IGF1R and clinical outcomes have been also reported in HNSCC [94]. Thus, in addition to unveiling alterations within the IGF system in tumours, the identification of alterations outside the IGF axis (*e.g.* upstream regulators), which may affect the IGF signalling, would be relevant to establish additional predictive markers for patient stratification and clinical management.

The controversial clinical data on the prognostic impact of the IGF system in HNSCC may reflect the high histopathological heterogeneity within this disease that includes tumours arising from various anatomical sites. Whether or not deregulation of the IGF signalling network and the positive regulation of IRS1 by ΔNp63 may have a prognostic significance for HNSCC are still relevant questions in the field, and further studies are needed to clarify these issues.

MATERIALS AND METHODS

Cells and culture conditions

Neonatal normal human epidermal keratinocytes (NHEKs, Life Technologies) were cultured in EpiLife medium with human keratinocyte growth supplements added (Life Technologies). FaDu (pharynx squamous cell carcinoma), SSC-090 (oral squamous cell carcinoma) and SSC-154 (tongue squamous cell carcinoma) cells were grown in Eagle's minimum essential medium (EMEM, Lonza, Basel, Switzerland); A253 cells (submaxillary salivary gland carcinoma) were cultured in McCoy's medium (Gibco, Invitrogen); SCC-9 cells (tongue squamous cell carcinoma) were cultured in1:1

mixture of Dulbecco's Modified Eagle's Medium (DMEM) and Ham's F-12 medium (DMEM F12, Gibco, Invitrogen) supplemented with 400 ng/mL hydrocortisone; CAL27 (tongue squamous cell carcinoma) and SCC-104 (oral squamous cell carcinoma) cells were grown in DMEM. All media were supplemented with 10% FBS, 100 U penicillin, and 100 µg/mL streptomycin (Gibco, Life Technologies). All HNSCC cell lines were purchased from ATCC and routinely tested for mycoplasma contaminations.

For p63 siRNA-mediated knockdown, NHEK and HNSCC cells were transfected with the following siRNAs: sip63#1 (SASI_Hs02_00326864) and sip63#2 (SASI_Hs02_00326867) oligos were purchased from Sigma-Aldrich; the sense strand of the siΔNp63 is: 5'-GAAGAAAGGACAGCAGCATTG -3'. The Negative Control siRNA (Qiagen, AATTCTCCGAACGTGTCA CGT) was used as a silencing control. All transfections were performed using the Lipofectamine RNAiMAX transfection reagent (Invitrogen) according to manufacturer's protocols.

RNA sequencing

RNA sequencing was performed as previously described [95]. Briefly, total RNA was extracted using a mirVana miRNA isolation kit (Thermo Fisher). rRNA was removed from each RNA extraction before proceeding with RNA seq library construction. Sequencing was performed on a SOLiD sequencer 5500XL (Applied Biosystems) with 75-base-pair single-end reads by Genomnia s.r.l. (Milan, Italy). Sequencing reads in SOLID "xsq" format were mapped to the hg19 genome built and analysed with the Lifetech Lifescope 2.5.1 Whole Transcriptomic analysis pipeline with the Integromics Seqsolve software and proprietary Genomnia procedures.

Real-time qPCR

Total RNA was extracted by the RNAeasy kit (Qiagen, Hilden, Germany). Total RNA (500ng) was used for reverse transcription using GoScript Reverse Transcription System kit (Promega, Fritchburg, WI, USA) following the manufacturer's instructions. Human *Tbp* mRNA was used as housekeeping gene for quantity normalization. qRT-PCR was performed using the Platinum SYBR Green qPCR SuperMix UDG (Invitrogen), using the following primer pairs: *Irs1* 5′-CTCAACTGGACATCACAGCAG -3′ (sense) and 5′-AGGTCCTAGTTGTGAATCATG -3′ (antisense); *TAp63* 5′- TCAGAAGATGGTGCGACAAAC -3′ (sense) and 5′- GTTCAGGAGCCCCAGGTTCG-3′ (antisense); *ΔNp63* 5′- GAAGAAAGGACAGCAGCA TTG -3′ (sense) and 5′- GGGACTGGTGGACGAGGA G -3′ (antisense). The PCR was monitored by a melting curve protocol according to the specifications of the ABI 7500 instrument (Applied Biosystems). Relative quantification of gene expression was calculated according to the $2^{-\Delta\Delta Ct}$ method. IRS1 expression was normalized on *Tbp* housekeeper.

Western blot analysis

Cells were lysed in SDS lysis buffer (100 mM Tris pH 8.8, 1% SDS, 5 mM EDTA, 20 mM DTT, and 2 mM AEBSF). Total protein extracts were resolved in SDS polyacrylamide gel and blotted onto a Hybond PVDF membrane (GE Healthcare, Chicago, IL, USA). After being blocked with PBST 5% non-fat dry milk (Bio-Rad), membranes were incubated over night with primary antibodies at +4°C, washed and hybridized for 1 h at room temperature using the appropriate horseradish peroxidase-conjugated secondary antibody (rabbit and mouse, Bio-Rad, Hercules, California, USA). Detection was performed with the ECL chemiluminescence kit (Perkin Elmer, Waltham, Massachusetts, USA). The following antibodies were used: anti-IRS1 (D32G12, Cell Signaling), anti-p63 (clone 4A4, Santa Cruz Biotechnology), anti-p-IRS1 (Ser612, clone C15H5, Cell Signaling), anti-p-AKT (Ser473, clone D9E, Cell Signaling), anti-AKT (clone #9272, Cell Signaling), anti-p-S6 Ribosomal Protein (Ser235/236, clone #2211, Cell Signaling), anti-S6 (Clone 5G10, Cell Signaling), anti-p44/42 MAPK (p-ERK1/2) (Thr202/Tyr204, Clone E10, Cell Signaling), anti-ERK1/2 (Clone 137F5, Cell Signaling).

Chromatin immunoprecipitation assay

Fadu cells were used for ChIP assay. Cells were collected, fixed in 1% formaldehyde, and subjected to sonication for DNA shearing. The ChIP assay was performed with an anti-p63 antibody (H129, Santa Cruz Biotechnology) or unspecific immunoglobulin G (IgG) (Invitrogen) using a ChIP assay Kit (Invitrogen). PCR validation was performed using primers spanning the p63-binding sites located within the genomic regions identified by ChIP-seq assays.

Luciferase assay

For luciferase assays, a total of 1.2×10^6 H1299 cells were seeded in 12-well dishes 24 h before transfection. In total, 30 ng of pGL3 reporter vector, 5 ng of pRL-CMV-*Renilla* luciferase vector (Promega) and 150 ng of HA-ΔNp63α expression vectors or empty pcDNA-HA vector (as a control) were cotransfected using the Effectene transfection reagent according to the manufacturer's instructions (Qiagen). The luciferase activities of cellular extracts were measured 24 h after trans-

fection using a Dual Luciferase Reporter Assay System (Promega). The light emission was measured over 10 sec using a Lumat LB9507 luminometer (EG&GBerthold). The transfection efficiency was normalized to *Renilla* luciferase activity. The p63 RE was mutated by site-directed mutagenesis using the forward primer: 5'-ATAAGGGCCTTCCTGTTCCGA GGCAGCCGTGTGAACCACC-3' and reverse primer: 5' - GGTGGTTCACACGGCTGCCTCGGAACAGGA AGGCCCTTAT-3'.

Human HNSCC tumour tissues

Tissue arrays including paraffin-embedded HNSCC (n=60), adenoid cystic carcinomas (n=7), adenocarcinomas (n=1), mucoepidermoid carcinomas (n=1), and normal tissues. (n=10) were purchased from US Biomax, Inc. (Rockville, MD). Samples were deparaffinized and rehydrated in 1x PBS for 10 min. Tissue sections were stained with anti-p63 (clone 4A4, Ventana) and IRS1 (Clone EP263Y, Abcam) antibodies. Immunoistochemistry (IHC) scoring was performed by two independent pathologists. The percentage of positive cells was rated as follows: 0, negative; 1, 1–25% positive cells; 2, 26–50% positive cells; 3, 51–75% positive cells; and 4, >75% positive cells. The staining intensity was scored as 0, negative; 1, weak; 2, moderate; and 3, intensive. For both stainings, the scores for the percentage of positive cells and those for the expression intensities were combined to calculate immunoreactive scores (IRSs) that are summarised in Table S1. According to the IRS, we grouped patients into five groups: 0 (no expression), 0,5 (low expression), 1 (moderate expression), 1,5-2 (high expression), and 2,5-3 (very high expression). Non squamous cell carcinomas of the head and neck were excluded from the analysis.

Computational methods

Publicly available gene expression data from TCGA were downloaded from the Genomic Data Commons (GDC) Data Portal and pre-processed via the *TCGAbiolinks* R package [96]. Harmonized and normalized RPKM data from GDC was downloaded for Head and Neck Squamous Cell Carcinomas (TCGA-HNSC).

RPKM distributions for each of the genes of interest have been analyzed either for tumor and normal samples in the HNSC cohort. A discrimination cutpoint between tumor and normal expression distributions either for TP63 and IRS1 has been detected using *OptimalCutpoints* R package [97]. The identified optimal cutoffs represent the RPKM values that maxi-mize the separation of gene expression distributions in tumor and normal samples. Data mining, statistical tests (Wilcoxon and Fisher's exact tests) and plots on TCGA gene expression data were performed in R.

Statistical analysis

The significance of differences between two experimental groups was calculated using the two-tailed Student's t-test. Values with $P<0.05$ were considered significant.

CONFLICTS OF INTEREST

The authors of this manuscript declare no conflicts of interest.

FUNDING

This work was partially supported by "Mission Sustainability" 2017 ("Head and neck squamous cell tumours: the identification of new biomarkers") to FB, by MFAG 2014 Id.15523 to AP, by the Medical Research Council (to GM), Associazione Italiana per la Ricerca contro il Cancro (AIRC) to GM IG#20473 (2018-2022), Fondazione Luigi Maria Monti IDI-IRCCS (RC to EC), Ministry of Health Italy-China cooperation grant. Work has been also supported by Regione Lazio through Lazio Innova Progetto Gruppo di Ricerca n 85-2017-14986.

REFERENCES

1. Lin MC, Chien PH, Wu HY, Chen ST, Juan HF, Lou PJ, Huang MC. C1GALT1 predicts poor prognosis and is a potential therapeutic target in head and neck cancer. Oncogene. 2018; 37:5780–93. https://doi.org/10.1038/s41388-018-0375-0

2. Aggarwal M, Saxena R, Sinclair E, Fu Y, Jacobs A, Dyba M, Wang X, Cruz I, Berry D, Kallakury B, Mueller SC, Agostino SD, Blandino G, et al. Reactivation of mutant p53 by a dietary-related compound phenethyl isothiocyanate inhibits tumor growth. Cell Death Differ. 2016; 23:1615–27. https://doi.org/10.1038/cdd.2016.48

3. Amelio I, Knight RA, Lisitsa A, Melino G, Antonov AV. p53MutaGene: an online tool to estimate the effect of p53 mutational status on gene regulation in cancer. Cell Death Dis. 2016; 7:e2148. https://doi.org/10.1038/cddis.2016.42

4. Alexandrova EM, Moll UM. Depleting stabilized GOF mutant p53 proteins by inhibiting molecular folding chaperones: a new promise in cancer therapy. Cell

Death Differ. 2017; 24:3–5. https://doi.org/10.1038/cdd.2016.145

5. Ghosh S, Salot S, Sengupta S, Navalkar A, Ghosh D, Jacob R, Das S, Kumar R, Jha NN, Sahay S, Mehra S, Mohite GM, Ghosh SK, et al. p53 amyloid formation leading to its loss of function: implications in cancer pathogenesis. Cell Death Differ. 2017; 24:1784–98. https://doi.org/10.1038/cdd.2017.105

6. Flores ER, Sengupta S, Miller JB, Newman JJ, Bronson R, Crowley D, Yang A, McKeon F, Jacks T. Tumor predisposition in mice mutant for p63 and p73: evidence for broader tumor suppressor functions for the p53 family. Cancer Cell. 2005; 7:363–73. https://doi.org/10.1016/j.ccr.2005.02.019

7. Galluzzi L, Vitale I, Aaronson SA, Abrams JM, Adam D, Agostinis P, Alnemri ES, Altucci L, Amelio I, Andrews DW, Annicchiarico-Petruzzelli M, Antonov AV, Arama E, et al. Molecular mechanisms of cell death: recommendations of the Nomenclature Committee on Cell Death 2018. Cell Death Differ. 2018; 25:486–541. https://doi.org/10.1038/s41418-017-0012-4

8. Gressner O, Schilling T, Lorenz K, Schulze Schleithoff E, Koch A, Schulze-Bergkamen H, Lena AM, Candi E, Terrinoni A, Catani MV, Oren M, Melino G, Krammer PH, et al. TAp63alpha induces apoptosis by activating signaling via death receptors and mitochondria. EMBO J. 2005; 24:2458–71. https://doi.org/10.1038/sj.emboj.7600708

9. Inoue S, Tomasini R, Rufini A, Elia AJ, Agostini M, Amelio I, Cescon D, Dinsdale D, Zhou L, Harris IS, Lac S, Silvester J, Li WY, et al. TAp73 is required for spermatogenesis and the maintenance of male fertility. Proc Natl Acad Sci USA. 2014; 111:1843–48. https://doi.org/10.1073/pnas.1323416111

10. Levine AJ, Tomasini R, McKeon FD, Mak TW, Melino G. The p53 family: guardians of maternal reproduction. Nat Rev Mol Cell Biol. 2011; 12:259–65. https://doi.org/10.1038/nrm3086

11. Marini A, Rotblat B, Sbarrato T, Niklison-Chirou MV, Knight JR, Dudek K, Jones C, Bushell M, Knight RA, Amelio I, Willis AE, Melino G. TAp73 contributes to the oxidative stress response by regulating protein synthesis. Proc Natl Acad Sci USA. 2018; 115:6219–24. https://doi.org/10.1073/pnas.1718531115

12. Baldelli S, Ciriolo MR. Altered S-nitrosylation of p53 is responsible for impaired antioxidant response in skeletal muscle during aging. Aging (Albany NY). 2016; 8:3450–67. https://doi.org/10.18632/aging.101139

13. Bourgeois B, Madl T. Regulation of cellular senescence via the FOXO4-p53 axis. FEBS Lett. 2018; 592:2083–97. https://doi.org/10.1002/1873-3468.13057

14. Guo X, Keyes WM, Papazoglu C, Zuber J, Li W, Lowe SW, Vogel H, Mills AA. TAp63 induces senescence and suppresses tumorigenesis in vivo. Nat Cell Biol. 2009; 11:1451–57. https://doi.org/10.1038/ncb1988

15. Regina C, Compagnone M, Peschiaroli A, Lena AM, Melino G, Candi E. ΔNp63α modulates histone methyl transferase SETDB1 to transcriptionally repress target genes in cancers. Cell Death Discov. 2016; 2:16015. https://doi.org/10.1038/cddiscovery.2016.15

16. Rivetti di Val Cervo P, Lena AM, Nicoloso M, Rossi S, Mancini M, Zhou H, Saintigny G, Dellambra E, Odorisio T, Mahé C, Calin GA, Candi E, Melino G. p63-microRNA feedback in keratinocyte senescence. Proc Natl Acad Sci USA. 2012; 109:1133–38. https://doi.org/10.1073/pnas.1112257109

17. Rufini A, Niklison-Chirou MV, Inoue S, Tomasini R, Harris IS, Marino A, Federici M, Dinsdale D, Knight RA, Melino G, Mak TW. TAp73 depletion accelerates aging through metabolic dysregulation. Genes Dev. 2012; 26:2009–14. https://doi.org/10.1101/gad.197640.112

18. Artigas N, Gámez B, Cubillos-Rojas M, Sánchez-de Diego C, Valer JA, Pons G, Rosa JL, Ventura F. p53 inhibits SP7/Osterix activity in the transcriptional program of osteoblast differentiation. Cell Death Differ. 2017; 24:2022–31. https://doi.org/10.1038/cdd.2017.113

19. Belle JI, Petrov JC, Langlais D, Robert F, Cencic R, Shen S, Pelletier J, Gros P, Nijnik A. Repression of p53-target gene Bbc3/PUMA by MYSM1 is essential for the survival of hematopoietic multipotent progenitors and contributes to stem cell maintenance. Cell Death Differ. 2016; 23:759–75. https://doi.org/10.1038/cdd.2015.140

20. Agostini M, Romeo F, Inoue S, Niklison-Chirou MV, Elia AJ, Dinsdale D, Morone N, Knight RA, Mak TW, Melino G. Metabolic reprogramming during neuronal differentiation. Cell Death Differ. 2016; 23:1502–14. https://doi.org/10.1038/cdd.2016.36

21. Charni M, Aloni-Grinstein R, Molchadsky A, Rotter V. p53 on the crossroad between regeneration and cancer. Cell Death Differ. 2017; 24:8–14. https://doi.org/10.1038/cdd.2016.117

22. Di Franco S, Sala G, Todaro M. p63 role in breast cancer. Aging (Albany NY). 2016; 8:2256–57. https://doi.org/10.18632/aging.101042

23. Gross A, Zaltsman Y, Maryanovich M. The ATM-BID pathway plays a critical role in the DNA damage response by regulating mitochondria metabolism. Cell

Death Differ. 2016; 23:182.
https://doi.org/10.1038/cdd.2015.154

24. Giacomello M, Pellegrini L. The coming of age of the mitochondria-ER contact: a matter of thickness. Cell Death Differ. 2016; 23:1417–27.
https://doi.org/10.1038/cdd.2016.52

25. Kagan VE, Jiang J, Huang Z, Tyurina YY, Desbourdes C, Cottet-Rousselle C, Dar HH, Verma M, Tyurin VA, Kapralov AA, Cheikhi A, Mao G, Stolz D, et al. NDPK-D (NM23-H4)-mediated externalization of cardiolipin enables elimination of depolarized mitochondria by mitophagy. Cell Death Differ. 2016; 23:1140–51.
https://doi.org/10.1038/cdd.2015.160

26. Martin-Lopez M, Maeso-Alonso L, Fuertes-Alvarez S, Balboa D, Rodríguez-Cortez V, Weltner J, Diez-Prieto I, Davis A, Wu Y, Otonkoski T, Flores ER, Menéndez P, Marques MM, Marin MC. p73 is required for appropriate BMP-induced mesenchymal-to-epithelial transition during somatic cell reprogramming. Cell Death Dis. 2017; 8:e3034.
https://doi.org/10.1038/cddis.2017.432

27. Lovat PE, Ranalli M, Annichiarrico-Petruzzelli M, Bernassola F, Piacentini M, Malcolm AJ, Pearson AD, Melino G, Redfern CP. Effector mechanisms of fenretinide-induced apoptosis in neuroblastoma. Exp Cell Res. 2000; 260:50–60.
https://doi.org/10.1006/excr.2000.4988

28. Tóth B, Garabuczi E, Sarang Z, Vereb G, Vámosi G, Aeschlimann D, Blaskó B, Bécsi B, Erdõdi F, Lacy-Hulbert A, Zhang A, Falasca L, Birge RB, et al. Transglutaminase 2 is needed for the formation of an efficient phagocyte portal in macrophages engulfing apoptotic cells. J Immunol. 2009; 182:2084–92.
https://doi.org/10.4049/jimmunol.0803444

29. Zhao J, Yin M, Deng H, Jin FQ, Xu S, Lu Y, Mastrangelo MA, Luo H, Jin ZG. Cardiac Gab1 deletion leads to dilated cardiomyopathy associated with mitochondrial damage and cardiomyocyte apoptosis. Cell Death Differ. 2016; 23:695–706.
https://doi.org/10.1038/cdd.2015.143

30. Van Nostrand JL, Bowen ME, Vogel H, Barna M, Attardi LD. The p53 family members have distinct roles during mammalian embryonic development. Cell Death Differ. 2017; 24:575–79.
https://doi.org/10.1038/cdd.2016.128

31. Xu-Monette ZY, Zhang S, Li X, Manyam GC, Wang XX, Xia Y, Visco C, Tzankov A, Zhang L, Montes-Moreno S, Dybkaer K, Chiu A, Orazi A, et al. p63 expression confers significantly better survival outcomes in high-risk diffuse large B-cell lymphoma and demonstrates p53-like and p53-independent tumor suppressor function. Aging (Albany NY). 2016; 8:345–65.
https://doi.org/10.18632/aging.100898

32. Tak H, Eun JW, Kim J, Park SJ, Kim C, Ji E, Lee H, Kang H, Cho DH, Lee K, Kim W, Nam SW, Lee EK. T-cell-restricted intracellular antigen 1 facilitates mitochondrial fragmentation by enhancing the expression of mitochondrial fission factor. Cell Death Differ. 2017; 24:49–58.
https://doi.org/10.1038/cdd.2016.90

33. Dey-Rao R, Sinha AA. Interactome analysis of gene expression profile reveals potential novel key transcriptional regulators of skin pathology in vitiligo. Genes Immun. 2016; 17:30–45.
https://doi.org/10.1038/gene.2015.48

34. Gianfrancesco MA, Balzer L, Taylor KE, Trupin L, Nititham J, Seldin MF, Singer AW, Criswell LA, Barcellos LF. Genetic risk and longitudinal disease activity in systemic lupus erythematosus using targeted maximum likelihood estimation. Genes Immun. 2016; 17:358–62.
https://doi.org/10.1038/gene.2016.33

35. Greschik H, Duteil D, Messaddeq N, Willmann D, Arrigoni L, Sum M, Jung M, Metzger D, Manke T, Günther T, Schüle R. The histone code reader Spin1 controls skeletal muscle development. Cell Death Dis. 2017; 8:e3173.
https://doi.org/10.1038/cddis.2017.468

36. Hussman JP, Beecham AH, Schmidt M, Martin ER, McCauley JL, Vance JM, Haines JL, Pericak-Vance MA. GWAS analysis implicates NF-κB-mediated induction of inflammatory T cells in multiple sclerosis. Genes Immun. 2016; 17:305–12.
https://doi.org/10.1038/gene.2016.23

37. Salsman J, Rapkin LM, Margam NN, Duncan R, Bazett-Jones DP, Dellaire G. Myogenic differentiation triggers PML nuclear body loss and DAXX relocalization to chromocentres. Cell Death Dis. 2017; 8:e2724. https://doi.org/10.1038/cddis.2017.151

38. Baraibar MA, Hyzewicz J, Rogowska-Wrzesinska A, Bulteau AL, Prip-Buus C, Butler-Browne G, Friguet B. Impaired energy metabolism of senescent muscle satellite cells is associated with oxidative modifications of glycolytic enzymes. Aging (Albany NY). 2016; 8:3375–89.
https://doi.org/10.18632/aging.101126

39. Brzeszczyńska J, Johns N, Schilb A, Degen S, Degen M, Langen R, Schols A, Glass DJ, Roubenoff R, Greig CA, Jacobi C, Fearon KC, Ross JA. Loss of oxidative defense and potential blockade of satellite cell maturation in the skeletal muscle of patients with cancer but not in the healthy elderly. Aging (Albany NY). 2016; 8:1690–702.
https://doi.org/10.18632/aging.101006

40. Choi JY, Hwang CY, Lee B, Lee SM, Bahn YJ, Lee KP, Kang M, Kim YS, Woo SH, Lim JY, Kim E, Kwon KS. Age-associated repression of type 1 inositol 1, 4, 5-triphosphate receptor impairs muscle regeneration. Aging (Albany NY). 2016; 8:2062–80. https://doi.org/10.18632/aging.101039

41. Fiacco E, Castagnetti F, Bianconi V, Madaro L, De Bardi M, Nazio F, D'Amico A, Bertini E, Cecconi F, Puri PL, Latella L. Autophagy regulates satellite cell ability to regenerate normal and dystrophic muscles. Cell Death Differ. 2016; 23:1839–49. https://doi.org/10.1038/cdd.2016.70

42. Honrath B, Matschke L, Meyer T, Magerhans L, Perocchi F, Ganjam GK, Zischka H, Krasel C, Gerding A, Bakker BM, Bünemann M, Strack S, Decher N, et al. SK2 channels regulate mitochondrial respiration and mitochondrial Ca2+ uptake. Cell Death Differ. 2017; 24:761–73. https://doi.org/10.1038/cdd.2017.2

43. Kaufman DM, Wu X, Scott BA, Itani OA, Van Gilst MR, Bruce JE, Crowder CM. Ageing and hypoxia cause protein aggregation in mitochondria. Cell Death Differ. 2017; 24:1730–38. https://doi.org/10.1038/cdd.2017.101

44. Pinto M, Pickrell AM, Wang X, Bacman SR, Yu A, Hida A, Dillon LM, Morton PD, Malek TR, Williams SL, Moraes CT. Transient mitochondrial DNA double strand breaks in mice cause accelerated aging phenotypes in a ROS-dependent but p53/p21-independent manner. Cell Death Differ. 2017; 24:288–99. https://doi.org/10.1038/cdd.2016.123

45. Qi Y, Liu H, Daniels MP, Zhang G, Xu H. Loss of Drosophila i-AAA protease, dYME1L, causes abnormal mitochondria and apoptotic degeneration. Cell Death Differ. 2016; 23:291–302. https://doi.org/10.1038/cdd.2015.94

46. Kaestner L, Minetti G. The potential of erythrocytes as cellular aging models. Cell Death Differ. 2017; 24:1475–77. https://doi.org/10.1038/cdd.2017.100

47. Kanemaru K, Nakamura Y, Totoki K, Fukuyama T, Shoji M, Kaneko H, Shiratori K, Yoneda A, Inoue T, Iwakura Y, Kabashima K, Fukami K. Phospholipase Cδ1 regulates p38 MAPK activity and skin barrier integrity. Cell Death Differ. 2017; 24:1079–90. https://doi.org/10.1038/cdd.2017.56

48. Fortini P, Ferretti C, Iorio E, Cagnin M, Garribba L, Pietraforte D, Falchi M, Pascucci B, Baccarini S, Morani F, Phadngam S, De Luca G, Isidoro C, Dogliotti E. The fine tuning of metabolism, autophagy and differentiation during in vitro myogenesis. Cell Death Dis. 2016; 7:e2168. https://doi.org/10.1038/cddis.2016.50

49. Lee SJ, Hwang J, Jeong HJ, Yoo M, Go GY, Lee JR, Leem YE, Park JW, Seo DW, Kim YK, Hahn MJ, Han JW, Kang JS, Bae GU. PKN2 and Cdo interact to activate AKT and promote myoblast differentiation. Cell Death Dis. 2016; 7:e2431. https://doi.org/10.1038/cddis.2016.296

50. Li G, Luo W, Abdalla BA, Ouyang H, Yu J, Hu F, Nie Q, Zhang X. miRNA-223 upregulated by MYOD inhibits myoblast proliferation by repressing IGF2 and facilitates myoblast differentiation by inhibiting ZEB1. Cell Death Dis. 2017; 8:e3094. https://doi.org/10.1038/cddis.2017.479

51. Palazzo E, Kellett MD, Cataisson C, Bible PW, Bhattacharya S, Sun HW, Gormley AC, Yuspa SH, Morasso MI. A novel DLX3-PKC integrated signaling network drives keratinocyte differentiation. Cell Death Differ. 2017; 24:717–30. https://doi.org/10.1038/cdd.2017.5

52. Shao AW, Sun H, Geng Y, Peng Q, Wang P, Chen J,

Xiong T, Cao R, Tang J. Bclaf1 is an important NF-κB signaling transducer and C/EBPβ regulator in DNA damage-induced senescence. Cell Death Differ. 2016; 23:865–75. https://doi.org/10.1038/cdd.2015.150

53. Tajhya RB, Hu X, Tanner MR, Huq R, Kongchan N, Neilson JR, Rodney GG, Horrigan FT, Timchenko LT, Beeton C. Functional KCa1.1 channels are crucial for regulating the proliferation, migration and differentiation of human primary skeletal myoblasts. Cell Death Dis. 2016; 7:e2426. https://doi.org/10.1038/cddis.2016.324

54. Wei X, Li H, Yang J, Hao D, Dong D, Huang Y, Lan X, Plath M, Lei C, Lin F, Bai Y, Chen H. Circular RNA profiling reveals an abundant circLMO7 that regulates myoblasts differentiation and survival by sponging miR-378a-3p. Cell Death Dis. 2017; 8:e3153. https://doi.org/10.1038/cddis.2017.541

55. Zhai L, Wu R, Han W, Zhang Y, Zhu D. miR-127 enhances myogenic cell differentiation by targeting S1PR3. Cell Death Dis. 2017; 8:e2707. https://doi.org/10.1038/cddis.2017.128

56. De Laurenzi V, Melino G. Evolution of functions within the p53/p63/p73 family. Ann N Y Acad Sci. 2000; 926:90–100. https://doi.org/10.1111/j.1749-6632.2000.tb05602.x

57. Candi E, Schmidt R, Melino G. The cornified envelope: a model of cell death in the skin. Nat Rev Mol Cell Biol. 2005; 6:328–40. https://doi.org/10.1038/nrm1619

58. Candi E, Terrinoni A, Rufini A, Chikh A, Lena AM, Suzuki Y, Sayan BS, Knight RA, Melino G. p63 is upstream of IKK α in epidermal development. J Cell Sci. 2006; 119:4617–22.

https://doi.org/10.1242/jcs.03265

59. Compagnone M, Gatti V, Presutti D, Ruberti G, Fierro C, Markert EK, Vousden KH, Zhou H, Mauriello A, Anemone L, Bongiorno-Borbone L, Melino G, Peschiaroli A. ΔNp63-mediated regulation of hyaluronic acid metabolism and signaling supports HNSCC tumorigenesis. Proc Natl Acad Sci USA. 2017; 114:13254–59. https://doi.org/10.1073/pnas.1711777114

60. Novelli F, Lena AM, Panatta E, Nasser W, Shalom-Feuerstein R, Candi E, Melino G. Allele-specific silencing of EEC p63 mutant R304W restores p63 transcriptional activity. Cell Death Dis. 2016; 7:e2227. https://doi.org/10.1038/cddis.2016.118

61. Candi E, Amelio I, Agostini M, Melino G. MicroRNAs and p63 in epithelial stemness. Cell Death Differ. 2015; 22:12–21. https://doi.org/10.1038/cdd.2014.113

62. Candi E, Rufini A, Terrinoni A, Dinsdale D, Ranalli M, Paradisi A, De Laurenzi V, Spagnoli LG, Catani MV, Ramadan S, Knight RA, Melino G. Differential roles of p63 isoforms in epidermal development: selective genetic complementation in p63 null mice. Cell Death Differ. 2006; 13:1037–47. https://doi.org/10.1038/sj.cdd.4401926

63. Chakrabarti R, Wei Y, Hwang J, Hang X, Andres Blanco M, Choudhury A, Tiede B, Romano RA, DeCoste C, Mercatali L, Ibrahim T, Amadori D, Kannan N, et al. ΔNp63 promotes stem cell activity in mammary gland development and basal-like breast cancer by enhancing Fzd7 expression and Wnt signalling. Nat Cell Biol. 2014; 16:1004–15, 1–13. https://doi.org/10.1038/ncb3040

64. Memmi EM, Sanarico AG, Giacobbe A, Peschiaroli A, Frezza V, Cicalese A, Pisati F, Tosoni D, Zhou H, Tonon G, Antonov A, Melino G, Pelicci PG, Bernassola F. p63 Sustains self-renewal of mammary cancer stem cells through regulation of Sonic Hedgehog signaling. Proc Natl Acad Sci USA. 2015; 112:3499–504. https://doi.org/10.1073/pnas.1500762112

65. Cancer Genome Atlas N, and Cancer Genome Atlas Network. Comprehensive genomic characterization of head and neck squamous cell carcinomas. Nature. 2015; 517:576–82. https://doi.org/10.1038/nature14129

66. Saladi SV, Ross K, Karaayvaz M, Tata PR, Mou H, Rajagopal J, Ramaswamy S, Ellisen LW. ACTL6A Is co-Amplified with p63 in squamous cell carcinoma to drive YAP activation, regenerative proliferation, and poor prognosis. Cancer Cell. 2017; 31:35–49. https://doi.org/10.1016/j.ccell.2016.12.001

67. Campbell JD, Yau C, Bowlby R, Liu Y, Brennan K, Fan H, Taylor AM, Wang C, Walter V, Akbani R, Byers LA, Creighton CJ, Coarfa C, et al, and Cancer Genome Atlas Research Network. Genomic, Pathway Network, and Immunologic Features Distinguishing Squamous Carcinomas. Cell Reports. 2018; 23:194–212.e6. https://doi.org/10.1016/j.celrep.2018.03.063

68. Rocco JW, Leong CO, Kuperwasser N, DeYoung MP, Ellisen LW. p63 mediates survival in squamous cell carcinoma by suppression of p73-dependent apoptosis. Cancer Cell. 2006; 9:45–56. https://doi.org/10.1016/j.ccr.2005.12.013

69. Yang X, Lu H, Yan B, Romano RA, Bian Y, Friedman J, Duggal P, Allen C, Chuang R, Ehsanian R, Si H, Sinha S, Van Waes C, Chen Z. ΔNp63 versatilely regulates a Broad NF-κB gene program and promotes squamous epithelial proliferation, migration, and inflammation. Cancer Res. 2011; 71:3688–700. https://doi.org/10.1158/0008-5472.CAN-10-3445

70. Lo Muzio L, Santarelli A, Caltabiano R, Rubini C, Pieramici T, Trevisiol L, Carinci F, Leonardi R, De Lillo A, Lanzafame S, Bufo P, Piattelli A. p63 over-expression associates with poor prognosis in head and neck squamous cell carcinoma. Hum Pathol. 2005; 36:187–94. https://doi.org/10.1016/j.humpath.2004.12.003

71. Chen Y, Li Y, Peng Y, Zheng X, Fan S, Yi Y, Zeng P, Chen H, Kang H, Zhang Y, Xiao ZX, Li C. ΔNp63α down-regulates c-Myc modulator MM1 via E3 ligase HERC3 in the regulation of cell senescence. Cell Death Differ. 2018; 25:2118-29. https://doi.org/10.1038/s41418-018-0132-5

72. Si H, Lu H, Yang X, Mattox A, Jang M, Bian Y, Sano E, Viadiu H, Yan B, Yau C, Ng S, Lee SK, Romano RA, et al. TNF-α modulates genome-wide redistribution of ΔNp63α/TAp73 and NF-κB cREL interactive binding on TP53 and AP-1 motifs to promote an oncogenic gene program in squamous cancer. Oncogene. 2016; 35:5781–94. https://doi.org/10.1038/onc.2016.112

73. Carvalho E, Jansson PA, Axelsen M, Eriksson JW, Huang X, Groop L, Rondinone C, Sjöström L, Smith U. Low cellular IRS 1 gene and protein expression predict insulin resistance and NIDDM. FASEB J. 1999; 13:2173–78. https://doi.org/10.1096/fasebj.13.15.2173

74. Zhou Y, Zhang Z, Wang N, Chen J, Zhang X, Guo M, John Zhong L, Wang Q. Suppressor of cytokine signalling-2 limits IGF1R-mediated regulation of epithelial-mesenchymal transition in lung adeno-carcinoma. Cell Death Dis. 2018; 9:429. https://doi.org/10.1038/s41419-018-0457-5

75. Law JH, Habibi G, Hu K, Masoudi H, Wang MY, Stratford AL, Park E, Gee JM, Finlay P, Jones HE,

Nicholson RI, Carboni J, Gottardis M, et al. Phosphorylated insulin-like growth factor-i/insulin receptor is present in all breast cancer subtypes and is related to poor survival. Cancer Res. 2008; 68:10238–46. https://doi.org/10.1158/0008-5472.CAN-08-2755

76. Jameson MJ, Beckler AD, Taniguchi LE, Allak A, Vanwagner LB, Lee NG, Thomsen WC, Hubbard MA, Thomas CY. Activation of the insulin-like growth factor-1 receptor induces resistance to epidermal growth factor receptor antagonism in head and neck squamous carcinoma cells. Mol Cancer Ther. 2011; 10:2124–34. https://doi.org/10.1158/1535-7163.MCT-11-0294

77. Chang Q, Li Y, White MF, Fletcher JA, Xiao S. Constitutive activation of insulin receptor substrate 1 is a frequent event in human tumors: therapeutic implications. Cancer Res. 2002; 62:6035–38.

78. Koda M, Sulkowska M, Kanczuga-Koda L, Sulkowski S. Expression of insulin receptor substrate 1 in primary breast cancer and lymph node metastases. J Clin Pathol. 2005; 58:645–49. https://doi.org/10.1136/jcp.2004.022590

79. Chan JM, Stampfer MJ, Giovannucci E, Gann PH, Ma J, Wilkinson P, Hennekens CH, Pollak M. Plasma insulin-like growth factor-I and prostate cancer risk: a prospective study. Science. 1998; 279:563–66. https://doi.org/10.1126/science.279.5350.563

80. Luo J, Wen Q, Li J, Xu L, Chu S, Wang W, Shi L, Xie G, Huang D, Fan S. Increased expression of IRS-1 is associated with lymph node metastasis in nasopharyngeal carcinoma. Int J Clin Exp Pathol. 2014; 7:6117–24.

81. Dale OT, Aleksic T, Shah KA, Han C, Mehanna H, Rapozo DC, Sheard JD, Goodyear P, Upile NS, Robinson M, Jones TM, Winter S, Macaulay VM. IGF-1R expression is associated with HPV-negative status and adverse survival in head and neck squamous cell cancer. Carcinogenesis. 2015; 36:648–55. https://doi.org/10.1093/carcin/bgv053

82. Lara PC, Bordón E, Rey A, Moreno M, Lloret M, Henríquez-Hernández LA. IGF-1R expression predicts clinical outcome in patients with locally advanced oral squamous cell carcinoma. Oral Oncol. 2011; 47:615–19. https://doi.org/10.1016/j.oraloncology.2011.05.005

83. Wu X, Zhao H, Do KA, Johnson MM, Dong Q, Hong WK, Spitz MR. Serum levels of insulin growth factor (IGF-I) and IGF-binding protein predict risk of second primary tumors in patients with head and neck cancer. Clin Cancer Res. 2004; 10:3988–95. https://doi.org/10.1158/1078-0432.CCR-03-0762

84. Sun JM, Jun HJ, Ko YH, Park YH, Ahn YC, Son YI, Baek JH, Park K, Ahn MJ. Insulin-like growth factor binding protein-3, in association with IGF-1 receptor, can predict prognosis in squamous cell carcinoma of the head and neck. Oral Oncol. 2011; 47:714–19. https://doi.org/10.1016/j.oraloncology.2011.06.007

85. Nahor I, Abramovitch S, Engeland K, Werner H. The p53-family members p63 and p73 inhibit insulin-like growth factor-I receptor gene expression in colon cancer cells. Growth Horm IGF Res. 2005; 15:388–96. https://doi.org/10.1016/j.ghir.2005.07.005

86. Barbieri CE, Perez CA, Johnson KN, Ely KA, Billheimer D, Pietenpol JA. IGFBP-3 is a direct target of transcriptional regulation by DeltaNp63alpha in squamous epithelium. Cancer Res. 2005; 65:2314–20. https://doi.org/10.1158/0008-5472.CAN-04-3449

87. Kouwenhoven EN, van Heeringen SJ, Tena JJ, Oti M, Dutilh BE, Alonso ME, de la Calle-Mustienes E, Smeenk L, Rinne T, Parsaulian L, Bolat E, Jurgelenaite R, Huynen MA, et al. Genome-wide profiling of p63 DNA-binding sites identifies an element that regulates gene expression during limb development in the 7q21 SHFM1 locus. PLoS Genet. 2010; 6:e1001065. https://doi.org/10.1371/journal.pgen.1001065

88. Weinstein JN, Collisson EA, Mills GB, Shaw KR, Ozenberger BA, Ellrott K, Shmulevich I, Sander C, Stuart JM, and Cancer Genome Atlas Research Network. The Cancer Genome Atlas Pan-Cancer analysis project. Nat Genet. 2013; 45:1113–20. https://doi.org/10.1038/ng.2764

89. Candi E, Agostini M, Melino G, Bernassola F. How the TP53 family proteins TP63 and TP73 contribute to tumorigenesis: regulators and effectors. Hum Mutat. 2014; 35:702–14. https://doi.org/10.1002/humu.22523

90. Abraham CG, Ludwig MP, Andrysik Z, Pandey A, Joshi M, Galbraith MD, Sullivan KD, Espinosa JM. ΔNp63α Suppresses TGFB2 Expression and RHOA Activity to Drive Cell Proliferation in Squamous Cell Carcinomas. Cell Reports. 2018; 24:3224–36. https://doi.org/10.1016/j.celrep.2018.08.058

91. Tanaka S, Wands JR. Insulin receptor substrate 1 overexpression in human hepatocellular carcinoma cells prevents transforming growth factor beta1-induced apoptosis. Cancer Res. 1996; 56:3391–94.

92. Xu H, Lee MS, Tsai PY, Adler AS, Curry NL, Challa S, Freinkman E, Hitchcock DS, Copps KD, White MF, Bronson RT, Marcotrigiano M, Wu Y, et al. Ablation of insulin receptor substrates 1 and 2 suppresses Kras-driven lung tumorigenesis. Proc Natl Acad Sci USA. 2018; 115:4228–33.

https://doi.org/10.1073/pnas.1718414115

93. Luo J, Feng J, Wen Q, Qoyawayma C, Wang W, Chen L, Lu J, Zhan Y, Xu L, Zang H, Fan S, Chu S. Elevated expression of IRS-1 associates with phosphorylated Akt expression and predicts poor prognosis of breast invasive ductal carcinoma. Hum Pathol. 2018; 79:9–17. https://doi.org/10.1016/j.humpath.2018.03.003

94. Matuschek C, Rudoy M, Peiper M, Gerber PA, Hoff NP, Buhren BA, Flehmig B, Budach W, Knoefel WT, Bojar H, Prisack HB, Steinbach G, Shukla V, et al. Do insulin-like growth factor associated proteins qualify as a tumor marker? Results of a prospective study in 163 cancer patients. Eur J Med Res. 2011; 16:451–56. https://doi.org/10.1186/2047-783X-16-10-451

95. Smirnov A, Lena AM, Cappello A, Panatta E, Anemona L, Bischetti S, Annicchiarico-Petruzzelli M, Mauriello A, Melino G, Candi E. ZNF185 is a p63 target gene critical for epidermal differentiation and squamous cell carcinoma development. Oncogene; 2018. https://doi.org/10.1038/s41388-018-0509-4. Epub ahead of print

96. Colaprico A, Silva TC, Olsen C, Garofano L, Cava C, Garolini D, Sabedot TS, Malta TM, Pagnotta SM, Castiglioni I, Ceccarelli M, Bontempi G, Noushmehr H. TCGAbiolinks: an R/Bioconductor package for integrative analysis of TCGA data. Nucleic Acids Res. 2016; 44:e71. https://doi.org/10.1093/nar/gkv1507

97. Lopez-Raton M, Cadarso-Suarez C, Rodriguez-Alvarez MX, Gude-Sampedro F. Optimal cutpoints: an R package for selecting optimal cutpoints in diagnostic tests. J Stat Softw. 2014; 61:1–36. https://doi.org/10.18637/jss.v061.i08

SUPPLEMENTARY MATERIAL

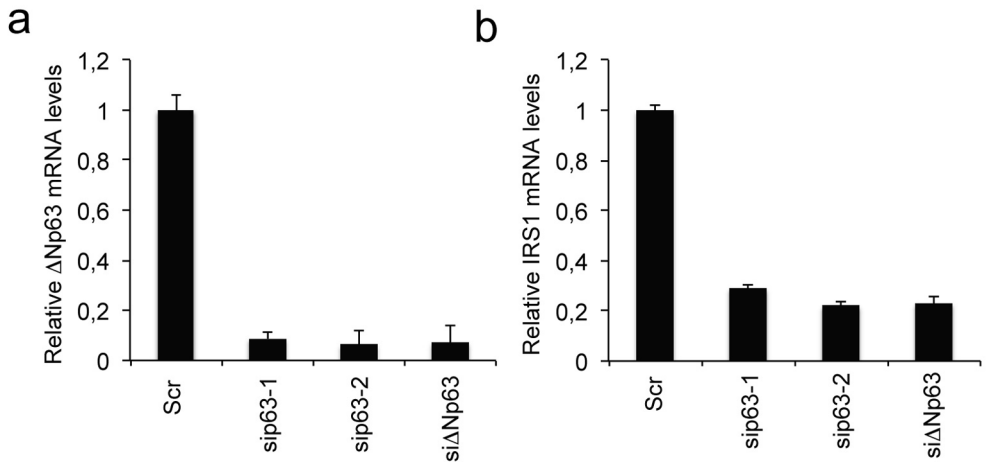

Supplementary Figure 1. Effect of distinct siRNAs against p63 on IRS1 expression.

Supplementary Table S1. Clinical features of HNSCC patients (as provided by Biomax), whose tumour samples were analysed for p63/IRS1 expression levels.

Patient sample	p63 Score	IRS1 Score	Organ	PATHOLOGY DIAGNOSIS	GRADE	STAGE	TNM	TYPE †	SEX	AGE
A1	0	0,5	Lip	Squamous cell carcinoma of right lower lip	1	IIA	T2N0M0	Malignant	F	60
A2	2	1	Nose	Squamous cell carcinoma of right nasal cavity	1	I	T1N0M0	Malignant	F	45
A3	0,5	1	Tongue	Squamous cell carcinoma	1	III	T3N1M0	Malignant	M	28
A4	0,5	0,5	Tongue	Squamous cell carcinoma	1	II	T2N0M0	Malignant	M	42
A5	1	1	Tongue	Squamous cell carcinoma	1	IIA	T2N0M0	Malignant	M	50
A6	1,5	0,5	Larynx	Squamous cell carcinoma	1	II	T2N0M0	Malignant	M	45
A7	0,5	1	Larynx	Squamous cell carcinoma	1	IVA	T4N0M0	Malignant	M	49
A8	1,5	1	Larynx	Squamous cell carcinoma	1	II	T2N0M0	Malignant	M	66
A9	0,5	1,5	Larynx	Squamous cell carcinoma	1	IVA	T4N0M0	Malignant	M	47
A10	0,5	0,5	Larynx	Squamous cell carcinoma	–	IV	T4N0M0	Malignant	M	60
B1	0,5	0,5	Larynx	Squamous cell carcinoma	1	II	T2N0M0	Malignant	M	51
B2	1,5	1,5	Larynx	Squamous cell carcinoma	2	IIB	T2N1M0	Malignant	M	59
B3	0,5	2	Cheek	Squamous cell carcinoma of left cheek	1	II	T2N0M0	Malignant	M	37
B4	3	3	Face	Squamous cell carcinoma	1	III	T3N0M0	Malignant	M	83
B5	1,5	1	Face	Squamous cell carcinoma of mandible	1	III	T3N0M0	Malignant	M	57
B6	0	1	Cheek	Squamous cell carcinoma of buccal region	1	II	T2N0M0	Malignant	M	70
B7	2	0,5	Oral cavity	Squamous cell carcinoma of gingiva	1	III	T3N0M0	Malignant	M	60
B8	0,5	1	Oral cavity	Squamous cell carcinoma of left maxillary sinus	1	III	T3N0M0	Malignant	M	55
B9	2,5	0,5	Oral cavity	Squamous cell carcinoma of upper jaw	1	IV	T4N0M0	Malignant	M	40
B10	1,5	1	Tongue	Squamous cell carcinoma	1	II	T2N0M0	Malignant	M	58
C1	3	0	Larynx	Squamous cell carcinoma	2	IIB	T2N1M0	Malignant	M	45
C2	1,5	0,5	Larynx	Squamous cell carcinoma	2	IV	T4N0M0	Malignant	M	50
C3	2,5	0	Larynx	Squamous cell carcinoma	2	IV	T2N2M0	Malignant	M	54
C4	1	0	Larynx	Squamous cell carcinoma	2	II	T2N0M0	Malignant	M	64
C5	3	1	Face	Squamous cell carcinoma of left face	2	I	T1N0M0	Malignant	M	65
C6	2,5	0	Larynx	Squamous cell carcinoma	2	IVA	T4N0M0	Malignant	M	49
C7	1	0	Larynx	Squamous cell carcinoma	3	I	T1N0M0	Malignant	M	48
C8	0	1	Larynx	Squamous cell carcinoma	2	II	T2N0M0	Malignant	M	55
C9	2	0,5	Larynx	Squamous cell carcinoma	2	III	T3N0M0	Malignant	M	72
C10	1	0	Larynx	Squamous cell carcinoma	3	IV	T4N0M0	Malignant	M	59
D1	1	1	Larynx	Squamous cell carcinoma	2	II	T2N0M0	Malignant	M	55
D2	1	1	Larynx	Squamous cell carcinoma	2	II	T2N0M0	Malignant	M	54

D4	1,5	0,5	Larynx	Squamous cell carcinoma	2	IV	T4N0M0	Malignant	M	65
D5	3	0,5	Larynx	Squamous cell carcinoma	2	III	T3N0M0	Malignant	M	75
D6	3	0,5	Larynx	Squamous cell carcinoma	2	IVA	T4N1M0	Malignant	M	64
D7	3	1,5	Larynx	Squamous cell carcinoma	3	III	T3N1M0	Malignant	F	70
D8	1	0	Oral cavity	Squamous cell carcinoma of hypopharynx	3	IV	T1N1M1	Malignant	M	53
D9	0	0,5	Larynx	Squamous cell carcinoma	3	III	T2N1M0	Malignant	M	54
D10	0	0,5	Nose	Squamous cell carcinoma of sinus piriformis	3	II	T2N0M0	Malignant	M	50
E1	1	0,5	Oral cavity	Squamous cell carcinoma of maxillary sinus	3	IIB	T2N1M0	Malignant	F	72
E2	1,5	0,5	Oral cavity	Squamous cell carcinoma of left maxillary sinus	3	I	T1N0M0	Malignant	F	51
E3	3	1	Larynx	Squamous cell carcinoma	2	IIA	T2N0M0	Malignant	M	71
E4	1,5	0	Larynx	Squamous cell carcinoma	3	IIA	T2N0M0	Malignant	F	62
E5	3	0,5	Larynx	Squamous cell carcinoma	3	III	T3N0M0	Malignant	M	58
E6	2,5	0,5	Larynx	Squamous cell carcinoma of left mandible	3	IIA	T2N0M0	Malignant	M	62
E7	2	0,5	Larynx	Squamous cell carcinoma	3	IIA	T2N0M0	Malignant	M	72
E8	2	0,5	Larynx	Squamous cell carcinoma	2	IIA	T2N0M0	Malignant	M	73
E10	3	0,5	Larynx	Squamous cell carcinoma	3	IVA	T4N0M0	Malignant	M	64
F1	3	0	Larynx	Squamous cell carcinoma	2	–	T3N2M0	Malignant	M	57
F2	1,5	0,5	Larynx	Squamous cell carcinoma of left nasal cavity	2	III	T3N0M0	Malignant	M	43
F3	3	0,5	Larynx	Squamous cell carcinoma	3	III	T3N0M0	Malignant	M	71
F4	1,5	0	Larynx	Squamous cell carcinoma	3	IV	T4N1M0	Malignant	M	67
F5	3	0	Larynx	Squamous cell carcinoma	3	IV	T3N2M0	Malignant	M	65
F6	1,5	0,5	Larynx	Squamous cell carcinoma	3	IV	T4N0M0	Malignant	M	68
F7	2	1	Larynx	Squamous cell carcinoma	2	II	T2N0M0	Malignant	M	60
F8	2,5	1	Larynx	Squamous cell carcinoma	3	IVA	T4N1M0	Malignant	M	53
F9	3	3	Oral cavity	Squamous cell carcinoma of mandible	3	–	–	Malignant	M	56
F10	2,5	0	Larynx	Squamous cell carcinoma	3	IV	T4N2M0	Malignant	M	53
G1	0	0,5	Larynx	Squamous cell carcinoma of laryngopharynx	3	IV	T4N1M0	Malignant	M	47
H1	0,5	0,5	Epiglottis	Epiglottis tissue	–	–	–	Normal	M	28
H4	0,5	0,5	Epiglottis	Epiglottis tissue	–	–	–	Normal	F	41
H4	3	1	Salivary gland	Salivary gland tissue	–	–	–	Normal	M	22
H5	0	0,5	Salivary gland	Salivary gland tissue	–	–	–	Normal	M	22
H6	0	0,5	Salivary gland	Salivary gland tissue	–	–	–	Normal	M	43
H7	0	0,5	Salivary gland	Salivary gland tissue	–	–	–	Normal	F	15
H8	0,5	0,5	Larynx	Larynx tissue	–	–	–	Normal	M	45
H9	0,5	0,5	Tongue	Tongue tissue	–	–	–	Normal	M	16
H10	0,5	0,5	Tongue	Tongue tissue	–	–	–	Normal	M	48

https://www.biomax.us/tissue-arrays/Head_and_Neck/HN802a

Review

Impaired ribosome biogenesis: mechanisms and relevance to cancer and aging

Zsofia Turi[1], Matthew Lacey[1], Martin Mistrik[1], Pavel Moudry[1]

[1]Institute of Molecular and Translational Medicine, Faculty of Medicine and Dentistry, Palacky University, 779 00 Olomouc, Czech Republic

Correspondence to: Pavel Moudry; **email:** pavel.moudry@upol.cz
Keywords: ribosome biogenesis, ribosomopathy, aging, cancer, p53
Received: December 11, 2018 **Accepted:** April 4, 2019 **Published:** April 26, 2019

ABSTRACT

The biosynthesis of ribosomes is a complex process that requires the coordinated action of many factors and a huge energy investment from the cell. Ribosomes are essential for protein production, and thus for cellular survival, growth and proliferation. Ribosome biogenesis is initiated in the nucleolus and includes: the synthesis and processing of ribosomal RNAs, assembly of ribosomal proteins, transport to the cytoplasm and association of ribosomal subunits. The disruption of ribosome biogenesis at various steps, with either increased or decreased expression of different ribosomal components, can promote cell cycle arrest, senescence or apoptosis. Additionally, interference with ribosomal biogenesis is often associated with cancer, aging and age-related degenerative diseases. Here, we review current knowledge on impaired ribosome biogenesis, discuss the main factors involved in stress responses under such circumstances and focus on examples with clinical relevance.

INTRODUCTION

The nucleolus has gained prominent attention in molecular research over the past two decades, due to its emerging role in various cellular processes. Among them, the production of ribosomes is seemingly the most important, as it controls translation of all proteins in the cell and thus governs cell growth and proliferation [1]. The nucleolus is a subnuclear, membrane-less organelle, formed in early G1 phase of the cell cycle around the short arms of acrocentric chromosomes (chromosome 13, 14, 15, 21 and 22), in nucleolar organizer regions (NORs). These NORs contain the ribosomal DNA (rDNA) genes, arranged in tandem repeats and transcribed by RNA Polymerase I (Pol I) [2]. The resulting single polycistronic transcript, known as 47S pre-rRNA, is further modified in the nucleolus. The maturation of the primary transcript is initiated co-transcriptionally and the main processing steps involve endo- and exonucleolytic cleavages, pseudouridylation and 2'-*O*-methylation which lead to the emergence of three ribosomal RNA (rRNA) species: 18S, 5.8S and 28S rRNAs. While 18S rRNA is incorporated into the small ribosomal subunit (SSU), 5.8S and 28S rRNAs, along with 5S rRNA, are members of the large ribosomal subunit (LSU) [3]. The gene encoding 5S rRNA is an exception when compared to other rRNA genes as it is located on chromosome 1 and transcribed by RNA Polymerase III (Pol III) in the nucleus [4, 5]. The protein components of the ribosome are 80 ribosomal proteins (RPs), which are transcribed in the nucleus by RNA Polymerase II (Pol II) and translated in the cytoplasm. However, both the 5S rRNA and the RPs need to be imported into the nucleolus in order to be incorporated into the ribosome [6]. During late ribosome maturation, the forming subunits are first moved into the nucleus, followed by transport to the cytoplasm where ribosomes can fully assemble and assume their protein-translation function [3].

It can be readily accepted that ribosome biosynthesis consumes most of the cell's energy, particularly when compared to other biological processes, as it requires the synthesis of the most abundant RNA and protein species in the cell. This not only includes the concerted action of all three RNA polymerases and the cell's translation apparatus, but also the activity of more than 200 non-ribosomal factors within the nucleolus [7, 8]. Therefore, it is not surprising that cellular signaling networks which sense the nutrient status, growth factors, extra- and intracellular stress levels affect the rate of ribosome biogenesis, mainly by altering the activity of Pol I [9, 10]. Disruption of ribosome biogenesis also promotes signaling pathways that lead to cell cycle arrest and cellular senescence or apoptosis [8, 11]. The earliest observation that impaired ribosome biogenesis halts cell cycle progression comes from a study by Volarevic et al., where they described that the conditional knockout of ribosomal protein *RPS6 (eS6)* causes cell cycle arrest in mouse liver cells [12]. Since then, a number of studies have demonstrated that the disruption of virtually any step in ribosome biogenesis can result in cell cycle arrest, primarily through activation of the tumor suppressor protein p53. This particular process was recently termed as the Impaired Ribosome Biogenesis Checkpoint (IRBC) [13].

Impaired ribosome biogenesis is usually best visible as structural alterations of the nucleolus which can be seen also in various human diseases [14-17]. Importantly, increased size of nucleoli usually reflects intense ribosome biogenesis and has been recognized by physicians for a long time as a hallmark of many tumor types [18]. Interestingly, despite excessive ribosome biogenesis being believed to drive the fast proliferation of cancer cells, some of the most rapidly dividing tumor cells do not display this phenotype [19]. Moreover, patients with another group of human diseases called ribosomopathies, are prone to developing various kinds of tumors. Ribosomopathies are characterized by mutations in RPs or ribosome biogenesis factors, showing a decreased rate of ribosome biosynthesis due to deficiencies of these components required in the ribosome biogenesis pathway. Symptoms of these disorders arise from tissue specific growth arrest and/or incompetent translation. There is a wide spectrum of phenotypes displayed by ribosomopathy patients and affected tissues frequently show upregulation of p53 as a consequence of IRBC [20, 21]. Altered ribosome biogenesis was also connected to aging and it is also relevant in neurodegenerative disorders such as: Alzheimer, Parkinson, Huntington and other advanced age-related diseases (for more details on this topic see the following reviews [16, 17]). However, the exact contribution of IRBC to these complex disorders and aging remains an intriguing question open to further research.

In this review, we summarize the most important steps of ribosome biogenesis, focusing mainly on human cell culture studies. Furthermore, we describe the main effectors of IRBC and review studies that provide evidence for the existence of this pathway as well as examining the clinical relevance of IRBC in aging and age-related diseases.

Ribosome biogenesis

Ribosome biogenesis begins with rRNA synthesis in the nucleolus. As a first step a pre-initiation complex (PIC) is formed around the rDNA promoter region. The PIC itself consists of the upstream binding factor (UBF), selectivity factor (SL1 also known as TIF1-B), transcription initiation factor 1A (TIF1-A or hRRN3) and Pol I. UBF marks the promoter regions by binding as a homodimer to the core promoter surrounding the transcription start site and to the upstream core element (UCE), thereby creating a DNA loop structure. Next, SL1 is recruited to the promoter: binding to both UBF and the rDNA. The interaction of TIF1-A with Pol I is essential for its recruitment to the promoter and formation of the complete PIC. Promoter opening and escape is also stimulated by UBF and is accompanied by the release of TIF1-A from the Pol I complex [22, 23]. Surprisingly, UBF was shown to bind the whole length of rDNA transcript units, and it has been suggested that it is involved in the control of elongation process as well [24]. Transcription termination occurs when Pol I encounters transcription termination factor 1 (TTF-1)-bound terminator elements, the stalled Pol I is subsequently removed by the polymerase I and transcript release factor (PTRF) [25].

In contrast to the synthesis of 47S rRNA, the precursor of 5S rRNA is transcribed by Pol III in the nucleoplasm. The main factors involved in this process are the transcription factors IIIA, IIIB and IIIC (TFIIIA, TFIIIB and TFIIIC), which are responsible for labeling of the promoter region and the recruitment of Pol III [5, 26].

The rate of ribosome production is regulated mainly on the level of rRNA synthesis. This is carried out by a number of factors and signaling pathways which are dependent on various cellular needs, such as the availability of nutrients, and the presence of mitogenic or stress signaling [10]. Mitogenic stimuli activate several, typically oncogenic pathways which upregulate rDNA transcription. For example, MAPK/ERK pathway phosphorylates UBF, TIF1-A and TFIIIB to stimulate Pol I and Pol III mediated rRNA transcription, respectively [27-30]. Moreover, both MAPK/ERK and PI3K/AKT signaling activate the expression of c-Myc [31, 32], which can boost ribosome biogenesis at multiple levels. It stimulates the formation of PIC by

recruiting SL1 to the rDNA promoter, increasing the activity of Pol II to drive transcription of RP genes while simultaneously upregulating Pol III transcription by activating TFIIIB [33-35]. Furthermore, growth factors also activate the mammalian target of rapamycin (mTOR) signaling network which contributes to the activation of UBF, TIF1-A and Pol III associated transcription factors TFIIIB and TFIIIC [36-38]. Additionally, p53 is also involved, both directly and indirectly, in the control of Pol I transcription. It interacts with SL1 to prevent its recruitment to rDNA promoters, thus inhibiting Pol I transcription [39], and also limits Pol III activity via the direct binding of TFIIIB [40]. One of the main transcriptional targets of p53 is p21, which is able to activate the retinoblastoma protein (pRb) through the inhibition of CDKs [41, 42]. Besides its well-known role in cell cycle regulation, pRb is able to bind to several ribosome biogenesis factors, like UBF and TFIIIB to suppress rRNA transcription [43-45].

Transcription of rDNA results in the emergence of a single polycistronic primary transcript, known as the 47S rRNA. This transcript contains 18S, 5.8S and 28S rRNAs separated by internal transcribed spacers (ITS1 and ITS2) and flanked by external transcribed spacers (5'-ETS and 3'-ETS). Over the course of rRNA maturation, the ITSs and ETSs are removed by the combined action of endo- and exonucleases. The processing of the 47S pre-rRNA is initiated co-transcriptionally by the formation of the so-called small subunit (SSU) processome [3]. The recruitment of the transcriptional U three protein (t-UTP) complex to the 5' end of the 47S pre-rRNA belongs among the earliest steps of SSU processome formation. t-UTPs strictly co-localize with the Pol I transcription machinery; forming bead-like structures during active transcription in the nucleolus [46]. Subsequently, t-UTPs and other SSU processome factors initiate the early processing steps of 18S rRNA [46]. Importantly, a cleavage in the ITS1 region separates the processing pathways of the two subunits (for more information on the topic of rRNA processing refer to one of the following reviews [3, 47]).

The maturation of rRNA is coordinated mainly by box C/D and box H/ACA small nucleolar ribonucleoprotein complexes (snoRNPs), named after a specific motif of the RNA component, which catalyze site-specific 2'-*O*-methylation and pseudouridylation of rRNA species respectively. Box C/D snoRNPs are composed of the methyltransferase fibrillarin (FBL), accessory proteins Nop56, Nop58, and 15.5K/NHPX along with the snoRNA component. The snoRNA hybridizes to the pre-rRNA to bring it into the proper conformation to be accessible for methylation by FBL. Furthermore, FBL's function is not limited to the methylation of pre-rRNA, when it forms a complex with e.g. U3, U8 or U14 box C/D snoRNAs, it is also involved in chaperoning and directing the pre-rRNA for endo- and exonucleolytic cleavages [48]. Box H/ACA snoRNPs consist of the pseudouridine synthase dyskerin, the accessory proteins Nhp2, Nop10, Gar1 and the H/ACA snoRNA component [48]. Box H/ACA snoRNPs operate similarly to box C/D snoRNPs, besides their function in site-specific pseudouridylation and cleavage of rRNA, box H/ACA RNPs are also involved in other cellular processes such as: mRNA splicing, production of miRNAs and telomere maintenance [48, 49].

In addition to snoRNPs, numerous other proteins (e.g. ATPases, GTPases, RNA helicases) are also implicated in rRNA processing. By chaperoning rRNA to facilitate proper folding, or by the removal of processing factors from the rRNA, these factors allow subsequent rRNA maturation steps and the assembly of RPs onto the rRNA to proceed [3]. An example of this is the multifunctional protein nucleolin (NCL), which is involved in multiple stages of ribosome biogenesis. NCL is recruited to the rRNA genes and interacts with both the promoter and the coding regions to facilitate transcription elongation by Pol I [50]. Furthermore, as a histone chaperone, NCL can bind to H2A-H2B dimers to promote their dissociation from the nucleosome and stimulate chromatin remodelers, like SWI/SNF and ACF, thereby increasing the rate of transcription [51]. NCL is also involved in rRNA maturation, as it binds to a specific site in the 5'-ETS region of the pre-rRNA and has a role in the cleavage of this site possibly by facilitating the action of its interaction partner, U3 snoRNA [52, 53]. Moreover, NCL was demonstrated to interact with a subset of RPs and have an important function in the pre-ribosome assembly [54, 55].

Nucleophosmin (NPM) is another multifunctional protein that is involved in ribosome biogenesis at multiple levels. Similarly to NCL, NPM is a histone chaperone, with the ability to stimulate rRNA transcription [56]. The requirement of NPM for rRNA processing was first described by Savkur and Olson in 1998. This study demonstrated that NPM is involved in the cleavage of pre-rRNA in the ITS2 region to promote the release of 28S rRNA [57]. These results were confirmed later on, as downregulation of NPM led to the impairment of this processing step [58]. Furthermore, NPM has been demonstrated to have a role in the nuclear export of RPL5 (uL18) and the pre-ribosomal subunits [59, 60]. Additionally, NPM has been implicated in numerous other cellular processes such as: centrosome duplication, regulation of cell cycle and maintenance of genome stability [61].

In parallel with the rRNA processing the newly synthesized RPs are imported into the nucleus and assemble onto the pre-ribosomal subunits [3]. Since nascent RPs in the cytoplasm are readily degraded by the proteasome, their nuclear import has to occur immediately following their synthesis [62, 63]. The nuclear import of RPs is an active, energy-dependent process facilitated by several proteins of the β-karyopherin family. Importin-β, transportin, RanBP5 and RanBP7 have been reported to promote the nuclear import of RPL23A (uL23), RPS7 (eS7) and RPL5 [64], while importin-11 was suggested to be a mediator of RPL12 (uL11) transport [65]. Furthermore, importin-7 was shown to participate in the nuclear import of several RPs, such as RPL4 (uL4), RPL6 (eL6) and RPL23A [66]. Once in the nucleus or nucleolus, RPs are believed to be actively involved in rRNA maturation presumably by stabilizing the secondary structure of the pre-rRNA. The incorporation of RPs into the pre-ribosome occurs in a highly hierarchical order, which correlates to the level of rRNA processing they are involved in, during either the early or late phases of maturation [3].

In addition to its synthesis, the maturation and assembly of 5S rRNA into the LSU is also exceptional. The pre-cursor of the 5S rRNA is matured in the nucleus and is assembled shortly after maturation; adding two LSU RPs, RPL5 and RPL11 (uL5) to the structure. As a ternary complex, the 5S RNP is incorporated into the pre-60S subunit [67, 68].

Similar to the nuclear import of RPs, the export of the pre-40S and pre-60S particles occurs through an energy-dependent process, which is also facilitated by β-karyopherins. Most importantly, exportin-1 is involved in the export of both of the pre-ribosomal subunits [69]. After their transport into the cytoplasm, pre-40S and pre-60S ribosomal subunits undergo the final maturation steps which include the dissociation of the remaining non-ribosomal proteins and the association of last RPs into their subunits [70]. Finally, the mature SSU and LSU particles can be joined together during translation initiation to fulfil their protein production function [71].

Impaired ribosome biogenesis

Ribosome biogenesis is an extremely energy-demanding process, which cells utilize for their growth and proliferation. In the case of impaired ribosome biogenesis, cells must immediately shut down their cell

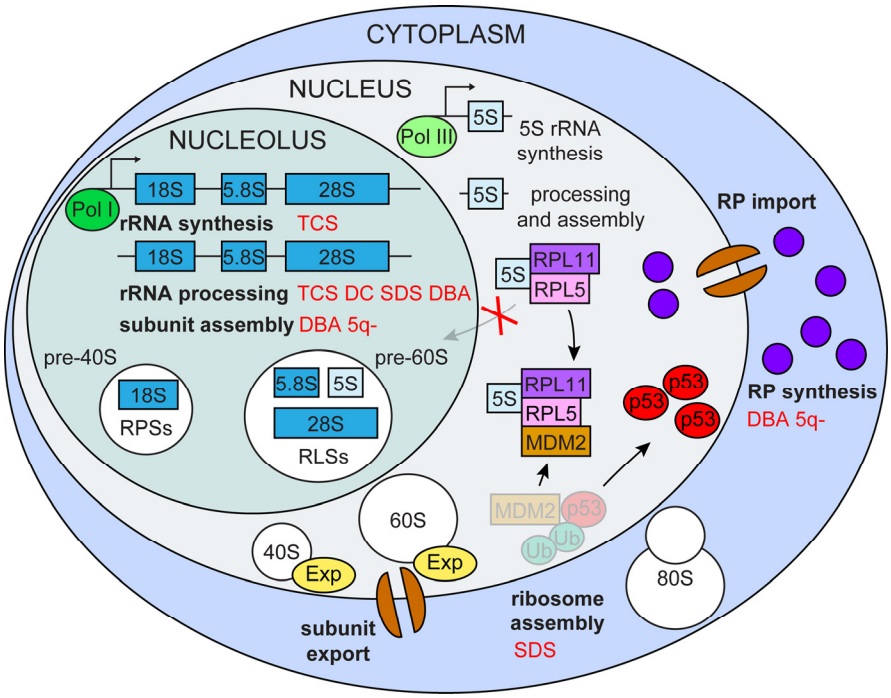

Figure 1. Impaired ribosome biogenesis. Impairment of multiple ribosome biogenesis stages (in bold black) activate p53 via the RPL5/RPL11/5S rRNA/Mdm2 pathway and is associated with various ribosomopathies (in red) TCS (Treacher Collins syndrome), DC (dyskeratosis congenital), SDS (Shwachman-Diamond syndrome), DBA (Diamond-Blackfan anemia) 5q- (5q- syndrome).

cycle to avoid incomplete growth and unprepared division. The central player in this control is the tumor suppressor protein p53 (Figure 1).

Activation of p53 by impaired ribosome biogenesis

Under normal conditions the level of p53 in cells is kept low, despite the fact that it is continuously expressed. Downregulation of p53 is ensured post-translationally by Mdm2, an E3 ubiquitin ligase [72-74]. Mdm2 forms a heterodimer with its inactive paralogue MdmX and their interaction is required for the stability of the complex [75]. Ubiquitylation of p53 by Mdm2 stimulates the nuclear export of p53 and its degradation by the 26S proteasome [76]. In addition, the interaction between Mdm2 and p53 counteracts p53's trans-activating activity; the ability to trigger the expression of its target genes [77]. Once stabilized, p53 is also responsible for the transactivation of Mdm2, providing a negative feedback loop to quench its own activity after the activating stress has been overcome [78, 79].

Perturbation of ribosome biogenesis promotes the recruitment and binding of a group of RPs and nucleolar factors to the Mdm2 central acidic domain, thereby disrupting its interaction with p53 which is then no longer degraded and thus becomes activated [8, 80]. Although Mdm2 binding activity, and thus the ability to induce p53 was shown for multiple RPs, it is generally accepted that RPL5 and RPL11 have major roles in p53 activation in response to ribosomal stress. This effect is best illustrated when Pol I is inhibited by, for example, a low dose of actinomycin D (ActD) treatment, which normally induces a p53 response. In the absence of RPL5 and/or RPL11 ActD induced p53 stabilization is largely inhibited. Interestingly, depletion of other RPs cannot abolish p53 activation in this manner [81, 82]. While most RPs are still synthesized during impaired ribosome biogenesis, they are rapidly degraded by the proteasome [63, 82, 83]. However, under these conditions RPL5 and RPL11 are able to accumulate in a ribosome free fraction, as a result of their mutual protection from proteasomal degradation, further supporting the central function of these proteins in IRBC [82]. Moreover, the assembly of RPL5 and RPL11 into the 5S RNP complex is continued even when ribosome biogenesis is impaired; the formation of this particle is essential for the binding of Mdm2 by these RPs [84]. Furthermore, the association of such a complex might render RPL5 and RPL11 more resistant to degradation when compared to other RPs.

The source of the Mdm2 binding RPs that are involved in IRBC is an intriguing question. In most cases, impairment of ribosome biogenesis leads to the disintegration of the nucleolar structure leading to spontaneous release of RPs and other nucleolar proteins into the nucleoplasm. Thus, disruption of the nucleoli seems to be an important prerequisite for p53 activation [85]. However, this logical proposal was questioned by Fumagalli et al. who demonstrated that RPS6 silencing, which inhibits SSU biogenesis, does not disrupt nucleolar structure, while p53 still accumulates via IRBC. It turned out that under these conditions translation of 5' terminal oligopyrimidin tract containing messenger RNAs (5'-TOP mRNAs), including RPL11 and RPL5 mRNA, is upregulated [81, 86]. The newly synthesized RPs are then actively imported into the nucleus to promote a p53-dependent response while nucleolar structure stays intact [8, 87]. Furthermore, it has been also demonstrated that even when disintegration of the nucleoli occurs upon impaired ribosome biogenesis, the induction of p53 relies on the presence of nascent RPL5 and RPL11 proteins [82]. Thus, while disruption of the nucleolus might be only a consequence of perturbed ribosome biogenesis, the conditions and mechanisms which induce such morphological changes remain unclear.

Besides RPL5 and RPL11, there is another nucleolar factor, called alternative reading frame protein (ARF), which is capable of binding to Mdm2 and thereby promotes the activation of p53 [88]. ARF is a tumor suppressor protein encoded by the *INK4A* locus, which also encodes a cyclin-dependent kinase (CDK) inhibitor termed p16 using alternative reading frame of the same genetic locus [88, 89]. Under normal conditions, ARF is expressed at low levels and sequestered into the nucleolus by NPM [90]. ARF is typically activated by oncogenes, which overstimulate ribosome biogenesis to gain excessive growth potential. Under such stimuli, ARF is released to the nucleoplasm where, similarly to RPs, it interacts with the central acidic domain of Mdm2 and indirectly promotes the stabilization of p53 [88, 91, 92]. Consequently, it was demonstrated that the absence of NPM triggers p53-mediated apoptosis through the activation of ARF [93]. Additionally, excessive quantities of ARF was shown to promote the degradation of NPM and therefore inhibit ribosome biogenesis [58]. This was suggested to induce 5S RNP mediated IRBC, implicating an interplay between the two pathways [87]. Moreover, ARF has a direct inhibitory effect on ribosome biogenesis; by suppressing the phosphorylation of UBF and the nucleolar import of TTF-1 it is able to shutdown rRNA synthesis, which triggers IRBC [87, 94, 95]. Surprisingly, one study demonstrated that overexpression of NPM also promotes the upregulation of p53, since NPM is also capable of interacting directly with Mdm2 to prevent p53's degradation [96]. Overexpression of NPM also inhibits the translocation of p53 from the nucleus to mitochondria, which prevents the activation of the so

called intrinsic apoptotic pathway [97]. However, upon apoptotic stimuli, NPM display pro-apoptotic activity as it translocates to the cytoplasm, where NPM binds the pro-apoptotic BAX protein, triggering cytochrome-c release from the mitochondria [98]. This dual function of NPM in the apoptotic process depicts the numerous functions of NPM in cells, which often differ depending on the conditions.

It is also worth mentioning that several studies have uncovered that activated IRBC also promotes cell cycle arrest through p53-independent pathways. For instance, RPL11 is capable of promoting the degradation of E2F-1 by binding to Mdm2 [99, 100]; E2F-1 is a transcription factor that is required for cell cycle progression [101]. Since nearly half of human cancers have inactivated p53 [102], discovering p53-independent pathways of IRBC, makes ribosome biogenesis relevant therapeutic target in cancer research (for more detailed reviews see [11, 87, 103, 104]).

Impaired rRNA synthesis

Perturbation of rRNA synthesis at multiple levels was shown to activate IRBC. It has been demonstrated by numerous studies that the induction of IRBC and the stabilization of p53 can be achieved by different conditions of inhibited Pol I transcription, including: the silencing of *POLR1A*, a gene encoding the catalytic subunit of Pol I [105]; knockout of the *TIF1-A* gene [106]; or inactivation of UBF by a monoclonal antibody [85]. Impairment of the Pol I transcription machinery can also be accomplished by using several small molecule inhibitors. For instance, the DNA intercalating agent ActD is a very potent inhibitor of rRNA synthesis; it intercalates into the DNA at guanosine-cytosine (GC) rich regions which are mainly present in rDNA genes. Therefore, at lower concentrations it preferentially inhibits transcription by Pol I [107, 108]. Several studies showed that ActD causes severe stress through this mechanism, disrupts the nucleolar structure and strongly induces p53 [11, 85, 104]. BMH-21, a newly identified drug has a similar mechanism of action, as it also intercalates into the GC-rich rDNA. Besides its incorporation into the rDNA, BMH-21 also promotes the proteasomal degradation of Pol I [109, 110]. Other chemical compounds employ different mechanisms to suppress rRNA synthesis. CX-3543 (quarfloxin) inhibits transcription elongation by disrupting the interaction of NCL with rDNA [111], and CX-5461 prevents the recruitment of SL1 to rDNA promoters [112]. Both drugs are potent inducers of the IRBC response. Furthermore, CX-5461 showed a preferential toxicity in some cancer cells compared to normal primary cells, causing p53-dependent apoptosis in Eμ-*Myc* lymphoma cells [113], as well as inducing p53-independent senescence and autophagy in solid tumor cell lines [112]. CX-5461 quickly advanced to phase I clinical trials [113-115], representing an example of therapeutic potential in targeting ribosome biogenesis. Of note, a recent study showed that in addition to their inhibitory effect on rDNA transcription, both CX-5461 and CX-3543 elicit cytotoxicity through induction of DNA damage [116]. Mechanistically, these drugs bind to and stabilize the four stranded DNA structures, G-quadruplexes (G4), thereby causing replication-dependent DNA damage [111, 116]. Elimination of G4 structures is carried out mainly by the homologous recombination (HR) machinery, therefore cancer cells deficient in HR components are particularly sensitive to these drugs [116]. Thus, besides the activation of IRBC, DNA damage induction also contributes to the increased sensitivity of cancer cells towards CX-5461 and CX-3543.

Impairment of the Pol III transcription machinery was also investigated by several research groups. Depletion of the *POLR3A* gene, which encodes the catalytic subunit of Pol III, impairs 5S rRNA biosynthesis and leads to cell cycle arrest in a p53-independent manner [117]. Since 5S rRNA is the essential component of 5S RNP, formed during both intact and impaired ribosome biogenesis, perturbation of its biosynthesis diminishes the formation of the ternary RNP complex which is involved in p53 stabilization. This may explain the lack of p53 induction in Pol III depleted cells [84]. Furthermore, deficiency of TFIIIA, which is involved exclusively in 5S rRNA transcription [118, 119], also led to p53-independent cell cycle arrest and could reverse the activation of p53 induced by Pol I depletion, supporting the hypothesis that 5S rRNA is essential for the induction of p53 in IRBC [68, 84, 117, 120].

Consequences of impaired rRNA synthesis and activated IRBC are well represented by patients suffering from Treacher Collins syndrome (TCS). TCS is a severe craniofacial disease with symptoms includeing: micrognathia, retrognathia, coloboma of the lower eyelids, loss of medial eyelashes, external ear aplasia or microtia, a large or protruding nose and zygomatic bone hypoplasia [121, 122]. TCS is an autosomal dominant disorder mainly caused by mutations in the *TCOF1* gene. A minority of TCS cases (~8%) are associated with mutations in the *POLR1C* and *POLR1D* genes, which encode the RPAC1 and RPAC2 proteins, respectively. Both RPAC1 and RPAC2 proteins are parts of the RNA polymerase I and III complexes. [123, 124]. The *TCOF1* gene encodes a protein named Treacle, which has a prominent role in both rRNA synthesis and the early processing steps [125, 126]. Haploinsufficiency of Treacle disrupts ribosome bio-

genesis, leading to the activation of IRBC and the initiation of p53-mediated apoptosis specific to the neural crest cells during early embryogenesis. The affected stem cell population is responsible for the formation of the bone, cartilage and connective tissue of the head [127, 128]. The strong connection of IRBC and p53-induced neural crest cell apoptosis with the pathogenesis of TCS was shown in the mouse model of the disease. Similarly to TCS patients, Treacle haploinsufficient mice display severe craniofacial abnormalities. Importantly, this phenotype can be reversed either by the chemical inhibition or genetic inactivation of p53 [129]. Recent findings suggest that TCOF1 is involved in the DNA damage response (DDR) and this might also contribute to TCS pathology. It was shown by several groups that upon DNA damage DDR protein NBS1 is relocated to the nucleolus, where it interacts with TCOF1 in a CK2- and ATM-dependent manner in order to suppress rRNA transcription [130, 131]. Interestingly, neuroepithelial cells, including progenitors of neural crest cells, have been reported to exhibit increased amount of DNA damage in a *Tcof1*$^{+/-}$ background. The accumulation of DNA damage has been suggested to be a consequence of the higher level of reactive oxygen species (ROS) produced in this tissue [132]. Since ROS are potent inducers of DNA damage [133, 134], proficient expression of TCOF1 in neural crest cells is essential. Indeed, the administration of the antioxidant N-acetyl-cysteine partially reduced craniofacial malformations in *Tcof1*$^{+/-}$ mouse embryos and accumulation of p53 [132], indicating that both DNA damage and the IRBC contribute to TCS pathology. Additionally, a recent study provides insight into pathogenesis and tissue-specificity of TCS. Calo et al. reported that upon TCOF1 depletion the nucleolar RNA helicase DDX21 redistributes to the nucleoplasm, leading to the inhibition of ribosome biogenesis [135]. Interestingly, such disruptions in the localization of DDX21 seem to be specific for cranial neural crest cells and depletion of DDX21 alone has been presented to induce craniofacial malformations [135]. The authors suggest that rDNA damage that occurs as a consequence of impaired Pol I transcription machinery induces p53 activation and DDX21 relocalization, followed by apoptosis in tissues, which are hypersensitive to elevated levels of p53 [135]. These findings add novel layers to the research of ribosomopathies and offer new therapeutic avenues for the small group of TCS patients.

Impaired rRNA maturation

rRNA processing is initiated co-transcriptionally and early processing factors, such as the t-UTP complex and Treacle, have been shown to have an important role in facilitating both rRNA synthesis and maturation. Therefore, perturbation of ribosome biogenesis due to the absence of these early processing factors leads to a drop in rRNA synthesis and impaired rRNA processing as well [46, 125, 126]. We have recently demonstrated that the depletion of one such early factor, HEAT repeat containing 1 (HEATR1) activates IRBC. Impaired expression of HEATR1 strongly induced p53 and p53-dependent cell cycle arrest. In this scenario activation of p53 was triggered by IRBC, evidenced by the robust disruption of the nucleolar structure and the emergence of Mdm2-RPL5 interaction. Furthermore, under these conditions p53 induction can be reversed by concomitant depletion of RPL5 or RPL11 [136]. UTP10, the yeast homolog of HEATR1 is a member of the t-UTP complex and has been demonstrated to have a role in rRNA synthesis as well as in early steps of pre-rRNA processing [137-139]. Correspondingly, we and others have demonstrated that human HEATR1 positively regulates rRNA synthesis and co-localizes with the Pol I transcription machinery regardless of active transcription [46, 136]. Upon impaired rRNA synthesis, HEATR1, along with other Pol I associated factors, is redistributed to the periphery of the nucleolus to form so-called nucleolar caps; structures characteristic for impaired rDNA transcription [46, 136, 140]. Moreover, this localization appears to be solely dependent on UBF [46]. In addition, similarly to UTP10, HEATR1 has also been shown to be involved in the early 18 S rRNA maturation [46]. The exact function of HEATR1 in rRNA synthesis and processing remains largely unknown. However, as it possesses a C-terminal HEAT repeat, a motif suggested to mediate protein-protein interactions, HEATR1 might promote connections between the Pol I transcription machinery and rRNA processing factors. Analogous results, i.e. repressed transcription and processing of rRNA and IRBC activation, were obtained for other yeast t-UTP homologs, such as: 1A6/DRIM [141], WDR43 [142] and NOL11 [143].

Depletion, mutation or overexpression of numerous subsequent processing factors have been shown to impair rRNA maturation and induce IRBC [144-147]. Downregulation of the box C/D snoRNP component FBL is one such an example; it has been shown to impair rRNA processing and activate the IRBC pathway which leads to p53-mediated apoptosis in embryonic stem cells [148]. Similarly, depletion of box C/D snoRNAs, such as U3 and U8 has been proposed to induce IRBC, resulting in a very potent induction of p53 [149]. Both, FBL and U3 or U8 expression has been shown to be upregulated in several cancer types, indicating their potential involvement in tumorigenesis [149-153]. High FBL expression led to the alteration of the 2'-*O*-methylation pattern of rRNA and translational infidelity. Moreover, the altered methylation of the

rRNA also promoted the internal ribosome entry site (IRES)-dependent translation of proto-oncogenic mRNAs, such as IGF1R, MYC, FGF1/2 and VEGFA [154]. An abnormal rRNA methylation pattern has been observed in aggressive breast cancer, where it induces a decrease in the IRES-dependent translation of p53, which contributes to tumor progression [153]. Additionally, opposing these effects, p53 was demonstrated to counteract such harmful methylation pattern by directly inhibiting the expression of FBL [154] Consistently, recent study by Sharma et al. showed that p53 depletion results in a robust increase in the level of FBL and introduces alterations in the methylation pattern of rRNAs. In addition, FBL ablation promotes the loss of mainly peripheral 2-O-methylated sites [155].

Mutations of the box H/ACA snoRNP component dyskerin encoding gene *DKC1* is associated with a rare genetic condition known as X-linked form of dyskeratosis congenita (X-DC). Dyskeratosis congenita (DC) is a premature aging syndrome characterized by the classical triad of mucocutaneous symptoms: abnormal pigmentation of the skin, nail dystrophy and leukoplakia of the oral mucosa. The most common cause of death is bone marrow failure, but further symptoms may also include: pulmonary fibrosis, increased risk for various malignancies, mental retardation, ophthalmic, skeletal, gastrointestinal and genitourinary abnormalities [156, 157]. The pathogenesis of DC was originally thought to be a consequence of impaired rRNA processing, caused by mutations of dyskerin [49]. However, dyskerin is also a component of the telomerase complex, formed from the box H/ACA telomerase RNA component (TERC), telomerase reverse transcriptase (TERT) and the box H/ACA snoRNA associated proteins [49, 156]. Patients with X-DC show accelerated telomere shortening, which mainly affects the rapidly dividing stem and progenitor cell populations. The possibility that DC is actually a telomerase dysfunction disorder is supported by the occurrence of DC due to mutations of TERT and TERC in the autosomal dominant form of the disease [49, 156, 158]. Furthermore, while depletion of dyskerin in human fibroblasts leads to early activation of p53, presumably through the IRBC pathway, similar upregulation of p53 was only observed later in the fibroblasts of patients with X-DC or autosomal dominant DC [159]. However, in the latter case p53 activation is actually the result of DNA damage arisen from telomere attrition after cells go through several cycles of population doubling [158, 159]. In agreement with this, most of the mutations in *DKC1* gene affect the RNA binding domain, which is involved in association with TERC, rather than affecting catalytic activity or the expression level of dyskerin in X-DC cases [156, 160]. *DKC1* mutations also seem to cause altered rRNA pseudouridylation, which impairs the IRES-dependent translation of a specific group of tumor suppressor mRNAs, including: p53, the CDK inhibitor p27 and the anti-apoptotic proteins XIAP and BCL-X_L. Thus, impaired rRNA processing might contribute to the cancer susceptibility observed in X-DC patients [161, 162]. In addition, similarly to FBL, the overexpression of dyskerin has also been associated with cancer [163, 164], likely contributing via the dysregulated rRNA pseudouridylation, but precise mechanism is not known.

Due to their importance in ribosome biogenesis, depletion of the multifunctional proteins NCL or NPM impairs this process at multiple levels; in the case of NCL, it has been demonstrated to result in the activation of p53, presumably via IRBC [51, 165]. Importantly, overexpression of NCL has been documented in many types of cancer [166]. This upregulation of NCL might promote tumorigenesis by increasing the rate of rRNA transcription and thus enhance ribosome production [167-169]. Apart from that, NCL was shown to also be involved in other cellular processes such as: chromatin organization, DNA and RNA metabolism, angiogenesis, cytokinesis, telomere maintenance, cell growth and proliferation, all of which can contribute to the tumorigenic potential of upregulated NCL [166, 167, 170]. Due to its high expression level NCL represents an interesting target for cancer therapy [167]. Indeed, aptameric compound AS1411, a G-rich oligonucleotide which binds to NCL with high affinity, counteracts NCL's RNA binding activity and induces apoptosis in various cancer cells [171, 172]. The therapeutic potential of AS1411 was already presented in a phase I trial for patients with different kinds of advanced cancer [173, 174] and phase II trials for patients with advanced renal cell carcinoma and acute myeloid leukemia (AML) [175, 176].

In contrast to other nucleolar processing factors, by binding to Mdm2, NPM has been shown to be actively involved in IRBC [96]. While another study reported that ablation of NPM also induces the upregulation of p53 through the activation of ARF [93]. Consistent with these rather conflicting results, NPM has been demonstrated to display both pro-oncogenic and tumor suppressive functions during tumorigenesis [61, 177, 178]. Overexpression of NPM has in fact been reported in many types of solid tumors [179-189]. Its role in tumorigenesis is commonly linked to its function in ribosome biogenesis. Interestingly, low levels of NPM have also been reported for certain cancers; such as gastric or breast cancer [190, 191]. Furthermore, mutations and rearrangements of the *NPM1* gene are often seen in numerous hematological malignancies

[177, 192, 193]. The involvement and importance of NPM in tumorigenesis, particularly in cases when it is upregulated, makes it an attractive target for cancer therapy. Indeed, several small molecule inhibitors of NPM have been tested in preclinical studies and clinical trials [194]. One such promising compound is NSC348884 which, by binding to NPM, is able to dissociate ARF from the complex with NPM; thereby inducing the upregulation of p53, which subsequently triggers apoptosis [195]. Furthermore, this compound has been shown to efficiently induce cytotoxicity in preclinical studies involving solid and hematological cancers [195, 196], however clinical trials of NSC348884 has not been initiated to date.

RP imbalance and impaired pre-ribosome assembly

The activation of p53 via the downregulation of both SSU and LSU RPs has been consistently demonstrated by multiple studies [81, 82, 86, 197-204]. Phenotypic consequences of the RP deficiency are well represented by a rare autosomal dominant disorder called Diamond Blackfan anemia (DBA), which is a bone marrow failure syndrome due to elevated apoptosis of the erythroid progenitor cells [202, 205, 206]. Patients suffering from DBA often show other symptoms as well, including: short stature, craniofacial, cardiac or genitourinary abnormalities and predisposition to cancer [157, 206]. Mutations in a subset of both 40S and 60S RP genes are observed in approximately 50% of DBA cases; the molecular background of the remaining cases is unknown [206-208]. In the most cases of DBA, disruption of the *RPS19 (eS19)* gene is observed, however several patients show mutations of: *RPL5*, *RPL11*, *RPL15 (eL15)*, *RPL36 (eL36)*, *RPL35A (eL33)*, *RPS7*, *RPS10 (eS10)*, *RPS17(eS17)*, *RPS24 (eS24)*, *RPS26 (eS26)* or *RPS27A (eS31)* genes. These mutations cause the haploinsufficiency of the certain RP and most likely impair the global translational capacity of the cells [205, 207]. In erythroid progenitors such insufficiency reduces the production of hemoglobin, leading to increased amount of free heme which has strong pro-oxidative potential. Elevated oxidative stress then leads to p53-independent apoptosis of these cells [209, 210]. This theory was well supported by a mouse model where the gene for Feline Leukemia Virus Subgroup Receptor 1 (FLVCR1), a heme exporter protein, was deleted. FLVCR1-null mice exhibit increased intracellular heme and show a phenotype resembling DBA [211]. Since the RPs which are commonly mutated in DBA patients are involved also in several diverse steps of ribosome biogenesis, their reduced expression also activates the IRBC and subsequent p53-dependent apoptosis [21, 210]. Such IRBC activation is indeed detectable as accumulation of p53 has been shown in DBA-patients' bone marrow samples [202]. Similarly, some mouse and zebrafish models of DBA, which show a similar, but not completely overlapping phenotype with impaired erythropoiesis, also have upregulated p53 [212-215]. The contribution of IRBC- and heme-induced apoptosis to the resulting DBA phenotype was studied by p53 inactivation in various models. While in zebrafish p53 inactivation only rescued developmental abnormalities, but did not affect the observed defective erythropoiesis, in mouse models inactivation of p53 reversed the apoptosis of erythroid progenitors [212, 214, 215].

Another ribosomopathy characterized by the reduced expression of an RP is $5q^{-}$ syndrome, which is often referred to as a somatically acquired form of DBA. The $5q^{-}$ syndrome is a myelodysplastic disease, which is predominantly present in women of advanced age and is caused by the deletion of the long arm of chromosome 5. Similarly to DBA, it is also characterized by disrupted erythropoiesis in the bone marrow, causing macrocytic anemia and a predisposition to AML. Although the extensive deletion of chromosome 5 q arm results in the loss of about 40 genes, *RPS14 (uS11)* seems to be particularly important for the pathogenesis of the disease [205, 216-219]. This is illustrated by mouse models with haploinsufficiency of *RPS14* which recapitulate the human phenotype and also show upregulation of p53. In these mouse models, genetic inactivation of p53 was sufficient to rescue apoptosis of bone marrow progenitors [219]. Additionally, an increased level of p53 was also represented in hematopoietic cells of $5q^{-}$ patients [202, 217].

Overall, due to the involvement of RPs in ribosome biogenesis a decrease in their expression leads to the initiation of the IRBC pathway. The subsequent stabilization and activation of p53 resulting in p53-dependent apoptosis seems to be the main cause of the pathogenesis of these diseases. However, active IRBC alone does not explain the tissue-specific effects of defective RPs in either of the aforementioned diseases. The sensitivity of erythroid progenitors is explained by an increased dependence on ribosome biogenesis due to rapid cell division combined with additional oxidative stress caused by the heme overload [21, 209]. The relative contribution of IRBC *versus* oxidative stress to the apoptosis of erythroid progenitors remains an unanswered question.

In contrast to the decreased expression of RPs, the selective overexpression of certain RPs has been observed in multiple types of cancer, suggesting an active role in tumorigenesis [6]. For instance, RPS13 (uS15) and RPL23 (uL14) were shown to be up-

regulated in gastric cancer contributing to the multidrug resistance of these cells [220].

Impaired RP import and pre-ribosome export

Golomb et al. demonstrated that depletion of β-karyopherin importin-7, not only disrupts the nuclear import of some RPs, but also causes the disruption of the nucleolar structure and activates IRBC, leading to p53 stabilization and activation [221]. In addition to β-karyopherins, other transport adaptor proteins might also be involved in the nuclear import of RPs. Lately, symportin-1 was identified as a crucial protein required for the co-import of RPL5 and RPL11 in yeast [222]. Furthermore, symportin-1 in *Chaetomium thermophilum* might also serve as a molecular chaperon for the assembly of RPL5 and RPL11 with 5S rRNA, to form the 5S RNP complex, which is able to subsequently incorporate into the LSU [223]. Whether human homolog of symportin-1, HEAT repeat containing protein 3 (HEATR3), has analogous functions remains to be investigated. Since 5S RNP is the main mediator of IRBC (as discussed above), impairment of the chaperoning of this complex might counteract the activation of the IRBC pathway and as a consequence could potentially lead to tumorigenesis.

Depletion or leptomycin-B-mediated pharmacological inhibition of exportin-1 inhibits the nuclear export of the premature subunits, induces morphological alterations of the nucleolus and activates p53 through IRBC [221]. Therefore, the disruption of either the import of RPs or the export of the pre-ribosomal particles is able to elicit the IRBC response.

As with the other steps of ribosome biogenesis, the transport of RPs and pre-ribosomal subunits also appears to be upregulated in cancer. For instance, the nuclear import of RPs was reported to be upregulated by the mTOR and c-Myc oncogenic pathways [221, 224]. Moreover, c-Myc is also required for the upregulation of exportin-1 expression [221]. Thus, targeting β-karyopherins involved in ribosome biogenesis might be an appealing approach for cancer therapy; although, it is important to bear in mind that these transport adaptor proteins have a large subset of cargo proteins which are involved in other cellular processes as well.

Impaired assembly of ribosomal subunits

One of the most important steps to initiate the subunit assembly is the release of the eukaryotic translation initiation factor 6 (eIF6) from the LSU, which is promoted by the GTPase activity of elongation factor like-1 (EFL1). Interestingly, ribosome maturation is abrogated at this step in a human autosomal recessive disorder, called Shwachman-Diamond syndrome (SDS) [225-227]. SDS is another bone marrow failure syndrome, with additional symptoms, including: exocrine pancreatic insufficiency, gastrointestinal, skeletal, immune system abnormalities and predisposition to AML [208, 228, 229]. Biallelic mutations in the *SBDS* gene is present in 90% of SDS cases. Ribosome maturation protein SBDS is required for the EFL1-promoted removal of eIF6 from the 60S ribosomal subunit, thus governing the final assembly of the ribosome [225-227]. Furthermore, SBDS was also reported to localize into the nucleolus [230], where it interacts with the 28S rRNA and NPM, which implies that it might have additional functions in the earlier steps of ribosome biogenesis as well [231]. The involvement of SBDS in both early and late steps of ribosome biogenesis is consistent with the observation of upregulated p53 in SDS patient-derived samples, presumably a consequence of active IRBC [232, 233]. However, concomitant depletion of p53 in zebrafish and mouse models of SDS only partially rescues the pathologic phenotype; indicating that insufficient translation, alongside with activated IRBC and upregulated p53, has a prominent role in the pathogenesis of the disease [234, 235].

Aberrant ribosome biogenesis and aging

Numerous studies presented a direct connection between dysregulated ribosome biogenesis and aging. For instance, the downregulation of ribosome biogenesis components or nutrient sensing pathways, which stimulate ribosome production, have been shown to increase the lifespan of multiple organisms including *C. elegans*, *D. melanogaster,* yeast, mice and human [236-249]. Therefore, enhanced ribosome biogenesis, visualized by enlarged nucleoli, is believed to accelerate aging. Indeed, consistent with this idea, the size of the nucleoli and the amount of rRNA increases during aging in human primary fibroblasts and a single, large nucleolus is often observed in senescent cells [250, 251]. Furthermore, fibroblasts isolated from patients suffering from the premature aging disease Hutchinson-Gilford progeria, have enlarged nucleoli and upregulated ribosome biogenesis [251]. Since the rate of protein translation is proportional to the rate of ribosome biogenesis [22, 252] it was suggested that upregulation of protein synthesis and disruption of global proteostasis is the mechanism through which ribosome biogenesis promotes aging [253]. This theory is supported by studies showing that reduction in the rate of translation can increase lifespan, and furthermore that altered proteostasis is a hallmark of aging [238, 254-258]. Additionally, caloric restriction that has been

shown to promote longevity [259-261], leads to the downregulation of ribosome biogenesis by several mechanisms [262-264]. Under such dietary conditions, deacetylase SIRT1 is induced [265, 266]. SIRT1, as a component of the energy dependent nucleolar silencing complex (eNoSC), is responsible for the epigenetic silencing of rDNA gene expression [264] and its overexpression can extend the lifespan [267]. Furthermore, a higher rate of metabolism and reduced amount of the tumor suppressors p53 and ARF might also contribute to aging [268, 269].

Accumulation of DNA damage in rDNA

Besides direct changes in rDNA expression level and/or rate of ribosome biogenesis, another theory relates to the accumulation of rDNA damage for aging. The repetitive nature of rDNA and the high rate of rRNA synthesis cause the rDNA repeats to be subject to recombination events and DNA damage, possibly due to collisions between the replication and transcription machineries and R-loop formations [270-274]. As a result, DNA damage can accumulate in rDNA, this in turn can lead to genome instability, which has also been implicated in cellular aging [258, 275]. Indeed, it has been recently demonstrated that hematopoietic stem cells, which are highly proliferative, and thus have upregulated ribosome biogenesis, accumulate DNA damage in their rDNA genes during aging [276]. Moreover, premature aging diseases, such as Bloom and Werner syndromes are associated with increased rDNA instability [277-279]. BLM and WRN helicases, that are mutated in Bloom and Werner syndromes, respectively have been shown to associate with the Pol I transcription machinery and promote rRNA synthesis [280, 281]. These findings indicate that rDNA instability in these diseases can be attributed to disrupted rRNA transcription and consequent accumulation of rDNA damage due to unresolved rDNA structures.

Deregulation of ribosome biogenesis in aging

Several studies have reported the downregulation of ribosome biogenesis in aged tissues. A progressive decrease in the expression of RPs or rRNA has been observed during the aging process [282, 283], inefficient ribosome biogenesis has been accounted for age-related cataract [284] and diminished skeletal muscle hypertrophy [285]. On the other hand, it has been suggested that such decrease of ribosome biosynthesis may be a compensatory mechanism in aged tissues to prolong lifespan [283].

Being an age-related disease, upregulation of ribosome biogenesis and increased size of the nucleoli have been observed in various types of cancer cells [18]. Numerous reports suggests that rather than being a passive consequence of tumorigenesis, upregulation of ribosome biogenesis is a key step to promote this process [113, 162, 286]. The increase in the rate of ribosome biogenesis drives translation, excess growth and proliferation [287] and the selective upregulation of certain ribosome biogenesis components in many cases contributes to tumorigenesis. For instance, overexpression of key rRNA processing factors, such as FBL or dyskerin has been reported in various cancers [150-153, 163, 164]. Upregulation of FBL or dyskerin alters the posttranscriptional modification of the rRNAs, thus changes the structure of the ribosomes. These altered ribosomes presumably do not change the amount of total protein production, however they affect the quality of translation [288]. Marcel et al. designated these altered complexes 'cancer ribosomes' in FBL upregulated cells, because of their active involvement in tumorigenesis due to preference for IRES-dependent translation of oncogene mRNAs [154]. Moreover, FBL overexpression has been observed in aged mice [289] and lower expression of it seems to be associated with increased lifespan in humans [262]. Additionally, similarly to FBL and dyskerin, selective overexpression of certain RPs has been reported to promote tumorigenesis [220, 290, 291]. Changes in the balance of the RPs might change the structure of the ribosome; however, since many of these RPs possess extra-ribosomal functions, these cannot be excluded from contribution to tumorigenesis.

A high rate of ribosome biogenesis and enlarged nucleoli are the main characteristics of stem cells as well as cancer cells. Similarly to cancer cells, stem cells rely on ribosome biogenesis for their growth and proliferation and it also ensures pluripotency [148, 292-294]. During differentiation these cells lose high expression of ribosome biogenesis factors and obtain shrunken nucleoli [295]. Several studies have demonstrated that partial depletion of certain nucleolar factors involved in ribosome biosynthesis induces differentiation of pluripotent stem cells [148, 292, 294, 296, 297]. Furthermore, complete loss of some ribosome biogenesis components affects stem cells more drastically, when compared to differentiated cells [148, 297]. Consistently, decreased expression of ribosome biosynthesis factors observed in ribosomopathies induces growth arrest and apoptosis in hematopoietic or other stem cell types, while differentiated cells remain mostly unaffected. Furthermore, although upregulation of ribosome biogenesis is traditionally associated with aging and cancer, downregulation of this process can also promote tumorigenesis, as patients with ribosomopathies are predisposed to development of certain cancer types [20, 205, 208]. This can be explained as a result of a lower amount of available

mature ribosomes introducing competition between various mRNAs. Thus tumor suppressors encoding mRNAs with lower affinity to the ribosome may lose their translational capacity [287]. High and stable expression of p53 can decrease lifespan in mice and humans [298-300], therefore it is possible that upregulated p53 usually observed in ribosomopathies can also contribute to accelerated aging of those patients. Indeed, one of the ribosomopathies, dyskeratosis congenita has been associated with premature aging. Whether this is a more general feature that is also shared by other ribosomopathies needs further investtigation. Although, both upregulation and downregulation of ribosome biogenesis can accelerate aging process, timing of the downregulation of the ribosome biogenesis is important factor that must be considered. While numerous studies show that an overall decrease in ribosome biogenesis promotes longevity, it must occur in the post-developmental phase. When it is downregulated early in life, as in the case of ribosomopathies, it has more severe consequences, which reduce lifespan [301].

Although differentiated, non-dividing cells usually display shrunken nucleoli and reduced rate of ribosome biogenesis, prominent nucleoli can be observed in terminally differentiated neurons [17]. It has been demonstrated that during development, post-mitotic neurons rely on increased ribosome biogenesis for their somatoneuritic growth [302, 303]. Specifically, neurotrophics, such as the brain-derived neurotrophic factor (BDNF) stimulate ribosome biosynthesis, through the ERK1/2 signaling cascade [302]. Consequently, upregulated ribosome biogenesis supply developing neurites with a sufficient number of ribosomes for the increased local protein synthesis to promote morphogenesis of the neurons [17, 302]. Furthermore, it has been also suggested that neurite outgrowth, which is promoted in mature neurons during regeneration of the nerves following injury, depends on the upregulation of ribosome biogenesis [304, 305].

Ribosome biogenesis and neurodegenerative diseases

The importance of active ribosome biogenesis in mature neurons is further supported by the observation that it is frequently impaired in neurodegenerative diseases. For instance, Alzheimer's disease (AD) has been reported to associate with reduced number of the ribosomes [306], which may be the linked to the increased oxidation of rRNA [307, 308] and/or epigenetic silencing of rDNA, seen in AD patient's brains [309, 310]. Furthermore, aberrant NORs have been also observed in AD patients [311]. Additionally, the microtubule-associated protein, tau, whose function is severely impaired in AD, has been reported to localize to the nucleolus, where it interacts with several nucleolar proteins and may have a role in several nucleolus-associated functions under normal conditions [312-315]. Downregulation of ribosome biogenesis has also been documented in Parkinson's disease (PD), which is often accompanied with disrupted nucleolar structure of the affected dopaminergic neurons [316, 317]. This phenotype may be mediated by NCL, since its expression has been reported to be decreased in the *substantia nigra* of PD patients [318]. Furthermore, NCL has been also documented to interact with α-synuclein and DJ-1, the two major proteins involved in the pathogenesis of familial PD [319]. Moreover, a mutation of DJ-1 has been presented to impair ribosome biogenesis by the exclusion of TNF receptor associated protein (TTRAP) from the nucleolus [320]. Whereas another study on PD has been reported that the overexpression of parkin associated substrate (PARIS) represses rRNA transcription by direct interaction with the Pol I transcription machinery [321]. Several factors perturbing ribosome biogenesis have been observed in Huntington's disease (HD) as well. For instance, the PIC component, UBF has been shown to be downregulated in HD patients [322]. UBF's function and thus rRNA synthesis has been also suggested to be inhibited via the decreased acetylation and/or increased methylation of UBF, both mediated by the mutant huntingtin protein [322, 323]. Furthermore, it has been also suggested that the CAG triplet expansion containing transcripts, characteristic of HD, are able to associate with NCL and this interaction leads to the reduced recruitment and binding of NCL to the rDNA promoter, followed by promoter hypermethylation and results in the rRNA synthesis suppression [324]. Overall, numerous studies indicate that impaired ribosome biogenesis is a key feature of neurodegeneration. The diversity and complexity of mechanisms that perturb this process indicate the existence of more factors capable of impairing ribosome biogenesis in these syndromes with a rather heterogeneous genetic background. Additionally, since the accumulation of p53 has been reported in AD, PD and HD [325-327], the activation of IRBC is evident and may be fundamental for the pathology of these diseases.

Although the complex relationship between aging, age-related diseases and ribosome biogenesis and the regulation thereof is just being elucidated, the importance of the tight regulation of these processes is evident from these examples.

CONCLUSION

In the past decades, a tremendous effort was made to explore the various steps of ribosome biogenesis and the regulation of this process. It has long been acknowledged that due to its complexity, ribosome biogenesis

requires a huge energy investment from cells. Therefore, it is regulated by numerous complex pathways. The impairment of ribosome biogenesis, at any step from rRNA synthesis to ribosome assembly, has been demonstrated to result in severe consequences such as: cell cycle arrest, senescence or apoptosis mainly through the RPL5/RPL11/5S rRNA/Mdm2/p53 axis. Although the process of IRBC is well-established and widely accepted, further research is ongoing. For instance, it is not fully understood how the defects in various steps of ribosome biogenesis are sensed and transduced to uniformly induce IRBC.

The dependence of ribosome biogenesis on the nutrient and energy status of cells renders the entire process highly vulnerable to internal and external stress stimuli. Indeed, multiple studies have reported that a number of typical cellular stressors, such as: DNA damaging agents (UV- and γ-irradiation, genotoxic chemotherapeutics); hypoxia, nutrient and growth factor deprivation; heat shock and oncogene activation induce alterations in ribosome biogenesis and ultimately activate the IRBC [328]. Consistently, a report from Burger and colleagues showed that a diverse group of commonly used chemotherapeutic drugs (e.g. alkylating agents, antimetabolites, mitosis inhibitors, kinase inhibitors, translation inhibitors, etc.), are all capable of perturbing ribosome biogenesis [108]. Interestingly, the stage of ribosome biogenesis inhibition differed between these compounds; some of them suppressed the process earlier while others inhibited later steps [108]. These results suggest that chemotherapeutic agents induce IRBC, which might contribute to their cytotoxicity. IRBC-induced apoptosis or senescence might be beneficial for cancer therapeutics, since cancer cells highly rely on ribosome production for their growth and proliferation. However, traditional chemotherapeutic drugs possess other cytotoxic effects such as: genotoxicity, nucleotide deprivation, inhibition of signal transduction, and others which poison non-cancerous cells as well. Therefore, it might be more favorable to take advantage of those compounds, which are rather specific and exclusively inhibit ribosome biogenesis. However, these agents must still be treated with caution, as other populations of rapidly dividing cells, such as stem cells might be sensitive to the perturbation of ribosome biogenesis. Other therapeutic approaches, targeting the various steps of ribosome biogenesis may be a valid therapeutic strategy, as selective upregulation of some ribosome biosynthesis factors is observed in various cancers.

CONFLICTS OF INTEREST

The authors declare no conflicts of interest.

FUNDING

The work was supported by the Grant Agency of the Czech Republic (17-14743S and 17-25976S), the Internal Grant of Palacky University (IGA-LF-2019-026) and the European Regional Development Fund - Project ENOCH (No. CZ.02.1.01/0.0/0.0/16_019/0000868

REFERENCES

1. Rudra D, Warner JR. What better measure than ribosome synthesis? Genes Dev. 2004; 18:2431–36. https://doi.org/10.1101/gad.1256704
2. McStay B. Nucleolar organizer regions: genomic 'dark matter' requiring illumination. Genes Dev. 2016; 30:1598–610. https://doi.org/10.1101/gad.283838.116
3. Henras AK, Plisson-Chastang C, O'Donohue MF, Chakraborty A, Gleizes PE. An overview of pre-ribosomal RNA processing in eukaryotes. Wiley Interdiscip Rev RNA. 2015; 6:225–42. https://doi.org/10.1002/wrna.1269
4. Sørensen PD, Frederiksen S. Characterization of human 5S rRNA genes. Nucleic Acids Res. 1991; 19:4147–51. https://doi.org/10.1093/nar/19.15.4147
5. Paule MR, White RJ. Survey and summary: transcription by RNA polymerases I and III. Nucleic Acids Res. 2000; 28:1283–98. https://doi.org/10.1093/nar/28.6.1283
6. Wang W, Nag S, Zhang X, Wang MH, Wang H, Zhou J, Zhang R. Ribosomal proteins and human diseases: pathogenesis, molecular mechanisms, and therapeutic implications. Med Res Rev. 2015; 35:225–85. https://doi.org/10.1002/med.21327
7. Fromont-Racine M, Senger B, Saveanu C, Fasiolo F. Ribosome assembly in eukaryotes. Gene. 2003; 313:17–42. https://doi.org/10.1016/S0378-1119(03)00629-2
8. Golomb L, Volarevic S, Oren M. p53 and ribosome biogenesis stress: the essentials. FEBS Lett. 2014; 588:2571–79. https://doi.org/10.1016/j.febslet.2014.04.014
9. Grummt I. Life on a planet of its own: regulation of RNA polymerase I transcription in the nucleolus. Genes Dev. 2003; 17:1691–702. https://doi.org/10.1101/gad.1098503R
10. Grummt I. Wisely chosen paths--regulation of rRNA synthesis: delivered on 30 June 2010 at the 35th FEBS Congress in Gothenburg, Sweden. FEBS J. 2010; 277:4626–39.

https://doi.org/10.1111/j.1742-4658.2010.07892.x

11. James A, Wang Y, Raje H, Rosby R, DiMario P. Nucleolar stress with and without p53. Nucleus. 2014; 5:402–26. https://doi.org/10.4161/nucl.32235

12. Volarević S, Stewart MJ, Ledermann B, Zilberman F, Terracciano L, Montini E, Grompe M, Kozma SC, Thomas G. Proliferation, but not growth, blocked by conditional deletion of 40S ribosomal protein S6. Science. 2000; 288:2045–47. https://doi.org/10.1126/science.288.5473.2045

13. Gentilella A, Morón-Duran FD, Fuentes P, Zweig-Rocha G, Riaño-Canalias F, Pelletier J, Ruiz M, Turón G, Castaño J, Tauler A, Bueno C, Menéndez P, Kozma SC, Thomas G. Autogenous Control of 5′TOP mRNA Stability by 40S Ribosomes. Mol Cell. 2017; 67:55–70.e4. https://doi.org/10.1016/j.molcel.2017.06.005

14. Hariharan N, Sussman MA. Stressing on the nucleolus in cardiovascular disease. Biochim Biophys Acta. 2014; 1842:798–801. https://doi.org/10.1016/j.bbadis.2013.09.016

15. Salvetti A, Greco A. Viruses and the nucleolus: the fatal attraction. Biochim Biophys Acta. 2014; 1842:840–47. https://doi.org/10.1016/j.bbadis.2013.12.010

16. Parlato R, Liss B. How Parkinson's disease meets nucleolar stress. Biochim Biophys Acta. 2014; 1842:791–97. https://doi.org/10.1016/j.bbadis.2013.12.014

17. Hetman M, Pietrzak M. Emerging roles of the neuronal nucleolus. Trends Neurosci. 2012; 35:305–14. https://doi.org/10.1016/j.tins.2012.01.002

18. Montanaro L, Treré D, Derenzini M. Nucleolus, ribosomes, and cancer. Am J Pathol. 2008; 173:301–10. https://doi.org/10.2353/ajpath.2008.070752

19. Zink D, Fischer AH, Nickerson JA. Nuclear structure in cancer cells. Nat Rev Cancer. 2004; 4:677–87. https://doi.org/10.1038/nrc1430

20. Armistead J, Triggs-Raine B. Diverse diseases from a ubiquitous process: the ribosomopathy paradox. FEBS Lett. 2014; 588:1491–500. https://doi.org/10.1016/j.febslet.2014.03.024

21. Danilova N, Gazda HT. Ribosomopathies: how a common root can cause a tree of pathologies. Dis Model Mech. 2015; 8:1013–26. https://doi.org/10.1242/dmm.020529

22. Russell J, Zomerdijk JC. RNA-polymerase-I-directed rDNA transcription, life and works. Trends Biochem Sci. 2005; 30:87–96. https://doi.org/10.1016/j.tibs.2004.12.008

23. Albert B, Perez-Fernandez J, Léger-Silvestre I, Gadal O. Regulation of ribosomal RNA production by RNA polymerase I: does elongation come first? Genet Res Int. 2012; 2012:276948. https://doi.org/10.1155/2012/276948

24. O'Sullivan AC, Sullivan GJ, McStay B. UBF binding in vivo is not restricted to regulatory sequences within the vertebrate ribosomal DNA repeat. Mol Cell Biol. 2002; 22:657–68. https://doi.org/10.1128/MCB.22.2.657-668.2002

25. Jansa P, Grummt I. Mechanism of transcription termination: PTRF interacts with the largest subunit of RNA polymerase I and dissociates paused transcription complexes from yeast and mouse. Mol Gen Genet. 1999; 262:508–14. https://doi.org/10.1007/s004380051112

26. Ciganda M, Williams N. Eukaryotic 5S rRNA biogenesis. Wiley Interdiscip Rev RNA. 2011; 2:523–33. https://doi.org/10.1002/wrna.74

27. Stefanovsky V, Langlois F, Gagnon-Kugler T, Rothblum LI, Moss T. Growth factor signaling regulates elongation of RNA polymerase I transcription in mammals via UBF phosphorylation and r-chromatin remodeling. Mol Cell. 2006; 21:629–39. https://doi.org/10.1016/j.molcel.2006.01.023

28. Stefanovsky VY, Moss T. The splice variants of UBF differentially regulate RNA polymerase I transcription elongation in response to ERK phosphorylation. Nucleic Acids Res. 2008; 36:5093–101. https://doi.org/10.1093/nar/gkn484

29. Zhao J, Yuan X, Frödin M, Grummt I. ERK-dependent phosphorylation of the transcription initiation factor TIF-IA is required for RNA polymerase I transcription and cell growth. Mol Cell. 2003; 11:405–13. https://doi.org/10.1016/S1097-2765(03)00036-4

30. Felton-Edkins ZA, Fairley JA, Graham EL, Johnston IM, White RJ, Scott PH. The mitogen-activated protein (MAP) kinase ERK induces tRNA synthesis by phosphorylating TFIIIB. EMBO J. 2003; 22:2422–32. https://doi.org/10.1093/emboj/cdg240

31. Zhu J, Blenis J, Yuan J. Activation of PI3K/Akt and MAPK pathways regulates Myc-mediated transcription by phosphorylating and promoting the degradation of Mad1. Proc Natl Acad Sci USA. 2008; 105:6584–89. https://doi.org/10.1073/pnas.0802785105

32. Mendoza MC, Er EE, Blenis J. The Ras-ERK and PI3K-mTOR pathways: cross-talk and compensation. Trends Biochem Sci. 2011; 36:320–28. https://doi.org/10.1016/j.tibs.2011.03.006

33. Gomez-Roman N, Felton-Edkins ZA, Kenneth NS, Goodfellow SJ, Athineos D, Zhang J, Ramsbottom BA, Innes F, Kantidakis T, Kerr ER, Brodie J, Grandori C, White RJ. Activation by c-Myc of transcription by RNA polymerases I, II and III. Biochem Soc Symp. 2006; 73:141–54. https://doi.org/10.1042/bss0730141

34. van Riggelen J, Yetil A, Felsher DW. MYC as a regulator of ribosome biogenesis and protein synthesis. Nat Rev Cancer. 2010; 10:301–09. https://doi.org/10.1038/nrc2819

35. White RJ. RNA polymerases I and III, growth control and cancer. Nat Rev Mol Cell Biol. 2005; 6:69–78. https://doi.org/10.1038/nrm1551

36. Mayer C, Grummt I. Ribosome biogenesis and cell growth: mTOR coordinates transcription by all three classes of nuclear RNA polymerases. Oncogene. 2006; 25:6384–91. https://doi.org/10.1038/sj.onc.1209883

37. Woiwode A, Johnson SA, Zhong S, Zhang C, Roeder RG, Teichmann M, Johnson DL. PTEN represses RNA polymerase III-dependent transcription by targeting the TFIIIB complex. Mol Cell Biol. 2008; 28:4204–14. https://doi.org/10.1128/MCB.01912-07

38. Kantidakis T, Ramsbottom BA, Birch JL, Dowding SN, White RJ. mTOR associates with TFIIIC, is found at tRNA and 5S rRNA genes, and targets their repressor Maf1. Proc Natl Acad Sci USA. 2010; 107:11823–28. https://doi.org/10.1073/pnas.1005188107

39. Zhai W, Comai L. Repression of RNA polymerase I transcription by the tumor suppressor p53. Mol Cell Biol. 2000; 20:5930–38. https://doi.org/10.1128/MCB.20.16.5930-5938.2000

40. Crighton D, Woiwode A, Zhang C, Mandavia N, Morton JP, Warnock LJ, Milner J, White RJ, Johnson DL. p53 represses RNA polymerase III transcription by targeting TBP and inhibiting promoter occupancy by TFIIIB. EMBO J. 2003; 22:2810–20. https://doi.org/10.1093/emboj/cdg265

41. Gartel AL, Tyner AL. Transcriptional regulation of the p21((WAF1/CIP1)) gene. Exp Cell Res. 1999; 246:280–89. https://doi.org/10.1006/excr.1998.4319

42. Harper JW, Elledge SJ, Keyomarsi K, Dynlacht B, Tsai LH, Zhang P, Dobrowolski S, Bai C, Connell-Crowley L, Swindell E. Inhibition of cyclin-dependent kinases by p21. Mol Biol Cell. 1995; 6:387–400. https://doi.org/10.1091/mbc.6.4.387

43. Cavanaugh AH, Hempel WM, Taylor LJ, Rogalsky V, Todorov G, Rothblum LI. Activity of RNA polymerase I transcription factor UBF blocked by Rb gene product. Nature. 1995; 374:177–80. https://doi.org/10.1038/374177a0

44. Hannan KM, Hannan RD, Smith SD, Jefferson LS, Lun M, Rothblum LI. Rb and p130 regulate RNA polymerase I transcription: rb disrupts the interaction between UBF and SL-1. Oncogene. 2000; 19:4988–99. https://doi.org/10.1038/sj.onc.1203875

45. Scott PH, Cairns CA, Sutcliffe JE, Alzuherri HM, McLees A, Winter AG, White RJ. Regulation of RNA polymerase III transcription during cell cycle entry. J Biol Chem. 2001; 276:1005–14. https://doi.org/10.1074/jbc.M005417200

46. Prieto JL, McStay B. Recruitment of factors linking transcription and processing of pre-rRNA to NOR chromatin is UBF-dependent and occurs independent of transcription in human cells. Genes Dev. 2007; 21:2041–54. https://doi.org/10.1101/gad.436707

47. Mullineux ST, Lafontaine DL. Mapping the cleavage sites on mammalian pre-rRNAs: where do we stand? Biochimie. 2012; 94:1521–32. https://doi.org/10.1016/j.biochi.2012.02.001

48. Watkins NJ, Bohnsack MT. The box C/D and H/ACA snoRNPs: key players in the modification, processing and the dynamic folding of ribosomal RNA. Wiley Interdiscip Rev RNA. 2012; 3:397–414. https://doi.org/10.1002/wrna.117

49. Angrisani A, Vicidomini R, Turano M, Furia M. Human dyskerin: beyond telomeres. Biol Chem. 2014; 395:593–610. https://doi.org/10.1515/hsz-2013-0287

50. Cong R, Das S, Ugrinova I, Kumar S, Mongelard F, Wong J, Bouvet P. Interaction of nucleolin with ribosomal RNA genes and its role in RNA polymerase I transcription. Nucleic Acids Res. 2012; 40:9441–54. https://doi.org/10.1093/nar/gks720

51. Angelov D, Bondarenko VA, Almagro S, Menoni H, Mongélard F, Hans F, Mietton F, Studitsky VM, Hamiche A, Dimitrov S, Bouvet P. Nucleolin is a histone chaperone with FACT-like activity and assists remodeling of nucleosomes. EMBO J. 2006; 25:1669–79. https://doi.org/10.1038/sj.emboj.7601046

52. Ginisty H, Amalric F, Bouvet P. Nucleolin functions in the first step of ribosomal RNA processing. EMBO J. 1998; 17:1476–86. https://doi.org/10.1093/emboj/17.5.1476

53. Ginisty H, Serin G, Ghisolfi-Nieto L, Roger B, Libante V, Amalric F, Bouvet P. Interaction of nucleolin with an evolutionarily conserved pre-ribosomal RNA sequence is required for the assembly of the primary processing complex. J Biol Chem. 2000; 275:18845–50. https://doi.org/10.1074/jbc.M002350200

54. Bouvet P, Diaz JJ, Kindbeiter K, Madjar JJ, Amalric F. Nucleolin interacts with several ribosomal proteins through its RGG domain. J Biol Chem. 1998; 273:19025–29.

https://doi.org/10.1074/jbc.273.30.19025

55. Roger B, Moisand A, Amalric F, Bouvet P. Nucleolin provides a link between RNA polymerase I transcription and pre-ribosome assembly. Chromosoma. 2003; 111:399–407. https://doi.org/10.1007/s00412-002-0221-5

56. Murano K, Okuwaki M, Hisaoka M, Nagata K. Transcription regulation of the rRNA gene by a multifunctional nucleolar protein, B23/nucleophosmin, through its histone chaperone activity. Mol Cell Biol. 2008; 28:3114–26. https://doi.org/10.1128/MCB.02078-07

57. Savkur RS, Olson MO. Preferential cleavage in pre-ribosomal RNA byprotein B23 endoribonuclease. Nucleic Acids Res. 1998; 26:4508–15. https://doi.org/10.1093/nar/26.19.4508

58. Itahana K, Bhat KP, Jin A, Itahana Y, Hawke D, Kobayashi R, Zhang Y. Tumor suppressor ARF degrades B23, a nucleolar protein involved in ribosome biogenesis and cell proliferation. Mol Cell. 2003; 12:1151–64. https://doi.org/10.1016/S1097-2765(03)00431-3

59. Yu Y, Maggi LB Jr, Brady SN, Apicelli AJ, Dai MS, Lu H, Weber JD. Nucleophosmin is essential for ribosomal protein L5 nuclear export. Mol Cell Biol. 2006; 26:3798–809. https://doi.org/10.1128/MCB.26.10.3798-3809.2006

60. Maggi LB Jr, Kuchenruether M, Dadey DY, Schwope RM, Grisendi S, Townsend RR, Pandolfi PP, Weber JD. Nucleophosmin serves as a rate-limiting nuclear export chaperone for the Mammalian ribosome. Mol Cell Biol. 2008; 28:7050–65. https://doi.org/10.1128/MCB.01548-07

61. Box JK, Paquet N, Adams MN, Boucher D, Bolderson E, O'Byrne KJ, Richard DJ. Nucleophosmin: from structure and function to disease development. BMC Mol Biol. 2016; 17:19. https://doi.org/10.1186/s12867-016-0073-9

62. Warner JR, Mitra G, Schwindinger WF, Studeny M, Fried HM. Saccharomyces cerevisiae coordinates accumulation of yeast ribosomal proteins by modulating mRNA splicing, translational initiation, and protein turnover. Mol Cell Biol. 1985; 5:1512–21. https://doi.org/10.1128/MCB.5.6.1512

63. Lam YW, Lamond AI, Mann M, Andersen JS. Analysis of nucleolar protein dynamics reveals the nuclear degradation of ribosomal proteins. Curr Biol. 2007; 17:749–60. https://doi.org/10.1016/j.cub.2007.03.064

64. Jäkel S, Görlich D. Importin beta, transportin, RanBP5 and RanBP7 mediate nuclear import of ribosomal proteins in mammalian cells. EMBO J. 1998; 17:4491–502. https://doi.org/10.1093/emboj/17.15.4491

65. Plafker SM, Macara IG. Ribosomal protein L12 uses a distinct nuclear import pathway mediated by importin 11. Mol Cell Biol. 2002; 22:1266–75. https://doi.org/10.1128/MCB.22.4.1266-1275.2002

66. Jäkel S, Mingot JM, Schwarzmaier P, Hartmann E, Görlich D. Importins fulfil a dual function as nuclear import receptors and cytoplasmic chaperones for exposed basic domains. EMBO J. 2002; 21:377–86. https://doi.org/10.1093/emboj/21.3.377

67. Zhang J, Harnpicharnchai P, Jakovljevic J, Tang L, Guo Y, Oeffinger M, Rout MP, Hiley SL, Hughes T, Woolford JL Jr. Assembly factors Rpf2 and Rrs1 recruit 5S rRNA and ribosomal proteins rpL5 and rpL11 into nascent ribosomes. Genes Dev. 2007; 21:2580–92. https://doi.org/10.1101/gad.1569307

68. Sloan KE, Bohnsack MT, Watkins NJ. The 5S RNP couples p53 homeostasis to ribosome biogenesis and nucleolar stress. Cell Reports. 2013; 5:237–47. https://doi.org/10.1016/j.celrep.2013.08.049

69. Thomas F, Kutay U. Biogenesis and nuclear export of ribosomal subunits in higher eukaryotes depend on the CRM1 export pathway. J Cell Sci. 2003; 116:2409–19. https://doi.org/10.1242/jcs.00464

70. Henras AK, Soudet J, Gérus M, Lebaron S, Caizergues-Ferrer M, Mougin A, Henry Y. The post-transcriptional steps of eukaryotic ribosome biogenesis. Cell Mol Life Sci. 2008; 65:2334–59. https://doi.org/10.1007/s00018-008-8027-0

71. Jackson RJ, Hellen CU, Pestova TV. The mechanism of eukaryotic translation initiation and principles of its regulation. Nat Rev Mol Cell Biol. 2010; 11:113–27. https://doi.org/10.1038/nrm2838

72. Honda R, Tanaka H, Yasuda H. Oncoprotein MDM2 is a ubiquitin ligase E3 for tumor suppressor p53. FEBS Lett. 1997; 420:25–27. https://doi.org/10.1016/S0014-5793(97)01480-4

73. Michael D, Oren M. The p53-Mdm2 module and the ubiquitin system. Semin Cancer Biol. 2003; 13:49–58. https://doi.org/10.1016/S1044-579X(02)00099-8

74. Haupt Y, Maya R, Kazaz A, Oren M. Mdm2 promotes the rapid degradation of p53. Nature. 1997; 387:296–99. https://doi.org/10.1038/387296a0

75. Gu J, Kawai H, Nie L, Kitao H, Wiederschain D, Jochemsen AG, Parant J, Lozano G, Yuan ZM. Mutual dependence of MDM2 and MDMX in their functional inactivation of p53. J Biol Chem. 2002; 277:19251–54. https://doi.org/10.1074/jbc.C200150200

76. Hock AK, Vousden KH. The role of ubiquitin modifica-

tion in the regulation of p53. Biochim Biophys Acta. 2014; 1843:137–49. https://doi.org/10.1016/j.bbamcr.2013.05.022

77. Toledo F, Wahl GM. Regulating the p53 pathway: in vitro hypotheses, in vivo veritas. Nat Rev Cancer. 2006; 6:909–23. https://doi.org/10.1038/nrc2012

78. Picksley SM, Lane DP. The p53-mdm2 autoregulatory feedback loop: a paradigm for the regulation of growth control by p53? BioEssays. 1993; 15:689–90. https://doi.org/10.1002/bies.950151008

79. Murray-Zmijewski F, Slee EA, Lu X. A complex barcode underlies the heterogeneous response of p53 to stress. Nat Rev Mol Cell Biol. 2008; 9:702–12. https://doi.org/10.1038/nrm2451

80. Zhang Y, Lu H. Signaling to p53: ribosomal proteins find their way. Cancer Cell. 2009; 16:369–77. https://doi.org/10.1016/j.ccr.2009.09.024

81. Fumagalli S, Ivanenkov VV, Teng T, Thomas G. Suprainduction of p53 by disruption of 40S and 60S ribosome biogenesis leads to the activation of a novel G2/M checkpoint. Genes Dev. 2012; 26:1028–40. https://doi.org/10.1101/gad.189951.112

82. Bursać S, Brdovčak MC, Pfannkuchen M, Orsolić I, Golomb L, Zhu Y, Katz C, Daftuar L, Grabušić K, Vukelić I, Filić V, Oren M, Prives C, Volarevic S. Mutual protection of ribosomal proteins L5 and L11 from degradation is essential for p53 activation upon ribosomal biogenesis stress. Proc Natl Acad Sci USA. 2012; 109:20467–72. https://doi.org/10.1073/pnas.1218535109

83. Warner JR. In the absence of ribosomal RNA synthesis, the ribosomal proteins of HeLa cells are synthesized normally and degraded rapidly. J Mol Biol. 1977; 115:315–33. https://doi.org/10.1016/0022-2836(77)90157-7

84. Donati G, Peddigari S, Mercer CA, Thomas G. 5S ribosomal RNA is an essential component of a nascent ribosomal precursor complex that regulates the Hdm2-p53 checkpoint. Cell Reports. 2013; 4:87–98. https://doi.org/10.1016/j.celrep.2013.05.045

85. Rubbi CP, Milner J. Disruption of the nucleolus mediates stabilization of p53 in response to DNA damage and other stresses. EMBO J. 2003; 22:6068–77. https://doi.org/10.1093/emboj/cdg579

86. Fumagalli S, Di Cara A, Neb-Gulati A, Natt F, Schwemberger S, Hall J, Babcock GF, Bernardi R, Pandolfi PP, Thomas G. Absence of nucleolar disruption after impairment of 40S ribosome biogenesis reveals an rpL11-translation-dependent mechanism of p53 induction. Nat Cell Biol. 2009; 11:501–08. https://doi.org/10.1038/ncb1858

87. Bursac S, Brdovcak MC, Donati G, Volarevic S. Activation of the tumor suppressor p53 upon impairment of ribosome biogenesis. Biochim Biophys Acta. 2014; 1842:817–30. https://doi.org/10.1016/j.bbadis.2013.08.014

88. Sherr CJ. Divorcing ARF and p53: an unsettled case. Nat Rev Cancer. 2006; 6:663–73. https://doi.org/10.1038/nrc1954

89. Quelle DE, Zindy F, Ashmun RA, Sherr CJ. Alternative reading frames of the INK4a tumor suppressor gene encode two unrelated proteins capable of inducing cell cycle arrest. Cell. 1995; 83:993–1000. https://doi.org/10.1016/0092-8674(95)90214-7

90. Korgaonkar C, Hagen J, Tompkins V, Frazier AA, Allamargot C, Quelle FW, Quelle DE. Nucleophosmin (B23) targets ARF to nucleoli and inhibits its function. Mol Cell Biol. 2005; 25:1258–71. https://doi.org/10.1128/MCB.25.4.1258-1271.2005

91. Sherr CJ. Ink4-Arf locus in cancer and aging. Wiley Interdiscip Rev Dev Biol. 2012; 1:731–41. https://doi.org/10.1002/wdev.40

92. Midgley CA, Desterro JM, Saville MK, Howard S, Sparks A, Hay RT, Lane DP. An N-terminal p14ARF peptide blocks Mdm2-dependent ubiquitination in vitro and can activate p53 in vivo. Oncogene. 2000; 19:2312–23. https://doi.org/10.1038/sj.onc.1203593

93. Qin FX, Shao HY, Chen XC, Tan S, Zhang HJ, Miao ZY, Wang L, Hui-Chen, Zhang L. Knockdown of NPM1 by RNA interference inhibits cells proliferation and induces apoptosis in leukemic cell line. Int J Med Sci. 2011; 8:287–94. https://doi.org/10.7150/ijms.8.287

94. Lessard F, Morin F, Ivanchuk S, Langlois F, Stefanovsky V, Rutka J, Moss T. The ARF tumor suppressor controls ribosome biogenesis by regulating the RNA polymerase I transcription factor TTF-I. Mol Cell. 2010; 38:539–50. https://doi.org/10.1016/j.molcel.2010.03.015

95. Ayrault O, Andrique L, Fauvin D, Eymin B, Gazzeri S, Séité P. Human tumor suppressor p14ARF negatively regulates rRNA transcription and inhibits UBF1 transcription factor phosphorylation. Oncogene. 2006; 25:7577–86. https://doi.org/10.1038/sj.onc.1209743

96. Kurki S, Peltonen K, Latonen L, Kiviharju TM, Ojala PM, Meek D, Laiho M. Nucleolar protein NPM interacts with HDM2 and protects tumor suppressor protein p53 from HDM2-mediated degradation. Cancer Cell. 2004; 5:465–75. https://doi.org/10.1016/S1535-6108(04)00110-2

97. Dhar SK, St Clair DK. Nucleophosmin blocks mitochondrial localization of p53 and apoptosis. J Biol Chem.

2009; 284:16409–18. https://doi.org/10.1074/jbc.M109.005736

98. Kerr LE, Birse-Archbold JL, Short DM, McGregor AL, Heron I, Macdonald DC, Thompson J, Carlson GJ, Kelly JS, McCulloch J, Sharkey J. Nucleophosmin is a novel Bax chaperone that regulates apoptotic cell death. Oncogene. 2007; 26:2554–62. https://doi.org/10.1038/sj.onc.1210044

99. Donati G, Brighenti E, Vici M, Mazzini G, Treré D, Montanaro L, Derenzini M. Selective inhibition of rRNA transcription downregulates E2F-1: a new p53-independent mechanism linking cell growth to cell proliferation. J Cell Sci. 2011; 124:3017–28. https://doi.org/10.1242/jcs.086074

100. Zhang Z, Wang H, Li M, Rayburn ER, Agrawal S, Zhang R. Stabilization of E2F1 protein by MDM2 through the E2F1 ubiquitination pathway. Oncogene. 2005; 24:7238–47. https://doi.org/10.1038/sj.onc.1208814

101. Crosby ME, Almasan A. Opposing roles of E2Fs in cell proliferation and death. Cancer Biol Ther. 2004; 3:1208–11. https://doi.org/10.4161/cbt.3.12.1494

102. Hollstein M, Sidransky D, Vogelstein B, Harris CC. p53 mutations in human cancers. Science. 1991; 253:49–53. https://doi.org/10.1126/science.1905840

103. Orsolic I, Jurada D, Pullen N, Oren M, Eliopoulos AG, Volarevic S. The relationship between the nucleolus and cancer: current evidence and emerging paradigms. Semin Cancer Biol. 2016; 37-38:36–50. https://doi.org/10.1016/j.semcancer.2015.12.004

104. Holmberg Olausson K, Nistér M, Lindström MS. p53 -Dependent and -Independent Nucleolar Stress Responses. Cells. 2012; 1:774–98. https://doi.org/10.3390/cells1040774

105. Donati G, Bertoni S, Brighenti E, Vici M, Treré D, Volarevic S, Montanaro L, Derenzini M. The balance between rRNA and ribosomal protein synthesis up- and downregulates the tumour suppressor p53 in mammalian cells. Oncogene. 2011; 30:3274–88. https://doi.org/10.1038/onc.2011.48

106. Yuan X, Zhou Y, Casanova E, Chai M, Kiss E, Gröne HJ, Schütz G, Grummt I. Genetic inactivation of the transcription factor TIF-IA leads to nucleolar disruption, cell cycle arrest, and p53-mediated apoptosis. Mol Cell. 2005; 19:77–87. https://doi.org/10.1016/j.molcel.2005.05.023

107. Hernandez-Verdun D, Roussel P, Thiry M, Sirri V, Lafontaine DL. The nucleolus: structure/function relationship in RNA metabolism. Wiley Interdiscip Rev RNA. 2010; 1:415–31. https://doi.org/10.1002/wrna.39

108. Burger K, Mühl B, Harasim T, Rohrmoser M, Malamoussi A, Orban M, Kellner M, Gruber-Eber A, Kremmer E, Hölzel M, Eick D. Chemotherapeutic drugs inhibit ribosome biogenesis at various levels. J Biol Chem. 2010; 285:12416–25. https://doi.org/10.1074/jbc.M109.074211

109. Peltonen K, Colis L, Liu H, Jäämaa S, Moore HM, Enbäck J, Laakkonen P, Vaahtokari A, Jones RJ, af Hällström TM, Laiho M. Identification of novel p53 pathway activating small-molecule compounds reveals unexpected similarities with known therapeutic agents. PLoS One. 2010; 5:e12996. https://doi.org/10.1371/journal.pone.0012996

110. Peltonen K, Colis L, Liu H, Trivedi R, Moubarek MS, Moore HM, Bai B, Rudek MA, Bieberich CJ, Laiho M. A targeting modality for destruction of RNA polymerase I that possesses anticancer activity. Cancer Cell. 2014; 25:77–90. https://doi.org/10.1016/j.ccr.2013.12.009

111. Drygin D, Siddiqui-Jain A, O'Brien S, Schwaebe M, Lin A, Bliesath J, Ho CB, Proffitt C, Trent K, Whitten JP, Lim JK, Von Hoff D, Anderes K, Rice WG. Anticancer activity of CX-3543: a direct inhibitor of rRNA biogenesis. Cancer Res. 2009; 69:7653–61. https://doi.org/10.1158/0008-5472.CAN-09-1304

112. Drygin D, Lin A, Bliesath J, Ho CB, O'Brien SE, Proffitt C, Omori M, Haddach M, Schwaebe MK, Siddiqui-Jain A, Streiner N, Quin JE, Sanij E, et al. Targeting RNA polymerase I with an oral small molecule CX-5461 inhibits ribosomal RNA synthesis and solid tumor growth. Cancer Res. 2011; 71:1418–30. https://doi.org/10.1158/0008-5472.CAN-10-1728

113. Bywater MJ, Poortinga G, Sanij E, Hein N, Peck A, Cullinane C, Wall M, Cluse L, Drygin D, Anderes K, Huser N, Proffitt C, Bliesath J, et al. Inhibition of RNA polymerase I as a therapeutic strategy to promote cancer-specific activation of p53. Cancer Cell. 2012; 22:51–65. https://doi.org/10.1016/j.ccr.2012.05.019

114. National Health and Medical Research Council. (2013). A Phase 1, Open-Label, Dose Escalation, Safety, Pharmacokinetic, and Pharmacodynamic Study of Intravenously Administered CX-5461 in Patients with Advanced Haematologic Malignancies. https://www.anzctr.org.au/Trial/Registration/TrialReview.aspx?id=364713 Registration number: ACTRN12613001061729. Australian New Zealand Clinical Trials Registry.

115. Canadian Cancer Trials Group. (2016). A Phase I Study of CX5461. Available from: https://ClinicalTrials.gov/show/NCT02719977. NLM identifier: NCT02719977

116. Xu H, Di Antonio M, McKinney S, Mathew V, Ho B, O'Neil NJ, Santos ND, Silvester J, Wei V, Garcia J, Kabeer F, Lai D, Soriano P, et al. CX-5461 is a DNA G-quadruplex stabilizer with selective lethality in

BRCA1/2 deficient tumours. Nat Commun. 2017; 8:14432. https://doi.org/10.1038/ncomms14432

117. Onofrillo C. (2013). Ribosome Biogenesis and cell cycle regulation: Effect of RNA Polymerase III inhibition [dissertation]. Oncologia e Patologia Sperimentale: Uniiversiittà dii Bollogna.

118. Engelke DR, Ng SY, Shastry BS, Roeder RG. Specific interaction of a purified transcription factor with an internal control region of 5S RNA genes. Cell. 1980; 19:717–28. https://doi.org/10.1016/S0092-8674(80)80048-1

119. Shastry BS, Honda BM, Roeder RG. Altered levels of a 5 S gene-specific transcription factor (TFIIIA) during oogenesis and embryonic development of Xenopus laevis. J Biol Chem. 1984; 259:11373–82.

120. Nishimura K, Kumazawa T, Kuroda T, Katagiri N, Tsuchiya M, Goto N, Furumai R, Murayama A, Yanagisawa J, Kimura K. Perturbation of ribosome biogenesis drives cells into senescence through 5S RNP-mediated p53 activation. Cell Reports. 2015; 10:1310–23. https://doi.org/10.1016/j.celrep.2015.01.055

121. Chang CC, Steinbacher DM. Treacher collins syndrome. Semin Plast Surg. 2012; 26:83–90. https://doi.org/10.1055/s-0032-1320066

122. Posnick JC. 2013. Principles and Practice of Orthognathic Surgery. Elsevier Health Sciences. Chapter 4, Frequently Seen Malformations with Dentofacial Deformity. p. 1059-94.

123. Kadakia S, Helman SN, Badhey AK, Saman M, Ducic Y. Treacher Collins Syndrome: the genetics of a craniofacial disease. Int J Pediatr Otorhinolaryngol. 2014; 78:893–98. https://doi.org/10.1016/j.ijporl.2014.03.006

124. Ahmed MK, Ye X, Taub PJ. Review of the Genetic Basis of Jaw Malformations. J Pediatr Genet. 2016; 5:209–19. https://doi.org/10.1055/s-0036-1593505

125. Valdez BC, Henning D, So RB, Dixon J, Dixon MJ. The Treacher Collins syndrome (TCOF1) gene product is involved in ribosomal DNA gene transcription by interacting with upstream binding factor. Proc Natl Acad Sci USA. 2004; 101:10709–14. https://doi.org/10.1073/pnas.0402492101

126. Gonzales B, Henning D, So RB, Dixon J, Dixon MJ, Valdez BC. The Treacher Collins syndrome (TCOF1) gene product is involved in pre-rRNA methylation. Hum Mol Genet. 2005; 14:2035–43. https://doi.org/10.1093/hmg/ddi208

127. Dixon J, Jones NC, Sandell LL, Jayasinghe SM, Crane J, Rey JP, Dixon MJ, Trainor PA. Tcof1/Treacle is required for neural crest cell formation and proliferation deficiencies that cause craniofacial abnormalities. Proc Natl Acad Sci USA. 2006; 103:13403–08. https://doi.org/10.1073/pnas.0603730103

128. Graham A, Koentges G, Lumsden A. Neural Crest Apoptosis and the Establishment of Craniofacial Pattern: An Honorable Death. Mol Cell Neurosci. 1996; 8:76–83. https://doi.org/10.1006/mcne.1996.0046

129. Jones NC, Lynn ML, Gaudenz K, Sakai D, Aoto K, Rey JP, Glynn EF, Ellington L, Du C, Dixon J, Dixon MJ, Trainor PA. Prevention of the neurocristopathy Treacher Collins syndrome through inhibition of p53 function. Nat Med. 2008; 14:125–33. https://doi.org/10.1038/nm1725

130. Larsen DH, Hari F, Clapperton JA, Gwerder M, Gutsche K, Altmeyer M, Jungmichel S, Toledo LI, Fink D, Rask MB, Grøfte M, Lukas C, Nielsen ML, et al. The NBS1-Treacle complex controls ribosomal RNA transcription in response to DNA damage. Nat Cell Biol. 2014; 16:792–803. https://doi.org/10.1038/ncb3007

131. Ciccia A, Huang JW, Izhar L, Sowa ME, Harper JW, Elledge SJ. Treacher Collins syndrome TCOF1 protein cooperates with NBS1 in the DNA damage response. Proc Natl Acad Sci USA. 2014; 111:18631–36. https://doi.org/10.1073/pnas.1422488112

132. Sakai D, Dixon J, Achilleos A, Dixon M, Trainor PA. Prevention of Treacher Collins syndrome craniofacial anomalies in mouse models via maternal antioxidant supplementation. Nat Commun. 2016; 7:10328. https://doi.org/10.1038/ncomms10328

133. Cadet J, Wagner JR. DNA base damage by reactive oxygen species, oxidizing agents, and UV radiation. Cold Spring Harb Perspect Biol. 2013; 5:a012559. https://doi.org/10.1101/cshperspect.a012559

134. Jena NR. DNA damage by reactive species: Mechanisms, mutation and repair. J Biosci. 2012; 37:503–17. https://doi.org/10.1007/s12038-012-9218-2

135. Calo E, Gu B, Bowen ME, Aryan F, Zalc A, Liang J, Flynn RA, Swigut T, Chang HY, Attardi LD, Wysocka J. Tissue-selective effects of nucleolar stress and rDNA damage in developmental disorders. Nature. 2018; 554:112–17. https://doi.org/10.1038/nature25449

136. Turi Z, Senkyrikova M, Mistrik M, Bartek J, Moudry P. Perturbation of RNA Polymerase I transcription machinery by ablation of HEATR1 triggers the RPL5/RPL11-MDM2-p53 ribosome biogenesis stress checkpoint pathway in human cells. Cell Cycle. 2018; 17:92–101.

https://doi.org/10.1080/15384101.2017.1403685

137. Gallagher JE, Dunbar DA, Granneman S, Mitchell BM, Osheim Y, Beyer AL, Baserga SJ. RNA polymerase I transcription and pre-rRNA processing are linked by specific SSU processome components. Genes Dev. 2004; 18:2506–17. https://doi.org/10.1101/gad.1226604

138. Dez C, Dlakić M, Tollervey D. Roles of the HEAT repeat proteins Utp10 and Utp20 in 40S ribosome maturation. RNA. 2007; 13:1516–27. https://doi.org/10.1261/rna.609807

139. Krogan NJ, Peng WT, Cagney G, Robinson MD, Haw R, Zhong G, Guo X, Zhang X, Canadien V, Richards DP, Beattie BK, Lalev A, Zhang W, et al. High-definition macromolecular composition of yeast RNA-processing complexes. Mol Cell. 2004; 13:225–39. https://doi.org/10.1016/S1097-2765(04)00003-6

140. Shav-Tal Y, Blechman J, Darzacq X, Montagna C, Dye BT, Patton JG, Singer RH, Zipori D. Dynamic sorting of nuclear components into distinct nucleolar caps during transcriptional inhibition. Mol Biol Cell. 2005; 16:2395–413. https://doi.org/10.1091/mbc.e04-11-0992

141. Peng Q, Wu J, Zhang Y, Liu Y, Kong R, Hu L, Du X, Ke Y. 1A6/DRIM, a novel t-UTP, activates RNA polymerase I transcription and promotes cell proliferation. PLoS One. 2010; 5:e14244. https://doi.org/10.1371/journal.pone.0014244

142. Zhao C, Andreeva V, Gibert Y, LaBonty M, Lattanzi V, Prabhudesai S, Zhou Y, Zon L, McCann KL, Baserga S, Yelick PC. Tissue specific roles for the ribosome biogenesis factor Wdr43 in zebrafish development. PLoS Genet. 2014; 10:e1004074. https://doi.org/10.1371/journal.pgen.1004074

143. Griffin JN, Sondalle SB, Del Viso F, Baserga SJ, Khokha MK. The ribosome biogenesis factor Nol11 is required for optimal rDNA transcription and craniofacial development in Xenopus. PLoS Genet. 2015; 11:e1005018. https://doi.org/10.1371/journal.pgen.1005018

144. Hölzel M, Rohrmoser M, Schlee M, Grimm T, Harasim T, Malamoussi A, Gruber-Eber A, Kremmer E, Hiddemann W, Bornkamm GW, Eick D. Mammalian WDR12 is a novel member of the Pes1-Bop1 complex and is required for ribosome biogenesis and cell proliferation. J Cell Biol. 2005; 170:367–78. https://doi.org/10.1083/jcb.200501141

145. Yu W, Qiu Z, Gao N, Wang L, Cui H, Qian Y, Jiang L, Luo J, Yi Z, Lu H, Li D, Liu M. PAK1IP1, a ribosomal stress-induced nucleolar protein, regulates cell proliferation via the p53-MDM2 loop. Nucleic Acids Res. 2011; 39:2234–48. https://doi.org/10.1093/nar/gkq1117

146. McMahon M, Ayllón V, Panov KI, O'Connor R. Ribosomal 18 S RNA processing by the IGF-I-responsive WDR3 protein is integrated with p53 function in cancer cell proliferation. J Biol Chem. 2010; 285:18309–18. https://doi.org/10.1074/jbc.M110.108555

147. Skarie JM, Link BA. The primary open-angle glaucoma gene WDR36 functions in ribosomal RNA processing and interacts with the p53 stress-response pathway. Hum Mol Genet. 2008; 17:2474–85. https://doi.org/10.1093/hmg/ddn147

148. Watanabe-Susaki K, Takada H, Enomoto K, Miwata K, Ishimine H, Intoh A, Ohtaka M, Nakanishi M, Sugino H, Asashima M, Kurisaki A. Biosynthesis of ribosomal RNA in nucleoli regulates pluripotency and differentiation ability of pluripotent stem cells. Stem Cells. 2014; 32:3099–111. https://doi.org/10.1002/stem.1825

149. Langhendries JL, Nicolas E, Doumont G, Goldman S, Lafontaine DL. The human box C/D snoRNAs U3 and U8 are required for pre-rRNA processing and tumorigenesis. Oncotarget. 2016; 7:59519–34. https://doi.org/10.18632/oncotarget.11148

150. Choi YW, Kim YW, Bae SM, Kwak SY, Chun HJ, Tong SY, Lee HN, Shin JC, Kim KT, Kim YJ, Ahn WS. Identification of differentially expressed genes using annealing control primer-based GeneFishing in human squamous cell cervical carcinoma. Clin Oncol (R Coll Radiol). 2007; 19:308–18. https://doi.org/10.1016/j.clon.2007.02.010

151. Koh CM, Gurel B, Sutcliffe S, Aryee MJ, Schultz D, Iwata T, Uemura M, Zeller KI, Anele U, Zheng Q, Hicks JL, Nelson WG, Dang CV, et al. Alterations in nucleolar structure and gene expression programs in prostatic neoplasia are driven by the MYC oncogene. Am J Pathol. 2011; 178:1824–34. https://doi.org/10.1016/j.ajpath.2010.12.040

152. Su H, Xu T, Ganapathy S, Shadfan M, Long M, Huang TH, Thompson I, Yuan ZM. Elevated snoRNA biogenesis is essential in breast cancer. Oncogene. 2014; 33:1348–58. https://doi.org/10.1038/onc.2013.89

153. Belin S, Beghin A, Solano-Gonzàlez E, Bezin L, Brunet-Manquat S, Textoris J, Prats AC, Mertani HC, Dumontet C, Diaz JJ. Dysregulation of ribosome biogenesis and translational capacity is associated with tumor progression of human breast cancer cells. PLoS One. 2009; 4:e7147. https://doi.org/10.1371/journal.pone.0007147

154. Marcel V, Ghayad SE, Belin S, Therizols G, Morel AP, Solano-Gonzàlez E, Vendrell JA, Hacot S, Mertani HC,

Albaret MA, Bourdon JC, Jordan L, Thompson A, et al. p53 acts as a safeguard of translational control by regulating fibrillarin and rRNA methylation in cancer. Cancer Cell. 2013; 24:318–30. https://doi.org/10.1016/j.ccr.2013.08.013

155. Sharma S, Marchand V, Motorin Y, Lafontaine DL. Identification of sites of 2′-O-methylation vulnerability in human ribosomal RNAs by systematic mapping. Sci Rep. 2017; 7:11490. https://doi.org/10.1038/s41598-017-09734-9

156. Kirwan M, Dokal I. Dyskeratosis congenita: a genetic disorder of many faces. Clin Genet. 2008; 73:103–12. https://doi.org/10.1111/j.1399-0004.2007.00923.x

157. Wilson DB, Link DC, Mason PJ, Bessler M. Inherited bone marrow failure syndromes in adolescents and young adults. Ann Med. 2014; 46:353–63. https://doi.org/10.3109/07853890.2014.915579

158. Fok WC, Niero EL, Dege C, Brenner KA, Sturgeon CM, Batista LF. p53 Mediates Failure of Human Definitive Hematopoiesis in Dyskeratosis Congenita. Stem Cell Reports. 2017; 9:409–18. https://doi.org/10.1016/j.stemcr.2017.06.015

159. Carrillo J, González A, Manguán-García C, Pintado-Berninches L, Perona R. p53 pathway activation by telomere attrition in X-DC primary fibroblasts occurs in the absence of ribosome biogenesis failure and as a consequence of DNA damage. Clin Transl Oncol. 2014; 16:529–38. https://doi.org/10.1007/s12094-013-1112-3

160. Mason PJ, Bessler M. The genetics of dyskeratosis congenita. Cancer Genet. 2011; 204:635–45. https://doi.org/10.1016/j.cancergen.2011.11.002

161. Bellodi C, Kopmar N, Ruggero D. Deregulation of oncogene-induced senescence and p53 translational control in X-linked dyskeratosis congenita. EMBO J. 2010; 29:1865–76. https://doi.org/10.1038/emboj.2010.83

162. Yoon A, Peng G, Brandenburger Y, Zollo O, Xu W, Rego E, Ruggero D. Impaired control of IRES-mediated translation in X-linked dyskeratosis congenita. Science. 2006; 312:902–06. https://doi.org/10.1126/science.1123835

163. Liu B, Zhang J, Huang C, Liu H. Dyskerin overexpression in human hepatocellular carcinoma is associated with advanced clinical stage and poor patient prognosis. PLoS One. 2012; 7:e43147. https://doi.org/10.1371/journal.pone.0043147

164. Sieron P, Hader C, Hatina J, Engers R, Wlazlinski A, Müller M, Schulz WA. DKC1 overexpression associated with prostate cancer progression. Br J Cancer. 2009; 101:1410–16. https://doi.org/10.1038/sj.bjc.6605299

165. Takagi M, Absalon MJ, McLure KG, Kastan MB. Regulation of p53 translation and induction after DNA damage by ribosomal protein L26 and nucleolin. Cell. 2005; 123:49–63. https://doi.org/10.1016/j.cell.2005.07.034

166. Jia W, Yao Z, Zhao J, Guan Q, Gao L. New perspectives of physiological and pathological functions of nucleolin (NCL). Life Sci. 2017; 186:1–10. https://doi.org/10.1016/j.lfs.2017.07.025

167. Abdelmohsen K, Gorospe M. RNA-binding protein nucleolin in disease. RNA Biol. 2012; 9:799–808. https://doi.org/10.4161/rna.19718

168. Berger CM, Gaume X, Bouvet P. The roles of nucleolin subcellular localization in cancer. Biochimie. 2015; 113:78–85. https://doi.org/10.1016/j.biochi.2015.03.023

169. Farin K, Schokoroy S, Haklai R, Cohen-Or I, Elad-Sfadia G, Reyes-Reyes ME, Bates PJ, Cox AD, Kloog Y, Pinkas-Kramarski R. Oncogenic synergism between ErbB1, nucleolin, and mutant Ras. Cancer Res. 2011; 71:2140–51. https://doi.org/10.1158/0008-5472.CAN-10-2887

170. Tajrishi MM, Tuteja R, Tuteja N. Nucleolin: the most abundant multifunctional phosphoprotein of nucleolus. Commun Integr Biol. 2011; 4:267–75. https://doi.org/10.4161/cib.4.3.14884

171. Soundararajan S, Chen W, Spicer EK, Courtenay-Luck N, Fernandes DJ. The nucleolin targeting aptamer AS1411 destabilizes Bcl-2 messenger RNA in human breast cancer cells. Cancer Res. 2008; 68:2358–65. https://doi.org/10.1158/0008-5472.CAN-07-5723

172. Bates PJ, Laber DA, Miller DM, Thomas SD, Trent JO. Discovery and development of the G-rich oligonucleotide AS1411 as a novel treatment for cancer. Exp Mol Pathol. 2009; 86:151–64. https://doi.org/10.1016/j.yexmp.2009.01.004

173. Laber DA, Taft BS, Kloecker GH, Bates PJ, Trent JO, Miller DM. Extended phase I study of AS1411 in renal and non-small cell lung cancers. J Clin Oncol. 2006; 24:13098.

174. Laber DA, Choudry MA, Taft BS, Bhupalam L, Sharma VR, Hendler FJ, Barnhart KM. A phase I study of AGRO100 in advanced cancer. J Clin Oncol. 2004; 22:3112. https://doi.org/10.1200/jco.2004.22.14_suppl.3112

175. Rosenberg JE, Bambury RM, Van Allen EM, Drabkin HA, Lara PN Jr, Harzstark AL, Wagle N, Figlin RA, Smith GW, Garraway LA, Choueiri T, Erlandsson F, Laber DA. A phase II trial of AS1411 (a novel nucleolin-targeted DNA aptamer) in metastatic renal cell carcinoma.

Invest New Drugs. 2014; 32:178–87. https://doi.org/10.1007/s10637-013-0045-6

176. Stuart RK, Stockerl-Goldstein K, Cooper M, Devetten M, Herzig R, Medeiros B, Schiller G, Wei A, Acton G, Rizzieri D. Randomized phase II trial of the nucleolin targeting aptamer AS1411 combined with high-dose cytarabine in relapsed/refractory acute myeloid leukemia (AML). J Clin Oncol. 2009; 27:7019.

177. Colombo E, Alcalay M, Pelicci PG. Nucleophosmin and its complex network: a possible therapeutic target in hematological diseases. Oncogene. 2011; 30:2595–609. https://doi.org/10.1038/onc.2010.646

178. Lim MJ, Wang XW. Nucleophosmin and human cancer. Cancer Detect Prev. 2006; 30:481–90. https://doi.org/10.1016/j.cdp.2006.10.008

179. Holmberg Olausson K, Elsir T, Moazemi Goudarzi K, Nistér M, Lindström MS. NPM1 histone chaperone is upregulated in glioblastoma to promote cell survival and maintain nucleolar shape. Sci Rep. 2015; 5:16495. https://doi.org/10.1038/srep16495

180. Coutinho-Camillo CM, Lourenço SV, Nishimoto IN, Kowalski LP, Soares FA. Nucleophosmin, p53, and Ki-67 expression patterns on an oral squamous cell carcinoma tissue microarray. Hum Pathol. 2010; 41:1079–86. https://doi.org/10.1016/j.humpath.2009.12.010

181. Sekhar KR, Benamar M, Venkateswaran A, Sasi S, Penthala NR, Crooks PA, Hann SR, Geng L, Balusu R, Abbas T, Freeman ML. Targeting nucleophosmin 1 represents a rational strategy for radiation sensitization. Int J Radiat Oncol Biol Phys. 2014; 89:1106–14. https://doi.org/10.1016/j.ijrobp.2014.04.012

182. Liu X, Liu D, Qian D, Dai J, An Y, Jiang S, Stanley B, Yang J, Wang B, Liu X, Liu DX. Nucleophosmin (NPM1/B23) interacts with activating transcription factor 5 (ATF5) protein and promotes proteasome- and caspase-dependent ATF5 degradation in hepatocellular carcinoma cells. J Biol Chem. 2012; 287:19599–609. https://doi.org/10.1074/jbc.M112.363622

183. Kim KH, Yoo BC, Kim WK, Hong JP, Kim K, Song EY, Lee JY, Cho JY, Ku JL. CD133 and CD133-regulated nucleophosmin linked to 5-fluorouracil susceptibility in human colon cancer cell line SW620. Electrophoresis. 2014; 35:522–32. https://doi.org/10.1002/elps.201300364

184. Wong JC, Hasan MR, Rahman M, Yu AC, Chan SK, Schaeffer DF, Kennecke HF, Lim HJ, Owen D, Tai IT. Nucleophosmin 1, upregulated in adenomas and cancers of the colon, inhibits p53-mediated cellular senescence. Int J Cancer. 2013; 133:1567–77. https://doi.org/10.1002/ijc.28180

185. Kalra RS, Bapat SA. Enhanced levels of double-strand DNA break repair proteins protect ovarian cancer cells against genotoxic stress-induced apoptosis. J Ovarian Res. 2013; 6:66. https://doi.org/10.1186/1757-2215-6-66

186. Zhou Y, Shen J, Xia L, Wang Y. Estrogen mediated expression of nucleophosmin 1 in human endometrial carcinoma clinical stages through estrogen receptor-α signaling. Cancer Cell Int. 2014; 14:540. https://doi.org/10.1186/s12935-014-0145-1

187. Léotoing L, Meunier L, Manin M, Mauduit C, Decaussin M, Verrijdt G, Claessens F, Benahmed M, Veyssière G, Morel L, Beaudoin C. Influence of nucleophosmin/B23 on DNA binding and transcriptional activity of the androgen receptor in prostate cancer cell. Oncogene. 2008; 27:2858–67. https://doi.org/10.1038/sj.onc.1210942

188. Tsui KH, Cheng AJ, Chang P, Pan TL, Yung BY. Association of nucleophosmin/B23 mRNA expression with clinical outcome in patients with bladder carcinoma. Urology. 2004; 64:839–44. https://doi.org/10.1016/j.urology.2004.05.020

189. Pianta A, Puppin C, Franzoni A, Fabbro D, Di Loreto C, Bulotta S, Deganuto M, Paron I, Tell G, Puxeddu E, Filetti S, Russo D, Damante G. Nucleophosmin is overexpressed in thyroid tumors. Biochem Biophys Res Commun. 2010; 397:499–504. https://doi.org/10.1016/j.bbrc.2010.05.142

190. Leal MF, Mazzotti TK, Calcagno DQ, Cirilo PD, Martinez MC, Demachki S, Assumpção PP, Chammas R, Burbano RR, Smith MC. Deregulated expression of Nucleophosmin 1 in gastric cancer and its clinicopathological implications. BMC Gastroenterol. 2014; 14:9. https://doi.org/10.1186/1471-230X-14-9

191. Karhemo PR, Rivinoja A, Lundin J, Hyvönen M, Chernenko A, Lammi J, Sihto H, Lundin M, Heikkilä P, Joensuu H, Bono P, Laakkonen P. An extensive tumor array analysis supports tumor suppressive role for nucleophosmin in breast cancer. Am J Pathol. 2011; 179:1004–14. https://doi.org/10.1016/j.ajpath.2011.04.009

192. Falini B, Martelli MP, Bolli N, Sportoletti P, Liso A, Tiacci E, Haferlach T. Acute myeloid leukemia with mutated nucleophosmin (NPM1): is it a distinct entity? Blood. 2011; 117:1109–20. https://doi.org/10.1182/blood-2010-08-299990

193. Naoe T, Suzuki T, Kiyoi H, Urano T. Nucleophosmin: a versatile molecule associated with hematological malignancies. Cancer Sci. 2006; 97:963–69. https://doi.org/10.1111/j.1349-7006.2006.00270.x

194. Di Matteo A, Franceschini M, Chiarella S, Rocchio S, Travaglini-Allocatelli C, Federici L. Molecules that target nucleophosmin for cancer treatment: an update. Oncotarget. 2016; 7:44821–40. https://doi.org/10.18632/oncotarget.8599

195. Qi W, Shakalya K, Stejskal A, Goldman A, Beeck S, Cooke L, Mahadevan D. NSC348884, a nucleophosmin inhibitor disrupts oligomer formation and induces apoptosis in human cancer cells. Oncogene. 2008; 27:4210–20. https://doi.org/10.1038/onc.2008.54

196. Balusu R, Fiskus W, Rao R, Chong DG, Nalluri S, Mudunuru U, Ma H, Chen L, Venkannagari S, Ha K, Abhyankar S, Williams C, McGuirk J, et al. Targeting levels or oligomerization of nucleophosmin 1 induces differentiation and loss of survival of human AML cells with mutant NPM1. Blood. 2011; 118:3096–106. https://doi.org/10.1182/blood-2010-09-309674

197. Lindström MS, Nistér M. Silencing of ribosomal protein S9 elicits a multitude of cellular responses inhibiting the growth of cancer cells subsequent to p53 activation. PLoS One. 2010; 5:e9578. https://doi.org/10.1371/journal.pone.0009578

198. Jin A, Itahana K, O'Keefe K, Zhang Y. Inhibition of HDM2 and activation of p53 by ribosomal protein L23. Mol Cell Biol. 2004; 24:7669–80. https://doi.org/10.1128/MCB.24.17.7669-7680.2004

199. Barkić M, Crnomarković S, Grabusić K, Bogetić I, Panić L, Tamarut S, Cokarić M, Jerić I, Vidak S, Volarević S. The p53 tumor suppressor causes congenital malformations in Rpl24-deficient mice and promotes their survival. Mol Cell Biol. 2009; 29:2489–504. https://doi.org/10.1128/MCB.01588-08

200. Sun XX, Wang YG, Xirodimas DP, Dai MS. Perturbation of 60 S ribosomal biogenesis results in ribosomal protein L5- and L11-dependent p53 activation. J Biol Chem. 2010; 285:25812–21. https://doi.org/10.1074/jbc.M109.098442

201. Llanos S, Serrano M. Depletion of ribosomal protein L37 occurs in response to DNA damage and activates p53 through the L11/MDM2 pathway. Cell Cycle. 2010; 9:4005–12. https://doi.org/10.4161/cc.9.19.13299

202. Dutt S, Narla A, Lin K, Mullally A, Abayasekara N, Megerdichian C, Wilson FH, Currie T, Khanna-Gupta A, Berliner N, Kutok JL, Ebert BL. Haploinsufficiency for ribosomal protein genes causes selective activation of p53 in human erythroid progenitor cells. Blood. 2011; 117:2567–76. https://doi.org/10.1182/blood-2010-07-295238

203. Zhou X, Hao Q, Liao J, Zhang Q, Lu H. Ribosomal protein S14 unties the MDM2-p53 loop upon ribosomal stress. Oncogene. 2013; 32:388–96. https://doi.org/10.1038/onc.2012.63

204. Daftuar L, Zhu Y, Jacq X, Prives C. Ribosomal proteins RPL37, RPS15 and RPS20 regulate the Mdm2-p53-MdmX network. PLoS One. 2013; 8:e68667. https://doi.org/10.1371/journal.pone.0068667

205. Narla A, Ebert BL. Ribosomopathies: human disorders of ribosome dysfunction. Blood. 2010; 115:3196–205. https://doi.org/10.1182/blood-2009-10-178129

206. Lipton JM, Ellis SR. Diamond-Blackfan anemia: diagnosis, treatment, and molecular pathogenesis. Hematol Oncol Clin North Am. 2009; 23:261–82. https://doi.org/10.1016/j.hoc.2009.01.004

207. Ellis SR, Gleizes PE. Diamond Blackfan anemia: ribosomal proteins going rogue. Semin Hematol. 2011; 48:89–96. https://doi.org/10.1053/j.seminhematol.2011.02.005

208. Nakhoul H, Ke J, Zhou X, Liao W, Zeng SX, Lu H. Ribosomopathies: mechanisms of disease. Clin Med Insights Blood Disord. 2014; 7:7–16. https://doi.org/10.4137/CMBD.S16952

209. Chiabrando D, Tolosano E. Diamond Blackfan Anemia at the Crossroad between Ribosome Biogenesis and Heme Metabolism. Adv Hematol. 2010; 2010:790632. https://doi.org/10.1155/2010/790632

210. Ellis SR. Nucleolar stress in Diamond Blackfan anemia pathophysiology. Biochim Biophys Acta. 2014; 1842:765–68. https://doi.org/10.1016/j.bbadis.2013.12.013

211. Keel SB, Doty RT, Yang Z, Quigley JG, Chen J, Knoblaugh S, Kingsley PD, De Domenico I, Vaughn MB, Kaplan J, Palis J, Abkowitz JL. A heme export protein is required for red blood cell differentiation and iron homeostasis. Science. 2008; 319:825–28. https://doi.org/10.1126/science.1151133

212. McGowan KA, Li JZ, Park CY, Beaudry V, Tabor HK, Sabnis AJ, Zhang W, Fuchs H, de Angelis MH, Myers RM, Attardi LD, Barsh GS. Ribosomal mutations cause p53-mediated dark skin and pleiotropic effects. Nat Genet. 2008; 40:963–70. https://doi.org/10.1038/ng.188

213. Jaako P, Flygare J, Olsson K, Quere R, Ehinger M, Henson A, Ellis S, Schambach A, Baum C, Richter J, Larsson J, Bryder D, Karlsson S. Mice with ribosomal protein S19 deficiency develop bone marrow failure and symptoms like patients with Diamond-Blackfan anemia. Blood. 2011; 118:6087–96. https://doi.org/10.1182/blood-2011-08-371963

214. Danilova N, Sakamoto KM, Lin S. Ribosomal protein S19 deficiency in zebrafish leads to developmental abnormalities and defective erythropoiesis through

activation of p53 protein family. Blood. 2008; 112:5228–37. https://doi.org/10.1182/blood-2008-01-132290

215. Torihara H, Uechi T, Chakraborty A, Shinya M, Sakai N, Kenmochi N. Erythropoiesis failure due to RPS19 deficiency is independent of an activated Tp53 response in a zebrafish model of Diamond-Blackfan anaemia. Br J Haematol. 2011; 152:648–54. https://doi.org/10.1111/j.1365-2141.2010.08535.x

216. Padron E, Komrokji R, List AF. Biology and treatment of the 5q- syndrome. Expert Rev Hematol. 2011; 4:61–69. https://doi.org/10.1586/ehm.11.2

217. Pellagatti A, Boultwood J. Recent Advances in the 5q-Syndrome. Mediterr J Hematol Infect Dis. 2015; 7:e2015037. https://doi.org/10.4084/mjhid.2015.037

218. Ebert BL, Pretz J, Bosco J, Chang CY, Tamayo P, Galili N, Raza A, Root DE, Attar E, Ellis SR, Golub TR. Identification of RPS14 as a 5q- syndrome gene by RNA interference screen. Nature. 2008; 451:335–39. https://doi.org/10.1038/nature06494

219. Barlow JL, Drynan LF, Hewett DR, Holmes LR, Lorenzo-Abalde S, Lane AL, Jolin HE, Pannell R, Middleton AJ, Wong SH, Warren AJ, Wainscoat JS, Boultwood J, McKenzie AN. A p53-dependent mechanism underlies macrocytic anemia in a mouse model of human 5q-syndrome. Nat Med. 2010; 16:59–66. https://doi.org/10.1038/nm.2063

220. Shi Y, Zhai H, Wang X, Han Z, Liu C, Lan M, Du J, Guo C, Zhang Y, Wu K, Fan D. Ribosomal proteins S13 and L23 promote multidrug resistance in gastric cancer cells by suppressing drug-induced apoptosis. Exp Cell Res. 2004; 296:337–46. https://doi.org/10.1016/j.yexcr.2004.02.009

221. Golomb L, Bublik DR, Wilder S, Nevo R, Kiss V, Grabusic K, Volarevic S, Oren M. Importin 7 and exportin 1 link c-Myc and p53 to regulation of ribosomal biogenesis. Mol Cell. 2012; 45:222–32. https://doi.org/10.1016/j.molcel.2011.11.022

222. Kressler D, Bange G, Ogawa Y, Stjepanovic G, Bradatsch B, Pratte D, Amlacher S, Strauß D, Yoneda Y, Katahira J, Sinning I, Hurt E. Synchronizing nuclear import of ribosomal proteins with ribosome assembly. Science. 2012; 338:666–71. https://doi.org/10.1126/science.1226960

223. Calviño FR, Kharde S, Ori A, Hendricks A, Wild K, Kressler D, Bange G, Hurt E, Beck M, Sinning I. Symportin 1 chaperones 5S RNP assembly during ribosome biogenesis by occupying an essential rRNA-binding site. Nat Commun. 2015; 6:6510. https://doi.org/10.1038/ncomms7510

224. Kazyken D, Kaz Y, Kiyan V, Zhylkibayev AA, Chen CH, Agarwal NK, Sarbassov D. The nuclear import of ribosomal proteins is regulated by mTOR. Oncotarget. 2014; 5:9577–93. https://doi.org/10.18632/oncotarget.2473

225. Finch AJ, Hilcenko C, Basse N, Drynan LF, Goyenechea B, Menne TF, González Fernández A, Simpson P, D'Santos CS, Arends MJ, Donadieu J, Bellanné-Chantelot C, Costanzo M, et al. Uncoupling of GTP hydrolysis from eIF6 release on the ribosome causes Shwachman-Diamond syndrome. Genes Dev. 2011; 25:917–29. https://doi.org/10.1101/gad.623011

226. Wong CC, Traynor D, Basse N, Kay RR, Warren AJ. Defective ribosome assembly in Shwachman-Diamond syndrome. Blood. 2011; 118:4305–12. https://doi.org/10.1182/blood-2011-06-353938

227. Burwick N, Coats SA, Nakamura T, Shimamura A. Impaired ribosomal subunit association in Shwachman-Diamond syndrome. Blood. 2012; 120:5143–52. https://doi.org/10.1182/blood-2012-04-420166

228. Burroughs L, Woolfrey A, Shimamura A. Shwachman-Diamond syndrome: a review of the clinical presentation, molecular pathogenesis, diagnosis, and treatment. Hematol Oncol Clin North Am. 2009; 23:233–48. https://doi.org/10.1016/j.hoc.2009.01.007

229. Nelson AS, Myers KC. Diagnosis, Treatment, and Molecular Pathology of Shwachman-Diamond Syndrome. Hematol Oncol Clin North Am. 2018; 32:687–700. https://doi.org/10.1016/j.hoc.2018.04.006

230. Austin KM, Leary RJ, Shimamura A. The Shwachman-Diamond SBDS protein localizes to the nucleolus. Blood. 2005; 106:1253–58. https://doi.org/10.1182/blood-2005-02-0807

231. Ganapathi KA, Austin KM, Lee CS, Dias A, Malsch MM, Reed R, Shimamura A. The human Shwachman-Diamond syndrome protein, SBDS, associates with ribosomal RNA. Blood. 2007; 110:1458–65. https://doi.org/10.1182/blood-2007-02-075184

232. Elghetany MT, Alter BP. p53 protein overexpression in bone marrow biopsies of patients with Shwachman-Diamond syndrome has a prevalence similar to that of patients with refractory anemia. Arch Pathol Lab Med. 2002; 126:452–55.

233. Dror Y. P53 protein overexpression in Shwachman-Diamond syndrome. Arch Pathol Lab Med. 2002; 126:1157–58.

234. Provost E, Wehner KA, Zhong X, Ashar F, Nguyen E, Green R, Parsons MJ, Leach SD. Ribosomal biogenesis genes play an essential and p53-independent role in

zebrafish pancreas development. Development. 2012; 139:3232–41. https://doi.org/10.1242/dev.077107

235. Tourlakis ME, Zhang S, Ball HL, Gandhi R, Liu H, Zhong J, Yuan JS, Guidos CJ, Durie PR, Rommens JM. In Vivo Senescence in the Sbds-Deficient Murine Pancreas: Cell-Type Specific Consequences of Translation Insufficiency. PLoS Genet. 2015; 11:e1005288. https://doi.org/10.1371/journal.pgen.1005288

236. Evans DS, Kapahi P, Hsueh WC, Kockel L. TOR signaling never gets old: aging, longevity and TORC1 activity. Ageing Res Rev. 2011; 10:225–37. https://doi.org/10.1016/j.arr.2010.04.001

237. Steffen KK, MacKay VL, Kerr EO, Tsuchiya M, Hu D, Fox LA, Dang N, Johnston ED, Oakes JA, Tchao BN, Pak DN, Fields S, Kennedy BK, Kaeberlein M. Yeast life span extension by depletion of 60s ribosomal subunits is mediated by Gcn4. Cell. 2008; 133:292–302. https://doi.org/10.1016/j.cell.2008.02.037

238. Hansen M, Taubert S, Crawford D, Libina N, Lee SJ, Kenyon C. Lifespan extension by conditions that inhibit translation in Caenorhabditis elegans. Aging Cell. 2007; 6:95–110. https://doi.org/10.1111/j.1474-9726.2006.00267.x

239. Chen D, Pan KZ, Palter JE, Kapahi P. Longevity determined by developmental arrest genes in Caenorhabditis elegans. Aging Cell. 2007; 6:525–33. https://doi.org/10.1111/j.1474-9726.2007.00305.x

240. Chiocchetti A, Zhou J, Zhu H, Karl T, Haubenreisser O, Rinnerthaler M, Heeren G, Oender K, Bauer J, Hintner H, Breitenbach M, Breitenbach-Koller L. Ribosomal proteins Rpl10 and Rps6 are potent regulators of yeast replicative life span. Exp Gerontol. 2007; 42:275–86. https://doi.org/10.1016/j.exger.2006.11.002

241. Curran SP, Ruvkun G. Lifespan regulation by evolutionarily conserved genes essential for viability. PLoS Genet. 2007; 3:e56. https://doi.org/10.1371/journal.pgen.0030056

242. Kaeberlein M, Powers RW 3rd, Steffen KK, Westman EA, Hu D, Dang N, Kerr EO, Kirkland KT, Fields S, Kennedy BK. Regulation of yeast replicative life span by TOR and Sch9 in response to nutrients. Science. 2005; 310:1193–96. https://doi.org/10.1126/science.1115535

243. Powers RW 3rd, Kaeberlein M, Caldwell SD, Kennedy BK, Fields S. Extension of chronological life span in yeast by decreased TOR pathway signaling. Genes Dev. 2006; 20:174–84. https://doi.org/10.1101/gad.1381406

244. Kapahi P, Zid BM, Harper T, Koslover D, Sapin V, Benzer S. Regulation of lifespan in Drosophila by modulation of genes in the TOR signaling pathway. Curr Biol. 2004; 14:885–90. https://doi.org/10.1016/j.cub.2004.03.059

245. Harrison DE, Strong R, Sharp ZD, Nelson JF, Astle CM, Flurkey K, Nadon NL, Wilkinson JE, Frenkel K, Carter CS, Pahor M, Javors MA, Fernandez E, Miller RA. Rapamycin fed late in life extends lifespan in genetically heterogeneous mice. Nature. 2009; 460:392–95. https://doi.org/10.1038/nature08221

246. Passtoors WM, Beekman M, Deelen J, van der Breggen R, Maier AB, Guigas B, Derhovanessian E, van Heemst D, de Craen AJ, Gunn DA, Pawelec G, Slagboom PE. Gene expression analysis of mTOR pathway: association with human longevity. Aging Cell. 2013; 12:24–31. https://doi.org/10.1111/acel.12015

247. Miller RA, Harrison DE, Astle CM, Baur JA, Boyd AR, de Cabo R, Fernandez E, Flurkey K, Javors MA, Nelson JF, Orihuela CJ, Pletcher S, Sharp ZD, et al. Rapamycin, but not resveratrol or simvastatin, extends life span of genetically heterogeneous mice. J Gerontol A Biol Sci Med Sci. 2011; 66:191–201. https://doi.org/10.1093/gerona/glq178

248. Hofmann JW, Zhao X, De Cecco M, Peterson AL, Pagliaroli L, Manivannan J, Hubbard GB, Ikeno Y, Zhang Y, Feng B, Li X, Serre T, Qi W, et al. Reduced expression of MYC increases longevity and enhances healthspan. Cell. 2015; 160:477–88. https://doi.org/10.1016/j.cell.2014.12.016

249. Schosserer M, Minois N, Angerer TB, Amring M, Dellago H, Harreither E, Calle-Perez A, Pircher A, Gerstl MP, Pfeifenberger S, Brandl C, Sonntagbauer M, Kriegner A, et al. Methylation of ribosomal RNA by NSUN5 is a conserved mechanism modulating organismal lifespan. Nat Commun. 2015; 6:6158. https://doi.org/10.1038/ncomms7158

250. Bemiller PM, Lee LH. Nucleolar changes in senescing WI-38 cells. Mech Ageing Dev. 1978; 8:417–27. https://doi.org/10.1016/0047-6374(78)90041-6

251. Buchwalter A, Hetzer MW. Nucleolar expansion and elevated protein translation in premature aging. Nat Commun. 2017; 8:328. https://doi.org/10.1038/s41467-017-00322-z

252. Ruggero D, Pandolfi PP. Does the ribosome translate cancer? Nat Rev Cancer. 2003; 3:179–92. https://doi.org/10.1038/nrc1015

253. Tiku V, Antebi A. Nucleolar Function in Lifespan Regulation. Trends Cell Biol. 2018; 28:662–72. https://doi.org/10.1016/j.tcb.2018.03.007

254. Syntichaki P, Troulinaki K, Tavernarakis N. Protein

synthesis is a novel determinant of aging in Caenorhabditis elegans. Ann N Y Acad Sci. 2007; 1119:289–95. https://doi.org/10.1196/annals.1404.001

255. Syntichaki P, Troulinaki K, Tavernarakis N. eIF4E function in somatic cells modulates ageing in Caenorhabditis elegans. Nature. 2007; 445:922–26. https://doi.org/10.1038/nature05603

256. Kaushik S, Cuervo AM. Proteostasis and aging. Nat Med. 2015; 21:1406–15. https://doi.org/10.1038/nm.4001

257. Pan KZ, Palter JE, Rogers AN, Olsen A, Chen D, Lithgow GJ, Kapahi P. Inhibition of mRNA translation extends lifespan in Caenorhabditis elegans. Aging Cell. 2007; 6:111–19. https://doi.org/10.1111/j.1474-9726.2006.00266.x

258. López-Otín C, Blasco MA, Partridge L, Serrano M, Kroemer G. The hallmarks of aging. Cell. 2013; 153:1194–217. https://doi.org/10.1016/j.cell.2013.05.039

259. McCay C, Crowell M, Maynard LA. The effect of retarded growth upon the length of life span and upon the ultimate body size. J Nutr. 1935; 10:63–79. https://doi.org/10.1093/jn/10.1.63

260. Al-Regaiey KA. The effects of calorie restriction on aging: a brief review. Eur Rev Med Pharmacol Sci. 2016; 20:2468–73.

261. Heilbronn LK, Ravussin E. Calorie restriction and aging: review of the literature and implications for studies in humans. Am J Clin Nutr. 2003; 78:361–69. https://doi.org/10.1093/ajcn/78.3.361

262. Tiku V, Jain C, Raz Y, Nakamura S, Heestand B, Liu W, Späth M, Suchiman HE, Müller RU, Slagboom PE, Partridge L, Antebi A. Small nucleoli are a cellular hallmark of longevity. Nat Commun. 2017; 8:16083. https://doi.org/10.1038/ncomms16083

263. Jack CV, Cruz C, Hull RM, Keller MA, Ralser M, Houseley J. Regulation of ribosomal DNA amplification by the TOR pathway. Proc Natl Acad Sci USA. 2015; 112:9674–79. https://doi.org/10.1073/pnas.1505015112

264. Murayama A, Ohmori K, Fujimura A, Minami H, Yasuzawa-Tanaka K, Kuroda T, Oie S, Daitoku H, Okuwaki M, Nagata K, Fukamizu A, Kimura K, Shimizu T, Yanagisawa J. Epigenetic control of rDNA loci in response to intracellular energy status. Cell. 2008; 133:627–39. https://doi.org/10.1016/j.cell.2008.03.030

265. Cohen HY, Miller C, Bitterman KJ, Wall NR, Hekking B, Kessler B, Howitz KT, Gorospe M, de Cabo R, Sinclair DA. Calorie restriction promotes mammalian cell survival by inducing the SIRT1 deacetylase. Science. 2004; 305:390–92. https://doi.org/10.1126/science.1099196

266. Nemoto S, Fergusson MM, Finkel T. Nutrient availability regulates SIRT1 through a forkhead-dependent pathway. Science. 2004; 306:2105–08. https://doi.org/10.1126/science.1101731

267. Satoh A, Brace CS, Rensing N, Cliften P, Wozniak DF, Herzog ED, Yamada KA, Imai S. Sirt1 extends life span and delays aging in mice through the regulation of Nk2 homeobox 1 in the DMH and LH. Cell Metab. 2013; 18:416–30. https://doi.org/10.1016/j.cmet.2013.07.013

268. Matheu A, Maraver A, Klatt P, Flores I, Garcia-Cao I, Borras C, Flores JM, Viña J, Blasco MA, Serrano M. Delayed ageing through damage protection by the Arf/p53 pathway. Nature. 2007; 448:375–79. https://doi.org/10.1038/nature05949

269. Hulbert AJ, Pamplona R, Buffenstein R, Buttemer WA. Life and death: metabolic rate, membrane composition, and life span of animals. Physiol Rev. 2007; 87:1175–213. https://doi.org/10.1152/physrev.00047.2006

270. Takeuchi Y, Horiuchi T, Kobayashi T. Transcription-dependent recombination and the role of fork collision in yeast rDNA. Genes Dev. 2003; 17:1497–506. https://doi.org/10.1101/gad.1085403

271. Ginno PA, Lott PL, Christensen HC, Korf I, Chédin F. R-loop formation is a distinctive characteristic of unmethylated human CpG island promoters. Mol Cell. 2012; 45:814–25. https://doi.org/10.1016/j.molcel.2012.01.017

272. Helmrich A, Ballarino M, Tora L. Collisions between replication and transcription complexes cause common fragile site instability at the longest human genes. Mol Cell. 2011; 44:966–77. https://doi.org/10.1016/j.molcel.2011.10.013

273. El Hage A, French SL, Beyer AL, Tollervey D. Loss of Topoisomerase I leads to R-loop-mediated transcriptional blocks during ribosomal RNA synthesis. Genes Dev. 2010; 24:1546–58. https://doi.org/10.1101/gad.573310

274. Wahba L, Costantino L, Tan FJ, Zimmer A, Koshland D. S1-DRIP-seq identifies high expression and polyA tracts as major contributors to R-loop formation. Genes Dev. 2016; 30:1327–38. https://doi.org/10.1101/gad.280834.116

275. Vijg J, Suh Y. Genome instability and aging. Annu Rev Physiol. 2013; 75:645–68. https://doi.org/10.1146/annurev-physiol-030212-183715

276. Flach J, Bakker ST, Mohrin M, Conroy PC, Pietras EM, Reynaud D, Alvarez S, Diolaiti ME, Ugarte F, Forsberg EC, Le Beau MM, Stohr BA, Méndez J, et al. Replication stress is a potent driver of functional decline in ageing haematopoietic stem cells. Nature. 2014; 512:198–202. https://doi.org/10.1038/nature13619

277. Schawalder J, Paric E, Neff NF. Telomere and ribosomal DNA repeats are chromosomal targets of the bloom syndrome DNA helicase. BMC Cell Biol. 2003; 4:15. https://doi.org/10.1186/1471-2121-4-15

278. Sinclair DA, Mills K, Guarente L. Accelerated aging and nucleolar fragmentation in yeast sgs1 mutants. Science. 1997; 277:1313–16. https://doi.org/10.1126/science.277.5330.1313

279. Sinclair DA, Guarente L. Extrachromosomal rDNA circles--a cause of aging in yeast. Cell. 1997; 91:1033–42. https://doi.org/10.1016/S0092-8674(00)80493-6

280. Grierson PM, Lillard K, Behbehani GK, Combs KA, Bhattacharyya S, Acharya S, Groden J. BLM helicase facilitates RNA polymerase I-mediated ribosomal RNA transcription. Hum Mol Genet. 2012; 21:1172–83. https://doi.org/10.1093/hmg/ddr545

281. Shiratori M, Suzuki T, Itoh C, Goto M, Furuichi Y, Matsumoto T. WRN helicase accelerates the transcription of ribosomal RNA as a component of an RNA polymerase I-associated complex. Oncogene. 2002; 21:2447–54. https://doi.org/10.1038/sj.onc.1205334

282. D'Aquila P, Montesanto A, Mandalà M, Garasto S, Mari V, Corsonello A, Bellizzi D, Passarino G. Methylation of the ribosomal RNA gene promoter is associated with aging and age-related decline. Aging Cell. 2017; 16:966–75. https://doi.org/10.1111/acel.12603

283. Jung M, Jin SG, Zhang X, Xiong W, Gogoshin G, Rodin AS, Pfeifer GP. Longitudinal epigenetic and gene expression profiles analyzed by three-component analysis reveal down-regulation of genes involved in protein translation in human aging. Nucleic Acids Res. 2015; 43:e100. https://doi.org/10.1093/nar/gkv473

284. Zhang W, Hawse J, Huang Q, Sheets N, Miller KM, Horwitz J, Kantorow M. Decreased expression of ribosomal proteins in human age-related cataract. Invest Ophthalmol Vis Sci. 2002; 43:198–204.

285. Kirby TJ, Lee JD, England JH, Chaillou T, Esser KA, McCarthy JJ. Blunted hypertrophic response in aged skeletal muscle is associated with decreased ribosome biogenesis. J Appl Physiol (1985). 2015; 119:321–27. https://doi.org/10.1152/japplphysiol.00296.2015

286. Barna M, Pusic A, Zollo O, Costa M, Kondrashov N, Rego E, Rao PH, Ruggero D. Suppression of Myc oncogenic activity by ribosomal protein haploinsufficiency. Nature. 2008; 456:971–75. https://doi.org/10.1038/nature07449

287. Ruggero D. Translational control in cancer etiology. Cold Spring Harb Perspect Biol. 2013; 5:5. https://doi.org/10.1101/cshperspect.a012336

288. Xue S, Barna M. Specialized ribosomes: a new frontier in gene regulation and organismal biology. Nat Rev Mol Cell Biol. 2012; 13:355–69. https://doi.org/10.1038/nrm3359

289. Duncan FE, Jasti S, Paulson A, Kelsh JM, Fegley B, Gerton JL. Age-associated dysregulation of protein metabolism in the mammalian oocyte. Aging Cell. 2017; 16:1381–93. https://doi.org/10.1111/acel.12676

290. Guo X, Shi Y, Gou Y, Li J, Han S, Zhang Y, Huo J, Ning X, Sun L, Chen Y, Sun S, Fan D. Human ribosomal protein S13 promotes gastric cancer growth through down-regulating p27(Kip1). J Cell Mol Med. 2011; 15:296–306. https://doi.org/10.1111/j.1582-4934.2009.00969.x

291. Du J, Shi Y, Pan Y, Jin X, Liu C, Liu N, Han Q, Lu Y, Qiao T, Fan D. Regulation of multidrug resistance by ribosomal protein l6 in gastric cancer cells. Cancer Biol Ther. 2005; 4:242–47. https://doi.org/10.4161/cbt.4.2.1477

292. Qu J, Bishop JM. Nucleostemin maintains self-renewal of embryonic stem cells and promotes reprogram-ming of somatic cells to pluripotency. J Cell Biol. 2012; 197:731–45. https://doi.org/10.1083/jcb.201103071

293. Le Bouteiller M, Souilhol C, Beck-Cormier S, Stedman A, Burlen-Defranoux O, Vandormael-Pournin S, Bernex F, Cumano A, Cohen-Tannoudji M. Notchless-dependent ribosome synthesis is required for the maintenance of adult hematopoietic stem cells. J Exp Med. 2013; 210:2351–69. https://doi.org/10.1084/jem.20122019

294. Yang A, Shi G, Zhou C, Lu R, Li H, Sun L, Jin Y. Nucleolin maintains embryonic stem cell self-renewal by suppression of p53 protein-dependent pathway. J Biol Chem. 2011; 286:43370–82. https://doi.org/10.1074/jbc.M111.225185

295. Meshorer E, Misteli T. Chromatin in pluripotent embryonic stem cells and differentiation. Nat Rev Mol Cell Biol. 2006; 7:540–46. https://doi.org/10.1038/nrm1938

296. Hayashi Y, Kuroda T, Kishimoto H, Wang C, Iwama A, Kimura K. Downregulation of rRNA transcription

triggers cell differentiation. PLoS One. 2014; 9:e98586. https://doi.org/10.1371/journal.pone.0098586

297. Stedman A, Beck-Cormier S, Le Bouteiller M, Raveux A, Vandormael-Pournin S, Coqueran S, Lejour V, Jarzebowski L, Toledo F, Robine S, Cohen-Tannoudji M. Ribosome biogenesis dysfunction leads to p53-mediated apoptosis and goblet cell differentiation of mouse intestinal stem/progenitor cells. Cell Death Differ. 2015; 22:1865–76. https://doi.org/10.1038/cdd.2015.57

298. Tyner SD, Venkatachalam S, Choi J, Jones S, Ghebranious N, Igelmann H, Lu X, Soron G, Cooper B, Brayton C, Park SH, Thompson T, Karsenty G, et al. p53 mutant mice that display early ageing-associated phenotypes. Nature. 2002; 415:45–53. https://doi.org/10.1038/415045a

299. Maier B, Gluba W, Bernier B, Turner T, Mohammad K, Guise T, Sutherland A, Thorner M, Scrable H. Modulation of mammalian life span by the short isoform of p53. Genes Dev. 2004; 18:306–19. https://doi.org/10.1101/gad.1162404

300. van Heemst D, Mooijaart SP, Beekman M, Schreuder J, de Craen AJ, Brandt BW, Slagboom PE, Westendorp RG, and Long Life study group. Variation in the human TP53 gene affects old age survival and cancer mortality. Exp Gerontol. 2005; 40:11–15. https://doi.org/10.1016/j.exger.2004.10.001

301. Steffen KK, Dillin A. A Ribosomal Perspective on Proteostasis and Aging. Cell Metab. 2016; 23:1004–12. https://doi.org/10.1016/j.cmet.2016.05.013

302. Gomes C, Smith SC, Youssef MN, Zheng JJ, Hagg T, Hetman M. RNA polymerase 1-driven transcription as a mediator of BDNF-induced neurite outgrowth. J Biol Chem. 2011; 286:4357–63. https://doi.org/10.1074/jbc.M110.170134

303. Slomnicki LP, Pietrzak M, Vashishta A, Jones J, Lynch N, Elliot S, Poulos E, Malicote D, Morris BE, Hallgren J, Hetman M. Requirement of Neuronal Ribosome Synthesis for Growth and Maintenance of the Dendritic Tree. J Biol Chem. 2016; 291:5721–39. https://doi.org/10.1074/jbc.M115.682161

304. Kinderman NB, Harrington CA, Drengler SM, Jones KJ. Ribosomal RNA transcriptional activation and processing in hamster facial motoneurons: effects of axotomy with or without exposure to testosterone. J Comp Neurol. 1998; 401:205–16. https://doi.org/10.1002/(SICI)1096-9861(19981116)401:2<205::AID-CNE4>3.0.CO;2-4

305. Storer PD, Jones KJ. Ribosomal RNA transcriptional activation and processing in hamster rubrospinal motoneurons: effects of axotomy and testosterone treatment. J Comp Neurol. 2003; 458:326–33. https://doi.org/10.1002/cne.10623

306. Ding Q, Markesbery WR, Chen Q, Li F, Keller JN. Ribosome dysfunction is an early event in Alzheimer's disease. J Neurosci. 2005; 25:9171–75.

https://doi.org/10.1523/JNEUROSCI.3040-05.2005

307. Honda K, Smith MA, Zhu X, Baus D, Merrick WC, Tartakoff AM, Hattier T, Harris PL, Siedlak SL, Fujioka H, Liu Q, Moreira PI, Miller FP, et al. Ribosomal RNA in Alzheimer disease is oxidized by bound redox-active iron. J Biol Chem. 2005; 280:20978–86. https://doi.org/10.1074/jbc.M500526200

308. Ding Q, Markesbery WR, Cecarini V, Keller JN. Decreased RNA, and increased RNA oxidation, in ribosomes from early Alzheimer's disease. Neurochem Res. 2006; 31:705–10. https://doi.org/10.1007/s11064-006-9071-5

309. Pietrzak M, Rempala G, Nelson PT, Zheng JJ, Hetman M. Epigenetic silencing of nucleolar rRNA genes in Alzheimer's disease. PLoS One. 2011; 6:e22585. https://doi.org/10.1371/journal.pone.0022585

310. Zeng J, Libien J, Shaik F, Wolk J, Hernández AI. Nucleolar PARP-1 Expression Is Decreased in Alzheimer's Disease: Consequences for Epigenetic Regulation of rDNA and Cognition. Neural Plast. 2016; 2016:8987928. https://doi.org/10.1155/2016/8987928

311. Dönmez-Altuntaş H, Akalin H, Karaman Y, Demirtaş H, Imamoğlu N, Özkul Y. Evaluation of the nucleolar organizer regions in Alzheimer's disease. Gerontology. 2005; 51:297–301. https://doi.org/10.1159/000086365

312. Bou Samra E, Buhagiar-Labarchède G, Machon C, Guitton J, Onclercq-Delic R, Green MR, Alibert O, Gazin C, Veaute X, Amor-Guéret M. A role for Tau protein in maintaining ribosomal DNA stability and cytidine deaminase-deficient cell survival. Nat Commun. 2017; 8:693. https://doi.org/10.1038/s41467-017-00633-1

313. Sjöberg MK, Shestakova E, Mansuroglu Z, Maccioni RB, Bonnefoy E. Tau protein binds to pericentromeric DNA: a putative role for nuclear tau in nucleolar organization. J Cell Sci. 2006; 119:2025–34. https://doi.org/10.1242/jcs.02907

314. Vanderweyde T, Apicco DJ, Youmans-Kidder K, Ash PE, Cook C, Lummertz da Rocha E, Jansen-West K, Frame AA, Citro A, Leszyk JD, Ivanov P, Abisambra JF, Steffen M, et al. Interaction of tau with the RNA-Binding Protein TIA1 Regulates tau Pathophysiology and Toxicity. Cell Reports. 2016; 15:1455–66. https://doi.org/10.1016/j.celrep.2016.04.045

315. Maina MB, Bailey LJ, Wagih S, Biasetti L, Pollack SJ, Quinn JP, Thorpe JR, Doherty AJ, Serpell LC. The involvement of tau in nucleolar transcription and the stress response. Acta Neuropathol Commun. 2018; 6:70. https://doi.org/10.1186/s40478-018-0565-6

316. Rieker C, Engblom D, Kreiner G, Domanskyi A, Schober A, Stotz S, Neumann M, Yuan X, Grummt I, Schütz G, Parlato R. Nucleolar disruption in dopaminergic neurons leads to oxidative damage and parkinsonism through repression of mammalian target of rapamycin signaling. J Neurosci. 2011; 31:453–60. https://doi.org/10.1523/JNEUROSCI.0590-10.2011

317. Healy-Stoffel M, Ahmad SO, Stanford JA, Levant B. Altered nucleolar morphology in substantia nigra dopamine neurons following 6-hydroxydopamine lesion in rats. Neurosci Lett. 2013; 546:26–30. https://doi.org/10.1016/j.neulet.2013.04.033

318. Caudle WM, Kitsou E, Li J, Bradner J, Zhang J. A role for a novel protein, nucleolin, in Parkinson's disease. Neurosci Lett. 2009; 459:11–15. https://doi.org/10.1016/j.neulet.2009.04.060

319. Jin J, Li GJ, Davis J, Zhu D, Wang Y, Pan C, Zhang J. Identification of novel proteins associated with both α-synuclein and DJ-1. Mol Cell Proteomics. 2007; 6:845–59. https://doi.org/10.1074/mcp.M600182-MCP200

320. Vilotti S, Codrich M, Dal Ferro M, Pinto M, Ferrer I, Collavin L, Gustincich S, Zucchelli S. Parkinson's disease DJ-1 L166P alters rRNA biogenesis by exclusion of TTRAP from the nucleolus and sequestration into cytoplasmic aggregates via TRAF6. PLoS One. 2012; 7:e35051. https://doi.org/10.1371/journal.pone.0035051

321. Kang H, Shin JH. Repression of rRNA transcription by PARIS contributes to Parkinson's disease. Neurobiol Dis. 2015; 73:220–28. https://doi.org/10.1016/j.nbd.2014.10.003

322. Lee J, Hwang YJ, Boo JH, Han D, Kwon OK, Todorova K, Kowall NW, Kim Y, Ryu H. Dysregulation of upstream binding factor-1 acetylation at K352 is linked to impaired ribosomal DNA transcription in Huntington's disease. Cell Death Differ. 2011; 18:1726–35. https://doi.org/10.1038/cdd.2011.38

323. Lee J, Hwang YJ, Ryu H, Kowall NW, Ryu H. Nucleolar dysfunction in Huntington's disease. Biochim Biophys Acta. 2014; 1842:785–90. https://doi.org/10.1016/j.bbadis.2013.09.017

324. Tsoi H, Lau TC, Tsang SY, Lau KF, Chan HY. CAG expansion induces nucleolar stress in polyglutamine diseases. Proc Natl Acad Sci USA. 2012; 109:13428–33. https://doi.org/10.1073/pnas.1204089109

325. Bae BI, Xu H, Igarashi S, Fujimuro M, Agrawal N, Taya Y, Hayward SD, Moran TH, Montell C, Ross CA, Snyder SH, Sawa A. p53 mediates cellular dysfunction and behavioral abnormalities in Huntington's disease. Neuron. 2005; 47:29–41. https://doi.org/10.1016/j.neuron.2005.06.005

326. Kitamura Y, Shimohama S, Kamoshima W, Matsuoka Y, Nomura Y, Taniguchi T. Changes of p53 in the brains of patients with Alzheimer's disease. Biochem Biophys Res Commun. 1997; 232:418–21. https://doi.org/10.1006/bbrc.1997.6301

327. Nair VD, McNaught KS, González-Maeso J, Sealfon SC, Olanow CW. p53 mediates nontranscriptional cell death in dopaminergic cells in response to proteasome inhibition. J Biol Chem. 2006; 281:39550–60. https://doi.org/10.1074/jbc.M603950200

328. Boulon S, Westman BJ, Hutten S, Boisvert FM, Lamond AI. The nucleolus under stress. Mol Cell. 2010; 40:216–27. https://doi.org/10.1016/j.molcel.2010.09.024

Research Paper

Overexpressed methyltransferase-like 1 (METTL1) increased chemosensitivity of colon cancer cells to cisplatin by regulating miR-149-3p/S100A4/p53 axis

Yang Liu[1,*], Chunyan Yang[2,*], Yong Zhao[1,*], Qiang Chi[1], Zhen Wang[1], Boshi Sun[1]

[1]The 3rd Department of General Surgery, The 2nd Affiliated Hospital of Harbin Medical University, Harbin 150001, Heilong Jiang, China
[2]Department of Oral and Maxillofacial Surgery, The 2nd Affiliated Hospital of Harbin Medical University, Harbin 150001, Heilong Jiang, China
*Co-first authors

Correspondence to: Boshi Sun; **email:** sun_boshi562@163.com
Keywords: colon cancer, METTL1, cisplatin, miR-149-3p, S100A4
Received: September 3, 2019 **Accepted:** November 24, 2019 **Published:** December 20, 2019

ABSTRACT

Methyltransferase-like 1 (METTL1) mediated 7-methylguanosine (m7G) is crucial for the regulation of chemoresistance in cancer treatment. However, the role of METTL1 in regulating chemoresistance of colon cancer (CC) cells to cisplatin is still unclear. This study established the cisplatin-resistant CC (CR-CC) cells and found that METTL1 was low-expressed in CR-CC cells compared to their paired cisplatin-sensitive CC (CS-CC) cells. Besides, overexpressed METTL1 enhanced the cytotoxic effects of cisplatin on CR-CC cells. In addition, miR-149-3p was the downstream target of METTL1, which could be positively regulated by METTL1. Further results validated that miR-149-3p was low-expressed in CR-CC cells comparing to the CS-CC cells. In addition, the promoting effects of overexpressed METTL1 on cisplatin induced CR-CC cell death were abrogated by synergistically knocking down miR-149-3p. Furthermore, S100A4/p53 axis was the downstream target of METTL1 and miR-149-3p, and either overexpressed METTL1 or miR-149-3p increased p53 protein levels in CR-CC cells, which were reversed by upregulating S100A4. Similarly, the promoting effects of overexpressed METTL1 on cisplatin-induced CR-CC cell death were abrogated by overexpressing S100A4. Taken together, overexpression of METTL1 sensitized CR-CC cells to cisplatin by modulating miR-149-3p/S100A4/p53 axis.

INTRODUCTION

Cisplatin was the first-line chemotherapeutic drug for colon cancer (CC) treatment in clinic [1, 2]. However, continuous cisplatin treatment induced chemoresistance of CC cells to cisplatin, which seriously limited its therapeutic efficacy [3–5], but the underlying mechanisms were still not fully delineated. Methyltransferase-like 1 (METTL1) was crucial for RNA processing (splicing, stability and localization) in a 7-methylguanosine (m7G) dependent manner [6–8], which served as a tumor suppressor and participated in the development of multiple cancers [9, 10]. Notably, METTL1 also determined sensitivity of cervical cancer cells to 5-fluorouracil (5-FU) [9], however, it is still unclear whether METTL1 participated in the regulation of chemoresistance of CC cells to Cisplatin.

MicroRNAs (miRNAs) were closely related with cancer progression and regulated chemoresistance generated by cancer cells to cisplatin according to their biological functions [11–13]. Recent studies have identified miR-149-3p as a tumor suppressor in multiple cancers, such as prostate cancer [14, 15], pancreatic cancer [16], colon cancer [17] and so on. Besides, overexpressed miR-149-3p abrogated cisplatin-resistance of ovarian cancer cells

[18], esophageal cancer cells [19], gastric cancer cells [20] and non-small cell lung cancer cells [21], however, only a few publications reported the role of miR-149-3p in regulating CC cells' resistance to cisplatin. In addition, previous studies proved that microRNAs could be regulated by METTL1 in a m7G dependent manner [22], and miR-149-3p was the potential downstream target of METTL1 [10], but the role of METTL1/miR-149-3p axis in regulating CC cell functions are still unclear.

S100A4 was a small calcium-binding protein and played an oncogenic role in the development of multiple cancers, such as prostate cancer [23], breast cancer [24] and colon cancer [25, 26]. Besides, S100A4 participated in the regulation of Cisplatin-resistance of different cancer cells in a p53-dependent manner [27, 28]. Since Cisplatin promoted cancer cell death and inhibited cell viability by inducing DNA double-strand break (DSB) [29, 30], and p53 was the hub gene of DSB-induced cell death [31], it was reasonable to hypothesize that S100A4/p53 axis was crucial for regulating Cisplatin-resistance of CC cells. Interestingly, previous study found that miR-149-3p inhibited bladder cancer cell proliferation and migration by downregulating S100A4 expression levels [15], which indicated that S100A4/p53 axis might be regulated by miR-149-3p.

Taken together, this study aimed to investigate the role of METTL1/miR-149-3p/S100A4/p53 cascade in the regulation of cisplatin-resistance of CC cells, which will provide new potential therapeutic agents for CC treatment in clinic.

RESULTS

The expression levels of METTL1 and miR-149-3p in CS-CC and CR-CC cells

The CC cells (HCT116, SW480 and SW620) were continuously exposed to low-dose cisplatin starting from 0.5μg/ml to 5μg/ml in a stepwise manner to induct the cisplatin-resistant CC (CR-CC) cell lines (Figure 1A). The CCK-8 results showed that the CR-CC cells were successfully inducted by this method (Figure 1B–1D). Specifically, high-dose cisplatin (20μg/ml) significantly inhibited CS-CC cell viability, but had little effects on CR-CC cell proliferation (Figure 1B–1D). Further results showed that both METTL1 mRNA (Figure 1F) and miR-149-3p (Figure 1E) were lowly expressed in CR-CC cells comparing to their paried CS-CC cells, and the Western Blot results validated that the expression levels of METTL1 were lower in CR-CC cells comparing to the CS-CC cells (Figure 1G–1H). In addition, METTL1 was successfully overexpressed and downregulated in CR-HCT116, CR-SW480 and CR-SW620 cells respectively (Supplementary Figure 1A–1B). The results showed that overexpressed METTL1 significantly increased miR-149-3p levels in CR-CC cells, and downregulation of METTL1 had opposite effects on miR-149-3p levels (Figure 1I). However, miR-149-3p did not regulate METTL1 expressions in CS-CC cells (Supplementary Figure1C, 1D), which were in accordance with the previous study [10] and indicated that METTL1 positively regulated miR-149-3p levels in CR-CC cells.

Overexpressed METTL1 enhanced the cytotoxic effects of high-dose cisplatin on CR-CC cells by targeting miR-149-3p

Further experiments delved the effects of METTL1 on high-dose cisplatin induced CR-CC cell death. The colony formation assay results showed that overexpressed METTL1 significantly enhanced the inhibiting effects of high-dose cisplatin on CR-CC cell proliferation, which were abrogated by synergistically knocking down miR-149-3p (Figure 2A, 2B). In addition, upregulation of METTL1 decreased the expression levels of Cyclin D1 and CDK2, increased p27 expression levels in CR-HCT116 cells (Figure 2C, 2D), CR-SW480 cells (Figure 2E, 2F) and CR-SW620 cells (Figure 2G, 2H) respectively. Of note, the effects of overexpressed METTL1 on the above proteins were reversed by synergistically downregulating miR-149-3p (Figure 2C–2H). Further results showed that high-dose cisplatin (20 μg/ml) had little effects on CR-CC cell apoptosis ratio, which were significantly increased by synergistically overexpressing METTL1 in CR-CC cells (Figure 3A, 3B), and the effects of overexpressed METTL1 on cell apoptosis were abrogated by co-transfecting cells with miR-149-3p inhibitor (Figure 3A, 3B). In parallel, overexpressed METTL1 increased the expression levels of cleaved Caspase 3 in cisplatin treated CR-CC cells, which were also abrogated by knocking down miR-149-3p (Figure 3C, 3D).

S100A4/p53 axis was regulated by METTL1 and miR-149-3p in CS-CC cells

The results showed that either overexpressed METTL1 or miR-149-3p decreased S100A4 expression levels in both mRNA levels (Figure 4A) and protein levels (Figure 4C–4H), and merely increased p53 protein expression levels in CS-CC cells (Figure 4C–4H), but had little effects on p53 mRNA levels (Figure 4B). Besides, the online starBase software predicted the binding sites of miR-149-3p and 3'UTR regions of S100A4 (Figure 4I), and the dual-luciferase reporter gene syetem assay validated that miR-149-3p inhibited S100A4 expression levels by binding to its 3' UTR regions (Figure 4J, 4K). In addition, knock-down of

miR-149-3p abrogated the effects of overexpressed METTL1 on the expression levels of S100A4 and p53 in CR-HCT116 cells (Figure 4L–4M), CR-SW480 cells (Figure 4N–4O) and CR-SW620 cells (Figure 4P–4Q). Interestingly, the results showed that S100A4 was high-expressed, and p53 was low-expressed in CR-CC cells comparing to their paired CS-CC cells (Supplementary Figure 2).

Targeting S100A4/p53 axis enhanced high-dose cisplatin induced CR-CC cell death

The study next explored the effects of S100A4/p53 axis on high-dose cisplatin induced CR-CC cell death. The results showed that upregulation of S100A4 decreased p53 protein levels (Supplementary Figure 3B–3G) instead of mRNA levels (Supplementary Figure 3A) in CS-CC cells, which was in line with the previous study and indirectly reflected that S100A4 promoted p53 protein degradation [28]. In addition, either downregulated S100A4 or upregulated p53 enhanced the cytotoxic effects of high-dose cisplatin on CR-CC cells (Figure 5). Specifically, the TUNEL assay results showed that the apoptosis ratio of cisplatin treated CR-CC cells was significantly increased by either knocking down S100A4 or overexpressing p53 (Figure 5A, 5B). Besides, the expression levels of cleaved Caspase 3 were increased by knocking down S100A4 or upregulating p53 in cisplatin treated CR-CC cells (Figure 5C, 5D). Furthermore, the CCK-8 results

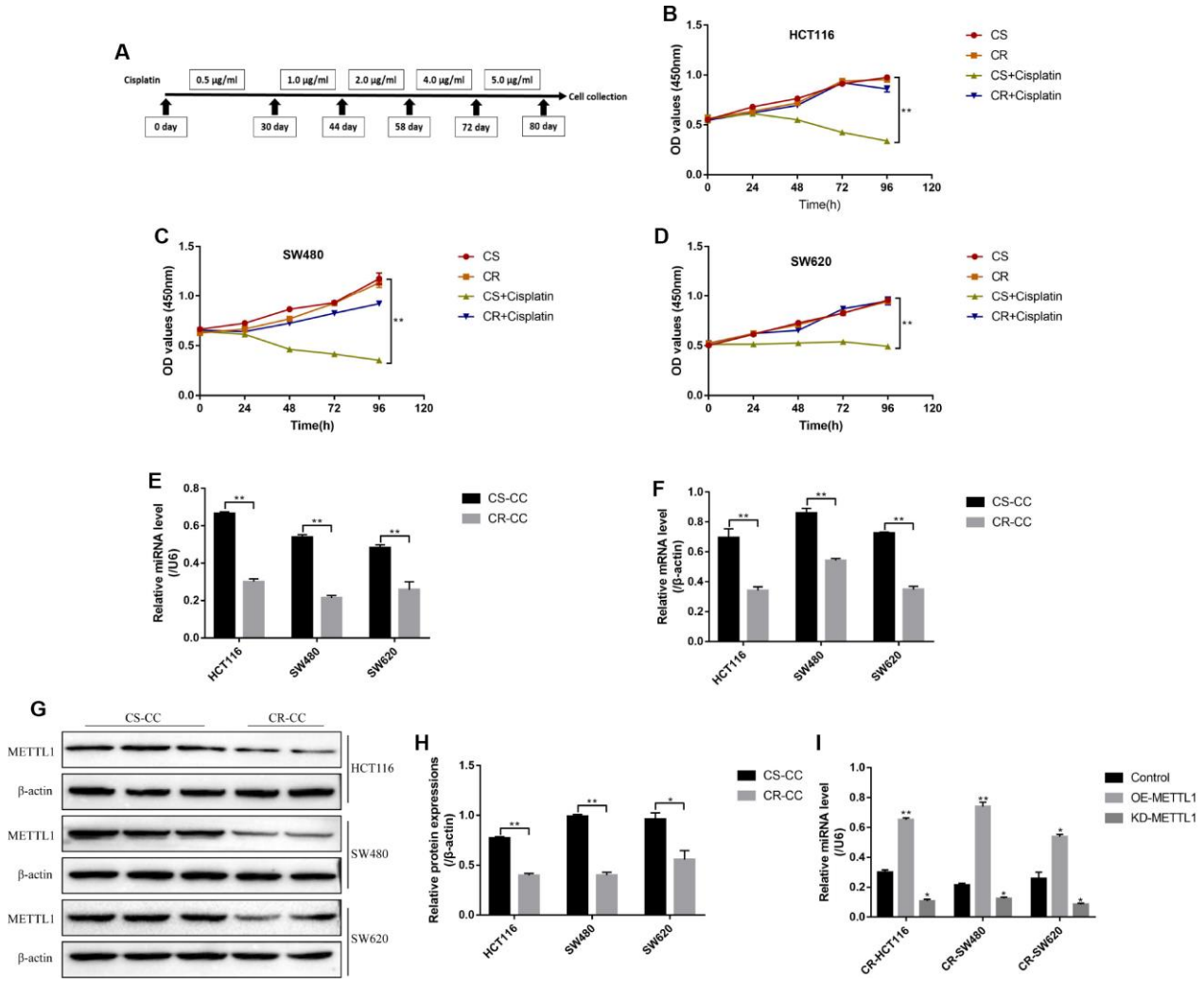

Figure 1. The expression levels of METTL1 and miR-149-3p in CR-CC cell lines. (**A**) The schematic procedures of the induction of CR-HCT116, CR-SW480 and CR-SW620 respectively. CCK-8 assay was conducted to detect (**B**) HCT116 cells, (**C**) SW480 cells and (**D**) SW620 cells proliferation respectively. Real-Time qPCR was performed to determine the levels of (**E**) miR-149-3p and (**F**) METTL1 mRNA in CC cells. (**G**, **H**) Western Blot was used to determine the expression levels of METTL1 in Cisplatin-sensitive colon cancer (CS-CC) and Cisplatin-resistant colon cancer (CR-CC) cells. (**I**) Real-Time qPCR was employed to investigate the effects of METTL1 on miR-149-3p levels in CR-CC cells. All the experiments repeated at least 3 times. "*" means $p < 0.05$, "**" means $p < 0.01$ and "NS" means no statistical significance.

showed that either downregulated S100A4 or upregulated p53 enhanced the inhibiting effects of high-dose cisplatin treatment on CR-CC cells proliferation (Figure 5E–5G).

The effects of METTL1 on cisplatin-induced CR-CC cell death were abrogated by upregulating S100A4

The colony formation assay results showed that overexpressed METTL1 aggravated the inhibiting effects of high-dose cisplatin treatment on CR-CC cell proliferation, which were abrogated by synergistically upregulating S100A4 (Figure 6A, 6B). Similarly, overexpressed METTL1 decreased the expression levels of Cyclin D1 as well as CDK2, and increased p27 levels in cisplatin treated CR-HCT116 cells (Figure 6C, 6D), CR-SW480 cells (Figure 6E, 6F) and CR-SW620 cells (Figure 6G, 6H), which were also reversed by upregulation of S100A4 (Figure 6C–6H). Consistently, the FCM results showed that the promoting effects of

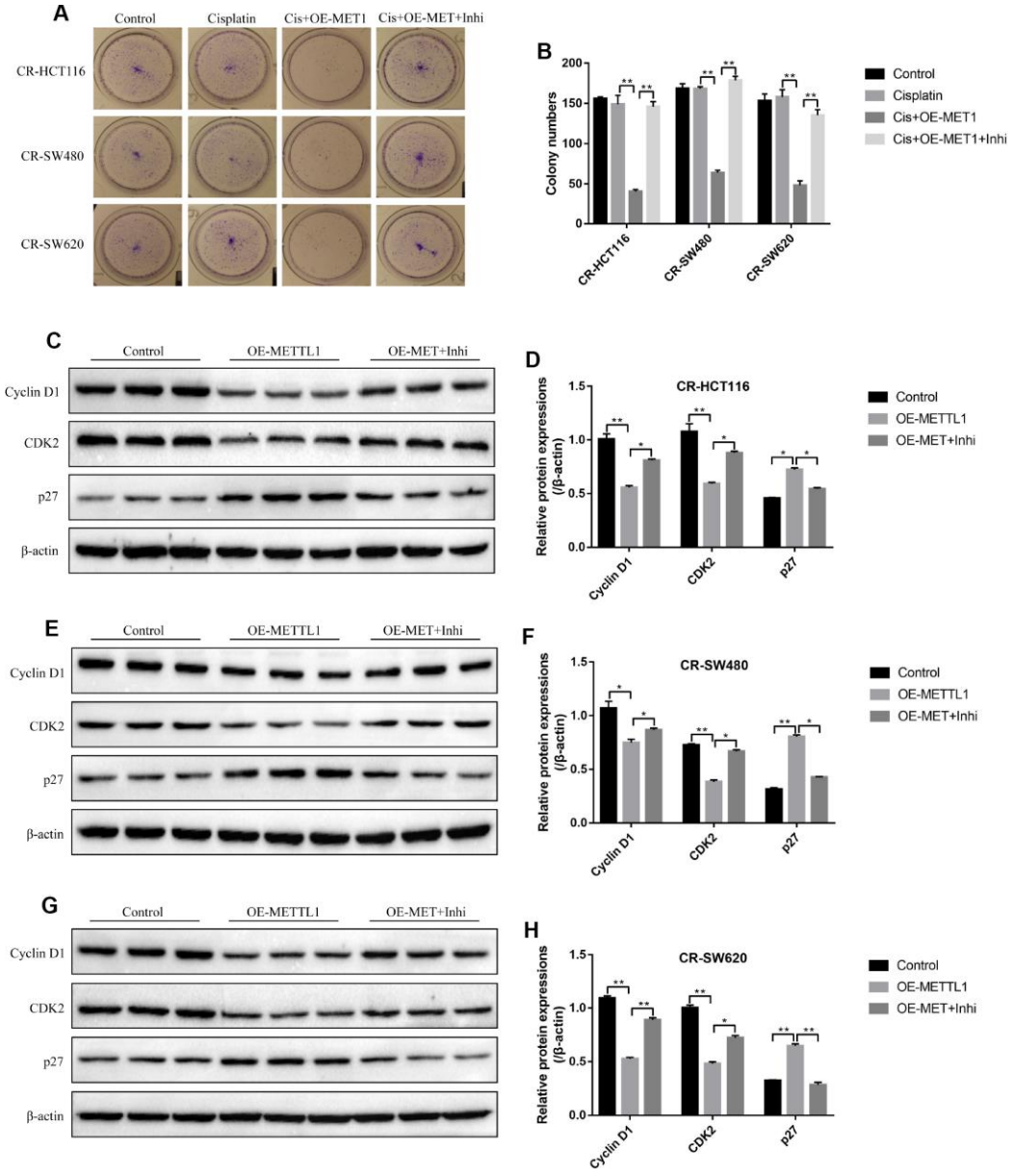

Figure 2. METTL1 regulated CR-CC cell proliferation by targeting miR-149-3p. (**A**, **B**) Colony formation assay was performed to evaluate the colony formation abilities in CC cells. Western Blot was conducted to detect the expression levels of Cyclin D1, CDK2 and p27 in (**C**, **D**) CR-HCT116 cells, (**E**, **F**) CR-SW480 cells and (**G**, **H**) CR-SW620 cells. ("OE-METTL1" represented "Overexpressed METTL1 group", and "OE-METTL1+Inhi" represented "Overexpressed METTL1 plus miR-149-3p inhibitor group"). All the experiments repeated at least 3 times. "*" means $p < 0.05$, "**" means $p < 0.01$ and "NS" means no statistical significance.

overexpressed METTL1 on the apoptosis ratio of cisplatin treated CR-CC cells were also reversed by upregulation of S100A4 (Figure 7A, 7B), which were further validated by the Western Blot results by determining the expression levels of cleaved Caspase 3 (Figure 7C, 7D).

DISCUSSION

Chemoresistance of CC cells to cisplatin seriously limited the utilization and therapeutic efficiency of this chemotherapeutic drug for CC treatment in clinic [3–5], and uncovering the underlying mechanisms might help to solve this problem. Methyltransferase-like 1 (METTL1) was the best characterized enzyme mediating m7G methylation [6–8], which was crucial for the regulation of cancer development [9, 10] and chemosensitivity [9]. In addition, microRNAs could be regulated by METTL1 in a m7G dependent manner [22]. MiR-149-3p served as a tumor suppressor in multiple cancers [14–17], and upregulated METTL1 increased miR-149-3p levels in lung cancer cells in a m7G dependent manner [10]. However, it is still unclear whether METTL1 and miR-149-3p participated in the regulation of CC cells' chemoresistance to cisplatin. This study found that both METTL1 and miR-149-3p were low-expressed in CR-CC cells comparing to the CS-CC cells. Besides, overexpressed METTL1 increased miR-149-3p levels in CR-CC cells, but upregulation of miR-149-3p did not affect METTL1. levels, which indicated that miR-149-3p was the downstream target of METTL1 and in accordance with

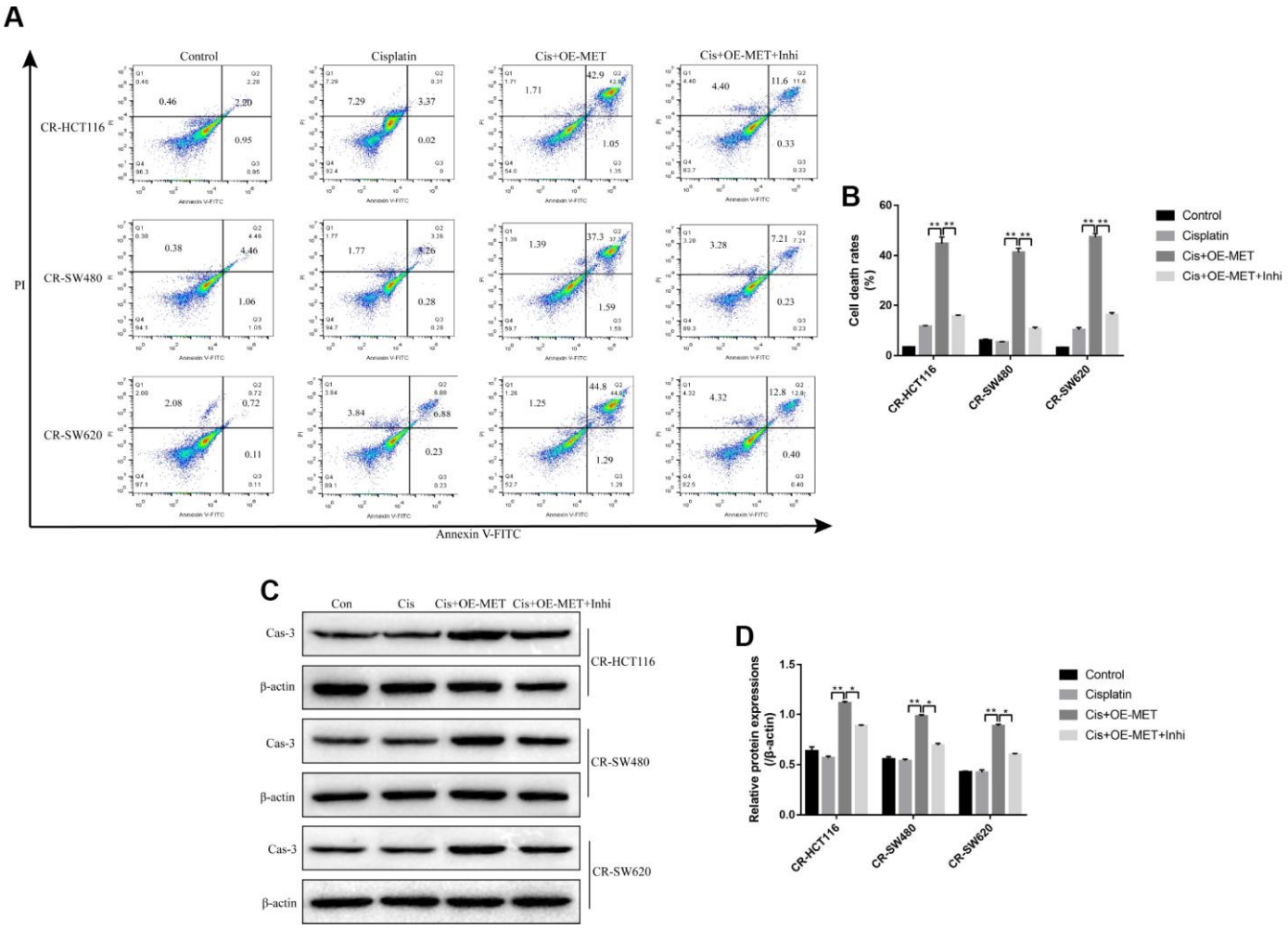

Figure 3. The involvement of METTL1/miR-149-3p axis in the regulation of CR-CC cell apoptosis. (**A**, **B**) FCM was employed to determine the apoptosis ratio of CR-CC cells. (**C**, **D**) Western Blot was used to detect the expression levels of cleaved Caspase-3 in CR-HCT116 cells, CR-SW480 cells and CR-SW620 cells respectively. ("Con" represented "Control group", "Cis" indicated "Cisplatin treated group", "Cis+OE-MET" represented "Cisplatin plus overexpressed METTL1 treated group", "Cis+OE-MET+Inhi" represented "Cisplatin plus overexpressed METTL1 and miR-149-3p inhibitor treated group"). All the experiments repeated at least 3 times. "*" means $p < 0.05$, "**" means $p < 0.01$ and "NS" means no statistical significance.

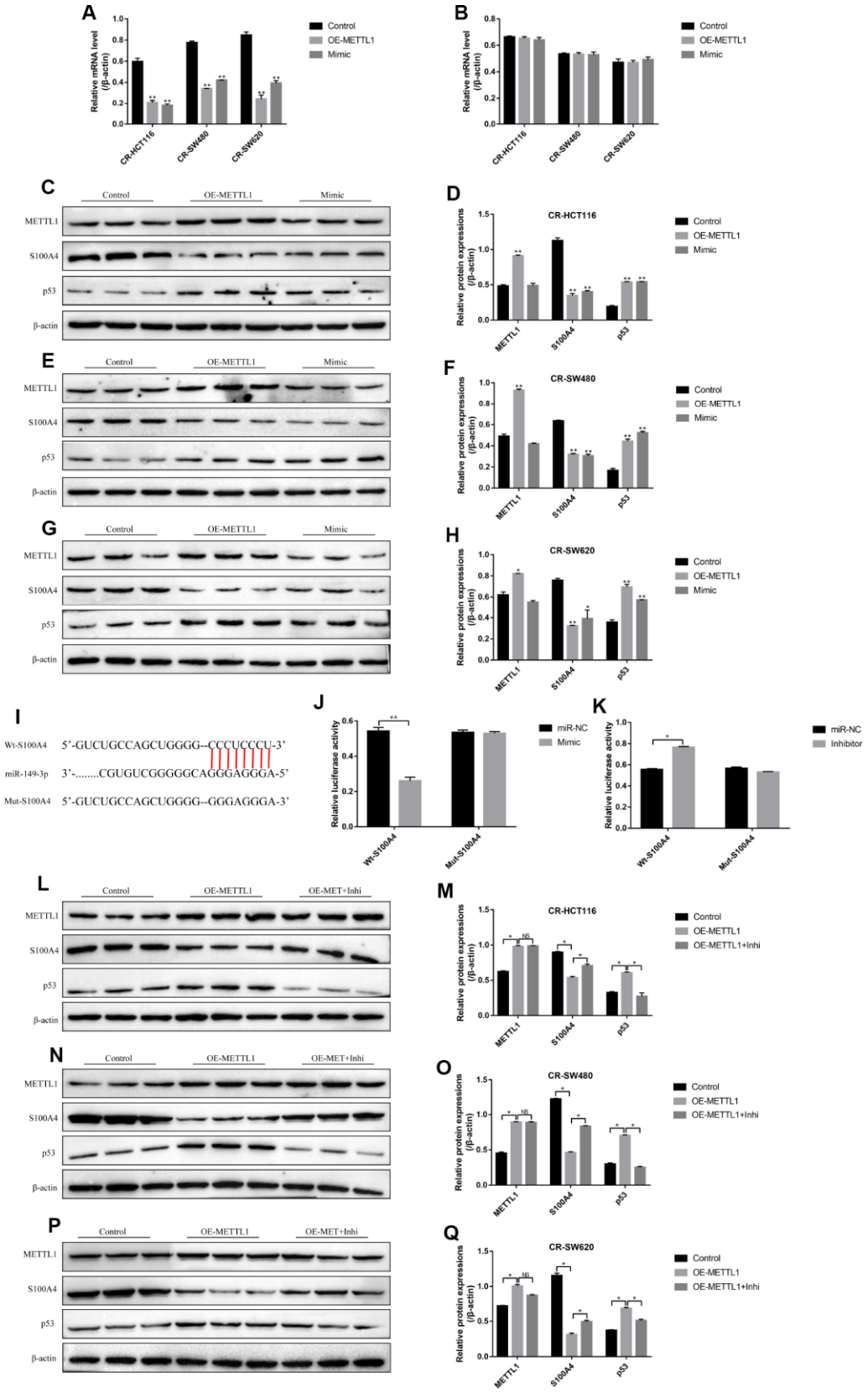

Figure 4. S100A4/p53 axis was the downstream target of METTL1 and miR-149-3p. Real-Time qPCR was conducted to detect the mRNA levels of (**A**) S100A4 and (**B**) p53 in CR-CC cells. Western Blot was performed to determine the expression levels of METTL1, S100A4 and p53 in (**C**, **D**) CR-HCT116 cells, (**E**, **F**) CR-SW480 cells and (**G**, **H**) CR-SW620 cells. (**I**) The binding sites of miR-149-3p and the 3'UTR regions

of S100A4 were predicted by online starBase software. Western Blot was used to detect the expression levels of METTL1, S100A4 and p53 in (**L**, **M**) CR-HCT116 cells, (**N**, **O**) CR-SW480 cells and (**P**, **Q**) CR-SW620 cells. ("OE-METTL1" represented "Overexpressed METTL1 group", and "OE-METTL1+Inhi" represented "Overexpressed METTL1 plus miR-149-3p inhibitor group"). All the experiments repeated at least 3 times. "*" means $p < 0.05$, "**" means $p < 0.01$ and "NS" means no statistical significance.

the previous study [10]. However, further experiments are still needed to explore whether METTL1 regulated miR-149-3p levels in colon cancer in a m7G dependent manner.

Further results showed that overexpressed METTL1 enhanced the cytotoxic effects of high-dose cisplatin on CR-CC cells, which indicated that upregulation of METTL1 enhanced the chemosensitivity of CR-CC cells to cisplatin. The above results were in accordance with the previous studies [9, 10] and indicated that METTL1 sensitized CR-CC cells to cisplatin treatment. Besides, miR-149-3p was the downstream target of METTL1 [10], and overexpression of miR-149-3p decreased chemoresistance of multiple cancers to cisplatin, such as ovarian cancer [18], esophageal cancer

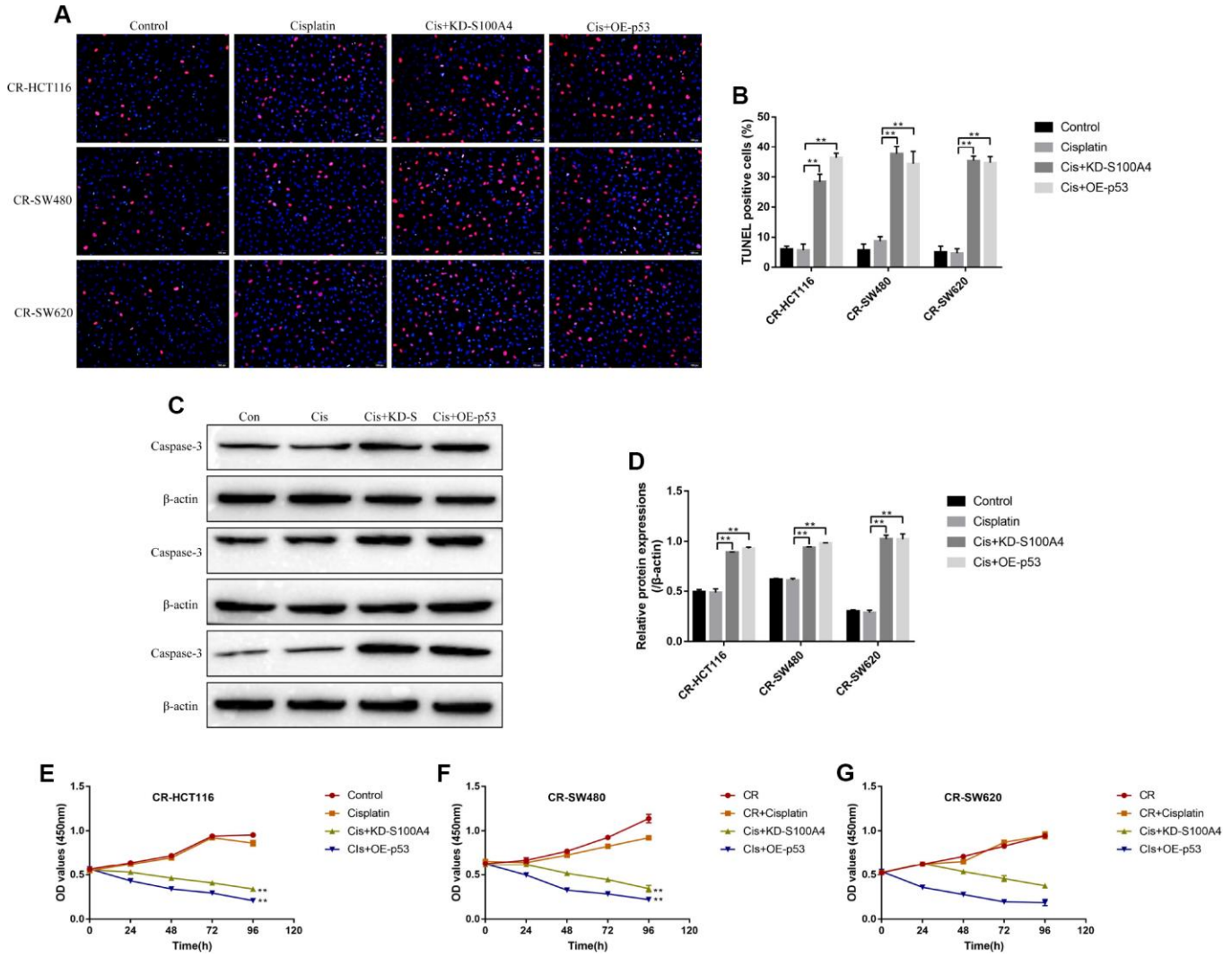

Figure 5. The effects of S100A4 and p53 on CR-CC cell viability. (**A**, **B**) TUNEL assay was conducted to detect cell apoptosis ratio in CC cells. (**C**, **D**) Western Blot was used to determine the expression levels of cleaved Caspase-3 in CR-CC cells. CCK-8 assay was performed to detect the proliferation ability of (**E**) CR-HCT116 cells, (**F**) CR-SW480 cells and (**G**) CR-SW620 cells. ("Con" represented "Control group", "Cis" indicated "Cisplatin treated group", "Cis+KD-S" represented "Cisplatin plus downregulated S100A4 treated group", "Cis+OE-p53" represented "Cisplatin plus overexpressed p53 treated group"). All the experiments repeated at least 3 times. "*" means $p < 0.05$, "**" means $p < 0.01$ and "NS" means no statistical significance.

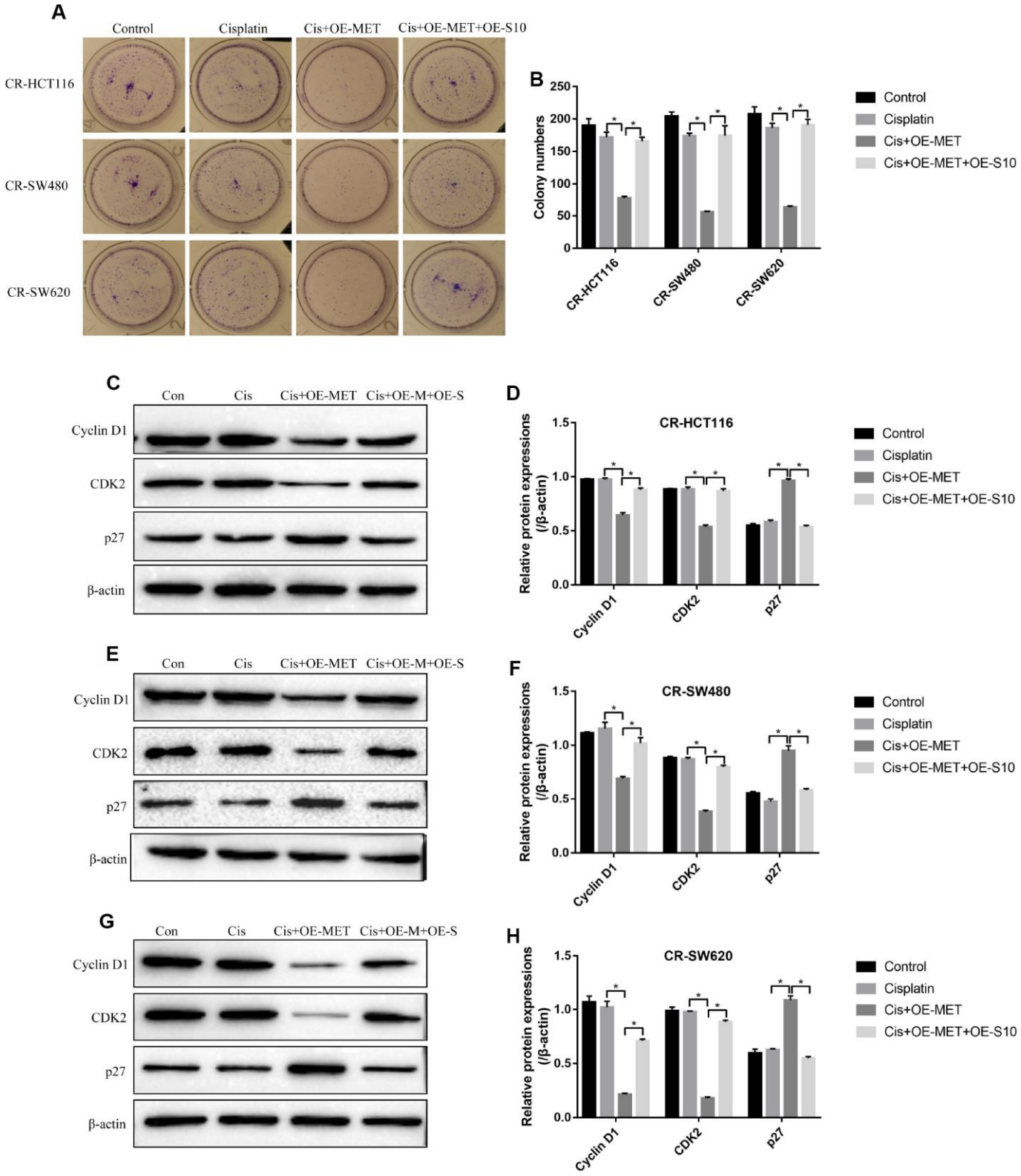

Figure 6. METTL1 regulated cell proliferation by targeting S100A4. (**A**, **B**) Colony formation assay was performed to detect cell proliferation. Western Blot was used to determine the expression levels of Cyclin D1, CDK2 and p27 in (**C**, **D**) CR-HCT116 cells, (**E**, **F**) CR-SW480 cells and (**G**–**H**) CR-SW620 cells. ("Con" represented "Control group", "Cis" indicated "Cisplatin treated group", "Cis+OE-MET" represented "Cisplatin plus overexpressed METTL1 treated group", "Cis+OE-M+OE-S" represented "Cisplatin plus overexpressed METTL1 and overexpressed S100A4 treated group"). All the experiments repeated at least 3 times. "*" means $p < 0.05$, "**" means $p < 0.01$ and "NS" means no statistical significance.

[19], gastric cancer [20] and non-small cell lung cancer [21]. Of note, this study found that the cytotoxic effects of overexpressed METTL1 on CR-CC cells treated with high-dose cisplatin were all abrogated by synergistically knocking down miR-149-3p, which suggested that overexpressed METTL1 sensitized CR-CC cells to high-dose cisplatin treatment by upregulating miR-149-3p and in line with the previous studies [10, 18–21].

S100A4 participated in the regulation of cisplatin-resistance of different cancer cells in a p53-dependent manner [27, 28], and upregulation of S100A4 promoted p53 protein degradation [28]. This study showed that overexpressed S100A4 and downregulated p53 were observed in CR-CC cells compared to CS-CC cells. In addition, overexpressed S100A4 mediated p53 degradation in CR-CC cells, which was in line with the previous study [28]. Notably, either downregulated S100A4 or upregulated p53 promoted high-dose cisplatin induced CR-CC cells death, which suggested that targeting S100A4/p53 axis increased chemosensitivity of CR-CC cells to cisplatin treatment and validated by the previous studies [27, 28]. Furthermore, S100A4/p53 axis was the downstream target of miR-149-3p [15], and overexpressed METTL1 inactivated S100A4/p53 axis in a miR-149-3p dependent manner. Besides, upregulation of S100A4 abrogated the cytotoxic effects of overexpressed METTL1 on CR-CC cells treated with high-dose cisplatin, which suggested that upregulation of METTL1 increased chemosensitivity of CR-CC cells to cisplatin by downregulating S100A4.

Taken together, this study found that overexpressed METTL1 increased chemosensitivity of CR-CC cells to cisplatin by regulating miR-149-3p/S100A4/p53 signaling pathway. Our work will provide new therapeutic strategies for CC treatment in clinic.

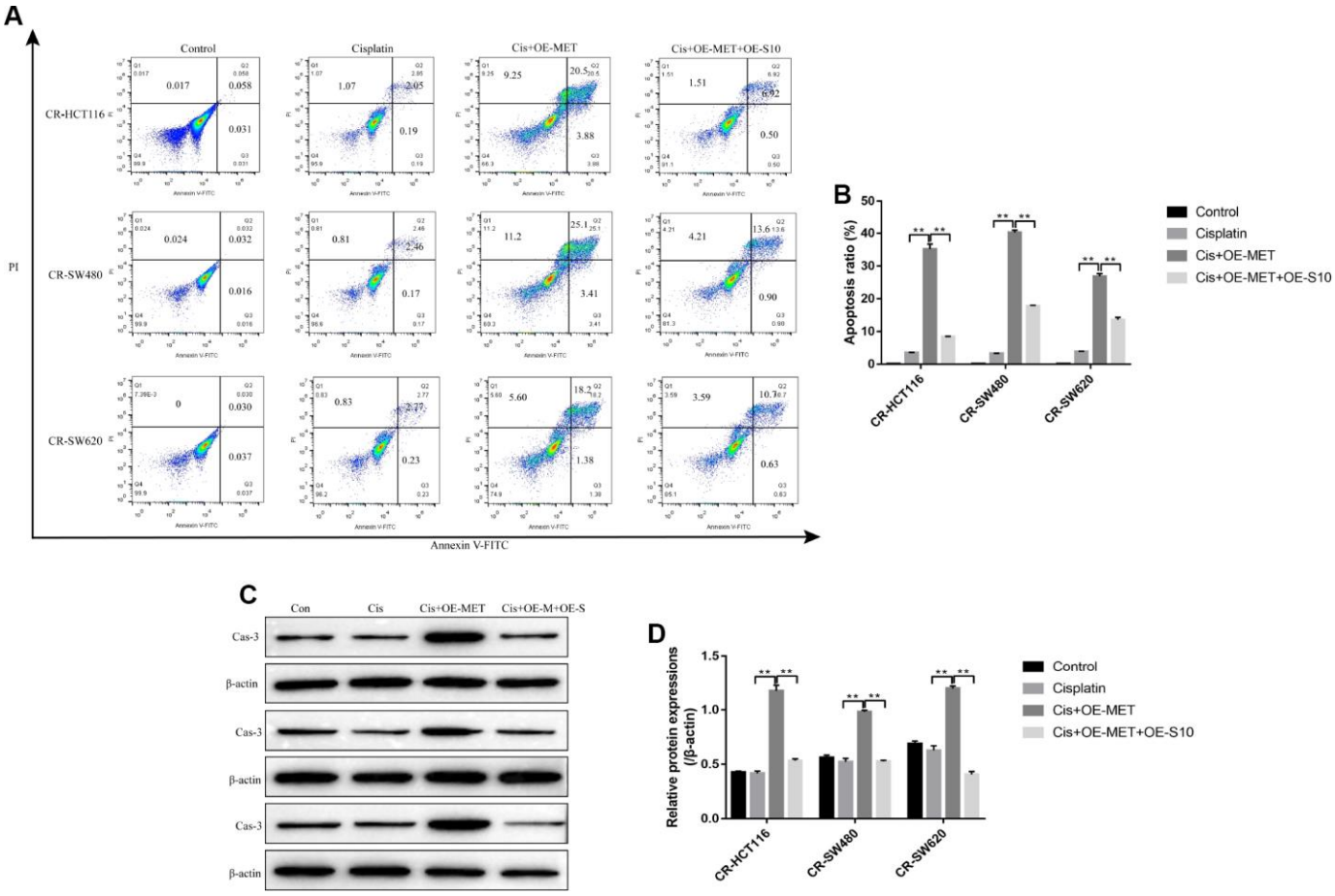

Figure 7. Overexpressed METTL1 promoted CR-CC cells apoptosis by regulating S100A4. (**A**, **B**) FCM was conducted to determine cell apoptosis ratio in CC cells. (**C**, **D**) Western Blot was employed to detect the expression levels of cleaved Caspase-3 in CR-CC cells. ("Con" represented "Control group", "Cis" indicated "Cisplatin treated group", "Cis+OE-MET" represented "Cisplatin plus overexpressed METTL1 treated group", "Cis+OE-M+OE-S" represented "Cisplatin plus overexpressed METTL1 and overexpressed S100A4 treated group"). "*" means $p < 0.05$, "**" means $p < 0.01$ and "NS" means no statistical significance.

MATERIALS AND METHODS

Cell culture and induction of Cisplatin-resistant CC (CR-CC) cells

Colon cancer (CC) cell lines (HCT116, SW480 and SW620) and HEK-293T cells were purchased from American Type Culture Collection (ATCC, USA). All the cells were cultured in the Dulbecco's modified Eagle medium (DMEM, Gibco Company, USA) containing 10% fetal bovine serum (FBS, Gibco Company, USA). The cells were cultured under the standard conditions with humidified atmosphere containing 5% CO_2 at 37°C. The CC cell lines were continuously exposed to low-dose cisplatin starting from 0.5μg/ml to 5μg/ml to generate cisplatin-resistant CC (CR-CC) cells according to the previous study [1]. After that, the above cells were collected and exposed to high-dose cisplatin (20μg/ml) to verify successful induction of CR-CC cells. The cisplatin-resistant CC (CR-CC) cells were named as CR-HCT116, CR-SW480 and CR-SW620 respectively. Similarly, the cisplatin-sensitive CC (CS-CC) cells were named as CS-HCT116, CS-SW480 and CS-SW620.

Vectors transfection

The cDNA fragments of METTL1, S100A4 and p53 were prepared by using the EcoRV/Xhol double enzymes digestion method. The above cDNAs sequences were next cloned into the pcDNA3.1 vectors to generate overexpressed METTL1 (OE-METTL1), S100A4 (OE-S100A4) and p53 (OE-p53) vectors respectively. The small interfering RNAs (siRNAs) for S100A4 were obtained from Sangon Biotech (Shanghai, China). In addition, the miR-149-3p mimic and inhibitor were also synthesized by Sangon Biotech (Shanghai, China). The above vectors were transfected into CR-CC cells by using the Lipofectamine 2000 reagent (Invitrogen, CA, USA) according to the manufacturer's protocol. After 24 hours post-transfection, Real-Time qPCR was used to detect the transfection efficiency.

Real-time qPCR

The CR-CC cells (CR-HCT116, CR-SW480 and CR-SW620) and CS-CC cells (CS-HCT116, CS-SW480 and CS-SW620) were collected and the total RNA were extracted by using the TakaRa MiniBEST Universal RNA Extraction Kit (Takara, Japan) according to the manufacturer's protocol. The total RNA were dissolved in the diethyl pyrocarbonate (DEPC) water and reversely transcribed into complementary DNA (cDNA) by using the TaqMan Reverse Transcription Reagents (Applied Biosystems, USA). After that, the SYBR Green SuperMix Kit (Takara, Japan) was used to amplify and quantify the involved genes including miR-149-3p and the mRNA levels of METTL1, S100A4 as well as p53. The primer sequences for the above genes were listed in Table 1.

Western blot

The CR-CC and CS-CC cells were collected and the total proteins were extracted by using the RIPA lysis buffer purchased from Beyotime Biotechnology (Shanghai, China). The 10% sodium dodecyl sulfate (SDS)-polyacrylamide gel electrophoresis (PAGE) was next employed to separate the target proteins according to their molecular weight. After that, the separated proteins were transferred to the poly vinylidene difluoride (PVDF) membranes and blocked by 5% skim milk solution. The membranes were probed with the primary antibodies including anti-METTL1 (1:1000, Abcam, UK), anti-β-actin (1:2000, Abcam, UK), anti-Cyclin D1 (1:1500, Abcam, UK), anti-CDK2(1:1500, Abcam, UK), anti-p27 (1:1000, Abcam, UK), anti-cleaved Caspase 3 (1:1000, Abcam, UK), anti-S100A4 (1:1000, Abcam, UK) and anti-p53 (1:1000, Abcam, UK) for 2 hours at room temperature. The secondary antibody purchased from Abcam (1:1000) was sequentially incubated with the PVDF membranes. The protein bands were visualized by using the ECL luminescence reagent (ThermoFisher Scientific, USA) and quantified by performing the Image J software (NIH, USA).

Cell counting kit-8 (CCK-8) assay

The CR-CC cells (CR-HCT116, CR-SW480 and CR-SW620) and CS-CC cells (CS-HCT116, CS-SW480 and CS-SW620) were all cultured under the standard cuture conditions. The above vectors were transfected into the cells until the cell confluency reached about 60-70%. The transfection efficiency of the vectors were determined by using the Real-Time qPCR and Western Blot technologies. About 24 hours post-transfection, the cells were collected and seeded into the 96-well plates at the density of 3000 cells per well. After 4 hours, the cells were incubated with high-dose cisplatin (20μg/ml) for 0h, 24h, 48h, 72h and 96h respectively. The CCK-8 kit (YEASEN, Shanghai, China) was used to determine cell proliferation according to the manufacturer's instruction. Briefly, 10μl of the CCK-8 solution were added to each well and incubated with the cells for 2 hours. After that, the optical density (OD) values in the wavelength of 450nm were detected to evaluate cell proliferation.

Colony formation assay

The CR-CC cells (CR-HCT116, CR-SW480 and CR-SW629) were transfected with the above vectors for 24

Table 1. Primer sequences for Real-Time qPCR.

Gene	Primer sequences (strand)
β-actin	Forward: 5′-CTCCATCCTGGCCTCGCTGT-3′ Reverse: 5′-GCTGCTACCTTCACCGTTCC-3′
U6	Forward: 5′-GACTATCATATGCTTACCGT-3′ Reverse: 5′-GGGCAGGAAGAGGGCCTAT-3′
miR-149-3p	Forward: 5′-GGCTCTGGCTCCGTGTCTT-3′ Reverse: 5′-CAGTGCAGGGTCCGAGGTATT-3′
METTL1	Forward: 5′-GAACATCGCCTGTCTCCGAA-3′ Reverse: 5′-TCGCTTAAAGTGTGGGTCCG-3′
S100A4	Forward: 5′-GATGTGATGGTGTCCACCTT-3′ Reverse: 5′-ATTTCTTCCTGGGCTGCTTA-3′
p53	Forward: 5′-CAGCCAAGTCTGTGACTTGCACGTAC-3′ Reverse: 5′-CTATGTCGAAAAGTGTTTCTGTCATC-3′

The genes included β-actin, U6, miR-149-3p, METTL1, S100A4 and p53.

hours and collected for further experiments. The cells were plated in 24-well plates at the density of 1000 cells per well, and cultured routinely at the standard conditions for 14 days according to the previous study [32]. After that, the cells were fixed with paraformaldehyde and stained with crystal violet (Beyotime Technology, Shanghai, China) for 10 min. Finally, the colonies containing at least 10 cells were counted under the light microscopy.

Flow cytometry (FCM)

The CR-CC cells (CR-HCT116, CR-SW480 and CR-SW629) were treated with high-dose cisplatin for 48 hours and cells were collected for apoptosis analysis. The Annexin V/Propidium iodide (PI) double stain kit (HaiGene Corporation, China) were purchased to determine the apoptosis ratio of the above cells according to the manufacturer's instruction. In brief, the above cells were diluted into cell suspensions at the density of 1×10^4/ml. The cell suspensions were next incubated with the Annexin V-FITC and PI double staining solution for 15-20 min at room temperature without light. Finally, the FCM machine (BD Biosciences, NJ, USA) was employed to determine the apoptosis ratio of the above cells.

Dual-luciferase reporter gene system

The online StarBase software (http://starbase.sysu.edu.cn/) was used to predict the binding sites of miR-149-3p and 3′UTR regions of S100A4. The 3′UTR regions of S100A4 were mutated according to the S100A4 sequences. After that, the wild-type (Wt) and mutant (Mut) 3′UTR regions of S100A4 were synthesized and cloned into the pmirGLO Expression Vector by Sangon Biotech (Shanghai, China) to generate Wt-S100A4 and Mut-S100A4 vectors respectively. Besides, the miR-149-3p mimic and inhibitor were obtained from Sangon Biotech (Shanghai, China). The above vectors were co-transfected into the HEK-293T cells by using the Lipofectamine 2000 reagent (Invitrogen, CA, USA) according to the manufacturer's protocol. After 24 hours post transfection, the luciferase activities were detected by using the dual-luciferase reporter gene system (Promega, USA) to validate the binding sites of miR-149-3p and 3'UTR regions of S100A4.

Terminal Deoxynucleotidyl Transferase (TdT)-mediated dUTP Nick-End Labeling (TUNEL) assay

The TUNEL assay was performed to determine cell apoptosis by using a TUNEL fluorescence kit (Rohce, Switzerland) according to the manufacturer's protocol. Briefly, the CR-CC cells were fixed with 4% paraformaldehyde for 30 min at room temperature. The cell membranes were next broken by treating cells with phosphate buffer saline (PBS) buffer containing 0.3% Triton X-100 (PBST), and the TdT mixed with dUTP was added to the cells. Finally, the cells were stained with DAPI for nuclei, and the Laser Scanning Confocal Microscope (Leica, Japan) was employed to determine cell apoptosis ratio according to the percentages of TUNEL positive cells.

Statistical analysis

All the data were collected and represented as Mean ± Standard Deviation (SD). The data analysis was conducted by using the SPSS 18.0 software. Specifically, the student's t-test was used to compare

the two groups, and the ANOVA was employed to analyse the differences among multiple groups. "$P < 0.05$" was regarded as statistical significance.

CONFLICTS OF INTEREST

These authors declare no Conflicts of interests in this research.

FUNDING

This work was financially supported by Natural Science Foundation of China (No. 81802990), Heilongjiang Province Postdoctoral First Aid funding (No. LBH-Z17114), Health and Family Planning Commission Research Project in Heilongjiang Province (No. 2018345) and Chenxiaoping Science and Technology (No. HE-201907).

REFERENCES

1. Xiong Z, Fu Z, Shi J, Jiang X, Wan H. HtrA1 Down-regulation Induces Cisplatin Resistance in Colon Cancer by Increasing XIAP and Activating PI3K/Akt Pathway. Ann Clin Lab Sci. 2017; 47:264–70. PMID:28667026

2. Wang ZK, Yang L, Wu LL, Mao H, Zhou YH, Zhang PF, Dai GH. Long non-coding RNA LINC00261 sensitizes human colon cancer cells to cisplatin therapy. Braz J Med Biol Res. 2017; 51:e6793. https://doi.org/10.1590/1414-431x20176793 PMID:29267503

3. Chen X, Xu H, Yu X, Wang X, Zhu X, Xu X. Apigenin inhibits in vitro and in vivo tumorigenesis in cisplatin-resistant colon cancer cells by inducing autophagy, programmed cell death and targeting m-TOR/PI3K/Akt signalling pathway. J BUON. 2019; 24:488–93. PMID:31127995

4. Shen F, Feng L, Zhou J, Zhang H, Xu Y, Jiang R, Zhang H, Chen Y. Overexpression of CASC11 in ovarian squamous cell carcinoma mediates the development of cancer cell resistance to chemotherapy. Gene. 2019; 710:363–66. https://doi.org/10.1016/j.gene.2019.06.011 PMID:31181314

5. Yadav SS, Kumar M, Varshney A, Yadava PK. KLF4 sensitizes the colon cancer cell HCT-15 to cisplatin by altering the expression of HMGB1 and hTERT. Life Sci. 2019; 220:169–76. https://doi.org/10.1016/j.lfs.2019.02.005 PMID:30716337

6. Alexandrov A, Martzen MR, Phizicky EM. Two proteins that form a complex are required for 7-methylguanosine modification of yeast tRNA. RNA. 2002; 8:1253–66. https://doi.org/10.1017/S1355838202024019 PMID:12403464

7. Cartlidge RA, Knebel A, Peggie M, Alexandrov A, Phizicky EM, Cohen P. The tRNA methylase METTL1 is phosphorylated and inactivated by PKB and RSK in vitro and in cells. EMBO J. 2005; 24:1696–705. https://doi.org/10.1038/sj.emboj.7600648 PMID:15861136

8. Lin S, Liu Q, Lelyveld VS, Choe J, Szostak JW, Gregory RI. Mettl1/Wdr4-Mediated m^7G tRNA Methylome Is Required for Normal mRNA Translation and Embryonic Stem Cell Self-Renewal and Differentiation. Mol Cell. 2018; 71:244–255.e5. https://doi.org/10.1016/j.molcel.2018.06.001 PMID:29983320

9. Okamoto M, Fujiwara M, Hori M, Okada K, Yazama F, Konishi H, Xiao Y, Qi G, Shimamoto F, Ota T, Temme A, Tatsuka M. tRNA modifying enzymes, NSUN2 and METTL1, determine sensitivity to 5-fluorouracil in HeLa cells. PLoS Genet. 2014; 10:e1004639. https://doi.org/10.1371/journal.pgen.1004639 PMID:25233213

10. Pandolfini L, Barbieri I, Bannister AJ, Hendrick A, Andrews B, Webster N, Murat P, Mach P, Brandi R, Robson SC, Migliori V, Alendar A, d'Onofrio M, et al. METTL1 Promotes let-7 MicroRNA Processing via m7G Methylation. Mol Cell. 2019; 74:1278–1290.e9. https://doi.org/10.1016/j.molcel.2019.03.040 PMID:31031083

11. Chen S, Yang C, Sun C, Sun Y, Yang Z, Cheng S, Zhuge B. miR-21-5p Suppressed the Sensitivity of Hepatocellular Carcinoma Cells to Cisplatin by Targeting FASLG. DNA Cell Biol. 2019; 38:865–73. https://doi.org/10.1089/dna.2018.4529 PMID:31225740

12. Li M, Gao M, Xie X, Zhang Y, Ning J, Liu P, Gu K. MicroRNA-200c reverses drug resistance of human gastric cancer cells by targeting regulation of the NER-ERCC3/4 pathway. Oncol Lett. 2019; 18:145–52. https://doi.org/10.3892/ol.2019.10304 PMID:31289483

13. Wu K, Hu Y, Yan K, Qi Y, Zhang C, Zhu D, Liu D, Zhao S. microRNA-10b confers cisplatin resistance by activating AKT/mTOR/P70S6K signaling via targeting PPARγ in esophageal cancer. J Cell Physiol. 2020; 235:1247–1258. https://doi.org/10.1002/jcp.29040 PMID:31267531

14. Bellazzo A, Di Minin G, Valentino E, Sicari D, Torre D, Marchionni L, Serpi F, Stadler MB, Taverna D, Zuccolotto G, Montagner IM, Rosato A, Tonon F, et al. Cell-autonomous and cell non-autonomous

downregulation of tumor suppressor DAB2IP by microRNA-149-3p promotes aggressiveness of cancer cells. Cell Death Differ. 2018; 25:1224–38. https://doi.org/10.1038/s41418-018-0088-5 PMID:29568059

15. Yang D, Du G, Xu A, Xi X, Li D. Expression of miR-149-3p inhibits proliferation, migration, and invasion of bladder cancer by targeting S100A4. Am J Cancer Res. 2017; 7:2209–19. PMID:29218245

16. Si L, Xu L, Yin L, Qi Y, Han X, Xu Y, Zhao Y, Liu K, Peng J. Potent effects of dioscin against pancreatic cancer via miR-149-3P-mediated inhibition of the Akt1 signalling pathway. Br J Pharmacol. 2017; 174:553–68. https://doi.org/10.1111/bph.13718 PMID:28095588

17. Zhang G, Liu X, Li Y, Wang Y, Liang H, Li K, Li L, Chen C, Sun W, Ren S, Zhu P, Zhang L. EphB3-targeted regulation of miR-149 in the migration and invasion of human colonic carcinoma HCT116 and SW620 cells. Cancer Sci. 2017; 108:408–18. https://doi.org/10.1111/cas.13161 PMID:28370854

18. Sun L, Zhai R, Zhang L, Zhao S. MicroRNA-149 suppresses the proliferation and increases the sensitivity of ovarian cancer cells to cisplatin by targeting X-linked inhibitor of apoptosis. Oncol Lett. 2018; 15:7328–34. https://doi.org/10.3892/ol.2018.8240 PMID:29731888

19. Wang Y, Chen J, Zhang M, Zhang W, Li M, Zang W, Dong Z, Zhao G. MiR-149 sensitizes esophageal cancer cell lines to cisplatin by targeting DNA polymerase β. J Cell Mol Med. 2018; 22:3857–65. https://doi.org/10.1111/jcmm.13659 PMID:29726631

20. Li X, Liang J, Liu YX, Wang Y, Yang XH, Luan BH, Zhang GL, Du J, Wu XH. miR-149 reverses cisplatin resistance of gastric cancer SGC7901/DDP cells by targeting FoxM1. Pharmazie. 2016; 71:640–43. https://doi.org/10.1691/ph.2016.6696 PMID:29441968

21. Berghmans T, Ameye L, Willems L, Paesmans M, Mascaux C, Lafitte JJ, Meert AP, Scherpereel A, Cortot AB, Cstoth I, Dernies T, Toussaint L, Leclercq N, Sculier JP, and European Lung Cancer Working Party. Identification of microRNA-based signatures for response and survival for non-small cell lung cancer treated with cisplatin-vinorelbine A ELCWP prospective study. Lung Cancer. 2013; 82:340–45. https://doi.org/10.1016/j.lungcan.2013.07.020 PMID:24007627

22. Boulias K, Greer EL. Put the Pedal to the METTL1: Adding Internal m^7G Increases mRNA Translation Efficiency and Augments miRNA Processing. Mol Cell. 2019; 74:1105–07. https://doi.org/10.1016/j.molcel.2019.06.004 PMID:31226274

23. Ruma IM, Kinoshita R, Tomonobu N, Inoue Y, Kondo E, Yamauchi A, Sato H, Sumardika IW, Chen Y, Yamamoto KI, Murata H, Toyooka S, Nishibori M, Sakaguchi M. Embigin Promotes Prostate Cancer Progression by S100A4-Dependent and-Independent Mechanisms. Cancers (Basel). 2018; 10:E239. https://doi.org/10.3390/cancers10070239 PMID:30041429

24. Egeland EV, Boye K, Park D, Synnestvedt M, Sauer T, Naume B, Borgen E, Mælandsmo GM, and Oslo Breast Cancer Consortium (OSBREAC). Prognostic significance of S100A4-expression and subcellular localization in early-stage breast cancer. Breast Cancer Res Treat. 2017; 162:127–37. https://doi.org/10.1007/s10549-016-4096-1 PMID:28058579

25. Dukhanina EA, Portseva TN, Kotnova AP, Pankratova EV, Georgieva SG. The Expression Level of S100A4 Protein Affects the Migration Activity of Breast Cancer Cells. Dokl Biochem Biophys. 2019; 485:104–06. https://doi.org/10.1134/S1607672919020030 PMID:31201625

26. Destek S, Gul VO. S100A4 May Be a Good Prognostic Marker and a Therapeutic Target for Colon Cancer. J Oncol. 2018; 2018:1828791. https://doi.org/10.1155/2018/1828791 PMID:30111999

27. Liang DP, Huang TQ, Li SJ, Chen ZJ. Knockdown of S100A4 chemosensitizes human laryngeal carcinoma cells in vitro through inhibition of Slug. Eur Rev Med Pharmacol Sci. 2014; 18:3484–90. PMID:25491625

28. Orre LM, Panizza E, Kaminskyy VO, Vernet E, Gräslund T, Zhivotovsky B, Lehtiö J. S100A4 interacts with p53 in the nucleus and promotes p53 degradation. Oncogene. 2013; 32:5531–40. https://doi.org/10.1038/onc.2013.213 PMID:23752197

29. Rezaee M, Sanche L, Hunting DJ. Cisplatin enhances the formation of DNA single- and double-strand breaks by hydrated electrons and hydroxyl radicals. Radiat Res. 2013; 179:323–31. https://doi.org/10.1667/RR3185.1 PMID:23368416

30. Wang L, Valiskova B, Forejt J. Cisplatin-induced DNA double-strand breaks promote meiotic chromosome synapsis in PRDM9-controlled mouse hybrid sterility. eLife. 2018; 7:7. https://doi.org/10.7554/eLife.42511

PMID:30592461

31. Gong L, Chen J. Δ113p53/Δ133p53 converts P53 from a repressor to a promoter of DNA double-stand break repair. Mol Cell Oncol. 2015; 3:e1033587. https://doi.org/10.1080/23723556.2015.1033587 PMID:27308550

32. Liu J, Song S, Lin S, Zhang M, Du Y, Zhang D, Xu W, Wang H. Circ-SERPINE2 promotes the development of gastric carcinoma by sponging miR-375 and modulating YWHAZ. Cell Prolif. 2019; 52:e12648. https://doi.org/10.1111/cpr.12648 PMID:31199037

SUPPLEMENTARY MATERIALS

Supplementary Figures

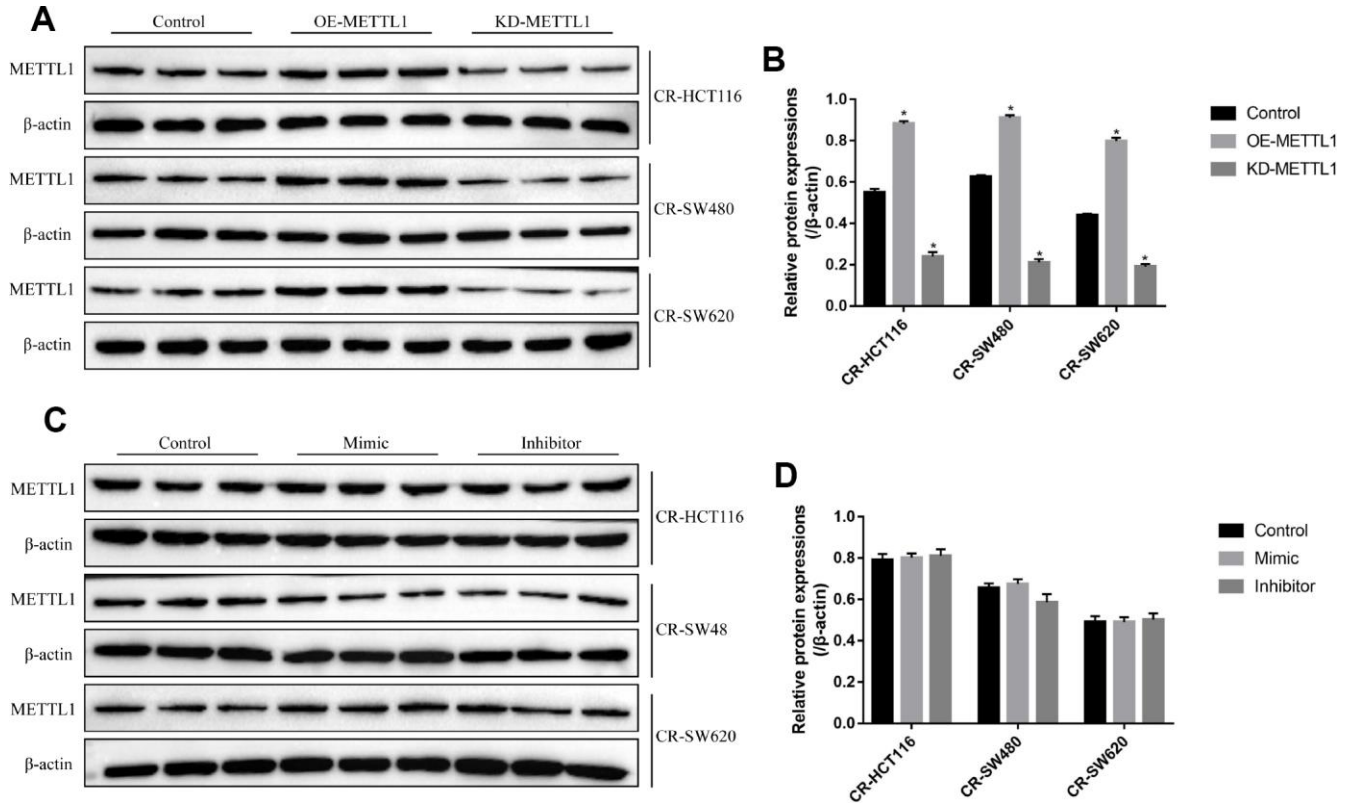

Supplementary Figure 1. Western Blot was used to determine (**A**) the expression levels of METTL1 in CR-CC cells and (**B**) the effects of miR-149-3p on METTL1 levels in CR-CC cells. All the experiments repeated at least 3 times. "*" means $p < 0.05$, "**" means $p < 0.01$ and "NS" means no statistical significance.

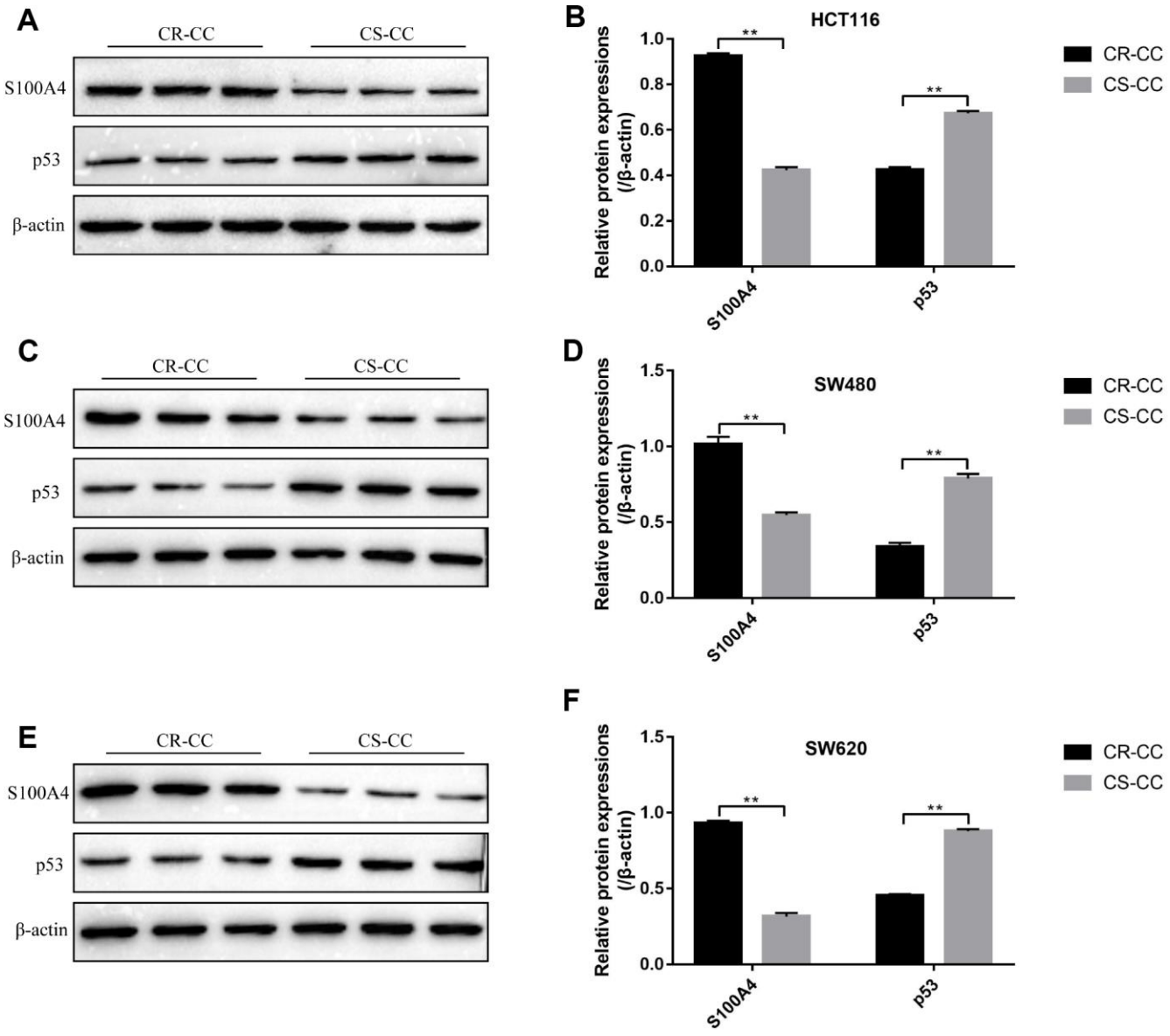

Supplementary Figure 2. Western Blot was used to determine the expression levels of S100A4 and p53 in (**A**, **B**) HCT116 cells, (**C**, **D**) SW480 cells and (**E**, **F**) SW620 cells. All the experiments repeated at least 3 times. "*" means $p < 0.05$, "**" means $p < 0.01$ and "NS" means no statistical significance.

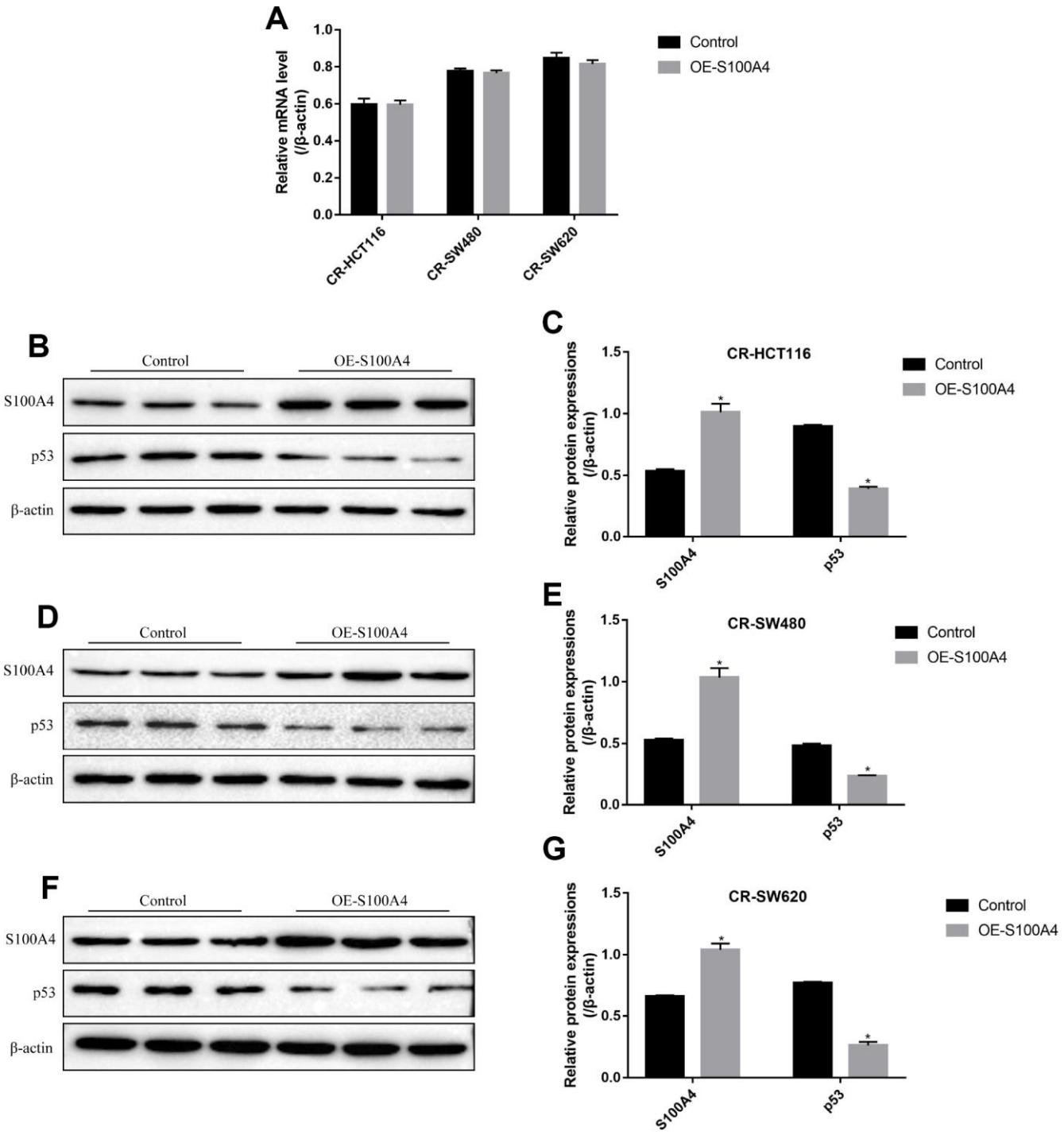

Supplementary Figure 3. The effects of S100A4 on p53 levels in CR-CC cells. (**A**) Real-Time qPCR was used to detect S100A4 mRNA levels. Western Blot was used to determine the expression levels of S100A4 and p53 in (**B**, **C**) CR-HCT116 cells, (**D**, **E**) CR-SW480 cells and (**F**, **G**) CR-SW620 cells. All the experiments repeated at least 3 times. "*" means $p < 0.05$, "**" means $p < 0.01$ and "NS" means no statistical significance.

Research Paper

TP53/miR-34a-associated signaling targets *SERPINE1* expression in human pancreatic cancer

Shaw M. Akula[1], Peter P. Ruvolo[2], James A. McCubrey[1]

[1]Department of Microbiology and Immunology, Brody School of Medicine, East Carolina University, Greenville, NC 27834, USA
[2]Department of Leukemia, University of Texas MD Anderson Cancer Center, Houston, TX 77030, USA

Correspondence to: Shaw M. Akula, James A. McCubrey; **email:** akulas@ecu.edu, mccubreyj@ecu.edu
Keywords: PDAC, aging, cancer, TP53, miR-34a, *SERPINE1*
Received: December 4, 2019 **Accepted:** January 12, 2020 **Published:** January 27, 2020

ABSTRACT

Pancreatic ductal adenocarcinoma (PDAC) is a disease of aging. The *TP53* gene product regulates cell growth, aging, and cancer. To determine the important targets of TP53 in PDAC, we examined the expression of 440 proteins on a reverse phase protein array (RPPA) in PDAC-derived MIA-PaCa-2 cells which either had WT-*TP53* or lacked WT-*TP53*. MIA-PaCa-2 cells have a *TP53* mutation as well as mutant *KRAS* and represent a good *in vitro* model to study PDAC. RPPA analysis demonstrated expression of tumor promoting proteins in cells that lacked WT-*TP53*; and this feature could be reversed significantly when the cells were transfected with vector encoding WT-*TP53* or treated with berberine or a modified berberine (BBR). Expression of miR-34a-associated signaling was elevated in cells expressing WT-*TP53* compared to cells expressing *mTP53*. Results from *in vivo* studies using human PDAC specimens confirmed the *in vitro* results as the expression of miR-34a and associated signaling was significantly decreased in PDAC specimens compared to non-cancerous tissues. This study determined *SERPINE1* as a miR-34a target with relevance to the biology of PDAC. Thus, we have identified a key target (*SERPINE1*) of the TP53/miR-34a axis that may serve as a potential biomarker for early detection of pancreatic cancer.

INTRODUCTION

The risk of developing cancer of the pancreas increases with age; it was estimated that only 13% of all patients with pancreatic cancer are diagnosed before the age of 60 [1]. The increasing incidence and mortality from pancreatic ductal adenocarcinoma (PDAC) are medical issues of paramount importance [2, 3]. Current treatments combining surgical resection and chemotherapy are only minimally effective [4, 5]. In most cases, by the time PDAC is diagnosed, it has already spread to distant sites, making treatment an impossible task. PDAC is the ninth most common cancer in the USA, has the highest mortality of any cancer, and will soon be the second most common cause of cancer death in USA [6, 7].

Two of the key genes involved in the development of PDAC are *KRAS* and *TP53* [8]. *KRAS* (activation) mutations occur in about 90% of PDAC while *TP53* (inactivation) mutations occur in approximately 75% of pancreatic cancers [9]. Apart from mutations in these genes, host cell microRNAs (miRNAs) also have crucial roles to play in various biological processes, including: inflammation, cell growth, aging, differentiation, proliferation, and metastasis [10, 11]. Increasing evidence in recent years suggests that miRNAs control the development and progression of inflammation and cancer [12–15]. In this study we focused on miR-34a over other miRNAs because of the following reasons: (i) Expression of miR-34a is significantly down-regulated or absent in a variety of cancers including hepatocellular and renal cell carcinomas, colon, breast, lung, prostate, ovarian, and pancreatic cancers [16–22]; (ii) The two major oncogenes that are mutated in PDAC are *KRAS* and *TP53* [23]; (iii) *TP53* directly transactivates miR-34a

expression [24] while mutated *KRAS* indirectly lowers expression of miR-34a via the transcription factor, ZEB1 [25, 26]. Therefore, inactivation of *TP53* and increases in mutated *KRAS* expression result in a sharp decline in miR-34a expression during tumorigenesis.

The miR-34 family contains three members and is encoded by two genes located on chromosomes 1 and 11 [27]. The mature miR-34a shares 86% identity (19/22 nt) with miR-34b and 82% identity (18/22 nt) with miR-34c, respectively. The position 2-9 adjacent at the 5' end (8 nt) is considered the "seed region" for all three members [27–29]. Among these members, miR-34a is expressed at higher levels than miR-34b/c, with the exception of the lung [30].

miR-34a is a key regulator of tumor suppression and is considered to have a broad anti-oncogenic activity [30]. We hypothesize miR-34a to play a major role in the development of PDAC. As of this date, there are limited investigations conducted to understand the roles of miR-34a in the biology of PDAC. Therefore, the focus of this study was to decipher a potential role for TP53>miR-34a-associated signaling in pancreatic cancer using *in vitro* and *in vivo* models. Our study determined a decrease in the expression of miR-34a in human PDAC specimens. Using *in vitro* and *in vivo* approaches, we ascertained *SERPINE1* to be a target of miR-34a and their patho-physiological significance is discussed.

RESULTS

Profiling of tumor promoting and suppressor proteins in response to expression of wild-type TP53 in MIA-PaCa-2 cells

RPPA assay was performed to elucidate the effects of expressing WT-*TP53* in MIA-PaCa-2 cells. The crucial step prior to performing the RPPA assay was to characterize the MIA-PaCa-2 cells used in this study. This is important as these cells expressing the *mTP53* and WT-*TP53* form the basis for the *in vitro* experiments conducted in this study. The MIA-PaCa-2+WT-*TP53* cells were more sensitive to the chemotherapeutic drugs compared to MIA-PaCa-2+pLXSN cells (Supplementary Figure 1). Similar results have been reported by earlier studies [23, 31–33]. The above results authenticate the physiological effects of expressing different forms of TP53 and associated cell signaling. RPPA is a high-throughput technology based on the detection of proteins along with their post-translational protein modifications, e.g., cleavage and phosphorylation [34]. To this end, we performed RPPA using a selection of 446 antibodies (Supplementary Table 1). RPPA analysis revealed a *mTP53*-dependent modulation of multiple cell signaling molecules involved in cell proliferation and survival (Figure 1A). Further, the analysis documented an increase and decrease in the expression of specific proteins that promoted tumor formation (Table 1) in MIA-PaCa-2 cells with mutated *TP53* (MIA-PaCa-2+pLXSN) compared to MIA-PaCa-2 cells expressing WT-*TP53* (MIA-PaCa-2+WT-*TP53*). The expression of proteins in parental MIA-PaCa-2 untransfected cells followed a similar pattern as expressed in MIA-PaCa-2+pLXSN cells (data not shown).

Expression of DNMT1, S6 (phosphorylated on serine residues at 240 and 244), and GSK-3α/3β (phosphorylated on serine residue at 21 of GSK3α or serine 9 of GSK-3β) were elevated in MIA-PaCa-2 cells with *mTP53* (MIA-PaCa-2+pLXSN) (Table 2) and MIA-PaCa-2 cells (data not shown). On the same lines, expression of Bax, cleaved caspase-3, and cleaved caspase-8 were down-regulated in MIA-PaCa-2 cells expressing WT-*TP53* (MIA-PaCa-2+WT-*TP53*) (Table 2). Thus, the cellular events seem to promote cell survival while actually inhibiting apoptosis in cells expressing *mTP53* (Figure 1B). RPPA analysis demonstrated a crucial role for the WT-*TP53* in mediating anti-tumor activity via modulating cell signaling.

Effect of treating MIA-PaCa-2 cells with BBR and MBBR on cell division, proliferation, survival, migration, and apoptosis

Earlier studies by us determined that BBR and MBBR inhibited proliferation of pancreatic cancer cells [31, 32]. In the current study, we determined the effect of treating MIA-PaCa-2+pLXSN cells with BBR and MBBR (NAX060) on cell signaling using RPPA. Treatment of MIA-PaCa-2+pLXSN cells (carrying *mTP3*) with BBR and MBBR altered the expression of 11 proteins to varying extents (Table 3). Each of these proteins influence tumorigenesis by regulating cell cycle progression, survival, proliferation, apoptosis and DNA repair. The effects of BBR and MBBR on the proliferation of MIA-PaCa-2+pLXSN cells is presented in the schematic (Figure 2). The schematic also represents the manner by which BBR and MBBR may directly or indirectly alter the expression of *mTP53*-associated signaling molecules (Figure 1A). RPPA analysis demonstrated the ability of BBR and MBBR to promote anti-tumor activity in MIA-PaCa-2+pLXSN and MIA-PaCa-2 (data not shown) cells by inhibiting cell cycle progression, proliferation, and survival to varying extents.

WT-TP53 enhances expression of miR-34a in MIA-PaCa2 cells

TP53 directly transactivates miR-34a expression [24]. Therefore, we set out to compare the expression levels of

miR-34a in MIA-PaCa-2 cells *in vitro*. The expression levels of miR-34a were significantly lower in the pancreatic cancer cell lines MIA-PaCa-2 and MIA-PaCa-2+pLXSN than those of MIA-PaCa2 cells that were stably transfected with vector encoding WT-*TP53* (MIA-PaCa-2+WT-*TP53*) (Figure 3A). Mock transfection (data not shown) did not significantly alter the expression profile of miR-34a. These results indicate the following: a) miR-34a levels are inherently lower in cells derived from pancreatic cancer which have a *mTP53*; and b) There is a direct positive correlation between the expression of WT-*TP53* and miR-34a.

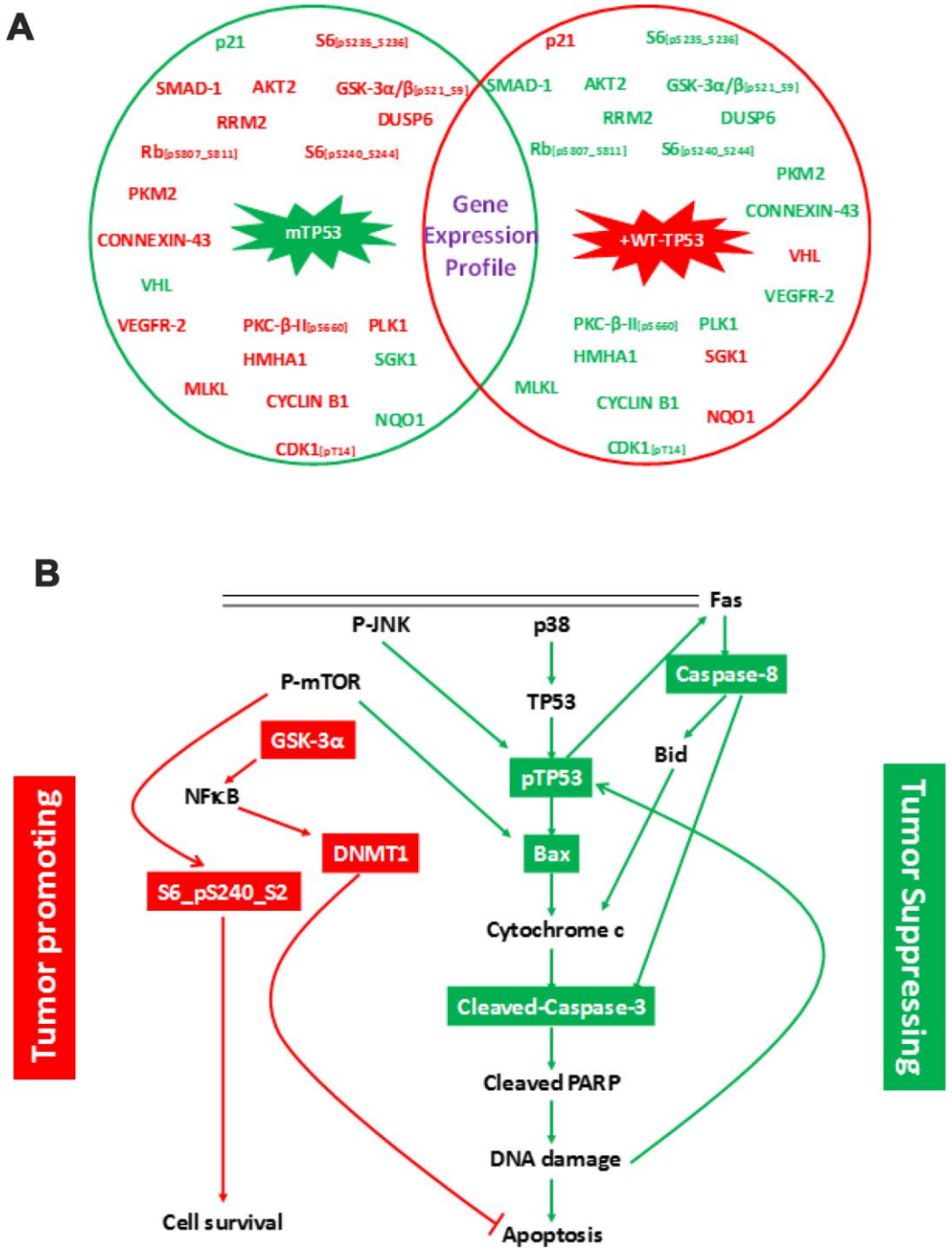

Figure 1. Changes in protein expression profile in MIA-PaCa-2 cells expressing pLXSN compared to WT-TP53. (**A**) Protein expression was assayed by RPPA. Proteins indicated in red and green denotes increased and decreased expression, respectively. Genes in red and green indicate tumor promoting and suppressor activities, respectively. (**B**) Schematic demonstrating cell signaling in MIA-PaCa-2+pLXSN cells promoting cell survival (in red) while significantly inhibiting apoptosis (in green).

Table 1. RPPA analysis demonstrating the tumor promoting milieu in MIA-PaCa-2+pLXSN cells compared to MIA-PaCa-2+WT-*TP53* cells.

Protein name, and phosphorylation status	Gene symbol	Function	GenBank accession no.	Fold change in protein expression
INCREASE IN EXPRESSION:				
AKT serine/threonine kinase 2 (AKT2)	AKT2	Promotes cancer formation	AAI20996.1	2.0
Cyclin dependent kinase 1 (CDK1_pT14))	CDK1	Promotes cell division	NP_001777.1	2.8
Connexin-43 (Cx43)	GJA1	Correlates with cancer metastasis	AAA52131.1	5.0
Cyclin-B1	CCNB1	Promotes cell survival	EAW51306.1	2.4
Dual specificity phosphatase 6 (DUSP6)	DUSP6	Drives poor prognosis in cancer	BAA34369.1	3.2
Glycogen synthase kinase 3α/β (GSK-3α/β_pS21_S9)	GSK-3α/β	Promotes cell growth & invasion	NP_063937.2	2.1
Minor histocompatibility protein HA-1 (HMHA1)	HMHA1	Induces cell spread	AAH48129.1	5.3
mitogen-activated protein kinase kinase kinase 9 (MLK1)	MLK1	Induces necroptosis	AAB26359.1	2.7
Protein kinase-β II (PKC-β-II_pS660)	PRKCB	Promotes signaling to cause cancer	P05771.4	2.0
Pyruvate kinase M1/2 (PKM2)	PKM2	Drives poor prognosis in cancer	AAH94767.1	2.1
Polo like kinase 1 (PLK1)	PLK1	Promotes proliferation and suppress apoptosis	NP_005021.2	3.1
Retinoblastoma protein (Rb_pS807_S811)	Rb1	Phosphorylation of Rb inactivates the protein	AAH40540.1	2.7
Ribonucleotide reductase regulatory subunit M2 (RRM2)	RRM2	Drives poor prognosis in cancer	NP_001025.1	2.4
40S ribosomal protein S6 (S6_pS235_S236)	S6	Promotes cell survival	NP_001001.2	3.4
40S ribosomal protein S6 (S6_pS240-S244)	S6	Promotes cell survival	NP_001001.2	3.8
SMAD family member 1 (SMAD1)	SMAD1	A crucial role in development of cancer	AAC50790.1	2.0
Vascular endothelial growth factor receptor-2 (VEGFR-2)	VEGFR-2	Induces angiogenesis	P35968.2	2.5
DECREASE IN EXPRESSION:				
NAD(P)H quinone dehydrogenase 1	NQO1	Regulates autophagy	AAI07740.1	0.3
p21	P21	Tumor suppressor	AAB29246.1	0.5
Serum/Glucocorticoid Regulated Kinase 1 (SGK1)	SGK1	Inhibits cancer cell invasion and migration	AAH01263.1	0.4
von Hippel-Lindau tumor suppressor (VHL)	VHL	Tumor suppressor	AAH58831.1	0.4

Table 2. RPPA analysis demonstrating changes in the expression of proteins that promote cell survival while decreasing apoptosis in MIA-PaCa-2+pLXSN cells compared to MIA-PaCa-2+WT-TP53 cells.

Protein name, and phosphorylation status	Gene symbol	Function	GenBank accession no.	Fold change in protein expression
PROMOTING CELL SURVIVAL:				
DNA methyltransferase 1 (DNMT1)	DNMT1	Promotes cell survival	AAI26228.1	2.4
40S ribosomal protein S6 (S6_pS240-S244)	S6	Promotes cell survival	NP_001001.2	3.8
Glycogen synthase kinase 3α/β (GSK-3α/β_pS21_S9)	GSK-3α/β	Promotes cell survival	NP_063937.2	2.1
DECREASING TUMOR SUPPRESSION:				
BCL2 associated X, apoptosis regulator (BAX)	BAX	Promotes apoptosis	Q07812.1	0.3
Cleaved caspase-3 (Caspase-3)	CASP3	Promotes apoptosis	CAC88866.1	0.4
Cleaved caspase-8 (Caspase-8)	CASP8	Promotes apoptosis	BAB32555.1	0.3

Table 3. RPPA analysis demonstrating the fold change in activity of proteins in response to treating MIA-PaCa-2+pLXSN cells with BBR and MBBR.

Protein name, and phosphorylation status	Gene symbol	Function	GenBank accession no.	% drop in expression	
				BBR	MBBR
AXL receptor tyrosine kinase (AXL)	AXL	Promotes proliferation, stem cell phenotype	AAH32229.1	34%	46%
Dynamin-related protein 1 (DRP-1)	DRP-1	Promotes cell survival, migration	O00429.2	44%	43%
Eukaryotic elongation factor 2 kinase (eEf2K)	eEf2K	Promotes cell survival, proliferation	AAH32665.1	31%	38%
Glycogen synthase kinase 3α/β (GSK-3α/β_pS21_S9)	GSK-3α/β	Promotes cell growth & invasion	NP_063937.2	92%	33%
Human epidermal growth factor receptor 2 (HER2)	HER2	Correlates with worse survival	P04626.1	39%	92%
Jagged canonical Notch ligand 1 (JAG1)	JAG1	Promotes migration and invasion of cells	NP_000205.1	38%	42%
Paired box 8 (PAX8)	PAX8	Promotes cell proliferation	AAB34216.1	54%	44%
Pyruvate dehydrogenase kinase 1 (PDK1)	PDK1	Promotes cell growth and survival	AAH39158.1	86%	35%
Ribosomal protein S6 kinase B1 (S6K1)	S6K1	Promotes cell proliferation	P23443.2	52%	37%
X-linked inhibitor of apoptosis (XIAP)	XIAP	Inhibitor of apoptosis	NP_001191330.1	70%	33%

One miRNA may target several genes. By using the miRmap and PiCTar tool algorithms [35, 36], we identified potential targets for miR-34a (Supplementary Tables 2 and 3). Analysis of RPPA data identified expression of a few of the miR-34a target proteins was altered in MIA-PaCa-2 cells. We determined a significant decrease in the expression of putative miR-34a targets (*ATG4B*, *AXL*, *GATA3*, *JAG1*, *LDHA*, *MAP2K1*, *MYT1*, *NOTCH1*, *PEA-15*, *SERPINE1*, and *SNAIL*) in MIA-PaCa-2+WT-*TP53* compared to MIA-PaCa-2+pLXSN (Figure 3B). Expression of putative miR-34a targets (PCD4 and MAPT) were significantly elevated in MIA-PaCa-2+WT-*TP53* compared to MIA-PaCa-2+pLXSN (Figure 3B). The effect of expressing

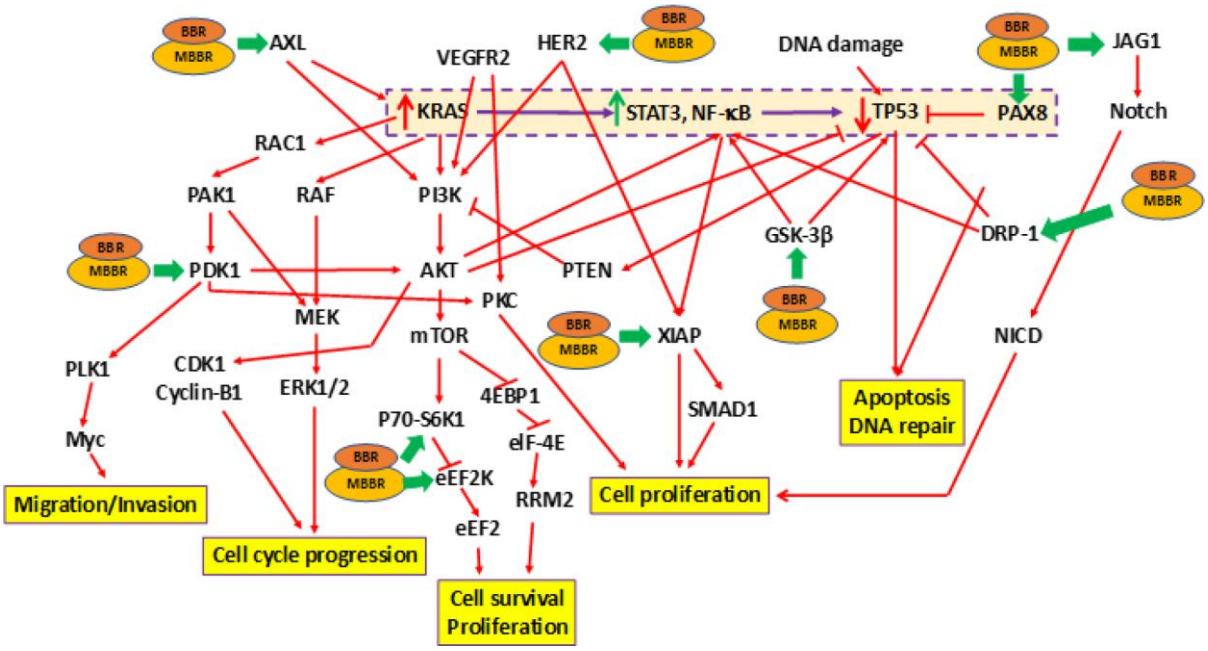

Figure 2. Effects of treating MIA-PaCa-2 cells with BBR and NAX060 on cell division, proliferation, survival, migration, and apoptosis. A schematic depicting the effects of BBR and NAX060 on the *N-RAS*/*TP53*-associated signaling critical to PDAC development. The model is based on the fact that over-expression of mutated *KRAS* significantly enhances STAT3, NF-κB signaling which in turn lowers the TP53 expression (highlighted and boxed in dotted purple line). Green bold arrows denote inhibiting effects of BBR/MBBR on the signaling molecule.

WT-*TP53* on the miR-34a targets at the level of transcription was monitored in cells by qRT-PCR. qRT-PCR data (Figure 3C) corroborated the RPPA analysis. The study established an inverse correlation between the expression of miR-34a and its target genes.

In vivo expression profile of miR-34a reflects its *in vitro* expression pattern

To monitor *in vivo* expression of miR-34a, we used human pancreas samples obtained from PDAC patients with appropriate controls. The expression levels of miR-34a were measured employing qRT-PCR with the SYBR green detection and specific forward primer for the mature miRNA sequence [74] and the universal adaptor reverse primer (GeneCopoeia, USA). Our preliminary results (Figure 4A) demonstrate a significant decrease in the levels of miR-34a in PDAC tumors when compared to healthy pancreas controls. The next obvious question was to understand the expression profiles of the set of putative miR-34a target genes that were significantly altered *in vitro* (Figure 3B, 3C). The expression profile of the miR-34a target genes (*ATG4B*, *AXL*, *GATA3*, *JAG1*, *LDHA*, *MAP2K1*, *MYT1*, *NOTCH1*, *PEA-15*, *SERPINE1*, and *SNAIL*) followed an identical expression pattern (Figure 4B). Expression of *PCD4* was at undetectable levels *in vivo* (Figure 4B). Interestingly, expression of *SERPINE1* was significantly greater than

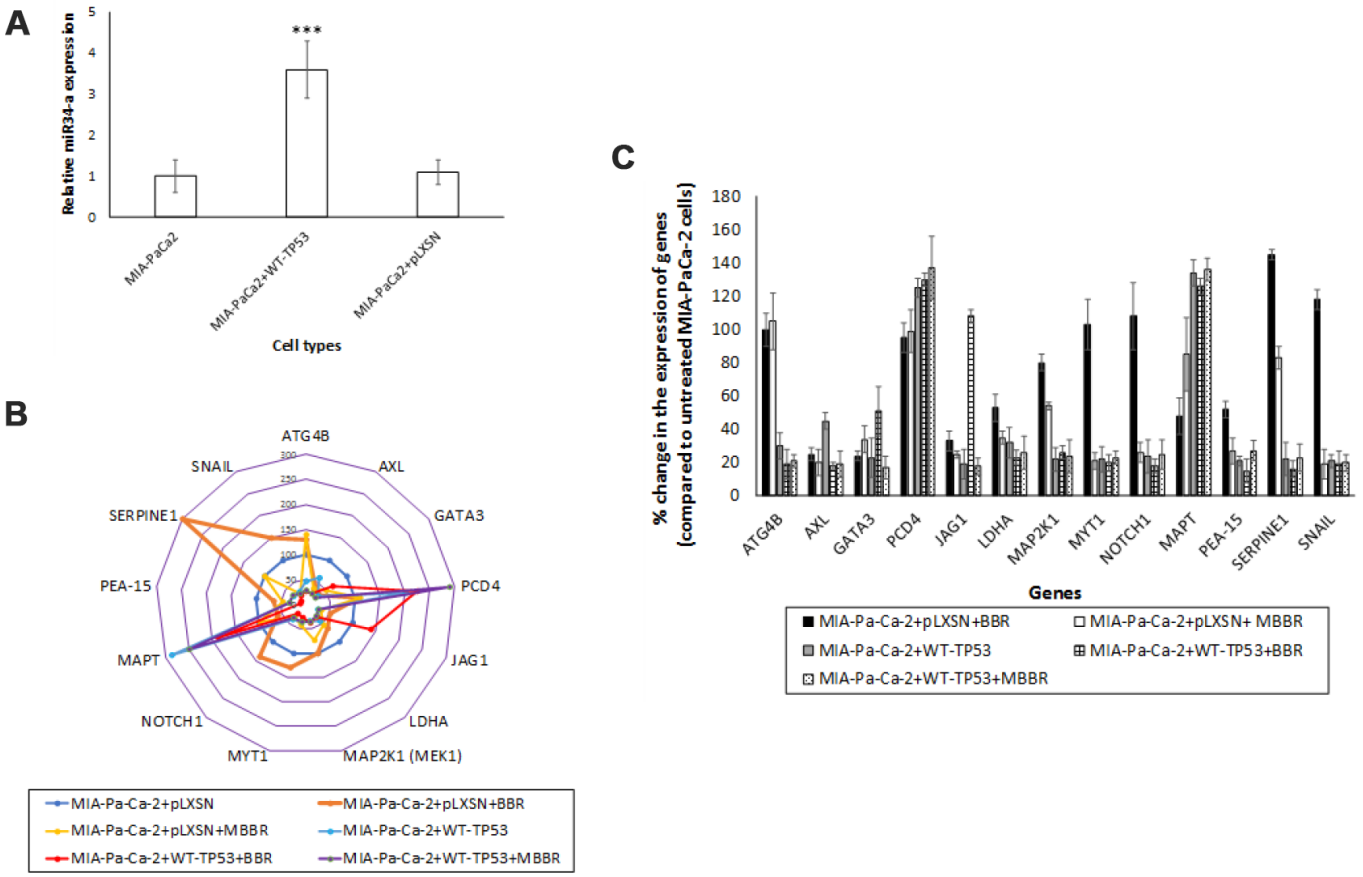

Figure 3. miR-34a expression in MIA-PaCa-2+pLXSN cells. (**A**) qRT-PCR was conducted to determine the miR-34a expression in MIA-PaCa-2+WT-TP53 and MIA-PaCa-2+pLXSN cells. Briefly, approximately 500 ng of RNA was reverse transcribed in a 25 µl reaction volume using the All-in-one miRNA qRT-PCR detection kit (GeneCopoeia, Rockville, MD). The synthesized cDNAs were used in the PCR reaction. The expression levels of miR-34a were measured employing the SYBR green detection and specific forward primer for the mature miRNA sequence and the universal adaptor reverse primer (GeneCopoeia, USA). Two-tailed P value of 0.05 or less was considered statistically significant; ***$p < 0.001$. (**B**) The putative targets of miR-34a that were significantly altered in MIA-PaCa-2+pLXSN and MIA-PaCa-2+WT-TP53 cells when the cells were treated with BBR and MBBR. A select few of the miR-34a target proteins that were significantly altered by treatment of MIA-PaCa-2 cells with BBR and NAX060 are projected. The data represent average of three individual experiments. (**C**) qRT-PCR was conducted to determine the expression of miR-34a-target genes in MIA-PaCa2+pLXSN and MIA-PaCa-2+WT-*TP53* cells. qRT-PCR was performed to monitor expression of the different miR-34a-putative target genes in untreated MIA-PaCa-2+pLXSN cells and MIA-PaCa-2 expressing WT-*TP53* or those treated with BBR and MBBR, respectively, using specific primers and SYBR green detection as per standard protocols. Bars represent average ± s.d. of three individual experiments.

any other miR-34a target genes of interest. This along with the fact that little is known about miR-34a>SERPINE1 associated signaling led us to further investigate the biology of this interaction in pancreatic cancer.

miR-34a targets *SERPINE1*

The secondary structure of the pre-miR-34a was predicted using the RNAstructure software [37] (Supplementary Figure 2). By using the DIANA and MiRmap tool algorithms, we identified a putative miR-34a binding site located in the 3′-UTR of *SERPINE1* mRNA (Supplementary Figure 3). To confirm the ability of miR-34a to specifically inhibit *SERPINE1* expression, we monitored the expression of *SERPINE1* in target cells that were untransfected, transfected with miR-34A mimic, or miR-NC. The range of doses tested in this study is comparable to those reported in the earlier studies [38–40]. The doses of the mimic and inhibitor used in the study did not significantly induce cell death in MIApaCa-2+pLXSN cells (Figure 5A, 5B). Transfection of MIA-PaCa-2+pLXSN cells with the miR-34a mimic significantly lowered the expression of *SERPINE1* and *SERPINE1* encoded protein, plasminogen activator inhibitor (PAI-1) levels at 24h post transfection compared to untransfected cells and cells transfected with miR-NC (Figure 5C, 5D). There was an inverse correlation observed in the expression of miR-34a and *SERPINE1* and PAI-1 levels in MIA-PaCa-2+pLXSN cells (Figure 5D, 5E). These results authenticate the fact that *SERPINE1* expression may well be regulated by miR-34a.

In order to determine the *bona fide* target of miR-34a, a luciferase reporter assay was performed. In this assay, two quantifiable genes encoding luciferase proteins were cloned in a vector. The *SERPINE1* 3′ UTR with the target region was placed downstream GLuc to regulate its translation, and SEAP was placed under no regulation for normalization. 293 cells were co-transfected with the *SERPINE1* 3′ UTR vector plasmid and miR-34a mimic. miR-34a mimic significantly decreased the relative luciferase activity compared to the cells that were transfected with miR-NC (Figure 6). In contrast, transfection of cells with miR-inhibitor reversed the ability of miR-34a mimic from lowering the luciferase activity (Figure 6). These results suggest that miR-34a directly targets *SERPINE1* and thereby downregulates its expression.

DISCUSSION

The *TP53* tumor suppressor gene is also known as the "guardian of the genome" as it serves to identify DNA damage, pause cell cycle progression to allow for repair, and when repair is not possible, to induce apoptosis [41, 42]. The multiplatform molecular analysis of the PDAC-derived target cells exhibits a range of neoplastic cellularity representative of the clinico-pathologic

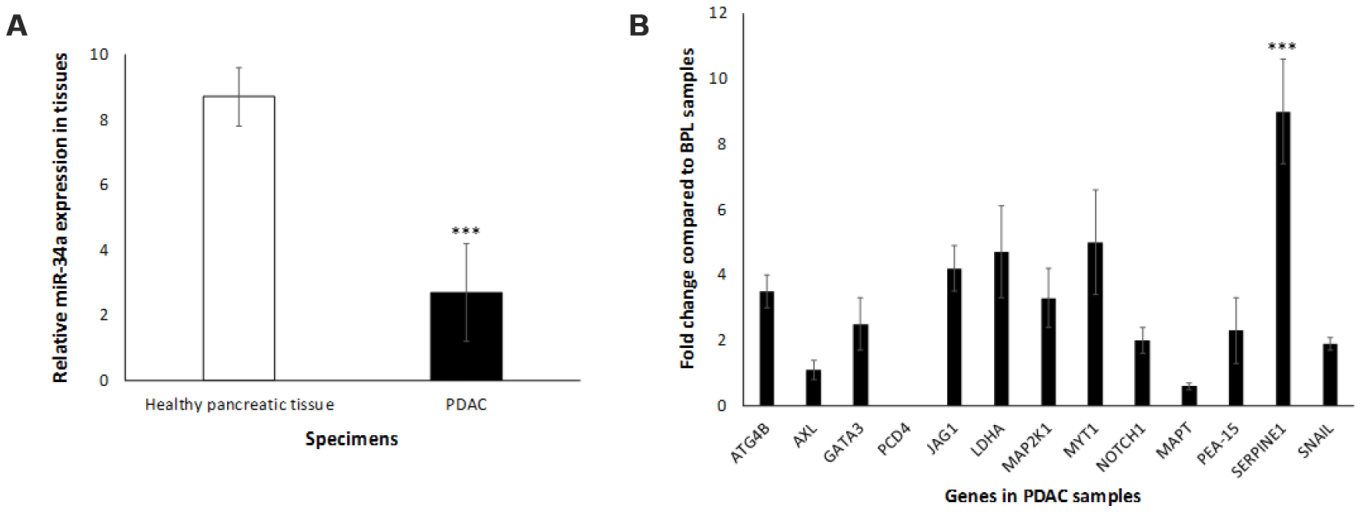

Figure 4. Expression profile of miR-34a in human PDAC samples. (**A**) miR34-a expression levels are lower in PDAC specimens compared to healthy pancreas controls. We compared the expression of miR-34a in 10 specimens in each group. Student t test was performed to compare groups. Two-tailed *P* value of 0.05 or less was considered statistically significant. ***$p < 0.001$. (**B**) qRT-PCR was conducted to determine the expression of miR-34a-target genes in human PDAC or healthy pancreas control specimens. Expression of miR-34a-target genes in human PDAC and healthy pancreas control specimens were detected by qRT-PCR using specific primers and SYBR green detection as per standard protocols. Bars represent average ± s.d. of three individual experiments. Two-tailed P value of 0.05 or less was considered statistically significant; ***$p < 0.001$.

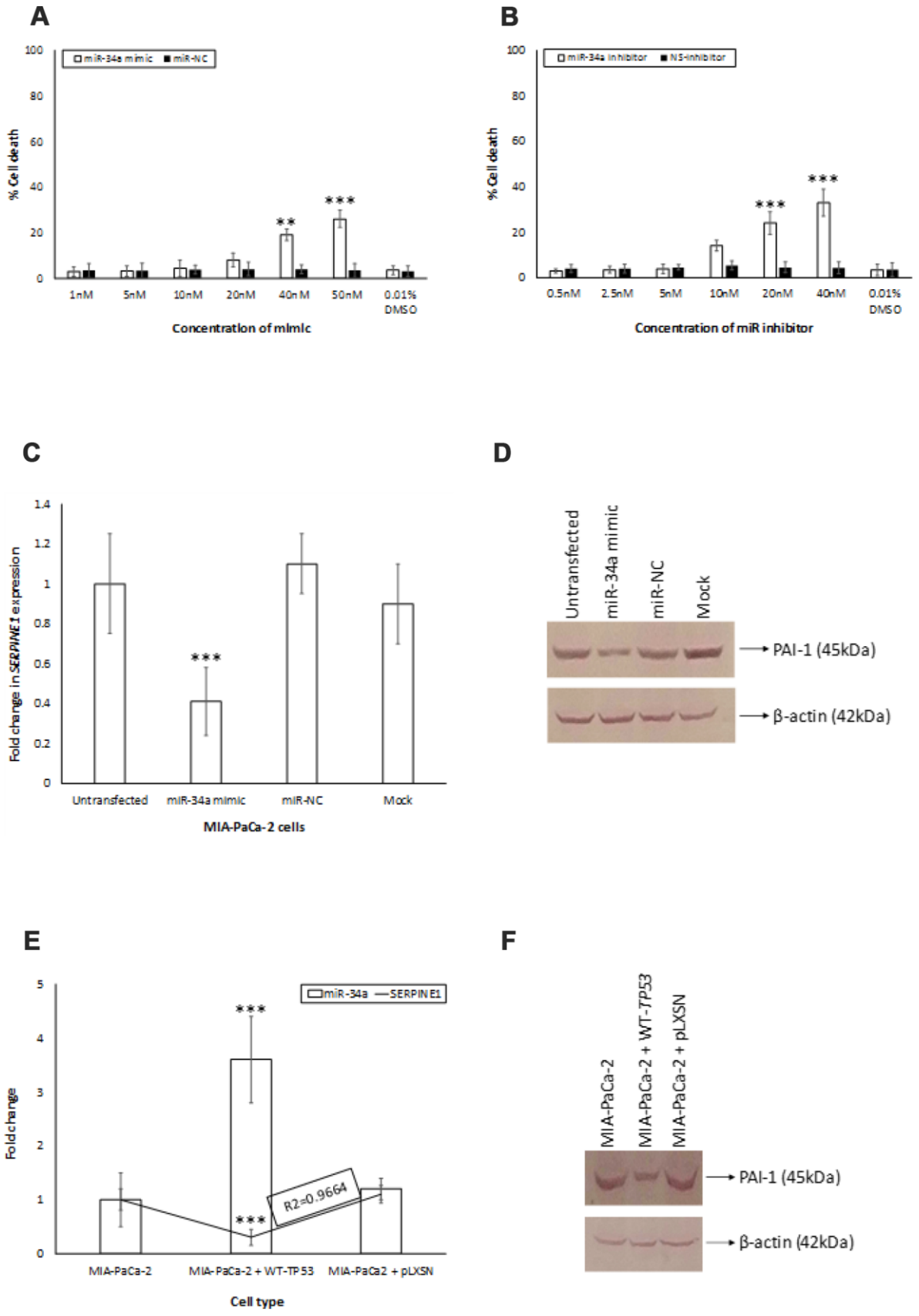

Figure 5. miR-34a targets *SERPINE1*. (**A**, **B**) To determine the cytotoxic effect of miR-34a mimic and inhibitor, MIA-PaCa2+pLXSN cells were transfected with different concentrations of miR-34a mimic and inhibitor. At 24 h post transfection, MTT was added to each well and

the absorption was measured. Percentage of cell death was monitored for miR-34a mimic (miR-mimic) (**A**) and miR-inhibitor (**B**) compared with 0.01% DMSO as control. (**C**, **D**) miR-34a mimic significantly decreased expression of *SERPINE1* and PAI-1 in MIA-PaCa-2+pLXSN cells. MIA-PaCa-2+pLXSN cells were untransfected, mock transfected, or transfected with miR-34a mimic or miR-NC. At the end of 24h of incubation at 37˚C, the cells were lysed, RNA extracted (panel **C**), cDNA synthesized, and *SERPINE1* expression monitored by qRT-PCR. In another set of experiments, the cells were lysed were probed for PAI-1 expression by Western blotting (panel **D**). (**E**) The relative expression of *SERPINE1* and miR-34a in MIA-PaCa-2 target cells was monitored by qRT-PCR. The expression was measured in terms of cycle threshold value (Ct) and normalized to expression of β-actin and snRNA RNU6B, respectively. The x-axis denotes the cell type and y-axis denotes fold change in expression of *SERPINE1* and miR-34a. The R2 values for the miRNA expression are provided. (**F**) In another set of experiments, the above cells were lysed and probed for PAI-1 expression by Western blotting (panel **F**). Bars (**A**–**C**, **E**) represent average ± s.d. of five individual experiments. Student t test was performed to compare groups. Two-tailed P value of 0.05 or less was considered statistically significant. **p,0.01; ***p < 0.001; NS-not significant.

spectrum of this disease (Figure 1). The RPPA analysis demonstrated the following: (i) expression of *mTP53*-associated signaling promoted cell survival and proliferation while inhibiting apoptosis (Figure 1; Tables 1, 2). Cells with *mTP53* alone (MIA-PaCa-2+pLXSN) had an increase in the expression DUSP6 (Figure 1). The role of DUSP6 in tumor formation depends on the micro-environment [43]. Recent studies demonstrated over-expression of DUSP6 to induce tumor formation [44]; (ii) expression of WT-*TP53*

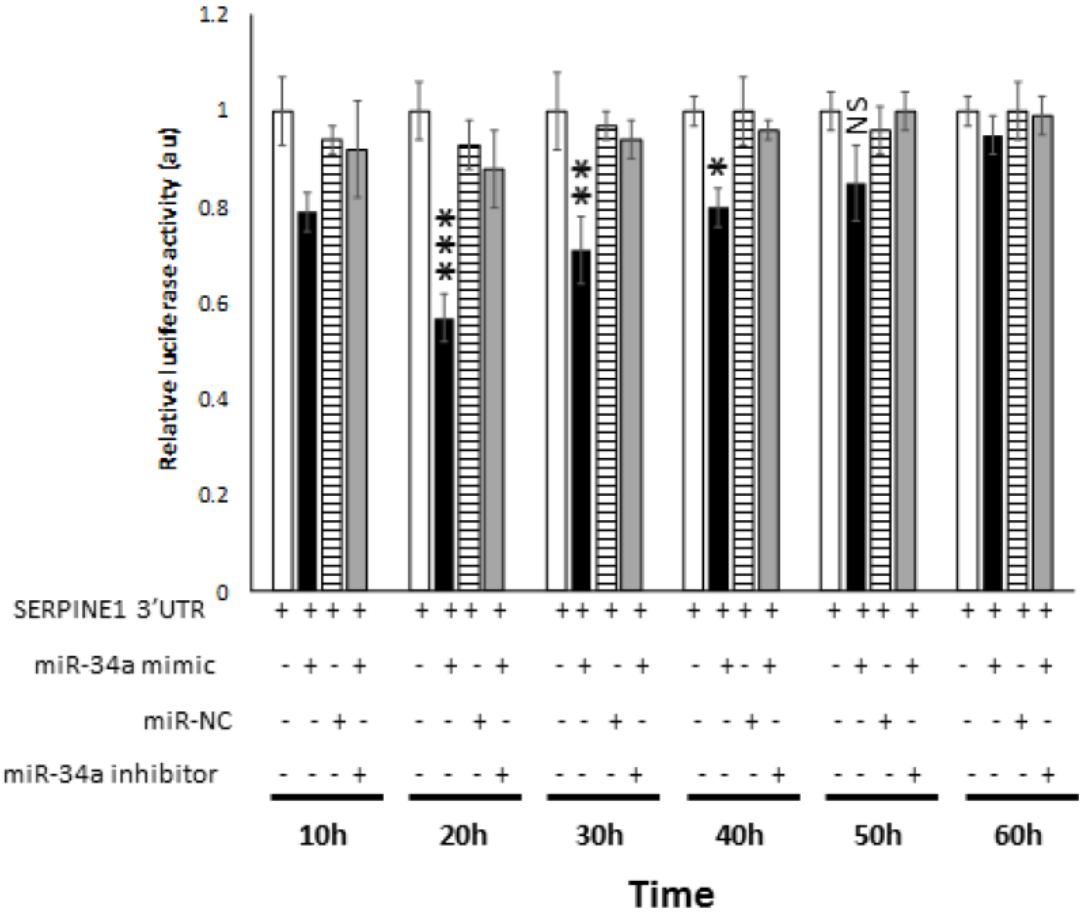

Figure 6. miR-34a specifically binds and interact with *SERPINE1*. Luciferase activity in 293 cells transfected with Dual-luciferase vector encoding Gaussia Luciferase (GLuc) and secreted alkaline phosphatase (SEAP) with 3'UR of *SERPINE1* placed downstream of Glu luciferase reporter (*SERPINE1* 3'UTR). 293 cells were either transfected with *SERPINE1* 3'UTR, co-transfected with *SERPINE1* 3'UTR and miR-34a mimic, co-transfected with *SERPINE1* 3'UTR and control mimic (miR-NC), or co-transfected with *SERPINE1* 3'UTR, miR-34a mimic and miR-34a inhibitor. GLuc activity was monitored at 10 h, 22 h, 30 h, 40h, 50 h, and 60 h post-transfection and was normalized to SEAP. Data is plotted as GLuc/SEAP ratio where the x-axis indicates the transfection and time points, and y-axis indicates the relative luciferase activity. Bars represent average ± s.d. of five individual experiments. Student t test was performed to compare groups. Two-tailed P value of 0.05 or less was considered statistically significant. *p < 0.05; **p,0.01; ***p < 0.001; NS-not significant.

had an opposing effect on *mTP53*-associated signaling (Figure 1); (iii) Treatment of cells expressing *mTP53* with BBR and MBBR can reverse cell signaling critical to tumor formation (Figure 2; Table 3). Inactivation of *TP53* is believed to be a critical step in pancreatic cancer progression. The above results are a crucial piece of evidence to this work on miRNA as this allowed us to establish a cell culture model to study the effects of TP53 on miR-34a and associated signaling.

TP53 mutations frequently occur during the transition from benign pancreatic intra-epithelial neoplasia to the highly-aggressive, invasive and metastatic PDAC [45]. TP53 is a transcription factor that controls the expression of many key genes and miRNAs that are involved in the regulation of cell cycle progression, apoptosis, cellular senescence and other critical biological processes [46–48]. miR-34a expression in PDAC-derived cell lines like MIA-PaCa-2 cells is relatively low [49]. It was demonstrated in this study that miR-34a levels could be significantly increased in the same MIA-PaCa-2 cells when they were transfected with vector expressing WT-*TP53* (Figure 3A). RPPA analysis also demonstrated a sharp decline in the expression of miR-34a-associated target genes in MIA-PaCa-2 cells over-expressing WT-*TP53* compared to cells expressing *mTP53* (Figure 3B, 3C). Overall, this is the first report to demonstrate a direct correlation between the WT-*TP53* and miR-34a expression in PDAC-derived cells.

In order to appreciate the clinical relevance of the expression of miR-34a and its cognate targets *in vivo*, we monitored the expression profiles of miR-34a and associated signaling *in vivo* using PDAC specimens derived from human participants. miR-34a levels were significantly lower in PDAC specimens compared to healthy pancreatic tissues (Figure 4A). Also, we observed an increase in the expression of majority of the miR-34a targets (Figure 4B) that were analyzed by RPPA using lysates from MIA-PaCa-2 cells (Figure 3B, 3C). The only difference observed was as follows: (i) *in vivo* expression of *PCD4* was at undetectable levels; and (ii) expression of *SERPINE1* was significantly elevated compared to the rest of the miR-34a targets (Figure 5B). *SERPINE1* levels have been identified to be significantly increased in colorectal cancer [50], lung cancer [51], gastric cancer [52], bladder cancer [53], head and neck squamous cell carcinoma [54], and others. Interestingly, earlier studies demonstrated ability of the *SERPINE1* encoded protein, plasminogen activator inhibitor (PAI-1), to mediate proliferation and invasion of PDAC-derived cell lines, including MIA-PaCa-2 cells [55]. A recent study also concluded that the expression of *SERPINE1* is negatively-related to the survival of PDAC patients [56]. Nonetheless, there are only three manuscripts that describe the expression of *SERPINE1* and its association with PDAC and they were all performed with cell line models [55–57]. This is the first report of that links miR-34a>*SERPINE1* expressions to PDAC using an *in vivo* patient-derived sample model.

It is a known fact that multiple genes may be regulated by one miRNA [58]. On the same note, a single mRNA transcript may be regulated by multiple miRNAs [59]. It is more than likely that the relationships between miRNAs and their targets are not one-to-one but multiple-to-multiple in cancers as reported in gastric carcinogenesis [60]. Earlier studies have demonstrated *SERPINE1* as a target of miR-34a in colorectal [61] and non-small cell lung cancer [62]. Using bioinformatics tools, we identified *SERPINE1* to be a promising target to miR-34a (Supplementary Figure 3). The results from luciferase reporter assays confirmed *SERPINE1* to be a target for miR-34a (Figure 6). Accordingly, there was an inverse correlation between the expression of miR-34a and *SERPINE1* (Figure 5E). Taken together, our results for the first time demonstrates a direct link between TP53, miR-34a, and SERPINE1 expression profiles in the pathobiology of PDAC.

The *SERPINE1* gene is located at 7q21.2-q22 and encodes a single-chain glycoprotein of about 50kDa. The *SERPINE1* gene is one of the main regulators of the plasminogen activator system (PAs). SERPINE1 inhibits the urokinase-type plasminogen (uPA) and tissue-type plasminogen activator (tPA), which in turn, reduce the conversion of plasminogen to the active protease plasmin [21]. Thus, the plasminogen activator inhibitor-1 (PAI-1) encoded by the *SERPINE1* gene regulates tumor cell migration and invasion crucial to tissue remodeling and tumorigenesis [63, 64]. PAI-1 protein can exist in two distinct forms: active and inactive forms. This is crucial because depending on the conformation, PAI-1 can activate distinct cell signaling pathways critical to development of tumors [65].

miR-34a expression inhibits components of inflammatory response [66]. miR-34a downregulates expression of NF-κB via APE1/Ref-1 or SEMA4B [67, 68]. Importantly, miR-34a targets more TP53 network genes compared to miR-34b/c [24]. miR-34a is a key regulator of tumor suppression and is considered to have a broad anti-oncogenic activity [30]. Expression of miR-34a is significantly down-regulated or absent in a variety of cancers including hepatocellular and renal cell carcinomas, colon, breast, lung, prostate, ovarian, and pancreatic cancers [16–22]. The focus of this study was on miR-34a; which is the target of TP53 [69]. In the process, we were able to identify a key link between

miR-34a, *SERPINE1*, and PDAC. Just as the age is a risk factor for the development of PDAC [70], PAI-1 is a part of the senescence-associated secretory phenotype (SASP) [71] and its expression is accordingly elevated in the elderly [72, 73]. Future studies are aimed at delineating the interactions between miR-34a and *SERPINE1* in the context of PDAC and aging.

MATERIALS AND METHODS

Cells

The MIA-PaCa-2 (ATCC® CRM-CRL-1420™) carcinoma cell line was derived from a 65-year old Caucasian male [74]. MIA-PaCa-2 cells have the R248W *TP53* GOF mutation. The R248W *TP53* mutation present in MIA-PaCa-2 cells is a missense point mutation in the central DNA binding domain which abrogates its DNA contact [75]. This *TP53* mutation results in a TP53 protein that is unable to bind to all TP53 target sequences in TP53-responsive genes and 2results in loss of its tumor suppressor properties [76, 77]. MIA-PaCa-2 cells also have an activating mutation at *KRAS* (G12C) and an elevated PI3K/AKT pathway activity. MIA-PaCa-2 cells were purchased from the ATCC (Rockville, MD, USA). Cells were cultured in medium containing 5% fetal bovine serum (FBS) purchased from (Atlanta Biologicals, Atlanta, GA, USA) as described in [33]. Tissue culture medium (Dulbecco's modified Eagles medium, DMEM), antibiotics containing l-glutamine and trypsin were obtained from Invitrogen (Carlsbad, CA, USA).

BBR and modified BBR (NAX060)

BBR was purchased from Sigma-Aldrich (Saint Louis, MO, USA). NAX060 compound was synthesized, purified and provided as a gift by Dr. Paolo Lombardi (Naxospharma, Milan, Italy) [78, 79].

Infection of cells with a retroviral vector encoding WT-*TP53*

The MIA-PaCa-2 cell line was infected with either a retroviral vector encoding WT-*TP53* (MIA-PaCa-2+WT-*TP53*) or the empty pLXSN vector (MIA-PaCa-2+pLXSN) as a control as described [23]. Stably infected cell lines were isolated in the presence of 2 mg/ml G418 (geneticin; Sigma-Aldrich). Pools were established after approximately four weeks in culture as per standard protocols [31].

Reverse phase protein array (RPPA)

Target cells were either untreated or treated with 1,000 nM BBR or 1,000 nM NAX060 for 24h at 37˚C. Cells were lysed 24 h later, denatured with 1% SDS and beta-mercaptoethanol, and five 2-fold serial dilutions of the samples were arrayed on nitrocellulose-coated slides (Grace Bio Lab, Bend, OR, USA) by an Aushon 2470 Arrayer (Aushon BioSystems, Bellerica, MA, USA). Each slide was probed with 419 primary antibodies and a biotin-conjugated secondary antibody. The stained samples were precipitated with 3,3' diaminobenzidine tetrahydrochloride (DAB) and quantified for spot intensity by using customized software. The signals were amplified with a Catalyzed Signal Amplification System (DakoCytomation, Glostrup, Denmark). Only target antibodies with a Pearson correlation coefficient (RPPA: western blotting) greater than 0.7 were used in the RPPA analysis. Each dilution curve was fitted with a logistic model ("Supercurve Fitting," developed by the Department of Bioinformatics and Computational Biology at MD Anderson Cancer Center). R software and the package Ggplot2 were used to visualize the heatmap.

Human PDAC specimens

A total of ten frozen PDAC human specimens were used in this study. We also used a total of ten frozen healthy pancreas specimens as controls. A total of these 20 samples were obtained from the North Carolina Tissue Consortium, Division of Surgical Oncology, Brody Medical Sciences Building, Greenville, NC. All these specimens were preserved in a liquid nitrogen container.

Monitoring expression of miR-34a

RNA was extracted from the cells and the tissues as per standard laboratory procedures using TRIzol (Invitrogen) [38]. The RNA concentrations were measured with a NanoDrop ND-2000 spectrophotometer (Thermo Fisher Scientific, Waltham, MA, USA), and then verified for quality using an Agilent 2100 Bioanalyzer (Agilent Technologies, Santa Clara, CA, USA). Only the RNA samples with 260/280 ratios of 1.8 to 2.0 were used in the study.

Approximately 500 ng of RNA was reverse transcribed in a 25 µl reaction volume using the All-in-oneTM miRNA qRT-PCR detection kit (GeneCopoeia, Rockville, MD, USA). Briefly, the cDNA was synthesized in a 25 µl reaction mix containing 5 µl of 5x reaction buffer, 2.5U/µl poly A polymerase, 10ng/µl MS2 RNA, and 1µl RTase mix. The reaction was performed at 37°C for 60 min and terminated at 85°C for 5 min. cDNA that was produced in the RT reaction was diluted ten-fold and was used as the template for the PCR reaction in an Applied Biosystems ViiA 7 Real-Time PCR System (Thermo Fisher Scientific). In this system, MS2 RNA

was used as an external reference for the quality of the extracted miRNAs, and RNU6B, RNU44, RNU48, and RNU49 were used for normalization. The expression levels of miRNAs were measured employing qRT-PCR with the SYBR green detection and specific forward primer for the mature miRNA sequence and the universal adaptor reverse primer (GeneCopoeia, USA). The specific forward primer to amplify miR-34a was 5'-TGGCAGTGTCTTAGCTGGTTGT-3'.

qRT-PCR to monitor expression of miR-34a putative targets

RNA was extracted from the cells and the tissues as per standard laboratory procedures using TRIzol [38]. Expression of *ATG4B*, *AXL*, *GATA3*, *JAG1*, *LDHA*, *MAP2K1*, *MYT1*, *NOTCH1*, *PEA-15*, *SERPINE1*, and *SNAIL* mRNAs by qRT-PCR was conducted as per earlier protocols [58] using appropriate primers (Supplementary Table 4).

Cytotoxicity assay

The 3-(4,5-dimethylthiazol-2-yl)-2,5-diphenyl-tetrazolium bromide (MTT) assays were performed to assess the sensitivity of cells to drugs, as previously described [23, 31, 80]. Target cells were treated with different concentrations of miR-34a mimic, inhibitor, or with appropriate controls at 37°C in a V-bottom 96-well plate. After a 24 h incubation, the percentage viable cells were assayed with MTT (Sigma-Aldrich). The optical density (OD) at the wavelength of 570 nm was used to calculate cell viability.

Western blotting

All the buffers used in this project were made with water that was endotoxin and pyrogen free. Western blotting was conducted as per earlier studies using the following primary antibodies: rabbit anti-PAI-1 polyclonal antibody (ThermoFisher Scientific) and mouse anti-actin antibodies (Clone AC-74; Sigma-Aldridge).

Dual-luciferase reporter assay

Luciferase reporter plasmids with wild-type *SERPINE1* 3′-UTR were purchased from GeneCopoeia. 293 cells were plated in 6-well plates. At 24 h post-plating, 293 cells were co-transfected with *SERPINE1* 3′-UTR luciferase reporter plasmid and miR-34a mimic, a scramble control (miR-NC), and/or miR-34a inhibitor using FuGene HD (Promega, Madison, WI, USA). At 10, 20, 30, 40, 50, and 60 h post transfection, supernatants were collected from each treatment and the luciferase activity measured using the Secrete-Pair Dual Luminescence Assay Kit (GeneCopoeia) as per the manufacturers' recommendations.

AUTHOR CONTRIBUTIONS

SMA and JAM designed the hypothesis; JAM and PPR designed and conducted the RPPA experiments; SMA designed and conducted miRNA experiments; SMA and JAM contributed equally in analyzing the data and writing the manuscript.

CONFLICTS OF INTEREST

The authors declare no conflicts of interest.

FUNDING

SMA and JAM were supported in part by East Carolina University Grants [grant numbers 111104 and 11110-668715-0000).

REFERENCES

1. Higuera O, Ghanem I, Nasimi R, Prieto I, Koren L, Feliu J. Management of pancreatic cancer in the elderly. World J Gastroenterol. 2016; 22:764–75. https://doi.org/10.3748/wjg.v22.i2.764 PMID:26811623

2. Idachaba S, Dada O, Abimbola O, Olayinka O, Uma A, Olunu E, Fakoya AO. A Review of Pancreatic Cancer: Epidemiology, Genetics, Screening, and Management. Open Access Maced J Med Sci. 2019; 7:663–71. https://doi.org/10.3889/oamjms.2019.104 PMID:30894932

3. Patel N, Khorolsky C, Benipal B. Incidence of Pancreatic Adenocarcinoma in the United States from 2001 to 2015: A United States Cancer Statistics Analysis of 50 States. Cureus. 2018; 10:e3796. https://doi.org/10.7759/cureus.3796 PMID:30868010

4. Jeune F, Coriat R, Prat F, Dousset B, Vaillant JC, Gaujoux S. Pancreatic cancer surgical management. Presse Med. 2019; 48:e147–58. https://doi.org/10.1016/j.lpm.2019.02.027 PMID:30905395

5. Falzone L, Salomone S, Libra M. Evolution of Cancer Pharmacological Treatments at the Turn of the Third Millennium. Front Pharmacol. 2018; 9:1300. https://doi.org/10.3389/fphar.2018.01300 PMID:30483135

6. Rahib L, Smith BD, Aizenberg R, Rosenzweig AB, Fleshman JM, Matrisian LM. Projecting cancer incidence and deaths to 2030: the unexpected burden

of thyroid, liver, and pancreas cancers in the United States. Cancer Res. 2014; 74:2913–21. https://doi.org/10.1158/0008-5472.CAN-14-0155 PMID:24840647

7. Saad AM, Turk T, Al-Husseini MJ, Abdel-Rahman O. Trends in pancreatic adenocarcinoma incidence and mortality in the United States in the last four decades; a SEER-based study. BMC Cancer. 2018; 18:688. https://doi.org/10.1186/s12885-018-4610-4 PMID:29940910

8. Waters AM, Der CJ. KRAS: The Critical Driver and Therapeutic Target for Pancreatic Cancer. Cold Spring Harb Perspect Med. 2018; 8:8. https://doi.org/10.1101/cshperspect.a031435 PMID:29229669

9. Bryant KL, Mancias JD, Kimmelman AC, Der CJ. KRAS: feeding pancreatic cancer proliferation. Trends Biochem Sci. 2014; 39:91–100. https://doi.org/10.1016/j.tibs.2013.12.004 PMID:24388967

10. Braun T, Gautel M. Transcriptional mechanisms regulating skeletal muscle differentiation, growth and homeostasis. Nat Rev Mol Cell Biol. 2011; 12:349–61. https://doi.org/10.1038/nrm3118 PMID:21602905

11. Shenoy A, Blelloch RH. Regulation of microRNA function in somatic stem cell proliferation and differentiation. Nat Rev Mol Cell Biol. 2014; 15:565–76. https://doi.org/10.1038/nrm3854 PMID:25118717

12. Tahamtan A, Teymoori-Rad M, Nakstad B, Salimi V. Anti-Inflammatory MicroRNAs and Their Potential for Inflammatory Diseases Treatment. Front Immunol. 2018; 9:1377. https://doi.org/10.3389/fimmu.2018.01377 PMID:29988529

13. Sonkoly E, Pivarcsi A. microRNAs in inflammation. Int Rev Immunol. 2009; 28:535–61. https://doi.org/10.3109/08830180903208303 PMID:19954362

14. Sethi S, Li Y, Sarkar FH. Regulating miRNA by natural agents as a new strategy for cancer treatment. Curr Drug Targets. 2013; 14:1167–74. https://doi.org/10.2174/13894501113149990189 PMID:23834152

15. Peng Y, Croce CM. The role of MicroRNAs in human cancer. Signal Transduct Target Ther. 2016; 1:15004. https://doi.org/10.1038/sigtrans.2015.4 PMID:29263891

16. Bharali D, Jebur HB, Baishya D, Kumar S, Sarma MP, Masroor M, Akhter J, Husain SA, Kar P. Expression Analysis of Serum microRNA-34a and microRNA-183 in Hepatocellular Carcinoma. Asian Pac J Cancer Prev. 2018; 19:2561–68. https://doi.org/10.22034/APJCP.2018.19.9.2561 PMID:30256056

17. Vogt M, Munding J, Grüner M, Liffers ST, Verdoodt B, Hauk J, Steinstraesser L, Tannapfel A, Hermeking H. Frequent concomitant inactivation of miR-34a and miR-34b/c by CpG methylation in colorectal, pancreatic, mammary, ovarian, urothelial, and renal cell carcinomas and soft tissue sarcomas. Virchows Arch. 2011; 458:313–22. https://doi.org/10.1007/s00428-010-1030-5 PMID:21225432

18. Toraih EA, Alghamdi SA, El-Wazir A, Hosny MM, Hussein MH, Khashana MS, Fawzy MS. Dual biomarkers long non-coding RNA GAS5 and microRNA-34a co-expression signature in common solid tumors. PLoS One. 2018; 13:e0198231. https://doi.org/10.1371/journal.pone.0198231 PMID:30289954

19. Orosz E, Kiss I, Gyöngyi Z, Varjas T. Expression of Circulating *miR-155, miR-21, miR-221, miR-30a, miR-34a* and *miR-29a*: Comparison of Colonic and Rectal Cancer. In Vivo. 2018; 32:1333–37. https://doi.org/10.21873/invivo.11383 PMID:30348685

20. Imani S, Wu RC, Fu J. MicroRNA-34 family in breast cancer: from research to therapeutic potential. J Cancer. 2018; 9:3765–75. https://doi.org/10.7150/jca.25576 PMID:30405848

21. Wang L, Yu J, Xu J, Zheng C, Li X, Du J. The analysis of microRNA-34 family expression in human cancer studies comparing cancer tissues with corresponding pericarcinous tissues. Gene. 2015; 554:1–8. https://doi.org/10.1016/j.gene.2014.10.032 PMID:25452192

22. Zhao K, Cheng J, Chen B, Liu Q, Xu D, Zhang Y. Circulating microRNA-34 family low expression correlates with poor prognosis in patients with non-small cell lung cancer. J Thorac Dis. 2017; 9:3735–46. https://doi.org/10.21037/jtd.2017.09.01 PMID:29268381

23. Abrams SL, Lertpiriyapong K, Yang LV, Martelli AM, Cocco L, Ratti S, Falasca M, Murata RM, Rosalen PL, Lombardi P, Libra M, Candido S, Montalto G, et al. Introduction of WT-TP53 into pancreatic cancer cells alters sensitivity to chemotherapeutic drugs, targeted therapeutics and nutraceuticals. Adv Biol Regul. 2018; 69:16–34. https://doi.org/10.1016/j.jbior.2018.06.002 PMID:29980405

24. Navarro F, Lieberman J. miR-34 and p53: New Insights into a Complex Functional Relationship. PLoS One.

2015; 10:e0132767.
https://doi.org/10.1371/journal.pone.0132767
PMID:26177460

25. Slabáková E, Culig Z, Remšík J, Souček K. Alternative mechanisms of miR-34a regulation in cancer. Cell Death Dis. 2017; 8:e3100.
https://doi.org/10.1038/cddis.2017.495
PMID:29022903

26. Sangrador I, Molero X, Campbell F, Franch-Expósito S, Rovira-Rigau M, Samper E, Domínguez-Fraile M, Fillat C, Castells A, Vaquero EC. Zeb1 in Stromal Myofibroblasts Promotes *Kras*-Driven Development of Pancreatic Cancer. Cancer Res. 2018; 78:2624–37.
https://doi.org/10.1158/0008-5472.CAN-17-1882
PMID:29490942

27. Hermeking H. The miR-34 family in cancer and apoptosis. Cell Death Differ. 2010; 17:193–99.
https://doi.org/10.1038/cdd.2009.56 PMID:19461653

28. Agostini M, Knight RA. miR-34: from bench to bedside. Oncotarget. 2014; 5:872–81.
https://doi.org/10.18632/oncotarget.1825
PMID:24657911

29. Rokavec M, Li H, Jiang L, Hermeking H. The p53/miR-34 axis in development and disease. J Mol Cell Biol. 2014; 6:214–30.
https://doi.org/10.1093/jmcb/mju003 PMID:24815299

30. Misso G, Di Martino MT, De Rosa G, Farooqi AA, Lombardi A, Campani V, Zarone MR, Gullà A, Tagliaferri P, Tassone P, Caraglia M. Mir-34: a new weapon against cancer? Mol Ther Nucleic Acids. 2014; 3:e194.
https://doi.org/10.1038/mtna.2014.47
PMID:25247240

31. Abrams SL, Follo MY, Steelman LS, Lertpiriyapong K, Cocco L, Ratti S, Martelli AM, Candido S, Libra M, Murata RM, Rosalen PL, Montalto G, Cervello M, et al. Abilities of berberine and chemically modified berberines to inhibit proliferation of pancreatic cancer cells. Adv Biol Regul. 2019; 71:172–82.
https://doi.org/10.1016/j.jbior.2018.10.003
PMID:30361003

32. Akula SM, Candido S, Libra M, Abrams SL, Steelman LS, Lertpiriyapong K, Ramazzotti G, Ratti S, Follo MY, Martelli AM, Murata RM, Rosalen PL, Bueno-Silva B, et al. Abilities of berberine and chemically modified berberines to interact with metformin and inhibit proliferation of pancreatic cancer cells. Adv Biol Regul. 2019; 73:100633.
https://doi.org/10.1016/j.jbior.2019.04.003
PMID:31047842

33. Candido S, Abrams SL, Steelman LS, Lertpiriyapong K, Martelli AM, Cocco L, Ratti S, Follo MY, Murata RM, Rosalen PL, Bueno-Silva B, de Alencar SM, Lombardi P, et al. Effects of the MDM-2 inhibitor Nutlin-3a on PDAC cells containing and lacking WT-TP53 on sensitivity to chemotherapy, signal transduction inhibitors and nutraceuticals. Adv Biol Regul. 2019; 72:22–40.
https://doi.org/10.1016/j.jbior.2019.03.002
PMID:30898612

34. Espina V, Wulfkuhle J, Calvert VS, Liotta LA, Petricoin EF 3rd. Reverse phase protein microarrays for theranostics and patient-tailored therapy. Methods Mol Biol. 2008; 441:113–28.
https://doi.org/10.1007/978-1-60327-047-2_8
PMID:18370315

35. Vejnar CE, Zdobnov EM. MiRmap: comprehensive prediction of microRNA target repression strength. Nucleic Acids Res. 2012; 40:11673–83.
https://doi.org/10.1093/nar/gks901
PMID:23034802

36. Chen K, Rajewsky N. Natural selection on human microRNA binding sites inferred from SNP data. Nat Genet. 2006; 38:1452–6.
https://doi.org/10.1038/ng1910 PMID:17072316

37. Reuter JS, Mathews DH. RNAstructure: software for RNA secondary structure prediction and analysis. BMC Bioinformatics. 2010; 11:129.
https://doi.org/10.1186/1471-2105-11-129
PMID:20230624

38. Hussein HA, Akula SM. miRNA-36 inhibits KSHV, EBV, HSV-2 infection of cells via stifling expression of interferon induced transmembrane protein 1 (IFITM1). Sci Rep. 2017; 7:17972.
https://doi.org/10.1038/s41598-017-18225-w
PMID:29269892

39. Goldgraben MA, Russell R, Rueda OM, Caldas C, Git A. Double-stranded microRNA mimics can induce length- and passenger strand-dependent effects in a cell type-specific manner. RNA. 2016; 22:193–203.
https://doi.org/10.1261/rna.054072.115
PMID:26670622

40. Kiener M, Chen L, Krebs M, Grosjean J, Klima I, Kalogirou C, Riedmiller H, Kneitz B, Thalmann GN, Snaar-Jagalska E, Spahn M, Kruithof-de Julio M, Zoni E. miR-221-5p regulates proliferation and migration in human prostate cancer cells and reduces tumor growth in vivo. BMC Cancer. 2019; 19:627.
https://doi.org/10.1186/s12885-019-5819-6
PMID:31238903

41. Aubrey BJ, Kelly GL, Janic A, Herold MJ, Strasser A. How does p53 induce apoptosis and how does this relate to p53-mediated tumour suppression? Cell Death Differ. 2018; 25:104–13.
https://doi.org/10.1038/cdd.2017.169
PMID:29149101

42. Frum RA, Love IM, Damle PK, Mukhopadhyay ND, Palit Deb S, Deb S, Grossman SR. Constitutive Activation of DNA Damage Checkpoint Signaling Contributes to Mutant p53 Accumulation via Modulation of p53 Ubiquitination. Mol Cancer Res. 2016; 14:423–36. https://doi.org/10.1158/1541-7786.MCR-15-0363 PMID:26965143

43. Kidger AM, Keyse SM. The regulation of oncogenic Ras/ERK signalling by dual-specificity mitogen activated protein kinase phosphatases (MKPs). Semin Cell Dev Biol. 2016; 50:125–32. https://doi.org/10.1016/j.semcdb.2016.01.009 PMID:26791049

44. Wu QN, Liao YF, Lu YX, Wang Y, Lu JH, Zeng ZL, Huang QT, Sheng H, Yun JP, Xie D, Ju HQ, Xu RH. Pharmacological inhibition of DUSP6 suppresses gastric cancer growth and metastasis and overcomes cisplatin resistance. Cancer Lett. 2018; 412:243–55. https://doi.org/10.1016/j.canlet.2017.10.007 PMID:29050982

45. Weissmueller S, Manchado E, Saborowski M, Morris JP 4th, Wagenblast E, Davis CA, Moon SH, Pfister NT, Tschaharganeh DF, Kitzing T, Aust D, Markert EK, Wu J, et al. Mutant p53 drives pancreatic cancer metastasis through cell-autonomous PDGF receptor β signaling. Cell. 2014; 157:382–94. https://doi.org/10.1016/j.cell.2014.01.066 PMID:24725405

46. Issler MV, Mombach JC. MicroRNA-16 feedback loop with p53 and Wip1 can regulate cell fate determination between apoptosis and senescence in DNA damage response. PLoS One. 2017; 12:e0185794. https://doi.org/10.1371/journal.pone.0185794 PMID:28968438

47. Yue Z, Zhou Y, Zhao P, Chen Y, Yuan Y, Jing Y, Wang X. p53 Deletion promotes myeloma cells invasion by upregulating miR19a/CXCR5. Leuk Res. 2017; 60:115–22. https://doi.org/10.1016/j.leukres.2017.07.003 PMID:28783539

48. Olivier M, Eeles R, Hollstein M, Khan MA, Harris CC, Hainaut P. The IARC TP53 database: new online mutation analysis and recommendations to users. Hum Mutat. 2002; 19:607–14. https://doi.org/10.1002/humu.10081 PMID:12007217

49. Kent OA, Mullendore M, Wentzel EA, López-Romero P, Tan AC, Alvarez H, West K, Ochs MF, Hidalgo M, Arking DE, Maitra A, Mendell JT. A resource for analysis of microRNA expression and function in pancreatic ductal adenocarcinoma cells. Cancer Biol Ther. 2009; 8:2013–24. https://doi.org/10.4161/cbt.8.21.9685 PMID:20037478

50. Zeng C, Chen Y. HTR1D, TIMP1, SERPINE1, MMP3 and CNR2 affect the survival of patients with colon adenocarcinoma. Oncol Lett. 2019; 18:2448–54. https://doi.org/10.3892/ol.2019.10545 PMID:31452735

51. Arroyo-Solera I, Pavón MA, León X, López M, Gallardo A, Céspedes MV, Casanova I, Pallarès V, López-Pousa A, Mangues MA, Barnadas A, Quer M, Mangues R. Effect of serpinE1 overexpression on the primary tumor and lymph node, and lung metastases in head and neck squamous cell carcinoma. Head Neck. 2019; 41:429–39. https://doi.org/10.1002/hed.25437 PMID:30548470

52. Li L, Zhu Z, Zhao Y, Zhang Q, Wu X, Miao B, Cao J, Fei S. FN1, SPARC, and SERPINE1 are highly expressed and significantly related to a poor prognosis of gastric adenocarcinoma revealed by microarray and bioinformatics. Sci Rep. 2019; 9:7827. https://doi.org/10.1038/s41598-019-43924-x PMID:31127138

53. Li X, Dong P, Wei W, Jiang L, Guo S, Huang C, Liu Z, Chen J, Zhou F, Xie D, Liu Z. Overexpression of CEP72 Promotes Bladder Urothelial Carcinoma Cell Aggressiveness via Epigenetic CREB-Mediated Induction of SERPINE1. Am J Pathol. 2019; 189:1284–97. https://doi.org/10.1016/j.ajpath.2019.02.014 PMID:30953603

54. Yang K, Zhang S, Zhang D, Tao Q, Zhang T, Liu G, Liu X, Zhao T. Identification of SERPINE1, PLAU and ACTA1 as biomarkers of head and neck squamous cell carcinoma based on integrated bioinformatics analysis. Int J Clin Oncol. 2019; 24:1030–41. https://doi.org/10.1007/s10147-019-01435-9 PMID:30937621

55. Botla SK, Savant S, Jandaghi P, Bauer AS, Mücke O, Moskalev EA, Neoptolemos JP, Costello E, Greenhalf W, Scarpa A, Gaida MM, Büchler MW, Strobel O, et al. Early Epigenetic Downregulation of microRNA-192 Expression Promotes Pancreatic Cancer Progression. Cancer Res. 2016; 76:4149–59. https://doi.org/10.1158/0008-5472.CAN-15-0390 PMID:27216198

56. Xiao Y. Construction of a circRNA-miRNA-mRNA network to explore the pathogenesis and treatment of pancreatic ductal adenocarcinoma. J Cell Biochem. 2020; 121:394–406. https://doi.org/10.1002/jcb.29194 PMID:31232492

57. Radke DI, Ling Q, Häsler R, Alp G, Ungefroren H, Trauzold A. Downregulation of TRAIL-Receptor 1 Increases TGFβ Type II Receptor Expression and TGFβ Signalling Via MicroRNA-370-3p in Pancreatic Cancer Cells. Cancers (Basel). 2018; 10:10.

https://doi.org/10.3390/cancers10110399
PMID:30366420

58. Hussein HA, Akula SM. Profiling of cellular microRNA responses during the early stages of KSHV infection. Arch Virol. 2017; 162:3293–303.
https://doi.org/10.1007/s00705-017-3478-y
PMID:28707270

59. Shivdasani RA. MicroRNAs: regulators of gene expression and cell differentiation. Blood. 2006; 108:3646–53.
https://doi.org/10.1182/blood-2006-01-030015
PMID:16882713

60. Hashimoto Y, Akiyama Y, Yuasa Y. Multiple-to-multiple relationships between microRNAs and target genes in gastric cancer. PLoS One. 2013; 8:e62589.
https://doi.org/10.1371/journal.pone.0062589
PMID:23667495

61. Wang T, Xu H, Liu X, Chen S, Zhou Y, Zhang X. Identification of Key Genes in Colorectal Cancer Regulated by miR-34a. Med Sci Monit. 2017; 23:5735–43.
https://doi.org/10.12659/MSM.904937
PMID:29197895

62. Lin X, Lin BW, Chen XL, Zhang BL, Xiao XJ, Shi JS, Lin JD, Chen X. PAI-1/PIAS3/Stat3/miR-34a forms a positive feedback loop to promote EMT-mediated metastasis through Stat3 signaling in Non-small cell lung cancer. Biochem Biophys Res Commun. 2017; 493:1464–70.
https://doi.org/10.1016/j.bbrc.2017.10.014
PMID:28988111

63. Wan J, Deng D, Wang X, Wang X, Jiang S, Cui R. LINC00491 as a new molecular marker can promote the proliferation, migration and invasion of colon adenocarcinoma cells. Onco Targets Ther. 2019; 12:6471–80.
https://doi.org/10.2147/OTT.S201233
PMID:31496744

64. Saleh AD, Cheng H, Martin SE, Si H, Ormanoglu P, Carlson S, Clavijo PE, Yang X, Das R, Cornelius S, Couper J, Chepeha D, Danilova L, et al. Integrated Genomic and Functional microRNA Analysis Identifies miR-30-5p as a Tumor Suppressor and Potential Therapeutic Nanomedicine in Head and Neck Cancer. Clin Cancer Res. 2019; 25:2860–73.
https://doi.org/10.1158/1078-0432.CCR-18-0716
PMID:30723145

65. Declerck PJ, De Mol M, Vaughan DE, Collen D. Identification of a conformationally distinct form of plasminogen activator inhibitor-1, acting as a noninhibitory substrate for tissue-type plasminogen activator. J Biol Chem. 1992; 267:11693–96.
PMID:1601844

66. Jiang P, Liu R, Zheng Y, Liu X, Chang L, Xiong S, Chu Y. MiR-34a inhibits lipopolysaccharide-induced inflammatory response through targeting Notch1 in murine macrophages. Exp Cell Res. 2012; 318:1175–84.
https://doi.org/10.1016/j.yexcr.2012.03.018
PMID:22483937

67. Ando K, Hirao S, Kabe Y, Ogura Y, Sato I, Yamaguchi Y, Wada T, Handa H. A new APE1/Ref-1-dependent pathway leading to reduction of NF-kappaB and AP-1, and activation of their DNA-binding activity. Nucleic Acids Res. 2008; 36:4327–36.
https://doi.org/10.1093/nar/gkn416
PMID:18586825

68. Jian H, Zhao Y, Liu B, Lu S. SEMA4B inhibits growth of non-small cell lung cancer in vitro and in vivo. Cell Signal. 2015; 27:1208–13.
https://doi.org/10.1016/j.cellsig.2015.02.027
PMID:25746385

69. Chang TC, Wentzel EA, Kent OA, Ramachandran K, Mullendore M, Lee KH, Feldmann G, Yamakuchi M, Ferlito M, Lowenstein CJ, Arking DE, Beer MA, Maitra A, Mendell JT. Transactivation of miR-34a by p53 broadly influences gene expression and promotes apoptosis. Mol Cell. 2007; 26:745–52.
https://doi.org/10.1016/j.molcel.2007.05.010
PMID:17540599

70. Bekkali NL, Oppong KW. Pancreatic ductal adenocarcinoma epidemiology and risk assessment: could we prevent? Possibility for an early diagnosis. Endosc Ultrasound. 2017 (Suppl 3); 6:S58–61.
https://doi.org/10.4103/eus.eus_60_17
PMID:29387690

71. Özcan S, Alessio N, Acar MB, Mert E, Omerli F, Peluso G, Galderisi U. Unbiased analysis of senescence associated secretory phenotype (SASP) to identify common components following different genotoxic stresses. Aging (Albany NY). 2016; 8:1316–29.
https://doi.org/10.18632/aging.100971
PMID:27288264

72. Khan SS, Shah SJ, Klyachko E, Baldridge AS, Eren M, Place AT, Aviv A, Puterman E, Lloyd-Jones DM, Heiman M, Miyata T, Gupta S, Shapiro AD, Vaughan DE. A null mutation in SERPINE1 protects against biological aging in humans. Sci Adv. 2017; 3:eaao1617.
https://doi.org/10.1126/sciadv.aao1617
PMID:29152572

73. Yamamoto K, Takeshita K, Kojima T, Takamatsu J, Saito H. Aging and plasminogen activator inhibitor-1 (PAI-1) regulation: implication in the pathogenesis of thrombotic disorders in the elderly. Cardiovasc Res. 2005; 66:276–85.
https://doi.org/10.1016/j.cardiores.2004.11.013
PMID:15820196

74. Deer EL, González-Hernández J, Coursen JD, Shea JE, Ngatia J, Scaife CL, Firpo MA, Mulvihill SJ. Phenotype and genotype of pancreatic cancer cell lines. Pancreas. 2010; 39:425–35. https://doi.org/10.1097/MPA.0b013e3181c15963 PMID:20418756

75. Liu DP, Song H, Xu Y. A common gain of function of p53 cancer mutants in inducing genetic instability. Oncogene. 2010; 29:949–56. https://doi.org/10.1038/onc.2009.376 PMID:19881536

76. Brosh R, Rotter V. When mutants gain new powers: news from the mutant p53 field. Nat Rev Cancer. 2009; 9:701–13. https://doi.org/10.1038/nrc2693 PMID:19693097

77. Solomon H, Buganim Y, Kogan-Sakin I, Pomeraniec L, Assia Y, Madar S, Goldstein I, Brosh R, Kalo E, Beatus T, Goldfinger N, Rotter V. Various p53 mutant proteins differently regulate the Ras circuit to induce a cancer-related gene signature. J Cell Sci. 2012; 125:3144–52. https://doi.org/10.1242/jcs.099663 PMID:22427690

78. Pierpaoli E, Arcamone AG, Buzzetti F, Lombardi P, Salvatore C, Provinciali M. Antitumor effect of novel berberine derivatives in breast cancer cells. Biofactors. 2013; 39:672–79. https://doi.org/10.1002/biof.1131 PMID:24000115

79. Pierpaoli E, Fiorillo G, Lombardi P, Salvatore C, Geroni C, Piacenza F, Provinciali M. Antitumor activity of NAX060: A novel semisynthetic berberine derivative in breast cancer cells. Biofactors. 2018; 44:443–52. https://doi.org/10.1002/biof.1440 PMID:30178609

80. Tang XJ, Huang KM, Gui H, Wang JJ, Lu JT, Dai LJ, Zhang L, Wang G. Pluronic-based micelle encapsulation potentiates myricetin-induced cytotoxicity in human glioblastoma cells. Int J Nanomedicine. 2016; 11:4991–5002. https://doi.org/10.2147/IJN.S114302 PMID:27757032

SUPPLEMENTARY MATERIALS

Supplementary Figures

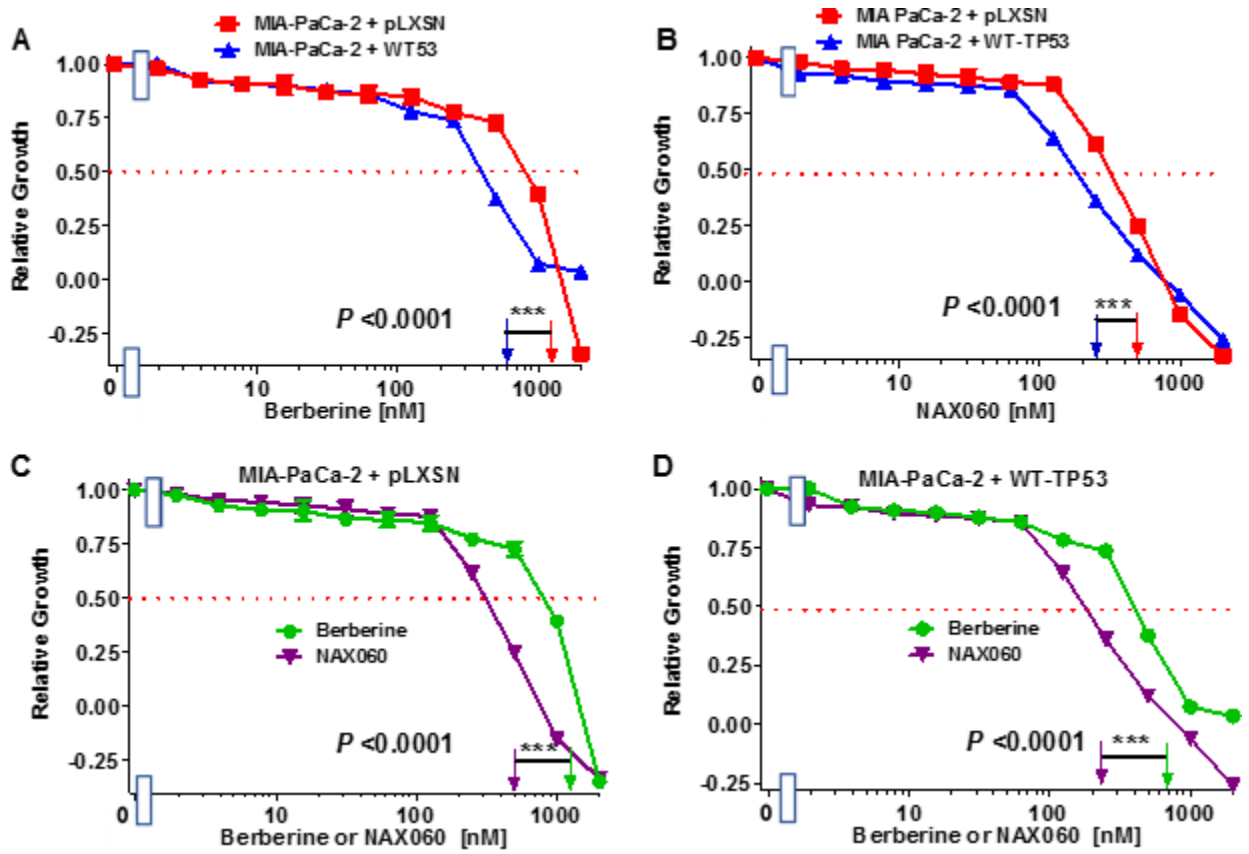

Supplementary Figure 1. Effects of Different doses of BBR and MBBR (NAX060) on MIA-PaCa-2+pLXSN and MIA-PaCa-2+WT-*TP53* Cells.

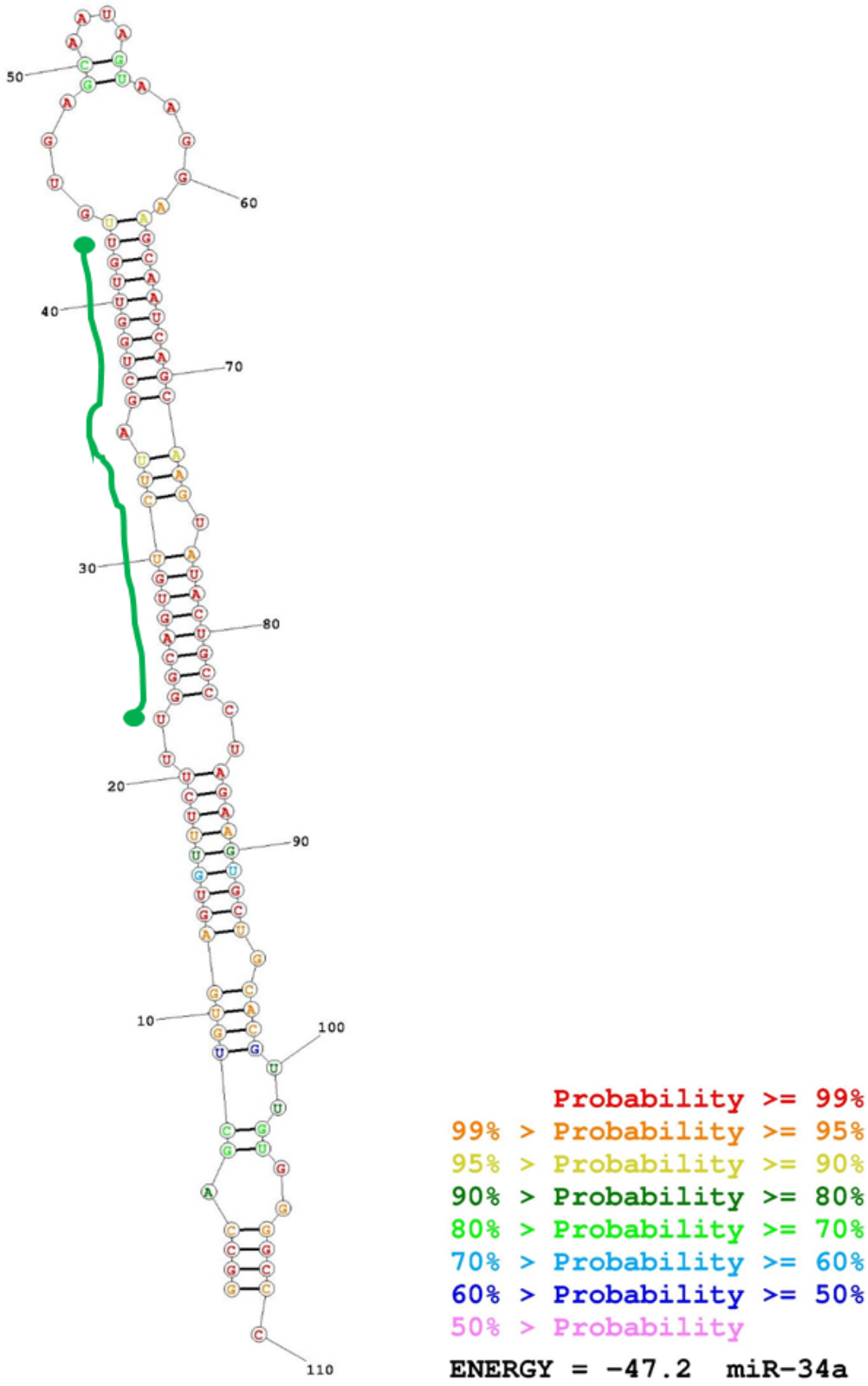

Supplementary Figure 2. Secondary structures of Pre-mir-34a. Structure was predicted using the RNAstructure software and base-pairing probability depicted in colors. Green line along the sequence denotes the mature sequence of hsa-miR-34a-5p (22 – 43).

```
(SERPINE1
Transcript) 5' CAU      GUGACG    CCC          3'
                  CCAGC       GAG    ACACUGCCA
                  |||||       .||    |||||||||
                  GGUCG       UUC    UGUGACGGU
(miR-34a)   3'   U      A                       5'
```

Transcript position: 940-965
Binding type: 9mer
Conserved species: panTro2,rheMac2,oryCun2,bosTau4,canFam2,dasNov2,loxAfr3,echTel1
miTG score: 0.906

Supplementary Figure 3. RNA hybrid analysis shows the miR-34a binding site located in 3'UTR of SERPINE1 mRNA. This is predicted using DIANA and MiRmap algorithms.

Supplementary Tables

Please browse Full Text version to see the data of Supplementary Tables 1–3

Supplementary Table 1. Description of antibodies used in RPPA assay.

Supplementary Table 2. comprehensive list of the putative targets of miR-34a as determined by miRmap.

Supplementary Table 3. comprehensive list of the putative targets of miR-34a as determined by PicTar.

Supplementary Table 4. Primers used to amplify miR-34a putative targets.

Target	Primer
ATG4B	F: 5'-TGAGTCTTGTGGTGTGTGGT-3'
	R: 5'-TACTTTCCCAGGACAGGCAG-3'
AXL	F: 5'-GAGGGAGAGTTTGGAGCTGT-3'
	R: 5'-GAAACAGACACCGATGAGCC-3'
GATA3	F: 5'-GGCGCCGTCTTGATACTTTC-3'
	R: 5'-AAGAGCAGAGAGGAGGAGGA-3'
PCD4	F: 5'-GCAGAAAATGCTGGGACTGAG-3'
	R: 5'-TGTACCCCAGACACCTTTGC-3'
JAG1	F: 5'-GTCCCACTGGTTTCTCTGGA-3'
	R: 5'-ATATACCGCACCCCTTCAGG-3'
LDHA	F: 5'-GGCTACACATCCTGGGCTAT-3'
	R: 5'-TCTTCTTCAAACGGGCCTCT-3'
MAP2K1	F: 5'-CAGAAGCAGAAGGTGGGAGA-3'
	R: 5'-GGATTGCGGGTTTGATCTCC-3'
MYT1	F: 5'-TTGATGTCAAGCCTGCCAAC-3'
	R: 5'-CAGACTGAACACATCCGCTG-3'
NOTCH1	F: 5'-ATGCAGAACAACAGGGAGGA-3'
	R: 5'-ACCAGGTTGTACTCGTCCAG-3'
MAPT	F: 5'- ACTCCAACAGCGGAAGATGT-3'
	R: 5'- GTGACCAGCAGCTTCGTCTT-3'
PEA-15	F: 5'- ACCCCTTCCTAATTGCAGCT-3'
	R: 5'-TGCTCTCTGGGCTCTGAAAA-3'
SERPINE1	F: 5'-CCGCCTCTTCCACAAATCAG-3'
	R: 5'-AATGTTGGTGAGGGCAGAGA-3'
SNAIL	F: 5'-CCCCAATCGGAAGCCTAACT-3'
	R: 5'-GACAGAGTCCCAGATGAGCA-3'

Research Paper

CTCF promotes colorectal cancer cell proliferation and chemotherapy resistance to 5-FU via the P53-Hedgehog axis

Qiuhua Lai[1,*], Qingyuan Li[1,*], Chengcheng He[1], Yuxin Fang[1], Simin Lin[1], Jianqun Cai[1], Jian Ding[1], Qian Zhong[1], Yue Zhang[1], Changjie Wu[1], Xinke Wang[1], Juan He[1], Yongfeng Liu[1], Qun Yan[1], Aimin Li[1,&], Side Liu[1,&]

[1]Guangdong Provincial Key Laboratory of Gastroenterology, Department of Gastroenterology, Nanfang Hospital, Southern Medical University, Guangzhou, Guangdong, China
*Equal contribution

Correspondence to: Side Liu, Aimin Li; **email:** liuside2011@163.com, lam0725@qq.com
Keywords: colorectal cancer, CTCF, Hedgehog, P53, chemotherapy resistance
Received: March 7, 2020 **Accepted:** June 19, 2020 **Published:** July 20, 2020

ABSTRACT

CTCF is overexpressed in several cancers and plays crucial roles in regulating aggressiveness, but little is known about whether CTCF drives colorectal cancer progression. Here, we identified a tumor-promoting role for CTCF in colorectal cancer. Our study demonstrated that CTCF was upregulated in colorectal cancer specimens compared with adjacent noncancerous colorectal tissues. The overexpression of CTCF promoted colorectal cancer cell proliferation and tumor growth, while the opposite effects were observed in CTCF knockdown cells. Increased GLI1, Shh, PTCH1, and PTCH2 levels were observed in CTCF-overexpressing cells using western blot analyses. CCK-8 and apoptosis assays revealed that 5-fluorouracil chemosensitivity was negatively associated with CTCF expression. Furthermore, we identified that P53 is a direct transcriptional target gene of CTCF in colorectal cancer. Western blot and nuclear extract assays showed that inhibition of P53 can counteract Hedgehog signaling pathway repression induced by CTCF knockdown. In conclusion, we uncovered a crucial role for CTCF regulation that possibly involves the P53-Hedgehog axis and highlighted the clinical utility of colorectal cancer-specific potential therapeutic target as disease progression or clinical response biomarkers.

INTRODUCTION

Colorectal cancer (CRC) is the third most malignant cancer worldwide and one of the most common tumors of the digestive tract, causing over 600 000 deaths annually [1–4]. Although progress has been made in the development of therapies, including various surgical methods, chemotherapy, radiotherapy and immunotherapy, the prognosis of CRC patients remains unsatisfactory; increasing rates of chemoradiotherapy resistance, local recurrence and distant metastasis result in a poor prognosis among CRC patients [5–9]. A large number of studies have shown that dysregulated genes and the abnormal activation or inhibition of tumor-associated signaling pathways are involved in the initiation and progression of CRC [10–12]. Therefore, we need to gain a more comprehensive understanding of the molecular mechanism involved in the development and progression of CRC and to develop more specific screening tests for the early detection and identification of colorectal tumors with a greater risk of progression.

CTCC-binding factor (CTCF), a transcription factor with 11 zinc fingers (ZFs), is highly conserved despite being over 700 amino acids long [13]. Many intensive studies have reported that CTCF functions as a versatile nuclear factor involved in transcriptional inhibition or activation [14–16], insulation [17, 18], silencers or enhancers [13, 18], gene imprinting [19, 20], controlling X chromosome inactivation in females [21], etc. Most CTCF functions are linked to its ability to regulate three-dimensional (3D) chromatin structure by forming sequence-specific

DNA loops [13, 19]. As a multifunctional transcription factor, CTCF was reported to be involved in the initiation of multiple cancers, including breast cancer [18], hepatocellular carcinoma [22], lung cancer [14], prostate cancer [23], etc., which could be attributed to the abnormal expression of CTCF or the dysregulation of its target genes. Some common observations involving CTCF function in cancers include the transcriptional activation of TERT, c-MYC, FOXM1, PLK, GAD1 and other genes [14, 22, 24–26] and the transcriptional repression of p53, BCL6, RASSF1A, CDH1 and others [27–30]. Additionally, chromatin immunoprecipitation (ChIP)-PCR analysis revealed that CTCF affects a number of metastasis-associated genes, including CTBP1, SERPINE1 and SRC [31]. Interestingly, a previous study showed that CTCF has one of the highest mutation rates in CRC [32]. However, the functional role of CTCF in CRC remains unclear.

In the present study, we observed abnormal CTCF expression in CRC. Additionally, we provided the first evidence of CTCF involvement in the P53-Hedgehog signaling pathway and confirmed the effects of aberrant CTCF expression on the cellular biological behavior, including proliferation and chemotherapy resistance to 5-fluorouracil (5-FU), of CRC cells *in vitro* as well as on tumor growth *in vivo*.

RESULTS

CTCF is a potential tumor-promoting gene in CRC

An online bioinformatics analysis website, Gene Expression Profiling Interactive Analysis (GEPIA, http://gepia.cancer-pku.cn/) [33], was used to explore the expression of CTCF in The Cancer Genome Atlas (TCGA) database, and the results indicated that CTCF was almost upregulated in all gastrointestinal tumors (Figure 1A). We divided CRC patients into two groups according to CTCF expression levels. Kaplan-Meier (K-M) survival analysis with PROGgeneV2 (http://genomics.jefferson.edu/proggene/) showed that the relapse-free survival time of patients with a high CTCF expression level was significantly shorter than that of patients with a low CTCF expression level in GSE31598 (Figure 1B). Analyses of CTCF-regulated gene set signatures with gene set enrichment analysis (GSEA) indicated that there is a positive correlation between high expression of CTCF and CRC gene set signatures (GSE17538 and TCGA, Figure 1C). Then, we assessed the expression level of CTCF in tumor and paracancerous normal colorectal tissues. CTCF expression in tumor and adjacent normal tissues was analyzed by qRT-PCR and western blot assays (Figure 1D, 1E), and the results showed that CTCF was upregulated in tumor specimens.

To further explore the function of CTCF *in vitro*, we examined CTCF expression in a human embryonic kidney cell line (293T), a human normal colon epithelial cell line (FHC) and six human CRC lines (SW480, SW620, RKO, HCT116 HT29 and LOVO). The expression level of CTCF was relatively high in SW480 cells and was comparatively low in the HCT116 cell line, which was confirmed by both qRT-PCR and western blot analyses (Supplementary Figure 1A, 1B). Herein, we selected SW480 and RKO cell lines to knock down endogenous CTCF expression. On the other hand, HCT116 and RKO cell lines were used to construct cell lines that stably overexpressed CTCF.

Overexpression of CTCF promotes human CRC cell proliferation

As a transcription factor, CTCF has been confirmed to play an essential role in the progression of multiple cancers [13]. To explore the role of CTCF in CRC, GSEA was performed to analyze the relationship between CTCF expression and cell cycle-relevant gene set signatures, and the results revealed that CTCF might promote cell proliferation (Figures 2A, 3A). As mentioned above, we chose two CRC cell lines (HCT-116 and RKO) to construct CTCF-overexpressing cell lines via lentivirus infection. Transfection efficiency was assessed by green fluorescent protein (GFP) (Supplementary Figure 1C). Overexpression effect was confirmed by qRT-PCR (Figure 2B) and western blot (Figure 2C) analyses. CCK-8 and colony formation assays suggested that CTCF upregulation enhanced the proliferative ability in both CRC cell lines (Figure 2D, 2E and Supplementary Figure 1D). In addition, the EdU incorporation assays further confirmed that upregulated CTCF increased the proportion of EdU-positive cells (Figure 2F, 2G).

To investigate whether CTCF is involved in promoting human CRC cell growth *in vivo*, HCT116-CTCF cells and HCT116-Vector cells were subcutaneously injected into the right and left back hips of nude mice (n = 4/group). As shown (Figure 2H, 2I and Supplementary Figure 1E), the tumors in the CTCF-overexpressing group grew more rapidly than the control group tumors. Immunohistochemical (IHC) staining of Ki67 (Figure 2J) further demonstrated that the tumors in the CTCF-overexpressing group displayed much more proliferation than those in the control group.

Downregulation of CTCF impairs the proliferative capacity of human CRC cells

As previously mentioned, the SW480 cell line, which had the highest CTCF expression level, and RKO cell line were transfected with CTCF-specific shRNA to

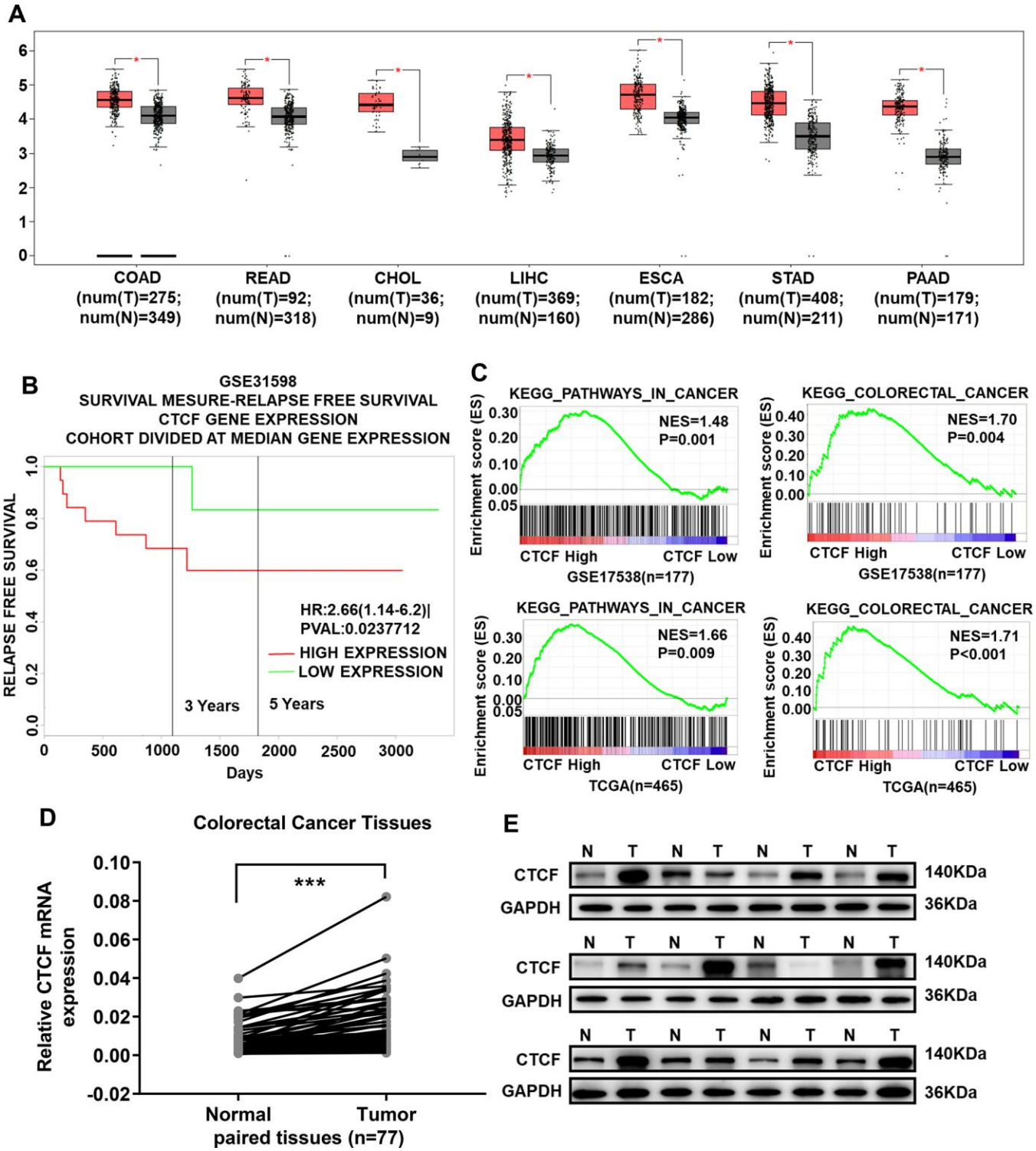

Figure 1. CTCF is significantly upregulated in CRC tissues and acts as a potential oncogenic gene. (**A**) CTCF is upregulated in all gastrointestinal tumors (GEPIA, http://gepia.cancer-pku.cn/). (**B**) Kaplan-Meier relapse free survival analysis in CRC patients with high or low expression of CTCF in GSE31598 via online website PROGgeneV2 (http://genomics.jefferson.edu/proggene/). (**C**) GSEA indicated that high expression of CTCF was positively correlated with the cancer related gene set signatures (KEGG_PATHWAYS_IN_CANCER, KEGG_COLORECTAL_CANCER) in CRC patient gene expression profiles (GSE17538, n = 177, and TCGA, n = 465). (**D**) qRT-PCR analysis of CTCF expression in 77 pairs of CRC patient specimens. (**E**) Western blot analyses of CTCF in 12 pairs of tumor and match adjacent normal tissues collected from clinical CRC patients. N for Normal, T for Tumor. The above data are presented as mean ± SEM. * P<0.05, **P<0.01, and ***P<0.001.

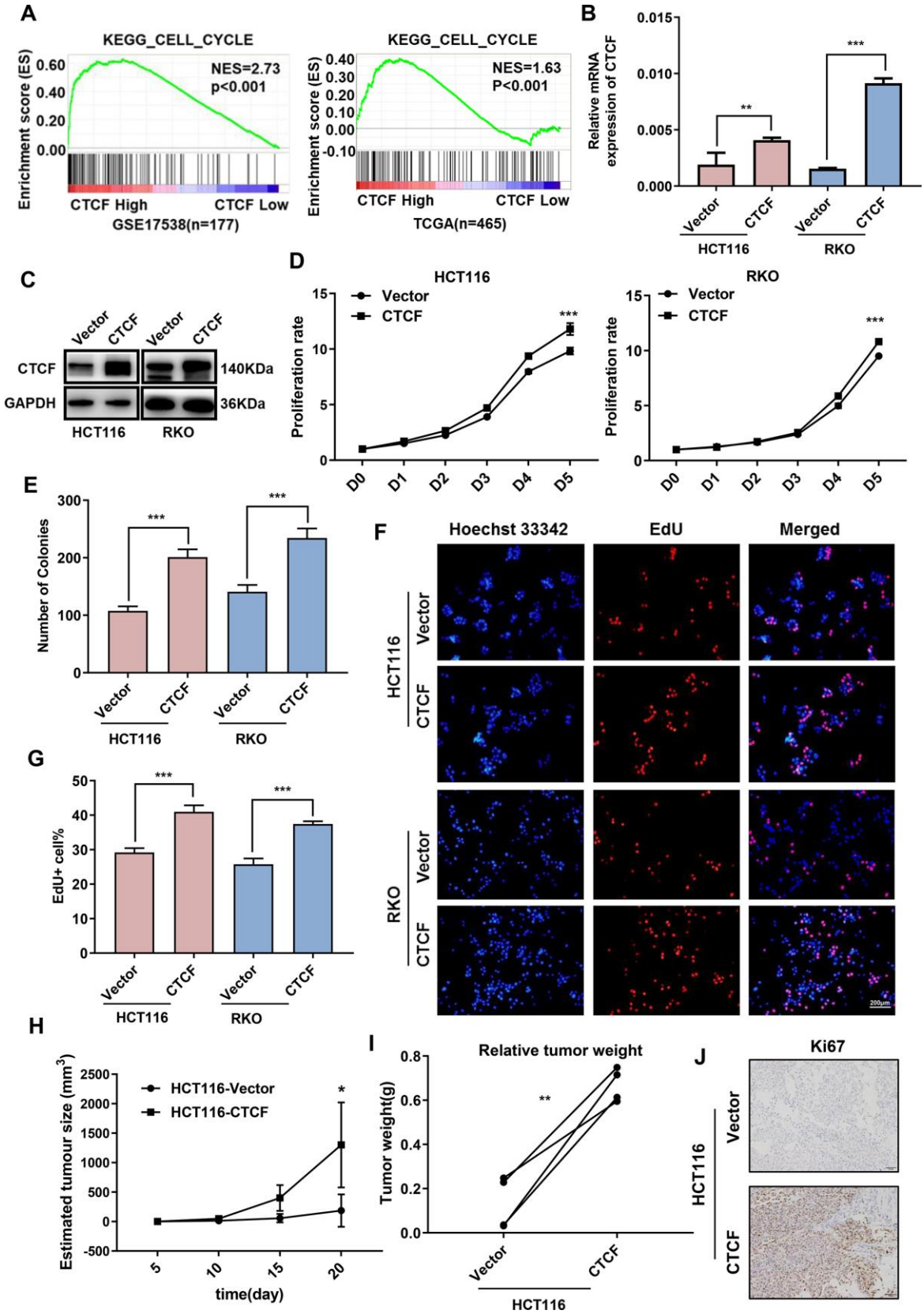

Figure 2. Upregulation of CTCF promotes human CRC cells proliferation. (**A**) GSEA plot indicated that high expression of CTCF is positively correlated with the cell cycle gene set signatures (KEGG_CELL_CYCLE) in published CRC patient gene expression profiles (GSE17538, n = 177, and TCGA, n = 465). (**B**, **C**) qRT-PCR and western blot analyses of CTCF expression level in constructed cell lines (HCT116 and RKO).

(**D**, **E**) The relative growth rates were measured using CCK8 and colony formation assays and compared between CTCF overexpressed group and Vector group at indicated times in HCT116 and RKO cell lines. (**F**) Images of EdU staining in both indicated cell lines, and the relative percentage of EdU-positive cells in images of related groups are shown (**G**). (**H**, **I**) Tumor volume and weight were measured and analyzed. (**J**) The tumor sections were under IHC staining using antibody against Ki-67. The above data are presented as mean ± SEM. * P<0.05, **P<0.01, and ***P<0.001.

knockdown endogenous CTCF expression. Similarly, lentiviral infection efficiency was assessed by GFP (Supplementary Figure 2A). Knockdown effect was confirmed by qRT-PCR (Figure 3B) and western blot (Figure 3C) analyses. CCK-8 (Figure 3D), colony formation (Figure 3E and Supplementary Figure 2B) and EdU incorporation assays (Figure 3F, 3G) revealed that the downregulation of endogenous CTCF impaired the proliferative ability in both CRC cell lines. Furthermore, subcutaneous tumorigenesis in nude mice consistently showed that tumors in the SW480-shCTCF group grew much more slowly than the SW480-Scramble group (Figure 3H–3J and Supplementary Figure 2C). Besides, CTCF expression was positively correlated with the expression of CDKs and Cyclins in GEPIA (http://gepia.cancer-pku.cn/, Supplementary Figure 2D).

Thus, these results strongly suggested that CTCF increases the proliferative capacity of CRC cells *in vitro* and in *vivo*.

CTCF induces chemoresistance in CRC

Furthermore, to explore the possible role of CTCF in chemotherapy resistance, Cell growth inhibition rate was detected after treatment with a concentration gradient of 5-FU, and the results demonstrated that CTCF weakened the cytostatic action of 5-FU (Figure 4A, 4B). Cell apoptosis rate was determined by an apoptosis kit and flow cytometry. The apoptosis rate was increased in the CTCF knockdown group, while it was dramatically decreased in the CTCF-overexpressing group during treatment with 5-FU (Figure 4C and Supplementary Figure 3A, 3B). In addition, we investigated the protein expression level of CTCF and found that CTCF was significantly upregulated after treatment with 5-FU (10 μM) in the HCT116 and RKO cell lines (Figure 4D). Consistently, the expression levels of crucial proteins in the apoptosis pathway were obviously reduced in the CTCF-overexpressing group, while they were increased in the CTCF-knockdown group (Figure 4E).

In further evaluations, the expression of ABCG2, which is a part of the superfamily of ATP-binding cassette (ABC) transporters and plays an important role in the chemotherapy resistance in various tumors [34], was positively related to CTCF expression (Figure 4F). Additionally, clinical specimens further confirmed there was a positive correlation between CTCF and ABCG2 (Figure 4G and Supplementary Figure 3C).

CTCF enhances malignant behavior in CRC via the Hedgehog signaling pathway

Previous studies reported that Hedgehog signaling pathway activation was closely associated with aggressive phenotypes and chemotherapy resistance in multiple malignancies, including lung cancer [35], pancreatic cancer [36], bladder cancer, etc. [37]. Hence, we examined whether there was a connection between CTCF and the Hedgehog signaling pathway. GSEA was performed to explore CTCF-regulated gene set signatures. The results demonstrated that "GCNP_SHH_UP_EARLY.V1_UP" and "GCNP_SHH_UP_LATE.V1_UP" and "GCNP_GLI1_UP.V1_UP" gene signatures enrich in the CTCF high expression group and "GCNP_SHH_UP_LATE.V1_DN" gene set enriches in the CTCF low expression group (GSE17538 and TCGA, Figure 5A). Then, we carried out western blot assays to investigate whether CTCF can activate Hedgehog signaling pathway in CRC. The results revealed that the expression levels of GLI1, Shh, PTCH1, and PTCH2 were increased in stable CTCF-overexpressing cell lines, while consistent phenomena was observed in the knockdown groups (Figure 5B). Also, correlation analysis in GEPIA revealed that CTCF was positively correlated with GLI1, Shh, PTCH1, and PTCH2 (Supplementary Figure 4A). K-M survival analysis with GEPIA revealed that high expression of GLI1 was accompanied by a shorter overall survival time (Supplementary Figure 4B). Moreover, GDC-0449, a Hedgehog signaling pathway inhibitor, was used for rescue assays, and western blot analyses showed that GDC-0449 counteracted the CTCF-induced activation of the Hedgehog signaling pathway (Figure 5B).

Subsequently, we explored whether the direct blockade of the Hedgehog signaling pathway could restore the function CTCF plays in CRC cell lines. Consistently, we found that treatment with GDC-0449 reversed the enhanced proliferation ability, which was induced by CTCF, based on CCK-8 (Figure 5C) and EdU staining assays (Figure 5D–5F).

CTCF activates the Hedgehog signaling pathway via transcriptional repression of P53

To predict the potential target genes involved in chemotherapy resistance to 5-FU, 3 bioinformatic target prediction programs (PubChem, STICH, and SuperPred Target-Prediction) were used to explore putative targets

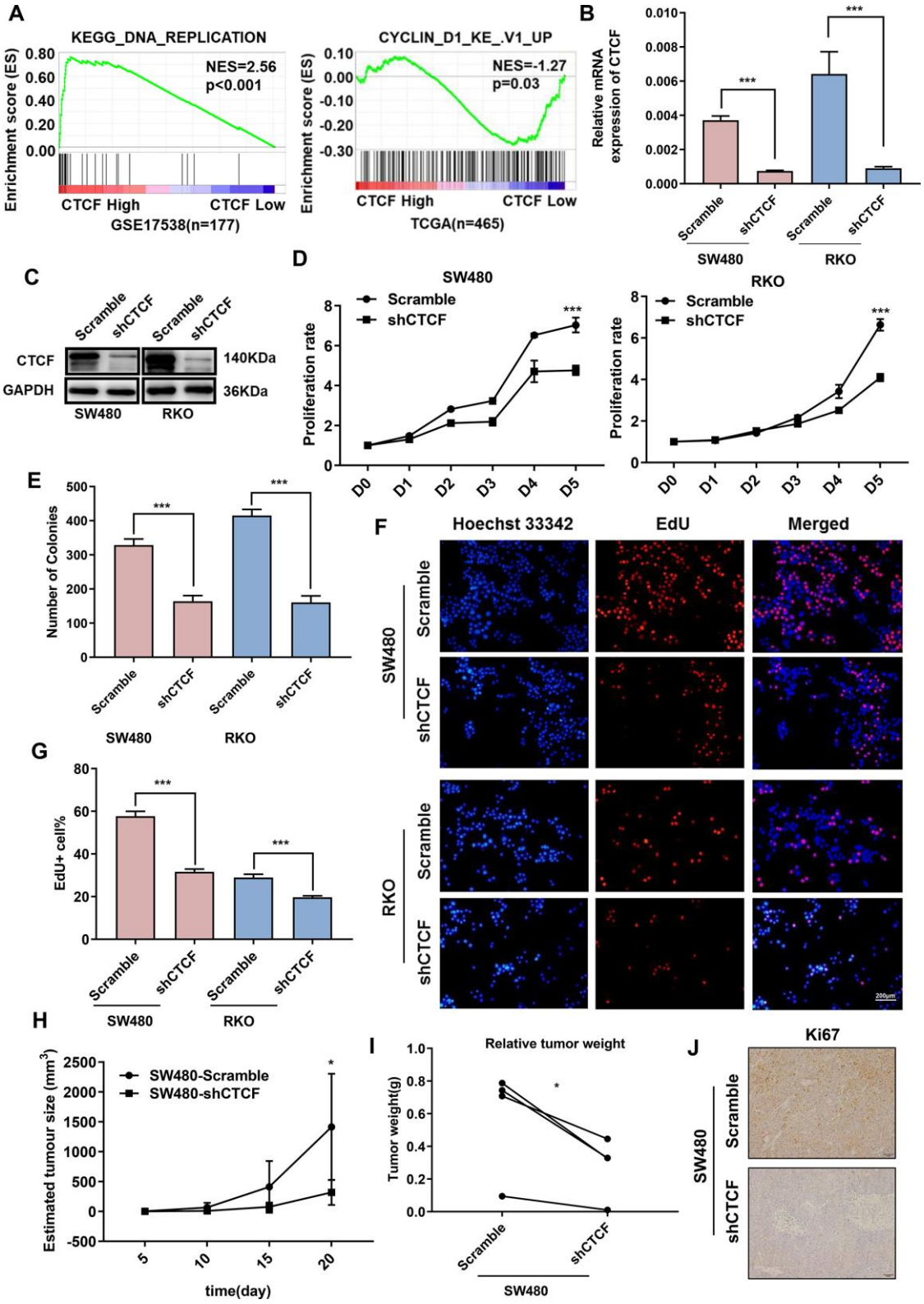

Figure 3. Inhibition of CTCF represses human CRC cells proliferation. (**A**) GSEA results showed that "KEGG_DNA_REPLICATION" gene set enriches in the CTCF high expression group and "CYCLIN_D1_KE_V1_UP" gene set enriches in the CTCF low expression group (GSE17538, n = 177, and TCGA, n = 465). (**B**, **C**) qRT-PCR and western blot analyses of CTCF expression level in the constructed cell lines (SW480 and RKO). (**D**–**G**) Cell reproductive capacity was examined by CCK8, colony formation and EdU staining assays. (**H**, **I**) Tumor volume and weight of subcutaneous tumor were measured and analysed. (**J**) Immunohistochemistry was performed to determine Ki-67 expression. The above data are presented as mean ± SEM. * P<0.05, **P<0.01, and ***P<0.001.

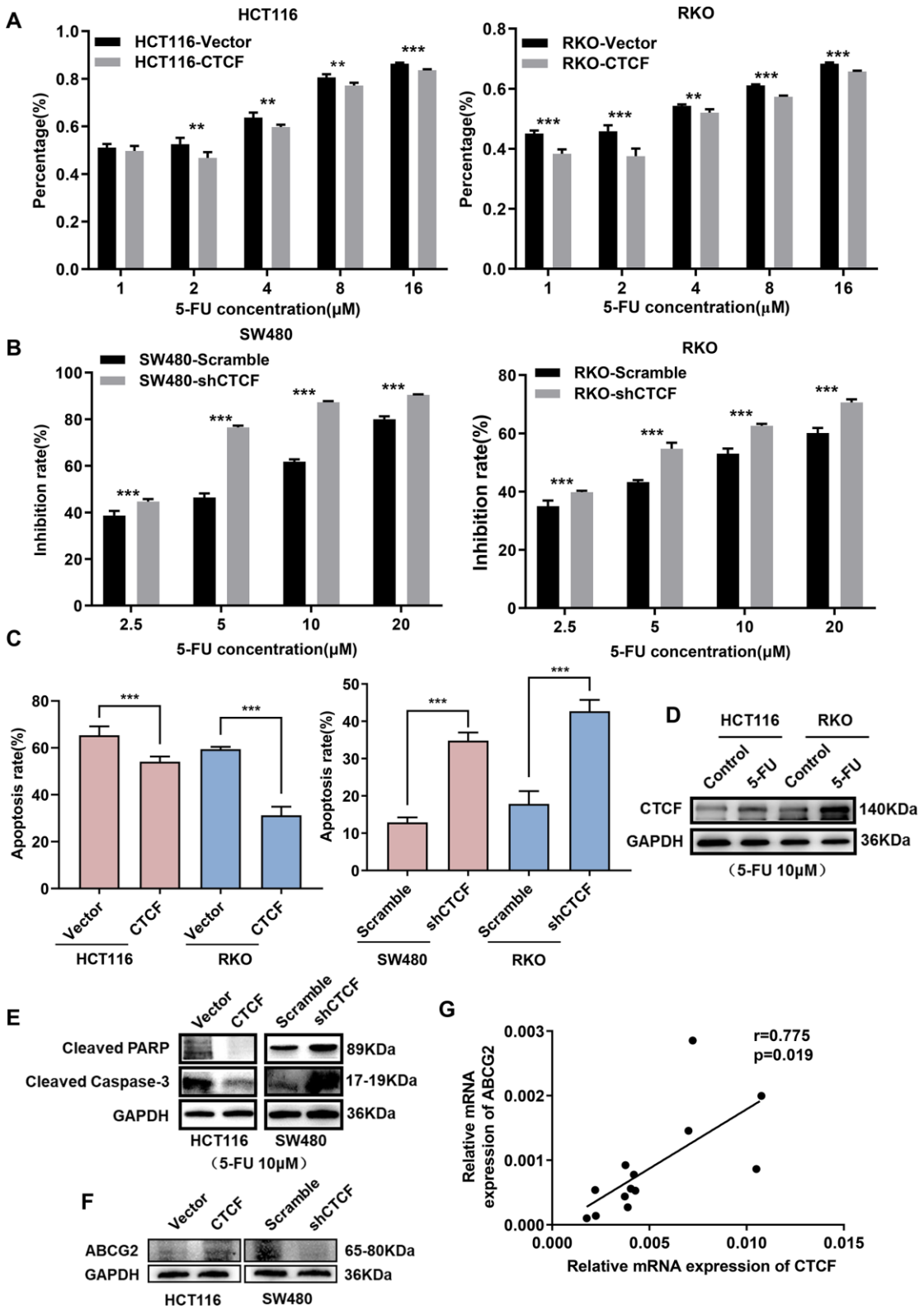

Figure 4. CTCF induces 5-FU-based chemoresistance in CRC. (**A**, **B**) Cell growth inhibition rate was measured via CCK8 analysis and compared between different groups with different treatment concentration at indicated time (48 hours). (**C**) The apoptosis rate of different transfected groups with 5-FU treatment were measured by flow cytometry. (**D**) Western blot analysis of CTCF in HCT116 and RKO cell lines after 5-FU (10 μM) treatment for 48 hours. (**E**, **F**) Western blot analyses of cleaved-PARP, cleaved Capase-3 and ABCG2 in HCT116 and SW480 cell lines. (**G**) Spearman correlation analyses between relative CTCF and ABCG2 mRNA expression in 13 fresh human CRC specimens. The above data are presented as mean ± SEM. * P<0.05, **P<0.01, and ***P<0.001.

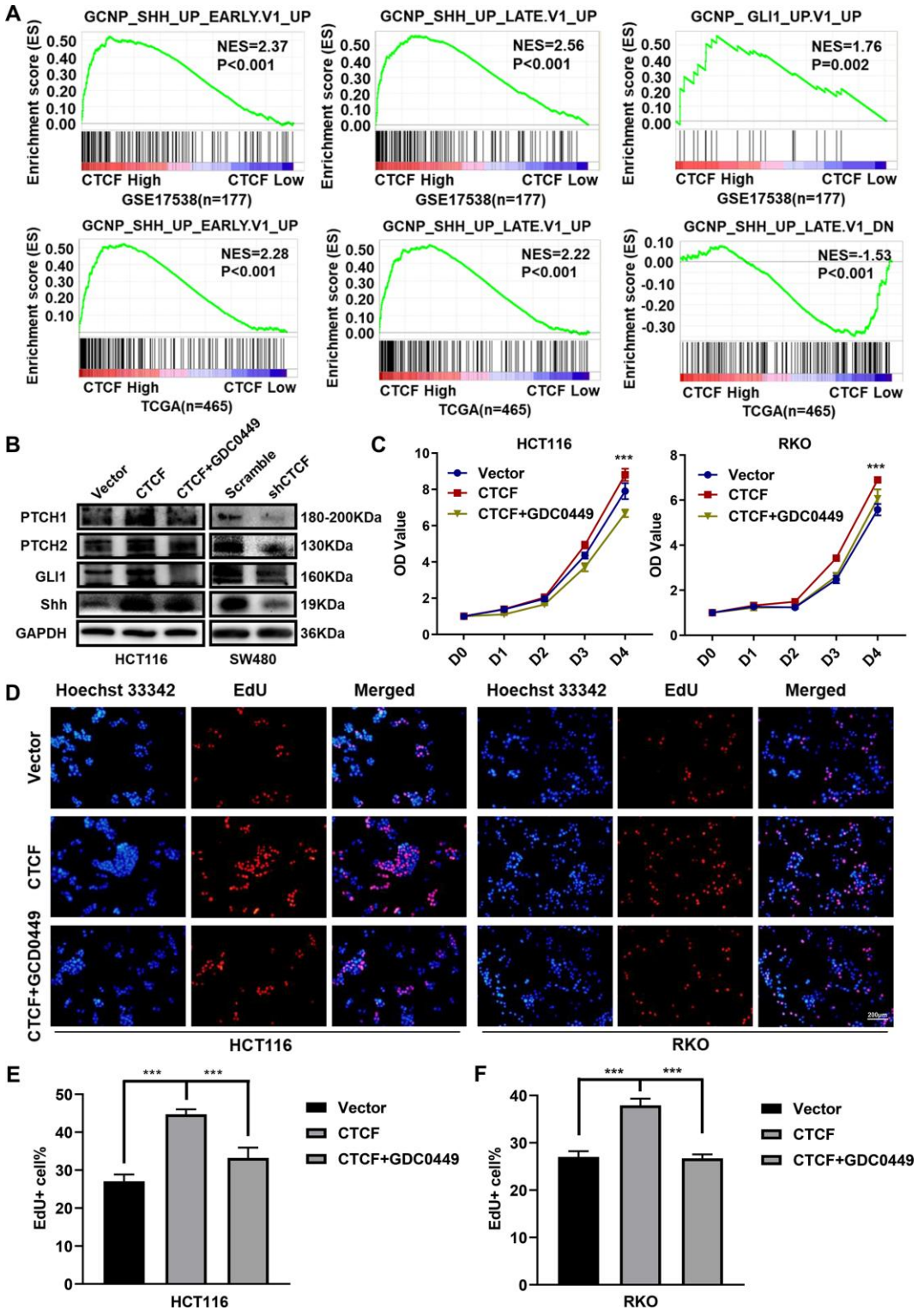

Figure 5. CTCF activates Hedgehog signaling pathway. (**A**) GSEA plots indicated that "GCNP_SHH_UP_EARLY.V1_UP" and "GCNP_SHH_UP_LATE.V1_UP" and "GCNP_GLI1_UP.V1_UP" gene signatures enrich in the CTCF high expression group and "GCNP_SHH_UP_LATE.V1_DN" gene set enriches in the CTCF low expression group (GSE17538, n = 177, and TCGA, n = 465). (**B**) Western blot analyses of Key molecules of Hedgehog signaling pathway in different transfected groups with or without the stimulation of Hedgehog signaling pathway inhibitor, GDC-0449 (2 μM). (**C**) Relative growth rate of different transfected groups with or without the administration of GDC-0449 (2 μM). (**D**–**F**) Images of EdU staining of both indicated cell lines with or without the administration of GDC-0449, and the relative percentage of EdU-positive cells in images of related groups is shown. The above data are presented as mean ± SEM. * P<0.05, **P<0.01, and ***P<0.001.

of 5-FU. Venn diagram enrichment analysis showed that TYMS and TP53 were theoretical target genes of 5-FU (Figure 6A). Then, we analyzed the interactions among CTCF, the above two target genes and the key molecules of the Hedgehog signaling pathway in functional protein association networks (STRING, https://string-db.org/, Figure 6B), the results suggested that P53 may be a "bridge" between CTCF and the Hedgehog signaling pathway. GSEA plots showed that CTCF was negatively correlated with P53-related gene set signatures (GSE17538, n = 177, Figure 6C). Moreover, GO enrichment were performed to analyze the top 30 similar genes of CTCF in GEPIA (http://gepia.cancer-pku.cn/). As the bubble diagram shown (Supplementary Figure 5A), "p53 binding" was in the top 20 of GO enrichment. qRT-PCR analyses showed that CTCF repressed P53 expression (Figure 6E). K-M survival analysis with GEPIA revealed that high expression of TP53 was accompanied by a longer survival time (Supplementary Figure 5B). Interestingly, high ratio of CTCF/TP53 was accompanied by a shorter disease free survival time while the prognosis of the high TP53/CTCF ratio group was good (Supplementary Figure 5C). A previous study [27] identified CTCF binding site (CBS) in the promoter region approximately 800 bp upstream of the P53 transcription start site (Figure 6D). Therefore, ChIP-qPCR and ChIP-PCR assays were performed to confirm whether CTCF can bind to the site in CRC (Supplementary Figure 6A and Figure 6F). Moreover, a dual luciferase reporter assay showed that the knockdown of CTCF enhanced P53 luciferase activity (Figure 6G). Clinical specimens further confirmed that there was a negative correlation between CTCF and P53 (Supplementary Figure 6B).

To further validate whether CTCF activates the Hedgehog signaling pathway via P53, siRNA targeting P53 was used for rescue assays. Western blot assays demonstrated that the knockdown of P53 counteracted the CTCF knockdown-induced repression of the Hedgehog signaling pathway (Figure 6H). Nuclear extract assays revealed that the inhibition of P53 blocked the CTCF knockdown-induced intranuclear reduction of GLI1 (Figure 6I, 6J). In addition, a colony formation assay showed that the decrease of P53 impaired changes in proliferative capacity caused by CTCF knockdown (Supplementary Figure 6C).

CTCF-induced chemoresistance is dependent on the P53-Hedgehog axis

The above results showed that CTCF can block 5-FU-stimulated cell apoptosis and activate the Hedgehog signaling pathway via transcriptional repression of P53. However, further information is needed to determine whether the associations are causal. Apoptosis assays indicated that administration of GDC-0449 dramatically increased 5-FU-stimulated cell apoptosis rate repressed by overexpression of CTCF (Figure 7A and Supplementary Figure 6D). Western blot analysis revealed that P53 restored the ABCG2 increase induced by CTCF (Figure 7B). Moreover, an *in vivo* tumor growth assay confirmed that the inhibition of the Hedgehog signaling pathway with JK184 recovered the stimulation of cell proliferation caused by upregulated CTCF (n=5/group, Figure 7D, 7E).

DISCUSSION

CRC is one of the most lethal cancers worldwide. Although progress has been made in CRC diagnosis and treatments, the prognosis of some CRC patients is still poor and is affected by chemotherapy resistance, postoperative recurrence, and metastasis [5, 38].

Studies have revealed that CTCF is robustly upregulated in several cancers and promotes the malignant characteristics of tumor cells [13, 18]. Moreover, Marois Giannakis et al. recently identified recurrently mutated genes in CRC, including TP53, KRAS, SMAD4, CTCF, etc., by performing whole-exome sequencing of 619 incident CRCs and integrating the results with tumor immunity, pathology, and survival data [32]. However, CTCF was not previously studied in CRC progression, which drove us to explore the exact role of CTCF in CRC. Herein, we demonstrated that CTCF was upregulated in CRC tissues by performing western blot and qRT-PCR assays. The overexpression of CTCF promoted malignant phenotypes in CRC by enhancing the proliferative potential and clonogenicity of CRC cells.

Although corresponding 5-FU-based chemotherapies, including FOLFIRI [39], FOLFOX [40], XELOX [41] and other regimens [38], have been developed in the past few years, the clinical outcome remains unsatisfactory, as some CRC patients suffer from chemotherapy resistance. Interestingly, our study indicated that CTCF overexpression reduced the sensitivity of CRC cells to 5-FU and decreased 5-FU-induced apoptosis, which offered a novel explanation for the emergence of chemo-resistance in CRC. ABCG2 has been suggested to be involved in clinical multidrug resistance (MDR) in cancer [42], and we found that ABCG2 was activated by CTCF in CRC. Hence, the inhibition of CTCF might be a new strategy to support chemotherapy in CRC patients.

The Hedgehog signaling pathway is involved in many aspects of tumorigenesis and malignant characteristics, including cell cycle progression, proliferation, angio-genesis, migration, invasion, and, in particular, chemotherapy resistance [43, 44]. For example, the

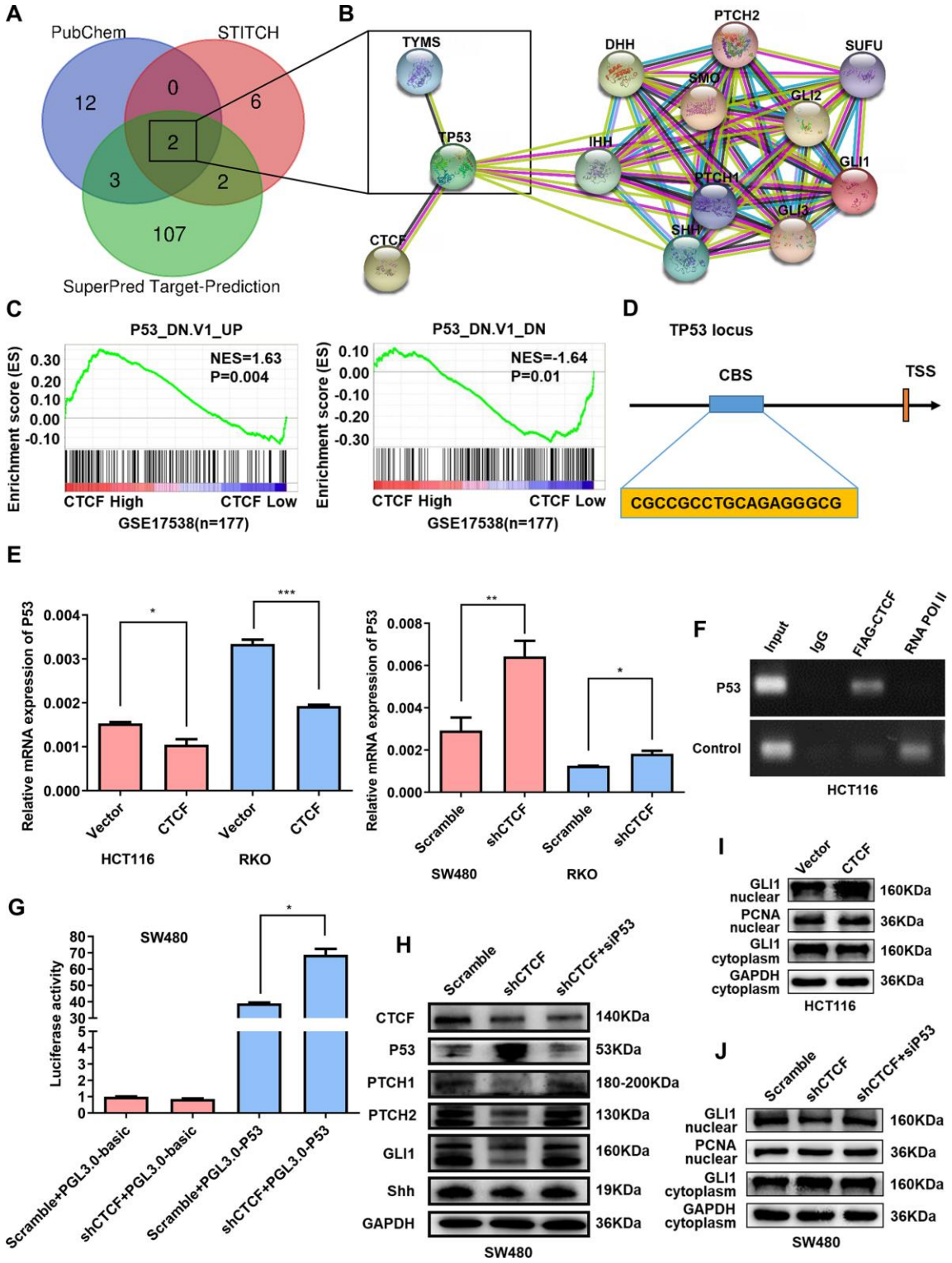

Figure 6. CTCF enhances Hedgehog signaling pathway activation via targeting P53. (**A**) Venn diagram enrichment analysis of the 5-FU putative target genes. (**B**) Protein-protein interaction analysis via STRING (https://string-db.org/). (**C**) GSEA plots indicated that "P53_DN.V1_UP" gene set signature enriches in the CTCF high expression group and "P53_DN.V1_DN" gene set enriches in the CTCF low expression group (GSE17538, n = 177). (**D**) Schematic view of the P53 gene transcription start site (TSS) with a CTCF-binding site (CBS). (**E**) qRT-PCR analysis of P53 expression level in constructed cell lines. (**F**) ChIP-PCR results for CTCF on the CBS in HCT116 cells. (**G**) P53 luciferase reporter activity was analyzed in SW480 cells. (**H**) Western blot analysis of Key molecules of Hedgehog signaling pathway and P53 in different transfected groups with or without the stimulation of P53-specific siRNA. (**I**, **J**) Nuclear extract assays and western blot analyses of GLI1 in indicated cells. The above data are presented as mean ± SEM. * P<0.05, **P<0.01, and ***P<0.001.

persistent activation of the Hedgehog pathway was confirmed to play a critical role in the chemoresistance and prognosis of cancer patients [45]. In addition, ABCG2 is a direct transcriptional target of the Hedgehog signaling pathway and is involved in drug tolerance in diffuse large B-cell lymphoma [46]. Hence, we performed GSEA to analyze the relationship between CTCF and the Hedgehog signaling pathway and found that the enrichment of Hedgehog pathway-related gene set signatures is notably related to CTCF expression. Furthermore, our results showed that the overexpression of CTCF increased GLI1, Shh, PTCH1, and PTCH2 levels, while silencing CTCF induced low GLI1, Shh, PTCH1, and PTCH2 expression. Additionally, the administration of the Hedgehog signaling pathway inhibitor GDC-0449 counteracted the increased proliferation and clonogenicity induced by CTCF up-regulation. Furthermore, rescue assays, including

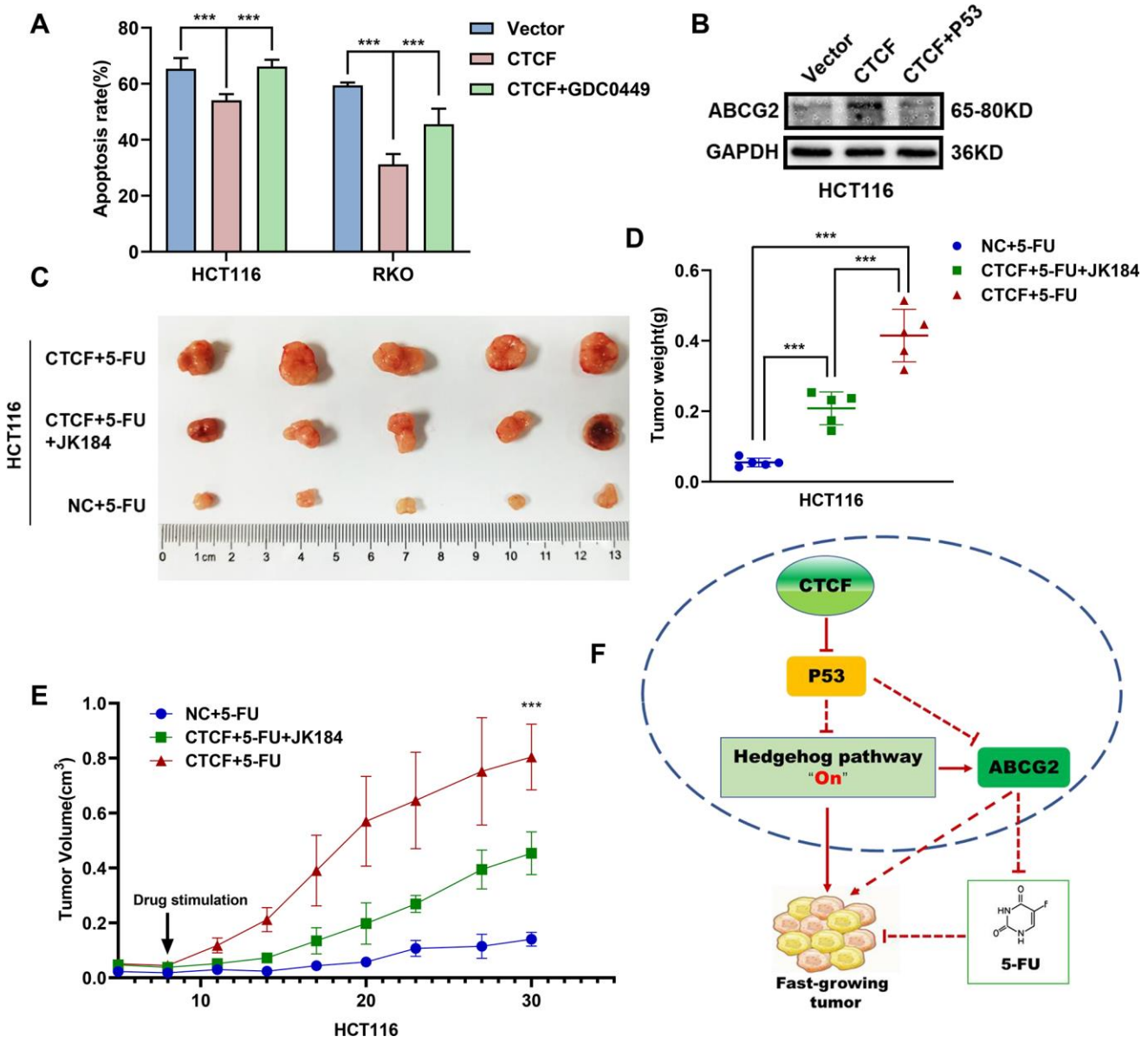

Figure 7. CTCF promotes chemoresistance by regulating P53-Hedgehog axis signaling. (**A**) Apoptosis assays showed the effect of GDC0449 on CTCF-mediated 5-FU stimulated apoptosis of CRC cells. (**B**) Western blot analysis of the effects of P53 on CTCF-mediated ABCG2 upregulation. (**C**) The representative images of subcutaneous tumors from different experimental groups are shown. (**D**, **E**) Tumor weight and volume analyses showed that JK184 recovered the stimulative cell proliferation caused by upregulated CTCF under stimulation of 5-FU. (**F**) A hypothetical model illustrating that CTCF transcriptionally represses P53 and activates the Hedgehog signaling pathway to promote proliferation and 5-FU chemotherapy resistance of CRC cells. The above data are presented as mean ± SEM. * P<0.05, **P<0.01, and ***P<0.001.

in vivo tumor growth assays and apoptosis assays, demonstrated that CTCF sustains CRC proliferation and chemotherapy resistance by activating the Hedgehog signaling pathway. However, the mechanism by which CTCF activates the Hedgehog signaling pathway is still unclear.

Thus, the above results indicated that CTCF promotes CRC proliferation and chemotherapy resistance via the Hedgehog signaling pathway. The mechanism by which CTCF activates the Hedgehog signaling pathway needs to be clarified, as previous studies have not reported this relationship. Through network pharmacologic analysis, we found that P53 and TYMS are the potential key target genes of 5-FU. In recent years, more and more studies have shown that TYMS and P53 are crucial molecules in 5-FU resistance [47, 48]. Furthermore, we found P53 might be a key molecule that connects CTCF and the Hedgehog signaling pathway by constructing a protein interaction network. P53 is a crucial molecule in the progression of virtually every malignant tumor [49]. Furthermore, it has been reported that P53 can suppress the Hedgehog signaling pathway [50]. GSEA revealed that CTCF expression is closely related to P53-related gene set signatures. A previous study reported that CTCF transcriptionally inhibits P53 in breast cancer [27]. Hence, we performed qRT-PCR, ChIP and dual luciferase reporter assays to investigate whether the regulatory mechanism between CTCF and P53 also exists in CRC cells. The results showed that CTCF can inhibit P53 transcription via bind to the promoter region of P53.

As mentioned above, studies showed that P53 can suppress the Hedgehog signaling pathway, and our study revealed that CTCF transcriptionally repressed P53 expression. Protein interaction network revealed that P53 is a "bridge" connecting CTCF to Hedgehog signaling pathway. However, whether CTCF activates Hedgehog signaling pathway is P53 dependent in CRC still should be clarified. Hence, we performed rescue assays, including western blot and nuclear extract assays, to investigate the relationship among CTCF, P53 and Hedgehog signaling pathway. Western blot assays demonstrated that CTCF activates the Hedgehog signaling pathway through the repression of P53. Furthermore, nuclear extract assays demonstrated that P53 repression increases the nuclear accumulation of GLI1 which is induced by CTCF. Most of all, subcutaneous xenotransplanted tumor model of human CRC in nude mice further confirmed that CTCF enhanced 5-FU resistance via activating Hedgehog signaling pathway.

In summary, our work provides evidence that CTCF facilitates malignant properties and induces chemo-therapy resistance to 5-FU in CRC by regulating the P53-Hedgehog axis. This work introduces a potential biomarker for CRC and a therapeutic target to reduce chemoresistance in patients with CRC.

MATERIALS AND METHODS

Clinical specimens and cell culture

With approval from the institutional review board of the hospital ethics committee (Nanfang Hospital, Southern Medical University), clinical CRC specimens and matched normal tissues were collected from 90 patients who underwent surgical treatment for CRC at Nanfang Hospital of Southern Medical University after obtaining informed consent. Additionally, the study was conducted in accordance with the Declaration of Helsinki. CRC was histopathologically confirmed in each patient. Cancer tissues and adjacent normal tissues were frozen at -80°C for storage.

A human embryonic kidney cell line (293T), human normal colon epithelial cell line (FHC) and six human CRC cell lines (SW480, SW620, RKO, HCT116 HT29 and LOVO) were purchased from the Cell Bank of Type Culture Collection (CBTCC, Chinese Academy of Sciences, Shanghai, China) and were cultured in DMEM (Gibco, Carlsbad, CA) supplemented with 10% fetal bovine serum (Gibco, Carlsbad, CA). Cells were maintained at 37°C in a humidified atmosphere with 5% CO2.

Plasmid construction, lentiviral construction and cell transfection

The overexpression and downregulation of CTCF were achieved by lentiviral delivery. To construct CTCF-overexpressing cell lines, full-length CTCF (NM_006565) was cloned into the expression vector pLenti-EF1a-EGFP-P2A-Puro-CMV (Obio Technology, Shanghai, China) and transfected into HCT116 and RKO cell lines according to the manufacturer's instructions. The knockdown of CTCF was accomplished with shRNA (Cyagen, Guangzhou, China) that were transfected into SW480 and RKO cell lines according to the manufacturer's instructions. The CTCF shRNA sequence was sense 5'-GCGAAAGCAGCATTCCTA TAT-3', and the scrambled sequence was sense 5'-CCTAAGGTTAAGTCGCCCTCG-3'. Transduced cells were selected in medium containing puromycin (#EZ2811D376, BioFrox, China) (2 μg/ml) and maintained in medium containing puromycin (1 μg/ml).

Plasmid and siRNA transfection

To exogenously overexpress TP53, full-length TP53 (NM_000546.6) was cloned into the expression vector

pENTER (Vigene, Shandong, China). The knockdown of TP53 was achieved by siRNA (Genecopoeia, Shanghai, China). The TP53 siRNA sequence was sense 5'-GAAGAAACCACUGGAUGGATT -3', and the negative control sequence was sense 5'-UUCUCCGAACGUGUCACGUTT-3'. Genomic DNA fragments from the TP53 locus (-1000-0 bp of the TP53 promoter region) were cloned into the pGL3-basic vector (Obio Technology, China). Plasmids or siRNA were transfected into CRC cells with LipofectamineTM 3000 (Invitrogen, Carlsbad, CA) according to the manufacturer's instructions.

Cell Counting Kit-8 (CCK-8), colony formation assays

CCK-8 (Dojindo, Japan) analysis was used to estimate cell proliferation. The transfected cell lines were cultured on the 96-well plates and then with culture medium containing 10ul CCK-8 each well and incubated for 2 hours. Proliferation was determined by absorbance measurement at 450 nm using a microplate reader.

Cells were seeded in 6-well plates at a density of 5×10^2 per well and incubated at 37 °C in a humidified atmosphere with 5% CO2 and the medium was replaced every 3-4 days. The colonies were counted and analysed in about two weeks. The experiment was performed with at least three replicates for each cell line.

5-Ethynyl-2'-deoxyuridine (EdU) incorporation and apoptosis assays

As the manufacturer's instructions for a Cell-Light EdU DNA cell proliferation kit (#C103010-1, RiboBio, China) described, transfected cell lines were seeded in 96-well plates and incubated with EdU in medium (50 μM) for 2 hours. Then, cells were washed twice and fixed in 4% paraformaldehyde for 10 min, permeabilized with 0.5% Triton-X 100, and stained with Apollo® fluorescent dye. Photographs of cells were independently taken with an OLYMPUS confocal microscope.

The cells were analyzed by FACS according to the standard protocol provided by the manufacturer (BD FACSAria II). Apoptosis was measured by using an Annexin V-PE/7-Amino-Actinomycin (7-AAD) Apoptosis Detection Kit (#559763, BD Biosciences Pharmingen, US). After treatment with 5-FU (#9648, TargetMol, China) at the indicated concentrations for 48 hours, cells were harvested by trypsinization, washed with cold PBS and then resuspended in 1X binding buffer. Then, 5 μl of PE Annexin V and 5 μl 7-AAD were added to each tube. The suspension was then mixed well and incubated for 15 min in the dark at room temperature (RT) (25°C). After resuspension, samples were analyzed by flow cytometry.

RNA isolation, cDNA synthesis, and quantitative real-time PCR (qRT-PCR)

Total RNAs were extracted from cells or fresh surgical CRC tissues with Trizol solution (TaKaRa). Quantitative real-time polymerase chain reaction (qRT-PCR) was performed in triplicate using the PrimeScript RT Reagent Kit, SYBR Premix Ex Taq (TaKaRa) and a Roche Light Cycler 480 Real-Time PCR System (Roche Diagnostics, Mannheim, Germany) following the manufacturer's instructions. Relative gene expression levels were normalized to the expression of GAPDH. qRT-PCR results were analyzed to obtain Ct values of amplified products, and data was analyzed by the 2-ΔΔCt method. The specific primers used for detection are listed in Supplementary Table 1.

Western blot and immunohistochemistry (IHC)

We performed western blot according to the previous study [51]. Protein lysates were prepared, subjected to SDS-PAGE, transferred onto PVDF membranes and blotted according to standard methods by using following antibodies: CTCF(#2899, Cell Signaling), PTCH1 (#2648, Cell Signaling), and PTCH2 (#2470, Cell Signaling), GLI1(#3538, Cell Signaling), Shh(#2207, Cell Signaling), GAPDH (60004-1-Ig, Proteintech), Cleaved PARP (BF9106, Affinity), Cleaved Caspase-3 (# 9661S, Cell Signaling), TP53 (AF0879, Affinity), ABCG2 (#42078T, Cell Signaling).

Immunohistochemistry was performed following the manufacturer's instructions (PV-6001, ZSGB-BIO, Beijing, China) and used the antibody (anti-Ki67, 27309-1-AP, Proteintech)

ChIP and dual luciferase reporter assays

ChIP assays were performed with a kit (#17–10085, Merck) as previously described [51]. The CTCF binding site (CBS) at the transcriptional start site of TP53 was amplified with qRT-PCR and PCR. The specific primers are included in Supplementary Table 1. Luciferase activity was detected with a dual luciferase assay kit (Promega, America), as previously described [52].

Network pharmacologic analysis

List of websites used as follows, PubChem: https://pubchem.ncbi.nlm.nih.gov/, STITCH: http://stitch.embl.de/, SuperPred Target-Prediction: http://prediction.charite.de/index.php?site=chemdoodle_search_target, STRING: https://string-db.org/. The Canonical SMILES of 5-FU is C1=C(C(=O)NC(=O)N1)F, and the InChI Key of 5-FU is GHASVSINZRGABV-UHFFFAOYSA-N.

In vivo experiments

Female athymic 4- to 5-week-old Balb/C (nu/nu) mice were purchased from the Laboratory Animal Services Centre of Guangdong Province and were maintained in a specific pathogen-free facility. For the tumor growth assay, 5×10^6 cells were subcutaneously injected into the right and left back of nude mice (n =4/group). For drug treatment assays, 1×10^7 cells were subcutaneously injected into the right back of nude mice (n =5/group). JK184 (5 mg/kg body weight, #315703-52-7, MCE) and 5-FU (23 mg/kg body weight, #51-21-8, MCE) were used to treat nude mice according to the manufacturer's instructions. The tumor volume was calculated using the following formula: $V = 0.5 \times D \times d2$ (V represents volume, D represents the longitudinal diameter, and d represents the latitudinal diameter). The use of animals was approved by the Nanfang Hospital Animal Ethics Committee (ethical code NFYY-2018-38; approval date-10 April 2018).

Statistical analysis

All experiments were performed at least thrice. The SPSS 17.0 (SPSS; Chicago, IL, USA) statistical analysis software was used for statistical analysis of experimental data. The significance of differences between groups was estimated by Student's t-test. Additionally, multiple group comparisons were analyzed with one-way ANOVA. * $P<0.05$, ** $P<0.01$, and *** $P<0.001$ were considered significant.

AUTHOR CONTRIBUTIONS

SDL and AML designed the experiments; QHL, QYL, CCH, YXF, SML, JQC and JD conducted experiments; YFL, YZ, XKW, QZ, JH and QY provided research materials and methods; QHL and QYL analyzed data; and QHL wrote the manuscript, SDL, AML and CJW reviewed the manuscript. All authors read and approved the final manuscript.

ACKNOWLEDGMENTS

We thank Junsheng Chen for helping us make a pathological diagnosis.

CONFLICTS OF INTEREST

The authors declare no conflicts of interest.

FUNDING

This study was supported by Guangdong Gastrointestinal Disease Research Center (No.2017B020209003), National Natural Science Funds of China (No.81772964), China's Postdoctoral Science Fund (2019M663005) and the Foundation for the President of Nanfang Hospital of Southern Medical University (2018C027 and 2019B014).

Editorial note

[&]This corresponding author has a verified history of publications using the personal email addresses for correspondence.

REFERENCES

1. Brenner H, Kloor M, Pox CP. Colorectal cancer. Lancet. 2014; 383:1490–502. https://doi.org/10.1016/S0140-6736(13)61649-9 PMID:24225001
2. Inadomi JM. Screening for Colorectal Neoplasia. 1533-4406 (Electronic).
3. Siegel RL, Miller KD, Fedewa SA, Ahnen DJ, Meester RG, Barzi A, Jemal A. Colorectal cancer statistics, 2017. CA Cancer J Clin. 2017; 67:177–93. https://doi.org/10.3322/caac.21395 PMID:28248415
4. Pfister DG, Benson AB 3rd, Somerfield MR. Clinical practice. Surveillance strategies after curative treatment of colorectal cancer. N Engl J Med. 2004; 350:2375–82. https://doi.org/10.1056/NEJMcp010529 PMID:15175439
5. Xiong M, Zhuang K, Luo Y, Lai Q, Luo X, Fang Y, Zhang Y, Li A, Liu S. KIF20A promotes cellular Malignant behavior and enhances resistance to chemotherapy in colorectal cancer through regulation of the JAK/STAT3 signaling pathway. Aging (Albany NY). 2019; 11:11905–21. https://doi.org/10.18632/aging.102505 PMID:31841120
6. Meyerhardt JA, Mayer RJ. Systemic therapy for colorectal cancer. N Engl J Med. 2005; 352:476–87. https://doi.org/10.1056/NEJMra040958 PMID:15689586
7. Kehlet H. Fast-track colorectal surgery. Lancet. 2008; 371:791–93. https://doi.org/10.1016/S0140-6736(08)60357-8 PMID:18328911
8. Maeda H, Kashiwabara K, Aoyama T, Oba K, Honda M, Mayanagi S, Kanda M, Hamada C, Sadahiro S, Sakamoto J, Saji S, Yoshikawa T. Hazard rate of tumor recurrence over time in patients with colon cancer: implications for postoperative surveillance from three Japanese foundation for multidisciplinary treatment of cancer (JFMC) clinical trials. J Cancer. 2017; 8:4057–64. https://doi.org/10.7150/jca.21365 PMID:29187881

9. Vecchione L, Gambino V, Raaijmakers J, Schlicker A, Fumagalli A, Russo M, Villanueva A, Beerling E, Bartolini A, Mollevi DG, El-Murr N, Chiron M, Calvet L, et al. A vulnerability of a subset of colon cancers with potential clinical utility. Cell. 2016; 165:317–30. https://doi.org/10.1016/j.cell.2016.02.059 PMID:27058664

10. Ma S, Yang D, Liu Y, Wang Y, Lin T, Li Y, Yang S, Zhang W, Zhang R. LncRNA BANCR promotes tumorigenesis and enhances adriamycin resistance in colorectal cancer. Aging (Albany NY). 2018; 10:2062–78. https://doi.org/10.18632/aging.101530 PMID:30144787

11. Yan L, You WQ, Sheng NQ, Gong JF, Hu LD, Tan GW, Chen HQ, Wang ZG. A CREB1/miR-433 reciprocal feedback loop modulates proliferation and metastasis in colorectal cancer. Aging (Albany NY). 2018; 10:3774–93. https://doi.org/10.18632/aging.101671 PMID:30523220

12. Liao W, Overman MJ, Boutin AT, Shang X, Zhao D, Dey P, Li J, Wang G, Lan Z, Li J, Tang M, Jiang S, Ma X, et al. KRAS-IRF2 axis drives immune suppression and immune therapy resistance in colorectal cancer. Cancer Cell. 2019; 35:559–72.e7. https://doi.org/10.1016/j.ccell.2019.02.008 PMID:30905761

13. Song SH, Kim TY. CTCF, cohesin, and chromatin in human cancer. Genomics Inform. 2017; 15:114–22. https://doi.org/10.5808/GI.2017.15.4.114 PMID:29307136

14. Eldholm V, Haugen A, Zienolddiny S. CTCF mediates the TERT enhancer-promoter interactions in lung cancer cells: identification of a novel enhancer region involved in the regulation of TERT gene. Int J Cancer. 2014; 134:2305–13. https://doi.org/10.1002/ijc.28570 PMID:24174344

15. Kim S, Yu NK, Kaang BK. CTCF as a multifunctional protein in genome regulation and gene expression. Exp Mol Med. 2015; 47:e166. https://doi.org/10.1038/emm.2015.33 PMID:26045254

16. Pérez-Juste G, García-Silva S, Aranda A. An element in the region responsible for premature termination of transcription mediates repression of c-myc gene expression by thyroid hormone in neuroblastoma cells. J Biol Chem. 2000; 275:1307–14. https://doi.org/10.1074/jbc.275.2.1307 PMID:10625678

17. Bell AC, West AG, Felsenfeld G. The protein CTCF is required for the enhancer blocking activity of vertebrate insulators. Cell. 1999; 98:387–96. https://doi.org/10.1016/s0092-8674(00)81967-4 PMID:10458613

18. Oh S, Oh C, Yoo KH. Functional roles of CTCF in breast cancer. BMB Rep. 2017; 50:445–53. https://doi.org/10.5483/bmbrep.2017.50.9.108 PMID:28648147

19. Holwerda SJ, de Laat W. CTCF: the protein, the binding partners, the binding sites and their chromatin loops. Philos Trans R Soc Lond B Biol Sci. 2013; 368:20120369. https://doi.org/10.1098/rstb.2012.0369 PMID:23650640

20. Yu X, Liu Q, He J, Huang Y, Jiang L, Xie X, Liu J, Chen L, Wei L, Qin Y. Vigilin interacts with CTCF and is involved in the maintenance of imprinting of IGF2 through a novel RNA-mediated mechanism. Int J Biol Macromol. 2018; 108:515–22. https://doi.org/10.1016/j.ijbiomac.2017.11.109 PMID:29157910

21. Chao W, Huynh KD, Spencer RJ, Davidow LS, Lee JT. CTCF, a candidate trans-acting factor for x-inactivation choice. Science. 2002; 295:345–47. https://doi.org/10.1126/science.1065982 PMID:11743158

22. Zhang B, Zhang Y, Zou X, Chan AW, Zhang R, Lee TK, Liu H, Lau EY, Ho NP, Lai PB, Cheung YS, To KF, Wong HK, et al. The CCCTC-binding factor (CTCF)-forkhead box protein M1 axis regulates tumour growth and metastasis in hepatocellular carcinoma. J Pathol. 2017; 243:418–30. https://doi.org/10.1002/path.4976 PMID:28862757

23. Guo Y, Perez AA, Hazelett DJ, Coetzee GA, Rhie SK, Farnham PJ. CRISPR-mediated deletion of prostate cancer risk-associated CTCF loop anchors identifies repressive chromatin loops. Genome Biol. 2018; 19:160. https://doi.org/10.1186/s13059-018-1531-0 PMID:30296942

24. Delgado MD, Chernukhin IV, Bigas A, Klenova EM, León J. Differential expression and phosphorylation of CTCF, a c-myc transcriptional regulator, during differentiation of human myeloid cells. FEBS Lett. 1999; 444:5–10. https://doi.org/10.1016/s0014-5793(99)00013-7 PMID:10037138

25. Klenova EM, Fagerlie S, Filippova GN, Kretzner L, Goodwin GH, Loring G, Neiman PE, Lobanenkov VV. Characterization of the chicken CTCF genomic locus, and initial study of the cell cycle-regulated promoter of the gene. J Biol Chem. 1998; 273:26571–79. https://doi.org/10.1074/jbc.273.41.26571 PMID:9756895

26. Yan H, Tang G, Wang H, Hao L, He T, Sun X, Ting AH, Deng A, Sun S. DNA methylation reactivates GAD1 expression in cancer by preventing CTCF-mediated polycomb repressive complex 2 recruitment. Oncogene. 2016; 35:3995–4008. https://doi.org/10.1038/onc.2015.423 PMID:26549033

27. Lee JY, Mustafa M, Kim CY, Kim MH. Depletion of CTCF in breast cancer cells selectively induces cancer cell death via p53. J Cancer. 2017; 8:2124–31. https://doi.org/10.7150/jca.18818 PMID:28819414

28. Batlle-López A, Cortiguera MG, Rosa-Garrido M, Blanco R, del Cerro E, Torrano V, Wagner SD, Delgado MD. Novel CTCF binding at a site in exon1A of BCL6 is associated with active histone marks and a transcriptionally active locus. Oncogene. 2015; 34:246–56. https://doi.org/10.1038/onc.2013.535 PMID:24362533

29. Chang JW, Hsu HS, Ni HJ, Chuang CT, Hsiung CH, Huang TH, Wang YC. Distinct epigenetic domains separated by a CTCF bound insulator between the tandem genes, BLU and RASSF1A. PLoS One. 2010; 5:e12847. https://doi.org/10.1371/journal.pone.0012847 PMID:20877461

30. Witcher M, Emerson BM. Epigenetic silencing of the p16(INK4a) tumor suppressor is associated with loss of CTCF binding and a chromatin boundary. Mol Cell. 2009; 34:271–84. https://doi.org/10.1016/j.molcel.2009.04.001 PMID:19450526

31. Zhao L, Yang Y, Yin S, Yang T, Luo J, Xie R, Long H, Jiang L, Zhu B. CTCF promotes epithelial ovarian cancer metastasis by broadly controlling the expression of metastasis-associated genes. Oncotarget. 2017; 8:62217–30. https://doi.org/10.18632/oncotarget.19216 PMID:28977939

32. Giannakis M, Mu XJ, Shukla SA, Qian ZR, Cohen O, Nishihara R, Bahl S, Cao Y, Amin-Mansour A, Yamauchi M, Sukawa Y, Stewart C, Rosenberg M, et al. Genomic correlates of immune-cell infiltrates in colorectal carcinoma. Cell Rep. 2016; 17:1206. https://doi.org/10.1016/j.celrep.2016.10.009 PMID:27760322

33. Tang Z, Li C, Kang B, Gao G, Li C, Zhang Z. GEPIA: a web server for cancer and normal gene expression profiling and interactive analyses. Nucleic Acids Res. 2017; 45:W98–102. https://doi.org/10.1093/nar/gkx247 PMID:28407145

34. Hsu HH, Chen MC, Baskaran R, Lin YM, Day CH, Lin YJ, Tu CC, Vijaya Padma V, Kuo WW, Huang CY. Oxaliplatin resistance in colorectal cancer cells is mediated via activation of ABCG2 to alleviate ER stress induced apoptosis. J Cell Physiol. 2018; 233:5458–67. https://doi.org/10.1002/jcp.26406 PMID:29247488

35. Giroux-Leprieur E, Costantini A, Ding VW, He B. Hedgehog signaling in lung cancer: from oncogenesis to cancer treatment resistance. Int J Mol Sci. 2018; 19:2835. https://doi.org/10.3390/ijms19092835 PMID:30235830

36. Huang FT, Zhuan-Sun YX, Zhuang YY, Wei SL, Tang J, Chen WB, Zhang SN. Inhibition of hedgehog signaling depresses self-renewal of pancreatic cancer stem cells and reverses chemoresistance. Int J Oncol. 2012; 41:1707–14. https://doi.org/10.3892/ijo.2012.1597 PMID:22923052

37. Amantini C, Morelli MB, Nabissi M, Cardinali C, Santoni M, Gismondi A, Santoni G. Capsaicin triggers autophagic cell survival which drives epithelial mesenchymal transition and chemoresistance in bladder cancer cells in an hedgehog-dependent manner. Oncotarget. 2016; 7:50180–94. https://doi.org/10.18632/oncotarget.10326 PMID:27367032

38. Allegra C, Sargent DJ. Adjuvant therapy for colon cancer—the pace quickens. N Engl J Med. 2005; 352:2746–48. https://doi.org/10.1056/NEJMe058117 PMID:15987925

39. Cremolini C, Loupakis F, Antoniotti C, Lupi C, Sensi E, Lonardi S, Mezi S, Tomasello G, Ronzoni M, Zaniboni A, Tonini G, Carlomagno C, Allegrini G, et al. FOLFOXIRI plus bevacizumab versus FOLFIRI plus bevacizumab as first-line treatment of patients with metastatic colorectal cancer: updated overall survival and molecular subgroup analyses of the open-label, phase 3 TRIBE study. Lancet Oncol. 2015; 16:1306–15. https://doi.org/10.1016/S1470-2045(15)00122-9 PMID:26338525

40. Limagne E, Euvrard R, Thibaudin M, Rébé C, Derangère V, Chevriaux A, Boidot R, Végran F, Bonnefoy N, Vincent J, Bengrine-Lefevre L, Ladoire S, Delmas D, et al. Accumulation of MDSC and Th17 cells in patients with metastatic colorectal cancer predicts the efficacy of a FOLFOX-bevacizumab drug treatment regimen. Cancer Res. 2016; 76:5241–52. https://doi.org/10.1158/0008-5472.CAN-15-3164 PMID:27496709

41. Guo Y, Xiong BH, Zhang T, Cheng Y, Ma L. XELOX vs. Folfox in metastatic colorectal cancer: an updated meta-analysis. Cancer Invest. 2016; 34:94–104. https://doi.org/10.3109/07357907.2015.1104689

PMID:26864862

42. Toyoda Y, Takada T, Suzuki H. Inhibitors of human ABCG2: from technical background to recent updates with clinical implications. Front Pharmacol. 2019; 10:208. https://doi.org/10.3389/fphar.2019.00208 PMID:30890942

43. Cai D, Yu J, Qiu J, He B, Chen Z, Yan M, Liu Q. Dynamic changes of sonic hedgehog signaling pathway in gastric mucosa of rats with MNNG-induced gastric precancerous lesions. J Cell Physiol. 2019; 234:10827–34. https://doi.org/10.1002/jcp.27908 PMID:30537251

44. Salaritabar A, Berindan-Neagoe I, Darvish B, Hadjiakhoondi F, Manayi A, Devi KP, Barreca D, Orhan IE, Süntar I, Farooqi AA, Gulei D, Nabavi SF, Sureda A, et al. Targeting hedgehog signaling pathway: paving the road for cancer therapy. Pharmacol Res. 2019; 141:466–80. https://doi.org/10.1016/j.phrs.2019.01.014 PMID:30639373

45. Giroux Leprieur E, Vieira T, Antoine M, Rozensztajn N, Rabbe N, Ruppert AM, Lavole A, Cadranel J, Wislez M. Sonic hedgehog pathway activation is associated with resistance to platinum-based chemotherapy in advanced non-small-cell lung carcinoma. Clin Lung Cancer. 2016; 17:301–08. https://doi.org/10.1016/j.cllc.2015.12.007 PMID:26762562

46. Singh RR, Kunkalla K, Qu C, Schlette E, Neelapu SS, Samaniego F, Vega F. ABCG2 is a direct transcriptional target of hedgehog signaling and involved in stroma-induced drug tolerance in diffuse large b-cell lymphoma. Oncogene. 2011; 30:4874–86. https://doi.org/10.1038/onc.2011.195 PMID:21625222

47. Xu F, Ye ML, Zhang YP, Li WJ, Li MT, Wang HZ, Qiu X, Xu Y, Yin JW, Hu Q, Wei WH, Chang Y, Liu L, Zhao Q. MicroRNA-375-3p enhances chemosensitivity to 5-fluorouracil by targeting thymidylate synthase in colorectal cancer. Cancer Sci. 2020; 111:1528–41. https://doi.org/10.1111/cas.14356 PMID:32073706

48. Liang Y, Hou L, Li L, Li L, Zhu L, Wang Y, Huang X, Hou Y, Zhu D, Zou H, Gu Y, Weng X, Wang Y, et al. Dichloroacetate restores colorectal cancer chemosensitivity through the p53/miR-149-3p/PDK2-mediated glucose metabolic pathway. Oncogene. 2020; 39:469–85. https://doi.org/10.1038/s41388-019-1035-8 PMID:31597953

49. Joerger AC, Fersht AR. The p53 pathway: origins, inactivation in cancer, and emerging therapeutic approaches. Annu Rev Biochem. 2016; 85:375–404. https://doi.org/10.1146/annurev-biochem-060815-014710 PMID:27145840

50. Chung JH, Larsen AR, Chen E, Bunz F. A PTCH1 homolog transcriptionally activated by p53 suppresses hedgehog signaling. J Biol Chem. 2014; 289:33020–31. https://doi.org/10.1074/jbc.M114.597203 PMID:25296753

51. Li Q, Lai Q, He C, Fang Y, Yan Q, Zhang Y, Wang X, Gu C, Wang Y, Ye L, Han L, Lin X, Chen J, et al. RUNX1 promotes tumour metastasis by activating the Wnt/β-catenin signalling pathway and EMT in colorectal cancer. J Exp Clin Cancer Res. 2019; 38:334. https://doi.org/10.1186/s13046-019-1330-9 PMID:31370857

52. Wang X, Lan Z, He J, Lai Q, Yao X, Li Q, Liu Y, Lai H, Gu C, Yan Q, Fang Y, Zhang Y, Li A, Liu S. LncRNA SNHG6 promotes chemoresistance through ULK1-induced autophagy by sponging miR-26a-5p in colorectal cancer cells. Cancer Cell Int. 2019; 19:234. https://doi.org/10.1186/s12935-019-0951-6 PMID:31516391

SUPPLEMENTARY MATERIALS

Supplementary Figures

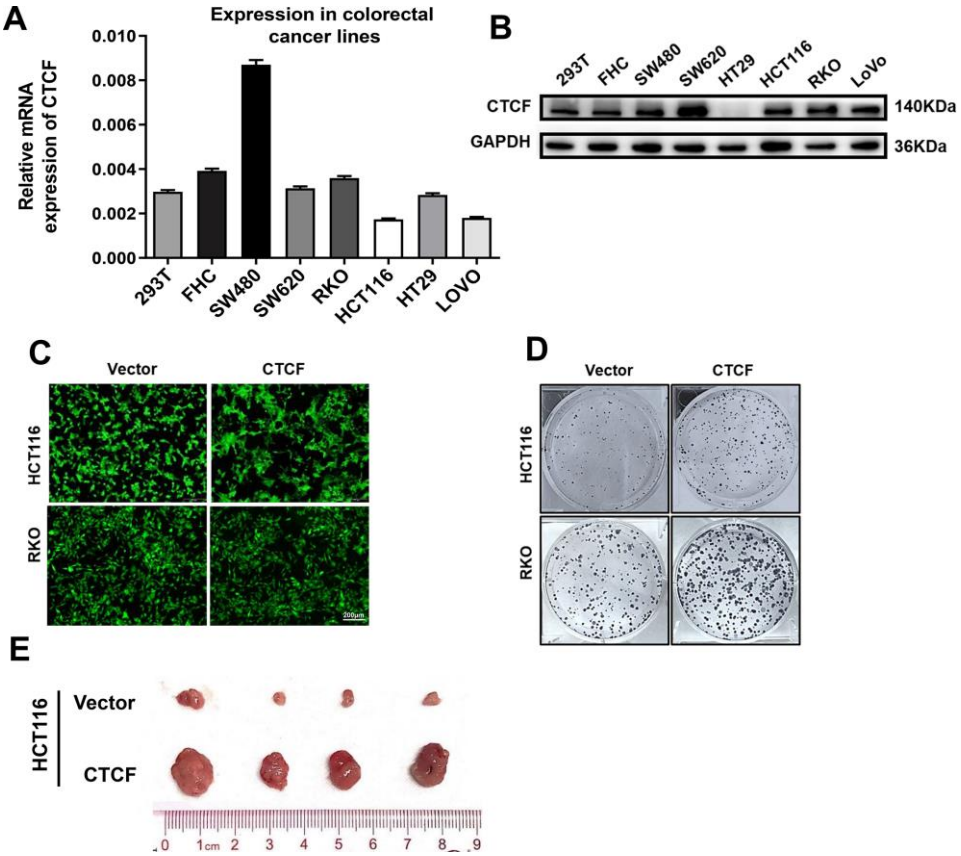

Supplementary Figure 1. Overexpression of CTCF enhances human CRC cells proliferative capacity. (**A**) mRNA level of CTCF in human embryonic kidney cell line (293T), human normal colon epithelial cell line (FHC) and six CRC cell lines. (**B**) Western blot analysis of human embryonic kidney cell line (293T), human normal colon epithelial cell line (FHC) and six CRC cell lines. The above data are presented as mean ± SEM. (**C**) Fluorescence assessment of the green fluorescent protein (GFP). Vector represents lentivirus-mediated control groups. CTCF represents lentivirus-mediated CTCF overexpressing groups. (**D**) The representative images of colony formation assay from different experimental groups are shown. (**E**) Corresponding cells were respectively injected subcutaneously into the right and left back hips of nude mice (n = 4). Representative images of the tumors are shown. * P<0.05, **P<0.01, and ***P<0.001.

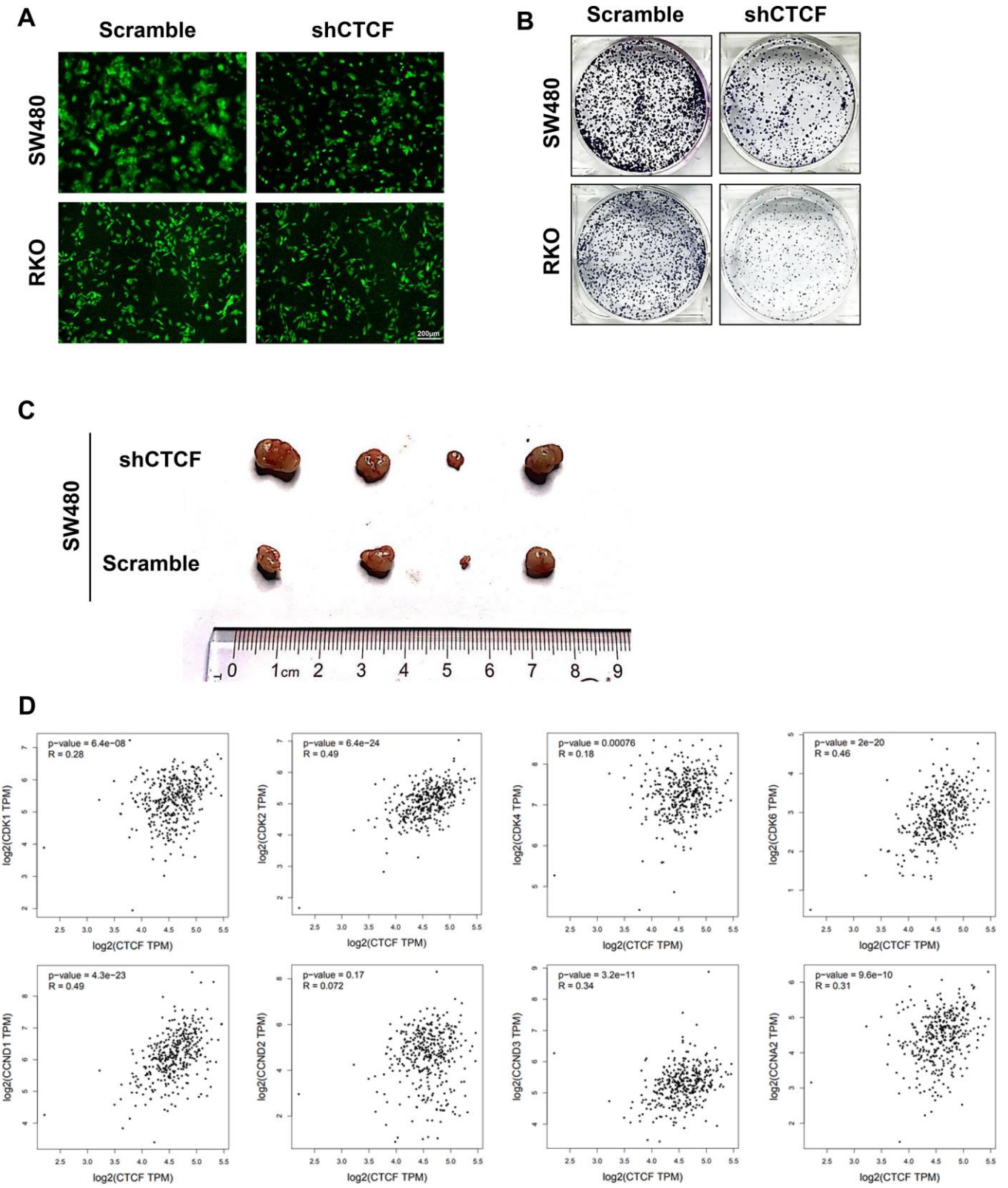

Supplementary Figure 2. Knockdown of CTCF inhibits human CRC cells proliferation. (**A**) Fluorescence assessment of the green fluorescent protein (GFP). Scramble represents lentivirus-mediated control groups. shCTCF represents lentivirus-mediated CTCF silencing groups. (**B**) The representative images of colony formation assays from different experimental groups are shown. (**C**) Corresponding cells were respectively injected subcutaneously into the right and left back hips of nude mice (n = 4). Representative images of the tumors are shown. (**D**) CTCF expression was positively correlated with the expression of CDKs and Cyclins in GEPIA (http://gepia.cancer-pku.cn/).

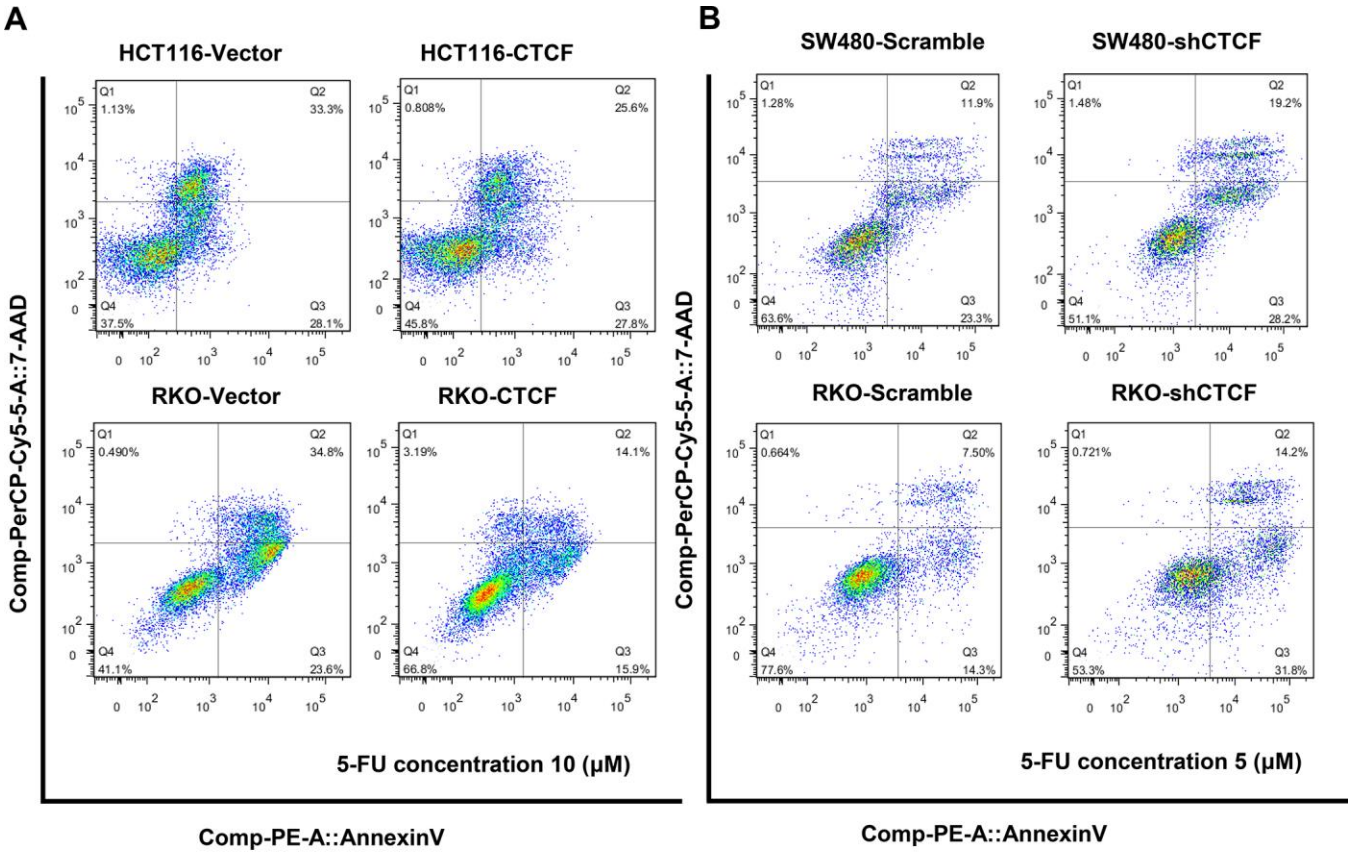

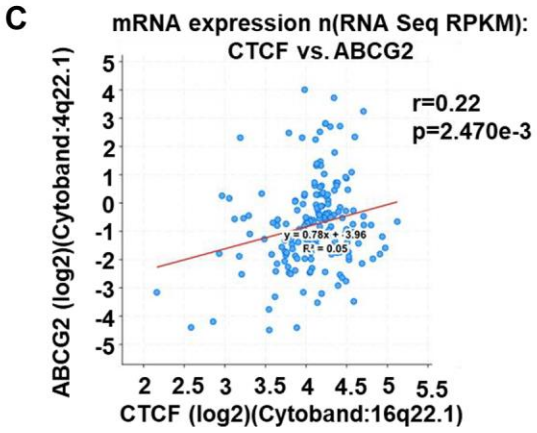

Supplementary Figure 3. CTCF causes CRC cells to be insensitive to 5-FU-based chemoresistance. (**A**, **B**) The representative images of apoptotic assays from different experimental groups are shown. Scramble and shCTCF cell lines were treated with 5-FU with a 5μM concentration, and the other cell lines were treated with 5-FU with a 10μM concentration. (**C**) Positive correlation between CTCF expression and ABCG2 by spearman correlation analysis in cBioPortal (http://www.cbioportal.org/).

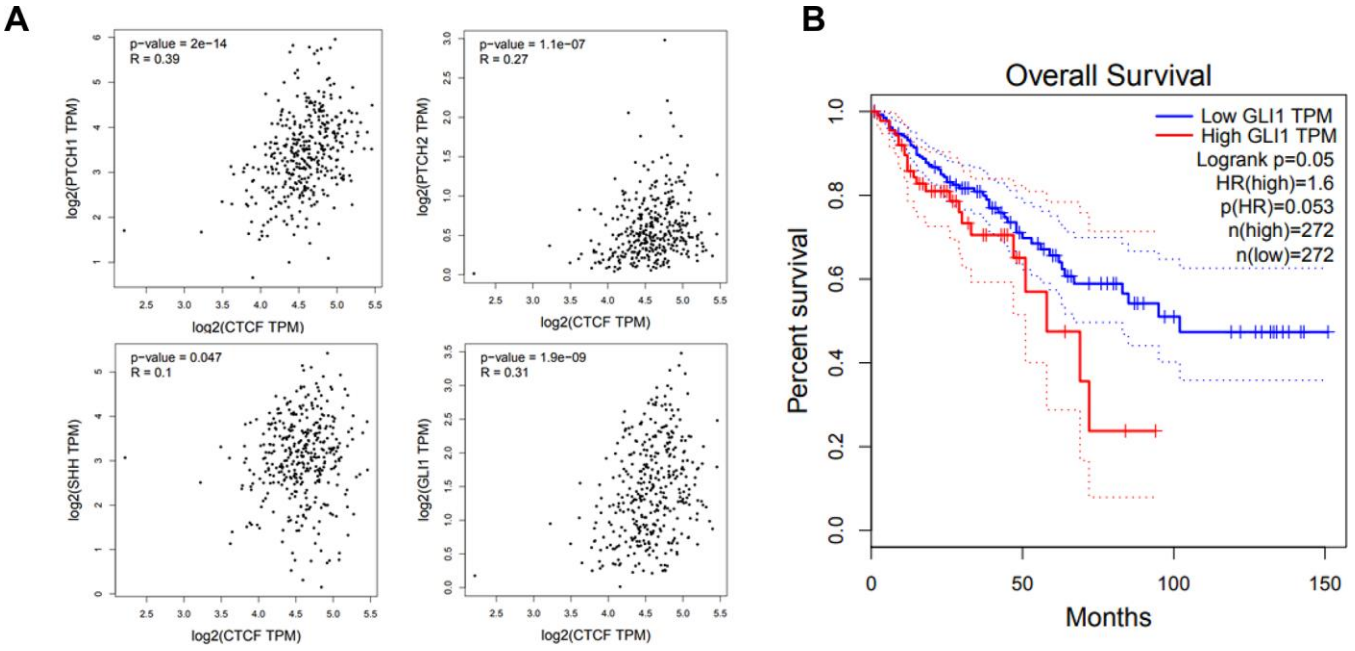

Supplementary Figure 4. CTCF activates Hedgehog signaling pathway. (**A**) Positive correlation between CTCF expression and the key molecules of Hedgehog signaling pathway by spearman correlation analsis in GEPIA (http://gepia.cancer-pku.cn/). (**B**) Kaplan-Meier survival analysis revealed that CRC patients in the GLI1 high expression group have shorter survival time in GEPIA.

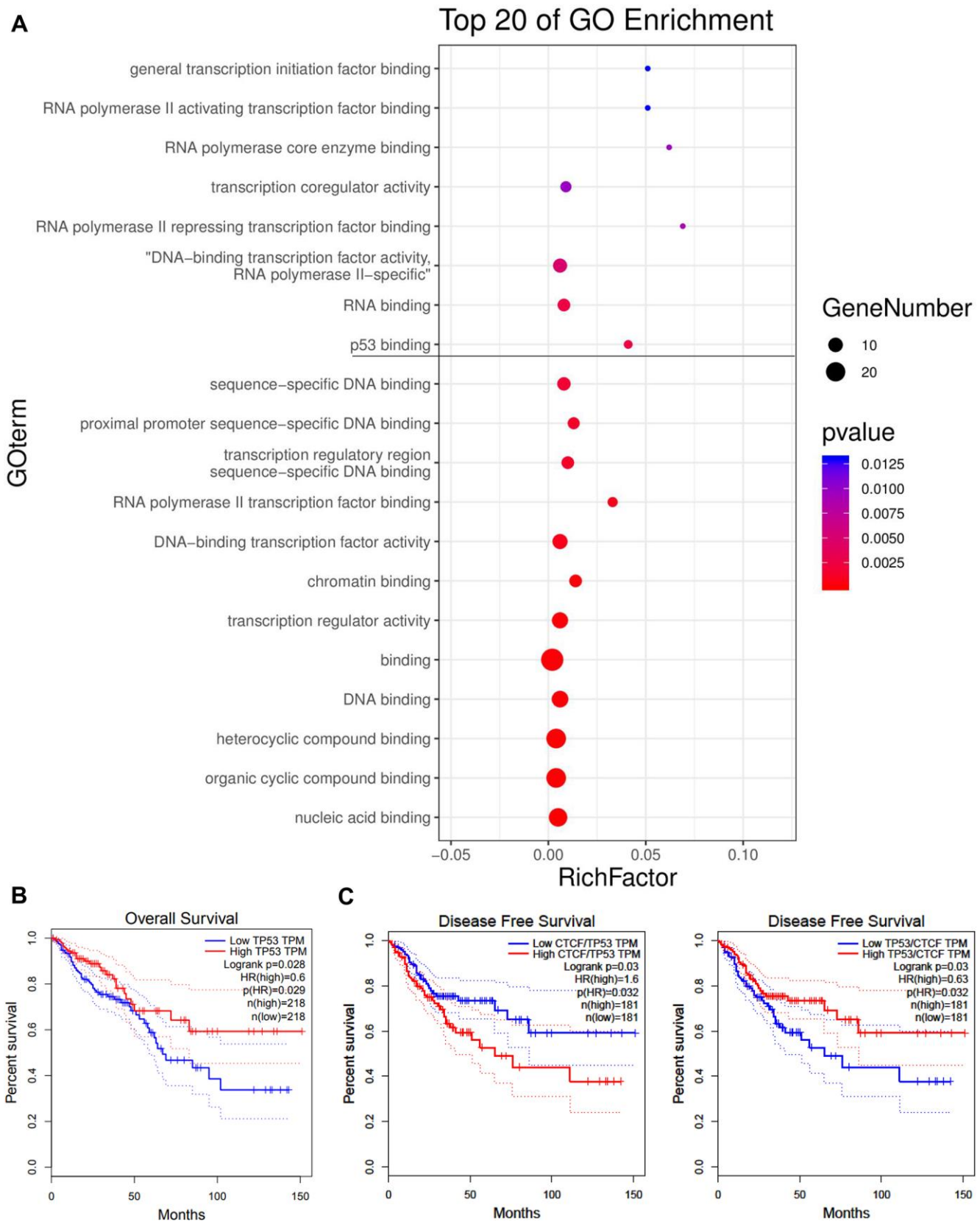

Supplementary Figure 5. CTCF might regulate P53 in CRC. (**A**) GO-molecular function enrichment analysis of the top 30 similar genes of CTCF in GEPIA is shown. (**B**) Kaplan-Meier survival analysis revealed that CRC patients in the TP53 high expression group have good prognosis in GEPIA. (**C**) Kaplan-Meier survival analysis showed that the ratio of CTCF/TP53 is positively related to disease free survival time.

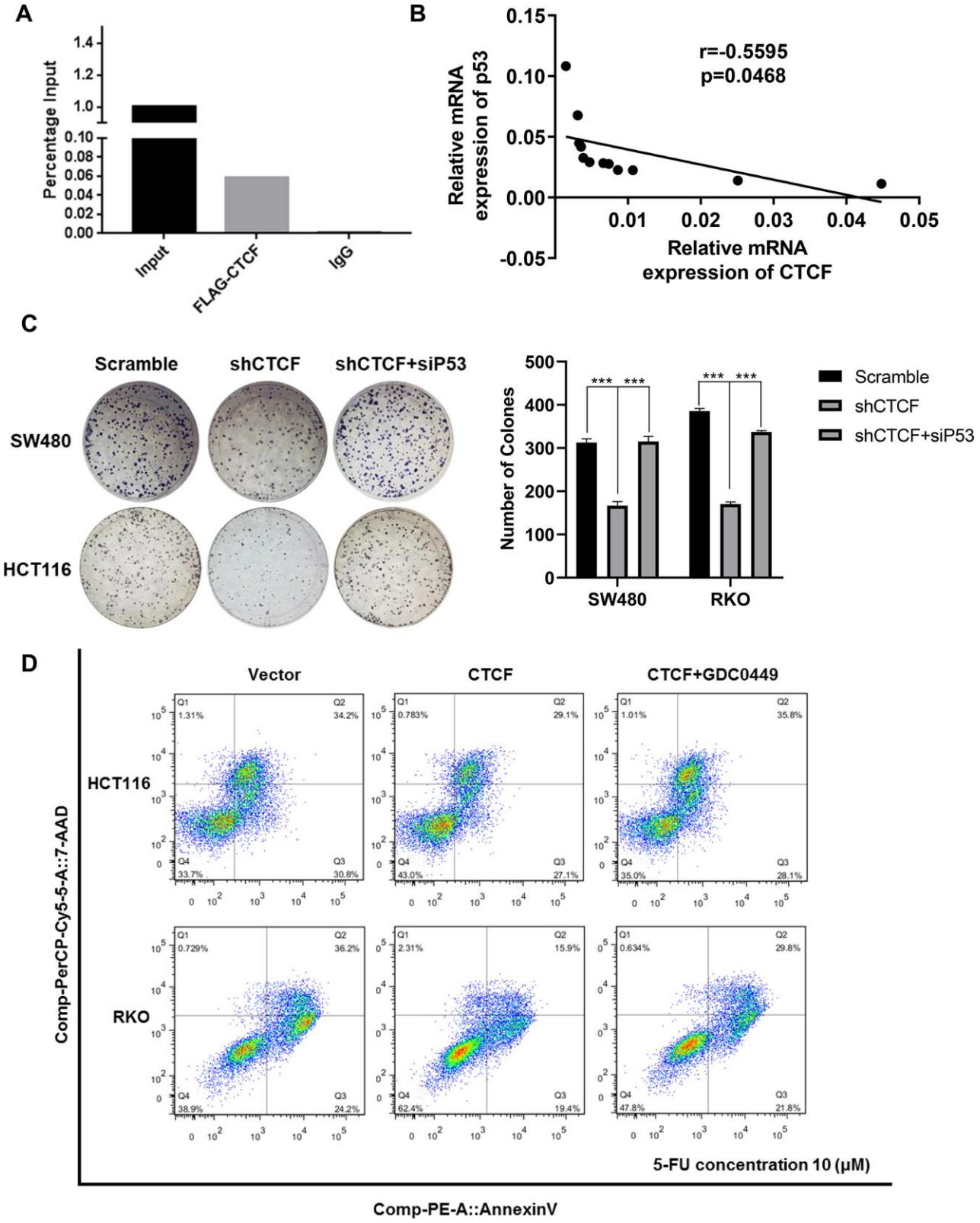

Supplementary Figure 6. CTCF facilitates CRC progression via P53-Hedgehog axis. (**A**) ChIP-qPCR results for CTCF on the CBS in HCT116 cells. (**B**) Spearman correlation analysis between relative CTCF and P53 mRNA expression in 13 fresh human CRC specimens. (**C**) Cell proliferative capacity was tested by colony formation assays and the representative images of colony formation assays from different experimental groups are shown. (**D**) The representative images of apoptotic assays from different experimental groups with or without administration of GDC-0449 are shown. The above data are presented as mean ± SEM. * P<0.05, **P<0.01, and ***P<0.001.

Supplementary Table

Supplementary Table 1. Primer sequences used for real-time PCR or ChIP-PCR (5′ to 3′).

Gene	Forward primer	Reverse primer
GAPDH	CGAGCCACATCGCTCAGACA	GTGGTGAAGACGCCAGTGGA
CTCF	CCCAAACAGAACCAGCCAAC	TCCTCTTCCTCTCCCTCTGC
ABCG2	CTCTTCTTCCTGACGACCAACCA	ATGACACTCTGTAGTATCCGCTGAT
TP53	CAGCACATGACGGAGGTTGT	TCATCCAAATACTCCACACGC
CTCF-CBS	CATTGTTGTATTCCTGAGTGCC	GAGTCCCGCGGTAAT TCTT

Research Paper

Knockdown of TXNDC9 induces apoptosis and autophagy in glioma and mediates cell differentiation by p53 activation

Tingting Zheng[1,*], Keke Chen[1,2,*], Xue Zhang[1,2,*], Huanhuan Feng[3], Yu Shi[1], Li Liu[1], Jun Zhang[4], Yun Chen[1,2]

[1]Shenzhen Key Laboratory for Drug Addiction and Medication Safety, Department of Ultrasound, Peking University Shenzhen Hospital, Shenzhen Peking University, The Hong Kong University of Science and Technology Medical Center, Shenzhen, Guangdong Province, China
[2]Clinical College of Shenzhen Hospital, Peking University, Anhui Medical University, Shenzhen, Guangdong Province, China
[3]School of Materials Science and Engineering, Harbin Institute of Technology Shenzhen, Shenzhen, Guangdong Province, China
[4]Queensland Micro- and Nanotechnology Centre, Griffith University, Brisbane, Australia
*Equal contribution

Correspondence to: Yun Chen; **email:** prof_yunchen@yeah.net, https://orcid.org/0000-0001-6442-4345
Keywords: glioma, TXNDC9, apoptosis, autophagy, differentiation
Received: April 17, 2020 **Accepted:** July 21, 2020 **Published:** September 8, 2020

ABSTRACT

Glioma is the most common malignant brain tumor. Because of its high degree of malignancy, the effect of surgical treatment, radiotherapy, chemotherapy, or immunotherapy is not ideal. TXNDC9 belongs to thioredoxin domain-containing proteins, which is involved in tumor progression. However, no research associated with TXNDC9 has been reported in glioma. In this study, we found that TXNDC9 was upregulated in glioma. Knockdown of TXNDC9 would prevent proliferation and metastasis, induce the apoptosis rate of glioma cells, and promote the expression Cleaved-caspase3, Cleaved-caspase8, Cleaved-caspase9. Meanwhile, knockdown of TXNDC9 induced autophagy by increasing the level of LC3 and Beclin-1. Cell morphology and expression analysis of GFAP, Vimentin, verified that TXNDC9 could regulate glioma cell differentiation. During this program, the expression of p53 changes dramatically. The apoptosis, autophagy, and cell differentiation program were blocked by p53 inhibitor treatment. In conclusion, the silencing of TXNDC9 induces apoptosis and autophagy in glioma and promotes cell differentiation by controlling p53 and may function as a new mechanism in glioma.

INTRODUCTION

Glioma is the most frequent primary tumor in the brain [1]. It has the characteristics of high incidence, invasive growth, and recurrence [2, 3]. It has become a significant problem affecting human health. Therefore, it is essential to investigate the mechanism involved in the development and progression of glioma.

The proliferation of tumor cells is regulated by programmed cell death. Autophagy and apoptosis are two forms of programmed cell death [4]. They have significant differences in morphology and function, but there are also many connections, which are related to the activation, expression, and regulation of a series of genes. It was reported that Licarin A induces autophagy and apoptosis in NSCLC cells [5]. Allavena G et al. found that targeting translational machinery can be made for the elimination of autophagy-deficient cells through the CASP8-dependent apoptotic signal pathway in NSCLC cells [6]. W09 would promote autophagy-dependent cell

apoptosis by regulating the Ras/MAPK signal pathway [7]. The silencing of cadherin-17 enhances apoptosis and inhibits autophagy in colorectal cancer cells [8]. With the deepening of research, more and more studies have proved that there is a specific relationship between apoptosis and autophagy. Whether autophagy can be regulated or not is closely related to the growth and apoptosis of tumor cells.

A malignant tumor is a common clinical disease, which seriously threatens people's life and quality of life. Since Pierce et al. first discovered that mouse testicular teratoma cells could spontaneously differentiate into normal cells in 1960, more and more studies have shown that dedifferentiated tumor cells can also be induced and re-differentiated into normal cells under the action of differentiation inducers, and their biological characteristics gradually move closer to normal cells and even transform into normal cells. It was reported that miR-146a/TRAF6 induced Th17 cell differentiation to control cervical cancer cell growth and apoptosis via NF-κB signaling [9]. NELL1 could regulate cell differentiation in lung cancer [10]. EGFR/AKT signaling pathway involved in ovarian cancer cell differentiation via regulating TSA [11].

Thioredoxin domain-containing 9 (TXNDC9) belongs to the TNX family. Recently research found that TXNDC9 benefited oxaliplatin resistance via regulation of autophagy and apoptosis in colorectal adeno-carcinoma [12]. TXNDC9 also accelerated the development of prostate cancer via regulating oxidative stress-induced androgen receptor signaling [13]. TXNDC9 facilitated the program of hepatocellular carcinoma [14]. TXNDC9 might be a potential bio-markers in Alzheimer's disease diagnosis [15].

In this study, we stated that TXNDC9 would be a tumor-associated gene, which involved in the development of glioma. Knockdown of TXNDC9 could prevent tumor program, induce apoptosis, and autophagy in U87 and U251 cells. Moreover, TXNDC9 prompted differentiation in U87 and U251 cells through the p53 signal pathway.

RESULTS

TXNDC9 was up-regulated in glioma tissues and cells

To explore the role of TXNDC9 in glioma, we first detected the expression of TXNDC9 in glioma tissue and normal tissue. The results showed that the mRNA and protein expression level of TXNDC9 was an upregulation in tumors compared with normal tissues (Figure 1A, 1B). Then we measured the mRNA and protein level of TXNDC9 in different human glioma cell lines (LN18, U87, U118, T98, U251) and human astrocytes (NHA) was used as a control. Compared with NHA, the expression of TXNDC9 was up-regulated in all glioma cell lines (Figure 1C, 1D).

Effects of TXNDC9 on cell metastasis and apoptosis in U87 and U251 cells

For further study, we constructed siRNA (si-TXNDC9) for inhibiting the function of TXNDC9, si-NC (negative control) was described as control. The clone formation experiment showed si-TXNDC9 reduced the number of clones (Figure 2A). Then we discussed the effect of TXNDC9 on glioma cell migration and invasion. Wound healing assay and transwell showed that si-TXNDC9 significantly inhibited cell migration and invasion (Figure 2B, 2C). After transfection with si-TXNDC9/si-NC, the cell apoptosis rate was measured by flow cytometry; the results showed that the percent of apoptosis cell was significantly increased in the si-TXNDC9 group (Figure 2D). Then the cell cycle assay was performed. The knockdown of TXNDC9 blocked cells from the G0 phase to the S phase (Figure 2E). Next, we determined the Caspase3 activity with the Caspase 3 Activity Assay Kit. The loss function of TXNDC9 induced caspase3 activation (Figure 2F). In previous studies, p53 played an essential role in regulating tumor progression [16–18]. Then we evaluated the expression of p53 in cells after transfecting with si-TXNDC9/si-NC; Down-regulated of TXNDC9 induced expression of p53 increased, and the apoptosis-associated protein (Cleaved-caspase3, Cleaved-caspase8, and Cleaved-caspase9) (Figure 2G).

Effects of TXNDC9 on cell autophagy in U87 and U251 cells

Autophagy degrades itself through the lysosome pathway, which is of considerable significance to the survival, development, balance, and differentiation of cells, and plays a protective role in the body. In the local hypoxic microenvironment of the tumor, it will promote the occurrence of autophagy. We constructed LC3 fused to green fluorescent protein (GFP-LC3) and transfected it into U87 and U251 cells. After transfection si-TXNDC9/si-NC, we found that knock-down of TXNDC9 induced the up-regulated of LC3, which showed induction of autophagy (Figure 3A). Beclin-1, LC3-I, and LC3-II were detected by western blot analysis, and the conversion of LC3 was demonstrated by LC3-II/LC3-I ratio. The results showed that si-TXNDC9 promoted the level of Beclin-1 and LC3-II/LC3-I (Figure 3B). In summary, si-TXNDC9 could induce autophagy in U87 and U251 cells.

Differentiation of U87 and U251 cells by TXNDC9

Inducing tumor cells to differentiate into normal cells or nearly normal cells has become a hot spot in the research of antineoplastic drugs. In vitro studies have shown that tumor cells can differentiate under the induction of some preparations, some have a normal phenotype, and some have restored some functions of normal cells. U87 and U251 cells observed by microscope showed that knockdown of TXNDC9 induced a significant change in structural morphology. Compared with the si-NC group, the shape of U87 and U251 glioma cells were long fusiform, the processes increase and become longer, and differentiate obviously, similar to normal astrocytes. (Figure 4A). We also explored whether morphology changed was corrective with GFAP expression; the image showed that si-TXNDC9 induced morphology changed accompanied by up-regulating of GFAP (Figure 4B). Vimentin and GFAP were indicated as markers of early and late glial differentiation [19], western blot results revealed that knockdown of TXNDC9 inhibited the expression of vimentin and promoted the expression of GFAP (Figure 4C). Taken together, knockdown of TXNDC9 would facilitate the differentiation of U87 and U251 cells.

TXNDC9 regulates procession of glioma cells via controlling p53

Based on the above results, we explored the mechanism of TXNDC9 in U87 and U251 cells. P53 has been deeply studied in a variety of human tumors. Most researchers believed that p53 is closely related to tumor

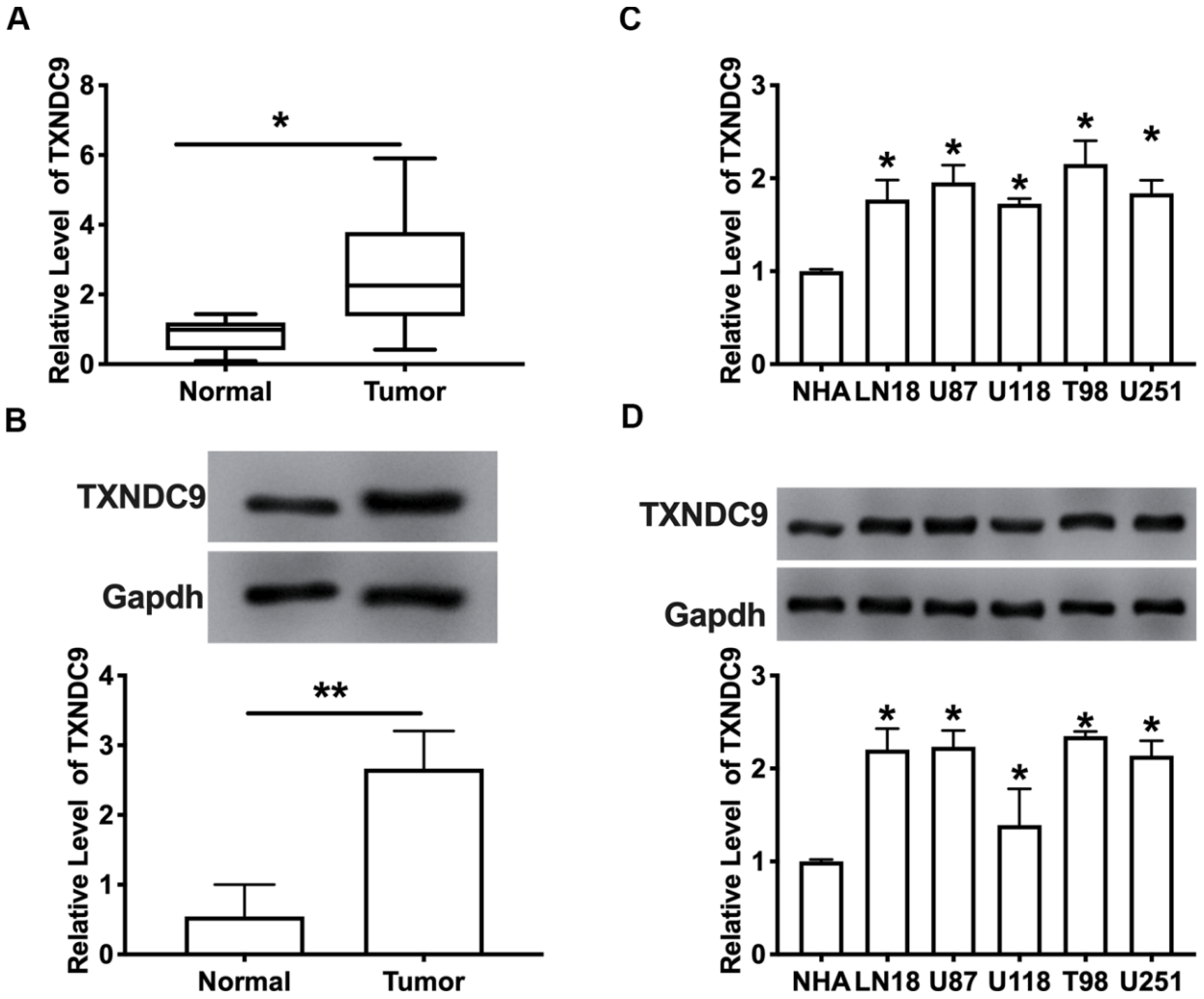

Figure 1. TXNDC9 was upregulated in glioma tissues and cells. (**A**) The mRNA level of TXNDC9 in tumor and normal samples was detected by RT-PCR. n=40, *P<0.05. (**B**) The protein level of TXNDC9 in tumor and normal samples was detected. n=6, *P<0.05. (**C**) The mRNA level of TXNDC9 in different glioma cell lines (LN18, U87, U118, T98, U251) were detected by RT-PCR. NHA cell was indicated as a control. n= 6, *P<0.05. (**D**) The protein level of TXNDC9 in different glioma cell lines. n= 4, *P<0.05.

invasion and metastasis and, to a certain extent, associated with the prognosis of patients. In previous studies, we found that si-TXNDC9 would induce the expression of p53 (Figure 2G). The U87 and U251 cells were treated with 10 μM p53 inhibitor (PFTα) for 48 h. As Figure 5A shown, PFTα additional treatment prevented the inhibition of si-TXNDC9 on the colony formation. Wound healing and transwell assay results showed that PFTα would restore the ability of migration and invasion (Figure 5B, 5C). In Figure 5D, PFTα additional treatment decreased the apoptosis rate. Meanwhile, si-TXNDC9 induced the expression of apoptosis-related protein that was inhibited by PFTα treated (Figure 5E).

PFTα also altered the fluorescence intensity of LC3 and decreased the level of Beclin-1 and the ratio of LC3-II/LC3-I (Figure 6A, 6B). Observed morphology through a microscope, PFTα reversed the change caused by si-TXNDC9 (Figure 6C). The level of vimentin and GFAP also showed that PFTα made cells in a state of low differentiation (Figure 6D). In conclusion, TXNDC9 involved in apoptosis, autophagy, and differentiation of glioma cells via regulating p53.

DISCUSSION

In this study, we found the up-regulated of TXNDC9 in U87 and U251 glioma cells. Knockdown of TXNDC9 could prevent cell metastasis and induced apoptosis, which was indicated by increasing the level of apoptosis-associated proteins. Meanwhile, the Knockdown of TXNDC9 could induce autophagy, which was described by the up-regulated of Beclin-2

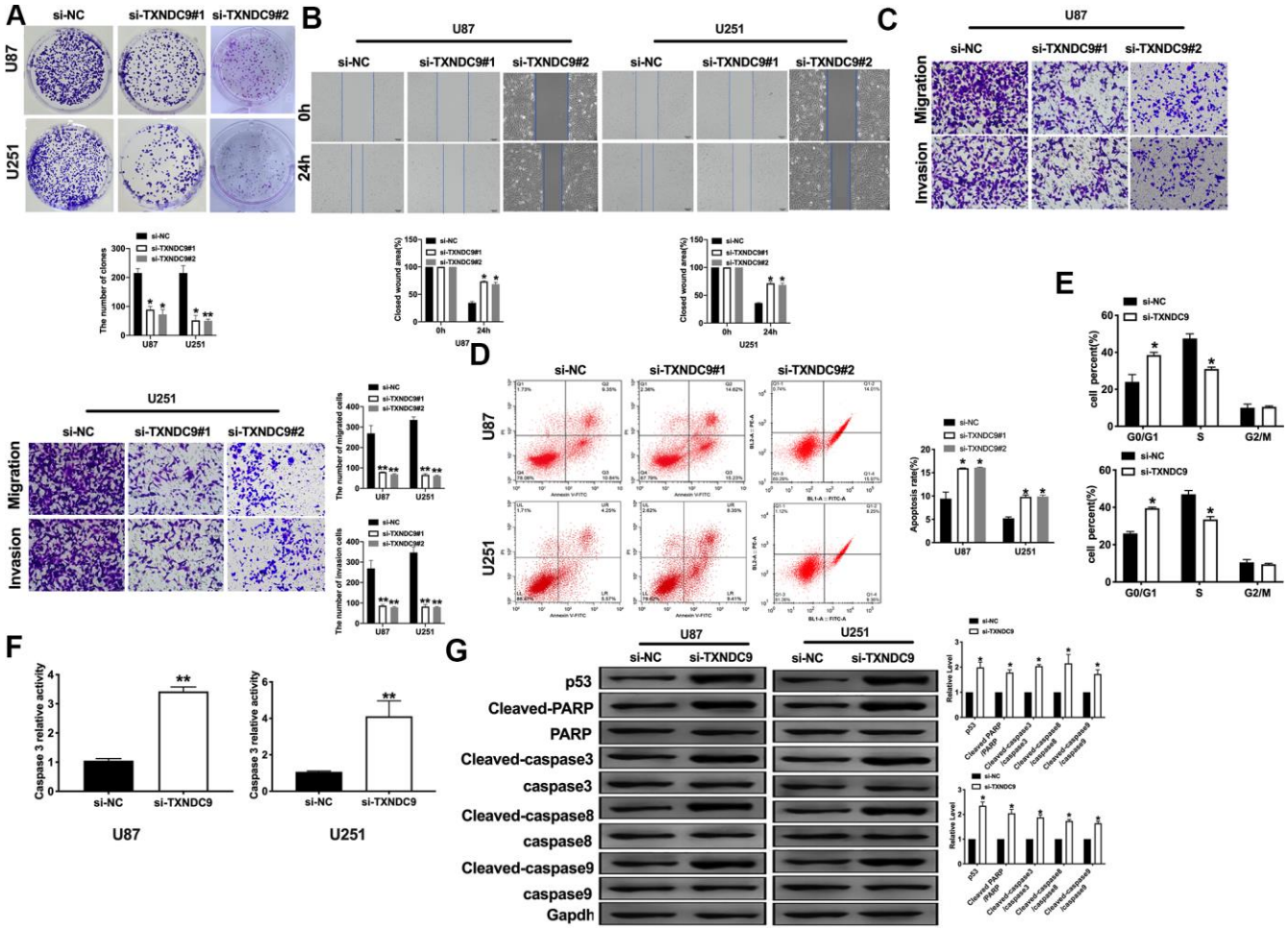

Figure 2. Knockdown of TXNDC9 prevented proliferation and induced apoptosis of U87 cells. (**A**) The colony formation assay. (**B**, **C**) Wound healing assay and transwell were performed for detecting the effect of TXNDC9 on migration and invasion. (**D**) The apoptosis rate of U87 and U251 cells were measured by flow cytometry. The histogram at the right is a statistical graph. n=4, *P<0.05. (**E**) Flow cytometry was performed to determine the cell cycle in U87 and U251 cells after transfection si-TXNDC9/si-NC. n= 4, *P<0.05. (**F**) The caspase3 activity of U87 and U251 cells was evaluated by the caspase3 activity kit. n= 6, **P<0.01. (**G**) The protein level of p53, Cleaved-caspase3, Cleaved-caspase8, and Cleaved-caspase9 were detected by western blot, Gapdh was indicated as a loading control. n= 6, *P<0.05.

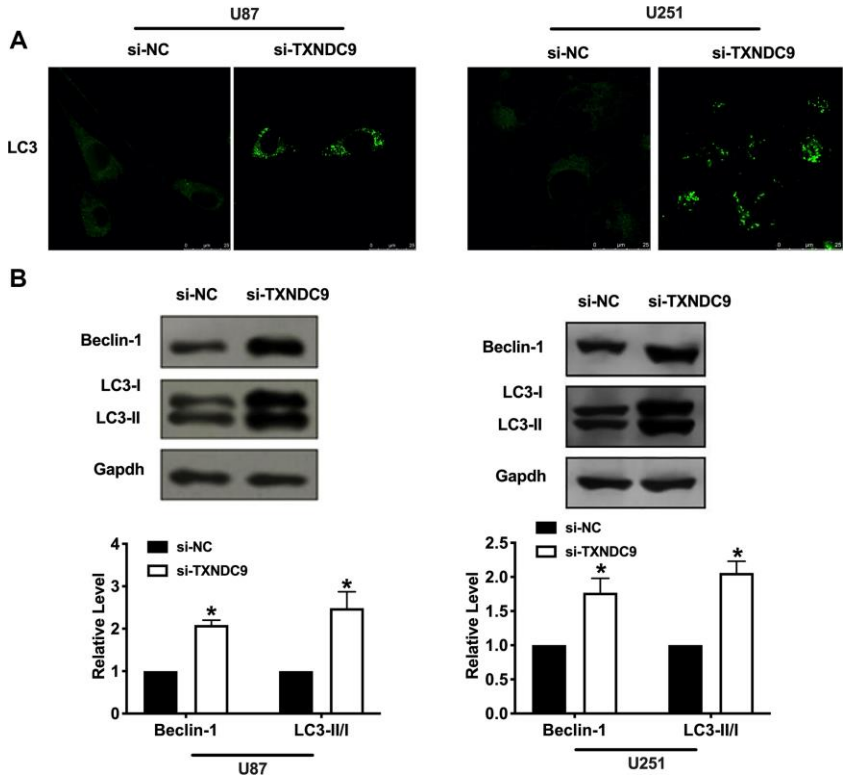

Figure 3. Knockdown of TXNDC9 promoted autophagy in U87 cells. (**A**) The level of GFP-LC3 and localization in U87 and U251 cells after transfecting with si-TXNDC9/si-NC. Representative immunofluorescence images were shown. (**B**) The protein level of Beclin-1 and LC3-I/II was detected in U87 and U251 cells, Gapdh was indicated as a loading control. n= 6, *P<0.05.

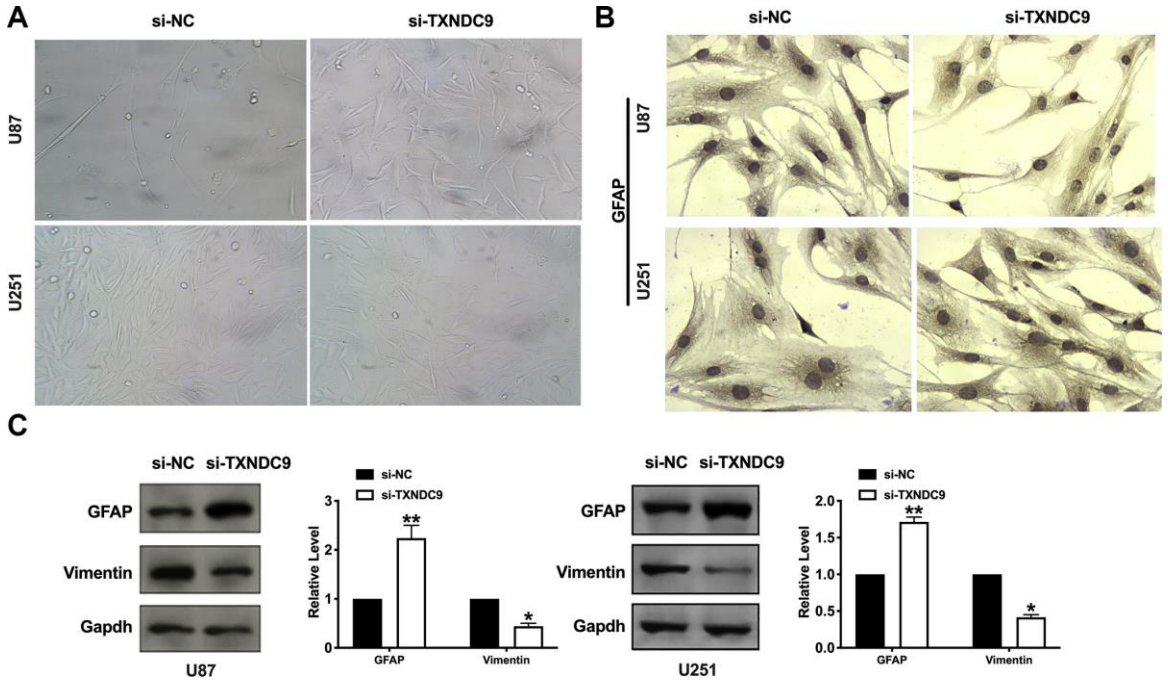

Figure 4. Knockdown of TXNDC9 induced differentiation of glioma cells. (**A**) U87 cell morphology was scanned after transfecting with si-TXNDC9/si-NC. (**B**) The immunocytochemical assay was performed for GFAP expression. (**C**). The protein level of vimentin and GFAP were measured in U87 and U251 cells, Gapdh was indicated as a loading control. n= 6, *P<0.05, **P<0.01.

and the LC3-II/LC3-I ratio. As the morphological changed and increasing vimentin, GFAP, si-TXNDC9 induced differentiation of U87 and U251 cells. During this program, the activation of p53 played a key role.

In recent years, intracranial tumors account for an increasing proportion of nervous system diseases, of which glioma accounts for more than half. Patients with low-grade glioma still cannot avoid recurrence after treatment. Still, for patients with high-level glioma, it brings specific challenges to clinical workers and patients whether to treat and what kind of treatment to take [20, 21]. Even if surgery plus radiotherapy and chemotherapy are adopted, the prognosis is not optimistic in the later stage [22]. This is not only an excellent challenge for clinical workers and researchers at home and abroad but also a heavy burden for patients and their families [23]. But the research on glioma has not stopped.

Inducing tumor cell apoptosis and autophagy is a convenient means to inhibit tumor development [24, 25]. Tumor suppressor p53 family proteins widely regulate phagocytosis, apoptosis, cell cycle, metabolism, DNA repair, and so on. They all play an inhibitory role in the tumor. P53 is down-regulated or deleted in most human tumors. The regulation of p53 on autophagy is related to its spatial distribution and plays a dual role. P53 in the nucleus mainly inhibits mTOR and induces autophagy through AMPK and TSC1/2 pathways [26]. P53 also induces tumor suppressor gene PTEN to inhibit PI3K/AKT signal pathway, induce apoptosis, and inhibit cancer cell migration [27]. Polychlorinated biphenyl quinone induced signaling

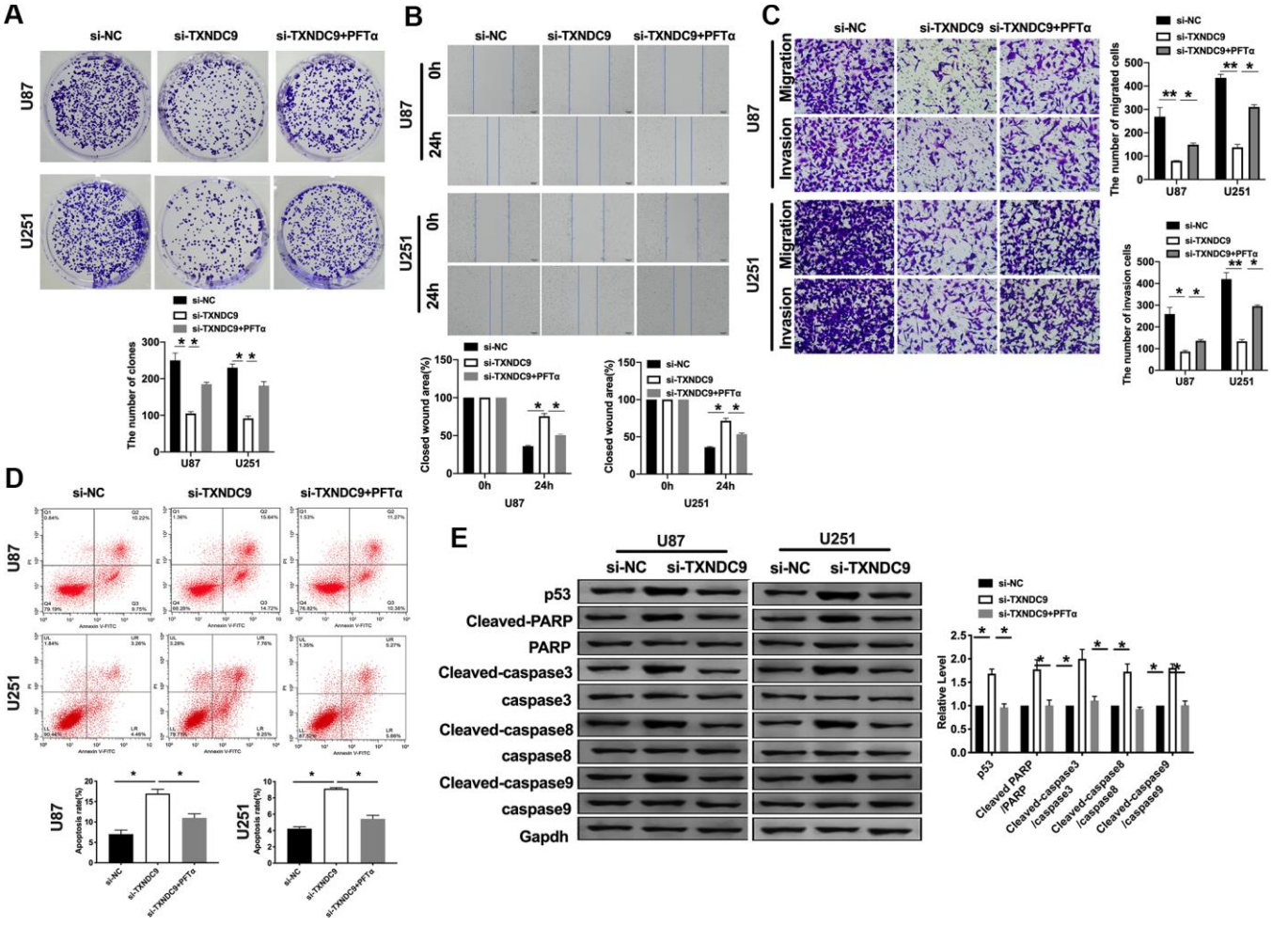

Figure 5. TXNDC9 regulated glioma program via controlling p53. (**A**) The colony formation assay. (**B**, **C**) Wound healing assay and transwell were performed for detecting the effect of p53 on migration and invasion. (**D**) The apoptosis rate of U87 and U251 cells was measured after si-TXNDC9/si-NC transfection and PFTα treatment. The histogram at the right is a statistical graph. n=6, *P<0.05. (**E**) The protein level of p53, Cleaved-caspase3, Cleaved-caspase8, and Cleaved-caspase9 were detected by western blot, Gapdh was indicated as a loading control. n= 6, *P<0.05.

transition from autophagy to apoptosis is regulated via p53 in human hepatoma HepG2 cells [28].

At present, inducing tumor cell differentiation is an effective way of treatment, and some key issues regulating the signal pathway of tumor cell differentiation are gradually being clarified: the entanglement and dialogue between different signal pathways; the preventive and regulatory effects of various kinases on different stimuli in the signal pathway; and the dose-effect and the time-effect relationship between cell differentiation and signal kinase activation. It was reported that notch signaling regulates oral neoplasm cell differentiation [29]. Inhibition of the EGFR/AKT signaling pathway promotes ovarian cancer cell differentiation via regulating TSA [11]. Prostaglandin E2 promotes immune escape via the inhibition of natural killer cell differentiation [30]. In our study, we found that TXNDC9 can affect the differentiation of glioma cells.

TXNDC9 is a member of the thioredoxin family. It can bind to ATP and maintain the redox state in the cell. The TXNDC9 gene is located at 2q11.2. It consists of 17,374 base pairs. It encodes a protein with a molecular weight of 27 ku and contains 226 amino acid residues. The protein is distributed in the cytoplasm. It includes the N-terminal and acidic C-terminal of the helical structure. It gets its name because it contains the same domain as thioredoxin in the center. In recent years, studies have found that. Many members of the Thioredoxin family are mainly involved in the redox reaction of the body. It is highly expressed in many solid tumors such as liver cancer [14], colon cancer [31], breast cancer [32] and so on. Other experiments showed that TXNDC9 was up-regulated in some

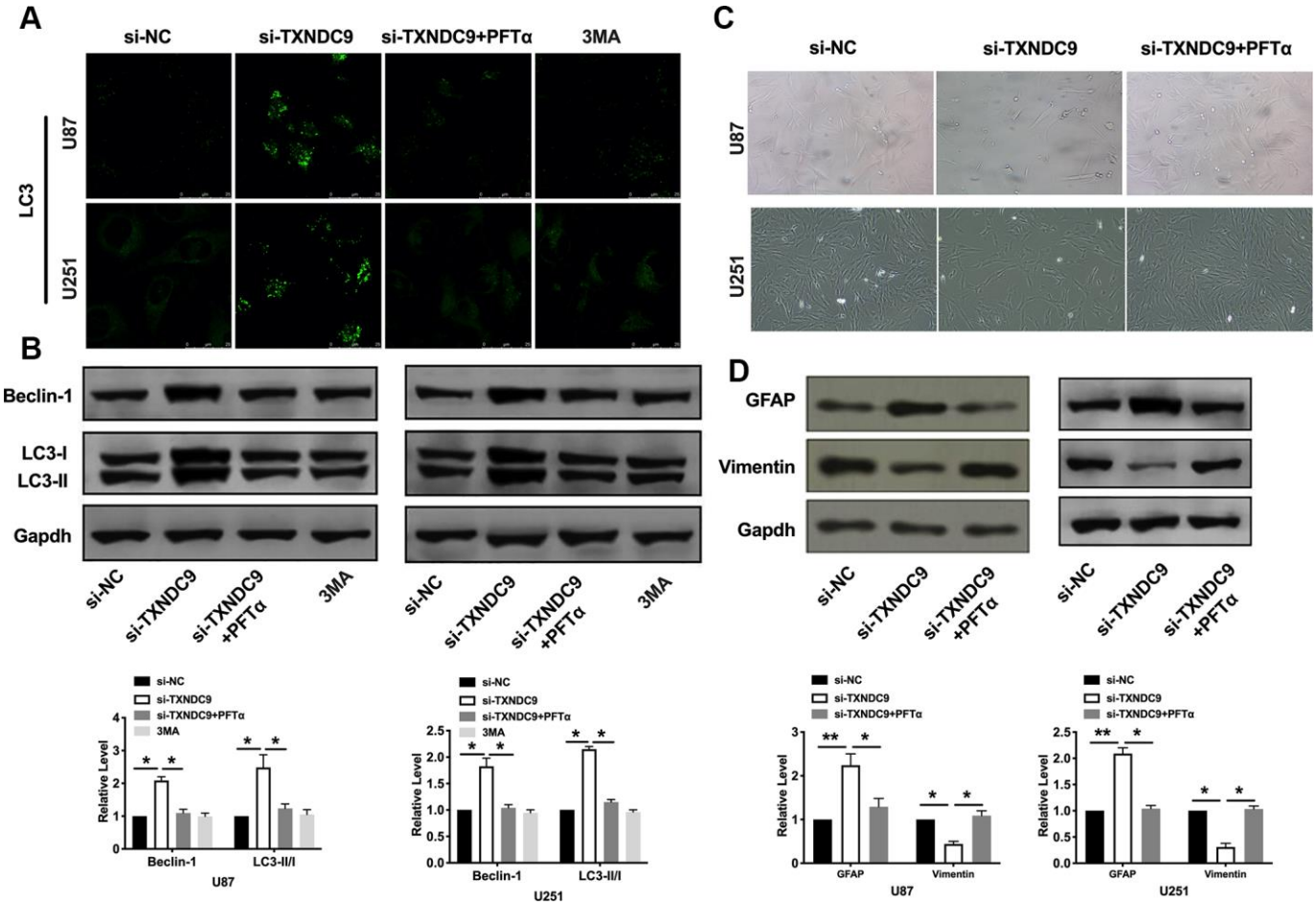

Figure 6. TXNDC9 regulated glioma autophagy and differentiation via controlling p53. (**A**) The level of LC3 and localization in U87 and U251 cells after si-TXNDC9/si-NC transfection, PFTα, and 3MA (5 mM) treatment. Representative immunofluorescence images were shown. (**B**) The protein level of Beclin-1 and LC3-I/II was detected in U87 and U251cells; Gapdh was indicated as a loading control. n= 6, *P<0.05. (**C**) U87 and U251 cell morphology were scanned after si-TXNDC9/si-NC transfection and PFTα treatment. (**D**) The protein level of vimentin and GFAP were measured in U87 and U251 cells, Gapdh was indicated as a loading control. n= 6, *P<0.05, **P<0.01.

oxaliplatin-resistant strains. At present, there are few studies on the role of TXNDC9 protein in eukaryotic cells. The specific function of the protein is not known. The expression and function of TXNDC9 in glioma cells have not been reported.

In this study, for the first, the function of TXNDC9 was revealed in glioma cells. Knockdown of TXNDC induced apoptosis and autophagy of glioma cells and promoted differentiation through regulating p53.

MATERIALS AND METHODS

Clinical samples

The tumor samples were collected from 35 glioma patients at Peking University Shenzhen Hospital. The characteristics of the 35 cases of newly diagnosed glioma patients involved in the study cohort. The mean age was 51.5 years, with a range of 24 to 79. There were 21 (60%) males and 14 (40%) females. According to the WHO classifications in 2007, 7 (20%),13(37.1%), 10 (28.6%), and 5 (14.3%) of 35 glioma patients were classified as WHO grade I, II, III, and IV. The normal tissues were collected from paired adjacent tissues. All of the patients or their guardians provided written consent. This research has got the approval of the Medical Ethics Committee of Peking University Shenzhen Hospital, and this study is in line with the Declaration of Helsinki.

Cell culture

The cell lines (NHA, LN18, U87, U118, T98, U251) were purchased from the Science Cell Laboratory. Cell lines were cultured in PRIM 1640 (Thermo-life, United States) with 10 % FBS (Thermo Fisher, USA) and 100 μL/mL penicillin and streptomycin (Beyotime, China) and placed at 37°C with 5% CO2. The cells were treated with 10 μM p53 inhibitor, Pifithrin-α (PFTα) (Selleck, USA) for 48 h and 5mM 3MA for 12 h.

Western blot

Total protein was collected from cells with RIPA lysis Mix (Beyotime, China). Briefly, 60 μg protein extraction was loaded via SDS-PAGE and transferred onto nitrocellulose membranes (MILLIPORE, USA), then put them into a 5% blocking solution for 3 h. The membranes were incubated with primary antibodies at 4 °C for one night. After incubation with secondary antibodies, the membranes were scanned using an Odyssey, and data were analyzed with Odyssey software (LI-COR, USA). p53 (60283-2-Ig, 1:500), Cleaved-caspase3 25546-1-AP, 1:500), LC3I/II(14600-1-AP, 1:1000), Beclin-1 (11306-1-AP, 1:500), Vimentin (60330-1-Ig, 1:500) and GFAP (16825-1-AP, 1:500) were purchased from proteintech; Cleaved-caspase8 (WL0153,1:500), Cleaved-caspase9 (WL01838, 1:500) were purchased from Wanlei (Wanleibio, China), Gapdh (60004-1-Ig, 1:2000) was used as an internal control.

Real time-PCR

Total RNA was isolated from glioma cells according to a standard protocol. And then, the purity and concentration of RNA were detected, and all the samples were converted into cDNA using reverse transcription kit. We used SYBR Green (Thermo Fisher Scientific) system to perform the qRT-PCR. Data were analyzed by GraphPad 7.

Wound-healing assay

The wound-healing assay was carried out on U87 and U251 cells. 5 $\times 10^5$ cells were cultured in trans-well plates, and then the cells were gently scratched with a pipette tip. The fresh medium was changed. After columbamine treatment, the scratched spaces on the plate were evaluated by microscopy.

Matrigel invasion assay

Cells in the logarithmic growth phase were adjusted to 2 $\times 10^5$ cells/well of medium (without serum) and plated 1μg/μl Matrigel into the upper chamber. The lower chamber was added with 500 μL of the medium, and then incubate the plate at 37°C for 48 h. Then the invading cells were visualized by the crystal violet and inverted microscope.

Immunocytochemistry

2×10^5 of U87 cells and U251 were cultured in 24-well plates. Then cells were fixed in paraformaldehyde (4%) for 0.5 h at room temperature. The endogenous peroxidase activity was abolished with H_2O_2 (3%) in methanol (10%)/PBS for 10 min, and 15 min for permeabilization with Triton X-100 (0.5%). After 1 h incubation with serum, it was added with primary mouse anti-GFAP antibody (16825-1-AP, 1:200) for 2 h. Cells were then incubated with diaminobenzidine substrate for 5 min and then finally counterstained with hematoxylin and mounted with glycerol (50%).

Confocal imaging

Cells were seeded in 24-well plates and transfected with GFP-LC3 for U87 and U251 cells. 24 h after transfection, the cells were transfected with siRNA for an additional 48 h. Cells were fixed with 4%

paraformaldehyde in PBS for 30 min at room temperature; the cells were mounted in anti-fading solution and stored at 4°C. The plates were examined under a laser microscope.

Caspase3 activity assay

Caspase3 activity assay was performed by the Caspase 3 Activity Assay Kit (Beyotime, China). Absorb the cell culture medium and set aside. The adherent cells were digested with trypsin and collected into a spare cell culture medium. The cells were collected by centrifugation at 600g at 4 °C for 5 minutes, and the supernatant was carefully removed. At the same time, no cells were absorbed as far as possible, and PBS was washed once. After absorbing the supernatant as before, add the lysate according to the proportion of 100 microliter lysate for every 2 million cells, re-suspension precipitation, ice bath cracking for 15 minutes. Operate according to instructions. Take out the right amount of Ac-DEVD-pNA (2mM) and set aside on the ice bath. Add Ac-DEVD-pNA (2mM) and mix well note. Incubate for 120 minutes at 37 °C. A405 can be determined when the color change is obvious. The A405 of the sample deducts the A405 of the blank control, that is, the absorbance produced by the pNA catalyzed by caspase 3 in the sample.

Cell apoptosis assay

The cells were counted about 5×105cells/mL. Then, 1 mL cells were centrifuged, 1000 rpm, 10 min, 4°C, and the medium was throw away. The cells were washed with PBS and dropped medium. The cells were resuspended and avoid light for 15 min, 200 μL Binding Buffer with 10 μL Annexin V-FITC, and 10 μL PI. Flow cytometry was used to measure the apoptosis rate within 1 h.

Cell cycle assay

Cells were collected with 1ml trypsin for 2min, suspension the cell with 5ml PBS, centrifuge at 1000 RPM for 5 min at 4°C. 10ml PBS buffer was used to re-washed and dropping medium, Then the cells were fixed with 70% ethanol overnight. The next day, the cell medium was filtered with a 300-mesh sieve, centrifuged at 1000 RPM at 4°C for 5min, and the supernatant was discarded. The cells were avoided light and fixed with 1ml PI solution and stated at 4°C for 30 min. Flow cytometer was used to evaluate the cell cycle.

Statistical analysis

All values are expressed as the mean ± SEM. Statistical significances were measured by Student's t-test and ANOVA. A two-tailed value of $P < 0.05$ was indicated as a statistically significant difference. Data statistics were used the GraphPad 7.0.

AUTHOR CONTRIBUTIONS

Tingting Zheng, Keke Chen, Xue Zhang designed and coordinated the study and prepared the manuscript. Huanhuan Feng and Yu Shi provided assistance in the design of the study and participated in manuscript preparation. Li Liu, Jun Zhang, and Yun Chen participated in data gathering. All authors have read and approved the content of the manuscript.

CONFLICTS OF INTEREST

The author reports no conflicts of interest in this work.

FUNDING

This work was supported by the National Natural Science Foundation (No.81901767, 81871358); Natural Science Foundation of Guangdong Province (No.2018M640807); Shenzhen Science and Technology Innovation Committee (JCYJ20180223181216494, JCYJ20180507183224565, JCYJ2017041217856582); China Postdoctoral Foundation (2018M640807); Ministry of Science and Technology (Key R & D Program) (No.2016YFC0104707); Griffith University-Peking University Collaborative Travel Grants Scheme, Project No. 036 Research Internal; Shenzhen Municipal Health Commission (No.SZSM201512026); Shenzhen Key Medical Discipline Construction Fund.

REFERENCES

1. Huang YT, Zhang Y, Wu Z, Michaud DS. Genotype-based gene signature of glioma risk. Neuro Oncol. 2017; 19:940–50. https://doi.org/10.1093/neuonc/now288 PMID:28339748
2. Ostrom QT, Bauchet L, Davis FG, Deltour I, Fisher JL, Langer CE, Pekmezci M, Schwartzbaum JA, Turner MC, Walsh KM, Wrensch MR, Barnholtz-Sloan JS. The epidemiology of glioma in adults: a "state of the science" review. Neuro Oncol. 2014; 16:896–913. https://doi.org/10.1093/neuonc/nou087 PMID:24842956
3. Wiedmann MK, Brunborg C, Di Ieva A, Lindemann K, Johannesen TB, Vatten L, Helseth E, Zwart JA. The impact of body mass index and height on the risk for glioblastoma and other glioma subgroups: a large prospective cohort study. Neuro Oncol. 2017; 19:976–85. https://doi.org/10.1093/neuonc/now272 PMID:28040713

4. Peters MA, Walenkamp AM, Kema IP, Meijer C, de Vries EG, Oosting SF. Dopamine and serotonin regulate tumor behavior by affecting angiogenesis. Drug Resist Updat. 2014; 17:96–104. https://doi.org/10.1016/j.drup.2014.09.001 PMID:25269824

5. Maheswari U, Ghosh K, Sadras SR. Licarin a induces cell death by activation of autophagy and apoptosis in non-small cell lung cancer cells. Apoptosis. 2018; 23:210–25. https://doi.org/10.1007/s10495-018-1449-8 PMID:29468481

6. Allavena G, Cuomo F, Baumgartner G, Bele T, Sellgren AY, Oo KS, Johnson K, Gogvadze V, Zhivotovsky B, Kaminskyy VO. Suppressed translation as a mechanism of initiation of CASP8 (caspase 8)-dependent apoptosis in autophagy-deficient NSCLC cells under nutrient limitation. Autophagy. 2018; 14:252–268. https://doi.org/10.1080/15548627.2017.1405192 PMID:29165042

7. Zhang P, Zheng Z, Ling L, Yang X, Zhang N, Wang X, Hu M, Xia Y, Ma Y, Yang H, Wang Y, Liu H. W09, a novel autophagy enhancer, induces autophagy-dependent cell apoptosis via activation of the EGFR-mediated RAS-RAF1-MAP2K-MAPK1/3 pathway. Autophagy. 2017; 13:1093–112. https://doi.org/10.1080/15548627.2017.1319039 PMID:28513279

8. Tian X, Han Z, Zhu Q, Tan J, Liu W, Wang Y, Chen W, Zou Y, Cai Y, Huang S, Chen A, Zhan T, Huang M, et al. Silencing of cadherin-17 enhances apoptosis and inhibits autophagy in colorectal cancer cells. Biomed Pharmacother. 2018; 108:331–37. https://doi.org/10.1016/j.biopha.2018.09.020 PMID:30227326

9. Li T, Li M, Xu C, Xu X, Ding J, Cheng L, Ou R. miR-146a regulates the function of Th17 cell differentiation to modulate cervical cancer cell growth and apoptosis through NF-κB signaling by targeting TRAF6. Oncol Rep. 2019; 41:2897–908. https://doi.org/10.3892/or.2019.7046 PMID:30864722

10. Zhai Y, Wei R, Sha S, Lin C, Wang H, Jiang X, Liu G. Effect of NELL1 on lung cancer stem-like cell differentiation. Oncol Rep. 2019; 41:1817–26. https://doi.org/10.3892/or.2019.6954 PMID:30628703

11. Shao G, Lai W, Wan X, Xue J, Wei Y, Jin J, Zhang L, Lin Q, Shao Q, Zou S. Inactivation of EGFR/AKT signaling enhances TSA-induced ovarian cancer cell differentiation. Oncol Rep. 2017; 37:2891–96. https://doi.org/10.3892/or.2017.5556 PMID:28393191

12. Zhou W, Fang C, Zhang L, Wang Q, Li D, Zhu D. Thioredoxin domain-containing protein 9 (TXNDC9) contributes to oxaliplatin resistance through regulation of autophagy-apoptosis in colorectal adenocarcinoma. Biochem Biophys Res Commun. 2020; 524:582–588. https://doi.org/10.1016/j.bbrc.2020.01.092 PMID:32029274

13. Feng T, Zhao R, Sun F, Lu Q, Wang X, Hu J, Wang S, Gao L, Zhou Q, Xiong X, Dong X, Wang L, Han B. TXNDC9 regulates oxidative stress-induced androgen receptor signaling to promote prostate cancer progression. Oncogene. 2020; 39:356–67. https://doi.org/10.1038/s41388-019-0991-3 PMID:31477836

14. Chen D, Zou J, Zhao Z, Tang X, Deng Z, Jia J, Liu S. TXNDC9 promotes hepatocellular carcinoma progression by positive regulation of MYC-mediated transcriptional network. Cell Death Dis. 2018; 9:1110. https://doi.org/10.1038/s41419-018-1150-4 PMID:30382079

15. Wang Y, Wang Z. Identification of dysregulated genes and pathways of different brain regions in Alzheimer's disease. Int J Neurosci. 2020; 1-13. https://doi.org/10.1080/00207454.2020.1720677 PMID:32019384

16. Karakostis K, Fåhraeus R. Shaping the regulation of the p53 mRNA tumour suppressor: the co-evolution of genetic signatures. BMC Cancer. 2019; 19:915. https://doi.org/10.1186/s12885-019-6118-y PMID:31519161

17. Muñoz-Fontela C, Mandinova A, Aaronson SA, Lee SW. Emerging roles of p53 and other tumour-suppressor genes in immune regulation. Nat Rev Immunol. 2016; 16:741–50. https://doi.org/10.1038/nri.2016.99 PMID:27667712

18. Bykov VJ, Eriksson SE, Bianchi J, Wiman KG. Targeting mutant p53 for efficient cancer therapy. Nat Rev Cancer. 2018; 18:89–102. https://doi.org/10.1038/nrc.2017.109 PMID:29242642

19. Zhou R, Skalli O. TGF-alpha differentially regulates GFAP, vimentin, and nestin gene expression in U-373 MG glioblastoma cells: correlation with cell shape and motility. Exp Cell Res. 2000; 254:269–78. https://doi.org/10.1006/excr.1999.4762 PMID:10640425

20. GLASS Consortium. Glioma through the looking GLASS: molecular evolution of diffuse gliomas and the Glioma Longitudinal Analysis Consortium. Neuro Oncol. 2018; 20:873–884. https://doi.org/10.1093/neuonc/noy020 PMID:29432615

21. Jones C, Karajannis MA, Jones DT, Kieran MW, Monje M, Baker SJ, Becher OJ, Cho YJ, Gupta N, Hawkins C, Hargrave D, Haas-Kogan DA, Jabado N, et al. Pediatric

high-grade glioma: biologically and clinically in need of new thinking. Neuro Oncol. 2017; 19:153–61. https://doi.org/10.1093/neuonc/now101 PMID:27282398

22. Meel MH, Kaspers GJ, Hulleman E. Preclinical therapeutic targets in diffuse midline glioma. Drug Resist Updat. 2019; 44:15–25. https://doi.org/10.1016/j.drup.2019.06.001 PMID:31202081

23. Ellingson BM, Wen PY, Cloughesy TF. Evidence and context of use for contrast enhancement as a surrogate of disease burden and treatment response in Malignant glioma. Neuro Oncol. 2018; 20:457–71. https://doi.org/10.1093/neuonc/nox193 PMID:29040703

24. Ravegnini G, Sammarini G, Nannini M, Pantaleo MA, Biasco G, Hrelia P, Angelini S. Gastrointestinal stromal tumors (GIST): Facing cell death between autophagy and apoptosis. Autophagy. 2017; 13:452–463. https://doi.org/10.1080/15548627.2016.1256522 PMID:28055310

25. Patra S, Panigrahi DP, Praharaj PP, Bhol CS, Mahapatra KK, Mishra SR, Behera BP, Jena M, Bhutia SK. Dysregulation of histone deacetylases in carcinogenesis and tumor progression: a possible link to apoptosis and autophagy. Cell Mol Life Sci. 2019; 76:3263–82. https://doi.org/10.1007/s00018-019-03098-1 PMID:30982077

26. Vadlakonda L, Pasupuleti M, Pallu R. Role of PI3K-AKT-mTOR and Wnt signaling pathways in transition of G1-S phase of cell cycle in cancer cells. Front Oncol. 2013; 3:85. https://doi.org/10.3389/fonc.2013.00085 PMID:23596569

27. Bernard M, Yang B, Migneault F, Turgeon J, Dieudé M, Olivier MA, Cardin GB, El-Diwany M, Underwood K, Rodier F, Hébert MJ. Autophagy drives fibroblast senescence through MTORC2 regulation. Autophagy. 2020; 1-13. https://doi.org/10.1080/15548627.2020.1713640 PMID:31931659

28. Shi Q, Wang Y, Dong W, Song E, Song Y. Polychlorinated biphenyl quinone-induced signaling transition from autophagy to apoptosis is regulated by HMGB1 and p53 in human hepatoma HepG2 cells. Toxicol Lett. 2019; 306:25–34. https://doi.org/10.1016/j.toxlet.2019.02.002 PMID:30742880

29. Nakano K, Takabatake K, Kawai H, Yoshida S, Maeda H, Kawakami T, Nagatsuka H. Notch Signaling Affects Oral Neoplasm Cell Differentiation and Acquisition of Tumor-Specific Characteristics. Int J Mol Sci. 2019; 20:1973. https://doi.org/10.3390/ijms20081973 PMID:31018488

30. Park A, Lee Y, Kim MS, Kang YJ, Park YJ, Jung H, Kim TD, Lee HG, Choi I, Yoon SR. Prostaglandin E2 secreted by thyroid cancer cells contributes to immune escape through the suppression of natural killer (NK) cell cytotoxicity and NK cell differentiation. Front Immunol. 2018; 9:1859. https://doi.org/10.3389/fimmu.2018.01859 PMID:30140269

31. Lu A, Wangpu X, Han D, Feng H, Zhao J, Ma J, Qu S, Chen X, Liu B, Zheng M. TXNDC9 expression in colorectal cancer cells and its influence on colorectal cancer prognosis. Cancer Invest. 2012; 30:721–26. https://doi.org/10.3109/07357907.2012.732160 PMID:23210642

32. Garcia SA, Nagai MA. Transcriptional regulation of bidirectional gene pairs by 17-β-estradiol in MCF-7 breast cancer cells. Braz J Med Biol Res. 2011; 44:112–22. https://doi.org/10.1590/s0100-879x2010007500149 PMID:21180879

Priority Research Paper

p21 can be a barrier to ferroptosis independent of p53

Divya Venkatesh[1], Brent R. Stockwell[1,2], Carol Prives[1]

[1]Department of Biological Sciences, Columbia University, New York, NY 10027, USA
[2]Department of Chemistry, Columbia University, New York, NY 10027, USA

Correspondence to: Brent R. Stockwell, Carol Prives; **email:** bstockwell@columbia.edu, clp3@columbia.edu
Keywords: p21, ferroptosis, cancer, p53-independent, organ damage
Received: June 1, 2020 **Accepted:** August 3, 2020 **Published:** September 24, 2020

ABSTRACT

Traditionally, the p21 protein has been viewed as limiting cancer progression and promoting aging. In contrast, there are reports that p21 can enhance cancer survival and limit tissue damage, depending on the tissue of origin and type of stressor involved. Here, we provide evidence to support these latter two roles of p21 by exploring its ability to regulate ferroptosis. Ferroptosis is a form of cell death that is associated with certain degenerative diseases, some of which are aging-related. Our results reveal a correlation between p21 protein levels in cell lines that are resistant to ferroptosis (p21 high) versus cell lines that are sensitive and easily undergo ferroptosis (p21 low). We also show that p21 levels themselves are differentially regulated in response to ferroptosis in a p53-independent manner. Further, experimentally altering the abundance of p21 protein inverts the ferroptosis-sensitivity of both resistant and sensitive human cancer cell lines. Our data also indicate that the interaction of p21 with CDKs is crucial for its ability to restrict the progression of ferroptosis. While this study was performed in cancer cell lines, our results support the potential of p21 to aid in maintenance of healthy tissues by blocking the damage incurred due to ferroptosis.

INTRODUCTION

The tumor suppressor protein, p53 is a crucial factor in determining the response of cancer cells to drug treatment [1, 2]. Notably, p53 has been shown to induce different forms of cell death in cancers including ferroptosis [3–5], a form of iron-dependent cell death that results from lipid peroxidation [6]. Several reports have linked dysregulated ferroptotic death to various other diseases as well. Ferroptotic death has been implicated in multiple neurodegenerative disorders such as Huntington's, Alzheimer's, Parkinson's and ischemic stroke [7]. Excessive ferroptosis has also been shown to be a key effector of cardiomyopathy [8], renal damage and failure [9, 10] and can also potentially mediate the loss of immunity against infection [11]. Each one of the abovementioned cases has been linked to aging-related disorders.

While several reports have demonstrated the ability of p53 to modulate the ferroptotic sensitivity of cancer cells, the directionality of this regulation is complex and context-specific, which is not unlike the other known stress-responses of p53 [5]. Therefore, as most of the differential responses of p53 to other stresses depend on its activation of appropriate target genes, we have examined the ability of p53 target genes to regulate ferroptosis. Since p53 can also promote premature aging [12, 13], neurodegenerative disorders [14–16] and developmental syndromes [17, 18] through its target genes, such a study would also give further insight into understanding the regulation of ferroptosis in these contexts. In line with this goal, we recently discovered that two key proteins of the p53 network, MDM2 and MDMX (the negative regulators of p53) are capable of promoting ferroptosis both in human cancer cells and in the context of neurodegeneration [19]. In the current study, we examine another well-validated target of the p53 network, p21, which is a cyclin dependent kinase that often mediates p53-induced cell cycle arrest [20].

As a consequence of the ability of p21 to induce cell cycle arrest, p21 may mediate cellular senescence, although whether p21 is a major regulator of this process is somewhat unclear [21, 22]. While stress-induced senescence is beneficial by blocking tumorigenesis due to unchecked proliferation of damaged cells, as well as by aiding tissue repair, it can also lead to undesirable effects on longevity due to prolonged accretion of senescent cells that are associated with tissue damage and aging [23].

Relatedly, in the context of some stressors, the loss of p21 has been shown to limit tissue damage and promote tissue regeneration [24] without necessarily leading to tumorigenesis [25]. On the other hand, while the function of p21 is mostly tumor suppressive, there are reports that suggest that when activated in a p53-independent manner, p21 can turn tumorigenic by protecting damaged cells from death [26]. In support of the tumorigenic potential of p21, a recent report demonstrated that the type of activation of p21 in response to chemotherapy dictates its behavior as a tumor suppressor by promoting senescence or as a tumor-driver by causing enhanced survival of so treated cancer cells [27]. In light of these conflicting roles in cancer, it is possible that the type of damage incurred would also dictate whether p21 could limit physiological tissue damage. In support of this prospect, p21 could either delay aging or promote tissue damage based on the type of tissue involved in a model of progeria [28]. Thus, examining the relationship of p21 and ferroptosis is important in the context of cancer as well as aging phenotypes.

Based on prior reports, p21 does have some potential links to ferroptosis. p21 can mediate the p53-ROS signaling pathway by helping sustain higher levels of ROS to effect senescence in some cancer cells [29]. High levels of heme-oxygenase-1 have been known to confer a resistance to apoptosis by altering cellular growth possibly due to upregulation of p21 levels [30]. It has also been shown that heme-oxygenase can enhance ferroptotic death [31, 32] but the possibility that p21 could also modulate this type of death is yet to be explored. Of direct relevance to ferroptosis, p21 has been shown to mediate the resistance of liver cells to treatment with sorafenib [33], a chemotherapeutic kinase inhibitor that has been shown to induce ferroptotic death [34]. In fact, sorafenib treatment triggers an induction of p21 and a knock-down of p21 can increase cellular killing by sorafenib [33]. Since at least a part of the death due to sorafenib can be attributed to ferroptosis, this strongly suggests a role for p21 in regulating ferroptosis. A more recent report effectively showed that p53 poses an impediment to the kinetics of ferroptosis in some human cancer cells via the p21-dependent maintenance of the intracellular glutathione pool [35].

In this study, we suggest another potential mechanism for p21 to promote tumorigenesis by serving as a barrier to ferroptosis, even in the absence of p53. In agreement with previous reports regarding the ability of p21 to enhance tumorigenesis [36], our study also shows that ferroptosis induction leads to a p53-independent regulation of *p21*. Given the prominent roles of ferroptosis in promoting organ damage, our study also supports the possibility that in damages incurred through ferroptosis, p21 could actually aid longevity instead of being a barrier to the organismal lifespan.

It is well known that the major roles of p21 in growth inhibition are mediated by its two main interactions with CDKs and the proliferating cell nuclear antigen (PCNA) [36]. The inhibitory effect of p21 on CDKs mediates its effect on the different cell cycle stages, whereas its abrogation of the role of PCNA mediates its ability to block damaged-DNA replication [37]. Since both CDKs and PCNA have roles that extend beyond just growth inhibition, p21 is able to control other processes as well. For example, p21 mediates a significant portion of the ability of p53 to repress transcription [38–40]. Further, previous reports suggest that the oncogenic role of p21 in preventing death of cancer cells is through its interaction with the CDKs [36]. Since our results reveal a potential for cyclin-dependent kinases (CDKs) to be involved in ferroptosis, they identify a new pathway involved in regulating ferroptosis.

RESULTS

The directionality of regulation of ferroptosis by p53 is highly context specific

We analyzed the response of several human cancer cell lines to the ferroptosis inducer erastin that belongs to the class I ferroptosis inducers (FINs) [41] and categorized them based on the degree of response (Figure 1A). In line with previous reports, even cell lines having the same tissue of origin varied in their response to ferroptosis [42]. The main aim of the current study was to identify if p53 or its targets could be responsible for the dichotomy between at least some of the resistant and sensitive cells. Although we had previously surmised that p53 status was not always predictive of the ferroptosis sensitivity of a given cancer cell line [19], we wanted to determine if the loss of p53 in a given cancer type would then alter its sensitivity to ferroptosis.

We chose two colon cancer cell lines with varying ferroptosis sensitivities- RKO and HCT-116 (Figure

1A) for which isogenic derivatives with respect to their p53 status were already available. These isogenic cell lines were created by the deletion of a functional domain of *p53* [43]. In both cell lines, the loss of p53 made them less sensitive to the chemotherapeutic doxorubicin (Left panels of Figure 1B, 1C), which is thought to elicit at least part of its effects on cancer cell survival through the activation of p53 [44]. On the other hand, the loss of p53 only slightly decreased the ferroptosis sensitivity of HCT-116 cells, while the RKO cells actually became more sensitive upon the loss of p53 (Right panels of Figure 1B, 1C). These results highlight the complexity in defining a set direction of regulation of ferroptosis by p53. Our findings are in line with the current literature in the field showing that p53 can either promote or block ferroptosis [5].

p21 is differentially regulated between cells that are sensitive and resistant in response to ferroptosis

We reasoned that the nuanced roles of p53 in ferroptosis might be indirect and perhaps based on one or more p53 targets being activated in response to ferroptosis induction. To this end, we sought to examine the protein levels of p21, as it is one of the key downstream targets of p53. In fact, one key difference between the HCT-116 and RKO cells used above was their relative p21 protein abundance (Figure 1D).

We found that upon the induction of ferroptosis using two class 1 FINs (erastin or IKE), three different ferroptosis-sensitive cell lines (HT-1080, SK-HEP1 and U2OS) showed decreased levels of p21 protein (as well as p53) as a function of erastin concentration (Figure 2A–2C). On the other hand, there was an increase in p21 protein levels in two ferroptosis-resistant cell lines (HCT-116, H1299) (Figure 2D, 2E). This increase in the levels of p21 was p53-independent since it was observed even in the p53-null H1299 cell line and in HCT-116 cells that were engineered to lose p53 (p53 KO HCT116).

We also evaluated the effect of FINs on the p21 protein levels of p53 KO derivatives of the sensitive cells, HT-1080 and SK-HEP1. As we had reported previously, the loss of p53 impairs the ferroptosis-response of these cells to some extent [19]. While the HT-1080 p53 KO cells still fall within the ferroptosis-sensitive category defined in Figure 1A, the increase in ferroptosis-resistance caused by the loss of p53, places SK-HEP1 p53 KO cells on the upper edge of the moderate class. Accordingly, p21 levels were decreased in the ferroptosis-sensitive HT-1080 p53 KO upon treatment with FINs, while they were enhanced in the SK-HEP1 p53 KO cells, which moderately resist ferroptosis (Supplementary Figure 1). These results further support that the resistance to ferroptosis and the ability of the cell line to promote FIN-dependent augmentation of p21 protein levels are linked independent of the p53 status.

We then wanted to understand the nature of regulation of p21 upon ferroptosis induction. To this end we compared ferroptosis-sensitive HT-1080 (p53 wild-type) cells and ferroptosis-resistant H1299 and HCT116 cells. To our surprise, we found that in both sensitive and resistant cells, *p21* mRNA expression was upregulated at the mRNA level (Figure 3). As controls, increases in the levels of *chac1* and *ptgs2*, known to be induced during ferroptosis [6], were documented as well. Note that there was not a universal reduction in protein levels upon ferroptosis induction as evidenced by constant levels of our loading control, as well as the additional control of expected increase in levels of ferritin in ferroptosis [45]. This result indicates that the process of ferroptosis induces *p21* gene expression in a p53-independent manner and that the subsequent loss of p21 protein in the sensitive cells is most likely a consequence of a post-transcriptional event. It also suggests that this differential regulation of p21 protein may then determine the extent of death achieved.

Altering p21 protein levels changes the sensitivity of cells to ferroptosis

The above results indicated a potential role for p21 in determining the sensitivity of cells to ferroptosis. To validate this hypothesis, we experimentally altered p21 levels and examined the changes in ferroptosis sensitivity of both resistant and sensitive cells.

In the resistant cell lines, HCT-116 and H1299, our goal was to determine if ferroptosis resistance can be lowered upon loss of p21. We used RNA interference against *p21* in these resistant cells and indeed observed a reduction in the resistance to ferroptosis (Figure 4A, 4B). We tested the possibility that a more complete and non-transient loss of *p21* might be required to further enhance the sensitivity of these cells, as it was reported that p21 can alter the metabolic pathways involved in ferroptosis [35]. Indeed, the HCT-116 derived *p21* -/- cell line [46], had a much-enhanced sensitivity to ferroptosis compared to its wild-type counterpart (Figure 4C).

As a reciprocal approach we increased p21 levels in the HT-1080 cell line that is ferroptosis-sensitive. Overexpression of a construct expressing wild-type p21 did suppress this form of cell death in the HT-1080 cells (Figure 4D).

Thus, the results in Figure 4A–4D demonstrate that the capacity of cells to regulate p21 when treated with FINs

A

Sensitive	Moderate	Resistant
BJeLR*- *impaired p53* (engineered fibrosarcoma)	RKO (Colon carcinoma)	HCT116 (Colorectal carcinoma)
HT-1080 (Fibrosarcoma)	U2OS (Osteosarcoma)	H1299*- *p53 null* (Non-small cell lung carcinoma)
SK-Hep1 (Hepatic adenocarcinoma)	HEPG2 (Hepatocellular carcinoma)	MCF-7 (Breast adenocarcinoma)
DoHH-2 WSU-NHL*- *mutant p53* SUDHL6 (Diffuse large B cell lymphoma)	HBL (Diffuse large B cell lymphoma)	LY7 (Diffuse large B cell lymphoma)

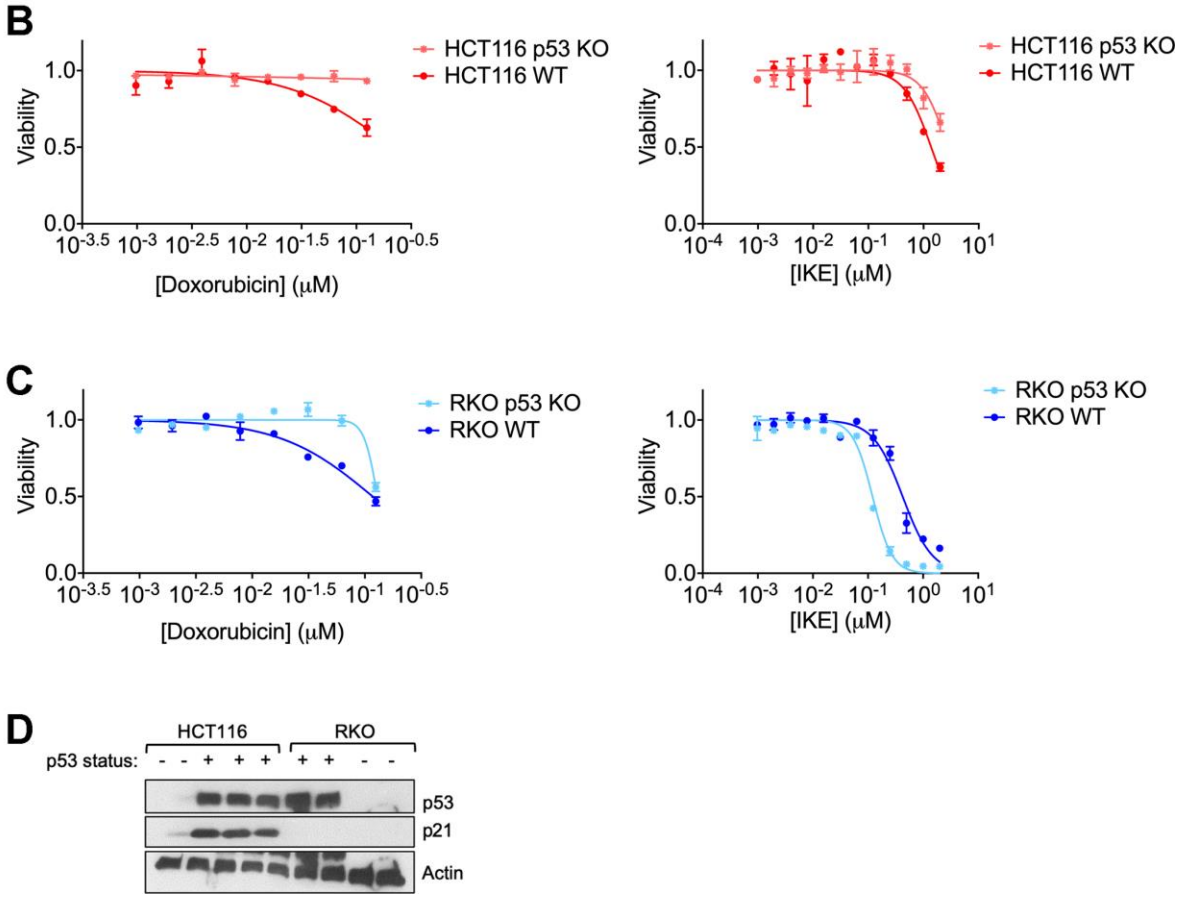

Figure 1. Regulation of ferroptosis by p53 is highly context specific. (**A**) The indicated cell lines were categorized based on the relative amount of cell death observed in response to 24 hours treatment with erastin in a 6-well format. After 24 hours of treatment, the sensitive cell lines had an EC50 of less than 2 μM of erastin, while the moderately sensitive cell lines had an EC50 that was greater than 2 μM, but lesser than 10 μM of erastin. In the resistant cell lines, erastin did not achieve 50% killing at this time point. (**B**, **C**) Viability of isogenic cell lines with wild-type (WT) p53 or no p53 (KO) in (**B**) HCT-116 and (**C**) RKO when treated with indicated doses of either doxorubicin (left panel) or IKE (right panel) for 24 hours. (**D**) Immunoblot showing p53 and p21 protein levels in HCT-116 and RKO cells. Multiple replicates of the wild-type and p53 KO cell lines cultured in separate dishes were used. Actin was used as a loading control. The data in (**B**, **C**) represent the mean ± SE for two of four independent experiments. The viability data have been normalized to that of the DMSO control.

crucially impacts the extent of response to ferroptosis. However, it is unclear if the ferroptosis-associated reduction of p21 in sensitive cells takes place as a consequence of translational or post-translational signals. The results in Figure 4D suggests that it is unlikely for the loss of p21 protein abundance to be a result of enhanced degradation of p21, as then the ectopic p21 protein would have also faced the same fate and should then have been rendered incapable of altering the degree of ferroptotic death. In further support of this hypothesis, we observed that proteasome inhibitor MG132 is unable to block any part of the reduction in p21 expression caused by erastin (Supplementary Figure 2A left panel). Note that MG132 treatment did slightly increase the sensitivity of ferroptosis, although this was found to be p21 independent (Supplementary Figure 2A right panel). Thus, based on these results we posit that p21 is more likely to be translationally regulated in response to ferroptosis.

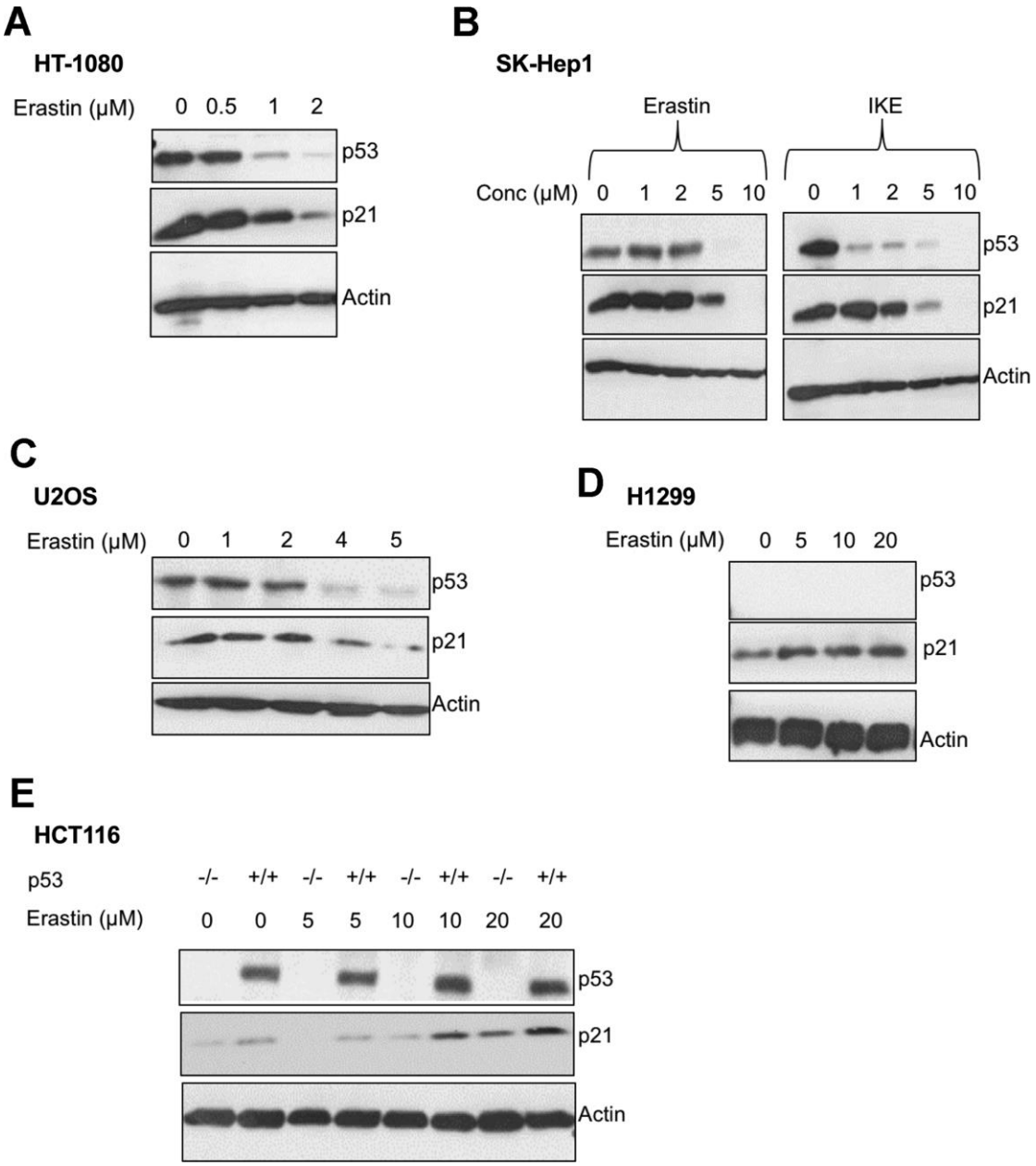

Figure 2. p21 protein is differentially regulated between cells that are sensitive and resistant in response to ferroptosis. (**A**–**E**) Impact of treatment with erastin/IKE on the protein levels of p21 and p53. (**A**) HT-1080 cells, (**B**) SK-HEP1 cells and (**C**) U2OS cells were treated for 16 hours whereas (**D**) H1299 cells and (**E**) HCT116 cells (+/+ and -/- isogenic lines with respect to p53 status) were treated for 48 hours.

The experiment in Figure 4D, further allowed us to determine which interactions of p21 may aid its role in ferroptosis. For this, we used two key mutant versions of p21, which disable either its CDK binding or PCNA binding domains [47, 48] and found that they differed in their ability to suppress ferroptosis. Specifically, the CDK binding-defective version of p21 was unable to block ferroptosis, while mutating the PCNA binding

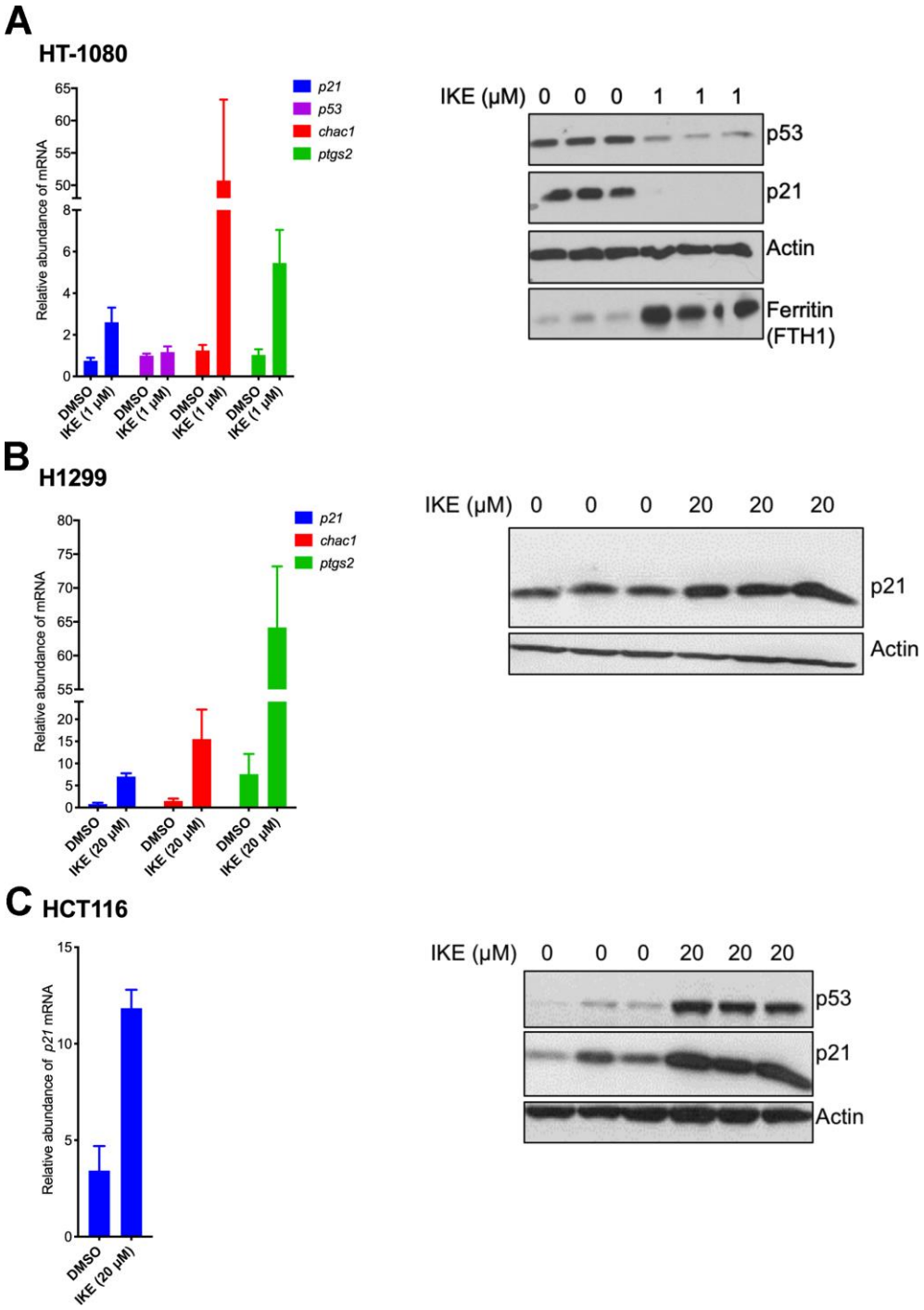

Figure 3. p21 mRNA is upregulated in both ferroptosis-sensitive and ferroptosis-resistant cells after treatment with IKE. (**A**–**C**) Left panels: Impact of IKE treatment on the mRNA levels of p21. (**A**) HT-1080 cells were treated for 16 hours while (**B**, **C**) H1299 and HCT-116 cells were treated for 48 hours. mRNA levels of *ptgs2* and *chac1* were measured in (**A**, **B**) as markers of ferroptosis. Right panels: the corresponding protein levels in the cells used in the left panels are shown. The data in left panels of (**A**–**C**) represent the mean ± SE for three biological replicates with two technical replicates each.

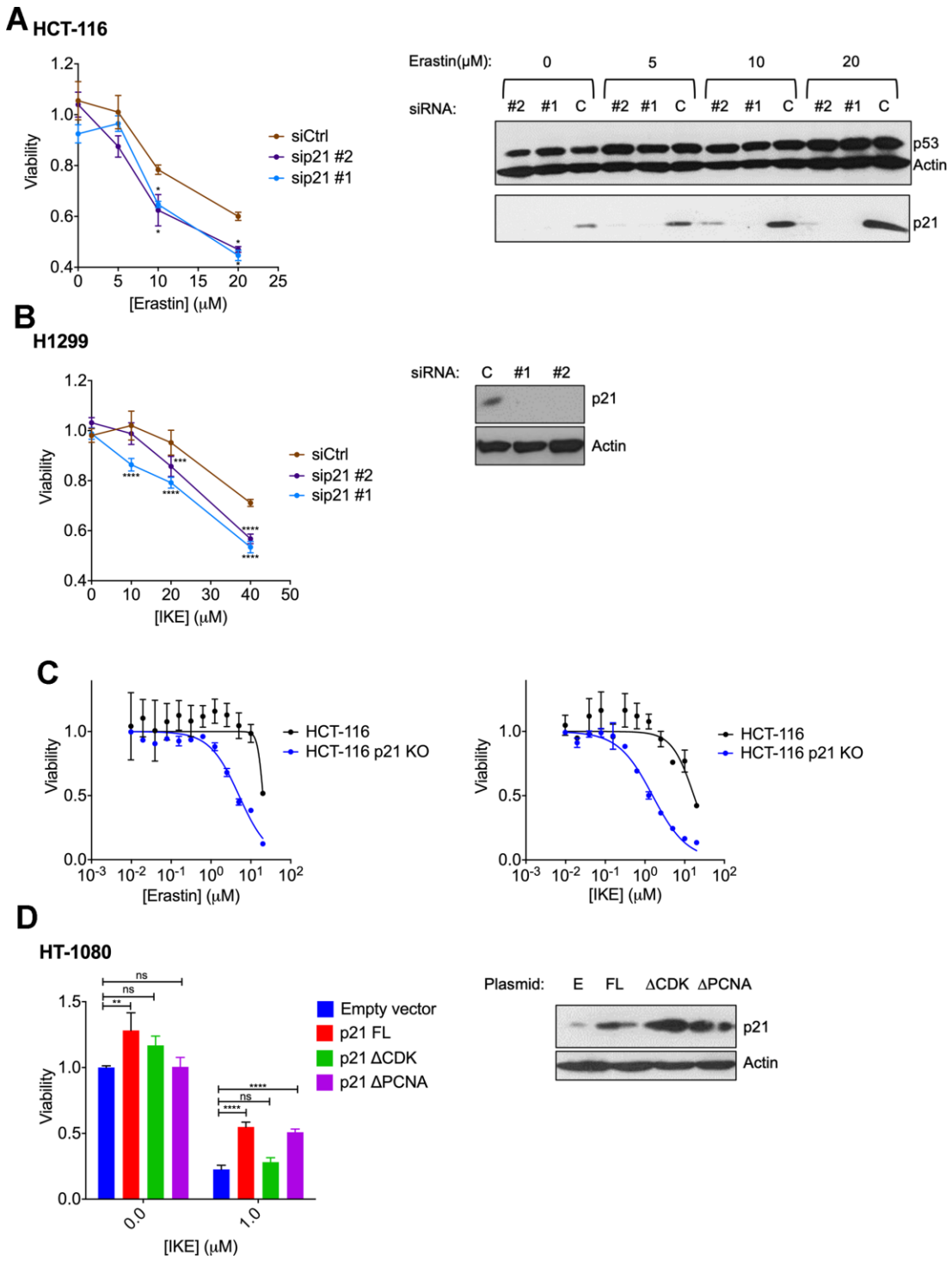

Figure 4. Altering p21 protein levels changes the sensitivity of cells to ferroptosis. (**A**, **B**) HCT116 (**A**) or H1299 (**B**) cells were transfected with two different siRNAs (#1, #2) directed against *p21* mRNA for 24 hours, and then treated with erastin or IKE as indicated for an additional 48 hours. As a control, cells were transfected with luciferase siRNA a (siCtrl/C). The right panels in A and B show the corresponding changes in p21 protein levels. (**C**) HCT-116 cells and HCT116 p21 (-/-) cells were treated with increasing doses of either erastin (left panel) or IKE (right panel) for 48 hours. (**D**) Left panel: Viability of HT-1080 cells that were transfected with the indicated plasmids expressing p21 variants or an empty vector and then treated with either DMSO or IKE for 48 hours. The panel on the right shows the corresponding immunoblot detecting p21 protein levels. The data in (**A**, **B**) represent the mean ± SE for two of three independent experiments, in (**C**) represent the mean ± SE for two out of four independent experiments, in (**D**) represent the mean ± SE for three independent experiments. The viability data have been normalized to the DMSO control in (**A**–**C**) and to their respective untreated control in (**D**).

region impaired p21 to a much lesser extent in that regard (although the levels of expression of this mutant were slightly lower). This result suggests the possibility that p21 alters sensitivity to ferroptosis by affecting CDK-mediated functions.

Taken together, we demonstrate that differential regulation of p21 protein can serve as a determining factor of ferroptosis sensitivity in many human cancer cells and that this regulation is independent of p53. Our results further emphasize the importance of p53-targets in the regulation of cell survival, even in the absence of p53.

DISCUSSION

There is growing literature on the complex roles of p53 in ferroptosis [5]. Given the highly context-specific regulation of ferroptosis by p53, we focused on elucidating the ability of p53-target genes to regulate this form of cell death. In line with that, our study has revealed the ability of p21, a major downstream target of p53, to block ferroptosis in several cancer cell lines. We demonstrate that cells which effectively undergo ferroptosis reduce the expression of p21 protein. Further the sensitivity of these cells can be suppressed by re-expressing p21, suggesting that the loss of p21 is essential to allow for a complete response to ferroptosis. Conversely the resistant cells that we tested were dependent on the presence of p21 to counteract ferroptotic death. Taken together, we believe that at least in some cancer cells, the regulation of p21 protein can be the determining factor of their ferroptotic sensitivity.

Although we sought to identify p53-target genes that may help determine the directionality of the regulation of p53 in ferroptosis, this work complements our previous work [19] in identifying members of the p53 network, namely p21, MDM2 and MDMX, which can modulate ferroptosis independent of p53. It is certainly possible that these proteins perhaps coordinate with p53 to ultimately dictate the ferroptosis-sensitivity in some contexts.

Mechanistically, our results indicate that the ability of p21 to interact with CDKs is important for its role in ferroptosis. The inhibition of CDK activity by p21 can have multiple effects that impact cellular growth including altered transcription, cell cycle changes and even dedifferentiation to a certain degree [36]. Our finding that complete ablation of *p21* has a more pronounced change in ferroptotic sensitivity than a transient yet highly effective siRNA against *p21*, suggests that the mechanism of resistance likely requires prolonged presence of p21. For example, if cancer cells underwent some extent of p21-dependent dedifferentiation in order to become ferroptosis-resistant, then it is likely that these changes would need more time to get reverted. Reports showing that dedifferentiation of melanoma cells as well as further differentiation of neurons enhance ferroptosis sensitivity [49, 50] lend some support to this theory.

We speculate that cell cycle changes alone may not explain the role of p21 in ferroptosis. Relatedly, it was reported that while that p53 can prevent ferroptosis through p21, cell cycle arrest alone is insufficient to cause this suppression [35]. It is definitely possible that p21 has a myriad of effects with cell cycle changes just being a subset of them. Taken together, a future study to better understand the molecular regulation of ferroptosis by p21, should evaluate the involvement of CDKs as a key factor. It is also unclear which proteins/pathways control the regulation of p21 in response to ferroptosis, both at the transcriptional and post-transcriptional levels. Studying these could further yield more regulators of ferroptosis.

Our data also indicate that p21 can have a potential to be used as a biomarker for ferroptosis sensitivity of cancer cells. If not merely the abundance of p21 protein, the protein levels of p21 post ferroptosis induction strongly track with the sensitivity of a wide range of cancer cell lines tested. Therefore, this study identifies another important regulator of ferroptosis sensitivity in cancer.

Our data also sparks the need to further examine the role of p21 in mediating the ability of ferroptosis to cause organ damage. If p21 can indeed control the differentiation of cells through CDKs as hypothesized above, then this provides a potential mechanism for p21 to promote tissue regeneration by inhibiting ferroptosis even in physiological conditions. While this is counter-intuitive to the traditional roles of p21 in aging, it adds a new perspective to the wide variety of roles that can be played by p21 in multiple contexts.

MATERIALS AND METHODS

Cells

HCT116, H1299, SK-HEP1, and U2OS cells were maintained in Dulbecco's modified Eagle's medium supplemented with 10% heat-inactivated fetal bovine serum (Gemini Bioproducts, cat# 900-108). HT-1080 cells were maintained in Dulbecco's modified Eagle's medium supplemented with 10% heat-inactivated fetal bovine serum (Gemini Bioproducts, cat# 900-108), and 1% non-essential amino acids (Sigma-Aldrich, cat# M7145). RKO cells were grown in McCoy's 5A

modified medium (Gibco, cat# 16600-082) supplemented with 10% heat-inactivated fetal bovine serum (Gemini Bioproducts, cat# 900-108). The HCT116 and RKO isogenic cell lines that were created by the deletion of a functional domain of *p53* [43] were a gift from Dr. Vogelstein. The HT-1080 p53 KO, HT-1080 p21 KO and SK-HEP1 p53 KO cell lines were genetically engineered using CRISPR technology [19]. All other cell lines were obtained from ATCC.

Drugs and chemicals

The commercially available compounds used were: erastin (Selleckchem, cat# S7242), doxorubicin (Sigma-Aldrich, cat#D1515) and MG132 (Selleckchem, cat# S2619). IKE (imidazole ketone erastin) was synthesized as in Larraufie MH et al., by Yan Zhang in Stockwell lab [51].

All the compounds were dissolved in DMSO (Sigma-Aldrich, cat# D8418).

Quantitative reverse transcription PCR

RNA was isolated from cells using the Qiagen RNeasy minikit. cDNA was generated using the Qiagen Quantitect reverse transcription kit with 0.5 µg of input RNA as measured with a NanoDrop (Thermo Scientific). Real-time PCR was carried out on an ABI StepOne Plus machine using the power SYBR Green dye (Thermo Scientific). Transcript levels were assayed in triplicate and normalized to *L32* mRNA levels. Relative changes in cDNA levels were calculated using the comparative Ct method ($\Delta\Delta C_T$ method).

Primer sequences

L32 F: TTCCTGGTCCACAACGTCAAG, L32 R: TGTGAGCGATCTCGGCAC; p21 F: GGCGGCAGA CCAGCATGACAGATT, p21 R: GCAGGGGGCGG CCAGGGTAT; chac1 F: GAACCCTGGTTACCT GGG, chac1 R: CGCAGCAAGTATTCAGGTGT; ptgs2 F: TAAGTGCGATTGTACCCGGAC, ptgs2 R: TCTCCAAAGGAGGTTACCTGC.

The p53 primer was obtained as premixed solution from Qiagen (Quantitech primer, HS_TP53_1_SG, cat# QT00060235) and the rest were individually ordered from Invitrogen.

Immunoblot

Cells were lysed with TEB lysis buffer (10mM Tris HCL pH 7.5-8, 137 mM sodium chloride, 10% glycerol, 1% NP-40) supplemented with 1mM magnesium chloride, 1mM calcium chloride and protease inhibitors (Roche). Protein concentrations were assayed using the Bio-Rad protein assay dye reagent and results were read using a spectrophotometer.

Protein extracts were run on in-house made Tris-Glycine SDS Polyacrylamide gels. Proteins were then electro-transferred at 360 mA for 70 min onto a nitrocellulose or PVDF membrane. Membranes were blocked with 5% milk in PBST (Phosphate-Buffered Saline with Tween) for 30 min, prior to being incubated overnight with primary antibodies (1:100-1:1000 dilution according to the specific antibody). The membranes were then washed three times with PBST and incubated with secondary antibody (1:5000 dilution) for 1 hour at room temperature. After three more washes with PBST, the membranes were imaged using ECL (Thermo Fisher, Pierce, cat# 32106 or EMD Millipore, Immobilon, cat# WBKLS0050). The primary and secondary antibodies were diluted with 1% milk in PBST.

The following primary antibodies were used: p53 (mAb 1801/mAb DO.1, in-house produced); p21 (C-19, Santa Cruz biotech, cat# sc-397); actin (Sigma-Aldrich, cat# A2066); ferritin/FTH1 (Cell Signaling Technology cat# 3998). Actin was used as loading control for all the blots.

Transfection: RNA interference

siRNA (15 nM) was used for each well in a 6-well plate. Lipofectamine RNAiMAX (Thermo Scientific) was used as the transfection reagent for all siRNA experiments (according to the manufacturer's instructions). After 18 hours, the media was changed and cells were treated with drugs 24 hours post transfection. Cells were plated prior to transfection such that they were only 80% confluent by the end of the drug treatment period.

The following siRNAs were used: siLuciferase [52], sip21 #1 (HS_CDKN1A_6 Flexitube siRNA from Qiagen), sip21 #2 (HS_CDKN1A_7 Flexitube siRNA from Qiagen).

Transfection: Ectopic expression of proteins

Plasmids were transfected into cells using Lipofectamine 3000 (Thermo Scientific) according to the manufacturer's instructions, with a ratio of 1 µg:1.7 µl lipofectamine reagent. After 18 hours, the media was changed and cells were treated with drugs 24 hours post transfection. The cells were plated prior to transfection such that they are only a maximum of 80% confluent by the end of the drug treatment period. The plasmids for full length and mutants of p21 were a kind

gift from Dr. Vanessa Gottifredi and have been previously described [47, 48].

Note

Cells became more resistant to ferroptosis inducers post transfection. In order to obtain cell death post transfection, three key factors need to be controlled: cell density must be lower than normal, lipofectamine reagent needs to be washed off as soon as possible, and a three to four-fold higher dose of FINs must be used to induce ferroptosis.

Cell viability assay

For the dose response curves, 1800 cells were plated in 36 µl per well of a 384 well plate on day one. Drugs were dissolved in DMSO and a 12 point, two-fold series was prepared. The drugs were then dissolved 1:33 in media and 4 µl was added to each well of the plates on day two. After 24-48 hours of drug treatment (based on the cell line), the viability of cells was measured using a 1:1 dilution of the CellTiter-Glo Luminescent reagent (Promega, cat# G7573) with media, which was read on a Victor 5 plate reader after 10 minutes shaking at room temperature. The intensity of luminescence was normalized to that of the DMSO control. Experiments were performed twice in duplicates each time.

For viability assays when the experiment was performed in 6-well plates, cells were harvested using trypsin (0.5 ml per well) and the media was saved from each well. The trypsinized cells were resuspended with the saved media and 2-3 aliquots (0.05 ml each) sampling different regions of this suspension were transferred into a 96-well plate to serve as technical replicates for the measurement. CellTiter-Glo Luminescent Viability assay was used to measure the viability of these aliquots. The rest of the cultures were used to extract protein to be analyzed using western blots.

Statistical analysis

Prism (version 8, GraphPad) was used to make all the graphs in the paper and for performing all the statistical analysis shown. The GraphPad style (0.1234(ns), <0.0332(*), < 0.0021(**), <0.0002(***), <0.0001 (****),) was used to represent the p values. The p values were calculated by ANOVA and appropriate multiple testing correction was done where required.

AUTHOR CONTRIBUTIONS

DV designed and conducted all experiments in the paper under the guidance of CLP and BRS. DV, CLP and BRS wrote and edited the manuscript.

ACKNOWLEDGMENTS

We are grateful to Ella Freulich for technical assistance. Chen Katz for advice, and Yan Zhang for synthesizing IKE that is used in this study. We thank Dr. Vanessa Gottifredi for providing the p21 plasmids and advice. We also thank Dr. Vogelstein for providing RKO and HCT-116 isogenic cells.

CONFLICTS OF INTEREST

Disclosure of financial interests: CLP is a member of the SAB of Aileron Therapeutics. BRS is an inventor on patents and patent applications related to ferroptosis, and is a consultant to and co-founder of Inzen Therapeutics and Nevrox Limited.

FUNDING

This study was supported by CA87497 (to BRS and CP), R35CA220526 (to CP), R35CA209896 and R61NS109407 (to BRS).

REFERENCES

1. O'Connor PM, Jackman J, Bae I, Myers TG, Fan S, Mutoh M, Scudiero DA, Monks A, Sausville EA, Weinstein JN, Friend S, Fornace AJ Jr, Kohn KW. Characterization of the p53 tumor suppressor pathway in cell lines of the national cancer institute anticancer drug screen and correlations with the growth-inhibitory potency of 123 anticancer agents. Cancer Res. 1997; 57:4285–300. PMID:9331090
2. Hientz K, Mohr A, Bhakta-Guha D, Efferth T. The role of p53 in cancer drug resistance and targeted chemotherapy. Oncotarget. 2017; 8:8921–46. https://doi.org/10.18632/oncotarget.13475 PMID:27888811
3. Ranjan A, Iwakuma T. Non-canonical cell death induced by p53. Int J Mol Sci. 2016; 17:2068. https://doi.org/10.3390/ijms17122068 PMID:27941671
4. Kang R, Kroemer G, Tang D. The tumor suppressor protein p53 and the ferroptosis network. Free Radic Biol Med. 2019; 133:162–68. https://doi.org/10.1016/j.freeradbiomed.2018.05.074 PMID:29800655
5. Gnanapradeepan K, Basu S, Barnoud T, Budina-Kolomets A, Kung CP, Murphy ME. The p53 tumor suppressor in the control of metabolism and ferroptosis. Front Endocrinol (Lausanne). 2018; 9:124. https://doi.org/10.3389/fendo.2018.00124 PMID:29695998

6. Stockwell BR, Friedmann Angeli JP, Bayir H, Bush AI, Conrad M, Dixon SJ, Fulda S, Gascón S, Hatzios SK, Kagan VE, Noel K, Jiang X, Linkermann A, et al. Ferroptosis: a regulated cell death nexus linking metabolism, redox biology, and disease. Cell. 2017; 171:273–85. https://doi.org/10.1016/j.cell.2017.09.021 PMID:28985560

7. Wu JR, Tuo QZ, Lei P. Ferroptosis, a recent defined form of critical cell death in neurological disorders. J Mol Neurosci. 2018; 66:197–206. https://doi.org/10.1007/s12031-018-1155-6 PMID:30145632

8. Fang X, Wang H, Han D, Xie E, Yang X, Wei J, Gu S, Gao F, Zhu N, Yin X, Cheng Q, Zhang P, Dai W, et al. Ferroptosis as a target for protection against cardiomyopathy. Proc Natl Acad Sci USA. 2019; 116:2672–80. https://doi.org/10.1073/pnas.1821022116 PMID:30692261

9. Friedmann Angeli JP, Schneider M, Proneth B, Tyurina YY, Tyurin VA, Hammond VJ, Herbach N, Aichler M, Walch A, Eggenhofer E, Basavarajappa D, Rådmark O, Kobayashi S, et al. Inactivation of the ferroptosis regulator Gpx4 triggers acute renal failure in mice. Nat Cell Biol. 2014; 16:1180–91. https://doi.org/10.1038/ncb3064 PMID:25402683

10. Müller T, Dewitz C, Schmitz J, Schröder AS, Bräsen JH, Stockwell BR, Murphy JM, Kunzendorf U, Krautwald S. Necroptosis and ferroptosis are alternative cell death pathways that operate in acute kidney failure. Cell Mol Life Sci. 2017; 74:3631–45. https://doi.org/10.1007/s00018-017-2547-4 PMID:28551825

11. Matsushita M, Freigang S, Schneider C, Conrad M, Bornkamm GW, Kopf M. T cell lipid peroxidation induces ferroptosis and prevents immunity to infection. J Exp Med. 2015; 212:555–68. https://doi.org/10.1084/jem.20140857 PMID:25824823

12. Wu D, Prives C. Relevance of the p53-MDM2 axis to aging. Cell Death Differ. 2018; 25:169–79. https://doi.org/10.1038/cdd.2017.187 PMID:29192902

13. Rufini A, Tucci P, Celardo I, Melino G. Senescence and aging: the critical roles of p53. Oncogene. 2013; 32:5129–43. https://doi.org/10.1038/onc.2012.640 PMID:23416979

14. Steffan JS, Kazantsev A, Spasic-Boskovic O, Greenwald M, Zhu YZ, Gohler H, Wanker EE, Bates GP, Housman DE, Thompson LM. The Huntington's disease protein interacts with p53 and CREB-binding protein and represses transcription. Proc Natl Acad Sci USA. 2000; 97:6763–68. https://doi.org/10.1073/pnas.100110097 PMID:10823891

15. Hooper C, Meimaridou E, Tavassoli M, Melino G, Lovestone S, Killick R. P53 is upregulated in Alzheimer's disease and induces tau phosphorylation in HEK293a cells. Neurosci Lett. 2007; 418:34–37. https://doi.org/10.1016/j.neulet.2007.03.026 PMID:17399897

16. Szybińska A, Leśniak W. P53 dysfunction in neurodegenerative diseases - the cause or effect of pathological changes? Aging Dis. 2017; 8:506–18. https://doi.org/10.14336/AD.2016.1120 PMID:28840063

17. Van Nostrand JL, Brady CA, Jung H, Fuentes DR, Kozak MM, Johnson TM, Lin CY, Lin CJ, Swiderski DL, Vogel H, Bernstein JA, Attié-Bitach T, Chang CP, et al. Inappropriate p53 activation during development induces features of CHARGE syndrome. Nature. 2014; 514:228–32. https://doi.org/10.1038/nature13585 PMID:25119037

18. Bowen ME, Attardi LD. The role of p53 in developmental syndromes. J Mol Cell Biol. 2019; 11:200–11. https://doi.org/10.1093/jmcb/mjy087 PMID:30624728

19. Venkatesh D, O'Brien NA, Zandkarimi F, Tong DR, Stokes ME, Dunn DE, Kengmana ES, Aron AT, Klein AM, Csuka JM, Moon SH, Conrad M, Chang CJ, et al. MDM2 and MDMX promote ferroptosis by PPARα-mediated lipid remodeling. Genes Dev. 2020; 34:526–43. https://doi.org/10.1101/gad.334219.119 PMID:32079652

20. Warfel NA, El-Deiry WS. p21WAF1 and tumourigenesis: 20 years after. Curr Opin Oncol. 2013; 25:52–58. https://doi.org/10.1097/CCO.0b013e32835b639e PMID:23159848

21. Qian Y, Chen X. Senescence regulation by the p53 protein family. Methods Mol Biol. 2013; 965:37–61. https://doi.org/10.1007/978-1-62703-239-1_3 PMID:23296650

22. Sharpless NE, Sherr CJ. Forging a signature of in vivo senescence. Nat Rev Cancer. 2015; 15:397–408. https://doi.org/10.1038/nrc3960 PMID:26105537

23. Burton DG, Krizhanovsky V. Physiological and pathological consequences of cellular senescence. Cell Mol Life Sci. 2014; 71:4373–86. https://doi.org/10.1007/s00018-014-1691-3 PMID:25080110

24. Papismadov N, Gal H, Krizhanovsky V. The anti-aging promise of p21. Cell Cycle. 2017; 16:1997–98. https://doi.org/10.1080/15384101.2017.1377500 PMID:28956690

25. Bell JF, Sharpless NE. Telomeres, p21 and the cancer-aging hypothesis. Nat Genet. 2007; 39:11–12. https://doi.org/10.1038/ng0107-11 PMID:17192782

26. Georgakilas AG, Martin OA, Bonner WM. P21: a two-faced genome guardian. Trends Mol Med. 2017; 23:310–19. https://doi.org/10.1016/j.molmed.2017.02.001 PMID:28279624

27. Hsu CH, Altschuler SJ, Wu LF. Patterns of early p21 dynamics determine proliferation-senescence cell fate after chemotherapy. Cell. 2019; 178:361–73.e12. https://doi.org/10.1016/j.cell.2019.05.041 PMID:31204100

28. Baker DJ, Weaver RL, van Deursen JM. P21 both attenuates and drives senescence and aging in BubR1 progeroid mice. Cell Rep. 2013; 3:1164–74. https://doi.org/10.1016/j.celrep.2013.03.028 PMID:23602569

29. Fitzgerald AL, Osman AA, Xie TX, Patel A, Skinner H, Sandulache V, Myers JN. Reactive oxygen species and p21Waf1/Cip1 are both essential for p53-mediated senescence of head and neck cancer cells. Cell Death Dis. 2015; 6:e1678. https://doi.org/10.1038/cddis.2015.44 PMID:25766317

30. Inguaggiato P, Gonzalez-Michaca L, Croatt AJ, Haggard JJ, Alam J, Nath KA. Cellular overexpression of heme oxygenase-1 up-regulates p21 and confers resistance to apoptosis. Kidney Int. 2001; 60:2181–91. https://doi.org/10.1046/j.1523-1755.2001.00046.x PMID:11737592

31. Chang LC, Chiang SK, Chen SE, Yu YL, Chou RH, Chang WC. Heme oxygenase-1 mediates BAY 11-7085 induced ferroptosis. Cancer Lett. 2018; 416:124–37. https://doi.org/10.1016/j.canlet.2017.12.025 PMID:29274359

32. Kwon MY, Park E, Lee SJ, Chung SW. Heme oxygenase-1 accelerates erastin-induced ferroptotic cell death. Oncotarget. 2015; 6:24393–403. https://doi.org/10.18632/oncotarget.5162 PMID:26405158

33. Giovannini C, Baglioni M, Baron Toaldo M, Ventrucci C, D'Adamo S, Cipone M, Chieco P, Gramantieri L, Bolondi L. Notch3 inhibition enhances sorafenib cytotoxic efficacy by promoting GSK3b phosphorylation and p21 down-regulation in hepatocellular carcinoma. Oncotarget. 2013; 4:1618–31. https://doi.org/10.18632/oncotarget.1221 PMID:24113128

34. Dixon SJ, Patel DN, Welsch M, Skouta R, Lee ED, Hayano M, Thomas AG, Gleason CE, Tatonetti NP, Slusher BS, Stockwell BR. Pharmacological inhibition of cystine-glutamate exchange induces endoplasmic reticulum stress and ferroptosis. Elife. 2014; 3:e02523. https://doi.org/10.7554/eLife.02523 PMID:24844246

35. Tarangelo A, Magtanong L, Bieging-Rolett KT, Li Y, Ye J, Attardi LD, Dixon SJ. P53 suppresses metabolic stress-induced ferroptosis in cancer cells. Cell Rep. 2018; 22:569–75. https://doi.org/10.1016/j.celrep.2017.12.077 PMID:29346757

36. Abbas T, Dutta A. P21 in cancer: intricate networks and multiple activities. Nat Rev Cancer. 2009; 9:400–14. https://doi.org/10.1038/nrc2657 PMID:19440234

37. Mansilla SF, de la Vega MB, Calzetta NL, Siri SO, Gottifredi V. CDK-independent and PCNA-dependent functions of p21 in DNA replication. Genes (Basel). 2020; 11:593. https://doi.org/10.3390/genes11060593 PMID:32481484

38. Löhr K, Möritz C, Contente A, Dobbelstein M. p21/CDKN1A mediates negative regulation of transcription by p53. J Biol Chem. 2003; 278:32507–16. https://doi.org/10.1074/jbc.M212517200 PMID:12748190

39. Laptenko O, Prives C. Transcriptional regulation by p53: one protein, many possibilities. Cell Death Differ. 2006; 13:951–61. https://doi.org/10.1038/sj.cdd.4401916 PMID:16575405

40. Engeland K. Cell cycle arrest through indirect transcriptional repression by p53: I have a DREAM. Cell Death Differ. 2018; 25:114–32. https://doi.org/10.1038/cdd.2017.172 PMID:29125603

41. Dixon SJ, Lemberg KM, Lamprecht MR, Skouta R, Zaitsev EM, Gleason CE, Patel DN, Bauer AJ, Cantley AM, Yang WS, Morrison B 3rd, Stockwell BR. Ferroptosis: an iron-dependent form of nonapoptotic cell death. Cell. 2012; 149:1060–72. https://doi.org/10.1016/j.cell.2012.03.042 PMID:22632970

42. Yang WS, SriRamaratnam R, Welsch ME, Shimada K, Skouta R, Viswanathan VS, Cheah JH, Clemons PA, Shamji AF, Clish CB, Brown LM, Girotti AW, Cornish VW, et al. Regulation of ferroptotic cancer cell death by GPX4. Cell. 2014; 156:317–31. https://doi.org/10.1016/j.cell.2013.12.010 PMID:24439385

43. Bunz F, Fauth C, Speicher MR, Dutriaux A, Sedivy JM, Kinzler KW, Vogelstein B, Lengauer C. Targeted inactivation of p53 in human cells does not result in aneuploidy. Cancer Res. 2002; 62:1129–33. PMID:11861393

44. Wang S, Konorev EA, Kotamraju S, Joseph J, Kalivendi S, Kalyanaraman B. Doxorubicin induces apoptosis in normal and tumor cells via distinctly different mechanisms. Intermediacy of H(2)O(2)- and p53-dependent pathways. J Biol Chem. 2004; 279:25535–43. https://doi.org/10.1074/jbc.M400944200 PMID:15054096

45. Hou W, Xie Y, Song X, Sun X, Lotze MT, Zeh HJ 3rd, Kang R, Tang D. Autophagy promotes ferroptosis by degradation of ferritin. Autophagy. 2016; 12:1425–28. https://doi.org/10.1080/15548627.2016.1187366 PMID:27245739

46. Waldman T, Kinzler KW, Vogelstein B. P21 is necessary for the p53-mediated G1 arrest in human cancer cells. Cancer Res. 1995; 55:5187–90. PMID:7585571

47. Soria G, Podhajcer O, Prives C, Gottifredi V. P21Cip1/WAF1 downregulation is required for efficient PCNA ubiquitination after UV irradiation. Oncogene. 2006; 25:2829–38. https://doi.org/10.1038/sj.onc.1209315 PMID:16407842

48. Mansilla SF, Bertolin AP, Bergoglio V, Pillaire MJ, González Besteiro MA, Luzzani C, Miriuka SG, Cazaux C, Hoffmann JS, Gottifredi V. Cyclin kinase-independent role of $p21^{CDKN1A}$ in the promotion of nascent DNA elongation in unstressed cells. Elife. 2016; 5:e18020. https://doi.org/10.7554/eLife.18020 PMID:27740454

49. Chonghaile TN. Ironing out dedifferentiation in melanoma. Science Translational Medicine. 2018; 10:eaau0461. https://doi.org/10.1126/scitranslmed.aau0461

50. Martinez AM, Mirkovic J, Stanisz ZA, Patwari FS, Yang WS. NSC-34 motor neuron-like cells are sensitized to ferroptosis upon differentiation. FEBS Open Bio. 2019; 9:582–93. https://doi.org/10.1002/2211-5463.12577 PMID:30984534

51. Larraufie MH, Yang WS, Jiang E, Thomas AG, Slusher BS, Stockwell BR. Incorporation of metabolically stable ketones into a small molecule probe to increase potency and water solubility. Bioorg Med Chem Lett. 2015; 25:4787–92. https://doi.org/10.1016/j.bmcl.2015.07.018 PMID:26231156

52. Urist M, Tanaka T, Poyurovsky MV, Prives C. P73 induction after DNA damage is regulated by checkpoint kinases Chk1 and Chk2. Genes Dev. 2004; 18:3041–54. https://doi.org/10.1101/gad.1221004 PMID:15601819

SUPPLEMENTARY MATERIALS

Supplementary Figures

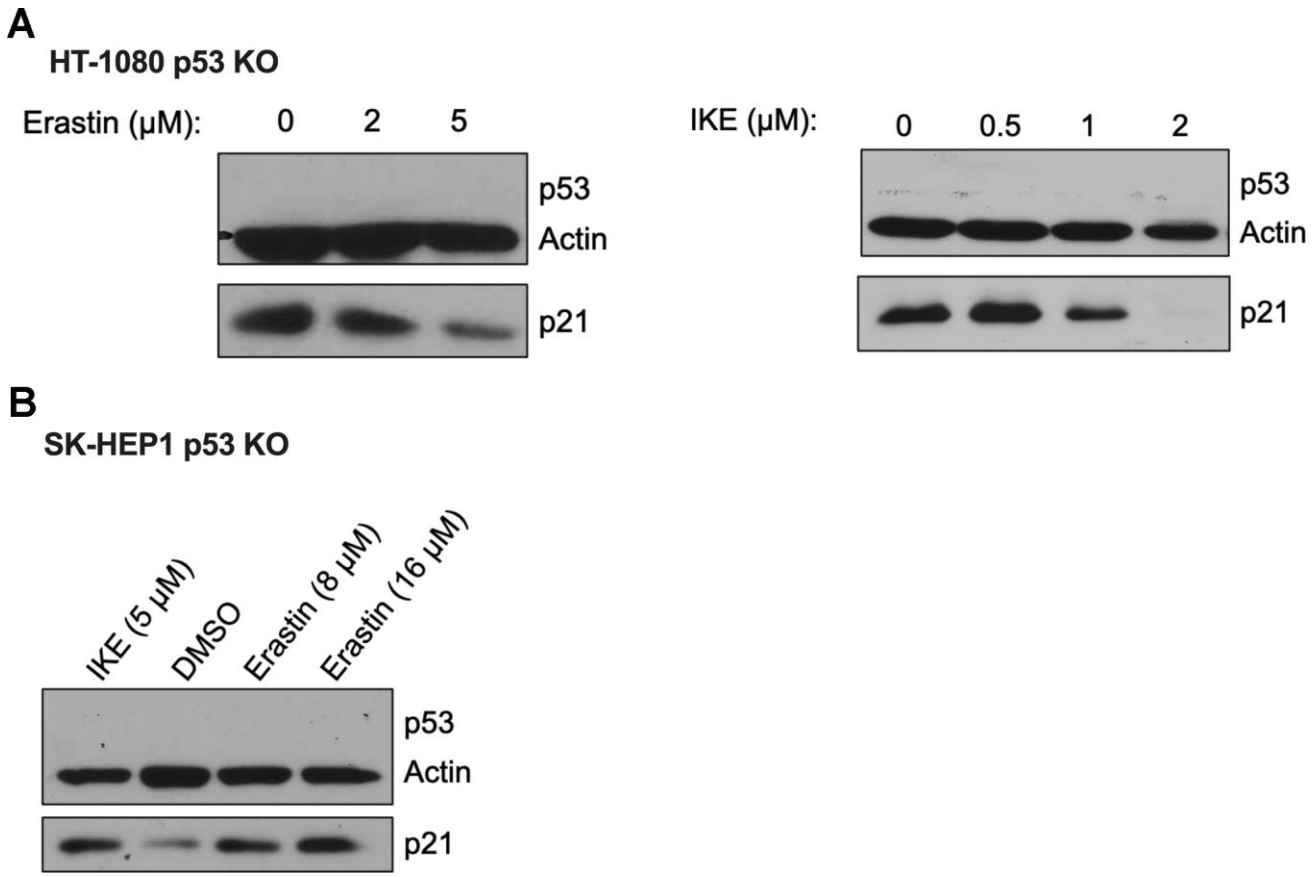

Supplementary Figure 1. Ferroptosis-driven differential regulation of p21 protein is independent of p53. (**A**, **B**) Impact of treatment with erastin/IKE on the protein levels of p21in (**A**) HT-1080 p53 KO cells and (**B**) SK-HEP1 p53 KO cells. Cells in (**A**) were treated with erastin/IKE for 16 hours and in (**B**) for 18 hrs.

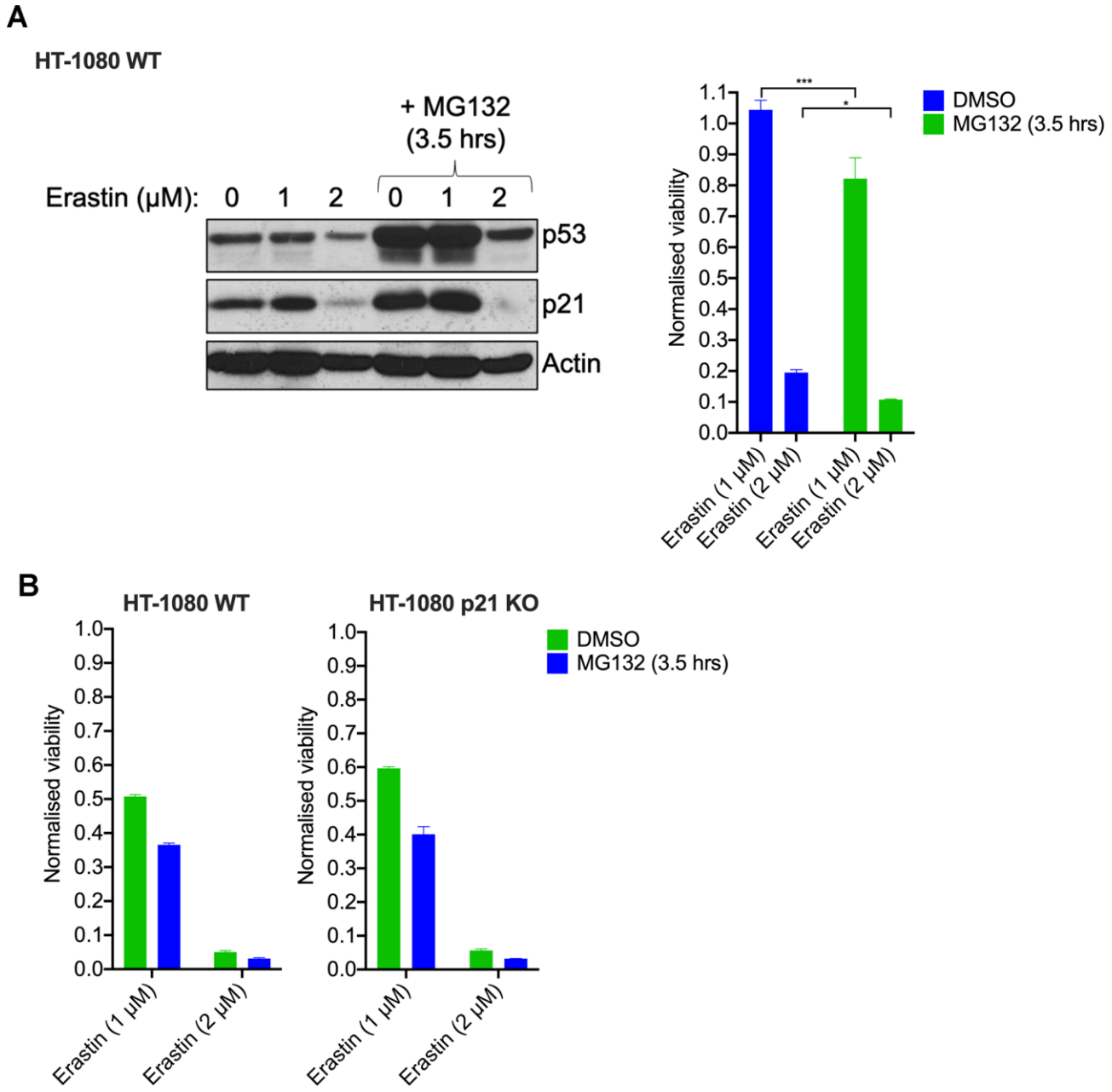

Supplementary Figure 2. Suppression of the proteasome does not revert the reduction in p21 protein levels due to ferroptosis. (**A**) Left panel- effect of addition of MG132 on protein levels of p21 and p53 in HT-1080 wild-type cells treated with erastin. Right panel- viability of HT-1080 wild-type cells when treated with MG132 in conjugation with erastin. (**B**) Comparison of responses of HT-1080 wild-type and p21 KO derivatives to combination treatment of erastin and MG132. Cells were treated with erastin for 16 hrs and MG132 (20μM) was added after 12.5 hours post erastin treatment. The data in right panel of (**A**) represent the mean ± SE for three biological replicates of one representative of three independent experiments, in (**B**) represent the mean ± SD for one out of two independent experiments. The viability data have been normalized to the respective controls not treated with ferroptosis.

Research Paper

Caspase-3 knockout attenuates radiation-induced tumor repopulation via impairing the ATM/p53/Cox-2/PGE_2 pathway in non-small cell lung cancer

Minghui Zhao[1,*], Yiwei Wang[1,*], Yucui Zhao[1,*], Sijia He[1], Ruyi Zhao[1], Yanwei Song[1], Jin Cheng[1], Yanping Gong[1], Jianzhu Xie[1], Yulan Wang[1], Binjie Hu[1], Ling Tian[2,3], Qian Huang[1]

[1]Cancer Center, Shanghai General Hospital, Shanghai Jiao Tong University School of Medicine, Shanghai 201620, China
[2]Shanghai Key Laboratory for Pancreatic Diseases, Shanghai General Hospital, Shanghai Jiao Tong University School of Medicine, Shanghai 201620, China
[3]Department of Central Laboratory, Shanghai Chest Hospital, Shanghai Jiao Tong University School of Medicine, Shanghai 200030, China
*Equal contribution

Correspondence to: Qian Huang; **email:** qhuang@sjtu.edu.cn
Keywords: radiotherapy, non-small cell lung cancer, tumor repopulation, caspase-3, DNA damage response
Received: May 15, 2020 **Accepted:** July 14, 2020 **Published:** November 7, 2020

ABSTRACT

Radiotherapy is an effective treatment for non-small cell lung cancer (NSCLC). However, irradiated, dying tumor cells generate potent growth stimulatory signals during radiotherapy that promote the repopulation of adjacent surviving tumor cells to cause tumor recurrence. We investigated the function of caspase-3 in NSCLC repopulation after radiotherapy. We found that radiotherapy induced a DNA damage response (DDR), activated caspase-3, and promoted tumor repopulation in NSCLC cells. Unexpectedly, caspase-3 knockout attenuated the ataxia-telangiectasia mutated (ATM)/p53-initiated DDR by decreasing nuclear migration of endonuclease G (EndoG), thereby reducing the growth-promoting effect of irradiated, dying tumor cells. We also identified p53 as a regulator of the Cox-2/PGE_2 axis and its involvement in caspase-3-induced tumor repopulation after radiotherapy. In addition, injection of caspase-3 knockout NSCLC cells impaired tumor growth in a nude mouse model. Our findings reveal that caspase-3 promotes tumor repopulation in NSCLC cells by activating DDR and the downstream Cox-2/PGE_2 axis. Thus, caspase-3-induced ATM/p53/Cox-2/PGE_2 signaling pathway could provide potential therapeutic targets to reduce NSCLC recurrence after radiotherapy.

INTRODUCTION

With over a million deaths reported worldwide annually, lung cancer ranks among the top causes of cancer-related mortality [1]. According to a study, non-small cell lung cancer (NSCLC) accounts for approximately 85% of all lung cancers [2]. Radiotherapy has remained an effective treatment throughout the continuum of NSCLC care. Despite remarkable advances in the treatment of NSCLC using a combination of surgical techniques and systemic chemotherapy or radiotherapy, it has a dismal prognosis due to resistance to the therapy and local recurrence. Consequently, NSCLC has a median survival of less than a year and a 2-year survival rate of less than 20% [3].

Radiotherapy uses high-energy waves to kill tumor cells and shrink the gross tumor mass. However, the surviving tumor cells can repopulate because they can proliferate during the intervals between the radiotherapy sessions [4, 5]. The possible factors underlying this phenomenon include tumor hypoxia

[6], inflammation [7], angiogenesis [8], and tumor stemness [9].

In our previous studies, we demonstrated the involvement of apoptosis in tumor repopulation during radiotherapy [10, 11]. Activated caspase-3 not only executes apoptosis but also promotes the release of several growth factors from irradiated, dying tumor cells that stimulate the proliferation of adjacent living tumor cells [10]. We found that activated caspase-3 cleaved cytosolic calcium-independent phospholipase A_2 ($iPLA_2$) and subsequently increased the production of arachidonic acid (AA), a known precursor of prostaglandin E_2 (PGE_2). PGE_2 is a potent mitotic factor and involved in acute inflammatory responses [12]. We named this counterintuitive caspase-induced tumor repopulation mechanism as the "Phoenix Rising" pathway. Caspase-3 is increasingly becoming recognized as a stimulator of cellular proliferation and carcinogenesis. For instance, we previously reported that caspase-3 in dying glioma cells promoted endothelial cell mitosis by activating the NF-κB/Cox-2/PGE_2 axis to establish a pro-angiogenic microenvironment that promoted tumor repopulation [11]. Similarly, another study demonstrated that activated caspase-3/7 contributed to self-inflicted DNA double-strand breaks (DSBs), elevating the expression of CD133 in glioma cancer stem cells (CSCs) [13].

Because radiations kill tumor cells by inducing DNA lesions, we investigated if the DNA damage repair pathway participated in tumor repopulation. DNA DSBs can arise from exogenous or endogenous stressors. To repair DNA lesions, cells have evolved a complex network called DNA damage response (DDR). DDR pathways consist of numerous proteins that function as part of cell cycle checkpoints and DNA damage repair. The ataxia-telangiectasia mutated (ATM)/p53 cascade participates in DNA damage repair and is the most commonly activated DDR pathway in response to DSBs or errors occurring during the cell cycle [14, 15]. The sensor kinase ATM is recruited to the damaged sites and autophosphorylated at Ser-1981. Next, the activated ATM directly phosphorylates checkpoint kinase 2 (Chk2) on Thr-68 and p53 on Ser-15. The phosphorylated p53 is resistant to ubiquitination and induces cell cycle arrest, apoptosis, or senescence [15–17]. Irradiated cells use the DDR to repair DNA lesions and recover. Radiotherapy works on the principle that irreparable DNA damage may trigger cell death. Moreover, defects in DDR have been reported to cause genetic instability and drive carcinogenesis [18].

We conducted experiments to study the hypothesis that caspase-3 coordinates with the DDR to induce tumor repopulation during radiotherapy in NSCLC. We found that treatment with ionizing radiations induced DDR and apoptosis by activating apoptotic caspase-3 and the ATM/p53 axis. Unexpectedly, activated p53 increased the production of Cox-2/PGE_2 in the presence of activated caspase-3 in irradiated NSCLC cells. Further, the production of Cox-2/PGE_2 was remarkably suppressed in caspase-3 knockout (Casp3 KO) NSCLC cells despite the elevated expression of p53. Overall, our findings reveal that the caspase-3-induced ATM/p53/Cox-2/PGE_2 signaling pathway participates in tumor repopulation in NSCLC. These results suggest that this pathway could be exploited to develop novel therapeutic strategies to counteract tumor recurrence during radiotherapy.

RESULTS

Radiations induce DNA damage, caspase-3 activation, and tumor repopulation in NSCLC cells

We first performed a colony formation assay to find the optimal X-ray dose that induced tumor cell death. As shown in Supplementary Figure 1, the surviving fractions of A549 and H460 cells irradiated with 8 Gy X-ray were 0.043% ± 0.014% and 0.355% ± 0.018%, respectively. Thus, we selected 8 Gy dose to generate dying NSCLC cells. Phosphorylated histone H2AX (γH2AX) is a well-characterized marker of DSBs [19]. As shown in Figure 1A, compared with the control cells, the levels of γH2AX foci greatly increased in the 8 Gy-irradiated cells at 48 h after irradiation. Cell death was measured using Annexin V-fluorescein isothiocyanate (FITC) and propidium iodide (PI) double staining by flow cytometry. Compared with the control group, the percentage of early apoptotic cells (Annexin V-FITC positive and PI negative) and total dead cells (Annexin V-FITC positive) increased in both the 8 Gy-irradiated A549 and H460 groups on day 3 (Figure 1B, 1C). Because caspase-3 functions in the execution phase of apoptosis, we next used western blotting to determine whether it was activated following irradiation. We observed that 8 Gy irradiation generated cleaved caspase-3 (CC3) in a time-dependent manner in both A549 and H460 cells (Figure 1D). Moreover, immunofluorescence analysis revealed markedly enhanced expression of CC3 after 8 Gy irradiation (Figure 1E). These results demonstrate that 8 Gy irradiation induced DNA damage accompanied by cell death in NSCLC cells.

To investigate the effect of irradiated, dying NSCLC cells on living tumor cells, we conducted an *in vitro* repopulation experiment. The firefly luciferase (Fluc)-green fluorescent protein (GFP)-labeled cells were named Fluc cells (reporter cells). We observed that the luciferase activity of A549 Fluc or H460 Fluc cells

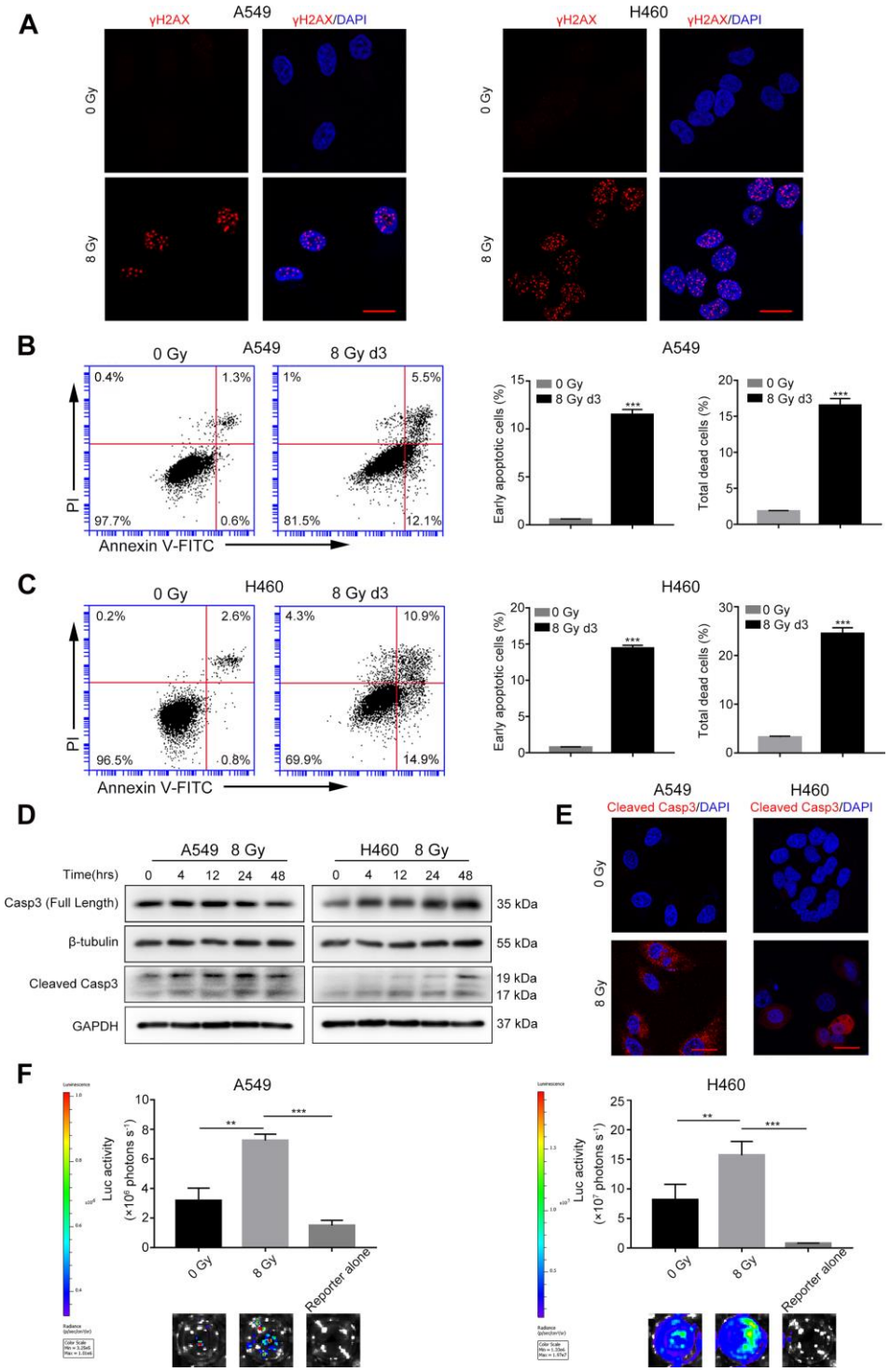

Figure 1. Radiations induce DNA damage, caspase-3 activation, and tumor repopulation in NSCLC cells. (**A**) Confocal images of immunostained A549 and H460 cells showing γH2AX foci following 8 Gy irradiation at 48 h. Scale bars: 25 µm. (**B**, **C**) The left panel shows flow cytometry analysis of A549 (**B**) and H460 (**C**) cell death after 0 Gy or 8 Gy irradiation on day 3. Apoptosis was monitored by Annexin V/propidium iodide (PI) double staining. The right panel shows quantitative analysis of early apoptosis and total cell death in 0 Gy- or 8 Gy-irradiated A549 (**B**) and H460 (**C**) cells (***p<0.001, Student's t test, n = 3). (**D**) Cleaved caspase-3 induced by 8 Gy radiations was assayed by western blotting, and β-tubulin and glyceraldehyde 3-phosphate dehydrogenase (GAPDH) served as loading controls. (**E**) Representative confocal images of immunostained A549 and H460 cells showing cleaved caspase-3 following exposure to 8 Gy radiations on day 3. Scale bars: 25 µm. (**F**) The 8 Gy-irradiated NSCLC cells promoted the growth of living NSCLC reporter cells. The upper panel depicts luciferase activities showing the growth of A549 Fluc and H460 Fluc cells that were seeded alone or with 0 Gy- or 8 Gy-irradiated NSCLC cells. The lower panel shows the representative bioluminescence images (**p<0.01, ***p<0.001, one-way analysis of variance [ANOVA], n = 4).

linearly correlated with the cell numbers (Supplementary Figure 2); thus, we used luciferase assay to measure the proliferation of Fluc-GFP-labeled cells. Subsequent results demonstrated that 8 Gy-irradiated A549 feeder cells promoted the proliferation of A549 Fluc reporter cells as compared with A549 Fluc reporter cells growing on sham-irradiated feeder cells or no feeder cells (Figure 1F). Similarly, 8 Gy-irradiated H460 feeder cells exerted potent growth-stimulating effects on H460 Fluc reporter cells (Figure 1F).

Casp3 KO attenuates the growth-promoting effect of dying NSCLC cells *in vitro*

We have previously reported a critical function of caspase-3 in breast and melanoma tumor cell repopulation [10, 20]. In the present study, we investigated whether caspase-3 exerted a growth-promoting effect of dying NSCLC cells. Using CRISPR/Cas9 technology, we generated A549 and H460 cells with genetic ablation of caspase-3 (Casp3 KO cells). First, we performed immunoblotting assays to assess the efficiency of Casp3 KO cells in different mutant single-cell clones (data not shown) and subsequently selected a clone with a sufficient Casp3 KO effect. As shown in Figure 2A, compared with the control A549 or H460 cells (wild-type), the levels of caspase-3 were reduced in selected Casp3 KO clones. Furthermore, we found that compared with the control group, the percentage of early apoptotic cells and total dead cells decreased in both 8 Gy-irradiated A549/Casp3 KO and H460/Casp3 KO groups on day 3 (Figure 2B, 2C). Using the *in vitro* repopulation model, we observed that 8 Gy-irradiated Casp3 KO feeder cells diminished the growth-stimulating effect of caspase-3 on both A549 and H460 living reporter cells (Figure 2D).

Activated Cox-2/PGE_2 signaling in dying cells promotes adjacent living tumor cell growth

Because Cox-2 is involved in the production of bioactive lipid PGE_2, and we previously identified PGE_2 as a downstream effector of caspase-3 in tissue regeneration [21], angiogenesis [11], and breast tumor repopulation [10], we hypothesized that caspase-3 could promote PGE_2 production by increasing Cox-2 expression in dying NSCLC cells. Western blotting and quantitative real-time polymerase chain reaction (qPCR) showed elevated expression and transcription of Cox-2 in both A549 and H460 cells after exposure to 8 Gy radiations in a time-dependent manner (Figure 3A, 3B). However, the expression and transcription of Cox-2 were markedly inhibited in Casp3 KO cells following 8 Gy irradiation (Figure 3A, 3B). We next analyzed the production of PGE_2 in supernatants obtained from irradiated A549 and A549/Casp3 KO cells using enzyme-linked immunosorbent assay (ELISA). As shown in Figure 3C, the levels of PGE_2 in 8 Gy-irradiated A549 cells on day 2 increased approximately fourfold as compared with those in non-irradiated A549 cells. However, the secretion of PGE_2 was considerably lower in Casp3 KO cells with or without 8 Gy irradiation. Moreover, similar results were obtained in H460 and H460/Casp3 KO cells. To determine the function of PGE_2 in regulating the growth-stimulating effect of dying NSCLC cells *in vitro*, we next studied whether the growth of living NSCLC cells was inhibited with the downregulation of Cox-2. Treatment with celecoxib (1 μM or 5 μM), a selective Cox-2 inhibitor, dramatically decreased the growth-stimulating effect of dying A549 or H460 feeder cells on A549 Fluc or H460 Fluc reporter cells in a dose-dependent manner (Figure 3D). In summary, these results demonstrate that PGE_2 is involved in caspase-3-induced NSCLC cell repopulation after irradiation.

Casp3 KO attenuates DDR, ATM/p53 signaling, and p53-induced Cox-2 expression in dying NSCLC cells

We next studied the mechanisms by which caspase-3 enhanced the expression of Cox-2. During apoptosis, the mitochondrial protein endonuclease G (EndoG) migrates to the nucleus and cleaves the DNA [22]. The distribution of EndoG was determined through an immunofluorescence assay. As shown in Figure 4A, compared with the poor staining observed in the cytoplasmic regions of non-irradiated cells, radiotherapy increased the nuclear EndoG staining in NSCLC cells. Interestingly, caspase-3 activity regulates the cytoplasmic to nuclear migration of EndoG. The EndoG nuclear migration was suppressed in irradiated Casp3 KO cells, as evident from poor nuclear EndoG staining. Moreover, we found that irradiated wild-type cells with nuclear EndoG staining showed higher formation of γH2AX foci. However, the nuclear EndoG and γH2AX foci double staining was mostly absent in irradiated Casp3 KO cells. Next, we performed western blotting to examine the location of EndoG before and after irradiation of NSCLC cells (Figure 4B).

As ATM is a major sensor of DSBs [23], we assessed the protein levels of pATM (S1981) following irradiation. We observed robust ATM phosphorylation in parental A549 and H460 cells after irradiation. Interestingly, Casp3 KO reduced the levels of pATM and total ATM after irradiation (Figure 4C). Activated ATM phosphorylates several substrates, such as Chk2 and p53, thereby propagating the damage signal to numerous cellular pathways [23]. We next investigated whether activated ATM in A549 cells triggered the activation of Chk2 and p53. The levels of pChk2 (T68), p53, and pp53 (S15) were considerably higher after

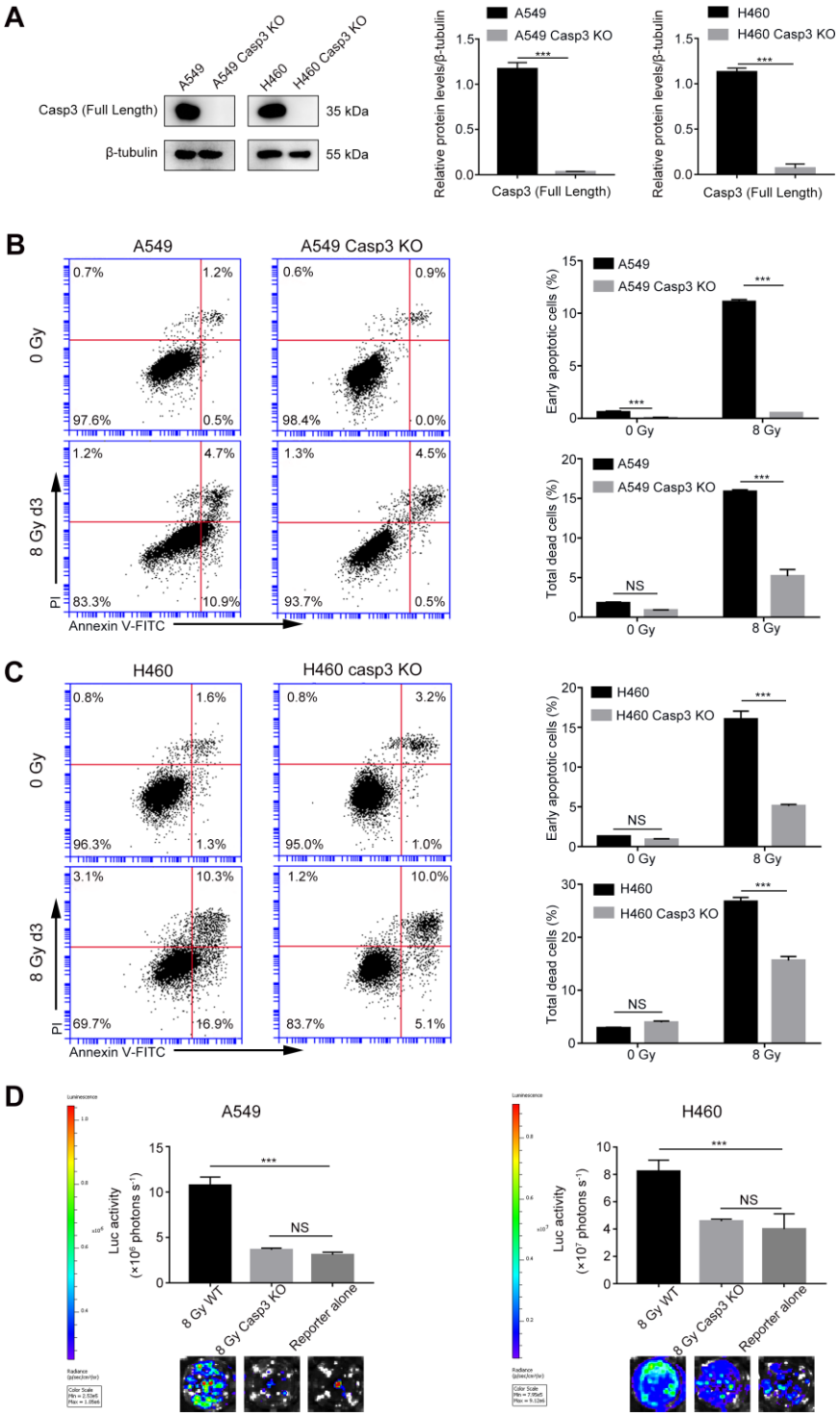

Figure 2. Casp3 KO attenuates radiation-induced apoptosis and growth-promoting effect of dying NSCLC cells. (**A**) Western blot analysis of the expression of caspase-3 in Casp3 KO A549 and H460 cells generated using the CRISPR/Cas9 system. β-tubulin was used as the loading control (***p<0.001, Student's t test, n = 3). (**B**, **C**) The left panel shows the flow cytometry analysis of cell death in A549 and A549/Casp3 KO (**B**) and H460 and H460/Casp3 KO (**C**) cells following irradiation. Apoptotic cells were analyzed by Annexin V/propidium iodide (PI) double staining. The right panel shows the quantitative analysis of early apoptosis and total cell death in 0 Gy- or 8 Gy-irradiated control and A549/Casp3 KO (**B**) and H460/Casp3 KO (**C**) cells (***p<0.001, NS = not significant, Student's t test, n = 3). (**D**) Casp3 KO significantly decreased the growth-promoting effect of 8 Gy-irradiated NSCLC cells on living NSCLC reporter cells. The upper panel depicts the luciferase activities showing the growth of A549 Fluc or H460 Fluc cells that were seeded with 8 Gy-irradiated wild-type or Casp3 KO cells or alone. The lower panel shows the representative bioluminescence images (***p<0.001, NS = not significant, one-way analysis of variance [ANOVA], n = 4).

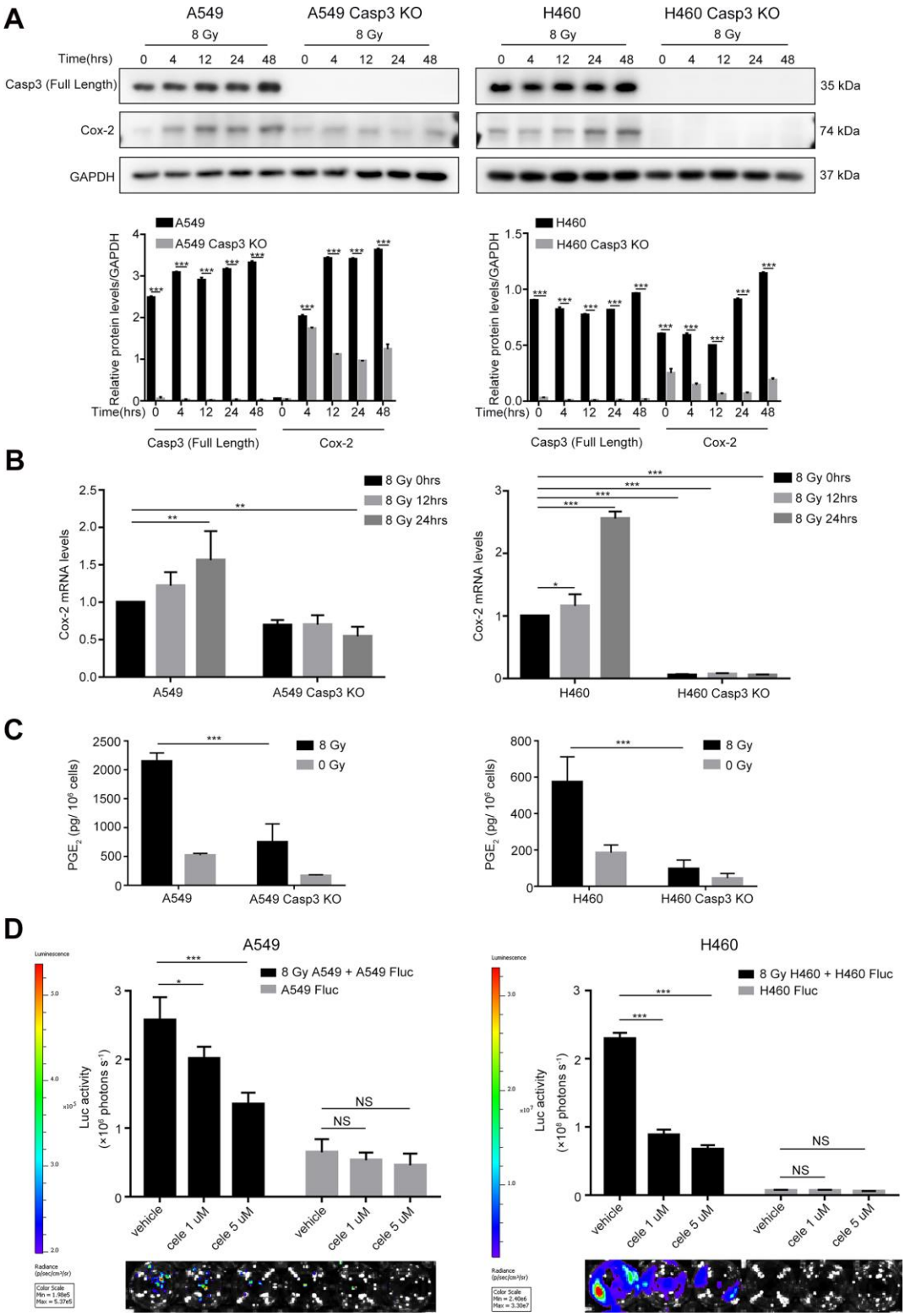

Figure 3. Caspase-3-dependent PGE_2 production in dying NSCLC cells induces tumor repopulation. (**A**) Western blot analysis of Cox-2 levels at various time intervals after 8 Gy irradiation of wild-type and Casp3 KO NSCLC cells (***p<0.001, one-way analysis of variance [ANOVA], n = 3). (**B**) Quantitative polymerase chain reaction (qPCR) analysis of Cox-2 in wild-type and Casp3 KO NSCLC cells at indicated times after 8 Gy irradiation (*p<0.05, **p<0.01, ***p<0.001, one-way ANOVA, n = 3). (**C**) Levels of prostaglandin E_2 (PGE_2) in culture supernatants of wild-type and Casp3 KO NSCLC cells at 48 h after 8 Gy irradiation were measured using enzyme-linked immunosorbent assay (ELISA) (***p<0.001, one-way ANOVA, n = 3). (**D**) A selective Cox-2 inhibitor, celecoxib, abrogated the pro-proliferation effects of dying NSCLC cells on Fluc cells in a dose-dependent manner (*p<0.05, ***p<0.001, NS = not significant, one-way ANOVA, n = 4).

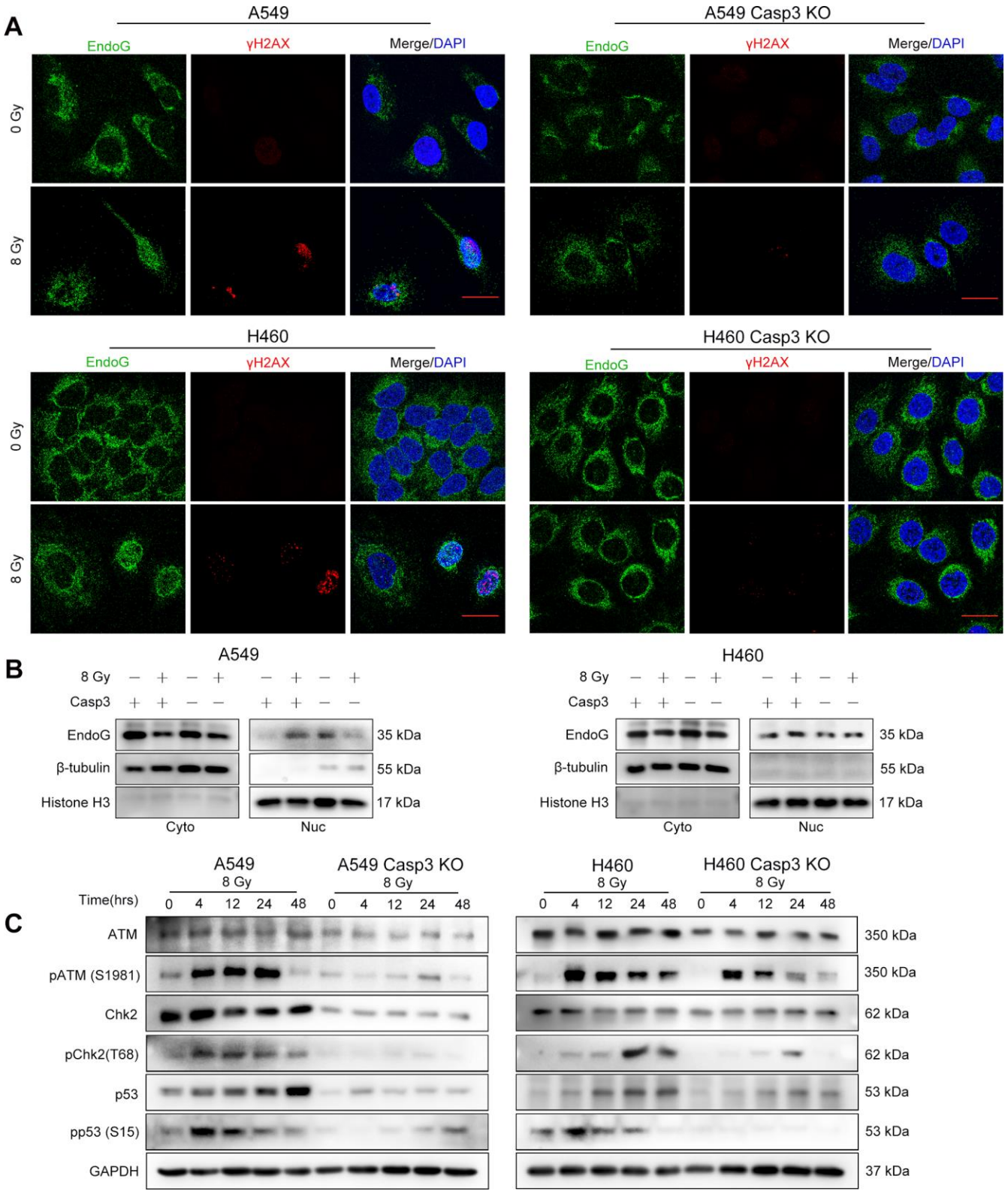

Figure 4. Casp3 KO attenuates the DDR *via* ATM/p53 signaling in irradiated NSCLC cells. (**A**) Immunofluorescence analysis of 8 Gy-irradiated wild-type and Casp3 KO NSCLC cells co-stained for EndoG and γH2AX foci at 48 h. Scale bars: 25 μm. (**B**) Western blot analysis of EndoG in the cytoplasmic and nuclear fractions of 8 Gy-irradiated wild-type and Casp3 KO NSCLC cells at 48 h. β-tubulin and Histone H3 were used as cytoplasmic and nuclear loading controls, respectively. (**C**) Levels of DNA damage response (DDR)-related proteins ATM, pATM (S1981), Chk2, pChk2 (T68), p53, and pp53 (S15) were measured by western blotting at indicated times after 8 Gy irradiation of wild-type and Casp3 KO NSCLC cells. GAPDH was used as the loading control.

irradiation than in the control cells, whereas Casp3 KO reduced the levels of these proteins (Figure 4C). In addition, H460 cells showed similar results with or without Casp3 KO after irradiation (Figure 4C). These results suggest that caspase-3 induces DDR *via* ATM/p53 signaling.

It was previously demonstrated that the tumor suppressor p53 induced the expression of Cox-2 in response to DNA damage [24]. To elucidate whether p53 regulated the transcription of the *PTGS2* gene (encodes Cox-2), we first searched the JASPAR database (http://jaspar.genereg.net) to predict p53 binding sites in the PTGS2 promoter (Supplementary Figure 3). Next, we constructed a luciferase reporter plasmid encoding the PTGS2 promoter sequence (PTGS2-WT) or mutant sequence (PTGS2-Mut) in a region between −1251 bp and −1238 bp (Figure 5A). As shown in Figure 5B, p53-overexpressing cells exhibited higher luciferase activity in the PTGS2-WT group than in the control group. However, in the PTGS2-Mut group, the overexpression of p53 did not result in a major difference as compared with the controls. Next, we examined the transcript levels of Cox-2 following the overexpression of p53. As shown in Figure 5C, 24 h after transfection in A549 and H460 cells, the levels of Cox-2 transcript increased by more than 10-fold. We found a markedly less p53-induced expression of Cox-2 in Casp3 KO cell lines (Figure 5C). Further, western blotting results showed that the expression of Cox-2 in p53-overexpressing A549 and H460 cells was considerably higher than in p53-overexpressing Casp3

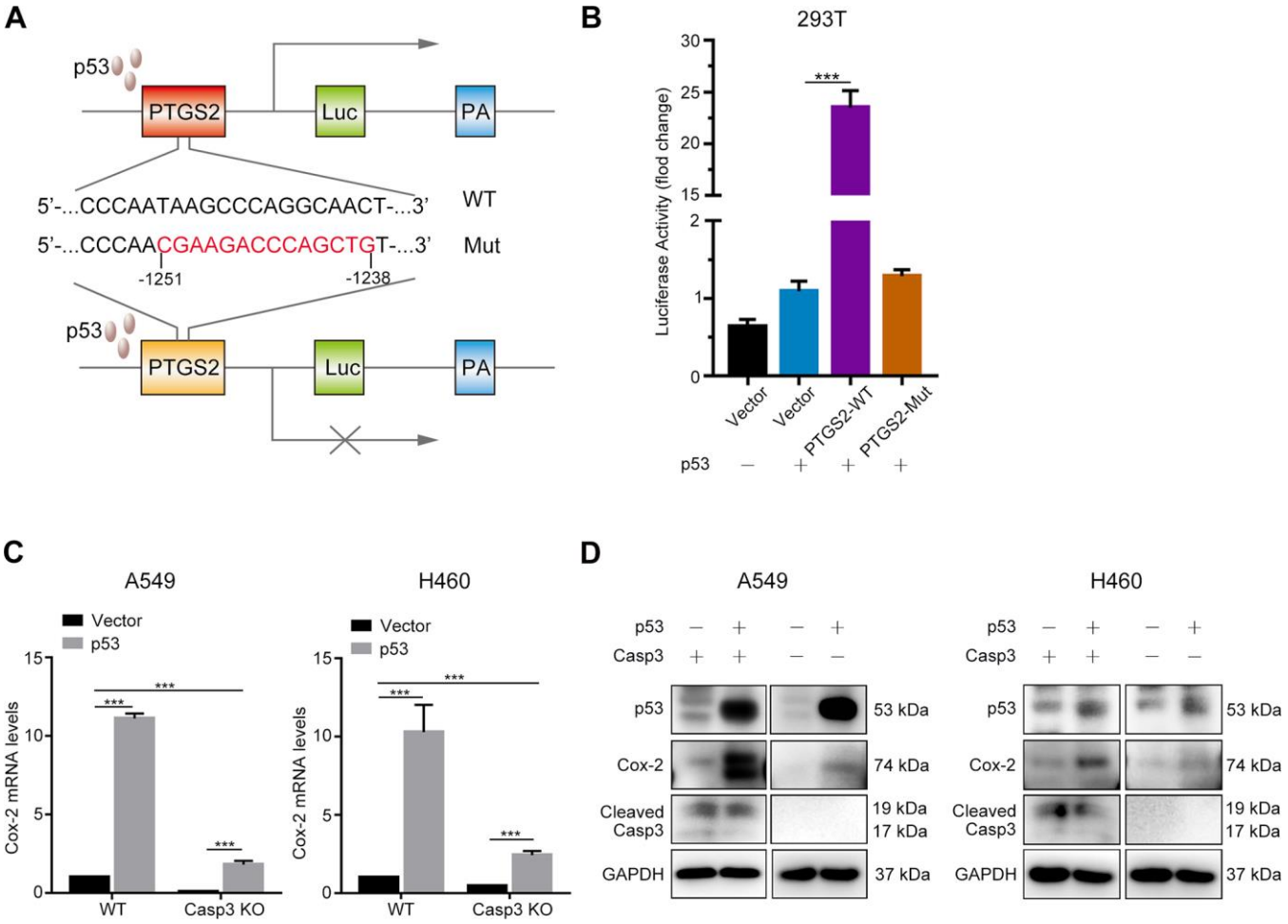

Figure 5. p53 induces Cox-2 in NSCLC cells. (**A**) Schematic representation of the luciferase reporter plasmid with the wild-type PTGS2 promoter sequence (PTGS2-WT) or mutant sequence (PTGS2-Mut). (**B**) A p53-dependent stimulation of PTGS2 promoter activity was demonstrated by luciferase assay. The 293T cells were co-transfected with p53 overexpression plasmid and PTGS2-WT plasmid, PTGS2-Mut plasmid, or vector alone. The pGMR-TK reporter was used as an internal transfection standard (***p<0.001, one-way analysis of variance [ANOVA], n = 3). (**C**, **D**) Quantitative polymerase chain reaction (qPCR) and western blot analysis showed that the mRNA and protein levels of Cox-2 were elevated by overexpression of p53 in wild-type and Casp3 KO NSCLC cells. Total RNA and proteins were extracted after transfection for 24 h and 48 h, respectively (***p<0.001, Student's t test, n = 3).

KO cells (Figure 5D). Based on these results, we conclude that p53, as a transcription factor, activates the expression of *PTGS2* in NSCLC.

Caspase-3 knockout decreases tumorigenicity, and radiations activate the ATM/p53/Cox-2 axis *in vivo*

To determine the effect of Casp3 KO on tumorigenicity *in vivo*, we subcutaneously inoculated wild-type and Casp3 KO H460 cells into nude mice. After 22 days, the volumes of the implanted tumors reached approximately 2000 mm^3 in mice in the wild-type group (left armpit, 7/7). However, no tumor formation was observed in mice in the Casp3 KO group (right armpit, 0/7) (Figure 6A–6C). These data suggested that the knockout of caspase-3 inhibited tumorigenicity *in vivo*. Next, mice were randomly divided into two groups and exposed to either 0 Gy or 8 Gy radiations. Consistent with the *in vitro* results, immunohistochemistry showed enhanced levels of CC3 48 h after irradiation (Figure 6D). Moreover, a high number of pATM (S1981)-, pChk2 (T68)-, p53-, pp53 (S15)-, and Cox-2-positive cells were observed in mice in the 8 Gy radiation group (Figure 6D). The mRNA levels of p53 and Cox-2 were elevated in tumor tissues after irradiation (Supplementary Figure 4). Altogether, these results imply that the activation of caspase-3 and the ATM/p53 signaling pathway following irradiation induces the expression of Cox-2 (Figure 7).

DISCUSSION

Radiotherapy treats cancer by triggering tumor cell death *via* apoptosis and/or necrosis [25, 26]. Caspase-3 is one of the core effector caspases responsible for apoptosis [27], and caspase-3 activity is widely used to evaluate the efficacy of anticancer therapeutics [28, 29]. In the present study, we demonstrated that caspase-3 coupled with DDR stimulated the proliferation of living tumor cells present adjacent to dying NSCLC cells, suggesting its involvement in tumor relapse following radiotherapy. A comparison of Casp3 KO cells with wild-type cells demonstrated that apoptotic caspase-3 induced tumor repopulation in NSCLC by 1) inducing DDR *via* activation of the ATM/p53 signaling pathway and by 2) activating the Cox-2/PGE_2 axis *via* p53.

DDR is essential for the maintenance of genome integrity, and any defect in this repair process increases the predisposition to cancer [30]. DNA damage repair system comprises two main pathways: homologous recombination (HR) [31] and non-homologous end joining (NHEJ) [32]. In HR, cells use a homologous DNA sequence to guide accurate repair, whereas NHEJ involves ligating the broken ends after removing the damaged nucleotides at the end of DNA break sites. As a master regulator of DDR, ATM activates both HR- and NHEJ-mediated DNA repair pathways. Mutations in ATM have been implicated in NSCLC [33], and its loss has been reported as an early event in NSCLC carcinogenesis [34]. In addition, an ongoing phase I clinical trial (NCT03225105) is evaluating the efficiency of ATM inhibitor M3541 in combination with radiotherapy in patients with solid tumors [35]. Moreover, other DDR inhibitors in preclinical and clinical studies have been shown to improve antitumor activity in HR-deficient (HRD) tumors [36]. For example, olaparib, a pharmaceutical inhibitor of poly (ADP-ribose) polymerase (PARP), has been used successfully to treat BRCA-mutant ovarian [37], breast [38], prostate [39], and pancreatic cancers [40]. Although PARP inhibitors as single agents have been unsuccessful in treating BRCA-proficient cancers, including NSCLC [41], a recent study has reported that a combination of DNA methyltransferase inhibitors and PARP inhibitors enhanced the sensitivity of NSCLC cells to radiations [42].

Because DNA damage inducers, such as radiations, trigger apoptosis, the finding that apoptotic caspase-3 reversely promoted DSBs following irradiation in NSCLC cells was surprising [43]. The results of our study revealed a novel function of activated caspase-3, i.e., activation of DDR by promoting nuclear translocation of EndoG following irradiation. Our results are consistent with those of other studies. For instance, Liu et al. reported that a moderate radiation dose ($\leq$ 6 Gy) sublethally activated caspase-3, causing DNA damage [44]. Similarly, Liu et al. found that activation of caspase-3 and nucleases resulted from spontaneous cytochrome C leakage, causing DNA damage and ATM activation, and leading to cancer stemness and tumorigenicity [13]. Another study reported that lethally activated caspase-3, in etoposide- or tumor necrosis factor (TNF)α-treated Hela cells, cleaved Cdc6 at D^{290}/S and D^{442}/G sites to activate ATM/ATR kinase and apoptosis [45]. Our findings demonstrated that lethally activated caspase-3 induced DDR following irradiation in an ATM/p53 pathway-dependent manner in NSCLC.

The Cox-2/PGE_2 axis is involved in tumor initiation, progression, and recurrence [46]. In our study, compared with irradiated wild-type cells, caspase-3 knockout impaired the expression of Cox-2/PGE_2 with a concurrent decrease in tumor repopulation. However, studies have reported controversial findings regarding the relationship between p53 and Cox-2 [24, 47–49]. In this study, the overexpression of p53 induced Cox-2, as revealed by a luciferase reporter assay, suggesting that Cox-2 acted as a transcriptional target of p53 in

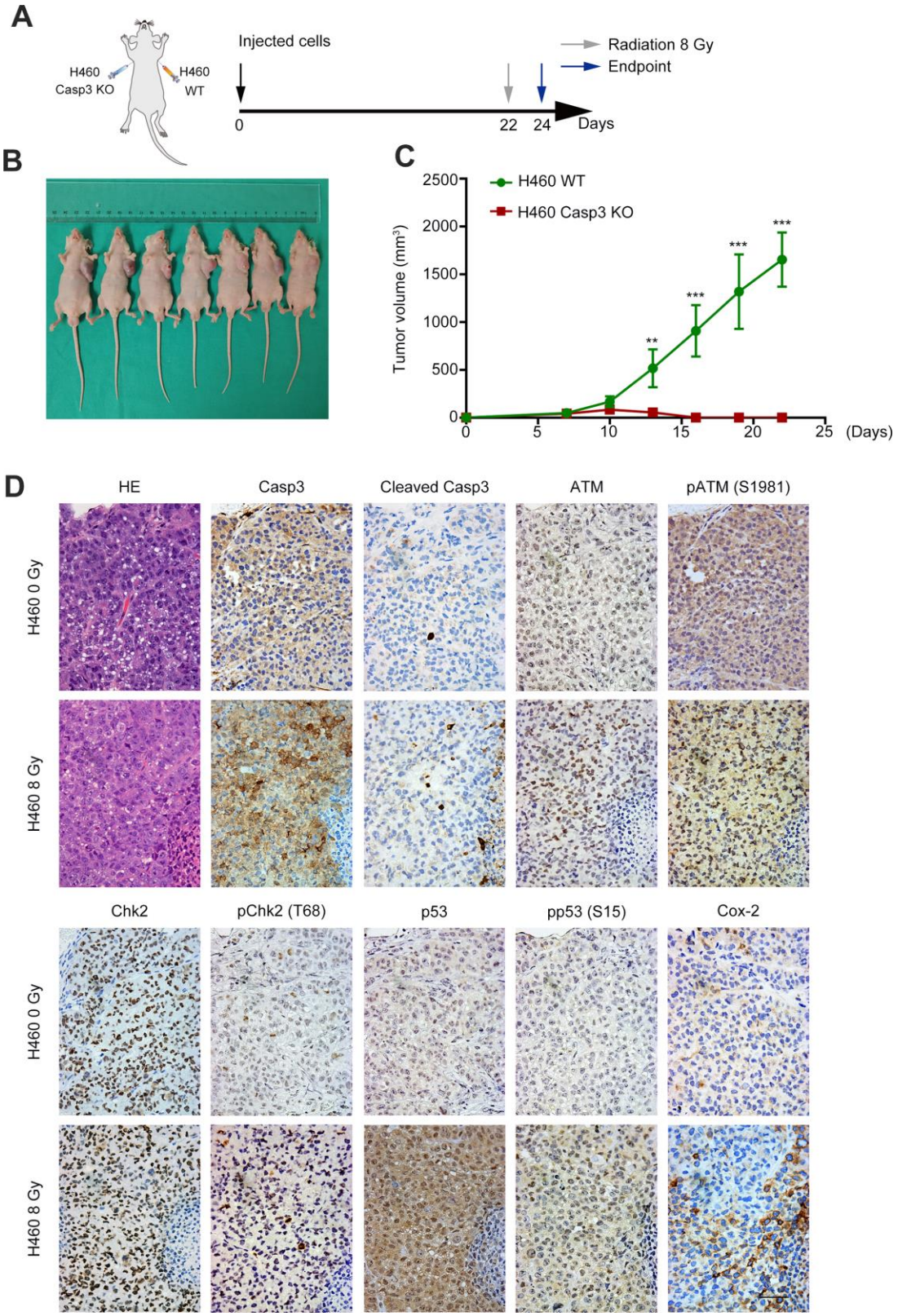

Figure 6. Casp3 KO inhibits tumor formation, and radiations activate the ATM/p53/Cox-2 axis *in vivo*. (**A**) Treatment scheme for nude mice. (**B**) Images of tumors obtained on day 22. (**C**) The tumor volume of xenografts was measured with calipers every 2 or 3 days (**p<0.01, ***p<0.001, Student's t test, n = 7). (**D**) Representative photomicrographs of hematoxylin and eosin (H&E) and immunohistochemical staining of caspase-3, cleaved caspase-3, ATM, pATM (S1981), Chk2, pChk2 (T68), p53, pp53 (S15), and Cox-2 in tumor tissues. Scale bars: 50 µm.

NSCLC. Our data showed that the absence of caspase-3 suppressed the expression of Cox-2, indicating a critical function of caspase-3 in the Cox-2 regulation. In addition, the protein levels of CC3 did not change after p53 overexpression in A549 and H460 cells (Figure 5D). This was consistent with the findings of previous studies, which demonstrated that the restoration of p53 in solid organ tumors primarily caused cell senescence than apoptosis [50, 51]. These results suggest that the Cox-2/PGE_2 axis is a downstream target of the caspase-3-centered DDR pathway, which participates in radiation-induced tumor repopulation.

Although our study focuses on Cox-2/PGE_2 as the downstream effector of caspase-3, radiation-induced dying NSCLC cells may also secrete additional growth-stimulating factors, such as vascular endothelial growth factor A (VEGF-A), to contribute to tumor relapse after radiotherapy [11, 52]. In addition, caspase-3 may modulate Cox-2 expression through other pathways [10, 11].

In summary, caspase-3 functions with DDR to induce tumor repopulation after radiotherapy in NSCLC, and the Cox-2/PGE_2 axis controls the progression of

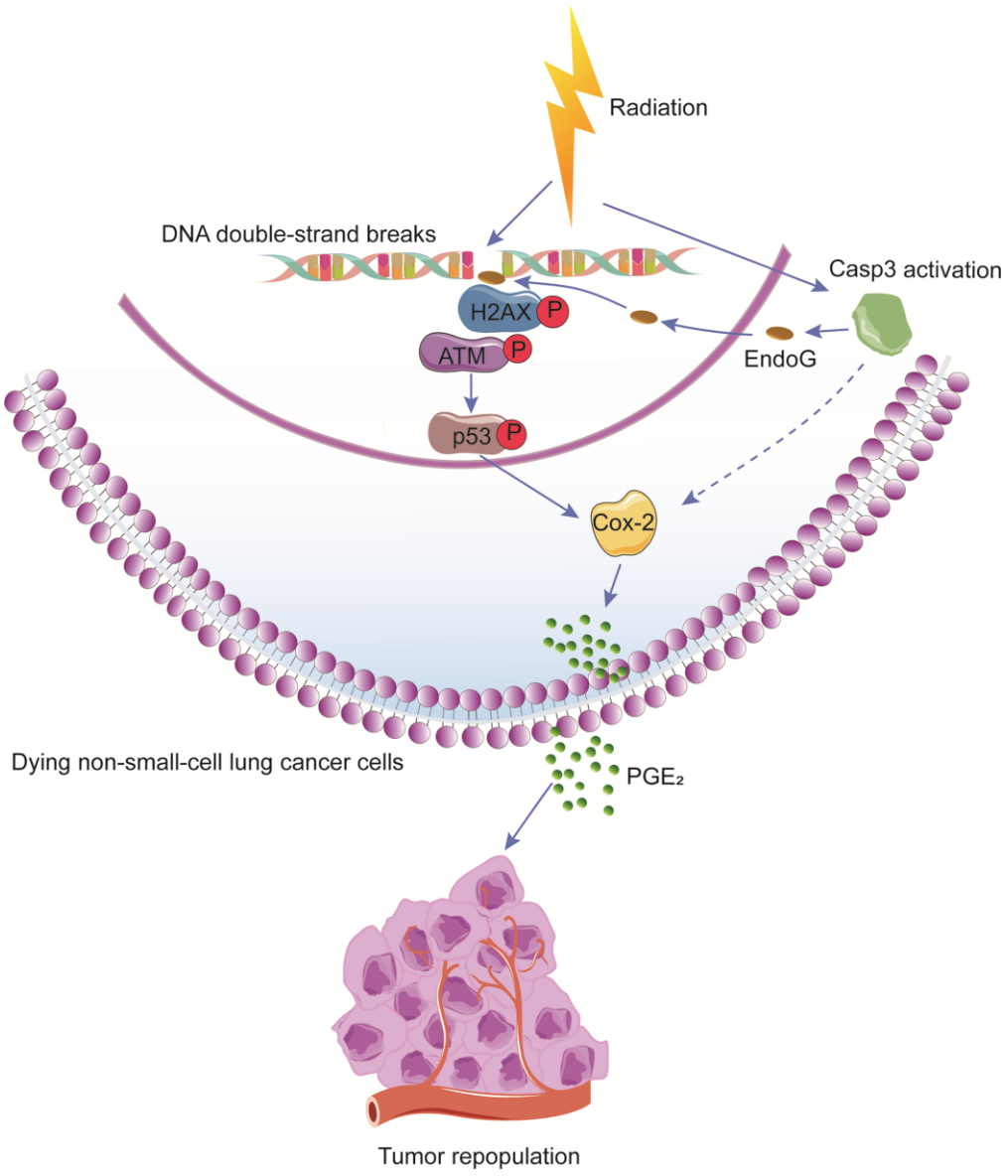

Figure 7. Schematic illustration of the proposed mechanism of radiation-induced tumor repopulation in NSCLC. Radiation-induced DNA double-strand breaks (DSBs) activate the DNA damage response (DDR) and caspase-3. Activated caspase-3 regulates the EndoG nuclear translocation and thus participates in the DDR by regulating ATM/p53 signaling, which activates the Cox-2/PGE_2 axis in dying NSCLC cells, consequently enhancing the proliferation of living tumor cells.

NSCLC after radiotherapy. These molecules could provide promising therapeutic targets for NSCLC.

MATERIALS AND METHODS

Cell culture and irradiation

Human 293T cells and NSCLC cell lines H460 and A549 were purchased from the American Type Culture Collection. The 293T cells were cultured in Dulbecco's Modified Eagle's medium (DMEM), and H460 and A549 cells were cultured in Roswell Park Memorial Institute (RPMI) 1640 medium supplemented with 10% fetal bovine serum (FBS), and 100 units/mL penicillin and 100 μg/mL streptomycin (both from Thermo Fisher Scientific) at 37°C in a humidified incubator with 5% CO_2. Cells or mice were irradiated in a cabinet X-ray generator (Faxitron) operated at 180 kVp and 10 mA with a dose rate of 3.0 Gy/min for the time required to apply a prescribed dose at room temperature.

Lentivirus packaging and transduction

To construct lentivirus particles, the pLEX lentiviral system (Open BioSystems) was used to transduce genes into the target cells. The Fluc and GFP fusion gene was kindly provided by Prof. Chuan-Yuan Li. Fluc- and GFP-labeled cells were generated *via* lentivirus infection, as previously described [10]. Subsequently, the cells were cultured in RPMI 1640 medium supplemented with 10% FBS, and transfected cells were selected using 1 μg/mL puromycin for 2 weeks.

Establishment of caspase-3 knockout cells

Casp3 KO A549 and H460 cells were established using the CRISPR/Cas9 genome editing system. The Casp3 KO lentivirus-based CRISPR plasmid [13, 53] (designated as the Casp3 KO plasmid) was also a kind gift from Prof. Li. The single guide RNA (sgRNA) sequence used to disrupt the *CASP3* gene was 5'-TAGTTAATAAAGGTATCCA-3'. This plasmid was packaged according to an established protocol [54]. A549 and H460 cells were seeded into a 6-well plate at a density of 5×10^5 cells, and subsequently infected with the Casp3 KO plasmid-encoding lentivirus for 24 h and cultured in RPMI 1640 medium supplemented with 10% FBS. Forty-eight hours after infection, cells were selected in a culture medium containing 1 μg/mL puromycin for 2 weeks. Surviving cells were then trypsinized (Gibco) to obtain single cells that were seeded into 96-well plates at 1 cell per well. Clones derived from single cells were selected, and western blotting was used to identify the efficiency of genome editing after a clone expansion period. Clones with no detectable caspase-3 signal were selected for further study.

Clonogenic assay

Cells were counted and seeded into 6-well plates. Next, the cells were exposed to different radiation doses (0, 2, 4, 6, or 8 Gy with 100 to 10,000 cells per well). After 10 to 14 days, cells were fixed with 4% paraformaldehyde (Sangon Biotech) and stained with crystal violet (Beyotime). Colonies containing more than 50 cells were scored under a Leica light microscope. The assay was performed in triplicate. The surviving fraction was calculated as previously described [55].

Flow cytometry

Cells were treated with 8 Gy radiations for 72 h and subsequently stained with fluorescein isothiocyanate (FITC)–Annexin V and propidium iodide (PI) using a FITC Annexin V Apoptosis Detection Kit (BD Biosciences) following the manufacturer's instructions. Apoptosis was measured on a BD Accuri C6 flow cytometer.

Western blotting

Whole cell lysates were prepared in radioimmunoprecipitation assay (RIPA) buffer with protease and phosphatase inhibitors (Roche) at 4°C. Protein concentrations were determined using a bicinchoninic acid (BCA) protein assay kit (Thermo Scientific). Western blotting was performed as previously described [56]. Primary antibodies against β-tubulin, glyceraldehyde 3-phosphate dehydrogenase (GAPDH), caspase-3, CC3, Cox-2, ATM, pATM-S1981, pChk2-T68, pp53-S15 (#2128, #5174, #9662, #9664, #12282, #2873, #5883, #2197, #9286, respectively, Cell Signaling Technology), p53, EndoG, Histone H3 (#ab1101, #ab9647, #ab1791, respectively, Abcam), and Chk2 (#A19543, ABclonal) were used.

Tumor repopulation model and bioluminescence imaging

In our *in vitro* repopulation model, 1 to 2.5×10^5 irradiated cells (feeder cells) were co-cultured with a small number (200 or 500) of non-irradiated Fluc cells (reporter cells). During co-culturing, the culture medium was replaced with fresh RPMI 1640 medium containing 2% FBS every 2 days. After 6 to 10 days, the growth of Fluc cells was measured by bioluminescence imaging. D-Luciferin potassium salt (0.15 mg/mL; Synchem) was used as the bioluminescent substrate, and the bioluminescence was measured using the IVIS Lumin Series III imaging system (PerkinElmer).

Quantitative real-time polymerase chain reaction

Total RNA was extracted from the cells using the RNA extracting reagent RNAiso Plus (#9109, Takara) and reverse transcribed into cDNA using the PrimeScrip RT Master Mix Kit (#RR036A, Takara). Quantitative real-time polymerase chain reaction (qPCR) was performed using the TB Green Premix Ex Taq Kit (#RR420A, Takara) according to the manufacturer's instructions. The primers for *Cox-2* were 5'-GAAGTCCCTGAGC ATCTACGG-3' (forward) and 5'-CCTATCAGTATTA GCCTGCTTGTCT-3' (reverse). The primers for *p53* were 5'-ACCTATGGAAACTACTTCCTGAAA-3' (forward) and 5'-CTGGCATTCTGGGAGCTTCA-3' (reverse). The primers for *GAPDH* were 5'-CCGGGA AACTGTGGCGTGATGG-3' (forward) and 5'-AG GTGGAGGAGTGGGTGTCGCTGTT-3' (reverse). GAPDH was used as the loading control. The qPCR procedure was performed under the following conditions: 30 s at 95°C, followed by 40 cycles of 5 s at 95°C and 30 s at 60°C. The results were obtained from three independent experiments. Differences in the relative expression were calculated using the $2^{-\Delta\Delta CT}$ method.

Transient transfection

For p53 overexpression, we transiently transfected the pcDNA3-p53 (WT) plasmid into cells using Lipofectamine 2000 reagent (Life Technologies) following the recommended protocol. The pcDNA3-p53 (WT) plasmid was synthesized by HarO Life, and the empty pcDNA3 plasmid (Invitrogen) was used as the control. Cells were incubated with Opti-MEM (Gibco) without FBS during transfections, and the transfection medium was replaced with RPMI 1640 medium after 6 h.

PGE_2 enzyme-linked immunosorbent assay

Cells were cultured in RPMI 1640 medium supplemented with 10% FBS and treated with 8 Gy radiations. Culture media were removed and replaced with fresh media containing 2% FBS for 16 h before the collection of supernatants at 48 h following irradiation. The levels of PGE_2 in the supernatants were measured using the Prostaglandin E_2 Express ELISA Kit (Cayman Chemical) according to the manufacturer's instructions.

Reagents

Celecoxib was purchased from Selleck (#S1261).

Immunofluorescence staining

Cells were incubated with antibodies against γH2AX (#80312, Cell Signaling Technology), caspase-3 (#9662, Cell Signaling Technology), or EndoG (#ab9647, Abcam) overnight at 4°C, followed by incubation with an Alexa Fluor 488- or 594-conjugated secondary antibody (Proteintech) for 1 h at room temperature. Nuclei were counterstained with DAPI (Yeasen). Images were captured using a confocal laser scanning microscope (Leica Microsystems).

Luciferase reporter assay

The upstream 2 kb promoter region of *PTGS2* (Cox-2) containing the potential p53 binding site was cloned into the GV238 (GeneChem) luciferase reporter vector (PTGS2-WT). Further, this region with a mutated p53 binding site was cloned into the same luciferase reporter vector (PTGS2-Mut). Next, 293T cells were co-transfected with the p53 overexpression (pcDNA3-p53) plasmid and PTGS2-WT plasmid, PTGS2-Mut plasmid, or empty vector for 24 h. Luciferase activity was determined using the dual luciferase reporter assay system (Promega), and the firefly luciferase activity was normalized to that of Renilla luciferase activity.

Xenograft tumor model

All animal protocols were approved by the Shanghai General Hospital Institutional Animal Care and Use Committee and were conducted in accordance with the guidelines from the Directive 2010/63/EU of the European Parliament on the protection of animals used for scientific purposes. Five-week-old BALB/c mice were housed in specific pathogen-free (SPF) facilities with free access to normal chow and water. Wild-type or Casp3 KO H460 cells (5×10^6 cells) were injected subcutaneously into the left and right armpit regions, respectively, of seven nude mice. The tumor volume (volume = length × width^2/2) was determined using calipers every 2 to 3 days. When the mean tumor volumes reached approximately 2000 mm^3, the mice were randomly divided into two groups: 0 Gy radiation (n = 3) and 8 Gy radiation (n = 4). Forty-eight hours after radiation treatment, all experimental mice were sacrificed, and tumor sections were collected for further pathologic examination.

Hematoxylin and eosin staining and immunohistochemistry

Hematoxylin and eosin (H&E) staining and immunohistochemistry (IHC) were performed as previously described [57, 58]. Primary antibodies against caspase-3, CC3, Cox-2, ATM, pATM-S1981, pChk2-T68, pp53-S15 (#9662, #9664, #12282, #2873, #5883, #2197, #9286, respectively, Cell Signaling Technology), p53 (#ab1101, Abcam), and Chk2 (#A19543, ABclonal) were used. The sections were incubated with horseradish

peroxidase-conjugated secondary antibody (EnVision III Detection System; GK500705; GeneTech), and counterstained with hematoxylin before visualized using a Leica light microscope.

Statistical analysis

All data are expressed as mean ± standard error (SE). Statistical analysis was performed using unpaired Student's *t* test or one-way analysis of variance (ANOVA) with SPSS version 18.0. A P-value < 0.05 was considered significant.

Abbreviations

AA: arachidonic acid; ATM: ataxia-telangiectasia mutated; Chk2: checkpoint kinase 2; DDR: DNA damage response; DSBs: DNA double-strand breaks; ELISA: enzyme-linked immunosorbent assay; EndoG: endonuclease G; Fluc: firefly luciferase; GFP: green fluorescent protein; H&E: hematoxylin and eosin; HR: homologous recombination; IHC: immunohistochemistry; $iPLA_2$: calcium-independent phospholipase A_2; NHEJ: non-homologous end joining; NSCLC: non-small cell lung cancer; PARP: poly (ADP-ribose) polymerase; PGE_2: prostaglandin E_2; qPCR: quantitative real-time polymerase chain reaction.

AUTHOR CONTRIBUTIONS

QH and MZ conceived and designed the study; MZ, YW, YZ, and YS performed the experiments; MZ, SH, RZ, JC, YG, JX, YW, and BH analyzed the data; MZ, QH, YZ, and YW wrote the manuscript; and LT supervised the study. All authors read and approved the final manuscript.

ACKNOWLEDGMENTS

We would like to thank Wenzhi Tu and Junjian Li (Shanghai General Hospital) for insightful discussions. We also thank the Institute of Translational Medicine at Shanghai General Hospital for providing service and technical support required for this study.

CONFLICTS OF INTEREST

The authors declare no conflicts of interest.

FUNDING

This study was supported by grants from the National Natural Science Foundation of China (grant nos. 81572951 and 81972843) to Qian Huang.

REFERENCES

1. Jemal A, Siegel R, Ward E, Hao Y, Xu J, Thun MJ. Cancer statistics, 2009. CA Cancer J Clin. 2009; 59:225–49. https://doi.org/10.3322/caac.20006 PMID:19474385
2. Herbst RS, Heymach JV, Lippman SM. Lung cancer. N Engl J Med. 2008; 359:1367–80. https://doi.org/10.1056/NEJMra0802714 PMID:18815398
3. Dağoğlu N, Karaman Ş, Arifoğlu A, Küçücük S, Oral EN. Definitive radiotherapy in locally advanced non-small cell lung cancer: dose and fractionation. Balkan Med J. 2014; 31:278–85. https://doi.org/10.5152/balkanmedj.2014.14496 PMID:25667780
4. Withers HR, Taylor JM, Maciejewski B. The hazard of accelerated tumor clonogen repopulation during radiotherapy. Acta Oncol. 1988; 27:131–46. https://doi.org/10.3109/02841868809090333 PMID:3390344
5. Kim JJ, Tannock IF. Repopulation of cancer cells during therapy: an important cause of treatment failure. Nat Rev Cancer. 2005; 5:516–25. https://doi.org/10.1038/nrc1650 PMID:15965493
6. Saggar JK, Tannock IF. Chemotherapy rescues hypoxic tumor cells and induces their reoxygenation and repopulation-an effect that is inhibited by the hypoxia-activated prodrug TH-302. Clin Cancer Res. 2015; 21:2107–14. https://doi.org/10.1158/1078-0432.CCR-14-2298 PMID:25677696
7. Reuter S, Gupta SC, Chaturvedi MM, Aggarwal BB. Oxidative stress, inflammation, and cancer: how are they linked? Free Radic Biol Med. 2010; 49:1603–16. https://doi.org/10.1016/j.freeradbiomed.2010.09.006 PMID:20840865
8. Asuthkar S, Velpula KK, Nalla AK, Gogineni VR, Gondi CS, Rao JS. Irradiation-induced angiogenesis is associated with an MMP-9-miR-494-syndecan-1 regulatory loop in medulloblastoma cells. Oncogene. 2014; 33:1922–33. https://doi.org/10.1038/onc.2013.151 PMID:23728345
9. Duru N, Candas D, Jiang G, Li JJ. Breast cancer adaptive resistance: HER2 and cancer stem cell repopulation in a heterogeneous tumor society. J Cancer Res Clin Oncol. 2014; 140:1–14. https://doi.org/10.1007/s00432-013-1494-1 PMID:23990015
10. Huang Q, Li F, Liu X, Li W, Shi W, Liu FF, O'Sullivan B, He Z, Peng Y, Tan AC, Zhou L, Shen J, Han G, et al. Caspase 3-mediated stimulation of tumor cell

repopulation during cancer radiotherapy. Nat Med. 2011; 17:860–66. https://doi.org/10.1038/nm.2385 PMID:21725296

11. Feng X, Yu Y, He S, Cheng J, Gong Y, Zhang Z, Yang X, Xu B, Liu X, Li CY, Tian L, Huang Q. Dying glioma cells establish a proangiogenic microenvironment through a caspase 3 dependent mechanism. Cancer Lett. 2017; 385:12–20. https://doi.org/10.1016/j.canlet.2016.10.042 PMID:27826040

12. Wang D, Dubois RN. Prostaglandins and cancer. Gut. 2006; 55:115–22. https://doi.org/10.1136/gut.2004.047100 PMID:16118353

13. Liu X, Li F, Huang Q, Zhang Z, Zhou L, Deng Y, Zhou M, Fleenor DE, Wang H, Kastan MB, Li CY. Self-inflicted DNA double-strand breaks sustain tumorigenicity and stemness of cancer cells. Cell Res. 2017; 27:764–83. https://doi.org/10.1038/cr.2017.41 PMID:28337983

14. Bartek J, Lukas J. Chk1 and Chk2 kinases in checkpoint control and cancer. Cancer Cell. 2003; 3:421–29. https://doi.org/10.1016/s1535-6108(03)00110-7 PMID:12781359

15. Kastan MB, Bartek J. Cell-cycle checkpoints and cancer. Nature. 2004; 432:316–23. https://doi.org/10.1038/nature03097 PMID:15549093

16. Hirao A, Kong YY, Matsuoka S, Wakeham A, Ruland J, Yoshida H, Liu D, Elledge SJ, Mak TW. DNA damage-induced activation of p53 by the checkpoint kinase Chk2. Science. 2000; 287:1824–27. https://doi.org/10.1126/science.287.5459.1824 PMID:10710310

17. Matsuoka S, Huang M, Elledge SJ. Linkage of ATM to cell cycle regulation by the Chk2 protein kinase. Science. 1998; 282:1893–97. https://doi.org/10.1126/science.282.5395.1893 PMID:9836640

18. Ciccia A, Elledge SJ. The DNA damage response: making it safe to play with knives. Mol Cell. 2010; 40:179–204. https://doi.org/10.1016/j.molcel.2010.09.019 PMID:20965415

19. Rogakou EP, Pilch DR, Orr AH, Ivanova VS, Bonner WM. DNA double-stranded breaks induce histone H2AX phosphorylation on serine 139. J Biol Chem. 1998; 273:5858–68. https://doi.org/10.1074/jbc.273.10.5858 PMID:9488723

20. Donato AL, Huang Q, Liu X, Li F, Zimmerman MA, Li CY. Caspase 3 promotes surviving melanoma tumor cell growth after cytotoxic therapy. J Invest Dermatol. 2014; 134:1686–92. https://doi.org/10.1038/jid.2014.18 PMID:24434746

21. Li F, Huang Q, Chen J, Peng Y, Roop DR, Bedford JS, Li CY. Apoptotic cells activate the "phoenix rising" pathway to promote wound healing and tissue regeneration. Sci Signal. 2010; 3:ra13. https://doi.org/10.1126/scisignal.2000634 PMID:20179271

22. Parrish J, Li L, Klotz K, Ledwich D, Wang X, Xue D. Mitochondrial endonuclease G is important for apoptosis in C. Elegans. Nature. 2001; 412:90–94. https://doi.org/10.1038/35083608 PMID:11452313

23. Matt S, Hofmann TG. The DNA damage-induced cell death response: a roadmap to kill cancer cells. Cell Mol Life Sci. 2016; 73:2829–50. https://doi.org/10.1007/s00018-016-2130-4 PMID:26791483

24. Han JA, Kim JI, Ongusaha PP, Hwang DH, Ballou LR, Mahale A, Aaronson SA, Lee SW. P53-mediated induction of cox-2 counteracts p53- or genotoxic stress-induced apoptosis. EMBO J. 2002; 21:5635–44. https://doi.org/10.1093/emboj/cdf591 PMID:12411481

25. Baskar R, Lee KA, Yeo R, Yeoh KW. Cancer and radiation therapy: current advances and future directions. Int J Med Sci. 2012; 9:193–99. https://doi.org/10.7150/ijms.3635 PMID:22408567

26. Dewey WC, Ling CC, Meyn RE. Radiation-induced apoptosis: relevance to radiotherapy. Int J Radiat Oncol Biol Phys. 1995; 33:781–96. https://doi.org/10.1016/0360-3016(95)00214-8 PMID:7591884

27. Poreba M, Szalek A, Kasperkiewicz P, Rut W, Salvesen GS, Drag M. Small molecule active site directed tools for studying human caspases. Chem Rev. 2015; 115:12546–629. https://doi.org/10.1021/acs.chemrev.5b00434 PMID:26551511

28. Dubash SR, Merchant S, Heinzmann K, Mauri F, Lavdas I, Inglese M, Kozlowski K, Rama N, Masrour N, Steel JF, Thornton A, Lim AK, Lewanski C, et al. Clinical translation of [^{18}F]ICMT-11 for measuring chemotherapy-induced caspase 3/7 activation in breast and lung cancer. Eur J Nucl Med Mol Imaging. 2018; 45:2285–99. https://doi.org/10.1007/s00259-018-4098-9 PMID:30259091

29. Cogo F, Poreba M, Rut W, Groborz K, Smyth P, Johnston MC, Williams R, Longley DB, Burden RE, Salvesen GS, Drag M, Scott CJ. Development of an advanced nanoformulation for the intracellular

delivery of a caspase-3 selective activity-based probe. Nanoscale. 2019; 11:742–51. https://doi.org/10.1039/c8nr07859a PMID:30566168

30. Futreal PA, Coin L, Marshall M, Down T, Hubbard T, Wooster R, Rahman N, Stratton MR. A census of human cancer genes. Nat Rev Cancer. 2004; 4:177–83. https://doi.org/10.1038/nrc1299 PMID:14993899

31. Daley JM, Kwon Y, Niu H, Sung P. Investigations of homologous recombination pathways and their regulation. Yale J Biol Med. 2013; 86:453–61. PMID:24348209

32. Lieber MR, Ma Y, Pannicke U, Schwarz K. Mechanism and regulation of human non-homologous DNA end-joining. Nat Rev Mol Cell Biol. 2003; 4:712–20. https://doi.org/10.1038/nrm1202 PMID:14506474

33. Schneider J, Illig T, Rosenberger A, Bickeböller H, Wichmann HE. Detection of ATM gene mutations in young lung cancer patients: a population-based control study. Arch Med Res. 2008; 39:226–31. https://doi.org/10.1016/j.arcmed.2007.08.004 PMID:18164969

34. Petersen LF, Klimowicz AC, Otsuka S, Elegbede AA, Petrillo SK, Williamson T, Williamson CT, Konno M, Lees-Miller SP, Hao D, Morris D, Magliocco AM, Bebb DG. Loss of tumour-specific ATM protein expression is an independent prognostic factor in early resected NSCLC. Oncotarget. 2017; 8:38326–36. https://doi.org/10.18632/oncotarget.16215 PMID:28418844

35. Yum S, Li M, Chen ZJ. Old dogs, new trick: classic cancer therapies activate cGAS. Cell Res. 2020; 30:639–48. https://doi.org/10.1038/s41422-020-0346-1 PMID:32541866

36. Pilié PG, Tang C, Mills GB, Yap TA. State-of-the-art strategies for targeting the DNA damage response in cancer. Nat Rev Clin Oncol. 2019; 16:81–104. https://doi.org/10.1038/s41571-018-0114-z PMID:30356138

37. Moore K, Colombo N, Scambia G, Kim BG, Oaknin A, Friedlander M, Lisyanskaya A, Floquet A, Leary A, Sonke GS, Gourley C, Banerjee S, Oza A, et al. Maintenance olaparib in patients with newly diagnosed advanced ovarian cancer. N Engl J Med. 2018; 379:2495–505. https://doi.org/10.1056/NEJMoa1810858 PMID:30345884

38. Robson M, Im SA, Senkus E, Xu B, Domchek SM, Masuda N, Delaloge S, Li W, Tung N, Armstrong A, Wu W, Goessl C, Runswick S, et al. Olaparib for Metastatic Breast Cancer in Patients with a Germline BRCA Mutation. N Engl J Med. 2017; 377:523–533. https://doi.org/10.1056/NEJMoa1706450 PMID:28578601

39. Mateo J, Carreira S, Sandhu S, Miranda S, Mossop H, Perez-Lopez R, Nava Rodrigues D, Robinson D, Omlin A, Tunariu N, Boysen G, Porta N, Flohr P, et al. DNA-repair defects and olaparib in metastatic prostate cancer. N Engl J Med. 2015; 373:1697–708. https://doi.org/10.1056/NEJMoa1506859 PMID:26510020

40. Kaufman B, Shapira-Frommer R, Schmutzler RK, Audeh MW, Friedlander M, Balmaña J, Mitchell G, Fried G, Stemmer SM, Hubert A, Rosengarten O, Steiner M, Loman N, et al. Olaparib monotherapy in patients with advanced cancer and a germline BRCA1/2 mutation. J Clin Oncol. 2015; 33:244–50. https://doi.org/10.1200/JCO.2014.56.2728 PMID:25366685

41. Levra MG, Olaussen KA, Novello S, Soria JC. PARP inhibitors: an interesting pathway also for non-small cell lung cancer? Curr Pharm Des. 2014; 20:3875–82. https://doi.org/10.2174/13816128113196660765 PMID:24191958

42. Abbotts R, Topper MJ, Biondi C, Fontaine D, Goswami R, Stojanovic L, Choi EY, McLaughlin L, Kogan AA, Xia L, Lapidus R, Mahmood J, Baylin SB, Rassool FV. DNA methyltransferase inhibitors induce a BRCAness phenotype that sensitizes NSCLC to PARP inhibitor and ionizing radiation. Proc Natl Acad Sci USA. 2019; 116:22609–18. https://doi.org/10.1073/pnas.1903765116 PMID:31591209

43. Branzei D, Foiani M. Regulation of DNA repair throughout the cell cycle. Nat Rev Mol Cell Biol. 2008; 9:297–308. https://doi.org/10.1038/nrm2351 PMID:18285803

44. Liu X, He Y, Li F, Huang Q, Kato TA, Hall RP, Li CY. Caspase-3 promotes genetic instability and carcinogenesis. Mol Cell. 2015; 58:284–96. https://doi.org/10.1016/j.molcel.2015.03.003 PMID:25866249

45. Yim H, Hwang IS, Choi JS, Chun KH, Jin YH, Ham YM, Lee KY, Lee SK. Cleavage of Cdc6 by caspase-3 promotes ATM/ATR kinase-mediated apoptosis of HeLa cells. J Cell Biol. 2006; 174:77–88. https://doi.org/10.1083/jcb.200509141 PMID:16801388

46. Wu WK, Sung JJ, Lee CW, Yu J, Cho CH. Cyclooxygenase-2 in tumorigenesis of gastrointestinal cancers: an update on the molecular mechanisms. Cancer Lett. 2010; 295:7–16. https://doi.org/10.1016/j.canlet.2010.03.015 PMID:20381235

47. Benoit V, de Moraes E, Dar NA, Taranchon E, Bours V, Hautefeuille A, Tanière P, Chariot A, Scoazec JY, de Moura Gallo CV, Merville MP, Hainaut P. Transcriptional activation of cyclooxygenase-2 by tumor suppressor p53 requires nuclear factor-kappaB. Oncogene. 2006; 25:5708–18. https://doi.org/10.1038/sj.onc.1209579 PMID:16682957

48. Subbaramaiah K, Dannenberg AJ. Cyclooxygenase 2: a molecular target for cancer prevention and treatment. Trends Pharmacol Sci. 2003; 24:96–102. https://doi.org/10.1016/S0165-6147(02)00043-3 PMID:12559775

49. Gallo O, Schiavone N, Papucci L, Sardi I, Magnelli L, Franchi A, Masini E, Capaccioli S. Down-regulation of nitric oxide synthase-2 and cyclooxygenase-2 pathways by p53 in squamous cell carcinoma. Am J Pathol. 2003; 163:723–32. https://doi.org/10.1016/S0002-9440(10)63699-1 PMID:12875991

50. Ventura A, Kirsch DG, McLaughlin ME, Tuveson DA, Grimm J, Lintault L, Newman J, Reczek EE, Weissleder R, Jacks T. Restoration of p53 function leads to tumour regression in vivo. Nature. 2007; 445:661–65. https://doi.org/10.1038/nature05541 PMID:17251932

51. Xue W, Zender L, Miething C, Dickins RA, Hernando E, Krizhanovsky V, Cordon-Cardo C, Lowe SW. Senescence and tumour clearance is triggered by p53 restoration in murine liver carcinomas. Nature. 2007; 445:656–60. https://doi.org/10.1038/nature05529 PMID:17251933

52. Cheng J, He S, Wang M, Zhou L, Zhang Z, Feng X, Yu Y, Ma J, Dai C, Zhang S, Sun L, Gong Y, Wang Y, et al. The caspase-3/PKCδ/Akt/VEGF-A signaling pathway mediates tumor repopulation during radiotherapy. Clin Cancer Res. 2019; 25:3732–43. https://doi.org/10.1158/1078-0432.CCR-18-3001 PMID:30890550

53. Zhou M, Liu X, Li Z, Huang Q, Li F, Li CY. Caspase-3 regulates the migration, invasion and metastasis of colon cancer cells. Int J Cancer. 2018; 143:921–30. https://doi.org/10.1002/ijc.31374 PMID:29524226

54. Cong L, Zhang F. Genome engineering using CRISPR-Cas9 system. Methods Mol Biol. 2015; 1239:197–217. https://doi.org/10.1007/978-1-4939-1862-1_10 PMID:25408407

55. Franken NA, Rodermond HM, Stap J, Haveman J, van Bree C. Clonogenic assay of cells in vitro. Nat Protoc. 2006; 1:2315–19. https://doi.org/10.1038/nprot.2006.339 PMID:17406473

56. Cheng J, Tian L, Ma J, Gong Y, Zhang Z, Chen Z, Xu B, Xiong H, Li C, Huang Q. Dying tumor cells stimulate proliferation of living tumor cells via caspase-dependent protein kinase Cδ activation in pancreatic ductal adenocarcinoma. Mol Oncol. 2015; 9:105–14. https://doi.org/10.1016/j.molonc.2014.07.024 PMID:25156550

57. Feldman AT, Wolfe D. Tissue processing and hematoxylin and eosin staining. Methods Mol Biol. 2014; 1180:31–43. https://doi.org/10.1007/978-1-4939-1050-2_3 PMID:25015141

58. Zhang Z, Wang M, Zhou L, Feng X, Cheng J, Yu Y, Gong Y, Zhu Y, Li C, Tian L, Huang Q. Increased HMGB1 and cleaved caspase-3 stimulate the proliferation of tumor cells and are correlated with the poor prognosis in colorectal cancer. J Exp Clin Cancer Res. 2015; 34:51. https://doi.org/10.1186/s13046-015-0166-1 PMID:25986235

SUPPLEMENTARY MATERIALS

Supplementary Figures

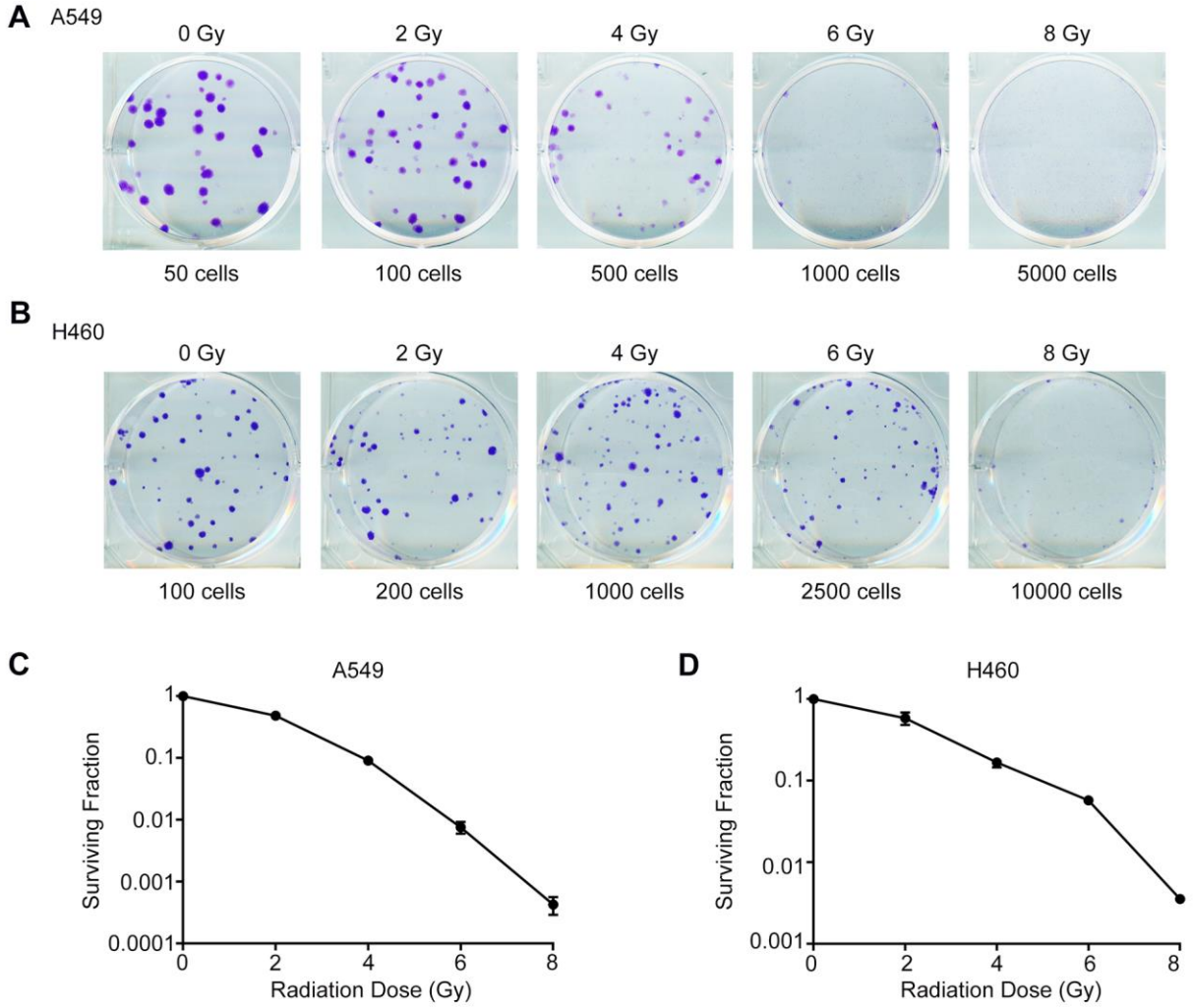

Supplementary Figure 1. Clonogenic cell survival assays in A549 and H460 cell lines after exposure to ionizing radiations. (**A**, **B**) The corresponding images of surviving colonies (>50 cells per colony) in A549 and H460 cells. (**C**, **D**) Surviving fractions of irradiated A549 and H460 cells, *n* = 3.

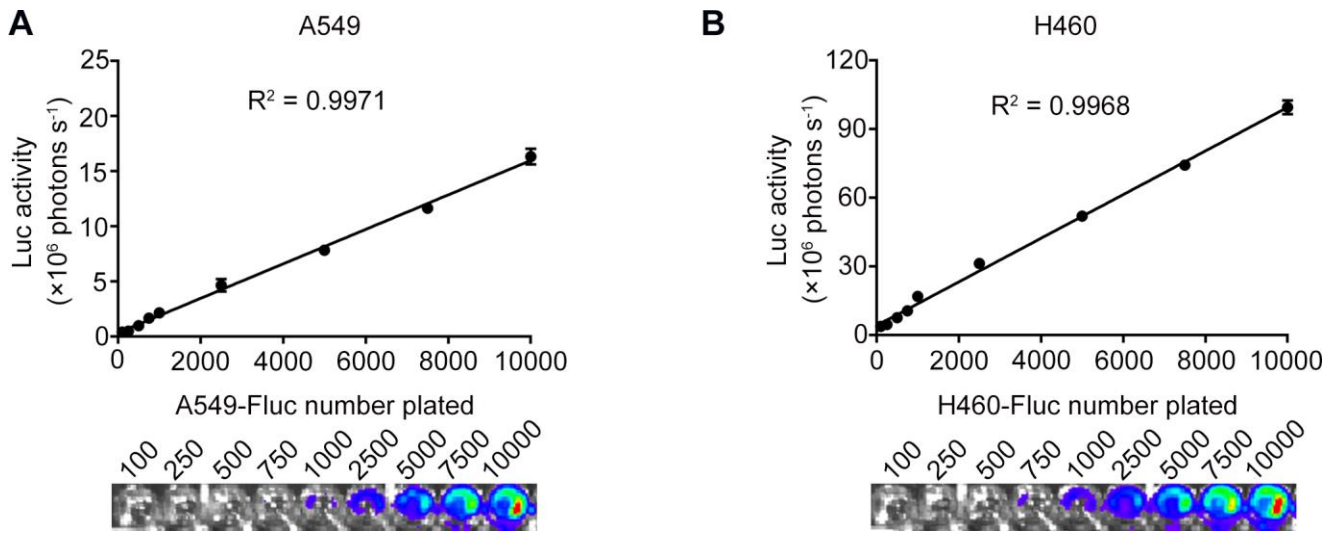

Supplementary Figure 2. A linear correlation was observed between the luciferase activity of A549 Fluc or H460 Fluc cells with seeded cell numbers. (**A**, **B**) Upper panel shows luciferase activities of different numbers of A549 Fluc and H460 Fluc cells. Lower panel shows the representative bioluminescence images, *n* = 4.

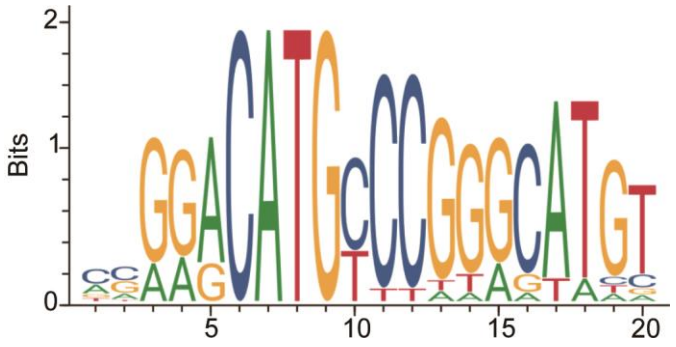

Supplementary Figure 3. The JASPAR database shows the potential p53 binding sites in the promoter region of *PTGS2*.

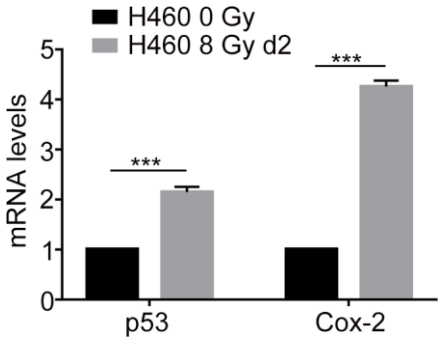

Supplementary Figure 4. The mRNA levels of p53 and Cox-2 in a xenograft mouse model after exposure to 8 Gy radiations (**p*<0.001, Student's *t* test, *n* = 3).**

Research Paper

Overexpression of hsa_circ_0002874 promotes resistance of non-small cell lung cancer to paclitaxel by modulating miR-1273f/MDM2/p53 pathway

Jianhao Xu[1,*], Liwei Ni[2,*], Fenglun Zhao[3,*], Xiaoxiao Dai[4], Jialong Tao[5], Jia Pan[3], Aiming Shi[3], Zhu Shen[3], Cunjin Su[3], Yusong Zhang[5]

[1] Department of Pathology, Kunshan First People's Hospital Affiliated to Jiangsu University, Kunshan 215300, Jiangsu, PR China
[2] Department of Medical Oncology, Hangzhou Cancer Hospital, Hangzhou 310002, Zhejiang, PR China
[3] Department of Pharmacy, The Second Affiliated Hospital of Soochow University, Suzhou 215004, Jiangsu, PR China
[4] Department of Pathology, The Second Affiliated Hospital of Soochow University, Suzhou 215004, Jiangsu, PR China
[5] Department of Oncology, The Second Affiliated Hospital of Soochow University, Suzhou 215004, Jiangsu, PR China
*Equal contribution

Correspondence to: Yusong Zhang, Cunjin Su; **email:** zhangyusong19@163.com, https://orcid.org/0000-0003-0474-5870; sucjgh@vip.163.com, https://orcid.org/0000-0003-3728-3377
Keywords: hsa_circ_0002874, miR1273f, MDM2, P53, paclitaxel-resistance
Received: July 17, 2020 **Accepted:** December 19, 2020 **Published:** February 17, 2021

ABSTRACT

Background: This study aimed to investigate the aberrant expression of hsa_circ_0002874 in non-small cell lung cancer (NSCLC) and elucidate associated molecular mechanisms that influence apoptosis and induce paclitaxel (PTX) resistance.
Methods: Inhibitors were used to downregulate circRNA or miRNA expression. pCDNA plasmid transfection and mimics were used to upregulate circRNA or miRNA expression. Dual-luciferase reporter assays were conducted to evaluate interactions between miR1273f and MDM2. Xenograft tumor models were used to assess the effect of hsa_circ_0002874 and miR1273f on tumor growth. NSCLC tissues and matched non-cancerous tissues were also collected for correlation analysis.
Results: hsa_circ_0002874 acts as a sponge for miR1273f which targets MDM2/P53. The stability of the hsa_circ_0002874/miR1273f/MDM2/P53 pathway was verified by upregulating and downregulating the expression of hsa_circ_0002874 and miR1273f. hsa_circ_0002874 downregulation or miR1273f upregulation reversed the resistance of the A549/Taxol cells in xenograft models. The expression of hsa_circ_0002874 was high, and the level of MDM2 was low in NSCLC tissues. P53 was only weakly expressed in NSCLC tissues with high expression of MDM2.
Conclusions: hsa_circ_0002874 is strongly expressed in NSCLC tissues and maybe a potential marker for PTX resistance. hsa_circ_0002874 downregulation could regulate miR1273f/MDM2/P53 signaling pathway to reverse the PTX resistance of NSCLC and induce apoptosis *in vitro* and *vivo*.

INTRODUCTION

Lung cancer (LC) is one of the most common causes of cancer-related death worldwide [1–3] and ranked second and first among new cancer cases and cancer-related death in 2018, respectively [4, 5]. Non-small cell LC (NSCLC) accounts for 80% of all LC cases with a 5-year survival rate of approximately 10%–15% [6, 7]. For patients with advanced NSCLC who do not receive molecular targeted therapy or immune checkpoint therapy, the standard first-line treatment remains cytotoxic chemotherapy [8]. Paclitaxel (PTX) is an

important first-line treatment of advanced NSCLC [9] and interferes with cell division by promoting microtubule polymerization and apoptosis [10]. However, other anti-tumor mechanisms for PTX remain undiscovered. One shortcoming of PTX is the emergence of drug resistance, but the underlying molecular mechanism still under investigation.

Unlike linear RNA, circular RNA (circRNA) forms a covalently closed continuous loop. That is, the 3' and 5' ends usually present in RNA molecules are connected in circular RNA [11]. In molecular biology, competition for endogenous RNA (ceRNA) is based on the function of miRNA to regulate other RNA transcripts [12, 13]. The circRNA hsa_circ_0002874 has been reported to be closely associated with doxorubicin resistance in the breast cancer cell line MCF-7 [14]. It was predicted by the software circMir 1.0 and RegRNA that its target miRNA is miR1273f. However, the miR-1273 family has 33-1074 mRNA target genes (free hybridization energy ≥90%), of which miR-1273f alone has >400 target genes, playing an important role in many different molecular pathways [15].

In this study, we investigated the aberrant expression of hsa_circ_0002874 in NSCLC and elucidated the molecular mechanisms underlying its influence on apoptosis and PTX resistance induction. Our findings provide novel viewpoints for the anti-tumor mechanisms of PTX and the molecular mechanism of PTX resistance in NSCLC.

RESULTS

In A549 cells, PTX treatment downregulates the expression of hsa_circ_0002874 which is predicted to act as a sponge for miR1273f

We designed primers for 18 circRNAs based on the reported microarray results from the doxorubicin-resistant breast cancer cell line MCF-7 [14] (Table 1). Screening by qPCR identified circRNA hsa_circ_ 0002874 as having the largest and most reproducible change of expression level after PTX exposure. Its target miRNAs were predicted by circMir 1.0, RegRNA 2.0 and MirTrap, and target genes of these screened miRNAs were predicted by literature review and miRBase webpage analysis. These were then confirmed by qPCR after PTX administration.

To accomplish this, we first excluded candidates with cycle threshold values (Ct value) of circRNA >30, which is considered too small when the Ct value of GAPDH is 18-20. Among the 18 circRNAs screened, 10 failed this quality control step, namely, hsa_circ_ 0006528, hsa_circ_ 0007769, hsa_circ_ 0092276, hsa_circ_ 0044556, hsa_circ_0003183, hsa_circ_ 0008131, hsa_circ_ 0003838, hsa_circ_ 0007551, hsa_circ_0006903 and hsa_circ_0018293. As shown in Figure 1A, the expression of 4 of the remaining 8 circRNAs did not change significantly (P≥0.05) after PTX administration, namely, hsa_circ_0002168, hsa_circ_0086241, hsa_circ_ 0085567, and hsa_circ_ 0085495. Significant changes in expression after PTX were observed for hsa_circ_ 0002113 (P=0.031), hsa_circ_0001667 (P=0.021), hsa_circ_0005004 (P=0.005), and hsa_circ_ 0002874 (P<0.001) (Figure 1B). Although the most marked change was seen for hsa_circ_0005004, it was found by the technique of Suzhou Gemma Gene Company that its length was too short (spliced length=238 bp) to ensure that the overexpression plasmid was looped. Therefore, a more robust circRNA hsa_circ_ 0002874 (spliced length=486 bp, P<0.001) was selected as the target circRNA for further study. To verify stability, expression of hsa_circ_0002874 at different times after PTX treatment (10 μM) was analyzed by qPCR. A significant decrease in hsa_circ_0002874 expression was found on the 2nd and 3rd day of PTX exposure (P=0.004, P<0.001, respectively) (Figure 1C).

Next, after identifying the target circRNA, target miRNAs were predicted by circMir 1.0, RegRNA 2.0 and MirTrap as follows: hsa-miR-1273f, hsa-miR-4726-5p, hsa-miR-2115-5p and hsa-miR-4649-5p (Figure 1D). As shown in Figure 1E, after exposure to 10μM PTX for 48 h, only hsa-miR-1273f expression had a significant change (P =0.033).

Their target genes were predicted by reviewing the literature and miRBase and Targetscan web page analysis. They were identified as MDM2, SHP-1, Erbb2, and MLLT6 (Table 2). Changed expression of these putative target genes in PTX-sensitive A549 cells compared with the resistant strain A549/Taxol after PTX exposure was analyzed by qPCR. The expression of MDM2 decreased significantly in A549 cells on treatment with PTX (P=0.026), but its high level in A549/Taxol cells was not affected (Figure 1F).

Further bioinformatics prediction analysis was undertaken to explore the combination of hsa_circ_0002874 and hsa-miR-1273f, or miR1273f and MDM2. As shown in Figure 1G, RegRNA 2.0 predicted that hsa-miR-1273f is a putative target of hsa_circ_0002874, and Target Scan Human 7.2 that MDM2 is a putative target of hsa-miR-1273f (Figure 1H).

hsa_circ_0002874 acts as a sponge for miR1273f, thus regulating the expression of MDM2 and P53 in A549 cells and contributing to PTX resistance

To investigate the hsa_circ_0002874/miR1273f/MDM2/P53 pathway and its association with A549/Taxol

Table 1. Primer sequences used for qPCR.

Gene	Forward primer sequence 5'-3'	Reverse primer sequence 5'-3'
hsa_circ_0002113	ACAGATAGAAGAGCACCGACAGT	AGCTCGAAGGCGTAGAGTGA
hsa_circ_0001667	TGCAGGAAACACTGATGCCC	AGGGCAGGGCCAGGATAAAT
hsa_circ_0006528	CGGAGTCACTGCCTTACGTG	AGCAGCTACTGTGTTCACGC
hsa_circ_0002874	TGGAGGCATGTCAGGGTCAC	GTGGGTTATAAGCCTTTCCCAGG
hsa_circ_0002168	CTGCATCACCACAGTTGCAGG	CGGAAGGGTCGGATGAAAGC
hsa_circ_0086241	GGGATTCAGATGGGCGTCAC	TTGTTGTTCGGTGTCGCTGG
hsa_circ_0007769	GCCGACGAACAGAACCACTC	AGAGGAGCCAGCATTTTGCAT
hsa_circ_0092276	CCTAGGAACCTTGTGCTTGCC	CAACCACACACTCCAAGCTCC
hsa_circ_0044556	TGCCAAGGGTCTGACTGGAA	AGGGGGTCCTTGAACACCAA
hsa_circ_0003183	AGGTGAAGCTTTTGCACGAGA	TCTTGCCCTGCCTCTTCTACA
hsa_circ_0085567	GAGGGAACGCCAATCCAAGG	AAATGAATTACCTTCAGCCAGTGC
hsa_circ_0085495	TTGCAGGCTACGTTGAAGCA	AGCCAAACCCTATGAAAGGTATCG
hsa_circ_0008131	AAGAAGGCGTTCGATGCTCC	CAACCTGCGAGGTGGACATT
hsa_circ_0003838	CTGCAATTGGCCTCGAGCTG	CCTGTTCCGATGTGCGTTGA
hsa_circ_0007551	AAGGCATCGACTGGACCCC	GAGCTTTGGGAAGCGGTCAC
hsa_circ_0005004	AGGCAGCTGATGAGGTTTGAG	GATGGTCTTGAGGGCAGGGA
hsa_circ_0006903	ACCACGTCTGGCAGAAGATTT	CAAAGCCTCTTTCCGGGTCC
hsa_circ_0018293	GCAGGCGAGAAGATTCGTGG	TCCATCTGTGCCACCCCTTA
MDM2	CATTGAACCTTGTGTGATTTGTC	GCAGGGCTTATTCCTTTTCTTTA
hsa-miR-1273f	GCTAACAACCTCCATCTCA	CAGTGCGTGTCGTGGAGT
hsa-miR-4726-5p	CCACTCCGGGACTCCTGGCCCC	GGTGAGGCCCTGAGGACCGGGG
hsa-miR-2115-5p	AGCAGCAGGAGTTTGGAAGCC	TCATCGTCCTCAAACCTTCGG
hsa-miR-4649-5p	CTCCGGGACTCCTGGCCCCTCGCCCT	GAGGCCCTGAGGACCGGGGAGCGGGA
u6	GCGCGTCGTGAAGCGTTC	GTGCAGGGTCCGAGGT

PTX resistance, relationships between PTX and hsa_circ_0002874, miR1273f, MDM2, or P53 were respectively verified.

First, as shown in Figure 2A, after exposure to 10 μM PTX for 48 h, A549 cells appeared smaller and shrunken, whereas no morphological changes of A549/Taxol cells were evident. It was confirmed that PTX inhibited the proliferation of A549 in a dose-dependent manner and that A549/Taxol cells were partially resistant to PTX in this MTT assay (IC_{50} value=17.18 μM and 55.47 μM respectively) (Figure 2B). Intracellular RNA levels were analyzed via qPCR. Expression of hsa_circ_0002874 in A549 cells was significantly decreased after treatment with PTX (P=0.046), while the expression of hsa_circ_0002874 in A549/Taxol cells was very high, about 9-fold that in A549 cells (P=0.002). There was no significant change of hsa_circ_0002874 expression in A549/Taxol cells after PTX treatment, which increased to 15-fold in treated A549 cells (P<0.001) (Figure 2C). Expression of miR1273f was significantly increased in A549 cells treated with PTX (P=0.021), while the expression of miR1273f in A549/Taxol cells was deficient, only one-fifth of that in A549 cells (P=0.002). There was no significant change of miR1273f expression in A549/Taxol cells after PTX treatment, which was one-seventh of that in treated A549 cells (P<0.001) (Figure 2D).

Second, the regulation of MDM2 and P53 levels were analyzed by Western blotting. It was found that the amount of MDM2 protein was significantly decreased in A549 cells after treatment with PTX (P=0.004) (Figure 2E, 2F), while P53 protein was significantly increased (P<0.001) (Figure 2E, 2G). In contrast, the amount of MDM2 protein in A549/Taxol cells was high, almost 3-fold that in A549 cells (P<0.001) (Figure 2E, 2F), while P53 expression was low, about one-eighth of that in A549 cells (P<0.001) (Figure 2E, 2G). There were no significant changes of MDM2 and P53 expression in A549/Taxol cells after PTX treatment, and MDM2 was 6-fold that in treated A549 cells (P<0.001) (Figure 2E, 2F) while P53 was approximately one-twenty-fifth of that in treated A549 (P<0.001) (Figure 2E, 2G).

Third, based on the above results, the negative regulatory activity of miR1273f on MDM2 expression was verified by dual-luciferase reporter gene assays. It was predicted by miRBase and TargetScan that the target gene of miR1273f is MDM2. To test this, the predicted binding sites were mutated (Figure 2H), and a luciferase reporter plasmid containing wild-type or mutant MDM2 was used to observe effects after transfection of MDM2-WT (Wild-type) and MDM2-MT (Mutant-type) (Figure 2I). Luciferase activity was measured 48 hours after transfection. When MDM2-WT was co-transfected together with miR1273f, the relative luciferase activity was significantly lower than the control group or the miR-NC group (P=0.027, P=0.026 respectively) (Figure 2I). However, when co-transfected with MDM2-MT, there was no observable difference. These results indicate that miR1273f interacts with MDM2.

Knockdown or overexpression of hsa_circ_0002874 regulates the expression of miR1273f, MDM2, and P53 in A549 cells

To further analyze relationships among hsa_circ_0002874, miR1273f, MDM2, and P53, expression of hsa_circ_0002874 was downregulated or

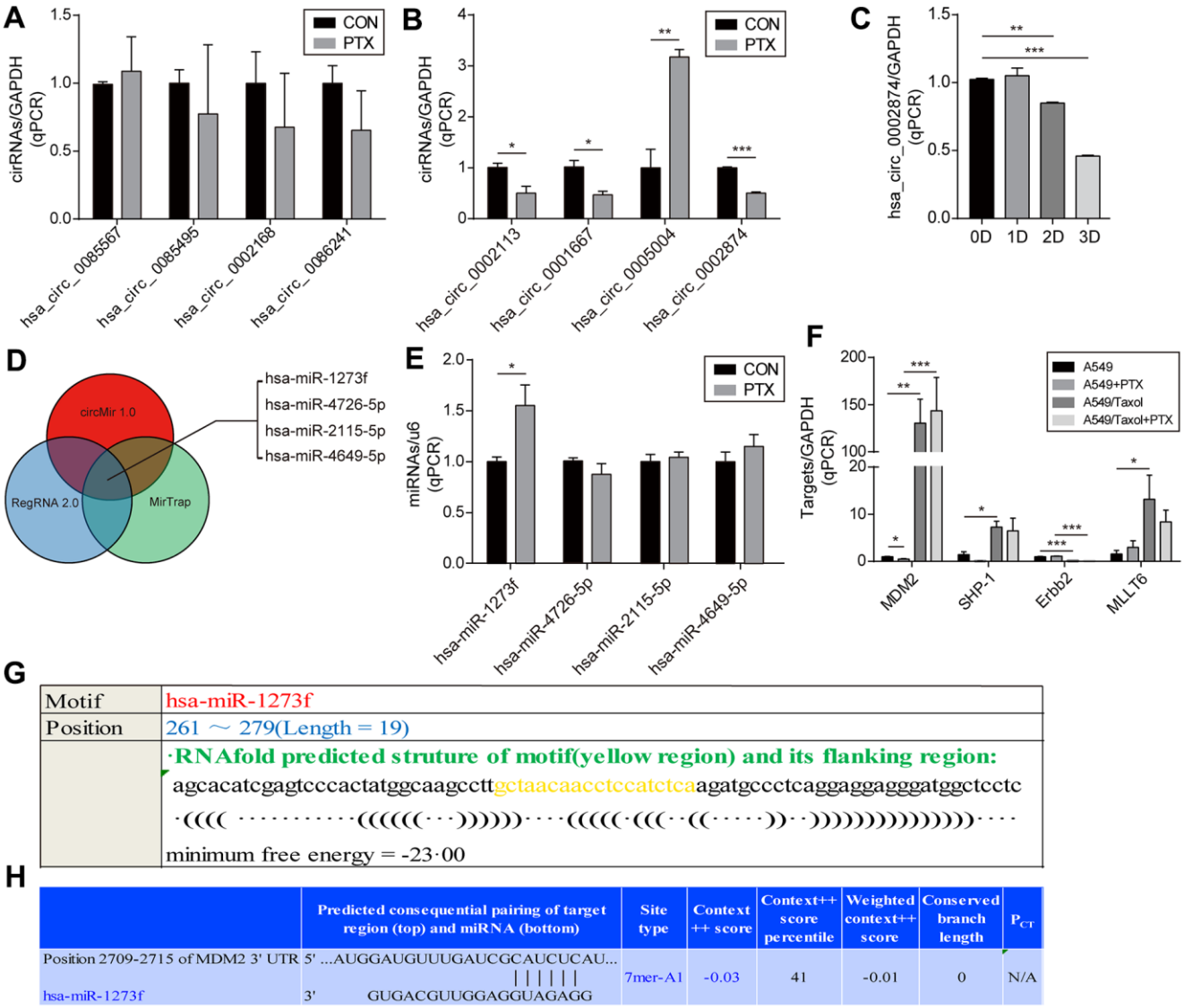

Figure 1. Screening of circRNA and determination of the downstream miRNA. (**A, B**) Screening for circRNA with the greatest change after PTX administration by qPCR. (**C**) Confirmation of the hsa_circ_0002874 expression at different time points after PTX administration by qPCR. (**D**) Prediction of target miRNAs for hsa_circ_0002874 by circMir 1.0, RegRNA 2.0 and MirTrap software. (**E**) Changes in the four predicted miRNAs expression after PTX administration by qPCR. (**F**) Changes in target genes expression for 4 predicted miRNAs after PTX administration by qPCR. (**G**) Prediction of the binding stability of hsa_circ_0002874 and miR1273f by Reg RNA2.0 website. (**H**) Prediction of the binding stability of miR1273f and MDM2 mRNA by TargetScan Human 7.2 website. *p <0.05, **p <0.01, ***p <0.001, n=3 in each group.

Table 2. Screening of target miRNAs for hsa_circ_0002874.

Name	Position	Length	Sequence	Minimum free energy (kcal/mol)	Target
hsa-miR-1273f	261~279	19	GCTAACAACCTCCATCTCA	-23.00	MDM2
hsa-miR-4726-5p	197~218	22	CCACTCCGGGACTCCTGGCCCC	-27.70	SHP-1
hsa-miR-2115-5p	442~462	21	AGCAGCAGGAGTTTGGAAGCC	-15.02	Erbb2
hsa-miR-4649-5p	200~225	26	CTCCGGGACTCCTGGCCCCTCGCCCT	-28.10	MLLT6

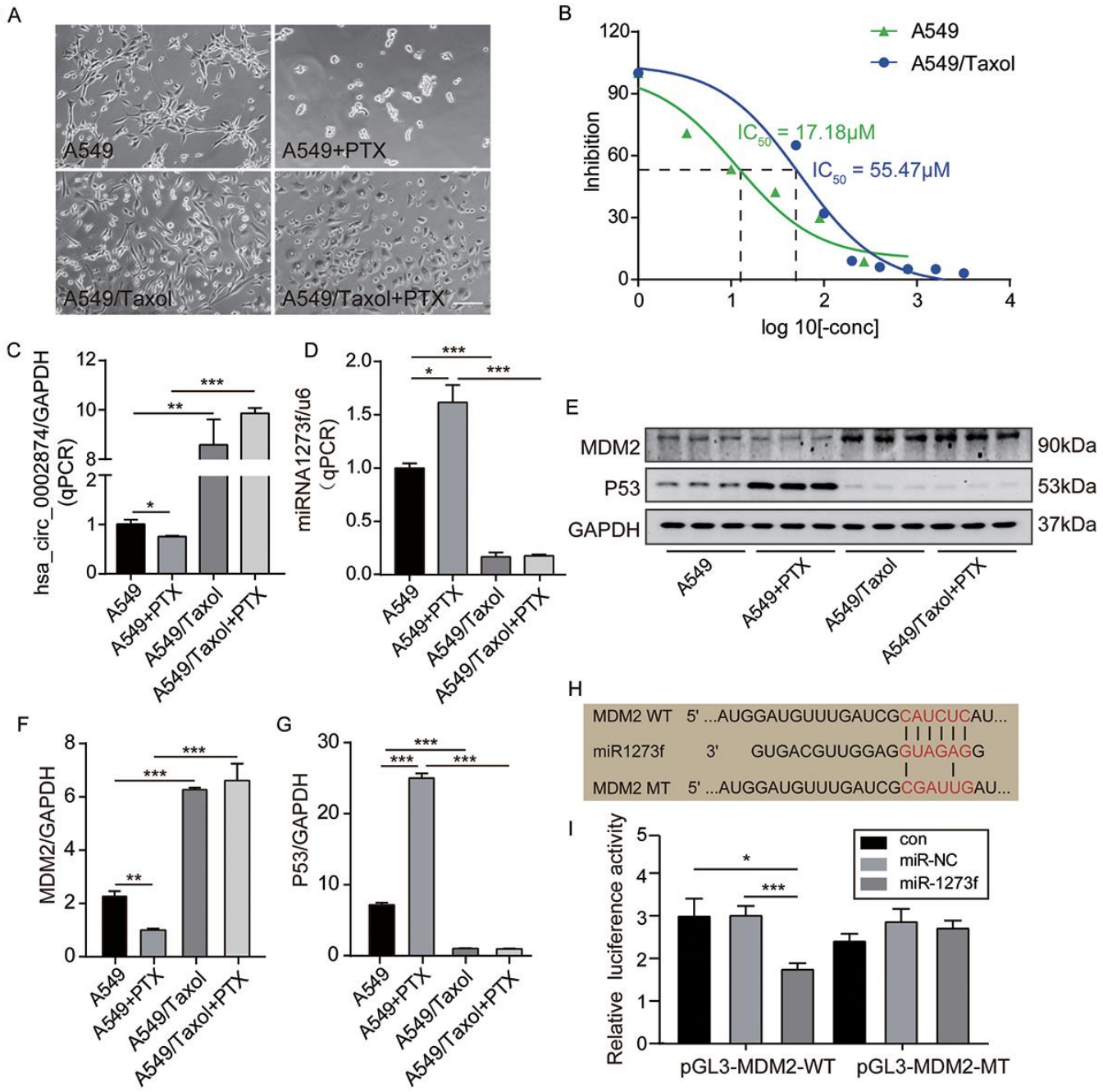

Figure 2. PTX downregulated the expression of hsa_circ_0002874 and MDM2 while upregulated the expression of miR1273f and P53 in A549 cells. (**A**) Cell morphology of A549 and A549/Taxol cells following 10μM PTX administration for 48h (images acquired at 10× magnification). (**B**) A549 or A549/Taxol cells viability was measured by MTT assay after the treatment of different concentrations of PTX. (**C**)

hsa_circ_0002874 expression was determined by qPCR method after 10μM PTX administration for 48h in A549 and A549/Taxol cells. (**D**) miR1273f expression was determined by qPCR method after 10μM PTX administration for 48h in A549 and A549/Taxol cells. (**E**) MDM2 and P53 expression were determined by western blot after 10μM PTX administration for 48h in A549 and A549/Taxol cells. (**F**) The quantification of MDM2 protein was analyzed according to bands in Figure 2E. (**G**) The quantification of P53 protein was analyzed according to bands in Figure 2E. (**H**) Sequence alignments between miR1273f and the seed sequence of MDM2. WT and MT represent wild-type and mutant sequences of MDM2. (**I**) Results of the dual-luciferase reporter gene assay in 293 cells. *p <0.05, **p <0.01, ***p <0.001, n=3 in each group. Scale bar=100μm.

upregulated in A549 cells by siRNAs-ciR interference or pCD25-ciR plasmid transfection. siRNAs-ciR is a group of short interfering RNAs used to down-regulate the expression of circular RNAs. pCD25-ciR is the fifth generation circRNA expression vector, which is used to overexpress circRNA. Thereafter, changes in the expression of miR1273f, MDM2 and P53 were analyzed by qPCR and western blotting.

First, as depicted in Figure 3A, we designed 3 hsa_circ_0002874 siRNAs specifically targeting the back-splice junction sequences at different binding sites in hsa_circ_0002874. As shown in Figure 3B, siRNAs-ciR transfection significantly downregulated the expression of hsa_circ_0002874 to one-third that of the negative control group, as assessed by qPCR (P=0.002), while pCD25-ciR transfection dramatically upregulated the expression of hsa_circ_0002874 to 700 times that in negative control group (P=0.001).

Second, intracellular RNA levels were analyzed via qPCR. As shown in Figure 3C, the expression of miR1273f was upregulated by siRNAs-ciR transfection (P=0.021), while pCD25-ciR transfection significantly decreased it (P=0.039). These results document the negative association of hsa_circ_0002874 with miR1273f. Accordingly, MDM2 mRNA was downregulated by siRNAs-ciR transfection (P=0.044), while it was upregulated by pCD25-ciR transfection (P=0.011) (Figure 3D). These results show that hsa_circ_0002874 is negatively correlated with miR1273f and positively with MDM2.

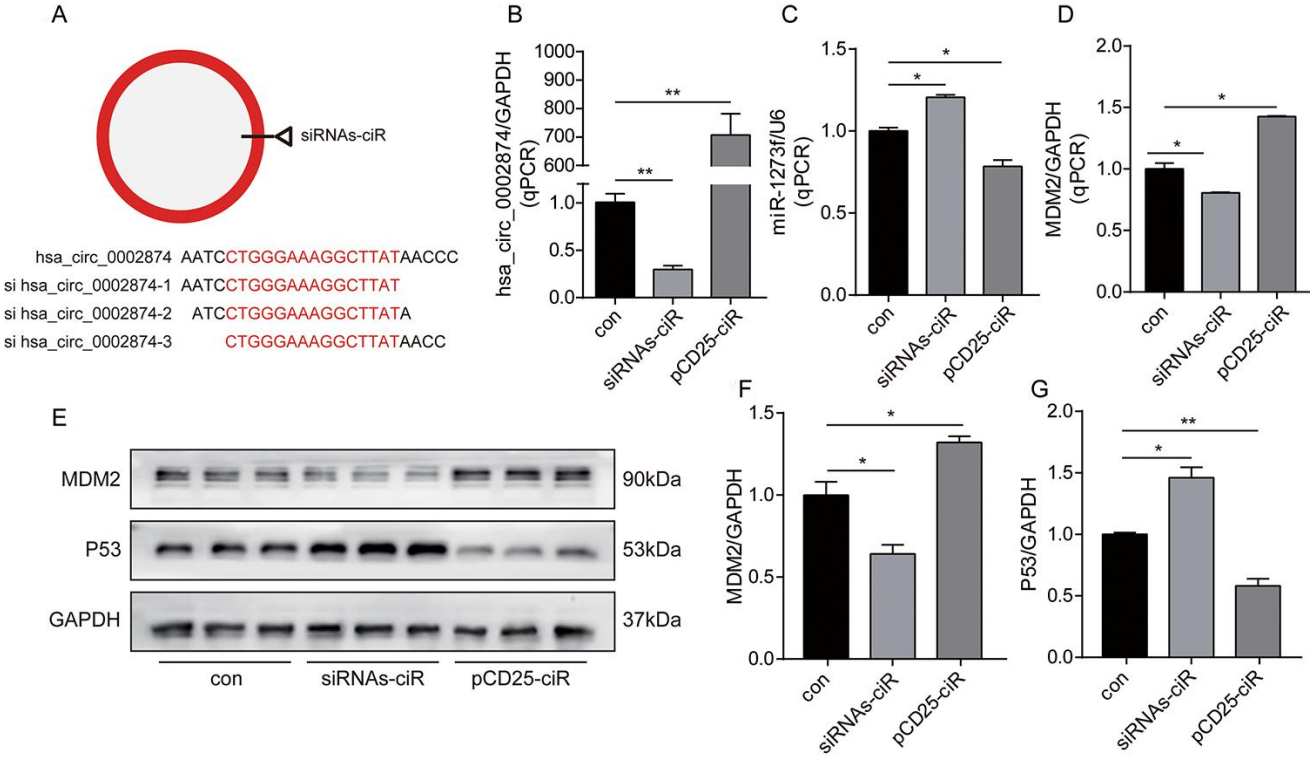

Figure 3. Knockdown or overexpression of hsa_circ_0002874 regulated the expression of miR1273f, MDM2 and P53 in A549 cell line. (**A**) 3 hsa_circ_0002874 siRNAs specifically targeting the backsplice junction sequences at different binding sites in hsa_circ_0002874 were designed. (**B**) hsa_circ_0002874 was determined by qPCR method after transfection of siRNAs-ciR and pCD25-ciR. (**C**) miR1273f was determined by qPCR method after transfection of siRNAs-ciR and pCD25-ciR. (**D**) MDM2 mRNA level was determined by qPCR method after transfection of siRNAs-ciR and pCD25-ciR. (**E**) MDM2 and P53 expression were determined by western blot after transfection of siRNAs-ciR and pCD25-ciR. (**F**) The quantification of MDM2 protein was analyzed according to bands in Figure 3E. (**G**) The quantification of P53 protein was analyzed according to bands in Figure 3E. *p <0.05, **p <0.01, ***p <0.001, n=3 in each group.

Next, MDM2 and P53 levels were analyzed by Western blotting. As shown in Figure 3E, siRNAs-ciR transfection downregulated MDM2 expression at the protein level to two-thirds of that in the negative control group (P=0.022) (Figure 3F) and upregulated P53 expression 1.5-fold (P=0.023) (Figure 3G). pCD25-ciR transfection increased MDM2 expression to 1.2-fold that of the negative control (P=0.016) (Figure 3F), and decreased P53 expression by one-half (P=0.006) (Figure 3G). These results indicate that hsa_circ_0002874 expression positively correlates with MDM2 protein levels but negatively with P53.

Knockdown and overexpression of miR1273f could reduce PTX sensitivity in A549 cell line and reverse PTX resistance in A549/Taxol cell line, respectively

Firstly, to further validate the hsa_circ_0002874 /miR1273f/MDM2/P53 pathway, miR1273f in A549 cells was downregulated or upregulated via transfection of inhibitor-miR1273f or mimic-miR1273f, and the expression changes of MDM2 and P53 were analyzed by qPCR and Western blot analysis to validate the miR1273f/MDM2/P53 pathway further. As shown in Figure 4A, miR1273f inhibitor was designed to target the binding sites in miR1273f specifically. qPCR results in Figure 4B showed that inhibitor-miR1273f and mimic-miR1273f transfections significantly down- and upregulated the expression of miR1273f to 1/2 (P=0.026) and 250000 times (P=0.011) of that in the negative control group, respectively. Therefore, transfection was successful. As shown in Figure 4C, the expression of MDM2 in A549 cells was upregulated to 1.5 times that in the negative control group (P=0.003) after inhibitor-miR1273f transfection, and mimic-miR1273f transfection significantly downregulated the expression of MDM2 to 2/3 of that in negative control group (P=0.035). As shown in Figure 4D, inhibitor-miR1273f transfection up- and downregulated MDM2 (P=0.044, Figure 4E) and P53 protein expressions (P=0.047, Figure 4F) respectively; whereas mimic-miR1273f transfection down- and upregulated MDM2 (P=0.004, Figure 4E) and P53 expressions (P=0.043, Figure 4F) respectively. The above results indicated that miR1273f was negatively and positively correlated with MDM2 and P53 respectively.

Secondly, to further analyze the association between hsa_circ_0002874/miR1273f/MDM2/P53 pathway and PTX resistance, we down- and upregulated miR1273f in A549 and A549/Taxol cells via the transfection of inhibitor- and mimic-miR1273f, respectively. Colony formation and CCK-8 assays were then employed to explore the changes in cell proliferation and cell viability in A549 and A549/Taxol cells after transfection. Figure 5A shows the cell proliferation ability of A549 and A549/Taxol cells after the transfection of inhibitor- and mimic-miR1273f via crystal violet staining, respectively. The stained cell area ratio was calculated by 15 random fields per well under 10× magnification. As shown in Figure 5B, inhibitor-miR1273f transfection increased the proliferation of A549 cells (P=0.020); however, this effect was not evident after PTX treatment (P=0.676). Mimic-miR1273f transfection significantly inhibited the proliferation of A549/Taxol cells (P<0.001) and increased the sensitivity of A549/Taxol cells to PTX (P<0.001). After dissolving crystal violet with 10% glacial acetic acid, optical density values were detected at 595 nm using the NanoDrop ND-1000 spectrophotometer. As shown in Figure 5C, inhibitor-miR1273f transfection increased the cellular survival of A549 cells (P=0.015); however, this effect was not evident after PTX treatment (P=0.621). As shown in Figure 5D, mimic-miR1273f transfection significantly inhibited cellular survival of A549/Taxol cells (P=0.046) and increased the sensitivity of A549/Taxol cells to PTX (P=0.028). The above results were consistent with the results shown in Figure 5B. The cell viability of A549 and A549/Taxol cells treated with PTX after the inhibitor's transfection and mimic-miR1273f was evaluated by CCK-8 assay. As shown in Figure 5E, the absorbance at 450 nm of each group indicated that inhibitor- and mimic-miR1273f transfection could attenuate (P=0.011) and strengthen (P<0.001) the cell viability inhibition of PTX in A549 and A549/Taxol cell lines, respectively. The above results indicated that inhibitor- and mimic-miR1273f transfections could reduce and reverse PTX sensitivity and resistance in A549 and A549/Taxol cell lines respectively.

hsa_circ_0002874 knockdown or miR1273f overexpression could reverse PTX resistance *in vivo*

To determine the important role of hsa_circ_ 0002874/miR1273f on PTX resistance in LC, we constructed drug-resistant xenografts by subcutaneously injecting A549/Taxol cells. Agomir is a small double-stranded RNA that has been specially labeled and chemically modified. It modulates the biological functions of target genes by simulating endogenous miRNA [16, 17]. As shown in Figure 6A and Figure 6B, the tumor size in the agomir-1273f group and siRNAs-ciR group were significantly smaller than those in the PTX group. The tumor size in the blank group was much larger than those in the PTX group. hsa_circ_0002874, miR1273f, and MDM2 expression levels were also detected by qPCR analysis (Figure 6C–6E). It was observed that the tumor growth was significantly suppressed by intratumorally injecting siRNAs-ciR and agomir-1273f (Figure 6B), with the

up- and downregulation of miR1273f (Figure 6D) and MDM2 expressions (Figure 6E) respectively, which validated the effect of hsa_circ_0002874/ miR1273f/MDM2/p53 pathway on PTX resistance *in vivo*.

hsa_circ_0002874 was upregulated in NSCLC tissues and correlated with poor TNM staging

To further validate the role of the hsa_circ _0002874/miR1273f/MDM2/P53 pathway in NSCLC, in addition to the above cellular and molecular experiments, we also collected 20 samples of resected NSCLC tissues. We matched paired non-cancerous tissues from patients diagnosed between September 2018 and May 2019.

First, qPCR was used to quantify hsa_circ_0002874, miR1273f, and MDM2 mRNA in these 20 paired NSCLC and neighboring non-cancerous tissues (Figure 7A–7C). As shown in Figure 7D, hsa_circ_0002874 was markedly upregulated in NSCLC tissues compared with the respective control (P=0.050). Although there was no significant difference in the amount of miR1273f in cancerous and non-cancerous tissues (P=0.770) (Figure 7E), MDM2 was significantly lower in the tumor (P=0.003) (Figure 7F). A negative relationship between miR1273f and MDM2 was found in paired non-cancerous matched tissues (P=0.044) (Figure 7G). No statistically significant correlation was found between hsa_circ_0002874 and miR1273f in the 20 paired NSCLC and non-cancerous tissues (P=0.874) (Figure 7H), or between hsa_circ_0002874 and MDM2

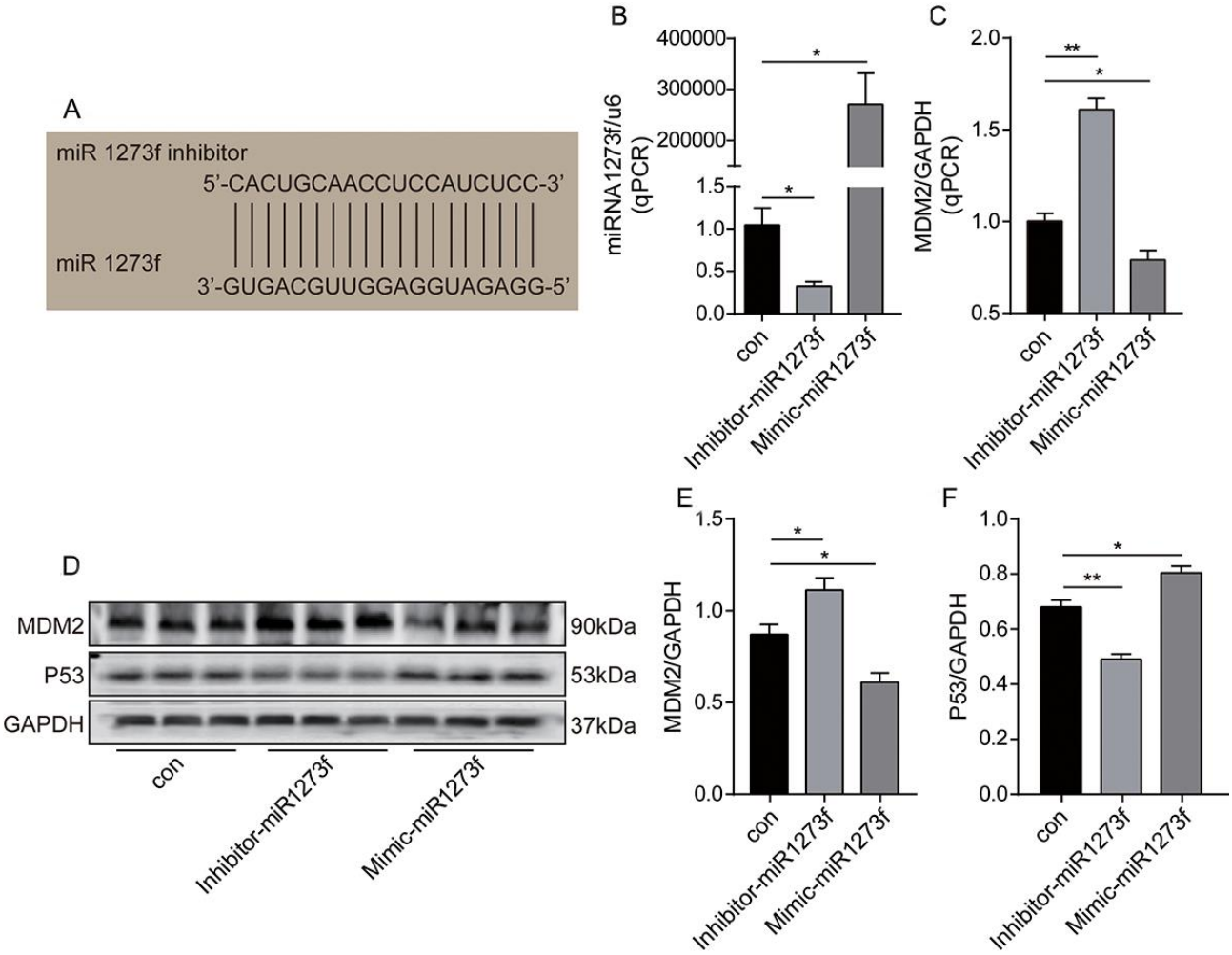

Figure 4. Knockdown or overexpression of miR1273f regulated the expression of MDM2 and P53 in A549 cell line. (**A**) miR1273f inhibitor specifically targeting the binding sites in miR1273f was designed. (**B**) miR1273f was determined by qPCR method after transfection of inhibitor-miR1273f and mimic-miR1273f. (**C**) MDM2 mRNA level was determined by qPCR method after transfection of inhibitor-miR1273f and mimic-miR1273f. (**D**) MDM2 and P53 expression were determined by western blot after transfection of inhibitor-miR1273f and mimic-miR1273f. (**E**) The quantification of MDM2 protein was analyzed according to bands in Figure 4D. (**F**) The quantification of P53 protein was analyzed according to bands in Figure 4D. *p <0.05, **p <0.01, ***p <0.001, n=3 in each group.

(P=0.369) (Figure 7I). The Oncomine database was employed to verify the expression of MDM2 in NSCLC tissue, which indicated that levels of MDM2 were decreased in certain pathological types of NSCLC (Figure 7J).

Second, correlations between hsa_circ_0002874/ miR1273f/MDM2 expression levels and other clinicopathological parameters in these NSCLC patients were also analyzed. The mean values of hsa_circ_0002874, miR1273f, or MDM2 in NSCLC tissues were used as the cut-off threshold for distinguishing high from low expression groups. It was found that increased expression of hsa_circ_0002874 was clearly related to advanced TNM stage (P=0.045, Table 3). Besides, the amount of hsa_circ_0002874 in tumor tissues was significantly higher than in the adjacent tissues in stage III/IV NSCLC (P=0.048, Table 4).

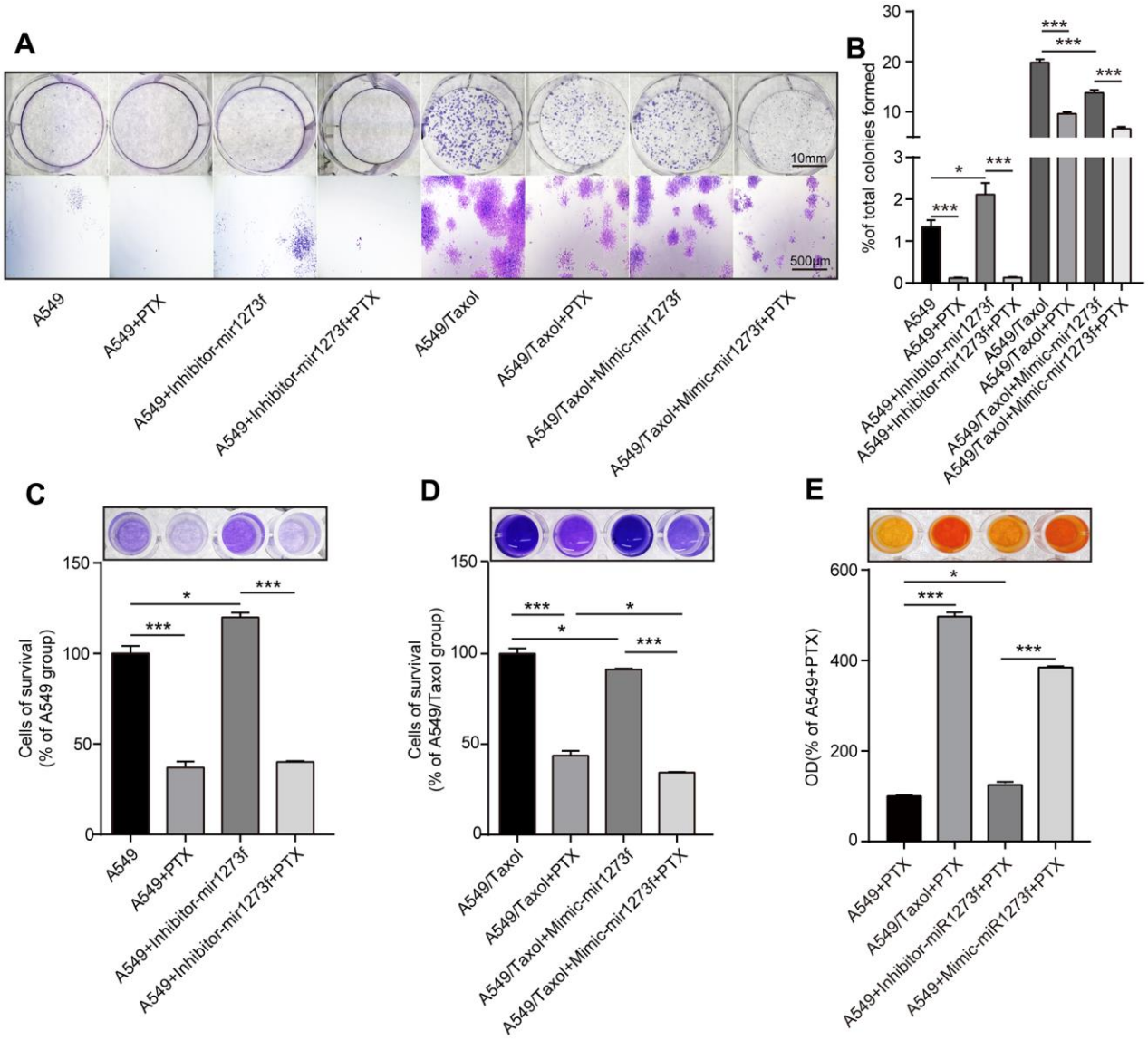

Figure 5. Knockdown of miR1273f could reduce PTX sensitivity in A549 cell line while overexpression of miR1273f could reverse PTX resistance in A549/Taxol cell line. (**A**) Cell proliferation ability of A549 and A549/Taxol cells treated with PTX after transfection of inhibitor-miR1273f and mimic-miR1273f was evaluated by colony formation assay and crystal violet staining assay. (**B**) The stained cell area ratio was calculated by 15 random fields per well in Figure 5A (images acquired at 10× magnification). (**C**) OD values of 4 groups with A549 cells were detected at 595 nm using the NanoDrop ND-1000 spectrophotometer. (**D**) OD values of 4 groups with A549/Taxol cells were detected at 595 nm using the NanoDrop ND-1000 spectrophotometer. (**E**) Cell viability of A549 and A549/Taxol cells treated with PTX after transfection of inhibitor-miR1273f and mimic-miR1273f was evaluated by CCK-8 assay. The absorbance at 450 nm of 4 groups was measured using NanoDrop ND-1000 spectrophotometer. *p <0.05, **p <0.01, ***p <0.001, n=3 in each group. Scale bar=10mm (upper) or 500μM (lower).

In contrast, for miR1273f, it was found that decreased expression was clearly associated with higher tumor grade (P=0.020, Table 5; P=0.027, Table 6) and advanced T stage (P=0.032, Table 6). Besides, the amount of miR1273f in tumor tissues was significantly lower than in adjacent tissues in node-positive NSCLC (P=0.045, Table 6) and stage III/IV NSCLC (P=0.034, Table 6).

Regarding MDM2, the increased expression of MDM2 was evidently related to advanced T stage (P=0.020, Table 7). In summary, the level of MDM2 expression in NSCLC tissues was significantly lower than that in paired non-cancerous matched tissues (P=0.004, Table 8).

Third, based on the qPCR results in Figure 7C, 20 paired NSCLC and paracancerous tissues were divided into 5 groups according to the sequence of MDM2 expression from low to high for western blotting experiments (Figure 8A). The levels of MDM2 and P53 protein are shown in Figures 8B, 8C, respectively. As shown in Figure 8D, MDM2 was markedly upregulated in NSCLC tissues compared with paracancerous tissues in MDM2 high-expression group (P=0.046). However, no significant difference was found between NSCLC and paracancerous tissues in the 4 relatively low-MDM2 expression groups (P=0.186, 0.131, 0.479, 0.470). As shown in Figure 8E, P53 was markedly downregulated in NSCLC tissues compared with that in paracancerous tissues in the two high-MDM2 expression groups (P=0.013, 0.026). However, no significant difference was found between NSCLC and paracancerous tissues in the 3 relatively low-MDM2 expression groups (P=0.201, 0.253, 0.514). A negative relationship between MDM2 and P53 was found in high-MDM2 expression group (R=-0.748, P=0.033; Figure 8F). No statistically significant correlation was found in another 4 relatively low-MDM2 expression groups between MDM2 and P53 (P=0.474, 0.790,

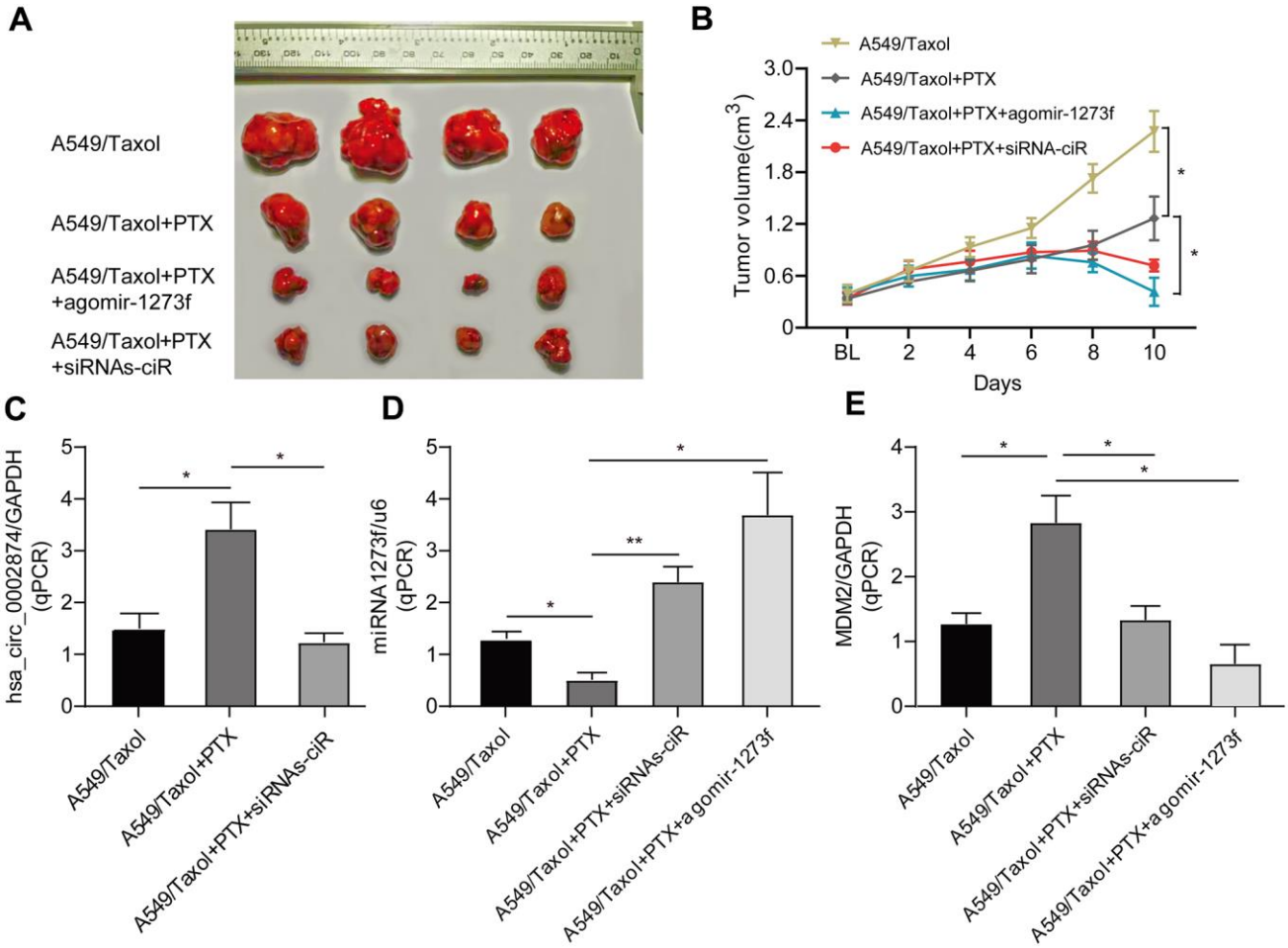

Figure 6. Effect of agomir-1273f and siRNAs-ciR on tumor growth in drug-resistant xenograft model. (**A**) The gross morphology of tumors measured on day 10 after injecting agomir-1273f plus PTX, siRNAs-ciR plus PTX or PTX. (**B**) Growth curves of subcutaneous xenograft tumors. Tumor volumes were calculated as length × (square of width) /2. (**C**–**E**) qPCR analysis was performed to detect the expression of hsa_circ_0002874, miR-1273f, and MDM2. BL, baseline tumor volume. *p <0.05, **p <0.01, n=4 in each group.

0.741, 0.409). The above results indicated that MDM2 could be associated with the progression of NSCLC in the high-MDM2 expression group, which was negatively correlated with P53.

DISCUSSION

The focus of this study was to determine whether the expression of hsa_circ_0002874 in NSCLC was aberrant and to elucidate molecular mechanisms influencing apoptosis and PTX resistance. Our results suggest that PTX exerted its effects in the A549 cell line by down-regulating the expression of hsa_circ_0002874, which in turn could regulate the expression of MDM2 and P53 via acting as a sponge for miR1273f. High expression of hsa_circ_0002874 is associated with PTX resistance in NSCLC cells, and downregulation of hsa_circ_0002874 or upregulation of

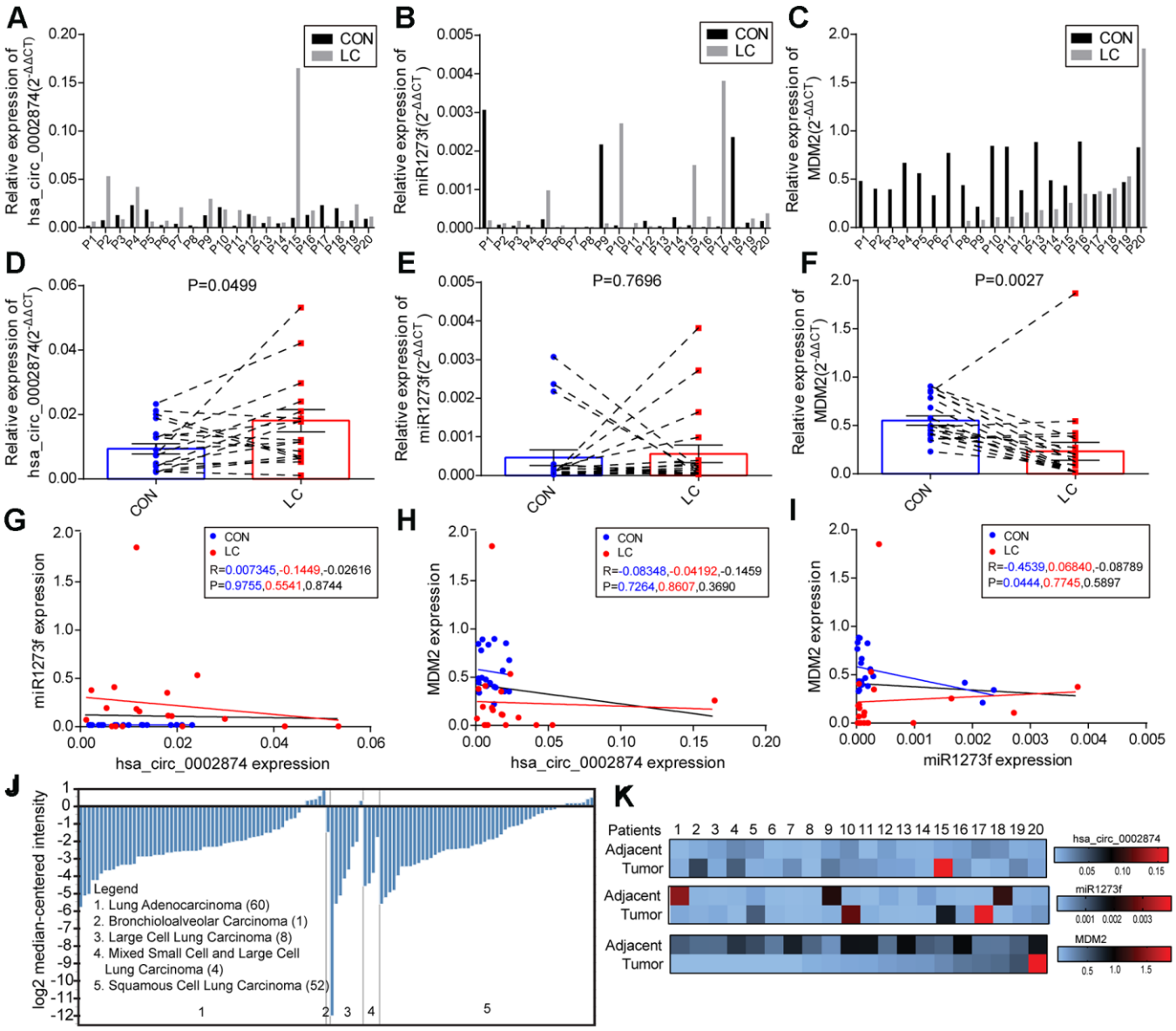

Figure 7. Levels of hsa_circ_0002874, miR1273f, and MDM2 in samples of NSCLC tissues and paired non-cancerous matched tissues. (**A**–**C**) Levels of hsa_circ_0002874, miR1273f, and MDM2 were measured using qPCR compared with GAPDH/U6 and calculated using the equation 2-ΔΔCT. (**D**–**F**) Schematic representation of the expression level of hsa_circ_0002874, miR1273f, and MDM2 in 20 NSCLC tissues compared with paired non-cancerous matched tissues. (**G**) Correlation analysis between hsa_circ_0002874 expression and miR1273f expression via Spearman Rank test. (**H**) Correlation analysis between hsa_circ_0002874 expression and MDM2 expression via Spearman Rank test. (**I**) Correlation analysis between miR1273f expression and MDM2 expression via Spearman Rank test. (**J**) Analysis of MDM2 expression in different pathological types of NSCLC via Oncomine database. (**K**) Heat map of the relative expression of hsa_circ_0002874, miR1273f, and MDM2 in 20 patients.

Table 3. Analysis of the correlation between expression of hsa_circ_0002874 in LC and its clinicopathological parameters.

Pathological characteristics	Cases (n)	hsa_circ_0002874 expression		P value
		High (5)	Low (15)	
Gender				0.606
Male	10 (50%)	3 (60%)	7 (46.7%)	
Female	10 (50%)	2 (40%)	8 (56.3%)	
Age				0.292
<65	8 (40%)	1 (20%)	7 (46.7%)	
≥65	12 (60%)	4 (80%)	8 (56.3%)	
Location				0.210
Left	6 (30%)	2 (40%)	4 (26.7%)	
Right	11 (55%)	1 (20%)	10 (66.7%)	
Others	3 (15%)	2 (40%)	1 (6.7%)	
T stage				0.347
1/2	15 (75%)	3 (60%)	12 (80%)	
3/4	2 (10%)	1 (20%)	1 (6.7%)	
Others	3 (15%)	1 (20%)	2 (13.3%)	
Lymph node metastasis				0.146
No	9 (45%)	1 (20%)	8 (53.3%)	
Yes	7 (35%)	3 (60%)	4 (26.7%)	
Others	4 (20%)	1 (20%)	3 (20%)	
Metastasis status				0.567
No	16 (80%)	4 (80%)	12 (80%)	
Yes	1 (5%)	0	1 (6.7%)	
Others	3 (15%)	1 (20%)	2 (13.3%)	
TNM stage				0.045
I/II	12 (60%)	1 (20%)	11 (73.3%)	
III/IV	6 (30%)	3 (60%)	3 (20%)	
Others	2 (10%)	1 (20%)	1 (6.7%)	
Histology				0.047
SCC	1 (5%)	1 (20%)	0	
Adenocarcinoma	18 (90%)	3 (60%)	15 (100%)	
Others	1 (5%)	1 (20%)	0	
Tumor grading*				0.166
2	2 (10%)	1 (20%)	1 (6.7%)	
3	10 (50%)	1 (20%)	9 (60%)	
Others	8 (40%)	3 (60%)	5 (33.3%)	

* No pathological grading of 1.

miR1273f could increase the chemosensitivity of A549/Taxol to PTX in xenograft models. According to our analysis of NSCLC and paired matched non-cancerous tissues, hsa_circ_0002874 was upregulated in NSCLC and correlated with poor TNM staging. These findings offer a new vista for research into the role of circular RNA in the development of NSCLC, and provide a new perspective for analyzing PTX resistance in this cancer. This study also explored the use of siRNAs-ciRs or mimic-miRs as new approaches to reverse PTX resistance.

The previous research of our group found that PTX depends on P53 protein to promote the apoptosis of

Table 4. Comparison of hsa_circ_0002874 expression according to patients' characteristics.

Pathological characteristics	Cases (n)	hsa_circ_0002874 in PNT ($\times 10^{-2}$)	P value	hsa_circ_0002874 in LC ($\times 10^{-2}$)	P value	P value between PNT and LC
Total	20	1.07±0.74		2.34±3.59		0.132
Gender			0.051		0.415	
Male	10	0.76±0.58		3.01±4.97		0.171
Female	10	1.39±0.76		1.66±1.22		0.561
Age			0.458		0.283	
<65	8	0.92±0.67		1.25±0.66		0.332
≥65	12	1.18±0.79		3.06±4.53		0.171
Location			0.269		0.410	
Left	6	1.34±0.98		1.93±2.23		0.572
Right	11	0.88±0.68		1.32±0.72		0.160
T stage			0.530		0.243	
1	8	1.23±0.84		1.24±0.91		0.981
2/3/4	9	0.98±0.76		2.06±1.71		0.101
Lymph node metastasis			0.508		0.323	
No	9	1.23±0.95		1.38±1.26		0.779
Yes	7	0.95±0.62		2.13±1.68		0.106
Metastasis status			0.000		0.007	
No	16	1.15±0.77		1.74±1.44		0.158
Yes	1	0.21		0.63		-
TNM stage			0.635		0.154	
I/II	12	1.14±0.84		1.25±1.11		0.801
III/IV	7	0.96±0.63		2.18±1.64		0.048
Histology			0.087		0.000	
SCC	1	0.76		5.32		-
Adenocarcinoma	18	1.09±0.78		1.38±1.05		0.356
Tumor grading*			0.009		0.216	
2	2	2.22±0.16		3.04±1.65		0.555
3	10	0.75±0.62		1.51±1.48		0.153

Note: PNT, Paired Noncancerous Tissues. Data were presented as means ± SD. * No pathological grading of 1.

A549 cells and can up-regulate P53 protein expression via up-regulating the level of long-chain ncRNA MEG3 [18]. Association studies between PTX and ncRNA non-coding RNA have often focused on PTX resistance. In terms of miRNAs, ursolic acid has recently been reported to reverse the chemical resistance of PTX to breast cancer cells by targeting miRNA-149-5p [19]. MiR-155-3p can also act as a tumor suppressor and reverse PTX resistance via the negative regulation of MYD88 in human breast cancer [20].

In studies of lncRNAs, it was recently reported that knockdown of LINC00511 could reduce the resistance of cervical cancer cells to PTX [21]. However, very few studies have examined associations between circRNAs and PTX resistance. Previous bioinformatics analysis suggested that 2909 significantly upregulated and 8372 downregulated circRNAs were detectable in A549/Taxol relative to parental A549 cells [22], leaving many unexplored areas for the roles of circular RNA in NSCLC. In our research, the expression of hsa_circ_0002874 was found to be downregulated by PTX in A549 cells, which could represent a new mechanism of action of PTX. Moreover, our results indicated that strong expression of hsa_circ_0002874 was associated with NSCLC PTX resistance. To explore

Table 5. Analysis of the correlation between expression of miR1273f in LC and its clinicopathological parameters.

Pathological characteristics	Cases (n)	miR1273f expression		P value
		High (4)	Low (16)	
Gender				0.264
Male	10 (50%)	1 (25%)	9 (56.3%)	
Female	10 (50%)	3 (75%)	7 (43.8%)	
Age				0.068
<65	8 (40%)	0	8 (50%)	
≥65	12 (60%)	4 (100%)	8 (50%)	
Location				0.938
Left	6 (30%)	1 (25%)	5 (31.3%)	
Right	11 (55%)	2 (50%)	9 (56.3%)	
Others	3 (15%)	1 (25%)	2 (12.5%)	
T stage				0.486
1/2	15 (75%)	3 (75%)	12 (75%)	
3/4	2 (10%)	0	2 (12.5%)	
Others	3 (15%)	1 (25%)	2 (12.5%)	
Lymph node metastasis				0.090
No	9 (45%)	3 (75%)	6 (37.5%)	
Yes	7 (35%)	0	7 (43.8%)	
Others	4 (20%)	1 (25%)	3 (18.8%)	
Metastasis status				0.633
No	16 (80%)	3 (75%)	13 (81.3%)	
Yes	1 (5%)	0	1 (6.3%)	
Others	3 (15%)	1 (25%)	2 (12.5%)	
TNM stage				0.180
I/II	12 (60%)	3 (75%)	9 (56.3%)	
III/IV	6 (30%)	0	6 (37.5%)	
Others	2 (10%)	1 (25%)	1 (6.3%)	
Histology				0.656
SCC	1 (5%)	0	1 (6.3%)	
Adenocarcinoma	18 (90%)	3 (75%)	15 (93.8%)	
Others	1 (5%)	1 (25%)	0	
Tumor grading*				0.020
2	2 (10%)	1 (25%)	1 (6.3%)	
3	10 (50%)	0	10 (62.5%)	
Others	8 (40%)	3 (75%)	5 (31.3%)	

* No pathological grading of 1.

methods to reverse the PTX resistance of NSCLC cells, transfection of inhibitor-miR1273f and mimic-miR1273f was performed. The results showed that knockdown of miR1273f could reduce PTX sensitivity in A549 cells while overexpression of miR1273f reversed PTX resistance in the A549/Taxol cell line.

An increased understanding of the biological roles of circRNA has resulted in questions on the relationship between circRNA and NSCLC becoming a hot topic. In 2017, some scholars analyzed the circRNA expression profile of patients with early lung adenocarcinoma [23]. A total of 357 dysregulated circRNAs were found in tumor samples, suggesting their potential role in lung

Table 6. Comparison of miR1273f expression according to patients' characteristics.

Pathological characteristics	Cases (n)	miR1273f in PNT ($\times 10^{-4}$)	P value	miR1273f in LC ($\times 10^{-4}$)	P value	P value between PNT and LC
Total	20	4.62±9.08		5.61±10.19		0.748
Gender			0.490		0.281	
Male	10	6.07±11.23		3.09±4.78		0.171
Female	10	3.17±6.58		8.13±13.51		0.561
Age			0.279		0.151	
<65	8	7.38±12.35		1.56±0.95		0.205
≥65	12	2.78±6.02		8.31±12.61		0.184
Location			0.038		0.663	
Left	6	9.88±13.57		7.12±15.22		0.748
Right	11	0.80±0.74		4.66±7.95		0.124
T stage			0.444		0.032	
1	8	7.12±12.02		13.57±15.49		0.396
2/3/4	9	3.31±7.63		1.37±1.22		0.460
Lymph node metastasis			0.031		0.174	
No	9	0.66±0.66		9.03±14.00		0.049
Yes	7	11.30±13.40		1.38±0.84		0.045
Metastasis status			0.000		0.185	
No	16	3.51±7.51		5.80±10.93		0.496
Yes	1	30.64		2.00		-
TNM stage			0.005		0.131	
I/II	12	0.941±0.887		9.58±13.68		0.041
III/IV	7	13.37±13.43		1.18±0.86		0.034
Histology			0.082		0.128	
SCC	1	0.90		1.32		-
Adenocarcinoma	18	5.04±9.50		5.25±10.40		0.950
Tumor grading*			0.554		0.027	
2	2	0.80±0.07		13.76±18.96		0.436
3	10	5.89±11.33		1.52±1.20		0.241

Note: PNT, Paired Noncancerous Tissues. Data were presented as means ± SD. * No pathological grading of 1.

cancer. Abnormal expression of circRNA clusters in early lung adenocarcinoma could provide potential targets for early diagnosis of the disease. More recently, many other circRNAs have been reported to be related to NSCLC. The expression of circ_0067934 was significantly increased in NSCLC tissues and was associated with poor prognosis of NSCLC. Silencing circ_0067934 inhibited proliferation, migration, and invasion of NSCLC cells [24]. NSCLC tumor specimens exhibited higher levels of circP4HB than paired healthy lung samples, which would promote NSCLC invasion and metastasis by adsorption of miR-133a-5p [25]. In our research, hsa_circ_0002874 was found to be strongly upregulated in NSCLC tissues compared to paired non-cancerous matched tissues.

In our study, the level of miR1273f, a downstream target of hsa_circ_0002874, did not differ significantly between NSCLC tissues and paired non-cancerous matched tissues. However, this could be due to the small sample size in this pilot study, with only 20 pairs of samples, or other pathways affecting the expression of miR1273f. There are many studies in the literature on the relationship between miRNA and NSCLC. A recent

Table 7. Analysis of the correlation between expression of MDM2 in LC and its clinicopathological parameters.

Pathological characteristics	Cases (n)	MDM2 expression		P value
		High (6)	Low (14)	
Gender				0.329
Male	10 (50%)	4 (66.7%)	6 (42.9%)	
Female	10 (50%)	2 (33.3%)	8 (57.1%)	
Age				0.550
<65	8 (40%)	3 (50%)	5 (35.7%)	
≥65	12 (60%)	3 (50%)	9 (64.3%)	
Location				0.394
Left	6 (30%)	2 (33.3%)	4 (28.6%)	
Right	11 (55%)	3 (50%)	8 (57.1%)	
Others	3 (15%)	1 (16.7%)	2 (14.3%)	
T stage				0.020
1/2	15 (75%)	3 (50%)	12 (85.7%)	
3/4	2 (10%)	2 (33.3%)	0	
Others	3 (15%)	1 (16.7%)	2 (14.3%)	
Lymph node metastasis				0.771
No	9 (45%)	2 (33.3%)	7 (50%)	
Yes	7 (35%)	2 (33.3%)	5 (35.8%)	
Others	4 (20%)	2 (33.3%)	2 (14.3%)	
Metastasis status				0.506
No	16 (80%)	5 (83.3%)	11 (78.6%)	
Yes	1 (5%)	0	1 (7.1%)	
Others	3 (15%)	1 (16.7%)	2 (14.3%)	
TNM stage				0.710
I/II	12 (60%)	3 (50%)	9 (64.3%)	
III/IV	6 (30%)	2 (33.3%)	4 (28.6%)	
Others	2 (10%)	1 (16.7%)	1 (7.1%)	
Histology				0.539
SCC	1 (5%)	0	1 (7.1%)	
Adenocarcinoma	18 (90%)	5 (83.3%)	13 (92.9%)	
Others	1 (5%)	1 (16.7%)	0	
Tumor grading*				0.273
2	2 (10%)	0	2 (14.3%)	
3	10 (50%)	4 (66.7%)	6 (42.9%)	
Others	8 (40%)	2 (33.3%)	6 (42.9%)	

* No pathological grading of 1.

report suggested that miRNA-621 is closely related to the pathological grade and poor prognosis of NSCLC. Furthermore, miRNA-621 could inhibit the malignant progression of NSCLC by modulating SIX4 expression [26]. miRNA could also be used as a candidate biomarker for early diagnosis of NSCLC. Recently, it has been reported that miRNA-23a and miRNA-451 may be useful as potential biomarkers for early diagnosis of NSCLC, and both together may be more effective for diagnosis than either alone [27]. MiRNA-17 and miRNA-222 can also be considered as non-invasive biomarkers for detecting early lung cancer development and metastasis in patients with NSCLC [28].

Regarding the relationship between MDM2 protein and NSCLC tissues, MDM2 is highly expressed as a proto-oncogene in cancer tissues. MDM2 is significantly upregulated in lung adenocarcinoma tissues compared with adjacent tissues [29]. However, MDM2 expression

Table 8. Comparison of MDM2 expression according to patients' characteristics.

Pathological characteristics	Cases (n)	MDM2 in PNT ($\times 10^{-1}$)	P value	MDM2 in LC ($\times 10^{-1}$)	P value	P value between PNT and LC
Total	20	5.50±0.21		0.23±0.41		0.004
Gender			0.275		0.346	
Male	10	4.96±1.81		3.22±5.70		0.370
Female	10	6.05±2.43		1.43±1.35		0.000
Age			0.587		0.740	
<65	8	5.17±2.21		1.94±2.07		0.009
≥65	12	5.73±2.22		2.59±5.16		0.049
Location			0.029		0.775	
Left	6	4.54±1.23		1.62±1.92		0.010
Right	11	6.59±2.20		1.34±1.76		0.000
T stage			0.972		0.392	
1	8	5.69±2.72		1.36±1.52		0.002
2/3/4	9	5.73±2.02		3.30±6.04		0.269
Lymph node metastasis			0.023		0.888	
No	9	6.44±2.33		1.32±1.43		0.000
Yes	7	4.39±1.71		1.45±2.25		0.017
Metastasis status			0.125		0.044	
No	16	5.76±2.36		2.53±4.6		0.018
Yes	1	4.80		0.00		-
TNM stage			0.015		0.627	
I/II	12	6.46±2.22		2.69±5.15		0.036
III/IV	7	3.82±0.97		1.67±2.16		0.046
Histology			0.006		0.029	
SCC	1	4.00		0.00		-
Adenocarcinoma	18	5.65±2.24		2.44±4.33		0.009
Tumor grading*			0.305		0.605	
2	2	7.57±2.29		0.53±0.75		0.020
3	10	5.72±2.29		2.79±5.73		0.151

Note: PNT, Paired Noncancerous Tissues. Data were presented as means ± SD. * No pathological grading of 1.

is not significantly different between cancer and paracancerous tissues in patients with NSCLC according to Western blot analysis results [30]. In our research, although the increased expression of MDM2 was evidently related to advanced T stage, the level of MDM2 expression in NSCLC tissues was significantly lower than that in paired non-cancerous matched tissues. The Oncomine database analysis indicated the low expression of MDM2 in different pathological subgroups. The above results showed that the expression of MDM2 in NSCLC remains uncertain. Besides, the contingency effect caused by the small sample size was also an interference factor.

Regarding the relationship between P53 protein and NSCLC tissues, the most common mutated gene in lung adenocarcinoma and lung squamous cell carcinoma is p53, found in 45%-70% of adenocarcinomas and 60%-80% of squamous cells cancer [31]. Due to the high mutation rate of p53 in NSCLC, targeting mutated p53 and restoring its wild-type function is a potential therapeutic strategy and is used to develop new compounds to treat cancer. Nutlin, for example, is a compound capable of increasing wild-type p53's anti-tumor activity by blocking the interaction between p53 and MDM2 *in vivo* (E3 ubiquitin ligase of p53) [32, 33]. Mammalian cell lines and mouse xenograft models

show that PRIMA (p53 reactivation and induction of massive apoptosis) can bind to and convert mutant p53 to its wild-type structure, leading to growth inhibition and apoptosis [34, 35]. RETRA (reactivation of transcriptional reporter activity) is another compound which inhibits mutant p53 activity by releasing p73 (p53 family protein with a high level of sequence similarity) from the p53 complex and activating target proteins associated with growth inhibition and apoptosis induction [36, 37]. Hence, developing and discovering

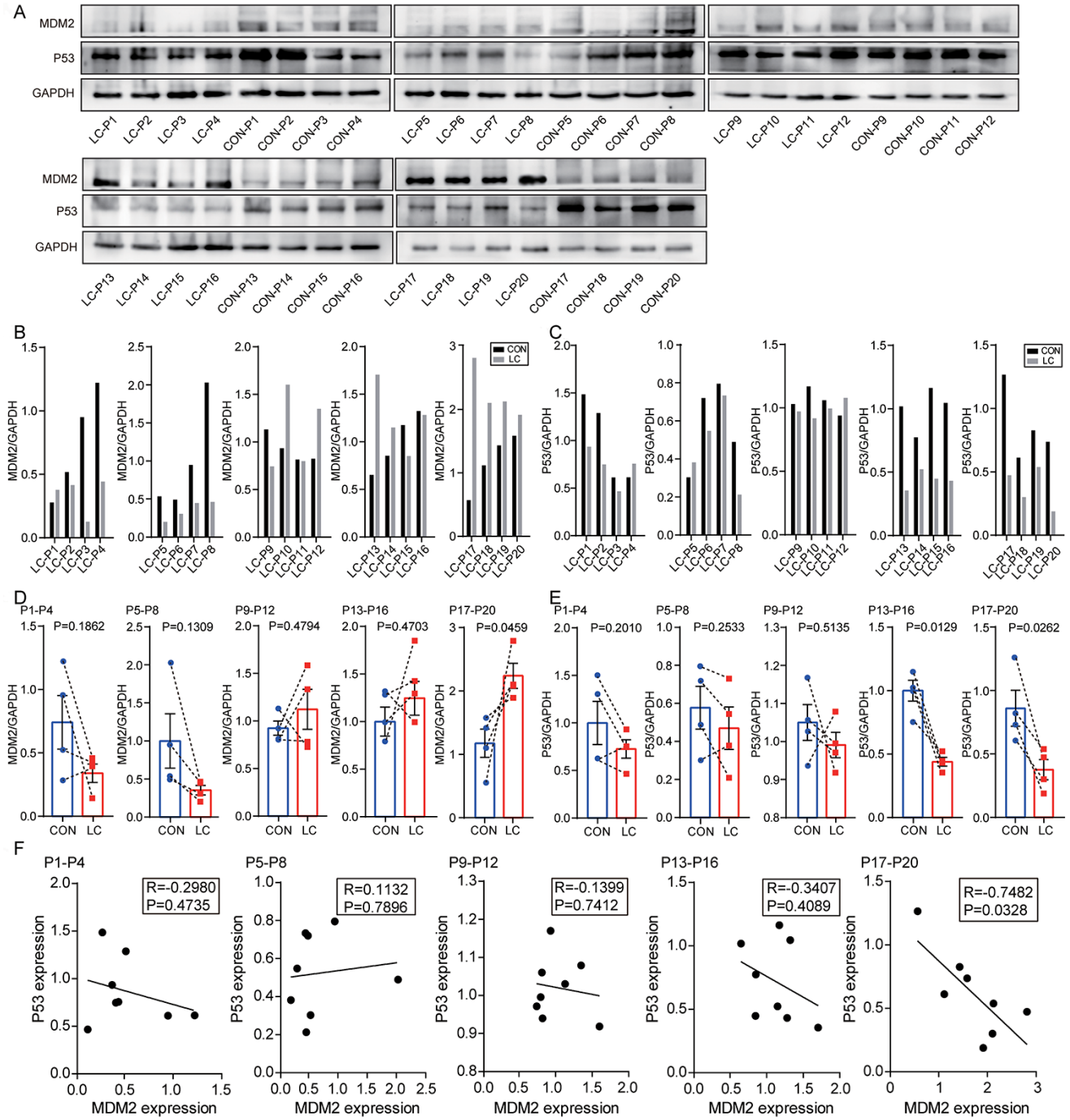

Figure 8. Levels of MDM2 and P53 protein in samples of NSCLC tissues and paired non-cancerous matched tissues. (**A**) MDM2 and P53 expression in 20 NSCLC tissues compared with paired non-cancerous matched tissues were determined by western blot. (**B**) The quantification of MDM2 protein was analyzed according to bands in Figure 8A. (**C**) The quantification of P53 protein was analyzed according to bands in Figure 8A. (**D**, **E**) Schematic representation of the expression level of MDM2 and P53 in 20 NSCLC tissues compared with paired non-cancerous matched tissues. (**F**) Correlation analysis between MDM2 expression and P53 expression via Spearman Rank test.

new molecules targeting abnormal p53 or promoting the pro-apoptotic role of wild-type p53 can aid clinical cancer therapy [38]. This research is dedicated to developing and discovering new molecules that enhance the pro-apoptotic effect of wild-type p53 via hsa_circ_0002874/miR1273f/MDM2/P53 pathway.

Limitations

There are some limitations to our analysis that deserve discussion. First, the mechanism study was carried out in a single pair of cell lines A549 and A549/Taxol, and more studies on other cell lines need to be further studied. Second, the mechanism of paclitaxel treatment regulating the expression of hsa_circ_0002874 needs further study. Third, only 20 NSCLC tissues and paired non-cancerous matched tissues were available for study. Limited sample size weakens conclusions on the abnormal expression of hsa_circ_0002874 in NSCLC. Forth, also due to the small sample size, there are many false positives in the chi-square test and the Student t-test in Table 3–8.

CONCLUSION

CircRNA hsa_circ_0002874 is strongly expressed in NSCLC tissues and maybe a potential marker of PTX resistance. CircRNA hsa_circ_0002874 acts as a sponge for miR1273f and thereby affects the level of MDM2, eventually acting as a tumor promoter in NSCLC.

MATERIALS AND METHODS

Reagents and antibodies

PTX was purchased from Aladdin. Dulbecco's Modified Eagle Medium (DMEM) /F12 was purchased from Gibco. Fetal bovine serum (FBS) was purchased from Biological Industries. Trypsin, crystal violet, 3- (4,5-dimethylthiazol-2-yl) -2,5-diphenyltetrazolium bromide (MTT) kit, Cell Counting Kit-8, and P53 antibody were purchased from Beyotime Biotechnology. Trizol was purchased from Ambion. RevertAid First Strand complementary DNA (cDNA) Synthesis Kit was purchased from Thermo. SYBR Green Polymerase Chain Reaction (PCR) kit was purchased from Biomake. Glyceraldehyde 3-phosphate dehydrogenase (GAPDH) antibody was purchased from Signalway Antibody. Goat anti-mouse IgG horseradish peroxidase horseradish peroxidase (HRP) -conjugated secondary antibody was purchased from Santa Cruz Biotecnology. MDM2 antibody was purchased from Affinity. Polyvinylidene difluoride (PVDF) membrane was purchased from Immobilon. 0.3% triton-X was purchased from Vetec. Lipofectamine 3000 transfection reagent was purchased from Invitrogen. Mimic-1273f and Inhibitor-1273f were synthesized by GenePharma (Shanghai, China). siRNAs-ciR and pCD25-ciR were synthesized by Geneseed (Guangzhou, China). The siRNAs-ciR used in this study is a mixture of 3 types of siRNA, and their sequences are 5'-AATCCTGGGAAAGGCTTAT-3', 5'-ATCCTGGGA AAGGCTTATA-3', and 5'-CTGGGAAAGGCTTA TAACC-3'. Dual luciferase reporter vector plasmid (miR1273f) was purchased by GenePharma (Shanghai, China). Dual luciferase reporter gene fluorescence detection kit was purchased by Promega. Agomir-1273f (catalog number: B06002) was purchased by GenePharma (Shanghai, China).

Tissue specimens

A total of 20 NSCLC tissues and paired non-cancerous matched tissues were collected through surgical resection from patients diagnosed between September 2018 and May 2019 at the The Second Affiliated Hospital of Suzhou University (Suzhou, Jiangsu, China). With the guidance of a skillful pathologist, we collected normal lung samples with a distance of ≥2 cm from the edge of cancer tissue. All patients did not receive radiotherapy and chemotherapy before surgery. All specimens were collected under the guidance of the HIPAA protocol. The study was approved by the Ethics Committee of Second Affiliated Hospital of Suzhou University, and written informed consent was obtained from all the patients. TNM stage classification complied with the NCCN Clinical Practice Guidelines in Oncology: Non-Small Cell Lung Cancer (Version 2.2019).

Cell lines and cell culture

Human A549 cell lines were supplied by the Cell Bank of Type Culture Collection of the Chinese Academy of Sciences, Shanghai, China (CBP60084). Human A549/Taxol cell lines were purchased from Yaji Biotechnology Company, Shanghai, China (YS421C). A549 cells were cultured in DMEM/F12 medium supplemented with 10% fetal bovine serum (which contained 100 U/ml penicillin and 100 mg/ml streptomycin). A549/Taxol cells were cultured in DMEM/F12 medium supplemented with 10% fetal bovine serum (which contained 5μM PTX, 100 U/mL penicillin, and 100 mg/mL streptomycin).

CircRNA and miRNA screening

Primers for 18 circRNAs resistant to breast cancer cell MCF-7 doxorubicin [14] were designed, and qPCR was used to screen for the most stable and robust circRNA expression after PTX administration. Subsequently, it was submitted to Suzhou Jima Gene Company for

technical evaluation to ensure that the length of the selected circRNA can ensure the synthesis of high-quality pCDNA and siRNAs for subsequent experimental steps. The 18 primary screening circRNAs were shown in Table 9.

Hsa_circ_0002874 was screened and its target miRNAs predicted by circMir 1.0, RegRNA 2.0 and MirTrap software were hsa-miR-1273f, hsa-miR-4726-5p, hsa-miR-2115-5p, and hsa-miR-4649-5p. The literature review, miRBase and TargetScan web analysis were used to predict the target genes of the four, and the downregulated protein expressions were: MDM2, SHP-1, Erbb2, MLLT6. The expressions of predicted miRNAs after the administration of PTX were verified by qPCR to estimate the true target miRNA of hsa_circ_0002874 (Table 2).

RNA extraction and quantitative polymerase chain reaction (qPCR) analysis

According to the manufacturer's protocol, total RNA was extracted with Trizol reagent. According to OD260/280 readings, the purity and concentration of RNA were determined by NanoDrop ND-1000 spectrophotometer. Total RNA (500ng) was reverse transcribed into cDNA with a final volume of 20 μl. RevertAid First Strand cDNA Synthesis Kit (Thermo) was used under standard conditions with random primers and oligo dT primers. Purity and concentration of DNA were determined by NanoDrop ND-1000 spectrophotometer. Then, the SYBR Green PCR kit was used for qPCR. The reaction was set as follows: 94° C for 3 min, 30 cycles at 94° C for 30 s, 55° C for 30 s, and 72° C for 30 s. Final extension was performed at 72° C for 7 min. The results of qPCR normalized to the expression of GAPDH. The results of qPCR were analyzed relative to the threshold cycle (Ct) value and converted into multiple values according to the rule of $2^{-\Delta\Delta CT}$. The primers used are shown in Table 1.

MTT assay

The cells were seeded into a 96-well plate (Corning) at a density of 5×10^3 cells/well in 200 μl culture medium. After treatment, the cells were incubated in 200 ml DMEM/F12 containing 0.5 mg/ml MTT at 37° C for 4 hours. Afterward, the supernatant was removed, and the cells were lysed in 200 μl dimethyl sulfoxide (DMSO) for 10 min at 37° C. Optical density (OD) values were detected at 490 nm. The obtained values were presented as folds of the control group.

Western blot analysis

Western blot analysis was performed using standard procedures. Briefly, total protein was extracted and isolated by 10% sodium dodecyl sulfate polyacrylamide gel electrophoresis (SDS-PAGE) and transferred to a PVDF membrane. To block non-specifically bound, the membrane was incubated with 5% skim milk powder for 1 hour at room temperature. Membranes were then incubated with primary antibody against MDM2 or P53 (1:1000) followed by HRP labeled secondary antibody and detected by chemiluminescence. An anti-GAPDH antibody (1:1000) was used as a protein loading control.

Dual-luciferase reporter assay

MDM2 3' UTR was amplified from cDNA of 293 cells and inserted into pGL-3 (Promega, USA). The 293 cells (GenePharma, Shanghai, China) were cotransfected with the wild-type 3'UTR of MDM2 containing the putative miR1273f binding site (Site 1: 2709-2715) and mutant MDM2 3' UTR with either NC mimics or miR1273f mimics via Lipofectamine 3000. After transfection, the cells were cultivated at 37° C, 5% CO2 for 4 h. Then, the luciferase activities were confirmed using a dual-luciferase reporter assay system according to the manufacturer's protocol.

Transfection

A549 cells were seeded into 6-well plates, incubated overnight and transfected with siRNAs-ciR/pCD25-ciR plasmid or miR1273f inhibitor/negative control. A549/Taxol cells were transfected with the miR1273f mimic/negative control under the same conditions. The sequences used for transfection were listed in Table 10. Lipofectamine 3000 was used as a transfection reagent according to the manufacturer's recommendations. After transfection for 48 hours, cells were used for functional analysis.

Colony formation assay

Transfected A549 or A549/Taxol cells were seeded in 6-well plates at 5×10^3 cells per well. After incubation for 36 hours at 37° C in a 5% CO_2 humidified incubator, the cells were incubated with medium supplemented with PTX (2μM) and cultured at 37° C in a 5% CO_2 humidified incubator for 7 days. After colony formation was observed, the medium was removed. The cells were washed twice with phosphate buffered saline (PBS), fixed with 4% formaldehyde for 10 minutes, and stained with 5% crystal violet for 10 minutes. The stained cell area ratio was calculated by randomly photographing 15 fields per well under a 10× microscope. Finally, after dissolving crystal violet with 10% glacial acetic acid, OD values were detected at 595 nm. The obtained values were presented as folds of the control group.

Table 9. 18 circRNAs* for primary screening.

CircRNA ID	CircRNA type	Chrom
Upregulated circRNAs		
hsa_circ_ 0002113	exonic	Chr21
hsa_circ_ 0001667	exonic	Chr7
hsa_circ_ 0006528	exonic	Chr5
hsa_circ_ 0002874	exonic	Chr9
hsa_circ_ 0002168	exonic	Chr20
hsa_circ_ 0086241	exonic	Chr9
hsa_circ_ 0007769	exonic	Chr6
hsa_circ_ 0092276	intronic	Chr3
hsa_circ_ 0044556	exonic	Chr17
hsa_circ_ 0003183	exonic	Chr8
hsa_circ_ 0085567	exonic	Chr8
hsa_circ_ 0085495	exonic	Chr8
Downregulated circRNAs		
hsa_circ_ 0008131	exonic	ChrX
hsa_circ_ 0003838	exonic	Chr15
hsa_circ_ 0007551	exonic	Chr5
hsa_circ_ 0005004	exonic	Chr7
hsa_circ_ 0006903	exonic	Chr12
hsa_circ_ 0018293	exonic	Chr10

* According to Screening circular RNA related to chemotherapeutic resistance in breast cancer [14].

Table 10. Transfected gene sequences.

Gene	Sequence (5'→3')
hsa_circ_0002874-siRNAs	AATCCTGGGAAAGGCTTAT
	ATCCTGGGA AAGGCTTATA
	CTGGGAAAGGCTTATAACC
Negative control (NC)	Sense UUCUCCGAACGUGUCACGUTT
	Antisense ACGUGACACGUUCGGAGAATT
miR-1273f mimic	Sense GGAGAUGGAGGUUGCAGUG
	Antisense CUGCAACCUCCAUCUCCUU
miRNA inhibitor NC	CAGUACUUUUGUGUAGUACAA
miR-1273f inhibitor	CACUGCAACCUCCAUCUCC

CCK8 assay

After 48 hours of transfection in 96-well plates, the freshly prepared medium contained PTX at a final concentration of 10μM. The medium was added to the wells with 7 replicate wells per set. After 48 hours of incubation, cell viability was measured using CCK-8 kit according to the manufacturer's instructions. The absorbance at 450 nm was measured using NanoDrop ND-1000 spectrophotometer.

Xenograft assay

All experimental protocols were approved by the Animal Ethics Committee of Second Affiliated Hospital of Soochow University. A total of 20 BALB/c nude mice (4 weeks old) weighing 20.75±1.2g were fed a pellet diet and housed under controlled environment with a temperature of 24±2˚C and air humidity of 60±2%. For the drug-resistant xenograft model, A549/Taxol cells were subcutaneously injected into the

armpits of nude mice (1×10^6 cells per animal). From the 10th day after cell injection, the engraftment of tumor was confirmed and the baseline tumor size was evaluated. The xenograft-bearing mouse models were randomized into four groups (n=5), five mice were were intraperitoneally injected with PTX (15mg/kg each time) and intratumorally injected with agomir-1273f (5 nmol each time); five mice were intraperitoneally injected with PTX and intratumorally injected with siRNAs-ciR; five mice were intraperitoneally injected with PTX and intratumorally injected with PBS; and the remaining five mice were intratumorally and intraperitoneally injected with PBS as a control once every 3 days. Tumor formations were monitored by measuring the length (L) and width (W) with calipers every 2 days, and the volumes were calculated using the following formula: (L×W×W)/2. All mice were sacrificed on 10 days, and the tumors were neatly excised. Tumor tissues were then subjected to RNA isolation for qPCR analysis.

Statistical analysis

All statistical analyses were performed using SPSS 22.0 software (IBM) and Graph pad Prism 5.0. Differences between NSCLC tissues and paired non-cancerous matched tissues were analyzed using the Student's t test. One-way ANOVA further analyzed the correlations between hsa_circ_0002874 expression levels and clinicopathological factors. The correlations among hsa_circ_0002874 expression, miR1273f expression, and MDM2 expression were explored by Pearson correlation analysis. $P < 0.05$ was considered statistically significant.

AUTHOR CONTRIBUTIONS

Conceptualization: ZYS, SCJ; Experiments: XJH, NLW, ZFL, DXX; Data analysis: TJL, PJ; Original draft writing: XJH, SAM; Review, editing, and final approval: NLW, SZ, SCJ; Research supervision: ZYS, SCJ.

CONFLICTS OF INTEREST

No editorial or financial conflicts of interest, and all authors have contributed to, read and approved the final manuscript for submission.

FUNDING

The current study was supported by grants from the National Science Foundation of China (No. 81601098), the Second Affiliated Hospital of Soochow University pre-research Project (SDFEYGJ1609), the Second Affiliated Hospital of Soochow University Clinical Discipline Group Project Funding (XKQ 2015008), the International Team of Gastrointestinal Tumor Project Funding (SZYJTD201804), Import Team of Hepatobiliary and Pancreatic Surgery Project Funding (SZYJTD201803), the Project of State Key Laboratory of Radiation Medicine and Protection (GZK1201820), the 2019 Kunshan Key R&D Plan (Ecological Agriculture and Social Development) -Social Development Science and Technology Project (KS1941), the second affiliate hospital of Soochow university science and technology innovation team project funding (XKTJ-TD 202009), and the Talent promotion project of the Second Affiliated Hospital of Suzhou University (XKTJ-RC202013).

REFERENCES

1. Jemal A, Siegel R, Xu J, Ward E. Cancer statistics, 2010. CA Cancer J Clin. 2010; 60:277–300. https://doi.org/10.3322/caac.20073 PMID:20610543
2. Siegel RL, Miller KD, Jemal A. Cancer statistics, 2018. CA Cancer J Clin. 2018; 68:7–30. https://doi.org/10.3322/caac.21442 PMID:29313949
3. Bray F, Ferlay J, Soerjomataram I, Siegel RL, Torre LA, Jemal A. Global cancer statistics 2018: GLOBOCAN estimates of incidence and mortality worldwide for 36 cancers in 185 countries. CA Cancer J Clin. 2018; 68:394–424. https://doi.org/10.3322/caac.21492 PMID:30207593
4. Devesa SS, Bray F, Vizcaino AP, Parkin DM. International lung cancer trends by histologic type: male:female differences diminishing and adenocarcinoma rates rising. Int J Cancer. 2005; 117:294–99. https://doi.org/10.1002/ijc.21183 PMID:15900604
5. Sánchez de Cos J, Sojo González MA, Montero MV, Pérez Calvo MC, Vicente MJ, Valle MH. Non-small cell lung cancer and silent brain metastasis. Survival and prognostic factors. Lung Cancer. 2009; 63:140–45. https://doi.org/10.1016/j.lungcan.2008.04.013 PMID:18556086
6. Fellner S, Bauer B, Miller DS, Schaffrik M, Fankhänel M, Spruss T, Bernhardt G, Graeff C, Färber L, Gschaidmeier H, Buschauer A, Fricker G. Transport of paclitaxel (Taxol) across the blood-brain barrier *in vitro* and *in vivo*. J Clin Invest. 2002; 110:1309–18. https://doi.org/10.1172/JCI15451 PMID:12417570
7. Klimaszewska-Wiśniewska A, Hałas-Wiśniewska M, Grzanka A, Grzanka D. Evaluation of anti-metastatic potential of the combination of fisetin with paclitaxel on A549 non-small cell lung cancer cells. Int J Mol Sci. 2018; 19:661.

https://doi.org/10.3390/ijms19030661
PMID:29495431

8. Razi SS, Rehmani S, Li X, Park K, Schwartz GS, Latif MJ, Bhora FY. Antitumor activity of paclitaxel is significantly enhanced by a novel proapoptotic agent in non-small cell lung cancer. J Surg Res. 2015; 194:622–30. https://doi.org/10.1016/j.jss.2014.11.004 PMID:25498514

9. Teow HM, Zhou Z, Najlah M, Yusof SR, Abbott NJ, D'Emanuele A. Delivery of paclitaxel across cellular barriers using a dendrimer-based nanocarrier. Int J Pharm. 2013; 441:701–11. https://doi.org/10.1016/j.ijpharm.2012.10.024 PMID:23089576

10. Reshma PL, Unnikrishnan BS, Preethi GU, Syama HP, Archana MG, Remya K, Shiji R, Sreekutty J, Sreelekha TT. Overcoming drug-resistance in lung cancer cells by paclitaxel loaded galactoxyloglucan nanoparticles. Int J Biol Macromol. 2019; 136:266–74. https://doi.org/10.1016/j.ijbiomac.2019.06.075 PMID:31201909

11. Jeck WR, Sorrentino JA, Wang K, Slevin MK, Burd CE, Liu J, Marzluff WF, Sharpless NE. Circular RNAs are abundant, conserved, and associated with ALU repeats. RNA. 2013; 19:141–57. https://doi.org/10.1261/rna.035667.112 PMID:23249747

12. Ding XC, Weiler J, Grosshans H. Regulating the regulators: mechanisms controlling the maturation of microRNAs. Trends Biotechnol. 2009; 27:27–36. https://doi.org/10.1016/j.tibtech.2008.09.006 PMID:19012978

13. Salmena L, Poliseno L, Tay Y, Kats L, Pandolfi PP. A ceRNA hypothesis: the rosetta stone of a hidden RNA language? Cell. 2011; 146:353–58. https://doi.org/10.1016/j.cell.2011.07.014 PMID:21802130

14. Gao D, Zhang X, Liu B, Meng D, Fang K, Guo Z, Li L. Screening circular RNA related to chemotherapeutic resistance in breast cancer. Epigenomics. 2017; 9:1175–88. https://doi.org/10.2217/epi-2017-0055 PMID:28803498

15. Ivashchenko A, Berillo O, Pyrkova A, Niyazova R. Binding sites of miR-1273 family on the mRNA of target genes. Biomed Res Int. 2014; 2014:620530. https://doi.org/10.1155/2014/620530 PMID:25243165

16. Mai H, Fan W, Wang Y, Cai Y, Li X, Chen F, Chen X, Yang J, Tang P, Chen H, Zou T, Hong T, Wan C, et al. Intranasal administration of miR-146a agomir rescued the pathological process and cognitive impairment in an AD mouse model. Mol Ther Nucleic Acids. 2019; 18:681–95. https://doi.org/10.1016/j.omtn.2019.10.002 PMID:31707205

17. Chen X, Gu S, Chen BF, Shen WL, Yin Z, Xu GW, Hu JJ, Zhu T, Li G, Wan C, Ouyang HW, Lee TL, Chan WY. Nanoparticle delivery of stable miR-199a-5p agomir improves the osteogenesis of human mesenchymal stem cells via the HIF1a pathway. Biomaterials. 2015; 53:239–50. https://doi.org/10.1016/j.biomaterials.2015.02.071 PMID:25890723

18. Xu J, Su C, Zhao F, Tao J, Hu D, Shi A, Pan J, Zhang Y. Paclitaxel promotes lung cancer cell apoptosis via MEG3-P53 pathway activation. Biochem Biophys Res Commun. 2018; 504:123–28. https://doi.org/10.1016/j.bbrc.2018.08.142 PMID:30173893

19. Xiang F, Fan Y, Ni Z, Liu Q, Zhu Z, Chen Z, Hao W, Yue H, Wu R, Kang X. Ursolic acid reverses the chemoresistance of breast cancer cells to paclitaxel by targeting MiRNA-149-5p/MyD88. Front Oncol. 2019; 9:501. https://doi.org/10.3389/fonc.2019.00501 PMID:31259152

20. Zhang L, Chen T, Yan L, Xu H, Wang Y, Li Y, Wang H, Chen S, Wang W, Chen C, Yang Q. MiR-155-3p acts as a tumor suppressor and reverses paclitaxel resistance via negative regulation of MYD88 in human breast cancer. Gene. 2019; 700:85–95. https://doi.org/10.1016/j.gene.2019.02.066 PMID:30878390

21. Mao BD, Xu P, Xu P, Zhong Y, Ding WW, Meng QZ. LINC00511 knockdown prevents cervical cancer cell proliferation and reduces resistance to paclitaxel. J Biosci. 2019; 44:44. https://doi.org/10.1007/s12038-019-9851-0 PMID:31180057

22. Xu N, Chen S, Liu Y, Li W, Liu Z, Bian X, Ling C, Jiang M. Profiles and bioinformatics analysis of differentially expressed circrnas in taxol-resistant non-small cell lung cancer cells. Cell Physiol Biochem. 2018; 48:2046–60. https://doi.org/10.1159/000492543 PMID:30099455

23. Zhao J, Li L, Wang Q, Han H, Zhan Q, Xu M. CircRNA expression profile in early-stage lung adenocarcinoma patients. Cell Physiol Biochem. 2017; 44:2138–46. https://doi.org/10.1159/000485953 PMID:29241190

24. Wang J, Li H. CircRNA circ_0067934 silencing inhibits the proliferation, migration and invasion of NSCLC cells and correlates with unfavorable prognosis in NSCLC. Eur Rev Med Pharmacol Sci. 2018; 22:3053–60.

https://doi.org/10.26355/eurrev_201805_15063
PMID:29863250

25. Wang T, Wang X, Du Q, Wu N, Liu X, Chen Y, Wang X. The circRNA circP4HB promotes NSCLC aggressiveness and metastasis by sponging miR-133a-5p. Biochem Biophys Res Commun. 2019; 513:904–11. https://doi.org/10.1016/j.bbrc.2019.04.108 PMID:31005252

26. Zhang M, Shi H, Zhang C, Zhang SQ. MiRNA-621 inhibits the Malignant progression of non-small cell lung cancer via targeting SIX4. Eur Rev Med Pharmacol Sci. 2019; 23:4807–14. https://doi.org/10.26355/eurrev_201906_18066 PMID:31210312

27. Cui S, Cao Z, Guo W, Yu H, Huang R, Wu Y, Zhou Y. [Plasma miRNA-23a and miRNA-451 as candidate biomarkers for early diagnosis of nonsmall cell lung cancer: a case-control study]. Nan Fang Yi Ke Da Xue Xue Bao. 2019; 39:705–11. https://doi.org/10.12122/j.issn.1673-4254.2019.06.12 PMID:31270050

28. Hetta HF, Zahran AM, El-Mahdy RI, Nabil EE, Esmaeel HM, Elkady OA, Elkady A, Mohareb DA, Mahmoud Mostafa M, John J. Assessment of circulating miRNA-17 and miRNA-222 expression profiles as non-invasive biomarkers in Egyptian patients with non-small-cell lung cancer. Asian Pac J Cancer Prev. 2019; 20:1927–33. https://doi.org/10.31557/APJCP.2019.20.6.1927 PMID:31244320

29. Tang Y, Xuan Y, Qiao G, Ou Z, He Z, Zhu Q, Liao M, Yin G. MDM2 promotes epithelial-mesenchymal transition through activation of Smad2/3 signaling pathway in lung adenocarcinoma. Onco Targets Ther. 2019; 12:2247–58. https://doi.org/10.2147/OTT.S185076 PMID:30988629

30. Wang B, Liu X, Liu H, Guo J, Zhang T, Zhou N, Ma Y, Yu H, Chen L, Ren Z, Fan K, Tian X. Differential expressions of MDM2 and TAP73 in cancer and cancer-adjacent tissues in patients with non-small-cell lung carcinoma. Pulmonology. 2018; 24:155–63. https://doi.org/10.1016/j.rppnen.2017.08.008 PMID:29452959

31. Liu G, Pei F, Yang F, Li L, Amin AD, Liu S, Buchan JR, Cho WC. Role of autophagy and apoptosis in non-small-cell lung cancer. Int J Mol Sci. 2017; 18:367. https://doi.org/10.3390/ijms18020367 PMID:28208579

32. Nietzold F, Rubner S, Berg T. The hydrophobically-tagged MDM2-p53 interaction inhibitor Nutlin-3a-HT is more potent against tumor cells than Nutlin-3a. Chem Commun (Camb). 2019; 55:14351–54. https://doi.org/10.1039/c9cc07795b PMID:31720601

33. Yee-Lin V, Pooi-Fong W, Soo-Beng AK. Nutlin-3, a p53-Mdm2 antagonist for nasopharyngeal carcinoma treatment. Mini Rev Med Chem. 2018; 18:173–83. https://doi.org/10.2174/1389557517666170717125821 PMID:28714398

34. Lambert JM, Gorzov P, Veprintsev DB, Söderqvist M, Segerbäck D, Bergman J, Fersht AR, Hainaut P, Wiman KG, Bykov VJ. PRIMA-1 reactivates mutant p53 by covalent binding to the core domain. Cancer Cell. 2009; 15:376–88. https://doi.org/10.1016/j.ccr.2009.03.003 PMID:19411067

35. Perdrix A, Najem A, Saussez S, Awada A, Journe F, Ghanem G, Krayem M. PRIMA-1 and PRIMA-1^{Met} (APR-246): from mutant/wild type p53 reactivation to unexpected mechanisms underlying their potent anti-tumor effect in combinatorial therapies. Cancers (Basel). 2017; 9:172. https://doi.org/10.3390/cancers9120172 PMID:29258181

36. Sonnemann J, Grauel D, Blümel L, Hentschel J, Marx C, Blumrich A, Focke K, Becker S, Wittig S, Schinkel S, Krämer OH, Beck JF. RETRA exerts anticancer activity in Ewing's sarcoma cells independent of their TP53 status. Eur J Cancer. 2015; 51:841–51. https://doi.org/10.1016/j.ejca.2015.02.016 PMID:25801700

37. Kravchenko JE, Ilyinskaya GV, Komarov PG, Agapova LS, Kochetkov DV, Strom E, Frolova EI, Kovriga I, Gudkov AV, Feinstein E, Chumakov PM. Small-molecule RETRA suppresses mutant p53-bearing cancer cells through a p73-dependent salvage pathway. Proc Natl Acad Sci USA. 2008; 105:6302–07. https://doi.org/10.1073/pnas.0802091105 PMID:18424558

38. Alsafadi S, Tourpin S, André F, Vassal G, Ahomadegbe JC. P53 family: at the crossroads in cancer therapy. Curr Med Chem. 2009; 16:4328–44. https://doi.org/10.2174/092986709789578196 PMID:19754415

Research Paper

ITPKA induces cell senescence, inhibits ovarian cancer tumorigenesis and can be downregulated by miR-203

Wang Shaosheng[1,*], Wang Shaochuang[2,*], Fan Lichun[3], Xie Na[4], Zhao Xiaohong[3]

[1]Maternity Service Center of Pengzhou Maternal & Children Health Care Hospital, Chengdu, Sichuan Province 611930, People's Republic of China
[2]Department of Hepatobiliary and Pancreatic Surgery, Huai'an First People's Hospital, Nanjing Medical University, Huai'an 223300, Jiangsu Province, People's Republic of China
[3]Hainan Maternal and Children's Medical Center, Haikou 570206, Hainan Province, People's Republic of China
[4]Department of Pathology, The Affiliated Hospital of Hainan Medical University, Haikou 571101, Hainan Province, People's Republic of China
*Equal contribution

Correspondence to: Zhao Xiaohong; **email:** zhaoxiaohx@163.com, https://orcid.org/0000-0001-6641-0510
Keywords: ovarian cancer, ITPKA, cell senescence, MDM2
Received: November 16, 2020 **Accepted:** March 14, 2021 **Published:** April 20, 2021

ABSTRACT

Overcoming senescence is a feature of ovarian cancer cells; however, the mechanisms underlying senescence regulation in ovarian cancer cells remain largely unknown. In this study, we found that ITPKA was downregulated in ovarian cancer samples, and the lower expression correlated with poor survival. Overexpression of ITPKA inhibited the anchorage-independent growth of ovarian cancer cells and induced senescence. However, knockdown of ITPKA promoted the anchorage-independent growth of ovarian cancer cells and inhibited senescence. Mechanistically, ITPKA was found to interact with MDM2, which stabilized P53, an essential regulator of senescence. Moreover, ITPKA was negatively regulated by miR-203, a microRNA that has been previously reported to be upregulated in ovarian cancer. Taken together, the results of this study demonstrated the tumor suppressive roles of ITPKA in ovarian cancer and provided a good explanation for the oncogenic roles of miR-203.

INTRODUCTION

Ovarian cancer is a common malignancy for women worldwide [1, 2], and although surgical resection, chemotherapy, radiotherapy and other therapeutic strategies have been used to treat this malignancy, the outlook for this disease is still not optimistic [3, 4]. A better understanding of the molecular mechanism guiding this disease would definitely benefit therapies.

Senescence is considered a state that inhibits tumor growth [5, 6]. P53, P21, P27 and P16 are the key regulators of senescence [7–9]. MDM2 is an E3 ubiquitin ligase that promotes the degradation of P53 to tightly control P53 protein levels [10, 11]. Numerous studies have shown that the induction of senescence inhibits the growth, colony formation and tumorigenesis of ovarian cancer [12, 13]. Therefore, the identification of novel regulators of senescence might provide therapeutic targets for ovarian cancer.

Inositol-trisphosphate 3-kinase A (ITPKA) promotes the motility of cancer cells by controlling the dynamics of the cytoskeleton [14–17]. Although previous studies have shown that ITPKA is expressed in a broad range of tumor types and that ITPKA gene body methylation inhibits its expression, thus serving as a novel and potential biomarker for early cancer detection, the

expression pattern of ITPKA in ovarian cancer remains unknown [14–17]. The biological functions of ITPKA in lung cancer and breast cancer have attracted considerable attention. In lung cancer, ITPKA has been reported as a marker of growth pattern-specific gene signatures in pulmonary adenocarcinoma [14, 18, 19], and ITPKA exhibits oncogenic activity in lung cancer cells by regulating Ins(1,4,5)P_3-mediated calcium release and cytoskeletal dynamics [20]. In addition, inositol-trisphosphate 3-kinase A (ITPKA) was a significantly enriched differentially expressed gene associated with the inositol phosphate metabolism pathway in glioma cells [21, 22]. However, whether the expression and function of ITPKA are context-dependent remains unknown.

Our previous study demonstrated the upregulation of miR-203 in ovarian cancer [23]. However, the target genes of miR-203 in ovarian cancer remain largely unknown. In this study, we examined the expression pattern and functions of ITPKA in ovarian cancer and investigated the underlying molecular mechanisms. Moreover, we explored the regulation of ITPKA by miR-203 in ovarian cancer.

RESULTS

ITPKA inhibited the colony formation of cancer cells and induced cell senescence

To investigate the functions of ITPKA in ovarian cancer, we transfected the ovarian cancer cell lines OVCA429 and OVCAR3 with a vector (Flag-ITPKA) to overexpress ITPKA (Figure 1A). The effects of ITPKA expression on colony formation were examined using a soft agar assay. As shown in Figure 1B–1C, forced expression of ITPKA inhibited the anchorage-independent growth of OVCA429 and OVCAR3 cells on soft agar. Moreover, β-gal staining revealed that ITPKA induced cell senescence (Figure 1D–1E).

To further understand the functions of ITPKA in the progression of ovarian cancer, the expression of ITPKA was knocked down in OVCA429 and OVCAR3 cells (Figure 2A). Knockdown of ITPKA expression enhanced the anchorage-independent growth of ovarian cancer cells and inhibited cell senescence (Figure 2B–2E). Taken together, these results demonstrated that ITPKA inhibited the colony formation of cancer cells and induced cell senescence.

ITPKA inhibited the ovarian cancer cell tumorigenesis *in vivo*

To extend our study to an *in vivo* system, we injected OVCAR3 control cells (OVCAR3/pLVX) and ITPKA-overexpressing cells (OVCAR3/Flag-ITPKA) into nude mice. Consistent with the *in vitro* study, overexpression of ITPKA impaired the tumorigenicity of OVCAR3 cells, as demonstrated by the tumor weight values (Figure 3A–3B). Examination of the tumors using immunohistochemistry (IHC) for Ki67 revealed less Ki67 staining in the tumors formed by the OVCAR3/Flag-ITPKA cells (Figure 3C–3D) compared to that in the control cells, suggesting that ITPKA inhibited cell proliferation. Moreover, P53 protein levels were increased in the tumors formed by OVCAR3/Flag-ITPKA cells (Figure 3E).

ITPKA interacted with MDM2 and stabilized P53

We next explored the molecular mechanisms through which ITPKA inhibited the tumorigenicity of ovarian cancer cells. Considering the induction of cell senescence by ITPKA, a GST pull-down assay was performed, and then the interactions between ITPKA and a major component of senescence-related pathways were examined. Interestingly, in the GST pull-down assay, the interaction between the fusion protein GST-MDM2 and ITPKA was detected (Figure 4A), which was further demonstrated by an immunoprecipitation assay (Figure 4B–4C). Next, the effects of ITPKA on the stability of P53 were assessed. ITPKA induced the accumulation of P53 upon CHX treatment as well as the expression of P21, the downstream target of P53 (Figure 4D–4F). Therefore, ITPKA interacted with MDM2 and stabilized P53 to inhibit cell growth and induce senescence.

To further investigate the mechanism in detail, we examined the ubiquitination of P53. Overexpression of ITPKA inhibited the interaction of MDM2 and P53 and the ubiquitination of P53 (Figure 4G–4H). In the functional study, knockdown of P53 blocked cell senescence induced by ITPKA (Figure 4I), indicating that the functions of ITPKA were dependent on P53.

ITPKA was downregulated in ovarian cancer and negatively regulated by miR-203

The expression of ITPKA was evaluated in ovarian cancer samples. IHC staining clearly showed the downregulation of ITPKA in ovarian cancer tissues (Figure 5A). Mining the GEPIA database showed that lower ITPKA expression was associated with poor survival (Figure 5B). Consistent with this observation, downregulation of ITPKA mRNA was observed in ovarian cancer tissues (Figure 5C). Moreover, the protein level of ITPKA was higher in the normal ovarian epithelial cell lines (IOSE80 and IOSE144) (Figure 5D). These results confirmed the down-regulation of ITPKA in ovarian cancer.

In a previous study, we demonstrated that miR-203 is upregulated in ovarian cancer. Therefore, we tested whether miR-203 inhibited the expression of ITPKA. As shown in Figure 5E–5F, miR-203 negatively regulated the mRNA level of ITPKA in OVCA429 and OVCAR3 cells (Figure 5E–5F). Moreover, the ability of miR-203 to promote colony formation of OVCAR3 cells was abolished by ITPKA (Figure 5G). In addition,

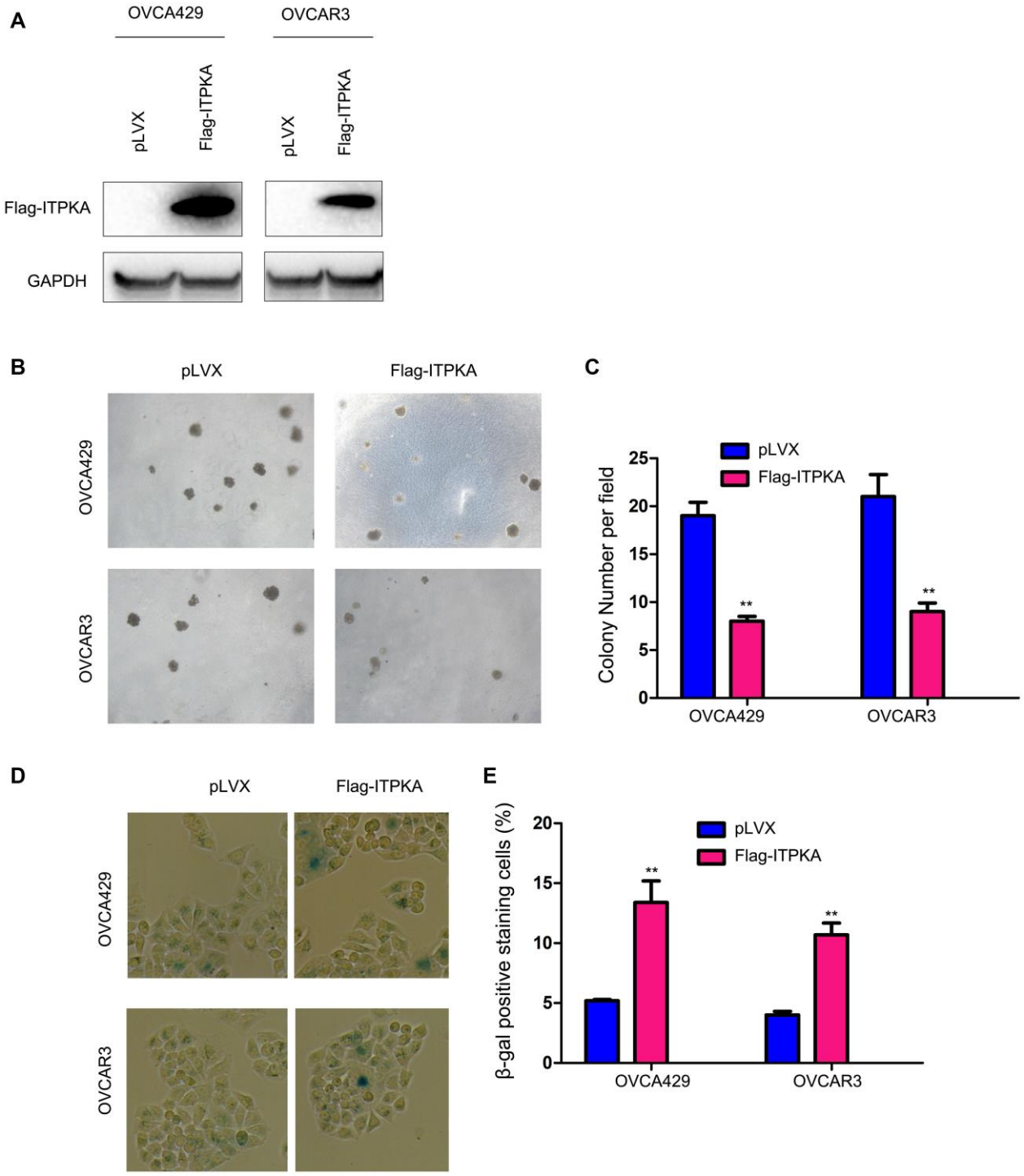

Figure 1. ITPKA inhibited colony formation and induced cell senescence in ovarian cancer. (**A**) Overexpression of ITPKA in OVCAR3 and OVCA429 cells. Cells were transfected with pLVX plasmids or pLVX-Flag-ITPKA plasmids. After selection, the resistant cells were examined for the expression of Flag-tagged ITPKA. (**B**) Effects of ITPKA on the colony formation of OVCAR3 and OVCA429 cells were examined using a soft agar assay. (**C**) Statistical analysis of (**B**). (**D**) Effects of ITPKA on the senescence of OVCAR3 and OVCA429 cells were examined using β-gal staining. (**E**) Statistical analysis of (**D**). $^{**}P < 0.01$.

we found a negative association between the expression of miR-203 and the mRNA levels of ITPKA (Figure 5H). In summary, ITPKA was downregulated in ovarian cancer and negatively regulated by miR-203.

DISCUSSION

Although several studies have shown that ITPKA is upregulated in some cancer types [14], our study clearly demonstrated that ITPKA is downregulated in ovarian cancer, suggesting that the expression of ITPKA in cancer is dependent on the context of the tumor. Moreover, we have provided evidence that ITPKA possesses tumor suppressor activity in ovarian cancer cells. ITPKA inhibited ovarian cancer cell colony formation and tumorigenesis and induced cell senescence. Moreover, we have provided evidence that ITPKA stabilizes P53. These results confirmed the tumor suppressive roles of ITPKA in ovarian cancer.

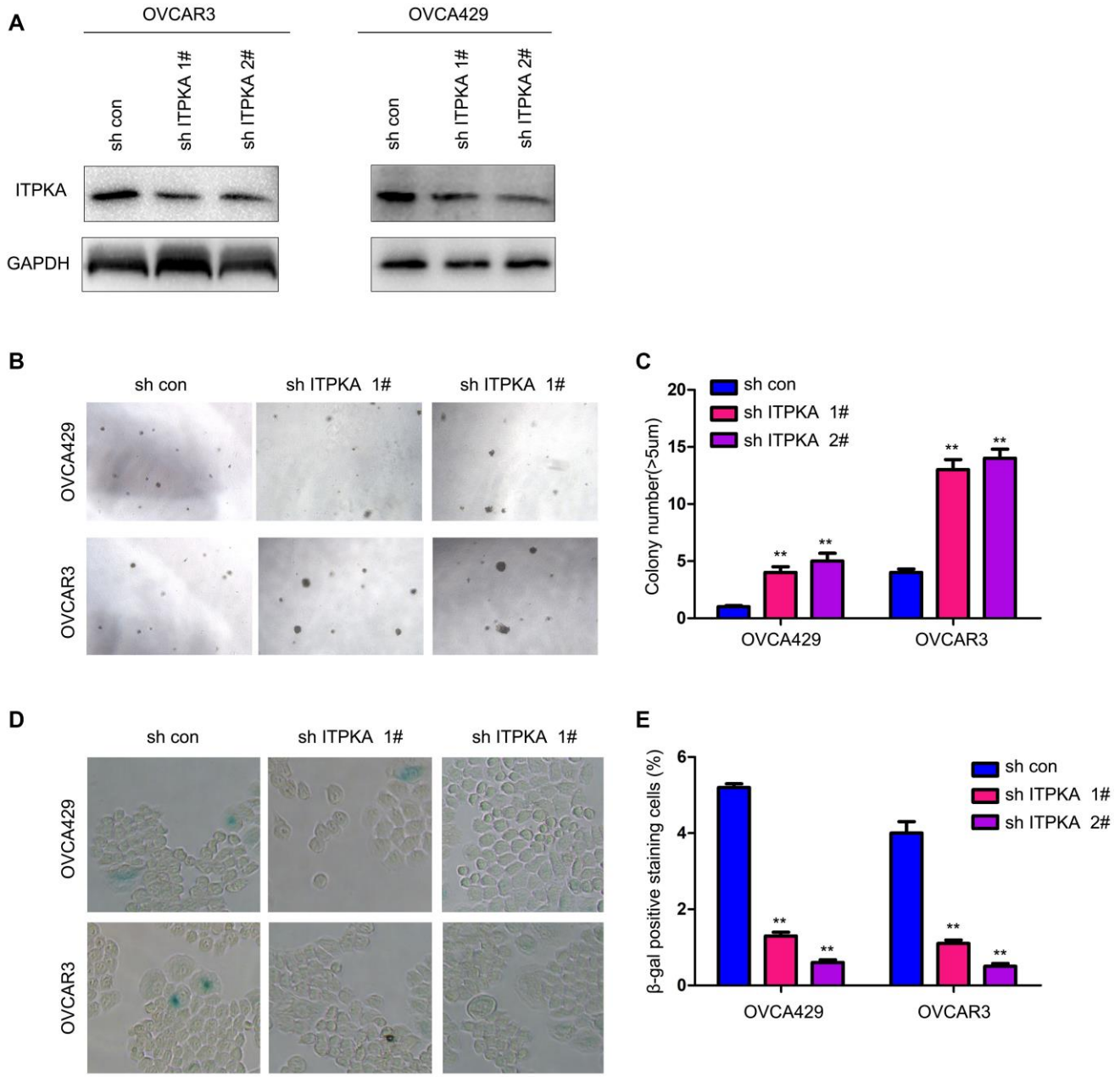

Figure 2. Knocking down ITPKA promoted colony formation and inhibited cell senescence in ovarian cancer. (**A**) Knockdown of ITPKA in OVCAR3 and OVCA429 cells. Cells were infected with a lentivirus for 8 hours. After selection, the resistant cells were examined for ITPKA expression. (**B**) Effects of ITPKA knockdown on the colony formation of OVCAR3 and OVCA429 cells were examined using a soft agar assay. (**C**) Statistical analysis of (**B**). (**D**) Effects of ITPKA knockdown on the senescence of OVCAR3 and OVCA429 cells were examined using β-gal staining. (**E**) Statistical analysis of (**D**). $^{**}P < 0.01$.

One interesting finding of this study is the induction of cell senescence by ITPKA. To our knowledge, this is the first report of the role of ITPKA in cell senescence. Numerous studies have demonstrated that cancer cells can overcome senescence and that senescence induction might be a therapeutic strategy for treating ovarian cancer [24, 25]. In this study, ITPKA was shown to induce senescence possibly by antagonizing the functions of MDM2.

Another interesting aspect of this study is the negative regulation of ITPKA by miR-203. In our previous work, we showed that miR-203 was upregulated in ovarian cancer and associated with poor survival [23]. However, the downstream targets of miR-203 have not been fully elucidated. In this study, we showed that ITPKA expression was inhibited by miR-203 and that the functions of miR-203 were abolished by overexpressing ITPKA. These results indicate that downregulation of ITPKA mediates the biological functions of miR-203 in ovarian cancer.

In fact, the roles of miR-203 in ovarian cancer are controversial. Although two studies have reported that miR-203 inhibits ovarian tumor metastasis by targeting BIRC5, attenuating the TGFβ pathway, and inhibiting

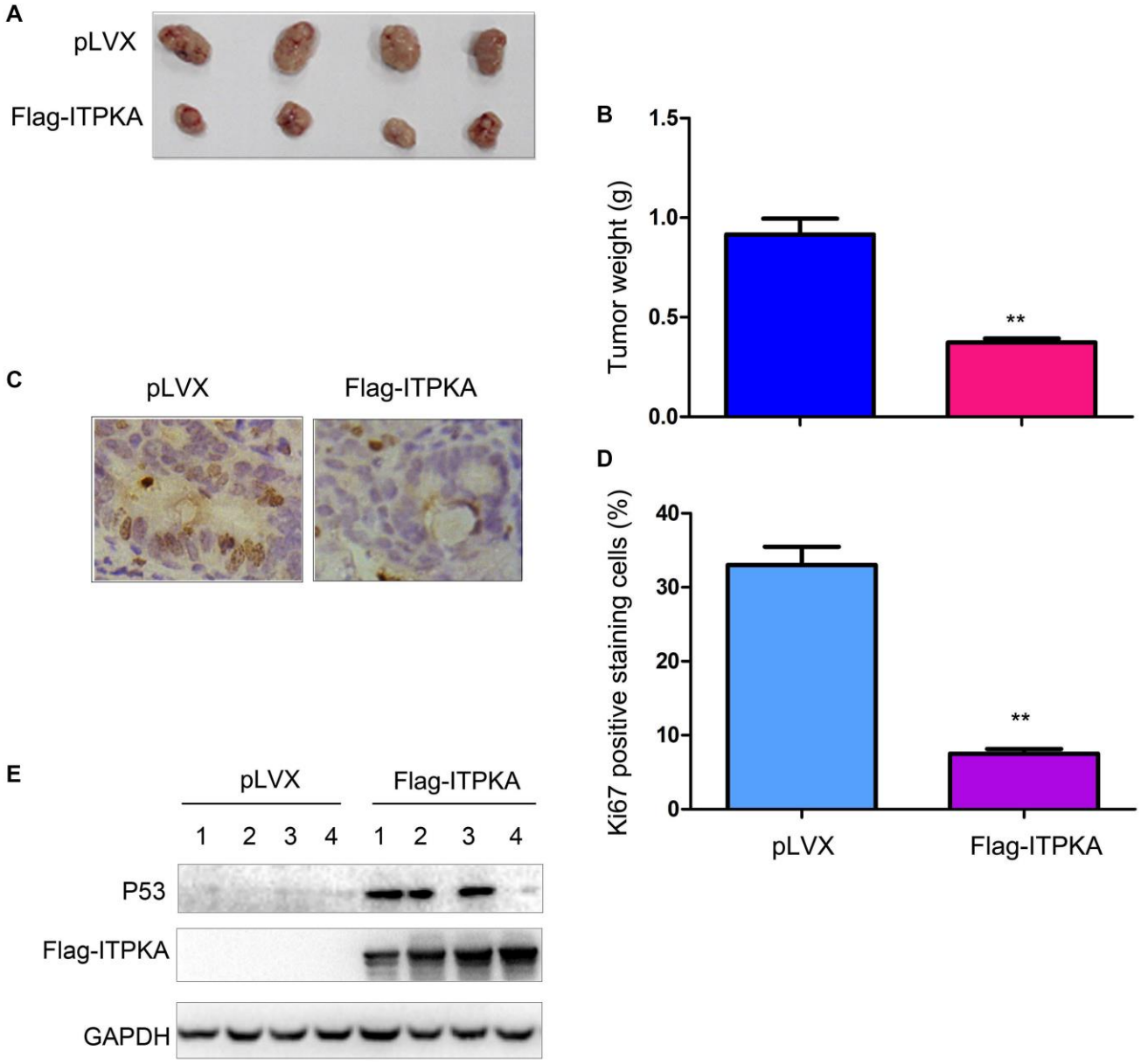

Figure 3. ITPKA inhibited the tumorigenicity of ovarian cancer. (**A**) Gross images of the tumors formed by OVCAR3 control cells and OVCAR3/Flag-ITPKA cells in nude mice. (**B**) Tumor weight as shown in (**A**). (**C**) Immunostaining was performed to examine Ki67 expression. (**D**) Statistical analysis of (**C**). (**E**) Expression of P53 and Flag-ITPKA in the tumors was examined via western blot. $^{**}P < 0.01$.

epithelial to mesenchymal transition [26, 27], one of these studies did not examine the expression of miR-203 in clinical ovarian cancer samples, and the other study was performed using human ovarian serous carcinoma tissues. Moreover, both studies focused on the metastasis of ovarian cancer. These observations only supported the notion that miR-203 promoted metastasis and did not indicate that miR-203 was a tumor suppressor in primary tumor formation.

The oncogenic roles of miR-203 in ovarian cancer are supported by several critical studies. A multi-institutional study demonstrated that miR-203 was an independent molecular predictor of poor prognosis and outcome in ovarian cancer [28], which was consistent

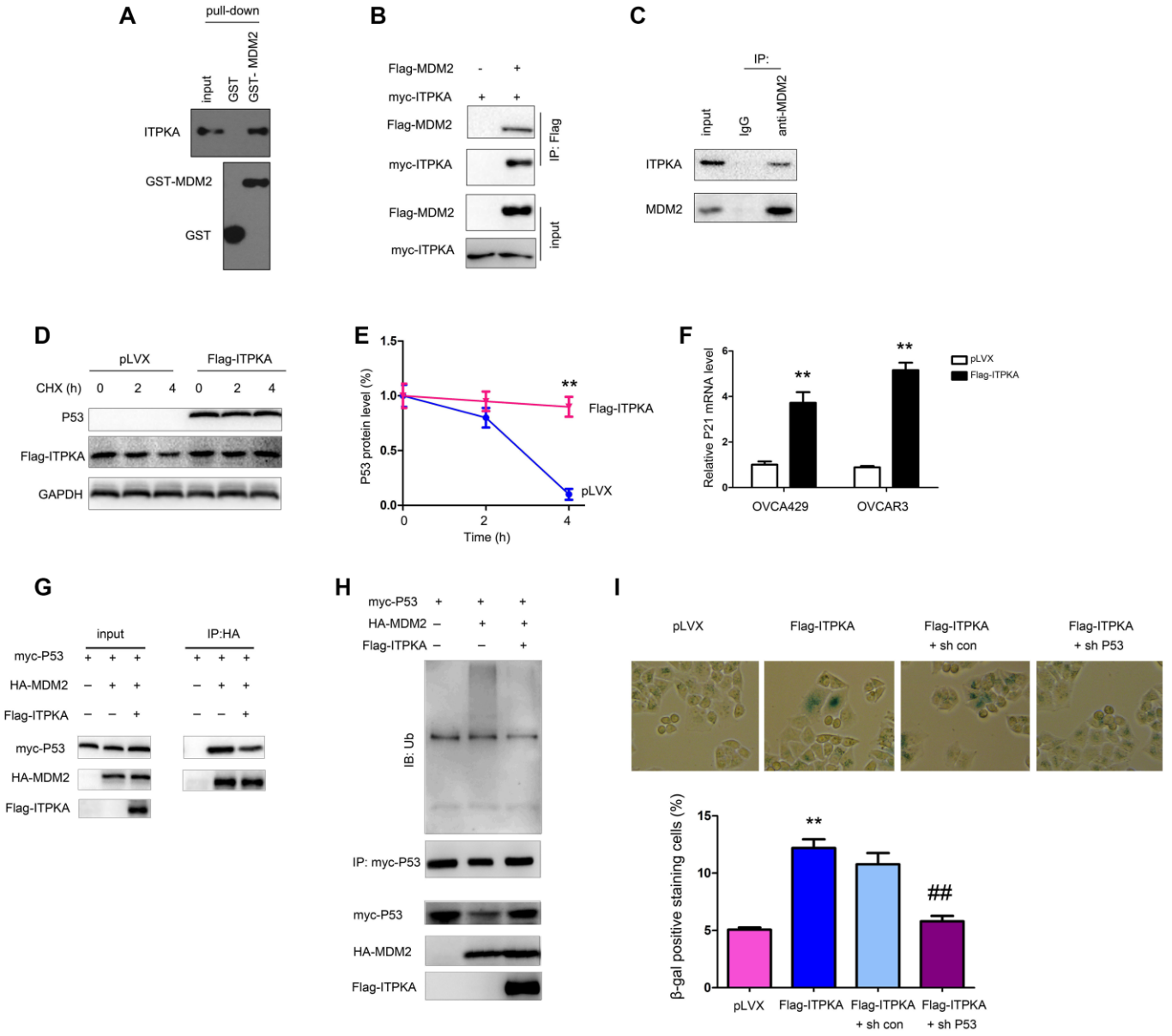

Figure 4. ITPKA interacted with MDM2. (**A**) GST pull-down assays were performed to examine the interaction between the fusion proteins GST-MDM2 and ITPKA. OVCAR3 cell lysates were used. (**B**) Immunoprecipitation assay was performed to examine the interaction between flag-tagged MDM2 and myc-tagged ITPKA. Flag-MDM2 and myc-ITPKA were transfected into OVCAR3 cells. Forty-eight hours later, the cells were harvested, and immunoprecipitation assays were performed using an anti-Flag antibody. (**C**) Immunoprecipitation assay was performed to examine the interaction between endogenous MDM2 and ITPKA. Protein from OVCAR3 cells was harvested, and immunoprecipitation assays were performed using an anti-MDM2 antibody. (**D–E**) Stability of P53 was examined after the cells were treated with CHX at the indicated time points. (**F**) mRNA level of P21 was examined using q-PCR. (**G**) Immunoprecipitation was performed to examine the interaction between P53 and MDM2 in OVCAR3 cells. (**H**) Ubiquitination of P53 was examined in OVCAR3 cells. (**I**) P53 knockdown abolished the function of ITPKA in cell senescence. $^{**}P < 0.01$; $^{\#\#}P < 0.01$.

with our study showing that upregulation of microRNA-203 is associated with advanced tumor progression and poor prognosis in epithelial ovarian cancer [23]. Moreover, we have shown the molecular mechanism by which miR-203 enhances the glycolytic pathway [29]. Taken together, we think that miR-203 (oncogene or tumor suppressor) might play different roles at different stages (primary and metastasis) of cancer.

The induction of senescence by IPTKA suggested that restoring the expression of ITPKA (using an inhibitor of miR-203) and treatment with an agonist of ITPKA would be promising strategies for ovarian cancer therapy. Additionally, in future studies, it is necessary to verify the effects of ITPKA on senescence using an ovarian cancer mouse model.

In summary, this study has demonstrated the tumor suppressive roles of ITPKA in ovarian cancer, which suggests that activation of ITPKA might be beneficial for the treatment of ovarian cancer.

MATERIALS AND METHODS

Cell culture

The ovarian cancer cell lines OVCAR3, OVCA429 and HEK293T were purchased from the cell bank of the Chinese Academy of Science (Shanghai, China). Cells were placed in an incubator at 37°C with 5% CO_2 and maintained in DMEM containing 10% FBS and antibiotics.

Clinical samples

Clinical samples were collected from the Hainan Maternal and Children's Medical Center after obtaining patients' written informed consent. The pathology of each sample was confirmed by two pathologists.

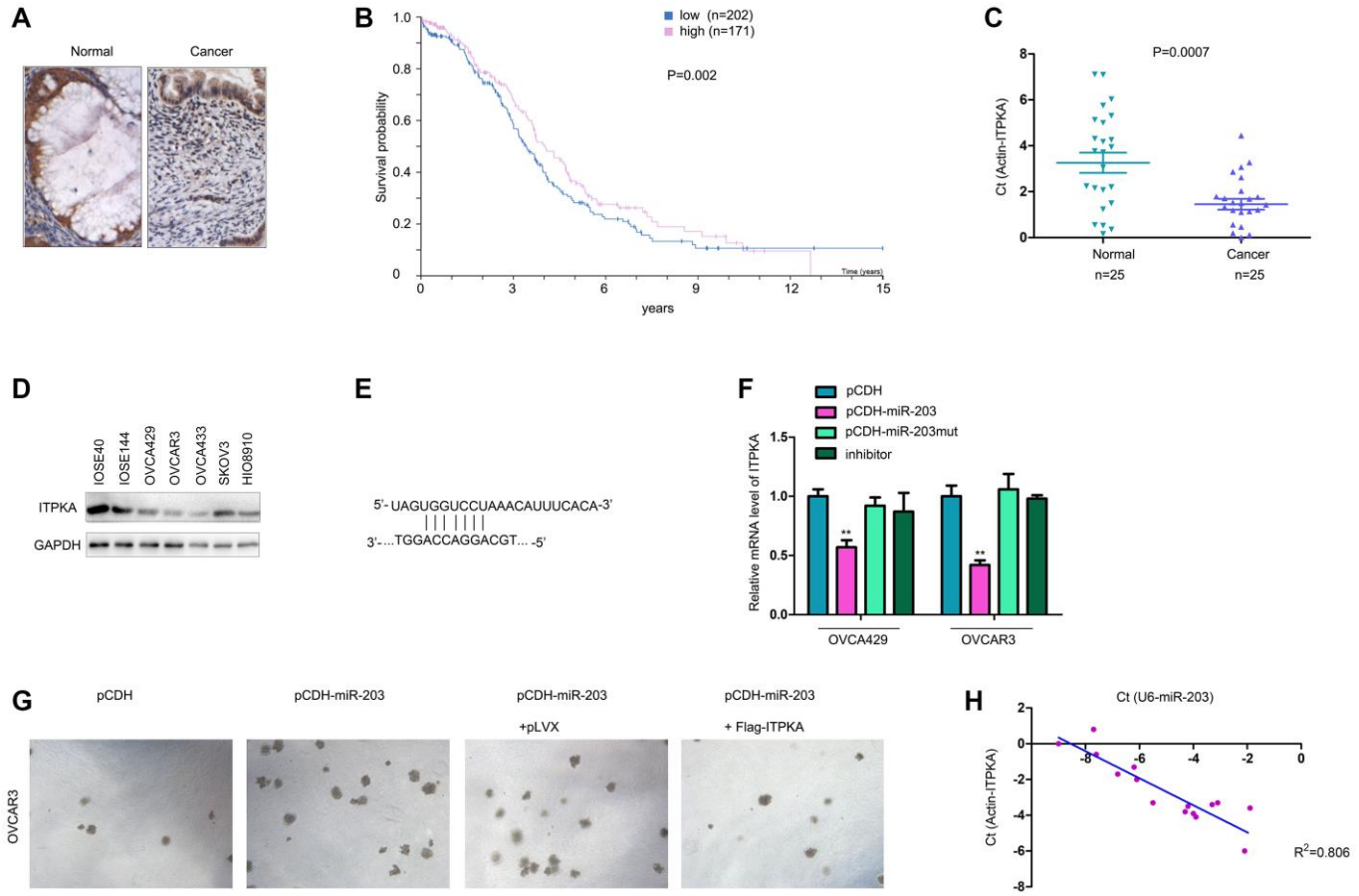

Figure 5. ITPKA was downregulated in ovarian cancer and negatively regulated by miR-203. (**A**) IHC was performed to examine the protein levels in ovarian cancer and normal tissues. (**B**) GEPIA database mining was performed to determine the correlation between ITPKA expression and survival. (**C**) q-PCR was performed to examine the mRNA levels of ITPKA in ovarian cancer samples and normal tissues. (**D**) Western blotting was performed to examine the ITPKA protein level in ovarian cancer cell lines and normal ovarian epithelial cell lines (IOSE80 and IOSE144). (**E**) Illustration of miR-203 and ITPKA. (**F**) Effects of miR-203, mutant miR-203 and inhibitor on the expression of ITPKA were examined using q-PCR. (**G**) Soft agar assays were performed to examine the effects of ITPKA on the tumorigenicity of OVCAR3 cells. (**H**) Expression of miR-203 and ITPKA in ovarian cancer samples. $^{**}P < 0.01$.

Plasmids

The coding sequence of ITPKA (NM002220.3) was cloned into the pLVX (containing the Flag tag) and pcDNA3.1 (containing the myc tag) vectors. The coding sequence of MDM2 (NM002392.6) was cloned into pGEX-4T-1 (containing the GST tag) to produce the fusion protein GST-MDM2. The sh RNA sequences were inserted into the cassette of the pLKO.1 vector. The sequences for sh ITPKA were as follows: sh ITPKA #1, 3′-aacgtgcagctggaagcgggc-5′; and sh ITPKA #2, 3′- aagctacctgcagctgcagga-5′.

qPCR

Twenty microliters of Hieff qPCR SYBR® Green Master Mix (No Rox Plus) was used for the amplification reaction. The system included 10 μL of PCR MIX, 0.4 μL of 10 μm forward primer, 0.4 μL of 10 μm reverse primer, and 3 μL of cDNA template, and it was supplemented with ddH_2O to a volume of 20 μL. All reactions were performed in duplicate and detected on a Thermo Scientific™ PikoReal™ Real-Time PCR Detection System. The reaction conditions were as follows: 95°C for 3 minutes; 40 cycles of 94°C for 30 seconds and 60°C for 30 seconds; 95°C for 15 s; 60°C for 60 s; and 95°C for 15 s. The melt curve was plotted to determine the specificity of amplification. The forward primer of ITPKA was 5′-CTTCGACGGACCTTGTGTG-3′, and the reverse primer was 5′-CACCGCCAGCATTTTCTTGT-3′. The forward primer of P21 was 5′-TGTCCGTCAGAACCCATGC-3′, and the reverse primer was 5′- AAAGTCGAAGTTCCATCGCTC-3′.

Cell transfection

For virus packaging, HEK293T cells were transfected using Lipofectamine 2000 according to the manufacturer's instructions. The virus was harvested 24 and 48 hours after transfection. After filtration, the virus was used to infect OVCAR3 and OVCA429 cells. Forty-eight hours later, the infected OVCAR3 and OVCA429 cells were selected by treatment with puromycin for 1 week. Then, the resistant cells were pooled and the expression of ITPKA was examined.

Soft agar assay

A bottom layer was generated that contained 0.5% agarose and 10% FBS in DMEM, and it was used to coat a 12-well plate. The upper layer in the 12-well plates contained 0.35% agarose and 10% FBS in DMEM. Then, 2×10^3 cells were suspended in the upper layer. Colonies that formed were photographed and counted after 14 days of incubation. All experiments were performed at least three times.

β-Gal staining

Cells were plated in 24-well plates at a density of 2×10^5/well. Twenty-four hours later, the senescence of the cells was examined using a kit (Beyond, Shanghai) according to the instructions.

Immunohistochemistry

IHC was performed as previously described [30]. Briefly, the tissues were treated with xylol to remove paraffin. Then, the sections were treated with ethanol (from a 100% to 75% gradient). After extensive washing with 0.1 M PBS, antigen recovery was performed by incubating tissues in 1 M citrate sodium solution (pH 6.0) at 100°C for 20 minutes. Then, the tissues were blocked with 5% BSA at room temperature for 1 hour. Each primary antibody (1:200) was incubated with tissues overnight at 4°C. The next day, the tissues were washed with PBS before incubating again with the secondary antibody at room temperature for 1 hour. The tissues were then developed using DAB and counterstained with hematoxylin.

GST-MDM2 fusion protein

The coding sequence of MDM2 (NM002392.6) was cloned into pGEX-4T-1 (containing the GST tag). BL21 competent cells were transformed with pGEX-4T-1 empty vectors or pGEX-4T-1 vectors containing the MDM2 coding sequence. An overnight culture was set up in 50 ml 2*TY with 150 mg/ml ampicillin. The next day, 5 ml of the overnight culture was seeded in 500 ml 2*TY with 150 mg/ml ampicillin and grown at 37°C to an A600 of 0.6–0.8, and then the culture was induced with 0.1 mM to 2 mM IPTG and grown for another 3 hours at 37°C. The cells were pelleted by centrifugation at 3000 g and 4°C for 10 min. The medium was decanted, and then the cells were resuspended and washed in 30 ml ice-cold PBS, transferred to a 40-ml Oak Ridge tube and centrifuged at 3000 g and 4°C for 10 min. The supernatant was discarded and the pellet was resuspended in 10 ml of ice-cold STE buffer. Then, 100 ml of freshly prepared lysozyme solution was added to the suspension and incubated on ice for 15 min. Immediately before sonication, 100 ml of 1 M DTT and 1.4 ml of 10% sarkosyl were added and mixed thoroughly by inversion and sonicated for a total of 1 min. Debris was pelleted via centrifugation at 16000 rpm for 20 min on an SS34 rotor. The supernatant was transferred to a 50-ml conical tube, and the pellet was discarded. Then, 4 ml of 10% Triton X-100 and STE buffer to a volume of 20 ml were added. The effective

concentrations of sarkosyl and Triton X-100 were 0.7% and 2%, respectively. The suspension was incubated at room temperature for 30 min and poured into a 1 ml bed of prepared glutathione Sepharose in PBS. Incubation was performed at room temperature for 30 min to 1 hour with agitation. The beads were washed with 150 ml of PBS, resuspended in 5 ml of PBS and poured into a dispo-column. The beads were washed in a 50-ml conical tube with an additional 5 ml of PBS and pooled with the first 5 ml in the dispo-column. The fusion protein was eluted with 10* 1 ml fractions of elution buffer. The desired fractions were determined via SDS-PAGE.

Western blot

Cells were harvested with RIPA buffer. The protein concentration was determined using BCA. Then, SDS-PAGE was performed, and the proteins were transferred to a PVDF membrane. After blocking with 5% BSA at room temperature for 1 hour, the membrane was incubated with the primary antibody for 4 hours and sequentially with the secondary antibody for 1 hour. Then, the signals were examined using an ECL kit. The following antibodies were used: anti-ITPKA (Sigma, HPA040454), anti-GAPDH (Santa Cruz, sc-47724), anti-GST (Santa Cruz, sc-138), anti-Flag (Proteintech, 80010-1-RR), anti-Myc (Santa Cruz, sc-40), anti-tubulin (Santa Cruz, sc-166729), anti-HA (Proteintech, 51064-2-AP), anti-P53 (CST, 48818), anti-MDM2 (CST, 86934), and anti-ubiquitin (CST, 3936).

GST pull-down

Fusion proteins were purified using Sepharose 4B beads, which were incubated with lysates from OVCAR3 cells for 4 hours. The proteins that were pulled down were separated by SDS-PAGE.

Immunoprecipitation

Cells were transfected with the indicated vectors with Lipofectamine 2000. Forty-eight hours later, the protein was harvested from the cells using RIPA buffer. After centrifugation, the supernatant was incubated with the indicated antibody for 4 hours. Then, protein A beads were added and incubated for another 4 hours. After extensive washing, the immunoprecipitated proteins were examined using western blots.

Subcutaneous tumor formation in nude mice

Eight-week-old male nude mice (SLAC, Shanghai) were randomly divided into two groups, with 4 mice each. The mice in one group were injected with OVCAR3 cells (1×10^6 cells/site) containing pLVX, and the mice in the other group were injected with OVCAR3 cells (1×10^6 cells/site) containing Flag-ITPKA. The mice were sacrificed after 5 weeks, the tumor tissues were excised and weighed, and ITPKA expression was evaluated via western blot. This study was approved by the ethical committee of the Hainan Maternal and Children's Medical Center and complied with the ethical regulations of the ethical committee of the Hainan Maternal and Children's Medical Center.

Statistical analysis

All sample sizes were sufficient to ensure proper statistical analysis. Data are represented as the means ± SEM of at least three experiments. Statistical analyses were performed using GraphPad Prism 6 software, version 6 (GraphPad Software, Inc.). Statistical significance was calculated using Student's two-tailed unpaired *t*-tests. The log-rank (Mantel-Cox) test was used for survival comparisons; ns, not significant ($P > 0.05$); $^{*}P < 0.05$; $^{**}P < 0.01$; $^{***}P < 0.001$; $^{****}P < 0.0001$.

Ethics approval and consent to participate

All experimental protocols were approved by the Hainan Maternal and Children's Medical Center Institutional Committee. Informed consent was obtained from all subjects. The study was reviewed and approved by the China National Institutional Animal Care and Use Committee.

AUTHOR CONTRIBUTIONS

Zhao Xiaohong designed the experiments, Wang Shaosheng and Fan Lichun conducted PCR, Western blot and Immunohistochemistry; Wang Shaochuang and Xie Na conducted the cell and animal experiments; Wang Shaosheng and Wang Shaochuang wrote the manuscript. All authors read and approved the final version of the manuscript.

CONFLICTS OF INTEREST

The authors declare no conflicts of interest.

FUNDING

This work was supported by the National Natural Science Foundation of China (81460445) and Natural Science Foundation of Hainan Province (817362).

REFERENCES

1. Feng RM, Zong YN, Cao SM, Xu RH. Current cancer situation in China: good or bad news from the 2018

Global Cancer Statistics? Cancer Commun (Lond). 2019; 39:22.
https://doi.org/10.1186/s40880-019-0368-6
PMID:31030667

2. Siegel RL, Miller KD, Jemal A. Cancer statistics, 2018. CA Cancer J Clin. 2018; 68:7–30.
https://doi.org/10.3322/caac.21442
PMID:29313949

3. Torre LA, Trabert B, DeSantis CE, Miller KD, Samimi G, Runowicz CD, Gaudet MM, Jemal A, Siegel RL. Ovarian cancer statistics, 2018. CA Cancer J Clin. 2018; 68:284–96.
https://doi.org/10.3322/caac.21456
PMID:29809280

4. Ricci AD, Rizzo A, Novelli M, Tavolari S, Palloni A, Tober N, Abbati F, Mollica V, De Lorenzo S, Turchetti D, Di Marco M, Brandi G. Specific Toxicity of Maintenance Olaparib *Versus* Placebo in Advanced Malignancies: A Systematic Review and Meta-analysis. Anticancer Res. 2020; 40:597–608.
https://doi.org/10.21873/anticanres.13989
PMID:32014900

5. Lewis S. Targeting senescence. Nat Rev Neurosci. 2019; 20:317.
https://doi.org/10.1038/s41583-019-0173-x
PMID:30980064

6. Sturmlechner I, Durik M, Sieben CJ, Baker DJ, van Deursen JM. Cellular senescence in renal ageing and disease. Nat Rev Nephrol. 2017; 13:77–89.
https://doi.org/10.1038/nrneph.2016.183
PMID:28029153

7. Baumann K. Cellular senescence: Senescence and reprogramming go hand-in-hand. Nat Rev Mol Cell Biol. 2016; 18:4.
https://doi.org/10.1038/nrm.2016.165
PMID:27991508

8. Bennett MR, Clarke MC. Killing the old: cell senescence in atherosclerosis. Nat Rev Cardiol. 2017; 14:132.
https://doi.org/10.1038/nrcardio.2016.217
PMID:28079111

9. Strzyz P. Cell Senescence: A new role for ATM. Nat Rev Mol Cell Biol. 2017; 18:277.
https://doi.org/10.1038/nrm.2017.39
PMID:28377621

10. Prives C. Signaling to p53: breaking the MDM2-p53 circuit. Cell. 1998; 95:5–8.
https://doi.org/10.1016/s0092-8674(00)81774-2
PMID:9778240

11. Pomerantz J, Schreiber-Agus N, Liégeois NJ, Silverman A, Alland L, Chin L, Potes J, Chen K, Orlow I, Lee HW, Cordon-Cardo C, DePinho RA. The Ink4a tumor suppressor gene product, p19Arf, interacts with MDM2 and neutralizes MDM2's inhibition of p53. Cell. 1998; 92:713–23.
https://doi.org/10.1016/s0092-8674(00)81400-2
PMID:9529248

12. Brosens JJ, Lam EW. Progesterone and FOXO1 signaling: harnessing cellular senescence for the treatment of ovarian cancer. Cell Cycle. 2013; 12:1660–61.
https://doi.org/10.4161/cc.25070
PMID:23708447

13. Oesterreich S, Edwards R, Vlad A. Progestins: pro-senescence therapy for ovarian cancer? Cell Cycle. 2013; 12:1662–63.
https://doi.org/10.4161/cc.25072
PMID:23708445

14. Windhorst S, Song K, Gazdar AF. Inositol-1,4,5-trisphosphate 3-kinase-A (ITPKA) is frequently over-expressed and functions as an oncogene in several tumor types. Biochem Pharmacol. 2017; 137:1–9.
https://doi.org/10.1016/j.bcp.2017.03.023
PMID:28377279

15. Erneux C, Ghosh S, Koenig S. Inositol(1,4,5)P3 3-kinase isoenzymes: Catalytic properties and importance of targeting to F-actin to understand function. Adv Biol Regul. 2016; 60:135–43.
https://doi.org/10.1016/j.jbior.2015.09.004
PMID:26446452

16. Ashour DJ, Pelka B, Jaaks P, Wundenberg T, Blechner C, Zobiak B, Failla AV, Windhorst S. The catalytic domain of inositol-1,4,5-trisphosphate 3-kinase-a contributes to ITPKA-induced modulation of F-actin. Cytoskeleton (Hoboken). 2015; 72:93–100.
https://doi.org/10.1002/cm.21208
PMID:25620569

17. Windhorst S, Minge D, Bähring R, Hüser S, Schob C, Blechner C, Lin HY, Mayr GW, Kindler S. Inositol-1,4,5-trisphosphate 3-kinase A regulates dendritic morphology and shapes synaptic Ca2+ transients. Cell Signal. 2012; 24:750–57.
https://doi.org/10.1016/j.cellsig.2011.11.010
PMID:22120525

18. Bäder S, Glaubke E, Grüb S, Muhs S, Wellbrock J, Nalaskowski M, Lange T, Windhorst S. Effect of the actin- and calcium-regulating activities of ITPKB on the metastatic potential of lung cancer cells. Biochem J. 2018; 475:2057–71.
https://doi.org/10.1042/BCJ20180238
PMID:29871874

19. Wang YW, Ma X, Zhang YA, Wang MJ, Yatabe Y, Lam S, Girard L, Chen JY, Gazdar AF. ITPKA Gene Body

Methylation Regulates Gene Expression and Serves as an Early Diagnostic Marker in Lung and Other Cancers. J Thorac Oncol. 2016; 11:1469–81.
https://doi.org/10.1016/j.jtho.2016.05.010
PMID:27234602

20. Zabeck H, Dienemann H, Hoffmann H, Pfannschmidt J, Warth A, Schnabel PA, Muley T, Meister M, Sültmann H, Fröhlich H, Kuner R, Lasitschka F. Molecular signatures in IASLC/ATS/ERS classified growth patterns of lung adenocarcinoma. PLoS One. 2018; 13:e0206132.
https://doi.org/10.1371/journal.pone.0206132
PMID:30352093

21. Ma K, Cheng Z, Sun L, Li H. Identification of potential therapeutic targets for gliomas by bioinformatics analysis. Oncol Lett. 2017; 14:5203–10.
https://doi.org/10.3892/ol.2017.6850
PMID:29113156

22. Xi Y, Tang W, Yang S, Li M, He Y, Fu X. Mining the glioma susceptibility genes in children from gene expression profiles and a methylation database. Oncol Lett. 2017; 14:3473–79.
https://doi.org/10.3892/ol.2017.6579
PMID:28927102

23. Wang S, Zhao X, Wang J, Wen Y, Zhang L, Wang D, Chen H, Chen Q, Xiang W. Upregulation of microRNA-203 is associated with advanced tumor progression and poor prognosis in epithelial ovarian cancer. Med Oncol. 2013; 30:681.
https://doi.org/10.1007/s12032-013-0681-x
PMID:23918241

24. Pérez-Mancera PA, Young AR, Narita M. Inside and out: the activities of senescence in cancer. Nat Rev Cancer. 2014; 14:547–58.
https://doi.org/10.1038/nrc3773
PMID:25030953

25. Muñoz-Espín D, Serrano M. Cellular senescence: from physiology to pathology. Nat Rev Mol Cell Biol. 2014; 15:482–96.
https://doi.org/10.1038/nrm3823
PMID:24954210

26. Wang B, Li X, Zhao G, Yan H, Dong P, Watari H, Sims M, Li W, Pfeffer LM, Guo Y, Yue J. miR-203 inhibits ovarian tumor metastasis by targeting BIRC5 and attenuating the TGFβ pathway. J Exp Clin Cancer Res. 2018; 37:235.
https://doi.org/10.1186/s13046-018-0906-0
PMID:30241553

27. Zhao G, Guo Y, Chen Z, Wang Y, Yang C, Dudas A, Du Z, Liu W, Zou Y, Szabo E, Lee SC, Sims M, Gu W, et al. miR-203 Functions as a Tumor Suppressor by Inhibiting Epithelial to Mesenchymal Transition in Ovarian Cancer. J Cancer Sci Ther. 2015; 7:34–43.
https://doi.org/10.4172/1948-5956.1000322
PMID:26819680

28. Panoutsopoulou K, Avgeris M, Mavridis K, Dreyer T, Dorn J, Obermayr E, Reinthaller A, Michaelidou K, Mahner S, Vergote I, Vanderstichele A, Braicu I, Sehouli J, et al. miR-203 is an independent molecular predictor of prognosis and treatment outcome in ovarian cancer: a multi-institutional study. Carcinogenesis. 2020; 41:442–51.
https://doi.org/10.1093/carcin/bgz163
PMID:31586203

29. Xiaohong Z, Lichun F, Na X, Kejian Z, Xiaolan X, Shaosheng W. MiR-203 promotes the growth and migration of ovarian cancer cells by enhancing glycolytic pathway. Tumour Biol. 2016; 37:14989–97.
https://doi.org/10.1007/s13277-016-5415-1
PMID:27655286

30. Cai Z, Qian ZY, Jiang H, Ma N, Li Z, Liu LY, Ren XX, Shang YR, Wang JJ, Li JJ, Liu DP, Zhang XP, Feng D, et al. hPCL3s Promotes Hepatocellular Carcinoma Metastasis by Activating β-Catenin Signaling. Cancer Res. 2018; 78:2536–49.
https://doi.org/10.1158/0008-5472.CAN-17-0028
PMID:29483096

Research Paper

Expression profile, molecular functions, and prognostic significance of miRNAs in primary colorectal cancer stem cells

Chuan-Wen Fan[1,2,3,4], Ran Lu[4], Chao Fang[1], Xue-Li Zhang[5], Zhao-Ying Lv[1], Yuan Li[1], Hong Zhang[5], Zong-Guang Zhou[1,&], Xian-Ming Mo[4], Xiao-Feng Sun[3]

[1]Institute of Digestive Surgery, Sichuan University, and Department of Gastrointestinal Surgery, West China Hospital, West China School of Medicine, Sichuan University, Chengdu, China
[2]Department of Gastrointestinal Surgery and Breast and Thyroid Surgery, Minimally Invasive Surgery, West China Fourth Hospital, Sichuan University, Chengdu, China
[3]Department of Oncology and Department of Biomedical and Clinical Sciences, Linköping University, Linköping, Sweden
[4]Laboratory of Stem Cell Biology, West China Hospital, Sichuan University, Chengdu, China
[5]School of Medicine, Institute of Medical Sciences, Örebro University, Örebro, Sweden

Correspondence to: Zong-Guang Zhou, Xian-Ming Mo, Xiao-Feng Sun; **email:** zhou767@163.com, xmingmo@scu.edu.cn, xiao-feng.sun@liu.se
Keywords: miRNAs, cancer stem cells, progression, prognosis, colorectal cancer
Received: October 19, 2020 **Accepted:** March 13, 2021 **Published:** April 1, 2021

ABSTRACT

MicroRNAs (miRNAs) are known to drive the pathogenesis of colorectal cancer (CRC) via the regulation of cancer stem cells (CSCs). We studied the miRNA expression profile of primary CSCs isolated from patients with CRC (pCRCSCs). Compared to pCRCSC-derived differentiated cells, 98 differentially expressed miRNAs were identified in pCRCSCs. Target genes encoding pCRCSC-related miRNAs were identified using a combination of miRNA target databases and miRNA-mRNA regulatory networks from the same patient. The pCRCSC-related miRNA target genes were associated with pathways contributing to malignant phenotypes, including I-kappa B kinase/NF-kappa B signaling, signal transduction by p53 class mediator, Ras signaling, and cGMP-PKG signaling. The pCRCSC-related miRNA expression signature was independently associated with poor overall survival in both the training and validation cohorts. We have thus identified several pCRCSC-related miRNAs with oncogenic potential that could serve as prognostic biomarkers for CRC.

INTRODUCTION

Colorectal cancer (CRC) is one of the leading causes of cancer-related death worldwide due in large part to its strong recurrence and metastatic potentials [1]. Cancer stem cells (CSCs), a subset of cancer cells, are characterized by sphere formation, self-renewal, and multi-lineage differentiation, and contribute to cancer initiation and metastasis and resistance to chemo-therapy, radiotherapy, and targeted therapy in various cancer types, including CRC [2]. We previously isolated and identified primary rectal CSCs and showed their characteristic phenotypes [3]. Further studies indicated that these primary CSCs can transdifferentiate into endothelial cells and neurons to support the growth of CRC cells [4, 5]. Compared with CSCs derived from cancer cell lines, primary CSCs are practically more relevant and reflect the actual tumor conditions in cancer patients [6]. However, a detailed understanding of malignant characteristics of primary CSCs isolated from patients with CRC (pCRCSCs) and the underlying molecular mechanisms of development of CSCs is required to mimic the CSC characteristics *in vivo*.

MiRNAs are small non-coding RNAs of approximately 20 to 25 nucleotides in length that regulate the expression of more than 60% of human genes. Recent findings have implicated several miRNAs, such as miR-21 [7], miR-27a [8], miR-31 [9], miR-137 [10], miR-146a [11], miR-148a [12], miR-195-5p [13], miR-196b-5p [14], miR-199a/b [15], miR-215 [16], miR-372/373 [17], and miR-1246 [18], in the regulation of CSC characteristics including self-renewal and differentiation [19, 20]. MiRNAs execute these functions by targeting the genes of several essential signaling pathways, such as Wnt/β-catenin and Notch, associated with the maintenance, growth, and function of CSCs [21]. However, a global miRNA expression profile of CRCSCs, especially of pCRCSCs is still unavailable. Moreover, CSC-related signaling pathways do not function in isolation but as a coordinated network [22, 23], implying that CSC phenotypes are an output of several signaling networks. Similarly, a single miRNA can target multiple genes and signaling pathways. Therefore, a single agent targeting the rare CSC subpopulations, although can reduce the tumor volume, cannot eliminate the tumor, highlighting the need to elucidate the regulatory network of pCRCSCs.

We performed a comprehensive global miRNA expression analysis of differentiated pCRCSCs to identify differentially expressed miRNAs. Further, molecular functions of differentially expressed miRNAs were annotated and their prognostic significance in patients with CRC was analyzed. The study design is shown in Figure 1.

RESULTS

Expression profiles of miRNAs in pCRCSCs and their corresponding pCRCSC-derived differentiated cells

To isolate colon CSCs, primary CSCs from patients with CRC were enriched in serum-free medium supplemented with epidermal growth factor (EGF) and basic fibroblast growth factor (bFGF). After 3 to 4 weeks, a small fraction of tumor cells formed spheres (Figure 2A). Next, the serum-free CSC medium was replaced with 20% fetal bovine serum (FBS)-containing medium to differentiate the spheres [3, 24]. The spherical cells in the culture gradually aggregated into clusters of polygonal cells and exhibited typical epithelial-like tumor cell morphology (Figure 2A).

To study tumorigenesis between the expanded pCRCSCs and pCRCSC-derived differentiated cells (termed differentiated pCRCSCs in the following text), both cell types were injected into immunodeficient mice and xenograft growth was assessed. Compared to differentiated pCRCSCs, pCRCSCs formed bigger tumor masses, with a faster growth (Figure 2B, 2C). In addition, mice-bearing pCRCSCs lost more weight than those bearing differentiated pCRCSCs (Figure 2D).

To further investigate the difference in the potential miRNAs regulating tumorigenesis between pCRCSCs and differentiated pCRCSCs, a global miRNA expression profile analysis was performed in three pCRCSCs and paired differentiated pCRCSCs including one primary CSC isolated from a patient with CRC and two previously enriched primary CSCs isolated from patients with rectal cancer [3]. In total, 98 differentially expressed miRNAs were identified between pCRCSCs and differentiated pCRCSCs, of which 50 were up-regulated and 48 were downregulated (Figure 2E and Supplementary Table 1).

Identification of target genes and regulatory network of pCRCSC-related miRNAs

Because miRNAs function by binding to their specific target genes, we first used miRWalk, TargetScan, and miRDB databases to predict target genes for all 98 differentially expressed miRNAs in pCRCSCs. Only genes that were commonly predicted by all three databases were used as putative target genes. In total, 18,792 potential target genes were identified (Supplementary Table 2). To more accurately identify the miRNA targets, we analyzed the miRNA and mRNA differential expression profile datasets of the same patients using the TCGA database. We identified 745 miRNAs and 5,558 mRNAs ($|\log2\ FC| > 2$, $p < 0.05$) that were differentially expressed in normal and CRC samples (Supplementary Tables 3, 4). The negatively regulated miRNA/mRNA pairs (miRNA upregulated/mRNA downregulated or miRNA down-regulated/mRNA upregulated) were obtained and intersected with predictive target mRNAs in the database. The 1,103 miRNA/mRNA pairs were identified, including 35 miRNAs and 870 mRNAs, were believed to be related to miRNA-regulated target genes in pCRCSCs (Supplementary Table 5). The miRNA–mRNA regulatory network is shown in Figure 3.

Relevant biological functions and pathways affected by pCRCSC-related miRNAs

To assess the biological functions of pCRCSC-related miRNAs, the functions and pathways of targeted genes of pCRCSC-related miRNAs were analyzed using the DAVID database. In total, 868 genes were found enriched in 68 gene ontology (GO) terms including 23 biological processes, 31 cell components, and 14 molecular functions (Figure 4A–4C and Supplementary Table 6). The enriched biological processes included

mRNA splicing regulation, I-kappa B kinase/NF-kappa B signaling, and signal transduction by p53 class mediator, which were linked to malignant features of CSCs. Protein binding, poly(A) RNA binding, nucleotide binding, and ubiquitin protein ligase binding were highly enriched molecular functions.

The pCRCSC-related miRNAs were enriched in several cancer-related pathways, including Ras signaling pathway, actin cytoskeleton regulatory pathways, cGMP–PKG signaling pathway, and spliceosome pathways, which correlated with the malignant phenotype of cancer cells (Figure 4D and Supplementary Table 7).

Because pCRCSC-related miRNA targets were predicted by bioinformatics, certain potential targets involved in the key pathways were selected and examined by quantitative reverse transcription-polymerase chain reaction (RT-qPCR) for validation. The expression of selected potential targets was congruent with the results of predictive miRNA target databases, validating the involvement of predictive miRNA-related signaling pathways in CRC (Figure 4E, 4F).

Identification of potential prognostic miRNA signatures for CRC

To evaluate the prognostic function of pCRCSC-related miRNAs in patients with CRC, we first randomly grouped the TCGA–COREAD data into training and validation cohorts (Supplementary Table 8). The prognostic significance of 35 functionally annotated pCRCSC-related miRNAs was further investigated using univariate Cox proportional hazards regression analyses in the training cohort (Supplementary Table 9). Prognosis-related miRNAs were subsequently selected for multivariate Cox proportional hazards regression analyses. Finally, two pCRCSC-related miRNAs (miR-664b-3p [risky miRNA] and miR-200c-5p [protective]) were confirmed as independent prognostic miRNAs of patients with CRC in the training cohort (Supplementary Table 10). To facilitate the use of pCRCSC-related miRNAs as prognostic markers in routine clinical practice, we next developed a formula to calculate the risk score of overall survival (OS) using the Cox proportional hazard regression model for each patient based on the expression of two pCRCSC-related miRNAs, where risk score = (0.384 × expression of miR-664b-3p) – (0.270 × expression of miR-200c-5p).

Clinical significance of prognostic miRNA signature in CRC patients

The patients were classified into low- and high-risk groups in the training and validation cohorts using X-tile plots to generate the optimal cut-off score (Supplementary Figure 1). Correlation analysis of clinicopathological characteristics of patients between high- and low-risk groups revealed remarkable differences only in the stage and survival status of patients in both training and validation cohorts (Table 1). In addition, as shown in Figure 5A, 5B, the distribution of miRNA-based risk scores, OS time, OS status, and the expression of two pCRCSC-related miRNAs in the training and validation cohorts showed that high-risk patients were associated with higher mortality than low-risk patients. The heat map revealed that the risky miR-664b-3p was highly expressed in high-risk patients, whereas protective miR-200c-5p was highly expressed in low-risk patients in both training and validation cohorts (Figure 5A, 5B).

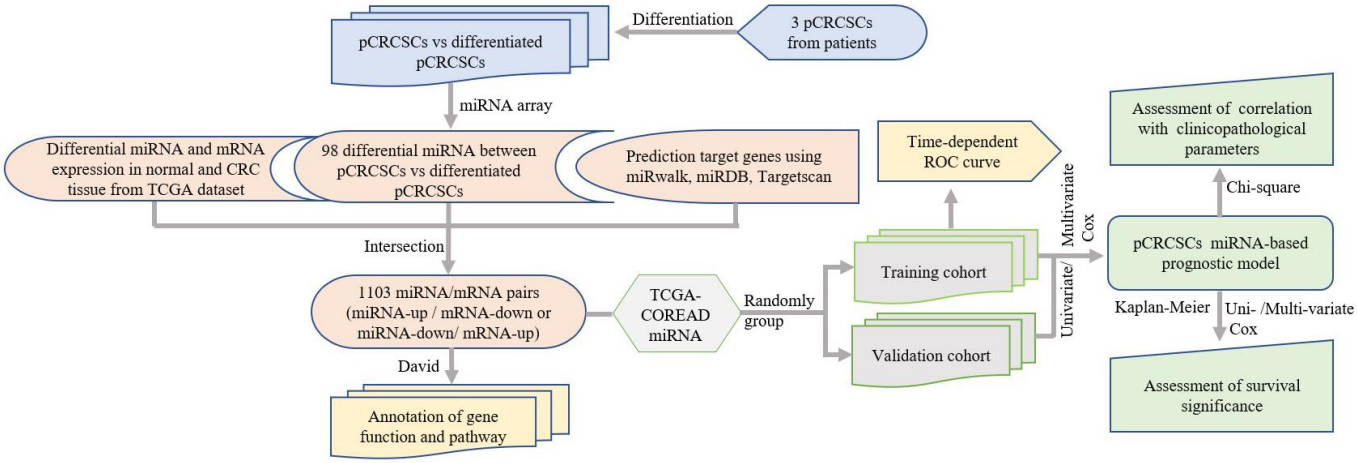

Figure 1. Study design. pCRCSCs: primary colorectal cancer stem cells.

Survival analyses showed that the 5-year OS was 56.3% (95% confidence interval [CI]: 42.7–74.2) for high-risk patients and 71.5% (95% CI: 57.8–88.3) for low-risk patients (Figure 5C; p = 0.003) after assessing the prognostic accuracy of two miRNA-based classifiers with time-dependent ROC analysis at varying follow-up times (Supplementary Figure 2A, 2B). The classifier universality of two pCRCSC-related miRNAs in different populations was confirmed by applying it to the validation cohort, thereby classifying 110 (41%) patients as high risk and 156 (59%) patients as low risk. Five-year OS was 28.1% (95% CI: 14.6–54.1) for high-risk patients and 71.4% (95% CI: 59.3–81.6) for low-risk patients (Figure 5D; $p < 0.001$).

Assessment of independent prognostic significance of miRNA signature in CRC patients

To further assess whether the pCRCSC-related miRNA signature could independently predict OS in patients with CRC, both univariate and multivariate Cox regression analyses were performed by adjusting for gender, age, tumor location, stage, microsatellite instability (MSI) status, and adjuvant

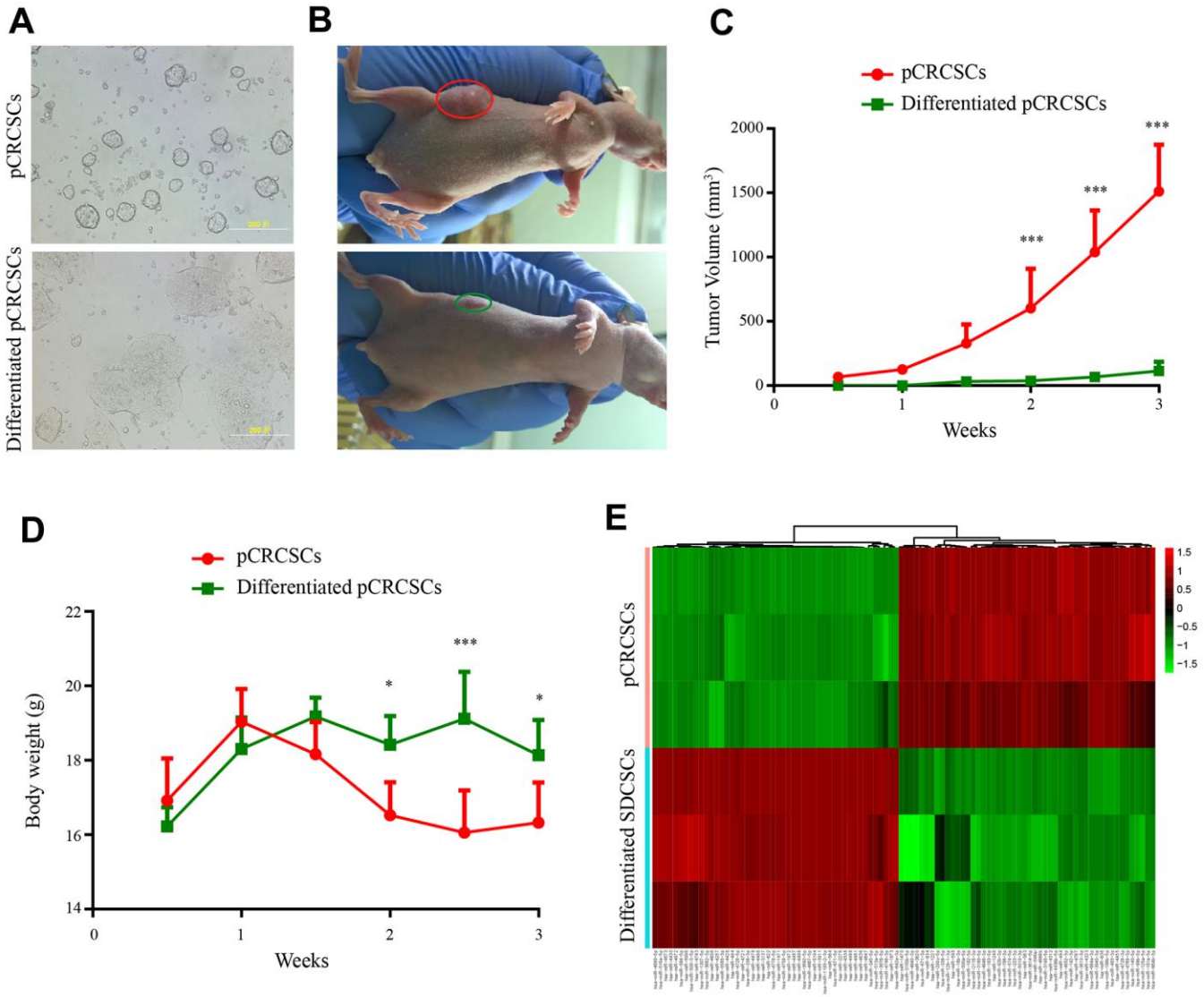

Figure 2. Differential tumorigenic capacity and distinct expression profiles of miRNAs between pCRCSCs and pCRCSCs-derived differentiated cells. (**A**) pCRCSCs generated from a human colon cancer sample and their corresponding differentiated pCRCSCs. Bars = 200 μM. (**B**) A tumor-bearing nude mouse showing a large xenograft tumor from pCRCSCs (red oval) and a small tumor from pCRCSC-derived differentiated cells (green oval). (**C**) Tumor volume of the subcutaneous tumor generated from 5×10^5 pCRCSCs and differentiated pCRCSCs. (**D**) Weight of tumor-bearing mice. Bars represent mean ± standard deviation (SD) (n = 5, $^{*}p < 0.05$, $^{***}p < 0.001$). (**E**) Heat map of differentially expressed miRNAs in pCRCSCs and pCRCSC-derived differentiated cells.

chemoradiotherapy as covariates. Univariate analyses revealed that the pCRCSC-related miRNA signature was significantly associated with OS (Supplementary Table 11; hazard ratio [HR] = 2.17, p = 0.015). Moreover, the pCRCSC-related miRNA signature was significant, even after adjusting for other covariates in the training cohort (Figure 6A, HR = 2.30, 95% CI: 1.17–4.60, p = 0.016). Similarly, the prognostic significance of pCRCSC-related miRNA signature with OS was validated in the validation cohort (Supplementary Table 12; HR = 3.71, p < 0.001). Multivariate analyses revealed that the pCRCSC-related miRNA signature remained a powerful prognostic factor in the validation cohort after adjusting for other covariates (Figure 6B, HR = 3.93, 95% CI: 2.09–7.40, p < 0.001).

DISCUSSION

Tumor resistance to traditional chemotherapy and radiotherapy is partially attributed to CSCs and results in cancer recurrence and metastasis [25]. We have previously shown that CSCs from primary rectal adenocarcinoma have a strong tumorigenic capacity and are resistant to common therapeutic drugs used for treating patients with advanced or metastatic CRC [3]. In this study, we further evaluated the tumorigenesis of CSCs of primary colon adenocarcinoma that exhibited strong tumorigenic potential, indicating the common malignant features of primary CSCs of both colon and rectal cancers.

Altered miRNA expression has been shown to contribute to the malignant behavior of CSCs [26]. A comprehensive analysis of the miRNA expression profile revealed 98 differentially expressed miRNAs in pCRCSCs, of which 50 were upregulated and 48 were downregulated. Some of these miRNAs, such as miRNA 200c [27, 28], miR-1246 [29], and miR-494 [30], are involved in the regulation of CSCs. For example, miR-1246 activates the Wnt/β-catenin pathway by inhibiting the expression of Axin-2 and GSK-3β to maintain the stemness of CSCs, including self-renewal, drug resistance, and tumorigenicity [29]. Similarly, miR-494 inhibits BMI-1 expression and prevents self-renewal of breast CSCs/progenitor cells [30]. Furthermore, miRNAs regulate four major signal transduction pathways that affect CSC characteristics: Wnt/β-catenin, BMI-1, Notch, and Hedgehog, and the corresponding pathways [8]. Therefore, we not only confirmed the potential significance of previously published miRNAs in CSCs but also identified certain novel miRNAs affecting the malignant features of pCRCSCs.

Pathway enrichment analysis revealed differentially expressed pCRCSC-related miRNAs to be enriched in I-kappa B kinase/NF-kappa B signaling, signal

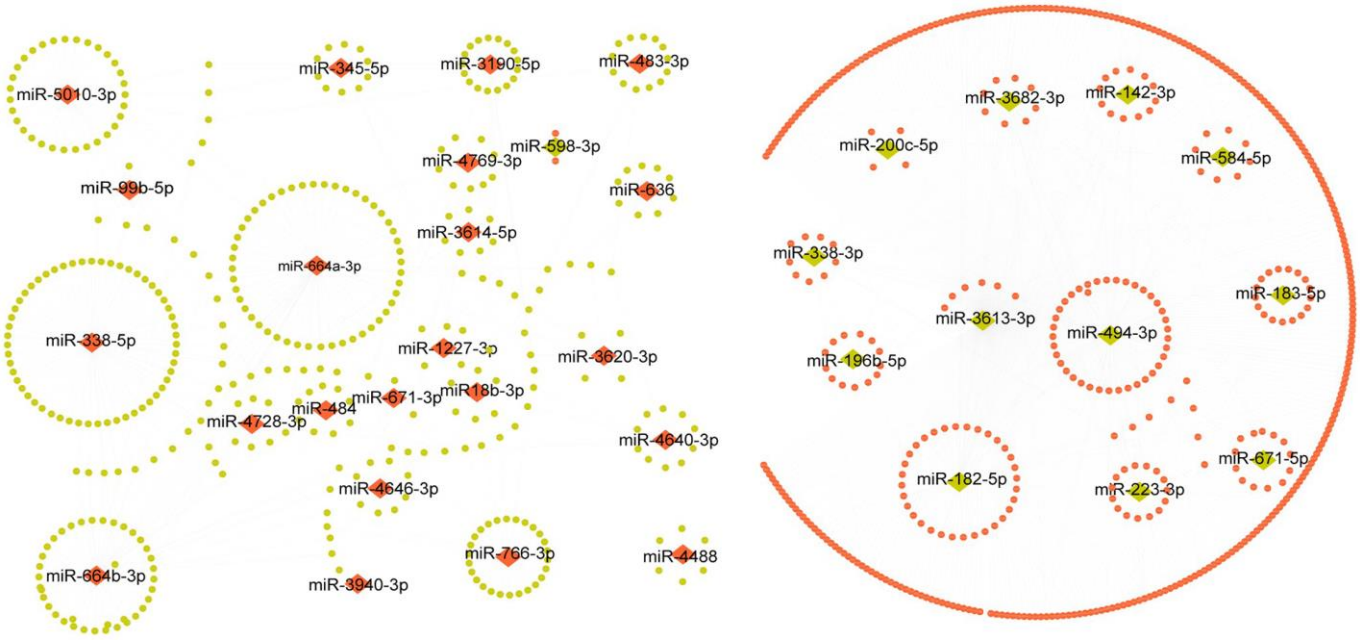

Figure 3. The regulatory network of pCRCSC-related miRNAs. Upregulated miRNAs are shown as red diamonds and the corresponding downregulated target genes in the TCGA database are shown as green ellipses. The downregulated miRNAs are shown as green diamonds and the corresponding upregulated target genes in the TCGA database are shown as red ellipses.

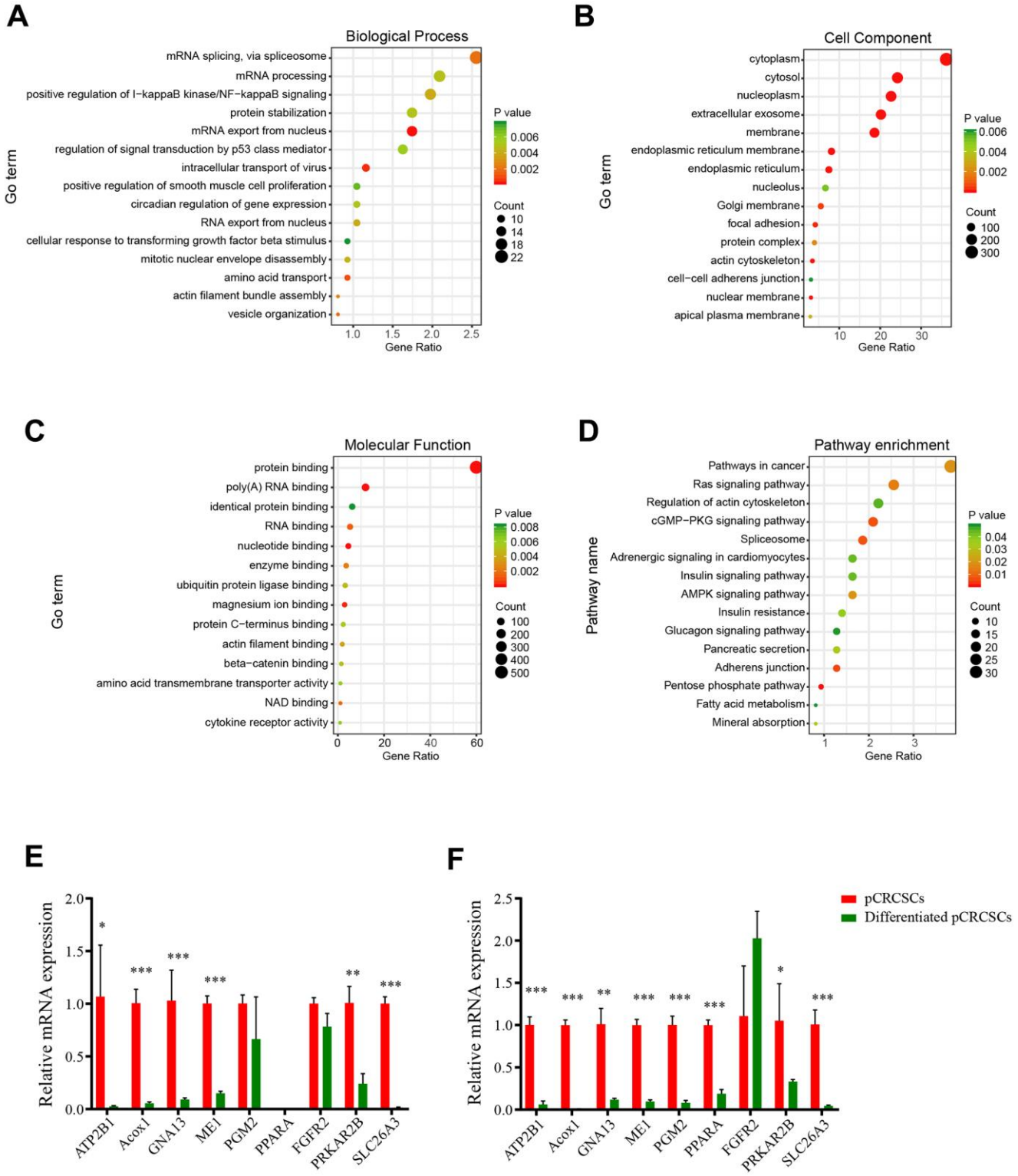

Figure 4. The GO and KEGG pathways of pCRCSC-related miRNAs. (**A**) The top 15 biological processes, (**B**) cell components, (**C**) molecular functions, and (**D**) the KEGG pathways of target genes based on the intersection of predicted downstream target genes and genes that negatively correlated with miRNA expression in the TCGA–COREAD dataset. (**E**) Nine potential target genes of pCRCSC-related miRNAs were validated by RT-qPCR in the primary CSCs derived from colon cancer and the corresponding differentiated cells. (**F**) Nine potential target genes of pCRCSC-related miRNAs were validated by RT-qPCR in the primary CSCs derived from rectal cancer and the corresponding differentiated cells. GAPDH was selected as the internal control. This experiment was repeated thrice. Bars represent mean ± standard deviation (SD) ($n = 3$, $^{*}p < 0.05$, $^{**}p < 0.01$, $^{***}p < 0.001$).

Table 1. Baseline characteristics of patients by miRNA assessment cohorts.

Parameters	Training set			Validation set		
	Low risk	High risk	p value	Low risk	High risk	p value
Gender						
Female	67 (43.8)	56 (49.6)	0.351	73 (45.9)	53 (49.5)	0.562
Male	86 (56.2)	57 (50.4)		86 (54.1)	54 (50.5)	
Age (years)						
≤65	68 (44.4)	55 (48.7)	0.494	69 (43.4)	49 (45.8)	0.700
>65	85 (55.6)	58 (51.3)		90 (56.6)	58 (54.2)	
Tumor location						
RSCC	81 (52.9)	39 (34.5)	0.004	65 (40.9)	43 (40.2)	0.959
LSCRC	67 (43.8)	68 (60.2)		91 (57.2)	61 (57.0)	
NA	5 (3.3)	6 (5.3)		3 (1.9)	3 (2.8)	
Stage						
Stage I	31 (20.3)	12 (10.6)	**0.032**	35 (22.0)	15 (14.0)	**0.001**
Stage II/III	103 (67.3)	79 (69.9)		106 (66.7)	63 (58.9)	
Stage IV	15 (9.8)	20 (17.7)		15 (9.4)	28 (26.2)	
NA	4 (2.6)	2 (1.8)		3 (1.9)	1 (0.9)	
MSI status						
MSS	118 (77.1)	107 (94.7)	<0.001	133 (83.6)	100 (93.5)	0.069
MSI	35 (22.9)	6 (5.3)		21 (13.2)	7 (6.5)	
NA				5 (3.1)		
Radiochemotherapy						
No	90 (58.8)	58 (51.3)	0.224	109 (68.6)	58 (54.2)	0.018
Yes	63 (41.2)	55 (48.7)		50 (31.4)	49 (45.8)	
Survival status						
Alive	134 (87.6)	82 (72.6)	**0.002**	134 (84.3)	68 (63.6)	**<0.001**
Dead	19 (12.4)	31 (27.4)		25 (15.7)	39 (36.4)	
Recurrence						
No	103 (67.3)	77 (68.1)	0.69	113 (71.1)	67 (62.6)	0.049
Yes	29 (19.0)	19 (16.8)		21 (13.2)	24 (22.4)	
NA	21 (13.7)	17 (15.0)		25 (15.7)	16 (15.0)	

Note: NA: Missing data; RSCC: right-sided colon cancer; LSCRC: left-sided colorectal cancer. Bold values indicate the statistical significance parameters in both training and validation sets (P<0.05).

transduction by p53 class mediator, Ras signaling pathway, actin cytoskeleton regulation, cGMP-PKG signaling pathway, and spliceosome pathways, which are known to correlate with the malignant phenotype of cancer cells [31–33]. Moreover, the majority of pathways reported to be related to pCRCSC-related miRNAs have functional implications in CSCs. For instance, p53 and Ras signaling pathways regulate stem cell differentiation and self-renewal [23, 34]. In addition, p53 regulates certain stem factors or miRNAs, including Bmi-1 and miR-34 [35]. Similarly, the NF-κB pathway has been implicated in inflammation, self-renewal, and maintenance and metastasis of CSCs [36]. Interestingly, a cross-talk among these CSC-related signaling pathways has been reported [22, 23, 37]. Further, univariate and multivariate Cox regression analyses revealed an association between pCRCSC-related miRNA expression and survival. MiR-664b-3p and miR-200c-5p were identified as independent prognostic biomarkers in patients with CRC. MiRNA-200c is a well-studied miRNA in a variety of tumors, including CRC, due to its involvement in epithelial-mesenchymal transition and drug resistance [28]. In addition, miRNA-200c is associated with patient clinicopathology and prognostic significance in certain specific cancer types [38–40]. Integration of two prognosis-related pCRCSC miRNAs into a pCRCSC miRNA signature by risk score method, based on their expression and relative contribution, successfully categorized patients into high- and low-risk groups with

large differences in OS. Furthermore, risk stratification showed a pCRCSC miRNA-based classifier as a strong prognostic factor that complements clinicopathological features and MSI status, thereby indicating the function of pCRCSC-related miRNAs in predicting the survival of CRC patients. A limitation of our study was that we only used the TCGA dataset due to the unavailability of the expression data of miR-664b-3p and miR-200c in other public databases. Nevertheless, because TCGA is a reliable database and our study included more than 500 patients, miRNAs identified as specifically expressed in CSCs can be used as promising biomarkers to predict the survival of cancer patients.

CONCLUSIONS

We performed a comprehensive pCRCSC miRNA expression profile analysis and identified a novel pCRCSC-based miRNA signature that was intricately associated with the survival of patients with CRC. Further, the patients were categorized into high- and low-risk groups with substantially different clinical

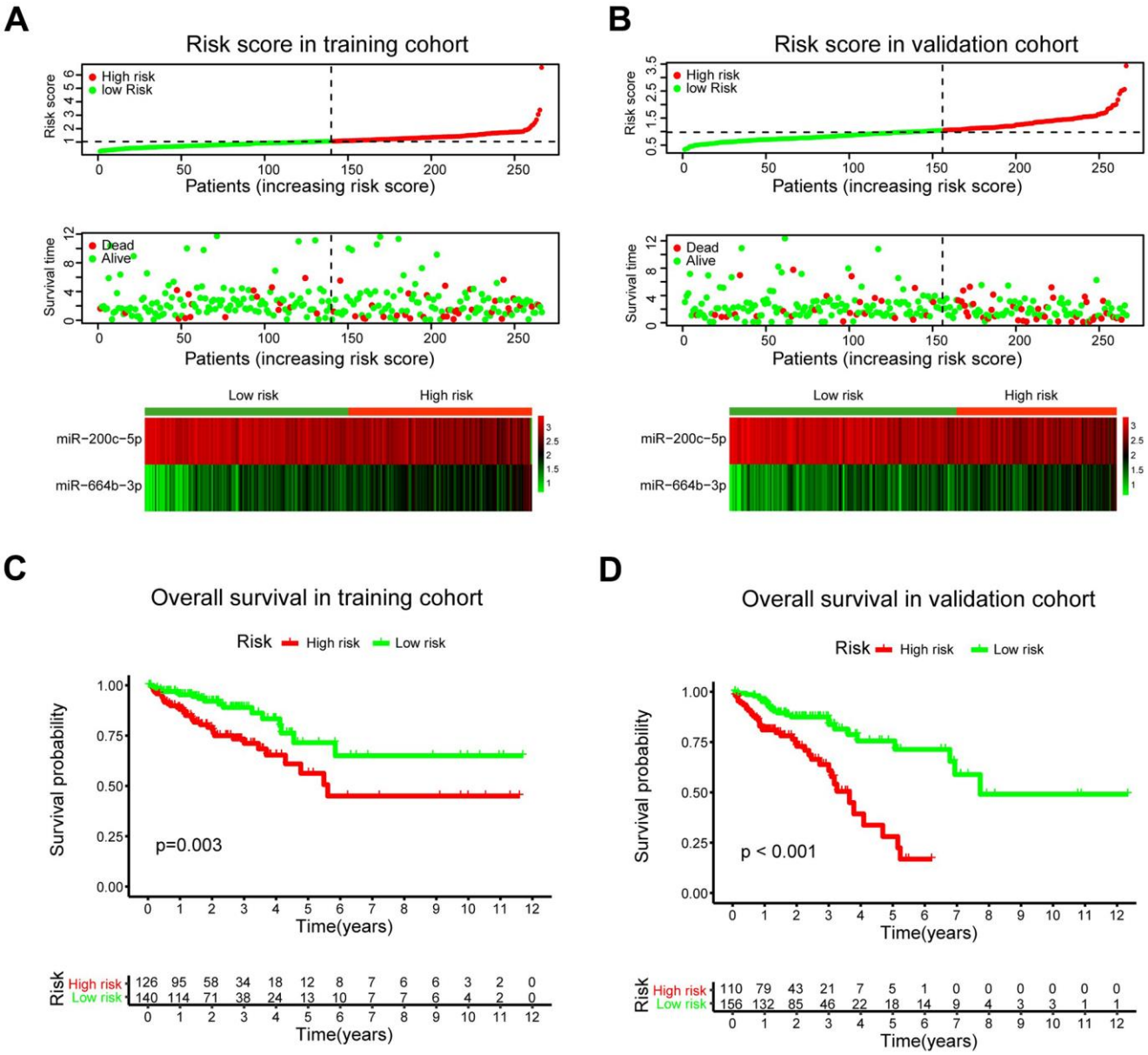

Figure 5. A prognostic model based on pCRCSC-related miRNA signature stratifies the OS in CRC patients. The distribution of risk score, overall survival (OS), OS status, and the heat map of prognostic pCRCSC miRNA signature in the training (**A**, **B**) validation cohorts. The dotted line indicates the cut-off point of the median risk score used to stratify the patients into low- and high-risk groups. Kaplan–Meier curves of OS for patients with CRC based on pCRCSC-related miRNA signature in the training (**C**, **D**) validation cohorts.

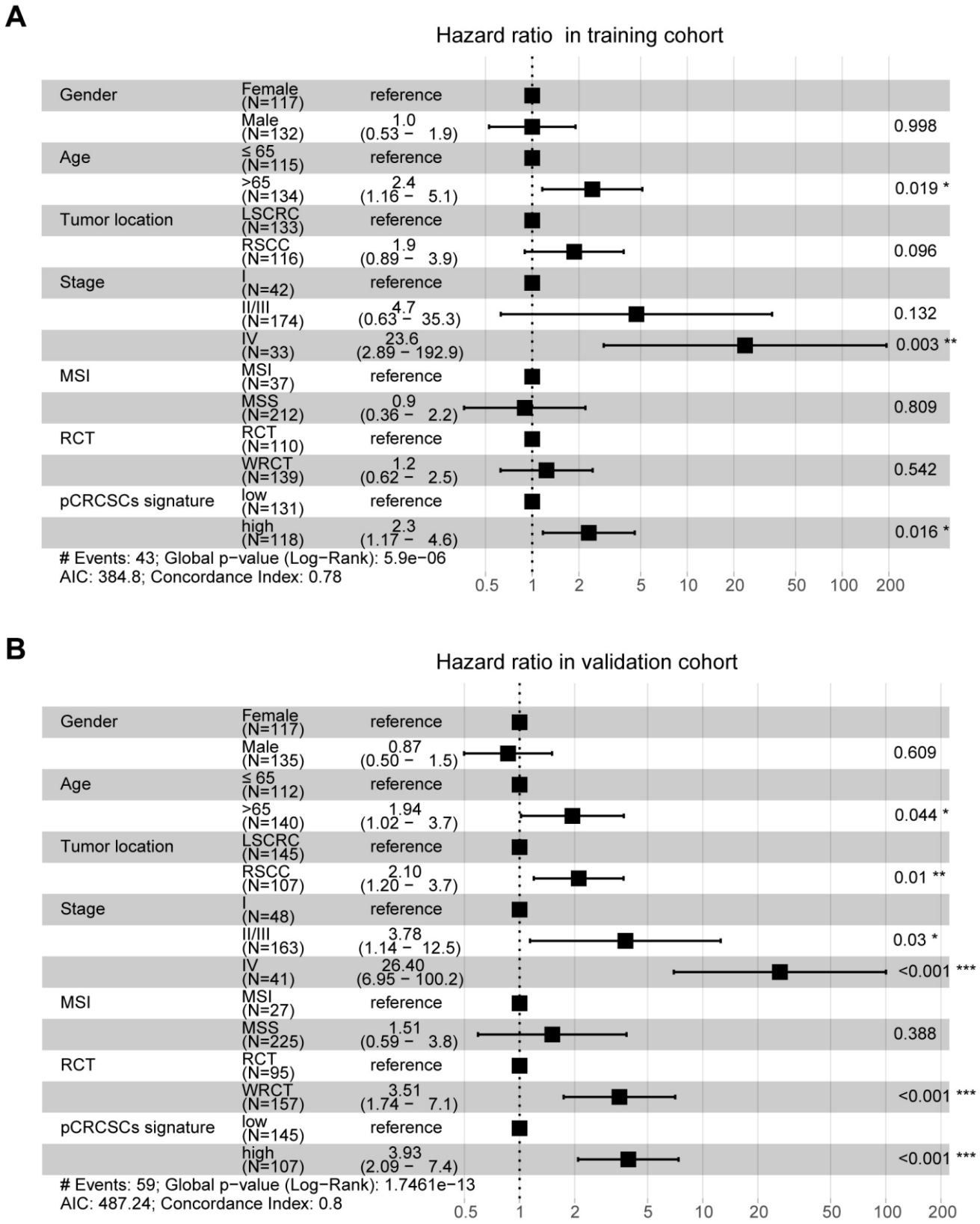

Figure 6. pCRCSC-related miRNA signature is an independent prognostic factor for OS in CRC patients. Forest plot summary of multivariate analyses for OS with gender, age, tumor location, tumor stage, MSI status, adjuvant chemoradiotherapy as covariates, and the risk based on pCRCSC-related miRNA signature in the training (**A**, **B**) validation cohorts. Squares on the transverse lines represent the hazard ratio (HR), whereas transverse lines represent 95% confidence interval (CI).

outcomes. Furthermore, the prognostic value of the pCRCSC-related miRNA signature was independent of other clinicopathological factors. Our study highlights the potential of pCRCSC-related miRNAs as alternative molecular markers, which could be used as promising therapeutic targets for CRC.

MATERIALS AND METHODS

Isolation, enrichment, and differentiation of CRCSC spheres from primary CRC

To isolate the primary CRCSC spheres, CRC samples were obtained from patients with primary colon adenocarcinoma who had undergone colon resection at the Department of Gastrointestinal Surgery, West China Hospital, Sichuan University. CRCSC spheres were isolated and expanded as described previously [3]. In brief, colon cancer tissues collected from surgical specimens were immediately minced on ice and suspended in the DMEM/F12 medium (HyClone, Logan, UT, USA). The tissue was mechanically and enzymatically dissociated, and the cell suspension was filtered. The dissociated single tumor cells were placed under stem cell conditions in serum-free DMEM/F12 medium supplemented with human recombinant EGF (PeproTech, Rocky Hill, NJ, USA) and bFGF (PeproTech) and cultured in ultra-low attachment plates (Corning, Corning, NY, USA). To obtain differentiated pCRCSCs, growth factors in the serum-free pCRCSC medium were removed and replaced with 20% FBS [3, 24].

Xenograft experiments in a nude mouse model

Female nude mice (BALB/c strain, 4- to 6-week-old) were purchased from the Beijing Experimental Animal Centre of the Chinese Academy of Sciences (Beijing, China). The mice were housed under pathogen-free conditions, and the animal studies were performed according to the protocol approved by the Sichuan University Institutional Animal Care and Use Committee. The pCRCSC spheres and differentiated cells were trypsinized using 0.05% trypsin; 5×10^5 cells were mixed with BD Matrigel (BD Biosciences, San Jose, CA, USA) at a 1:1 ratio and injected subcutaneously into the ventral wall of nude mice. Mice bearing the tumor were euthanized when the established criteria for the end-stage disease were reached, and the images were acquired.

MiRNA isolation, miRNA microarray, and data analyses

MiRNAs of three pairs of CRCSCs and the corresponding differentiated cells were carefully isolated using "mirVana miRNA Isolation Kit" (Ambion, Darmstadt, Germany) following the manufacturer's instructions. The purity and concentrations of miRNA samples were measured and determined spectro-photometrically with NanoDrop ND-2000c (Thermo Fisher Scientific, Inc., Wilmington, DE, USA).

Genome-wide miRNA profiles of three pairs of CRCSCs and their corresponding differentiated cells were analyzed using Agilent Human miRNA Microarray (V21) at Shanghai Biotechnology Corporation (Shanghai, China). The differential expression of miRNAs was identified using the Limma package in R 3.6.0 and selected based on adjusted *p*-values ($p < 0.05$). The absolute value of log2 fold change was >1.

Prediction of target genes of differential miRNAs

MiRNA target genes were identified using miRWalk 2.0 (http://zmf.umm.uni-heidelberg.de/apps/zmf/mirwalk2/miRretsys-self.html), TargetScan 7.1 (http://www.targetscan.org), and miRDB (http://mirdb.org/miRDB/, v4.0). The target genes were further reduced by selecting those commonly predicted by all three databases.

Gene ontology (GO) and kyoto encyclopedia of genes and genomes (KEGG) analyses

Biological process, cell component, molecular function, and KEGG pathways were annotated in the following way: the list of potential target transcripts for each pCRCSC-related miRNA was uploaded to the Database for Annotation, Visualization and Integrated Discovery (DAVID) (https://david.ncifcrf.gov) for functional annotation. A GO term and pathway were selected if miRNAs were significant ($p < 0.05$). The top 15 GO terms and pathways were visualized using the "ggplot2" package in R 3.6.0.

pCRCSC-related miRNA-based prognostic model development

Level-3 data of miRNA-seq, mRNA-seq, including Illumina HiSeq and Illumina GA platforms, as well as the potential batch effects were removed using the "combat" function of "sva" package of R. The clinico-pathological data of TCGA colorectal samples (COREAD) were obtained from UCSC Xena (https://xenabrowser.net/hub/). The adjuvant radiochemo-therapeutic data were downloaded from GDC (https://portal.gdc.cancer.gov/projects). The TCGA colorectal samples were randomly divided into training and validation cohorts using the "caret" R package in R 3.6.0.

MiRNAs sharing both differential pCRCSC miRNAs and TCGA-COREAD miRNA datasets were considered

as predictive prognostic markers for survival comparison, with the lowest log-rank $p < 0.05$. The candidate prognostic miRNA signature was identified using the multivariate Cox proportional hazard regression survival model. The prognostic risk scores for each patient were calculated using the formula based on the coefficient from the multivariate Cox proportional hazard regression model. The optimal cut-off was automatically selected by the X-tile software version 3.6.1 (Yale University School of Medicine, New Haven, CT, USA). The patients were subsequently divided into high- and low-risk groups using the optimal cut-off. Next, the area under the curve (AUC) was applied to assess the predictive accuracy of the pCRCSC miRNA prognostic model using the "survival ROC" package in R 3.6.0.

The differences in OS between the high and low pCRCSC-related miRNA scores were analyzed using the Kaplan–Meier (K–M) curve with a log-rank test based on the "survival" package in R 3.6.0.

Statistical analyses

We compared different clinicopathological parameters in low- and high-risk groups using the *t*-test for continuous variables and χ^2 test for categorical variables. The K–M method was used to compare the survival curves. The univariate and multivariate Cox regression model was used to study the prognostic significance of clinicopathological parameters and the CRCSC miRNA signature in the TCGA–COREAD data. All statistical tests were performed using the R software version 3.6.0. A p-value < 0.05 was considered significant.

Ethics statement

This study was approved by the Independent Ethics Committee of the West China Hospital of Sichuan University and was performed in accordance with the Declaration of Helsinki (1983). Informed consent was obtained from all patients who provided samples.

Editorial note

[&]This corresponding author has a verified history of publications using a personal email address for correspondence.

Abbreviations

miRNAs: microRNAs; CSCs: cancer stem cells; CRC: colorectal cancer; pCRCSCs: primary CSCs from CRC patients; GO: gene ontology; KEGG: Kyoto Encyclopedia of Genes and Genomes; OS: overall survival.

AUTHOR CONTRIBUTIONS

Conceptualization: C-W.F., Z-G.Z., H.Z., X-M.M., and X-F.S. Data curation: C-W.F., R.L., C.F., Z-Y.L., Y.L., Z-G.Z., H.Z., X-M.M., and X-F.S. Formal analysis: C-W.F., R.L., C.F., Z-Y.L., X-L.Z., and Y.L. Investigation: H.Z., X-M.M., and X-F.S. Methodology: C-W.F., R.L., X-L.Z., Z-Y.L., H.Z., X-M.M., and X-F.S. Project administration: Z-G.Z., H.Z., X-M.M., and X-F.S. Resources: Z-G.Z. and X-M.M. Software: C-W.F., R.L., C.F., and X-L.Z. Supervision: H.Z., X-M.M., and X-F.S. Validation: R.L., C.F., Z-Y.L., Y.L., Z-G.Z., X-M.M., and X-F.S. Visualization: C-W.F. and X-L.Z. Writing the original draft: C-W.F. and X-F.S. Writing, reviewing, and editing: R.L., C.F., X-L.Z., Z-Y.L., Y.L., Z-G.Z., H.Z., X-M.M., and X-F.S.

ACKNOWLEDGMENTS

The authors are grateful to the Institutional Ethics Committee, Sichuan University, China, for approving the study. We also thank the participants and their families for their kind cooperation, generosity, and patience.

CONFLICTS OF INTEREST

The authors declare that they have no conflicts of interest.

FUNDING

This work was supported by grants from the Sichuan Science and Technology Program (No. 2017JY0061), Science Fund for Creative Research Groups of the National Natural Science Foundation of China (No. 81821002), and Swedish Cancer Foundation, Swedish Research Council, and Oncology Clinics in Linköping.

REFERENCES

1. Siegel RL, Miller KD, Fedewa SA, Ahnen DJ, Meester RG, Barzi A, Jemal A. Colorectal cancer statistics, 2017. CA Cancer J Clin. 2017; 67:177–93. https://doi.org/10.3322/caac.21395 PMID:28248415
2. Phi LT, Sari IN, Yang YG, Lee SH, Jun N, Kim KS, Lee YK, Kwon HY. Cancer Stem Cells (CSCs) in Drug Resistance and their Therapeutic Implications in Cancer Treatment. Stem Cells Int. 2018; 2018:5416923. https://doi.org/10.1155/2018/5416923 PMID:29681949
3. Fan CW, Chen T, Shang YN, Gu YZ, Zhang SL, Lu R,

OuYang SR, Zhou X, Li Y, Meng WT, Hu JK, Lu Y, Sun XF, et al. Cancer-initiating cells derived from human rectal adenocarcinoma tissues carry mesenchymal phenotypes and resist drug therapies. Cell Death Dis. 2013; 4:e828.
https://doi.org/10.1038/cddis.2013.337
PMID:24091671

4. Shangguan W, Fan C, Chen X, Lu R, Liu Y, Li Y, Shang Y, Yin D, Zhang S, Huang Q, Li X, Meng W, Xu H, et al. Endothelium originated from colorectal cancer stem cells constitute cancer blood vessels. Cancer Sci. 2017; 108:1357–67.
https://doi.org/10.1111/cas.13262 PMID:28421697

5. Lu R, Fan C, Shangguan W, Liu Y, Li Y, Shang Y, Yin D, Zhang S, Huang Q, Li X, Meng W, Xu H, Zhou Z, et al. Neurons generated from carcinoma stem cells support cancer progression. Signal Transduct Target Ther. 2017; 2:16036.
https://doi.org/10.1038/sigtrans.2016.36
PMID:29263908

6. Pan C, Kumar C, Bohl S, Klingmueller U, Mann M. Comparative proteomic phenotyping of cell lines and primary cells to assess preservation of cell type-specific functions. Mol Cell Proteomics. 2009; 8:443–50.
https://doi.org/10.1074/mcp.M800258-MCP200
PMID:18952599

7. Mamoori A, Gopalan V, Smith RA, Lam AK. Modulatory roles of microRNAs in the regulation of different signalling pathways in large bowel cancer stem cells. Biol Cell. 2016; 108:51–64.
https://doi.org/10.1111/boc.201500062
PMID:26712035

8. Zhang R, Xu J, Zhao J, Bai J. Knockdown of miR-27a sensitizes colorectal cancer stem cells to TRAIL by promoting the formation of Apaf-1-caspase-9 complex. Oncotarget. 2017; 8:45213–23.
https://doi.org/10.18632/oncotarget.16779
PMID:28423356

9. De Robertis M, Mazza T, Fusilli C, Loiacono L, Poeta ML, Sanchez M, Massi E, Lamorte G, Diodoro MG, Pescarmona E, Signori E, Pesole G, Vescovi AL, et al. EphB2 stem-related and EphA2 progression-related miRNA-based networks in progressive stages of CRC evolution: clinical significance and potential miRNA drivers. Mol Cancer. 2018; 17:169.
https://doi.org/10.1186/s12943-018-0912-z
PMID:30501625

10. Sakaguchi M, Hisamori S, Oshima N, Sato F, Shimono Y, Sakai Y. miR-137 Regulates the Tumorigenicity of Colon Cancer Stem Cells through the Inhibition of DCLK1. Mol Cancer Res. 2016; 14:354–62.
https://doi.org/10.1158/1541-7786.MCR-15-0380
PMID:26747706

11. Wellner U, Schubert J, Burk UC, Schmalhofer O, Zhu F, Sonntag A, Waldvogel B, Vannier C, Darling D, zur Hausen A, Brunton VG, Morton J, Sansom O, et al. The EMT-activator ZEB1 promotes tumorigenicity by repressing stemness-inhibiting microRNAs. Nat Cell Biol. 2009; 11:1487–95.
https://doi.org/10.1038/ncb1998 PMID:19935649

12. Shi L, Xi J, Xu X, Peng B, Zhang B. MiR-148a suppressed cell invasion and migration via targeting WNT10b and modulating β-catenin signaling in cisplatin-resistant colorectal cancer cells. Biomed Pharmacother. 2019; 109:902–09.
https://doi.org/10.1016/j.biopha.2018.10.080
PMID:30551544

13. Jin Y, Wang M, Hu H, Huang Q, Chen Y, Wang G. Overcoming stemness and chemoresistance in colorectal cancer through miR-195-5p-modulated inhibition of notch signaling. Int J Biol Macromol. 2018; 117:445–53.
https://doi.org/10.1016/j.ijbiomac.2018.05.151
PMID:29852230

14. Ren D, Lin B, Zhang X, Peng Y, Ye Z, Ma Y, Liang Y, Cao L, Li X, Li R, Sun L, Liu Q, Wu J, et al. Maintenance of cancer stemness by miR-196b-5p contributes to chemoresistance of colorectal cancer cells via activating STAT3 signaling pathway. Oncotarget. 2017; 8:49807–23.
https://doi.org/10.18632/oncotarget.17971
PMID:28591704

15. Chen B, Zhang D, Kuai J, Cheng M, Fang X, Li G. Upregulation of miR-199a/b contributes to cisplatin resistance via Wnt/β-catenin-ABCG2 signaling pathway in ALDHA1^{+} colorectal cancer stem cells. Tumour Biol. 2017; 39:1010428317715155.
https://doi.org/10.1177/1010428317715155
PMID:28639895

16. Ju J. Implications of miRNAs in Colorectal Cancer Chemoresistance. Int Drug Discov. 2011; 2011:2063.
PMID:25750759

17. Wang LQ, Yu P, Li B, Guo YH, Liang ZR, Zheng LL, Yang JH, Xu H, Liu S, Zheng LS, Zhou H, Qu LH. miR-372 and miR-373 enhance the stemness of colorectal cancer cells by repressing differentiation signaling pathways. Mol Oncol. 2018; 12:1949–64.
https://doi.org/10.1002/1878-0261.12376
PMID:30171794

18. Toden S, Kunitoshi S, Cardenas J, Gu J, Hutchins E, Van Keuren-Jensen K, Uetake H, Toiyama Y, Goel A. Cancer stem cell-associated miRNAs serve as prognostic biomarkers in colorectal cancer. JCI Insight. 2019; 4:e125294.
https://doi.org/10.1172/jci.insight.125294
PMID:30895943

19. Asadzadeh Z, Mansoori B, Mohammadi A, Aghajani M, Haji-Asgarzadeh K, Safarzadeh E, Mokhtarzadeh A, Duijf PH, Baradaran B. microRNAs in cancer stem cells: Biology, pathways, and therapeutic opportunities. J Cell Physiol. 2019; 234:10002–17. https://doi.org/10.1002/jcp.27885 PMID:30537109

20. Khan AQ, Ahmed EI, Elareer NR, Junejo K, Steinhoff M, Uddin S. Role of miRNA-Regulated Cancer Stem Cells in the Pathogenesis of Human Malignancies. Cells. 2019; 8:840. https://doi.org/10.3390/cells8080840 PMID:31530793

21. Lou W, Liu J, Gao Y, Zhong G, Ding B, Xu L, Fan W. MicroRNA regulation of liver cancer stem cells. Am J Cancer Res. 2018; 8:1126–41. PMID:30094089

22. Takebe N, Miele L, Harris PJ, Jeong W, Bando H, Kahn M, Yang SX, Ivy SP. Targeting Notch, Hedgehog, and Wnt pathways in cancer stem cells: clinical update. Nat Rev Clin Oncol. 2015; 12:445–64. https://doi.org/10.1038/nrclinonc.2015.61 PMID:25850553

23. Yang L, Shi P, Zhao G, Xu J, Peng W, Zhang J, Zhang G, Wang X, Dong Z, Chen F, Cui H. Targeting cancer stem cell pathways for cancer therapy. Signal Transduct Target Ther. 2020; 5:8. https://doi.org/10.1038/s41392-020-0110-5 PMID:32296030

24. Ricci-Vitiani L, Lombardi DG, Pilozzi E, Biffoni M, Todaro M, Peschle C, De Maria R. Identification and expansion of human colon-cancer-initiating cells. Nature. 2007; 445:111–15. https://doi.org/10.1038/nature05384 PMID:17122771

25. Hu Y, Fu L. Targeting cancer stem cells: A new therapy to cure cancer patients. Am J Cancer Res. 2012; 2:340–56. PMID:22679565

26. Bertoli G, Cava C, Castiglioni I. MicroRNAs: New Biomarkers for Diagnosis, Prognosis, Therapy Prediction and Therapeutic Tools for Breast Cancer. Theranostics. 2015; 5:1122–43. https://doi.org/10.7150/thno.11543 PMID:26199650

27. Wu MJ, Kim MR, Chang CJ. Regulation of microRNA-200c in cancer stem cells. Oncoscience. 2015; 2:745–46. https://doi.org/10.18632/oncoscience.204 PMID:26501077

28. Shimono Y, Zabala M, Cho RW, Lobo N, Dalerba P, Qian D, Diehn M, Liu H, Panula SP, Chiao E, Dirbas FM, Somlo G, Pera RA, et al. Downregulation of miRNA-200c links breast cancer stem cells with normal stem cells. Cell. 2009; 138:592–603. https://doi.org/10.1016/j.cell.2009.07.011 PMID:19665978

29. Lin SS, Peng CY, Liao YW, Chou MY, Hsieh PL, Yu CC. miR-1246 Targets CCNG2 to Enhance Cancer Stemness and Chemoresistance in Oral Carcinomas. Cancers (Basel). 2018; 10:272. https://doi.org/10.3390/cancers10080272 PMID:30115848

30. Chen SM, Wang BY, Lee CH, Lee HT, Li JJ, Hong GC, Hung YC, Chien PJ, Chang CY, Hsu LS, Chang WW. Hinokitiol up-regulates miR-494-3p to suppress BMI1 expression and inhibits self-renewal of breast cancer stem/progenitor cells. Oncotarget. 2017; 8:76057–68. https://doi.org/10.18632/oncotarget.18648 PMID:29100291

31. Luo JL, Kamata H, Karin M. IKK/NF-kappaB signaling: balancing life and death--a new approach to cancer therapy. J Clin Invest. 2005; 115:2625–32. https://doi.org/10.1172/JCI26322 PMID:16200195

32. Stegh AH. Targeting the p53 signaling pathway in cancer therapy - the promises, challenges and perils. Expert Opin Ther Targets. 2012; 16:67–83. https://doi.org/10.1517/14728222.2011.643299 PMID:22239435

33. Tuttle TR, Mierzwa ML, Wells SI, Fox SR, Ben-Jonathan N. The cyclic GMP/protein kinase G pathway as a therapeutic target in head and neck squamous cell carcinoma. Cancer Lett. 2016; 370:279–85. https://doi.org/10.1016/j.canlet.2015.10.024 PMID:26551887

34. Fitzgerald TL, Lertpiriyapong K, Cocco L, Martelli AM, Libra M, Candido S, Montalto G, Cervello M, Steelman L, Abrams SL, McCubrey JA. Roles of EGFR and KRAS and their downstream signaling pathways in pancreatic cancer and pancreatic cancer stem cells. Adv Biol Regul. 2015; 59:65–81. https://doi.org/10.1016/j.jbior.2015.06.003 PMID:26257206

35. Prabhu VV, Allen JE, Hong B, Zhang S, Cheng H, El-Deiry WS. Therapeutic targeting of the p53 pathway in cancer stem cells. Expert Opin Ther Targets. 2012; 16:1161–74. https://doi.org/10.1517/14728222.2012.726985 PMID:22998602

36. Rinkenbaugh AL, Baldwin AS. The NF-κB Pathway and Cancer Stem Cells. Cells. 2016; 5:16. https://doi.org/10.3390/cells5020016 PMID:27058560

37. Matsui WH. Cancer stem cell signaling pathways. Medicine (Baltimore). 2016; 95:S8–19. https://doi.org/10.1097/MD.0000000000004765 PMID:27611937

38. Diaz T, Tejero R, Moreno I, Ferrer G, Cordeiro A, Artells R, Navarro A, Hernandez R, Tapia G, Monzo M. Role of miR-200 family members in survival of colorectal cancer patients treated with fluoropyrimidines. J Surg Oncol. 2014; 109:676–83. https://doi.org/10.1002/jso.23572 PMID:24510588

39. Toiyama Y, Hur K, Tanaka K, Inoue Y, Kusunoki M, Boland CR, Goel A. Serum miR-200c is a novel prognostic and metastasis-predictive biomarker in patients with colorectal cancer. Ann Surg. 2014; 259:735–43. https://doi.org/10.1097/SLA.0b013e3182a6909d PMID:23982750

40. Roh MS, Lee HW, Jung SB, Kim K, Lee EH, Park MI, Lee JS, Kim MS. Expression of miR-200c and its clinicopathological significance in patients with colorectal cancer. Pathol Res Pract. 2018; 214:350–55. https://doi.org/10.1016/j.prp.2018.01.005 PMID:29496312

SUPPLEMENTARY MATERIALS

Supplementary Figures

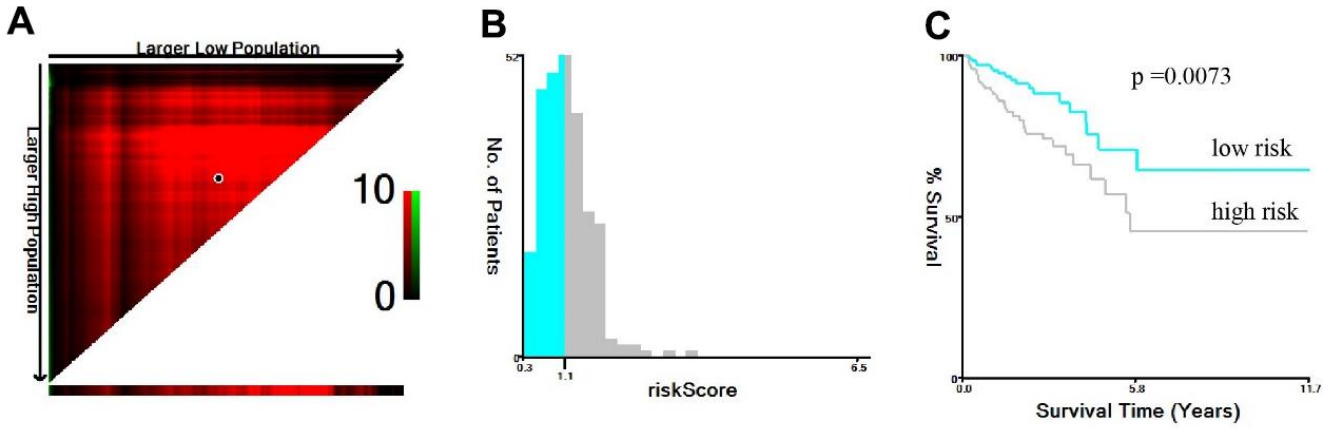

Supplementary Figure 1. X-tile plots of pCRCSCs-related miRNAs signature for optimal cut-off determination in training cohort. (**A**, **B**) The cut-off (IRS= 1.106) was optimized to separate low pCRCSCs-related miRNAs signature (blue) from high pCRCSCs-related miRNAs signature (gray) in the frequency histogram of training cohort. (**C**) Kaplan-Meier curve for testing the survival of sample subsets defined by optimized cutoff value of pCRCSCs-related miRNAs signature.

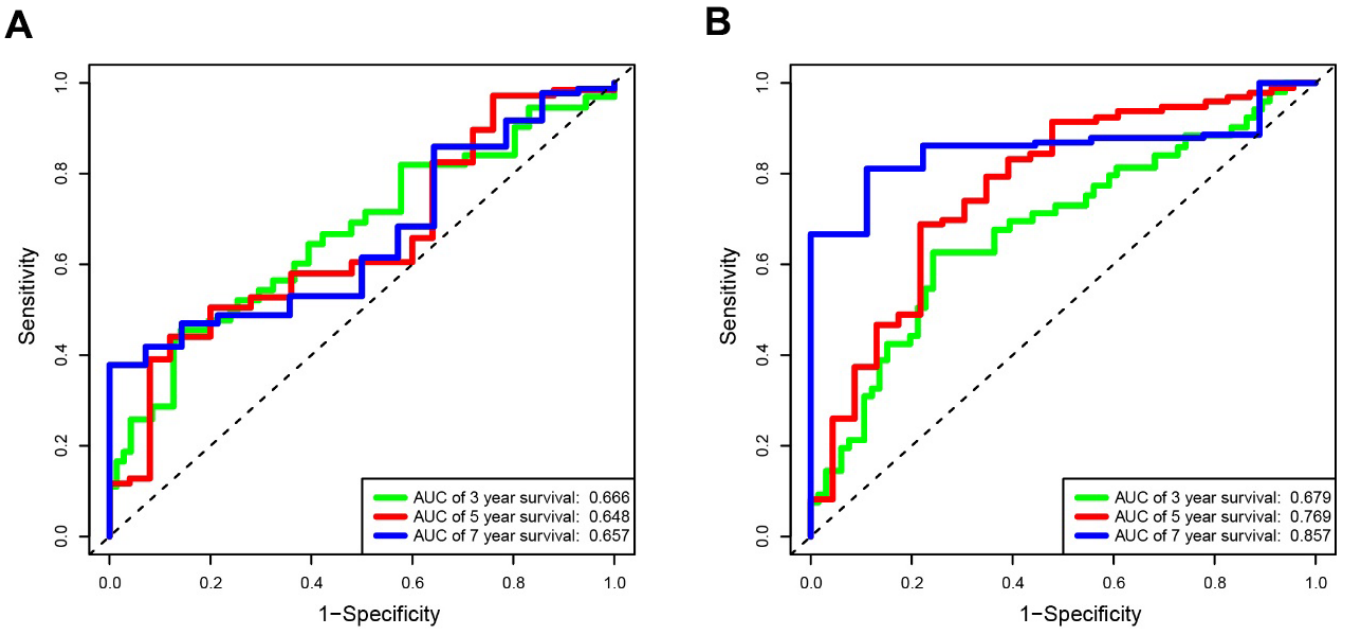

Supplementary Figure 2. Time-dependent ROC curves for OS-specific pCRCSC-related miRNA signature. (**A**) Time-dependent receiver operating characteristic curves at 3-, 5-, 7- years based on the pCRCSCs miRNAs signature in the training cohort. (**B**) Time-dependent receiver operating characteristic curves at 3-, 5-, 7- years based on the pCRCSCs miRNAs signature in the validation cohort.

Supplementary Tables

Please browse Full Text version to see the data of Supplementary Tables 1–6, 8.

Supplementary Table 1. Differentially expressed miRNAs between pCRCSCs and pCRCSC-derived differentiated cells.

Supplementary Table 2. Predictive target genes of pCRCSC-related miRNAs in different databases.

Supplementary Table 3. Differentially expressed miRNAs between normal and cancer tissues in patients from CRC from the TCGA dataset.

Supplementary Table 4. Differentially expressed mRNAs between normal and cancer tissues in patients with CRC from the TCGA dataset.

Supplementary Table 5. The integrated target genes of pCRCSC-related miRNAs using the database and TCGA miRNA–mRNA pairs.

Supplementary Table 6. GO analysis of target genes of pCSCSC-related miRNAs.

Supplementary Table 7. The KEGG pathway analysis of target genes of pCSCSC-related miRNAs.

Term	Count	%	p value	Genes
hsa00030:Pentose phosphate pathway	8	0.921659	8.55E-04	PGM2, GPI, RPE, PGM1, RPIA, PFKM, IDNK, PRPS1
hsa04520:Adherens junction	11	1.2672811	0.005685	PTPRJ, CDC42, SORBS1, BAIAP2, WASF2, MET, CTNND1, CDH1, WASL, INSR, TCF7L2
hsa04022:cGMP-PKG signaling pathway	18	2.0737327	0.006789	GNA13, KCNMA1, ATP1B3, PDE3A, ATP1A2, PPP1CB, VASP, KCNMB1, ATP2B1, EDNRB, ATP2B4, GNAQ, PLN, PDE5A, ADRA2A, INSR, MYLK, CALM1
hsa03040:Spliceosome	16	1.843318	0.006997	SRSF1, CHERP, SNRPB2, U2SURP, HNRNPU, SRSF3, HNRNPA3, SRSF2, SRSF5, TCERG1, SRSF7, SRSF6, SNRNP200, SNRPC, PRPF38B, RBM17
hsa04014:Ras signaling pathway	22	2.5345622	0.014486	FGFR2, PLD1, MET, KITLG, ARF6, KIT, FOXO4, STK4, CDC42, ETS2, RRAS2, GAB1, SOS2, PDGFRA, RALB, RAP1A, PDGFD, PRKACB, ABL1, INSR, GNG7, CALM1
hsa05200:Pathways in cancer	33	3.8018433	0.019088	GNA13, FGFR2, BID, E2F3, KITLG, FOXO1, EGLN1, CDH1, KIT, TCF7L2, PTEN, EDNRB, CDC42, BCL2, SOS2, RALB, TGFA, PRKACB, TPR, AXIN2, GNG7, PTGER4, EPAS1, MET, SKP2, ITGA2, FZD5, STK4, RAD51, HDAC2, GNAQ, PDGFRA, ABL1
hsa04152:AMPK signaling pathway	14	1.6129032	0.019246	PPP2R3A, PPP2R5A, FOXO1, ACACB, PFKM, PCK2, PPARGC1A, CPT1A, SLC2A4, PPP2CB, RAB14, RHEB, CAB39, INSR
hsa04972:Pancreatic secretion	11	1.2672811	0.03379	ATP2B1, KCNMA1, SLC26A3, CLCA1, ATP2B4, ATP1B3, SLC12A2, GNAQ, RAP1A, ATP1A2, SLC4A4
hsa04978:Mineral absorption	7	0.8064516	0.034055	SLC26A3, TRPM6, ATP1B3, SLC30A1, ATP1A2, SLC6A19, MT1G
hsa04931:Insulin resistance	12	1.3824885	0.037857	PPARA, SLC2A4, MLX, FOXO1, OGT, ACACB, PCK2, PTEN, PPARGC1A, INSR, PPP1CB, CPT1A
hsa04910:Insulin signaling pathway	14	1.6129032	0.043867	PRKAR2B, SORBS1, SLC2A4, SOS2, PHKA1, FOXO1, RHEB, PRKACB, ACACB, PCK2, PPARGC1A, INSR, PPP1CB, CALM1
hsa04261:Adrenergic signaling in cardiomyocytes	14	1.6129032	0.043867	PPP2R3A, ATP1B3, PPP2R5A, ATP1A2, PPP1CB, ATP2B1, ATP2B4, GNAQ, PLN, BCL2, PPP2CB, CAMK2D, PRKACB, CALM1
hsa04810:Regulation of actin cytoskeleton	19	2.1889401	0.045241	GNA13, FGFR2, ENAH, BAIAP2, PPP1R12B, WASF2, ITGA2, IQGAP2, PPP1CB, CDC42, DOCK1, EZR, CFL2, RRAS2, SOS2, PDGFRA, WASL, PDGFD, MYLK
hsa04922:Glucagon signaling pathway	11	1.2672811	0.048678	PPARA, GNAQ, PHKA1, CAMK2D, FOXO1, PRKACB, ACACB, PCK2, PPARGC1A, CPT1A, CALM1
hsa01212:Fatty acid metabolism	7	0.8064516	0.049232	ACOX1, ELOVL5, FADS1, HSD17B12, ACSL4, HADH, CPT1A
hsa01200:Carbon metabolism	12	1.3824885	0.049953	ME1, GPI, RPE, ME2, SUCLG2, ADPGK, RPIA, PFKM, IDNK, IDH3A, PC, PRPS1

Supplementary Table 8. List of TCGA IDs for randomly grouped training and validation cohorts.

Supplementary Table 9. Univariate screening of pCRCSC-related miRNAs for OS in the training cohort.

miRNAs	HR	HR.95L	HR.95H	p value
hsa-miR-142-3p	1.138066098	0.845905055	1.531134535	0.392881924
hsa-miR-182-5p	1.104825785	0.841234945	1.451009639	0.473486987
hsa-miR-183-5p	1.001026756	0.772377724	1.297363369	0.99381111
hsa-miR-196b-5p	0.879311673	0.729857866	1.059369303	0.175999667
hsa-miR-200c-5p	0.752123057	0.585874866	0.96554593	0.025412824
hsa-miR-223-3p	0.943087363	0.761021372	1.16871064	0.592357826
hsa-miR-338-3p	1.031115061	0.81146031	1.310228308	0.802055672
hsa-miR-338-5p	0.936520549	0.706315441	1.241755011	0.64864497
hsa-miR-345-5p	0.888078248	0.672958772	1.171963287	0.401630231
hsa-miR-3613-3p	1.135614061	0.730689762	1.764934125	0.571881692
hsa-miR-3614-5p	0.883264151	0.632935428	1.232598978	0.465361894
hsa-miR-3682-3p	1.18709029	0.769815217	1.830547545	0.437679937
hsa-miR-3940-3p	1.438622027	0.821532705	2.519234261	0.203279004
hsa-miR-4728-3p	1.061788613	0.716659991	1.573124038	0.764998501
hsa-miR-483-3p	0.896636456	0.764797104	1.0512029	0.17876179
hsa-miR-484	0.91859734	0.63191972	1.335329546	0.656421376
hsa-miR-5010-3p	1.100223917	0.656812919	1.842979384	0.716687824
hsa-miR-584-5p	0.83386517	0.679098374	1.023903382	0.082837655
hsa-miR-664b-3p	1.478618442	1.026965052	2.128906423	0.035462445
hsa-miR-664a-3p	1.106623781	0.731356495	1.674444955	0.631621212
hsa-miR-671-3p	0.96482922	0.658084789	1.41455241	0.854478312
hsa-miR-671-5p	1.086601465	0.761944892	1.549590733	0.646499192
hsa-miR-766-3p	0.931641917	0.643760078	1.348261087	0.707317911
hsa-miR-99b-5p	0.962351989	0.643240409	1.439774829	0.851897147
hsa-miR-494-3p	0.82117325	0.554024877	1.217139401	0.326458875
hsa-miR-598-3p	1.006536592	0.783515509	1.293038744	0.959340387

Supplementary Table 10. Multivariate screening of pCRCSC-related miRNAs for OS in the training cohort.

miRNA	coef	HR	HR.95L	HR.95H	p value
hsa-miR-200c-5p	-0.26960351	0.763682226	0.59521481	0.979832043	0.033990201
hsa-miR-664b-3p	0.383954209	1.468078215	1.003818613	2.147054873	0.047746837

Supplementary Table 11. Univariate analysis of pCRCSC-related miRNA signature for OS in the training cohort.

Parameters	HR	HR.95L	HR.95H	p value
Gender (Male vs Female)	1.409341027	0.767455353	2.588088183	0.268524673
Age (≤60 vs >60)	2.530791757	1.275012442	5.023407384	0.00794166
Location (RSCC vs LSCRC)	1.129825063	0.617866334	2.065988392	0.6918184
pTNM (II/III vs I)	5.209048044	0.707243848	38.36609056	0.105238693
pTNM (IV vs I)	20.28084515	2.677647553	153.6097159	0.003575243
MSI (MSS vs MSI)	1.015366899	0.451256094	2.284667076	0.970599452
RCT (WRCT vs RCT)	0.906118362	0.495940318	1.655542925	0.748521717
risk (High vs low)	2.17329531	1.160487595	4.070024121	0.015311349

Supplementary Table 12. Univariate analysis of pCRCSC-related miRNA signature for OS in the validation cohort.

Parameters	HR	HR.95L	HR.95H	p value
Gender (Male vs Female)	1.074137693	0.639349115	1.804603707	0.787025435
Age (≤60 vs >60)	2.510383032	1.396271857	4.51346415	0.002103413
Location (RSCC vs LSCRC)	1.754334544	1.049870147	2.931495576	0.031893283
pTNM (II/III vs I)	2.971275024	0.910809589	9.692997719	0.071057644
pTNM (IV vs I)	12.36401574	3.657776016	41.79285021	5.19E-05
MSI (MSS vs MSI)	1.252524391	0.534756327	2.933705079	0.604101677
RCT (WRCT vs RCT)	1.251448747	0.733429318	2.1353441	0.410642781
risk (High vs low)	3.709875215	2.114370252	6.509349107	4.87E-06

Priority Research Paper

Cdkn1a transcript variant 2 is a marker of aging and cellular senescence

José Alberto López-Domínguez[1,#,*], Sandra Rodríguez-López[2,*], Ulises Ahumada-Castro[3,4], Pierre-Yves Desprez[1], Maria Konovalenko[1], Remi-Martin Laberge[5], César Cárdenas[1,3,4,6], José Manuel Villalba[2], Judith Campisi[1,7]

[1]Buck Institute for Research on Aging, Novato, CA 94945, USA
[2]Departamento de Biología Celular, Fisiología e Inmunología, Universidad de Córdoba, Campus de Excelencia Internacional Agroalimentario, Córdoba 14071, Spain
[3]Center for Integrative Biology, Faculty of Sciences, Universidad Mayor, Santiago 2422, Chile
[4]Geroscience Center for Brain Health and Metabolism, Santiago, Chile
[5]Unity Biotechnology Inc., South San Francisco, CA 94080, USA
[6]Department of Chemistry and Biochemistry, University of California, Santa Barbara, CA 93106, USA
[7]Lawrence Berkeley National Laboratory, University of California, Berkeley, CA 94720, USA
*Equal contribution
[#]Current affiliation: Institute for Research in Biomedicine, Barcelona Institute of Science and Technology, Barcelona 08028, Spain

Correspondence to: Judith Campisi; **email:** jcampisi@buckinstitute.org
Keywords: p21, p53, mouse dermal fibroblast, ionizing radiation, doxorubicin
Received: March 16, 2021 **Accepted:** May 18, 2021 **Published:** May 25, 2021

ABSTRACT

Cellular senescence is a cell fate response characterized by a permanent cell cycle arrest driven primarily the by cell cycle inhibitor and tumor suppressor proteins p16^{Ink4a} and p21$^{Cip1/Waf1}$. In mice, the p21$^{Cip1/Waf1}$ encoding locus, *Cdkn1a*, is known to generate two transcripts that produce identical proteins, but one of these transcript variants is poorly characterized. We show that the *Cdkn1a* transcript variant 2, but not the better-studied variant 1, is selectively elevated during natural aging across multiple mouse tissues. Importantly, mouse cells induced to senescence in culture by genotoxic stress (ionizing radiation or doxorubicin) upregulated both transcripts, but with different temporal dynamics: variant 1 responded nearly immediately to genotoxic stress, whereas variant 2 increased much more slowly as cells acquired senescent characteristics. Upon treating mice systemically with doxorubicin, which induces widespread cellular senescence *in vivo*, variant 2 increased to a larger extent than variant 1. Variant 2 levels were also more sensitive to the senolytic drug ABT-263 in naturally aged mice. Thus, variant 2 is a novel and more sensitive marker than variant 1 or total p21$^{Cip1/Waf1}$ protein for assessing the senescent cell burden and clearance in mice.

INTRODUCTION

The stringent cell growth arrest associated with cellular senescence is determined, among other mechanisms, by activities of cyclin-dependent kinase inhibitor proteins p16^{Ink4a} and p21$^{Cip1/Waf1}$, encoded by the *Cdkn2a* and *Cdkn1a* loci, respectively [1]. The increased expression of these proteins is a major hallmark of senescence in most cells, and therefore have become markers of senescence both in culture and *in vivo*. Consistent with the fact that senescent cells increase with age in many mouse and human tissues, *Cdkn2a* (p16^{Ink4a}) mRNA levels also increase with age in these tissues [2]. Based on this association, transgenic mice have been generated

to detect [3] and selectively eliminate senescent cells *in vivo* [4, 5]. By contrast, despite having a key role in the senescence growth arrest, *Cdkn1a*/p21$^{Cip1/Waf1}$ upregulation during aging is often moderate or absent *in vivo*, and tissue-dependent [2, 6–8]. For example, p21$^{Cip1/Waf1}$ reporter mouse have shown increased reporter activity only in kidneys of 23.5 month-old mice [9]. Further, in most tissues, calorie restriction does not prevent the age-related increase in *Cdkn1a* expression, in contrast to *Cdkn2a* expression [7]. Consequently, the role of *Cdkn1a*/p21$^{Cip1/Waf1}$ as an *in vivo* marker of aging or cellular senescence remains uncertain.

Two transcript variants are currently annotated for the murine *Cdkn1a* gene (Figure 1A). The better-studied mRNA (*Cdkn1a* transcript variant 1, NM_007669.5, hereafter termed p21var1) contains three exons, the two latter of which encode the p21$^{Cip1/Waf1}$ protein. An alternative transcript (*Cdkn1a* transcript variant 2, NM_001111099.2, hereafter termed p21var2) differs from p21var1 in the first exon and therefore contains an almost entirely different 5' untranslated region (UTR), despite encoding the same protein [10]. Additionally, the p21var2 transcription start site (TSS) lies ~2.8 kb upstream of p21var1, and thus might be subject to regulation by elements not present in p21var1. Interestingly, the p21var2 is generally less abundant than p21var1, but the translation of the p21var2 transcript increases under nutrient stress; consequently, the relative contribution of each variant to the total pool of p21$^{Cip1/Waf1}$ protein likely varies depending on stress and possibly other conditions [11]. To date, possible changes in the expression of *Cdkn1a* transcript-specific variants during age or cellular senescence have not been explored.

To fill this gap in our knowledge, we explored the expression levels of each *Cdkn1a* transcript variant in several tissues from aged mice. We also analyze their expression levels in a cell culture model of mouse cells subjected to genotoxic stress-induced senescence to evaluate their relative utility as senescence markers both in culture and *in vivo*. Finally, we show that well-established regulators of *Cdkn1a* expression have variant-specific effects, which add a novel level of complexity to the biological roles of p21$^{Cip1/Waf1}$.

RESULTS

Cdkn1a transcript variant 2 is preferentially induced with age

To assess expression levels of the individual *Ckdn1a* mRNA transcript variants, we designed two primer sets in which the forward primers hybridize with the variant-specific first exons (Figure 1A). To determine whether differential regulation occurs during aging *in vivo*, we analyzed liver samples from male mice at 2, 11, 23, 25 and 30 months of age. Relative to 2 month-old mice, p21var2, but not p21var1, increased after 20 months of age (Figure 1B). We then obtained additional tissues from 2 and 24 month-old male and female animals (n = 12-15 per sex and age). p21var2 levels were higher than p21var1 levels in aged liver, white adipose tissue, kidney, heart and lung (Figure 1C–1G). Steady-state levels of p21var1 remained unaltered with age, and were even slightly reduced with age in liver. On average, p21var2 abundance increased 3-fold with age in liver, kidney and adipose tissue, and 2-fold in heart and lung. Mice at 4 months of age used as young control yielded equivalent results (data not shown). The transcript encoding p16^{Ink4a} also increased with age in all these tissues (Supplementary Figure 1A–1E).

When males and females were analyzed separately, p21var2 increased with age in all tissues and in both sexes (Supplementary Figure 2A–2J), with the only exception of heart in male mice, where the upwards trend did not reach statistical significance (Supplementary Figure 2D). Of note, we detected higher p21var1 levels in the kidney of aged females (Supplementary Figure 2H). Despite the propensity of p21var2 to increase with age, overall, in all organs tested, p21var1 was more abundant than p21var2, as reported [10]. In sum, p21var2 expression is consistently elevated with age, in contrast with an absence of age-related change in p21var1 levels.

Both *Cdnk1a* transcript variants are induced in cellular senescence

To determine whether either transcript variant is preferentially upregulated in senescent cells, we induced senescence in primary mouse dermal fibroblasts (MDFs) using 15 GY ionizing radiation (IR), which induces a senescence response in virtually all the irradiated cells. Seven days later, irradiated, but not sham-irradiated, MDFs showed hallmarks of senescence, including increased levels of the mRNA encoding p16^{Ink4a} and lower levels of the mRNA encoding lamin-B1, as expected [12] (Supplementary Figure 3A–3B). The levels of both p21var1 and p21var2 also increased. However, as reported [10], p21var2 levels were 6- to 8-fold lower compared to p21var1 (data not shown). These data show that both of the murine *Ckdn1a* transcript variants are valid readouts to evaluate cellular senescence in cultured MDFs.

We then tested the dynamics of *Cdkn1a* variant expression in MDFs after irradiation. Expression of p21var1 increased 3 hours after irradiation, then progressively declined to a level twice that of baseline

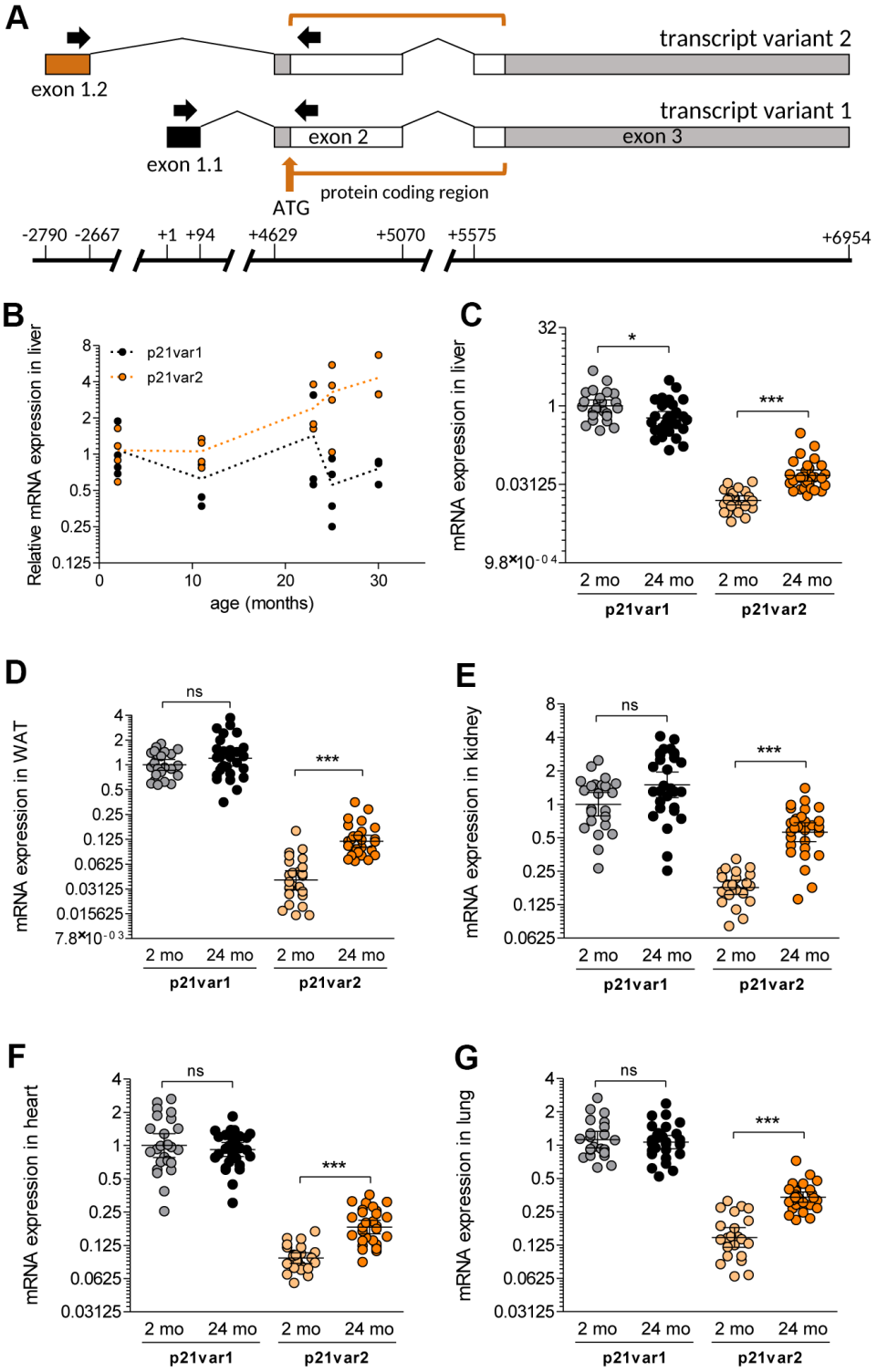

Figure 1. The *Cdkn1a* variant 2 transcript is preferentially induced during aging. (**A**) We designed primers (black arrows) to specifically detect *Cdkn1a* variant 1 and 2 transcripts, spanning the first and second exons in each case. The protein-coding region is indicated as well as the ATG start codon (brown arrow). Transcription starts at +1 for p21var1 and at -2790 for p21var2. The first and last bases of each exon are also indicated. (**B**) mRNA levels of p21var1 and p21var2 in the livers of male mice aged 2 to 30 months of age, normalized to levels in livers of 2 month-old animals. (**C–G**) Levels of each *Cdkn1a* transcript were assessed in 2 (young) and 24 (old) month-old mice. Animals were young males (n = 12), young females (n = 12), old males (n =14-15) and old females (n = 14-15). Results are shown for (**C**) liver, (**D**) adipose tissue, (**E**) kidney, (**F**) heart and (**G**) lung. In (**C–G**) data were normalized to p21var1 levels in young mice. Note Y axes are log-2 scales. 1-way ANOVA and Tukey post-tests were applied. * $p < 0.05$, ** $p < 0.01$, *** $p < 0.001$, ns = not-significant.

by 12 hours after irradiation. In contrast, p21var2 levels remained unaltered for the first 24 hours after irradiation (Figure 2A). Thereafter, both *Cdkn1a* variants steadily increased from day 3, without reaching a plateau by the end of the 12-day time course. Establishment of senescence was verified by increased p16^{Ink4a} and decreased lamin B1 mRNA levels (Figure 2B). Treatment of MDFs with 250 nM doxorubicin (doxo), a chemotherapeutic agent known to cause cellular senescence in culture and *in vivo* [13], increased p21var1 levels within the 24 hours, followed by a smaller increase in p21var2 levels (Figure 2C). Similar to the pattern in irradiated cells, from day 5 onwards both variants were coordinately and increasingly upregulated, concomitant with senescence-associated changes in p16^{Ink4a} and lamin B1 expression (Figure 2D). Together, our results show that p21var1 increases preferentially shortly after acute genotoxic stress, but both variants gradually rise as cells enter a senescent state.

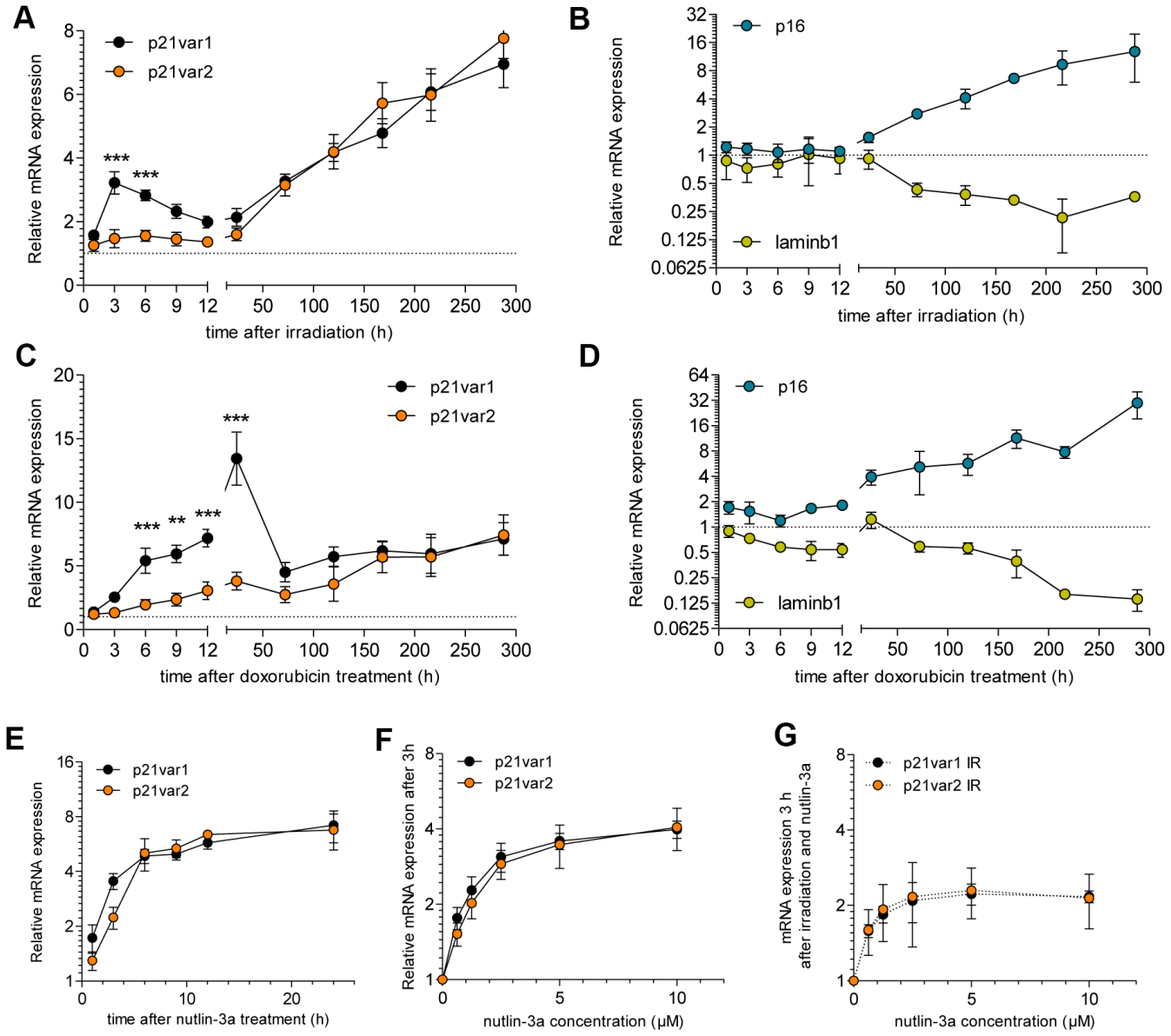

Figure 2. *Cdkn1a* variant 2 increases as cells acquire senescent phenotypes in culture. Time course of (**A**) p21var1 and p21var2 levels and (**B**) p16^{Ink4a} and lamin B1 mRNA levels after 15 Gy irradiation. 2-way ANOVA test was applied. Time course of (**C**) p21var1 and p21var2 levels and (**D**) p16^{Ink4a} and lamin B1 levels after a 24 h exposure to 250 nM doxorubicin. 2-way ANOVA test was applied. (**E**) p21var1 and p21var2 levels in MDFs after treatment with 10 μM nutlin-3a. (**F**) mRNA levels 3 hours after treatment with increasing doses of nutlin-3a. (**G**) mRNA levels 3 hours after irradiation (15 Gy) and treatment with increasing doses of nutlin-3a. Mean ± SEM is shown. Note Y axes are log-2 scales. * $p < 0.05$, ** $p < 0.01$, *** $p < 0.001$.

p53 stabilization upregulates both *Cdkn1a* transcript variants

The basal expression of p21var1 and p21var2 is differentially regulated by p53, likely due to the proximity of the p21var2 transcription start site (TSS) to a p53-response elements (p53-Res) [10]. We performed a promoter analysis (TRANSFAC version 2018.3) for both *Cdkn1a* TSSs, spanning 2.5 kb upstream and 0.5 kb downstream of each TSS (Supplementary Information). Among a plethora of predicted transcription factor binding sites, p53-REs were detected within 500 bases upstream of both TSSs, even when we applied the most stringent algorithm. To understand the p53 responsiveness of the *Cdkn1a* transcript variants, we treated MDFs with 10 μM nutlin-3a, an MDM-2 inhibitor that stabilizes p53 [14]. The levels of both variants increased within 1 hour, reaching a plateau approximately 12 hours later (Figure 2E). Lower concentrations of nutlin-3a failed to reveal any sensitivity differences between the variants. Three hours after treatment, the dose-response curves were similar in shape for both *Cdkn1a* transcripts (Figure 2F). The same was true for senescent (irradiated) MDFs treated with 10 μM nutlin-3a (Figure 2G). These results suggest that p21var1 and p21var2 are equally sensitive to transcriptional upregulation upon p53 stabilization.

Circadian regulation of $p21^{Cip1/Waf1}$ does not involve transcript variant 2

To further explore the expression pattern of p21var2 *in vivo*, we asked whether it is subject to circadian regulation, as described for $p21^{Cip1/Waf1}$ [15]. We euthanized 2 month-old male mice at 3 hour intervals for 12 hours. In liver samples, p21var1 mRNA levels were highest at the end of the dark cycle (6:00 am Pacific time) and progressively decreased 8-fold to a minimum in the afternoon (Figure 3A). The p21var2 remained unaltered, at lower levels, throughout the same period. A similar pattern was observed in adipose and kidney tissue (Figure 3B, 3C). These results indicate that the circadian regulation of $p21^{Cip1/Waf1}$ is driven solely by expression of *Cdkn1a* transcript variant 1.

Expression of p21var2 *in vivo* is increased by doxorubicin and decreased by ABT-263

To determine how *Cdkn1a* transcript variants are expressed when cellular senescence is induced *in vivo*, we induced cellular senescence *in vivo* by intraperitoneal injection of a single dose (10 mg/kg) of doxorubicin. After 6 weeks, p21var1 increased 3-fold while p21var2 increased 25-fold (reaching levels comparable to those of p21var1 at baseline) in the livers of treated mice (Figure 3D and Supplementary Figure 4A, 4B). Similar elevations were observed in the adipose tissue and kidneys (Figure 3E, 3F and Supplementary Figure 4C–4F) of male and female mice, consistent with the widespread luminescence reported in doxorubicin-treated p21-reporter mice [9]. Our data suggest that p21var2 is a more sensitive readout for doxorubicin-induced senescence *in vivo* than p21var1.

ABT-263 (navitoclax) has been shown to clear senescent cells by inhibiting Bcl-2 and related anti-apoptotic proteins [16, 17]. In a mixed cohort of 20-22 month-old male and female mice, ABT-263 specifically reduced p21var2 levels in adipose tissue and kidney, whereas p21var1 levels remained unaltered (Figure 3H–3L). There were no significant changes in the levels of either variant in liver (Figure 3G). Together, these results reinforce the idea p21var2 is a better marker than p21var1 for assessing the presence of senescent cells *in vivo*.

DISCUSSION

Cdkn1a transcript variant 2 has received little attention since it was first described, likely because the encoded protein is identical to that encoded by variant 1, and both variants are regulated by p53. Our results are, to our knowledge, the first to study *Ckdn1a* transcript variants in the context of aging. We show that, although tissue-specific exceptions may arise, p21var2 but not p21var1 is a better candidate marker of aging and senescence in mice.

Our findings help explain previous reports regarding changes in $p21^{Cip1/Waf1}$ with age. Thus, given the architecture of the promoters for both transcript variants, a $p21^{Cip1/Waf1}$ reporter mouse that included 2.5 kb of the *Cdkn1a* upstream sequence [9] would not detect p21var2, unlike a reporter mouse containing 4.5 kb of *Cdkn1a* upstream sequences [18] or a knock-in $p21^{FLuc}$ reporter mouse [19]. In line with our data, the reporter mouse containing 2.5 kb of the *Cdkn1a* promoter did not detect an age-related increase in expression, except for the kidney, in which we also observed an increase in p21var1 levels in old females. Our findings clarify the interpretation of previous and future results on the age-related changes in expression of this locus.

Key to understanding the biological context of *Cdkn1a* transcriptional regulation is the different circadian expression pattern between both transcript variants. Thus, comparisons among previous studies may be confounded by an absence of data regarding the time of euthanasia, a limitation that could be, in principle, avoided by measuring p21var2. In the liver, the wide

circadian oscillation of p21var1 contrasts with the more subtle age-related changes in p21var2. This disconnect suggests that p21var1 would be, in accordance to its higher relative contribution to the *Cdkn1a* mRNA pool, the main source of $p21^{Cip1/Waf1}$ for homeostatic functions [9], whereas p21var2 could be more selectively responsive to stress signals and ultimately more reflective of cellular senescence *in vivo*.

Our data do not explain why an increase in p21var2, but not p21var1, which is also observed in cultured senescent cells, is detected in aged animals. One possibility is that some transcriptional modulators are evident *in vivo*, but not necessarily in cultured cells. In addition, there may be cell type-specific expression of *Cdkn1a* variants in senescent cells. Our data show that p53 stabilization cannot explain the expression dynamics of *Cdkn1a* variants upon genotoxic-stress. However, the differences between the variant promoters, of which our analysis provides only an initial hint, may well affect which variant is expressed under different circumstances.

A recent report describes how the dynamics of $p21^{Cip1/Waf1}$ levels in response to DNA damage determine whether cancer cells enter a permanent cell

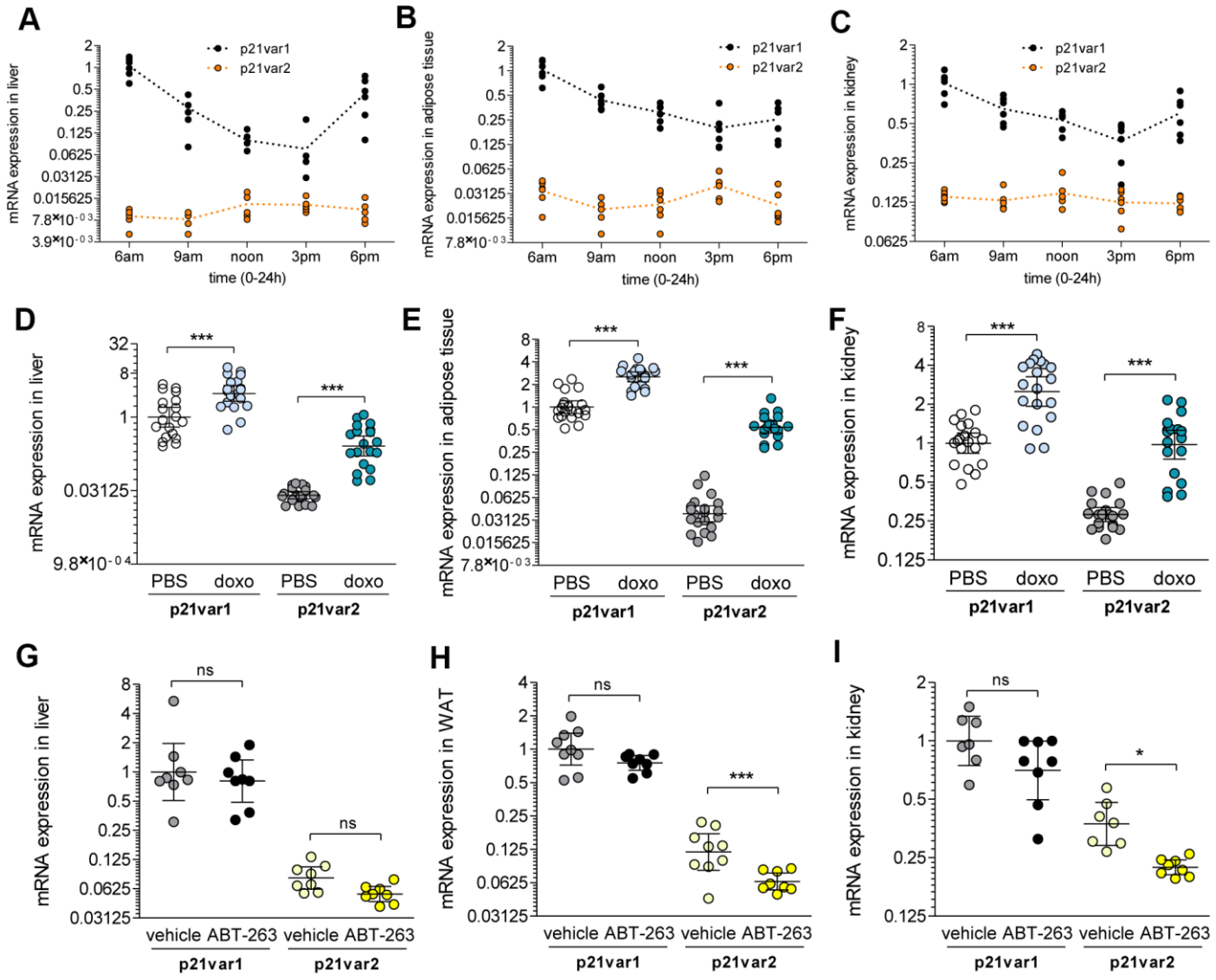

Figure 3. *Cdkn1a* variant 1 is circadian regulated, whereas variant 2 rises with senescence *in vivo*. (**A**) *Cdkn1a* variants expression throughout the light cycle (6 am to 6 pm) in the liver, (**B**) white adipose tissue and (**C**) kidney of 6 week-old male mice. (**D**–**F**) A cohort of 6 week-old mice were treated with doxorubicin or vehicle (n = 9-10 for either males or females, n = 9-10 for either vehicle or doxorubicin) and *Cdkn1a* variant levels were analyzed 6 weeks later. Results are shown for (**D**) liver, (**E**) adipose tissue and (**F**) kidney. (**G**–**I**) A cohort of 18 to 22 month-old mice were treated with ABT-263 or vehicle. Pooled results are shown for (**G**) liver, (**H**) adipose tissue and (**I**) kidney. 1-way ANOVA and Tukey post-tests were applied. * $p < 0.05$, ** $p < 0.01$, *** $p < 0.001$, ns = not significant.

cycle arrest or return to proliferation [20]. It remains unexplored the possibility that the different transcript variants are preferentially associated with one or other cell fate. Additionally, translational regulation at the 5' UTR of the variants has been shown to affect cell fate [11, 21]. Human cells also express several *Cdkn1a* transcript variants [22]. Among the ten human transcript variants currently annotated, at least one (transcript variant 4) shares translational regulatory mechanisms with the murine p21var2 [21]. Interestingly, even though murine variant 2 and human variant 4 do not appear to share sequence homology, the translational regulation in both transcripts is driven by the integrated stress response and results in cell cycle arrest [21]. The potential relevance of this mechanism for cellular senescence in humans remains unknown, and the functions and interrelations of the different *Cdkn1a* transcript variants have not been studied in depth. Our findings may thus lead to a better understanding of the age-related functions of p21 and improve our ability to monitor the effectiveness of anti-aging therapies.

MATERIALS AND METHODS

Mouse models

Animal husbandry

C56BL/6 mice were purchased from The Jackson Laboratory and allowed to acclimate to the Buck Institute facilities. The animals were group housed under controlled conditions of temperature (22-24° C), humidity (40-60%), and a 12 h light-dark cycle. All animal procedures were approved by the Buck Institute Institutional Animal Care and Use Committee (IACUC).

Aging cohorts

C56BL/6 were aged at the Buck Institute vivarium and male and female littermates derived from the same colony were used as young controls.

Doxorubicin treatment

6-week old male and female C57BL/6 littermates were intraperitoneally (IP) injected with a single dose of doxorubicin (10 mg/kg) to induce widespread senescence [13]. After 6 weeks, the animals were euthanized by CO_2 inhalation followed by cervical dislocation, and tissues were harvested and flash frozen in liquid nitrogen.

ABT-263 treatment

ABT-263 or vehicle (5% DMSO, 95% corn oil) was delivered to 20-month old C57BL/6 littermates via IP injection at 50 mg/kg for 7 consecutive days per cycle for two cycles, with a 2-week interval between cycles. Animals were sacrificed one week after the last treatment cycle and tissues were collected and flash frozen in liquid nitrogen.

Cell culture

Mouse dermal fibroblasts

Primary mouse dermal fibroblasts (MDF) were obtained from postnatal day 2-3 C57BL/6 mice. Skin was excised from the mice and incubated overnight in 0.25% trypsin-EDTA. The dermis was mechanically disengaged and incubated with 10 mg/ml collagenase for 30 min at room temperature. The mixture was filtered and plated. MDF were cultured in 3% oxygen in Dulbecco's modified Eagle's medium (DMEM) with 10% fetal bovine serum and 100 U/ml streptomycin and penicillin.

Irradiation and doxorubicin treatment

MDFs were induced to senesce by X-irradiation (15 Gy), as described [23], or mock-irradiated (control). Alternatively, MDF were treated with 250 nM doxorubicin or vehicle (DMSO, control) for 24 h, then washed and cultured in fresh complete medium. Senescence markers were tested at different times (1, 3, 6, 9, 12 h and 1, 3, 5, 7, 9, 12 days) after treatment.

Nutlin-3a treatment

MDFs were incubated with 10 μM nutlin-3a or vehicle (DMSO, control) and RNA was collected 1, 3, 6, 9, 12 and 24 h later. MDFs were also treated with different nutlin-3a concentrations (0.6-10 μM), irradiated (15 Gy X-rays) or mock-irradiated and RNA collected 3 h later.

RNA extraction and RT-qPCR

RNA was extracted using Tri-reagent and isolated with the Direct-Zol RNA miniprep kit (Genesee Scientific). For adipose tissue, the RNeasy Lipid Tissue mini kit (Qiagen) was used. cDNA was synthesized using the High Capacity cDNA RT kit (Life Technologies). Transcripts were analyzed using a Roche LightCycler 480 II in 384-well plates and the UPL probe system. Bioline SensiFast Probe No-ROX was used as a master mix. Primer sequences and respective probes were as follows: Cdkn2a (p16), forward 5'-TCCTCGCAGTTCGAATCTG, reverse 5'-AACTCTTTCGGTCGTACCCC, with a custom designed probe (5'- /56-FAM/AGG TGA TGA /ZEN/TGA TGG GCA ACG TTC AC/3IABkFQ/ -3'); *Cdkn1a* (p21) variant 1, forward 5'-TCCACAG CGATATCCAGACA, reverse 5'-GGACATCACCA GGATTGGAC, with UPL probe 21; *Cdkn1a* (p21) variant 2, forward 5'-TTGCCAGCAGAATAAA AGGTG, reverse 5'-TTTGCTCCTGTGCGGAAC, with UPL probe 9; β-actin: forward 5'- CTAAG GCCAACCGTGAAAAG, reverse 5'- ACCAGAGG

CATACAGGGACA, with UPL probe 64; tubulin: forward 5'- CTGGAACCCACGGTCATC, reverse 5'- GTGGCCACGAGCATAGTTATT, UPL probe 88. Results were normalized to β-actin and tubulin. ΔΔCt values prior to logarithmic transformation were used for statistical analyses.

Promoter analysis

Transcription factor binding sites were analyzed using TRANSFAC version 2018.3 (geneXplain) and sequences between -2500 and +500 for each variant. For each variant, two analyses were performed, either minimizing false positives (minFP) or balancing false positives and false negatives (minSUM), using algorithms provided by the software.

Statistical analysis

Unless otherwise noted, results are shown as individual data points with geometric means and 95% CIs. Comparisons between multiple groups were analyzed using 1-way ANOVA with Tukey post-tests, or 2-way ANOVA with Bonferroni post-tests if a second variant (usually time) was present. No statistical outliers were removed.

AUTHOR CONTRIBUTIONS

J.A.L.-D., S.R.L. and U.A.C performed the experimental work. M.K. performed the *in vivo* ABT-263 experiment. J.A.L.-D., U.A.C, R.-M.L. P.-Y.D. and J.C. designed experiments and interpreted the results. J.M.V. and C.C. contributed to interpretation of the results. J.A.L.-D., P.-Y.D. and J.C. wrote the paper.

CONFLICTS OF INTEREST

J.C. is a cofounder of Unity Biotechnology, which is developing senolytic agents. R.-M.L. and J.C. are co-inventors on patent applications licensed to or filed by Unity Biotechnology.

FUNDING

This work was supported by the Spanish Ministry of Economy project grant BFU2015-64630-R and pre-doctoral fellowship BES-2016-078229, and by UNITY Biotechnology.

REFERENCES

1. Campisi J, d'Adda di Fagagna F. Cellular senescence: when bad things happen to good cells. Nat Rev Mol Cell Biol. 2007; 8:729–40. https://doi.org/10.1038/nrm2233 PMID:17667954

2. Krishnamurthy J, Torrice C, Ramsey MR, Kovalev GI, Al-Regaiey K, Su L, Sharpless NE. Ink4a/Arf expression is a biomarker of aging. J Clin Invest. 2004; 114:1299–307. https://doi.org/10.1172/JCI22475 PMID:15520862

3. Sorrentino JA, Krishnamurthy J, Tilley S, Alb JG Jr, Burd CE, Sharpless NE. p16INK4a reporter mice reveal age-promoting effects of environmental toxicants. J Clin Invest. 2014; 124:169–73. https://doi.org/10.1172/JCI70960 PMID:24334456

4. Demaria M, Ohtani N, Youssef SA, Rodier F, Toussaint W, Mitchell JR, Laberge RM, Vijg J, Van Steeg H, Dollé ME, Hoeijmakers JH, de Bruin A, Hara E, Campisi J. An essential role for senescent cells in optimal wound healing through secretion of PDGF-AA. Dev Cell. 2014; 31:722–33. https://doi.org/10.1016/j.devcel.2014.11.012 PMID:25499914

5. Baker DJ, Wijshake T, Tchkonia T, LeBrasseur NK, Childs BG, van de Sluis B, Kirkland JL, van Deursen JM. Clearance of p16Ink4a-positive senescent cells delays ageing-associated disorders. Nature. 2011; 479:232–36. https://doi.org/10.1038/nature10600 PMID:22048312

6. Baker DJ, Childs BG, Durik M, Wijers ME, Sieben CJ, Zhong J, Saltness RA, Jeganathan KB, Verzosa GC, Pezeshki A, Khazaie K, Miller JD, van Deursen JM. Naturally occurring p16(Ink4a)-positive cells shorten healthy lifespan. Nature. 2016; 530:184–89. https://doi.org/10.1038/nature16932 PMID:26840489

7. Edwards MG, Anderson RM, Yuan M, Kendziorski CM, Weindruch R, Prolla TA. Gene expression profiling of aging reveals activation of a p53-mediated transcriptional program. BMC Genomics. 2007; 8:80. https://doi.org/10.1186/1471-2164-8-80 PMID:17381838

8. Hudgins AD, Tazearslan C, Tare A, Zhu Y, Huffman D, Suh Y. Age- and Tissue-Specific Expression of Senescence Biomarkers in Mice. Front Genet. 2018; 9:59. https://doi.org/10.3389/fgene.2018.00059 PMID:29527222

9. Ohtani N, Imamura Y, Yamakoshi K, Hirota F, Nakayama R, Kubo Y, Ishimaru N, Takahashi A, Hirao A, Shimizu T, Mann DJ, Saya H, Hayashi Y, et al. Visualizing the dynamics of p21(Waf1/Cip1) cyclin-dependent kinase inhibitor expression in living animals. Proc Natl Acad Sci USA. 2007; 104:15034–39. https://doi.org/10.1073/pnas.0706949104 PMID:17848507

10. Gartel AL, Radhakrishnan SK, Serfas MS, Kwon YH, Tyner AL. A novel p21WAF1/CIP1 transcript is highly dependent on p53 for its basal expression in mouse tissues. Oncogene. 2004; 23:8154–57. https://doi.org/10.1038/sj.onc.1207820 PMID:15361845

11. Lehman SL, Cerniglia GJ, Johannes GJ, Ye J, Ryeom S, Koumenis C. Translational Upregulation of an Individual p21Cip1 Transcript Variant by GCN2 Regulates Cell Proliferation and Survival under Nutrient Stress. PLoS Genet. 2015; 11:e1005212. https://doi.org/10.1371/journal.pgen.1005212 PMID:26102367

12. Freund A, Laberge RM, Demaria M, Campisi J. Lamin B1 loss is a senescence-associated biomarker. Mol Biol Cell. 2012; 23:2066–75. https://doi.org/10.1091/mbc.E11-10-0884 PMID:22496421

13. Demaria M, O'Leary MN, Chang J, Shao L, Liu S, Alimirah F, Koenig K, Le C, Mitin N, Deal AM, Alston S, Academia EC, Kilmarx S, et al. Cellular Senescence Promotes Adverse Effects of Chemotherapy and Cancer Relapse. Cancer Discov. 2017; 7:165–76. https://doi.org/10.1158/2159-8290.CD-16-0241 PMID:27979832

14. Kojima K, Konopleva M, McQueen T, O'Brien S, Plunkett W, Andreeff M. Mdm2 inhibitor Nutlin-3a induces p53-mediated apoptosis by transcription-dependent and transcription-independent mechanisms and may overcome Atm-mediated resistance to fludarabine in chronic lymphocytic leukemia. Blood. 2006; 108:993–1000. https://doi.org/10.1182/blood-2005-12-5148 PMID:16543464

15. Gréchez-Cassiau A, Rayet B, Guillaumond F, Teboul M, Delaunay F. The circadian clock component BMAL1 is a critical regulator of p21WAF1/CIP1 expression and hepatocyte proliferation. J Biol Chem. 2008; 283:4535–42. https://doi.org/10.1074/jbc.M705576200 PMID:18086663

16. Chang J, Wang Y, Shao L, Laberge RM, Demaria M, Campisi J, Janakiraman K, Sharpless NE, Ding S, Feng W, Luo Y, Wang X, Aykin-Burns N, et al. Clearance of senescent cells by ABT263 rejuvenates aged hematopoietic stem cells in mice. Nat Med. 2016; 22:78–83. https://doi.org/10.1038/nm.4010 PMID:26657143

17. Zhu Y, Tchkonia T, Fuhrmann-Stroissnigg H, Dai HM, Ling YY, Stout MB, Pirtskhalava T, Giorgadze N, Johnson KO, Giles CB, Wren JD, Niedernhofer LJ, Robbins PD, Kirkland JL. Identification of a novel senolytic agent, navitoclax, targeting the Bcl-2 family of anti-apoptotic factors. Aging Cell. 2016; 15:428–35 https://doi.org/10.1111/acel.12445 PMID:26711051

18. Vasey DB, Wolf CR, MacArtney T, Brown K, Whitelaw CB. p21-LacZ reporter mice reflect p53-dependent toxic insult. Toxicol Appl Pharmacol. 2008; 227:440–50. https://doi.org/10.1016/j.taap.2007.11.029 PMID:18215733

19. Tinkum KL, Marpegan L, White LS, Sun J, Herzog ED, Piwnica-Worms D, Piwnica-Worms H. Bioluminescence imaging captures the expression and dynamics of endogenous p21 promoter activity in living mice and intact cells. Mol Cell Biol. 2011; 31:3759–72. https://doi.org/10.1128/MCB.05243-11 PMID:21791610

20. Hsu CH, Altschuler SJ, Wu LF. Patterns of Early p21 Dynamics Determine Proliferation-Senescence Cell Fate after Chemotherapy. Cell. 2019; 178:361–73.e12. https://doi.org/10.1016/j.cell.2019.05.041 PMID:31204100

21. Collier AE, Spandau DF, Wek RC. Translational control of a human *Cdkn1a* mRNA splice variant regulates the fate of UVB-irradiated human keratinocytes. Mol Biol Cell. 2018; 29:29–41. https://doi.org/10.1091/mbc.E17-06-0362 PMID:29118075

22. Radhakrishnan SK, Gierut J, Gartel AL. Multiple alternate p21 transcripts are regulated by p53 in human cells. Oncogene. 2006; 25:1812–5. https://doi.org/10.1038/sj.onc.1209195 PMID:16261158

23. Rodier F, Coppé JP, Patil CK, Hoeijmakers WA, Muñoz DP, Raza SR, Freund A, Campeau E, Davalos AR, Campisi J. Persistent DNA damage signalling triggers senescence-associated inflammatory cytokine secretion. Nat Cell Biol. 2009; 11:973–9. https://doi.org/10.1038/ncb1909 PMID:19597488

SUPPLEMENTARY MATERIALS

Supplementary Figures

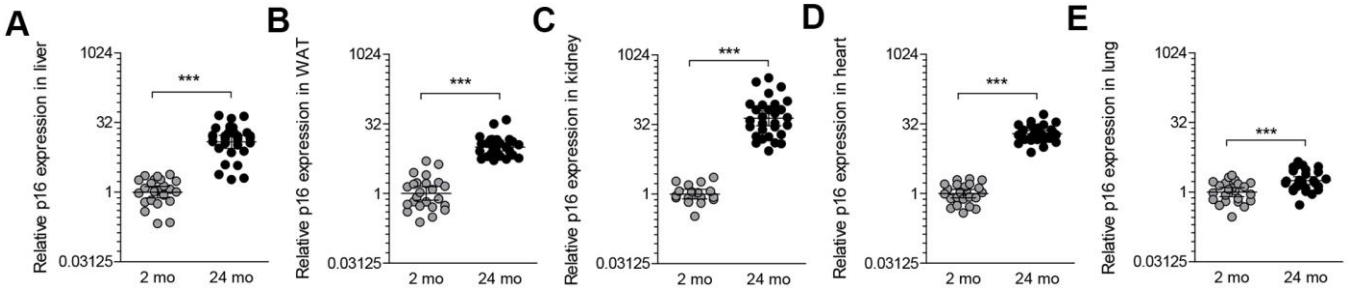

Supplementary Figure 1. p16^{Ink4a} mRNA levels increase with age in multiple tissues. mRNA levels were determined in (**A**) liver, (**B**) white adipose tissue, (**C**) kidney, (**D**) heart and (**E**) lung of 2 and 24 month old mice (n = 24-28). Males and females were pooled. Note Y axes are log-2 scales. t-tests were applied. *** $p < 0.001$.

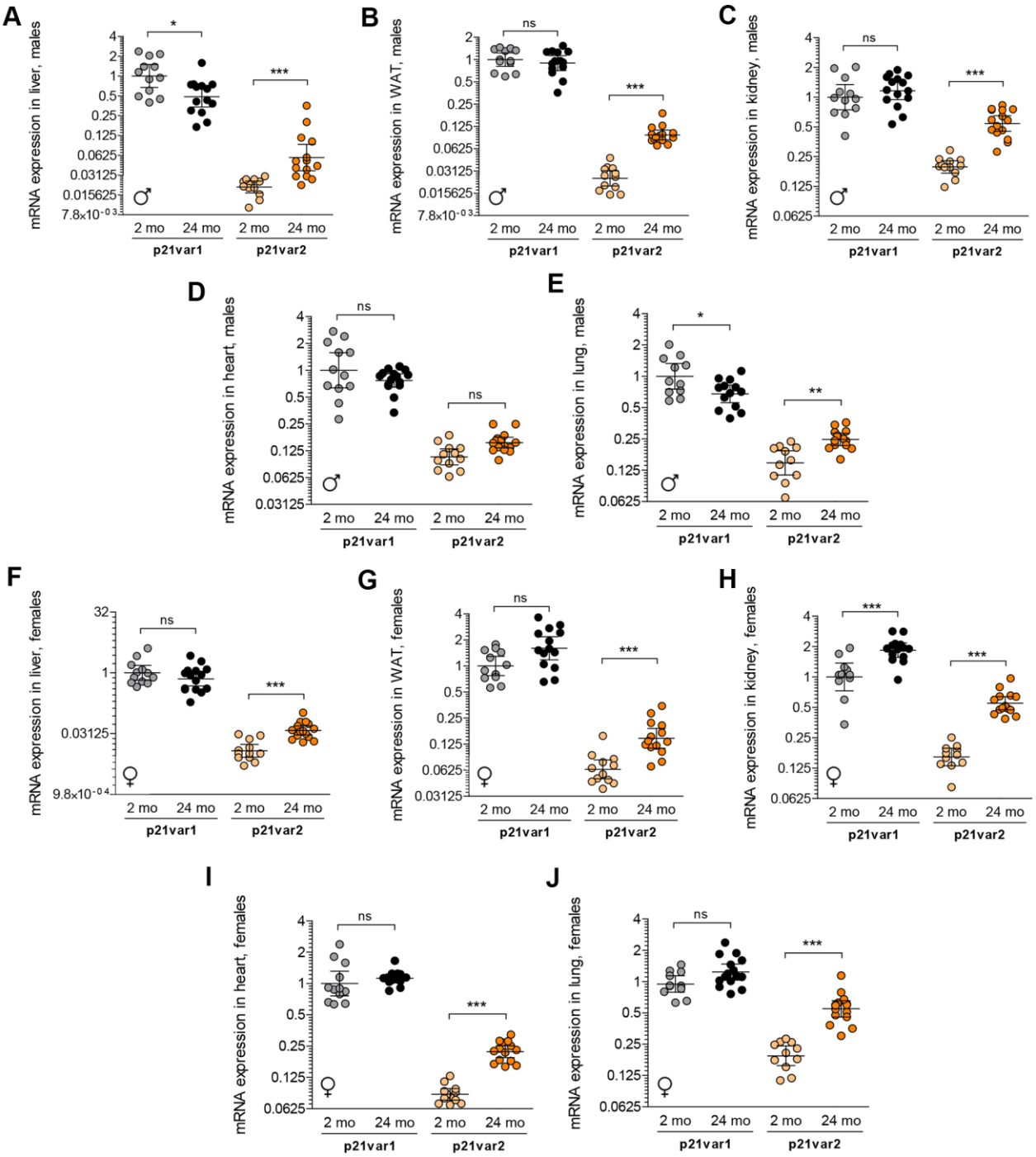

Supplementary Figure 2. *Cdkn1a* transcript variants in young and aged male and female mice. Levels of *Ckdn1a* variants in the (**A**) liver, (**B**) white adipose tissue, (**C**) kidney, (**D**) heart and (**E**) lung of male 2 and 24 month old mice from Figure 1. Expression levels in the (**F**) liver, (**G**) white adipose tissue, (**H**) kidney, (**I**) heart and (**J**) lung of female mice at the same ages. Note Y axes are log-2 scales. 1-way ANOVA and Tukey post-tests were applied. * $p < 0.05$, ** $p < 0.01$, *** $p < 0.001$, ns = not significant.

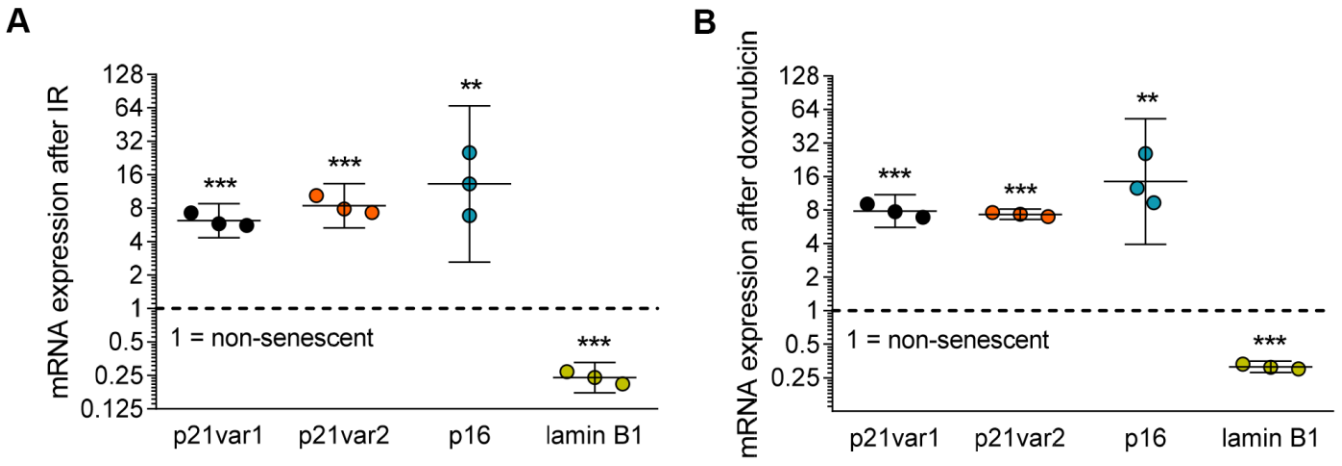

Supplementary Figure 3. Markers of senescence in cultured mouse dermal fibroblasts. (**A**) Levels of *Cdkn1a* transcript variants and p16Ink4a and lamin B1 mRNAs 7 days after irradiation (15 Gy). (**B**) Levels 7 days after a 24 h exposure to 250 nM doxorubicin. Note Y axes are log-2 scales. ** $p < 0.01$, *** $p < 0.001$ vs non-senescent control for each transcript (=1).

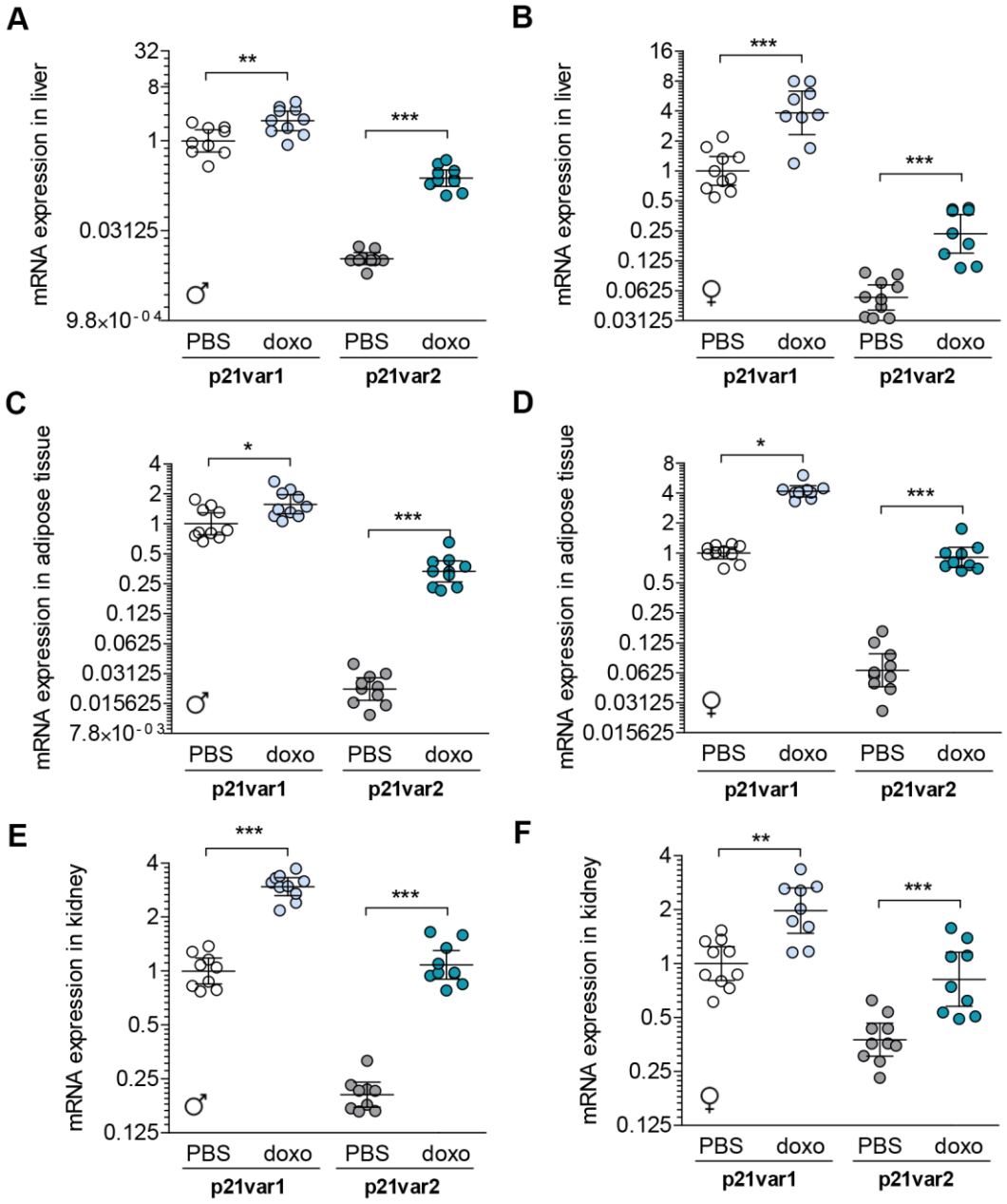

Supplementary Figure 4. *Cdkn1a* transcript variants in doxorubicin-treated male and female mice. Transcript levels were determined in (**A**, **B**) liver, (**C**, **D**) adipose tissue and (**E**, **F**) kidney of male or female 3.5 month old mice, 6 weeks after treatment with doxorubicin (n = 9-10 per sex or treatment). 1-way ANOVA and Tukey post-tests were applied. Note Y axes are log-2 scales. * $p < 0.05$, ** $p < 0.01$, *** $p < 0.001$, ns = not significant.

Research Paper

LHX9, a p53-binding protein, inhibits the progression of glioma by suppressing glycolysis

Xiangying Luo[1], Jianwei Ge[2], Tao Chen[3], Jinfang Liu[1], Ziyuan Liu[1], Changlong Bi[1], Song Lan[1]

[1]Department of Neurosurgery, XiangYa Hospital of Central South University, Changsha 410078, P.R. China
[2]Department of Neurosurgery, Renji Hospital, School of Medicine, Shanghai Jiaotong University, Shanghai 200127, P.R. China
[3]Department of Neurology, The First Affiliated Hospital of Guangzhou Medical University, Guangzhou 510120, P.R. China

Correspondence to: Song Lan; **email:** Lansong1988@csu.edu.cn
Keywords: LHX9, p53, glioma, glycolysis, PGK1
Received: November 24, 2020 **Accepted:** May 11, 2021 **Published:** September 17, 2021

ABSTRACT

Purpose: LHX9 methylation has been reported in many tumors, but its functions and related mechanisms in glioma are still unknown and need to be verified.
Methods: The protein level of LHX9 in glioma tissues was examined using western blotting and immunohistochemistry, and the functions of LHX9 in glioma cell lines were investigated using MTT and colony formation assays. In addition, the interaction between LHX9 and P53 was analyzed by immunoprecipitation, and the roles of LHX9 in cancer metabolism were explored by measuring metabolites.
Results: In this study, we found that the LHX9 expression level was decreased in glioma specimens, and the upregulation of LHX9 expression inhibited the growth of glioma cells in liquid medium and on soft agar. Regarding the molecular mechanism, we found that LHX9 interacted with p53, and downregulation of LHX9 promoted the expression of the glycolysis-related enzyme PGK1 and increased the lactic acid content. By interfering with the expression of LHX9, the tumorigenicity of glioma cells was promoted, an outcome blocked by further interference with PGK1 expression.
Conclusion: In summary, the decreased expression of LHX9 in gliomas activates the expression of the glycolysis-related enzyme PGK1, thereby promoting the development of gliomas, suggesting that the LHX9-PGK1 signaling axis can be used as a target for the treatment of glioma.

INTRODUCTION

In recent years, an increasing number of studies have shown that abnormally active glycolytic metabolism can significantly promote the proliferation and invasion abilities of tumor cells [1]. As the most common malignant tumor in the skull, glioma has glycolytic activity in tissues that is three-fold higher than that in normal brain tissues [2, 3]. However, the molecular basis and exact mechanism of this glycolysis remodeling remain to be investigated.

Phosphoglycerate kinase 1 (PGK1), an important rate-limiting enzyme in glycolysis, can catalyze the conversion of 3-phosphoglycerate to 3-phosphoglycerate phosphate [4]. In addition to cell metabolism regulation, PGK1 is involved in a variety of biological activities, including angiogenesis, autophagy and DNA repair [5–7]. With multiple functions, PGK1 is involved in very complicated mechanisms in the occurrence and development of tumors [8]. PGK1 is highly expressed and promotes the proliferation of tumor cells [9]. PGK1 is also

associated with radiochemotherapy resistance and poor prognosis [8]. Therefore, it is of great significance to investigate the regulatory mechanism of PGK1.

LHX9, LIM homeodomain (LIM-hd) transcription factor 9, is highly expressed in mesenchymal cells of the testis and ovary and plays important roles in determining the sex of animals and the differentiation of sex organs [10–13]. Valentina et al. found that LHX9 was also expressed in mouse embryonic brain tissues, especially in the diencephalon, the telencephalon, vesicles and the dorsal mesencephalon [13]. LHX9 consists of a linker region and two highly conserved cysteine-rich zinc finger structures that link to proteins [14]. According to their expression pattern and structural characteristics, LHX9-encoded transcription factors are very likely to control the differentiation fate of a variety of nerve cells [14–17].

Studies have shown LHX9 methylation in approximately 88% of high-grade gliomas and approximately 29% of nondiffuse fibroblastic astrogliomas [18]. In glioma tissues, LHX9 expression levels are significantly reduced [18]. Previous studies have shown that the expression of LHX9 significantly inhibits the migration and invasion of glioma cells [18]. However, other functions and mechanisms of LHX9 in glioma cells are still unknown.

In this study, we investigated novel functions of LHX9 in gliomas and LHX9 regulation of PGK1 and glycolysis.

RESULTS

Downregulation of LHX9 is associated with poor survival of glioma patients

To investigate the correlation between the expression pattern of LHX9 and the survival of glioma patients, we first searched public databases and analyzed the expression of LHX9 in glioma tissues (http://www.proteinatlas.org/ENSG00000143355-LHX9/pathology/glioma#ihc). As shown in Figure 1A, patients with high expression of LHX9 had a better prognosis. Then, we measured the expression of LHX9 in glioma tissues and paracarcinoma tissues. The experimental results showed negligible protein expression of LHX9 in most glioma tissues (Figure 1B, 1C). Consistent with this result, LHX9 was expressed at high levels in HEB normal human brain glial cells and at low levels in glioma cells (U87, SK-N-SH, A172, and SHG44 cells) (Figure 1D). These results suggest that LHX9 expression was downregulated in the gliomas.

LHX9 inhibited the growth and colony formation of glioma cells

To investigate the functions of LHX9 in glioma cells, we overexpressed flag-tagged LHX9 (Flag-LHX9) in glioma cells (Figure 2A) and measured the effect of LHX9 expression on the growth of glioma cells using MMT and soft agar assays. The results showed that upregulating the expression of LHX9 in glioma cells not only inhibited the growth of cells in liquid medium (Figure 2B) but also inhibited the anchorage-independent growth of glioma cells (Figure 2C, 2D). To confirm the roles of LHX9 in the proliferation of glioma cells, an EdU assay was performed. As shown in Figure 2E, 2F, overexpression of LHX9 decreased the percentage of EdU-positive cells (Figure 2E, 2F).

In addition, we investigated the biological functions of endogenously expressed LHX9 in gliomas. We knocked down the expression of LHX9 in SK-N-SH and A172 glioma cells (Figure 3A). The experimental results showed that downregulating the expression of LHX9 in SK-N-SH and A172 glioma cells accelerated the growth of the cells in liquid medium (Figure 3B) and colony formation on soft agar (Figure 3C, 3D).

Interaction of LHX9 and p53

To investigate the mechanism by which LHX9 regulates the growth and colony formation of glioma cells, we analyzed the interactions between LHX9 and a series of proteins involved in cell growth regulation. Figure 4A shows that the fusion protein GST-p53 interacted with endogenously expressed LHX9, as determined by the GST pull-down assay. In addition, coimmunoprecipitation assays showed that p53 and LHX9 formed a complex (Figure 4B, 4C). Subsequently, we constructed a series of p53 truncated mutants (Figure 4D), and these mutants were cotransfected with LHX9 into HEK293T cells. The experimental results showed that the DB (DNA binding) domain of p53 mediated its interaction with LHX9 (Figure 4E).

Downregulation of LHX9 expression activated glycolysis in tumor cells

P53 suppresses glycolysis of tumor cells. Considering the interaction between LHX9 and p53, we first investigated the effect of LHX9 on glycolysis in glioma cells. As shown in Figure 5A, hindered LHX9 expression led to the upregulated expression of PGK1. Knockdown of p53 induced the expression of PGK1, which was abolished by the overexpression of LHX9 (wild-type p53 in SK-N-SH cells and A172 cells) (Figure 5B). In the screening of the PGK1 promoter,

one-half of the P53-binding site sequence (AAGCAAG) was adjacent to the LHX9-binding site sequence (TTAACA) in the region from -655 bp to -668 bp (Figure 5C, left). This finding suggests the binding of P53 and LHX9 to the PGK1 promoter. Chromosome immunoprecipitation (ChIP) assays showed that p53 and LHX9 were bound to the PGK1 promoter at the same time (Figure 5C, right). However, interfering with LHX9 expression inhibited the binding of p53 to the PGK1 promoter, and vice versa (Figure 5D). Next, we investigated whether PGK1 mediated the biological functions of LHX9. In SK-N-SH cells with dampened LHX9 expression, interference of PGK1 expression restored the colony formation induced by the downregulation of LHX9 (Figure 5E, 5F). Moreover, interfering with the expression of LHX9 increased the lactic acid content, while interfering with the expression of PGK1 restored the lactic acid content (Figure 5G). To determine whether the promoting effects of LHX9 on the anchorage-independent growth of glioma cells were dependent on P53, we restored the expression of P53 in LHX9-knockdown cells. As shown in Figure 5H–5J, the restoration of P53 abolished the advantages of anchorage-independent growth and PGK1 expression caused by LHX9 knockdown.

Interfering with LHX9 expression promoted the tumorigenicity of glioma cells

Interfering with LHX9 promoted the growth of SK-N-SH cells in nude mice. Interfering with PGK1 restored the tumor volume and weight caused by downregulation

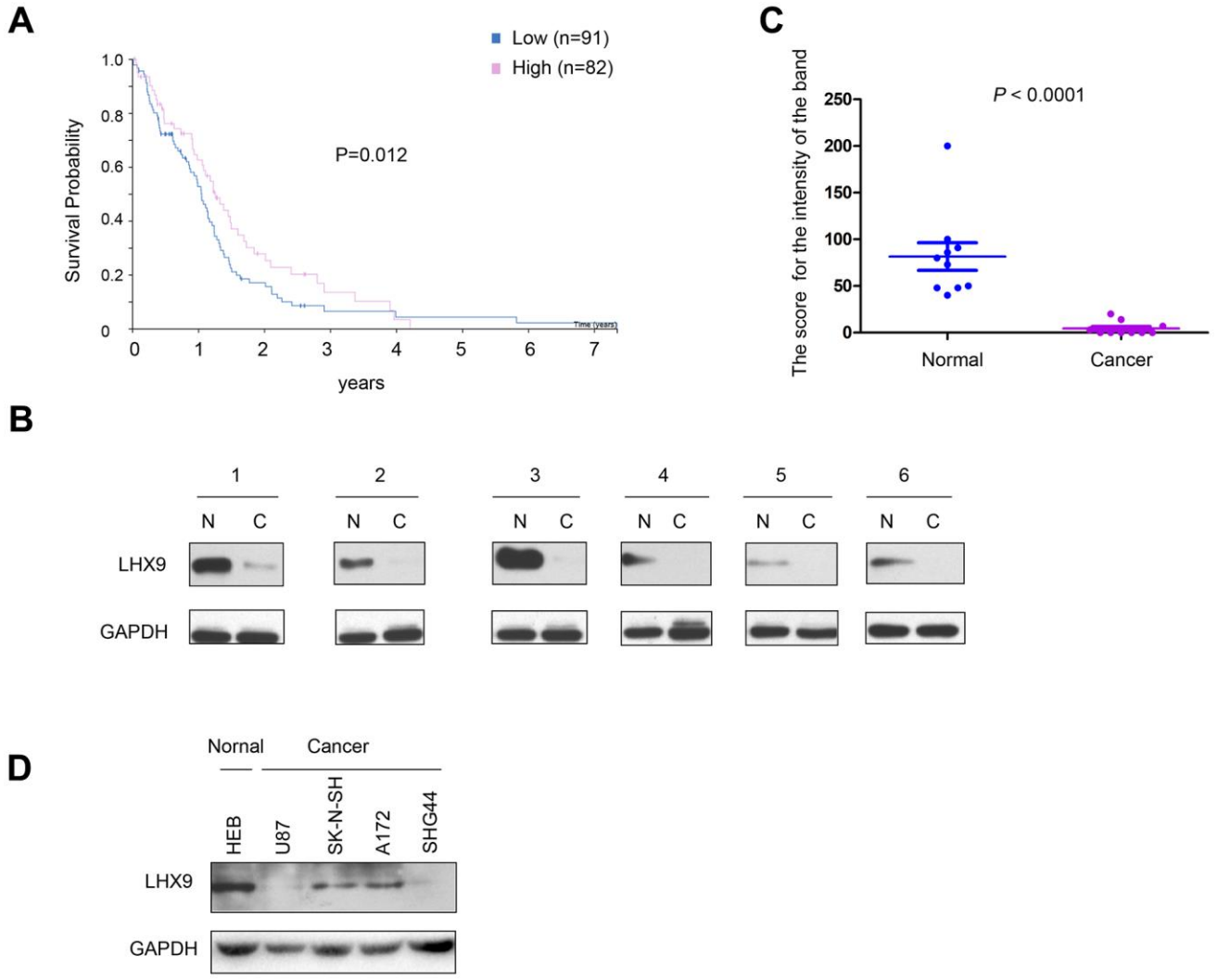

Figure 1. Down-regulation of LHX9 is associated with poorer survival of glioma patients. (**A**) GEPIA database analysis showed that LHX9 was positively correlated with survival time of patients. Patients with higher LHX9 expression levels survived better. (**B**, **C**) The expression levels of LHX9 in normal and glioma tissues were detected by Western blot, and quantified. (**D**) The expression levels of LHX9 in normal cells HEB and glioma cells were detected by Western blot.

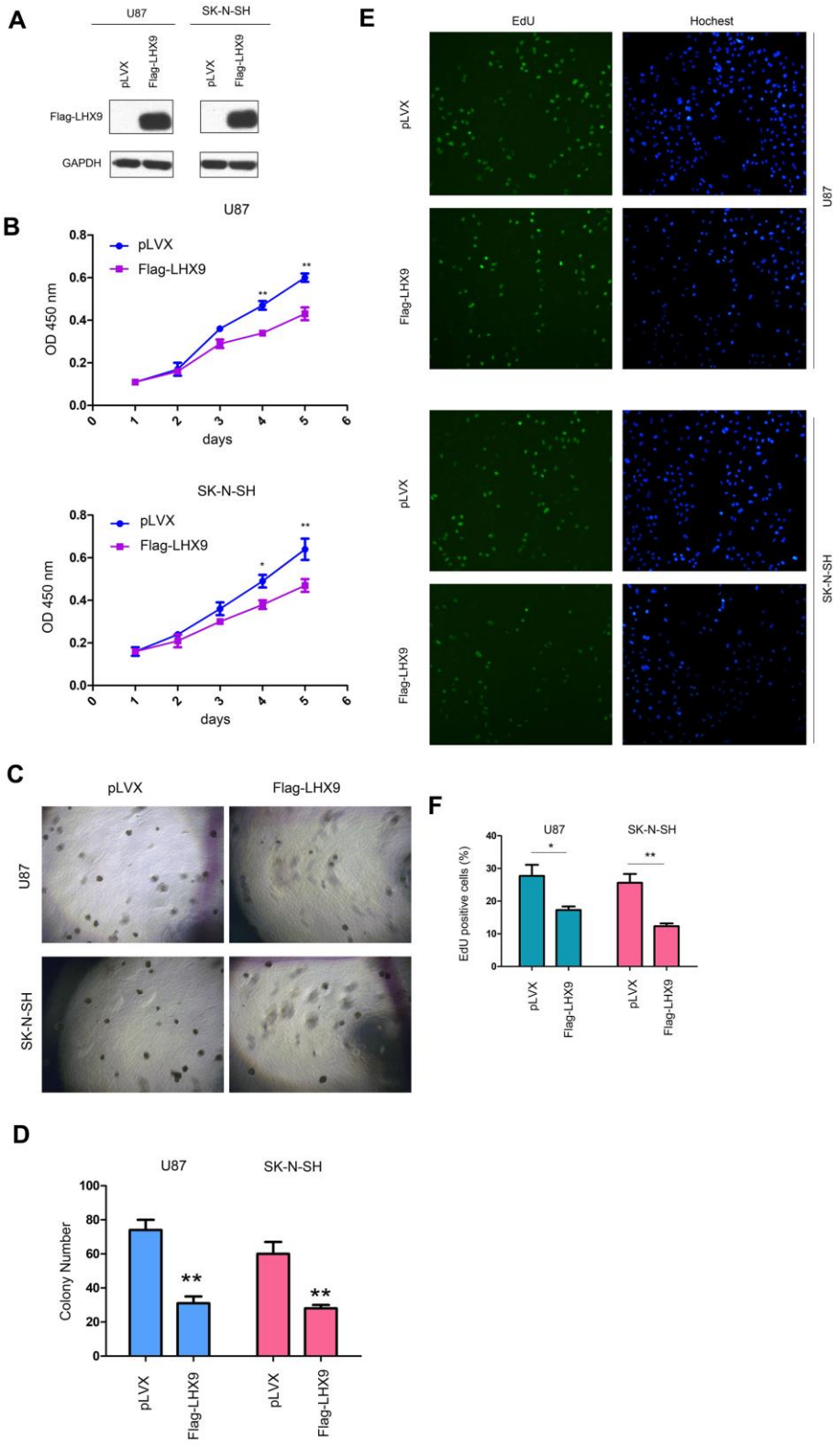

Figure 2. LHX9 overexpression inhibited the growth of glioma cells. (**A**) Overexpression of Flag-labeled LHX9 in U87 and SK-N-SH cells. Flag-LHX9 expression plasmid was transfected into U87 and SK-N-SH cells using lipofectamine 2000. Cells were screened with puromycin for 1 week, and then Flag-LHX9 expression was identified. (**B**) The effect of LHX9 expression on the growth of U87 and SK-N-SH cells was detected by CCK8 assay. (**C**, **D**) The effect of LHX9 expression on the anchorage-independent growth of U87 and SK-N-SH cells was detected by soft agar assay. (**E**, **F**) The EdU assay was performed. Details about the EdU assay were described in the "Materials and methods". *, $P<0.05$; **, $P<0.01$.

of LHX9 expression (Figure 6A–6C). We extracted proteins from the formed tumors to detect the expression of LHX9 and PGK1 (Figure 6D).

DISCUSSION

Gliomas are among the common malignancies in the skull [19]. Patients with gliomas have an extremely poor prognosis, and the need for new treatment methods is urgent [19]. Therefore, it is of significance to the treatment of glioma to study the molecular mechanism of glioma progression. Glycolysis is a basic feature of tumor cell metabolism [20, 21]. An in-depth analysis of the regulatory mechanism of glycolysis in glioma cells is expected to provide potential targets for the treatment of gliomas. In this study, we found that the transcription factor LHX9 was downregulated in gliomas. LHX9 interacted with p53 to inhibit the expression of PGK1, thereby inhibiting the progression of gliomas. This study suggests that PGK1 is very likely to be an important therapeutic target for gliomas.

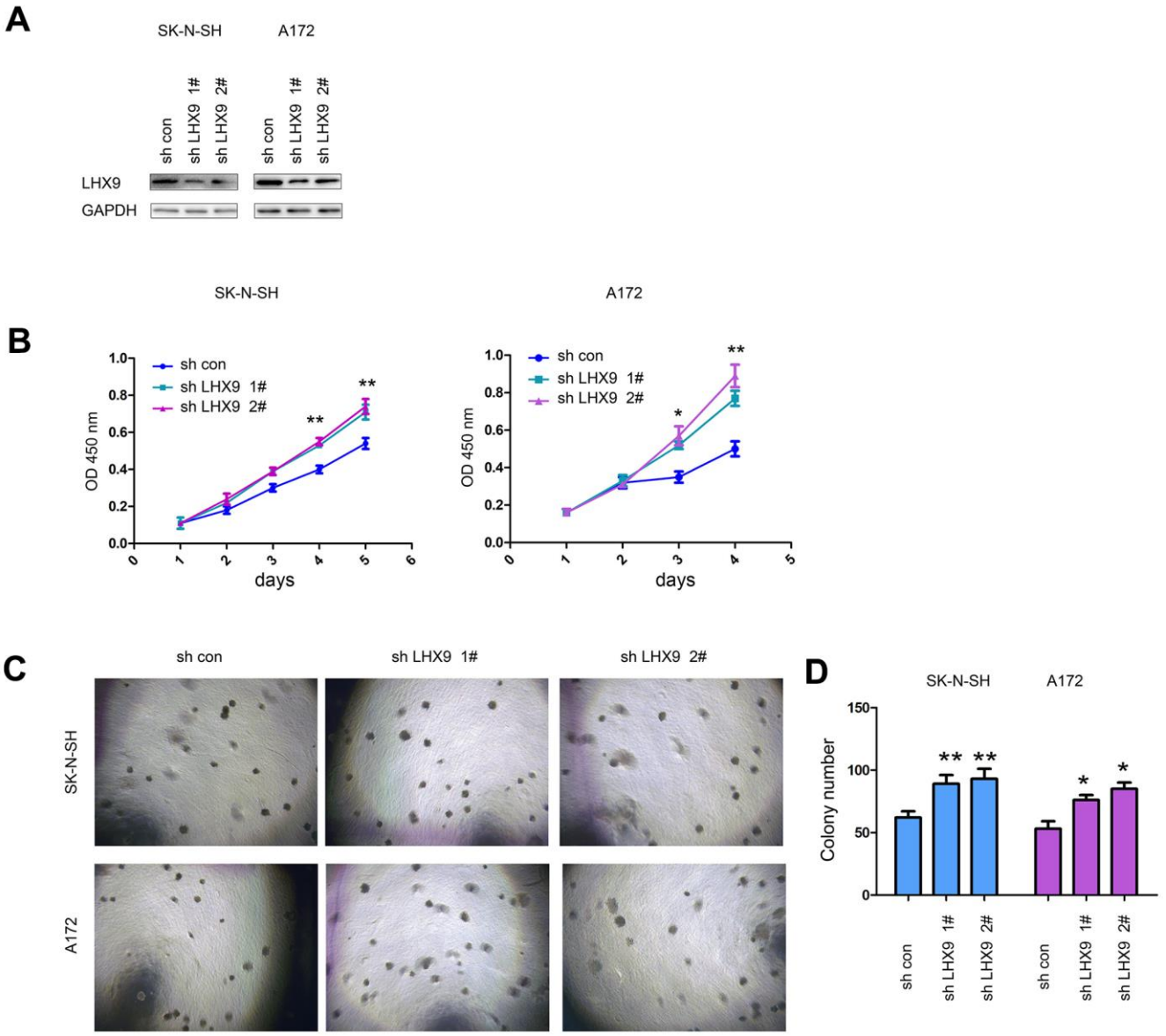

Figure 3. Interfering with LHX9 expression accelerated the growth of glioma cells. (**A**) Interference with LHX9 expression in A172 and SK-N-SH cells. The target sequence was cloned into the pL.KO.1 vector, the virus was packaged to infect A172 and SK-N-SH cells. Cells were screened with puromycin for 1 week, and then the expression of LHX9 was identified. (**B**) The effect of interference with LHX9 expression on the growth of A172 and SK-N-SH cells was detected by CCK8 assay. (**C**, **D**) The effect of interference with LHX9 expression on the anchorage-independent growth of A172 and SK-N-SH cells was detected by soft agar assays. *, $P<0.05$; **, $P<0.01$.

An important finding of this study is that LHX9 overexpression inhibits the colony-forming ability of glioma cells on soft agar. Although Vladimirova V. et al. found that LHX9 had no effect on the growth of glioma cells, their observation time window was 72 hours [18]. In our CCK-8 assay, we also observed that LHX9 expression had little effect on the growth of glioma cells in the first 72 hours, but within a time window of 96 hours (4 days), we observed that LHX9 had inhibitory effects on cell growth and that downregulation of LHX9 expression promoted the growth of glioma cells. In addition, we also observed that LHX9 inhibited the colony formation of glioma cells on soft agar, suggesting that LHX9 inhibited the anchorage-independent growth of glioma cells. None of these findings were not observed by Vladimirova V et al. [18].

Another important finding of this study is that LHX9 inhibits PGK1 expression by interacting with p53. LHX9 interacts with the p53 DNA-binding domain, suggesting that it very likely regulates the transcriptional activity of p53. In tumor formation experiments, we observed that interference with downstream PGK1 expression almost completely reversed the tumorigenicity caused by the downregulation of LHX9 expression, suggesting that treatment with inhibitors of PGK1 is highly likely to benefit patients with glioma. Consistent with this finding, PGK1 has been found to be upregulated in various tumors and to promote tumor progression.

In conclusion, we have revealed the molecular mechanism of glioma inhibition by LHX9 in this study. The LHX9/p53-PGK1 signaling pathway is likely to be an important target for the treatment of glioma.

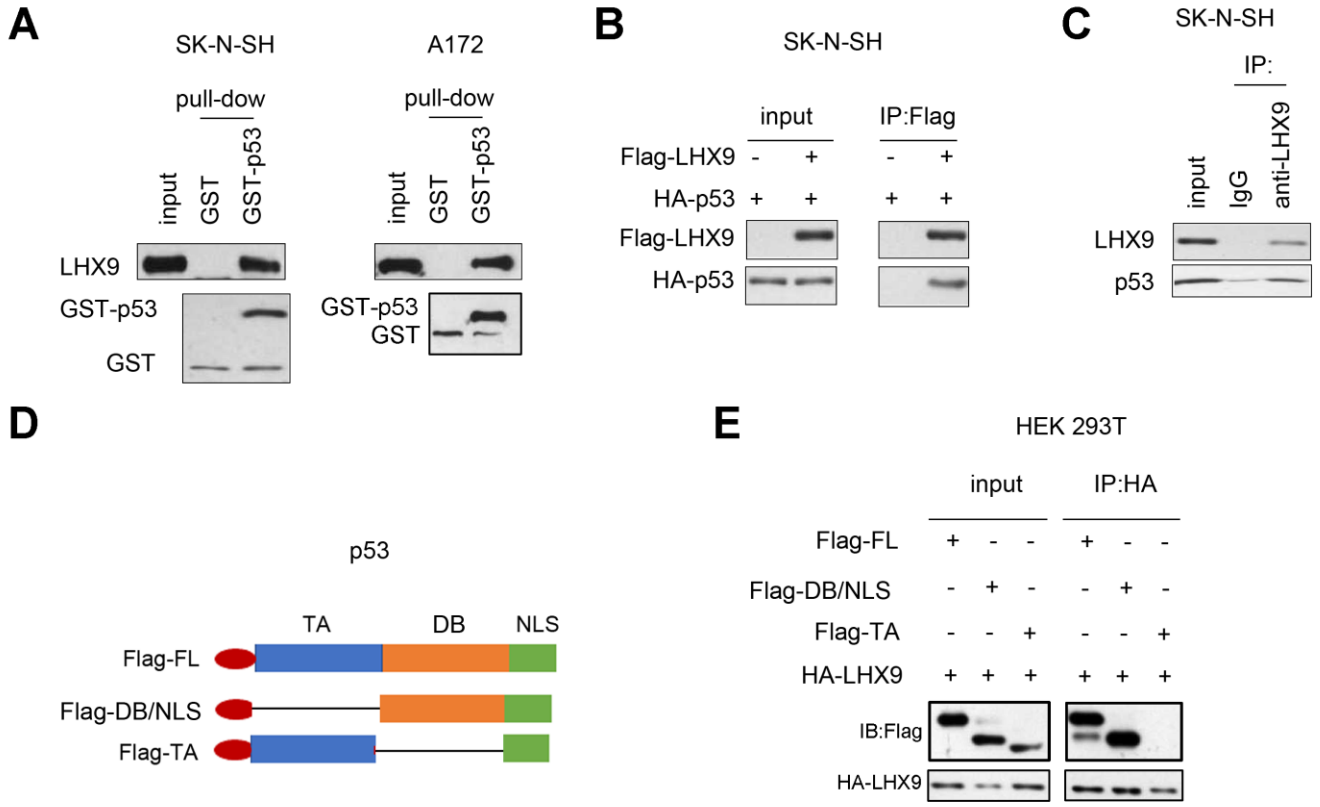

Figure 4. Interaction between LHX 9 and p53. (**A**) The interaction between LHX9 and fusion protein GST-p53 was detected by GST pull-down assay. 10 μg of GST-p53 fusion protein incubated with SK-N-SH and A172 cell lysis. (**B**) The interaction between the exogenously expressed Flag-LHX9 and HA-p53 was detected by co-immunoprecipitation assay. (**C**) The interaction between endogenously expressed LHX9 and p53 was detected by co-immunoprecipitation assay. (**D**) Schematic diagram of different truncated mutants of p53. (**E**) The domain of p53 that interacted with LHX9 was identified by co-immunoprecipitation.

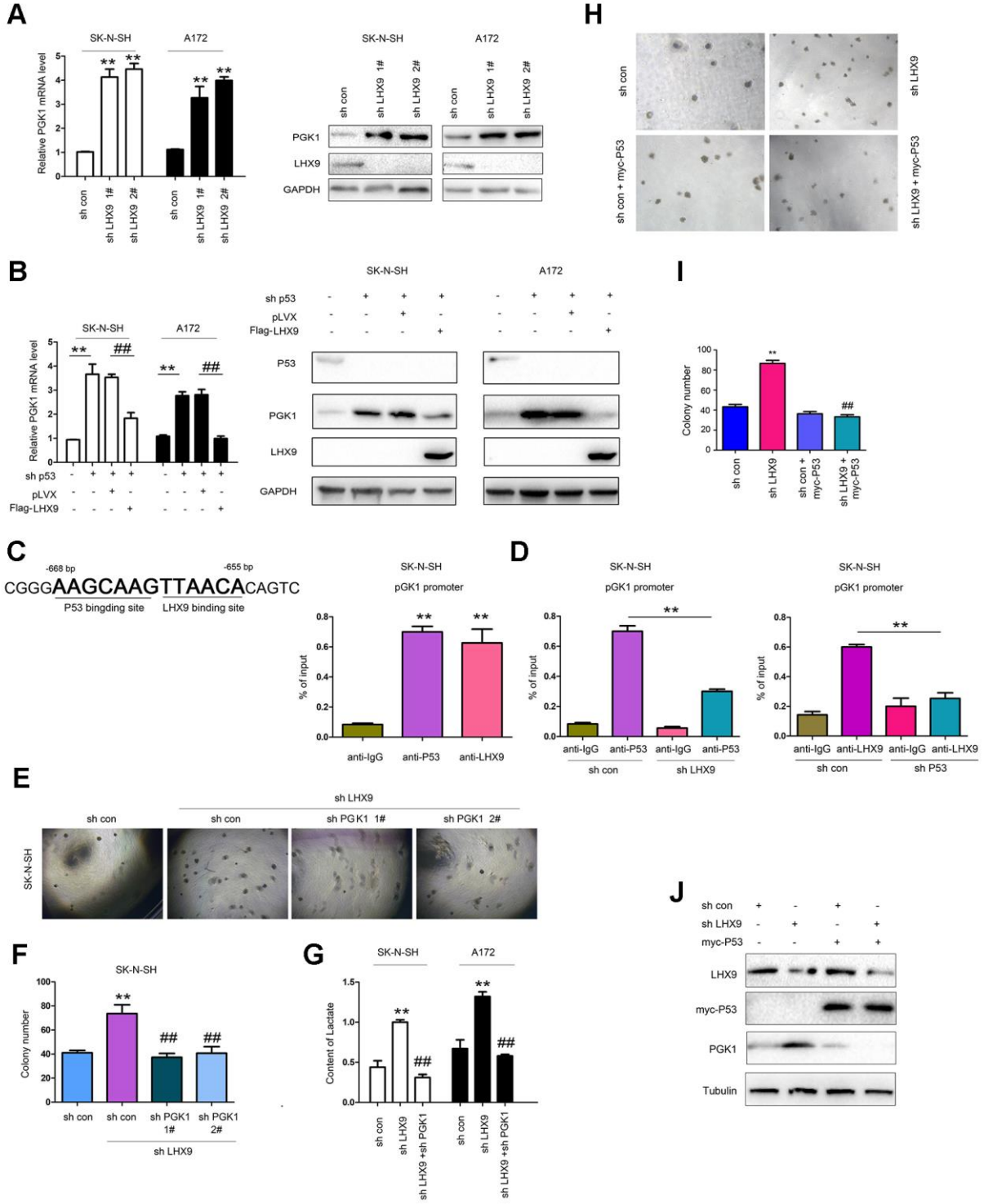

Figure 5. LHX9 inhibited glycolysis by down-regulating PGK1 expression. (**A**) Interfering with LHX9 expression up-regulated the mRNA level of PGK1. (**B**) Overexpression of LHX9 inhibited the induction of PGK1 by knockdown of p53. (**C**) Left: the schematic illustration of the PKG1 promoter with labeled p53 and LHX9 binding sites. Right: Chromosomal immunoprecipitation assay demonstrated that p53 and LHX9 bound to the PGK1 promoter. (**D**) Chromosomal immunoprecipitation assay demonstrated that down-regulating LHX9 expression inhibited the binding of p53 to the PGK1 promoter, and vice versa. (**E**, **F**) Soft agar assay demonstrated that down-regulating the expression of PGK1 abolished the increase in colony formation caused by down-regulation of LHX9. (**G**) Interfering with LHX9 expression increased the lactic acid content. This increase could be suppressed by interfering with PGK1. (**H**, **I**) The effects of P53 restoration on the anchorage-independent growth of SK-N-SH were examined. (**J**) The effects of P53 restoration on the PGK1 expression of SK-N-SH were examined. ##, *P*<0.01; **, *P*<0.01.

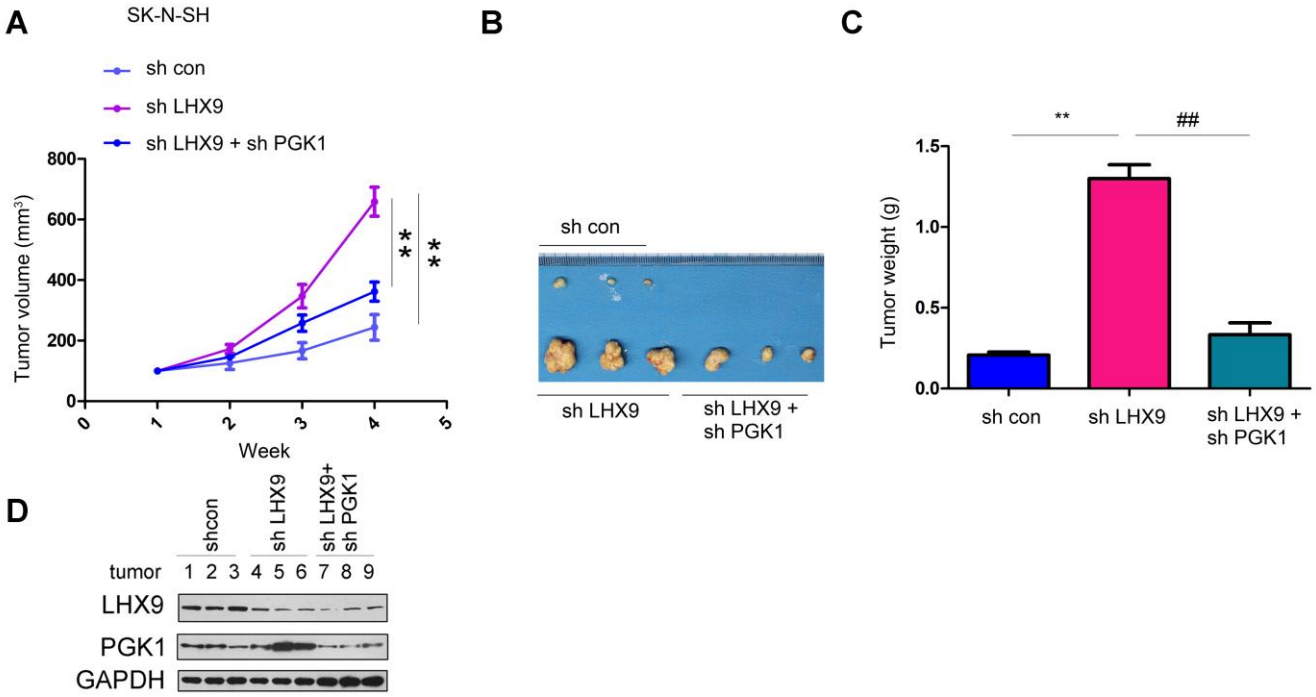

Figure 6. LHX9 down-regulation accelerated the *in vivo* tumorigenicity of glioma cells. (**A**) Tumor growth curve. SK-N-SH cells were interfered with the expression of LHX9 or the expressions of both LHX9 and PGK1. The *in-vivo* tumor formation experiments were performed in nude mice and the tumor volume was recorded. (**B**, **C**) Tumor morphology and tumor weight. (**D**) Expressions of LHX9 and PGK1 in tumors were detected by Western blot. ##, $P<0.01$; **, $P<0.01$.

MATERIALS AND METHODS

Cell culture and transfection

Glioma cells (U87, SK-N-SH, SHG44 and A172 cells) and normal HEB cells were purchased from Shanghai Cell Bank, Chinese Academy of Sciences. The cells were cultured in DMEM containing 10% serum and antibiotics.

Cells were cultured in an incubator at 37° C with 5% CO_2. The cells were transfected using Lipofectamine 2000 following the manufacturer's instructions. Screening was performed using 1 μg/ml puromycin 48 hours after cell transfection. Seven days later, the surviving cells were mixed, and gene expression was determined by Western blot analysis.

Clinical specimens

Clinical specimens were collected from the Department of Neurosurgery, XiangYa Hospital of Central South University, and informed consent was obtained from the patients from whom the specimens were collected. The specimens were fixed with formaldehyde, dehydrated with ethanol, embedded in paraffin, and cut into 5-μm sections for subsequent analysis.

Western blot analysis

After washing twice with PBS, cells were lysed with RIPA buffer (1% NP-40, 0.1% SDS, 0.5% deoxycholate, 50 mM Tris [pH 7.4], and a protease inhibitor cocktail) on ice for 15 min, scraped with a scraper, and centrifuged at 12,000 rpm for 15 min at 4° C. After measuring the protein concentration with Bradford reagent (Sigma), the protein samples were adjusted, 6× loading buffer was added, and the samples were boiled for 5 min. Then, electrophoresis was performed. Then, the proteins were transferred to a polyvinylidene difluoride membrane (Millipore). After incubation with TBST containing 5% skimmed milk (25 mM Tris, 150 mM NaCl, 0.05% Tween 20 [pH 7.5]) for 1 hour at room temperature, the primary antibody was incubated overnight with the membrane at 4° C. After washing the membrane three times with TBST, a horseradish peroxidase-conjugated secondary antibody was added, and the membrane was incubated for 1 hour at room temperature. The membrane was washed three times with TBST and developed with enhanced chemiluminescence (Pierce). Antibodies against GST (10000-0-AP), GAPDH (10494-1-AP), HA (51064-2-AP) and Flag (20543-1-AP) were obtained from Proteintech, and antibodies against LHX9 (ab224357), P53 (ab26) and PGK1 (ab199438) were obtained from Abcam.

Cell growth assay

One hundred microliters of cell suspension (containing 1000 cells) was inoculated into wells of a 96-well plate, and the time was recorded as "day 0". Ten microliters of CCK-8 solution was added to each well on days 1, 2, 3, and 4 and then incubated in an incubator for 4 hours. The absorbance at 450 nm was measured with a microplate reader.

Edu assay

Cells were plated into a 96-well plate (20000 cells/well). Cell proliferation was evaluated using a Cell-Light EdU Apollo 567 *in vitro* kit (RiboBio, C10310-1). A fluorescence microscope was used to acquire images for analysis. The percentage of positively stained cells was calculated.

Anchorage-independent growth assay

A soft agar assay was performed with 12-well plates. The soft agar consisted of two layers: the upper layer and the lower layer. The lower layer of agar was mainly used to embed the 12-well plates; the agar concentration was 0.5%, and the serum concentration was 10%. The upper agar was used for resuspending the cells; the agar concentration was 0.35%, and the serum concentration was 10%. An inhibitor was mixed in the upper agar. First, the agar was heated to 37° C, and the lower layer of agar was paved. After agar coagulation, 2,000 cells were added to the upper layer of agar, and after mixing well, cells were seeded on the lower layer of agar. The cells were photographed and counted after incubation for 14 days at 37° C.

Knockdown of LHX9 and PGK1 expression

Retroviruses that interfere with LHX9 expression were purchased from Shanghai GeneChem Biotechnology Co., Ltd. The viruses were removed after 8 hours of incubation with cell culture. Twenty-four hours later, puromycin (1 μg/ml) was added for screening. After seven days, surviving cells were collected, and the expression of LHX9 was verified.

GST pull-down assay

Cells were collected, lysed and centrifuged at 12,000 rpm for 20 min at 4° C, and then, the supernatant was collected. The supernatant was incubated with 10 μg of GST or GST-p53 fusion protein at 4° C overnight, and then, Sepharose 4B GST gel beads were added and incubated for another 4 hours. The gel beads were washed 3 times with PBST buffer for 5 min each time. Then, 30 μL of loading buffer was added and boiled for 5 min at 100° C, and the supernatant was collected for Western blotting.

Coimmunoprecipitation

SK-N-SH and A172 cells were collected, lysed and centrifuged at 12,000 rpm for 20 min at 4° C, and the supernatant was collected. The supernatant was mixed with the primary antibody and incubated overnight at 4° C. Then, protein A gel beads were added and incubated for another 4 hours. The gel beads were washed 3 times with PBST buffer for 5 min each time. Then, 30 μL of loading buffer was added and boiled for 5 min at 100° C. The supernatant was used in Western blot analysis.

qPCR

For qPCR, 20 μl of Hieff qPCR SYBR® Green Master Mix (No Rox Plus) was used for the amplification reaction. The system included 10 μL of PCR MIX, 0.4 μL of 10 μm forward primer, 0.4 μL of 10 μm reverse primer, and 3 μL of cDNA template and supplemented to 20 μL with ddH_2O. All reactions were performed in duplicate and detected with a Thermo Scientific™ PikoReal™ Real-Time PCR detection system. The reaction conditions were as follows: 95° C for 3 min; 40 cycles of 94° C for 30 s and 60° C for 30 s; and finally, 95° C for 15 s, 60° C for 60 s, and 95° C for 15 s. The melt curve was plotted to determine the specificity of the amplification. The forward primer of PGK1 was 5'-agataacaaacaaccagagg-3', and the reverse primer was 5'-acagacccagcagctgggtt-3'.

ChIP

ChIP assays were performed by using a ChIP kit from Cell Signaling Technology. Antibodies against p53 and LHX9 were used for ChIP. The IP results with normal IgG or specific antibody were then used to calculate the relative nonspecific background and specific occupancy. The ChIP primers were F, 5'-GATGTAATTTTTCAATGG-3', and R, 5'-TAACTGC CAAGATGTAAC-3'.

Determination of lactic acid content

Cells were cultured in Dulbecco's modified Eagle's medium without phenol red for 15 hours. Then, the culture medium was harvested to measure the lactate concentrations. Lactate levels were quantified using a lactate assay kit (BioVision, CA). All values were normalized to the relative protein levels measured using a bicinchoninic acid (BCA) protein assay.

Subcutaneous tumor formation experiments

Four-week-old male nude mice were assigned to 3 group, with 3 mice in each group. One group of mice was injected with sh control SK-N-SH cells ($1*10^6$ cells/injection), one group of mice was injected with sh LHX9 SK-N-SH cells ($1 * 10^6$ cells/injection), and the other group was injected with sh LHX9+sh PGK1 SK-N-SH cells ($1*10^6$ cells/injection). The mice were sacrificed 4 weeks after injection, tumor tissues were removed and weighed, and the expression of LHX9 and PGK1 was measured.

Ethics approval and consent to participate

Ethical approval Research involving animals: All applicable international, national, and/or institutional guidelines for the care and use of animals were followed.

Research Involving human participants: All procedures performed in studies involving human participants were in accordance with the ethical standards of the institutional and/or national research committee and with the 1964 Helsinki declaration and its later amendments or comparable ethical standards.

Consent for publication

Written informed consent for publication was obtained from all the authors.

Availability of data and materials

The data that support the findings of the study are available from the corresponding author upon reasonable request.

AUTHOR CONTRIBUTIONS

XL and SL designed the study. XL, JG and JL performed the experiments. ZL, TC and CB assisted the data analysis. XL and JG drafted the manuscript. SL revised the manuscript and supervised the work.

CONFLICTS OF INTEREST

The authors declare that they have no conflicts of interest.

FUNDING

This work was supported by grants from the National Natural Science Foundation of China (32070972).

REFERENCES

1. Koppenol WH, Bounds PL, Dang CV. Otto Warburg's contributions to current concepts of cancer metabolism. Nat Rev Cancer. 2011; 11:325–37. https://doi.org/10.1038/nrc3038 PMID:21508971
2. Crunkhorn S. Targeting cancer cell metabolism in glioblastoma. Nat Rev Drug Discov. 2019. [Epub ahead of print]. https://doi.org/10.1038/d41573-019-00054-3 PMID:31048798
3. Crunkhorn S. Targeting cancer cell metabolism in glioblastoma. Nat Rev Cancer. 2019; 19:250. https://doi.org/10.1038/s41568-019-0139-3 PMID:30944412
4. Hoekema A, Kastelein RA, Vasser M, de Boer HA. Codon replacement in the PGK1 gene of Saccharomyces cerevisiae: experimental approach to study the role of biased codon usage in gene expression. Mol Cell Biol. 1987; 7:2914–24. https://doi.org/10.1128/mcb.7.8.2914-2924.1987 PMID:2823108
5. Zhou JW, Tang JJ, Sun W, Wang H. PGK1 facilities cisplatin chemoresistance by triggering HSP90/ERK pathway mediated DNA repair and methylation in endometrial endometrioid adenocarcinoma. Mol Med. 2019; 25:11. https://doi.org/10.1186/s10020-019-0079-0 PMID:30925862
6. Wang J, Wang J, Dai J, Jung Y, Wei CL, Wang Y, Havens AM, Hogg PJ, Keller ET, Pienta KJ, Nor JE, Wang CY, Taichman RS. A glycolytic mechanism regulating an angiogenic switch in prostate cancer. Cancer Res. 2007; 67:149–59. https://doi.org/10.1158/0008-5472.CAN-06-2971 PMID:17210694
7. Qian X, Li X, Cai Q, Zhang C, Yu Q, Jiang Y, Lee JH, Hawke D, Wang Y, Xia Y, Zheng Y, Jiang BH, Liu DX, et al. Phosphoglycerate Kinase 1 Phosphorylates Beclin1 to Induce Autophagy. Mol Cell. 2017; 65:917–31.e6. https://doi.org/10.1016/j.molcel.2017.01.027 PMID:28238651
8. He Y, Luo Y, Zhang D, Wang X, Zhang P, Li H, Ejaz S, Liang S. PGK1-mediated cancer progression and drug resistance. Am J Cancer Res. 2019; 9:2280–302. PMID:31815035
9. Hu H, Zhu W, Qin J, Chen M, Gong L, Li L, Liu X, Tao Y, Yin H, Zhou H, Zhou L, Ye D, Ye Q, Gao D. Acetylation of PGK1 promotes liver cancer cell proliferation and tumorigenesis. Hepatology. 2017; 65:515–28. https://doi.org/10.1002/hep.28887 PMID:27774669

10. Failli V, Rogard M, Mattei MG, Vernier P, Rétaux S. Lhx9 and Lhx9alpha LIM-homeodomain factors: genomic structure, expression patterns, chromosomal localization, and phylogenetic analysis. Genomics. 2000; 64:307–17. https://doi.org/10.1006/geno.2000.6123 PMID:10756098

11. Birk OS, Casiano DE, Wassif CA, Cogliati T, Zhao L, Zhao Y, Grinberg A, Huang S, Kreidberg JA, Parker KL, Porter FD, Westphal H. The LIM homeobox gene Lhx9 is essential for mouse gonad formation. Nature. 2000; 403:909–13. https://doi.org/10.1038/35002622 PMID:10706291

12. Bertuzzi S, Porter FD, Pitts A, Kumar M, Agulnick A, Wassif C, Westphal H. Characterization of Lhx9, a novel LIM/homeobox gene expressed by the pioneer neurons in the mouse cerebral cortex. Mech Dev. 1999; 81:193–98. https://doi.org/10.1016/s0925-4773(98)00233-0 PMID:10330499

13. Rétaux S, Rogard M, Bach I, Failli V, Besson MJ. Lhx9: a novel LIM-homeodomain gene expressed in the developing forebrain. J Neurosci. 1999; 19:783–93. https://doi.org/10.1523/JNEUROSCI.19-02-00783.1999 PMID:9880598

14. Mazaud S, Oréal E, Guigon CJ, Carré-Eusèbe D, Magre S. Lhx9 expression during gonadal morphogenesis as related to the state of cell differentiation. Gene Expr Patterns. 2002; 2:373–77. https://doi.org/10.1016/s1567-133x(02)00050-9 PMID:12617828

15. Bieser KL, Wibbels T, Mourad G, Paladino F. The cloning and expression analysis of Lhx9 during gonadal sex differentiation in the red-eared slider turtle, Trachemys scripta, a species with temperature-dependent sex determination. J Exp Zool B Mol Dev Evol. 2013; 320:238–46. https://doi.org/10.1002/jez.b.22497 PMID:23671035

16. Peukert D, Weber S, Lumsden A, Scholpp S. Lhx2 and Lhx9 determine neuronal differentiation and compartition in the caudal forebrain by regulating Wnt signaling. PLoS Biol. 2011; 9:e1001218. https://doi.org/10.1371/journal.pbio.1001218 PMID:22180728

17. Mollé B, Père S, Failli V, Bach I, Rétaux S. Lhx9 and lhx9alpha: differential biochemical properties and effects on neuronal differentiation. DNA Cell Biol. 2004; 23:761–68. https://doi.org/10.1089/dna.2004.23.761 PMID:15585134

18. Vladimirova V, Mikeska T, Waha A, Soerensen N, Xu J, Reynolds PC, Pietsch T. Aberrant methylation and reduced expression of LHX9 in malignant gliomas of childhood. Neoplasia. 2009; 11:700–11. https://doi.org/10.1593/neo.09406 PMID:19568415

19. Siegel RL, Miller KD, Jemal A. Cancer statistics, 2019. CA Cancer J Clin. 2019; 69:7–34. https://doi.org/10.3322/caac.21551 PMID:30620402

20. Martinez-Outschoorn UE, Peiris-Pagés M, Pestell RG, Sotgia F, Lisanti MP. Cancer metabolism: a therapeutic perspective. Nat Rev Clin Oncol. 2017; 14:113. https://doi.org/10.1038/nrclinonc.2017.1 PMID:28094266

21. Mullard A. Cancer metabolism pipeline breaks new ground. Nat Rev Drug Discov. 2016; 15:735–37. https://doi.org/10.1038/nrd.2016.223 PMID:27807357

Research Paper

Metformin-induced chemosensitization to cisplatin depends on P53 status and is inhibited by Jarid1b overexpression in non-small cell lung cancer cells

Tharcisio Citrangulo Tortelli Jr[1], Rodrigo Esaki Tamura[1,2], Mara de Souza Junqueira[1], Janio da Silva Mororó[1], Silvina Odete Bustos[1], Renato Jose Mendonça Natalino[1], Shonagh Russell[3], Laurent Désaubry[4], Bryan Eric Strauss[1], Roger Chammas[1]

[1]Centro de Investigação Translacional em Oncologia (LIM24), Departamento de Radiologia e Oncologia, Faculdade de Medicina da Universidade de São Paulo and Instituto do Câncer do Estado de São Paulo, São Paulo, SP 01246-000, Brazil
[2]Laboratory of Cancer Molecular Biology, Federal University of São Paulo, São Paulo, SP 04039-002, Brazil
[3]Department of Cancer Physiology, H. Lee Moffitt Cancer Center and Research Institute, Tampa, FL 33612, USA
[4]Laboratory of Regenerative Nanomedicine (RNM), INSERM U 1260, University of Strasbourg, CRBS, Strasbourg 67000, France

Correspondence to: Tharcisio Citrangulo Tortelli Jr; **email:** tharcisio.junior@hc.fm.usp.br
Keywords: metformin, cisplatin, Jarid1b, p53, NSCLC
Received: June 16, 2020 **Accepted:** August 25, 2021 **Published:** September 16, 2021

ABSTRACT

Metformin has been tested as an anti-cancer therapy with potential to improve conventional chemotherapy. However, in some cases, metformin fails to sensitize tumors to chemotherapy. Here we test if the presence of P53 could predict the activity of metformin as an adjuvant for cisplatin-based therapy in non-small cell lung cancer (NSCLC). A549, HCC 827 (TP53 WT), H1299, and H358 (TP53 null) cell lines were used in this study. A549 cells were pre-treated with a sub-lethal dose of cisplatin to induce chemoresistance. The effects of metformin were tested both *in vitro* and *in vivo* and related to the ability of cells to accumulate Jarid1b, a histone demethylase involved in cisplatin resistance in different cancers. Metformin sensitized A549 and HCC 827 cells (but not H1299 and H358 cells) to cisplatin in a P53-dependent manner, changing its subcellular localization to the mitochondria. Treatment with a sub-lethal dose of cisplatin increased Jarid1b expression, yet downregulated P53 levels, protecting A549Res cells from metformin-induced chemosensitization to cisplatin and favored a glycolytic phenotype. Treatment with FL3, a synthetic flavagline, sensitized A549Res cells to cisplatin. In conclusion, metformin could potentially be used as an adjuvant for cisplatin-based therapy in NSCLC cells if wild type P53 is present.

INTRODUCTION

Lung cancers are among the most lethal types of cancer worldwide. Approximately 80% of all lung cancers are Non-Small Cell Lung Carcinomas (NSCLC), which present an overall survival rate of 15%-35% for stage III-A and 5%-10% for stage III-B in the 5 years following diagnosis [1]. As platinum-based therapy for stage III NSCLC fails, novel approaches have been tested. Immunotherapeutic agents, like the immune checkpoint blocker anti-PD-1 monoclonal antibodies (Pembrolizumab or Nivolumab), present promising results, improving overall survival [2, 3]. However, the cost of this relatively new immunotherapy still limits

access by most public health systems and patients around the world. Thus, new cost-affordable treatments are necessary.

Metformin, a biguanide derived from the plant *Galega officinalis*, has been used for many years to manage type-II diabetic patients [4, 5]. Metformin has become a candidate for repurposing to cancer therapy since the discovery that type-II diabetic patients treated with metformin have lower incidences of different types of cancer [6]. This effect has been studied successfully in many types of tumors [7, 8]. However, many other studies showed that metformin does not improve cancer treatment when in combination with chemotherapy [9, 10], demonstrating that more understanding is needed to determine when metformin can be used or not for cancer therapy.

Metformin accumulates in the mitochondrial matrix and blocks the complex-1 of the electron transport chain leading to a mitochondrial malfunction [11]. The resulting accumulation of ADP and AMP lead to the activation of the AMP-activated protein kinase (AMPK) that, among many other functions, inhibit AKT/mTOR pathway [12, 13]. Metformin also increases the glycolytic metabolism by enhancing glucose consumption, lactate production and by decreasing oxygen consumption [14]. Therefore, metformin could be used to chemosensitize subpopulations of tumor cells which depend preferentially on mitochondrial metabolism. This subpopulation is reprogrammed to escape the Warburg Effect, which relies on aerobic glycolysis. Mechanisms for metabolic reprogramming include the overexpression of the jumonji/ARID1 H3K4 histone demethylase Jarid1b/KDM5B/PLU-1, associated with the development of different types of tumors [15–17]. Jarid1b overexpressing cells are resistant to many types of chemotherapy (including cisplatin), display a mitochondrial-based primary metabolism and are responsible for tumor repopulation in melanoma [18]. Jarid1b overexpressing cells have a stem cell phenotype as demethylation of H3K4 blocks terminal differentiation of embryoid body and keeps high expression of stem cell markers like Oct-4 and Nanog [19].

Different responses of tumor cells to different treatments are related to circuitry rewiring of cancer gene signaling networks upon malignant transformation. For NSCLC, critical cancer driver gene networks involve *TP53* and EGFR-RAS-RAF-MEK-ERK pathways, which can be treated with EGFR inhibitors [20]. *TP53* is mutated in more than 50% of NSCLC. Patients harboring *TP53* mutations have a poorer prognosis than patients with wild type *TP53* [21]. Its major protein product is the multifunctional protein P53, which controls cell apoptosis at different levels. As a transcription factor, nuclear P53 induces the expression of apoptosis-related genes like *BAX*, *PUMA* and *NOXA* [22]. Cytoplasmic P53 can induce apoptosis when it is phosphorylated by AMPK- on serine 15. Ser^{15} –phosphorylated P53 translocate to mitochondria, where P53 can release BAX and BAK from BCL-XL, favoring the initiation of the apoptotic cascade [23].

FL3, a synthetic flavagline [24], has been reported as a stemness regulator by downregulating Oct4 in teratocarcinoma cell and selectively kills Oct-4 overexpressing cells and has little effect on normal cells. FL3-induced apoptosis depends on MAPK activation, as phosphorylation of p38 is necessary for FL3-iduced cell death [25]. Also, FL3 is a potent inhibitor of the EGFR-RAS-RAF axis, as it inhibits the activation of C-Raf by RAS through the inhibition of the interaction between C-Raf and the scaffold proteins prohibitin [26].

In the present study, we show that metformin chemosensitizes NSCLC cells to cisplatin in a P53-dependent manner. Sub-lethal treatment with cisplatin leads to Jarid1b overexpression and shifts the metabolism of A549 cells into glycolysis. Also, overexpression of Jarid1b leads to P53 downregulation, blocking the ability of metformin to sensitize to cisplatin-induced cell death. As Jarid1b overexpressing cells represent a chemoresistant population, FL3 could potentially be used to treat Jarid1b overexpressing cells. Therefore, P53-dependent pathways are critical for metformin-induced chemosensitization to cisplatin in NSCLC.

RESULTS

Metformin improves cisplatin-induced death in A549 and HCC 827 NSCLC cells in a P53 dependent manner

We first checked the ability of metformin to chemosensitize the A549 and HCC 827 human non-small cell lung cancer cells lines to cisplatin. Combination of metformin with cisplatin synergistically induced a high chemosensitization to cisplatin evidenced through DNA fragmentation assay (Figure 1A), caspase 3 and 7 activation assay (Figure 1B) and through cell viability assay (Figure 1C) in A549 and HCC 827 cells. Metformin treatment reduced the ability of A549 and HCC 827 cells to produce colonies and this ability was completely abolished when these cells were treated with cisplatin (with or without metformin) (Figure 1D). A549 tumors in NOD-SCID mice treated with cisplatin plus metformin had the lowest tumor volume and weight, (Figure 1E, 1F and Supplementary Figure 1), yet cisplatin-only treated mice had the tumors with the highest volume, and this volume was not related to

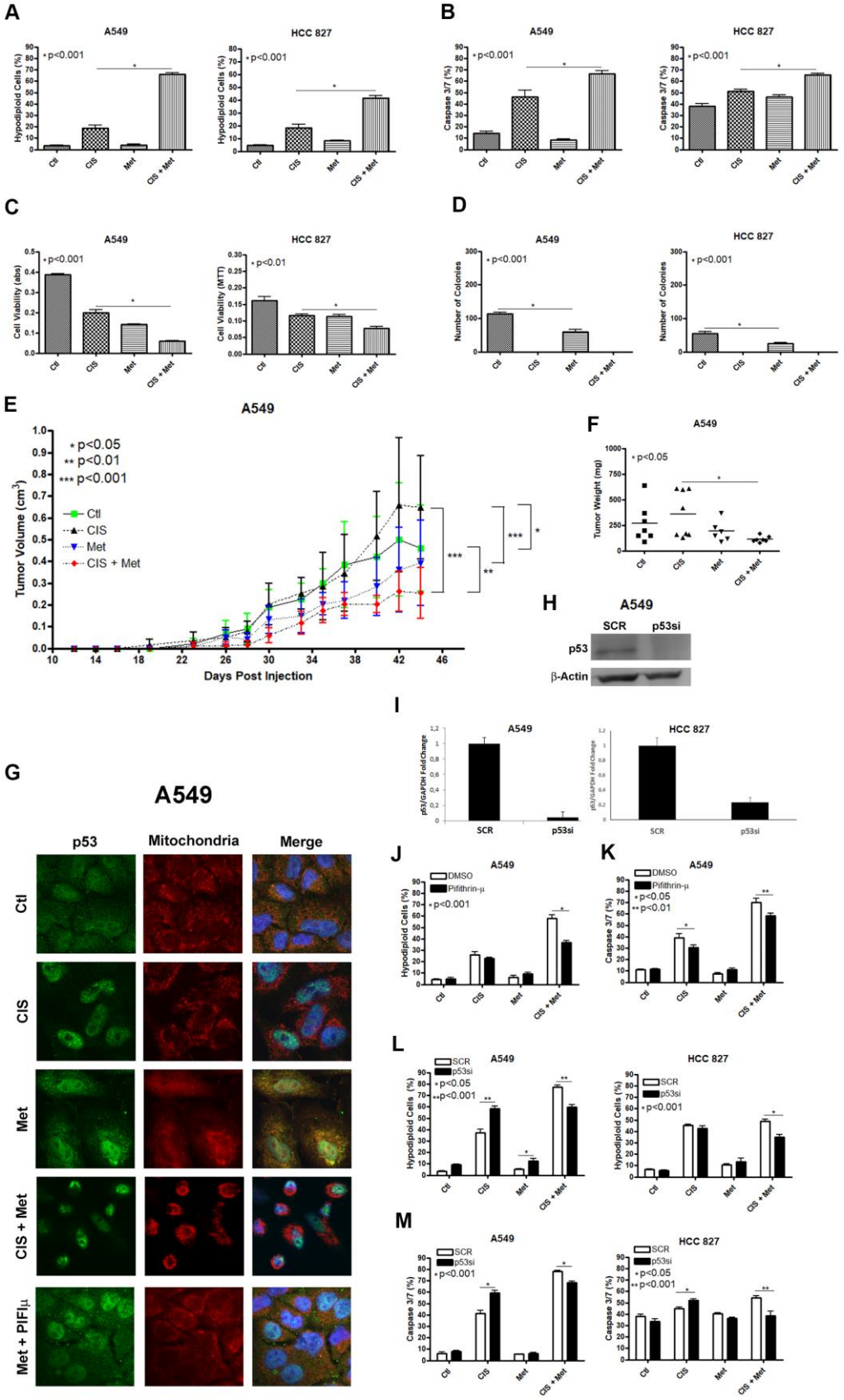

Figure 1. Metformin improves cisplatin-induced death in A549 and HCC 827 NSCLC cells in a P53 dependent manner. Combined treatment between cisplatin and metformin improves DNA fragmentation (p<0.001) (**A**), caspase 3 and 7 activation (p<0.001)

(**B**) and cell viability assay through MTT ($p<0.001$ and $p<0.01$ respectively) (**C**), when compared to both treatments alone in A549 and HCC 827 cells. Metformin decreased the number of colonies and no colonies was observed after cisplatin treatment in A549 and HCC 827 cells ($p<0.001$ and $p<0.01$, respectively) (**D**). A549 cells injected in NOD/SCID mice also have a smaller volume ($p<0.001$) (**E**) and weight ($p<0.05$) (**F**) after combined treatment between cisplatin and metformin. Data represent the mean of three independent experiments. Metformin treatment translocate P53 to the mitochondria in A549 cells and this translocation is blocked by pifithrin-μ (**G**). P53 inhibition by pifithrin-μ protects A549 cells to the metformin induced chemosensitization to cisplatin by decreasing DNA fragmentation ($p<0.001$) (**J**) and caspase 3 and 7 activation ($p<0.01$) (**K**). *TP53* inhibition by siRNA (**H**, **I**) also protects A549 and HCC 827 cell from metformin-induced chemosensitization to cisplatin by decreasing DNA fragmentation ($p<0.001$) (**L**) and caspase 3 and 7 activation ($p<0.001$) (**M**). Data represent the mean of three independent experiments. A549 cells were treated with 10mM of metformin for 72 h and 25μM of cisplatin (with or without metformin) for another 72 h. HCC 827 cells were treated with 20mM of metformin for 72 h and 20μM of cisplatin (with or without metformin) for another 72 h.

necrotic area (Supplementary Figure 2). As mentioned above, metformin-induced activation of AMPK leads to P53 phosphorylation, which promotes the induction of apoptosis. We first analyzed whether metformin treatment changes the subcellular localization of P53 to the mitochondria. Figure 1G shows that metformin increases P53 association with the mitochondria in A549 cells as seen by the yellowish color in the merged image. This accumulation can be partially blocked by pifithrin-μ, which specifically blocks P53 translocation to the mitochondria [27]. Also, cisplatin treatment accumulates p53 in the nucleus and no co-localization in the mitochondria was observed under cisplatin and metformin combination. To determine if the subcellular localization of P53 in the mitochondria is important for the metformin-induced chemosensitization to cisplatin we inhibited its localization with pifithrin-μ or inhibited its expression with siRNA. The inhibition of the subcellular localization of P53 by pifithrin-μ in A549 cells (Figure 1J, 1K) or the inhibition of its expression by siRNA in A549 and HCC 827 cells (Figure 1L, 1M), protected the A549 cells from metformin-induced chemosensitization to cisplatin after three days of combined treatment.

Treatment with sub-lethal dose of cisplatin leads to Jarid1b overexpression and chemoresistance in A549 cells

Jarid1b overexpression is part of the survival response against different types of chemotherapy in melanoma cells [18]. The concept of using a sub-lethal dose of chemotherapy for a few days differs from the usual manner of emerging resistant cells *in vitro*, by treating them with a very low dose of chemotherapy for weeks. By giving a single sub-lethal dose, it is possible to compare the regular regiment of treatment, where in many cases, a few doses of chemotherapeutic agent are given to the patients, and due to the irregular distribution of chemotherapy in the tumor micro-environment, some regions of the tumor will receive a sub-lethal dose of the given chemotherapeutic agent and cell resistance could rise even with one shot [28, 29]. To check if A549 cells increase Jarid1b expression after cisplatin treatment we pre-treated these cells with a sub-lethal dose of cisplatin and observed an increase in Jarid1b mRNA expression in a dose-dependent manner that remains high for at least 30 days after the sub-lethal dose of cisplatin was completely removed and cells were kept in normal culture media (Figure 2A). In the following assays, A549Res cells were treated with a higher dose of cisplatin in combination with metformin. In the A549Res cells, metformin lost the ability to chemosensitize to cisplatin, as DNA fragmentation or caspase 3 and 7 activation under cisplatin and metformin treatment had the same levels, when compared to cisplatin alone (Figure 2B, 2C). While A549Res cells show lower MTT staining as compared to A549, Figure 2D shows that metformin and cisplatin do not change the viability levels with the same efficiency as seen in Figure 1C. Metformin also lowered the number of colonies in A549Res cells while no colonies were observed in A549Res cells after cisplatin treatment. However, the colonies formed after 30 days in A549Res cells have the same cell morphology as observed in A549 cells (Supplementary Figure 1F). Inhibition of Jarid1b by its pharmacological inhibitor PBIT [30] chemosensitized A549Res to the combination of metformin and cisplatin as seen in the DNA fragmentation assay, while caspase 3/7 activity was not elevated indicating that PBIT may activate a cell death pathway other than apoptosis (Figure 2F, 2G). To confirm that Jarid1b is related to chemoresistance in A549Res cells, a siRNA approach was employed. As expected, the siRNA to Jarid1b reduced its mRNA expression level (Figure 2H) and restored metformin-induced chemosensitization to cisplatin in the A549Res cells, as measured by DNA fragmentation (Figure 2I) and caspase 3 and 7 activation assays (Figure 2J).

Sub-lethal dose of cisplatin inhibits P53 accumulation in a Jarid1b-dependent manner

As shown by other groups [31] and us, Jarid1b can inhibit P53 expression. Sub-lethal treatment with cisplatin inhibited P53 in A549Res cells at the mRNA and protein levels (Figure 3A, 3B). *TP53*

downregulation, in Figure 3A, remained low in A549Res cells in the same manner as Jarid1b expression remained high in Figure 2A. The western blot shows that metformin treatment increased P53 inhibition in A549Res cells. Jarid1b inhibition with PBIT blocked the metformin-induced downregulation of P53. To confirm if the increase of P53 is sufficient to sensitize the A549Res cells to the combination of cisplatin and metformin, we

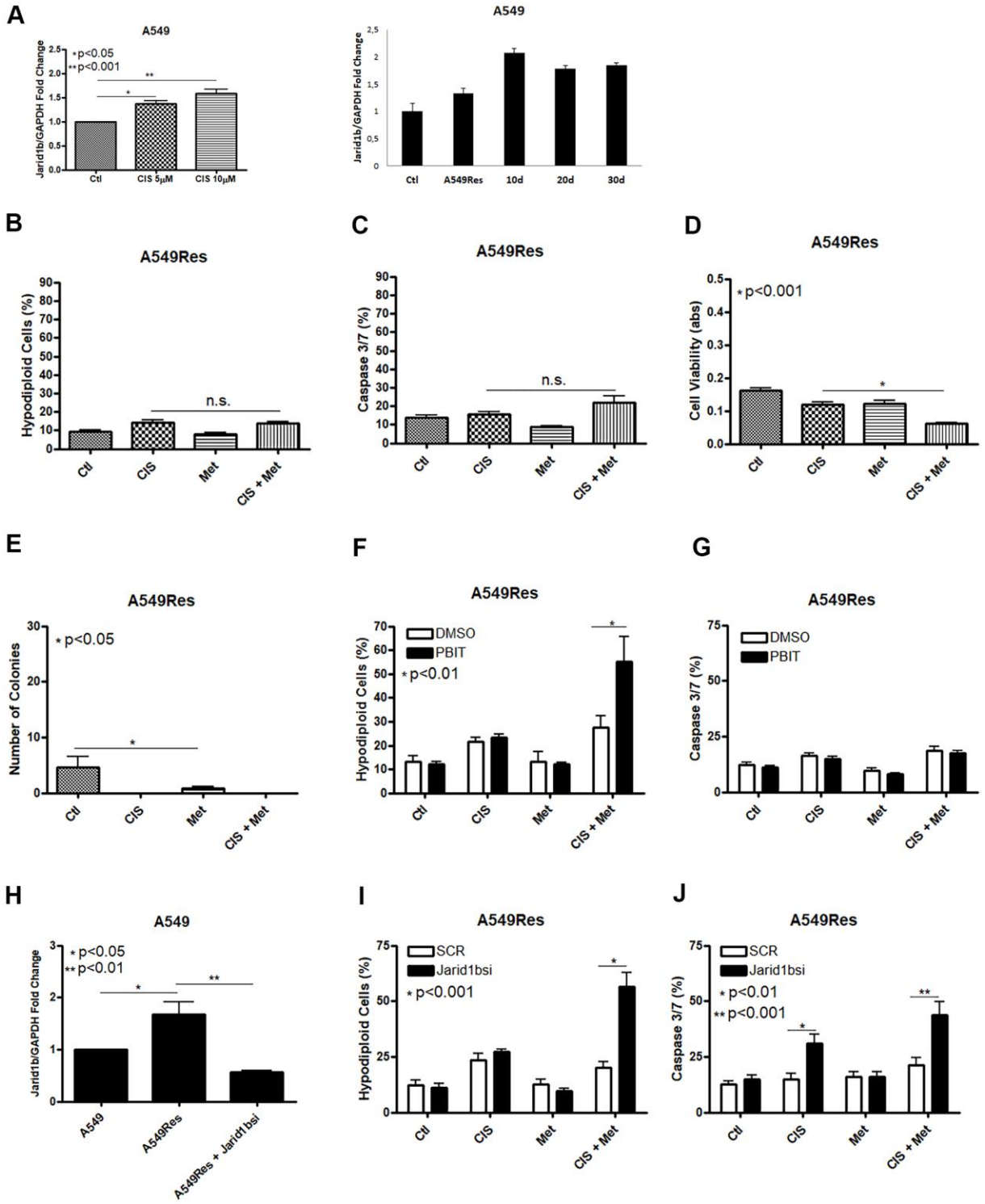

Figure 2. Treatment with sub-lethal dose of cisplatin leads to Jarid1b overexpression and chemoresistance in A549 cells. Sub-lethal treatment with cisplatin in A549 cells increases Jarid1b expression in a dose dependent manner and keeps overexpressed even

after 30 days post-treatment (**A**). A549Res cells become resistant to the combined treatment between metformin and cisplatin as no improvement in DNA fragmentation (**B**), caspase 3 and 7 activation (**C**) can be seen. Only through cell viability assay showed some difference in the metformin and cisplatin combination (p<0.001) (**D**). Metformin decreased the number of colonies in A549Res cells (p<0.05), and no colonies was observed upon cisplatin treatment (**E**). Inhibition of Jarid1b by the pharmacological inhibitor PBIT restores the ability of metformin to chemosensitize to cisplatin as measured by DNA fragmentation assay (p<0.01) (**F**), but caspase 3 and 7 activation was not observed (**G**). However, inhibition of Jarid1b by siRNA (p<0.01) (**H**) restores the ability of metformin to chemosensitize to cisplatin through DNA fragmentation (p<0.001) (**I**) and caspase 3 and 7 activation assay (p<0.001) (**J**). Jarid1b inhibition by siRNA, MTT assay, DNA fragmentation and caspase 3 and 7 activation assay data represent the mean of three independent experiments. A549 cells were pre-treated with 10µM of cisplatin for 72 h to generate A549Res cells. After pre-treatment, A549Res cells were treated with 10mM of metformin for 72 h and 25µM of cisplatin (with or without metformin) for another 72 h.

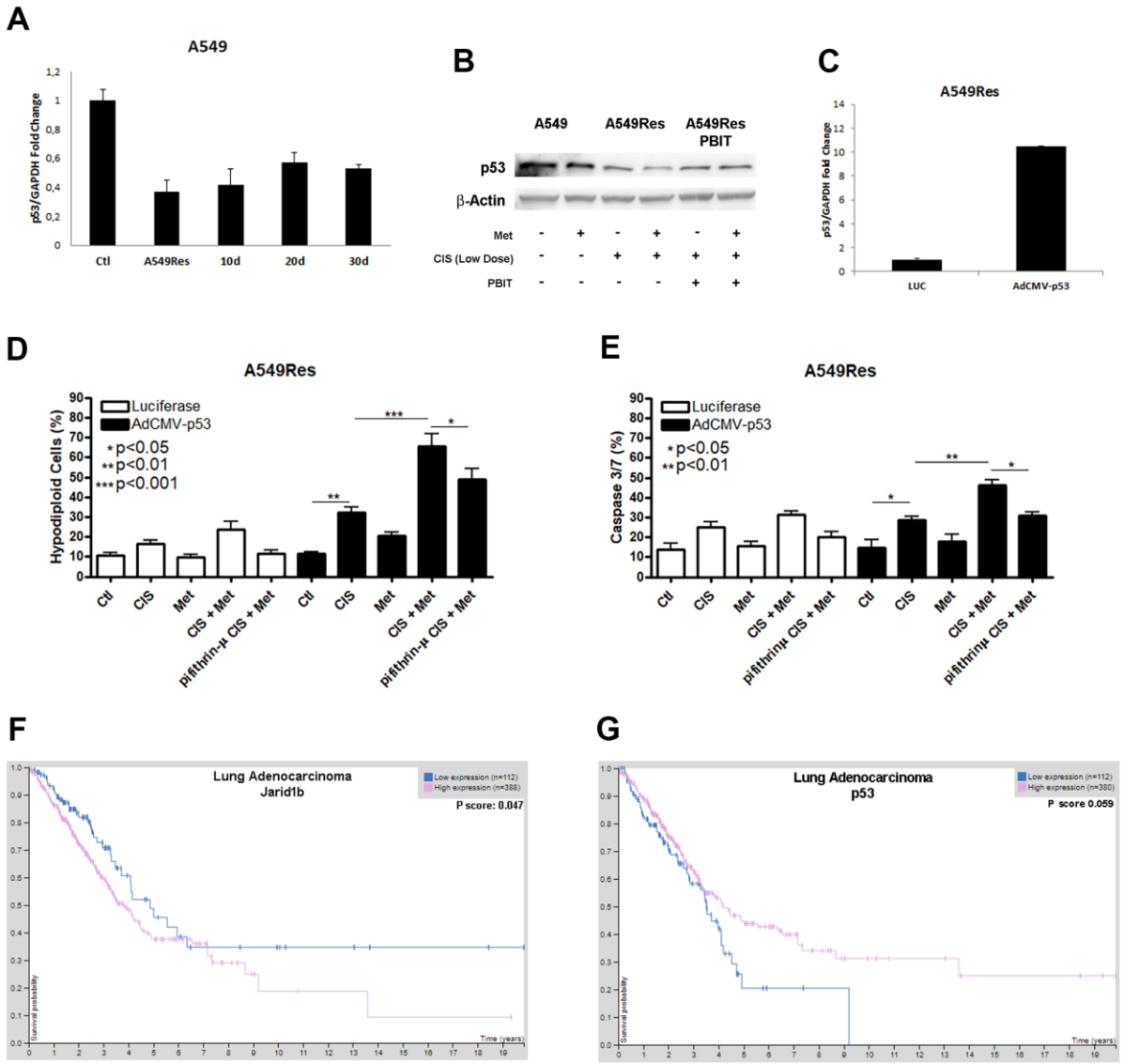

Figure 3. Sub-lethal dose of cisplatin inhibits P53 accumulation in a Jarid1b-dependent manner. Sub-lethal dose of cisplatin in the A549 cells downregulates *TP53* expression even after 30 days post-treatment (**A**). Western blot analysis shows that A549Res has lower expression of P53 compared to A549. Treatment with Jarid1b inhibitor PBIT avoid metformin-induced downregulation of P53 levels (**B**). Overexpression of *TP53* using AdCMVp53 expressing virus (**C**) restores metformin-induced chemosensitization to cisplatin on A549Res as seen by DNA fragmentation (p<0.001) (**D**) and caspase 3 and 7 activation assay (p<0.01) (**E**), while treatment with pifithrin-µ protect from metformin and cisplatin combination in the DNA fragmentation (p<0.05) and caspase 3 and 7 activation assay (p<0.05) (**D**, **E** respectively). High expression of Jarid1b (p<0.05) (**F**) or low expression of *TP53*, despite p=0.059 (**G**) indicate poor prognosis for patients with lung adenocarcinoma. DNA fragmentation assay data represents the mean of three independent experiments and caspase 3 and 7 activation assay represents the mean of two independent experiments.

transduced a virus expressing *TP53* in A549Res cells (Figure 3C). This higher level of *TP53* was enough to increase cell death in A549Res cells, as inhibiting P53 translocation to the mitochondria by pifithrin-μ protected from metformin-induced chemosensitization to cisplatin (Figure 3D, 3E). The same relation of high expression of Jarid1b (Figure 3F) or low expression of *TP53*, (despite p value, the curves clearly showed a difference between high and low expression of *TP53* in survival probability) (Figure 3G), as seen in Figures 2A, 3A for the A549 cells, leads to poor prognosis for patients. Also, KM Plot shows that high expression of Jarid1b indicates poor prognosis in stage 3 lung adenocarcinoma, while low expression indicates poor prognosis in stage 1 and 2 [32] (Supplementary Figure 3).

Sub-lethal treatment with cisplatin enhances glycolysis in A549 cells

Tumor metabolism is a potential target for chemosensitization. Jarid1b overexpressing cells have a mitochondrial-based metabolism in melanomas where the inhibition of the mitochondrial function successfully restores the sensitization to chemotherapy [18]. As metformin fails to inhibit the mitochondria and chemo-sensitize the A549Res cells to cisplatin, we decided to analyze the metabolism of the A549Res cells. Surprisingly, the sub-lethal treatment with cisplatin in the A549Res cells increased the glycolytic metabolism, and not the OXPHOS metabolism, as expected due to Jarid1b overexpression. Figure 4A, 4B show that the

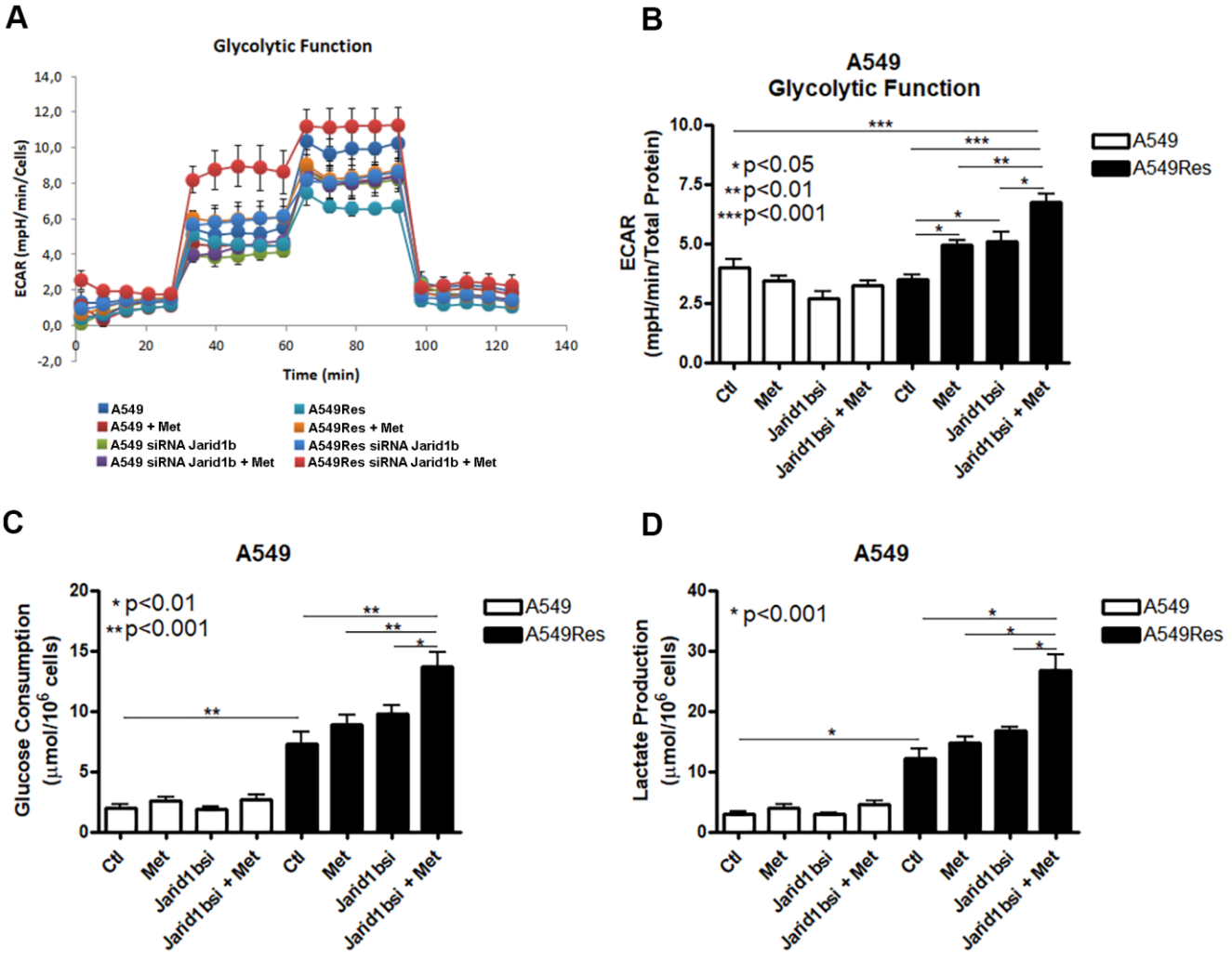

Figure 4. Sub-lethal treatment with cisplatin enhances glycolysis in A549 cells. A549 cells were treated with sub-lethal dose of cisplatin and treated with Jarid1b siRNA and metformin. Representative graph of glycolytic cell metabolism of A549 cells analyzed using the Seahorse XFe96 Analyzer (**A**). A549Res cells increase the extracellular acidification rate (ECAR) after metformin treatment ($p<0.05$) or Jarid1b inhibition by siRNA ($p<0.05$) or in the combination on both ($p<0.001$) (**B**). Glucose consumption ($p<0.001$) (**C**) or lactate production ($p<0.001$) (**D**) is increased after sub-lethal treatment with cisplatin for the generation of the A549Res cells. Data represent the mean of four independent experiments.

extracellular acidification rate (ECAR) was increased in the A549Res cells upon metformin and/or inhibition of Jarid1b by siRNA. The increase in ECAR after Jarid1b inhibition shows the role of Jarid1b in promoting OXPHOS and that sub-lethal treatment with cisplatin impedes this function (Figure 4B). The glycolytic metabolism of the A549Res cells could be confirmed by two other parameters. Glucose consumption (Figure 4C) and lactate production (Figure 4D) were also increased upon sub-lethal treatment with cisplatin and Jarid1b inhibition by siRNA increased these parameters even more when cells were treated with metformin. Also, sub-lethal treatment with cisplatin decreased the oxygen consumption rate (OCR) and the mitochondrial activity in A549Res cells (Supplementary Figure 4).

Metformin does not chemosensitize H1299 and H358 (P53 null) cells to cisplatin

We analyzed whether the combination of cisplatin and metformin could sensitize another NSCLC cell line. We decided to use the human NSCLC cell line H1299 and H358 as these cells lack expression of P53 (Figure 5A). The results were the opposite as seen in the A549 cells, where P53 is present. In H1299 and H358, the combination of cisplatin and metformin did not increase cell death as no additional DNA fragmentation (Figure 5B) or no caspase 3 and 7 activation (Figure 5C) was observed. Also, no decrease in cell viability was seen after combined cisplatin and metformin treatment (Figure 5D). As observed in A549, A549Res and HCC

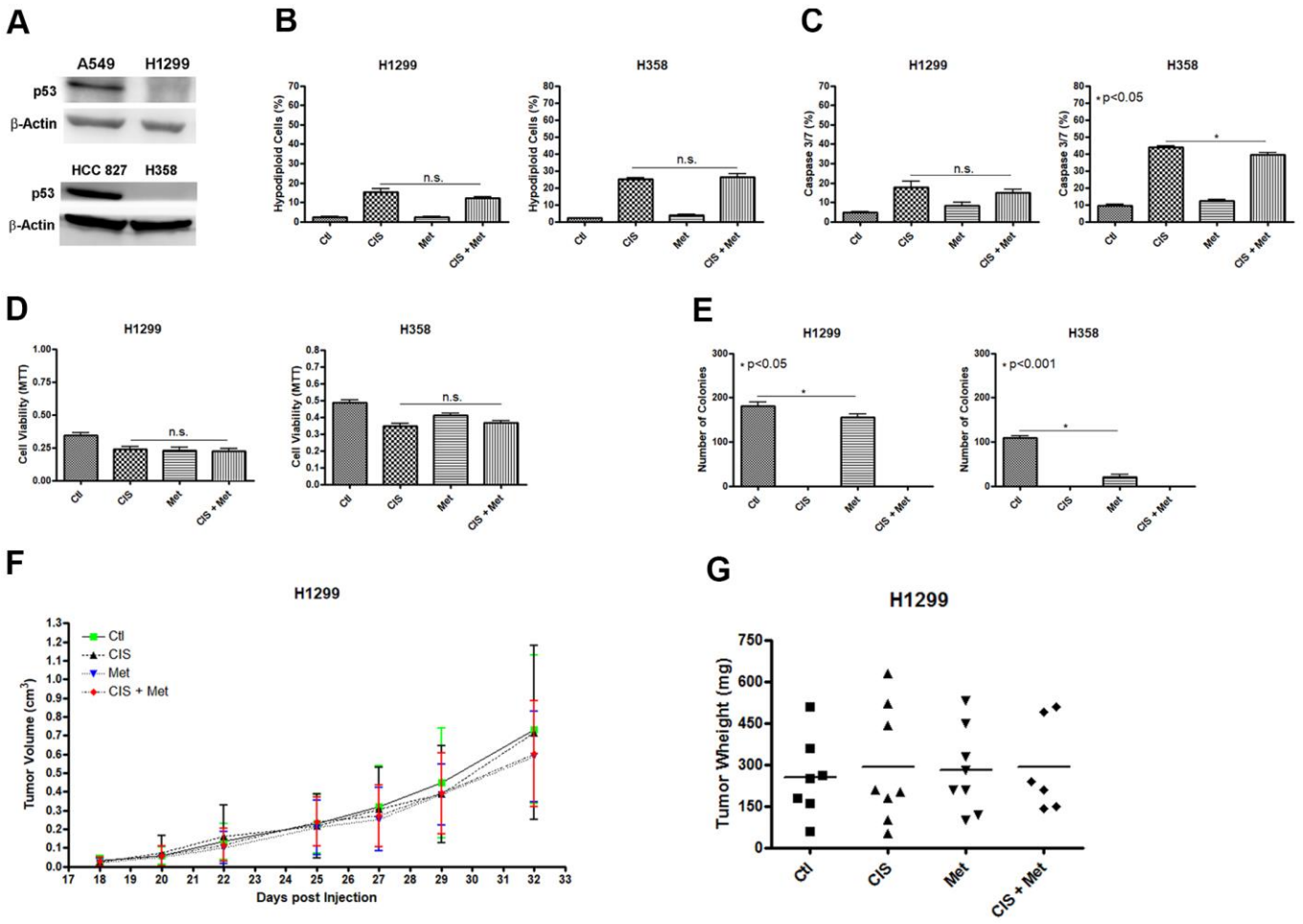

Figure 5. Metformin does not chemosensitize H1299 and H358 (P53 null) cells to cisplatin. The P53 null H1299 and H358 NSCLC cells (**A**) were not chemosensitized by combined treatment between cisplatin and metformin as it did not elevate DNA fragmentation (**B**), caspase 3 and 7 activation (**C**) or reduce cell viability as measured by MTT (**D**), when compared to either treatments alone. Metformin decreased the number of colonies and no colonies was observed after cisplatin treatment in H1299 and H358 cells ($p<0.05$ and $p<0.001$, respectively) (**E**). Combined treatment also did not decrease H1299 tumor growth (**F**) and weight in NOD/SCID mice (**G**). Data represent the mean of three independent experiments. Non-significance (n.s.). H1299 cells were treated with 2mM of metformin for 72 h and 12.5µM of cisplatin (with or without metformin) for another 72 h. H358 cells were treated with 20mM of metformin for 72 h and 20µM of cisplatin (with or without metformin) for another 72 h.

827 cells, metformin treatment decreased the ability of these cells to produce colonies and no colonies were observed when cisplatin was used as treatment (Figure 5E). To check if the H1299 cells could be chemosensitized to cisplatin by metformin *in vivo*, we used the same protocol previously applied to the A549 cells (Figure 1E, 1F). As expected, metformin did not chemosensitize the H1299 cells to cisplatin *in vivo* as no difference in tumor volume (Figure 5F) and weight (Figure 5G) was observed, despite a correlation between cisplatin and increased necrotic area in these tumors (Supplementary Figure 2). Differently than observed in A549 or HCC 827 and H1299 and H358 cells, the human ovary cancer cell lines SK-OV-3 and A2780 did not respond to cisplatin and metformin combination, independently of P53 status (Supplementary Figure 5).

FL3 sensitizes A549Res but not H1299 cells to cisplatin

In an attempt to chemosensitize the A549Res cells to cisplatin, we used the synthetic flavagline FL3, as FL3 has been shown to induce the death of oct-4 high-expressing cells, like Jarid1b overexpressing cancer cells. We first analyzed if the sub-lethal treatment with cisplatin increase oct-4 levels in A549Res cells. Figure 6A shows that oct-4 expression was increased in A549Res cells. Cisplatin alone is enough to kill the

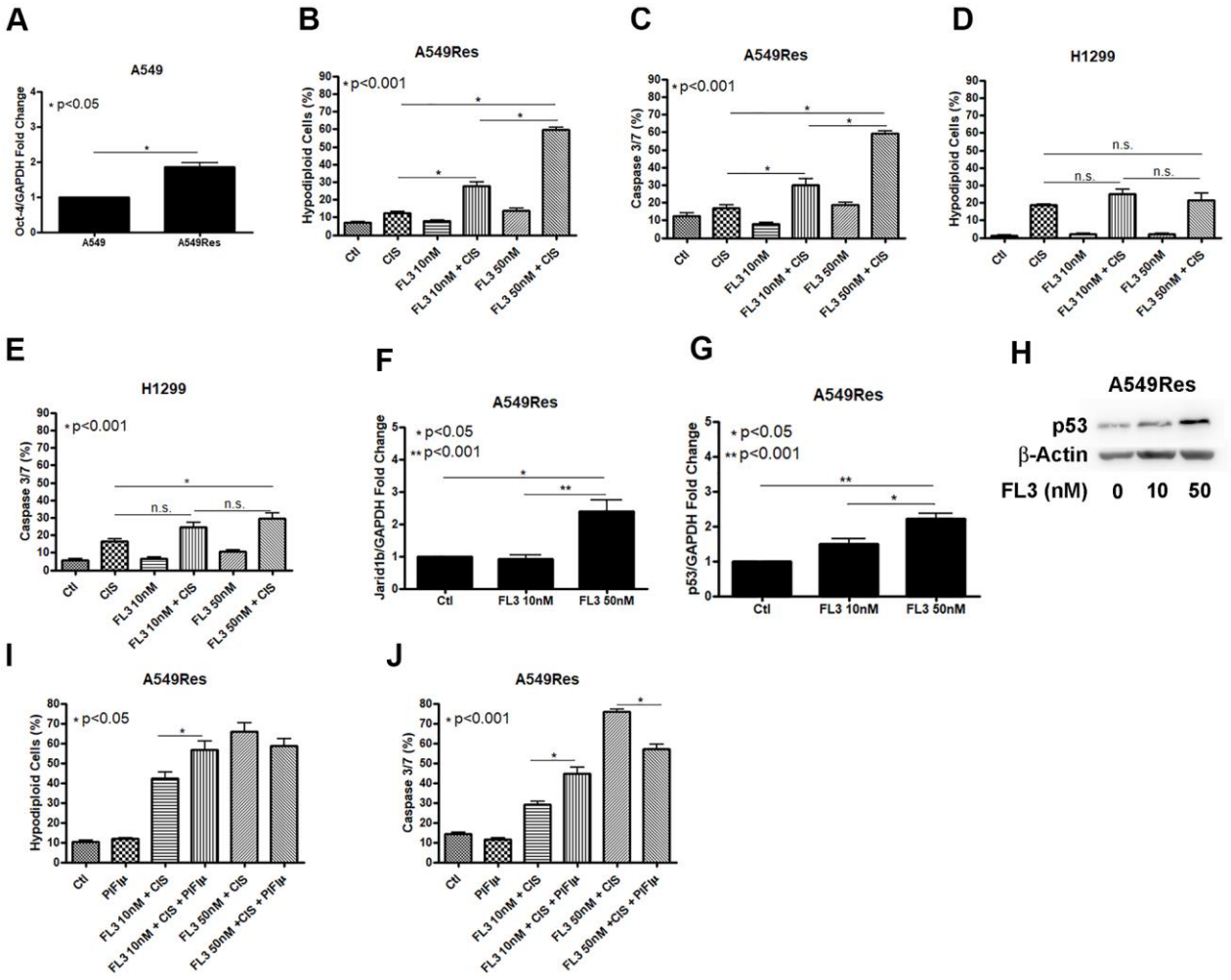

Figure 6. FL3 sensitizes A549Res cells but not H1299 cells to cisplatin. Sub-lethal treatment with cisplatin increased Oct-3 expression in A549Res cells (p<0.05) (**A**). The synthetic flavagline FL3 sensitized A549Res cells to cisplatin as measured by DNA fragmentation (p<0.001) (**B**) and caspase 3 and 7 activation (p<0.001) (**C**), Treatment with 50nM of FL3 combined with cisplatin did not increase DNA fragmentation on H1299, but increased caspase 3 and 7 activation, when compared to cisplatin alone (p<0.001) (**D**, **E**, respectively). In A549 cells, Jarid1b expression is increased upon FL3 treatment (p<0.05) (**F**). However, P53 expression is also increased upon FL3 treatment (p<0.001) (**G**, **H**). P53 inhibition by pifithrin-μ does not protects A549Res to cisplatin-induced cell death through DNA fragmentation assay but caspase 3 and 7 activation is lowered (p<0.001) (**I**, **J**, respectively). Data represent the mean of three independent experiments. FL3 treatment was kept during all experiment for H1299 and A549Res cells.

A549Res cells after FL3 treatment in A549Res cells (Figure 6B, 6C) but is not enough to sensitize the H1299 cells (Figure 6D, 6E). In A549 cells, FL3 treatment increased Jarid1b expression in a dose-dependent manner (Figure 6F). However, FL3 treatment did not downregulate P53 and, instead, P53 levels were elevated, even though Jarid1b was overexpressed (Figure 6G, 6H). We asked if P53 localization in the mitochondria is necessary for FL3-induced chemo-sensitization to cisplatin. Figure 6I, 6J shows that pifithrin-μ did not reduce DNA fragmentation, yet did decrease the apoptotic pathway in A549Res cells, raising the possibility that an alternative cell death pathway compensated for the decrease in caspase 3/7 activity. Interestingly, the chemosensitization seen with high dose of FL3 treatment was diminished in the presence of metformin (Supplementary Figure 6).

DISCUSSION

Non-small cell lung cancer is among the most lethal tumors and treatment frequently has a poor prognosis. A recent publication shows that metformin has no impact in platinum-based therapy for NSCLC [33]. Another publication shows that metformin enhances cisplatin-induced sensitivity to radiotherapy in two wild type P53 cell lines [34]. However, these two publications did not directly examine whether presence or not of P53 played a role in metformin-induced chemosensitization. Our work shows that the presence of P53 is necessary for the effectiveness of metformin-induced chemosensitization of cisplatin in NSCLC.

In this manuscript, we show that P53 is necessary for metformin-induced chemosensitization to cisplatin in NSCLC cells. In the A549 and HCC 827 cells, both wild type for P53, the combination of metformin and cisplatin increased the levels of DNA fragmentation and apoptosis activation, resulting in higher cell death, when compared to cisplatin and metformin treatment alone (Figure 1). In the H1299 and H358 cells, both P53 null, (Figure 5) and in the A549Res (Figure 2), no chemosensitization was seen. Therefore, using short-term treatment, as the doses used for cisplatin in all cells were too high to generate clones, P53 is necessary for metformin-induced chemosensitization to cisplatin in these cell lines. However, the same result was seen in the animal experiments for A549 and H1299 cells. We also show that Jarid1b overexpression is a cellular response to cisplatin, by downregulating P53 levels and protecting cells to the combined therapy. This *in vitro* and *in vivo* data is promising and warrants further investigation to work towards clinical studies.

The histone demethylase Jarid1b drives tumor metabolism towards OXPHOS and is a potential target for cancer therapy. Jarid1b overexpression is associated with poor prognosis in NSCLC [35] as seen by TCGA dataset (Figure 3F). Kaplan-Meier curve showed that Jarid1b is associated with poor prognosis in Stage 3 lung adenocarcinoma where the tumor is more resistant to treatment (Supplementary Figure 3C). In stage 1 and 2, Jarid1b low expression is associated with poor prognosis population (Supplementary Figure 3A, 3B) probably because Jarid1b can induce a slow-cycling and a long-term tumor maintaining population [18], making the tumors in these stages less aggressive. Biguanides like metformin and phenformin can target Jarid1b overexpressing cells, as these drugs can target the mitochondria, enhancing the effect of BRAF V600E inhibitors [36]. However, differently than expected, metformin works as a chemosensitizing agent to cisplatin in the A549 cells and not in the A549Res cells, where Jarid1b is overexpressed.

Roesch et al. showed that in melanomas, a biguanide like phenformin inhibited the mitochondria in Jarid1b overexpressing cells and restored the chemosensitivity of these cells [18]. In the A549 cells, metformin was not sufficient to restore the chemosensitivity of Jarid1b high expressing cells. The first reason could be because phenformin is a biguanide more powerful than metformin. However, phenformin increases lactic acidosis in patients, which can be potentially harmful. The second reason is because in the A549 cells, P53 is necessary for the ability of metformin to chemosensitize these cells to cisplatin. However, this mechanism still needs to be further explored as it seems to be tumor-context dependent as both the A2780 (P53 WT) and SK-OV-3 (P53 null) ovary cancer cell line does not respond to the combination of metformin and cisplatin (Supplementary Figure 5).

AMPK activation can phosphorylate and translocate P53 to the mitochondria and this translocation can be inhibited by pifithrin-μ [23, 37]. In a parallel study, metformin does not induce AMPK phosphorylation, using the same protocol used to generate the A549Res cells [38]. However, metformin treatment decreases mTOR activity in both A549 and A549Res cells, as expected. Thus, P53 translocate to the mitochondria in an AMPK-independent pathway in A549 cells. Figure 1 shows that P53 co-localization on the mitochondria is important for the chemosensitization of A549 cells as the inhibition of P53 translocation to the mitochondria by pifithrin-μ protects A549 cells from metformin-induced chemosensitization to cisplatin. It would be interesting to know whether *TP53* harboring any mutation will respond to cisplatin and metformin combination in NSCLC. One hypothesis is that even if a mutated *TP53* has lost its ability to transactivate target genes, it could chemosensitize NSCLC cells if the

mutated P53 still has the ability associate with the mitochondria.

Tumor cell metabolism is a hallmark of cancer and is an important target for therapy. A subpopulation of tumor cells that uses oxidative phosphorylation as the main ATP source is resistant to chemotherapy and is generated by sub-lethal doses of many types of chemotherapy. One of these subpopulations has overexpression of the transcriptional coactivator peroxisome proliferator-activated receptor gamma coactivator-1 alpha (PGC-1alpha) which turns metabolism towards OXPHOS and protects cells from chemotherapy [39, 40] and is also overexpressed in A549Res cells (data not shown). To our surprise, sub-lethal treatment with cisplatin turns the metabolism towards glycolysis, even in the presence of Jarid1b. Jarid1b inhibition increases glycolysis after metformin treatment, showing that Jarid1b overexpression in A549Res cells still tries to hold the metabolism in the oxidative phosphorylation, but is overcome by the cisplatin treatment.

A549Res cells are resistant to the combination of cisplatin and metformin, indicating that a change in metabolism (i.e., increase in glycolysis) is not enough to their chemosensitization. In A549 cells, metformin does not increase glycolysis and, yet metformin is able to chemosensitize to cisplatin. Hence, metformin is chemosensitizing the A549 cells to cisplatin not by modulating the metabolism, but, at least in part, by using P53 as a chemosensitizing agent. Also, the increase in glycolysis in cisplatin-treated cells could explain the increase in tumor volume of A549 cells injected in NOD/SCID mice (Figure 1E), where tumors from the cisplatin-treated group had the highest volumes and weights (Figure 1E, 1F).

The rise of Jarid1b overexpressing cells upon cisplatin treatment seems to be transitory. Roesch et al. showed in melanoma model that the Jarid1b overexpressing cells lose Jarid1b expression spontaneously and become sensitive again to chemotherapy [18]. We observed that Jardi1b expression keeps high after 30 days of cisplatin treatment and the morphology of these cells changes to the non-resistant A549 morphology and cell starts to proliferate again (Supplementary Figure 1F). It seems that the cost of the resistance is the loss of proliferation in the A549 cells line. The genetic and/or epigenetic basis of this behavior still need to be understood.

In a parallel study [38], applying a proteomic approach to analyze the very same cell population groups studied here, A549Res cells showed that metformin decreased the expression of Lactate Dehydrogenase B (LDHB) and Succinate-CoA Ligase GDP-Forming Subunit Beta (SUCLG2), which can convert lactate into pyruvate and catalyze the conversion of succinyl-CoA to succinate, respectively [41, 42], on A549 cells. Nevertheless, metformin was not able to increase the lactate production in this population. Interesting, metformin treatment in A549 cells could decrease fatty acid oxidation enzymes like Electron Transfer Flavoprotein Subunit Alpha (ETFA) and Enoyl-CoA Hydratase 1 (ECH1), while increased the expression of Hydroxyacyl-CoA Dehydrogenase Trifunctional Multienzyme Complex Subunit Alpha (HADHA) in A549Res cells (data not shown). A549 cells are highly dependent on fatty acid oxidation, such dependence increases upon cisplatin treatment as observed in A549Res cells (Supplementary Figure 4C). Taken together, fatty acid oxidation could be a potential target to sensitize A549 cells to chemotherapy. Evidence in the literature showed that A549 cells in co-culture with differentiated 3T3-L1 adipocytes or harvested with its conditioned media increased cell proliferation, migration, invasion and fatty acid metabolism [43].

H1299 and H358 P53 null cells are resistant to the cisplatin and metformin combination (Figure 5). Despite H1299 cells being more sensitive to metformin and to cisplatin than the A549 cells (Supplementary Figure 7), and metformin decreased the number of colonies *in vitro*, metformin did not chemosensitize H1299 cells to cisplatin *in vivo*, as no difference in tumor growth and weight was seen using the same cisplatin and metformin dosage and the same treatment protocol as used in A549 cells, where the combination decreased tumor volume and weight (Figure 1E, 1F). This result shows that the lower dose of cisplatin and metformin used *in vitro* for the H1299 cells is not the reason that the combined treatment did not work for this cell line.

One of the ways that cisplatin can induce cell death is by enhancing reactive oxygen species (ROS) production in the mitochondria. Even though cisplatin treatment does not turn the metabolism into OXPHOS in A549Res cells through Jardi1b and PGC-1alpha (data not shown) overexpression, cisplatin-induced chemoresistance could still increase ROS protection as a chemoresistance mechanism. ROS production that could lead to cell death in A549 cells is related to the cisplatin treatment during the generation of the resistant A549Res cells and not to Jarid1b overexpression. No increment in ROS production is seen when comparing metformin-treated cells between A549Res and A549Res under PBIT treatment. Furthermore, pifithrin-μ, which protects A549 cells by blocking P53 translocation to the mitochondria, does not modify ROS production after metformin treatment in any condition (Supplementary Figure 8). Also, Jarid1b inhibition by PBIT does not increase ROS levels in A549Res after cisplatin and

metformin combination (Supplementary Figure 8D). This evidence reinforces the idea that Jarid1b is protecting A549 cells through P53 downregulation and not by protecting them from ROS increase. Also, mitochondrial membrane potential and mitochondrial mass does not change under PBIT treatment (Supplementary Figure 8B, 8C).

In this work, we are showing that cisplatin treatment induces a chemoresistant subpopulation when the drug concentration is not strong enough to kill the tumor cells, that potentially will lead to treatment failure. It is urgent to find a way to block the rising of resistant cells after treatment. The stem cell behavior of Jarid1b overexpressing cells is related to the stem cell marker Oct4, as Jarid1b inhibition downregulates Oct4 [44]. The synthetic flavagline FL3 has been reported to selectively kill Oct4 overexpressing cells without affecting normal cells [25]. Therefore, FL3 could potentially kill cisplatin-induced chemoresistant cells in the tumor microenvironment, like Jarid1b overexpressing cells. FL3 was able to chemosensitize to cisplatin the A549Res cells but not H1299 cells (Figure 6), despite both cell lines expresses Oct4 [45]. Whether P53 is necessary or not for FL3 chemosensitization to cisplatin still need to be investigated. FL3 also prevent apoptosis in normal human skin cells, but not to malignant cells, through BAD activation [46] making it a good candidate for treatment where Jarid1b overexpressing subpopulation are present. This way, FL3 could be used in a treatment protocol, using cisplatin, where FL3 and metformin are not used at the same time as metformin protects from FL3-induced chemosensitization to cisplatin in A549Res cells when cells are treated with high doses of FL3 (Supplementary Figure 6).

MATERIALS AND METHODS

Cell culture, reagents, and primers for RT-PCR

A549, H1299 and HCC 827 NSCLC cells were purchased from Banco de Células do Rio de Janeiro. H358 cells were kindly provided by Dr. Daniela Basseres from Instituto de Química da USP. A549 cells were cultivated in Ham's F12 Nutrient Mixture media supplemented with 10% fetal bovine serum (FBS). H1299 NSCLC cells were cultivated in RPMI 1640 media supplemented with 10% FBS. HCC 827 and H358 were cultivated in RPMI 1640 media supplemented for 4000 mg/mL of glucose and 1mM of sodium pyruvate and supplemented with 10% fetal bovine serum. All experiments were made between passages 5 and 20 for A549 cells, between passages 28 to 40 for H1299 cells, between passages 35 to 50 for H358 and between passages 12 to 30 for HCC 827. All human cell lines were authenticated using Short Tandem Repeat (STR) profiling and pro filed within the last three years. All experiments were performed with mycoplasma-free cells. Cisplatin (cat: P4394), Metformin (cat: PHR1084), Pifithrin-μ (cat: P0122), PBIT (cat: sml1058), Thiazolyl Blue Tetrazolium Bromide (MTT) (cat: M2128) and Hoechst 33258 (cat: 94403) were purchased from Sigma-Aldrich. siRNA for *TP53* (cat: sc-29435) and Jarid1b (cat: sc-44522) were purchased from Santa Cruz Biotechnology. P53 antibody (cat: #9286) was purchased from Cell Signaling. Primers for Jarid1b (Forward: TGCTCCAGGTATCCCTTCCT Reverse: CCTCGGCAACAGTCATTCTTC); GAPDH (Forward: GGTGGTCTCCTCTGACTTCAACA Reverse: GGTG CTGTAGCCAAATTCGTTGT); *TP53* (Forward: CGC TTCGAGATGTTCCGAGA Reverse: CTTCAGGTGG CTGGAGTGAG); Oct-4 (Forward: TCTCCCATGCAT TCAAACTGAG Reverse: CCTTTGTGTGTTCCCAAT TCCTTC), CellEvent Caspase-3/7 Green Detection Reagent (cat: C10423), Opti-MEM (cat: 22600050), Mitotracker Red CMXRos (cat: M7512) and Alexa Fluor 488 (cat: A-11001) were purchased from Thermo-Scientific.

Generation of A549 resistant cells (A549Res) and cell treatment

A549 cells were treated with sub-lethal dose of cisplatin (10 μM for 72 h) to generate cisplatin resistant cells (A549Res). A549 or A549Res cells were treated with metformin (10 mM for 72 h), prior to high dose of cisplatin (25 μM) and/or metformin for another 72 h. PBIT (20 μM) was added before the sub-lethal treatment with cisplatin and pifithrin-μ (15 μM) was added before metformin treatment and both were kept during all the experiment. H1299 cells were treated with 2 mM of metformin for 72 h and then, treated with 12.5 μM of cisplatin, combined or not with metformin for another 72 h. H358 and HCC 827 cells were treated with 20 mM of metformin for 72 h and then treated with 20 μM of cisplatin combined or not with metformin for another 72 h.

Animal experiments

Seven weeks-old male NOD/SCID mice were divided in groups of eight animals with four animals per cage. In each cage, animals were randomized in different experimental group. Two million and a half cells/animal for the A549 cells and one million cells/animal for the H1299 cells were injected in the subcutaneous of the animals. Treatment started when palpable but not measurable tumors were detected. Commercial metformin, (Merck, lot number BR78614) was administered daily (350 mg/kg) diluted in 100 μL of regular mineral water through oral gavage for 14 days, starting one day before cisplatin treatment (four doses

every 72 h, 2 mg/kg in PBS, intraperitoneally). All animals were sacrificed when the first tumor reached 1 cm^3, for ethical reasons. Tumor volume was measured through the following equation: $V=d^2*D*0.52$ (V: volume, d: minor diameter and D: major diameter).

siRNA for *TP53* and Jarid1b

One hundred thousand cells/well of A549 or HCC 827 cells were plated on a 6 well plate. siRNA for Jarid1b (40 nM) or *TP53* (20 nM) was transfected with oligofectamine (8 µL/well) for 6h using Opti-Mem in the absence of fetal bovine serum. Oligofectamine and the siRNA were incubated alone in Opti-Mem media for 5 minutes alone and then were incubated together for 20 minutes for the oligofectamine-siRNA complex formation. After three washes with PBS, the Opti-Mem media containing the oligofectamine-siRNA complex was added to the 6 well plate (600 µL/well). After 6 hours, the Opti-Mem media containing the siRNA was replaced by the respective complete media. For a longer experiment using Jarid1b siRNA, a second inhibition was made after sub-lethal treatment with cisplatin.

DNA fragmentation and caspase 3/7 assay

Thirty thousand cells/well were plated on a 12 well plate. For the DNA fragmentation assay, cells were fixed in 70% ethanol for 2 h at room temperature, washed once with PBS and incubated in 200 µL of propidium iodide (PI) solution (0.1% Triton X-100, 200 µg/ml of RNAse A and 20 µg/ml of PI) for 30 min at room temperature, protected from light. The hypodiploid content was used to estimate cells that were in cell death process. For Caspase 3 and 7 activation, cells were incubated with CellEvent Caspase-3/7 Green Detection Reagent (2 µM) in Ham's F12 Nutrient Mixture media with 10% FBS for the A549 cells or RPMI 1640 with 10% FBS for the H1299 cells at 37° C 5% CO_2 incubator for 1h, protected from light. Caspase 3/7 positive cells was calculated through measurement of caspase 3/7 positive cells over caspase 3/7 positive and negative cells in flow cytometry.

P53 adenoviral transduction

The non-replicating, serotype 5 adenoviral vectors AdCMVp53 and AdPGLuc have been described previously [47]. Virus purification in a gradient of iodixanol and titration using the Adeno-Xtm Rapid Titer Kit (Clontech) followed the procedures described in these previous publications. One hundred thousand A549 cells were plated in a 6 well plate and treated with 10 µM of cisplatin to generate A549Res cells. After 72 h the A549Res cells were transduced with the adenoviral vectors, AdPGLuc or AdCMVp53, using a multiplicity of infection (MOI) of 3 in Ham's F12 Nutrient Mixture culture medium with 2% fetal bovine serum. After 16 hours incubation at 37° C, cells were washed with PBS and cultivated in Ham's F12 Nutrient Mixture medium containing 10% FBS. After 48 h, A549Res cells were treated accordingly to the protocol for chemosensitization to cisplatin by metformin.

Protein extraction and western blot

Cells were trypsinized and centrifuged at 370 g for 2 min. Cell pellet was resuspended in RIPA buffer with protease inhibitor cocktail (Sigma cat: S8830) and left to stand at 4° C for 30 min. The homogenate was centrifuged at 4° C for 15 min at 13200 g and supernatant was collected. Protein content was measured with the BCA reagent kit (ThermoScientific cat: 23225). About 100 µg of proteins were separated on 10% polyacrylamide gel (0.375 M Tris, pH 8.8, 0.1% SDS, 10% acrylamide, 0.03% ammonium persulfate (APS), and 0.06% N,N,N′,N′-tetramethylethylenediamine (TEMED)), and transfer-red to a hydrophobic polyvinylidene difluoride (PVDF) membrane. The nonspecific sites of the membrane were blocked with 5% fat-free milk in 0.1% PBS-Tween for 1 h at room temperature. PVDF membrane was incubated with the primary antibody overnight at 4° C. Membrane was washed three times with 5% fat-free milk in 0.1% PBS-Tween for 1 h at room temperature and the membrane was incubated with the secondary antibody for 1 hour at room temperature. The samples were visualized with the chemiluminescent substrate ECL (GE Healthcare).

Cell viability through MTT

One two, or five thousand cells for the H1299, A549, A549Res cells, respectively, were plated on a 96 well plate. MTT solution (0.45 mg/mL final concentration) was added in culture media for 2 h in 37° C 5% CO_2, protected from light. Cells were lysed in DMSO (150 µL/well), homogenized and the absorbance was read in 595 nm on a microplate reader.

Clonogenic assay

Cells were treated according to their respective protocol. After treatment, 300 cells were plated in a 6 well plate and when colonies in the control group reached around 50 cells (7 days for H1299 cells; 9 days for A549, HCC 827 and H358 cells; 30 days for A549Res cells) cells were the washed with PBS and fixed with PBS/formaldehyde 4% for 15 minutes. Cells were washed again with PBS and incubated with crystal violet 0.1% for 10 minutes. After three washes with PBS, the plate was left for dry and then colonies were counted.

Fluorescence microscopy

Ten thousand cells were plated onto a 24 well plate over a 30 mm coverslip where all treatments were made. For mitochondria labeling, Mitotracker Red CMXRos was diluted culture media (500 nM) and incubated at 37° C and 5% CO2 for 20 min. Cells were then fixed in 4% paraformaldehyde in PBS for 15 min and washed three times with PBS. 0.2% Triton X-100 in PBS was added for 5 min for cell permeabilization. Nonspecific sites were blocked in 5% PBS/BSA for 1 h. Primary antibody was incubated O.N. in 4° C. After three times washed in 1% PBS/BSA, secondary antibody conjugated with Alexa Fluor 488 (4 µg/mL) and Hoechst 33258 (0.5 mg/mL) were incubated for 1 h at room temperature in 5% PBS/BSA. After incubation, coverslips were mounted in a slide and cells were observed in the EVOS© microscope.

Glycolytic analysis, glucose consumption and lactate production

After respective treatment, A549's culture media was removed, and cells were washed with PBS. New Ham's F12 Nutrient Mixture media, supplemented with 10% of FBS, was added in a volume of 1 ml. Cells were incubated in a 37° C and 5% CO_2 for 1h. 200µL of the fresh A549 culture media was transferred to a 96 well plate in triplicate and the plate was transferred to the YSI 2950 Biochemistry Analyzer for glucose consumption and lactate production measurement Over 20000 cells of the remaining cells were plated in quintuplicate on the Seahorse XFe96 cell culture plate. Glycolysis Stress Test on the seahorse was made accordingly to user manual.

TCGA data analysis

The survival curve comparing high and low expression of Jarid1b and *TP53* in lung adenocarcinoma was made in the Human Protein Atlas website (https://www.proteinatlas.org/), using the Cancer Genome Atlas (TCGA) RNA samples. All parameters were set to default.

Statistical analysis

All statistical analysis was made in the GraphPad Prism software v4.03, using one or two-way ANOVA and Bonferroni for Post Test.

Ethical approval

All procedures were in accordance with the guidelines of the Brazilian Council on Animal Care (COBEA) and approved by the Ethical Committee for Animal Research of School of Medicine (registry number: 100/16), University of São Paulo and the National Technical Commission on Biosafety (CTNBio), process number: 98509/2015.

Abbreviations

A549Res: A549 cisplatin resistant cells; AMPK: AMP-activated protein kinase; CIS: Cisplatin; ECAR: Extracellular Acidification Rate; ECH1: Enoyl-CoA Hydratase 1; ETFA: Electron Transfer Flavoprotein Subunit Alpha; FBS: Fetal Bovine Serum; HADHA: Hydroxyacyl-CoA Dehydrogenase Trifunctional Multienzyme Complex Subunit Alpha; Jarid1b: Jumonji/ ARID1 H3K4 Histone Demethylase; LDHB: Lactate Dehydrogenase B; Met: Metformin; MOI: Multiplicity of Infection; NSCLC: Non-Small-Cell Lung Cancer; OCR: Oxygen Consumption Rate; Oct4: Octamer-Binding Transcription Factor 4; OXPHOS: Oxidative Phosphorylation; PGC-1alpha: Peroxisome Proliferator-Activated Receptor Gamma Coactivator-1 alpha; ROS: Reactive Oxygen Species; STR: Short Tandem Repeat; SUCLG2: Succinate-CoA Ligase GDP-Forming Subunit Beta; TCGA: The Cancer Genome Atlas.

AUTHOR CONTRIBUTIONS

Main Experiments and drafting article: T.C.T.J. Experimental procedures: R.E.T., M.S.J., J.S.M., S.O.B. Data analysis and interpretation: R.J.M.N., S.H. Critical review and discussion T.C.T.J., R.E.T., M.S.J., J.S.M., S.O.B., R.J.M.N., S.H., L.D., B.E.S., R.C.

ACKNOWLEDGMENTS

We thank Dr. Robert J. Gillies from H. Lee Moffitt Cancer Center and Research Institute, USA, for the experiments with the Seahorse XFe96 and the YSI 2950 Biochemistry Analyzer, Dr. Kirill Afonin from the department of chemistry of the University of Charlotte for the experiments with siRNA and Dr. Marsha Rosner from the University of Chicago for the discussions about metformin in cancer treatment.

CONFLICTS OF INTEREST

The authors declare no conflicts of interest.

FUNDING

This work was provided by Fundação de Amparo à Pesquisa do Estado de S. Paulo - FAPESP (Grant# 2015/26580-9; 2015/22814-5; 2019/08147-7), Conselho Nacional de Desenvolvimento Científico e Tecnológico - CNPq (Grant# 305700/2017-0) and UICC Yamagiwa-Yoshida Memorial International Cancer Study Grant.

REFERENCES

1. Yoon SM, Shaikh T, Hallman M. Therapeutic management options for stage III non-small cell lung cancer. World J Clin Oncol. 2017; 8:1–20. https://doi.org/10.5306/wjco.v8.i1.1 PMID:28246582

2. Paz-Ares L, Luft A, Vicente D, Tafreshi A, Gümüş M, Mazières J, Hermes B, Çay Şenler F, Csőszi T, Fülöp A, Rodríguez-Cid J, Wilson J, Sugawara S, et al, and KEYNOTE-407 Investigators. Pembrolizumab plus Chemotherapy for Squamous Non-Small-Cell Lung Cancer. N Engl J Med. 2018; 379:2040–51. https://doi.org/10.1056/NEJMoa1810865 PMID:30280635

3. Borghaei H, Paz-Ares L, Horn L, Spigel DR, Steins M, Ready NE, Chow LQ, Vokes EE, Felip E, Holgado E, Barlesi F, Kohlhäufl M, Arrieta O, et al. Nivolumab versus Docetaxel in Advanced Nonsquamous Non-Small-Cell Lung Cancer. N Engl J Med. 2015; 373:1627–39. https://doi.org/10.1056/NEJMoa1507643 PMID:26412456

4. Sanchez-Rangel E, Inzucchi SE. Metformin: clinical use in type 2 diabetes. Diabetologia. 2017; 60:1586–93. https://doi.org/10.1007/s00125-017-4336-x PMID:28770321

5. Zhou J, Massey S, Story D, Li L. Metformin: An Old Drug with New Applications. Int J Mol Sci. 2018; 19:2863. https://doi.org/10.3390/ijms19102863 PMID:30241400

6. Currie CJ, Poole CD, Gale EA. The influence of glucose-lowering therapies on cancer risk in type 2 diabetes. Diabetologia. 2009; 52:1766–77. https://doi.org/10.1007/s00125-009-1440-6 PMID:19572116

7. Bishnu A, Sakpal A, Ghosh N, Choudhury P, Chaudhury K, Ray P. Long term treatment of metformin impedes development of chemoresistance by regulating cancer stem cell differentiation through taurine generation in ovarian cancer cells. Int J Biochem Cell Biol. 2019; 107:116–27. https://doi.org/10.1016/j.biocel.2018.12.016 PMID:30593952

8. Zhang C, Wang Y. Metformin attenuates cells stemness and epithelial-mesenchymal transition in colorectal cancer cells by inhibiting the Wnt3a/β-catenin pathway. Mol Med Rep. 2019; 19:1203–09. https://doi.org/10.3892/mmr.2018.9765 PMID:30569135

9. Zhao Y, Gong C, Wang Z, Zhang J, Wang L, Zhang S, Cao J, Tao Z, Li T, Wang B, Hu X. A randomized phase II study of aromatase inhibitors plus metformin in pre-treated postmenopausal patients with hormone receptor positive metastatic breast cancer. Oncotarget. 2017; 8:84224–36. https://doi.org/10.18632/oncotarget.20478 PMID:29137418

10. Reni M, Dugnani E, Cereda S, Belli C, Balzano G, Nicoletti R, Liberati D, Pasquale V, Scavini M, Maggiora P, Sordi V, Lampasona V, Ceraulo D, et al. (Ir)relevance of Metformin Treatment in Patients with Metastatic Pancreatic Cancer: An Open-Label, Randomized Phase II Trial. Clin Cancer Res. 2016; 22:1076–85. https://doi.org/10.1158/1078-0432.CCR-15-1722 PMID:26459175

11. El-Mir MY, Nogueira V, Fontaine E, Avéret N, Rigoulet M, Leverve X. Dimethylbiguanide inhibits cell respiration via an indirect effect targeted on the respiratory chain complex I. J Biol Chem. 2000; 275:223–28. https://doi.org/10.1074/jbc.275.1.223 PMID:10617608

12. Gwinn DM, Shackelford DB, Egan DF, Mihaylova MM, Mery A, Vasquez DS, Turk BE, Shaw RJ. AMPK phosphorylation of raptor mediates a metabolic checkpoint. Mol Cell. 2008; 30:214–26. https://doi.org/10.1016/j.molcel.2008.03.003 PMID:18439900

13. Emami Riedmaier A, Fisel P, Nies AT, Schaeffeler E, Schwab M. Metformin and cancer: from the old medicine cabinet to pharmacological pitfalls and prospects. Trends Pharmacol Sci. 2013; 34:126–35. https://doi.org/10.1016/j.tips.2012.11.005 PMID:23277337

14. Scotland S, Saland E, Skuli N, de Toni F, Boutzen H, Micklow E, Sénégas I, Peyraud R, Peyriga L, Théodoro F, Dumon E, Martineau Y, Danet-Desnoyers G, et al. Mitochondrial energetic and AKT status mediate metabolic effects and apoptosis of metformin in human leukemic cells. Leukemia. 2013; 27:2129–38. https://doi.org/10.1038/leu.2013.107 PMID:23568147

15. Yamamoto S, Wu Z, Russnes HG, Takagi S, Peluffo G, Vaske C, Zhao X, Moen Vollan HK, Maruyama R, Ekram MB, Sun H, Kim JH, Carver K, et al. JARID1B is a luminal lineage-driving oncogene in breast cancer. Cancer Cell. 2014; 25:762–77. https://doi.org/10.1016/j.ccr.2014.04.024 PMID:24937458

16. Xiang Y, Zhu Z, Han G, Ye X, Xu B, Peng Z, Ma Y, Yu Y, Lin H, Chen AP, Chen CD. JARID1B is a histone H3 lysine 4 demethylase up-regulated in prostate cancer. Proc Natl Acad Sci USA. 2007; 104:19226–31. https://doi.org/10.1073/pnas.0700735104 PMID:18048344

17. Fang L, Zhao J, Wang D, Zhu L, Wang J, Jiang K. Jumonji AT-rich interactive domain 1B overexpression is associated with the development and progression of glioma. Int J Mol Med. 2016; 38:172–82. https://doi.org/10.3892/ijmm.2016.2614 PMID:27246838

18. Roesch A, Vultur A, Bogeski I, Wang H, Zimmermann KM, Speicher D, Körbel C, Laschke MW, Gimotty PA, Philipp SE, Krause E, Pätzold S, Villanueva J, et al. Overcoming intrinsic multidrug resistance in melanoma by blocking the mitochondrial respiratory chain of slow-cycling JARID1B(high) cells. Cancer Cell. 2013; 23:811–25. https://doi.org/10.1016/j.ccr.2013.05.003 PMID:23764003

19. Dey BK, Stalker L, Schnerch A, Bhatia M, Taylor-Papidimitriou J, Wynder C. The histone demethylase KDM5b/JARID1b plays a role in cell fate decisions by blocking terminal differentiation. Mol Cell Biol. 2008; 28:5312–27. https://doi.org/10.1128/MCB.00128-08 PMID:18591252

20. Lynch TJ, Bell DW, Sordella R, Gurubhagavatula S, Okimoto RA, Brannigan BW, Harris PL, Haserlat SM, Supko JG, Haluska FG, Louis DN, Christiani DC, Settleman J, Haber DA. Activating mutations in the epidermal growth factor receptor underlying responsiveness of non-small-cell lung cancer to gefitinib. N Engl J Med. 2004; 350:2129–39. https://doi.org/10.1056/NEJMoa040938 PMID:15118073

21. Skaug V, Ryberg D, Kure EH, Arab MO, Stangeland L, Myking AO, Haugen A. p53 mutations in defined structural and functional domains are related to poor clinical outcome in non-small cell lung cancer patients. Clin Cancer Res. 2000; 6:1031–37. PMID:10741731

22. Brady CA, Jiang D, Mello SS, Johnson TM, Jarvis LA, Kozak MM, Kenzelmann Broz D, Basak S, Park EJ, McLaughlin ME, Karnezis AN, Attardi LD. Distinct p53 transcriptional programs dictate acute DNA-damage responses and tumor suppression. Cell. 2011; 145:571–83. https://doi.org/10.1016/j.cell.2011.03.035 PMID:21565614

23. Nieminen AI, Eskelinen VM, Haikala HM, Tervonen TA, Yan Y, Partanen JI, Klefström J. Myc-induced AMPK-phospho p53 pathway activates Bak to sensitize mitochondrial apoptosis. Proc Natl Acad Sci USA. 2013; 110:E1839–48. https://doi.org/10.1073/pnas.1208530110 PMID:23589839

24. Thuaud F, Bernard Y, Türkeri G, Dirr R, Aubert G, Cresteil T, Baguet A, Tomasetto C, Svitkin Y, Sonenberg N, Nebigil CG, Désaubry L. Synthetic analogue of rocaglaol displays a potent and selective cytotoxicity in cancer cells: involvement of apoptosis inducing factor and caspase-12. J Med Chem. 2009; 52:5176–87. https://doi.org/10.1021/jm900365v PMID:19655762

25. Emhemmed F, Ali Azouaou S, Thuaud F, Schini-Kerth V, Désaubry L, Muller CD, Fuhrmann G. Selective anticancer effects of a synthetic flavagline on human Oct4-expressing cancer stem-like cells via a p38 MAPK-dependent caspase-3-dependent pathway. Biochem Pharmacol. 2014; 89:185–96. https://doi.org/10.1016/j.bcp.2014.02.020 PMID:24607276

26. Polier G, Neumann J, Thuaud F, Ribeiro N, Gelhaus C, Schmidt H, Giaisi M, Köhler R, Müller WW, Proksch P, Leippe M, Janssen O, Désaubry L, et al. The natural anticancer compounds rocaglamides inhibit the Raf-MEK-ERK pathway by targeting prohibitin 1 and 2. Chem Biol. 2012; 19:1093–104. https://doi.org/10.1016/j.chembiol.2012.07.012 PMID:22999878

27. Chiu GS, Maj MA, Rizvi S, Dantzer R, Vichaya EG, Laumet G, Kavelaars A, Heijnen CJ. Pifithrin-μ Prevents Cisplatin-Induced Chemobrain by Preserving Neuronal Mitochondrial Function. Cancer Res. 2017; 77:742–52. https://doi.org/10.1158/0008-5472.CAN-16-1817 PMID:27879267

28. Yu L, Fan Z, Fang S, Yang J, Gao T, Simões BM, Eyre R, Guo W, Clarke RB. Cisplatin selects for stem-like cells in osteosarcoma by activating Notch signaling. Oncotarget. 2016; 7:33055–68. https://doi.org/10.18632/oncotarget.8849 PMID:27102300

29. Sun NK, Huang SL, Chang TC, Chao CC. TLR4 and NFκB signaling is critical for taxol resistance in ovarian carcinoma cells. J Cell Physiol. 2018; 233:2489–501. https://doi.org/10.1002/jcp.26125 PMID:28771725

30. Sayegh J, Cao J, Zou MR, Morales A, Blair LP, Norcia M, Hoyer D, Tackett AJ, Merkel JS, Yan Q. Identification of small molecule inhibitors of Jumonji AT-rich interactive domain 1B (JARID1B) histone demethylase by a sensitive high throughput screen. J Biol Chem. 2013; 288:9408–17. https://doi.org/10.1074/jbc.M112.419861 PMID:23408432

31. Shen X, Zhuang Z, Zhang Y, Chen Z, Shen L, Pu W, Chen L, Xu Z. JARID1B modulates lung cancer cell proliferation and invasion by regulating p53 expression. Tumour Biol. 2015; 36:7133–42. https://doi.org/10.1007/s13277-015-3418-y PMID:25877751

32. Győrffy B, Surowiak P, Budczies J, Lánczky A. Online survival analysis software to assess the prognostic value of biomarkers using transcriptomic data in non-small-cell lung cancer. PLoS One. 2013; 8:e82241. https://doi.org/10.1371/journal.pone.0082241 PMID:24367507

33. Wen-Xiu X, Xiao-Wei Z, Hai-Ying D, Ying-Hui T, Si-Si K, Xiao-Fang Z, Huang P. Impact of metformin use on survival outcomes in non-small cell lung cancer treated with platinum. Medicine (Baltimore). 2018; 97:e13652. https://doi.org/10.1097/MD.0000000000013652 PMID:30572481

34. Riaz MA, Sak A, Erol YB, Groneberg M, Thomale J, Stuschke M. Metformin enhances the radiosensitizing effect of cisplatin in non-small cell lung cancer cell lines with different cisplatin sensitivities. Sci Rep. 2019; 9:1282. https://doi.org/10.1038/s41598-018-38004-5 PMID:30718758

35. Kuo KT, Huang WC, Bamodu OA, Lee WH, Wang CH, Hsiao M, Wang LS, Yeh CT. Histone demethylase JARID1B/KDM5B promotes aggressiveness of non-small cell lung cancer and serves as a good prognostic predictor. Clin Epigenetics. 2018; 10:107. https://doi.org/10.1186/s13148-018-0533-9 PMID:30092824

36. Yuan P, Ito K, Perez-Lorenzo R, Del Guzzo C, Lee JH, Shen CH, Bosenberg MW, McMahon M, Cantley LC, Zheng B. Phenformin enhances the therapeutic benefit of BRAF(V600E) inhibition in melanoma. Proc Natl Acad Sci USA. 2013; 110:18226–31. https://doi.org/10.1073/pnas.1317577110 PMID:24145418

37. Zhuang Y, Berens-Norman HM, Leser JS, Clarke P, Tyler KL. Mitochondrial p53 Contributes to Reovirus-Induced Neuronal Apoptosis and Central Nervous System Injury in a Mouse Model of Viral Encephalitis. J Virol. 2016; 90:7684–91. https://doi.org/10.1128/JVI.00583-16 PMID:27307572

38. Morelli AP, Tortelli TC Jr, Pavan IC, Silva FR, Granato DC, Peruca GF, Pauletti BA, Domingues RR, Bezerra RM, De Moura LP, Paes Leme AF, Chammas R, Simabuco FM. Metformin impairs cisplatin resistance effects in A549 lung cancer cells through mTOR signaling and other metabolic pathways. Int J Oncol. 2021; 58:28. https://doi.org/10.3892/ijo.2021.5208 PMID:33846781

39. Cruz-Bermúdez A, Laza-Briviesca R, Vicente-Blanco RJ, García-Grande A, Coronado MJ, Laine-Menéndez S, Palacios-Zambrano S, Moreno-Villa MR, Ruiz-Valdepeñas AM, Lendinez C, Romero A, Franco F, Calvo V, et al. Cisplatin resistance involves a metabolic reprogramming through ROS and PGC-1α in NSCLC which can be overcome by OXPHOS inhibition. Free Radic Biol Med. 2019; 135:167–81. https://doi.org/10.1016/j.freeradbiomed.2019.03.009 PMID:30880247

40. Vazquez F, Lim JH, Chim H, Bhalla K, Girnun G, Pierce K, Clish CB, Granter SR, Widlund HR, Spiegelman BM, Puigserver P. PGC1α expression defines a subset of human melanoma tumors with increased mitochondrial capacity and resistance to oxidative stress. Cancer Cell. 2013; 23:287–301. https://doi.org/10.1016/j.ccr.2012.11.020 PMID:23416000

41. Urbańska K, Orzechowski A. Unappreciated Role of LDHA and LDHB to Control Apoptosis and Autophagy in Tumor Cells. Int J Mol Sci. 2019; 20:2085. https://doi.org/10.3390/ijms20092085 PMID:31035592

42. Chinopoulos C, Batzios S, van den Heuvel LP, Rodenburg R, Smeets R, Waterham HR, Turkenburg M, Ruiter JP, Wanders RJ, Doczi J, Horvath G, Dobolyi A, Vargiami E, et al. Mutated SUCLG1 causes mislocalization of SUCLG2 protein, morphological alterations of mitochondria and an early-onset severe neurometabolic disorder. Mol Genet Metab. 2019; 126:43–52. https://doi.org/10.1016/j.ymgme.2018.11.009 PMID:30470562

43. Li FF, Zhang H, Li JJ, Cao YN, Dong X, Gao C. Interaction with adipocytes induces lung adenocarcinoma A549 cell migration and tumor growth. Mol Med Rep. 2018; 18:1973–80. https://doi.org/10.3892/mmr.2018.9226 PMID:29956800

44. Lin CS, Lin YC, Adebayo BO, Wu A, Chen JH, Peng YJ, Cheng MF, Lee WH, Hsiao M, Chao TY, Yeh CT. Silencing JARID1B suppresses oncogenicity, stemness and increases radiation sensitivity in human oral carcinoma. Cancer Lett. 2015; 368:36–45. https://doi.org/10.1016/j.canlet.2015.07.003 PMID:26184998

45. Leung EL, Fiscus RR, Tung JW, Tin VP, Cheng LC, Sihoe AD, Fink LM, Ma Y, Wong MP. Non-small cell lung cancer cells expressing CD44 are enriched for stem cell-like properties. PLoS One. 2010; 5:e14062. https://doi.org/10.1371/journal.pone.0014062 PMID:21124918

46. Emhemmed F, Azouaou SA, Hassan S, Lefevbre R, Désaubry L, Muller CD, Fuhrmann G. The synthetic flavagline FL3 spares normal human skin cells from its cytotoxic effect via an activation of Bad. Toxicol In Vitro. 2019; 60:27–35. https://doi.org/10.1016/j.tiv.2019.04.025 PMID:31028861

47. Tamura RE, da Silva Soares RB, Costanzi-Strauss E, Strauss BE. Autoregulated expression of p53 from an adenoviral vector confers superior tumor inhibition in a model of prostate carcinoma gene therapy. Cancer Biol Ther. 2016; 17:1221–30. https://doi.org/10.1080/15384047.2016.1235655 PMID:27646031

SUPPLEMENTARY MATERIALS

Supplementary Methods

Clonogenic assay

Cells were treated according to their respective protocol. After treatment, 300 cells were plated in a 6 well plate and when colonies in the control group reached around 50 cells (7 days for H1299 cells; 9 days for A549, HCC 827 and H358 cells; 30 days for A549Res cells) cells were the washed with PBS and fixed with PBS/formaldehyde 4% for 15 minutes. Cells were washed again with PBS and incubated with crystal violet 0.1% for 10 minutes. After three washes with PBS, the plate was left for dry and then colonies were counted.

Oxygen consumption rate and fatty acid dependence analysis on seahorse XFe96

Twenty thousand cells were plated in quintuplicate for each experimental condition on Seahorse XFe96 Cell Culture Microplates one day before the experiment. Seahorse XF Cell Mito Stress Test and dependency test of Seahorse XF Mito Fuel Flex Test were done according to user manual.

Detection of superoxide anions by MitoSOX and measurement of the mitochondrial membrane potential (Δψm) and mitochondrial mass

The fluorescent probes were purchased from Thermo Fisher, Waltham, MA USA. At the end of the experimental treatments, cells were loaded with 3 μM of MitoSOX for 30 min at 37° C in HBSS solution (Gibco). In order to analyze the mitochondrial potential and mitochondrial mass, cells were incubated with TMRE (100 nM) for 20 min at 37° C and with Mitotracker green (150 nM) for 30 min at 37° C in HBSS, respectively. The evaluation of these three probes was performed by flow cytometry. For cytometry experiments the cells were counted and normalized before the probe incubation and analyzed using the geometric mean of the median fluorescence intensity with FlowJo software (Tree Star Inc., Ashland, OR, USA).

Cell culture and reagents

A2780 human ovary carcinoma cells were purchased from Banco de Células do Rio de Janeiro and SK-OV-3 human ovary carcinoma cells were kindly provided by Dr. Érico Tosoni Costa from Hospital Sírio-Libanês. All human cell lines were authenticated using Short Tandem Repeat (STR) profiling and pro filed within the last three years. All experiments were performed with mycoplasma-free cells. A2780 were cultivated in RPMI-1640 medium containing 4500 mg/L of glucose and supplemented with 10% FBS. SK-OV-3 human ovary adenocarcinoma cells were cultivated in McCoy's 5a Medium Modified media and supplemented with 10% FBS. All experiments were made from passage 6 to 17 for A2780 cells and from passage 16 to 25 for SK-OV-3 cells. Cisplatin (cat: P4394) and Metformin (cat: PHR1084), were purchased from Sigma-Aldrich. P53 antibody (cat: #9286) was purchased from Cell Signaling.

Treatment with cisplatin and metformin on the SK-OV-3 and A2780 cells

Forty thousand SK-OV-3 cells (human ovary adenocarcinoma cell line) were plated on a 12 well plate and treated with 20 mM of metformin for 72 h prior to the treatment with cisplatin (4 μM), combined or not with metformin, for another 72 h. Five thousand A2780 cells (human ovary carcinoma cell line) were plated in a 12 well plate and treated with 5 mM of metformin for 72 h prior to the treatment with cisplatin (2.5 μM), combined or not with metformin, for another 72 h.

Kaplan-Meier plotter of lung adenocarcinoma and expression of Jarid1b in different types of tumors

Overview expression of Jarid1b in different tumors was done in The Human Protein Atlas website (https://www.proteinatlas.org/), using the The Cancer Genome Atlas (TCGA) RNA samples. All parameters were set to default. Kaplan-Meier plots for the analysis of stages 1, 2 and 3 of lung adenocarcinoma were created at the http://kmplot.com/analysis/index.php?p=service&cancer=lung website. All parameters were set to default, using all available cohorts. Green JetSet color was chosen for the best probe set for KDM5B (Jarid1b) gene.

Supplementary Figures

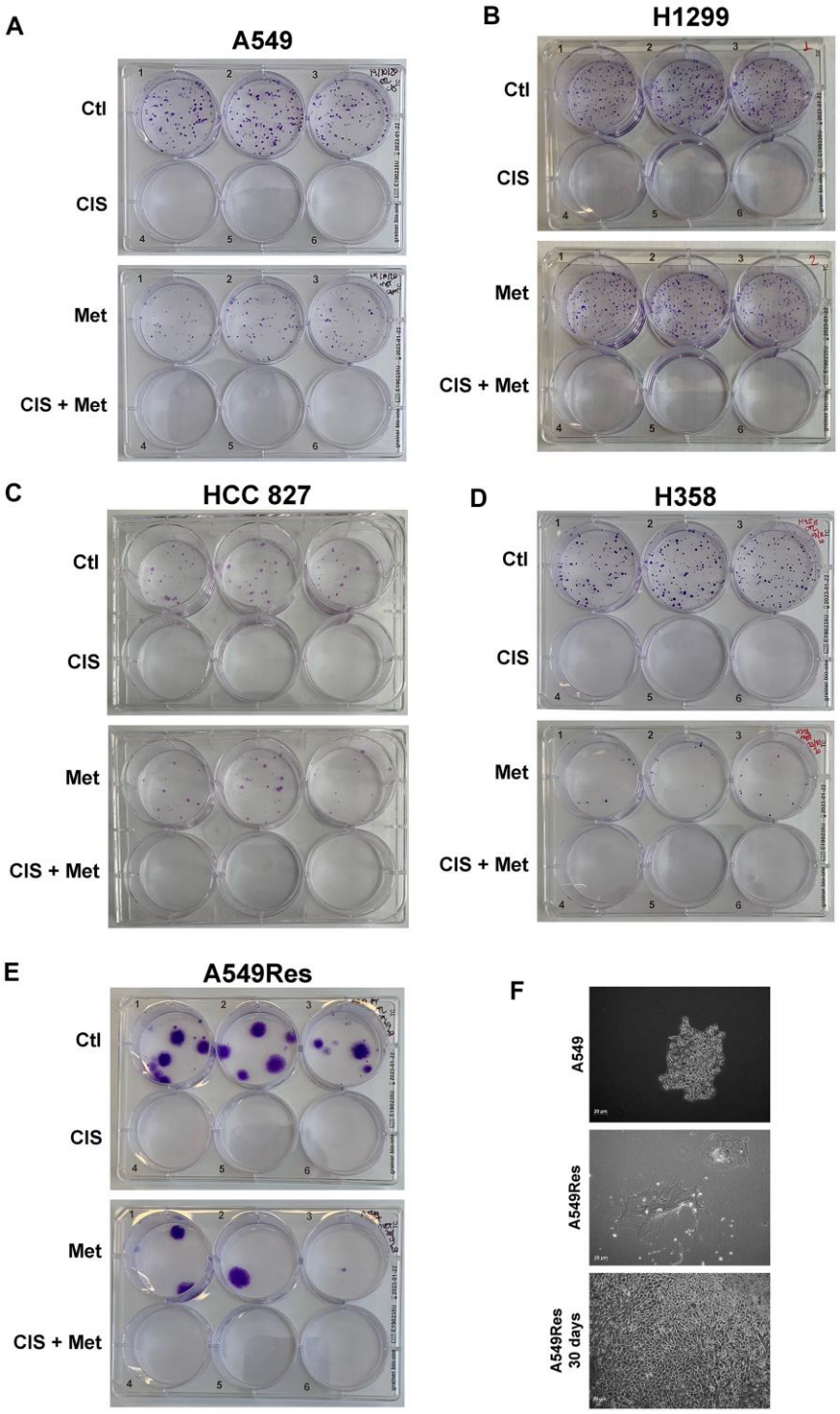

Supplementary Figure 1. Clonogenic assay in A549, H1299, HCC 827, H358 and A549Res cells. Cells were treated as described in methods section. After treatment, cells were detached from plate and 300 cells were plated in 6 well plate in triplicate. Colonies were then counted for A549 cells (**A**), H1299 cells (**B**), HCC 827 cells (**C**), H358 (**D**) and A549Res (**E**). In (**F**) a picture was taken to document the difference in morphology of the A549Res cells after 30 days when compared to A549 cells. Picture was taken from a Control group well in A549Res plate. All plates are representative of three independent experiments.

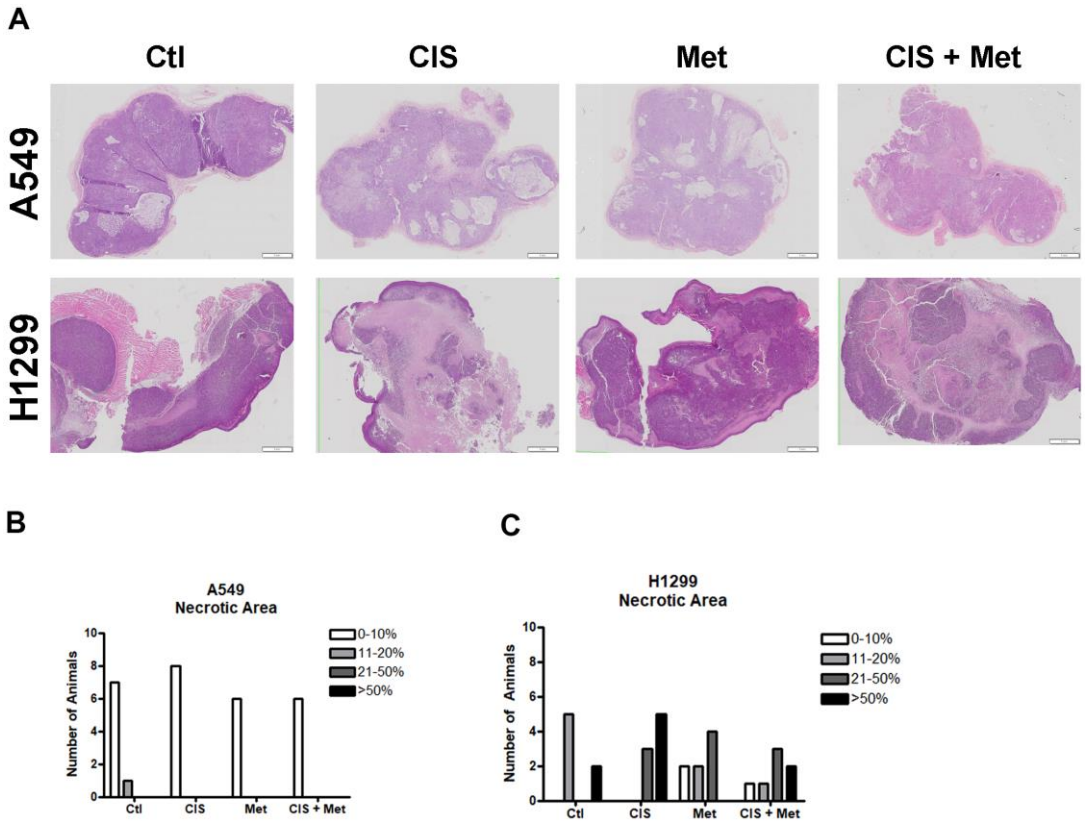

Supplementary Figure 2. Necrotic area in A549 and H1299 tumors injected in NOD/SCID mice. Histological section of A549 or H1299 derived tumors, stained with hematoxylin and eosin, after metformin, cisplatin and the combination of metformin and cisplatin treatment in NOD/SCID mice (**A**). Quantification of the necrotic area shows that in A549 derived-tumors, cisplatin does not increase the necrotic area (**B**). However, in H1299 derived-tumors, cisplatin increases the necrotic area when used alone in NOD/SCID mice and metformin decreases the necrotic area when combined with cisplatin (**C**).

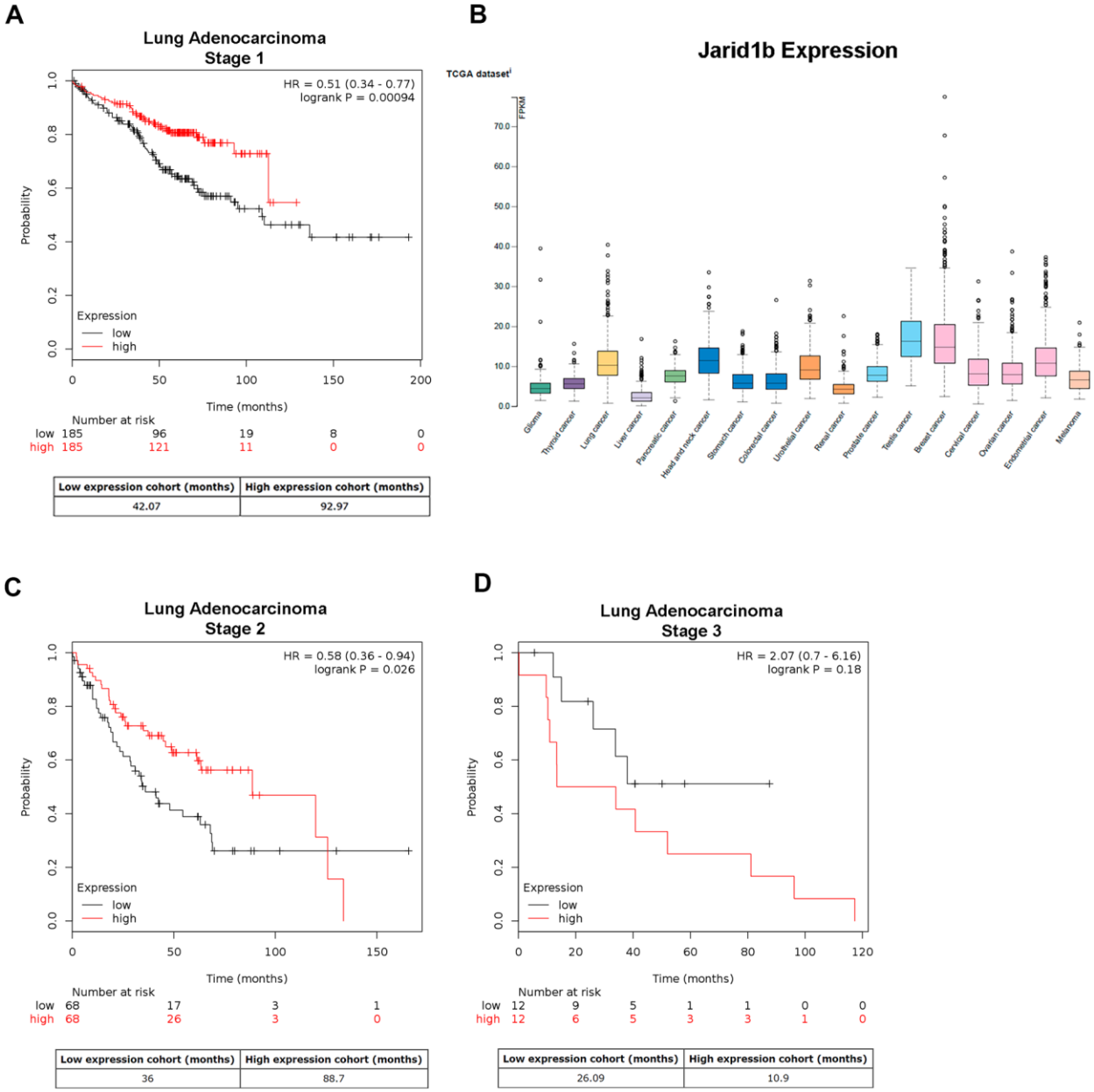

Supplementary Figure 3. Kaplan-Meier plotter of Jarid1b expression in lung adenocarcinoma. Jarid1b is highly expressed among different types of cancer (**A**). The Kaplan-Meier plotter shows that overexpression of Jarid1b in Lung Adenocarcinoma leads to a good prognosis in Stage 1 (p<0,001) (**B**), Stage 2 (p<0.05) (**C**) and has a tendency of poor prognosis in Stage 3 (p=0.18) due to the small number of patients (**D**).

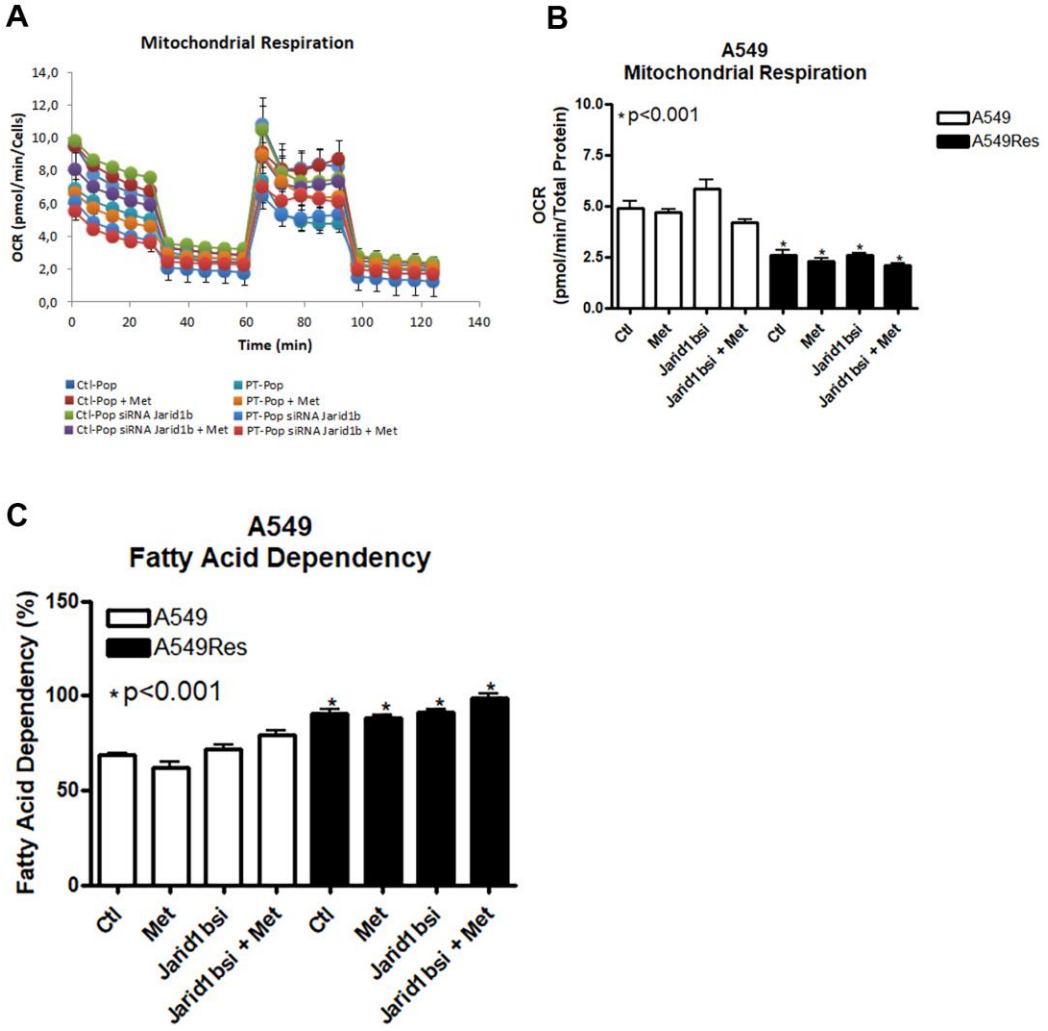

Supplementary Figure 4. Oxygen consumption rate (OCR) and fatty acid dependency in A549 cells. OCR in A549 cells or in A549Res cells were analyzed using the Seahorse XFe96. Cells were treated with metformin under Jarid1b inhibition by siRNA. Representative graph of four independent experiments from the measurement in A549 cells (**A**). Quantification of OCR in A549 and A549Res cells indicates that in the A549Res cells (when compared to the A549 Ctl group), OCR is decreased and metformin treatment and/or Jarid1b inhibition by siRNA did not increase its level ($p<0.001$) (**B**). A549 cells are highly dependent on fatty acid metabolism and this dependency increases after cisplatin treatment ($p<0.001$) (**C**). Sub-lethal treatment with cisplatin, metformin treatment and Jarid1b inhibition by siRNA was made according to materials and methods. OCR data represent the mean of four independent experiments and fatty acid dependence data represent the mean of three independent experiments.

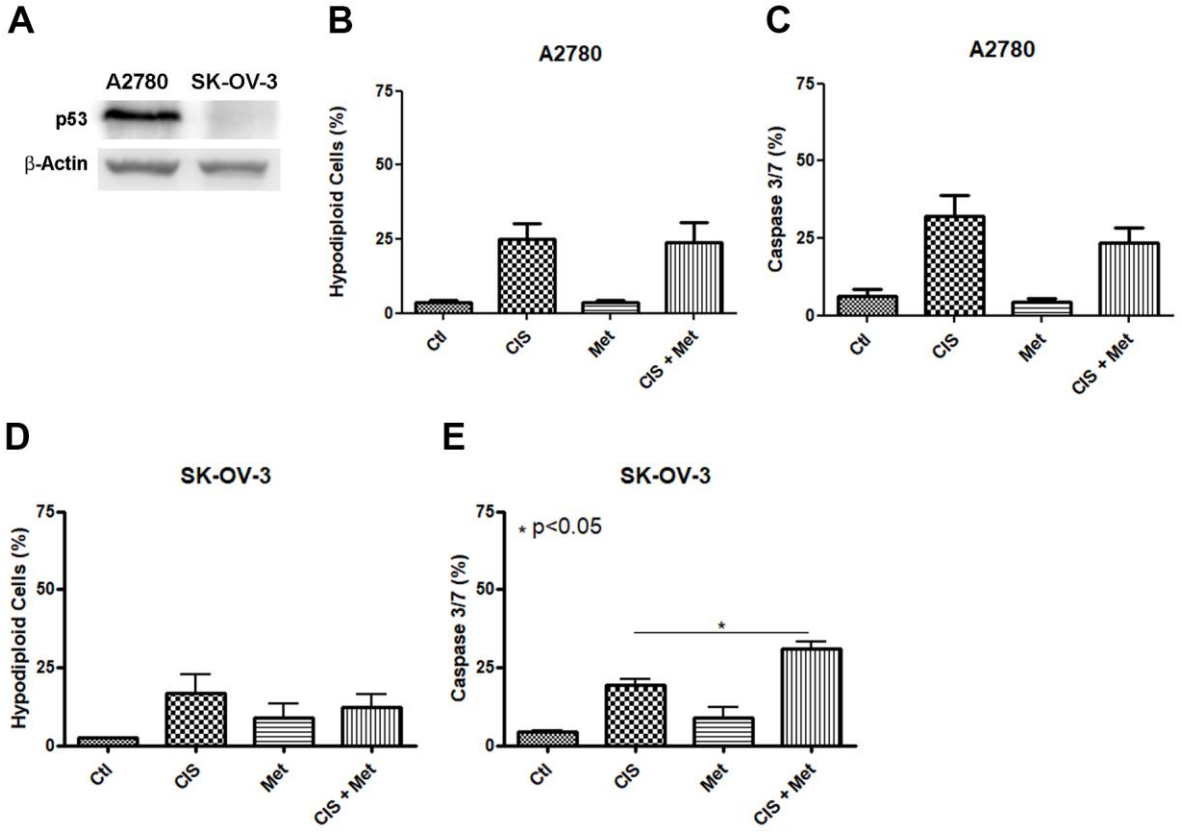

Supplementary Figure 5. Combination of metformin and cisplatin treatment in human ovarian carcinoma cells. Western blot showed that P53 is expressed in A2780 cells but not in SK-OV-3 cells (**A**). Combination of metformin and cisplatin treatment does not increase cell death, measured by hypodiploid cells and Caspase 3 and 7 activation in A2780 cells (**B**, **C**, respectively) and did not increased cell death by hypodiploid cells analysis in SK-OV-3 cells (**D**) but increased caspase 3 and 7 activation ($p<0.05$) (**E**). DNA fragmentation and Caspase 3 and 7 activation assays were performed according to materials and methods. Data represent the mean of three independent experiments. SK-OV-3 cells were treated with 20 mM of metformin for 72 h prior to the treatment with cisplatin (4 µM), combined or not with metformin, for another 72 h. A2780 cells were treated with 5 mM of metformin for 72 h prior to the treatment with cisplatin (2.5 µM), combined or not with metformin, for another 72 h.

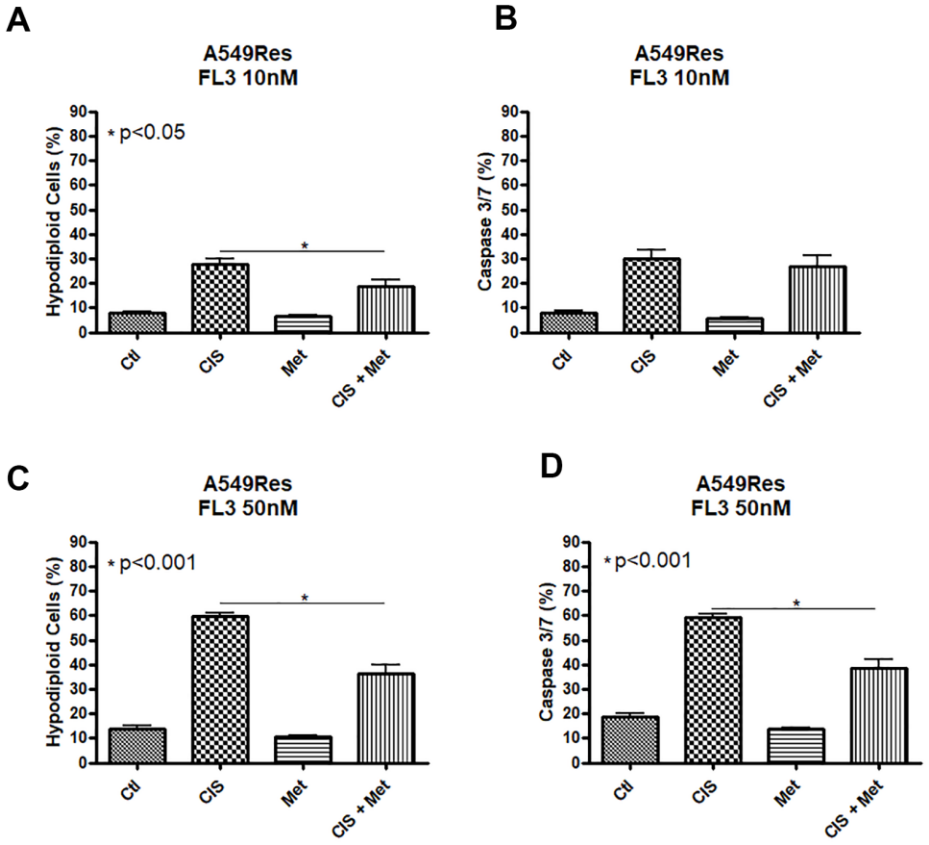

Supplementary Figure 6. FL3 protect A549Res cells to metformin and cisplatin combination. A549Res cells were treated with 10nM or 50nM of FL3 and then treated with the combination of metformin and cisplatin. Treatment with 10nM of FL3 protected the A549Res cells from cisplatin and metformin combination as seen by decreased DNA fragmentation ($p<0.05$) but did not change caspase 3 and 7 activation (**A**, **B**, respectively). When cells were treated with 50nM of FL3, the combination of cisplatin and metformin treatment decreased DNA fragmentation ($p<0.001$) and caspase 3 and 7 activation ($p<0.001$), when compared to cisplatin treatment alone, protecting A549Res cells (**C**, **D**, respectively). Sub-lethal treatment with cisplatin for generation of A549Res cells, treatment with FL3, cisplatin and metformin were made according to materials and methods. Data represent the mean of three independent experiments.

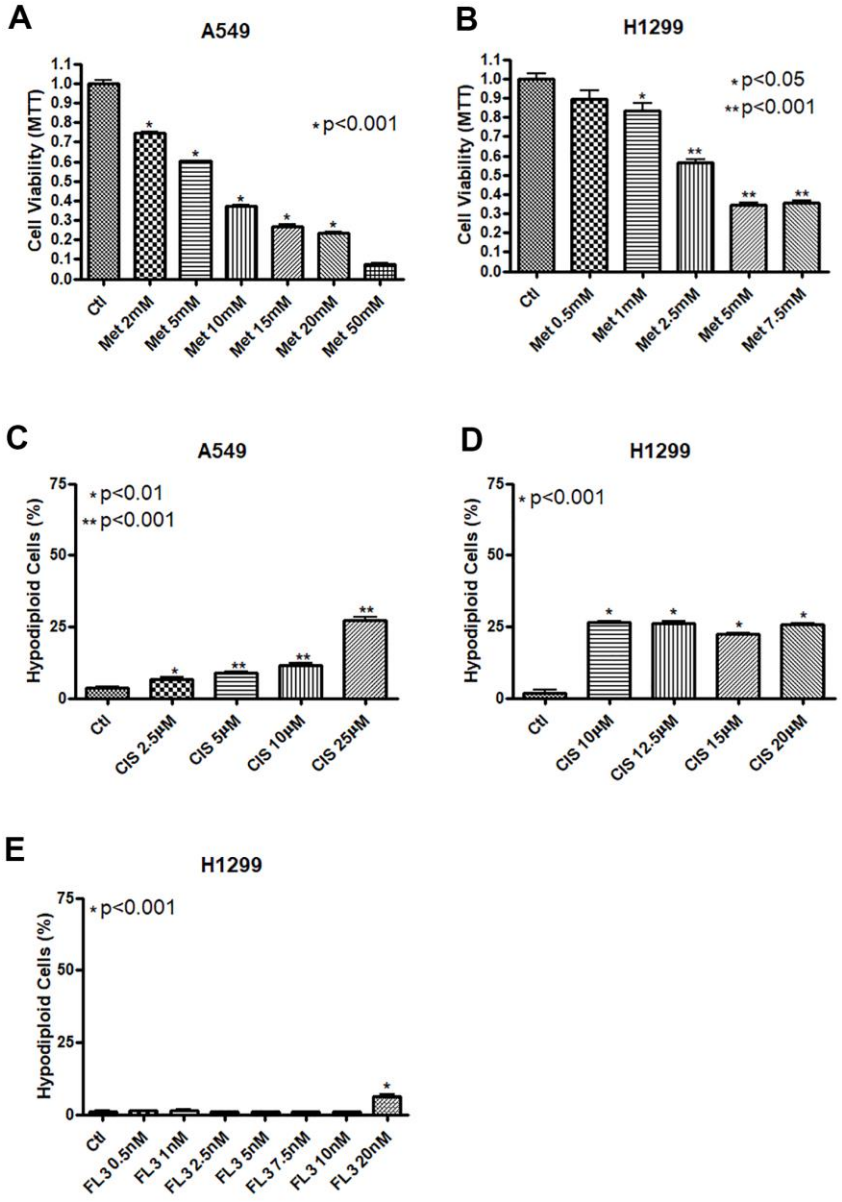

Supplementary Figure 7. Dose-response curves in A549 and H1299 cells for metformin, cisplatin and FL3. A549 and H1299 cells have different sensitivity to metformin and cisplatin. Cell viability for metformin treatment indicated that A549 cells are more resistant than H1299 cells (**A**, **B**). A549 cells were more resistant to cisplatin than H1299 cells (**C**, **D**). The smallest dose of FL3 before the induction of cell death (10nM), and a dose 5x higher (50 nM), was determined using the H1299 cells (**E**), and these concentrations were applied in the A549 cells. FL3, MTT and DNA fragmentation assay was made according to materials and methods. P value (*) or (**) is related to control (Ctl) group.

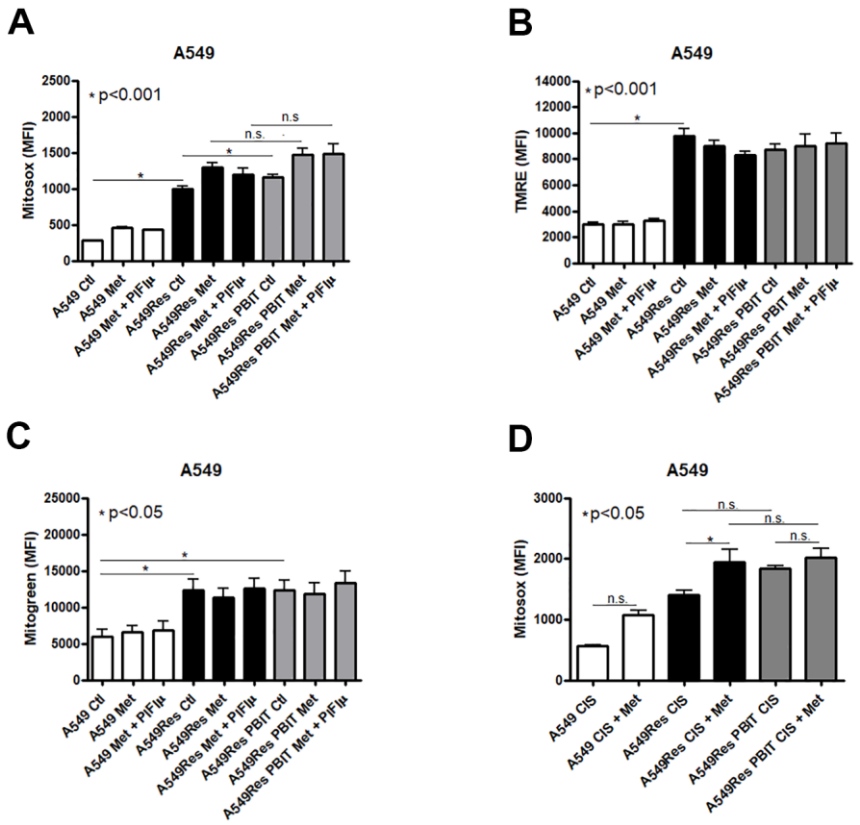

Supplementary Figure 8. Mitosox, TMRE and mitogreen analyses In A549 cells. Mitochondrial function was analyzed in A549 cells and in A549Res cells. Reactive oxygen species (ROS) increase was related to the sub-lethal treatment with cisplatin ($p<0.001$). PBIT treatment increased ROS levels, when compared to A549Res cells ($p<0.001$) but PBIT did not change ROS levels when cells were treated with metformin, even in the presence of pifithrin-μ (**A**). Mitochondrial membrane potential ($p<0.001$) and mitochondrial mass ($P<0.001$) increase was also related to the sub-lethal treatment with cisplatin and not to metformin treatment or by Jarid1b (**B**, **C**). Combined treatment with cisplatin and metformin increased ROS levels in A549Res cells ($p<0.05$) only when compared to cisplatin treatment alone, and PBIT treatment did no change ROS levels when compared to A549Res cells. (**D**). Sub-lethal treatment with cisplatin, combined treatment with cisplatin and metformin and Jarid1b inhibition by PBIT was made according to materials and methods. Non-significance (n.s.). Data represent the mean of three independent experiments.

Research Paper

The telomere-mitochondrial axis of aging in newborns

Charlotte Van Der Stukken[1], Tim S. Nawrot[1,2], Rossella Alfano[1], Congrong Wang[1], Sabine A.S. Langie[1], Michelle Plusquin[1], Bram G. Janssen[1], Dries S. Martens[1]

[1]Centre for Environmental Sciences, Hasselt University, Hasselt, Belgium
[2]Department of Public Health and Primary Care, University of Leuven, Leuven, Belgium

Correspondence to: Dries S. Martens; **email:** dries.martens@uhasselt.be
Keywords: telomere length, mitochondrial DNA content, p53, PGC-1α, aging
Received: October 20, 2021 **Accepted:** February 2, 2022 **Published:** February 15, 2022

ABSTRACT

Aging starts at the beginning of life as evidenced by high variability in telomere length (TL) and mitochondrial DNA content (mtDNAc) at birth. Whether p53 and PGC-1α are connected to these age-related markers in early life is unclear. In this study, we hypothesized that these hallmarks of aging are associated at birth.
In 613 newborns from the ENVIR*ON*AGE birth cohort, p53 and PGC-1α protein levels were measured in cord plasma, while TL and mtDNAc were measured in both cord blood and placental tissue. Cord blood methylation data of genes corresponding to the measured protein levels were available from the Human MethylationEPIC 850K BeadChip array. Pearson correlations and linear regression models were applied while accounting for selected covariates. In cord, a 10% increase in TL was associated with 5.22% (95% CI: 3.26 to 7.22; *p* < 0.0001) higher mtDNAc and −2.66% (95% CI: −5.04 to −0.23%; *p* = 0.032) lower p53 plasma level. In placenta, a 10% increase in TL was associated with 5.46% (95% CI: 3.82 to 7.13%; *p* < 0.0001) higher mtDNAc and −2.42% (95% CI: −4.29 to −0.52; *p* = 0.0098) lower p53 plasma level. Methylation level of TP53 was correlated with TL and mtDNAc in cord blood and with cord plasma p53 level.
Our study suggests that p53 may be an important factor both at the protein and methylation level for the telomere-mitochondrial axis of aging at birth.

INTRODUCTION

Aging is universal, unavoidable, and starts at the very beginning of life with an acceleration at middle-age. The general cause of aging is considered the time-dependent accumulation of cellular damage [1–3]. The aging phenotype can be determined by cellular and molecular hallmarks that are generally considered to contribute to the aging process. Recently, primary hallmarks of aging were defined, which include genomic instability, telomere attrition, epigenetic alterations, loss of proteostasis, deregulated nutrient sensing, mitochondrial dysfunction, cellular senescence, stem cell exhaustion and altered intercellular communication [4].These pathways have mainly been studied individually. A major challenge is to dissect the interconnection between the candidate hallmarks and their contribution to the aging-phenotype.

In an experimental study using mouse embryonic fibroblasts, Sahin et al. [5] revealed a direct connection between two primary hallmarks of aging i.e., dysfunctional telomeres which resulted in altered mitochondrial biogenesis and function via the tumor suppressor *TP53*, which in turn repressed peroxisome proliferator-activated receptor gamma, coactivator 1 alpha and beta (*PGC1A* and *PGC1B*), also known as master regulators of the mitochondria. Through observations from their experimental study, the "core axis of aging" was put forth, involving telomeres, mitochondria, p53 and PGC.

Until now, research on aging-mechanisms has mainly been limited to experimental research. Translation of these findings to population-based studies is scarce and focusses mostly on the older segment of the population [6]. However, human aging may start early and even from birth onward. It is therefore important to extent research on aging-mechanisms to the younger segment of the population. We evaluated the connection between TL and mtDNAc in 613 newborns from the ENVIR*ON*AGE birth cohort and we evaluated whether p53 and PGC-1α are on the path of this aging biomarker link as experimentally suggested.

METHODS

Study population

Mothers with a singleton full-term birth were selected from the ongoing population-based prospective ENVIR*ON*AGE (ENVIRonmental influence ON early AGEing) birth cohort study, which is located in Limburg, Belgium. Detailed study procedures have been described previously [7]. Between 2010 and 2017, 1530 mother newborn pairs were recruited. In 691 samples, cord plasma protein levels (p53 and PGC-1α) were measured. After removing 4 missing data, 18 outlying data (3 SDs from the mean) for protein levels and 10 outlying data for TL and mtDNAc, a total of 613 participants were used for statistical analysis. After delivery, mothers completed study questionnaires to provide detailed information on maternal age, paternal age, maternal education, smoking status, parity, and newborn's ethnicity. Maternal education was classified as "low" when mothers did not obtain any diploma, "middle" when they obtained a high school diploma, and "high" when they obtained a college or university diploma. Mothers were categorized as "never smoker", "former smoker" when they had quit smoking before pregnancy, and "smoker" if they had smoked at any time point during pregnancy. Parity was categorized in mothers having their first newborn, having their second newborn, or having their third or more newborn. Newborns were classified as either "European" when two or more grandparents were European, or as "non-European" when at least three grandparents were of non-European origin. Other maternal and perinatal parameters such as maternal pre-pregnancy Body Mass Index (BMI), newborns' sex, birth weight and birth date were collected from medical records after birth. Maternal pre-pregnancy BMI (kg/m²) was calculated based on data obtained during the first antenatal consultation. The date of conception was estimated by combining data on the first day of the mother's last menstrual period and the first ultrasonographic examination. The ENVIR*ON*AGE study protocol has been conducted according to the Helsinki Declaration and was approved by the Ethical Committees of Hasselt University in Diepenbeek, Belgium (reference no. B371201216090 and B371201524537) and East-Limburg Hospital in Genk, Belgium. Written informed consent was provided by all participating mothers.

Sample collection and preparation

Procedures for umbilical cord blood and placental tissue collection for TL and mtDNAc assessment have been described in detail previously [7]. BD Vacutainer® Plus plastic whole-blood tubes with spray-coated K2EDTA (BD, Franklin Lakes, NJ, USA) were used to collect umbilical cord blood samples immediately after delivery. To obtain buffy coat and retrieve blood plasma, samples were centrifuged at 3,200 rpm for 15 min and stored separately. Within 10 minutes after delivery, placentas were collected and stored at –20°C. Four different placental biopsies (approximately 1–2 cm^3) were taken at the fetal side at 4 cm from the umbilical cord and directly underneath the chorioamniotic membrane. Contamination by the chorioamniotic membrane was avoided by dissection followed by visual examination. All samples were stored at –80°C until DNA extraction. DNA was extracted using the QIAamp DNA Mini Kit (Qiagen Inc., Venlo, the Netherlands), according to the manufacturer's instructions. The quantity and purity of the sample was measured with the Nanodrop spectrophotometer (ND-1000; Isogen Life Science, the Netherlands). DNA samples were normalized to ensure a uniform DNA input of 5 ng for each qPCR reaction, and this was checked using the Quant-iT™ PicoGreen® dsDNA Assay Kit (Life Technologies, Europe). Extracted DNA was stored at –80°C until further use.

Average relative TL and mtDNAc measurement

TL and mtDNAc were measured in cord blood buffy coat and placental tissue using a previously described modified quantitative real-time polymerase chain reaction (qPCR) protocol [8–10]. Details are provided in supplement (Supplementary Material). On each run, a 6-point serial dilution of pooled buffy coat or placental DNA was used to assess PCR efficiency as well as eight inter-run calibrators (IRCs) to account for inter-run variability. Non-template controls were also used in each run. All samples were measured in triplicate on a 7900HT Fast Real-Time PCR System (Applied Biosystems) in a 384-well format. qPCR curves for each sample were visually inspected and when technical problems were detected or triplicates showed too high variability, samples were removed for further analysis. Using qBase plus software (Biogazelle, Zwijnaarde, Belgium), all measurements were processed and normalized to a reference gene, taking into account run-to-run

differences. Average relative TL was calculated by determining the ratio of one telomere gene copy number (T) to one reference gene (*36B4*) (S). Average mtDNAc was calculated by determining the average of the ratio of two mitochondrial gene copy numbers (*MTF3212/R3319* and *MT-ND1*) (M) to two nuclear reference genes (*36B4 and β-Actin*) (S). Telomere assay-reliability was assessed using an intra class correlation coefficient (ICC). The inter-assay ICC was 0.936 (95% CI: 0.808 to 0.969) and the intra-assay ICC was 0.952 (95% CI: 0.947 to 0.956).

p53, PGC-1α and SIRT-1 protein measurement

After thawing cord blood plasma, 100 µl of plasma was quantified for p53 protein levels (U/mL) using a Human p53 ELISA Kit according to the manufacturer's instructions (ref. ab46067, Abcam, Cambridge, United Kingdom). For PGC-1α (ng/mL), 100 µl of 1:250 diluted plasma was quantified according to the manufacturer's instructions (ref. E-EL-H1359, Elabscience, Texas, USA). Two commercially available Human SIRT1 ELISA Kits were tested for the detection of cord plasma SIRT-1 protein levels, but for none of them the limit of detection was reached (ref. ab171573, Abcam, Cambridge, United Kingdom and ref. E-EL-H1546, Elabscience, Texas, USA). All protein levels were measured in duplicate using a FLUOstar Omega microplate reader (BMG Labtech, Ortenberg, Germany). To minimize variability, all samples were randomized across 96 well plates and all ELISAs for one protein were measured in one day, while using the same serial dilution. Five IRCs per plate were taken into account to control for potential variability between plates. The intra-assay coefficient of variation was 5% for p53, and 10% for PGC-1α while the inter-assay coefficient of variation reached 14.5% for p53 and 25% for PGC-1α.

DNA methylation measurement

Cord blood DNA was used to determine the epigenome-wide DNA methylation levels. DNA samples were bisulfite-converted, amplified and then hybridized to the Illumina Infinium Human MethylationEPIC 850K BeadChip array (Illumina, San Diego, CA, USA) at the GenomeScan lab (Leiden, The Netherlands). The array measurements were scanned using an Illumina iScan and the data quality was assessed using the R script MethylAid. DNA methylation data preprocessing, quality control, outlier detection, batch effect removal and probe filtering were described previously [11]. In total, 57 CpG loci with their UCSC reference gene name referring to *TP53*, *PGC1A* or *SIRT1* were selected for the present study. Methylation levels of *TP53*, *PGC1A* and *SIRT1* were available for 205 participants and used for further analysis. Details are provided in Supplementary Table 1.

Statistical analysis

All statistical analyses were performed using R studio version 3.6.2 (R Core Team, Vienna, Austria). Shapiro-Wilk's test was used to check the normality of the distributions. Average relative TL, mtDNAc and cord plasma protein levels were $\log_{10}$-transformed to better approximate a normal distribution. For the descriptive statistics, continuous variables were presented as means ± standard deviation (SD) and categorical variables as numbers (frequency in percentage). Pearson correlation was used to systematically evaluate following correlations: (1) TL in cord blood and placenta and mtDNAc in the respective tissue, (2) TL in cord blood and placenta and cord plasma protein levels, (3) mtDNAc in cord blood and placenta and cord plasma protein levels and (4) cord plasma protein levels. Multiple linear regression was applied to further confirm the associations independent of potential confounding effects. We adjusted for a priori selected covariates based on known associations of these factors with TL, mtDNAc, and protein levels as shown previously in multiple studies [8, 12]: Technical covariates (sample storage and batch effects), newborn's sex, gestational age, maternal BMI, maternal and paternal age, ethnicity, parity, smoke status, maternal education and month of delivery. All model estimates were presented as percentage difference with 95% CI and expressed for a 10% increment in explanatory variable.

In a secondary explorative analysis, we evaluated in a subpopulation whether cord blood methylation levels of genes corresponding to our measured protein levels (p53, PGC-1α and SIRT1) were related to the studied age-related markers and protein levels, to further explore the interrelationship of the telomere-mitochondrial aging axis. We restricted these DNA methylation association studies to age-related markers measured in cord blood, as it is known that DNA methylation levels are highly tissue- and cell type-specific [13–15]. Since multiple CpGs were measured for each gene, we first made a correlation matrix showing the Pearson correlations between the CpGs for each gene. Second, we performed Principal Component Analysis (PCA) to reduce the dimensionality of our dataset [16]. To determine the number of Principal components (PCs) to retain in our analysis, we created scree plots for each gene (Supplementary Figure 1). PCs on the left side of the "elbow" of the graph were retained in the analysis. For all genes, this resulted in 5 PCs to retain. Next, we correlated the PCs with the CpGs, to determine their loadings (Supplementary Table 2). CpG loci were selected as relevant to a factor if the absolute value of their factor loadings were larger than 0.45 [16].

Table 1. Descriptive characteristics of mother-newborn pairs from a subset (*n* = 613) of the ENVIR*ON*AGE birth cohort.

Characteristic	Mean ± SD or *n* (%) (*n* = 613)
Mothers	
Age, y	29.3 ± 4.6
Pre-pregnancy BMI, kg/m^2	24.6 ± 4.8
Educational level	
Low	79 (12.9%)
Middle	227 (37.0%)
High	307 (50.1%)
Smoking status	
Never smoker	391 (63.8%)
Former smoker	154 (25.1%)
Current smoker	68 (11.1%)
Parity	
1	337 (55.0%)
2	206 (33.6%)
≥3	70 (11.4%)
Newborns	
Sex	
Female	321 (52.4%)
Gestational age, wk	39.2 ± 1.7
Birth weight, g	3420 ± 496
Ethnicity	
European-Caucasian	533 (86.9%)
Season of birth	
Winter	150 (24.5%)
Spring	149 (24.3%)
Summer	151 (24.6%)
Autumn	163 (26.6%)

First, these first five PCs were used to assess the Pearson correlations between methylation data and both cord blood age-related markers and cord plasma protein levels. Second, multiple linear regression was applied to confirm these associations while adjusting for the aforementioned covariates.

RESULTS

Study population characteristics

Demographic, pregnancy-related and perinatal characteristics of the mother-newborn pairs included in this study (*n* = 613) were summarized in Table 1. Our study subset was representative for the original study population (Supplementary Table 3). Mothers were on average 29.3 (SD: 4.6) years old and had an average pre-pregnancy BMI of 24.6 (SD: 4.8) kg/m^2. Half of the participating women were highly educated (50%). The majority of the pregnant women never smoked cigarettes (63%), 25% stopped smoking before pregnancy, and 11% kept smoking on the average 3.4 cigarettes/day during pregnancy. Among the newborns, 52% were girls. Newborns had an average gestational age of 39.2 (SD: 1.67) weeks, an average birth weight of 3420 (SD: 496) grams, and most were of European origin (86%). Information about the age-related and protein markers is given in

Table 2. Age-related markers measured in a subset (*n* = 613) of the ENVIR*ON*AGE birth cohort.

Age-related marker	Mean ± SD
Placenta	
TL (T/S ratio)	0.99 ± 0.26
mtDNAc (M/S ratio)	1.05 ± 0.65
Cord blood	
TL (T/S ratio)	0.99 ± 0.19
mtDNAc (M/S ratio)	1.03 ± 0.57
p53 plasma level (U/ml)	12.5 ± 9.72
PGC-1α plasma level (μg/ml)	1145 ± 360

Data presented as mean ± SD or number of participants (%). TL and mtDNAc are normalized separately in cord blood and placental tissue. Abbreviations: TL: telomere length; mtDNAc: Mitochondrial DNA content.

Table 2. Cord plasma SIRT-1 levels were excluded from the analysis since the measurements did not reach the limit of detection (LOD) of 0.31−0.63 ng/ml.

The telomere-mitochondrial axis of aging: links between TL, mtDNAc, p53 and PGC-1α

Unadjusted correlations

Cord blood and placental TL were positively correlated (r = 0.40, $p < 0.0001$, Supplementary Figure 2A), but no correlation between cord blood and placental mtDNAc was observed (Supplementary Figure 2B). The following correlations were systematically evaluated: (1) TL and mtDNAc, (2) TL and cord plasma protein levels, (3) mtDNAc and cord plasma protein levels and (4) between the cord plasma protein levels.

First, a positive correlation was found between TL and mtDNAc in both cord blood (r = 0.23, $p < 0.0001$, Supplementary Figure 3A) and placental tissue (r = 0.28, $p < 0.0001$, Supplementary Figure 3B).

Second, cord plasma p53 levels were negatively correlated with cord blood TL (r = −0.13, $p = 0.0015$, Supplementary Figure 4A) but not with placental TL (Supplementary Figure 4B). Cord plasma PGC-1α levels were negatively correlated with both cord blood TL (r = −0.10, $p = 0.013$, Supplementary Figure 4C) and placental TL (r = −0.09, $p = 0.029$, Supplementary Figure 4D).

Third, no correlation was observed between cord plasma p53 levels and cord blood mtDNAc (Supplementary Figure 5A), but tended to be negatively correlated with mtDNAc in placenta (r = −0.07, $p = 0.094$, Supplementary Figure 5B). No correlation was observed between cord plasma PGC-1α levels and cord blood mtDNAc (Supplementary Figure 5C), but a negative correlation was observed with placental mtDNAc (r = −0.11, $p = 0.0082$, Supplementary Figure 5D).

Fourth, cord plasma p53 and PGC-1α levels were not correlated (Supplementary Figure 6). In Figure 1, a visual summary of all correlations is presented, which is based on the experimentally derived telomere-mitochondrial axis of aging hypothesis.

Covariate adjusted linear models

Using adjusted regression models, we further evaluated the associations between TL and (1) mtDNAc and (2) cord plasma protein levels (Table 3). We furthermore evaluated the associations between mtDNAc and the cord plasma protein levels, and also the association between the cord plasma protein levels (Supplementary Table 4). All associations were adjusted for technical covariates (sample storage and batch effects), newborn's sex, gestational age, maternal BMI, maternal and paternal age, ethnicity, parity, smoke status, maternal education and month of delivery. First, an increase in cord blood and placental TL was associated with higher mtDNAc in the respective tissue. A 10% increase in cord blood TL was associated with 5.22% (95% CI: 3.26 to 7.22; $p < 0.0001$) higher cord blood mtDNAc and a 10% increase in placental TL was associated with 5.46% (95% CI: 3.82 to 7.13%; $p < 0.0001$) higher placental mtDNAc. Second, both cord blood and placental TL were associated with lower p53 levels, which is largely in line with the observed unadjusted correlations. A 10% increase in cord blood TL was associated with −2.66% (95% CI: −5.04 to −0.23%; $p = 0.032$) lower p53 plasma levels, while a 10% increase in placental TL was associated with –2.42% (95% CI: −4.29 to −0.52; $p = 0.0098$) lower p53 plasma levels. The observed correlations between TL and cord blood PGC-1α levels could not be confirmed in adjusted models. Furthermore, the correlations observed

Table 3. Association between TL in cord blood and placenta and (1) mtDNAc in the respective tissue and (2) cord plasma protein levels in the telomere-mitochondrial axis of aging.

	Cord TL (n = 603)		Placenta TL (n = 558)	
	% difference (95% CI)	*P*-value	% difference (95% CI)	*P*-value
Cord mtDNAc	5.22 (3.26, 7.22)	<0.0001	–0.45 (–1.96, 1.08)	0.56
Placenta mtDNAc	1.02 (–1.06, 3.16)	0.34	5.46 (3.82, 7.13)	<0.0001
Cord p53	–2.66 (–5.04, –0.23)	0.032	–2.42 (–4.29, –0.52)	0.0098
Cord PGC-1α	0.17 (–0.85, 1.21)	0.74	0.49 (–0.31, 1.29)	0.22

Estimates are presented as percentage difference with 95% CI for a 10% change in explanatory variable. All models are adjusted for technical covariates (sample storage and batch effects), newborn's sex, gestational age, maternal BMI, maternal and paternal age, ethnicity, parity, smoke status, maternal education and month of delivery. Cord blood and placental Telomere Length represent the response variables, while the markers in the first column represent the exposure variables. Abbreviations: TL: telomere length; mtDNAc: mitochondrial DNA content.

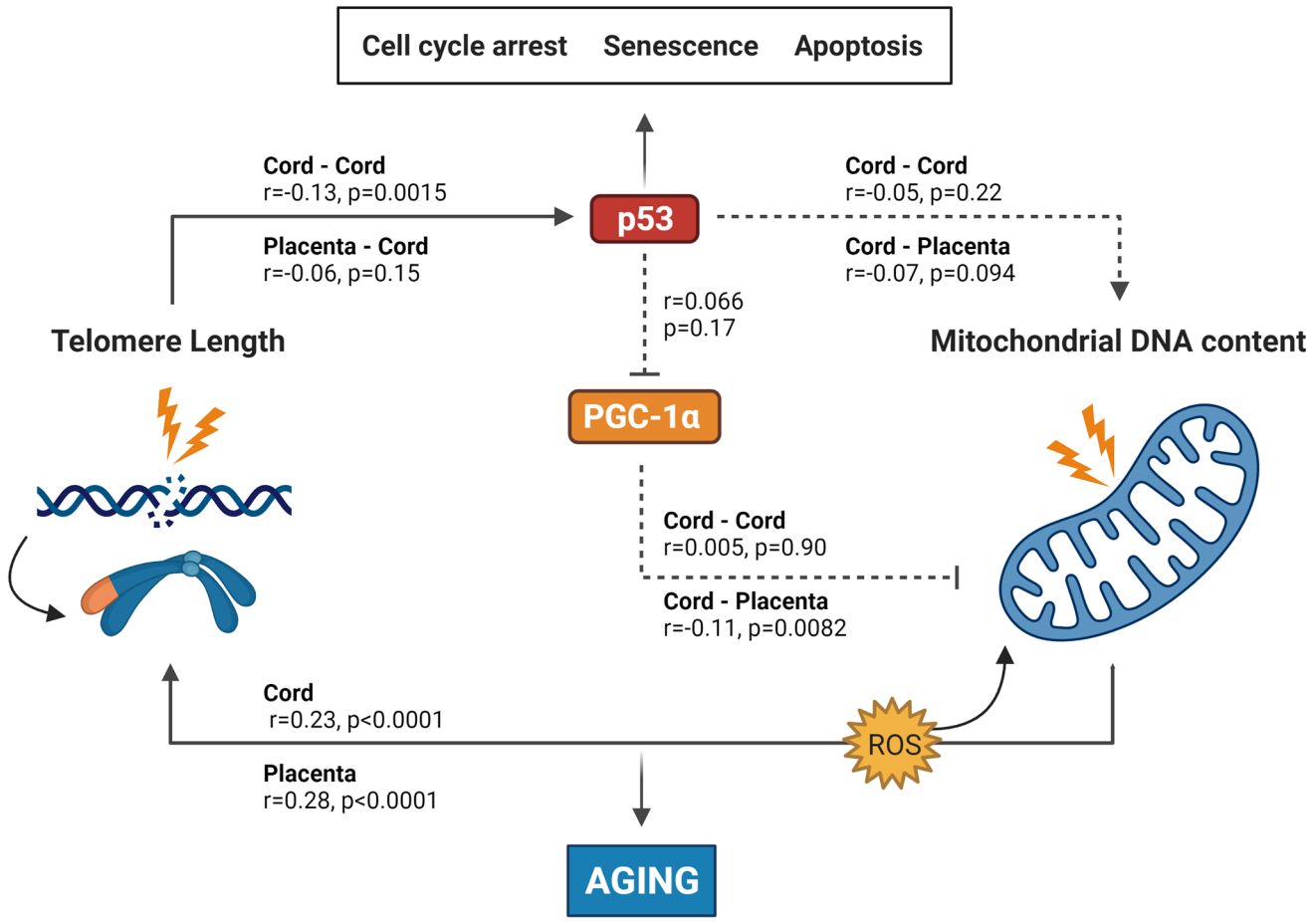

Figure 1. Summary of the results found in this study integrated into the experimentally based telomere-mitochondrial axis of biological aging hypothesis. DNA damage and telomere shortening activate p53 leading to growth arrest, senescence or apoptosis. p53 might also impair mitochondrial function and mitochondrial DNA content indirectly through suppression of PGC-1α – one of the master regulators of the mitochondria – leading to mitochondrial comprise and increased ROS levels, which leads to more DNA damage including telomere shortening. p53 and PGC-1α could therefore be central players in the association between telomere length and mitochondrial DNA content and subsequently in the aging process. Solid lines represent significant associations between age-related or protein markers, while non-significant associations are represented by dotted lines. p53 and PGC-1α levels were only measured in cord blood, while TL and mtDNAc were measured in both cord blood and placental tissue. Abbreviations: p53: tumor suppressor protein 53; PGC-1α: peroxisome proliferator-activated receptor gamma co-activator 1 alpha protein. Figure based on the experimental work of Sahin et al. [5, 33].

between mtDNAc and the protein levels, nor between the protein levels themselves could not be confirmed in full adjusted regression models (Supplementary Table 4).

Cord blood *TP53*, *PGC1A* and *SIRT1* methylation levels and the cord blood telomere-mitochondrial axis of aging

Unadjusted correlations

First, a Pearson correlation heatmap of the methylation levels of all CpGs for each gene (*TP53*, *PGC1A* and *SIRT1*, separately) is shown in Supplementary Figure 7. Second, the unadjusted Pearson correlation matrix between *TP53*, *PGC1A* and *SIRT1* methylation data (reflected by 5 PCs) and both cord blood age-related markers and protein levels in a subset of our study data (n = 205) is shown in Supplementary Figure 8. The first five PCs cumulatively explained 41%, 58% and 59% of the variation of *TP53*, *PGC1A* and *SIRT1,* respectively. In Supplementary Figures 9 and 10, significant correlations were additionally presented in correlations plots.

For *TP53* methylation data, PC1 was negatively correlated with cord plasma p53 level (r = −0.17, p = 0.038), PC2 was positively correlated with cord blood TL (r = 0.20, p = 0.010) and PC5 was negatively correlated with cord blood mtDNAc (r = −0.16, p = 0.00073). The most relevant CpG to PC1 based on factor loadings (cg12041429, Supplementary Table 2) was located within the 5′ untranslated region (5′UTR), meaning between the transcription start site (TSS) and the translation initiation codon (ATG) (Supplementary Table 1). The most relevant CpG for PC2 (cg18198734, Supplementary Table 2), was located in the gene body, meaning between the ATG and stop codon; irrespective of the presence of introns, exons, TSS or promoters (Supplementary Table 1). For PC5, absolute values of CpG factor loadings were not larger than 0.45, therefore, no CpG loci were selected as relevant to this factor.

For *PGC1A* methylation data, PC3 was positively correlated with cord blood TL (r = 0.18, p = 0.013). However, no CpG loci were selected as relevant to this factor.

For SIRT1 methylation data, no significant correlations were found with any of the measured markers.

Covariate adjusted linear models

The associations between *TP53*, *PGC1A* and *SIRT1* methylation data and cord blood age-related markers and cord plasma protein levels were further evaluated using regression models. All models were adjusted for technical covariates (sample storage and batch effects), newborn's sex, gestational age, maternal BMI, maternal and paternal age, ethnicity, parity, smoke status, maternal education and month of delivery (Supplementary Table 5). The observed unadjusted correlations between methylation levels and both cord blood age-related markers and cord plasma protein levels could be confirmed after adjustment.

DISCUSSION

Aging is a complex universal and unavoidable physiological phenomenon. Both telomere attrition and mitochondrial damage are main factors in this biological process, but have mostly been studied independently. We [9, 17] and others [18–20] already observed large variability in TL and mtDNAc among newborns and we found that TL at birth predicts later life TL [17]. In the current study with 613 mother-newborn pairs, we evaluated in cord blood and placenta if TL is connected to mtDNAc, whether p53 and PGC-1α are connected to these age-related markers and whether we may confirm the core axis of aging hypothesis in newborns.

Our study has two main findings: First, TL in cord blood and placenta is positively associated with mtDNAc in the respective tissue. Second, TL in cord blood and placenta is negatively associated with cord plasma p53 level, and the TL connection with p53 regulation is furthermore strengthened with the observed association with *TP53* methylation levels. These findings were confirmed after adjustment for potential confounding factors, and are in line with the proposed hypothesis as displayed in Figure 1. Our results partly confirmed the contribution of p53 in the telomere-mitochondrial axis of aging in early-life, however, the connection between p53 and mtDNAc and between the protein levels remains unconfirmed in our study.

Negative correlations between placental mtDNAc and both p53 and PGC1-α protein levels were found, but did not survive full adjustment for potential confounders. Also, p53 and PGC1-α were not correlated. However, methylation levels of the genes corresponding to the measured proteins show correlations with all markers that are in line with our hypothesis. As for the methylation levels, the highest contributing CpG loci were either located in the 5′UTR or in the gene body. In the 5′UTR, essential promotor elements are located and methylation of these promotor sequences will downregulate methylation, while gene-body methylation has been observed to be positively correlated with gene expression levels [21].

There was furthermore a strong positive association between cord blood and placental TL, but not between

cord blood and placental mtDNAc, which may indicate that tissue-specific differences in mtDNAc are larger than tissue-specific differences in TL. This finding is in line with observations that TLs are highly correlated in different tissues within the same individual [17, 22]. For mtDNAc, the difference largely depends on the difference in energy demand of each cell type [23].

How can our observations be explained based on the proposed hypothesis (Figure 1)? DNA damage and excessive telomere shortening caused by intracellular stresses or environmental signals activate p53 [12, 24], which has commonly been referred to as the 'guardian of the genome' due to its role in protecting the cell from DNA damage and acting as a central hub in many biological downstream pathways [25, 26]. It regulates the expression of a variety of genes involved in different cellular functions, including cell-cycle regulation, apoptosis, DNA replication and repair, cell proliferation, cellular stress response and negative regulation of p53 [27]. Its activation modulates cellular senescence and organismal aging [28], whereas loss or mutation within the *TP53* gene (which encodes p53) prevent cell death and increase cancer risk [29]. In this model, activated p53 directly suppresses PGC-1α, which alters the mitochondria (decreased mitochondrial function, impaired ATP generation and increased reactive oxygen species (ROS) production) which can lead to accelerated biological aging. Contradictory, there is growing evidence that p53 helps maintain the mitochondrial genome through translocation into mitochondria and interactions with mtDNA repair proteins. Park et al. [30] suggest that in unstressed cells, p53 functions as mito-checkpoint protein and regulates mtDNA copy number and mitochondrial biogenesis. Conversely, stress activated p53 (through DNA damage or telomere shortening) results in impaired mitochondrial biogenesis [30].

The findings of our study are supported by both experimental and population-based human studies. First of all, the link between telomeres and mitochondria was initially proposed in the experimental study of Sahin et al. [31], where telomerase-deficient mice (with a high level of dysfunctional telomeres) showed a strong activation of the *TP53* gene, which resulted in suppression of *PGC1A* and *PGC1B* genes – the master regulators of mitochondrial biogenesis and metabolism – leading to comprised mitochondrial biogenesis. The link between these age-related markers was also made in several human studies [6, 32]. In a community sample of 392 healthy adults, Tyrka et al. [32] showed a positive correlation between leukocyte TL and mtDNAc, but the underlying mechanism remained undetermined. In 166 elderly, an association has been demonstrated between leukocyte TL and mtDNAc with *SIRT1* as a key role player in the telomere-mitochondrial interactome [6]. *SIRT1* expression was also shown to be inversely associated with *TP53* expression, which subsequently altered the expression of *PGC1A* [6].

What is the importance of our findings? Excessive telomere shortening to a critical length (Hayflick limit) [9] can lead to genome instability and senescence. It is also associated with an increased risk of age-related diseases, such as cardiovascular diseases [10], metabolic diseases [11] and cancer [12]. Mitochondria are the biochemical power plants of eukaryotic cells. Compared with nuclear DNA (nDNA), mtDNA is more vulnerable to damage induced by endogenous and exogenous agents. This due to the lack of protective histones, the small mitochondrial genome, its close proximity to the respiratory chain and its limited DNA repair system [15]. Mitochondrial damage might result in metabolic changes such as impaired ATP generation, increased production of ROS and decreased levels of ROS-detoxifying enzymes, which cause additional genomic instability as observed in aging and cancer [16]. By unraveling the mechanisms underlying the association between age-related markers in an early life context, we can further investigate how these important regulators may be influenced by early life exposures, and how this may lead to vulnerability for disease in later life. In addition, more research is needed to determine whether tracking and fixed ranking of TL among newborns, as evidence by Martens et al. [17], can be explained by variations of key-regulator levels in the core axis of aging. By strengthening our knowledge about tracking and ranking mechanisms involved in the complete axis of aging, improved measures can be taken to promote healthy aging across the life course.

Our study has several strengths. First of all, this is to our knowledge the first study that has investigated the key regulators of the telomere-mitochondrial axis of aging at birth. Second, we used a relatively large sample size (n = 613) within the ENVIR*ON*AGE birth cohort, which is representative for the ENVIR*ON*AGE birth cohort at large [7]. The third strength is the availability of different biological matrices (placenta, cord blood and cord plasma), in which the age-related markers were measured over different biological levels (TL, mtDNAc, proteins levels and methylation levels). This made it possible to investigate the telomere-mitochondrial axis of aging independent of the biological matrix.

Besides our strengths, we also had to deal with some limitations. First, in addition to p53 and PGC-1α, SIRT-1 is also considered to be a major contributor in the telomere-mitochondrial axis of aging pathway [6].

Unfortunately, this could not be confirmed in our study, since were not able to detect cord plasma SIRT-1 levels above the limit of detection of several commercially available ELISA kits. As evidenced by other studies [6, 33], SIRT-1 plays a role in the molecular axis of aging and might provide interesting information to confirm our hypothesis. A second limitation is that p53 and PGC-1α were only measured in cord plasma but not in placental tissue, due to incompatibility with the measurement assays and due to limited placental tissue availability. As the aging process may be different for different tissues, the availability of placental protein levels of p53 and PGC-1α would provide more insight in the placental aging processes, this especially as placental tissue is a temporary end of life organ. Third, other non-studied markers playing a role in the telomere-mitochondrial axis of aging were not investigated and we can therefore not exclude that our findings are influenced by other important gene regulators. Fourth, our results only give an indication that p53 protein and methylation is linked with TL and mtDNAc.

In conclusion, we show that TL is connected to mtDNAc and that epigenetic and protein differences related to p53 might be involved in connecting these age-related markers at birth. This might be in line with the experimentally proposed telomere-mitochondrial axis of aging and gains important insight into the early life aging process.

AUTHOR CONTRIBUTIONS

TSN conceived and coordinates the ENVIR*ON*AGE birth cohort and designed the current study together with DSM, BGJ and CVDS. BGJ and DSM performed telomere and ELISA measurements. RA, MP and SASL performed quality control of the methylation data. CVDS and DSM processed and statistically analyzed all data and performed the quality control of the database. CVDS, TSN and DSM wrote the first draft of the manuscript. All authors were involved in data interpretation and critical revision of the manuscript.

CONFLICTS OF INTEREST

The authors declare they have no competing financial interests. None of the funding agencies had a role in the design and conduct of the study; in the collection, analysis, and interpretation of the data; or in the preparation, review, or approval of the manuscript.

FUNDING

The authors thank the participating women and neonates, as well as the staff of the maternity ward, midwives, and the staff of the clinical laboratory of East-Limburg Hospital in Genk. The ENVIR*ON*AGE birth cohort is supported by the Flemish Scientific Fund (FWO, Grant No. N1518119, No. G082317N and No. 1523817N) and Kom Op Tegen Kanker (KOTK). Dries S. Martens is a postdoctoral fellow funded by the Research Foundation Flanders (FWO, 12X9620N). Bram G. Janssen and Sabine A.S. Langie were the beneficiary of a post-doctoral fellowship (12W3218N and 12L5216N respectively) also provided by the FWO.

REFERENCES

1. Gems D, Partridge L. Genetics of longevity in model organisms: debates and paradigm shifts. Annu Rev Physiol. 2013; 75:621–44. https://doi.org/10.1146/annurev-physiol-030212-183712 PMID:23190075
2. Kirkwood TB. Understanding the odd science of aging. Cell. 2005; 120:437–47. https://doi.org/10.1016/j.cell.2005.01.027 PMID:15734677
3. Vijg J, Campisi J. Puzzles, promises and a cure for ageing. Nature. 2008; 454:1065–71. https://doi.org/10.1038/nature07216 PMID:18756247
4. López-Otín C, Blasco MA, Partridge L, Serrano M, Kroemer G. The hallmarks of aging. Cell. 2013; 153:1194–217. https://doi.org/10.1016/j.cell.2013.05.039 PMID:23746838
5. Sahin E, Colla S, Liesa M, Moslehi J, Müller FL, Guo M, Cooper M, Kotton D, Fabian AJ, Walkey C, Maser RS, Tonon G, Foerster F, et al. Telomere dysfunction induces metabolic and mitochondrial compromise. Nature. 2011; 470:359–65. https://doi.org/10.1038/nature09787 PMID:21307849
6. Pieters N, Janssen BG, Valeri L, Cox B, Cuypers A, Dewitte H, Plusquin M, Smeets K, Nawrot TS. Molecular responses in the telomere-mitochondrial axis of ageing in the elderly: a candidate gene approach. Mech Ageing Dev. 2015; 145:51–7. https://doi.org/10.1016/j.mad.2015.02.003 PMID:25736869
7. Janssen BG, Madhloum N, Gyselaers W, Bijnens E, Clemente DB, Cox B, Hogervorst J, Luyten L, Martens DS, Peusens M, Plusquin M, Provost EB, Roels HA, et al. Cohort Profile: The ENVIRonmental influence ON early AGEing (ENVIRONAGE): a birth cohort study. Int J Epidemiol. 2017; 46:1386–7m.

https://doi.org/10.1093/ije/dyw269
PMID:28089960

8. Janssen BG, Munters E, Pieters N, Smeets K, Cox B, Cuypers A, Fierens F, Penders J, Vangronsveld J, Gyselaers W, Nawrot TS. Placental mitochondrial DNA content and particulate air pollution during in utero life. Environ Health Perspect. 2012; 120:1346–52. https://doi.org/10.1289/ehp.1104458 PMID:22626541

9. Martens DS, Plusquin M, Gyselaers W, De Vivo I, Nawrot TS. Maternal pre-pregnancy body mass index and newborn telomere length. BMC Med. 2016; 14:148. https://doi.org/10.1186/s12916-016-0689-0 PMID:27751173

10. Cawthon RM. Telomere length measurement by a novel monochrome multiplex quantitative PCR method. Nucleic Acids Res. 2009; 37:e21. https://doi.org/10.1093/nar/gkn1027 PMID:19129229

11. Wang C, Nawrot TS, Van Der Stukken C, Tylus D, Sleurs H, Peusens M, Alfano R, Langie SAS, Plusquin M, Martens DS. Different epigenetic signatures of newborn telomere length and telomere attrition rate in early life. Aging (Albany NY). 2021; 13:14630–50. https://doi.org/10.18632/aging.203117 PMID:34086604

12. Martens DS, Nawrot TS. Air Pollution Stress and the Aging Phenotype: The Telomere Connection. Curr Environ Health Rep. 2016; 3:258–69. https://doi.org/10.1007/s40572-016-0098-8 PMID:27357566

13. Herzog E, Galvez J, Roks A, Stolk L, Verbiest M, Eilers P, Cornelissen J, Steegers E, Steegers-Theunissen R. Tissue-specific DNA methylation profiles in newborns. Clin Epigenetics. 2013; 5:8. https://doi.org/10.1186/1868-7083-5-8 PMID:23724794

14. Janssen BG, Byun HM, Cox B, Gyselaers W, Izzi B, Baccarelli AA, Nawrot TS. Variation of DNA methylation in candidate age-related targets on the mitochondrial-telomere axis in cord blood and placenta. Placenta. 2014; 35:665–72. https://doi.org/10.1016/j.placenta.2014.06.371 PMID:25047690

15. Nomura Y, Lambertini L, Rialdi A, Lee M, Mystal EY, Grabie M, Manaster I, Huynh N, Finik J, Davey M, Davey K, Ly J, Stone J, et al. Global methylation in the placenta and umbilical cord blood from pregnancies with maternal gestational diabetes, preeclampsia, and obesity. Reprod Sci. 2014; 21:131–7. https://doi.org/10.1177/1933719113492206 PMID:23765376

16. Wang C, Plusquin M, Ghantous A, Herceg Z, Alfano R, Cox B, Nawrot TS. DNA methylation of insulin-like growth factor 2 and H19 cluster in cord blood and prenatal air pollution exposure to fine particulate matter. Environ Health. 2020; 19:129. https://doi.org/10.1186/s12940-020-00677-9 PMID:33287817

17. Martens DS, Van Der Stukken C, Derom C, Thiery E, Bijnens EM, Nawrot TS. Newborn telomere length predicts later life telomere length: Tracking telomere length from birth to child- and adulthood. EBioMedicine. 2021; 63:103164. https://doi.org/10.1016/j.ebiom.2020.103164 PMID:33422989

18. Okuda K, Bardeguez A, Gardner JP, Rodriguez P, Ganesh V, Kimura M, Skurnick J, Awad G, Aviv A. Telomere length in the newborn. Pediatr Res. 2002; 52:377–81. https://doi.org/10.1203/00006450-200209000-00012 PMID:12193671

19. Vasu V, Turner KJ, George S, Greenall J, Slijepcevic P, Griffin DK. Preterm infants have significantly longer telomeres than their term born counterparts. PLoS One. 2017; 12:e0180082. https://doi.org/10.1371/journal.pone.0180082 PMID:28658264

20. Sanchez-Guerra M, Peng C, Trevisi L, Cardenas A, Wilson A, Osorio-Yáñez C, Niedzwiecki MM, Zhong J, Svensson K, Acevedo MT, Solano-Gonzalez M, Amarasiriwardena CJ, Estrada-Gutierrez G, et al. Altered cord blood mitochondrial DNA content and pregnancy lead exposure in the PROGRESS cohort. Environ Int. 2019; 125:437–44. https://doi.org/10.1016/j.envint.2019.01.077 PMID:30753999

21. Jjingo D, Conley AB, Yi SV, Lunyak VV, Jordan IK. On the presence and role of human gene-body DNA methylation. Oncotarget. 2012; 3:462–74. https://doi.org/10.18632/oncotarget.497 PMID:22577155

22. Daniali L, Benetos A, Susser E, Kark JD, Labat C, Kimura M, Desai K, Granick M, Aviv A. Telomeres shorten at equivalent rates in somatic tissues of adults. Nat Commun. 2013; 4:1597. https://doi.org/10.1038/ncomms2602 PMID:23511462

23. Bai RK, Chang J, Yeh KT, Lou MA, Lu JF, Tan DJ, Liu H, Wong LJ. Mitochondrial DNA content varies with pathological characteristics of breast cancer. J Oncol. 2011; 2011:496189.

https://doi.org/10.1155/2011/496189
PMID:22028711

24. Chin L, Artandi SE, Shen Q, Tam A, Lee SL, Gottlieb GJ, Greider CW, DePinho RA. p53 deficiency rescues the adverse effects of telomere loss and cooperates with telomere dysfunction to accelerate carcinogenesis. Cell. 1999; 97:527–38.
https://doi.org/10.1016/s0092-8674(00)80762-x
PMID:10338216

25. Ryan KM, Phillips AC, Vousden KH. Regulation and function of the p53 tumor suppressor protein. Curr Opin Cell Biol. 2001; 13:332–7.
https://doi.org/10.1016/s0955-0674(00)00216-7
PMID:11343904

26. Harris SL, Levine AJ. The p53 pathway: positive and negative feedback loops. Oncogene. 2005; 24:2899–908.
https://doi.org/10.1038/sj.onc.1208615
PMID:15838523

27. Tokino T, Nakamura Y. The role of p53-target genes in human cancer. Crit Rev Oncol Hematol. 2000; 33:1–6.
https://doi.org/10.1016/s1040-8428(99)00051-7
PMID:10714958

28. Rufini A, Tucci P, Celardo I, Melino G. Senescence and aging: the critical roles of p53. Oncogene. 2013; 32:5129–43.
https://doi.org/10.1038/onc.2012.640
PMID:23416979

29. Vousden KH, Lu X. Live or let die: the cell's response to p53. Nat Rev Cancer. 2002; 2:594–604.
https://doi.org/10.1038/nrc864
PMID:12154352

30. Park JH, Zhuang J, Li J, Hwang PM. p53 as guardian of the mitochondrial genome. FEBS Lett. 2016; 590:924–34.
https://doi.org/10.1002/1873-3468.12061
PMID:26780878

31. Tyrka AR, Carpenter LL, Kao HT, Porton B, Philip NS, Ridout SJ, Ridout KK, Price LH. Association of telomere length and mitochondrial DNA copy number in a community sample of healthy adults. Exp Gerontol. 2015; 66:17–20.
https://doi.org/10.1016/j.exger.2015.04.002
PMID:25845980

32. Yamamoto H, Schoonjans K, Auwerx J. Sirtuin functions in health and disease. Mol Endocrinol. 2007; 21:1745–55.
https://doi.org/10.1210/me.2007-0079
PMID:17456799

33. Sahin E, DePinho RA. Axis of ageing: telomeres, p53 and mitochondria. Nat Rev Mol Cell Biol. 2012; 13:397–404.
https://doi.org/10.1038/nrm3352
PMID:22588366

SUPPLEMENTARY MATERIALS

Supplementary Methods

Reaction mixtures and PCR cycling conditions for telomere length (TL) and mitochondrial DNA content (mtDNAc) measurements

The master mix for TL measurement contained 1× QuantiTect SYBR Green PCR master mix (Qiagen, Inc., Venlo, the Netherlands), 2 mM dithiothreitol (DTT), 300 nM telg primer (ACACTAAGGTTTGGGTTTGGGTT TGGGTTTGGGTTAGTGT) and 900 nM telc primer (TGTTAGGTATCCCTATCCCTATCCCTATCCCTAT CCCTAACA). Used cycling conditions were: 1 cycle at 95°C for 10 min, followed by 2 cycles at 94°C for 15 sec and 49°C for 2 min and 30 cycles at 94°C for 15 sec, 62°C for 20 sec, and 74°C for 1 min and 20 sec. The single-copy gene reaction mixture contained 1× QuantiTect SYBR Green PCR master mix, 300 nM 36B4u primer (CAGCAAGTGGGAAGGTGTAATCC) and 500 nM 36B4d primer (CCCATTCTATCAT CAACGGGTACAA). Used cycling conditions were: 1 cycle at 95°C for 10 min, followed by 40 cycles at 95°C for 15 sec, and 58°C for 1 min and 20 sec [1].

The master mix for mtDNAc measurement consisted of Fast SYBR® Green I dye 2× (Applied Biosystems; 5 µL/reaction), 300 nm forward (5′-CACCCAAGAA CAGGGTTTGT-3′ for MTF3212/3319, and 5′-ATGG CCAACCTCCTACTCCT-3′ for MT-ND1) and 300 nm reverse primer (5′-TGGCCATGGGTATGTTGTTAA-3′ for MTF3212/3319 and 5′-CTACAACGTTGGGGCC TTT-3′ for MT-ND1) and RNase free water (1.9 µL/ reaction). thermal cycling profile was the same for all transcripts: 20 sec at 95°C for activation of the AmpliTaq Gold® DNA-polymerase, followed by 40 cycles of 1 sec at 95°C for denaturation and 20 sec at 60°C for annealing/extension. Amplification specificity and absence of primer dimers was confirmed by melting curve analysis at the end of each run. After thermal cycling, raw data were collected and processed. CT (cycle threshold)–values of the two mitochondrial genes were normalized relative to the nuclear reference genes according to the qBase software (Biogazelle, Zwijnaarde, Belgium). The program uses modified software from the classic comparative CT method (ΔΔCT) that takes multiple reference genes into account and uses inter-run calibration algorithms to correct for run-to-run differences [2, 3].

REFERENCES

1. Martens DS, Plusquin M, Gyselaers W, De Vivo I, Nawrot TS. Maternal pre-pregnancy body mass index and newborn telomere length. BMC Med. 2016; 14:148. https://doi.org/10.1186/s12916-016-0689-0 PMID:27751173
2. Grevendonk L, Janssen BG, Vanpoucke C, Lefebvre W, Hoxha M, Bollati V, Nawrot TS. Mitochondrial oxidative DNA damage and exposure to particulate air pollution in mother-newborn pairs. Environ Health. 2016; 15:10. https://doi.org/10.1186/s12940-016-0095-2 PMID:26792633
3. Hellemans J, Mortier G, De Paepe A, Speleman F, Vandesompele J. qBase relative quantification framework and software for management and automated analysis of real-time quantitative PCR data. Genome Biol. 2007; 8:R19. https://doi.org/10.1186/gb-2007-8-2-r19 PMID:17291332

Supplementary Figures

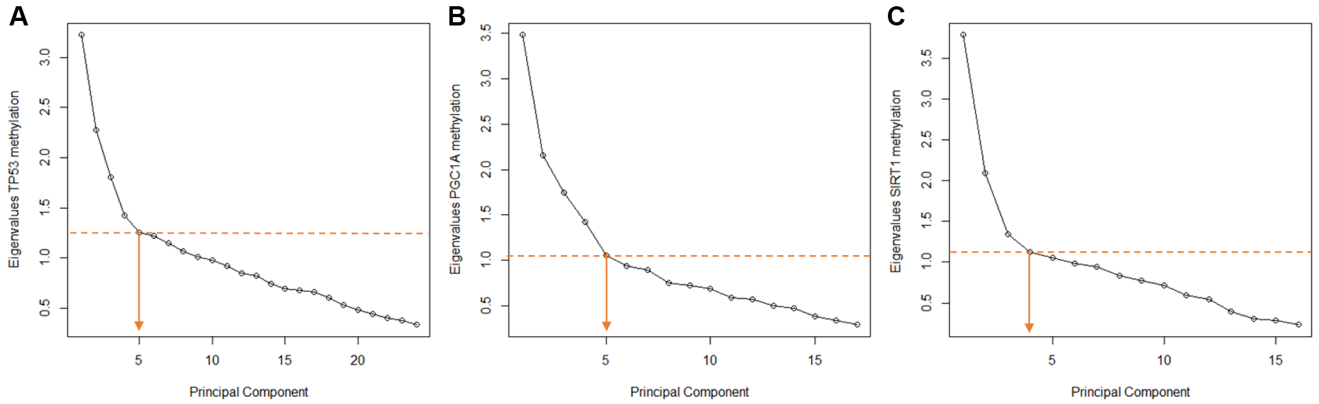

Supplementary Figure 1. Scree plots presenting eigenvalues of each Principal Component (PC). Eigenvalues represent the total amount of variance that can be explained by a given PC. Panel (**A**) displays the variance in *TP53* methylation explained by each PC. Panel (**B**) shows the variance in *PGC1A* methylation explained by each PC and panel (**C**) shows the variance in *SIRT1* methylation explained by each PC. Only PCs on the left side of the elbow in the curve were retained in the analysis.

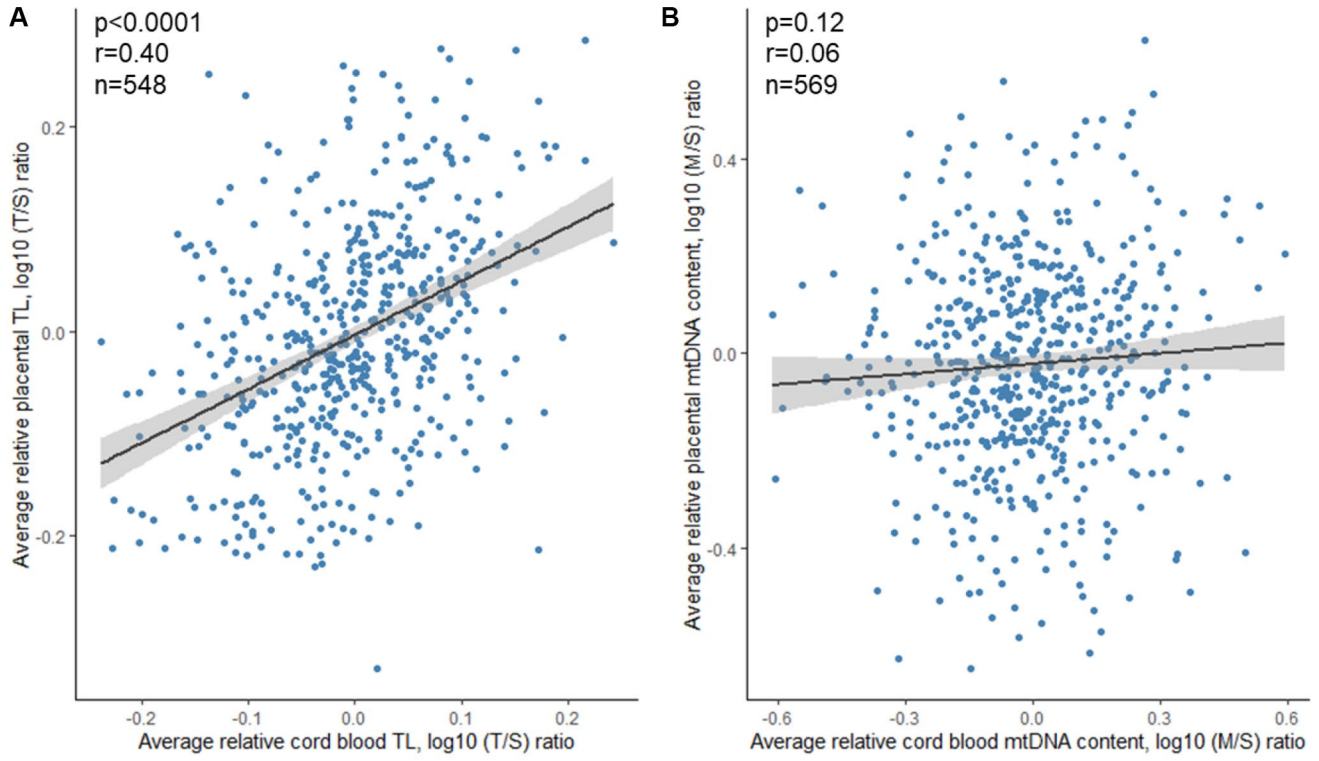

Supplementary Figure 2. Correlation between cord blood and placental age related markers. Panel (**A**) shows the correlation between average relative cord blood TL and average relative placental TL. Panel (**B**) shows the correlation between average relative cord blood mtDNAc and average relative placental mtDNAc. Abbreviations: TL: telomere length; T/S: telomere/single copy gene ratio; mtDNAc: mitochondrial DNA content; M/S: mitochondrial DNA/single copy gene ratio.

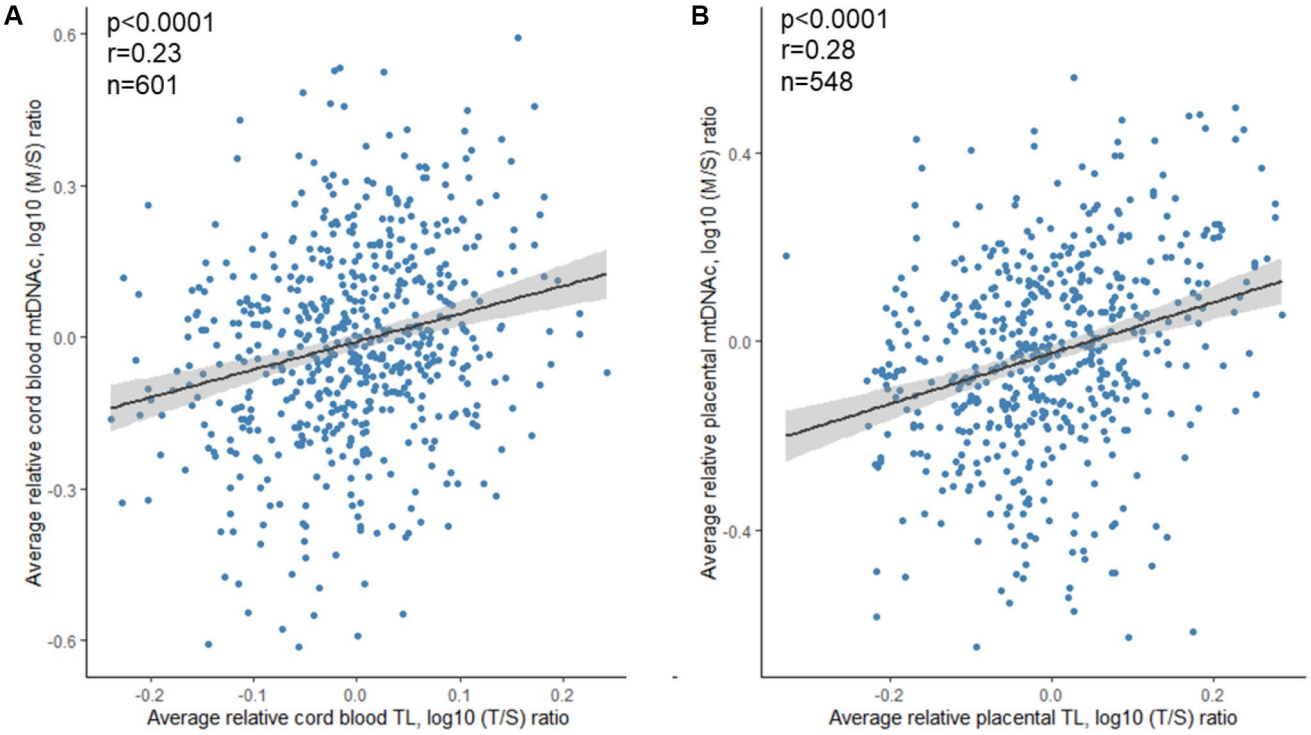

Supplementary Figure 3. Correlation between TL and mtDNAc. Panel (**A**) shows the correlation between average relative cord blood TL and mtDNAc. Panel (**B**) shows the correlation between average relative placental TL and mtDNAc. Abbreviations: TL: telomere length; T/S: telomere/single copy gene ratio; mtDNAc: mitochondrial DNA content; M/S: mitochondrial DNA/single copy gene ratio.

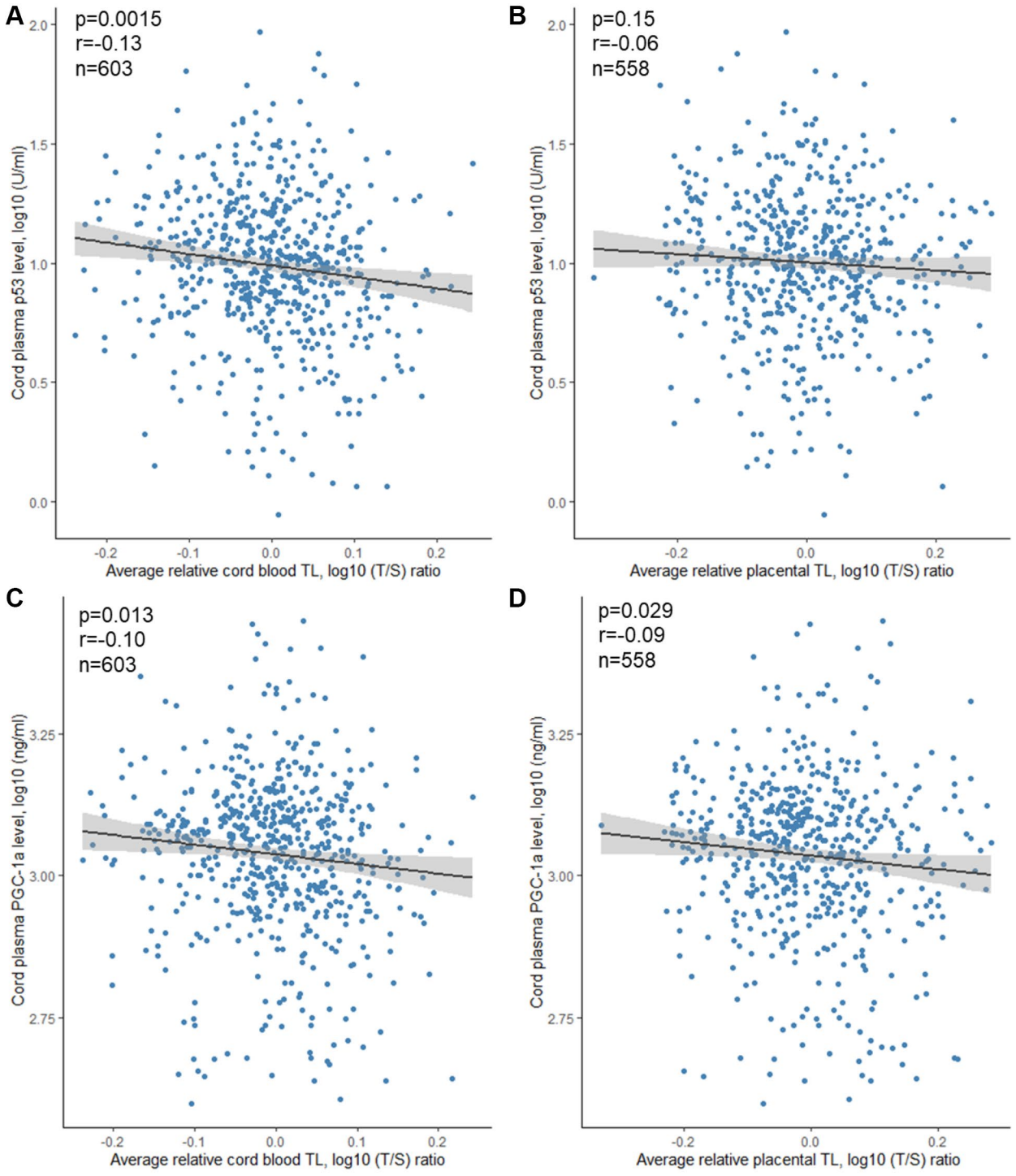

Supplementary Figure 4. Correlation between TL and cord plasma protein levels. Panel (**A**) shows the correlation between average relative cord blood TL and cord plasma p53 level. Panel (**B**) shows the correlation between average relative placental TL and cord plasma p53 level. Panel (**C**) shows the correlation between average relative cord blood TL and cord plasma PGC-1α level. Panel (**D**) shows the correlation between average relative placental TL and cord plasma PGC-1α level. Abbreviations: TL: telomere length; T/S: telomere/single copy gene ratio.

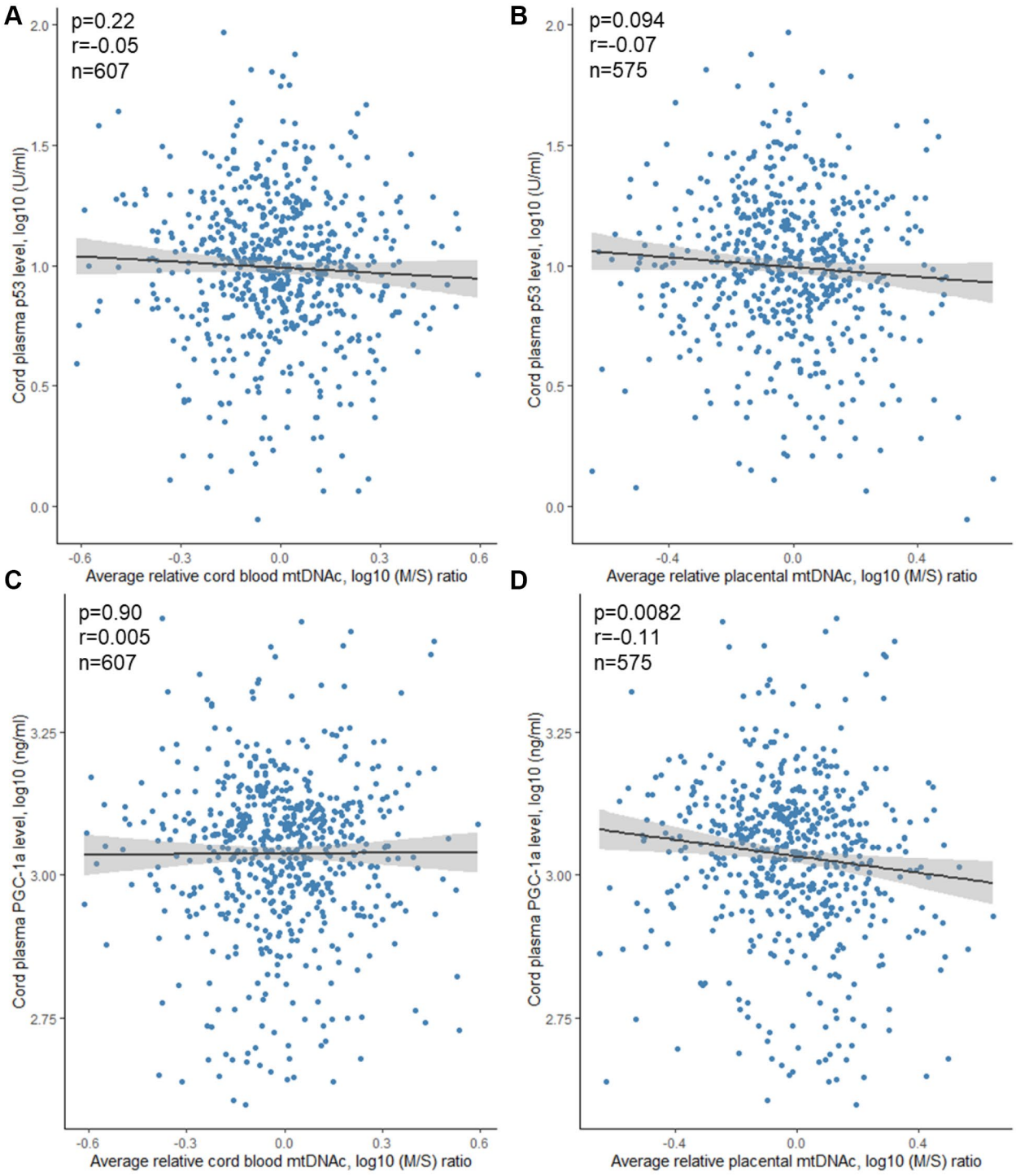

Supplementary Figure 5. Correlation between mtDNAc and cord plasma protein levels. Panel (**A**) shows the correlation between average relative cord blood mtDNAc and cord plasma p53 level. Panel (**B**) shows the correlation between average relative placental mtDNAc and cord plasma p53 level. Panel (**C**) shows the correlation between average relative cord blood mtDNAc and cord plasma PGC-1α level. Panel (**D**) shows the correlation between average relative placental mtDNAc and cord plasma PGC-1α level. Abbreviations: TL: telomere length; T/S: telomere/single copy gene ratio; mtDNAc: mitochondrial DNA content; M/S: mitochondrial DNA/single copy gene ratio.

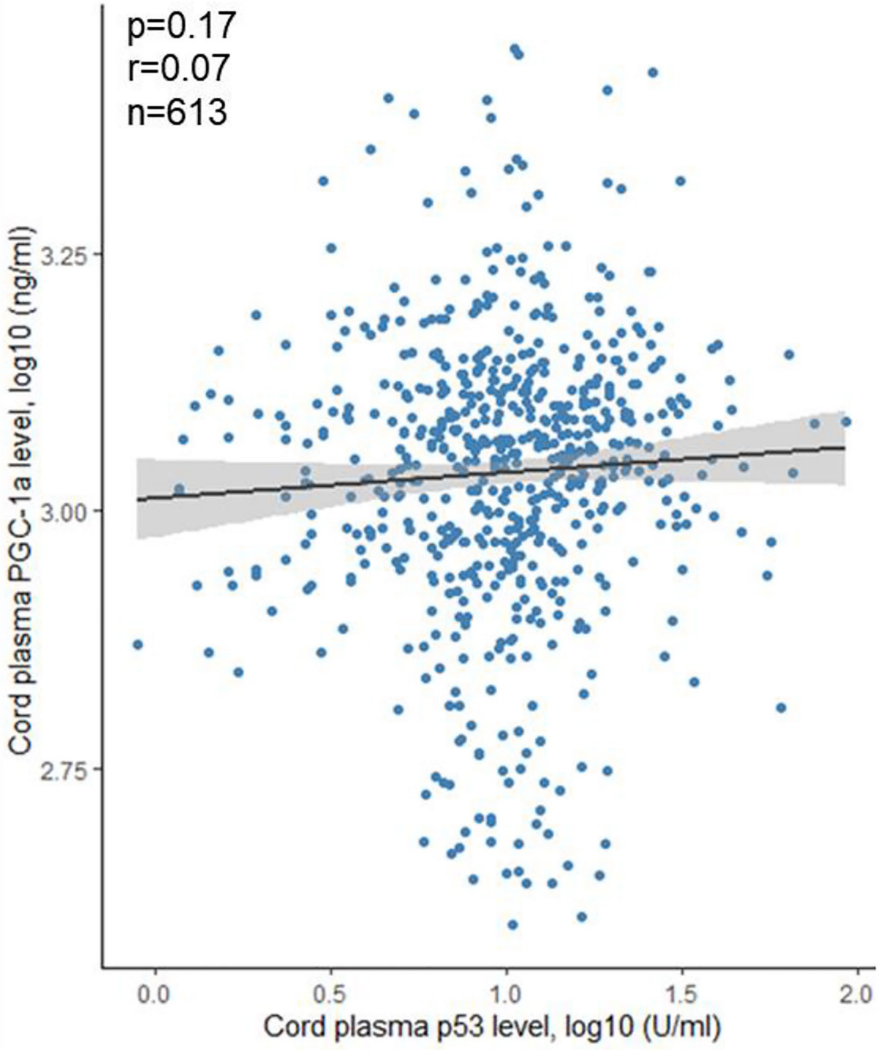

Supplementary Figure 6. Correlation between cord plasma p53 and cord plasma PGC-1α levels.

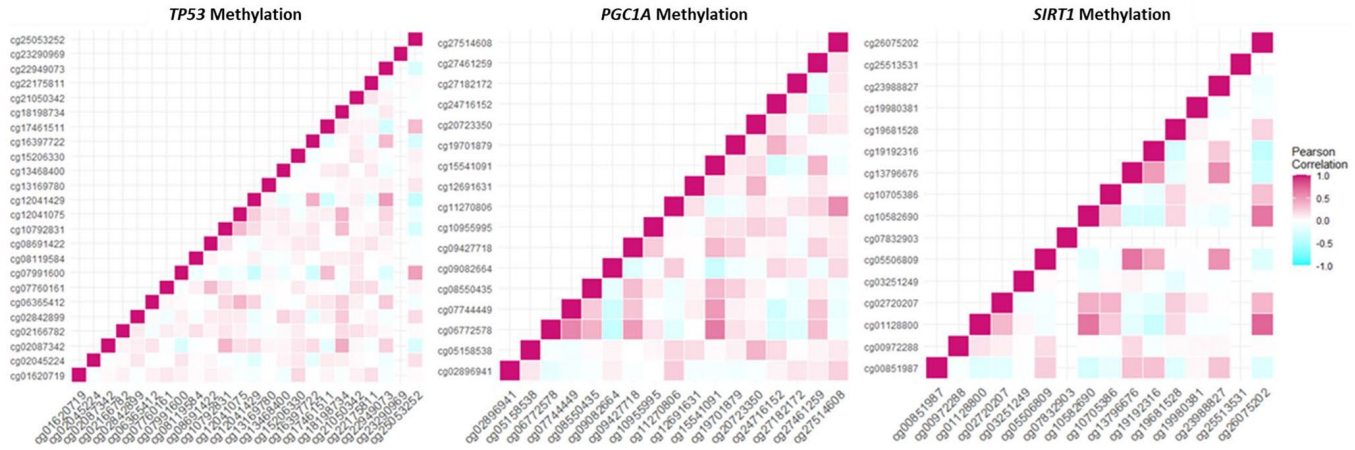

Supplementary Figure 7. Pearson correlation heatmap showing correlations between methylation levels of CpG regions for each gene separately. Methylation levels of *TP53*, *PGC1A* and *SIRT1* were obtained from the 850K array.

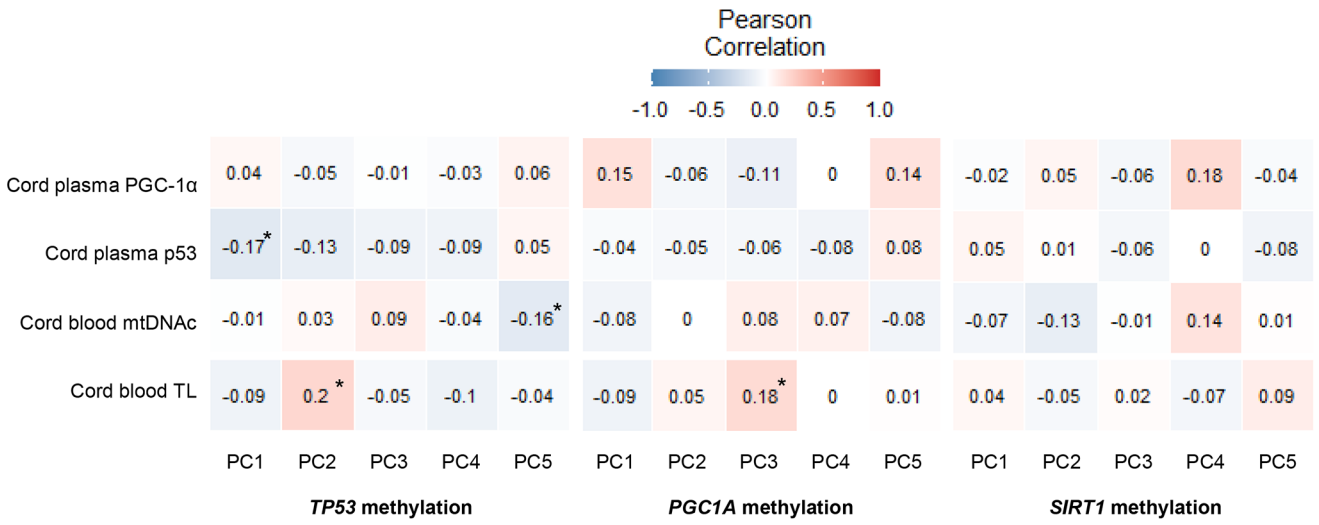

Supplementary Figure 8. Pearson correlation matrix showing correlations between age-related markers and methylation levels in cord blood. Methylation levels of *TP53*, *PGC1A* and *SIRT1* were obtained from the 850K array. All age-related markers are log-transformed. A star indicates *p*-values ≤0.05. Abbreviations: mtDNAc: Mitochondrial DNA content; TL: telomere length.

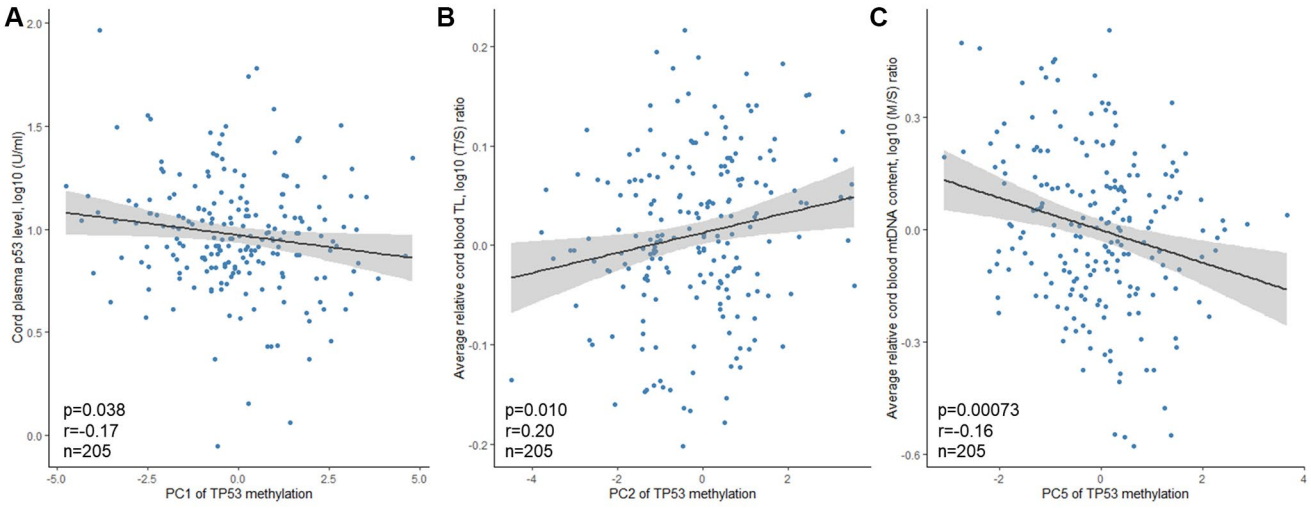

Supplementary Figure 9. Correlation between PCs of *TP53* methylation levels and cord blood age-related markers. Panel (**A**) shows a negative correlation between PC1 and cord plasma p53 level. Panel (**B**) shows a positive correlation between PC2 and average relative cord blood TL. Panel (**C**) shows a negative correlation between PC5 and average relative cord blood mtDNA content. Abbreviations: TL: telomere length; T/S: telomere/single copy gene ratio; mtDNAc: Mitochondrial DNA content; M/S: Mitochondrial DNA/single copy gene ratio.

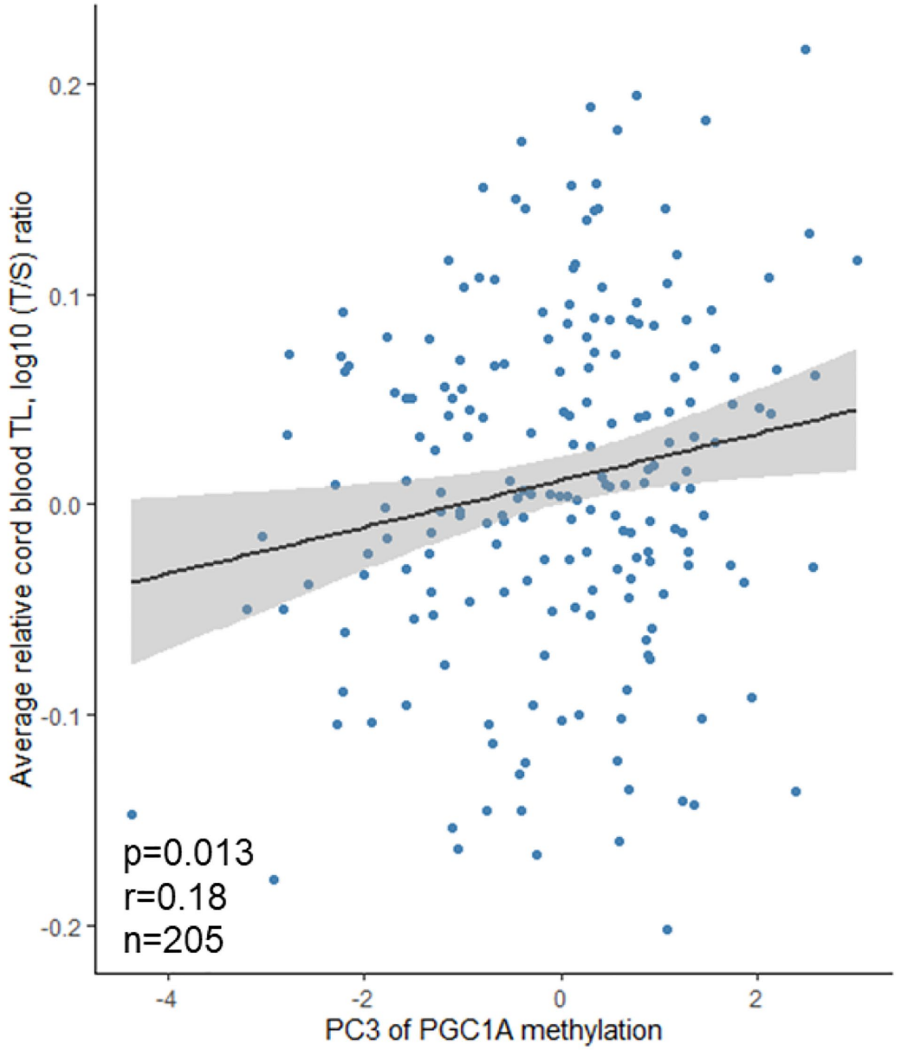

Supplementary Figure 10. Correlation between PCs of *PGC1A* methylation levels and cord blood TL. A positive correlation is shown between PC3 and average relative cord blood TL. Abbreviations: TL: telomere length; T/S: telomere/single copy gene ratio.

Supplementary Tables

Supplementary Table 1. 850K methylation information. Annotations were obtained using the BiocManager package in R.

850K methylation array							
CpG Name	**Annotation**	**Position**	**Relation to Island**	**UCSC Ref Gene Name**	**UCSC Ref Gene Accession**	**UCSC Ref Gene Group**	**Regulatory Feature Group**
cg25053252	chr17:7589290-7589503	7589358	Island	***TP53***	NM_000546	5′UTR	PA
cg17461511	chr17:7591494-7591839	7591552	Island	***TP53***	NM_000546	TSS1500	PA
cg02045224	chr17:7591494-7591839	7591618	Island	***TP53***	NM_000546	TSS1500	PA
cg07991600	chr17:7589290-7589503	7589380	Island	***TP53***	NM_000546	5′UTR	PA
cg02087342	NA	7579047	Open Sea	***TP53***	NM_000546	Body	
cg22949073	NA	7572391	Open Sea	***TP53***	NM_000546	3′UTR	
cg13169780	chr17:7591494-7591839	7591570	Island	***TP53***	NM_000546	TSS1500	PA
cg07760161	chr17:7589290-7589503	7588378	N Shore	***TP53***	NM_000546	5′UTR	PA; CTS
cg02166782	chr17:7591494-7591839	7591564	Island	***TP53***	NM_000546	TSS1500	PA
cg22175811	chr17:7591494-7591839	7590052	N Shore	***TP53***	NM_000546	5′UTR	PA
cg21050342	chr17:7591494-7591839	7591644	Island	***TP53***	NM_000546	TSS1500	PA
cg13468400	NA	7579546	Open Sea	***TP53***	NM_000546	Body	
cg08119584	chr17:7591494-7591839	7589976	N Shore	***TP53***	NM_000546	5′UTR	PA
cg18198734	**NA**	**7579263**	**Open Sea**	***TP53***	**NM_000546**	**Body**	
cg23290969	chr17:7589290-7589503	7589272	N Shore	***TP53***	NM_000546	5′UTR	PA
cg16397722	NA	7577090	Open Sea	***TP53***	NM_000546	Body	
cg12041075	NA	7579312	Open Sea	***TP53***	NM_000546	Body	
cg08691422	chr17:7589290-7589503	7588787	N Shore	***TP53***	NM_000546	5′UTR	
cg15206330	chr17:7591494-7591839	7591591	Island	***TP53***	NM_000546	TSS1500	PA
cg12041429	**chr17:7589290-7589503**	**7585875**	**N Shelf**	***TP53***	**NM_000546**	**5′UTR**	
cg02842899	chr17:7589290-7589503	7589491	Island	***TP53***	NM_000546	5′UTR	PA
cg01620719	chr17:7589290-7589503	7589251	N Shore	***TP53***	NM_000546	5′UTR	PA
cg10792831	NA	7578689	Open Sea	***TP53***	NM_000546	Body	
cg06365412	NA	7580709	Open Sea	***TP53***	NM_000546	5′UTR	
cg27182172	chr4:23890120-23890955	23890890	Open Sea	***PGC1A***	NM_013261	Body	
cg09082664	chr4:23499647-23499989	23890701	Open Sea	***PGC1A***	NM_013261	Body	
cg27514608	chr4:23892305-23892675	23892540	Open Sea	***PGC1A***	NM_013261	TSS1500	
cg05158538	chr4:23891440-23891870	23891486	Open Sea	***PGC1A***	NM_013261	Body	
cg10955995	chr4:23857865-23858250	23858146	Open Sea	***PGC1A***	NM_013261	Body	
cg27461259	chr4:23892305-23892675	23892621	Open Sea	***PGC1A***	NM_013261	TSS1500	
cg07744449	NA	23887314	Open Sea	***PGC1A***	NM_013261	Body	
cg08550435	chr4:23829600-23829910	23829879	Open Sea	***PGC1A***	NM_013261	Body	
cg02896941	chr4:23499647-23499989	23890659	Open Sea	***PGC1A***	NM_013261	Body	
cg19701879	chr4:23880820-23881155	23881105	Open Sea	***PGC1A***	NM_013261	Body	
cg11270806	chr4:23892305-23892675	23892515	Open Sea	***PGC1A***	NM_013261	TSS1500	

cg24716152	chr4:23879168-23881165	23879965	Open Sea	***PGC1A***	NM_013261	Body	
cg12691631	chr4:23891440-23891870	23891835	Open Sea	***PGC1A***	NM_013261	TSS200	
cg15541091	chr4:23812780-23813175	23813125	Open Sea	***PGC1A***	NM_013261	Body	
cg06772578	NA	23796624	Open Sea	***PGC1A***	NM_013261	3′UTR	
cg09427718	chr4:23819243-23820433	23819929	Open Sea	***PGC1A***	NM_013261	Body	
cg20723350	chr4:23891440-23891870	23891596	Open Sea	***PGC1A***	NM_013261; NM_013261	1stExon; 5′UTR	
cg10582690	chr10:69644169-69645178	69644422	Island	***SIRT1***	NM_012238	TSS200	PA
cg07832903	chr10:69644169-69645178	69644926	Island	***SIRT1***	NM_012238	Body	PA
cg00972288	chr10:69644169-69645178	69644348	Island	***SIRT1***	NM_012238	TSS200	PA
cg19681528	chr10:69644169-69645178	69644405	Island	***SIRT1***	NM_012238	TSS200	PA
cg02720207	chr10:69644169-69645178	69644399	Island	***SIRT1***	NM_012238	TSS200	PA
cg25513531	chr10:69644169-69645178	69644407	Island	***SIRT1***	NM_012238	TSS200	PA
cg26075202	chr10:69644169-69645178	69645177	Island	***SIRT1***	NM_012238	Body	
cg10705386	chr10:69644169-69645178	69644512	Island	***SIRT1***	NM_012238	1stExon	PA
cg01128800	chr10:69644169-69645178	69644938	Island	***SIRT1***	NM_012238	Body	PA
cg00851987	chr10:69662340-69664884	69664037	Open Sea	***SIRT1***	NM_012238	Body	
cg03251249	chr10:69644169-69645178	69645012	Island	***SIRT1***	NM_012238	Body	PA
cg05506809	chr10:69644169-69645178	69648299	S Shelf	***SIRT1***	NM_012238	Body	
cg19192316	chr10:69644169-69645178	69643020	N Shore	***SIRT1***	NM_012238	TSS1500	
cg23988827	NA	69676715	Open Sea	***SIRT1***	NM_012238	3'UTR	
cg19980381	chr10:69644169-69645178	69644128	N Shore	***SIRT1***	NM_012238	TSS1500	PA
cg13796676	chr10:69644169-69645178	69648687	S Shelf	***SIRT1***	NM_012238	Body	

Abbreviations: NA: not applicable; PA: Promotor Associated; CTS: Cell Type Specific.

Supplementary Table 2. Rotated loadings. Bold loadings have an absolute value larger than 0.45, meaning the CpG is selected as relevant for the specific PC.

			TP53		
CpG	**PC1**	**PC2**	**PC3**	**PC4**	**PC5**
cg01620719	–0.11	0.16	0.35	0.02	0.44
cg02045224	–0.20	0.27	–0.07	0.17	–0.16
cg02087342	**0.55**	0.27	0.06	–0.08	–0.16
cg02166782	–0.01	0.32	0.31	0.27	–0.26
cg02842899	–0.12	**0.47**	–0.05	0.04	–0.35
cg06365412	0.37	0.36	–0.27	–0.06	0.42
cg07760161	–0.01	0.18	**0.60**	–0.25	0.25
cg07991600	**–0.56**	0.26	–0.22	0.20	0.32
cg08119584	0.03	0.16	0.18	0.34	–0.23
cg08691422	0.04	0.21	**0.58**	–0.16	0.04
cg10792831	**0.49**	0.42	0.14	–0.32	0.03
cg12041075	0.43	**0.46**	–0.24	–0.15	0.09
cg12041429	**0.72**	–0.25	–0.02	0.24	0.09
cg13169780	0.04	0.14	0.04	0.26	0.03
cg13468400	–0.04	0.32	0.04	–0.44	–0.36

cg15206330	–0.07	0.23	0.36	0.20	–0.03
cg16397722	**0.54**	–0.21	0.17	0.00	0.03
cg17461511	–0.42	0.44	–0.25	–0.15	0.13
cg18198734	0.35	**0.61**	–0.25	–0.06	–0.21
cg21050342	0.05	0.25	0.31	**0.47**	0.25
cg22175811	–0.17	0.17	0.38	–0.06	0.33
cg22949073	**0.64**	–0.10	–0.05	0.34	0.07
cg23290969	–0.03	0.20	0.22	0.00	–0.40
cg25053252	**–0.62**	0.29	–0.19	0.10	–0.01
		PGC1A			
CpG	**PC1**	**PC2**	**PC3**	**PC4**	**PC5**
cg02896941	0.04	0.06	0.02	–0.07	0.02
cg05158538	0.08	0.07	–0.09	–0.10	–0.06
cg06772578	0.30	0.21	0.21	–0.12	–0.07
cg07744449	0.20	0.19	0.19	–0.09	–0.09
cg08550435	**0.45**	0.05	0.10	–0.08	–0.11
cg09082664	–0.04	–0.14	–0.14	0.07	–0.11
cg09427718	**0.54**	–0.05	0.10	0.06	0.08
cg10955995	0.20	–0.02	0.10	0.08	0.05
cg11270806	0.04	–0.02	–0.05	–0.08	0.04
cg12691631	0.06	0.03	–0.02	0.04	–0.16
cg15541091	0.20	0.32	0.20	–0.11	–0.19
cg19701879	**0.48**	–0.13	–0.14	0.06	–0.02
cg20723350	0.05	0.03	0.00	0.02	–0.09
cg24716152	0.29	–0.26	–0.22	0.14	0.02
cg27182172	–0.02	–0.07	–0.09	–0.01	0.03
cg27461259	0.04	0.12	0.01	–0.01	0.03
cg27514608	0.20	–0.11	–0.01	0.00	–0.08
		SIRT1			
CpG	**PC1**	**PC2**	**PC3**	**PC4**	**PC5**
cg00851987	**–0.51**	0.14	–0.10	–0.15	0.28
cg00972288	–0.01	0.28	–0.08	**0.68**	–0.22
cg01128800	**0.69**	**0.45**	–0.32	–0.08	–0.16
cg02720207	**0.49**	0.40	0.18	–0.17	0.04
cg03251249	0.00	–0.03	–0.22	**0.59**	**0.48**
cg05506809	**–0.56**	**0.60**	–0.12	0.13	–0.06
cg07832903	0.01	0.00	**0.55**	0.27	**–0.62**
cg10582690	**0.73**	0.34	–0.15	–0.21	–0.16
cg10705386	0.41	0.36	0.19	0.02	0.11
cg13796676	**–0.66**	**0.57**	–0.05	0.21	–0.01
cg19192316	**–0.65**	0.18	0.03	–0.07	0.25
cg19681528	0.35	0.23	0.25	–0.24	–0.08
cg19980381	–0.02	0.05	**0.64**	0.03	0.28
cg23988827	**–0.46**	**0.61**	–0.17	–0.09	–0.13
cg25513531	0.08	0.35	0.42	0.11	0.03
cg26075202	**0.76**	0.31	–0.27	–0.21	–0.14

Supplementary Table 3. Comparison of the characteristics between our study population (*n* = 613) and full ENVIR*ON*AGE data (*n* = 1530).

Characteristic	Analyzed population Mean ± SD or *n* (%) (*n* = 613)	Total population Mean ± SD or *n* (%) (*n* = 1530)	*P*-value
Mothers			
Age, y	29.3 ± 4.6	29.4 ± 4.55	0.64
Pre-pregnancy BMI, kg/m^2	24.6 ± 4.8	24.5 ± 4.76	0.66
Educational level			
Low	79 (12.9%)	160 (10.5%)	0.13
Middle	227 (37.0%)	500 (32.7%)	0.064
High	307 (50.1%)	726 (47.5%)	0.32
Smoking status			
Never smoker	391 (63.8%)	897 (58.6%)	0.030
Former smoker	154 (25.1%)	326 (21.3%)	0.064
Current smoker	68 (11.1%)	173 (11.3%)	0.95
Parity			
1	337 (55.0%)	751 (49.1%)	0.015
2	206 (33.6%)	507 (33.1%)	0.86
≥	70 (11.4%)	172 (11.2%)	0.95
Newborns			
Sex			
Female	321 (52.4%)	736 (48.1%)	0.10
Gestational age, wk	39.2 ± 1.7	39.2 ± 1.6	0.91
Birth weight, g	3420 ± 496	3400 ± 495	0.52
Ethnicity			
European-Caucasian	533 (86.9%)	1221 (79.8%)	0.0001
Season of birth			
Winter	150 (24.5%)	372 (24.3%)	0.97
Spring	149 (24.3%)	344 (22.5%)	0.40
Summer	151 (24.6%)	329 (21.5%)	0.13
Autumn	163 (26.6%)	385 (25.2%)	0.54

Supplementary Table 4. Association between mitochondrial DNA content (mtDNAc) and cord plasma protein levels (p53 and PGC-1α) and between the cord plasma protein levels.

	Cord p53 (*n* = 613)		Cord PGC-1α (*n* = 607)	
	% difference (95% CI)	*P*-value	% difference (95% CI)	*P*-value
Cord mtDNAc	–0.0082 (–0.51, 0.50)	0.99	0.27 (–0.91, 1.47)	0.26
Placenta mtDNAc*	–0.30 (–0.86, 0.27)	0.31	–0.74 (–2.05, 0.58)	0.27
Cord PGC-1α	0.12 (–0.21, 0.44)	0.51	NA	NA

Estimates are presented as percentage difference with 95% CI for a 10% change in explanatory variable. All models are adjusted for technical covariates (sample storage and batch effects), newborn's sex, gestational age, maternal BMI, maternal and paternal age, ethnicity, parity, smoke status, maternal education and month of delivery. Cord plasma p53 and PGC-1α represent the exposure variable, while the variables in the left column represent the outcome variable. *Data available for *n* = 575. Abbreviation: NA: not applicable.

Supplementary Table 5. Association between Principle Components (PCs) of *TP53*, *PGC1A* and *SIRT1* methylation levels and cord blood telomere length, cord blood mitochondrial DNA content (mtDNAc) and cord plasma protein levels (p53 and PGC-1α).

	Cord TL (*n* = 200)	Cord mtDNA (*n* = 205)	Cord p53 (*n* = 205)	Cord PGC-1α (*n* = 205)
	% difference (95% CI)	% difference (95% CI)	% difference (95% CI)	% difference (95% CI)
TP53				
PC1	−1.00 (−2.48, 0.50)	−0.48 (−4.43, 3.63)	**−5.58 (−1.25, −0.66)**	0.27 (−2.72, 3.35)
PC2	**1.74 (−0.073, 3.58)**	0.32 (−4.51, 5.39)	**−4.63 (−9.79, 0.83)**	−1.00 (−4.55, 2.68)
PC3	−1.38 (−3.36, 0.65)	−0.11 (−5.62, 5.71)	−3.23 (−9.73, 3.74)	0.13 (−3.90, 4.33)
PC4	**−2.46 (−4.84, -0.024)**	−2.96 (−9.28, 3.81)	−4.63 (−12.42, 3.85)	−0.20 (−5.10, 4.96)
PC5	−0.63 (−2.84, 1.64)	**−10.52 (−15.59,-5.14)**	2.59 (−5.16, 10.96)	0.77 (−3.79, 5.54)
PGC1A				
PC1	−0.31 (−1.88, 1.29)	−0.17 (4.06, 3.89)	−2.51 (7.33, 2.55)	1.15 (−1.82, 4.22)
PC2	−0.65 (-2.47, 1.21)	−0.34 (−5.24, 4.81)	−1.39 (−7.30, 4.89)	−0.26 (−3.82, 3.44)
PC3	**2.20 (0.11, 4.34)**	4.47 (−0.92, 10.78)	−0.18 (−7.08, 7.024)	−0.77 (−4.87, 3.52)
PC4	−0.77 (-2.99, 1.50)	2.50 (−3.38, 8.74)	−3.87 (−11.09, 3.93)	0.98 (−3.57, 5.74)
PC5	0.91 (-1.66, 3.54)	−3.98 (−10.38, 2.88)	3.58 (−5.27, 13.25)	2.71 (−2.55, 8.25)
SIRT1				
PC1	0.12 (-1.27, 1.52)	−2.43 (−5.96, 1.32)	0.73 (−3.80, 5.47)	−0.26 (−2.93, 2.48)
PC2	−0.41 (-2.25, 1.46)	**−4.15 (−8.42, 0.80)**	−0.76 (−6.84, 5.72)	−0.79 (−4.42, 2.97)
PC3	1.00 (-1.31, 3.37)	−1.18 (−6.97, 4.96)	−3.23 (−10.66, 4.81)	−2.57 (−7.04, 2.12)
PC4	0.52 (-1.99, 3.08)	4.20 (−2.30, 11.14)	0.48 (−7.79, 9.48)	4.41 (−0.70, 9.78)
PC5	1.10 (-1.63, 3.91)	0.11 (−6.92, 7.67)	−5.28 (−13.83, 4.12)	−0.77 (−6.16, 4.94)

Estimates are presented as percentage difference with 95% CI for a one-unit change in exposure variable. All models are adjusted for technical covariates (sample storage and batch effects), newborn's sex, gestational age, maternal BMI, maternal and paternal age, ethnicity, parity, smoke status, maternal education and month of delivery. The variables in columns represent the response variables, while the variables in the rows represent the explanatory variables. Bold values indicate significant estimates.

Research Paper

TP53/BRAF mutation as an aid in predicting response to immune-checkpoint inhibitor across multiple cancer types

Jia-Zheng Cao[1,*], Gao-Sheng Yao[2,*], Fei Liu[3,*], Yi-Ming Tang[2], Peng-Ju Li[2], Zi-Hao Feng[2], Jun-Hang Luo[2], Jin-Huan Wei[2]

[1]Department of Urology, Jiangmen Central Hospital, Jiangmen, Guangdong, China
[2]Department of Urology, The First Affiliated Hospital of Sun Yat-Sen University, Guangzhou, Guangdong, China
[3]Department of Urology, National Cancer Center, Cancer Hospital, Chinese Academy of Medical Sciences and Peking Union Medical College, Beijing, China
*Equal contribution

Correspondence to: Jun-Hang Luo, Jin-Huan Wei; **email:** luojunh@mail.sysu.edu.cn, weijh23@mail.sysu.edu.cn
Keywords: immune-checkpoint inhibitor therapies, TP53, BRAF, prognosis, precision medicine
Received: September 17, 2021 **Accepted:** February 11, 2022 **Published:** March 27, 2022

ABSTRACT

Immunotherapy with checkpoint inhibitors, such as PD-1/PD-L1 blockage, is becoming standard of practice for an increasing number of cancer types. However, the response rate is only 10%-40%. Thus, identifying biomarkers that could accurately predict the ICI-therapy response is critically important. We downloaded somatic mutation data for 46,697 patients and tumor-infiltrating immune cells levels data for 11070 patients, then combined TP53 and BRAF mutation status into a biomarker model and found that the predict ability of TP53/BRAF mutation model is more powerful than some past models. Commonly, patients with high-TMB status have better response to ICI therapy than patients with low-TMB status. However, the genotype of $TP53^{MUT}BRAF^{WT}$ in high-TMB status cohort have poorer response to ICI therapy than the genotype of $BRAF^{MUT}TP53^{WT}$ in low-TMB status (Median, 18 months vs 47 month). Thus, TP53/BRAF mutation model can add predictive value to TMB in identifying patients who benefited from ICI treatment, which can enable more informed treatment decisions.

INTRODUCTION

Immune-checkpoint inhibitor (ICI) therapies have shown unprecedented durable responses in patients with advanced-stage cancers, including the success of anti-programmed cell death protein 1 (PD-1), anti-programmed death-ligand 1 (PD-L1) and anti-cytotoxic T-lymphocyte-associated protein 4 (CTLA-4), but the response rate is only 10%-40% [1, 2]. Therefore, it is important to identify the biomarkers that can accurately predict the ICI-therapy response.

More and more studies showed tumor mutation burden (TMB) is a clinical useful biomarker for identifying patients who benefited from ICI treatment [3, 4]. Recently, a pan-cancer study showed combining POLE and POLD1 mutation status into a simple model also can efficiently predict response to ICI therapy [5]. TP53 is one of the most frequently mutated gene in human cancers and has been formulated in a large number of studies for functions and mechanisms [6]. In brief, wild-type p53 plays a vital role in maintaining genomic stability and preventing oncogenesis by regulating many cellular processes, including promoting cell growth arrest, DNA repair, modulating autophagy and cancer metabolism [7], and TP53 is highly mutated in about 50% of human cancers. BRAF, is located on human chromosome 7 and encodes a RAS-regulated serine-

threonine kinase that plays a part in ERK/MAPK signaling pathway. At the same time, the pathway is not only involved in regulating cellular biological functions, but is also related to tumor formation [8]. Up to this day, mutations in BRAF have been reported extensively in a variety of benign and malignant tumors [9, 10]. Comparing with POLE and POLD1, the mutation of TP53 and BRAF are more common in human cancer, and TP53 and BRAF had been shown to be linked to ICI therapies responses [11, 12].

In this study, we combined TP53 and BRAF mutation status into a biomarker model and found that the predict ability of TP53/BRAF mutation model is more powerful than POLE/POLD1 mutation model, and the combination of TP53/BRAF mutation model and TMB can more accurately predict the response to ICI therapy. Furthermore, we propose several possible molecular signaling pathways for the effect of TP53/BRAF mutations on the predictive value of ICI treatment response.

MATERIALS AND METHODS

In this study, somatic mutation data for 46,697 patients were downloaded from cBioPortal (https://www.cbioportal.org) [13]. All nonsynonymous mutations were taken into account. The overall survival (OS) of 1,661 patients who received ICI therapy was defined from the date of the first ICI treatment to the time of death or most recent follow-up, and TMB was defined as the total number of somatic nonsynonymous mutations normalized to the total number of megabases sequenced [14].

The data of tumor-infiltrating immune cells levels for 11070 patients from TCGA by CIBERSORT[14] was download from Tumor Immune Estimation Resource (TIMER) version 2.0 [15] (http://timer.cistrome.org/infiltration_estimation_for_tcga.csv.gz). The expression profiles of mRNAs and clinical survival data of 33 tumor types were obtained from the Pan-Cancer Atlas (https://gdc.cancer.gov/about-data/publications/pancanatlas).

The limma package V3.34.9 in R was used to identify differentially expressed mRNAs. Gene Ontology (GO) and Kyoto Encyclopedia of Genes and Genomes (KEGG) analyses were identified and visualized using R packages "clusterProfiler". The cBioPortal online analysis tool was used for mutual exclusivity analysis between TP53 mutation and BRAF mutation. For survival analysis, Kaplan-Meier survival curves were generated and compared using the log-rank test, and the Cox regression model was used for multivariate survival analysis. Statistical tests were done with R software (version 4.0.2). Statistical significance was set at p values less than 0.05. Ethical approval was waived because we used only publicly available data and materials in this study.

Availability of data and materials

The datasets presented in this study can be found in online repositories. The names of the repositories and accession numbers can be found in the article material.

RESULTS

TP53/BRAF mutation model has high frequency

The prevalence of TP53 and BRAF mutations in 46,697 patients with different cancer types is summarized in Figure 1. The mutation frequencies of TP53 and BRAF (33.51% and 5.30%) were significantly higher than that of POLE and POLD1 (2.74% and 1.45%). The relationships between TP53 mutation and BRAF mutation are mutually exclusive (Table 1).

TP53/BRAF mutation model can predict immunotherapeutic effect and prognosis of patients

Based on the mutually exclusive relationship between TP53 mutation and BRAF mutation, we explored the immunotherapy response in patients with different combinations of TP53 mutation and BRAF mutation. Patients were divided into four genotypes, patients with BRAF mutation alone ($BRAF^{MUT}TP53^{WT}$) showed favorable survival (Median, 47 months), while those with TP53 mutation alone ($TP53^{MUT}BRAF^{WT}$) had the worst survival (Median, 13 months). Patients with both mutations or neither mutation ($TP53^{MUT}BRAF^{MUT}$ or $TP53^{WT}BRAF^{WT}$) showed moderate survival (Median, 27 months and 20 months, respectively) (Figure 2A).

In multivariable Cox regression analysis, TP53/BRAF mutation model and TMB were independent predictive factors for identifying patients who benefited from ICI treatment (both $P<0.0001$). However, POLE/POLD1 mutation model and MSI were not independent predictive factors (both $P>0.05$) (Table 2).

Patients in high-TMB status group (the median TMB as cutoff) had longer OS than patients in low-TMB status group (median, 27 months vs 15 month; P =0.000031, Figure 2B). When stratified by TMB status, TP53/BRAF mutation model was still a statistically significant model for predicting ICI-therapy response. In both high-TMB status group and low-TMB status group, TP53/BRAF mutation model can successfully divide patients into three risk stratification: good response genotype ($BRAF^{MUT}TP53^{WT}$), intermediate response genotype ($TP53^{MUT}BRAF^{MUT}$ or $TP53^{WT}BRAF^{WT}$), and poor response genotype ($TP53^{MUT}BRAF^{WT}$) (Figure 2C, 2D).

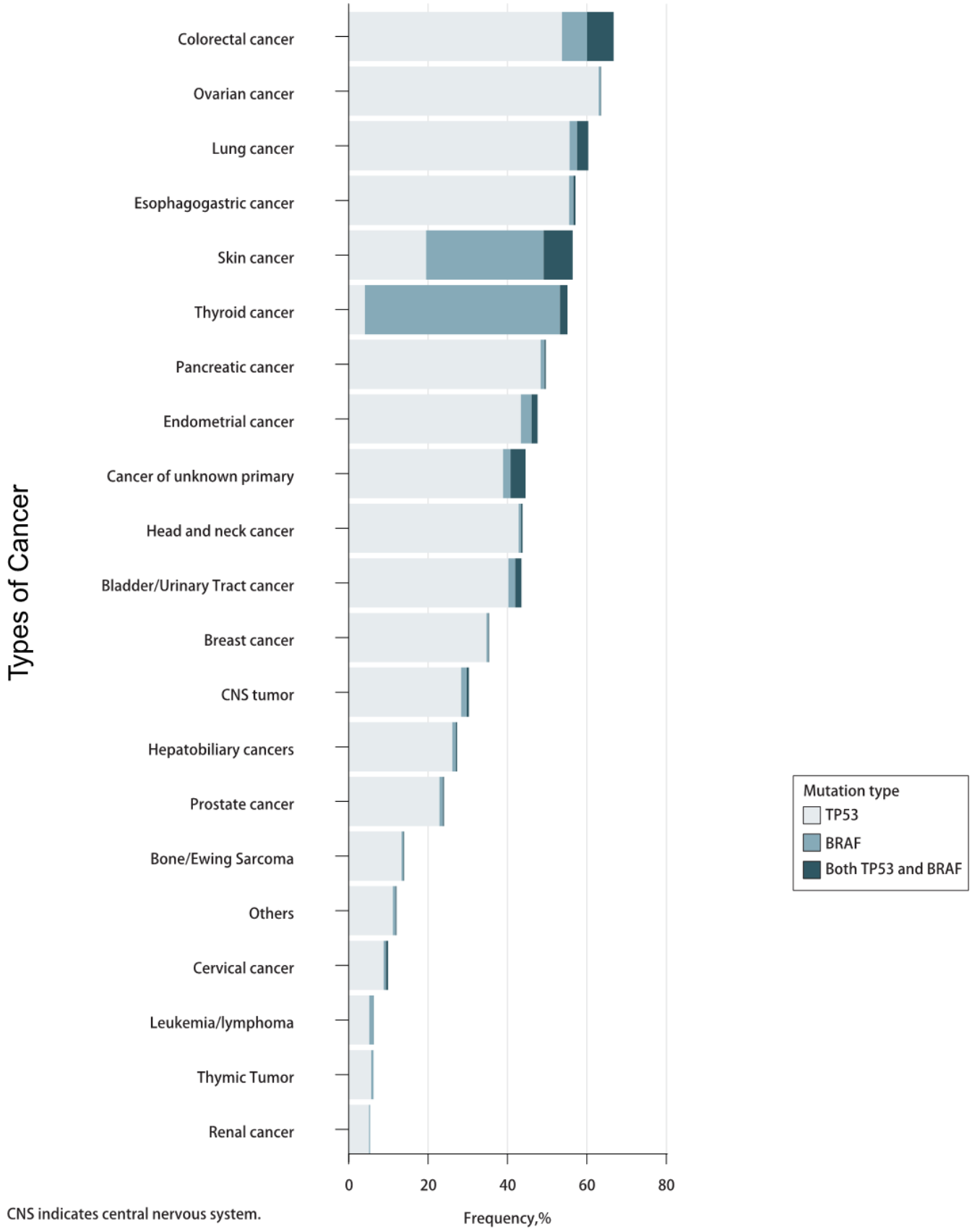

Figure 1. Prevalence of TP53/BRAF mutations in pan-cancer.

In addition, the TP53/BRAF mutation model remained a statistically significant model when stratified according to patients' clinical information. Regardless of gender or age, TP53/BRAF mutation model can still classify patients into three risk stratification (Supplementary Figure 1A–1D).

We further performed MSI analysis and found that the low-MSI status group had a better prognosis (median, 19 months vs 15 month; *P*=0.0095, Supplementary Figure 1E). Exactly like the TMB model, MSI status can also stratify patients with mutated genetic risk (Supplementary Figure 1F, 1G).

TP53/BRAF mutation is an immune-related model

It is generally admitted that CD8+ T cells are directly involved in antitumor cytotoxic responses, and accumulating evidence indicates that tumor-infiltrating CD8+ T cells predict the efficacy of ICI therapy [16–18].

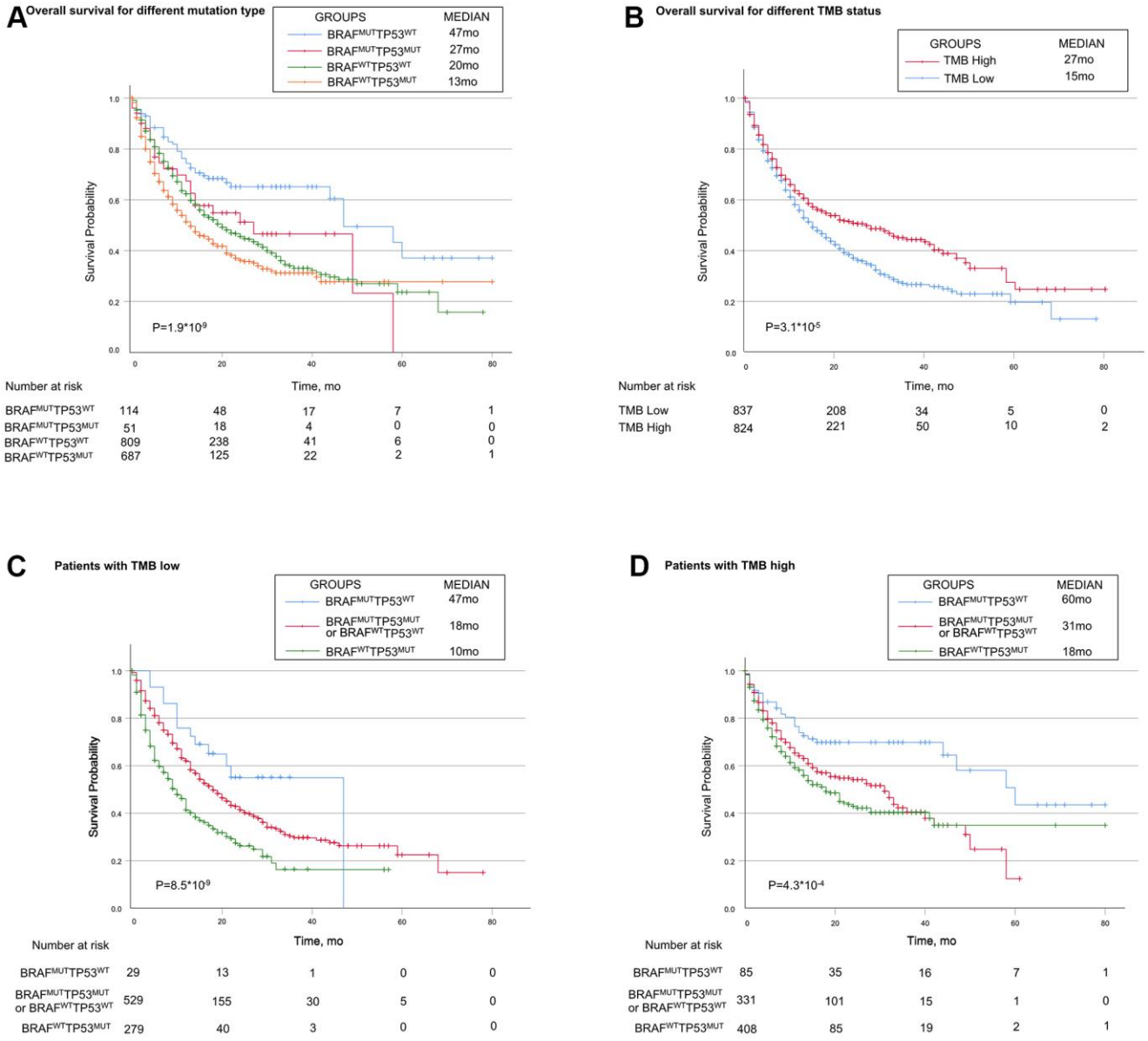

Figure 2. Associations of TP53 and BRAF mutation types with prognosis in patients treated with immune checkpoint inhibitors. (**A**) Patients with the BRAF mutation alone had the best prognosis, while patients with TP53 mutation alone had the worst prognosis. Patients with mutations in both or none had median survival. (**B**) Patients in high-TMB status group had longer OS than patients in low-TMB status group. (**C**, **D**) In both high-TMB/low-TMB status groups, $TP53^{MUT}BRAF^{WT}$ indicated poorer OS, while $BRAF^{MUT}TP53^{WT}$ did the opposite. BRAF indicates B-Raf Proto-Oncogene, Serine/Threonine Kinase gene; TP53 indicates tumor protein p53 gene; MUT indicates mutant genes; WT indicates wild type genes; TMB indicates tumor mutation burden; MSI indicates microsatellite instable.

Table 1. Mutual exclusivity analysis between TP53 mutation and BRAF mutation in the whole cohort, TCGA subset, and MSKCC subset.

Cohorts	$TP53^{WT}$ $BRAF^{WT}$	$TP53^{MUT}$ $BRAF^{WT}$	$BRAF^{MUT}$ $TP53^{WT}$	$TP53^{MUT}$ $BRAF^{MUT}$	Log2 odds ratio	p-value	q-value
Whole cohort	27745	13519	1642	646	-0.309	<0.001	<0.001
TCGA subset	5683	3661	636	209	-0.971	<0.001	<0.001
MSKCC subset	798	691	119	53	-0.959	<0.001	<0.001

TCGA, The Cancer Genome Atlas; MSKCC, Memorial Sloan Kettering Cancer Center.

Table 2. Univariate and multivariable association of the TP53/BRAF mutation model with overall survival in 1,661 patients who received ICI therapy.

Parameters	Univariate		Multivariable	
	HR (95%CI)	p value	HR (95%CI)	p value
Gender	0.88 (0.77-1.01)	0.078	0.89 (0.77-1.02)	0.09
Age	1.00 (0.99-1.00)	0.071	1.00 (0.99-1.00)	0.449
POLE/POLD1 mutation model	0.62 (0.45-0.84)	0.002	0.87 (0.63-1.21)	0.399
TMB	0.98 (0.98-0.99)	<0.0001	0.98 (0.97-0.99)	<0.0001
MSI	0.98 (0.97-1.00)	0.044	1.01 (0.99-1.03)	0.235
Cancer type	0.95 (0.93-0.98)	<0.0001	0.96 (0.94-0.98)	0.0003
TP53/BRAF mutation model	1.41 (1.26-1.58)	<0.0001	1.42 (1.26-1.60)	<0.0001

TMB, tumor mutation burden; MSI, microsatellite instable.

The data from TCGA showed that patients with high tumor-infiltrating CD8+ T cells had longer OS than patients with low tumor-infiltrating CD8+ T cells (Figure 3A). We investigated whether TP53/BRAF mutation was correlated with the level of tumor-infiltrating CD8+ T cells. Patients with $BRAF^{MUT}TP53^{WT}$ showed the highest level of tumor-infiltrating CD8+ T cells, patients with $TP53^{MUT}BRAF^{MUT}$ or $TP53^{WT}BRAF^{WT}$ showed moderate level of tumor-infiltrating CD8+ T cells, and patients with $TP53^{MUT}BRAF^{WT}$ showed the lowest level of CD8+ T cells (Figure 3E). In addition, we further analyzed the correlation between other typical tumor-infiltrating immune cells and patient outcomes (Figure 4B–4D), as well as TP53/BRAF mutation (Figure 3F–3H).

In addition to tumor-infiltrating immune cells, we also analyzed the relationship between TP53/BRAF mutation model and other immune-related genes. Several representative genes were selected, such as immune-suppress genes, like S100A8 and S100A9 in myeloid-derived suppressor cells (MDSC), LRP1 in Regulatory T cells; major histocompatibility complex (MHC) related genes (HlA.DPA1, HlA.DPB1); and immune checkpoints related gene PDCD1. And The violin diagrams about the relative expression quantity of each group was drawn (Supplementary Figure 2).

Mechanism prediction of TP53/BRAF mutation model

To understand the mechanism of oncogenesis underlying TP53/BRAF mutation correlates with response to ICI, functional enrichment characterization of different expression mRNAs between $TP53^{MUT}BRAF^{WT}$ and $BRAF^{MUT}TP53^{WT}$ was performed by GO and KEGG analysis. According to GO analysis, we found that the enriched GO terms were including T cell activation and lymphocyte differentiation. Moreover, KEGG pathway analysis indicated that most of different expression mRNAs were involved in PI3K−Akt signaling pathway, MAPK signaling pathway, Rap1 signaling pathway, chemokine signaling pathway, and AMPK signaling pathway in cancer (Figure 4).

DISCUSSION

Up to this day, ICI therapies have shown powerful responses in cancer patients. However, the rate is not ideal enough, and the methods have the potential to play a greater role in the clinic. It's critical to build more effective biomarker models and stratify the patients for predicting prognosis and applying better individualized treatments.

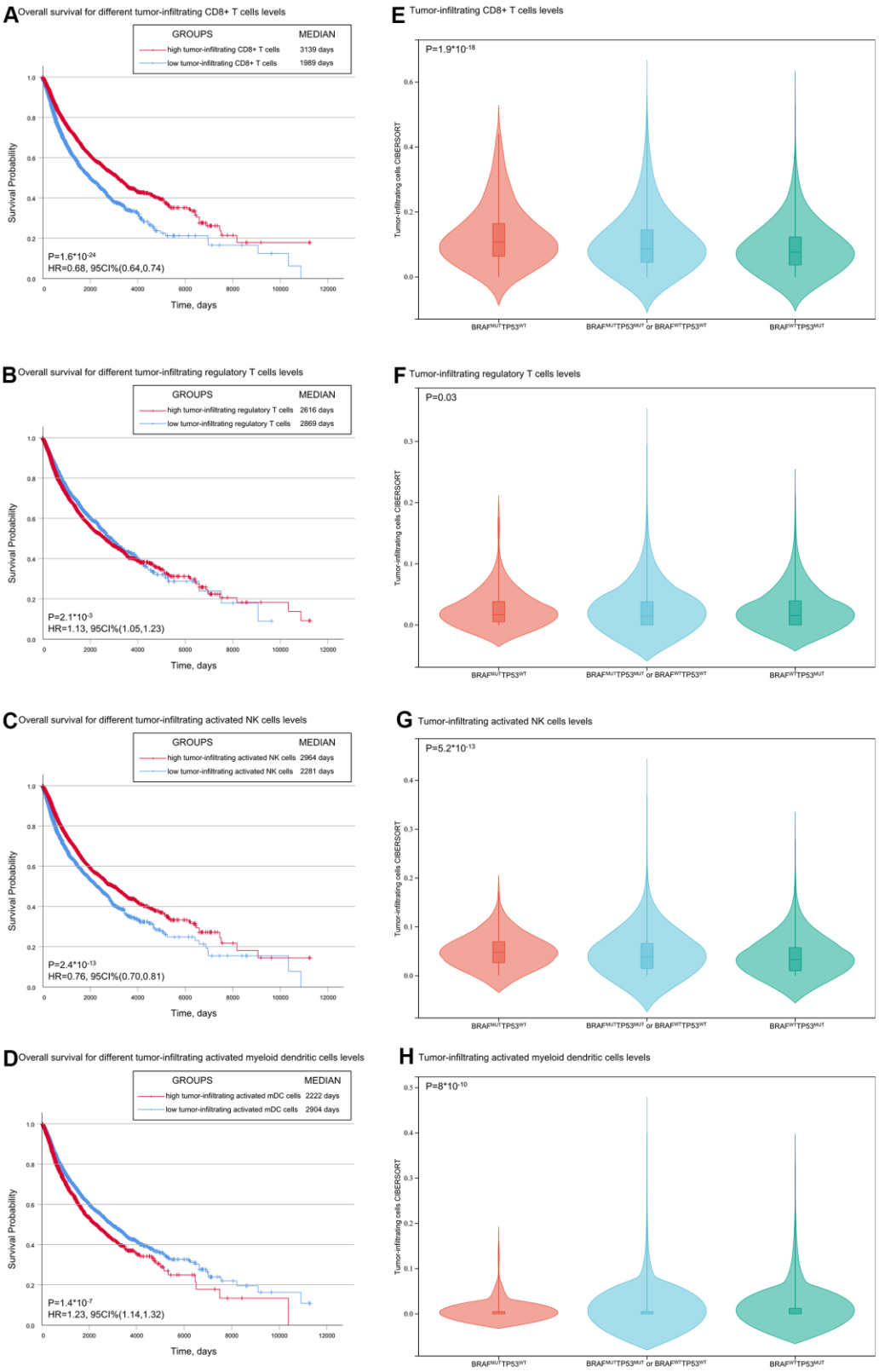

Figure 3. Associations of overall survival and TP53 and BRAF mutation types with tumor-infiltrating immune cells. (**A**, **B**) Patients with low tumor-infiltrating CD8+ T cells/activated NK cells had shorter OS than patients with high tumor-infiltrating CD8+ T cells/activated NK cells. (**C**, **D**) Patients with low tumor-infiltrating regulatory T cells /activated myeloid dendritic cells had shorter OS than patients with high regulatory T cells /activated myeloid dendritic cells. (**E**–**H**) The level of tumor infiltrating CD8+ T cells was correlated with the mutation of TP53/BRAF. Data was from TCGA database.

In the POLE/POLD1 mutation model, patients with either POLE or POLD1 mutations was associated with better ICI therapy response and longer OS than the wild-type population (34months vs 18months) [5]. However, the POLE/POLD1 mutation model was not a significant predictive factor for ICI therapy response after multi-variable adjustment of TMB and TP53/BRAF mutation model. TP53/BRAF mutation model was a powerful and independent predictive factor for identifying patients who benefited from ICI treatment. In advanced tumors, TP53 and BRAF mutations are more common than POLE and POLD1 mutations, and TP53/BRAF mutation model is better than POLE/POLD1 mutation model in predicting ICI treatment response.

The biological implications of a mutually exclusive TP53 mutation and BRAF mutation are not understood at present. As mentioned above, TP53 is a tumor suppressor gene involved in the regulation of cell growth [19], BRAF is an oncogene involved in cellular responses to growth signals [20]. Missense mutations, insertions or deletions of TP53 lead to TP53 inactivation are very common. BRAF mutations, such as BRAF V600E mutations, cause the continuous activation of the downstream MEK-ERK signaling pathway [21]. In this study, concurrent TP53 mutation and BRAF mutation was seen in a small number of patients. Tumors carrying both TP53 mutations and BRAF mutations are less likely to response to ICI therapy than those showing only BRAF mutation. This could account for the TP53 inactivation and BRAF activation might be genetically redundant, and that alteration in both genes does not confer a further advantage.

The molecular mechanisms explaining the effects of TP53/BRAF mutation on predictive value for ICI therapy response are presently unknown. Previously, we have shown statistically that the level of tumor-infiltrating CD8+ T cells is correlated with TP53/BRAF mutations, which may be one of the causes. According to KEGG analysis, we found five enriched signaling pathways closely related to tumor immunity. The PI3K−Akt signaling pathway plays a critical role in T and B cell development [22, 23]. The BRAF-MAPK signaling pathway correlates with the production of various immunosuppressive factors in regulating cancer-immune evasion [24]. The Rap1 signaling pathway activation leads to increased integrin affinity, leukocytes arrest rolling and actively lymphocyte migration and adhesion [25–27]. Chemokines signaling pathway are key molecules involved in the migration and homeostasis of immune cells [28]. The AMPK signaling pathway is involved in shaping the activity of lymphocytes [29, 30]. The above pathways may explain potential reasons why TP53/BRAF mutation of cancer patients contributes to the ICI therapy response. More detailed and specific studies are needed to elucidate the precise molecular mechanisms.

In this study, we show that a novel TP53/BRAF mutation model provides significant information about the stratification of response to ICI-therapy. Commonly, patients with high-TMB status have better response to ICI therapy than patients with low-TMB status. However, the genotype of $TP53^{MUT}BRAF^{WT}$ in high-TMB status cohort have poorer response to ICI therapy than the genotype of $BRAF^{MUT}TP53^{WT}$ in low-TMB status (Median, 18 months vs 47 month). Thus, TP53/BRAF mutation model can add predictive value to TMB in identifying patients who benefited from ICI treatment, which can enable more informed treatment decisions.

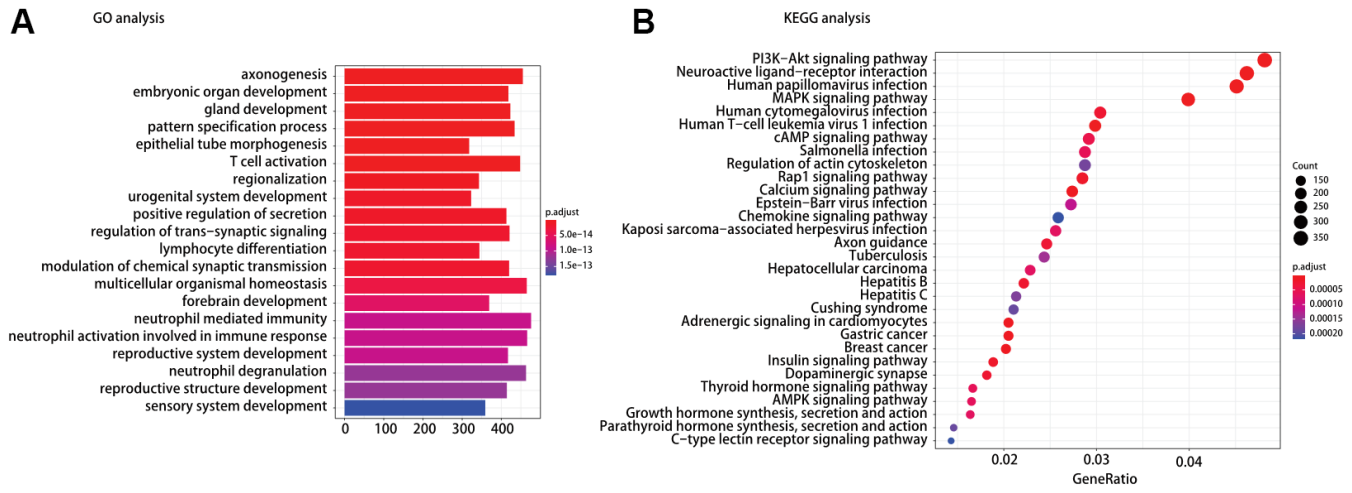

Figure 4. (**A**) Gene ontology (GO) and (**B**) Kyoto encyclopedia of gene and genomes (KEGG) pathway analysis of different expression mRNAs between $TP53^{MUT}BRAF^{WT}$ and $BRAF^{MUT}TP53^{WT}$.

CONCLUSIONS

we combined TP53 and BRAF mutation status into a biomarker model which owns the ability to be more efficient than the POLE/POLD1 mutation model, and the combination of TP53/BRAF mutation model and TMB can more accurately predict the response to ICI therapy.

AUTHOR CONTRIBUTIONS

Dr Luo and Dr Wei had full access to all of the data in the study and take responsibility for the integrity of the data and the accuracy of the data analysis. Drs Yao, Liu, and Cao contributed equally to this work. Concept and design: Yao, Liu, Wei, Luo. Acquisition, analysis, or interpretation of data: All authors. Drafting of the manuscript: Yao, Liu, Cao, Tang, Li, Wei. Critical revision of the manuscript for important intellectual content: Wei, Luo. Statistical analysis: Wei, Feng, Luo. Obtained funding: Wei, Luo. Administrative, technical, or material support: Liu, Cao, Tang, Li, Feng. Supervision: Luo.

CONFLICTS OF INTEREST

The authors declare that they have no conflicts of interest.

FUNDING

This study was supported by grants from National Natural Science Foundation of China (Award Number: 81725016, 81872094, 81602219), Natural Science Foundation of Guangdong Province (Award Number: 2017B020227004, 2017A030313538).

REFERENCES

1. Sharma P, Hu-Lieskovan S, Wargo JA, Ribas A. Primary, Adaptive, and Acquired Resistance to Cancer Immunotherapy. Cell. 2017; 168:707–23. https://doi.org/10.1016/j.cell.2017.01.017 PMID:28187290
2. Zou W, Wolchok JD, Chen L. PD-L1 (B7-H1) and PD-1 pathway blockade for cancer therapy: Mechanisms, response biomarkers, and combinations. Sci Transl Med. 2016; 8:328rv4. https://doi.org/10.1126/scitranslmed.aad7118 PMID:26936508
3. Samstein RM, Lee CH, Shoushtari AN, Hellmann MD, Shen R, Janjigian YY, Barron DA, Zehir A, Jordan EJ, Omuro A, Kaley TJ, Kendall SM, Motzer RJ, et al. Tumor mutational load predicts survival after immunotherapy across multiple cancer types. Nat Genet. 2019; 51:202–6. https://doi.org/10.1038/s41588-018-0312-8 PMID:30643254
4. Chan TA, Yarchoan M, Jaffee E, Swanton C, Quezada SA, Stenzinger A, Peters S. Development of tumor mutation burden as an immunotherapy biomarker: utility for the oncology clinic. Ann Oncol. 2019; 30:44–56. https://doi.org/10.1093/annonc/mdy495 PMID:30395155
5. Wang F, Zhao Q, Wang YN, Jin Y, He MM, Liu ZX, Xu RH. Evaluation of POLE and POLD1 Mutations as Biomarkers for Immunotherapy Outcomes Across Multiple Cancer Types. JAMA Oncol. 2019; 5:1504–6. https://doi.org/10.1001/jamaoncol.2019.2963 PMID:31415061
6. Levine AJ. p53: 800 million years of evolution and 40 years of discovery. Nat Rev Cancer. 2020; 20:471–80. https://doi.org/10.1038/s41568-020-0262-1 PMID:32404993
7. Kastenhuber ER, Lowe SW. Putting p53 in Context. Cell. 2017; 170:1062–78. https://doi.org/10.1016/j.cell.2017.08.028 PMID:28886379
8. Rubinfeld H, Seger R. The ERK cascade: a prototype of MAPK signaling. Mol Biotechnol. 2005; 31:151–74. https://doi.org/10.1385/MB:31:2:151 PMID:16170216
9. Davies H, Bignell GR, Cox C, Stephens P, Edkins S, Clegg S, Teague J, Woffendin H, Garnett MJ, Bottomley W, Davis N, Dicks E, Ewing R, et al. Mutations of the BRAF gene in human cancer. Nature. 2002; 417:949–54. https://doi.org/10.1038/nature00766 PMID:12068308
10. Choueiri TK, Cheville J, Palescandolo E, Fay AP, Kantoff PW, Atkins MB, McKenney JK, Brown V, Lampron ME, Zhou M, Hirsch MS, Signoretti S. BRAF mutations in metanephric adenoma of the kidney. Eur Urol. 2012; 62:917–22. https://doi.org/10.1016/j.eururo.2012.05.051 PMID:22727996
11. Long J, Wang A, Bai Y, Lin J, Yang X, Wang D, Yang X, Jiang Y, Zhao H. Development and validation of a TP53-associated immune prognostic model for hepatocellular carcinoma. EBioMedicine. 2019; 42:363–74. https://doi.org/10.1016/j.ebiom.2019.03.022 PMID:30885723
12. Mazieres J, Drilon A, Lusque A, Mhanna L, Cortot AB, Mezquita L, Thai AA, Mascaux C, Couraud S, Veillon R, Van den Heuvel M, Neal J, Peled N, et al. Immune checkpoint inhibitors for patients with advanced lung cancer and oncogenic driver alterations: results from the IMMUNOTARGET registry. Ann Oncol. 2019; 30:1321–8.

https://doi.org/10.1093/annonc/mdz167
PMID:31125062

13. Gao J, Aksoy BA, Dogrusoz U, Dresdner G, Gross B, Sumer SO, Sun Y, Jacobsen A, Sinha R, Larsson E, Cerami E, Sander C, Schultz N. Integrative analysis of complex cancer genomics and clinical profiles using the cBioPortal. Sci Signal. 2013; 6:pl1. https://doi.org/10.1126/scisignal.2004088 PMID:23550210

14. Newman AM, Liu CL, Green MR, Gentles AJ, Feng W, Xu Y, Hoang CD, Diehn M, Alizadeh AA. Robust enumeration of cell subsets from tissue expression profiles. Nat Methods. 2015; 12:453–7. https://doi.org/10.1038/nmeth.3337 PMID:25822800

15. Li T, Fu J, Zeng Z, Cohen D, Li J, Chen Q, Li B, Liu XS. TIMER2.0 for analysis of tumor-infiltrating immune cells. Nucleic Acids Res. 2020; 48:W509–14. https://doi.org/10.1093/nar/gkaa407 PMID:32442275

16. Snyder A, Makarov V, Merghoub T, Yuan J, Zaretsky JM, Desrichard A, Walsh LA, Postow MA, Wong P, Ho TS, Hollmann TJ, Bruggeman C, Kannan K, et al. Genetic basis for clinical response to CTLA-4 blockade in melanoma. N Engl J Med. 2014; 371:2189–99. https://doi.org/10.1056/NEJMoa1406498 PMID:25409260

17. Rizvi NA, Hellmann MD, Snyder A, Kvistborg P, Makarov V, Havel JJ, Lee W, Yuan J, Wong P, Ho TS, Miller ML, Rekhtman N, Moreira AL, et al. Cancer immunology. Mutational landscape determines sensitivity to PD-1 blockade in non-small cell lung cancer. Science. 2015; 348:124–8. https://doi.org/10.1126/science.aaa1348 PMID:25765070

18. McGranahan N, Furness AJ, Rosenthal R, Ramskov S, Lyngaa R, Saini SK, Jamal-Hanjani M, Wilson GA, Birkbak NJ, Hiley CT, Watkins TB, Shafi S, Murugaesu N, et al. Clonal neoantigens elicit T cell immunoreactivity and sensitivity to immune checkpoint blockade. Science. 2016; 351:1463–9. https://doi.org/10.1126/science.aaf1490 PMID:26940869

19. Aubrey BJ, Strasser A, Kelly GL. Tumor-Suppressor Functions of the TP53 Pathway. Cold Spring Harb Perspect Med. 2016; 6:a026062. https://doi.org/10.1101/cshperspect.a026062 PMID:27141080

20. Pratilas CA, Solit DB. Therapeutic strategies for targeting BRAF in human cancer. Rev Recent Clin Trials. 2007; 2:121–34. https://doi.org/10.2174/157488707780599393 PMID:18473997

21. Kotani H, Adachi Y, Kitai H, Tomida S, Bando H, Faber AC, Yoshino T, Voon DC, Yano S, Ebi H. Distinct dependencies on receptor tyrosine kinases in the regulation of MAPK signaling between BRAF V600E and non-V600E mutant lung cancers. Oncogene. 2018; 37:1775–87. https://doi.org/10.1038/s41388-017-0035-9 PMID:29348459

22. Lucas CL, Chandra A, Nejentsev S, Condliffe AM, Okkenhaug K. PI3Kδ and primary immunodeficiencies. Nat Rev Immunol. 2016; 16:702–14. https://doi.org/10.1038/nri.2016.93 PMID:27616589

23. Sobral-Leite M, Salomon I, Opdam M, Kruger DT, Beelen KJ, van der Noort V, van Vlierberghe RL, Blok EJ, Giardiello D, Sanders J, Van de Vijver K, Horlings HM, Kuppen PJ, et al. Cancer-immune interactions in ER-positive breast cancers: PI3K pathway alterations and tumor-infiltrating lymphocytes. Breast Cancer Res. 2019; 21:90. https://doi.org/10.1186/s13058-019-1176-2 PMID:31391067

24. Sumimoto H, Imabayashi F, Iwata T, Kawakami Y. The BRAF-MAPK signaling pathway is essential for cancer-immune evasion in human melanoma cells. J Exp Med. 2006; 203:1651–6. https://doi.org/10.1084/jem.20051848 PMID:16801397

25. Shimonaka M, Katagiri K, Nakayama T, Fujita N, Tsuruo T, Yoshie O, Kinashi T. Rap1 translates chemokine signals to integrin activation, cell polarization, and motility across vascular endothelium under flow. J Cell Biol. 2003; 161:417–27. https://doi.org/10.1083/jcb.200301133 PMID:12707305

26. Katagiri K, Maeda A, Shimonaka M, Kinashi T. RAPL, a Rap1-binding molecule that mediates Rap1-induced adhesion through spatial regulation of LFA-1. Nat Immunol. 2003; 4:741–8. https://doi.org/10.1038/ni950 PMID:12845325

27. Katagiri K, Imamura M, Kinashi T. Spatiotemporal regulation of the kinase Mst1 by binding protein RAPL is critical for lymphocyte polarity and adhesion. Nat Immunol. 2006; 7:919–28. https://doi.org/10.1038/ni1374 PMID:16892067

28. Krieg C, Boyman O. The role of chemokines in cancer immune surveillance by the adaptive immune system. Semin Cancer Biol. 2009; 19:76–83. https://doi.org/10.1016/j.semcancer.2008.10.011 PMID:19038343

29. Notarangelo LD. Combined immunodeficiencies with nonfunctional T lymphocytes. Adv Immunol. 2014; 121:121–90. https://doi.org/10.1016/B978-0-12-800100-4.00004-0 PMID:24388215

30. Wang J, Li Z, Gao L, Qi Y, Zhu H, Qin X. The regulation effect of AMPK in immune related diseases. Sci China Life Sci. 2018; 61:523–33. https://doi.org/10.1007/s11427-017-9169-6 PMID:29127585

SUPPLEMENTARY MATERIALS

Supplementary Figures

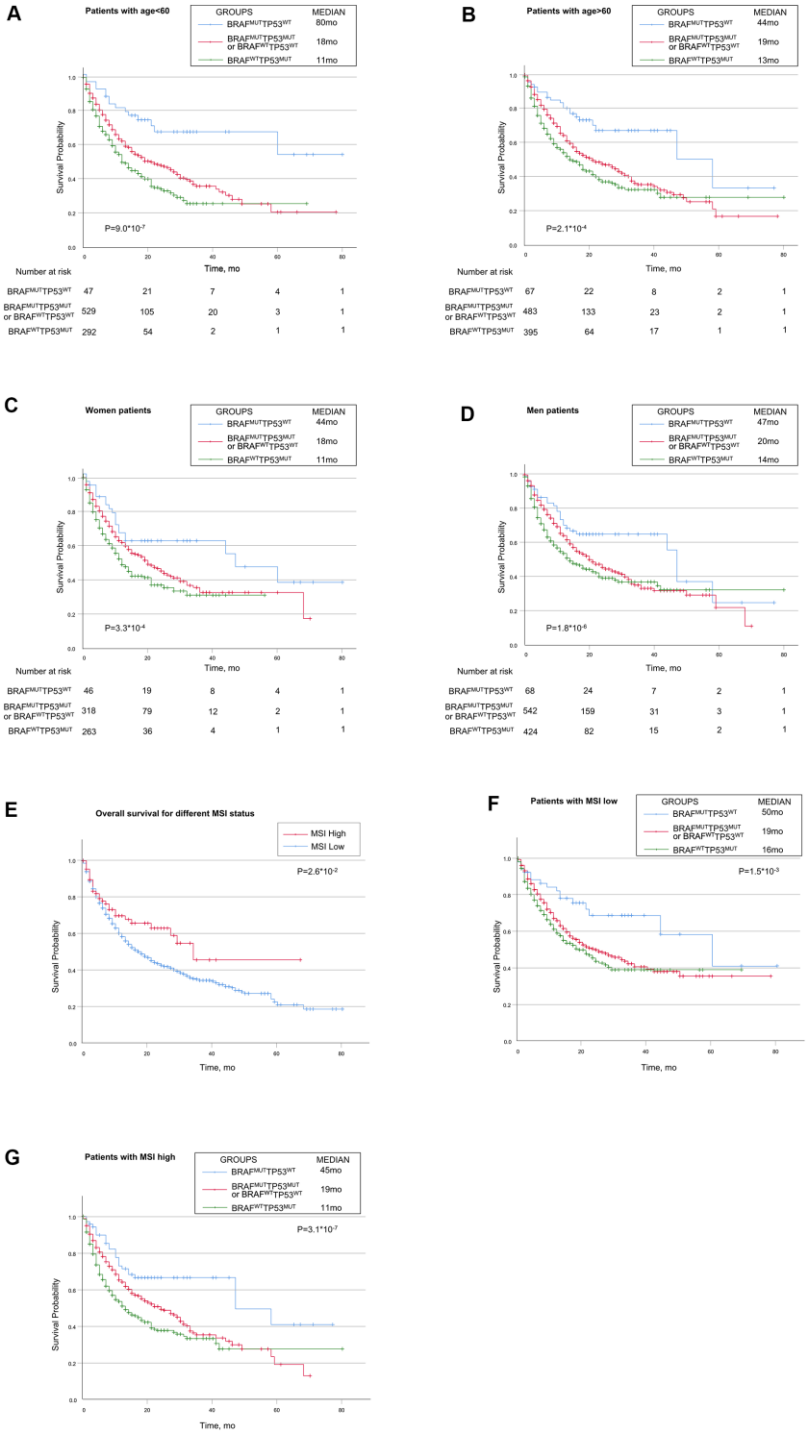

Supplementary Figure 1. Relationship between TP53 and BRAF Mutation Types and Prognosis in Patients Treated with Immune Checkpoint Inhibitors in Different Stratification of Clinical Parameters (**A**, **B**) Overall survival of different TP53/BRAF mutation types in different age groups (age<60 and >60). (**C**, **D**) Overall survival of different TP53/BRAF mutation types in different gender groups (women and men). (**E**) Patients in high-MSI status group had longer OS than patients in low-MSI status group. (**F**, **G**) Overall survival of different TP53/BRAF mutation types in high/low MSI groups.

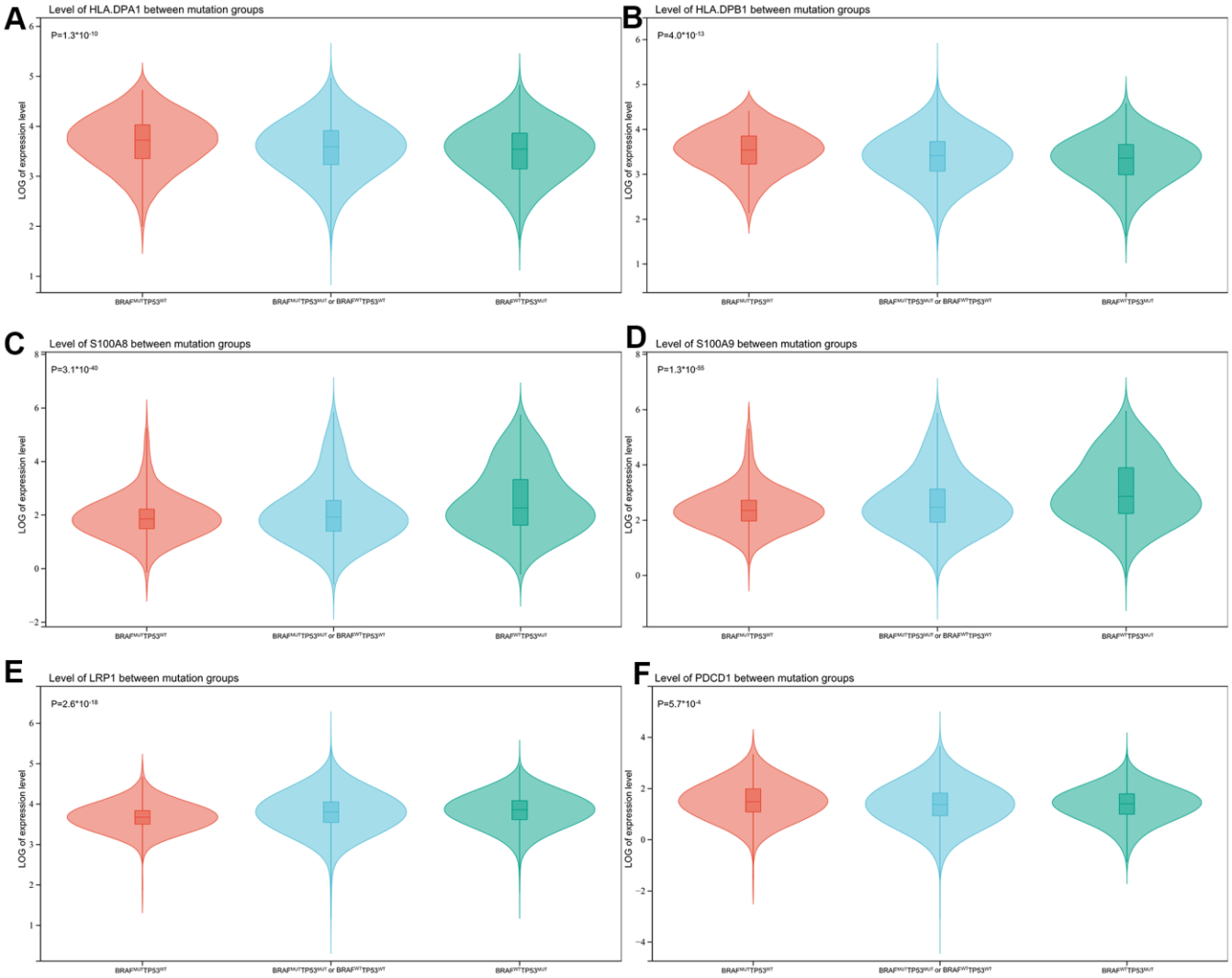

Supplementary Figure 2. Associations of TP53 and BRAF Mutation Types and Immune-related Genes (**A–F**) TP53/BRAF mutation model was significantly related to the expression of immune-related genes, that include myeloid-derived suppressor cells (MDSC), major histocompatibility complex (MHC), and immune checkpoints related genes.

Research Paper

Wild type and gain of function mutant TP53 can regulate the sensitivity of pancreatic cancer cells to chemotherapeutic drugs, EGFR/Ras/Raf/MEK, and PI3K/mTORC1/GSK-3 pathway inhibitors, nutraceuticals and alter metabolic properties

James A. McCubrey[1], Akshaya K. Meher[1], Shaw M. Akula[1], Stephen L. Abrams[1], Linda S. Steelman[1], Michelle M. LaHair[1], Richard A. Franklin[1], Alberto M. Martelli[2], Stefano Ratti[2], Lucio Cocco[2], Fulvio Barbaro[3], Przemysław Duda[4], Agnieszka Gizak[4]

[1]Department of Microbiology and Immunology, Brody School of Medicine at East Carolina University, Greenville, NC 27858, USA
[2]Department of Biomedical and Neuromotor Sciences, Università di Bologna, Bologna, Italy
[3]Department of Medicine and Surgery, Re.Mo.Bio.S. Laboratory, Anatomy Section, University of Parma, Parma, Italy
[4]Department of Molecular Physiology and Neurobiology, University of Wroclaw, Wroclaw, Poland

Correspondence to: James A. McCubrey; **email:** mccubreyj@ecu.edu
Keywords: TP53, targeted therapy, PDAC, chemotherapeutic drugs, metabolic properties
Received: December 3, 2021 **Accepted:** January 20, 2022 **Published:** April 27, 2022

ABSTRACT

TP53 is a master regulator of many signaling and apoptotic pathways involved in: aging, cell cycle progression, gene regulation, growth, apoptosis, cellular senescence, DNA repair, drug resistance, malignant transformation, metastasis, and metabolism. Most pancreatic cancers are classified as pancreatic ductal adenocarcinomas (PDAC). The tumor suppressor gene *TP53* is mutated frequently (50–75%) in PDAC. Different types of TP53 mutations have been observed including gain of function (GOF) point mutations and various deletions of the TP53 gene resulting in lack of the protein expression. Most PDACs have point mutations at the *KRAS* gene which result in constitutive activation of KRas and multiple downstream signaling pathways. It has been difficult to develop specific KRas inhibitors and/or methods that result in recovery of functional TP53 activity. To further elucidate the roles of TP53 in drug-resistance of pancreatic cancer cells, we introduced wild-type (WT) TP53 or a control vector into two different PDAC cell lines. Introduction of WT-TP53 increased the sensitivity of the cells to multiple chemotherapeutic drugs, signal transduction inhibitors, drugs and nutraceuticals and influenced key metabolic properties of the cells. Therefore, TP53 is a key molecule which is critical in drug sensitivity and metabolism of PDAC.

INTRODUCTION

Pancreatic cancer—a disease associated with aging that is diagnosed late in development and difficult to successfully treat

When a patient is diagnosed with pancreatic cancer, the outcome is poor [1–7]. There are four stages of pancreatic cancer. This cancer is often detected at stage IV, the most advanced stage [1, 2, 5]. The age of the patient will influence the survival rate as younger pancreatic cancer patients (15–49 years old) have a better survival rate than the older patients (50 and above) [7]. Thus, pancreatic cancer is a disease associated with aging [8, 9].

Therapeutic approaches for pancreatic cancer

Most pancreatic cancers consist of pancreatic ductal adenocarcinoma (PDAC). They are often refractive to classical chemotherapeutic drugs. PDAC patients undergo surgery to remove the diseased part of the pancreas. However, as PDAC is frequently diagnosed late in the course of the disease, the PDAC has often metastasized to other organs making therapy difficult and ineffective [10–12]. PDACs are often refractive to chemotherapeutic drugs and have modest effects in terms of treatments of the disease [13–17].

Genes implicated in PDAC

Many genes have been implicated in PDAC including *KRAS*, *TP53*, *CDKN2A*, *SMAD4* and *PDGFβR* [3, 8, 9, 18–22]. Changes in the expression of these genes has many different effects and contribute to PDAC progression and metastasis [23–26]. The *TP53* gene can become mutated by various genetic mechanisms. Two of the most common mechanisms of mutation of *TP53* are point mutations and deletions of part or the entire TP53 gene. Certain point mutations at the *TP53* gene alter the activity of the TP53 protein and give the TP53 protein different properties. This class of *TP53* mutation is referred to as a gain-of-function (GOF) mutation [27–31]. Another class of *TP53* mutation results in the lack of expression of the TP53. This class of *TP53* mutation is referred to TP53-null [27–31].

Interestingly, a novel class of compounds have been developed which alter the structure of mutant TP53 and restore some of its properties which are important is suppression of cell growth [32, 33]. APR-246 is one such compound which has been examined in clinical trials. A summary of the effects of TP53 on various processes important in cell growth and metastasis is present in Figure 1.

KRAS is another important gene which in mutated in >90% of PDAC. Although many potential Ras

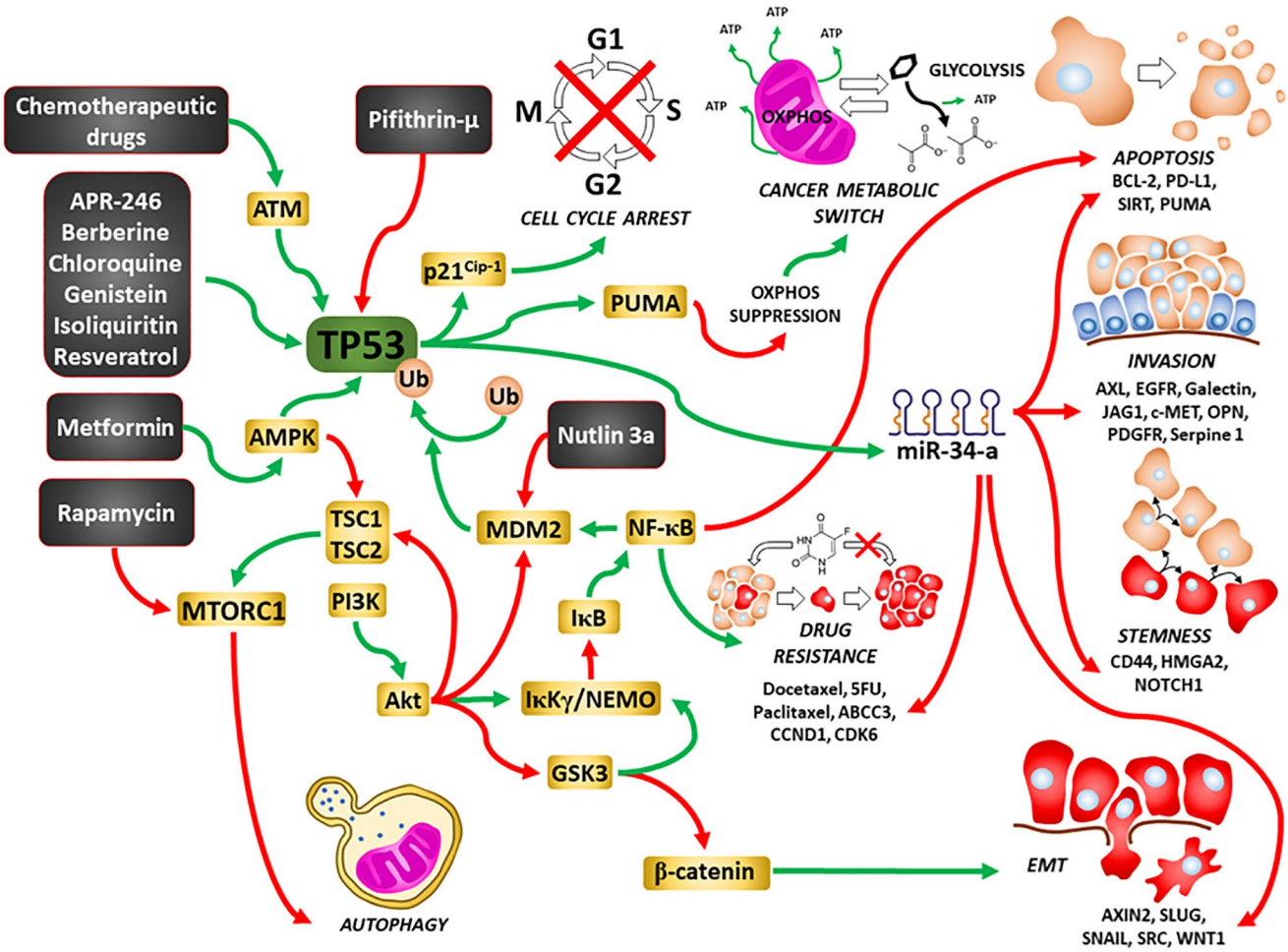

Figure 1. Illustration of TP53's interactions with other signaling pathways important in regulation of cell growth and sites of interaction for chemotherapeutic drugs, certain signal transduction inhibitors, natural products and nutraceuticals. Green arrows = induction of a pathway, red arrows = suppression of a pathway.

inhibitors were developed over the past 25 years, they were not specific to mutant KRas, recently, some have shown promise [34, 35]. As with most drugs, cancer cells have developed mechanisms to become resistant to these inhibitors [36]. In the following studies, we examined the consequences of introduction of WT-TP53 gene in two PDAC cell lines, one lacking TP53 expression (TP53-null) and one cell line with GOF-TP53 [37–39]. Earlier studies performed by us, indicated that inheritance of WT-TP53 increased the ability of some chemotherapeutic drugs, signal transduction inhibitors and natural products to inhibit cell proliferation [40, 41]. In the current studies, we examined the effects of inheritance of WT-TP53 on a larger panel of chemotherapeutic drugs as well the consequences of on other properties important in cancer progression such as clonogenicity, colony formation in soft agar and metabolic properties.

RESULTS

Restoration of WT-TP53 activity results in decreased resistance to various drugs, inhibitors, and natural products

MIA-PaCa-2 cells have GOF mutant TP53 alleles (R248W). A cDNA encoding WT-TP53 cDNA was inserted into the pLXSN vector [42]. MIA-PaCa-2 cells were transduced with the WT-TP53 vector and named MIA-PaCa-2 + WT-TP53 cells. As a negative control, the effects of the empty parental pLXSN plasmid [43] on MIA-PaCa-2 cells and named MIA-PaCa-2 + pLXSN.

Table 1 is a list of the various agents examined in this study as well as their targets and intersections with the TP53 pathway and a brief description of their mechanisms of action.

Docetaxel is a common chemotherapeutic drug used to treat various cancer types including PDAC. The IC_{50} for docetaxel in MIA-PaCa-2 + WT-TP53 cells was 3.8-fold lower than in MIA-PaCa-2 + pLXSN cells (Figure 2A). The effects of WT-TP53 on the sensitivity to three topoisomerase inhibitors used in cancer therapy were also examined (Figure 2B–2D). The IC_{50}s for all the inhibitors were lower (~ 2-fold for etoposide and daunorubicin, and 5-fold for aclacinomycin) in MIA-PaCa-2 + WT-TP53 cells than in MIA-PaCa-2 + pLXSN cells.

Restoration of WT-TP53 activity in MIA-PaCa-2 cells resulted in increased sensitivity to chemotherapeutic drugs used to treat cancer patients. Table 2 summarizes the effects of addition of WT-TP53 into Mia-PaCa-2 cells. Restoration of WT-TP53 activity increased sensitivity to the KRAS inhibitor ARS-1620 [44] 125-fold (Figure 3A).

Various signaling cascades are located downstream of KRas. Two important kinase cascades are the Raf/MEK/ERK and PI3K/PTEN/Akt/mTORC1 pathways. They are often involved in regulation of cell growth and their aberrant regulation is often implicated in cancer [45–47]. Restoration of WT-TP53 activity in MIA-PaCa-2 cells increased the sensitivity to the MEK1 inhibitor PD0325901 3.3-fold. (Figure 3B).

Restoration of WT-TP53 activity in MIA-PaCa-2 cells led to a 33.3-fold lower IC_{50} for the PI3K inhibitor LY294002 inhibitor than that observed in MIA-PaCa-2 cells lacking WT-TP53 (Figure 3C). Thus, addition of WT-TP53 activity in MIA-PaCa-2 cells increased their sensitivity to small molecule inhibitors which target the Ras/Raf/MEK/ERK and PI3K/PTEN/Akt/mTORC1 pathways.

Pifithrin-μ is a small molecule that inhibits the interactions of TP53 with either BCL2 or BCLXL at the mitochondrial membrane. This results in the induction of apoptosis. However, Pifithrin-μ does not inhibit the effects that TP53 has on transcription [48]. Restoration of WT-TP53 in MIA-PaCa-2 cells resulted in a pifithrin-μ IC_{50} 240-fold lower than that detected in MIA-PaCa-2 cells which lack WT-TP53 activity (Figure 3D).

GSK-3 is a multifunctional kinase that is involved in the regulation of many processes both in normal physiological and malignant growth [49]. GSK-3 has been shown to be important for the interactions between KRas and NF-κB [50, 51]. GSK-3 is an important target in many cancers. GSK-3 inhibitors have been suggested for the treatment of PDAC [52]. The effects of GSK-3 inhibitors BIO, CHIR99021 and SB415286 on MIA-PaCa-2 cells containing and lacking WT activity were examined. Restoration of WT-TP53 activity in MIA-PaCa-2 cells resulted in over 13-fold lower IC_{50} for SB415286 and only about 2-fold lower IC50 for BIO and CHIR99021 than in cells lacking WT-TP53 activity (Figure 4A–4C).

The mTORC1 complex plays critical roles in many processes, including: cell growth, metabolism, cancer and aging [53, 54]. Restoration of WT-TP53 activity in MIA-PaCa-2 cells resulted in a rapamycin IC_{50} 6.7-fold lower than that observed in cells lacking WT-TP53 activity (Figure 4D).

EGFR, HER2, ALK, AXL, FLT3, PDGFR and other receptors and signal transducers (*e.g.*, Raf) are involved in the metastasis of various cancers [55–61]. The effects of: the AG1478 EGFR inhibitor, the multi-kinase ALK, AXL, FLT3 inhibitor gilteritinib and multi-kinase Raf, PDGFR, FLT3, VEGFR inhibitor sorafenib on the

Table 1. Chemotherapeutic drugs, signal transduction inhibitors, natural products used in this study and their targets, mode of action, and intersections with the TP53 pathway.[1,2]

Chemotherapeutic drugs[1]			
Drug↓	**Target[1]**	**Mode of action**	**Intersection with TP53 pathway**
Docetaxel	Microtubule Binder	Blocks mitosis by inhibiting mitotic spindle assembly.	Docetaxel intersects with TP53 pathway. WT-TP53 increases sensitivity, increases phosphorylation of S15-TP53.
5-Fluorouracil (5FU)	Nucleoside Analogue	Blocks the activity of thymidylate synthase, thus, inhibits DNA synthesis/replication.	5FU intersects with TP53 pathway. WT-TP53 increases sensitivity to FU. 5FU induces TP53 stabilization by blocking MDM2.
Gemcitabine (Gem)	Nucleoside Analogue	Gemcitabine exerts it antitumor effects by promoting apoptosis of cells undergoing DNA synthesis.	Gem intersects with TP53 pathway. WT-TP53 increases sensitivity. Gem can induce TP53 targets such as PUMA and Bax which leads to apoptosis.
Aclacinomycin (Aclarubicin)	DNA intercalator, Topoisomerase II	Topoisomerase inhibitor (inh.) thus, inhibits DNA replication.	As an anthracycline it probably insects with TP53 pathway. However, like most chemotherapeutic drugs, it can function in TP53 mutant cells.
Daunorubicin	DNA intercalators, Topoisomerase II	Topoisomerase inh. thus, inhibits DNA replication.	Daunorubicin intersects with TP53 pathway. It induces TP53 and downstream p21Cip1.
Doxorubicin (Dox)	DNA intercalator, Topoisomerase II	Topoisomerase inh. thus, inhibits DNA replication and induces many TP53-regulated genes, many induce apoptosis.	Dox intersects with TP53 pathway. It increases TP53 expression and phosphorylation at S15 and can induce p21Cip-1.
Etoposide	Binds to Topoisomerase II	Topoisomerase inh. thus, inhibits DNA replication and induces apoptosis. Complex form between etoposide and DNA and can prevent DNA repair.	Etoposide intersects with TP53 pathway. It increases TP53 and pro-apoptotic PUMA expression as well as Bax processing.
Cisplatin (Cis)	DNA	Crosslinks DNA to form DNA adducts. Preventing repair of DNA leading to DNA damage and subsequently apoptosis.	Cis intersects with TP53 pathway. Cis can enhance TP53, p21Cip-1, MDM2 and Fas expression.
Signal transduction inhibitors[1]			
Drug↓	**Target**	**Mode of action**	**Intersection with TP53 pathway**
ARS-1620	Mutant KRas	KRas-mediated catalysis of the chemical reaction with Cys12 in KRASG12C.	KRas interacts with the TP53 pathway. TP53 and KRas interact to modulate CREB1 expression to promote metastasis and tumor growth.
PD0325901	MEK1	A highly selective allosteric inh. that does not compete with either ATP or ERK1/2.	MEK1 interacts with the TP53 pathway. Downstream ERK can phosphorylate and activate TP53, resulting in many cellular responses.
LY294002	PI3K and others	Competition with ATP for binding the PI3K active site.	PI3K and downstream molecules can interact with the TP53 pathway. Downstream of PI3K are PTEN and Akt and they can regulate the TP53 pathway at various steps and processes.
Pifithrin-μ	TP53	Inhibits some of TP53 activities by binding to BCLXL and BCL2 at the mitochondria without affecting TP53 transcriptional activities.	Pifithrin-μ inhibits some proteins regulated by the TP53 pathway (BCL-XL and BCL2).
6-bromoindirubin-30-oxime (BIO)	GSK-3	BIO is a selective, reversible potent GSK-3 inh. It is an ATP-competitive inhibitor of GSK-3α/β. It interacts with ATP binding site of GSK-3.	GSK-3 interacts with TP53 pathway. GSK-3 phosphorylates sites on the proteasomal inhibitor MDM2. This phosphorylation is required for TP53 degradation. Inhibition of GSK-3 leads to an increase in TP53 levels.
SB415286	GSK-3	Targets ATP-binding site. It inhibits both GSK-3α and GSK-β.	GSK-3 interacts with TP53 pathway. GSK-3 phosphorylates sites on the proteasomal inhibitor MDM2. This phosphorylation is required for TP53 degradation. Inhibition of GSK-3 leads to an increase in TP53 levels.
CHIR99021	GSK-3	Targets ATP-binding site. It inhibits both GSK-3α and GSK-β.	GSK-3 interacts with TP53 pathway. GSK-3 phosphorylates sites on the proteasomal inhibitor MDM2. This phosphorylation is required for TP53 degradation. Inhibition of GSK-3 leads to an increase in TP53 levels.

Rapamycin	mTORC1	Binds and blocks mTORC1 complex.	mTORC1 interacts with the TP53 pathway. Activation of TP53 downregulates mTOR signaling. This occurs through AMPK.
AG1498	EGFR	AG1478 competitively binds to the ATP binding pocket in EGFR.	EGFR interacts with the TP53 pathway.TP53 mutations are associated with primary or acquired resistance to EGFR-tyrosine kinase inhibitors.
Gilteritinib	AXL/ALK/FLT3	Gilteritinib binds to the ATP binding site in the active pocket of the AXL/ALK/FLT3 kinases.	AXL/ALK/FLT3 interacts with the TP53 pathway. AXL suppresses TP53 expression by binding to DNA sequences upstream from the TP53 gene. AXL is also regulated by miR-34a which is regulated by TP53. ALK inhibitors are not as effective in lung cancer patients that have rearranged ALK genes and are also mutated at TP53 as in patients with germline genes. Also, FLT-3 and TP53 also interact.
Sorafenib	Multiple kinases (e.g., Raf, PDGFR, VEGFR, FLT-3 and others)	Sorafenib binds to the ATP binding site.	Many of these kinases and their downstream substrates interact with TP53 pathway by phosphorylating TP53 and other molecules regulated by TP53. Mutant TP53 can also regulate the expression of some of these kinases such as PDGFR.
OTX008	Galectin-1	OTX008 binds galectin-1 which leads to galectin-1 oxidation and proteasomal degradation.	Galectin-1 can interact with the TP53 pathway. TP53 can induce the expression of miRs which regulate galectin-1 expression.
Tiplaxtinin	Serpine-1	Tiplaxtinin binds to the active conformation of serpine-1 and induced reversible inactivation serpine-1.	TP53 regulates the expression of miR-34a which can down regulate serpine-1. Serpine1- is involvement of metastasis in various cancers.
Verapamil (Ver)	Calcium channel	Also, some transporters associated with chemotherapeutic drug resistance. Binds to sites on MDR1 glycoprotein preventing drug efflux. Also, downregulates MDR1 expression.	TP53 pathway and Ver interact. Ver interacts with the TP53 activator (MDM2 inhibitor) nutlin-3a which results in suppression of cell growth.
Vismodegib (Vis)	Hh pathway	Smoothened homologue (SMO) binds to Smoothened (SMO) and inhibits its activity.	Multiple interactions with TP53 pathway.
		Natural products[2]	
Cyclopamine	Sonic hedgehog (SHH) pathway	Cyclopamine binds to SMO and inhibits its activity.	Multiple interactions with TP53 pathway.
Parthenolide[2]	NF-κB (other targets)	Inhibition of activation of IκB, and direct binding to NF-κB, preventing its interaction with DNA.	NF-κB interacts with the TP53 pathway TP53 and NF-κB inhibit each other's ability to stimulate gene expression.
Isoliquiritin[2]	Induces apoptotic cell death through upregulating TP53 and p21Cip-1. Suppresses NF-κB, ERK and activation of other targets	Suppresses invasiveness and angiogenesis of cancer.	Isoliquiritin interacts with TP53 pathway. It induces TP53 and inhibits NF-κB and ERK. Both interact with TP53 pathway.
Genistein (isoflavone)[2]	Multiple targets	Genistein triggers the ER stress to induce apoptosis and other mechanisms of cell death.	Genistein interacts with TP53 pathway. Genistein increases the phosphorylation and activation of ATM/ATR-TP53-p21Cip-1 pathway.
Daidzein (isoflavone)[2]	Multiple targets	Daidzein and genistein induce cell cycle arrest in the G2/M phase. This is accompanied by activation of ATM/TP53, and p21Cip-1 and other cell cycle regulatory genes.	Daidzein interacts with TP53 pathway. Daidzein increases the phosphorylation and activation of ATM/ATR-TP53-p21Cip-1 pathway.

[1]Many chemotherapeutic drugs and signal transduction inhibitors have other effects and targets. We describe the targets that are most closely related to TP53.
[2]Most natural products have multiple targets. We describe some of the targets that are more closely related to TP53.

Table 2. Effects of WT-TP53 and pLXSN on sensitivity of MIA-PaCa-2 pancreatic cancer cells on chemotherapeutic drugs, signal transduction inhibitors and natural products as determined by IC_{50} analysis.[1]

Drug/Agent↓	+ pLXSN	+ WT-TP53	Fold change WT vs. LXSN
Docetaxel (microtubule binder)	0.3 nM	0.08 nM	3.8 X↓
Etoposide (topoisomerase inh.)	750 nM	400 nM	1.9 X↓
Aclacinomycin (topoisomerase inh.)	1 nM	0.2 nM	5 X↓
Daunorubicin (topoisomerase inh.)	120 nM	60 nM	2 X ↓
ARS-1620 (mutant KRas inh.)	10 nM	0.8 nM	12.5 X↓
PD0325901 (MEK1 inh.)	150 nM	45 nM	3.3 X↓
LY294002 (PI3K inh.)	5,000 nM	150 nM	33.3 X↓
Pifithrin-μ (TP53 inh.)	600 nM	2.5 nM	240 X↓
BIO (GSK-3 inh.)	210 nM	100 nM	2.1 X↓
SB415286 (GSK-3 inh.)	40 nM	3 nM	13.3 X↓
CHIR99021 (GSK-3 inh.)	500 nM	300 nM	1.7 X↓
Rapamycin (mTORC1 blocker)	2 nM	0.3 nM	6.7 X↓
AG1498 (EGFR inh.)	1,000 nM	200 nM	5 X↓
Gilteritinib (AXL/ALK/FLT3 inh.)	600 nM	220 nM	2.7 X↓
Sorafenib (multi-kinase inh.)	1,000 nM	700 nM	1.4 X↓
OTX008 (Galectin-1 inh.)	1,000 nM	10 nM	100 X↓
Tiplaxtinin (Serpine-1 inh.)	40 nM	10 nM	4 X↓
Cyclopamine (SHH inh.)	1,000 nM	500 nM	2 X↓
Parthenolide (NF-κB inh, other targets)	40 nM	3.5 nM	11.4 X↓
Isoliquiritin (multiple targets)	1,900 nM	600 nM	3.2 X↓
Genistein (isoflavone, many targets)	300 nM	70 nM	4.3 X↓
Daidzein (isoflavone, many targets)	1,000 nM	600 nM	1.7 X↓

[1]Determined by MTT analysis as previously described [40, 41].

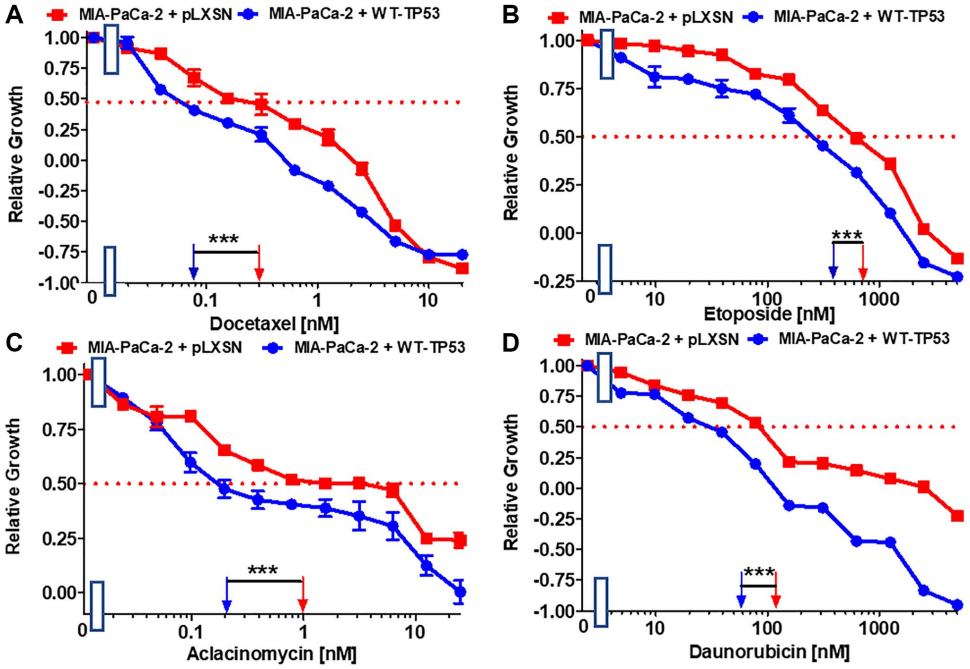

Figure 2. Effects of signal transduction inhibitors on the growth of MIA-PaCa-2 + WT-TP53 and MIA-PaCa-2 + pLXSN cells. The effects of docetaxel (**A**), etoposide (**B**) aclacinomycin (**C**) and daunorubicin (**D**) on MIA-PaCa-2 + pLXSN cells (solid red squares) and MIA-PaCa-2 + WT-TP53 cells (solid blue circles) were examined by MTT analysis. These experiments were repeated and similar results were obtained. Statistical analyses were performed by the Student *T* test on the means and standard deviations of various treatment groups. $^{***}P < 0.0001$.

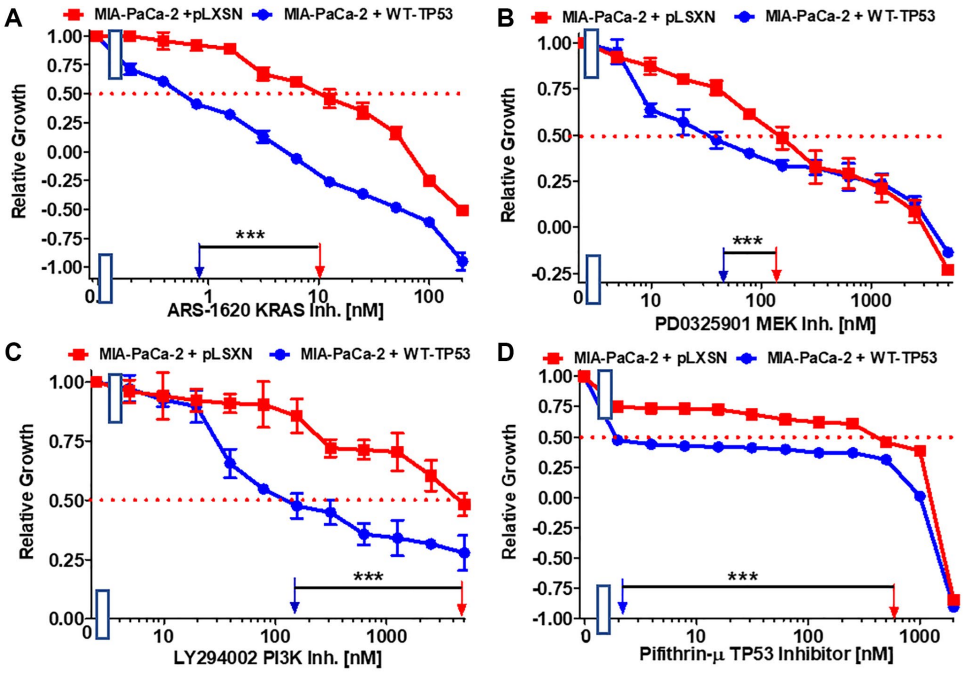

Figure 3. Effects of the Ras/MEK, PI3K/mTOR and TP53 inhibitors on the growth of MIA-PaCa-2 + WT-TP53 and MIA-PaCa-2 + pLXSN cells. The effects of the ARS-1620 mutant KRas inhibitor (**A**), the PD0325901 MEK1 inhibitor (**B**), the LY294002 PI3K inhibitor (**C**) and the TP53 inhibitor pifithrin-μ (**D**) on MIA-PaCa-2 + pLXSN cells (solid red squared) and MIA-PaCa-2 + WT-TP53 cells (solid blue circles) were examined by MTT analysis. The MIA-PaCa-2 + WT-TP53, and MIA-PaCa-2 + pLXSN cells in each panel were all examined at the same time period. These experiments were repeated and similar results were obtained. Statistical analyses were performed by the Student *T* test on the means and standard deviations of various treatment groups. $^{***}P < 0.0001$.

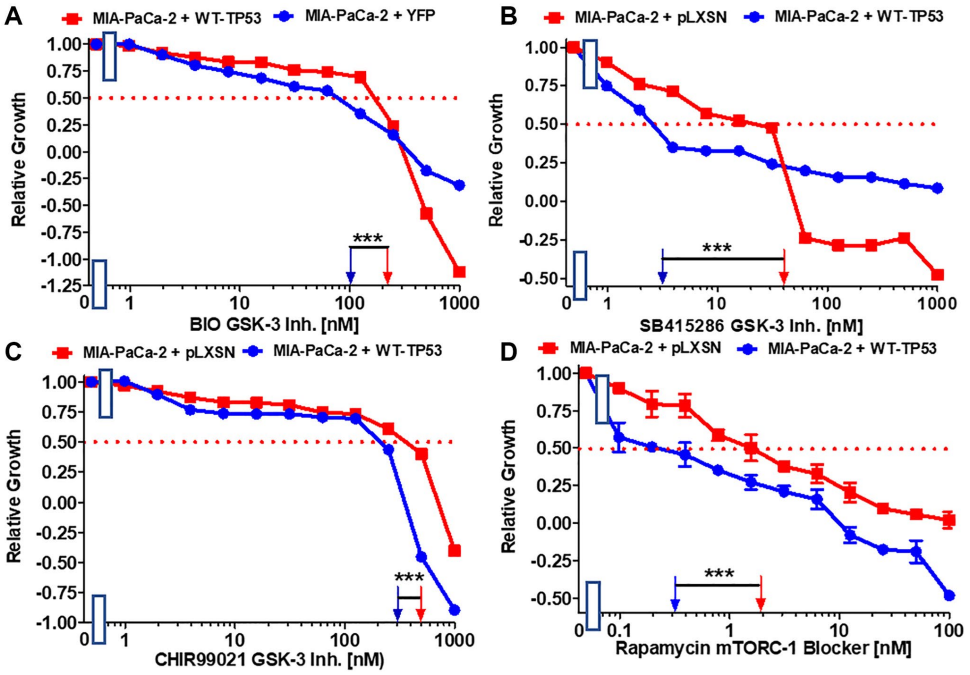

Figure 4. Effects of GSK-3 inhibitors and the mTORC1 blocker rapamycin on the growth of MIA-PaCa-2 + WT-TP53 and MIA-PaCa-2 + pLXSN cells. The effects of the BIO GSK-3 inhibitor (**A**), the SB415286 GSK-3 inhibitor (**B**), the CHIR99021 GSK-3 inhibitor (**C**) and the mTORC1 blocker rapamycin (**D**) on MIA-PaCa-2 + pLXSN cells (solid red squared) and MIA-PaCa-2 + WT-TP53 cells (solid blue circles) were examined by MTT analysis. The MIA-PaCa-2 + WT-TP53, and MIA-PaCa-2 + pLXSN cells in each panel were all examined at the same time period. These experiments were repeated and similar results were obtained. Statistical analyses were performed by the *T* test on the means and standard deviations of various treatment groups. $^{***}P < 0.0001$.

growth of MIA-PaCa-2 cells expressing WT-TP53 or not were ascertained. Introduction of WT-TP53 into MIA-PaCa-2 cells resulted in reduction of the IC_{50}s for all the inhibitors in comparison to the IC_{50}s in MIA-PaCa-2 cells lacking WT-TP53 expression (Figure 5A–5C) but the reduction was most pronounced for the AG1478 EGFR inhibitor.

Galectin-1 is involved in hedgehog (Hh) signaling, stromal remodeling and metastasis of PDAC [62]. Galectin-1 is negatively regulated by WT TP53 [63]. OTX008 inhibits the activity of galectin-1. Restoration of WT-TP53 activity in MIA-PaCa-2 cells sensitized the cells 100-fold in comparison to MIA-PaCa-2 cells which lacked WT-TP53 activity (Figure 5D).

The plasminogen activator inhibitor (PAI-1), serpine1 is negatively regulated by miR-34a in MIA-PaCa-2 upon restoration of WT-TP53 activity [64]. The small molecule tiplaxtinin inhibits serpine1 activity [65]. Upon restoration of WT-TP53 activity in MIA-PaCa-2 cells resulted in 4-fold enhanced sensitivity to tiplaxtinin in comparison to MIA-PaCa-2 cells lacking WT-TP53 activity (Figure 6A).

Effects of WT-TP53 on sensitivity to natural products and nutraceuticals

The ability of various natural products and nutraceuticals to inhibit the proliferation in MIA-PaCa-2 cells in the presence and absence of WT-TP53 activity was determined. These compounds were selected on the basis of literature data suggesting their targets and their influence on the development of PDAC.

A natural product that inhibits the Hh signaling pathway is cyclopamine. The Hh pathway is very important in PDAC and metastasis [66, 67]. Restoration of WT-TP53 activity in MIA-PaCa-2 cells increased the sensitivity 2-fold to cyclopamine (Figure 6B).

Extracts from the plant fever few contain parthenolide. One of its targets is NF-κB [68]. Parthenolide has been observed to suppress PDAC progression [69]. Restoration of WT-TP53 activity in MIA-PaCa-2 cells increased the sensitivity to parthenolide 11.4-fold in comparison to cells lacking WT-TP53 activity (Figure 6C).

Licorice contains the flavonoid isoliquiritin which has various biological activities including anti-cancer

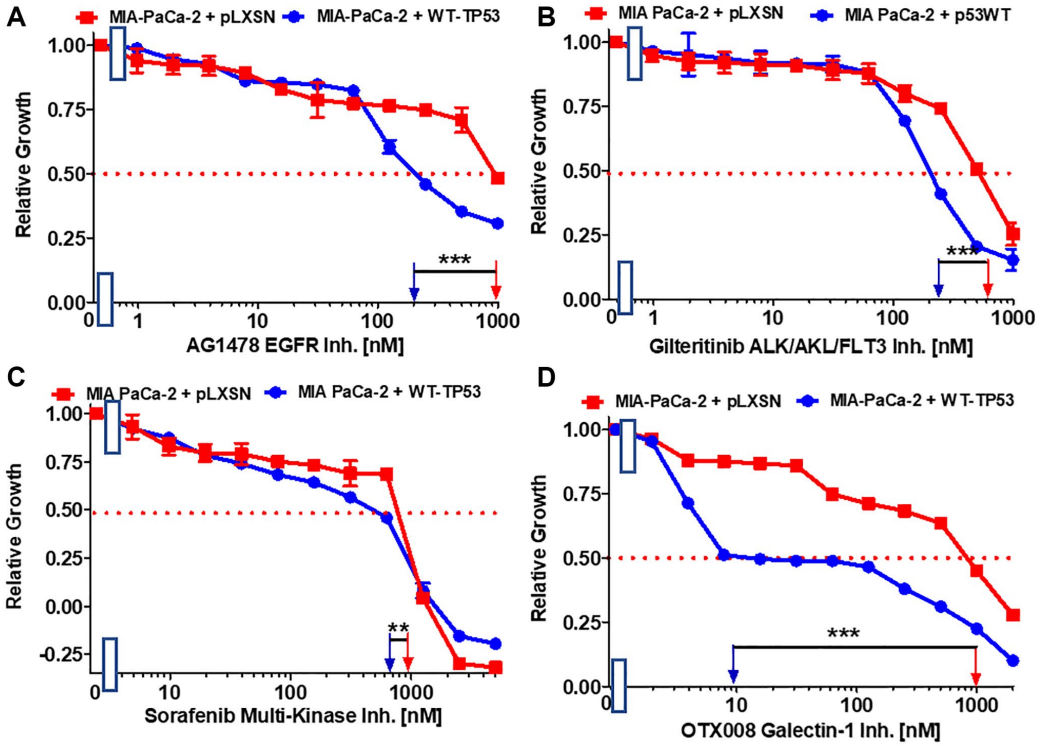

Figure 5. Effects of inhibitors which may suppress metastasis on the growth of MIA-PaCa-2 + WT-TP53 and MIA-PaCa-2 + pLXSN cells. The effects of the AG1478 EGFR inhibitor (**A**), the gilteritinib ALK/AXL/FLT3 inhibitor (**B**), the sorafenib multi-kinase inhibitor (**C**) and the galectin-1 inhibitor OTX008 (**D**) on MIA-PaCa-2 + pLXSN cells (solid red squares) and MIA-PaCa-2 + WT-TP53 cells (solid blue circles) were examined by MTT analysis. The MIA-PaCa-2 + WT-TP53, and MIA-PaCa-2 + pLXSN cells in each panel were all examined at the same time period. These experiments were repeated and similar results were obtained. Statistical analyses were performed by the *T* test on the means and standard deviations of various treatment groups. $^{***}P < 0.0001$, and $^{**}P < 0.005$.

activities [70, 71]. In lung cancer cells, it was shown that isoliquiritin can induce TP53 activity [71]. In pancreatic cancer cells it suppressed the invasiveness *in vitro* [72]. Restoration of WT-TP53 activity in MIA-PaCa-2 cells increased their sensitivity to isoliquiritin 3.2-fold (Figure 6D).

Genistein is an isoflavone. It possesses certain anti-cancer properties including inhibition of angiogenesis in PDAC [73]. It induces apoptosis in PDAC lines [74]. Restoration of WT-TP53 activity in MIA-PaCa-2 cells increased their sensitivity to genistein 4.3-fold in comparison to MIA-PaCa-2 cells lacking WT-TP53 (Figure 7A).

Daidzein is an additional isoflavone. It inhibited breast cancer growth in rodent models [75, 76]. Restoration of WT-TP53 activity in MIA-PaCa-2 cells increased the sensitivity to daidzein 1.7-fold (Figure 7B).

Summarizing, restoration of WT-TP53 activity in MIA-PaCa-2 cells increased the sensitivity to various chemotherapeutic drugs, signal transduction inhibitors and natural products.

Restoration of WT-TP53 decreases clonogenicity in the presence of chemotherapeutic drugs

The ability of WT-TP53 to suppress clonogenicity in 5-fluorouracil, gemcitabine and cisplatin was determined in MIA-PaCa-2 and PANC-28 cell containing and lacking WT-TP53. Upon restoration of WT-TP53 activity in MIA-PaCa-2 and PANC-28 cells, clonogenicity decreased in a dose-dependent fashion more dramatically in cells containing WT-TP53 activity (Figure 8). Although gemcitabine inhibited clonogenicity in cells containing and lacking WT-TP53 activity. Thus, restoration of WT-TP53 suppressed clonogenicity in larger culture volumes containing chemotherapeutic drugs carried out for 14–21 days and it reduced the IC_{50}s for chemotherapeutic drugs in smaller cultures carried out over 5 days [40, 41].

Effects of WT-TP53 on the ability of cells to form colonies in medium containing soft agar

The ability of cells to form colonies in medium containing soft agar in the absence of adhesion to the bottom of the tissue culture plate (anchorage-independent growth) is often considered as a measure of the extent of transformation of malignant transformation as most "normal" cells do not [77].

The effects of restoration of WT-TP53 activity on the ability to form colonies in increasing concentrations of 5FU were compared. As documented in Figure 9, restoration of WT-TP53 activity in MIA-PaCa-2 cells inhibited their ability to form colonies in soft agar in the presence of 5FU.

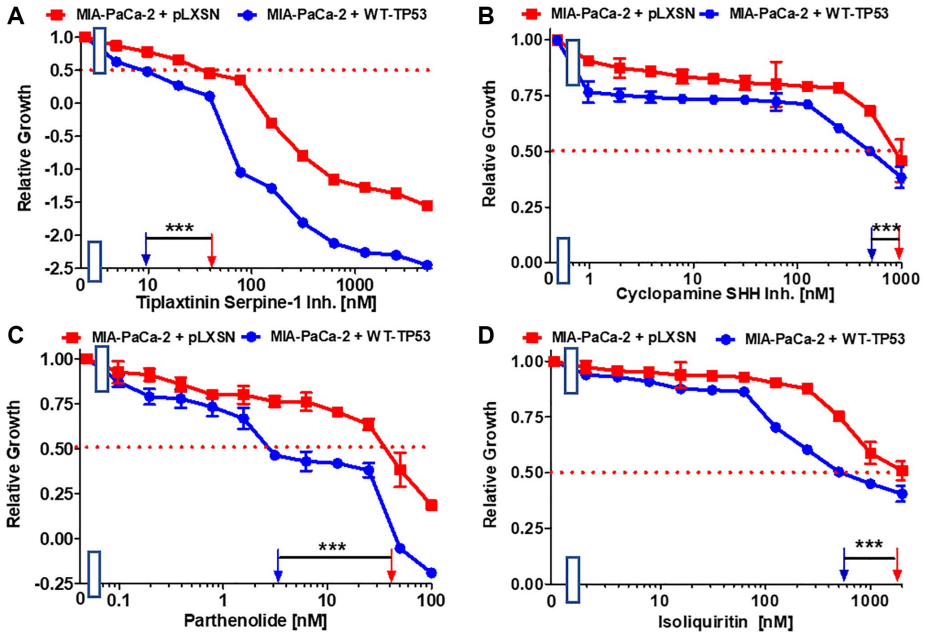

Figure 6. Effects of inhibitors/natural products which may suppress metastasis on the growth of MIA-PaCa-2 + WT-TP53 and MIA-PaCa-2 + pLXSN cells. The effects of the tiplaxtinin Serpine-1 inhibitor (**A**), the natural product cyclopamine, a SHH inhibitor (**B**), the natural product parthenolide, a NF-κB inhibitor (**C**), and the natural product/nutraceutical isoliquiritin (**D**) were examined by MTT analysis. The MIA-PaCa-2 + WT-TP53, and MIA-PaCa-2 + pLXSN cells in each panel were all examined at the same time period. These experiments were repeated and similar results were obtained. Statistical analyses were performed by the *T* test on the means and standard deviations of various treatment groups. $^{***}P < 0.0001$.

Figure 10 presents photographs of colonies stained with crystal violet, not only were there less colonies in soft agar when WT-TP53 activity was restored to MIA-PaCa-2 cells but the colony sizes were also smaller. When there was no 5FU in the culture medium, MIA-PaCa-2 cells containing or lacking WT-TP53 formed similar numbers of colonies of roughly equal sizes. However, even at the lowest dose of 5FU (1.25 µM), there was a massive drop in the number of colonies observed in MIA-PaCa-2 cells containing WT-TP3 activity while the decline in MIA-PaCa-2 cells lacking WT-TP53 activity, was not as extreme.

Restoration of WT-TP53 activity in both MIA-PaCa-2 and PANC-28 cells decreased their ability to form colonies in soft agar containing docetaxel (Figure 11). Introduction of WT-TP53 activity decreased the ability of MIA-PaCa-2 cells to form colonies in soft agar containing doxorubicin (Figure 12A).

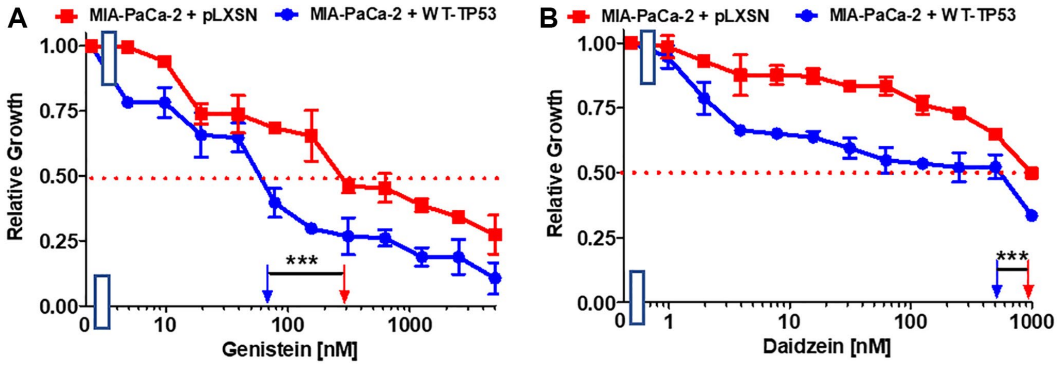

Figure 7. Effects of nutraceuticals on the growth of MIA-PaCa-2 + WT-TP53 and MIA-PaCa-2 + pLXSN cells. The effects of genistein (**A**), and daidzein (**B**), on MIA-PaCa-2 + pLXSN cells (solid red squared) and MIA-PaCa-2 + WT-TP53 cells (solid blue circles) were examined by MTT analysis. The MIA-PaCa-2 + WT-TP53, and MIA-PaCa-2 + pLXSN cells in each panel were all examined at the same time period. These experiments were repeated and similar results were obtained. Statistical analyses were performed by the *T* test on the means and standard deviations of various treatment groups. $^{***}P < 0.0001$.

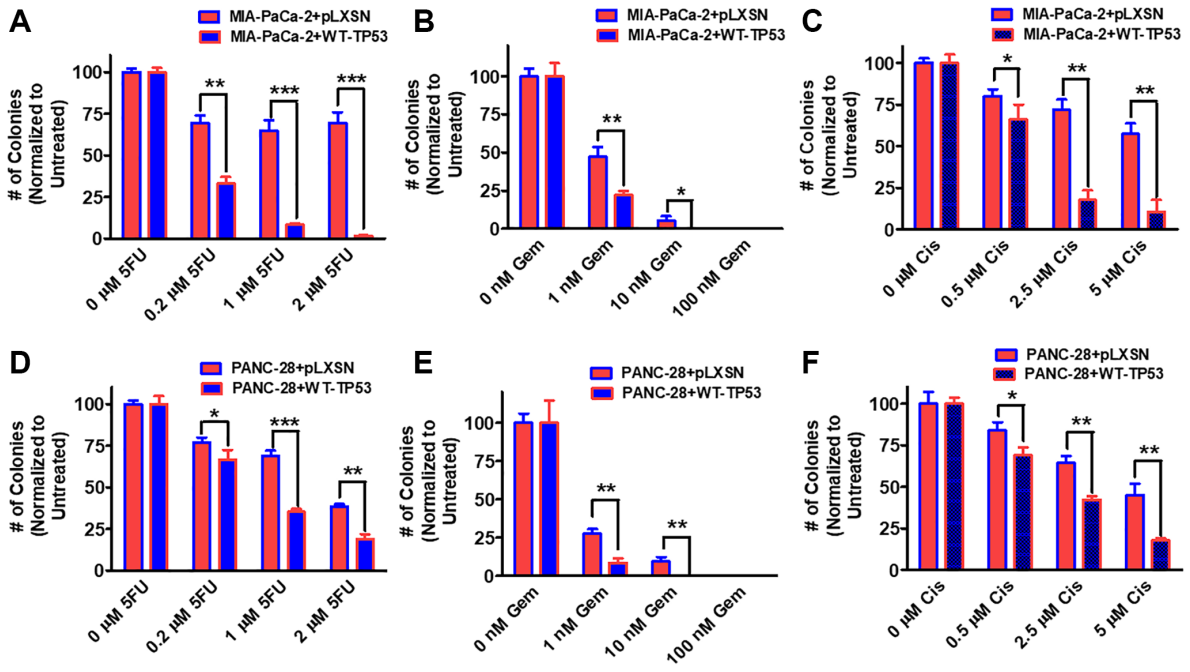

Figure 8. Effects of pLXSN and WT-TP53 on clonogenicity in the presence of 5-Fluorouracil, gemcitabine or cisplatin in two PDAC cell lines. The clonogenicity in the presence of increasing concentrations of 5-fluorouracil (5FU), gemcitabine (Gem) and cisplatin (Cis) were examined in: MIA-PaCa-2 + pLXSN and MIA-PaCa-2 + WT-TP53 (**A–C**), PANC-28 + pLXSN, and PANC-28 + WT-TP53 (**D–F**). Red horizontal bars = MIA-PaCa-2 or PANC-28 containing pLXSN. Blue horizontal bars = MIA-PaCa-2 or PANC-28 containing WT-TP53. These experiments were repeated and similar results were observed. The colonies for each cell line were normalized to untreated so that the results from pLXSN and WT-TP53 could be compared. $^{***}P < 0.0001$, $^{**}P < 0.005$ and $^{*}P < 0.05$.

Drug transporters such as MDR1 are often upregulated in drug resistant cells [78–80]. Verapamil will inhibit the activity of certain drug transporters such as MDR1. Addition of WT-TP53 activity to MIA-PaCa-2 cells increased their sensitivity to verapamil as determined by colony formation in soft agar (Figure 12B).

Hh signaling is critical in differentiation and in some cases, cancer metastasis [81]. Hh pathway inhibitors have been evaluated in PDAC patients [82]. Restoration of WT-TP53 activity in MIA-PaCa-2 cells made them more sensitive to the Hh pathway vismodegib in soft agar colony formation assays (Figure 12C). Thus, restoration of WT-TP53 activity in both MIA-PaCa-2 and PANC-28 cells resulted in the cells becoming more sensitive to chemotherapeutic drugs.

Restoration of WT-TP53 activity in MIA-PaCa-2 cells alters their metabolic properties

For their rapid growth, cancer cells require a large amount of ATP that occurs by glycolysis and mitochondrial oxidative phosphorylation. To determine the consequence of restoration of WT-TP53 activity in energy metabolism in MIA-PaCa-2 cells, stress tests were done with the Seahorse analyzer. This machine determines the extent of glycolysis by determining the

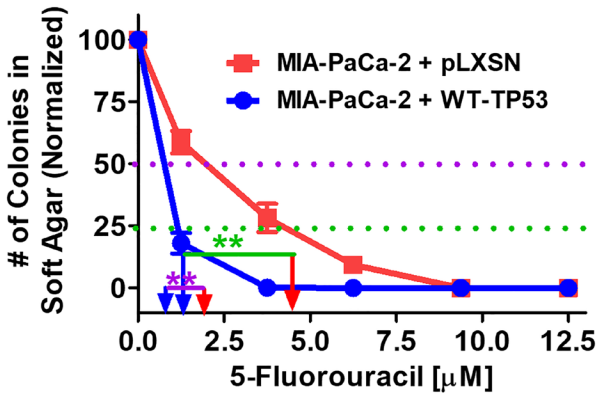

Figure 9. Effects of pLXSN and WT-TP53 on the colony formation in soft agar in the presence of 5-Fluorouracil. The effects of pLXSN and WT-TP53 on the colony formation in soft agar were examined. Red squares = MIA-PaCa-2 + pLXSN cells, blue circles = MIA-PaCa-2 + WT-TP53 cells. IC_{50} is indicated with a purple dotted line and IC_{25} is indicated with a green dotted line. IC_{25} is a term to indicate inhibition of colony formation at 25%. These experiments were repeated performed and similar results were observed. The colonies for each cell line were normalized to untreated cells so that the results from the MIA-PaCa-2 + pLXSN and MIA-PaCa-2 + WT-TP53 could be compared. $^{**}P < 0.005$.

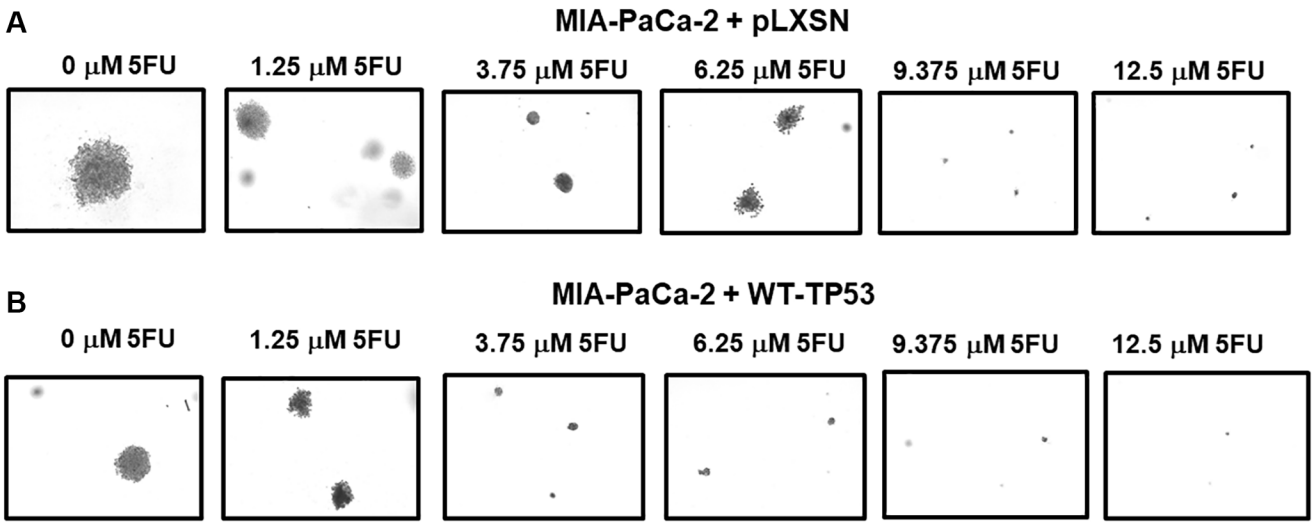

Figure 10. Crystal violet-stained colonies in soft agar in the presence of 5-Fluorouracil. The effects of pLXSN and WT-TP53 on the colony formation in soft agar were photographed after staining. Photographs were taken at the same day and at the same magnification on the microscope. (**A**) MIA-PaCa-2 + pLXSN cells treated with increasing concentration of 5FU, (**B**) MIA-PaCa-2 + WT-TP53 cells treated with increasing concentrations of 5FU.

extracellular acidification (ECAR) and can also analyze mitochondrial oxidative phosphorylation by measuring the real-time oxygen consumption rate (OCR).

TP53 has been shown to be a cellular energy metabolism regulator [83–88]. It can influence both glycolysis and mitochondrial metabolism through multiple mechanisms [88]. Some studies have shown that mutant TP53 can have more effects on mitochondrial metabolism than glycolysis [89]. The effects of restoration of WT-TP53 activity on mitochondrial activity in PDAC cells have not been documented well.

The effects of WT-TP53 activity on metabolic parameters were determined in MIA-PaCa-2 cells containing and lacking WT-TP53 activity were determined as we previously described [90] using the Seahorse analyzer. The results presented here indicated that restoration of WT-TP53 activity led to a decrease in glycolytic capacity in comparison to cells lacking WT-TP53 activity (Figures 13–15). Moreover, the effects on mitochondrial respiration also were more pronounced in MIA-PaCa-2 cells containing WT-TP53 activity.

Upon restoration of WT-TP53 activity in MIA-PaCa-2 cells, the level of basal mitochondrial respiration was significantly lower than in MIA-PaCa-2 lacking WT-TP53 activity. Also, their maximal respiratory and spare respiratory capacity levels were significantly reduced in contrast to cells lacking WT-TP53 (Figures 13 and 14).

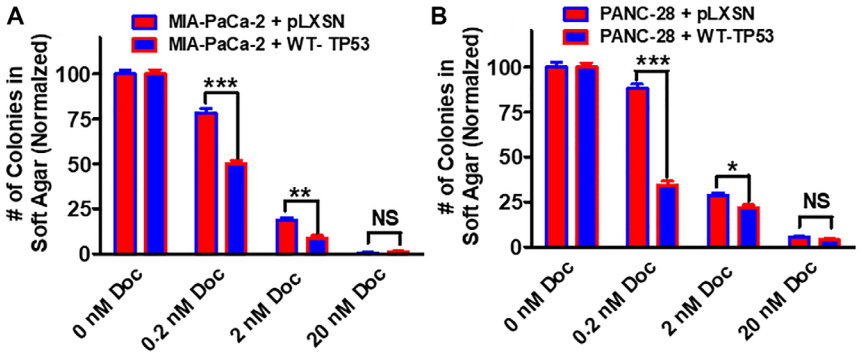

Figure 11. Effects of pLXSN and WT-TP53 on the colony formation in soft agar in the presence of docetaxel. The effects of pLXSN and WT-TP53 on the colony formation in soft agar in MIA-PaCa-2 and PANC-28 cells were examined. (**A**) MIA-PaCa-2 + pLXSN (red bars) and MIA-PaCa-2 + WT-TP53 (blue bars) were compared in response to docetaxel. (**B**) PANC-28 + pLXSN (red bars) and PANC-28 + WT-TP53 (blue bars) were compared in response to docetaxel. The colonies for each cell line were normalized to untreated so that the results from pLXSN and WT-TP53 could be compared. These studies were repeated and similar results were observed. $^{***}P < 0.0001$, $^{**}P < 0.005$ and $^{*}P < 0.05$, NS = not statistically significant.

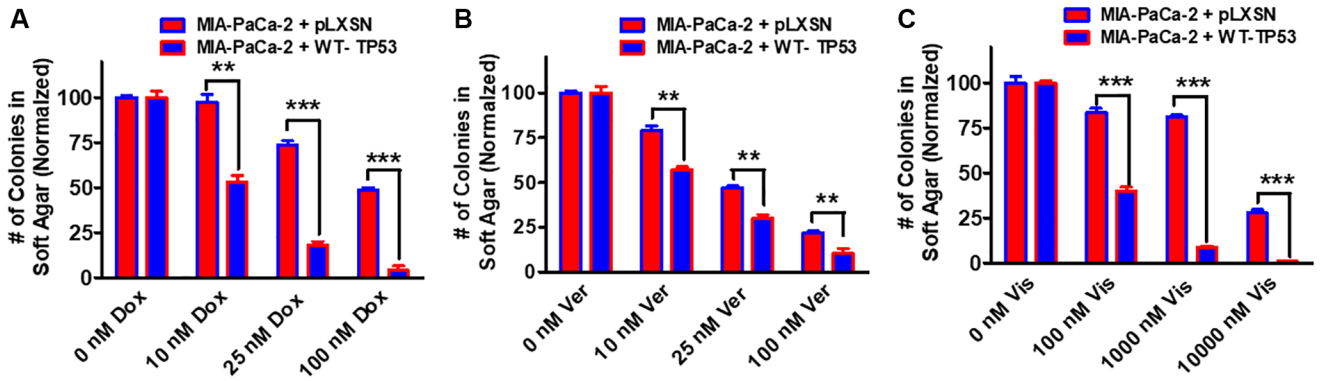

Figure 12. Effects of pLXSN and WT-TP53 on the colony formation in soft agar in the presence of doxorubicin, verapamil and vismodegib. The effects of pLXSN and WT-TP53 on the colony formation in soft agar in MIA-PaCa-2 in response to drugs was examined. (**A**) Colony formation abilities of MIA-PaCa-2 + pLXSN (red bars) and MIA-PaCa-2 + WT-TP53 (blue bars) were compared in response to treatment with doxorubicin. (**B**) Colony formation abilities of MIA-PaCa-2 + pLXSN (red bars) and MIA-PaCa-2 + WT-TP53 (blue bars) were compared in response to verapamil. (**C**) Colony formation abilities of MIA-PaCa-2 + pLXSN (red bars) and MIA-PaCa-2 + WT-TP53 (blue bars) were compared in response to treatment with vismodegib. The number of colonies for each cell line were normalized to untreated so that the results from pLXSN and WT-TP53 could be compared. These studies were repeated and similar results were observed. $^{***}P < 0.0001$, and $^{**}P < 0.005$.

DISCUSSION

TP53 is one of the most frequently mutated genes in human cancer, including pancreatic cancer. The *TP53* genes are altered in the two PDAC cell lines examined. MIA-PaCa-2 cells have GOF TP53 mutations and PANC-28 cells lack TP53 expression. Both PDAC cell lines have activating mutations in the *KRAS* gene which results in constitutive KRas expression. Interactions between mutant TP53 and KRas have been observed

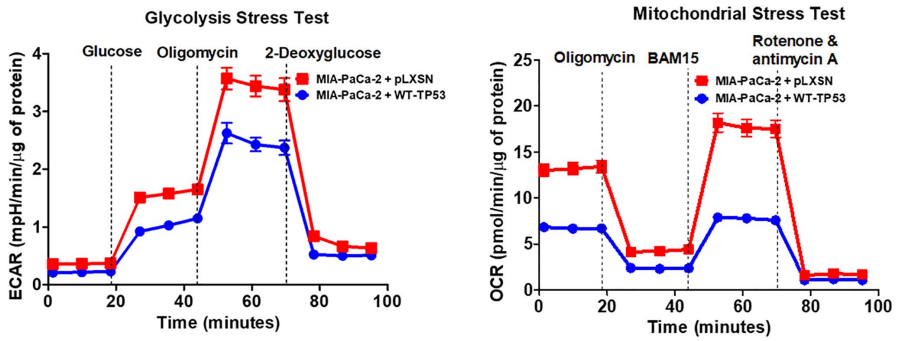

Figure 13. Effects of presence of WT-TP53 on glycolysis and mitochondrial respiration. The data for MIA-PaCa-2 + pLXSN is the same control as presented in [91]. Both MIA-PaCa-2 + pLXSN and MIA-PaCa-2 + WT-TP53 cells were examined the same time on the Seahorse machine as were MIA-PaCa-2 + WT-GSK-3β and MIA-PaCa-2 + KD-GSK-3β cells (all four cell lines done at same time). The data presented in Figure 14 are the means and standard error of the means (SEM).

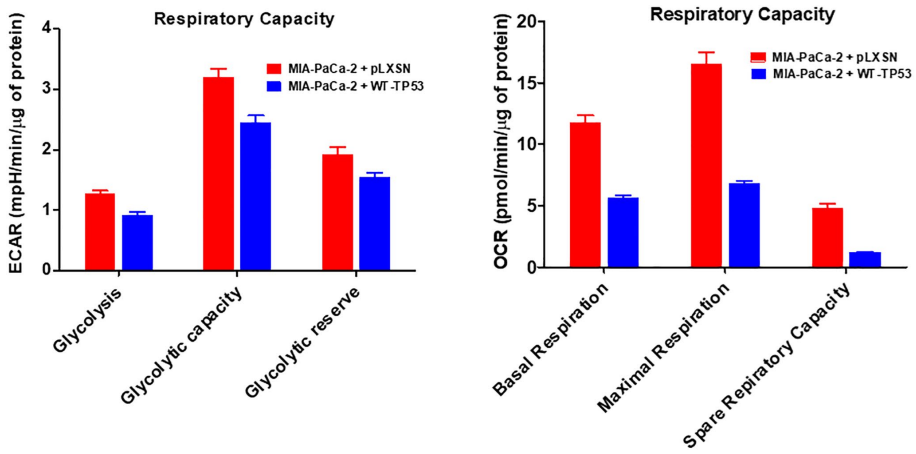

Figure 14. Effects of presence of WT-TP53 on respiratory capacity. The data for MIA-PaCa-2 + pLXSN is the same control as presented in [91]. Both MIA-PaCa-2 + pLXSN and MIA-PaCa-2 + WT-TP53 were examined the same time on the Seahorse machine. The measurements were made 5 times (5 replicates). The data presented in Figure 14 are the means and standard error of the means (SEM).

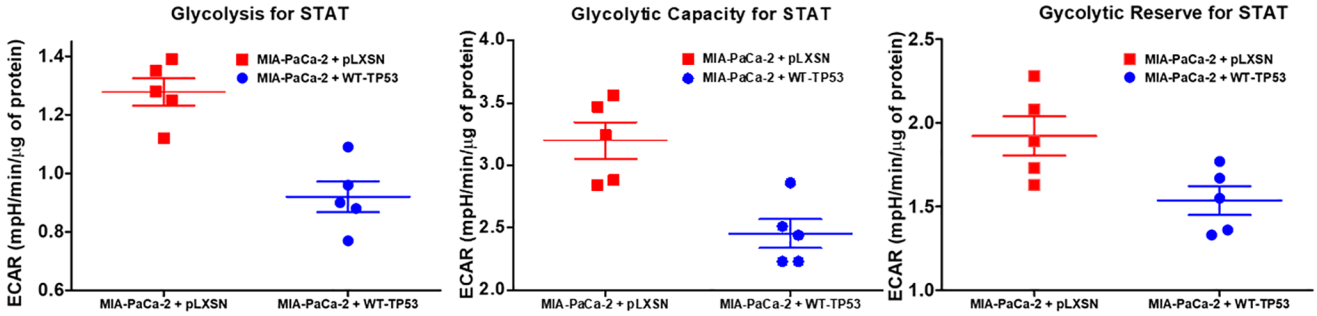

Figure 15. Effects of presence of WT-TP53 on glycolysis. Glycolysis for STAT, glycolytic capacity, and glycolytic reserve for STAT were measured by the Seahorse instrument. The data for MIA-PaCa-2 + pLXSN is the same control as presented in [91]. Both MIA-PaCa-2 + MIA-PaCa-2 + WT-TP53 were examined the same time on the Seahorse machine. STAT is an abbreviation for statistics used in study which was the Mann–Whitney test.

which led to increased KRas functions [51]. GSK-3β may regulate KRas activity in these cells [51]. Thus, TP53 can interact with many signaling pathways important in cancer development.

In this manuscript, the consequences of restoration of WT-TP53 activity on the response to therapeutic agents have been documented. Restoration of WT-TP53 activity augmented the ability of PDAC cells to various agents used in the therapy of many different cancer types.

Interestingly, restoration of WT-TP53 activity augmented the responsive of MIA-PaCa-2 cells to multiple small molecule inhibitors which target critical signal molecules which are often aberrantly regulated in various cancers. These kinases and GTPases are often associated with cell growth and metastasis.

When WT-TP53 activity was restored to MIA-PaCa-2 cells they became more sensitive to small molecule inhibitors that target mutant KRas and downstream MEK1 than cells containing pLXSN. Thus, WT-TP53 could increase the sensitivity of cells which contain mutant KRas to MEK1 inhibitors. ERK1,2 lies downstream of MEK1. ERK1,2 phosphorylates many important substrates which are involved in various aspects of cell proliferation. Combination of ERK1,2 and autophagy inhibition with a MEK1 inhibitor and chloroquine may be an additional treatment option for some PDAC patients [91].

The presence of functional WT-TP53 is important for the sensitivity of FL5.12 hematopoietic cells to the mTORC1 blocker rapamycin [92]. FL5.12 cells normally have WT-TP53 activity [93]. Upon insertion of dominant negative (DN) TP53 into FL5.12 cells, their sensitivity to rapamycin was eliminated [92]. Likewise, in this current study, restoration of WT-TP53 activity in MIA-PaCa-2 cells increased the sensitivity to rapamycin. Thus, TP53 intersects with the mTORC1 pathway.

Clearly, the presence of WT-TP53 is critical for the sensitivity of various cancers, including PDAC to many drugs used in cancer therapy [94]. Additional studies on methods and approaches to reactivate mutant TP53 and other mutated genes implicated cancer should be undertaken.

TP53 can influence glycolytic and mitochondrial metabolism both through transcriptional and non-transcriptional regulation. This influence is important for the tumor suppressor role of the protein. An overview of the effects of WT and mutant TP53 on metabolic properties, together with the effects of metformin and rapamycin, and drugs used to inhibit pancreatic cancer growth, is presented in Figure 16.

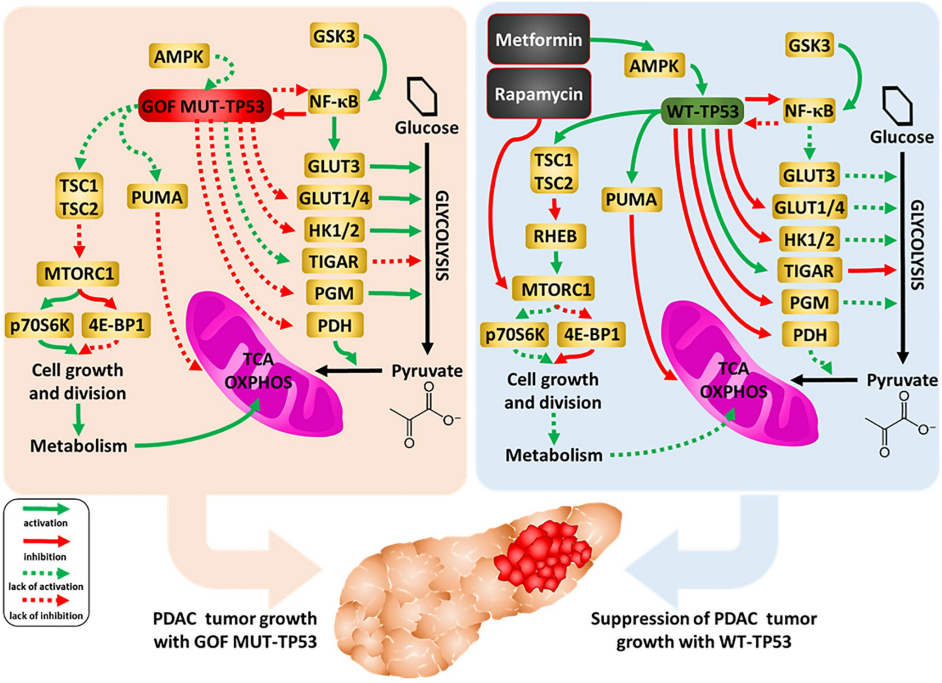

Figure 16. Influences of mutant and WT-TP53 on mitochondrial activity and glucose metabolism and effects of rapamycin and metformin. The effects of WT and mutant TP53 on key enzymes important in glycolysis and how they can influence metabolism and PDAC tumor growth. In our studies, we have examined the effect of GOF mutant TP53 and in some cases WT TP53. In addition, sites of interaction of the type 2 diabetes drug metformin and the immunosuppressive drug rapamycin and their effects on AMPK and mTORC1 are indicated. TP53 can induce mitochondrial apoptosis pathway by regulating the expression of PUMA and other proteins.

Enhanced glucose metabolism via glycolysis is the predominant source of ATP in numerous cancers. TP53 represses expression of, for example, glucose transporters, hexokinase and inhibits nuclear factor-kappa B cell (NF-κB), a protein that regulates many genes, including genes encoding glycolytic enzymes. Thus, restoration of WT TP53 activity can lead to reduction of glycolysis and impairment of cancer cell growth. On the other hand, TP53 is known to induce oxidative phosphorylation and mitochondrial production of intermediates for biosynthesis [for review see 89]. In our work, however, we observed a decrease of both glycolysis and mitochondrial respiration after the restoration of WT TP53 activity in PDAC. Other studies with breast cancer cell lines, which differ in TP53 status as well as other genes, were observed to increase both glycolytic and mitochondrial activity when mutant TP53 was present [95]. Knock-in of certain TP53 GOF mutations in mice was observed to augment mitochondrial activity, promote survival, and increased maximal treadmill exercise times [96].

TP53 has been shown to induce pro-oxidant enzymes and mitochondrial apoptosis pathway (by regulating the expression of PUMA, BAK, BAX, BCL2, BCLXL), and block anti-oxidant pathways [88]. Thus, the observed reduction of mitochondrial respiration might result from the oxidative-stress-induced impairment of function of the organelles in the WT-TP53-expressing cells. The observed value of the maximum respiration of these cells, only slightly higher than the basal respiration, seems to confirm the impairment of mitochondrial function, but it should be kept in mind that the reduction of the glycolytic rate leads to a reduction in the number of mitochondrial substrates.

Regardless of which of the above processes contributes more to the reduction of mitochondrial metabolism in comparison with the same cells that only express GOF TP53, together the observed changes suggest restoration of WT-TP3 activity confers increased sensitization to various drugs and therapeutic molecules, natural products as well as nutraceuticals. Mutant TP53 can affect the activity of mTORC1 which is important in cellular growth and metabolism. Mutant TP53 may make the PDAC cells more resistant to rapamycin than cells containing WT-TP53. Rapamycin and metformin can interfere with some of the important pathways in the mitochondria, some of which are regulated by TP53 [96–98].

MATERIALS AND METHODS

Cell culture and sources of therapeutic agents

The MIA-PaCa-2 and PANC-28 cells have been described in previous publications [37, 39, 99]. Cell culture conditions and sources of chemotherapeutic drugs, small molecule inhibitors, natural products and nutraceuticals have been described in our previous publications [40, 41, 47, 80, 90, 100]. Aclacinomycin was obtained from the US National Cancer Institute, (Bethesda, Maryland, USA).

Restoration of WT-TP53 activity

Restoration of WT-TP53 activity and sources of plasmid DNAs have been previously described [40, 41, 90].

Cell proliferation assays-MTT assays

MTT assays were performed as described previously [40].

Clonogenicity assays

Clonogenicity Assays were performed as described in our previous publication [100].

Semi-solid colony formation

Semi-solid colony formation in agar has been described in our previous publications [100, 101].

Analysis of cell metabolism

Cellular metabolism and statistical analysis were performed as described in our previous publication [90].

AUTHOR CONTRIBUTIONS

J.A.M., A.K.M., S.M.A., L.S.S., M.M.L., and R.A.F. researched various topics, carried out the experiments and analyzed some of the data, A.M.M., S.R., L.C., F.B., researched the many of the topics and wrote various sections, P.D. and A.G generated some of the artwork, researched various topics and wrote multiple sections. All of the authors have read the manuscript and accepted the final version of the manuscript.

CONFLICTS OF INTEREST

The authors declare no conflicts of interest related to this study.

FUNDING

J.A.M., S.L.A. and M.M.L were supported in part from East Carolina University Grants (#111104 and #111110-668715-0000). A.K.M. was supported in part by NIH grant (R01-HL146685).

REFERENCES

1. Rawla P, Sunkara T, Gaduputi V. Epidemiology of Pancreatic Cancer: Global Trends, Etiology and Risk Factors. World J Oncol. 2019; 10:10–27. https://doi.org/10.14740/wjon1166 PMID:30834048

2. Siegel R, Naishadham D, Jemal A. Cancer statistics, 2013. CA Cancer J Clin. 2013; 63:11–30. https://doi.org/10.3322/caac.21166 PMID:23335087

3. Hidalgo M, Cascinu S, Kleeff J, Labianca R, Löhr JM, Neoptolemos J, Real FX, Van Laethem JL, Heinemann V. Addressing the challenges of pancreatic cancer: future directions for improving outcomes. Pancreatology. 2015; 15:8–18. https://doi.org/10.1016/j.pan.2014.10.001 PMID:25547205

4. Fitzgerald TL, McCubrey JA. Pancreatic cancer stem cells: association with cell surface markers, prognosis, resistance, metastasis and treatment. Adv Biol Regul. 2014; 56:45–50. https://doi.org/10.1016/j.jbior.2014.05.001 PMID:24925031

5. McGuigan A, Kelly P, Turkington RC, Jones C, Coleman HG, McCain RS. Pancreatic cancer: A review of clinical diagnosis, epidemiology, treatment and outcomes. World J Gastroenterol. 2018; 24:4846–61. https://doi.org/10.3748/wjg.v24.i43.4846 PMID:30487695

6. Muniraj T, Jamidar PA, Aslanian HR. Pancreatic cancer: a comprehensive review and update. Dis Mon. 2013; 59:368–402. https://doi.org/10.1016/j.disamonth.2013.08.001 PMID:24183261

7. Wang H, Liu J, Xia G, Lei S, Huang X, Huang X. Survival of pancreatic cancer patients is negatively correlated with age at diagnosis: a population-based retrospective study. Sci Rep. 2020; 10:7048. https://doi.org/10.1038/s41598-020-64068-3 PMID:32341400

8. Morton JP, Timpson P, Karim SA, Ridgway RA, Athineos D, Doyle B, Jamieson NB, Oien KA, Lowy AM, Brunton VG, Frame MC, Evans TR, Sansom OJ. Mutant p53 drives metastasis and overcomes growth arrest/senescence in pancreatic cancer. Proc Natl Acad Sci U S A. 2010; 107:246–51. https://doi.org/10.1073/pnas.0908428107 PMID:20018721

9. Fitzgerald TL, Lertpiriyapong K, Cocco L, Martelli AM, Libra M, Candido S, Montalto G, Cervello M, Steelman L, Abrams SL, McCubrey JA. Roles of EGFR and KRAS and their downstream signaling pathways in pancreatic cancer and pancreatic cancer stem cells. Adv Biol Regul. 2015; 59:65–81. https://doi.org/10.1016/j.jbior.2015.06.003 PMID:26257206

10. Singh RR, O'Reilly EM. New Treatment Strategies for Metastatic Pancreatic Ductal Adenocarcinoma. Drugs. 2020; 80:647–69. https://doi.org/10.1007/s40265-020-01304-0 PMID:32306207

11. Skelton RA, Javed A, Zheng L, He J. Overcoming the resistance of pancreatic cancer to immune checkpoint inhibitors. J Surg Oncol. 2017; 116:55–62. https://doi.org/10.1002/jso.24642 PMID:28628715

12. Ruarus A, Vroomen L, Puijk R, Scheffer H, Meijerink M. Locally Advanced Pancreatic Cancer: A Review of Local Ablative Therapies. Cancers (Basel). 2018; 10:E16. https://doi.org/10.3390/cancers10010016 PMID:29320420

13. Conroy T, Desseigne F, Ychou M, Bouché O, Guimbaud R, Bécouarn Y, Adenis A, Raoul JL, Gourgou-Bourgade S, de la Fouchardière C, Bennouna J, Bachet JB, Khemissa-Akouz F, et al, and Groupe Tumeurs Digestives of Unicancer, and PRODIGE Intergroup. FOLFIRINOX versus gemcitabine for metastatic pancreatic cancer. N Engl J Med. 2011; 364:1817–25. https://doi.org/10.1056/NEJMoa1011923 PMID:21561347

14. Conroy T, Gavoille C, Samalin E, Ychou M, Ducreux M. The role of the FOLFIRINOX regimen for advanced pancreatic cancer. Curr Oncol Rep. 2013; 15:182–9. https://doi.org/10.1007/s11912-012-0290-4 PMID:23341367

15. Faris JE, Blaszkowsky LS, McDermott S, Guimaraes AR, Szymonifka J, Huynh MA, Ferrone CR, Wargo JA, Allen JN, Dias LE, Kwak EL, Lillemoe KD, Thayer SP, et al. FOLFIRINOX in locally advanced pancreatic cancer: the Massachusetts General Hospital Cancer Center experience. Oncologist. 2013; 18:543–8. https://doi.org/10.1634/theoncologist.2012-0435 PMID:23657686

16. Thota R, Pauff JM, Berlin JD. Treatment of metastatic pancreatic adenocarcinoma: a review. Oncology (Williston Park). 2014; 28:70–4. PMID:24683721

17. Von Hoff DD, Ramanathan RK, Borad MJ, Laheru DA, Smith LS, Wood TE, Korn RL, Desai N, Trieu V, Iglesias JL, Zhang H, Soon-Shiong P, Shi T, et al. Gemcitabine plus nab-paclitaxel is an active regimen in patients

with advanced pancreatic cancer: a phase I/II trial. J Clin Oncol. 2011; 29:4548–54.
https://doi.org/10.1200/JCO.2011.36.5742
PMID:21969517

18. Rasheed ZA, Yang J, Wang Q, Kowalski J, Freed I, Murter C, Hong SM, Koorstra JB, Rajeshkumar NV, He X, Goggins M, Iacobuzio-Donahue C, Berman DM, et al. Prognostic significance of tumorigenic cells with mesenchymal features in pancreatic adenocarcinoma. J Natl Cancer Inst. 2010; 102:340–51.
https://doi.org/10.1093/jnci/djp535
PMID:20164446

19. Klein AP. Genetic susceptibility to pancreatic cancer. Mol Carcinog. 2012; 51:14–24.
https://doi.org/10.1002/mc.20855
PMID:22162228

20. Klein AP. Identifying people at a high risk of developing pancreatic cancer. Nat Rev Cancer. 2013; 13:66–74.
https://doi.org/10.1038/nrc3420
PMID:23222481

21. McCubrey JA, Abrams SL, Fitzgerald TL, Cocco L, Martelli AM, Montalto G, Cervello M, Scalisi A, Candido S, Libra M, Steelman LS. Roles of signaling pathways in drug resistance, cancer initiating cells and cancer progression and metastasis. Adv Biol Regul. 2015; 57:75–101.
https://doi.org/10.1016/j.jbior.2014.09.016
PMID:25453219

22. Masetti M, Acquaviva G, Visani M, Tallini G, Fornelli A, Ragazzi M, Vasuri F, Grifoni D, Di Giacomo S, Fiorino S, Lombardi R, Tuminati D, Ravaioli M, et al. Long-term survivors of pancreatic adenocarcinoma show low rates of genetic alterations in KRAS, TP53 and SMAD4. Cancer Biomark. 2018; 21:323–34.
https://doi.org/10.3233/CBM-170464
PMID:29103024

23. Chen X, Ko LJ, Jayaraman L, Prives C. p53 levels, functional domains, and DNA damage determine the extent of the apoptotic response of tumor cells. Genes Dev. 1996; 10:2438–51.
https://doi.org/10.1101/gad.10.19.2438
PMID:8843196

24. Ko LJ, Prives C. p53: puzzle and paradigm. Genes Dev. 1996; 10:1054–72.
https://doi.org/10.1101/gad.10.9.1054
PMID:8654922

25. Olivier M, Eeles R, Hollstein M, Khan MA, Harris CC, Hainaut P. The IARC TP53 database: new online mutation analysis and recommendations to users. Hum Mutat. 2002; 19:607–14.
https://doi.org/10.1002/humu.10081
PMID:12007217

26. Saison-Ridinger M, DelGiorno KE, Zhang T, Kraus A, French R, Jaquish D, Tsui C, Erikson G, Spike BT, Shokhirev MN, Liddle C, Yu RT, Downes M, et al. Reprogramming pancreatic stellate cells via p53 activation: A putative target for pancreatic cancer therapy. PLoS One. 2017; 12:e0189051.
https://doi.org/10.1371/journal.pone.0189051
PMID:29211796

27. Dittmer D, Pati S, Zambetti G, Chu S, Teresky AK, Moore M, Finlay C, Levine AJ. Gain of function mutations in p53. Nat Genet. 1993; 4:42–6.
https://doi.org/10.1038/ng0593-42
PMID:8099841

28. Weissmueller S, Manchado E, Saborowski M, Morris JP 4th, Wagenblast E, Davis CA, Moon SH, Pfister NT, Tschaharganeh DF, Kitzing T, Aust D, Markert EK, Wu J, et al. Mutant p53 drives pancreatic cancer metastasis through cell-autonomous PDGF receptor β signaling. Cell. 2014; 157:382–94.
https://doi.org/10.1016/j.cell.2014.01.066
PMID:24725405

29. Stein Y, Rotter V, Aloni-Grinstein R. Gain-of-Function Mutant p53: All the Roads Lead to Tumorigenesis. Int J Mol Sci. 2019; 20:E6197.
https://doi.org/10.3390/ijms20246197
PMID:31817996

30. Roszkowska KA, Gizinski S, Sady M, Gajewski Z, Olszewski MB. Gain-of-Function Mutations in p53 in Cancer Invasiveness and Metastasis. Int J Mol Sci. 2020; 21:E1334.
https://doi.org/10.3390/ijms21041334
PMID:32079237

31. Vogiatzi F, Brandt DT, Schneikert J, Fuchs J, Grikscheit K, Wanzel M, Pavlakis E, Charles JP, Timofeev O, Nist A, Mernberger M, Kantelhardt EJ, Siebolts U, et al. Mutant p53 promotes tumor progression and metastasis by the endoplasmic reticulum UDPase ENTPD5. Proc Natl Acad Sci U S A. 2016; 113:E8433–42.
https://doi.org/10.1073/pnas.1612711114
PMID:27956623

32. Parrales A, Iwakuma T. Targeting Oncogenic Mutant p53 for Cancer Therapy. Front Oncol. 2015; 5:288.
https://doi.org/10.3389/fonc.2015.00288
PMID:26732534

33. Sallman DA. To target the untargetable: elucidation of synergy of APR-246 and azacitidine in *TP53* mutant myelodysplastic syndromes and acute myeloid leukemia. Haematologica. 2020; 105:1470–2.
https://doi.org/10.3324/haematol.2020.249060
PMID:32482751

34. Janes MR, Zhang J, Li LS, Hansen R, Peters U, Guo X, Chen Y, Babbar A, Firdaus SJ, Darjania L, Feng J, Chen JH, Li S, et al. Targeting KRAS Mutant Cancers with a Covalent G12C-Specific Inhibitor. Cell. 2018; 172:578–89.e17.
https://doi.org/10.1016/j.cell.2018.01.006
PMID:29373830

35. Goebel L, Müller MP, Goody RS, Rauh D. KRasG12C inhibitors in clinical trials: a short historical perspective. RSC Med Chem. 2020; 11:760–70.
https://doi.org/10.1039/d0md00096e
PMID:33479673

36. Jiao D, Yang S. Overcoming Resistance to Drugs Targeting *KRASG12C* Mutation. Innovation (N Y). 2020; 1:100035.
https://doi.org/10.1016/j.xinn.2020.100035
PMID:32939510

37. Deer EL, González-Hernández J, Coursen JD, Shea JE, Ngatia J, Scaife CL, Firpo MA, Mulvihill SJ. Phenotype and genotype of pancreatic cancer cell lines. Pancreas. 2010; 39:425–35.
https://doi.org/10.1097/MPA.0b013e3181c15963
PMID:20418756

38. Gradiz R, Silva HC, Carvalho L, Botelho MF, Mota-Pinto A. MIA PaCa-2 and PANC-1 - pancreas ductal adenocarcinoma cell lines with neuroendocrine differentiation and somatostatin receptors. Sci Rep. 2016; 6:21648.
https://doi.org/10.1038/srep21648
PMID:26884312

39. Zhu J, Abbruzzese JL, Izzo J, Hittelman WN, Li D. AURKA amplification, chromosome instability, and centrosome abnormality in human pancreatic carcinoma cells. Cancer Genet Cytogenet. 2005; 159:10–7.
https://doi.org/10.1016/j.cancergencyto.2004.09.008
PMID:15860351

40. Abrams SL, Lertpiriyapong K, Yang LV, Martelli AM, Cocco L, Ratti S, Falasca M, Murata RM, Rosalen PL, Lombardi P, Libra M, Candido S, Montalto G, et al. Introduction of WT-TP53 into pancreatic cancer cells alters sensitivity to chemotherapeutic drugs, targeted therapeutics and nutraceuticals. Adv Biol Regul. 2018; 69:16–34.
https://doi.org/10.1016/j.jbior.2018.06.002
PMID:29980405

41. Abrams SL, Akula SM, Martelli AM, Cocco L, Ratti S, Libra M, Candido S, Montalto G, Cervello M, Gizak A, Rakus D, Steelman LS, McCubrey JA. Sensitivity of pancreatic cancer cells to chemotherapeutic drugs, signal transduction inhibitors and nutraceuticals can be regulated by WT-TP53. Adv Biol Regul. 2021; 79:100780.
https://doi.org/10.1016/j.jbior.2020.100780
PMID:33451973

42. Eliyahu D, Michalovitz D, Eliyahu S, Pinhasi-Kimhi O, Oren M. Wild-type p53 can inhibit oncogene-mediated focus formation. Proc Natl Acad Sci U S A. 1989; 86:8763–7.
https://doi.org/10.1073/pnas.86.22.8763
PMID:2530586

43. Miller AD, Rosman GJ. Improved retroviral vectors for gene transfer and expression. Biotechniques. 1989; 7:980-90.
PMID:2631796

44. Padavano J, Henkhaus RS, Chen H, Skovan BA, Cui H, Ignatenko NA. Mutant K-RAS Promotes Invasion and Metastasis in Pancreatic Cancer Through GTPase Signaling Pathways. Cancer Growth Metastasis. 2015; 8:95–113.
https://doi.org/10.4137/CGM.S29407
PMID:26512205

45. McCubrey JA, Steelman LS, Chappell WH, Abrams SL, Montalto G, Cervello M, Nicoletti F, Fagone P, Malaponte G, Mazzarino MC, Candido S, Libra M, Bäsecke J, et al. Mutations and deregulation of Ras/Raf/MEK/ERK and PI3K/PTEN/Akt/mTOR cascades which alter therapy response. Oncotarget. 2012; 3:954–87.
https://doi.org/10.18632/oncotarget.652
PMID:23006971

46. Zhang Y, Liu JL, Wang J. KRAS gene silencing inhibits the activation of PI3K-Akt-mTOR signaling pathway to regulate breast cancer cell epithelial-mesenchymal transition, proliferation and apoptosis. Eur Rev Med Pharmacol Sci. 2020; 24:3085–96.
https://doi.org/10.26355/eurrev_202003_20673
PMID:32271426

47. Candido S, Abrams SL, Steelman LS, Lertpiriyapong K, Martelli AM, Cocco L, Ratti S, Follo MY, Murata RM, Rosalen PL, Bueno-Silva B, de Alencar SM, Lombardi P, et al. Effects of the MDM-2 inhibitor Nutlin-3a on PDAC cells containing and lacking WT-TP53 on sensitivity to chemotherapy, signal transduction inhibitors and nutraceuticals. Adv Biol Regul. 2019; 72:22–40.
https://doi.org/10.1016/j.jbior.2019.03.002
PMID:30898612

48. Strom E, Sathe S, Komarov PG, Chernova OB, Pavlovska I, Shyshynova I, Bosykh DA, Burdelya LG, Macklis RM, Skaliter R, Komarova EA, Gudkov AV. Small-molecule inhibitor of p53 binding to mitochondria protects mice from gamma radiation. Nat Chem Biol. 2006; 2:474–9.
https://doi.org/10.1038/nchembio809
PMID:16862141

49. McCubrey JA, Steelman LS, Bertrand FE, Davis NM, Sokolosky M, Abrams SL, Montalto G, D'Assoro AB, Libra M, Nicoletti F, Maestro R, Basecke J, Rakus D, et al. GSK-3 as potential target for therapeutic intervention in cancer. Oncotarget. 2014; 5:2881–911. https://doi.org/10.18632/oncotarget.2037 PMID:24931005

50. Ougolkov AV, Fernandez-Zapico ME, Savoy DN, Urrutia RA, Billadeau DD. Glycogen synthase kinase-3beta participates in nuclear factor kappaB-mediated gene transcription and cell survival in pancreatic cancer cells. Cancer Res. 2005; 65:2076–81. https://doi.org/10.1158/0008-5472.CAN-04-3642 PMID:15781615

51. Kazi A, Xiang S, Yang H, Delitto D, Trevino J, Jiang RHY, Ayaz M, Lawrence HR, Kennedy P, Sebti SM. GSK3 suppression upregulates β-catenin and c-Myc to abrogate KRas-dependent tumors. Nat Commun. 2018; 9:5154. https://doi.org/10.1038/s41467-018-07644-6 PMID:30514931

52. Ding L, Billadeau DD. Glycogen synthase kinase-3β: a novel therapeutic target for pancreatic cancer. Expert Opin Ther Targets. 2020; 24:417–26. https://doi.org/10.1080/14728222.2020.1743681 PMID:32178549

53. Morran DC, Wu J, Jamieson NB, Mrowinska A, Kalna G, Karim SA, Au AY, Scarlett CJ, Chang DK, Pajak MZ, Oien KA, McKay CJ, Carter CR, et al, and Australian Pancreatic Cancer Genome Initiative (APGI). Targeting mTOR dependency in pancreatic cancer. Gut. 2014; 63:1481–9. https://doi.org/10.1136/gutjnl-2013-306202 PMID:24717934

54. Leontieva OV, Blagosklonny MV. DNA damaging agents and p53 do not cause senescence in quiescent cells, while consecutive re-activation of mTOR is associated with conversion to senescence. Aging (Albany NY). 2010; 2:924–35. https://doi.org/10.18632/aging.100265 PMID:21212465

55. Wu H, Zhu L, Zhang H, Shi X, Zhang L, Wang W, Xue H, Liang Z. Coexpression of EGFR and CXCR4 predicts poor prognosis in resected pancreatic ductal adenocarcinoma. PLoS One. 2015; 10:e0116803. https://doi.org/10.1371/journal.pone.0116803 PMID:25679210

56. Xie ZB, Zhang YF, Jin C, Mao YS, Fu DL. LRG-1 promotes pancreatic cancer growth and metastasis via modulation of the EGFR/p38 signaling. J Exp Clin Cancer Res. 2019; 38:75. https://doi.org/10.1186/s13046-019-1088-0 PMID:30760292

57. Raj D, Yang MH, Rodgers D, Hampton EN, Begum J, Mustafa A, Lorizio D, Garces I, Propper D, Kench JG, Kocher HM, Young TS, Aicher A, Heeschen C. Switchable CAR-T cells mediate remission in metastatic pancreatic ductal adenocarcinoma. Gut. 2019; 68:1052–64. https://doi.org/10.1136/gutjnl-2018-316595 PMID:30121627

58. Avan A, Quint K, Nicolini F, Funel N, Frampton AE, Maftouh M, Pelliccioni S, Schuurhuis GJ, Peters GJ, Giovannetti E. Enhancement of the antiproliferative activity of gemcitabine by modulation of c-Met pathway in pancreatic cancer. Curr Pharm Des. 2013; 19:940–50. PMID:22973962

59. He X, Zheng Z, Li J, Ben Q, Liu J, Zhang J, Ji J, Yu B, Chen X, Su L, Zhou L, Liu B, Yuan Y. DJ-1 promotes invasion and metastasis of pancreatic cancer cells by activating SRC/ERK/uPA. Carcinogenesis. 2012; 33:555–62. https://doi.org/10.1093/carcin/bgs002 PMID:22223849

60. Botla SK, Savant S, Jandaghi P, Bauer AS, Mücke O, Moskalev EA, Neoptolemos JP, Costello E, Greenhalf W, Scarpa A, Gaida MM, Büchler MW, Strobel O, et al. Early Epigenetic Downregulation of microRNA-192 Expression Promotes Pancreatic Cancer Progression. Cancer Res. 2016; 76:4149–59. https://doi.org/10.1158/0008-5472.CAN-15-0390 PMID:27216198

61. Awasthi N, Zhang C, Hinz S, Schwarz MA, Schwarz RE. Enhancing sorafenib-mediated sensitization to gemcitabine in experimental pancreatic cancer through EMAP II. J Exp Clin Cancer Res. 2013; 32:12. https://doi.org/10.1186/1756-9966-32-12 PMID:23497499

62. Martínez-Bosch N, Fernández-Barrena MG, Moreno M, Ortiz-Zapater E, Munné-Collado J, Iglesias M, André S, Gabius HJ, Hwang RF, Poirier F, Navas C, Guerra C, Fernández-Zapico ME, Navarro P. Galectin-1 drives pancreatic carcinogenesis through stroma remodeling and Hedgehog signaling activation. Cancer Res. 2014; 74:3512–24. https://doi.org/10.1158/0008-5472.CAN-13-3013 PMID:24812270

63. Puchades M, Nilsson CL, Emmett MR, Aldape KD, Ji Y, Lang FF, Liu TJ, Conrad CA. Proteomic investigation of glioblastoma cell lines treated with wild-type p53 and cytotoxic chemotherapy demonstrates an association between galectin-1 and p53 expression. J Proteome Res. 2007; 6:869–75. https://doi.org/10.1021/pr060302l PMID:17269744

64. Akula SM, Ruvolo PP, McCubrey JA. TP53/miR-34a-associated signaling targets *SERPINE1* expression in human pancreatic cancer. Aging (Albany NY). 2020; 12:2777–97.
https://doi.org/10.18632/aging.102776
PMID:31986125

65. Elokdah H, Abou-Gharbia M, Hennan JK, McFarlane G, Mugford CP, Krishnamurthy G, Crandall DL. Tiplaxtinin, a novel, orally efficacious inhibitor of plasminogen activator inhibitor-1: design, synthesis, and preclinical characterization. J Med Chem. 2004; 47:3491–4.
https://doi.org/10.1021/jm049766q
PMID:15214776

66. Zhao J, Wang H, Hsiao CH, Chow DS, Koay EJ, Kang Y, Wen X, Huang Q, Ma Y, Bankson JA, Ullrich SE, Overwijk W, Maitra A, et al. Simultaneous inhibition of hedgehog signaling and tumor proliferation remodels stroma and enhances pancreatic cancer therapy. Biomaterials. 2018; 159:215–28.
https://doi.org/10.1016/j.biomaterials.2018.01.014
PMID:29331808

67. Rosow DE, Liss AS, Strobel O, Fritz S, Bausch D, Valsangkar NP, Alsina J, Kulemann B, Park JK, Yamaguchi J, LaFemina J, Thayer SP. Sonic Hedgehog in pancreatic cancer: from bench to bedside, then back to the bench. Surgery. 2012; 152:S19–32.
https://doi.org/10.1016/j.surg.2012.05.030
PMID:22770959

68. Sohma I, Fujiwara Y, Sugita Y, Yoshioka A, Shirakawa M, Moon JH, Takiguchi S, Miyata H, Yamasaki M, Mori M, Doki Y. Parthenolide, an NF-κB inhibitor, suppresses tumor growth and enhances response to chemotherapy in gastric cancer. Cancer Genomics Proteomics. 2011; 8:39–47.
PMID:21289336

69. Liu W, Wang X, Sun J, Yang Y, Li W, Song J. Parthenolide suppresses pancreatic cell growth by autophagy-mediated apoptosis. Onco Targets Ther. 2017; 10:453–61.
https://doi.org/10.2147/OTT.S117250
PMID:28176967

70. Tang ZH, Li T, Tong YG, Chen XJ, Chen XP, Wang YT, Lu JJ. A Systematic Review of the Anticancer Properties of Compounds Isolated from Licorice (Gancao). Planta Med. 2015; 81:1670–87.
https://doi.org/10.1055/s-0035-1558227
PMID:26695708

71. Zhou Y, Ho WS. Combination of liquiritin, isoliquiritin and isoliquirigenin induce apoptotic cell death through upregulating p53 and p21 in the A549 non-small cell lung cancer cells. Oncol Rep. 2014; 31:298–304.
https://doi.org/10.3892/or.2013.2849
PMID:24247527

72. Kim A, Ma JY. Isoliquiritin Apioside Suppresses *in vitro* Invasiveness and Angiogenesis of Cancer Cells and Endothelial Cells. Front Pharmacol. 2018; 9:1455.
https://doi.org/10.3389/fphar.2018.01455
PMID:30618749

73. Tuli HS, Tuorkey MJ, Thakral F, Sak K, Kumar M, Sharma AK, Sharma U, Jain A, Aggarwal V, Bishayee A. Molecular Mechanisms of Action of Genistein in Cancer: Recent Advances. Front Pharmacol. 2019; 10:1336.
https://doi.org/10.3389/fphar.2019.01336
PMID:31866857

74. Bi YL, Min M, Shen W, Liu Y. Genistein induced anticancer effects on pancreatic cancer cell lines involves mitochondrial apoptosis, G_0/G_1cell cycle arrest and regulation of STAT3 signalling pathway. Phytomedicine. 2018; 39:10–6.
https://doi.org/10.1016/j.phymed.2017.12.001
PMID:29433670

75. Liu X, Suzuki N, Santosh Laxmi YR, Okamoto Y, Shibutani S. Anti-breast cancer potential of daidzein in rodents. Life Sci. 2012; 91:415–9.
https://doi.org/10.1016/j.lfs.2012.08.022
PMID:23227466

76. Guo JM, Xiao BX, Dai DJ, Liu Q, Ma HH. Effects of daidzein on estrogen-receptor-positive and negative pancreatic cancer cells in vitro. World J Gastroenterol. 2004; 10:860–3.
https://doi.org/10.3748/wjg.v10.i6.860
PMID:15040033

77. Shin SI, Freedman VH, Risser R, Pollack R. Tumorigenicity of virus-transformed cells in nude mice is correlated specifically with anchorage independent growth in vitro. Proc Natl Acad Sci U S A. 1975; 72:4435–9.
https://doi.org/10.1073/pnas.72.11.4435
PMID:172908

78. Creemers SG, van Koetsveld PM, De Herder WW, Dogan F, Franssen GJH, Feelders RA, Hofland LJ. MDR1 inhibition increases sensitivity to doxorubicin and etoposide in adrenocortical cancer. Endocr Relat Cancer. 2019; 26:367–78.
https://doi.org/10.1530/ERC-18-0500
PMID:30650062

79. Steelman LS, Abrams SL, Ruvolo P, Ruvolo V, Cocco L, Ratti S, Martelli AM, Neri LM, Candido S, Libra M, McCubrey JA. Drug-resistance in doxorubicin-resistant FL5.12 hematopoietic cells: elevated MDR1, drug efflux and side-population positive and decreased BCL2-family member expression. Oncotarget. 2017; 8:113013–33.

https://doi.org/10.18632/oncotarget.22956
PMID:29348885

80. Abrams SL, Ruvolo PP, Ruvolo VR, Ligresti G, Martelli AM, Cocco L, Ratti S, Tafuri A, Steelman LS, Candido S, Libra M, McCubrey JA. Targeting signaling and apoptotic pathways involved in chemotherapeutic drug-resistance of hematopoietic cells. Oncotarget. 2017; 8:76525–57.
https://doi.org/10.18632/oncotarget.20408
PMID:29100331

81. Gu D, Schlotman KE, Xie J. Deciphering the role of hedgehog signaling in pancreatic cancer. J Biomed Res. 2016; 30:353–60.
https://doi.org/10.7555/JBR.30.20150107
PMID:27346466

82. De Jesus-Acosta A, Sugar EA, O'Dwyer PJ, Ramanathan RK, Von Hoff DD, Rasheed Z, Zheng L, Begum A, Anders R, Maitra A, McAllister F, Rajeshkumar NV, Yabuuchi S, et al. Phase 2 study of vismodegib, a hedgehog inhibitor, combined with gemcitabine and nab-paclitaxel in patients with untreated metastatic pancreatic adenocarcinoma. Br J Cancer. 2020; 122:498–505.
https://doi.org/10.1038/s41416-019-0683-3
PMID:31857726

83. Berkers CR, Maddocks OD, Cheung EC, Mor I, Vousden KH. Metabolic regulation by p53 family members. Cell Metab. 2013; 18:617–33.
https://doi.org/10.1016/j.cmet.2013.06.019
PMID:23954639

84. Puzio-Kuter AM. The Role of p53 in Metabolic Regulation. Genes Cancer. 2011; 2:385–91.
https://doi.org/10.1177/1947601911409738
PMID:21779507

85. Humpton TJ, Vousden KH. Regulation of Cellular Metabolism and Hypoxia by p53. Cold Spring Harb Perspect Med. 2016; 6:a026146.
https://doi.org/10.1101/cshperspect.a026146
PMID:27371670

86. Kawauchi K, Araki K, Tobiume K, Tanaka N. p53 regulates glucose metabolism through an IKK-NF-kappaB pathway and inhibits cell transformation. Nat Cell Biol. 2008; 10:611–8.
https://doi.org/10.1038/ncb1724
PMID:18391940

87. Matoba S, Kang JG, Patino WD, Wragg A, Boehm M, Gavrilova O, Hurley PJ, Bunz F, Hwang PM. p53 regulates mitochondrial respiration. Science. 2006; 312:1650–3.
https://doi.org/10.1126/science.1126863
PMID:16728594

88. Flöter J, Kaymak I, Schulze A. Regulation of Metabolic Activity by p53. Metabolites. 2017; 7:E21.
https://doi.org/10.3390/metabo7020021
PMID:28531108

89. Eriksson M, Ambroise G, Ouchida AT, Lima Queiroz A, Smith D, Gimenez-Cassina A, Iwanicki MP, Muller PA, Norberg E, Vakifahmetoglu-Norberg H. Effect of Mutant p53 Proteins on Glycolysis and Mitochondrial Metabolism. Mol Cell Biol. 2017; 37:e00328–17.
https://doi.org/10.1128/MCB.00328-17
PMID:28993478

90. Abrams SL, Akula SM, Meher AK, Steelman LS, Gizak A, Duda P, Rakus D, Martelli AM, Ratti S, Cocco L, Montalto G, Cervello M, Ruvolo P, et al. GSK-3β Can Regulate the Sensitivity of MIA-PaCa-2 Pancreatic and MCF-7 Breast Cancer Cells to Chemotherapeutic Drugs, Targeted Therapeutics and Nutraceuticals. Cells. 2021; 10:816.
https://doi.org/10.3390/cells10040816
PMID:33917370

91. Zhao H, Zheng B. Dual Targeting of Autophagy and MEK in KRAS Mutant Cancer. Trends Cancer. 2019; 5:327–9.
https://doi.org/10.1016/j.trecan.2019.04.003
PMID:31208693

92. Abrams SL, Duda P, Akula SM, Steelman LS, Follo ML, Cocco L, Ratti S, Martelli AM, Montalto G, Emma MR, Cervello M, Rakus D, Gizak A, McCubrey JA. Effects of the Mutant TP53 Reactivator APR-246 on Therapeutic Sensitivity of Pancreatic Cancer Cells in the Presence and Absence of WT-TP53. Cells. 2022; 11:794.
https://doi.org/10.3390/cells11050794
PMID:35269416

93. McCubrey JA, Abrams SL, Ligresti G, Misaghian N, Wong EW, Steelman LS, Bäsecke J, Troppmair J, Libra M, Nicoletti F, Molton S, McMahon M, Evangelisti C, Martelli AM. Involvement of p53 and Raf/MEK/ERK pathways in hematopoietic drug resistance. Leukemia. 2008; 22:2080–90.
https://doi.org/10.1038/leu.2008.207
PMID:18685611

94. Balmer MT, Katz RD, Liao S, Goodwine JS, Gal S. Doxorubicin and 5-fluorouracil induced accumulation and transcriptional activity of p53 are independent of the phosphorylation at serine 15 in MCF-7 breast cancer cells. Cancer Biol Ther. 2014; 15:1000–12.
https://doi.org/10.4161/cbt.29112
PMID:24801380

95. Harami-Papp H, Pongor LS, Munkácsy G, Horváth G, Nagy ÁM, Ambrus A, Hauser P, Szabó A, Tretter L, Győrffy B. TP53 mutation hits energy metabolism and increases glycolysis in breast cancer. Oncotarget. 2016; 7:67183–95.
https://doi.org/10.18632/oncotarget.11594
PMID:27582538

96. Kamp WM, Wang PY, Hwang PM. TP53 mutation, mitochondria and cancer. Curr Opin Genet Dev. 2016; 38:16–22.
https://doi.org/10.1016/j.gde.2016.02.007
PMID:27003724

97. Abu El Maaty MA, Strassburger W, Qaiser T, Dabiri Y, Wölfl S. Differences in p53 status significantly influence the cellular response and cell survival to 1,25-dihydroxyvitamin D3-metformin cotreatment in colorectal cancer cells. Mol Carcinog. 2017; 56:2486–98.
https://doi.org/10.1002/mc.22696
PMID:28618116

98. Agarwal S, Bell CM, Taylor SM, Moran RG. p53 Deletion or Hotspot Mutations Enhance mTORC1 Activity by Altering Lysosomal Dynamics of TSC2 and Rheb. Mol Cancer Res. 2016; 14:66–77.
https://doi.org/10.1158/1541-7786.MCR-15-0159
PMID:26385560

99. Frazier ML, Fernández E, de Llorens R, Brown NM, Pathak S, Cleary KR, Abbruzzese JL, Berry K, Olive M, Le Maistre A, Evans DB. Pancreatic adenocarcinoma cell line, MDAPanc-28, with features of both acinar and ductal cells. Int J Pancreatol. 1996; 19:31–8.
https://doi.org/10.1007/BF02788373
PMID:8656025

100. Sokolosky M, Chappell WH, Stadelman K, Abrams SL, Davis NM, Steelman LS, McCubrey JA. Inhibition of GSK-3β activity can result in drug and hormonal resistance and alter sensitivity to targeted therapy in MCF-7 breast cancer cells. Cell Cycle. 2014; 13:820–33.
https://doi.org/10.4161/cc.27728
PMID:24407515

101. Chappell WH, Candido S, Abrams SL, Russo S, Ove R, Martelli AM, Cocco L, Ramazzotti G, Cervello M, Montalto G, Steelman LS, Leng X, Arlinghaus RB, et al. Roles of p53, NF-κB and the androgen receptor in controlling NGAL expression in prostate cancer cell lines. Adv Biol Regul. 2018; 69:43–62.
https://doi.org/10.1016/j.jbior.2018.05.002
PMID:29861174